

ALBRIGHT'S CHEMICAL ENGINEERING HANDBOOK

Edited by
Lyle F. Albright



CRC Press
Taylor & Francis Group

CRC Press
Taylor & Francis Group
6000 Broken Sound Parkway NW, Suite 300
Boca Raton, FL 33487-2742

© 2009 by Taylor & Francis Group, LLC
CRC Press is an imprint of Taylor & Francis Group, an Informa business

No claim to original U.S. Government works
Printed in the United States of America on acid-free paper
10 9 8 7 6 5 4 3 2 1

International Standard Book Number-13: 978-0-8247-5362-7 (Hardcover)

This book contains information obtained from authentic and highly regarded sources. Reasonable efforts have been made to publish reliable data and information, but the author and publisher cannot assume responsibility for the validity of all materials or the consequences of their use. The authors and publishers have attempted to trace the copyright holders of all material reproduced in this publication and apologize to copyright holders if permission to publish in this form has not been obtained. If any copyright material has not been acknowledged please write and let us know so we may rectify in any future reprint.

Except as permitted under U.S. Copyright Law, no part of this book may be reprinted, reproduced, transmitted, or utilized in any form by any electronic, mechanical, or other means, now known or hereafter invented, including photocopying, microfilming, and recording, or in any information storage or retrieval system, without written permission from the publishers.

For permission to photocopy or use material electronically from this work, please access www.copyright.com (<http://www.copyright.com/>) or contact the Copyright Clearance Center, Inc. (CCC), 222 Rosewood Drive, Danvers, MA 01923, 978-750-8400. CCC is a not-for-profit organization that provides licenses and registration for a variety of users. For organizations that have been granted a photocopy license by the CCC, a separate system of payment has been arranged.

Trademark Notice: Product or corporate names may be trademarks or registered trademarks, and are used only for identification and explanation without intent to infringe.

Library of Congress Cataloging-in-Publication Data

Albright's chemical engineering handbook / editor Lyle Albright.
p. cm.

Includes bibliographical references and index.

ISBN 978-0-8247-5362-7 (alk. paper)

1. Chemical engineering--Handbooks, manuals, etc. I. Albright, Lyle Frederick, 1921- II. Title.

TP151.A565 2008
660--dc22

2007020174

Visit the Taylor & Francis Web site at
<http://www.taylorandfrancis.com>

and the CRC Press Web site at
<http://www.crcpress.com>

Chapter 11 Chemical Reaction Engineering.....	737
<i>J. B. Joshi and L. K. Doraiswamy</i>	
Chapter 12 Distillation	969
<i>James R. Fair</i>	
Chapter 13 Absorption and Stripping	1073
<i>James R. Fair</i>	
Chapter 14 Adsorption	1119
<i>Kent S. Knaebel</i>	
Chapter 15 Process Control.....	1173
<i>James B. Riggs, William J. Korchinski, and Arkan Kayihan</i>	
Chapter 16 Conceptual Process Design, Process Improvement, and Troubleshooting	1267
<i>Donald R. Woods, Andrew N. Hrymak, and James R. Couger</i>	
Chapter 17 Chemical Process Safety	1437
<i>Richard W. Prugh</i>	
Chapter 18 Environmental Engineering: A Review of Issues, Regulations, and Resources ...	1485
<i>Bradly P. Carpenter, Douglas E. Watson, and Brooks C. Carpenter</i>	
Chapter 19 Biochemical Engineering	1501
<i>James M. Lee</i>	
Chapter 20 Measuring Physical Properties.....	1531
<i>Lyle F. Albright</i>	
Chapter 21 Selecting Materials of Construction (Steels and Other Metals).....	1539
<i>David A. Hansen</i>	
Chapter 22 Solid/Liquid Separation.....	1597
<i>Frank M. Tiller, Wenping Li, and Wu Chen</i>	
Chapter 23 Drying: Principles and Practice	1667
<i>Arun S. Mujumdar</i>	

Sanjeev S. Katti

The Dow Chemical Company
Midland, Michigan

Arkan Kayihan

Expedia, Inc.
Seattle, Washington

Kent S. Knaebel

Adsorption Research, Inc.
Dublin, Ohio

William J. Korchinski

Advanced Industrial Modeling, Inc.
Santa Barbara, California

James M. Lee

Chemical Engineering Department
and Division of Bioengineering Environmental
Systems
Washington State University
Pullman, Washington

Douglas E. Leng

Leng Associates
Midland, Michigan

Wenping Li

Chemical Engineering Department
University of Houston
Houston, Texas

Richard G. Mallinson

School of Chemical Engineering and Materials
Science
University of Oklahoma
Norman, Oklahoma

Nash McCauley

Retired from Rotex, Inc.
Cincinnati, Ohio

Arun S. Mujumdar

Mechanical Engineering Department
National University of Singapore
Singapore, Indonesia

Nandkishor Nere

School of Chemical Engineering
Purdue University
West Lafayette, Indiana

Frank Oreovicz

Purdue University (retired)
West Lafayette, Indiana

Peter N. Pintauro

Department of Chemical and Biomolecular
Engineering
Vanderbilt University
Nashville, Tennessee

Richard W. Prugh

Chilworth Technology, Inc.
Monmouth Junction, New Jersey

Doraiswami Ramkrishna

School of Chemical Engineering
Purdue University
West Lafayette, Indiana

James B. Riggs

Chemical Engineering Department
Texas Tech
Lubbock, Texas

Daniel W. Siderius

Department of Chemistry
Washington University
St. Louis, Missouri

D. William Tedder

School of Chemical Engineering
Georgia Institute of Technology
Atlanta, Georgia

Fred Thomson (deceased)

Landenberg, Pennsylvania

Frank M. Tiller (deceased)

Chemical Engineering Department
University of Houston
Houston, Texas

Sinh Trinh

Rentech, Inc.
Denver, Colorado

Douglas E. Watson

Greenfield Environmental, Inc.
Downers Grove, Illinois

1.8.7	Liquid-Liquid Equilibria	25
1.8.8	Viscosity	25
1.8.9	Thermal Conductivity	26
1.8.10	Electrolyte Solutions	27
1.9.	Overview of Major Data Sources	27
1.9.1	Introductory Comments	27
1.9.2	NIST (Including TRC)	28
1.9.3	DIPPR	28
1.9.4	DECHEMA	29
1.9.5	DDB	29
1.9.6	NEL	29
1.9.7	Landolt-Börnstein	29
1.9.8	Beilstein	29
1.9.9	Gmelin	30
1.9.10	Process Simulation Software	30
	Acknowledgments	30
	References	30

1.1 INTRODUCTION

No single handbook could tabulate more than a small fraction of the physical and chemical property data needed by engineers. Therefore, this chapter does not contain extensive tables of data, but instead points readers to reliable sources of data and to methods for extrapolation, estimation, or measurement of data.

We cannot emphasize enough the importance of *quality* of data. Much data—whether in handbooks, on the Internet, or in scientific journals—are inaccurate or simply wrong. This can be due to problems with experiments, errors in processing measurements, misuse of extrapolation or estimation techniques, or something as simple as a copying error. For the responsible engineer, the goal is not just to “get a number,” but to get a *reliable* number. Obtaining reliable physical and chemical property data requires *evaluation* of data. This involves expert evaluation of experimental techniques (including sample purity), consistency tests, comparisons among multiple data sets and multiple measurements for the same substance, and other factors such as trends within chemical families. It is preferable to use sources where the data are evaluated and where some indication of their quality is given.

A related issue is *uncertainty*. A datum has little value if one does not know whether it is uncertain by 1% or 100%. Ideally, all data would have a quantitative uncertainty given, which could be propagated into engineering design calculations. In practice, we often have to settle for approximate or qualitative estimates of uncertainties, but the more that can be said about uncertainty, the better.

Data sources listed here range from those that are free, to data available at low cost (for example in a single book or inexpensive database), to databases that may cost thousands of dollars. Of course, engineers want to save money, but often “you get what you pay for.” While one can sometimes take advantage of free products from government agencies or academic groups, reliable data often cost money, because data collection and evaluation require skilled labor. The engineer who uses free data (perhaps from a Web search) of unknown quality as the basis for a multimillion-dollar design is being foolish if more trustworthy data could be obtained for a reasonable price.

As process simulation programs become routine tools, many engineers treat their thermodynamic calculations as a “black box” without giving thought to the underlying data or models. To their credit, developers of process simulators have spent much effort to validate both data and models. However, it is unwise to put blind trust in numbers merely because they are produced by

TABLE 1.1
Thermodynamic Properties of Saturated Water and Steam as a Function
of Temperature

$T, ^\circ\text{C}$	p, MPa	Density, kg/m^3		Enthalpy, kJ/kg		Entropy, $\text{kJ}/(\text{kg}\cdot\text{K})$	
		ρ_L	ρ_V	h_L	h_V	s_L	s_V
0.01	0.000 612	999.79	0.004 855	0.00	2500.9	0.0000	9.1555
5	0.000 873	999.92	0.006 802	21.02	2510.1	0.0763	9.0248
10	0.001 228	999.65	0.009 407	42.02	2519.2	0.1511	8.8998
15	0.001 706	999.06	0.012 841	62.98	2528.3	0.2245	8.7803
20	0.002 339	998.16	0.017 314	83.91	2537.4	0.2965	8.6660
25	0.003 170	997.00	0.023 075	104.83	2546.5	0.3672	8.5566
30	0.004 247	995.61	0.030 415	125.73	2555.5	0.4368	8.4520
35	0.005 629	993.99	0.039 674	146.63	2564.5	0.5051	8.3517
40	0.007 385	992.18	0.051 242	167.53	2573.5	0.5724	8.2555
45	0.009 595	990.17	0.065 565	188.43	2582.4	0.6386	8.1633
50	0.012 352	988.00	0.083 147	209.34	2591.3	0.7038	8.0748
55	0.015 762	985.66	0.104 56	230.26	2600.1	0.7680	7.9898
60	0.019 946	983.16	0.130 43	251.18	2608.8	0.8313	7.9081
65	0.025 042	980.52	0.161 46	272.12	2617.5	0.8937	7.8296
70	0.031 201	977.73	0.198 43	293.07	2626.1	0.9551	7.7540
75	0.038 595	974.81	0.242 19	314.03	2634.6	1.0158	7.6812
80	0.047 414	971.77	0.293 67	335.01	2643.0	1.0756	7.6111
85	0.057 867	968.59	0.353 88	356.01	2651.3	1.1346	7.5434
90	0.070 182	965.30	0.423 90	377.04	2659.5	1.1929	7.4781
95	0.084 608	961.88	0.504 91	398.09	2667.6	1.2504	7.4151
100	0.101 42	958.35	0.598 17	419.17	2675.6	1.3072	7.3541
110	0.143 38	950.95	0.826 93	461.42	2691.1	1.4188	7.2381
120	0.198 67	943.11	1.1221	503.81	2705.9	1.5279	7.1291
130	0.270 28	934.83	1.4970	546.38	2720.1	1.6346	7.0264
140	0.361 54	926.13	1.9667	589.16	2733.4	1.7392	6.9293
150	0.476 16	917.01	2.5481	632.18	2745.9	1.8418	6.8371
160	0.618 23	907.45	3.2596	675.47	2757.4	1.9426	6.7491
170	0.792 19	897.45	4.1222	719.08	2767.9	2.0417	6.6650
180	1.0028	887.00	5.1588	763.05	2777.2	2.1392	6.5840
190	1.2552	876.08	6.3954	807.43	2785.3	2.2355	6.5059
200	1.5549	864.66	7.8610	852.27	2792.0	2.3305	6.4302
210	1.9077	852.72	9.5885	897.63	2797.3	2.4245	6.3563
220	2.3196	840.22	11.615	943.58	2800.9	2.5177	6.2840
230	2.7971	827.12	13.985	990.19	2802.9	2.6101	6.2128
240	3.3469	813.37	16.749	1037.6	2803.0	2.7020	6.1423
250	3.9762	798.89	19.967	1085.8	2800.9	2.7935	6.0721
260	4.6923	783.63	23.712	1135.0	2796.6	2.8849	6.0016
270	5.5030	767.46	28.073	1185.3	2789.7	2.9765	5.9304
280	6.4166	750.28	33.165	1236.9	2779.9	3.0685	5.8579
290	7.4418	731.91	39.132	1290.0	2766.7	3.1612	5.7834
300	8.5879	712.14	46.168	1345.0	2749.6	3.2552	5.7059
310	9.8651	690.67	54.541	1402.2	2727.9	3.3510	5.6244
320	11.284	667.09	64.638	1462.2	2700.6	3.4494	5.5372
330	12.858	640.77	77.050	1525.9	2666.0	3.5518	5.4422
340	14.601	610.67	92.759	1594.5	2621.8	3.6601	5.3356
350	16.529	574.71	113.61	1670.9	2563.6	3.7784	5.2110

[16, 17], liquid densities [18], liquid heat capacities [19, 20], liquid heat capacities at 298.15 K [21], and enthalpies of vaporization [22].

For the vapor pressure, the Antoine equation is widely used:

$$\ln\left(\frac{p^{\text{sat}}}{p_0}\right) = A - \frac{B}{T + C} \quad (1.1)$$

where p^{sat} is the vapor pressure; p_0 is a reference pressure (typically 1 in the units of pressure being used); T is the absolute temperature in kelvins, and A , B , and C are parameters fitted to the data. Sometimes Equation (1.1) is written with a base-10 logarithm, and sometimes with the denominator written as $(T + C - 273.15)$, so when using reported Antoine parameters, one must be careful to use the correct equation format. Because the Antoine equation has a physical basis (it is derived from the Clausius-Clapeyron equation), it can be extrapolated for small distances in temperature, as long as one stays well below the critical temperature. Extended versions of the Antoine equation, with more parameters, are sometimes used to cover a wider temperature range.

The Wagner equation for vapor pressure is capable of covering a wide range of temperatures:

$$\ln\left(\frac{p^{\text{sat}}}{p_c}\right) = \frac{1}{T_r}(a\tau + b\tau^{1.5} + c\tau^3 + d\tau^6) \quad (1.2a)$$

where $T_r = T/T_c$; T_c and p_c are the critical temperature and pressure of the fluid, respectively; $\tau = 1 - T_r$; and a , b , c , and d are adjustable parameters. Because the Wagner equation is constrained to give the correct critical pressure, it is better suited for extrapolation to high temperatures. Unlike the Antoine equation, it requires reliable values of T_c and p_c . Sometimes a slightly different Wagner form gives better results:

$$\ln\left(\frac{p^{\text{sat}}}{p_c}\right) = \frac{1}{T_r}(a\tau + b\tau^{1.5} + c\tau^{2.5} + d\tau^5) \quad (1.2b)$$

Use of the Wagner equations requires relatively extensive and internally consistent data; they may produce unphysical slopes of the vapor-pressure curve if fitted to inconsistent data. Neither the Wagner nor the Antoine equation should be extrapolated far below the temperature range in which it was fitted. Vapor-pressure data at low temperatures (where the vapor pressures are small) are scarce. Often, better estimates of the vapor pressure at low temperatures may be obtained from extrapolation techniques that make use of heat-capacity data, as discussed in *The Properties of Gases and Liquids* [15].

The second approach for calculating thermodynamic properties when some data are available is to use an equation of state (see Chapter 4, "Thermodynamics of Fluid Phase and Chemical Equilibria"). The most popular EOS are cubic equations, especially the Soave-Redlich-Kwong (SRK) and Peng-Robinson (PR) equations. The parameters in these equations were originally computed from the critical parameters and the acentric factor. However, it is also possible to fit the EOS parameters directly to experimental data; it has become common practice to fit parameters in advanced versions of these EOS to vapor-pressure data. Such fitting is generally necessary to get a good representation of the vapor pressure for polar fluids. Twu et al. [23] provide an overview of modern cubic EOS technology.

Because software for cubic EOS calculations is widely available, it is tempting to use these EOS for everything without considering that choice. This is unwise, because these methods have limitations. The common EOS forms like SRK and PR were optimized primarily for hydrocarbons;

An additional alternative is to measure the needed data. The difficulty and cost will depend on the fluid and on the property and conditions of interest. Experiments may well be needed if an important project is at stake, especially if you do not have high confidence in the available estimation methods. Measurement of fluid properties is discussed in Section 1.8 of this chapter.

1.2.7 IDEAL-GAS PROPERTIES

For gases at relatively low pressures, the ideal-gas law is often sufficient to calculate the density. The ideal-gas heat capacity (and its integrated form, the ideal-gas enthalpy) are used not only for calculating the properties of gases assumed to be ideal, but also as a starting point in many calculations of the heat capacity and enthalpy of nonideal fluids.

Ideal-gas heat capacities may be estimated from gas-phase heat-capacity measurements, but more often they are calculated from statistical mechanics based on molecular information, usually obtained by spectroscopy [27–29]. The results of such calculations have been tabulated for many molecules [5, 11–15, 28–30]. Predictive methods also exist based on molecular structure; the leading methods are reviewed in *The Properties of Gases & Liquids* [15]. Calculations from one of these methods (that of Benson) are available in the *NIST Chemistry Webbook* [5].

1.2.8 CRITICAL CONSTANTS AND ACENTRIC FACTORS FOR PURE FLUIDS

The values of temperature, pressure, and density at the critical point, and the acentric factor (which characterizes the shape of the vapor-pressure curve) are seldom of direct interest. However, they are used in many correlations and equations of state.

The critical temperature and pressure have been measured for a few hundred fluids; these are mostly relatively small molecules because most larger molecules with high critical temperatures begin to decompose before the critical temperature is reached. The critical density is less often measured but is seldom used in correlations. Extensive tabulations of critical parameters exist [5, 11–15, 31]; in some cases these sources supplement measured values with those obtained from estimation techniques. Some sources [11, 12, 14, 15] also contain values for the acentric factor. It is also possible to calculate the acentric factor from its definition (see Chapter 4, “Thermodynamics”) from the vapor pressure and values of the critical temperature and pressure.

Techniques exist to estimate the critical parameters and acentric factor from molecular structure; these are reviewed in *The Properties of Gases and Liquids* [15]. Since these techniques depend on the regression of experimental data to assign contributions to individual groups within the molecule, they are reliable only when the functional groups in the molecule for which the prediction is made are present in similar molecules in the dataset used to develop the correlation.

1.3 THERMODYNAMIC PROPERTIES OF SINGLE-PHASE MIXTURES

1.3.1 DENSITY

Three major approaches are used to predict the density of a multicomponent vapor or liquid. Many methods may be enhanced if some mixture data are available.

One approach is to use a mixture equation of state (EOS). This could be one of the cubic EOS mentioned in Section 1.2.5, but their poor performance for pure-fluid densities also carries over to mixtures. More sophisticated mixture EOS are available that make use of the reference-quality equations of state described in Section 1.2.4. If such an EOS exists for each component in a mixture, such an approach can produce good densities. A computer database is available [9] that implements this approach for common refrigerants and light hydrocarbons.

Mixture EOS models generally contain adjustable binary parameters that can improve the predictions if some experimental mixture data are available. Often, these models have been optimized to reproduce vapor-liquid equilibria rather than densities, although such parameters still

this temperature and pressure, the definition of an “ideal” mixture volume in Equation (1.3) loses its usefulness. In practice, Equation (1.5) is useful only for liquid mixtures where all the components are liquids in their pure state at the condition of interest. Equation (1.5) also tends to be less useful in mixtures containing dissimilar components and/or many different functional groups. More parameters are usually needed in such systems, and the implicit assumption that the pair interactions are unaffected by other components in the mixture is less likely to be true.

To use Equation (1.5), reliable data are needed for v^E in binary mixtures. These data are also useful in equation-of-state or corresponding-states approaches if it is desired to fit a binary parameter to improve the performance. References to many binary excess-volume data (but not the data themselves) may be found in the series of books by Wisniak and Tamir [33], and data may be found in the Dortmund Data Bank [13] and a volume of the Landolt-Börnstein series [34].

1.3.2 CALORIC PROPERTIES

The three approaches mentioned in the previous section may also be used to describe caloric properties (enthalpy, entropy, heat capacity) of mixtures. The same considerations mentioned earlier are also true for the application of mixture equations of state and corresponding-states methods for the prediction of caloric properties.

For the third approach mentioned in Section 1.3.1 (modeling a liquid solution in terms of deviation from ideality), one can use Equations (1.3) to (1.5), substituting the excess enthalpy h^E for the excess volume. As with density, such an approach is useful primarily for mixtures of liquids, and for cases where the interactions in solution are not too complex. Strong interactions in solution, such as hydrogen bonding, have a greater effect on h^E than on v^E . h^E data can be found through the bibliography by Wisniak and Tamir [33] and in some additional databases and compilations [13, 31, 35].

The excess enthalpy of a liquid mixture can be rigorously related to the excess Gibbs energy g^E of the solution; models for g^E are typically used for calculating phase equilibria with activity coefficients. The relationship is

$$h^E = -RT^2 \left[\frac{\partial(g^E/RT)}{\partial T} \right]_{p,x} \quad (1.6)$$

where R is the molar gas constant. Equation (1.6) seldom provides a successful approach in practice, probably because the temperature dependence of g^E models is often not very accurate (especially if the parameters have been fitted at only a single temperature). However, it provides a reasonable approximation if good phase-equilibrium data exist over a range of temperatures. Conversely, if measurements of h^E are available, Equation (1.6) may be used to find the temperature dependence of g^E (and therefore the temperature dependence of activity coefficients).

1.4 PHASE EQUILIBRIA FOR MIXTURES

1.4.1 TYPES OF PHASE-EQUILIBRIUM CALCULATIONS

The basic principles of phase equilibria are discussed in the chapter covering thermodynamics (Chapter 4). In general, two or more phases are in equilibrium when they have the same temperature, pressure, and fugacity (or, equivalently, chemical potential) for each species.

While an enormous variety of phase equilibria exist, if we restrict ourselves to fluids, we need consider only the possible presence of a vapor and one or more liquid phases. The case most commonly encountered in chemical engineering (for example, in distillation) is vapor-liquid equilibrium (VLE). Multiple liquid phases (such as oil and water) can be in equilibrium, so one

A German academic group has provided a software package called PE [43] that may be used to perform phase-equilibrium and density calculations with many different equations of state and mixing rules. Parameters are built in for a limited number of components and mixtures, but the software also has the capability to fit parameters to pure-component and mixture data.

It is also possible to calculate mixture phase equilibria based on the reference-quality equations of state described in Section 1.2.4. In this approach, the Helmholtz energy is written as the sum of pure-component contributions (given by the reference-quality EOS for each pure component) plus a residual term. The residual term contains one or more adjustable parameters for each binary. Software implementing this approach is available [9].

For some important classes of compounds, methods have been developed to predict EOS parameters, including binary interaction parameters, from molecular structure. The PSRK method [44] has found significant use, and a promising new method is known as VTPR [45].

1.4.3 ACTIVITY-COEFFICIENT METHODS

The use of activity coefficients for phase equilibria is based on writing the fugacity f_i of each component in the liquid phase as the product of an ideal term and a correction (activity coefficient γ_i) for nonideality:

$$f_i^L = \gamma_i x_i f_i^{0L} \quad (1.9)$$

where the standard-state fugacity f_i^{0L} is the fugacity of pure component i at the temperature and pressure of interest. Fugacity f_i^{0L} is related to the pure-component vapor pressure p_i^{sat} by

$$f_i^{0L} = p_i^{\text{sat}} \phi_i^{\text{sat}} \exp \left[\int_{p_i^{\text{sat}}}^p \frac{v_i^L}{RT} dp \right] \quad (1.10)$$

where ϕ_i^{sat} is the fugacity coefficient of component i at saturation, v_i^L is the liquid molar volume of pure component i , and the exponential is the Poynting factor, which accounts for the effect of pressure on liquid fugacity. Fugacity coefficient ϕ_i^{sat} can be assumed to be unity in many cases (exceptions would be if p_i^{sat} is significantly above atmospheric pressure or if component i associates strongly in the vapor phase [i.e., carboxylic acids, HF]). The Poynting factor can also be taken as unity at pressures near atmospheric; for higher pressures, it may be simplified by assuming that v_i^L is independent of pressure.

The activity coefficients γ_i are typically computed from a model for the excess Gibbs energy g^E , as described in the thermodynamics chapter (Chapter 4). The most popular are the Wilson, NRTL, and Uniquac models, described in detail in many places [15, 36–40]. They contain two or three adjustable (and possibly temperature-dependent) parameters per binary. One cannot predict which model will be best for a given system; however, the Wilson equation is incapable of describing LLE.

For binary pairs where no data exist to which to fit parameters in activity-coefficient models, group-contribution methods have been developed to estimate these parameters based on molecular structure. The leading method, UNIFAC [46], usually provides reasonable estimates for mixtures of organic compounds.

A recent alternative to group-contribution activity-coefficient estimation methods is based on interactions between surface charge distributions (determined by quantum-mechanical calculations) of molecules in solution. The solvation model used for the charge-distribution calculation is known as COSMO; the most widely used method based on this technique is called COSMO-RS [47].

When using binary interaction parameters, it is best to use parameters fitted to binary data at or near the temperature of interest. If data are available at multiple temperatures, it is possible to include limited temperature dependence. It is also possible to fit parameters for a binary pair to ternary data, but only if parameters for the other two binary pairs in the ternary system are already known. Binary interaction parameters are not interchangeable between methods, so it is important to use exactly the same EOS or activity-coefficient model in both data regression and phase-equilibrium calculations.

Finally, VLLE calculations can sometimes be simplified in systems containing water and hydrocarbons. Because the solubility of hydrocarbons in water is very small, simplified calculations can be made by assuming a pure liquid water phase. Methods exist [4] to estimate the amount of water present in the vapor and dissolved in the liquid hydrocarbon phase. Such a simplification could not be performed if the amount of hydrocarbon in the water were important (for example, if wastewater contamination were a key design variable), but it is often adequate for calculations in petroleum refining.

1.4.5 SOURCES OF DATA

Both EOS and activity-coefficient methods require binary interaction parameters. In process simulation software, the necessary parameters may already be built into a data bank. Sometimes, parameters for the system of interest may be found in the literature. If not, however, the parameters must be fitted to mixture data.

The Dortmund Data Bank (DDB) [13] contains a large amount of mixture VLE and LLE data. A large collection of printed data is the DECHEMA Chemistry Data Series [31]; another printed source is the *International Data Series: Selected Data on Mixtures* [49]. Knowledge of an azeotrope (where the coexisting vapor and liquid have the same composition) can be an important piece of VLE data; azeotropic data may be found in the DDB [13] and in a printed compilation [50]. Extensive data for solubility, primarily of gases in various solvents, are in the *IUPAC Solubility Data Series* [51]; some data from this series are now available on the Internet [52]. Solubility data for organic compounds in water are collected in the AQUASOL database [53]; a large subset of these data is available in book form [54]. Some Henry's constants of solutes in water are available in the *NIST Chemistry Webbook* [5], and high-quality correlations have been produced [55] for the Henry's constants of common gases in water over a wide range of temperatures. The compilation of Linke and Seidell [56], while old, is still a valuable source of data for solubilities of inorganic compounds (including salts and other solids) in various liquids.

1.5 TRANSPORT PROPERTIES

1.5.1 KINETIC THEORY FOR TRANSPORT PROPERTIES

For simple approximations to intermolecular interactions, the kinetic theory of gases has been well developed for the computation of transport properties at low densities. Theory and theory-based correlations are reviewed in references [15] and [57]. If the molecules are modeled as hard spheres of diameter σ and molar mass M , kinetic theory gives the following relations for the viscosity η , thermal conductivity λ , and diffusivity D of dilute gases:

$$\eta = C_{\eta} \frac{T^{1/2} M^{1/2}}{\sigma^2} \quad (1.12)$$

$$\lambda = C_{\lambda} \frac{T^{1/2}}{M^{1/2} \sigma^2} \quad (1.13)$$

$$\ln \eta_{\text{mix}} = \sum_i x_i \ln \eta_i + \frac{1}{2} \sum_i \sum_j x_i x_j G_{ij} \quad (1.16)$$

where the sums extend over all species. The G_{ij} parameter may be fitted to binary data where available or else set to zero; structure-based estimation techniques for G_{ij} have also been developed. *The Properties of Gases and Liquids* [15] discusses the merits of this and similar mixing rules. All obtain reasonable results (within about 10% if the pure-component viscosities are accurately known) for most classes of fluids *if* all the mixture components are liquids well below their critical temperatures. Such mixing rules are notoriously unreliable for mixtures of light and heavy components, such as crude oil containing dissolved methane.

The methods in the preceding paragraphs are effective for gases at moderately low densities and for dense liquids well below the critical temperature. For intermediate densities (high-temperature liquids, compressed gases, supercritical fluids), a corresponding-states approach is preferred. In this approach, the properties of the fluid are mapped onto those of a well-known reference fluid such as propane. The mapping parameters may depend on the fluid's critical properties, acentric factor, and/or vapor-pressure curve; one-fluid mixing rules for these quantities are used to map mixtures onto the reference fluid. The most commonly used such approach, SUPERTRAPP [58], has been implemented in NIST databases [9, 59].

For a few fluids (water, air components, light hydrocarbons, common refrigerants), extensive viscosity data exist and have been fitted to comprehensive equations. These reference-quality correlations are available in the pure-fluid property databases mentioned in Section 1.2.4.

For completeness, we mention that the viscosity of a fluid diverges to infinity in the limit as the critical point is approached. The effects of this viscosity divergence are confined to such a tiny region around the critical point that it can usually be ignored.

Viscosity data for pure components are available in several places [11–14, 60–64], and some collections of mixture data (mostly for binaries) also exist [31, 63, 65]. Some additional data references are cited in *The Properties of Gases and Liquids* [15].

1.5.3 THERMAL CONDUCTIVITY

Kinetic theory is useful for vapor-phase thermal conductivities, but a complication (compared to the viscosity) is that molecules can store thermal energy in internal modes. Almost always, an approach due to Eucken is used in which the correlated quantity is $(\lambda M / \eta C_V)$, where λ is the thermal conductivity, M is the molar mass, η is the viscosity (computed as described in Section 1.5.2), and C_V is the constant-volume heat capacity that contains contributions from molecular rotation and vibration. *The Properties of Gases and Liquids* [15] reviews several methods for estimating this factor, and also a group-contribution corresponding-states method that is useful for predictions for some classes of organic compounds. Methods exist [15] for extending the low-density results to somewhat higher pressures.

As with the viscosity, simplistic mole-fraction averaging of pure-component values is not advisable for gas-phase thermal conductivities. The most common method for predicting mixture values has the form

$$\lambda_{\text{mix}} = \sum_i \frac{y_i \lambda_i}{\sum_j y_j A_{ij}} \quad (1.17)$$

where various methods exist [15] for estimating A_{ij} (which is unity if $i = j$). A corresponding-states approach, similar to that for pure components, can also be used.

modeling of electrolytes in mixed solvents is especially difficult and is beyond the scope of this chapter. The thermodynamics of electrolyte solutions is discussed in most physical chemistry textbooks. The key quantities are the osmotic coefficient (which describes the effect of the dissolved electrolyte on the vapor pressure of the solvent) and the activity coefficient (which is related to the chemical potential of the solute).

Correlations for the activity and osmotic coefficients of aqueous electrolytes begin with the theoretically rigorous Debye-Hückel limiting law for dilute solutions. Because the Debye-Hückel theory is accurate only at very low concentrations, it is supplemented by semiempirical terms. The most widely used are the Pitzer model and the electrolyte-NRTL model, both of which may be extended (perhaps with additional parameters) to systems containing multiple salts. A thorough description of the Pitzer model and a listing of parameters is in the monograph edited by Pitzer [70]. Sources for the electrolyte-NRTL model include the original journal article [71] and the book by Zemaitis et al. [72].

Several sources exist [72–74] containing evaluated data for the activity and/or osmotic coefficients of single electrolytes in water at 25°C. Data at other temperatures, or for mixed salts, are more scarce, but some compilations and databases exist [13, 74–76].

If data are lacking on the system of interest, it is often a fair approximation (especially at low and moderate concentrations) to use a “model-substance” approach. The behavior of an electrolyte is assumed to be similar to that of a known electrolyte of the same charge type. For example, NaCl is a model substance for 1:1 salts. This approach is particularly useful in estimating the temperature dependence of activity and osmotic coefficients; when these coefficients are known only at 25°C, the model-substance approach may be used to estimate the effect of temperature.

1.6.2 DENSITY AND ENTHALPY

The methods described in Section 1.3 are generally unsuitable for electrolyte solutions. Electrolytes cannot be simply incorporated into equations of state, and simple mixing rules or corresponding-states approaches do not work because the properties of the pure electrolyte have little relationship to the contributions their ions make to mixture properties.

Typically, density and enthalpy are modeled by starting with a definition of ideal mixing in which each solute contributes as it does at infinite dilution:

$$v^{\text{id}} = x_1 v_1 + \sum_i x_i v_i^{\circ} \quad (1.18)$$

where subscript 1 denotes the solvent, the sum includes all the solutes, and v_i° is the *standard-state* volume of solute i , which is the infinite-dilution limit of the solute's partial molar volume. Additional multiplicative factors appear in the equations if, as is commonly the case for electrolytes, concentration is expressed in molality (moles per kilogram of solvent) instead of mole fraction. An analogous equation applies for the enthalpy:

$$h^{\text{id}} = x_1 h_1 + \sum_i x_i h_i^{\circ} \quad (1.19)$$

For dilute solutions, Equation (1.18) and Equation (1.19) are sufficient to describe the density and enthalpy. For more concentrated solutions, corrections must be applied. The corrections to the density are obtained from the pressure derivative of an activity-coefficient expression, while those for enthalpy are obtained from a temperature derivative. Details are given by Zemaitis et al. [72] and Pitzer [70]; the latter also tabulates parameters for temperature dependence in the Pitzer activity-

Experimental data for the transport properties of aqueous electrolytes are found in several sources [29, 75, 76]. Tables based on smoothed data are in the book by Zaytsev and Aseyev [74]. Values of the viscosity for many electrolyte solutions at 20°C are tabulated in the *CRC Handbook* [26]. While now somewhat dated, the book by Horvath [83] discusses additional correlation methods, data sources, and parameters for transport properties of electrolyte solutions, including material on diffusion coefficients and electrical conductivity.

1.7 PROPERTIES FOR CHEMICAL REACTION EQUILIBRIA

The thermodynamic equilibrium constant for a chemical reaction is a function of temperature only and is related to the standard-state Gibbs energy change for the reaction. The standard state for each component is typically that of the pure substance at the temperature of interest and 0.1 MPa. The standard-state Gibbs energy for each component is taken as that corresponding to the formation of each compound from its elements. Standard-state Gibbs energies are typically tabulated at 298.15 K. Values of the standard-state enthalpy of formation and the heat capacity are used to calculate the standard-state Gibbs energy (and thence the thermodynamic equilibrium constant) at other temperatures.

For many species, thermochemical properties (Gibbs energy and enthalpy of formation, heat capacity) can be found in the *NIST Chemistry Webbook* [5]. A good written source, especially for small molecules, is the *JANAF Tables* [30]. The *NBS Tables of Chemical Thermodynamic Properties* [84] provides thermochemical properties at 298.15 K for many species, including ions in aqueous solution. Many pure-component thermodynamic databases include enthalpy and Gibbs energy of formation for the compounds included [11–14]. For vapor species, ideal-gas properties are often adequate; these may be obtained from the sources described in Section 1.2.7.

It is also possible to estimate standard-state thermodynamic properties from molecular structures, particularly for gas-phase species. Group-contribution methods for such estimations are reviewed in *The Properties of Gases and Liquids* [15]. The most widely used method is that of Benson, for which software is available [85]; more limited calculations are available in the *NIST Chemistry Webbook* [5].

For relatively small molecules, it is becoming routine to calculate thermochemical properties in the ideal-gas state with computational quantum mechanics. For organic species with fewer than about 10 nonhydrogen atoms, the methods are sufficiently well developed that they can rival or even surpass the accuracy that can be obtained from experiment.

Reaction equilibria in solution (acid-base neutralization, etc.) significantly affect phase equilibria and other properties mentioned in previous sections, rendering those calculations much more difficult. In many aqueous electrolyte systems, properly accounting for the speciation in solution is the most important part of the problem.

1.8 MEASUREMENT OF FLUID THERMOPHYSICAL PROPERTIES

1.8.1 WHEN EXPERIMENTS ARE NECESSARY

When data are needed, the option of measurement should always be considered. Even for those without experimental facilities, there is the option of contracting the work. Experiments may be more time-consuming than computerized estimation techniques, but if the data are of sufficient importance, the effort may be a good investment.

When deciding whether experiments are needed when data are lacking, one must weigh the merits of measurement versus estimation. One important factor is the reliability of available estimation methods. If a method has been demonstrated to be reliable for systems very similar to the one of interest, then measurement may be unnecessary. On the other hand, if the only available

reference materials for different property measurements. Many reference materials for calibrations are available through the NIST Standard Reference Materials program [<http://www.nist.gov/srm/>] and other national metrology laboratories.

1.8.3 DENSITY

For liquids at ambient conditions, one can obtain a reasonably accurate density simply by weighing a known volume of the liquid. For rough work, one can use something as simple as a volumetric flask; for more precise work, calibrated volumes (known as pycnometers) are used. One can easily obtain 1% accuracy, and careful pycnometry can obtain 0.1%.

More accurate density measurements may be made by instruments that take advantage of the principle of Archimedes, where the apparent weight of an object immersed in a fluid is diminished by that of the fluid displaced. In the simplest version of this experiment, a “sinker” of known mass and volume is immersed in the fluid while suspended by a wire from an analytical balance. More sophisticated versions may use a magnet to suspend the sinker or measure the difference between two sinkers of similar mass and surface area but different volume. With care and good control of temperature and pressure, such instruments can achieve uncertainties of 0.02% or lower for both vapor and liquid densities.

Another method of measuring density relies on the change in the resonant frequency of a tube (often U-shaped) when it is filled with a fluid. Vibrating-tube densimeters are commercially available; they can be a convenient measuring tool in many circumstances. These instruments must be calibrated (usually with water if liquids are being measured, although for liquids whose density is significantly different from water a calibration fluid with a similar density is preferable) at the temperature and pressure of interest. While the precision of these instruments is often better than 0.01%, very careful calibration and temperature control are required to obtain better than 0.1% uncertainty in practice.

Another alternative, particularly for high-pressure measurements, is the isochoric method. A cell of known volume is filled with the fluid, and then the pressure is measured as the temperature of the cell is changed. This provides data along curves of approximately constant density, known as isochors. Corrections are made for the expansion of the vessel due to temperature and pressure. This method is most useful for supercritical fluids and other situations where the fluid is fairly compressible. Uncertainties with this method can be on the order of 0.1%, but are often higher at elevated temperatures and pressures.

Expansion methods are often used for measuring gas densities. In these methods, a sample is expanded from a small volume to a larger volume (where the ratio of volumes is accurately known), holding the temperature constant and measuring the pressure ratio. Typically, multiple expansions are used (a successive expansion technique known as the Burnett method is popular), with the final state being at a pressure sufficiently low that the density is accurately known by other means (such as correction of the ideal-gas law by the second virial coefficient). The Burnett expansion method may achieve uncertainties in density as low as 0.01%.

1.8.4 HEAT CAPACITY AND CALORIC PROPERTIES

The measurement of heat capacity and related quantities is known as *calorimetry*. Most often the constant-pressure heat capacity C_p is measured; some instruments measure the constant-volume heat capacity C_V . Often, what is actually measured is not the derivatives C_p and C_V but an energy change divided by a small but finite temperature change. In some cases, the original “enthalpy increment” data may be more useful than the approximate heat capacities derived from them. In addition to the IUPAC books referenced in Section 1.8.1, the monograph of Hemminger and Höhne [93] has extensive information about calorimetry.

One category of calorimetric measurements is *batch* or *static calorimetry*, where, in the simplest implementation, the sample is contained in a vessel, a measured amount of energy is

accuracy of ebulliometry can exceed that for static methods, but it is more difficult to extend ebulliometry to high pressures.

Sometimes *comparative* measurements are used, where a substance whose vapor pressure is well known (such as water) serves as a reference. This can be done either by measuring the temperatures of the sample and the reference fluid boiling under the same pressure (comparative ebulliometry), or by measuring the pressure difference between the sample and reference fluid at a common temperature. Comparative measurements can be relatively fast and convenient if a suitable reference fluid is available. With good temperature measurement and an accurately known reference fluid, the accuracy of comparative ebulliometry can be better than 0.1%.

In the *gas saturation* method, a carrier gas such as helium or air is bubbled slowly through the sample, coming to equilibrium with it. The material exiting the apparatus is collected, and the amount of sample dissolved can be measured at the end of the experiment. Knowledge of the number of moles carried away, the number of moles of carrier gas used, and the pressure of equilibration allows calculation of the partial pressure of the sample at equilibrium, which is approximately its vapor pressure. Care must be taken to ensure that all of the carrier gas is equilibrated with the sample and to prevent premature condensation before the solute is collected. This method is typically applied for vapor pressures below about 3 kPa, and may achieve 1% accuracy with careful use.

For very low vapor pressures (below about 10 Pa), the vapor pressure can be measured by the *Knudsen* method, in which the rate of escape of vapor through a small hole is measured. The kinetic theory of gases (with correction factors for hole geometry, etc.) is used to relate the rate of effusion to the vapor pressure. The attainable accuracy of such methods is around 1% to 10% at best, but it is often the only experimental option for substances of very low volatility.

1.8.6 MIXTURE VAPOR-LIQUID EQUILIBRIA

The experimental measurement of vapor-liquid equilibria in mixtures is a huge subject; space considerations dictate that we only briefly discuss the major categories of techniques. More information may be found in some books [87, 90, 94].

The *analytic* method involves confining a mixture in a two-phase state, measuring its temperature and pressure, and analyzing samples from each phase to obtain the equilibrium compositions. This is challenging in practice, largely due to the difficulty of sampling. Samples must be small to avoid disturbing the equilibrium, and they must be extracted without changing their composition. Often, internal stirring or mixing is needed to obtain equilibrium in a reasonable period of time. This approach is widely used and can provide accurate data if done carefully. Sometimes only the liquid composition is measured; while this provides less information, it may suffice if the vapor phase is predominantly a single component whose solubility in the liquid is the quantity of most interest. Sometimes measurement of the total pressure and the liquid composition are combined with approximate thermodynamic analysis of the vapor (for example, with the virial equation) to yield a complete picture of the vapor-liquid equilibrium.

In some cases, it is possible to measure the composition of one or both phases without withdrawing a sample. Techniques for *in situ* composition measurements include various forms of spectroscopy and measurements of other properties such as the refractive index.

A related *dynamic* method makes use of a recirculating still to produce equilibrated samples of vapor and liquid. This method is often used at low and moderate pressures; it is particularly suited for mixtures where the volatilities of the components are similar.

A dynamic technique known as *differential ebulliometry* can measure the effect of small amounts of solute on a solvent. The difference in temperature is measured between a pure fluid and a solution, both of which are boiling at the same pressure. Differential ebulliometry is a common technique for determining infinite-dilution activity coefficients, particularly when the solute is less volatile than the solvent.

sealed instruments may be used. A different analysis must be applied to obtain correct results with a sealed capillary viscometer [96]. Sealed capillary viscometers have not yet been commercialized, and the uncertainty is currently 2% at best.

A second type of capillary viscometer generates a constant volumetric flow rate with a pumping device, and the viscosity is determined by measuring the pressure drop. Such viscometers have been used mostly in research, but some commercial instruments are available. These viscometers may be used over a wide range of conditions for both gases and liquids, and in some cases the uncertainty can be reduced to less than 0.1%.

Another simple method is to measure the falling or rolling of a sphere through a liquid; this motion is described by Stokes's law under certain simplifying assumptions. This method is commonly used for viscous liquids, with an accuracy on the order of 3%. It can also be used for liquids at high pressures, with some loss of accuracy.

A more sophisticated technique involves measuring the damping of the oscillations of a body immersed in a fluid. The oscillating body may be a sphere, a thin disk, or a cylinder. Research instruments of this type can attain better than 0.5% accuracy (0.05% in the best cases) for both vapors and liquids over a wide range of conditions. In a variant known as the oscillating-cup method, the fluid is contained inside a hollow body; this method is more often used for high-temperature measurements on fluids such as molten metals or molten salts.

Three techniques related to oscillating-body methods can be mentioned. One involves measuring the torsional oscillations of a piezoelectric crystal immersed in a fluid; it can achieve accuracies of about 2% and has been used in a variety of conditions. A second involves measuring the drag on a rotating cylinder magnetically suspended in the fluid; it can achieve uncertainties as low as 0.15% in the dilute-gas region and 0.4% for higher densities. A third technique involves measuring the damping of a vibrating wire due to shear and to its inertia; this can yield simultaneous measurements of density and viscosity, with uncertainties in viscosity near 4% if both properties are being measured, or near 0.5% if the density is already accurately known. The first two techniques have been implemented in commercially available viscometers.

Finally, there are industrial rheological instruments in common use that allow determination of viscosities for liquids to within a few percent, which is sufficient for many purposes. These involve measuring the torque required to maintain a given velocity for a fluid confined in the annulus between two concentric cylinders, one of which is rotated (*Couette* viscometer), or a fluid confined between a flat plate and a rotating cone (*cone-and-plate* viscometer).

1.8.9 THERMAL CONDUCTIVITY

The traditional way to measure thermal conductivity is with *steady-state* instruments, in which a measured heat flux is compared to a temperature difference between surfaces. Most often the geometry is coaxial cylinders, a thin wire inside a cylinder, or parallel plates. In such instruments, eliminating convection currents is crucial; many old data taken with steady-state instruments are unreliable because of convection. Multiple experiments at different heat fluxes are often performed to verify the absence of convection. With good design and operation, such instruments may achieve accuracy in the 1% to 3% range.

A newer method is the *transient hot-wire* method, where an electric current is passed through a metal wire immersed in the fluid. The resistance of the wire is affected by its temperature, which in turn is affected by the dissipation of heat from the wire's surface, which depends on the thermal conductivity of the fluid. These instruments require sophisticated data analysis, but that is no longer an obstacle with the ready availability of personal computers. The absence of convection is relatively easy to verify. The best research instruments can achieve an accuracy of better than 1%. Measurements on conducting fluids (such as polar liquids) are more difficult because of the need to electrically insulate the wire. Other geometries, such as needle-shaped cylinders and thin strips, are also sometimes used for transient measurements.

1.9.2 NIST (INCLUDING TRC)

One of the mandates of the U.S. National Institute of Standards and Technology (NIST) is to provide reliable data to meet the needs of industry, including the physical and chemical property data that are the subject of this chapter.

One of the main sources of data from the NIST is the Standard Reference Database program [<http://www.nist.gov/srd/>]. Computer databases are available for the thermophysical properties of a variety of industrially important fluids and fluid mixtures, including water, air, cryogenic fluids, common refrigerants (including refrigerant blends), and natural gas [8,9]. These are available as stand-alone programs or as source code for integration into other software.

The *NIST Chemistry Webbook* [5] provides information on a large number of chemical compounds. This includes thermophysical property information (a subset of that available in the Standard Reference Databases) for several important pure fluids. Structural information is available for a large number of compounds, and for many of these data are given for vapor pressure, heats of formation and phase change, and/or ideal-gas heat capacity.

The NIST's Thermodynamics Research Center (TRC) has a large collection of pure-fluid thermodynamic and transport properties; tables of recommended values and correlations exist both in paper form and in a computer database [12]. The TRC has also produced books with comprehensive compilations for organic compounds (sometimes also available as software) for vapor pressure [17], liquid density [18], and ideal-gas heat capacity [29], in addition to a compilation on virial coefficients [32]. Their major archival database of experimental pure-component and mixture data is called Source [97]; it is currently available only to members of their consortium. Some data for mixtures of organic compounds are published in the periodical *Selected Data on Mixtures* [49]. More information is at <http://trc.nist.gov>.

Other sources of data from the NIST include the *JANAF Tables* for standard-state properties of small molecules [30], *The NBS Tables of Chemical Thermodynamic Properties* for species (including aqueous ions) at 298.15 K [84], and the *Journal of Physical and Chemical Reference Data* (jointly published by NIST and the American Institute of Physics).

1.9.3 DIPPR

The Design Institute for Physical Properties (DIPPR) of the American Institute of Chemical Engineers (AIChE) sponsors a variety of projects to provide data for the chemical industries. The DIPPR's Project 801 produces a database containing pure-component thermodynamic and transport properties for over 1900 industrially important chemicals. Recommended values are given for a number of single-valued properties (such as critical parameters, normal boiling point, standard-state Gibbs energy, and enthalpy of formation), and correlations are given for 15 temperature-dependent properties (such as vapor pressure, heat of vaporization, and transport properties for the saturated liquid and vapor). Evaluated experimental data are used where possible, but sometimes estimation techniques are used to fill in missing values so that a complete set of recommended and evaluated data is given for each compound included in the database. The original data used to develop the recommended values are also available. DIPPR 801 data are available in both book and electronic form [11]. The most recent data are restricted to the project's industrial sponsors; the version available to the general public lags behind by about two years.

DIPPR Project 911 compiles and evaluates data for environmental and health purposes. This includes data on flammability, toxicity, biological oxygen demand, and related properties, and data for air/water and octanol/water partitioning. A discontinued project compiled several volumes of data for transport properties of mixtures [65]. Information about the DIPPR, including other projects relevant to physical and chemical properties, may be found at <http://www.aiche.org/dippr/>.

While many technical reference libraries have *Beilstein* in print form, it is more convenient to search for information in the electronic form of the database. In addition, the printed series is no longer being updated. The electronic database allows a variety of searches on compounds and properties. Access to the electronic database is offered through CrossFire Beilstein [see <http://www.mdl.com>] or through the STN database system of the Chemical Abstracts Service [<http://www.cas.org/stn.html>]. Some details given in the print version (such as experimental methods) were not carried over to the electronic version, so in some cases it may be necessary to consult the print version or the literature citation for further information.

1.9.9 GMELIN

Gmelin's Handbook of Inorganic and Organometallic Chemistry, first published in German in the 1700s, is to inorganic and organometallic chemistry what *Beilstein* is to organic chemistry. Like *Beilstein*, it is more focused on chemical aspects, but contains some thermodynamic property information. Also like *Beilstein*, much of the data (without some supplementary information) has been carried over into an electronic database that continues to be updated. Access to the electronic database is offered through CrossFire Gmelin [see <http://www.mdl.com>] or the STN database system of the Chemical Abstracts Service [<http://www.cas.org/stn.html>].

1.9.10 PROCESS SIMULATION SOFTWARE

In chemical process design, it is common to obtain property data via process simulation software. This is sometimes a good option; the major simulation packages incorporate data from NIST, DIPPR, and other reliable sources. Caution is in order, however, especially for temperature-dependent properties and for mixture quantities such as binary interaction parameters in activity-coefficient models or equations of state. The danger is that the parameters in the simulation software may be fitted at conditions other than those of interest, and often it is difficult to tell where the parameters came from or under what conditions they are applicable. It is important to verify that the parameters in the software are appropriate for the conditions in which they are being used; that might involve a query to the vendor or doing some sample calculations to validate them against data.

ACKNOWLEDGMENTS

This chapter is a contribution of the National Institute of Standards and Technology, not subject to copyright in the United States. The identification of certain commercial products in this chapter neither constitutes nor implies recommendation or endorsement by the U.S. government or the National Institute of Standards and Technology. Material for some sections was supplied by Dr. Arno Laesecke of NIST (Section 1.8.8) and Dr. Song Yu of Columbia University (Sections 1.9.8 and 1.9.9). Several members of the NIST Experimental Properties of Fluids Group provided helpful input for Section 1.8.

REFERENCES

1. Brandrup, J., E. H. Immergut, and E. A. Grulke, eds., *Polymer Handbook*, 4th ed., John Wiley & Sons, New York, 1999.
2. Danner, R. P., and M. S. High, *Handbook of Polymer Solution Thermodynamics*, AIChE, New York, 1993.
3. Caruthers, J. M. (ed.), *Handbook of Diffusion and Thermal Properties of Polymers and Polymer Solutions*, AIChE, New York, 1998.
4. American Petroleum Institute, *Technical Data Book: Petroleum Refining*, 6th ed., API, Washington, DC, 1997; available on-line at <http://www.epcon.com>.

30. Chase, M. W., Jr., ed., *NIST-JANAF Thermochemical Tables*, 4th ed., American Institute of Physics, Melville, NY, 1998.
31. Society for Chemical Engineering and Biotechnology, *DECHEMA Chemistry Data Series*; <http://www.dechema.de/CDS-design-1.html>.
32. Dymond, J. D., K. N. Marsh, and R. C. Wilhoit, *Virial Coefficients of Pure Gases and Mixtures* (subvols. A and B), in *Landolt-Börnstein: Numerical Data and Functional Relationships in Science and Technology—New Series*, vol. 4/21, Springer-Verlag, Berlin, 2002–2003.
33. Wisniak, J., and A. Tamir, *Mixing and Excess Thermodynamic Properties: A Literature Source Book*, Elsevier, Amsterdam, 1978; see also *Supplement 1*, Elsevier, Amsterdam, 1982; *Supplement 2*, Elsevier, Amsterdam, 1986.
34. *Densities of Liquid Systems* (subvols. A and B), in *Landolt-Börnstein: Numerical Data and Functional Relationships in Science and Technology—New Series*, vol. 4/1, Springer-Verlag, Berlin, 1974–1977.
35. Christensen, J. J., R. W. Hanks, and R. M. Izatt, *Handbook of Heats of Mixing*, Wiley, New York, 1982; J. J. Christensen, R. L. Rowley, and R. M. Izatt, *Handbook of Heats of Mixing (Supplementary Volume)*, Wiley, New York, 1988.
36. Prausnitz, J. M., R. N. Lichtenthaler, and E. Gomes de Azevedo, *Molecular Thermodynamics of Fluid-Phase Equilibria*, 3rd ed., Prentice Hall, Upper Saddle River, NJ, 1999.
37. Walas, S., *Phase Equilibria in Chemical Engineering*, Butterworth, Boston, 1985.
38. Sandler, S. I., *Chemical and Engineering Thermodynamics*, 3rd ed., Wiley, New York, 1998.
39. Elliott, J. R., and C. T. Lira, *Introductory Chemical Engineering Thermodynamics*, Prentice Hall, Upper Saddle River, NJ, 1999.
40. Smith, J. M., H. C. Van Ness, and M. M. Abbott, *Introduction to Chemical Engineering Thermodynamics*, 6th ed., McGraw-Hill, New York, 2001.
41. Anderko, A., in *Equations of State for Fluids and Fluid Mixtures* (J. V. Sengers, R. F. Kayser, C. J. Peters, and H. J. White, Jr., eds.), 75–126, Elsevier, Amsterdam, 2000.
42. Sandler, S. I., and H. Orbey, in *Equations of State for Fluids and Fluid Mixtures* (J. V. Sengers, R. F. Kayser, C. J. Peters, and H. J. White, Jr., eds.), 321–357, Elsevier, Amsterdam, 2000.
43. Thermische Verfahrenstechnik; available on-line at <http://www.tu-harburg.de/vt2/pe2000/>.
44. Horstmann, S., K. Fischer, and J. Gmehling, *Fluid Phase Equil.* 167: 173 (2000), and references therein.
45. Ahlers, J., and J. Gmehling, *Ind. Eng. Chem. Res.* 41: 5890 (2002).
46. Wittig, R., J. Lohmann, and J. Gmehling, *Ind. Eng. Chem. Res.* 42: 183 (2003), and references therein.
47. Klamt, A., and F. Eckert, *Fluid Phase Equil.* 172: 43 (2000); F. Eckert and A. Klamt, *Ind. Eng. Chem. Res.* 40: 2371 (2001); O. Spuhl and W. Arlt, *Ind. Eng. Chem. Res.* 43: 852 (2004); see also <http://www.cosmologic.de>.
48. Hayden, J. G., and J. P. O'Connell, *Ind. Eng. Chem. Process Des. Dev.* 14: 209 (1975).
49. International Data Series, Selected Data on Mixtures, Series A: Thermodynamic Properties of Non-Reacting Binary Systems of Organic Substances. Quarterly publication with annual index, 1973–present; see <http://trc.nist.gov/IDS/ids.htm>.
50. Gmehling, J., J. Menke, J. Krafczyk, and K. Fischer, *Azeotropic Data*, 3 vols., Wiley-VCH, Weinheim, 2004.
51. *IUPAC Solubility Data Series*. Over 80 volumes published beginning in 1979; a listing is given at <http://www.iupac.org/publications/sds/volumes.html>. Beginning with vol. 66 (1998), new volumes are published in the *Journal of Physical and Chemical Reference Data*.
52. IUPAC-NIST Solubility Database, <http://srdata.nist.gov/solubility/>.
53. AQUASOL Database; <http://www.pharmacy.arizona.edu/outreach/aquasol/>.
54. Yalkowsky, S. H., and Y. He, *Handbook of Aqueous Solubility Data*, CRC Press, Boca Raton, FL, 2003.
55. Fernández-Prini, R., J. L. Alvarez, and A. H. Harvey, *J. Phys. Chem. Ref. Data* 32: 903 (2003).
56. Linke, W. F., and A. Seidell, *Solubilities: Inorganic and Metal-Organic Compounds*, American Chemical Society, Washington, DC, vol. 1, 1958; vol. 2, 1965.
57. Millat, J., J. H. Dymond, and C. A. Nieto de Castro (eds.), *Transport Properties of Fluids: Their Correlation, Prediction and Estimation*, Cambridge University Press, Cambridge, 1996.
58. Huber, M. L., and H. J. M. Hanley, in *Transport Properties of Fluids: Their Correlation, Prediction and Estimation* (J. Millat, J. H. Dymond, and C. A. Nieto de Castro, eds.), pp. 283–295, Cambridge University Press, Cambridge, 1996.

86. McCullough, J. P., and D. W. Scott, eds., *Calorimetry of Non-reacting Systems*, vol. 1 of *Experimental Thermodynamics*, Butterworths, London, 1968.
87. Le Neindre, B., and B. Vodar, eds., *Experimental Thermodynamics of Non-reacting Fluids*, vol. 2 of *Experimental Thermodynamics*, Butterworths, London, 1975.
88. Marsh, K. N., and P. A. G. O'Hare, eds., *Solution Calorimetry*, vol. 4 of *Experimental Thermodynamics*, Blackwell Scientific, Oxford, 1994.
89. Goodwin, A. R. H., K. N. Marsh, and W. A. Wakeham, eds., *Measurement of the Thermodynamic Properties of Single Phases*, vol. 6 of *Experimental Thermodynamics*, Elsevier, Amsterdam, 2003.
90. Weir, R. D., and T. W. de Loos, eds., *Measurement of the Thermodynamic Properties of Multiple Phases*, vol. 7 of *Experimental Thermodynamics*, Elsevier, Amsterdam, 2005.
91. Armarego, W. L. F., and C. L. L. Chai, *Purification of Laboratory Chemicals*, 5th ed., Butterworth-Heinemann, Amsterdam, 2003.
92. Marsh, K. N., ed., *Recommended Reference Materials for the Realization of Physicochemical Properties*, Blackwell Scientific, New York, 1987.
93. Hemminger, W., and G. Höhne, *Calorimetry: Fundamentals and Practice*, Verlag Chemie, Weinheim, 1984.
94. Raal, J. D., and A. L. Mühlbauer, *Phase Equilibria: Measurement and Computation*, Taylor & Francis, Bristol, PA, 1998.
95. Novák, J. P., J. Matou, and J. Pick, *Liquid-Liquid Equilibria*, vol. 7 of *Studies in Modern Thermodynamics*, Elsevier, Amsterdam, 1987.
96. Laesecke, A., T. O. D. Luddecke, R. F. Hafer, and D. J. Morris, *Int. J. Thermophys.* 20: 401 (1999).
97. Frenkel, M., Q. Dong, R. C. Wilhoit, and K. R. Hall, *Int. J. Thermophys.* 22: 215 (2001).

2.3.5	Binomial Theorem.....	58
2.3.6	Inequalities.....	58
2.3.6.1	Algebraic Inequalities	58
2.3.6.2	Integral Inequalities.....	59
2.4	Differential and Integral Calculus.....	60
2.4.1	Functions, Limits, and Continuity	60
2.4.2	The Derivative	61
2.4.2.1	An Example Application of the Derivatives.....	62
2.4.3	The Mean Value Theorem.....	62
2.4.3.1	An Example Application of the Mean Value Theorem.....	62
2.4.4	L'Hôspital's Rule.....	63
2.4.5	Implicit Function Theorem.....	64
2.4.6	The Integral	64
2.4.6.1	Improper Integrals.....	65
2.4.6.2	An Example Application of the Integrals.....	66
2.5	Vector Analysis.....	66
2.5.1	Vector Algebra.....	66
2.5.2	Vector Calculus.....	68
2.5.3	Orthogonal Curvilinear Coordinate Systems	69
2.5.3.1	Scale Factors and Metric Tensors.....	69
2.5.3.2	Differential Operators in Curvilinear Coordinate System	70
2.5.3.3	Circular Cylindrical Coordinates	71
2.5.3.4	Spherical Coordinates	71
2.5.3.5	Elliptic Cylindrical Coordinates	72
2.5.3.6	Prolate Spheroidal Coordinates	72
2.5.3.7	Oblate Spheroidal Coordinates	73
2.5.3.8	Parabolic Cylinder Coordinates	73
2.5.3.9	Parabolic Coordinates	74
2.5.3.10	Conical Coordinates.....	74
2.5.3.11	Ellipsoidal Coordinates.....	75
2.5.3.12	Paraboloidal Coordinates	75
2.5.3.13	Bispherical Coordinates	76
2.5.3.14	Toroidal Coordinates.....	76
2.5.4	Vector Integral Theorems	76
2.5.5	Gradients of Sum and Product.....	77
2.6	Dimensional Analysis.....	78
2.6.1	Theory of Dimensional Analysis	78
2.6.2	Applications of Dimensional Analysis.....	79
2.7	Algebraic Equations	81
2.7.1	System of Linear Equations	81
2.7.1.1	Solution of Linear Equations.....	83
2.7.2	Nonlinear Equations	85
2.7.2.1	Polynomial Equations	85
2.7.2.2	Numerical Solutions of Nonlinear Equations.....	88
2.8	Difference Equations	92
2.8.1	Method of Solution for Homogeneous Equations.....	92
2.8.2	Method of Solution for Inhomogeneous Equations.....	92
2.8.3	Numerical Solutions to Ordinary Differential Equations	94
2.8.3.1	Explicit Methods	96
2.8.3.2	Implicit Methods	99

2.11.4	Methods of Solution for Fredholm Equations	136
2.11.4.1	Degenerate Kernels	136
2.11.4.2	Method of Fredholm Resolvent Kernels	137
2.11.4.3	Method of Iterated Kernels	138
2.11.4.4	Symmetric Kernels	139
2.11.4.5	Numerical Solution of Nonhomogeneous Fredholm Equation of the Second Kind	139
2.11.4.6	Solution of Ill-Posed Fredholm Equations of the First Kind	140
2.11.4.7	Method of Regularization	142
2.12.	Complex Variables	143
2.12.1	Properties of Complex Numbers	143
2.12.2	Analytic Functions	144
2.12.2.1	Elementary Functions	147
2.12.2.2	Multivalued Functions	147
2.12.2.3	Logarithmic Functions	148
2.12.2.4	Cauchy Integral Formula	148
2.12.2.5	Laurent Series	149
2.12.3	Residue Theorem	149
2.12.3.1	Calculus of Residues	149
2.12.3.2	Application of Complex Integration	150
2.12.4	Argument Principle and Rouché Theorem	151
2.12.5	Conformal Mapping	152
2.13	Integral Transforms	155
2.13.1	Laplace Transform	156
2.13.1.1	Convolution Property	156
2.13.1.2	Application of Laplace Transform	156
2.13.2	Fourier Transform	157
2.13.2.1	Convolution Property	157
2.13.2.2	Application of Fourier Transform	158
2.13.2.3	Application of Fourier Sine Transform	159
2.13.2.4	Application of Fourier Cosine Transform	160
2.13.3	Mellin Transform	160
2.13.3.1	Convolution Property	160
2.13.3.2	Application of Mellin Transform	161
2.13.4	Hankel Transform	162
2.13.4.1	Property of Hankel Transform	162
2.13.4.2	Application of Hankel Transform	162
2.14	Calculus of Variations	163
2.14.1	Euler-Lagrange Differential Equation	163
2.14.2	Euler-Lagrange Equations for a Functional of n -Dependent Variables	164
2.14.3	Euler-Lagrange Equations for a Functional Involving n -Order Derivative	165
2.14.4	Euler-Lagrange Equations for a Functional of Two Independent Variables	165
2.14.5	Application of Calculus of Variations	165
2.15	Stochastic Differential Equations	166
2.15.1	Differential Chapman-Kolmogorov Equation	167
2.15.2	Connection between the Fokker-Planck Equation and Stochastic Differential Equation	167
2.15.3	Itô Stochastic Integral	168
2.15.3.1	One-Dimensional Itô Formula	169
2.15.3.2	An Example Application of a Stochastic Differential Equation	169
2.16	Asymptotic Approximations and Expansions	170

When multiple steady states exist, the stability of these solutions and the startup condition must be contemplated to ensure that the desired steady state is attained.

Continuity with respect to small perturbations in the governing equations is more difficult to ascertain. It can arise in problems where the mathematical equations are structurally unstable. Typical examples of these problems are systems undergoing bifurcation. In structurally unstable systems, small perturbations in system parameters lead to large changes in the solution. For example, slight perturbations can alter the stability characteristics of the solutions. In addition to these structurally unstable systems, there is a class of engineering problems that is sensitive with respect to small errors due to, perhaps, uncertainties in measurements or other fluctuations in the surrounding environments. These problems arise in determining unknown functions of interest from experimental data. They are known broadly as inverse problems.

A particular class of problems whose solutions are sensitive to initial conditions is known as chaotic problems. The phenomenon of chaos has been observed in fluid mechanics, chemical reactions, and biological systems (Cvitanovic, 1987). A special feature of these systems is unpredictability. The chaotic solutions are so sensitive to initial conditions that two systems with minute differences in their initial states can eventually diverge from each other. Thus their long-term dynamics are unpredictable.

The foregoing issues are clearly important, since understanding them can affect the engineering designs and operations, but they have not received adequate attention from practicing engineers. In this chapter, various mathematical tools for investigation and computation of chemical engineering problems are introduced to help the practicing engineer to adapt to the modern approach to the design and operation of chemical engineering equipment. The special features of this chapter are to bring these issues to the attention of the readers and address some of them in sections where they are encountered using the techniques currently available in the literature. Special focus is placed on (a) simple analyses of equations to ensure that numerical solutions are reliable and (b) the formulation of a class of ill-posed problems, the inverse problems.

The specific objectives of this chapter are to

1. Sensitize the reader to the issues of well-posedness of a mathematical problem
2. Provide concise coverage of solution techniques in linear and nonlinear problems and provide directions for more detailed treatment
3. Introduce the engineer briefly to symbolic and numerical software for solving mathematical problems of interest. It should be noted that we have not cited literature in the text, however, pertinent references are included in the bibliography.

The organization of this chapter preserves the hierarchy of topics generally followed in the applied mathematics literature. However, the reader is encouraged to refer to Table 2.1 for general guidelines on what chemical engineering activity would lead to each of the itemized sections.

2.2 EQUATIONS ENCOUNTERED IN CHEMICAL ENGINEERING

The mathematical equations arising in chemical engineering are obtained by applying the conservation principles of mass, energy, and momentum to chemical reaction systems. These equations express the accumulation of mass, energy, or momentum in the system as a result of the combined effects of net fluxes across the boundary and the consumption or production of these quantities in the system. These equations can be classified as algebraic equations, ordinary differential equations, partial differential equations, integral equations, and integrodifferential equations. The reader is referred to various free Web sources (e.g., <http://en.wikipedia.org/wiki/Trigonometry>, etc.) for the details pertaining to the trigonometry that has not been covered in this chapter.

Algebraic equations arise in systems that are independent of space and time variations, and ordinary differential equations govern systems that either vary with space or vary with time. In

ified at the entrance and exit of the reactor (boundary-value problems). The existence and uniqueness of a solution for an initial-value problem are guaranteed by a general theorem. Partial differential equations arise in steady-state systems with variations in more than one spatial coordinate. Unsteady-state systems may include temporal variations. Transient equations for tubular reactors are examples of partial differential equations.

Integral equations are equations that contain the integral of the unknown functions. There are two types of integral equations: Volterra and Fredholm integral equations. Fredholm equations feature integrals with *fixed* limits, while Volterra equations have integrals in which the limits of integration are the independent variables. These equations can be obtained by direct formulation or by the reduction of differential equations. Volterra equations are reduced from initial-value problems, and Fredholm equations from boundary-value problems.

Integrodifferential equations involve both derivatives and integrals of the unknown functions. These equations arise in radiative transport problems in weakly absorbing media and naturally arise in the modeling of particulate systems. For more information, see the monograph by Ramkrishna (2000).

There are many systems that can fluctuate randomly in space and time and cannot be described by deterministic equations. For example, Brownian motion of small particles occurs randomly because of random collisions with molecules of the medium in which the particles are suspended. It is useful to model such systems with what are known as stochastic differential equations. Stochastic differential equations feature “noise” terms representing the behavior of random elements in the system. Other examples of stochastic behavior arise in chemical reaction systems involving a small number of molecules, such as in a living cell or in the formation of particles in emulsion drops, and so on. A useful reference on stochastic methods is Gardiner (2003).

The different equations encountered in mathematical modeling can be further classified as linear and nonlinear equations. Linear equations arise in systems where the unknowns in the equations are present in the first power. Linear equations enjoy the principle of superposition, i.e., the sum of the solutions is also a solution of the equations. Linearity allows the original problem to be partitioned into simpler component problems that can be solved separately and superimposed to obtain the solution to the original problem.

In what follows, we present representative chemical engineering applications arising in each of the foregoing classes of equations so as to familiarize the reader with their scope. Introductory discussion is deferred to the individual sections covering each topic.

2.2.1 PROCESSES GOVERNED BY DIFFERENCE EQUATIONS

We may classify the difference equations encountered in chemical engineering applications into two types, namely, scalar and vector difference equations. The unknowns in difference equations are functions of discrete independent variables.

2.2.1.1 Scalar Difference Equations

Dissolution of a species: We consider the dynamics of dissolution of a solid mounted on a revolving assembly to show that the mathematical description of its dissolution gives rise to a simple scalar difference equation.

Let x_0 = initial concentration of the dissolved solid in the solution; x_s = solubility of the solid species in a solvent; x_n = concentration of dissolved species at time $t_n = (\Delta t)n$, where n stands for the number of discrete time steps, (Δt) . For dissolution to occur, we must of course assume that $x_0 < x_s$. The rate law for the concentration of dissolved solid in the solution follows the equation

$$\frac{x_{n+1} - x_n}{\Delta t} = K_{La}(x_s - x_n) \quad (2.1)$$

Also, we have

$$X_{0,i} = p_i, \quad i = 1, 2, \dots, m \quad (2.8)$$

If $X_{n,i}$ are known, the original variables $x_{n,i}$ are then recovered from

$$x_{n,i} = \frac{X_{n,i}x_{0,i}}{\sum_{j=1}^m X_{n,j}x_{0,j}} \quad (2.9)$$

To solve for $X_{n,i}$, it is convenient to define the vector $\mathbf{X}_n = (X_{n,1}, X_{n,2}, \dots, X_{n,m})$ and the matrix operator \mathbf{A} , whose elements are given by

$$a_{ij} \equiv Rp_i\delta_{ij} + p_ix_{0,j} \quad (2.10)$$

\mathbf{X}_n is then satisfied by a difference equation of the form

$$\mathbf{X}_n = \mathbf{A}\mathbf{X}_{n-1} \quad (2.11)$$

The solution of Equation (2.11) is given by

$$\mathbf{X}_n = \mathbf{A}^n\mathbf{X}_0 \quad (2.12)$$

where $\mathbf{X}_0 = (p_0, p_1, \dots, p_m)$. The solution of the vector difference Equation (2.12) is expressed in terms of the eigenvalues of the matrix \mathbf{A} (for details, see Amundson, 1966 or Ramkrishna and Amundson, 1985). Similarly, one can obtain a vector difference equation for the stripping section.

2.2.2 PROCESSES GOVERNED BY LINEAR EQUATIONS

2.2.2.1 Steady-State Continuous Countercurrent Staged Extraction

Consider a sequence of n equilibrium extraction stages, which are countercurrently fed with the extracting solvent phase entering stage 1, and the raffinate stream entering stage n (Ramkrishna and Amundson, 1985). The flow rates of the solute-free extract and raffinate are denoted as S and R , respectively. The solute concentration in the j th stage measured in mole ratios is Y_j in the extract phase and X_j in raffinate. The equilibrium relationship between Y and X is assumed to be $Y = KX$. The steady-state mass balance is given by the following equations:

$$\text{Stage 1: } SY_0 - (SK + R)X_1 + RX_2 = 0 \quad (2.13)$$

$$\text{Stages } 2, 3, \dots, n-1: SKX_{j-1} - (SK + R)X_j + RX_{j+1} = 0, \quad j = 2, 3, \dots, n-1 \quad (2.14)$$

$$\text{Stage } n: SKX_{n-1} - (SK + R)X_n + RX_{n+1} = 0 \quad (2.15)$$

which are clearly the linear equations that can be concisely written as

By stoichiometry $P_{\text{H}_2} = 3P_{\text{N}_2}$. Hence

$$P_{\text{N}_2} = \frac{1}{4}(P_t - x), \quad P_{\text{H}_2} = \frac{3}{4}(P_t - x)$$

The equilibrium constant for the chemical reaction is given by

$$\frac{P_{\text{NH}_3}^2}{P_{\text{N}_2} P_{\text{H}_2}^3} = K$$

Substituting the partial pressure in terms of equilibrium partial pressure gives

$$\frac{256x^2}{27(P_t - x)^4} = K$$

or

$$x = \frac{3}{16} \sqrt{3K} (P_t - x)^2$$

that is a quadratic equation in x .

2.2.3.2 Vapor-Liquid Equilibria

Consider one mole per hour of a stream consisting of n volatile liquids with known compositions, and $x_{f,i}$ to be continuously separated into vapor and liquid streams at a given temperature and pressure (Reklaitis, 1983). It is desired to determine the steady-state flow rates of the vapor stream and of the liquid stream and their compositions. Let K_i be the vapor-liquid equilibrium constants, $K_i = y_i/x_i$, where x_i and y_i are the liquid and vapor fractions, respectively. K_i is calculated from Raoult's law, $K_i = p_i(T)/P$, where p_i is the vapor pressure obtained from the Antoine equation. The flow rate of vapor stream, V , is obtained by solving the following nonlinear equation resulting out of the material balance on each of the species:

$$\sum_{i=1}^n \frac{x_{f,i}(1-K_i)}{1+V(K_i-1)} = 0 \quad (2.18)$$

The flow rate of the liquid stream is

$$L = 1 - V$$

The mole fractions are obtained from

$$x_i = \frac{x_{f,i}}{1+V(K_i-1)} \quad (2.19)$$

and the mole fractions in the vapor phase are given by

2.2.4.2 Steady State of a Tubular Reactor

Consider the reaction in Section 2.2.3.3 occurring in a homogeneous tubular reactor of length l , cross-sectional area A , and the perimeter P . The reactant is fed into the reactor with velocity v , which is assumed to be uniform over the tube cross section. The constant mass-dispersion coefficient and the thermal conductivity are denoted by D_m and k , respectively. Heat exchange takes place through the wall of the reactor maintained at the coolant temperature of T_c with the heat-transfer coefficient U . We assume here no radial variation of temperature, i.e., $T \equiv T(z)$. The mass and energy balance are given by the following differential equations:

$$D_m \frac{d^2 C}{dz^2} - v \frac{dC}{dz} - r(C, T) = 0, \quad 0 < z < l \quad (2.25)$$

$$k \frac{d^2 T}{dz^2} - \rho C_p \frac{dT}{dz} - \frac{UP}{A} (T - T_c) + (-\Delta H) r(C, T) = 0, \quad 0 \leq z \leq l \quad (2.26)$$

The boundary conditions are

$$-D_m \frac{dC}{dz} = v(C_f - C), \quad z = 0$$

$$\frac{dC}{dz} = 0, \quad z = l$$

$$-k \frac{dT}{dz} = \rho C_p v (T_f - T), \quad z = 0$$

$$\frac{dT}{dz} = 0, \quad z = l$$

For an adiabatic reactor, i.e., $U = 0$, T can be solved in terms of C , and these equations are combined into one nonlinear differential equation to be solved for C .

2.2.5 PROCESSES GOVERNED BY PARTIAL DIFFERENTIAL EQUATIONS

2.2.5.1 Dynamics of a Tubular Reactor

We reflect on the more involved case of a tubular reactor described in Section 2.2.4.2, where we will consider the radial variation of temperature in addition to its axial variation. Thus $T \equiv T(r, z)$. Furthermore, we also assume that the diffusion coefficient D_m is constant. Consequently, the mass and energy balance are given by the following partial differential equations:

$$\frac{DC}{Dt} = D_m \nabla^2 C - r(C, T) = 0, \quad 0 < z < l, \quad 0 < r < R \quad (2.27)$$

$$\rho C_p \frac{DT}{Dt} = k \nabla^2 T + (-\Delta H) r(c, T) = 0, \quad 0 < z < l, \quad 0 < r < R \quad (2.28)$$

where

$$n_i = f_i(c_i)$$

Differentiating this relationship gives

$$\frac{\partial n_i}{\partial t} = f'(c_i) \frac{\partial c_i}{\partial t} \quad (2.30)$$

Substituting the above equation in the mass balances yields the partial differential equation for the concentration dynamics:

$$\frac{\partial c_i}{\partial t} [\varepsilon + (1 - \varepsilon) f'(c_i)] + \varepsilon \frac{\partial v c_i}{\partial z} = 0 \quad (2.31)$$

2.2.6 PROCESSES GOVERNED BY INTEGRAL EQUATIONS

2.2.6.1 Particle Size Distribution in Continuous Comminution Process

Consider a continuous comminution process in which the feed consists of large particles and the smaller comminuted particles are being removed at the same mass flow rate as the feed. Following Ramkrishna (2000), the population balance equation may be written as

$$\frac{\partial n(x, t)}{\partial t} = \frac{n_f(x) - n(x, t)}{\theta} + \int_x^\infty v(y) g(y) P(x|y) n(y, t) dy - g(x) n(x, t) \quad (2.32)$$

where $n(x, t)$ is the number density (assumed to be spatially uniform), $n_f(x, t)$ is the number density in the feed and θ is the mean residence time. The comminution process is described by the breakage frequency $g(x)$ and the size distribution of particles of size x formed from the breakage of a particle size y is defined by $P(x|y)$. The steady state integro-differential equation may be written in terms of the so-called "breakage kernel," $K(x, y) \equiv v(y) g(y) P(x|y)$ as follows.

$$g(x) n_s(x) = \frac{n_f(x) - n_s(x)}{\theta} + \int_x^\infty K(x, y) n_s(y) dy \quad (2.33)$$

where $n_s(x)$ is the steady-state exit number density.

2.2.6.2 Determination of Pore Size Distribution in Porous Media

The pore size distribution in a porous medium is determined by measuring the counterdiffusion rates of two gases across the medium in a Wicke-Kallenbach experiment (Brown and Travis, 1983). The experiments are carried out without a temperature or pressure gradient across the pellet.

The thickness of the porous medium is L . The mole fractions of a gaseous species A at the near face and a distant face at L are denoted by y_{A0} and y_{AL} , respectively. Define α as a function of molecular weights of the gases A and B as follows:

$$\alpha = \frac{M_A + M_B}{M_B}$$

The boundary condition in Equation (2.37) represents a mixed derivative boundary condition, which can be written in the form

$$\frac{dt}{dx} = \beta[T(x, b) - t], \quad t(0) = t_0, \quad \beta \equiv \frac{hP}{WC_p} \quad (2.40)$$

and can be rewritten as

$$t(x) = t_0 e^{-\beta x} + \beta \int_0^x T(\xi, b) e^{-\beta(x-\xi)} d\xi \quad (2.41)$$

Substitution for $T(\xi, b)$ from Equation (2.39) results in the Fredholm integral equation:

$$t(x) = g(x) + \lambda \int_0^1 K(x, \xi) t(\xi) d\xi \quad (2.42)$$

where the expressions for the functions $g(x)$ and $K(x, \xi)$ can be readily obtained from Equations (2.41) and (2.39). Thus, solution of the integral Equation (2.42) completely specifies the solution to the boundary-value problem of Equation (2.39).

2.2.7 PROCESSES GOVERNED BY INTEGRODIFFERENTIAL EQUATIONS

Most chemical systems involve multiple phases. The description of the interaction between them leads to both the differential as well as integral terms. The *population balance equations* form an important class of integrodifferential equations.

The population balance equation is a framework for the modeling of particulate systems. These include dispersions involving solid particles, liquid drops, and gas bubbles spanning a variety of systems of chemical engineering interest. The detailed derivation of the population balance equation and its applications can be found in Ramkrishna (1985, 2000). Publications pioneering the general application of population balance are by Hulburt and Katz (1964), Randolph and Larson (1964), and Frederickson et al. (1967).

Let $f(\mathbf{x}, \mathbf{r}, t)$ be the number density of particles with the particle state, \mathbf{x} , called as internal coordinate at a spatial location \mathbf{r} at time t . Let $\dot{\mathbf{X}}(\mathbf{x}, \mathbf{r}, \mathbf{Y}, t)$ and $\dot{\mathbf{R}}(\mathbf{x}, \mathbf{r}, \mathbf{Y}, t)$ be the velocities along the internal and external coordinates, respectively, at time t in an environment of state \mathbf{Y} . Let $P(\mathbf{x}, \mathbf{r}, \mathbf{Y}, t)$ and $D(\mathbf{x}, \mathbf{r}, \mathbf{Y}, t)$ be the rates of production and destruction of particles. Then, following Ramkrishna (2000), the population balance equation for the number density is written as

$$\frac{\partial f}{\partial t} + \nabla \cdot \dot{\mathbf{X}} f + \frac{1}{V_0} \int_{A_i} f \dot{\mathbf{R}} \cdot d\mathbf{A} + \frac{1}{V_0} \int_{A_o} f \dot{\mathbf{R}} \cdot d\mathbf{A} = P - D$$

where V_0 is the system volume, and A_i and A_o are the areas of inlet and outlet, respectively. The production and destruction terms most commonly resulting out of aggregation and breakage involve integral terms imparting population balance equations as a class of the integrodifferential equations.

2.2.8 PROCESSES GOVERNED BY STOCHASTIC DIFFERENTIAL EQUATIONS

In industrial operations, there often exist random fluctuations in the operating conditions from a variety of sources. Aris and Amundson (1958) show how fluctuations in the outputs of a continuous reactor caused by specified fluctuations in the input variables can be estimated by linearization.

$$a^{-n} = \frac{1}{a^n}, \quad a \neq 0$$

The n th root of a real number is defined as

$$x = a^{1/n} = \sqrt[n]{a} \text{ if and only if } x^n = a$$

Properties of powers and roots are as follows:

$$a^n a^m = a^{m+n}; \quad \frac{a^n}{a^m} = a^{n-m}; \quad (ab)^n = a^n b^n; \quad \left(\frac{a}{b}\right)^n = \frac{a^n}{b^n}$$

$$a^{n/m} = \sqrt[m]{a^n} = (\sqrt[n]{a})^m; \quad \sqrt[n]{\sqrt[m]{a}} = \sqrt[m]{\sqrt[n]{a}}; \quad \sqrt[n]{ab} = \sqrt[n]{a} \sqrt[n]{b}$$

$$\sqrt[n]{\frac{a}{b}} = \frac{\sqrt[n]{a}}{\sqrt[n]{b}} \quad (b \neq 0)$$

2.3.1.2 Logarithm

The logarithm to the base $c > 0$,

$$x = \log_c a$$

is defined by

$$c^x = a \quad \text{or} \quad c^{\log_c a} = a$$

Properties of logarithms:

$$\log_c a = 1; \quad \log_c c^p = p$$

$$\log_c(ab) = \log_c a + \log_c b; \quad \log_c \left(\frac{a}{b}\right) = \log_c a - \log_c b$$

$$\log_c(a^n) = n \log_c a; \quad \log_c(\sqrt[n]{a}) = \frac{1}{n} \log_c a$$

2.3.2 SEQUENCES AND SERIES

A sequence is a function that maps integers to a subset of real numbers. A sequence can be viewed as a set of numbers indexed by integers. A finite sequence terminates after a finite number of terms. The following is an example of a finite sequence:

$$\{a_i\}_{i=0}^5 = \{2i+1\}_{i=0}^5 = \{1, 3, 5, 7, 9, 11\}$$

$$\sum_{n=1}^{\infty} \frac{1}{n}$$

is divergent because

$$\int_1^{\infty} \frac{1}{x} dx = \infty$$

2.3.3.2 Ratio Test

$$\rho = \lim_{n \rightarrow \infty} \frac{a_{n+1}}{a_n}$$

The series is convergent if $\rho < 1$; divergent if $\rho > 1$. It is indeterminate if $\rho = 1$. For example, the series

$$\sum_{n=0}^{\infty} \frac{1}{n!}$$

is convergent because

$$\lim_{n \rightarrow \infty} \frac{a_{n+1}}{a_n} = \lim_{n \rightarrow \infty} \frac{1}{n+1} = 0 < 1$$

2.3.3.3 Root Test

$$\rho = \lim_{n \rightarrow \infty} \sqrt[n]{a_n}$$

The series is convergent if $\rho < 1$; divergent if $\rho > 1$. It is indeterminate if $\rho = 1$. For example, the series

$$\sum_{n=1}^{\infty} \frac{1}{n^n}$$

is convergent because

$$\lim_{n \rightarrow \infty} \sqrt[n]{a_n} = \lim_{n \rightarrow \infty} \frac{1}{n} = 0 < 1$$

2.3.3.4 Comparison Test

If $0 < a_n < (>)b_n$ and the series

2.3.5 BINOMIAL THEOREM

For any positive integer n ,

$$\begin{aligned}(a+b)^n &= a^n + na^{n-1}b + \frac{n(n-1)}{2!}a^{n-2}b^2 + \frac{n(n-1)(n-2)}{3!}a^{n-3}b^3 + \cdots + \\ &= \sum_{m=0}^n C_m^n a^{n-m} b^m\end{aligned}$$

where

$$\begin{aligned}C_m^n &= \frac{n!}{(n-m)!m!} = C_{n-m}^n \\ n! &= n(n-1)(n-2)\cdots 1, \quad 0! = 1\end{aligned}$$

C_m^n satisfies the following identity:

$$2^n = 1 + C_1^n + C_2^n + \cdots + C_n^n$$

that is obtained by letting $a = b = 1$. The expansion of binomial terminates when n is an integer. A similar expansion holds for $b = 1$ and noninteger n ,

$$(1+a)^n = 1 + na + \frac{n(n-1)}{2!}a^2 + \frac{n(n-1)(n-2)}{3!}a^3 + \cdots +$$

2.3.6 INEQUALITIES

We list here some of the important inequalities followed by an example showing the use of one of the inequalities in the context of a chemical reaction. Let $\{a_i\}_{i=1}^n$ and $\{b_i\}_{i=1}^n$ be sequences of real numbers and $p, q \geq 1$.

2.3.6.1 Algebraic Inequalities

$$\text{Triangular inequality: } \left| \sum_{i=1}^n a_i \right| \leq \sum_{i=1}^n |b_i| \quad (2.46)$$

$$\text{Hölder's inequality: } \sum_{i=1}^n |a_i b_i| \leq \left(\sum_{i=1}^n |a_i|^p \right)^{1/p} \left(\sum_{i=1}^n |b_i|^q \right)^{1/q}, \quad \frac{1}{p} + \frac{1}{q} = 1 \quad (2.47)$$

For $p = q = 2$, Holder's inequality is known as the Cauchy–Schwartz inequality.

$$k\bar{c}^n = k \left[\int_0^{c_0} cf(c)dc \right]^n$$

It is easy to show that the rate of reaction as described by the lumped dispersed phase analysis underestimates the actual rate by using the Hölder's inequality. Let $g(c) = cf^{1/p}$ and $h(c) = f^{1/q}$. Thus,

$$\int_0^{c_0} c[f(c)]^{1/p+1/q} dc \leq \left(\int_0^{c_0} c^p f(c) \right)^{1/p} \left(\int_0^{c_0} f(c)dc \right)^{1/q}$$

The second integral on the right-hand side of the inequality is unity by definition. Hence, with $p = n$ and $q = 1/(n - 1)$,

$$k\bar{c}^n \leq \overline{kc^n}, \quad n > 1$$

2.4 DIFFERENTIAL AND INTEGRAL CALCULUS

2.4.1 FUNCTIONS, LIMITS, AND CONTINUITY

A function $y = f(x)$ is a rule that assigns a unique value of y for each of the given values of x in the definition of a domain of f , and x is said to be an independent variable and y the dependent variable. There may exist more than one value of x for a given value of y . The set of values of x is called the domain of a function, and the corresponding set of y is called the range of a function.

A function $f(x)$ approaches a limit y_0 as x approaches x_0 ; for any given $\epsilon > 0$, then there exists a $\delta > 0$ such that $|f(x) - y_0| < \epsilon$ for $|x - x_0| < \delta$. Symbolically,

$$\lim_{x \rightarrow x_0} f(x) = y_0$$

The limits follow simple arithmetic operations, e.g., the sum of the limits is the limit of the sums, etc.

A function is said to be continuous at x_0 if

$$\lim_{x \rightarrow x_0} f(x) = f(x_0)$$

For example,

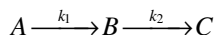
$$f(x) = \begin{cases} \frac{1}{x}, & x > 0 \\ 0, & x = 0 \end{cases}$$

is not continuous at $x = 0$ because

$$\lim_{x \rightarrow 0} f(x) = \infty \neq f(0) = 0$$

2.4.2.1 An Example Application of the Derivatives

The concentration of the intermediate product, B , at any time, t , as a result of the following reactions in series



with first-order reaction kinetics with respect to A and B and with the initial concentration of the reactant, A , equal to C_{A0} , is given by

$$C_B(t) = \frac{k_1 C_{A0}}{k_2 - k_1} [e^{-k_1 t} - e^{-k_2 t}]$$

To find out the space-time, τ , that maximizes the concentration of B , the derivative of C_B with respect to time t is set equal to zero at $t = \tau$ to yield

$$\left. \frac{dC_B}{dt} \right|_{t=\tau} = 0 \Rightarrow \tau = \frac{\ln k_2 - \ln k_1}{k_2 - k_1}$$

$$\left. \frac{d^2 C_B}{dt^2} \right|_{t=\tau} < 0, \text{ at } t = \tau$$

Hence, the maximum concentration of the species B , $C_{B,m}$ is given by

$$C_{B,m} = \frac{k_1 C_{A0}}{k_2 - k_1} \left[\left(\frac{k_1}{k_2} \right)^{k_1/k_2 - k_1} - \left(\frac{k_1}{k_2} \right)^{k_2/k_2 - k_1} \right]$$

2.4.3 THE MEAN VALUE THEOREM

Let $f(x)$ and $g(x)$ be the differentiable functions on $[a, b]$. If $g(b) \neq g(a)$ and $g'(x) \neq 0$, then there exists $c \in (a, b)$ such that

$$\frac{f'(c)}{g'(c)} = \frac{f(b) - f(a)}{g(b) - g(a)}$$

In particular, if $g(x) = x$, then

$$f'(c) = \frac{f(b) - f(a)}{b - a}$$

which is the familiar form of the mean value theorem.

2.4.3.1 An Example Application of the Mean Value Theorem

To account for the effects of transport resistance in a catalyst pellet, effectiveness factors (defined as the ratio between the observed reaction rate to that obtained when neither concentration nor temperature gradients exist between the ambient phase and any point in the catalyst pellet) are used

$$\lim_{x \rightarrow x_0} \frac{f(x)}{g(x)} = \lim_{x \rightarrow x_0} \frac{f'(x)}{g'(x)}$$

since $\infty - 1/0$, $0 \cdot \infty$ can be stated as the first two forms. Limit of the form $\infty - \infty$ is equivalent to $1 - \infty/\infty$.

Logarithms of the limits can be used to find the limits involving exponents using L'Hôspital's rule.

Example 2.2: Application of L'Hôspital's Rule

$$\lim_{x \rightarrow \infty} \left(\cos \frac{1}{x} \right)^x$$

Let

$$y = \left(\cos \frac{1}{x} \right)^x \Rightarrow \ln y = x \ln \cos \frac{1}{x}$$

$$\lim_{x \rightarrow \infty} \ln y = \lim_{x \rightarrow \infty} x \ln \cos \frac{1}{x} = \lim_{x \rightarrow \infty} \frac{\ln \cos \frac{1}{x}}{\frac{1}{x}} = - \lim_{x \rightarrow \infty} \frac{\sin \frac{1}{x}}{\cos \frac{1}{x}} = 0$$

$$\lim_{x \rightarrow \infty} \left(\cos \frac{1}{x} \right)^x = 1$$

2.4.5 IMPLICIT FUNCTION THEOREM

Given a function $f(x,y)$ such that

$$f(x_0, y_0) = 0, \quad \text{and} \quad \left. \frac{\partial f}{\partial y} \right|_{(x_0, y_0)} \neq 0$$

then there exists a neighborhood $B(x_0)$ and a unique function $g(x)$ such that $y = g(x)$ for $x \in B(x_0)$, $f(x, g(x)) = 0$.

2.4.6 THE INTEGRAL

Given a bounded function $f(x)$ defined on a bounded interval $[a, b]$, the definite Riemann integral of $f(x)$ is defined as

$$\int_a^b f(x) dx = \lim_{\|\Delta x_i\|} \sum_{i=1}^n f(\xi_i) \Delta x_i$$

where

$$x_{i-1} < \xi_i < x_i, \quad \|\Delta x_i\| = \max_{i=1}^n (x_i - x_{i-1}), \quad a = x_0 < x_1 < \cdots < x_n = b$$

$$\int_a^b f(x)dx = \lim_{x \rightarrow a} \int_x^b f(\xi)d\xi$$

The improper integrals are said to be convergent if and only if the limits are convergent.

The Riemann integral is convergent for a bounded function with a finite number of discontinuities. It is possible to construct a pathological function that has an infinite number of discontinuities. Although such a function is bounded, its Riemann integral does not exist. The Lebesgue integral is designed to overcome such a deficiency.

2.4.6.2 An Example Application of the Integrals

We reproduce here some useful formulae for the determination of area under the curve, the arc length, volume of solid revolution, and the surface area that are the results of the application of the integrals. Let $f(x)$ be a real valued function defined on an interval (a,b) . Let A be the area bounded by the function, the x -axis, and the lines $x = a$ and $x = b$. Then

$$A = \int_a^b f(x)dx \quad (2.56)$$

and the arclength, S , of the curve defined by the function is

$$S = \int_a^b \sqrt{1 + \left(\frac{df}{dx}\right)^2} dx \quad (2.57)$$

The volume of the solid generated by revolving the curve $f(x)$ about the x -axis is

$$\pi \int_a^b [f(x)]^2 dx$$

and the surface area of the solid body is given by

$$2\pi \int_a^b f(x) \sqrt{1 + \left(\frac{df}{dx}\right)^2} dx \quad (2.58)$$

2.5 VECTOR ANALYSIS

2.5.1 VECTOR ALGEBRA

A vector \mathbf{v} in n -dimensional space is an array consisting of n scalar quantities, i.e., $\mathbf{v} = [v_1 \ v_2 \ \dots \ v_n]^T$. In three-dimensional space, a vector, \mathbf{v} , can be represented geometrically as directed line segments with directions and magnitudes. The terms v_x , v_y , and v_z are the components

of the vector \mathbf{v} along the x -, y -, and z -axes, respectively. The magnitude of \mathbf{v} , $|\mathbf{v}|$, is $\sqrt{v_x^2 + v_y^2 + v_z^2}$, which measures the length of the vector or the distance from the origin to the tip of the vector. The angles α , β , and γ between the vector \mathbf{v} and basis vectors δ_x , δ_y , and δ_z of the coordinate axes x , y , and z , respectively, are calculated from the direction cosines of the vector,

$$\epsilon_{123} = \epsilon_{231} = \epsilon_{312} = 1 \quad (2.62)$$

$$\epsilon_{132} = \epsilon_{321} = \epsilon_{213} = -1 \quad (2.63)$$

$$\epsilon_{ijk} = \epsilon_{ijj} = \epsilon_{iji} = 0 \quad (2.64)$$

Scalar triple product:

$$(\mathbf{a} \times \mathbf{b}) \cdot \mathbf{c} = \begin{vmatrix} a_x & a_y & a_z \\ b_x & b_y & b_z \\ c_x & c_y & c_z \end{vmatrix}$$

Vector triple product:

$$\mathbf{a} \times (\mathbf{b} \times \mathbf{c}) = (\mathbf{a} \cdot \mathbf{c})\mathbf{b} - (\mathbf{a} \cdot \mathbf{b})\mathbf{c}$$

Quadruple scalar product:

$$(\mathbf{a} \times \mathbf{b}) \cdot (\mathbf{c} \times \mathbf{d}) = (\mathbf{a} \cdot \mathbf{c})(\mathbf{b} \cdot \mathbf{d}) - (\mathbf{a} \cdot \mathbf{d})(\mathbf{b} \cdot \mathbf{c})$$

Quadruple vector product:

$$(\mathbf{a} \times \mathbf{b}) \times (\mathbf{c} \times \mathbf{d}) = [(\mathbf{a} \times \mathbf{b}) \cdot \mathbf{d}]\mathbf{c} - [(\mathbf{a} \times \mathbf{b}) \cdot \mathbf{c}]\mathbf{d}$$

2.5.2 VECTOR CALCULUS

We list here some of the useful vector operations in a differential setting that are generally encountered in chemical engineering:

$$\frac{d\mathbf{a}}{dt} = \frac{da_x}{dt}\boldsymbol{\delta}_x + \frac{da_y}{dt}\boldsymbol{\delta}_y + \frac{da_z}{dt}\boldsymbol{\delta}_z$$

$$\frac{d}{dt}(\mathbf{a} + \mathbf{b}) = \frac{d\mathbf{a}}{dt} + \frac{d\mathbf{b}}{dt}$$

$$\frac{d}{dt}(\phi\mathbf{a}) = \phi \frac{d\mathbf{a}}{dt} + \mathbf{a} \frac{d\phi}{dt}$$

$$\frac{d}{dt}(\mathbf{a} \cdot \mathbf{b}) = \frac{d\mathbf{a}}{dt} \cdot \mathbf{b} + \mathbf{a} \cdot \frac{d\mathbf{b}}{dt}$$

$$\frac{d}{dt}(\mathbf{a} \times \mathbf{b}) = \frac{d\mathbf{a}}{dt} \times \mathbf{b} + \mathbf{a} \times \frac{d\mathbf{b}}{dt}$$

$$\frac{d}{dt}(\mathbf{a} \times \mathbf{b} \cdot \mathbf{c}) = \frac{d\mathbf{a}}{dt} \times \mathbf{b} \cdot \mathbf{c} + \mathbf{a} \times \frac{d\mathbf{b}}{dt} \cdot \mathbf{c} + \mathbf{a} \times \mathbf{b} \cdot \frac{d\mathbf{c}}{dt}$$

$$\frac{d}{dt}(\mathbf{a} \times \mathbf{b} \times \mathbf{c}) = \frac{d\mathbf{a}}{dt} \times (\mathbf{b} \times \mathbf{c}) + \mathbf{a} \times \left(\frac{d\mathbf{b}}{dt} \times \mathbf{c} \right) + \mathbf{a} \times \left(\mathbf{b} \times \frac{d\mathbf{c}}{dt} \right)$$

$$ds_1 = h_2 h_3 d\xi_1 d\xi_3; \quad ds_2 = h_1 h_3 d\xi_1 d\xi_3; \quad ds_3 = h_1 h_2 d\xi_2 d\xi_3$$

2.5.3.2 Differential Operators in Curvilinear Coordinate System

We present here the expressions for various differential vector operators that can be of great utility for transforming the equations in different coordinate systems. Given a curvilinear coordinate system with basis vectors ($h_1\delta_1 \quad h_2\delta_2 \quad h_3\delta_3$),

$$\begin{aligned} \frac{\partial \delta_1}{\partial \xi_1} &= -\frac{\delta_2}{h_2} \frac{\partial h_1}{\partial \xi_2} - \frac{\delta_3}{h_3} \frac{\partial h_1}{\partial \xi_3} & \frac{\partial \delta_1}{\partial \xi_2} &= \frac{\delta_2}{h_1} \frac{\partial h_2}{\partial \xi_1} & \frac{\partial \delta_1}{\partial \xi_3} &= \frac{\delta_3}{h_1} \frac{\partial h_3}{\partial \xi_1} \\ \frac{\partial \delta_2}{\partial \xi_2} &= -\frac{\delta_1}{h_1} \frac{\partial h_2}{\partial \xi_1} - \frac{\delta_3}{h_3} \frac{\partial h_2}{\partial \xi_3} & \frac{\partial \delta_2}{\partial \xi_1} &= \frac{\delta_1}{h_2} \frac{\partial h_1}{\partial \xi_2} & \frac{\partial \delta_2}{\partial \xi_3} &= \frac{\delta_3}{h_2} \frac{\partial h_3}{\partial \xi_2} \\ \frac{\partial \delta_3}{\partial \xi_3} &= -\frac{\delta_1}{h_1} \frac{\partial h_3}{\partial \xi_1} - \frac{\delta_2}{h_2} \frac{\partial h_3}{\partial \xi_2} & \frac{\partial \delta_3}{\partial \xi_1} &= \frac{\delta_1}{h_3} \frac{\partial h_1}{\partial \xi_3} & \frac{\partial \delta_3}{\partial \xi_2} &= \frac{\delta_2}{h_3} \frac{\partial h_2}{\partial \xi_3} \end{aligned}$$

let

$$\mathbf{f} = f_1\delta_1 + f_2\delta_2 + f_3\delta_3$$

$$\nabla\Phi = \delta_1 \frac{\partial \Phi}{\partial \xi_1} + \delta_2 \frac{\partial \Phi}{\partial \xi_2} + \delta_3 \frac{\partial \Phi}{\partial \xi_3}$$

$$\nabla \cdot \mathbf{f} = \frac{1}{h_1 h_2 h_3} \left(\frac{\partial}{\partial \xi_1} (h_2 h_3 f_1) + \frac{\partial}{\partial \xi_2} (h_1 h_3 f_2) + \frac{\partial}{\partial \xi_3} (h_1 h_2 f_3) \right)$$

$$\nabla \times \mathbf{f} = \frac{1}{h_1 h_2 h_3} \begin{vmatrix} h_1 \delta_1 & h_2 \delta_2 & h_3 \delta_3 \\ \frac{\partial}{\partial \xi_1} & \frac{\partial}{\partial \xi_2} & \frac{\partial}{\partial \xi_3} \\ h_1 f_1 & h_2 f_2 & h_3 f_3 \end{vmatrix}$$

$$\nabla^2 = \frac{1}{h_1 h_2 h_3} \left(\frac{\partial}{\partial \xi_1} \left(\frac{h_2 h_3}{h_1} \frac{\partial}{\partial \xi_1} \right) + \frac{\partial}{\partial \xi_2} \left(\frac{h_1 h_3}{h_2} \frac{\partial}{\partial \xi_2} \right) + \frac{\partial}{\partial \xi_3} \left(\frac{h_1 h_2}{h_3} \frac{\partial}{\partial \xi_3} \right) \right)$$

$$\nabla(\nabla \cdot \mathbf{f}) = \sum_{i=1}^3 \frac{1}{h_i} \frac{\partial}{\partial \xi_i} \left\{ \frac{1}{h_1 h_2 h_3} \left[\frac{\partial f_i h_2 h_3}{\partial \xi_1} + \frac{\partial f_2 h_1 h_3}{\partial \xi_2} + \frac{\partial f_3 h_1 h_2}{\partial \xi_3} \right] \right\} \delta_i$$

$$\nabla\Phi = \frac{\partial\Phi}{\partial r}\delta_r + \frac{1}{r}\frac{\partial\Phi}{\partial\theta}\delta_\theta + \frac{1}{r\sin\theta}\frac{\partial\Phi}{\partial\phi}\delta_\phi$$

$$\nabla \cdot \mathbf{f} = \frac{1}{r^2}\frac{\partial}{\partial r}(r^2 f_r) + \frac{1}{r\sin\theta}\frac{\partial}{\partial\theta}(f_\theta \sin\theta) + \frac{1}{r\sin\theta}\frac{\partial f_\phi}{\partial\phi}$$

$$\nabla \times \mathbf{f} = \frac{1}{r^2 \sin\theta} \begin{vmatrix} \delta_r & r\delta_\theta & r\sin\theta\delta_\phi \\ \frac{\partial}{\partial r} & \frac{\partial}{\partial\theta} & \frac{\partial}{\partial\phi} \\ f_r & rf_\theta & r\sin\theta f_\phi \end{vmatrix}$$

$$\nabla^2 = \frac{1}{r^2}\frac{\partial}{\partial r}\left(r^2\frac{\partial}{\partial r}\right) + \frac{1}{r^2\sin\theta}\frac{\partial}{\partial\theta}\left(\sin\theta\frac{\partial}{\partial\theta}\right) + \frac{1}{r^2\sin^2\theta}\frac{\partial^2}{\partial\phi^2}$$

2.5.3.5 Elliptic Cylindrical Coordinates

$$x = a \cosh \xi_1 \cos \xi_2, \quad y = a \sinh \xi_1 \sin \xi_2$$

where $\xi_1 = \text{constant}$ is a confocal ellipse described by

$$\left(\frac{x}{a \cosh \xi_1}\right)^2 + \left(\frac{y}{a \sinh \xi_1}\right)^2 = 1$$

and $\xi_2 = \text{constant}$ is a confocal hyperbola described by

$$\left(\frac{x}{a \cosh \xi_2}\right)^2 - \left(\frac{y}{a \sinh \xi_2}\right)^2 = 1$$

$$h_1 = h_2 = a\sqrt{\cosh^2 \xi_1 - \cos^2 \xi_2} \quad h_3 = 1$$

2.5.3.6 Prolate Spheroidal Coordinates

$$x = a \cosh \xi_1 \cos \xi_2, \quad y = a \sinh \xi_1 \sin \xi_2 \sin \xi_3, \quad z = a \sinh \xi_1 \sin \xi_2 \cos \xi_3$$

where $\xi_1 = \text{constant}$ is a prolate spheroid described by

$$\left(\frac{x}{a \cosh \xi_1}\right)^2 + \left(\frac{y}{a \sinh \xi_1}\right)^2 + \left(\frac{z}{a \sinh \xi_1}\right)^2 = 1$$

$\xi_2 = \text{constant}$ is a hyperboloid two sheets described by

$$y^2 = \xi_1^2 (\xi_1^2 - 2x)$$

$$h_1 = h_2 = \sqrt{\xi_1^2 + \xi_2^2} \quad h_3 = 1$$

2.5.3.9 Parabolic Coordinates

$$x = \frac{1}{2} (\xi_2^2 - \xi_1^2), \quad y = \xi_1 \xi_2 \sin \xi_3, \quad z = \xi_1 \xi_2 \cos \xi_3$$

where $\xi_1 = \text{constant}$ is a paraboloid of revolution described by

$$y^2 + z^2 = \xi_1^2 (\xi_1^2 + 2x)$$

and $\xi_2 = \text{constant}$ is a paraboloid of revolution described by

$$y^2 + z^2 = \xi_1^2 (\xi_1^2 - 2x)$$

$$\tan \xi_3 = \frac{y}{z}$$

$$h_1 = h_2 = \sqrt{\xi_1^2 + \xi_2^2} \quad h_3 = \xi_1 \xi_2$$

2.5.3.10 Conical Coordinates

$$x^2 = \left(\frac{\xi_1 \xi_2 \xi_3}{bc} \right)^2 \quad y^2 = \frac{\xi_1^2 (b^2 - \xi_2^2) (\xi_3^2 - b^2)}{b^2 (c^2 - b^2)} \quad z^2 = \frac{\xi_1^2 (c^2 - \xi_2^2) (c^2 - \xi_3^2)}{b^2 (c^2 - b^2)}$$

$$0 < \xi_2^2 < b^2 < \xi_3^2 < c^2$$

where $\xi_1 = \text{constant}$ is a sphere described by

$$x^2 + y^2 + z^2 = r^2 = \xi_1^2$$

$\xi_2 = \text{constant}$ is an elliptic cone described by

$$\frac{x^2}{\xi_2^2} - \frac{y^2}{b^2 - \xi_2^2} - \frac{z^2}{c^2 - \xi_2^2} = 0$$

and $\xi_3 = \text{constant}$ is an elliptic cone described by

$$\frac{x^2}{\xi_3^2} - \frac{y^2}{b^2 - \xi_3^2} - \frac{z^2}{c^2 - \xi_3^2} = 0$$

$$h_1 = 1 \quad h_2 = \sqrt{\frac{\xi_1^2 (\xi_3^2 - \xi_2^2)}{(b^2 - \xi_2^2) (c^2 - \xi_2^2)}}, \quad h_3 = \sqrt{\frac{\xi_1^2 (\xi_3^2 - \xi_2^2)}{(\xi_2^2 - b^2) (c^2 - \xi_3^2)}}$$

$$\frac{x^2}{a-\xi_3} - \frac{y^2}{\xi_3-b} = 4(z-\xi_3)$$

$$h_1 = \left[\frac{(\xi_2 - \xi_1)(\xi_2 - \xi_3)}{(\xi_2 - a)(\xi_2 - b)} \right]^{1/2} \quad h_2 = \left[\frac{(\xi_2 - \xi_1)(\xi_3 - \xi_1)}{(a - \xi_1)(b - \xi_1)} \right]^{1/2} \quad h_3 = \left[\frac{(\xi_3 - \xi_1)(\xi_2 - \xi_1)}{(a - \xi_3)(\xi_3 - b)} \right]^{1/2}$$

2.5.3.13 Bispherical Coordinates

$$x = a\xi_3 \frac{\sqrt{1-\xi_2^2}}{\xi_1 - \xi_2}; \quad y = a \frac{\sqrt{(1-\xi_2^2)(1-\xi_3^2)}}{\xi_1 - \xi_2}; \quad z = a \frac{\sqrt{\xi_1^2 - 1}}{\xi_1 - \xi_2}$$

$$h_1 = \frac{a}{(\xi_1 - \xi_2)\sqrt{\xi_1^2 - 1}}; \quad h_2 = \frac{a}{(\xi_1 - \xi_2)\sqrt{1 - \xi_2^2}}; \quad h_3 = \frac{a}{\xi_1 - \xi_2} \sqrt{\frac{1 - \xi_2^2}{1 - \xi_3^2}}$$

2.5.3.14 Toroidal Coordinates

$$x = a \frac{\sqrt{\xi_1^2 - 1}}{\xi_1 - \xi_2}; \quad y = a \frac{\sqrt{(\xi_1^2 - 1)(1 - \xi_3^2)}}{\xi_1 - \xi_2}; \quad z = a \frac{\sqrt{1 - \xi_3^2}}{\xi_1 - \xi_2}$$

$$h_1 = \frac{a}{(\xi_1 - \xi_2)\sqrt{\xi_1^2 - 1}}; \quad h_2 = \frac{a}{(\xi_1 - \xi_2)\sqrt{1 - \xi_3^2}}; \quad h_3 = \frac{a}{\xi_1 - \xi_2} \sqrt{\frac{\xi_2^2 - 1}{1 - \xi_3^2}}$$

2.5.4 VECTOR INTEGRAL THEOREMS

Let V be a volume bounded by a closed surface S , and let \mathbf{f} be a continuously differentiable vector field in V and S . If $d\mathbf{s}$ is an outward normal vector to the differential area, then we have the following equations as per various useful theorems.

Gauss's divergence theorem:

$$\iiint_V \nabla \cdot \mathbf{f} dv = \iint_S \mathbf{f} \cdot d\mathbf{s}$$

Gradient theorem:

$$\iiint_V \nabla \mathbf{f} dv = \iint_S \mathbf{f} d\mathbf{s}$$

Curl theorem:

$$\iiint_V \nabla \times \mathbf{f} dv = - \iint_S \mathbf{f} \times d\mathbf{s}$$

Stokes's theorem: Let S be a surface bounded by a closed curve C and $d\mathbf{r}$ be the tangent vector. Then

$$\nabla(\phi\psi) = \psi\nabla\phi + \phi\nabla\psi$$

$$\nabla(\mathbf{f} \cdot \mathbf{g}) = (\mathbf{f} \cdot \nabla)\mathbf{g} + (\mathbf{g} \cdot \nabla)\mathbf{f} + \mathbf{f} \times (\nabla \times \mathbf{g}) + \mathbf{g} \times (\nabla \times \mathbf{f})$$

$$\nabla \cdot (\phi \cdot \mathbf{f}) = \phi(\nabla \cdot \mathbf{f}) + \mathbf{f} \cdot \nabla\phi$$

$$(\mathbf{a} \cdot \nabla)(\phi\mathbf{f}) = \phi[(\mathbf{a} \cdot \nabla)\mathbf{f}] + \mathbf{f}[(\mathbf{a} \cdot \nabla)\phi]$$

$$(\mathbf{a} \cdot \nabla)(\mathbf{f} \times \mathbf{g}) = \mathbf{f} \times [(\mathbf{a} \cdot \nabla)\mathbf{g}] + [(\mathbf{a} \cdot \nabla)\mathbf{f}] \times \mathbf{g}$$

$$\nabla \cdot (\phi\mathbf{f}) = \mathbf{f} \cdot \nabla\phi + \phi\nabla \cdot \mathbf{f}$$

$$\nabla \cdot (\mathbf{f} \times \mathbf{g}) = \mathbf{g} \cdot (\nabla \times \mathbf{f}) - \mathbf{f} \cdot (\nabla \times \mathbf{g})$$

$$\nabla \times (\phi\mathbf{f}) = \nabla\phi \times \mathbf{f} + \phi\nabla \times \mathbf{f}$$

$$\nabla \times (\mathbf{f} \times \mathbf{g}) = (\mathbf{g} \cdot \nabla)\mathbf{f} - (\mathbf{f} \cdot \nabla)\mathbf{g} + \mathbf{f}\nabla \cdot \mathbf{g} - \mathbf{g}\nabla \cdot \mathbf{f}$$

2.6 DIMENSIONAL ANALYSIS

Dimensional homogeneity is fundamental to equations relating variables in the description of natural processes. The recognition of this basic attribute is the substance of dimensional analysis, which results in the reduction of relevant parameters to the essential minimum. Physical quantities comprise combinations of one or more basic dimensions. Table 2.2 shows some commonly used physical quantities in engineering expressed in terms of basic dimensions (mass, M ; length, L ; time, T ; temperature, θ).

2.6.1 THEORY OF DIMENSIONAL ANALYSIS

Consider a specific process that involves n physical quantities comprising m basic dimensions among them. The dimension of each physical quantity is defined as the product of each of the basic dimensions raised to an appropriate exponent. For example, velocity can be expressed as LT^{-1} . Each physical quantity is then viewed as a vector of elements representing the respective exponents. Thus in the MLT system involving mass (M)-length (L)-time (T) as basic dimensions, velocity would be represented by the row vector $[0 \ 1 \ -1]$. By lining up the vectors representing the different physical quantities (in columns), we obtain the *dimensional matrix*. A dimensionless group is a multiplicative combination of physical quantities with no net dimension and has the zero vector as its representative. Thus the formation of a dimensionless group can be identified with expressing the zero vector as a linear combination of vectors representing physical quantities in the group. From linear algebra, it follows that the number of independent dimensionless groups that can be formed is $n - r$, where r is the rank of the dimensional matrix, which is known as Buckingham's π -theorem. If the basic dimensions are independent, then $r = m$. Once the dimensionless groups $\pi_1, \pi_2, \dots, \pi_{n-r}$ are determined, the physical process is described abstractly by an equation of the form $f(\pi_1, \pi_2, \dots, \pi_{n-r}) = 0$. A couple of examples follow.

According to Buckingham's π -theorem, there exist two dimensionless groups. Thus there are two linearly independent solutions to Equation (2.67), and these are $k_1 = k_2 = -2$, $k_3 = 1$, $k_4 = -1$, $k_5 = 0$ and $k_1 = k_2 = k_4 = 1$, $k_3 = 0$, $k_5 = -1$. The resulting dimensionless groups are given by

$$\pi_1 = \frac{F}{\rho V^2 D^2} \quad \pi_2 = \frac{VD\rho}{\mu}$$

Experimental data are, however, correlated as $C_D = (8/\pi)\pi_1$, known as the drag coefficient, while π_2 is the well-known Reynolds number.

Example 2.4

The objective of this example is to show the utility of dimensional analysis in the interpretation of experimental data. Bose and coworkers (Barenblatt, 1996) performed experiments with various fluids, namely, water, chloroform, bromoform, and mercury. The fluids were allowed to flow through a pipe in the turbulent regime. The times τ required for the fluids of density ρ and viscosity μ to attain a certain specified total discharge (volume) of Q under an imposed pressure drop P were measured. A graph of $\log P$ as a function of $\log(1/\tau)$ showed four separate curves representing four different fluids. The same data can be plotted in terms of the new dimensionless groups, showing the collapse of all the data on a single curve through dimensional analysis, as was first shown by Von Kármán (1957):

The dimensional matrix may be written as

	P	τ	Q	ρ	μ
M	1	0	0	1	1
L	-1	0	3	-3	-1
T	-2	1	0	0	-1

The dimensionless groups are formed using $P^{k_1} \tau^{k_2} Q^{k_3} \rho^{k_4} \mu^{k_5}$:

$$\begin{aligned} k_1 + k_4 + k_5 &= 0 \\ -k_1 + 3k_3 - 3k_4 - k_5 &= 0 \\ -2k_1 + k_2 - k_5 &= 0 \end{aligned} \quad (2.68)$$

The two linearly independent solutions are $k_1 = 0$, $k_2 = -1$, $k_3 = 2/3$, $k_4 = 1$, $k_5 = -1$ and $k_1 = k_2 = 1$, $k_3 = -1$, $k_4 = k_5 = 0$. The two dimensionless groups are

$$\frac{\tau P}{\mu} \quad \text{and} \quad \frac{\rho Q^{2/3}}{\tau \mu}$$

The functional relation is

$$f\left(\frac{\tau P}{\mu}, \frac{\rho Q^{2/3}}{\tau \mu}\right)$$

When the number of equations is less than the number of unknowns ($m < n$), at least $m - n$ of the unknowns must be assumed arbitrarily in terms of which the remaining unknowns can be calculated. When $m = n$, the number of equations is equal to the number of unknowns, a situation generally viewed to be sufficient for solving for all the unknowns. However, this issue is connected with situations when solutions exist in general. When $m > n$, the number of equations exceeds the number of unknowns, raising concerns about the consistency of the set of equations. The question of when a set of equations can be solved for the unknowns regardless of the relative values of m and n is answered elegantly by matrix theory. A few preliminary definitions are necessary before the necessary and sufficient conditions for the existence of the solution to a set of algebraic equations can be understood.

Vectors: The collection of all vectors containing n elements satisfying basic axioms (see, for example, Ramkrishna and Amundson (1985)) is called a linear space denoted by \mathfrak{R}^n . The basic axioms define scalar multiplication, vector addition (from which evolves the concept of linear combination), and a null vector that has all elements zero. Thus a linear combination of vectors \mathbf{x}_j , $j = 1, 2, \dots, k$, is expressed as the vector $\sum_{j=1}^k \alpha_j \mathbf{x}_j$, where the α_j 's are numbers. If the α_j 's are all zero, the linear combination gives the zero vector, 0. Linear spaces contain (linear) subspaces that are subsets in which linear combinations are contained within the set. Linear subspaces are also linear spaces.

Linear dependence: A set of vectors such as \mathbf{x}_i , $i = 1, 2, \dots, k$, is said to be linearly dependent if it is possible to find scalars not all zeroes such that the linear combination gives the zero vector. If this is not possible, the set is said to be linearly independent. No vector in a linearly independent set can be expressed as a linear combination of the remaining vectors.

The maximum number of linearly independent vectors in a linear space or subspace is said to be the dimension of the space. Such a linearly independent set of vectors is said to be a *basis* for that space, by which it is meant that any arbitrary vector in the space can be expressed as a linear combination of the basis set.

Matrices: We consider the matrix \mathbf{A} defined in Equation (2.72). If it has only one column ($n = 1$), it is the same as a column vector. If it has only one row, then it is a row vector. Thus vectors may be regarded as matrices themselves. The following properties are of interest.

Rank of a matrix: The rank of matrix \mathbf{A} is the largest order of square array whose determinant is nonzero. Clearly, the rank of the matrix above cannot exceed the minimum of m and n . The definition of a determinant can be found in Amundson (1966). The matrix \mathbf{A} may be regarded as a *transformation* of vectors in \mathfrak{R}^n into a range of vectors, denoted $R(\mathbf{A})$, a subspace of \mathfrak{R}^m . The rank of \mathbf{A} may also be seen to be the dimension of $R(\mathbf{A})$. When $m = n$, \mathbf{A} is said to be a *square* matrix of order n . If its rank is less than n , it is said to be *singular*. Clearly, the determinant of the singular matrix is zero.

A square matrix that has only nonzero elements along its diagonal is called a diagonal matrix. If the diagonal matrix has all its diagonal elements equal to unity, it is called the identity matrix, denoted by \mathbf{I} . The diagonal matrix \mathbf{D} and the identity matrix \mathbf{I} are shown below:

$$\mathbf{D} = \begin{bmatrix} d_{11} & 0 & \cdots & 0 \\ 0 & d_{22} & \cdots & 0 \\ \vdots & \vdots & \ddots & \vdots \\ 0 & 0 & \cdots & d_{mm} \end{bmatrix}, \quad \mathbf{I} = \begin{bmatrix} 1 & 0 & \cdots & 0 \\ 0 & 1 & \cdots & 0 \\ \vdots & \vdots & \ddots & \vdots \\ 0 & 0 & \cdots & 1 \end{bmatrix}$$

Matrix addition/subtraction: Two matrices \mathbf{A} and \mathbf{B} are said to be compatible for addition/subtraction if both the matrices have the same numbers of rows and columns. The addition/subtraction of two matrices is carried out elementwise and simply follows

where \mathbf{z}_j are the $(m - r)$ linearly independent solutions of the homogeneous equation $\mathbf{b}^T \mathbf{z}_j = \mathbf{0}$. In this case, the solution to the inhomogeneous Equation (2.71) is not unique, since a particular solution to the inhomogeneous equation plus an arbitrary nontrivial solution of its homogeneous version is also a solution to the inhomogeneous Equation (2.71).

It should be noted that the calculation of an inverse matrix requires considerable computational time, and hence various methods have been proposed for the solution of a set of linear equations that take advantage of the structure of the matrix \mathbf{A} . The methods may be divided into two classes, namely, direct and iterative methods.

Cramer's rule, LU decomposition, and Gauss elimination methods form the class of *direct methods*, whereas Jacobi, Gauss-Seidel, and successive overrelaxation methods constitute the class of *iterative methods*. Among the direct methods, the Gauss elimination method, especially its partial pivoting variant, is the preferred method for large problems when sufficient computer memory is available for matrix storage. It relies on the transformation of the coefficient matrix into an upper triangular matrix problem and solving it by back substitution.

Iterative methods are sometimes used due to ease of computer coding and lesser computational storage requirements. The Jacobi method is the simplest iterative method but has slower convergence in comparison with the Gauss-Seidel method. In the Gauss-Seidel method, the $(k+1)$ th iteration of the value of the unknown x_i is given by

$$x_i^{(k+1)} = \left(- \sum_{j=1}^{i-1} a_{ij} x_j^{(k+1)} - \sum_{j=i+1}^{n} a_{ij} x_j^{(k)} + b_i \right) / a_{ii}, \quad i = 1, 2, \dots, m$$

The successive overrelaxation method is a variant of the Gauss-Seidel method, wherein the $(k+1)$ th iteration is a weighted average of the Gauss Seidel k th and $(k+1)$ th estimates x_i and $x_i^{(k+1)}$, respectively. The reader is referred to Jensen and Jeffreys (1977) for a detailed account on the matrices and solution methods.

Generalized inverse (pseudoinverse): To obtain an approximate solution of an overdetermined system of linear equations, i.e., when the number of equations is greater than the number of unknowns ($m > n$), a vector \mathbf{x} is sought to minimize the square of residuals, $\mathbf{r}^T \mathbf{r}$, where

$$\mathbf{r} = \mathbf{Ax} - \mathbf{b}$$

The condition for minimization can be written as

$$d\mathbf{r}^T \mathbf{r} = 0$$

than implies

$$\mathbf{A}^T \mathbf{Ax} = \mathbf{A}^T \mathbf{b}$$

The matrix $\mathbf{B} = \mathbf{A}^T \mathbf{A}$ is symmetric and positive definite. If its inverse exists, then the least square solution is given by

$$\mathbf{x} = \mathbf{B}^{-1} \mathbf{A}^T \mathbf{b} = (\mathbf{A}^T \mathbf{A})^{-1} \mathbf{A}^T \mathbf{b}$$

$$D_1 = a_1 D_2 = \begin{vmatrix} a_1 & a_0 \\ a_3 & a_2 \end{vmatrix} \quad D_3 = \begin{vmatrix} a_1 & a_0 & 0 \\ a_3 & a_2 & a_1 \\ a_5 & a_4 & a_3 \end{vmatrix} \quad D_4 = \begin{vmatrix} a_1 & a_0 & 0 & 0 \\ a_3 & a_2 & a_1 & a_0 \\ a_5 & a_4 & a_3 & a_2 \\ a_7 & a_6 & a_5 & a_4 \end{vmatrix} \dots$$

$$D_n = \begin{vmatrix} a_1 & a_0 & 0 & 0 & \dots & 0 \\ a_3 & a_2 & a_1 & 0 & \dots & 0 \\ \dots & \dots & \dots & \dots & \dots & \dots \\ a_{2n-1} & a_{2n-2} & a_{2n-3} & a_{2n-4} & \dots & a_n \end{vmatrix}$$

Descartes's rule of signs: The number of positive real roots of a real polynomial equation is either equal to the number of sign changes in the sequence of coefficients $\{a_n, a_{n-1}, \dots, a_0\}$, or it is less by an even number. Application of this rule to $P(-x)$ gives the number of negative real roots.

Budan's rule of signs: The number of zeroes in the interval (a, b) is either equal to $V(a) - V(b)$ or less by an even number, where $V(x)$ is the number of sign changes in the sequence

$$\{P_n(x), P'_n(x), P''_n(x), \dots, P_n^{(n)}(x)\}$$

Bounds on real roots: If the first k coefficients $(a_n, a_{n-1}, \dots, a_{k-1})$ of a real polynomial are nonnegative, then all the real roots are less than U where

$$U = 1 + \sqrt[k]{\frac{M}{a_n}}$$

$$M = \max_{0 \leq j \leq k} |a_j|, \quad a_j < 0$$

Application of this bound to $P_n(-x)$ gives the lower bound L on the roots. Thus, all the real roots of a real polynomial are located in the interval (L, U) .

Polynomials of degree $n \leq 4$ can be solved by the following formulae.

Quadratic formula: The roots of a polynomial of degree $n = 2$ are given by the quadratic formula

$$x_1 = \frac{-a_1 + \sqrt{D}}{2a_2}$$

$$x_2 = \frac{-a_1 - \sqrt{D}}{2a_2}$$

where

$$D = a_1^2 - 4a_2a_0$$

$$\rho = \sqrt[3]{-\left(\frac{p}{3}\right)^3} \quad \text{and} \quad \cos \phi = -\frac{q}{2\rho}$$

Then the roots are given by

$$x_1 = 2\sqrt[3]{\rho \cos\left(\frac{\phi}{3}\right)} - \frac{a_2}{3a_3} \quad (2.77)$$

$$x_2 = 2\sqrt[3]{\rho \cos\left(\frac{\phi}{3} + \frac{2\pi}{3}\right)} - \frac{a_2}{3a_3} \quad (2.78)$$

$$x_3 = 2\sqrt[3]{\rho \cos\left(\frac{\phi}{3} + \frac{4\pi}{3}\right)} - \frac{a_2}{3a_3} \quad (2.79)$$

Quartic formula: For $n = 4$, the roots are obtained by solving the cubic resolvent equation (Harris and Stocker, 1998):

$$8y^3 - 4\frac{a_2}{a_4}y^2 + \frac{2a_3a_1 - 8a_0}{a_4}y + 4\frac{a_2a_0 - a_3^2a_0 - a_1^2}{a_4} = 0$$

The roots to the quartic equation are obtained by solving

$$x^2 + \frac{a_3 + a_4D}{2a_4} + \left(y + \frac{a_3y - a_1}{a_4D}\right) = 0$$

where

$$D = \pm \sqrt{8y + \frac{a_3^2}{a_4} - 4\frac{a_2}{a_4}}$$

If $a_3 = a_1 = 0$, then the quartic equation is reduced to a quadratic equation by substituting $y = x^2$.

2.7.2.2 Numerical Solutions of Nonlinear Equations

We discuss here the use of two most prominent iterative methods of solutions of nonlinear equations through illustrations that are relevant to chemical engineers.

2.7.2.2.1 Successive Substitution

The steady-state mass and energy balances in a CSTR are given by Equations (2.20) and (2.21), respectively, which are reproduced here for ready reference:

$$|g'(x)|_{x=x_\infty} < 1$$

where x_∞ is the solution. Thus, the condition ensures that the iteration converges to a stable solution.

In general, the system of n equations in n unknowns is written in vector form as

$$\mathbf{f}(\mathbf{x}) = \mathbf{0} \quad (2.88)$$

which can be solved by iterating the following equation:

$$\mathbf{x}_{n+1} = \mathbf{g}(\mathbf{x}_n)$$

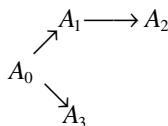
The criterion for the convergence of such a sequence is that the absolute eigenvalues of the following Jacobian matrix evaluated at the root are less than 1:

$$\mathbf{Jg}(\mathbf{x})|_{\mathbf{x}=\mathbf{x}_\infty} = \begin{bmatrix} \frac{\partial g_1}{\partial x_1} & \frac{\partial g_1}{\partial x_2} & \cdots & \frac{\partial g_1}{\partial x_n} \\ \frac{\partial g_2}{\partial x_1} & \vdots & \cdots & \frac{\partial g_2}{\partial x_n} \\ \frac{\partial g_n}{\partial x_1} & \frac{\partial g_n}{\partial x_2} & \cdots & \frac{\partial g_n}{\partial x_n} \end{bmatrix}_{\mathbf{x}=\mathbf{x}_\infty}$$

The convergence condition stated above is difficult to ascertain, since it requires eigenvalues of the Jacobian to be evaluated at the root. A relatively loose condition is to ensure that the eigenvalues of the Jacobian are less than unity in the interval where the expected root is located. Using this condition and the application of the Gershgorin theorem (Bell, 1965), the condition for the convergence of iterations can be ensured for the function $g(x)$.

Example 2.5: Application of the Convergence Condition

Consider first-order reactions represented by



The first-order rate constants k_1 and k_3 associated with the reactions producing A_1 and A_3 , respectively, are determined by measuring the rate of consumption of the reactant A_0 and the production of A_3 . The rate constant, k_2 , for the reaction producing A_2 is determined by solving a nonlinear equation that is derived as follows.

The concentrations of A_0 , A_1 , and A_3 as functions of time are obtained by integrating the following equations:

$$\frac{dA_0}{dt} = -(k_1 + k_3)A_0 \quad (2.89)$$

$$\mathbf{Jf}(\mathbf{x}_n)[\mathbf{x}_{n+1} - \mathbf{x}_n] = \mathbf{f}(\mathbf{x}_n) \quad (2.98)$$

where

$$\mathbf{Jf}(\mathbf{x}) = \begin{bmatrix} \frac{\partial f_1}{\partial x_1} & \frac{\partial f_1}{\partial x_2} & \cdots & \frac{\partial f_1}{\partial x_n} \\ \frac{\partial f_2}{\partial x_1} & \vdots & \cdots & \frac{\partial f_2}{\partial x_n} \\ \frac{\partial f_n}{\partial x_1} & \frac{\partial f_n}{\partial x_2} & \cdots & \frac{\partial f_n}{\partial x_n} \end{bmatrix}$$

The sequence \mathbf{x}_{n+1} is generated by solving the system of linear equations defined by Equation (2.98). This sequence converges faster but requires a more accurate initial guess for x_0 .

2.8 DIFFERENCE EQUATIONS

Difference equations are discrete analogues of differential equations. In this section, we present the methods of solving linear difference equations.

2.8.1 METHOD OF SOLUTION FOR HOMOGENEOUS EQUATIONS

Given a homogeneous k th-order linear difference equation

$$a_k y_{n+k} + a_{k-1} y_{n+k-1} + \cdots + a_0 y_n = 0 \quad (2.99)$$

the general solution of Equation (2.99) is determined by the solutions of the characteristic equation

$$a_k r^k + a_{k-1} r^{k-1} + \cdots + a_0 = 0 \quad (2.100)$$

If r_1, r_2, \dots, r_k are distinct roots of the characteristic equation, then the general solution is given by

$$y_n = \sum_{m=1}^k C_m r_m^n \quad (2.101)$$

where C_m 's are constants to be determined from the boundary conditions.

If r_1, r_2, \dots, r_{m-p} are real but not distinct, and if r_p is a root of p -multiplicity, then the general solution is

$$y_n = \sum_{m=1}^m \sum_{k_j=0}^{k_p-1} C_{m,k_j} r_{m-p}^n k_j^m r_p^n \quad (2.102)$$

2.8.2 METHOD OF SOLUTION FOR INHOMOGENEOUS EQUATIONS

Given the following inhomogeneous linear equations:

The constants C_1 and C_2 can be calculated through the application of boundary conditions, enabling the complete specification of the solution.

2.8.3 NUMERICAL SOLUTIONS TO ORDINARY DIFFERENTIAL EQUATIONS

In this subsection, some commonly used numerical schemes that involve difference equations to solve ordinary differential equations are presented along with their stability characteristics. Simple examples to illustrate the effects of step size on the convergence of numerical methods are shown.

A simple discretization of the first-order linear differential equation

$$\frac{dy}{dz} = -\lambda y, \quad a \leq x \leq b, \quad y(a) = y_0$$

by a straightforward discretization using Euler's rule yields the following difference equation:

$$y_{n+1} = y_n - h\lambda y_n = (1 - h\lambda)y_n$$

where $h = (b - a)/n$. The solution is given by

$$y_n = (1 - h\lambda)^n y_0$$

The solution of the differential equation approaches zero as x approaches infinity. The solution of the difference equation clearly depends on h , and it approaches zero only if $h\lambda < 1$. For $h\lambda > 1$, the solution of the difference equation oscillates between very large positive and negative values for large n . Thus, the solution of the difference equation converges only for values h that satisfy $h\lambda < 1$.

For a nonlinear equation,

$$\frac{dy}{dx} = f(x, y), \quad a \leq x \leq b, \quad y(a) = y_0$$

the necessary and sufficient condition through convergence of Euler's rule is (Lambert, 1973)

$$\sup_{x \in (a, b); y \in (-\infty, \infty)} \left(h \left| \frac{\partial f}{\partial y} \right| \right) < 1$$

This example illustrates that the step size, h , plays a crucial role in the convergence of the numerical solution of a differential equation. Depending on the equation to be solved and the method of discretization, h can be adjusted to obtain convergence of a numerical solution.

A general method of solving a differential equation is to divide the interval of integration into n subintervals and then approximate the derivative by a one-step difference quotient, as in the Euler method or k -step difference quotient:

$$\frac{dy}{dx} = \frac{1}{h} \sum_{i=0}^k \alpha_i y_i \quad (2.104)$$

where α_i 's are constants with values ensuring the limit of the right-hand side of Equation (2.104) to the derivative of y at $x = 0$. Such an approximation introduces errors in computation. It also introduces

TABLE 2.4
Theoretical and Numerical Solutions of Equation
(2.108) by Four-Stage Runge-Kutta Method (y_{rk})

x	y , Equation (2.109)	y_{rk} , $h = 0.02$	y_{rk} , $h = 0.04$
0	1	1	1
0.04	0.3333	0.326900	-0.3333
0.08	0.2	0.197676	-0.958119
0.12	0.142857	0.141669	-578.994

The interval of absolute stability for four-stage Runge-Kutta is $(-2.78, 0)$. If the numerical solution is to converge to the theoretical solution, the step size h must be selected such that $-2.78 < \bar{h} < 0$. Because $dy/dx < 0$, the solution is a monotonically decreasing function of x , the maximum value of y is $y(0) = 1$, and the minimum of $\bar{h} = -100h < 2.78$. For $h = 0.01$ and 0.02 , $\bar{h} = -1, -2$, respectively, which remain in the interval of absolute stability. For $h = 0.04$, $\bar{h} = -4$, which falls outside of the interval of absolute stability. Hence, the numerical solution diverges for $h = 0.04$.

The extension of a single equation to a system is accomplished with vector-dependent variables. In principle, the stability condition is still valid with the replacement of \bar{h} by $h\rho$, where ρ is the maximum among all the absolute eigenvalues of the Jacobian of the vector $\mathbf{f}(x, \mathbf{y})$.

The reader is referred to Lambert (1973) for an excellent treatise on the computational methods for ordinary differential equations.

In what follows, we list the explicit and implicit methods for ready reference. The differences will be obvious through the formulations.

2.8.3.1 Explicit Methods

2.8.3.1.1 Runge-Kutta Methods

There exists a family of Runge-Kutta methods that differs by the number of functional evaluations of $f(x_r, y_r)$. A method that requires R functional evaluations is known as the R -stage Runge-Kutta method.

Two-stage Runge-Kutta method

1. Modified Euler method:

$$y_{n+1} - y_n = hf \left(x_n + \frac{1}{2}h, y_n + \frac{1}{2}hf(x_n, y_n) \right)$$

Interval of absolute stability: $(-2, 0)$

2. Improved Euler method:

$$y_{n+1} - y_n = \frac{1}{2}h[f(x_n, y_n) + f(x_n + h, y_n + hf(x_n, y_n))]$$

Interval of absolute stability: $(-2, 0)$

Three-stage Runge-Kutta method

1. Heun's third-order formula:

Interval of absolute stability: $(-2.78, 0)$

2.

$$y_{n+1} - y_n = \frac{h}{8}(k_1 + 3k_2 + 3k_3 + k_4) \quad (2.123)$$

$$k_1 = f(x_n, y_n) \quad (2.124)$$

$$k_2 = f\left(x_n + \frac{1}{3}h, y_n + \frac{1}{3}hk_1\right) \quad (2.125)$$

$$k_3 = f\left(x_n + \frac{2}{3}h, y_n - \frac{1}{3}hk_1 + hk_2\right) \quad (2.126)$$

$$k_4 = f(x_n + h, y_n + hk_1 - hk_2 + hk_3) \quad (2.127)$$

Interval of absolute stability: $(-2.78, 0)$

Fifth-order six-stage Runge-Kutta method

$$y_{n+1} - y_n = \frac{h}{90}(7k_1 + 32k_3 + 12k_4 + 32k_5 + 7k_6) \quad (2.128)$$

$$k_1 = f(x_n, y_n) \quad (2.129)$$

$$k_2 = f\left(x_n + \frac{1}{2}h, y_n + \frac{1}{2}hk_1\right) \quad (2.130)$$

$$k_3 = f\left(x_n + \frac{1}{4}h, y_n + \frac{1}{16}h(3k_1 + k_2)\right) \quad (2.131)$$

$$k_4 = f\left(x_n + \frac{1}{2}h, y_n + \frac{1}{2}hk_3\right) \quad (2.132)$$

$$k_5 = f\left(x_n + \frac{3}{4}h, y_n + \frac{3}{16}h(-k_2 + 2k_3 + 3k_4)\right) \quad (2.133)$$

$$k_6 = f\left(x_n + h, y_n + \frac{1}{7}h(k_1 + 4k_2 + 6k_3 - 12k_4 + 8k_5)\right) \quad (2.134)$$

Interval of absolute stability: $(-5.7, 0)$

Fourth-order two-stage implicit Runge-Kutta method

$$y_{n+1} - y_n = \frac{h}{2}(k_1 + k_2) \quad (2.141)$$

$$k_1 = f\left(x_n + \left(\frac{1}{2} + \frac{\sqrt{3}}{6}\right)h, y_n + \frac{1}{4}hk_1 + \left(\frac{1}{4} + \frac{\sqrt{3}}{6}\right)hk_2\right) \quad (2.142)$$

$$k_2 = f\left(x_n + \left(\frac{1}{2} - \frac{\sqrt{3}}{6}\right)h, y_n + \left(\frac{1}{4} - \frac{\sqrt{3}}{6}\right)hk_1 + \frac{1}{4}hk_2\right) \quad (2.143)$$

Interval of absolute stability: $(-\infty, 0)$.

*2.8.3.2.2 Adams-Moulton Family of Methods**One-step Adams-Moulton, backward Euler's rule*

$$y_{n+1} - y_n = hf_{n+1} \quad (2.144)$$

Interval of absolute stability: $(-\infty, 0)$

Two-step Adams-Moulton, trapezoidal rule

$$y_{n+2} - y_{n+1} = \frac{h}{2}(f_{n+2} + f_{n+1}) \quad (2.145)$$

Interval of absolute stability: $(-\infty, 0)$

Three-step Adams-Moulton

$$y_{n+3} - y_{n+2} = \frac{h}{12}(5f_{n+2} + 8f_{n+1} - f_{n+1}) \quad (2.146)$$

Interval of absolute stability: $(-6, 0)$

Four-step Adams-Moulton

$$y_{n+4} - y_{n+3} = \frac{h}{24}(9f_{n+4} + 19f_{n+3} - 5f_{n+2} + f_{n+1}) \quad (2.147)$$

Interval of absolute stability: $(-3, 0)$

Software: The method chosen of course depends on the nature of the equation. The analysis presented earlier may be of great help in selecting the right kind of step size balancing the stability and convergence.

$$y = f\left(\frac{dy}{dx}\right) \quad (2.149)$$

$$\text{Let } p = \frac{dy}{dx} \quad \text{thus} \quad dy = p dx$$

From Equation (2.149),

$$dy = f'(p) dp = p dx$$

The solution is given by

$$y = f(p), \quad x = \int \frac{f'(p) dp}{p} + c \quad (2.150)$$

$$x = f\left(\frac{dy}{dx}\right)$$

$$\text{Let } p = \frac{dy}{dx} \quad \text{thus} \quad dy = p dx$$

From Equation (2.150),

$$dx = f'(p) dp$$

$$dy = p dx = p f'(p) dp$$

The solution is given by

$$y = \int p f'(p) dp + c, \quad x = f(p)$$

2.9.2.3 Lagrange Equation

$$y = x f\left(\frac{dy}{dx}\right) + g\left(\frac{dy}{dx}\right)$$

$$\text{Let } p = \frac{dy}{dx} \quad \text{thus} \quad dy = p dx$$

$$p dx = f(p) dx + x f'(p) dp + g'(p) dp$$

Dividing throughout by dp gives

The mass balance for the species A is given by

$$\frac{dA}{dt} = -k_1 A - nk_n A^n, \quad A(0) = A_0$$

The solution is given by

$$A(t) = \left[\left(A_0^{1-n} + \frac{nk_n}{k_1} \right) e^{(n-1)k_1 t} - \frac{nk_n}{k_1} \right]^{1/(1-n)}, \quad n > 1$$

2.9.2.6 Exact Differential Equations

$$N(x, y) \frac{dy}{dx} + M(x, y) = 0, \quad y(0) = y_0$$

This is often written in the form

$$M(x, y)dx + N(x, y)dy = 0$$

The equation is said to be exact if

$$\frac{\partial M}{\partial y} = \frac{\partial N}{\partial x}$$

Then the solution is given by the implicit function, $\psi(x, y)$, where

$$\psi(x, y) = 0 \int_0^x M(t, y) dt + \int_{y_0}^y \left[N(x, s) - \int_0^x \frac{\partial M(t, s)}{\partial s} dt \right] ds$$

2.9.2.7 Homogeneous Equations

A nonlinear differential equation

$$\frac{dy}{dx} = f(x, y)$$

is said to be homogeneous of degree 0 if

$$f(tx, ty) = f(x, y) = tF\left(\frac{y}{x}\right)$$

The transformation $y = xv$ converts the equation to

$$x \frac{dv}{dx} = F(v) - v$$

2.9.3 SECOND-ORDER DIFFERENTIAL EQUATIONS

2.9.3.1 Homogeneous Linear Equations with Constant Coefficients

The mass balance for a first-order reaction in a tubular reactor with a flow velocity of v and the concentration of reactant in feed, C_f , undergoing a reaction with the rate constant of k is governed by the following second-order linear equation with constant coefficients:

$$D \frac{d^2 C}{dx^2} - v \frac{dC}{dx} - kC = 0 \quad (2.153)$$

subjected to boundary conditions:

$$-D \frac{dC}{dx} = v(C_f - C), \quad x = 0$$

$$\frac{dC}{dx} = 0, \quad x = L$$

where L is the reactor length and D is the diffusion coefficient. The solutions are determined by the roots of the characteristic equation,

$$D\lambda^2 - v\lambda - k = 0$$

that is given by

$$\lambda_{1,2} = \frac{v \pm \sqrt{v^2 + 4Dk}}{2D}$$

$$C(x) = A \exp(\lambda_1 x) + B \exp(\lambda_2 x)$$

Equivalently,

$$C(x) = \exp\left(\frac{v}{2D}x\right) [A \cosh(\gamma x) + B \sinh(\gamma x)] \quad (2.154)$$

where

$$\gamma = \frac{\sqrt{v^2 + 4Dk}}{2D}$$

$$A = \frac{vC_f(v \sinh(\gamma L) + 2D\gamma \cosh(\gamma L))}{(v^2 + 2Dk) \sinh(\gamma L) + 2Dv\gamma \cosh(\gamma L)}$$

$$B = -\frac{vC_f(v \cosh(\gamma L) + 2D\gamma \sinh(\gamma L))}{(v^2 + 2Dk) \sinh(\gamma L) + 2Dv\gamma \cosh(\gamma L)}$$

$$\alpha(x) = - \int^x \frac{S(\xi)}{y_1(\xi)y_2'(\xi) - y_1'(\xi)y_2(\xi)} y_2(\xi) d\xi$$

$$\beta(x) = \int^x \frac{S(\xi)}{y_1(\xi)y_2'(\xi) - y_1'(\xi)y_2(\xi)} y_1(\xi) d\xi$$

Substituting $\alpha(x)$ and $\beta(x)$ in $C_p(x)$ gives the particular solution

$$C_p(x) = \int^x \frac{y_1(t)y_2(x) - y_1(x)y_2(t)}{y_1(t)y_2'(t) - y_1'(t)y_2(t)} S(t) dt$$

and the general solution

$$C(x) = Ay_1 + By_2 + \int^x \frac{y_1(t)y_2(x) - y_1(x)y_2(t)}{y_1(t)y_2'(t) - y_1'(t)y_2(t)} S(t) dt$$

where A and B are constants that can be determined on the specification of boundary conditions.

2.9.3.3 Green's Function

The method of Green's function expresses the solution of the inhomogeneous boundary-value problem as the integral representation of the inhomogeneous function (Friedman, 1956; Stakgold, 1979). Given the boundary-value problem,

$$a_2 \frac{d^2 y}{dx^2} + a_1 \frac{dy}{dx} + a_0 y = g(x)$$

$$\alpha_1 \frac{dy}{dx} + \beta_1 y = 0, \quad x = 0$$

$$\alpha_2 \frac{dy}{dx} + \beta_2 y = 0, \quad x = 1$$
(2.156)

The above boundary-value problem is transformed to the following self-adjoint forms:

$$\frac{d}{dx} \left(p(x) \frac{dy}{dx} \right) + q(x)y = f(x)$$

$$B_1(y) = \alpha_1 \frac{dy}{dx} + \beta_1 y = 0, \quad x = 0$$

$$B_2(y) = \alpha_2 \frac{dy}{dx} + \beta_2 y = 0, \quad x = 1$$

$$p(x) = \exp \left(\int^x \frac{a_1}{a_2} dx \right), \quad q(x) = \frac{a_0(x)p(x)}{a_2(x)}, \quad f(x) = \frac{p(x)g(x)}{a_2(x)}$$
(2.157)

Green's function for Equation (2.157) is given by

The solution is given by

$$C(x) = C_1(x) + \int_0^1 \exp\left(-\frac{\nu}{D}x\right) G(x, \xi) S(\xi) d\xi$$

where $C_1(x)$ is the solution of the homogeneous equation and $C_0 \neq 0$ is given by Equation (2.154), and the Green's function $G(x, \xi)$ for $C_0 = 0$ is given by

$$G(x, \xi) = \begin{cases} -\frac{4D^2 q v_1(x) v_2(\xi)}{4Dq\nu \cosh(qL) + (4D^2 q^2 + \nu^2) \sinh(q)} & x < \xi \\ -\frac{4D^2 q v_1(\xi) v_2(x)}{4Dq\nu \cosh(qL) + (4D^2 q^2 + \nu^2) \sinh(q)} & x \geq \xi \end{cases} \quad (2.158)$$

where the two linearly independent solutions v_1 and v_2 satisfying $B_i(v_i)$ are

$$v_1(x) = \exp\left(\frac{\nu}{2D}x\right) \left[\cosh(qx) + \frac{\nu L}{2Dq} \sinh(qx) \right]$$

$$v_2(x) = \exp\left(\frac{\nu}{2D}x\right) \left[\cosh(q(x-L)) - \frac{\nu L}{2Dq} \sinh(q(x-L)) \right]$$

2.9.3.4 Green's Function by Eigenfunction (Mercer's) Expansions

Consider the Green's function defined by the following differential equations:

$$\frac{d}{dx} \left(p(x) \frac{dG}{dx} \right) + q(x)G - \lambda r(x)G = \delta(x - \xi)$$

$$\alpha_1 \frac{dG(a, \xi; \lambda)}{dx} + \beta_1 G(a, \xi; \lambda) = 0, \quad x = a$$

$$\alpha_2 \frac{dG(b, \xi; \lambda)}{dx} + \beta_2 G(b, \xi; \lambda) = 0, \quad x = b$$
(2.159)

where $\delta(x - \xi)$ is the dirac delta function (see Appendix 2.B). Let $y_i(x)$ be the normalized eigenfunctions corresponding to the eigenvalues λ_i of the operator, then we have, $Ly_i = \lambda_i y_i$ where

$$L \equiv -\frac{1}{r(x)} \left[\frac{d}{dx} \left(p(x) \frac{d}{dx} \right) + r(x)q(x) \right] \quad (2.160)$$

Since L is self-adjoint, the eigenfunctions y_i and y_j , corresponding to different eigenvalues λ_i and λ_j , respectively, are orthogonal, i.e.,

$$\int_a^b y_i(x) y_j(x) r(x) dx = \delta_{i,j} = \begin{cases} 1 & \text{if } i = j \\ 0 & \text{if } i \neq j \end{cases}$$

$$y(x) = \sum_{i=1}^m \left(\sum_{k_j=0}^{k_i-1} c_{i,k_j} t^{k_j} \right) \exp(\lambda_i x)$$

2.9.4.2 Inhomogeneous Equation

$$\sum_{i=1}^n a_i \frac{d^i y}{dt^i} = f(t)$$

Let $y_i = \exp(\lambda_i x)$, $i = 1, 2, \dots, n$ be the n solutions of the homogeneous equation, i.e., the n solutions for $f(t) = 0$. Let us define the vectors

$$\mathbf{Y}_i = \begin{bmatrix} y_i \\ \frac{dy_i}{dx} \\ \dots \\ \frac{d^{n-1}y_i}{dx^{n-1}} \end{bmatrix} \quad \mathbf{\delta}_n = \begin{bmatrix} 0 \\ 0 \\ \vdots \\ 1 \end{bmatrix}$$

The Wronskian of these solutions is defined as

$$W(\mathbf{Y}_1, \mathbf{Y}_2, \dots, \mathbf{Y}_n) = \begin{vmatrix} y_1 & y_2 & \dots & y_n \\ \frac{dy_1}{dx} & \frac{dy_2}{dx} & \dots & \frac{dy_n}{dx} \\ \frac{d^2 y_1}{dx^2} & \vdots & \dots & \frac{d^2 y_n}{dx^2} \\ \vdots & \vdots & \vdots & \vdots \\ \frac{d^{n-1} y_1}{dx^{n-1}} & \frac{d^{n-1} y_2}{dx^{n-1}} & \dots & \frac{d^{n-1} y_n}{dx^{n-1}} \end{vmatrix}$$

and let

$$W_1 = W(\mathbf{\delta}_n, \mathbf{Y}_2, \dots, \mathbf{Y}_n) \cdots W_n = W(\mathbf{Y}_1, \mathbf{Y}_2, \dots, \mathbf{\delta}_n) \quad \text{and} \quad \mathbf{\delta}_n = [0 \quad 0 \quad \dots \quad 0 \quad 1]^T$$

$$y(x) = y_h(x) + \sum_{i=1}^n y_i(x) \int_0^x \frac{W_i}{W(\mathbf{Y}_1, \mathbf{Y}_2, \dots, \mathbf{Y}_n)} f(t) dt$$

where $y_h(x)$ is the solution of the homogeneous equation.

2.9.4.3 Application of Higher-Order Equations

Consider the sequence of reactions following the first-order kinetics

where the Green's function is given by Equation (2.158).

2.9.4.4 Finite Element Method

Various formulations of finite element methods have been proposed. For an exhaustive account on finite element methods, the reader is referred to Chen (2005), Donea (2003), Reddy (2005), etc. We present here one of the popular formulations known as the weak formulation of the governing differential equation that, instead of requiring the solution to be twice continuously differentiable, requires that the derivative of the solution be square integrable. We illustrate the weak formulation of the boundary-value problem, Equation (2.157).

To derive the weak formulation, multiplying Equation (2.157) by a test function, $\phi(x)$ (any member of a family of suitably smooth functions), and integrating by parts over an arbitrary element (x_1, x_2) we get

$$\begin{aligned} & - \int_{x_1}^{x_2} a \frac{dy}{dx} \frac{d\phi}{dx} dx + \int_{x_1}^{x_2} qy\phi dx - \int_{x_1}^{x_2} f\phi dx \cdots \\ & + \frac{a(x_2)\phi(x_2)}{\alpha_2} [-\beta_2 y(x_2) + \gamma_2] - \frac{a(x_1)\phi(x_1)}{\alpha_1} [-\beta_1 y(x_1) + \gamma_1] \end{aligned}$$

Let the approximation solution on the local element $y^{(e)}$ be

$$y^{(e)}(x) = \sum_{j=1}^n y_j^{(e)} \psi_j^{(e)}(x)$$

where $y_j^{(e)}$ are the parameters to be determined, and $\psi_j^{(e)}(x)$ are the approximation functions given by

$$\psi_1^{(e)}(x) = \frac{x_{e+1} - x}{x_{e+1} - x_e} \quad \psi_2^{(e)}(x) = \frac{x - x_e}{x_{e+1} - x_e} \quad x_e \leq x \leq x_{e+1}$$

The functions $\psi_j^{(e)}(x)$ are endowed with the following properties:

$$1. \quad \psi_i^{(e)}(x_j) = \begin{cases} 0 & \text{if } i \neq j \\ 1 & \text{if } i = j \end{cases} \quad x_1 = x_e \quad x_2 = x_{e+1} \quad (2.169)$$

$$2. \quad \sum_{i=1}^2 \psi_i^{(e)}(x) = 1 \quad (2.170)$$

Selecting $\phi = \psi_i$ and substituting the approximate solution into the weak formulation, one obtains the local Galerkin finite element equation,

$$\begin{aligned} & - \sum_{j=1}^n \left[\int_{x_1}^{x_2} \left(a \frac{d\psi_i}{dx} \frac{d\psi_j}{dx} + q\psi_i\psi_j \right) dx - \frac{a(x_2)\beta_2}{\alpha_2} \psi_i(x_2)\psi_j(x_2) + \frac{a(x_1)\beta_1}{\alpha_1} \psi_i(x_1)\psi_j(x_1) \right] y_j^{(e)} \cdots \\ & - \int_{x_1}^{x_2} f\psi_i dx + \frac{a(x_2)\psi_i(x_2)\gamma_2}{\alpha_2} - \frac{a(x_1)\psi_i(x_1)\gamma_1}{\alpha_1} \end{aligned}$$

equation to a system of ordinary differential equations and proceeds as follows. We define a characteristic direction on the plane $x - y$ by the differential equations

$$\frac{\partial x}{\partial t} = a(x, y, z), \quad \frac{\partial y}{\partial t} = b(x, y, z), \quad \frac{\partial z}{\partial t} = c(x, y, z) \quad (2.177)$$

the third of which follows from substituting the first two into the partial differential Equation (2.176). The ordinary differential equations are solved subject to the initial conditions $x(0, s) = f(s)$, $y(0, s) = g(s)$, $z(0, s) = h(s)$. The ordinary differential Equations (2.177) are solved by the methods used for ordinary differential equations to obtain the solution $x(t, s)$, $y(t, s)$, $z(t, s)$. The entire solution surface is generated by varying the parameter s over the range of the initial curve. If it is desired to get the solution in the form $z = Z(x, y)$, then we must invert (t, s) to obtain x, y . We consider the following example, from Rhee et al. (1986).

Example 2.8

The dynamics of a plug-flow reactor with a fluid velocity, v , and the first-order reaction kinetics is governed by

$$\begin{aligned} \frac{\partial c}{\partial t} + v \frac{\partial c}{\partial x} &= -kc \\ c(x, 0) &= f(x), \quad c(0, t) = g(t) \end{aligned}$$

The characteristic equations are

$$\begin{aligned} \frac{dt}{dx} &= 1 \\ \frac{dx}{ds} &= v \\ \frac{dc}{ds} &= -kc \end{aligned}$$

Figure 2.1 shows the space-time domain divided by the line $x = vt$ into two regions, $x > vt$ and $x < vt$. For the characteristic lines in the region $x > vt$, the characteristics intersect the x -axis on which the initial condition is specified. The initial condition is parameterized by ξ :

$$t = 0, \quad x = \xi, \quad c = f(\xi) \quad \text{for } s = 0$$

In the region $x < vt$, feed condition is used:

$$x = 0, \quad t = \eta, \quad c = g(\eta) \quad \text{for } s = 0$$

For $x > vt$, the characteristic line emanating from the condition $t = 0$, $x = \xi$ is $f(\xi)$, and integration from $t = 0$ to $t = s$ gives

$$t = s, \quad x = vs + \xi, \quad c(s, \xi) = f(\xi) \exp(-ks)$$

Eliminating s and ξ from the initial and boundary conditions,

The solution of the characteristic equations is parametrically represented by

$$x_i = f_i(s_1, \dots, s_{n-1}, t), \quad \text{for } i = 1, \dots, n$$

$$z = Z(s_1, \dots, s_{n-1}, t)$$

These equations form a parametric representation for the integral surface $z = z(x_1, \dots, x_n)$, provided that the parametric variables in the initial conditions can be inverted to obtain (s_1, \dots, s_{n-1}, t) as functions of (x_1, \dots, x_n) . This is the case when the Jacobian

$$J = \begin{vmatrix} \frac{\partial f_1}{\partial s_1} & \dots & \frac{\partial f_n}{\partial s_1} \\ \vdots & \dots & \vdots \\ \frac{\partial f_1}{\partial s_{n-1}} & \dots & \frac{\partial f_n}{\partial s_{n-1}} \\ a_1 & \dots & a_n \end{vmatrix}$$

does not vanish.

2.10.2 CLASSIFICATION OF SECOND-ORDER EQUATIONS

Second-order equations are classified into different types, depending on the coefficients of the second-order derivatives. The auxiliary conditions to determine a unique solution depend on the type of equation. Auxiliary conditions specified incorrectly with the type of equation lead to an ill-posed problem that may not reflect physical reality.

The general second-order partial differential equation in n -variables is written as

$$\sum_{i=1}^n \sum_{k=1}^n a_{ik}(x_1, x_2, \dots, x_n) \frac{\partial^2 \Phi}{\partial x_i \partial x_k} + B \frac{\partial^2 \Phi}{\partial t^2} + C \left(x_1, \dots, x_n; \Phi; \frac{\partial \Phi}{\partial x_1}, \dots, \frac{\partial \Phi}{\partial x_n} \right) = 0 \quad (2.178)$$

The equation is elliptic if and only if $B = 0$ and is hyperbolic if and only if $B < 0$. If $B = 0$ and the matrix $[a_{ik}]$ is nonnegative definite, the equation is parabolic.

For hyperbolic and parabolic equations, the conditions on (x_1, x_2, \dots, x_n) are prescribed on the boundary of the region, and the conditions on t must be prescribed at $t = 0$. These equations are often referred to as evolution equations. These equations describe the time evolution of a process from a given initial configuration.

As a consequence of the evolutionary nature of the hyperbolic and parabolic equations, boundary conditions are specified on the boundary of the spatial variables, and initial conditions are specified on the time variable, t .

Elliptic equations describe steady-state or equilibrium processes. For such equations, all auxiliary conditions must be prescribed on the boundary of the region of interest. Initial conditions given to elliptic equations lead to ill-posed problems. Solutions to these ill-posed problems exhibit sensitivity to the initial data. Small changes to the initial data cause large changes in the solution.

There are three kinds of boundary conditions for elliptic equations. If the values of the unknown function are prescribed on the boundary, then the problem is called the Dirichlet problem. If the derivatives of the unknown function are prescribed on the boundary, then it is called the Neumann problem. If a linear combination of the function values and the derivatives is specified, then it is called the Robin problem.

The methods for solving a second-order partial differential equation are separation of variables, similarity variable, Laplace transform, Fourier transform, and Hankel transform. Each of the

The expression for the coefficient A_n can be obtained as follows. The initial condition gives

$$u(x, 0) = u_0(x) = \sum_{n=1}^{\infty} A_n \sin(n\pi x)$$

Multiplying the above equation by $\sin(m\pi x)$ and integrating over $(0, 1)$ gives

$$A_n = 2 \int_0^1 u_0(x) \sin(n\pi x) dx$$

The answer is obtained by making use of the orthogonal property,

$$2 \int_0^1 \sin(n\pi x) \sin(m\pi x) dx = \delta_{m,n}, \quad \text{where } \delta_{m,n} \text{ is the Kronecker delta}$$

The method of separation of variables is applicable for higher-order and higher-dimensional equations, but it requires that the equation and boundary conditions be homogeneous in a finite domain.

2.10.3.2 Inhomogeneous Equation, Duhamel's Principle

Duhamel's principle helps to represent solutions to inhomogeneous initial boundary-value problems in terms of the solutions to homogeneous problems. The solution of the inhomogeneous equation,

$$\frac{\partial u}{\partial t} = \frac{\partial^2 u}{\partial x^2} + h(x, t) \quad (2.179)$$

subjected to boundary conditions

$$u(0, t) = u(1, t) = u(x, 0) = 0$$

is given by

$$u(x, t) = \int_0^t v(x, t - \tau; \tau) d\tau \quad (2.180)$$

where $v(x, t; \tau)$ is the solution of the following homogeneous equation:

$$\begin{aligned} \frac{\partial v}{\partial t} &= \frac{\partial^2 v}{\partial x^2} \\ v(0, t; \tau) &= v(1, t; \tau) = 0 \\ v(x, 0; \tau) &= h(x, \tau) \end{aligned}$$

the solution of which clearly follows:

2.10.3.3 Inhomogeneous Boundary Conditions

Generally, the initial boundary-value problem given by

$$\frac{\partial u}{\partial t} = \frac{\partial^2 u}{\partial x^2}$$

$$u(x, 0) = u_0(x), \quad u(0, t) = a(t), \quad u(1, t) = b(t)$$

is solved by letting $u(x, t) = v(x, t) + w(x, t)$ such that $v(0, t) = v(1, t) = 0$. Thus, $w(0, t) = a(t)$, $w(1, t) = b(t)$. The simplest function $w(x, t)$ that satisfies the boundary conditions is

$$w(x, t) = [b(t) - a(t)]x + a(t)$$

Substitution for $u(x, t)$ into the equation gives

$$\frac{\partial v}{\partial t} = \frac{\partial^2 v}{\partial x^2} + [a'(t) - b'(t)]x - a'(t)$$

$$v(0, t) = v(1, t) = 0$$

$$v(x, 0) = u_0(x) + [a(0) - b(0)]x - a(0)$$

The solution of the transformed equation can then be easily obtained using Duhamel's principle with $h(x, t) = [a'(t) - b'(t)]x - a'(t)$.

The methods presented here can be neatly integrated into the subject of linear operators (Ramkrishna and Amundson, 1985), extending considerably the variety of problems that can be solved. For the solution using the method of Fourier transforms, the reader is referred to Varma and Morbidelli (1997).

2.10.3.4 Similarity Solutions

The equation suggests a similarity solution when there is no characteristic length scale, i.e., the domain is either a semi-infinite or infinite region. Consider the diffusion equation in a positive real line:

$$\frac{\partial u}{\partial t} = \frac{\partial^2 u}{\partial x^2}, \quad 0 < x < \infty$$

$$u(x, 0) = 0, \quad u(0, t) = u_0(t)$$

Let the transformed variable be $\eta = x/(2\sqrt{t})$ and hence $u(x, t) = \Theta(\eta)F(\eta)$. Such a scaling behavior is typical of diffusion processes:

$$\frac{\partial u}{\partial x} = \frac{\partial u}{\partial \eta} \frac{\partial \eta}{\partial x} = \Theta F'(\eta) \frac{1}{2\sqrt{t}}; \quad \frac{\partial^2 u}{\partial x^2} = \Theta F''(\eta) \frac{1}{4t}$$

and

where $v_1(x, t)$ is the solution of

$$\frac{\partial v_1}{\partial t} = \frac{\partial^2 v_1}{\partial x^2}, \quad -\infty < x < \infty$$

$$v_1(x, 0) = u_0(x)$$

and $v_2(x, t)$ satisfies

$$\frac{\partial v_2}{\partial t} = \frac{\partial^2 v_2}{\partial x^2} + h(x, t), \quad -\infty < x < \infty$$

$$v_2(x, 0) = 0$$

For the inhomogeneous equation,

$$\frac{\partial v}{\partial t} = \frac{\partial^2 v}{\partial x^2} + h(x, t), \quad 0 < x < \infty$$

$$v(0, t) = a(t)$$

$$v(x, 0) = u_0(x)$$

the solution is given with the use of Duhamel's principle (Section 2.10.3.2):

$$v(x, t) = u_h(x, t) + \int_0^t \int_0^\infty [k(x-s, t-\tau) - k(x+s, t-\tau)] h(s, \tau) ds d\tau$$

where $u_h(x, t)$ is the solution of the homogeneous equation, and $k(x, t)$ is the fundamental solution.

2.10.4 HYPERBOLIC EQUATIONS

A prototype of a hyperbolic equation is the wave equation. The wave equation governs many physical phenomena such as the propagation of sound waves, water waves, vibration of a membrane in a two-dimensional setting, and vibration of a string in a one-dimensional setting.

2.10.4.1 d'Alembert's Solution

The one-dimensional wave equation in an infinite domain can be solved by a change of independent variables to reduce the wave equation that can be integrated to produce d'Alembert's solution. Consider a one-dimensional wave equation,

$$\frac{\partial^2 u}{\partial t^2} = \frac{\partial^2 u}{\partial x^2}, \quad -\infty < x < \infty$$

$$u(x, 0) = f(x) \tag{2.181}$$

$$\frac{\partial u(x, 0)}{\partial t} = g(x)$$

Let $\xi = x - t$ and $\eta = x + t$. Then the equation is transformed to

Defining $\xi = x - t$ and $\eta = x + t$ transforms the above equation to

$$\frac{\partial^2 u}{\partial \xi \partial \eta} = -\frac{1}{4} h\left(\frac{1}{2}(\xi + \eta), -\frac{1}{2}(\xi - \eta)\right)$$

$$w(s, s) = \frac{\partial w(s, s)}{\partial \xi} = \frac{\partial w(s, s)}{\partial \eta} = 0$$

the solution of which is

$$w(x, t) = \frac{1}{2} \int_0^t \int_{x-t}^{x+t} h(y, z) dy dz$$

Therefore, the solution of the inhomogeneous wave equation is given by

$$u(x, t) = \frac{1}{2} [f(x-t) + f(x+t)] + \frac{1}{2} \int_{x-t}^{x+t} g(s) ds + \frac{1}{2} \int_0^t \int_{x-t+\tau}^{x+t+\tau} h(y, z) dy dz$$

2.10.4.2 Separation of Variables

Consider a one-dimensional inhomogeneous equation

$$\frac{\partial^2 u}{\partial t^2} = \frac{\partial^2 u}{\partial x^2} + h$$

subjected to the boundary conditions

$$u(0, t) = a(t)$$

$$u(1, t) = b(t)$$

$$u(x, 0) = f(x)$$

$$\frac{\partial u(x, 0)}{\partial t} = g(x)$$

Let $u(x, t) = v(x, t) + x[b(t) - a(t)] + a(t)$, where $v(x, t)$ satisfies

$$\frac{\partial^2 v}{\partial t^2} = \frac{\partial^2 v}{\partial x^2} + h - x[b''(t) - a''(t)] - a''(t)$$

$$v(0, t) = v(1, t) = 0$$

$$v(x, 0) = f(x) - x[b(0) - a(0)] - a(0)$$

$$\frac{\partial v(x, 0)}{\partial t} = g(x) - x[b'(0) - a'(0)] - a'(0)$$

The problem for $v(x, t)$ is solved by defining

which is solved by Duhamel's principle (Section 2.10.3.2), which states that the solution of the inhomogeneous equation is given by

$$v_2(x, t) = \int_0^t w(x, t - \tau, \tau) d\tau$$

where $w(x, t)$ satisfies

$$\begin{aligned} \frac{\partial^2 w}{\partial t^2} &= \frac{\partial^2 w}{\partial x^2} \\ w(0, t, \tau) &= w(1, t, \tau) = w(x, 0, \tau) = 0 \\ \frac{\partial w(x, 0, \tau)}{\partial t} &= h(x, \tau) - x[b''(\tau) - a''(\tau)] - a''(\tau) \end{aligned}$$

The solution is given by

$$w(x, t, \tau) = \sum_1^{\infty} C_n(\tau) \sin(n\pi t) \sin(n\pi x)$$

where

$$C_n(\tau) = \frac{2}{n\pi} \int_0^1 \{h(x, \tau) - x[b''(\tau) - a''(\tau)] - a''(\tau)\} \sin(n\pi x) dx$$

Thus the solution of the inhomogeneous equation is given by

$$\begin{aligned} u(x, t) &= x[b(t) - a(t)] + a(t) + \sum_{n=1}^{\infty} [A_n \sin(n\pi t) + B_n \cos(n\pi t)] \sin(n\pi x) + \\ &\int_0^t \sum_{n=1}^{\infty} C_n(\tau) \sin(n\pi(t - \tau)) \sin(n\pi x) d\tau \end{aligned}$$

2.10.5 ELLIPTIC EQUATIONS

A prototype of the elliptic equation is the Laplace equation. The Laplace equation describes the steady-state distribution of energy or matter inside the domain given the distribution on the boundary. The dynamics of a given process may or may not come to a steady state. If the dynamics does not lead to an equilibrium, then the solution does not exist. Consider the steady-state temperature distribution in a unit cube governed by the following Poisson's equation:

$$\nabla^2 u = f(x, y, z), \quad (x, y, z) \in \mathcal{D}$$

where \mathcal{D} is the domain of the region. The general boundary condition is written as

To ensure that the solution is finite at $r = 0$, $D = 0$. Thus, by the superposition principle, the general solution is given by

$$u(r, \theta) = \frac{a_0}{2} + \sum_{n=1}^{\infty} r^n (a_n \cos(n\theta) + b_n \sin(n\theta))$$

where

$$a_n = \frac{1}{\pi} \int_0^{2\pi} f(\theta) \cos(n\theta) d\theta, \quad b_n = \frac{1}{\pi} \int_0^{2\pi} f(\theta) \sin(n\theta) d\theta$$

Substituting a_n and b_n into the solution, we get

$$\begin{aligned} u(r, \theta) &= \frac{1}{\pi} \int_0^{2\pi} \left\{ \frac{1}{2} + \sum_{n=1}^{\infty} r^n [\cos(n\theta) \cos(n\phi) + \sin(n\theta) \sin(n\phi)] \right\} f(\phi) d\phi \\ &= \frac{1}{\pi} \int_0^{2\pi} \left\{ \frac{1}{2} + \sum_{n=1}^{\infty} r^n \cos[n(\phi - \theta)] \right\} f(\phi) d\phi \\ &= \frac{1-r^2}{2\pi} \int_0^{2\pi} \frac{f(\phi) d\phi}{1-2r \cos(\phi - \theta) + r^2} \end{aligned}$$

that is obtained by summing the series in the braces.

The solution of the Laplace equation in a unit sphere with $f(\theta, \phi)$ prescribed on the surface of the sphere is given by

$$u(r, \theta, \phi) = \frac{1}{4\pi} \int_0^{2\pi} \int_0^{\pi} \frac{(1-r^2)f(\theta', \phi')}{(1-2r \cos \Theta + r^2)^{3/2}} \sin \phi' d\phi' d\theta'$$

where

$$\cos \Theta = \cos \phi \cos \phi' + \sin \phi \sin \phi' \cos(\theta - \theta')$$

2.10.5.2 Green's Function

The solution of the Poisson equation

$$\nabla^2 u = h, \quad 0 \leq r \leq 1, \quad 0 \leq \theta \leq 2\pi$$

$$u(1, \theta) = 0$$

is given by

$$u(r, \theta) = \int_0^1 \int_0^{2\pi} G(r, \theta; \rho, \phi) h(\rho, \phi) \rho d\rho d\phi$$

$$u(x) - \lambda \int_a^x K(x, y)u(y)dy = f(x) \quad (2.183)$$

$$p(x)u(x) - \lambda \int_a^x K(x, y)u(y)dy = f(x) \quad (2.184)$$

The first equation is known as a Volterra equation of the first kind, and the last two are of the second and the third kinds, respectively. An integral equation of the third kind can be transformed into an integral equation of the second kind if $p(x) \neq 0$.

Differentiating the integral equation of the first kind with respect to the independent variable x yields (under suitable continuity and differentiability conditions on various functions in the integral equation)

$$\frac{df}{dx} = \lambda \int_0^x \frac{\partial K(x, y)}{\partial x} u(y)dy + \lambda K(x, x)u(x) \quad (2.185)$$

If $K(x, x) \neq 0$, then the Volterra equation of the first kind can be converted to a Volterra equation of the second kind,

$$u(x) + \int_0^x H(x, t)u(t)dt = g(x)$$

where

$$g(x) \equiv \frac{1}{K(x, x)} \frac{df}{dx}, \quad H(x, t) \equiv \frac{1}{K(x, x)} \frac{\partial K(x, t)}{\partial x} \quad (2.186)$$

Volterra equations are classified as regular and singular integral equations. If $K(x, y) < \infty$, the equations are called regular; otherwise, they are defined as singular. If $f(x) = 0$, the equations are termed homogeneous.

Each type of equation is further categorized into linear and nonlinear equations based on whether or not the unknowns in the equations appear as a first power. The following is an example of a nonlinear Volterra equation:

$$u(x) = f(x) + \int_0^x K(x, y)F(u(y))dy \quad (2.187)$$

Other forms of nonlinear integral equations also arise in applications.

2.11.2 METHODS OF SOLUTION FOR VOLTERRA EQUATIONS

The monograph by Linz (1985) provides a good theoretical and practical treatment of Volterra integral equations. In what follows, we list the solutions in accordance with the kernel type.

2.11.2.1 Kernel Is Only a Function of Dependent Variable

For $K(x, y) = K(y)$,

$$u(x) = f(x) + \lambda \int_0^x K(x-y)u(y)dy \quad (2.196)$$

The equation is solved by Laplace transform with the help of the convolution theorem:

$$\bar{u}(s) = \frac{\bar{f}(s)}{1 - \lambda \bar{K}(s)}, \quad \lambda \bar{K} \neq 1$$

where $\bar{u}(s)$, $\bar{f}(s)$, and $\bar{K}(s)$ are the Laplace transforms of $u(x)$, $f(x)$, and $K(x)$, respectively.

Inverting the transform,

$$u(x) = \mathcal{L}^{-1} \left\{ \frac{\bar{f}(s)}{1 - \lambda \bar{K}(s)} \right\}$$

The inversion of the right hand side above would of course depend on the specific form of $K(s)$. The method of resolvent kernels in the section below can also be applied here.

$$u(x) = f(x) + \lambda \int_0^x K(x,y)u(y)dy$$

2.11.2.5 Method of Resolvent Kernels

$$u(x) = f(x) + \lambda \int_0^x K(x,y)f(y)dy \quad (2.197)$$

The solution of a Volterra equation is given in terms of a resolvent kernel,

$$u(x) = f(x) + \lambda \int_0^x \Gamma(x,y;\lambda)f(y)dy \quad (2.198)$$

where the resolvent kernel is given in terms of the Neumann series as

$$\Gamma(x,y;\lambda) = \sum_{i=0}^{\infty} \lambda^i K_{i+1}(x,y) \quad (2.199)$$

$$K_1(x,y) = K(x,y) \quad (2.200)$$

$$K_2(x,y) = \int_y^x K(x,s)K(s,y)ds \quad (2.201)$$

$$\vdots \quad (2.202)$$

$$K_{i+1}(x,y) = \int_y^x K(x,s)K_i(s,y)ds \quad (2.203)$$

$$u(x) = f(x) + \int_a^x K(x, y, u(y)) dy \quad (2.208)$$

Equation (2.209) is linearized by Newton's method to give

$$u_{k+1}(x) = f(x) + \int_a^x \left\{ K(x, y, u_k(y)) + \frac{\partial K}{\partial u}(x, y, u_k) u_{k+1}(y) - \frac{\partial K}{\partial u}(x, y, u_k) u_k(y) \right\} dy \quad (2.209)$$

Successive substitution is based on the following equation:

$$u_{k+1}(x) = f(x) + \int_a^x K(x, y, u_k(y)) dy \quad (2.210)$$

The trapezoidal rule is used to convert Equation (2.210) to a set of algebraic equations.

Jerry (1985) discusses the solution to the nonlinear Volterra equations. The existence of linear equations is discussed in Section 2.7.1.

2.11.3 FREDHOLM INTEGRAL EQUATIONS

The equations of the form

$$\int_a^b K(x, y) u(y) dy = f(x) \quad (2.211)$$

$$u(x) - \lambda \int_a^b K(x, y) u(y) dy = f(x) \quad (2.212)$$

$$a(x) u(x) - \lambda \int_a^b K(x, y) u(y) dy = f(x) \quad (2.213)$$

are called the Fredholm integral equations of the first, second, and third kinds, respectively. Every boundary-value problem can be reduced to a Fredholm equation via the Green's function. Fredholm equations can be further classified into regular and singular integral equations. If the kernel of the equation is finite everywhere in the domain of the integration, the equation is regular. Otherwise, it is singular.

2.11.4 METHODS OF SOLUTION FOR FREDHOLM EQUATIONS

We list here the solutions to Fredholm integral equations in accordance with the type of kernel.

2.11.4.1 Degenerate Kernels

The kernel $K(x, y)$ is said to be a degenerate kernel if it can be expressed as $\sum_{i=1}^n a_i(x) b_i(y)$:

$$u(x) = f(x) + \lambda \sum_{i=1}^n \int_a^b a_i(x) b_i(y) u(y) dy \quad (2.214)$$

The functions $\Gamma(x,y;\lambda)$, $D(x,y;\lambda)$, and $D(\lambda)$ are the Fredholm resolvents of the kernel, Fredholm minor, and Fredholm determinant, respectively. The $D(x,y;\lambda)$ is defined as

$$D(x,y;\lambda) = \sum_{n=0}^{\infty} \frac{(-\lambda)^n}{n!} B_n(x,y)$$

where

$$B_n(x,y) = C_n K(x,y) - n \int_a^b K(x,s) B_{n-1}(s,y) ds, \quad B_0(x,y) = K(x,y)$$

where

$$C_n = \int_a^b B_{n-1}(y,y) dy, \quad n=1,2,\dots, \quad C_0 = 1$$

and

$$D(\lambda) = \sum_{n=0}^{\infty} \frac{(-\lambda)^n}{n!} C_n, \quad C_0 = 1$$

2.11.4.3 Method of Iterated Kernels

The solution of

$$u(x) = f(x) + \lambda \int_a^b K(x,y) u(y) dy$$

is given by

$$u(x) = f(x) + \lambda \int_a^b \Gamma(x,y;\lambda) f(y) dy$$

The iterated kernel $\Gamma(x,y;\lambda)$ is defined as

$$\Gamma(x,y;\lambda) = \sum_{i=1}^{\infty} \lambda^{i-1} K_i(x,y) \quad (2.220)$$

where

$$K_1(x,y) \equiv K(x,y), \quad K_i(x,y) = \int_a^b K(x,s) K_{i-1}(s,y) ds$$

The series defined in Equation (2.220) is convergent for $\max |\lambda B_n| < 1$, where

$$u(x) = f(x) + \int_a^b K(x, y)u(y)dy \quad (2.221)$$

The equation is solved at discrete points $\{x_i\}$, and the integral is approximated by the trapezoidal rule to give the following system of equations:

$$u(x_i) = f(x_i) + \Delta x \left\{ \frac{1}{2} [K(x_i, a)u(a) + K(x_i, b)u(b)] + \sum_{j=1}^{n-1} K(x_i, y_j)u(y_j) \right\} \quad (2.222)$$

$$i = 0, 1, \dots, n$$

where $x_0 = a$, $x_n = b$, $\Delta x = (b - a)/n$. Equation (2.223) represents a system of $n + 1$ equations in $n + 1$ unknowns $\{u_i\}_{i=0}^n$.

For the nonlinear equation,

$$u(x) = f(x) + \int_a^b K(x, y, u(y))dy \quad (2.223)$$

The simplest way to solve Equation (2.223) is by successive substitution:

$$u_{k+1}(x) = f(x) + \int_a^b K(x, y, u_k(y))dy \quad (2.224)$$

Equation (2.224) is solved by discretizing the integral using the trapezoidal rule and iterating the resulting system of algebraic equations until convergence criteria are met.

The second method of solution is by linearization using Newton's method to give

$$u_{k+1}(x) = f(x) + \int_a^b \left\{ K(x, y, u_k(y)) + \frac{\partial K}{\partial u}(x, y, u_k(y))u_{k+1}(y) - \frac{\partial K}{\partial u}(x, y, u_k(y))u_k(y) \right\} dy \quad (2.225)$$

The trapezoidal rule is used to discretize Equation (2.225) to form a system of linear equations that is solved iteratively for a given closer initial guess of $u_0(x)$.

2.11.4.6 Solution of Ill-Posed Fredholm Equations of the First Kind

It is seen in Section 2.2.6 that Fredholm equations of the first kind arise from inverse problem formulation, i.e., the determination of model parameters from experimental measurements. Inverse problems are generally ill posed. They lack the one or more of the three properties required for reliable model predictions:

1. Existence of solution
2. Uniqueness of solution
3. Stability with respect to small perturbations in model parameters

In this subsection, the ill-posed nature of Fredholm integral equations of the first kind is demonstrated with an example equation. A technique known as *regularization* to overcome these issues is presented. The essential idea for regularization is to approximate the integral equation of

$$\mathbf{A}\mathbf{u} = \mathbf{c}$$

to be solved for u_i , which is used in the solution Equation (2.227).

2.11.4.7 Method of Regularization

This section presents a simplified treatment of the technique of Tikhonov regularization. The idea of regularization is to convert a original ill-posed problem (which means that the error in the solution is magnified by errors in the input data) into a well-posed problem for which the error in the solution is under control. More specifically, consider the solution of the following Fredholm integral equation of the first kind.

$$\int_a^b K(x, y)u(y)dy = f(x), \text{ i.e., } Au = f$$

where A is clearly a linear integral operator. By direct solution of the above equation we imply the minimization of the norm of the residual $Au - f$. This is ill-posed because small errors in f produce large errors in the solution u . To regularize this we ask to minimize

$$J(u) = \|Au - f\| + \alpha\|u\| \quad (2.229)$$

where $\alpha > 0$. This formulation is a well-posed problem because it prevents excessive detail in the solution. It is shown (Kress, 1989) that the minimizer u_α of Equation (2.231) is the unique solution of the equation

$$\alpha u + A^*Au = A^*f \quad (2.230)$$

where

$$A^*Au = \int_a^b K(y, x)K(x, y)u(y)dy$$

and

$$A^*f = \int_a^b K(y, x)f(y)dy$$

Thus, the ill-posed problem of a Fredholm equation of the first kind is approximated by the well-posed problem of the second kind.

The error of approximation is represented by the functional $J(u)$, which depends on the regularization parameter α . There are two components in this error. One component involves $\|Au - f\|$, which is due to the solution of the ill-posed problem, while the other component involves regularization $\alpha\|u\|$. The relative importance of each term in this functional is depicted in Figure 2.2. The strategy for choosing α is to minimize the functional $J(u)$. The criterion is called the L criterion in view of the shape of the function $J(u)$.

For the inverse problems of chemical engineering interest, the reader is referred to Ramkrishna and coworkers (Sathyagal et al. (1985), Muralidhar and Ramkrishna (1989), Wright and Ramkrishna (1992), etc.).

The term \bar{z} is said to be a complex conjugate of z . It follows that

$$z\bar{z} \equiv (x^2 + y^2, 0) = r^2 = (\operatorname{Re} z)^2 + (\operatorname{Im} z)^2$$

Complex numbers can also be represented in their polar form as

$$z \equiv (x, y) = re^{i\theta} = r(\cos \theta + i \sin \theta)$$

where

$$r = \sqrt{x^2 + y^2}, \quad \theta = \tan^{-1} \frac{y}{x}$$

The interpretation of r is the modulus (magnitude or the length) of the complex number, and θ (phase angle) is the argument of z , $\theta = \arg(z)$. Geometrically

$$z = re^{i\theta} = re^{i(\theta + 2n\pi)}$$

Thus $\arg(z)$ as a function should be restricted, such as

$$-\pi < \arg(z) < \pi$$

Such restriction defines the principal value of $\arg(z)$, which is denoted as $\operatorname{Arg}(z)$:

$$\operatorname{Arg}(z_1 z_2) = \operatorname{Arg}(z_1) + \operatorname{Arg}(z_2)$$

$$\operatorname{Arg}\left(\frac{z_1}{z_2}\right) = \operatorname{Arg}(z_1) - \operatorname{Arg}(z_2)$$

The n th root of unity is defined as

$$z^n = 1 \Rightarrow z = \cos\left(\frac{2k\pi}{n}\right) + i \sin\left(\frac{2k\pi}{n}\right), \quad k = 1, 2, \dots, n-1$$

2.12.2 ANALYTIC FUNCTIONS

A complex function $w = f(z)$ assigns a value of w in the complex plane to each value of z in the subset of the complex plane D . The set of complex numbers, D , is called the domain of definition of f . When the domain of definition is not specified, then it is understood that the function takes on all values of z for which f is defined. For example, the domain of $f(z) = 1/z$ is all of z such that $z \neq 0$.

Functions of a complex variable often encounter indefiniteness from being multivalued. To make a function single-valued, a function of a complex variable also includes its domain of definition.

Given a function of a complex variable $f(z)$, it is always possible to write

$$f(z) = f(x + iy) = u(x, y) + iv(x, y)$$

The addition rule:

$$\frac{d}{dz}(f(z) \pm g(z)) = \frac{df}{dz} \pm \frac{dg}{dz}$$

The product rule:

$$\frac{d}{dz}(f(z)g(z)) = f(z)\frac{dg}{dz} + g(z)\frac{df}{dz}$$

The quotient rule:

$$\frac{d}{dz} \frac{f(z)}{g(z)} = \frac{g(z)\frac{df}{dz} - f(z)\frac{dg}{dz}}{g^2(z)}$$

The derivative of a function of a complex variable $f(x + iy) = u(x,y) + iv(x,y)$ exists at $z_0 = (x_0, y_0)$ if and only if the following equations are satisfied:

$$\frac{\partial u}{\partial x} = \frac{\partial v}{\partial y} \quad \text{and} \quad \frac{\partial v}{\partial x} = -\frac{\partial u}{\partial y} \quad (2.231)$$

Equations (2.233) are known as Cauchy–Riemann equations. In polar coordinates, the $f(r_0 e^{i\theta}) = u(r_0, \theta_0) + iv(r_0, \theta_0)$ is differentiable at (r_0, θ_0) if and only if

$$\frac{\partial u}{\partial r} = \frac{1}{r} \frac{\partial v}{\partial \theta} \quad \text{and} \quad \frac{\partial v}{\partial r} = -\frac{1}{r} \frac{\partial u}{\partial \theta} \quad (2.232)$$

It follows that the real and imaginary parts of a differentiable function are not independent, i.e., given $u(x,y)$, $v(x,y)$ can be constructed with an arbitrary constant. Given a differentiable function $f(z)$, the real and imaginary parts of f satisfy the Laplace equation:

$$\frac{\partial^2 u}{\partial x^2} + \frac{\partial^2 u}{\partial y^2} = 0$$

$$\frac{\partial^2 v}{\partial x^2} + \frac{\partial^2 v}{\partial y^2} = 0$$

The $u(x,y)$ of a differentiable function $f(z)$ is also called a *harmonic function*, whereas $v(x,y)$ is called a conjugate harmonic function.

It also follows that if $f(z)$ is analytic, then the real and imaginary parts satisfy the Cauchy–Riemann equations, and it can be represented by a Taylor series in the neighborhood of z_0 . A complex-valued function that is analytic in the whole complex plane is called an *entire function*. If a complex-valued function fails to be analytic at z_0 but is analytic at every other point in the neighborhood of z_0 , then z_0 is said to be an isolated singular point of f . For example, 0 is an isolated singular point of $f(z) = 1/z$.

2.12.2.3 Logarithmic Functions

Given the entire function

$$z = re^{i\theta}$$

the function $\log z$ is

$$\log z = \log r + i\theta$$

where $r = |z|$ and $\theta = \arg(z)$. Because

$$re^{i\theta} = re^{i(\theta+2k\pi)}$$

$$\theta = \arg(z) = \arg(z) + 2k\pi$$

is not a single-valued function. The situation is similar to that in the previous section. Defining the principal value of the logarithmic function,

$$\text{Log } z = \text{Log } r + i\Theta, \quad (r > 0, -\pi < \Theta \leq \pi)$$

The mapping $w = \text{Log } z$ is a single-valued and continuous function in its domain of definition, which is the set of all nonzero complex numbers; its range is the strip $-\pi < \text{Im}(w) \leq \pi$. Thus the function $\text{Log } z$ is analytic.

2.12.2.4 Cauchy Integral Formula

Consider a curve C parameterized by t , $z(t) = x(t) + iy(t)$, $a \leq t \leq b$ and a complex function $f(x + iy) = u(x, y) + iv(x, y)$. The contour integral of $f(z)$ along the curve z is

$$\begin{aligned} \int_C f(z) dz &= \int_a^b (ux' - vy') dt + i \int_a^b (vx' + vy') dt \\ &= \int_C u dx - v dy + i \int_C v dx + u dy \end{aligned}$$

If $f(z)$ is analytic everywhere within and on a simple closed contour C , taken in the positive sense (i.e., traversing the curve, C , in counterclockwise direction), and if z_0 is any point interior to C , then

$$f(z_0) = \frac{1}{2\pi i} \int_C \frac{f(z) dz}{z - z_0} \quad (2.233)$$

A simple curve is a closed curve that does not intersect itself. Equation (2.235) is called the Cauchy integral formula. As a consequence of the Cauchy integral formula, we can write

$$\frac{d^n f(z_0)}{dz^n} = \frac{n!}{2\pi i} \int_C \frac{f(z) dz}{(z - z_0)^{n+1}}$$

$$b_1 = \frac{1}{(m-1)!} \frac{d^{m-1}\phi(z_0)}{dz^{m-1}}$$

If $m = 1$, then

$$b_1 = \phi(z_0) = \lim_{z \rightarrow z_0} (z - z_0) f(z)$$

Consequently,

$$f(z) = \frac{\phi(z_0)}{(z - z_0)^m} + \frac{\phi'(z_0)}{(z - z_0)^{m-1}} + \cdots + \frac{\phi^{(m-1)}(z_0)}{(m-1)!} \frac{1}{z - z_0} + \sum_{n=m}^{\infty} \frac{\phi^{(n)}(z_0)}{n!} (z - z_0)^{n-m}$$

For example, if $q(z_0) = 0$, then

$$\phi(z) = \frac{p(z_0) + p'(z_0)(z - z_0) + \cdots}{q''(z_0)/2! + q'''(z - z_0)/3! + \cdots}$$

and

$$b_1 = \phi'(z_0) = 2 \frac{p'(z_0)}{q''(z_0)} - \frac{2}{3} \frac{p(z_0)q'''(z_0)}{[q''(z_0)]^2}$$

2.12.3.2 Application of Complex Integration

One of the many applications of the theory of complex variables is the application of the residue theorem to evaluate definite real integrals. Another is to use conformal mapping to solve boundary-value problems involving harmonic functions. The residue theorem is also very useful in evaluating integrals resulting from solutions of differential equations by the method of integral transforms.

Evaluation of definite real integrals using the residue theorem requires proper specification of contours. For some problems, contours can be as simple as a semicircle in the upper half of the complex plane. Problems utilizing this contour are those with integration limits extending over the real line, i.e., $(-\infty, \infty)$, and the integrand being a rational function. We now illustrate the use of complex integration through an example (Fisher, 1999) as follows.

Example 2.9

Evaluate

$$\int_0^{\infty} \frac{\log x dx}{x^2 + b^2}$$

There are two simple poles, ib and $-ib$, on the imaginary axis. An appropriate contour for this integral is shown in Figure 2.3.

$$\frac{1}{2\pi} \Delta_C \arg(f(z)) = N - P$$

Rouché theorem: For two analytic functions $f(z)$ and $g(z)$, inside and on a simple closed contour C , if $|f(z)| > |g(z)|$ at each point on C , then the number of zeros of $f(z)$ is the same as the number of zeros of $f(z) + g(z)$, counting multiplicities inside the contour C .

2.12.5 CONFORMAL MAPPING

Conformal mapping provides a transformation of variables that converts one mathematical problem into another. Its importance lies in the greater ease with which the transformed problem may be solved than the original problem. Applications arise in steady-state conduction or diffusion problems.

Let C_1 and C_2 be two smooth curves in the z plane passing through z_0 , and let α be the angle between these two curves measured in the counterclockwise direction. Let Γ_1 and Γ_2 be the images of $w = f(z)$ of C_1 and C_2 in the w plane, respectively. If the angle between the curves Γ_1 and Γ_2 measured in the counterclockwise direction is α , then the mapping $w = f(z)$ is said to be conformal.

A mapping is said to be conformal at a point z_0 if it preserves the magnitude and sense of the angle between any two smooth arcs through the point z_0 . Thus, at each point z where a function $f(z)$ is analytic and $f'(z) \neq 0$, the mapping $w = f(z)$ is conformal.

Theorem 1: Suppose that the analytic function $f(z) = u(x,y) + iv(x,y)$ maps a domain D_z in the z plane onto a domain D_w in the w plane. If $h(u,v)$ is a harmonic function defined on D_w , then the function

$$H(x,y) = h[u(x,y), v(x,y)]$$

is harmonic in D_z .

Theorem 2: Suppose that the analytic function $f(z) = u(x,y) + iv(x,y)$ maps an arc C in the z plane onto an arc Γ in the w plane. Let $f(z)$ be conformal on C and let a function $h(u,v)$ be differentiable on Γ . If the function $h(u,v)$ satisfies either of the conditions

$$h = c \quad \text{or} \quad \frac{dh}{dn} = 0$$

along Γ , then the function $H(x,y) = h[u(x,y), v(x,y)]$ satisfies the corresponding condition, $H = c$ or $dH/dN = 0$ along C . Here dH/dN denotes the derivative normal to C .

Theorems 1 and 2 are useful for the construction of analytic functions satisfying given boundary conditions. We will now illustrate some of the applications taken from Brown and Churchill (1996).

Example 2.10: The Dirichlet Boundary-Value Problem

Consider a thin semi-infinite plate defined by $y \geq 0$ whose faces are insulated and whose edge $y = 0$ is kept at temperature zero except for the segment $-1 < x < 1$. The segment $(-1 < x < 1)$ is kept at temperature unity. The steady-state temperature distribution $T(x,y)$ is given by the Laplace equation

$$\nabla^2 T = 0$$

for $-\infty < x < \infty$, $y \geq 0$. Then

The solution of the Laplace equation is then expressed as

$$T(x, y) = \frac{1}{\pi} \tan^{-1} \left(\frac{2y}{x^2 + y^2 - 1} \right)$$

Example 2.11: The Neumann Boundary-Value Problem

Find the harmonic function in the first quadrant $x, y > 0$ satisfying

$$\begin{cases} \frac{\partial T(x, 0)}{\partial y} = 0 & \text{when } 0 < x < 1 \\ T(x, 0) = 0 & \text{when } x > 1 \end{cases}$$

$$T(0, y) = 0$$

The function

$$z = \sin w = \sin u \cosh v + i \cos u \sinh v = x + iy$$

maps the first quadrant onto the infinite strip,

$$0 \leq u \leq \frac{\pi}{2}, \quad v = 0 \text{ onto } 0 < x < 1$$

$$u = \frac{\pi}{2}, \quad v \geq 0 \text{ onto } v \geq 1$$

$$u = 0, \quad v \geq 0 \text{ onto } v \geq 1$$

The boundary conditions become

$$T(0, v) = 0$$

$$T(1, v) = 1$$

$$\frac{\partial T(u, 0)}{\partial v} = 0, \quad 0 < u < \frac{\pi}{2}$$

The harmonic function that satisfies the boundary conditions is

$$T(u, v) = \frac{2}{\pi} u$$

The mapping implies that

$$\frac{x^2}{\sin^2 u} - \frac{y^2}{\cos^2 u} = 1$$

Integral transforms can be used to solve ordinary differential equations by converting them to algebraic equations. In what follows, the convolution properties of the different transforms have been listed, followed by the methods of integral transform used to solve (a) one-dimensional diffusion equations in the infinite and semi-infinite domains and (b) Laplace equations in the cylindrical geometries.

2.13.1 LAPLACE TRANSFORM

The Laplace transform of $f(t)$ is denoted as $\mathcal{L}f(t)$, and the inversion is given by

$$f(t) = \frac{1}{2\pi i} \int_{\gamma-i\infty}^{\gamma+i\infty} e^{\lambda t} F(\lambda) d\lambda \quad (2.235)$$

where γ is chosen such that all singularities of the integrand lie to the left of γ .

2.13.1.1 Convolution Property

If $F(\lambda)$ and $G(\lambda)$ are the Laplace transforms of $f(t)$ and $g(t)$, respectively, then

$$\begin{aligned} \mathcal{L} \left[\int_0^t f(s)g(t-s)ds \right] &= \int_0^\infty e^{-\lambda t} \int_0^t f(s)g(t-s)ds dt \\ &= \int_0^\infty f(s)ds \int_s^\infty f(t-s)e^{-\lambda t} dt \\ &= \int_0^\infty f(s)e^{-\lambda s} ds \int_0^\infty g(y)e^{-\lambda y} dy \\ \mathcal{L} \left[\int_0^t f(s)g(t-s)ds \right] &= F(\lambda)G(\lambda) \end{aligned} \quad (2.236)$$

2.13.1.2 Application of Laplace Transform

The temperature distribution in a semi-infinite bar that is heated at one end is described by the solution of the following problem:

$$\frac{\partial u}{\partial t} = \frac{\partial^2 u}{\partial x^2} \quad (2.237)$$

subjected to the boundary conditions

$$-\frac{\partial u(0,t)}{\partial x} = q(t), \quad u(x,0) = 0$$

Define

$$U(x,\lambda) = \int_0^\infty u(x,t)e^{-\lambda t} dt$$

and

2.13.2.2 Application of Fourier Transform

The fundamental solution of the heat equation, i.e., the Dirichlet problem in infinite domain, $(-\infty, \infty)$, is obtained by solving

$$\frac{\partial u}{\partial t} = \frac{\partial^2 u}{\partial x^2}, \quad -\infty < x < \infty \quad (2.240)$$

subjected to the boundary conditions

$$u(x, 0) = u_0(x)$$

Define

$$U(\lambda, t) = \frac{1}{\sqrt{2\pi}} \int_{-\infty}^{\infty} u(x, t) \exp(i\lambda x) dx$$

Multiplying Equation (2.242) by $e^{i\lambda x}$ and integrating over $(-\infty, \infty)$ yields

$$\begin{aligned} \frac{dU}{dt} &= -\lambda^2 U \\ U(\lambda, 0) &= U_0(\lambda) \end{aligned}$$

where

$$U_0(\lambda) = \int_{-\infty}^{\infty} u_0(x) \exp(i\lambda x) dx$$

The solution is given by

$$U(\lambda, t) = U_0(\lambda) \exp(-\lambda^2 t)$$

Inverting the Fourier transform with the use of the convolution theorem yields

$$u(x, t) = \int_{-\infty}^{\infty} k(x - y, t) u_0(y) dy$$

where the function

$$k(x, t) = \mathcal{F}^{-1}[\exp(-\lambda^2 t - i\lambda x)] = \frac{1}{\sqrt{4\pi t}} \exp\left[-\frac{x^2}{4t}\right] \quad (2.241)$$

is called the fundamental solution of the diffusion equation.

$$u(x,t) = \frac{1}{\pi} \int_0^\infty \int_0^\infty e^{-\lambda^2 t} [\cos(\lambda(x-s)) - \cos(\lambda(x+s))] u_0(s) d\lambda ds \\ + \frac{2}{\pi} \int_0^t \int_0^\infty \lambda e^{-\lambda^2(t-\tau)} \sin(\lambda x) a(\tau) d\lambda d\tau$$

The definition of $k(x,t)$ [Equation (2.243)] can be used to arrive at the following:

$$u(x,t) = \int_0^\infty [k(x-s,t) - k(x+s,t)] u_0(s) ds - 2 \int_0^t \frac{\partial k(x,t-\tau)}{\partial x} a(\tau) d\tau$$

where $k(x,t)$ is given by Equation (2.243).

2.13.2.4 Application of Fourier Cosine Transform

The temperature distribution in a semi-infinite rod with prescribed heat flux applied at one end can be obtained as follows. The temperature distribution in the rod is governed by the following equation:

$$\frac{\partial u}{\partial t} = \frac{\partial^2 u}{\partial x^2} + h(x,t), \quad 0 < x < \infty \quad (2.243)$$

subjected to the boundary conditions

$$-\frac{\partial u(0,t)}{\partial x} = a(t) \\ u(x,0) = u_0(x)$$

Following the procedure similar to that described in the previous subsection, the solution obtained by the Fourier cosine transform is given as

$$u(x,t) = \int_0^\infty [k(x-s,t) + k(x+s,t)] u_0(s) ds - 2 \int_0^t k(x,t-\tau) a(\tau) d\tau + \\ \int_0^t \int_0^\infty [k(x-s,t-\tau) + k(x+s,t-\tau)] h(s,\tau) ds d\tau$$

where the $k(x,t)$ is defined by Equation (2.243)

2.13.3 MELLIN TRANSFORM

2.13.3.1 Convolution Property

Let $F(\lambda)$ and $G(\lambda)$ be the Mellin transforms of $f(x)$ and $g(x)$, respectively. Then

$$\mathcal{M} \left[\int_0^\infty f\left(\frac{x}{y}\right) \frac{g(y)}{y} dy \right] = F(\lambda) G(\lambda) \quad (2.244)$$

2.13.4 HANKEL TRANSFORM

2.13.4.1 Property of Hankel Transform

Let \mathcal{B}_k be the Bessel differential operator of order k , i.e.,

$$\mathcal{B}_k \equiv \frac{d^2}{dr^2} + \frac{1}{r} \frac{d}{dr} - \left(\frac{k}{r} \right)^2$$

If the Hankel transform of $f(r)$ is denoted as $\mathcal{H}_k f(r) = F_k(\lambda)$, then (Zauderer, 1983; Poularikas, 2000)

$$\mathcal{H}_k[\mathcal{B}_k f(r)] = -\lambda^2 \mathcal{H}_k[f(r)] + [rf'(r)J_k(\lambda r) - \lambda rf'_k(\lambda r)]_{r=0}^{r=\infty}$$

The second term on the right-hand side is specified using the boundary conditions. The inverse Hankel transform is given by

$$f(r) = \int_0^\infty \lambda F_k(\lambda) J_k(\lambda r) d\lambda$$

2.13.4.2 Application of Hankel Transform

The Hankel transform may be used to solve numerous boundary-value problems in a relatively straightforward way, using various properties of Bessel functions. We present here the solution to one of the boundary-value problems (Davies, 2002) of interest.

The axisymmetric steady-state temperature distribution in an infinite cylinder with one of its ends maintained at constant temperature is described by the solution of

$$\frac{\partial^2 u}{\partial r^2} + \frac{1}{r} \frac{\partial u}{\partial r} + \frac{\partial^2 u}{\partial z^2} = 0 \quad (2.246)$$

subjected to the boundary conditions

$$u(r, 0) = u_0(r)$$

$$\lim_{z \rightarrow \infty} u(r, z) = 0$$

Define

$$U(\lambda, z) = \int_0^\infty u(r, z) J_0(r, \lambda) r dr$$

In addition to the stated boundary conditions, it is assumed that

$$\lim_{r \rightarrow \infty} \left[r \frac{\partial u}{\partial r} J_0(\lambda r) \right] = \lim_{r \rightarrow \infty} r u J_0(\lambda r) = 0 \quad (2.247)$$

Multiply Equation (2.248) by $rJ_0(r\lambda)$ and integrate over $(0, \infty)$ to get

$$\delta \mathcal{F} = \int_a^b \left(\frac{\partial F}{\partial y} h + \frac{\partial F}{\partial y'} h' \right) dx = 0$$

Integrating the second term by parts yields

$$\delta \mathcal{F} = \int_a^b \left(\frac{\partial F}{\partial y} - \frac{d}{dx} \frac{\partial F}{\partial y'} \right) h dx + F_y h \Big|_{x=a}^{x=b} = 0 \quad (2.248)$$

There are two possibilities:

Case 1: The variational equation is subjected to the fixed end-point conditions

$$y(a) = y_a, \quad y(b) = y_b$$

that translate to

$$h(a) = h(b) = 0$$

Equation (2.250) becomes

$$\delta \mathcal{F} = \int_a^b \left(\frac{\partial F}{\partial y} - \frac{d}{dx} \frac{\partial F}{\partial y'} \right) h dx = 0 \quad (2.249)$$

Because $h(x)$ is an arbitrary continuously differentiable function, the variational equation of the *functional* requires

$$F_y - \frac{d}{dx} F_{y'} = 0 \quad (2.250)$$

that is known as a *Euler-Lagrange* equation establishing a necessary condition for $y(x)$ to be *optimal*.

Case 2: The variational equation is subjected to the conditions

$$F_{y'} \Big|_{x=a} = F_{y'} \Big|_{x=b} = 0$$

These conditions are known as the natural boundary conditions. In either case, the optimal function satisfies the Euler-Lagrange equation.

2.14.2 EULER-LAGRANGE EQUATIONS FOR A FUNCTIONAL OF n -DEPENDENT VARIABLES

An approach similar to the one adopted in the previous subsection can be used to derive the Euler-Lagrange equations for a functional that possesses n -dependent variables y_1, y_2, \dots, y_n to give the following system of equations:

$$F(y, y', x) = y\sqrt{1 + y'^2}, \quad F_{y'} = \frac{yy'}{\sqrt{1 + y'^2}}$$

$$y\sqrt{1 + y'^2} - \frac{yy'^2}{\sqrt{1 + y'^2}} = c_1$$

Solving for y' gives

$$y' = \sqrt{c_1 y^2 - 1}$$

the solution of which is given by

$$y = c_1 \cosh\left(\frac{x + c_2}{c_1}\right)$$

which is an equation describing a catenary curve, where c_2 is another constant. The constants c_1 and c_2 can be determined from the condition that the curve representing the solution should pass through the two (prescribed) end points.

2.15 STOCHASTIC DIFFERENTIAL EQUATIONS

Processes in which a certain time-dependent random variable $\mathbf{X}(t)$ exists are called *stochastic processes*. Loosely, these are the processes that evolve probabilistically in time. We can measure values $\mathbf{x}_1, \mathbf{x}_2, \mathbf{x}_3, \dots$, etc., of $\mathbf{X}(t)$ at times t_1, t_2, t_3, \dots , and we assume that a set of joint probability densities, $p(\mathbf{x}_1, t_1; \mathbf{x}_2, t_2; \mathbf{x}_3, t_3; \dots)$, exists that describes the system completely. For a treatise on stochastic processes, the reader is referred to Gardiner (2003). The applications related to chemical engineering can be followed from Rao et al. (1974a and 1974b).

The conditional probability densities can be defined in terms of the joint probability density functions as

$$p(\mathbf{x}_1, t_1; \mathbf{x}_2, t_2; \dots | \mathbf{y}_1, \tau_1; \mathbf{y}_2, \tau_2; \dots) = \frac{p(\mathbf{x}_1, t_1; \mathbf{x}_2, t_2; \dots; \mathbf{y}_1, \tau_1; \mathbf{y}_2, \tau_2; \dots)}{p(\mathbf{y}_1, \tau_1; \mathbf{y}_2, \tau_2; \dots)} \quad (2.251)$$

The definitions in Equation (2.253) are valid independently of the ordering of the times. However, it is usual to consider only times that increase from right to left, i.e.,

$$t_1 \geq t_2 \geq t_3 \cdots \geq t_1 \geq \tau_2 \cdots \quad (2.252)$$

Stochastic differential equations then obviously describe the evolution of stochastic processes in terms of a dependent random variable $\mathbf{X}(t)$.

Conditional probabilities can be seen as predictions of the future values of $\mathbf{X}(t)$ (i.e., $\mathbf{x}_1, \mathbf{x}_2, \dots$ at times t_1, t_2, \dots) given the knowledge of the past values ($\mathbf{y}_1, \mathbf{y}_2, \dots$ at times τ_1, τ_2, \dots). A stochastic process is said to be completely independent if

$$p(\mathbf{x}_1, t_1; \mathbf{x}_2, t_2; \dots | \mathbf{y}_1, \tau_1; \mathbf{y}_2, \tau_2; \dots) = \prod_i p(\mathbf{x}_i, t_i)$$

the conditional probability density function for the sample path is the Fokker-Planck equation,

$$\frac{\partial}{\partial t} p(x, t | x_0, t_0) = -\frac{\partial}{\partial x} [a(x, t) p(x, t | x_0, t_0)] + \frac{1}{2} \frac{\partial^2}{\partial x^2} [b(x, t)^2 p(x, t | x_0, t_0)]$$

For a stochastic differential equation for n variables,

$$d\mathbf{x} = \mathbf{A}(\mathbf{x}, t)dt + \mathbf{B}(\mathbf{x}, t)d\mathbf{W}(t)$$

where $\mathbf{W}(t)$ is an n -variable Wiener process, the Fokker-Planck equation for the conditional probability density $p \equiv p(\mathbf{x}, t | \mathbf{x}_0, t_0)$ is given by

$$\frac{\partial p}{\partial t} = -\sum_i \frac{\partial}{\partial x_i} [A_i(\mathbf{x}, t)p] + \sum_{i,j} \frac{1}{2} \frac{\partial^2}{\partial x_i \partial x_j} \{ [\mathbf{B}(\mathbf{x}, t)\mathbf{B}^T(\mathbf{x}, t)]_{i,j} p \}$$

2.15.3 ÎTO STOCHASTIC INTEGRAL

The solution of a stochastic differential equation is expressed in terms of the integral with respect to a sample function $\mathbf{W}(t)$. The stochastic integral

$$\int_{t_0}^t G(t')d\mathbf{W}(t')$$

is obtained by dividing the interval $[t_0, t]$ into n subintervals such that

$$t_0 \leq t_1 \leq \dots \leq t_{n-1} \leq t$$

where the intermediate points τ_i satisfy

$$t_{i-1} \leq \tau_i \leq t_i$$

The Îto stochastic integral is defined as a limit of the partial sum

$$\int_{t_0}^t G(t')d\mathbf{W}(t') = \text{ms-lim}_{n \rightarrow \infty} \sum_{i=1}^n G(t_{i-1})[W(t_i) - W(t_{i-1})]$$

where ms-lim is the mean square limit defined as

$$\text{ms-lim}_{n \rightarrow \infty} X_n = X \Leftrightarrow \lim_{n \rightarrow \infty} \int p(\omega) [X_n(\omega) - X(\omega)] d\omega = 0$$

The Îto integration formula, which is presented in the next subsection, is useful for the purpose of evaluating a stochastic integral.

$$\frac{dC}{dt} = -kC + C\alpha\xi(t) \quad t=0, \quad C = C_0$$

$$dC = -kCdt + C\alpha\xi(t)dt$$

2.16 ASYMPTOTIC APPROXIMATIONS AND EXPANSIONS

Many problems in transport and chemical reaction engineering are nonlinear and cannot be solved analytically. A powerful approach to solve such problems lies in the method of matched asymptotic expansions that often provide analytical expressions for the solution. The method is based on an expansion whose convergence is based on concepts somewhat different from that usually understood. An example is considered below to clarify the nature of such expansions. Such expansions can be used in the solution of nonlinear equations for limiting values of parameters associated with the problem. Several examples are available in the chemical engineering literature (Leal, 1992, 2007; Deen, 1998; Varma and Morbidelli, 1997).

Example 2.15

A detailed treatment of this example is given by Erdelyi (1956). Let

$$S(x) = \sum_{n=0}^{\infty} (-1)^n n! x^n \quad (2.256)$$

The foregoing sum is definitely divergent because of $n!$. However, let us proceed without regard for the divergence to invoke the well-known result from the theory of gamma functions,

$$n! = \int_0^{\infty} e^{-t} t^n dt \quad (2.257)$$

Using Equation (2.260) in Equation (2.59), one has

$$S(x) = \sum_{n=0}^{\infty} (-1)^n \int_0^{\infty} e^{-t} x^n t^n dt \quad (2.258)$$

Disregarding conditions required for interchanging the summation and integration, one obtains

$$S(x) = \int_0^{\infty} e^{-t} \sum_{n=0}^{\infty} (-1)^n (xt)^n dt \quad (2.259)$$

The alternating series within the integrand on the right-hand side of Equation (2.258) can now be summed exactly to write from Equation (2.259)

$$S(x) = \int_0^{\infty} \frac{e^{-t}}{1+xt} dt \quad (2.260)$$

Note that the right-hand side is a very well-behaved function for any real value of x . It was not legitimately obtained because the interchange of summation and integration cannot be performed

$$\lim_{N \rightarrow \infty} \left| T(\mathbf{x}, \epsilon) - \sum_{n=1}^N f_n(\epsilon) T_n(\mathbf{x}) \right| = 0 \quad (2.265)$$

but a necessary condition for asymptotic convergence is

$$\lim_{\epsilon \rightarrow 0} \left| T(\mathbf{x}, \epsilon) - \sum_{n=1}^N f_n(\epsilon) T_n(\mathbf{x}) \right| = 0, \quad \text{fixed } N \quad (2.266)$$

This definition is consistent with the example shown earlier. A necessary condition for asymptotic convergence is given by

$$\lim_{\epsilon \rightarrow 0} \frac{f_{n+1}(\epsilon)}{f_n(\epsilon)} \quad \text{for all } n \quad (2.267)$$

Suppose the expansion of $T(\mathbf{x}, \epsilon)$ is desired in a domain Ω . If the asymptotic convergence occurs for all \mathbf{x} in Ω , the expansion is said to be a *regular asymptotic expansion*.

Generally, the occurrence of the regular asymptotic expansions is in finite (bounded) domains. In other situations, the convergence of a particular expansion may occur only in a subdomain. For example, the entire domain may be made up of two separate subdomains, Ω^+ separated from another denoted Ω^- , with an intersection $\partial\Omega$ separating the two domains. This is also called the *overlap region*. Thus, we may have two separate expansions of the function $T(\mathbf{x}, \epsilon)$ as follows:

$$T(\mathbf{x}, \epsilon) = \sum_{n=0}^{N^+} f_n^+(\epsilon) T_n^+(\mathbf{x}), \quad \mathbf{x} \in \Omega^+ \quad (2.268)$$

$$T(\mathbf{x}, \epsilon) = \sum_{n=0}^{N^-} f_n^-(\epsilon) T_n^-(\mathbf{x}), \quad \mathbf{x} \in \Omega^- \quad (2.269)$$

The expansions in the individual subdomains are known as *singular expansions*. To determine the expansion in the entire domain, it is necessary to match the two expansions in the overlap region $\partial\Omega$. There are two strategies that are possible. One is referred to as a “matching” strategy, requiring the same functional forms for the gauge functions from either side in the overlap region. Thus in this case one has

$$N^+ = N^-, \quad f_n^+(\epsilon) = f_n^-(\epsilon), \quad T_n^+(\mathbf{x}) = T_n^-(\mathbf{x}), \quad \mathbf{x} \in \partial\Omega$$

A less rigorous strategy is satisfied by numerically equating the two solutions by “patching” as follows:

$$\sum_{n=0}^{N^+} f_n^+(\epsilon) T_n^+(\mathbf{x}) = \sum_{n=0}^{N^-} f_n^-(\epsilon) T_n^-(\mathbf{x}), \quad \mathbf{x} \in \partial\Omega$$

$$F(v) \equiv \frac{(1+\beta-v)^n}{v-1} \exp \left[\gamma \left(1 - \frac{1}{v} \right) \right] = \frac{\beta^{n-1}}{Da} \quad (2.274)$$

Because $F(1) = \infty$, $F(1+\beta) = 0$, and $F(v) > 0$ for $1 \leq v \leq 1+\beta$, Equation (2.292) admits a unique solution if $F(v)$ is monotonically decreasing, i.e.,

$$\frac{dF}{dv} \leq 0 \quad \text{for} \quad 1 \leq v \leq 1+\beta \quad (2.275)$$

If the condition in Equation (2.275) is violated, then uniqueness is assured if and only if

$$G(\bar{Z}) \geq \gamma \quad \text{for} \quad 0 < Z < 1 \quad (2.276)$$

where

$$G(Z; n, \beta) \equiv \frac{(1+\beta Z)^2 [(1+Z(n-1))]}{\beta Z(1-Z)}, \quad Z = \frac{v-1}{\beta}$$

and $z \equiv \bar{Z}$ is the one and only root in the interval (0,1) of the following equation:

$$\beta(n-1)Z^3 - (n-1)(2\beta+1)Z^2 - (2+\beta)Z + 1 = 0 \quad (2.277)$$

that is obtained from $G'(Z) = 0$. If the condition in Equation (2.276) is violated, then multiple solutions exist for $Da_* < Da < Da^*$, where

$$Da_* = \frac{\beta^{n-1}}{F(v_+)} \quad \text{and} \quad Da^* = \frac{\beta^{n-1}}{F(v_-)}$$

where $v_{\pm} = 1 + \beta Z_{\pm}$ and Z_{\pm} are the roots of $G(Z) = \gamma$.

2.17.1.2 Steady-State Multiplicity of a Tubular Reactor

The analysis of multiplicity for a tubular reactor is involved because its mass and energy balances are governed by nonlinear boundary-value problems. The uniqueness conditions for a tubular reactor are more conservative than those for a CSTR. The exact bounds for the uniqueness require numerical solutions.

The dimensionless mass and energy balance in a tubular reactor are (Morbidelli et al. 1986)

$$\frac{1}{Pe_m} \frac{d^2 u}{dx^2} - \frac{du}{dx} - Da r(u, v) = 0 \quad (2.278)$$

$$\frac{1}{Pe_t} \frac{d^2 v}{dx^2} - \frac{dv}{dx} - \delta(v - v_c) + \beta Da r(u, v) = 0 \quad (2.279)$$

where μ is the same parameter as defined in the previous case and

$$a_1 = \sup \frac{\partial r}{\partial u} > 0, \quad a_2 = \inf \frac{\partial r}{\partial u} \geq 0$$

Case 3: $Pe_m \neq Pe_p$ $\delta \neq 0$

$$Da \leq \frac{-\beta\mu_m a_3 + (\mu_t + \delta)a_2 + \sqrt{\Delta}}{a_3\beta[2a_2 + a_1 \exp(|Pe_t - Pe_m|)]}$$

where

$$\Delta = \beta\mu_m a_3 + (\mu_t + \delta)^2 + 2\beta\mu_m(\mu_m + \delta)a_1 a_3 \exp(|Pe_t - Pe_m|), \quad a_3 = \sup \frac{\partial r}{\partial v} \quad (2.283)$$

where $\mu_i = \lambda_i/Pe_i + Pe_i/4$, $i = m, t$ and λ_i is the same as previously defined.

The exact bounds for multiplicity can be determined by computationally solving the boundary-value problems with the use of the singularity theory.

2.17.2 ANALYSIS OF MULTIPLICITY BY SINGULARITY THEORY

Techniques based on the implicit function theorem have been used to predict the existence of multiple solutions in a CSTR (Chang and Calo, 1979). An extension of catastrophe theory known as singularity theory has also been effectively used to determine the conditions for the existence of multiple solutions in a CSTR and a tubular reactor (Balakotaiah and Luss, 1981, 1982; Witmer et al., 1986). In this subsection, the technique of singularity to find the maximum number of solutions of a single mathematical equation and its application to analysis of the multiplicity of a CSTR are presented (Luss, 1986; Balakotaiah et al., 1985). The details of singularity theory can be found in Golubitsky and Schaeffer (1985).

For the first-order reaction, the steady-state equations for mass and energy balance in a CSTR can be combined into a single equation represented as

$$f(x, \mathbf{p}) = 0 \quad (2.284)$$

where \mathbf{p} is a vector of physical quantities. A singular point (x_s, \mathbf{p}_s) of codimension k is defined as

$$f(x_s, \mathbf{p}_s) = \frac{df(x_s, \mathbf{p}_s)}{dx} = \dots = \frac{d^k f(x_s, \mathbf{p}_s)}{dx^k} = 0, \quad \frac{d^{k+1} f(x_s, \mathbf{p}_s)}{dx^{k+1}} \neq 0 \quad (2.285)$$

The application of catastrophe theory (Hopf, 1960) predicts that in the neighborhood of a singular point of codimension k , the qualitative features represented by Equation (2.284) are similar to that of the polynomial,

$$y^{k+1} - \sum_{i=0}^{k-1} \alpha_i y^i \quad (2.286)$$

In the neighborhood of such a singular point, Equation (2.284) admits $k+1$ solutions if

Multiplicity exists if and only if

$$B > \frac{4}{1-4/\gamma} > 0 \quad (2.289)$$

(i) Adiabatic CSTR, hysteresis variety

In addition to the condition for multiplicity in Equation (2.289), the condition for the existence of hysteresis variety is defined by

$$\frac{\partial^2 F}{\partial x^2}(x, Da, \mathbf{p}_s) = 0$$

that gives the solution

$$\alpha = \frac{1-x_h}{x_h} \left[\frac{4Bx_h(1-x_h)}{y^2(1-2x_h)} \right] \exp \left\{ \gamma - \frac{2}{1-2x_h} \right\}$$

where

$$x_h = \frac{\frac{4B}{\gamma} \left(1 + \frac{y_c}{\gamma} \right) + 4y_c - B \pm \sqrt{D}}{2 \left[4y_c - 2B + \frac{4B}{\gamma} \left(1 + \frac{y_c}{\gamma} \right) \right]}$$

and

$$D = \left[\frac{4B}{\gamma} \left(1 + \frac{y_c}{\gamma} \right) \right]^2 - 4y_c \left[4y_c - 2B + \frac{4B}{\gamma} \left(1 + \frac{y_c}{\gamma} \right) \right]$$

(ii) Isola variety

$$F(x, Da, \mathbf{p}_s) = \frac{\partial F}{\partial x}(x, Da, \mathbf{p}_s) = \frac{\partial F}{\partial Da}(x, Da, \mathbf{p}_s) = 0 \quad (2.290)$$

The condition in Equation (2.290) gives parametric representations by the equations

$$x_b^5 B^3 / \gamma^2 - x_b^3 [1 - x_b + y_c x_b / \gamma^2 - 2/\gamma] B^2 + x_b [1 + y_c(1 - x_b) - 2x_b y_c / \gamma] B - y_c = 0$$

$$\alpha = \frac{B(1-x_b)^2}{Bx_b^2 - y_c} \exp \left\{ \frac{Bx_b^2}{1 + Bx_b^2/\gamma} \right\}$$

where the parameter $0 < x_b < 1$.

The dynamics of the CSTR is governed by the following dimensionless equations:

$$\frac{du}{dt} = 1 - u - Dau^n e^{-\gamma/v} \quad (2.292)$$

$$\frac{dv}{dt} = (1 + \delta)(1 - v + \beta Dau^n e^{-\gamma/v}) \quad (2.293)$$

where the parameters are given by

$$u = \frac{C}{C_f} \quad \delta = \frac{UA}{F\rho C_p} \quad T_m = \frac{T_f + \delta T_c}{1 + \delta}$$

$$v = \frac{T}{T_m} \quad \gamma = \frac{E}{RT_m} \quad Da = \frac{kVC_f^{n-1}}{F} \quad \beta = \frac{(-\Delta H)C_f}{\rho C_p T_m}$$

The linearized equations about the steady-state solution (u_s, v_s) can be written as

$$\frac{du}{dt} = -[1 + Dae^{-\gamma/v_s}]u - \frac{Da\gamma u_s}{v_s^2} e^{-\gamma/v_s} v \quad (2.294)$$

$$\frac{dv}{dt} = (1 + \delta) \left\{ \beta Dae^{-\gamma/v_s} u - \left[1 - \frac{\beta Da\gamma u_s}{v_s^2} e^{-\gamma/v_s} \right] v \right\} \quad (2.295)$$

The eigenvalues of the system of Equations (2.294) and (2.295) are negative if and only if

$$1 + Dae^{-\gamma/v_s} - \beta Da\gamma u_s / v_s^2 e^{-\gamma/v_s} > 0$$

and

$$2 + \delta + Dae^{-\gamma/v_s} - (1 + \delta)(\beta Da\gamma u_s / v_s^2 e^{-\gamma/v_s}) >$$

which are the necessary conditions for the steady-state solution to be stable.

2.17.3.2 Method of Lyapunov's Function

The method of Lyapunov's function consists of constructing a function $V(x, y)$ with the following properties:

(i) $V(x, y) > 0$ for $x, y \neq 0$

(ii) $\frac{dV(x, y)}{dt} = \nabla V \cdot \mathbf{f} < 0$ where $\frac{dx}{dt} = \mathbf{f}$

APPENDIX 2.A: MATHEMATICAL SOFTWARE

The development of software over the decades has enabled engineers to perform increasingly complex calculations based on the solution of a variety of mathematical equations. While analytic solutions can be well handled by symbolic mathematical software, the system of equations requiring numerical solution can be tackled using a variety of software packages. Furthermore, one can recognize that some software packages are designed to address specific classes of mathematical problems and methods of solutions. The purpose of this brief appendix is to make the reader aware of such tools along with their specific utilities and their sources.

Table 2.A.1 lists various software packages along with their utility in reference to the relevant mathematics in chemical engineering. It should be noted that the table lists only the tools that the authors are aware of and that it is *not complete* by any means. Furthermore, the mathematical utility of the software packages represents only a *fraction* of their many capabilities.

TABLE 2.A.1
Software Packages Relevant to Mathematical Calculations in Chemical Engineering

Software	Mathematical Utility	Source
1. Aspen HYSYS and Aspen Plus	Process simulation and optimization	www.aspentech.com
2. Auto 2000	Continuation and bifurcation problems	www.acm.caltech.edu
3. CFD Solvers CFX and FLUENT FLOW-3D PHOENIX SPIKE, TINA, FINS List of free CFD software	Computational fluid dynamics	www.ansys.com www.flow3d.com www.cham.co.uk www.fluidgravity.co.uk www.icemcfd.com
4. Comsol	Finite element analysis, free equation-based modeling, general periodic boundary conditions, evaluation of material, energy balances	www.comsol.com
5. DIVA	Nonlinear equations, discrete algebraic equations, continuation and stability analysis, parameter analysis, and parameter estimation	www.mpi-magdeburg.mpg.de (see also Mangold et al., 2000)
6. gPROMS	Nonlinear equations, steady-state and dynamic simulations, steady-state and dynamic optimization, and parameter estimation	www.psenterprise.com
7. JACOBIAN	Ordinary differential equations, differential algebraic equations, partial differential equations, discrete/continuous dynamic simulation, sensitivity analysis, optimization, and parameter estimation	www.numericatech.com
8. Mathematica	Analytical integration and differentiation, algebraic and differential equations, and optimization problems	www.wolfram.com
9. Mathcad	Symbolic mathematics, calculus, algebra, differential equations, statistics, geometry, and transforms	www.mathsoft.com
10. Maple	Symbolic mathematics, calculus, algebra, differential equations, statistics, geometry, and transforms	www.maplesoft.com

Continued

APPENDIX 2.B: DIRAC DELTA FUNCTION

The Dirac delta or Dirac's delta, introduced by the theoretical physicist Paul Dirac is an interesting function with significant utility, which is formally denoted by δ and defined as follows:

$$\delta(x) = \begin{cases} \infty & x = 0 \\ 0 & x \neq 0 \end{cases}$$

that is constrained to satisfy

$$\int_{-\infty}^{\infty} \delta(x) dx = 1$$

Thus, the function may be visualized as the one representing an infinitely sharp peak bounding unit area.

Some of the important properties are listed below:

1. $\int_{-\infty}^{\infty} f(x) \delta(x-a) dx = f(a)$
2. $\int_{-\infty}^{\infty} \delta(\alpha x) dx = \frac{1}{|\alpha|}$ for a scalar α
3. $\int_{-\infty}^{\infty} f(t) \delta(t-\tau) dt = f(\tau)$
4. $\int_{-\infty}^{\infty} f(x) \delta^n(x) dx = - \int_{-\infty}^{\infty} \frac{df}{dx} \delta^{n-1}(x) dx$
5. $\int_{-1}^1 \delta\left(\frac{1}{x}\right) dx = 0$
6. $\delta(x) = \int_{-\infty}^{\infty} e^{-2\pi i \lambda x} d\lambda$

TABLE 2.C.1 (Continued)
Laplace Transforms

$F(\lambda) = \int_0^\infty e^{-\lambda x} f(x) dx$	$f(x) = \frac{1}{\sqrt{2\pi i}} \int_{\gamma-i\infty}^{\gamma+i\infty} F(\lambda) e^{\lambda x} d\lambda$
$\frac{e^{-a\sqrt{\lambda}}}{\lambda}$	$\frac{2}{\sqrt{\pi}} \int_{a/\sqrt{x}}^\infty e^{-y^2} dy = \operatorname{erfc}\left(\frac{a}{2\sqrt{x}}\right)$
$(-1)^n \frac{d^n F}{d\lambda^n}$	$x^n f(x)$
$\frac{F(\lambda)}{\lambda}$	$\int_0^x f(t) dt$
$F(\lambda - a)$	$e^{ax} f(x)$
$\lambda F(\lambda) - F(0)$	$\frac{df}{dx}$

TABLE 2.C.2
Fourier Transforms

$F(\lambda) = \frac{1}{\sqrt{2\pi}} \int_{-\infty}^\infty f(x) e^{i\lambda x} d\lambda$	$f(x) = \frac{1}{\sqrt{2\pi}} \int_{-\infty}^\infty F(\lambda) e^{-i\lambda x} d\lambda$
$\sqrt{2\pi} \delta(\lambda)$	1
$(\pi/2)^{1/2} i \operatorname{sing}(\lambda)$	1/x
$1/\sqrt{2\pi}$	$\delta(x)$
$1/ \lambda $	$1/ x $
$(2/\pi)^{1/2} \Gamma(1-a) \sin(\frac{1}{2}\pi) \lambda ^{1-a}$	$1/ x ^a$
$(2/\pi)^{1/2} \delta(1+a)$	e^{iax}
$a(2/\pi)^{1/2} / (a^2 + \lambda^2)$	$e^{-a x }, \quad a > 0$
$2ai\lambda(2/\pi)^{1/2} / (a^2 + \lambda^2)^2, \quad \lambda > 0$	$xe^{-a x }, \quad a > 0$
$(2/\pi)^{1/2} (a^2 - \lambda^2) / ((a^2 + \lambda^2)^2), \quad \lambda > 0$	$ x e^{-a x }, \quad a > 0$
$[a + (a^2 + \lambda^2)^{1/2}]^{1/2} / (a^2 + \lambda^2)^{1/2}, \quad \lambda > 0$	$e^{-a x } / x ^{1/2}, \quad a > 0$
$e^{-\lambda^2/4a^2} / (a\sqrt{2})$	$e^{-a^2x^2}$
$(2/\pi)^{1/2} e^{-a \lambda } / a$	$1/(a^2 + x^2), \quad \operatorname{Re} a > 0$
$-i(2/\pi)^{1/2} \lambda e^{-a \lambda } / 2a$	$x/(a^2 + x^2), \quad \operatorname{Re} a > 0$
$\frac{1}{(2a)^{1/2}} \sin\left(\frac{\lambda^2}{4a} + \frac{\pi}{4}\right)$	$\sin(ax^2)$

TABLE 2.C.3
Fourier Sine Transforms

$F(\lambda) = \sqrt{\frac{2}{\pi}} \int_0^\infty f(x) \sin(\lambda x) dx$	$f(x) = \sqrt{\frac{2}{\pi}} \int_0^\infty F(\lambda) \sin(\lambda x) d\lambda$
$1/x$	$(\pi/2)^{1/2} \operatorname{sign} \lambda, \quad \lambda > 0$
$(2/\pi)^{1/2} \lambda^{\nu-1} \Gamma(1-\nu) \cos(\nu\pi/2), \quad \lambda > 0$	$x^{-\nu}, \quad 0 < \operatorname{Re} \nu < 1$
$\frac{1}{(2\pi)^{1/2}} \ln \left \frac{\lambda+a}{\lambda-a} \right , \quad \lambda > 0$	$\frac{\sin(ax)}{x}, \quad a > 0$
$\begin{cases} \sqrt{\frac{\pi}{2}} \lambda & \text{for } \lambda < a \\ a \sqrt{\frac{\pi}{2}} & \text{for } \lambda > a \end{cases}$	$\frac{\sin(ax)}{x^2}$
$a \sqrt{\frac{\pi}{2}} \lambda^{-1/2} J_1(2a\lambda^{1/2}), \quad \lambda > 0$	$\sin \frac{a^2}{x}, \quad a > 0$
$\sqrt{\frac{\pi}{2}} \lambda^{-1/2} Y_0(2a\lambda^{1/2}) + K_0(2a\lambda^{1/2}), \quad \lambda > 0$	$x^{-1} \sin \frac{a^2}{x}, \quad a > 0$
$\sqrt{\frac{\pi}{2}} a^{-1} \lambda^{1/2} J_1(2a\lambda^{1/2}), \quad \lambda > 0$	$x^{-2} \sin \frac{a^2}{x}, \quad a > 0$
$\sqrt{\frac{\pi}{2}} e^{-a\lambda}, \quad \lambda > 0$	$\frac{x}{a^2 + x^2}, \quad a > 0$
$2\pi^{-1/2} a^{-1} \lambda e^{-a\lambda}, \quad \lambda > 0$	$\frac{x}{(a^2 + x^2)^2}$
$2\pi^{-1/2} a^{-1} \lambda e^{-a\lambda}, \quad \lambda > 0$	$\frac{x}{(a^2 + x^2)^2}$
$\pi/2^{1/2} a^{-2} (1 - e^{-a\lambda}), \quad \operatorname{Re} \lambda > 0$	$x^{-1} (a^2 + x^2)^{-1} \operatorname{Re} a > 0$
$2/\pi^{1/2} \lambda / (a^2 + \lambda^2), \quad \operatorname{Re} \lambda > 0$	$e^{-ax}, \quad \operatorname{Re} a > 0$
$2/\pi^{1/2} 2a\lambda / (a^2 + \lambda^2)^2, \quad \lambda > 0$	$xe^{-ax}, \quad \operatorname{Re} a > 0$
$2/\pi^{1/2} \tan^{-1} \frac{\lambda}{a}, \quad \lambda > 0$	$x^{-1} e^{-ax}, \quad \operatorname{Re} a > 0$
$(2/\pi)^{1/2} \Gamma(\nu) (a^2 + \lambda^2)^{-\nu/2} \sin \left[\nu \tan^{-1} \frac{\lambda}{a} \right], \quad \lambda > 0$	$x^{-\nu-1} e^{-ax}, \quad \operatorname{Re} a > 0, \quad \operatorname{Re} \nu > 0$
$(2/\pi)^{1/2} a^{-1} \tanh \frac{1}{2a} \pi \lambda, \quad \lambda > 0$	$\csc(ax), \quad \operatorname{Re} a > 0$
$(2/\pi)^{1/2} a^{-1} \frac{1}{\tan(\pi\lambda/a)} - \lambda, \quad \lambda > 0$	$\frac{1}{\tanh(ax)}, \quad \operatorname{Re} a > 0$

TABLE 2.C.5
Mellin Transforms

$F(\lambda) = \int_0^\infty x^{\lambda-1} f(x) dx$	$f(x) = \frac{1}{2\pi i} \int_{\gamma-i\delta}^{\gamma+i\delta} F(\lambda) x^{-\lambda} d\lambda$
$\Gamma(\lambda) \cos \frac{\pi}{2} \lambda, \quad 0 < \operatorname{Re} \lambda < 1$	$\cos x$
$\Gamma(\lambda) \sin \frac{\pi}{2} \lambda, \quad 0 < \operatorname{Re} \lambda < 1$	$\sin x$
$\Gamma(\lambda), \quad \operatorname{Re} \lambda > 0$	e^{-x}
$\frac{\Gamma(a-\lambda)\Gamma(\lambda)}{\Gamma(a)}, \quad 0 < \operatorname{Re} \lambda < \operatorname{Re} a$	$(1+x)^{-a}$
$\frac{\pi}{\sin \lambda \pi}, \quad 0 < \operatorname{Re} \lambda < 1$	$(1+x)^{-1}$
$\frac{\Gamma(\lambda) e^{i\lambda\pi/2}}{\alpha^\lambda}, \quad 0 < \operatorname{Re} \lambda < 1$	$e^{i\alpha x}$
$\frac{\pi}{\lambda \sin \lambda \pi}, \quad -1 < \operatorname{Re} \lambda < 0$	$\operatorname{Log}(1+x)$
$\frac{\Gamma(\lambda)}{2a^{\lambda/2}}$	$e^{-ax^2}, \quad a > 0$
$\frac{\pi \cos \lambda \theta}{\sin \lambda \pi}, \quad \lambda \neq k\pi, \quad k \in \mathbb{Z}$	$\frac{1+x \cos \theta}{1+2x \cos \theta + x^2}$
$\frac{\pi \sin \lambda \theta}{\sin \lambda \pi}, \quad \lambda \neq k\pi, \quad k \in \mathbb{Z}$	$\frac{x \sin \theta}{1+2x \cos \theta + x^2}$
$\frac{dF(\lambda)}{d\lambda}$	$(\log x) f(x)$
$F(\lambda + a)$	$x^a f(x), \quad a \in \mathbb{C}$
$a^{-\lambda} F(\lambda)$	$f(ax), \quad a > 0$
$\frac{1}{a} F\left(\frac{\lambda}{a}\right)$	$f(x^a), \quad a > 0$
$-\frac{1}{\lambda} F(\lambda + 1)$	$\int_0^x f(t) dt$
$\frac{1}{\lambda} F(\lambda + 1)$	$\int_x^\infty f(t) dt$

- Arnold, V. I., *Mathematical Methods of Classical Mechanics*, trans. K. Vogtmann and A. Weinstein, Berlin: Springer-Verlag, 1978.
- Balakotaiah, V., and Luss, D. "Analysis of the Multiplicity Patterns of a CSTR," *Chem. Eng. Comm.* 13 (1981): 111–132.
- Balakotaiah, V., and Luss, D. "Analysis of the Multiplicity Patterns of a CSTR," *Chem. Eng. Comm.* 15 (1982): 185–189.
- Balakotaiah, V., Luss, D., and Keyfitz, B., "Steady State Multiplicity Analysis of Lumped-Parameter Systems Described by a Set of Algebraic Equations," *Chem. Eng. Comm.* 36 (1982): 121–147.
- Balakotaiah, V., and Luss, D. "Steady-State Multiplicity Features of Chemical Reacting Systems," *Chem. Eng. Edu.* 24 (1986): 12–56.
- Banks, H. T., and Kunisch, K., *Estimation Techniques for Distributed Parameter Systems*, Boston: Birkhauser, 1989.
- Barenblatt, G. I., *Scaling Phenomena in Fluid Mechanics*, Cambridge, UK: Cambridge University Press, 1994.
- Barenblatt, G. I., *Scaling, Self-Similarity and Intermediate Asymptotics*, Cambridge, UK: Cambridge University Press, 1996.
- Bell, H. E., "Gerschgorin's Theorem and the Zeros of Polynomials," *Am. Math. Monthly* 72 (1965): 292–295.
- Bender, C. M., and Orszag, S. A., *Advanced Mathematical Methods for Scientists and Engineers*, New York: McGraw-Hill, 1978.
- Bleistein, N., and Handelsman, R. A., *Asymptotic Expansions of Integrals*, Mineola, NY: Dover Publications, 1986.
- Bluman, G. W., and Kumei, S., *Symmetries and Differential Equations*, Berlin: Springer-Verlag, 1989.
- Borisenko, A. I., and Tarapov, I. E., *Vector and Tensor Analysis with Applications*, Mineola, NY: Dover Publications, 1979.
- Boyce, W. E., and DiPrima, R. E., *Elementary Differential Equations and Boundary Value Problems*, 7th ed., New York: John Wiley and Sons, 2000.
- Brown, L. F., and Travis, B. J., "Using Diffusion Measurements To Determine Pore-Size Distributions in Porous Materials," *Chem. Eng. Sci.* 38 (6) (1983): 843–847.
- Carslaw, H. S., *An Introduction to the Theory of Fourier's Series and Integrals*, 3rd rev. ed., Mineola, NY: Dover Publications, 1950.
- Chen, Z., *Finite Element Methods and Their Applications*, Berlin: Springer-Verlag, 2005.
- Churchchill, R. V., Brown, J. W., and Verhey, R. F., *Complex Variables and Applications*, 3rd ed., New York: McGraw-Hill, 1976.
- Cloud, M. J., and Drachman, B. C., *Inequalities with Applications to Engineering*, Berlin: Springer-Verlag, 1998.
- Cochran, J. A., *Applied Mathematics, Principles, Techniques, and Applications*, Belmont, CA: Wadsworth, International Group, 1982.
- Coddington, E. A., and Levinson, N., *Theory of Ordinary Differential Equations*, New York: McGraw-Hill, 1955.
- Collatz, L., *Functional Analysis and Numerical Mathematics*, trans. H. Oser, New York: Academic Press, 1996.
- Collins, E. R., *Mathematical Methods for Physicists and Engineers*, Mineola, NY: Dover Publications, 1999.
- Colton, D., and Kress, R., *Inverse Acoustic and Electromagnetic Scattering Theory*, Berlin: Springer-Verlag, 1998.
- Corduneanu, C., *Integral Equations and Applications*, Cambridge: Cambridge University Press, 1991.
- Corduneanu, C., *Principles of Differential and Integral Equations*, London: Chelsea Publishing, 1977.
- Corduneanu, C., and Sandberg, I. W., *Volterra Equations and Applications*, Amsterdam: Gordon and Breach, 2000.
- Corduneanu, C., *Integral Equations and Applications*, Cambridge: Cambridge University Press, 1991.
- Dautray, R., and Lions, J., *Physical Origin and Classical Methods*, vol. 1 of *Mathematical Analysis and Numerical Methods for Science and Technology*, Berlin: Springer-Verlag, 1985.
- Dautray, R., and Lions, J., *Functional and Variational Methods*, vol. 2 of *Mathematical Analysis and Numerical Methods for Science and Technology*, Berlin: Springer-Verlag, 1985.
- Dautray, R., and Lions, J., *Spectral Theory and Applications*, vol. 3 of *Mathematical Analysis and Numerical Methods for Science and Technology*, Berlin: Springer-Verlag, 1985.
- Dautray, R., and Lions, J., *Integral Equations and Numerical Methods*, vol. 4 of *Mathematical Analysis and Numerical Methods for Science and Technology*, Berlin: Springer-Verlag, 1985.
- Dautray, R., and Lions, J., *Evolution Problems II: The Navier-Stokes and Transport Equations in Numerical Methods*, vol. 5 of *Mathematical Analysis and Numerical Methods for Science and Technology*, Berlin: Springer-Verlag, 1985.

- Hochstadt, H., *Integral Equations*, New York: John Wiley, 1973.
- Holmes, M. H., *Introduction to Perturbations Methods*, Berlin: Springer-Verlag, 1995.
- Hopf, H., "The work of R. Thom," in *Proceedings International Congress Mathematics*, 1958, New York, 1960.
- Hulburt, H. M., and Katz, S., "Some Problems in Particle Technology: A Statistical Mechanical Formulation", *Chem. Eng. Sci.* 19 (8) (1964): 555–574.
- Isaacson, E., and Keller, H. B., *Analysis of Numerical Methods*, New York: John Wiley & Sons, 1966.
- Isakov, V., *Inverse Problems for Partial Differential Equations*, Berlin: Springer-Verlag, 1998.
- Iooss, G., and Joseph, D. D., *Elementary Stability and Bifurcation Theory*, Berlin: Springer-Verlag, 1990.
- Jensen, V. G., and Jeffreys, G. V., *Mathematical Methods in Chemical Engineering*, New York: Academic Press, 1977.
- Jerri, A. J., *Introduction to Integral Equations with Applications*, New York: Marcel Dekker, 1985.
- John, F., *Partial Differential Equations*, 4th ed., Berlin: Springer-Verlag, 1982.
- Johnson, L. W., and Riess, R. D., *Numerical Analysis*, 2nd ed., Reading, MA: Addison Wesley, 1982.
- Jordan, D. W., and Smith, P., *Nonlinear Ordinary Differential Equations*, 2nd ed., Oxford: Oxford University Press, 1989.
- Kahn, P. J., *Introduction to Linear Algebra*, New York: Harper & Row, 1967.
- Karman, T. von, *Aerodynamics*, Ithaca, NY: Cornell University Press, 1957.
- Keener, J. P., *Principles of Applied Mathematics, Transformation and Approximation*, Reading, MA: Addison Wesley, 1988.
- Keller, H. B., *Numerical Methods for Two-Point Boundary Value Problems*, Mineola, NY: Dover Publications, 1992.
- Kevorkian, J., and Cole, J. D., *Multiple Scale and Singular Perturbation Methods*, Berlin: Springer-Verlag, 1996.
- Khalil, H. K., *Nonlinear Systems*, 2nd ed., Englewood Cliffs, NJ: Prentice-Hall, 1996.
- Kirsch, A., *An Introduction to the Mathematical Theory of Inverse Problems*, Berlin: Springer-Verlag, 1996.
- Kondo, J., *Integral Equations*, Oxford: Oxford University Press, 1991.
- Kress, R., *Linear Integral Equations*, Berlin: Springer-Verlag, 1989.
- Kubo, R., *Stochastic Processes in Chemical Physics*, ed. K. E. Shuler, New York: Wiley-Interscience, 1969.
- Lakin, W. D., and Sanchez, D. A., *Topics in Ordinary Differential Equations*, Mineola, NY: Dover Publications, 1982.
- Lakshmikantham, V., Leela, S., and Martynuk, A. A., *Stability Analysis of Nonlinear Systems*, New York: Marcel Dekker, 1989.
- Lamb, G. L., Jr., *Introductory Applications of Partial Differential Equations*, New York: John Wiley & Sons, 1995.
- Lambert, J. D., *Computational Methods in Ordinary Differential Equations*, New York: John Wiley & Sons, 1973.
- Lawrence, P., *Differential Equations and Dynamical Systems*, Berlin: Springer-Verlag, 1991.
- Leal, G., *Advanced Transport Phenomena: Fluid Mechanics and Convective Transport Processes*, New York: Cambridge University Press.
- LePage, W. R., *Complex Variables and the Laplace Transform for Engineers*, Mineola, NY: Dover Publications, 1961.
- Leal, G., *Laminar Flow and Convective Transport Processes: Scaling Principles and Asymptotic Analysis*, Boston: Butterworth-Heinemann, 1992.
- Lightstone, A. H., *Fundamentals of Linear Algebra*, New York: Appleton-Century-Crofts, 1969.
- Linz, P., *Analytical and Numerical Methods for Volterra Equations*, Philadelphia: SIAM (1985).
- Lord, R., "On the Viscosity of Argon as Affected by Temperature," *Proc. R. Soc. London* 66 (1899–1900): 68–74.
- Lord, R., "The Principle of Similitude," *Nature* 95 (1915): 66–68.
- Mangold, M., Kienle, A., Gilles, E. D., and Mohl, K. D., "Nonlinear Computation in DIVA Methods and Applications," *Chem. Eng. Sci.* 55 (2): 441–454 (2000).
- Markushevich, A. I., *The Theory of Analytic Functions: A Brief Course*, Moscow: MIR Publisher, 1983.
- Marsden, J., *Basic Complex Analysis*, New York: W.H. Freeman, 1973.
- Menzel, D., *Mathematical Physics*, Mineola, NY: Dover Publications, 1953.
- Mikhailov, V. P., *Partial Differential Equations*, Moscow: MIR Publisher, 1983.
- Moler, C., *Numerical Computing with MATLAB*, Philadelphia: SIAM, 2004.

- Ranade, V. V., *Computational Flow Modeling for Chemical Reactor Engineering*, New York: Academic Press, 2002.
- Randolph, A. D., and Larson, M. A., *Theory of Particulate Processes*, New York: Academic Press, 1971.
- Rao, N. J., Borwanker, J. D., and Ramkrishna, D., "Numerical Solution of Ito Integral Equations," *SIAM Journal on Control*, 12 (1974): 124–139.
- Rao, N. J., Ramkrishna, D., and Borwanker, J. D., "Nonlinear Stochastic Simulation of Stirred Tank Reactors," *Chem. Eng. Sci.* 29 (1974): 1193–1204.
- Rashevsky, N., *Mathematical Biophysics: Physico-Mathematical Foundations of Biology*, vol. 1, Mineola, NY: Dover Publications, 1960.
- Reddy, J. N., *An Introduction to the Finite Element Method*, New York: McGraw-Hill, 2005.
- Reklaitis, G. V., *Introduction to Material and Energy Balances*, New York: John Wiley & Sons, 1983.
- Rhee, H., Aris, R., and Amundson, N. R., *Theory and Application of Single Equations*, vol. 1 of *First-Order Partial Differential Equations*, Mineola, NY: Dover Publications, 2001.
- Rhee, H., Aris, R., and Amundson, N. R., *Theory and Application of Hyperbolic Systems of Quasi-linear Equations*, vol. 2 of *First-Order Partial Differential Equations*, Mineola, NY: Dover Publications, 2001.
- Richtmyer, R. D., *Principles of Advanced Mathematical Physics*, vol. 1, Berlin: Springer-Verlag, 1985.
- Richtmyer, R. D., *Principles of Advanced Mathematical Physics*, vol. 2, Berlin: Springer-Verlag, 1985.
- Robinson, J., *Infinite-Dimensional Dynamical Systems, from Basic Concepts to Actual Calculations*, Cambridge, UK: Cambridge University Press, 2001.
- Rubinstein, I., and Rubinstein, L., *Partial Differential Equations in Classical Mathematical Physics*, Cambridge, UK: Cambridge University Press, 1998.
- Sagan, H., *Boundary and Eigenvalue Problems in Mathematical Physics*, Mineola, NY: Dover Publications, 1961.
- Sagan, H., *Introduction to the Calculus of Variations*, Mineola, NY: Dover Publications, 1993.
- Sathyagal, A. N., Ramkrishna, D., and Narsimhan, G., "Solution of Inverse Problems in Population Balances, II: Particle Break-Up," *Computers Chem. Eng.* 19 (4): 437 (1995).
- Schneider, H., and Barker, G. P., *Matrices and Linear Algebra*, Mineola, NY: Dover Publications, 1989.
- Shilov, G. E., *Elementary Functional Analysis*, Mineola, NY: Dover Publications, 1995.
- Shilov, G. E., *Linear Algebra*, Mineola, NY: Dover Publications, 1971.
- Silverman, R. A., *Introductory Complex Analysis*, Mineola, NY: Dover Publications, 1972.
- Sirovich, L., *Introduction to Applied Mathematics*, Berlin: Springer-Verlag, 1988.
- Skufca, J. D., "Analysis Still Matters: A Surprising Instance of Failure of Runge-Kutta-Felberg ODE Solvers," *Siam Review* 46 (2004): 729.
- Smith, D. R., *Variation Methods in Optimization*, Mineola, NY: Dover Publications, 1998.
- Smoller, J., *Shock Waves and Reaction-Diffusion Equations*, 2nd ed., Berlin: Springer-Verlag, 1994.
- Sneddon, I. N., *Fourier Transforms*, Mineola, NY: Dover Publications, 1995.
- Sneddon, I. N., *The Use of Integral Transforms*, New York: McGraw-Hill, 1972.
- Sobolev, S. L., *Partial Differential Equations of Mathematical Physics*, Mineola, NY: Dover Publications, 1989.
- Sperb, R., *Maximum Principles and Their Applications*, New York: Academic Press, 1981.
- Stakgold, I., *Green's Functions and Boundary Value Problems*, New York: John Wiley, 1979.
- Starzhinskii, V. M., *Applied Methods in the Theory of Nonlinear Oscillations*, Moscow: MIR Publishers, 1980.
- Taylor, G. I., "The Formation of a Blast Wave by a Very Intense Explosion, I: Theoretical Discussion," *Proc. Roy. Soc. A* 201 (1950a): 159–174.
- Taylor, G. I., "The Formation of a Blast Wave by a Very Intense Explosion, II: The Atomic Explosion of 1945," *Proc. Roy. Soc. A* 201 (1950b): 175–186.
- Temam, R., *Infinite-Dimensional Dynamical Systems in Mechanics and Physics*, Berlin: Springer-Verlag, 1997.
- Titchmarsh, E. C., *The Theory of Functions*, Oxford: Oxford University Press, 1988.
- Titchmarsh, E. C., *Introduction to the Theory of Fourier Integrals*, Londn: Chelsea Publishing, 1986.
- Trujillo, D. M., and Busby, H. R., *Practical Inverse Analysis on Engineering*, Boca Raton, FL: CRC Press, 1997.
- Varma, A., and Amundson, N. R., "Some Problems Concerning the Non-Adiabatic Tubular Reactor," *Can. J. Chem. Eng.* 50: 470 (1972).
- Varma, A., and Morbidelli, M., *Mathematical Methods in Chemical Engineering*, New York, Oxford: Oxford University Press, 1997.

3.7.2.2	$\hat{y} = \beta_1 x$	248
3.7.2.3	$\hat{y} = \beta_0 + \beta_1 x$	248
3.7.3	Design for Several Factors	248
3.7.4	Factorial Design with More Levels	251
3.7.5	Blocks and New Duplicates	252
3.7.6	Computer-Aided Experimental Design	252
Appendix		253
Acknowledgment		254
References		254

3.1 INTRODUCTION

Statistics finds important applications by engineers, scientists, and industrial managers when planning and executing research, plant design and operation, marketing and sales programs. Improved operations, better and more uniform products, increased safety, and additional profitability often result. Experimental data contain errors or uncertainties for a variety of factors.

In analyzing a chemical process, it is important to first establish threshold knowledge of the key operating variables, or at least most of them. Such variables affect the operating costs, amount and quality of products formed, and of course profitability. Statistics are often employed to develop mathematical models for all of the above. Plant operators frequently need to be notified, because all of the following likely vary with time: sales of products, availability and cost of feed streams, character of desired product (varies with seasons, such as type of gasoline), etc. Statistics can indicate how to maximize profits.

Numerous resources are available that describe how statistics can be best employed. These include literature references (see list of references located at the end of this chapter), software packages, and the *Handbook of Statistical Methods* prepared by the National Institute of Standards and Testing [1]. The latter consists of about 3500 pages and contains coverage of topics of technical importance, including many examples. Its Internet address is <http://www.itl.nist.gov/div898/handbook/index.htm>. On the Internet, it is listed as *NIST/SEMATECH e-Handbook of Statistical Methods*. It is free to all and is highly recommended. The appendix at the end of this chapter provides an outline of the topics covered in the handbook. Suitable mathematical software packages are also available from several vendors, including (most commonly used) Microsoft Excel, Mathematica, MatLab®, and JMP. Several examples in this chapter refer to Microsoft Excel, because it simplifies many statistical tasks.

3.1.1 DATA TYPES

Data are of two categories: discrete and continuous. Each type has its own statistical parameters, probability models, and statistical tools. Some statistical tests are applicable to only one type. Data are discrete if there is a finite set of possible outcomes. A data set is continuous if the data may, at least theoretically, assume any value over an interval. Large sets of discrete data are often modeled as continuous, because statistical tools for continuous data are typically simpler.

3.1.2 RANDOM VARIABLES

A variable is random if it is associated with an experiment (a test in the broadest sense, such as throwing dice, measuring temperature, collecting poll data, etc.) in which the outcome may take on values according to its data type. For example, the outcome of throwing two six-sided dice and taking their sum is an integer between 2 and 12, one of several discrete outcomes. Measuring temperature at some point in a room, however, takes on a random value depending on the temperature profile of the room, since the random values are between the upper and lower temperatures in the room.

number is equal to that of any other number (both being between 0 and 3). Because the sum (or in the case of a continuous probability density distribution, the integral) of all probabilities is equal to unity, one can write

$$\int_0^3 f(\theta) d\theta = 1 \quad (3.1)$$

Therefore, since the distribution is uniform, $f(\theta) = 1/3$. Such distributions provide an evaluation of reproducibility for data, but not accuracy.

3.1.4 CUMULATIVE PROBABILITY DISTRIBUTION FUNCTIONS

A cumulative probability distribution function characterizes a set of outcomes between an upper and a lower bound. For a discrete distribution function, the associated distribution is usually denoted as $F(a \leq x \leq b)$, where a and b are the lower and upper bounds, respectively. The new function F is determined by summing the probability of independent outcomes that result in x between a and b . The distribution of a continuous probability density distribution can be written in the same manner and is determined by modifying the bounds of the integral appropriately. These properties of cumulative distribution functions are illustrated in the following example.

Example 3.2

When throwing two six-sided dice and taking their sum, determine the probability of observing a sum between 7 and 10, inclusive.

Solution

Probabilities are summed for face sums of 7, 8, 9, and 10 as follows:

$$F(7 \leq x \leq 10) = \sum_{i=7}^{10} P(i) = \frac{1}{6} + \frac{5}{36} + \frac{1}{9} + \frac{1}{12} = \frac{1}{2} \quad (3.2)$$

Example 3.3

For the random number generator mentioned in Section 3.1.3.2 (which generates a number between 0 and 3, such that $f(x) = 1/3$), determine the probability of observing a random number between 0.4 and 1.7.

Solution

The probability density distribution is integrated between 0.4 and 1.7:

$$F(0.4 \leq x \leq 1.7) = \int_{0.4}^{1.7} f(\theta) d\theta = \int_{0.4}^{1.7} \frac{1}{3} d\theta = 0.4333 \quad (3.3)$$

The bounds of a cumulative distribution might be $-\infty$ or ∞ if those bounds are mathematically meaningful to the probability model. For a lower bound $a = -\infty$, the cumulative distribution is interpreted as the probability of observing a value smaller than b . The positive infinity bound is exactly opposite.

3.1.5 CHARACTERISTIC PARAMETERS OF A PROBABILITY DISTRIBUTION

Probability distributions are characterized by several terms: the *mean* is the expected value of a population (denoted as μ) and the *variance* is the spread, or width, of a distribution (denoted as

TABLE 3.1
Definition of Population Statistical Parameters

	Discrete Random Variable	Continuous Random Variable
Population mean	$\mu = \sum_i x_i P(x_i)$	$\mu = \int_{-\infty}^{\infty} xf(x)dx$
Population variance	$\sigma^2 = \sum_i (x_i - \mu)^2 P(x_i)$	$\sigma^2 = \int_{-\infty}^{\infty} (x - \mu)^2 f(x)dx$

Sources: Montgomery, Douglas C., and Runger, George C. 2003. *Applied Statistics and Probability for Engineers*, 3rd ed., New York: John Wiley & Sons. Metcalfe, Andrew V., *Statistics in Engineering*, 1994. London: Chapman & Hall. Fraser, D.A.S., *Probability and Statistics: Theory and Applications*, 1976, North Scituate, MA: Duxbury Press.

3.2.1 BINOMIAL DISTRIBUTION—DISCRETE VARIABLE

The binomial distribution describes the probability of x successes in n trials when only success or failure occurs. This distribution assumes that each trial is independent and that the probability of a success in each trial is constant. This probability is denoted p . The probability function for a binomial distribution [2] is

$$P(x, n) = \binom{n}{x} p^x (1 - p)^{n-x} \quad (3.6)$$

$$\binom{n}{x} = \frac{n!}{x!(n-x)!} \quad (3.7)$$

Equation (3.6) can be derived using intuition. The probability of observing x successes and $n - x$ failures is $p^x(1 - p)^{n-x}$, and

$$\binom{n}{x}$$

is the binomial coefficient that equals the number of arrangements of subsets of size x given a total number of elements n . “(The binomial coefficient also equals the redundancy of the experiment.)” Using the appropriate equations in Table 3.1 along with the expression for $P(x, n)$ given in Equation (3.6), the mean value of x is $\mu = np$ and the variance of x is $\sigma^2 = np(1 - p)$.

Example 3.4

Suppose that a six-sided die is thrown 20 times. What is the probability of a particular number turning up 6 times? (A success is defined as that particular number turning up, and a failure is *any other* number turning up.)

Solution

The probability of any side is $p = 1/6$, $x = 6$, and $n = 20$. Using Equation (3.6),

Example 3.6

During continuous paper production, a tear occurs on average once every 500 feet. What is the probability that five tears will occur in 1000 feet?

Solution

The average rate of tears is $p = 1/500$ (ft⁻¹) and the interval size is $n = 1000$ ft. Therefore, the *expected* number of tears is

$$\lambda = 1000 \text{ ft} \cdot \left(\frac{1}{500 \text{ ft}} \right) = 2$$

Using Equation (3.9), the probability of $x = 5$ tears occurring in 1000 feet of product is

$$P(5) = \frac{e^{-2} 2^5}{5!} = 0.0361$$

3.2.4 NORMAL OR GAUSSIAN DISTRIBUTION—CONTINUOUS VARIABLE

The normal or Gaussian distribution is commonly employed for large data sets, since they generally resemble a characteristic bell-shaped curve. Although the shape of each distribution may be qualitatively different, all bell curves collapse to the same distribution when scaled appropriately. As discussed in Section 3.3, the normal distribution also describes the distribution of sample means when the population variance is known. The analytic form of the normal distribution [2] is

$$f(x) = \frac{1}{\sqrt{2\pi\sigma^2}} \exp\left(\frac{-(x-\mu)^2}{2\sigma^2}\right) \quad (3.10)$$

The mean and standard deviation of the normal distribution are μ and σ , respectively. Since the normal distribution is designed for continuous data, the cumulative distribution function is more practical than the probability density function. For a particular data population, the cumulative distribution [2] is as follows:

$$F(x) = \frac{1}{\sqrt{2\pi\sigma^2}} \int_{-\infty}^x \exp\left(\frac{-(x'-\mu)^2}{2\sigma^2}\right) dx' = \frac{1}{2} \left(1 + \operatorname{erf}\left(\frac{x-\mu}{\sqrt{2\sigma^2}}\right) \right) \quad (3.11)$$

The error function, $\operatorname{erf}(y)$, is introduced because the normal distribution cannot be integrated analytically. The error function is found in many mathematical tables and software packages [5–8]. Summarizing, $F(x)$ is the probability of an observation being less than or equal to x . Conversely, the probability of an observation exceeding x is $1 - F(x)$. From the properties of integrals, it is straightforward to show that the probability of an observation being between a and b , $F(a \leq x \leq b)$, can be expressed as $F(b) - F(a)$. Values of $F(x)$ are also available in the literature or suitable software. For example, the probability of an observation falling within one standard deviation of the mean, $F(\mu - \sigma \leq x \leq \mu + \sigma)$, is 0.683. The probability of an observation being within two standard deviations is 0.955, and that within three is 0.997, a progression often referred to as the 68-95-99 rule [2].

The normal distribution is reduced to the *standard* normal distribution by introducing the transformation variable z , defined [2] as follows:

of degrees of freedom and α being the percentage of the distribution lying above the particular t . The Microsoft Excel functions TDIST and TINV can be used to calculate t values or cumulative probabilities [5, 6]. The t distribution is most useful in determining the confidence interval of a measured sample mean and testing hypotheses, as described in Sections 3.3 and 3.4.

Example 3.8

Ten measurements are taken. Above what t value will 10% of the measurements fall?

Solution

As $n = 10$, $v = n - 1 = 9$. Because 10% of the distribution lies above the t value, $\alpha = 0.1$. Then, reading from Table 3.3, for $v = 9$ and $\alpha = 0.1$, $t = 1.3830$. Therefore $P(t > 1.3830) = 0.1$.

Example 3.9

Now six measurements are taken. What two t values define an area, centered at $t = 0$, in which 95% of measurements will fall?

Solution

If 95% of measurements are to be included in the t interval, 2.5% of values will fall above and below the upper and lower t values, respectively. For $v = 5$ and $\alpha = 0.025$, the t value is 2.5706. Therefore $F(-2.5706 < t < 2.5706) = 0.95$.

3.2.6 CHI-SQUARE DISTRIBUTION FOR THE SAMPLE VARIANCE— CONTINUOUS VARIABLE

As in the t distribution that describes the distribution of sample means, a specific probability distribution is necessary to describe the distribution of the variance of samples. The chi-square distribution [2] describes the probability distribution of the sample variance for a sample of size n , where the test statistic χ^2 is

$$\chi^2 = \frac{(n-1)s^2}{\sigma^2} \quad (3.14)$$

The chi-square distribution is used to perform statistical tests on the sample variance. It is highly asymmetric for small values of n , but becomes more symmetric and similar to a normal distribution as n becomes large, such as 20 or 30. The cumulative distribution function of the chi-square distribution is listed in Table 3.4 as a function of v and α , where $v = n - 1$ is the number of degrees of freedom and α is the percentage of the distribution above the particular χ^2 . Microsoft Excel has built-in functions, CHIDIST and CHIINV, that compute a chi-square distribution [5, 6].

Example 3.10

Twenty measurements are taken. Above what χ^2 value will 10% of the measurements fall?

Solution

Because $n = 20$, $v = n - 1 = 19$. From Table 3.4, for $v = 19$ and $\alpha = 0.1$, $\chi^2 = 27.2036$. Therefore, $F(\chi^2 > 27.2036) = 0.1$.

Example 3.11

Ten measurements are taken. Define the areas for which 10% of measurements will have lower χ^2 and 10% will have higher χ^2 .

Solution

The two χ^2 values to be found are those for $n = 10$ ($v = 9$), such that 10% of the distribution lies above the higher χ^2 value and 10% of the distribution lies below the smaller χ^2 value. The higher

Changes in variability are often quantified by examining the ratio of the variance of two samples, where a statistically significant (see Section 3.3) ratio not equal to unity indicates a change. The proper distribution to describe this ratio is the F distribution [2], which describes the ratio of two chi-square variables (e.g., a ratio of variances). The test statistic for this distribution is

$$F = \frac{s_1^2 / \sigma_1^2}{s_2^2 / \sigma_2^2} \quad (3.15)$$

where samples 1 and 2 have degrees of freedom $v_1 = n_1 - 1$ and $v_2 = n_2 - 1$, respectively. Owing to its form, the F distribution is used in statistical tests of the ratio of two sample variances. Multiple tables are required to calculate an F value because F depends on three parameters: the two degrees of freedom and the desired cumulative probability for that F value. The number of tables is reduced by the relationship [2]

$$F_{1-\alpha, v_1, v_2} = \frac{1}{F_{\alpha, v_2, v_1}} \quad (3.16)$$

where $F_{1-\alpha, v_1, v_2}$ is the F value for a cumulative probability of $1 - \alpha$ and degrees of freedom v_1 and v_2 in the numerator and denominator, respectively. The F distribution is highly asymmetric, but becomes normal as the number of degrees of freedom approaches infinity. Tables 3.5 through 3.9 display the F values for cumulative probabilities (α) of 0.01, 0.025, 0.05, 0.1, and 0.25, respectively. The Microsoft Excel functions FDIST and FINV provide F values and cumulative probabilities [5, 6]. Since the F distribution depends on three variables, these Excel functions are simpler to use than reading from tables.

Example 3.12

Five measurements are taken in sample 1 and seven measurements are taken in sample 2. Above what F value will 10% of the measurements fall?

Solution

Solving with a confidence level of 90% ($\alpha = 0.1$), with $v_1 = 5 - 1 = 4$ and $v_2 = 7 - 1 = 6$, and reading from Table 3.8, $F_{0.1, 4, 6} = 3.1808$. Therefore, 10% of F values fall above 3.1808 for the given degrees of freedom.

Example 3.13

For the same two sample sizes, what two F values define an interval for which 5% of measurements fall above the higher F value (95% fall above this F) and 5% fall below the lower F value?

Solution

We solve such that 5% of measurements fall below the lower F value and 95% fall above this F , 5% of measurements fall above the higher F value. Therefore, the two F values for this interval are $F_{0.95, 4, 6}$ and $F_{0.05, 4, 6}$. The lower F value is not listed in one of the tables, so the relationship shown in Equation (3.16) is used to replace $F_{0.95, 4, 6}$ with $1 / F_{0.05, 6, 4}$. Reading from Table 3.7, $F_{0.05, 4, 6} = 4.5337$ and $F_{0.05, 6, 4} = 6.1631$. Then, $F_{0.95, 4, 6} = 1 / F_{0.05, 6, 4} = 0.1623$. Therefore, 90% of F measurements fall between 0.1623 and 4.5337 for the specified samples.

3.3 CONFIDENCE INTERVALS OF POPULATION PARAMETERS

When collecting experimental data, experimental measurements are *sample* parameters and do not represent the true *population* parameters exactly. Hence, based on the experimental measurements of sample parameters, in what interval does the population parameter lie? Using the probability

TABLE 3.5
F Variable for F Distribution as a Function of Degrees of Freedom ν_1 and ν_2 for Cumulative Probability $\alpha = 0.01$

ν_1	ν_2	1	2	3	4	5	6	7	8	9	10	15	20	30	40	50	75	100
1	4052.181	4999.500	5403.352	5624.583	5763.650	5858.986	5928.356	5981.070	6022.473	6055.847	6157.285	6208.730	6260.649	6286.782	6302.517	6323.561	6334.110	
2	98.5025	99.0000	99.1662	99.2494	99.2993	99.3326	99.3564	99.3742	99.3881	99.3992	99.4325	99.4492	99.4658	99.4742	99.4792	99.4858	99.4892	
3	34.1162	30.8165	29.4567	28.7099	28.2371	27.9107	27.6717	27.4892	27.3452	27.2287	26.8722	26.6898	26.5045	26.4108	26.3542	26.2784	26.2402	
4	21.1977	18.0000	16.6944	15.9770	15.5219	15.2069	14.9758	14.7989	14.6591	14.5459	14.1982	14.0196	13.8377	13.7454	13.6896	13.6147	13.5770	
5	16.2582	13.2739	12.0600	11.3919	10.9670	10.6723	10.4555	10.2893	10.1578	10.0510	9.7222	9.5526	9.3793	9.2912	9.2378	9.1660	9.1299	
6	13.7450	10.9248	9.7795	9.1483	8.7459	8.4661	8.2600	8.1017	7.9761	7.8741	7.5590	7.3958	7.2285	7.1432	7.0915	7.0218	6.9867	
7	12.2464	9.5466	8.4513	7.8466	7.4604	7.1914	6.9928	6.8400	6.7188	6.6201	6.3143	6.1554	5.9920	5.9084	5.8577	5.7892	5.7547	
8	11.2586	8.6491	7.5910	7.0061	6.6318	6.3707	6.1776	6.0289	5.9106	5.8143	5.5151	5.3591	5.1981	5.1156	5.0654	4.9976	4.9633	
9	10.5614	8.0215	6.9919	6.4221	6.0569	5.8018	5.6129	5.4671	5.3511	5.2565	4.9621	4.8080	4.6486	4.5666	4.5167	4.4492	4.4150	

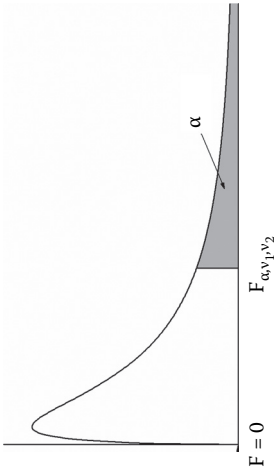
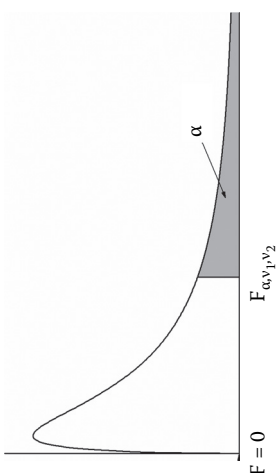


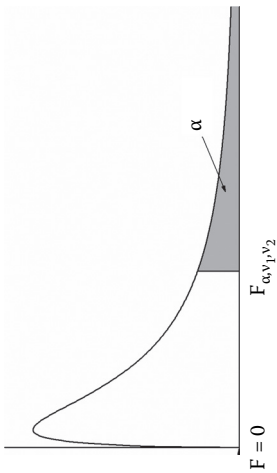
TABLE 3.6
F Variable for *F* Distribution as a Function of Degrees of Freedom *v*₁ and *v*₂ for Cumulative Probability $\alpha = 0.025$



The figure shows a graph of the probability density function of the F-distribution. The horizontal axis is labeled $F = 0$ at the origin. A vertical line is drawn at a point labeled F_{α, v_1, v_2} . The area under the curve to the right of this line is shaded and labeled α .

<i>v</i> ₁ <i>v</i> ₂	1	2	3	4	5	6	7	8	9	10	15	20	30	40	50	75	100
1	647.793	799.482	864.151	899.599	921.835	937.114	948.203	956.643	963.279	968.634	984.874	993.081	1001.405	1005.596	1008.098	1011.475	1013.163
2	38.5062	39.0000	39.1656	39.2483	39.2984	39.3311	39.3557	39.3729	39.3866	39.3984	39.4311	39.4475	39.4648	39.4730	39.4775	39.4848	39.4875
3	17.4434	16.0442	15.4391	15.1010	14.8848	14.7347	14.6244	14.5399	14.4730	14.4189	14.2527	14.1674	14.0806	14.0365	14.0099	13.9742	13.9562
4	12.2179	10.6490	9.9792	9.6045	9.3645	9.1973	9.0741	8.9796	8.9046	8.8439	8.6566	8.5599	8.4613	8.4111	8.3808	8.3400	8.3195
5	10.0069	8.4336	7.7636	7.3879	7.1464	6.9777	6.8530	6.7572	6.6810	6.6192	6.4277	6.3285	6.2269	6.1751	6.1436	6.1013	6.0800
6	8.8131	7.2599	6.5988	6.2271	5.9875	5.8197	5.6955	5.5996	5.5234	5.4613	5.2686	5.1684	5.0652	5.0125	4.9804	4.9372	4.9154
7	8.0727	6.5415	5.8898	5.5226	5.2852	5.1186	4.9949	4.8993	4.8232	4.7611	4.5678	4.4668	4.3624	4.3089	4.2763	4.2323	4.2101
8	7.5709	6.0595	5.4160	5.0526	4.8173	4.6517	4.5285	4.4333	4.3572	4.2951	4.1012	3.9994	3.8940	3.8398	3.8067	3.7620	3.7393
9	7.2093	5.7147	5.0781	4.7181	4.4844	4.3197	4.1970	4.1020	4.0260	3.9639	3.7693	3.6669	3.5604	3.5055	3.4719	3.4265	3.4034
10	6.9367	5.4564	4.8256	4.4683	4.2361	4.0721	3.9498	3.8549	3.7790	3.7168	3.5217	3.4185	3.3110	3.2554	3.2214	3.1752	3.1517

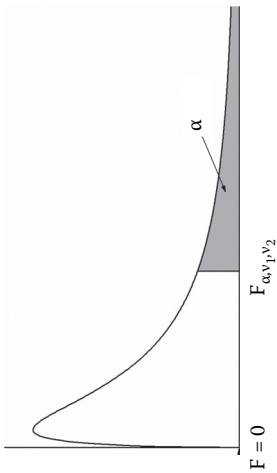
TABLE 3.7
F Variable for F Distribution as a Function of Degrees of Freedom v_1 and v_2 for cumulative probability $\alpha = 0.05$



The figure shows a graph of the F-distribution curve. The horizontal axis is labeled F and the vertical axis is labeled F_{α, v_1, v_2} . The area under the curve to the right of F_{α, v_1, v_2} is shaded and labeled α . The curve starts at $F = 0$ on the horizontal axis.

v_1	v_2	1	2	3	4	5	6	7	8	9	10	15	20	30	40	50	75	100
1	161.446	199.499	215.707	224.583	230.160	233.988	236.767	238.884	240.543	241.882	245.949	248.016	250.096	251.144	251.774	251.774	252.618	253.043
2	18.5128	19.0000	19.1642	19.2467	19.2963	19.3295	19.3531	19.3709	19.3847	19.3959	19.4291	19.4457	19.4625	19.4707	19.4757	19.4757	19.4823	19.4857
3	10.1280	9.5521	9.2766	9.1172	9.0134	8.9407	8.8867	8.8452	8.8123	8.7855	8.7028	8.6602	8.6166	8.5944	8.5810	8.5810	8.5630	8.5539
4	7.7086	6.9443	6.5914	6.3882	6.2561	6.1631	6.0942	6.0410	5.9988	5.9644	5.8578	5.8025	5.7459	5.7170	5.6995	5.6995	5.6759	5.6640
5	6.6079	5.7861	5.4094	5.1922	5.0503	4.9503	4.8759	4.8183	4.7725	4.7351	4.6188	4.5581	4.4957	4.4638	4.4444	4.4444	4.4183	4.4051
6	5.9874	5.1432	4.7571	4.5337	4.3874	4.2839	4.2067	4.1468	4.0990	4.0600	3.9381	3.8742	3.8082	3.7743	3.7537	3.7537	3.7258	3.7117
7	5.5915	4.7374	4.3468	4.1203	3.9715	3.8660	3.7871	3.7257	3.6767	3.6365	3.5107	3.4445	3.3758	3.3404	3.3189	3.3189	3.2897	3.2749
8	5.3176	4.4590	4.0662	3.8379	3.6875	3.5806	3.5005	3.4381	3.3881	3.3472	3.2184	3.1503	3.0794	3.0428	3.0204	3.0204	2.9901	2.9747
9	5.1174	4.2565	3.8625	3.6331	3.4817	3.3738	3.2927	3.2296	3.1789	3.1373	3.0061	2.9365	2.8637	2.8259	2.8028	2.8028	2.7715	2.7556
10	4.9646	4.1028	3.7083	3.4780	3.3258	3.2172	3.1355	3.0717	3.0204	2.9782	2.8450	2.7740	2.6996	2.6609	2.6371	2.6371	2.6048	2.5884

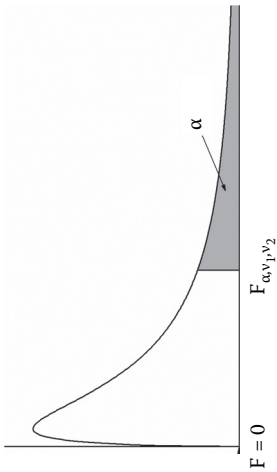
TABLE 3-8
F Variable for F Distribution as a Function of Degrees of Freedom v_1 and v_2 for Cumulative Probability $\alpha = 0.1$



The figure shows a graph of the probability density function of the F-distribution. The horizontal axis is labeled $F = 0$ at the origin. A curve starts at the origin, rises to a peak, and then tapers off to the right. A vertical line is drawn at a point labeled F_{α, v_1, v_2} . The area under the curve to the right of this line is shaded gray and labeled with the Greek letter α .

v_1 v_2	1	2	3	4	5	6	7	8	9	10	15	20	30	40	50	75	100
1	39.864	49.500	53.593	55.833	57.240	58.204	58.906	59.439	59.857	60.195	61.220	61.740	62.265	62.529	62.688	62.901	63.007
2	8.5263	9.0000	9.1618	9.2434	9.2926	9.3255	9.3491	9.3668	9.3805	9.3916	9.4247	9.4413	9.4579	9.4662	9.4713	9.4779	9.4813
3	5.5383	5.4624	5.3908	5.3427	5.3091	5.2847	5.2662	5.2517	5.2400	5.2304	5.2003	5.1845	5.1681	5.1597	5.1546	5.1477	5.1443
4	4.5448	4.3246	4.1909	4.1072	4.0506	4.0097	3.9790	3.9549	3.9357	3.9199	3.8704	3.8443	3.8174	3.8036	3.7952	3.7839	3.7782
5	4.0604	3.7797	3.6195	3.5202	3.4530	3.4045	3.3679	3.3393	3.3163	3.2974	3.2380	3.2067	3.1741	3.1573	3.1471	3.1333	3.1263
6	3.7760	3.4633	3.2888	3.1808	3.1075	3.0546	3.0145	2.9830	2.9577	2.9369	2.8712	2.8363	2.8000	2.7812	2.7697	2.7541	2.7463
7	3.5894	3.2574	3.0741	2.9605	2.8833	2.8274	2.7849	2.7516	2.7247	2.7025	2.6322	2.5947	2.5555	2.5351	2.5226	2.5057	2.4971
8	3.4579	3.1131	2.9238	2.8064	2.7264	2.6683	2.6241	2.5893	2.5612	2.5380	2.4642	2.4246	2.3830	2.3614	2.3481	2.3300	2.3208
9	3.3603	3.0064	2.8129	2.6927	2.6106	2.5509	2.5053	2.4694	2.4403	2.4163	2.3396	2.2983	2.2547	2.2320	2.2180	2.1989	2.1892
10	3.2850	2.9245	2.7277	2.6053	2.5216	2.4606	2.4140	2.3771	2.3473	2.3226	2.2435	2.2007	2.1554	2.1317	2.1171	2.0971	2.0869

TABLE 3.9
F Variable for F Distribution as a Function of Degrees of Freedom v_1 and v_2 for Cumulative Probability $\alpha = 0.25$



The figure shows a graph of the F-distribution curve. The horizontal axis is labeled F and the vertical axis is labeled F_{α, v_1, v_2} . The area under the curve to the right of F_{α, v_1, v_2} is shaded and labeled α . The curve starts at $F = 0$ on the horizontal axis.

v_1 v_2	1	2	3	4	5	6	7	8	9	10	15	20	30	40	50	75	100
1	5.8284	7.5000	8.1999	8.5809	8.8198	8.9832	9.1021	9.1923	9.2631	9.3202	9.4934	9.5812	9.6698	9.7144	9.7412	9.7771	9.7951
2	2.5714	3.0000	3.1534	3.2321	3.2799	3.3121	3.3352	3.3526	3.3661	3.3770	3.4098	3.4263	3.4428	3.4511	3.4561	3.4627	3.4661
3	2.0239	2.2798	2.3555	2.3901	2.4095	2.4218	2.4302	2.4364	2.4410	2.4447	2.4552	2.4602	2.4650	2.4674	2.4688	2.4706	2.4715
4	1.8074	2.0000	2.0467	2.0642	2.0723	2.0766	2.0790	2.0805	2.0814	2.0820	2.0829	2.0828	2.0825	2.0821	2.0819	2.0815	2.0813
5	1.6925	1.8528	1.8843	1.8927	1.8947	1.8945	1.8935	1.8923	1.8911	1.8899	1.8851	1.8820	1.8784	1.8763	1.8751	1.8733	1.8724
6	1.6214	1.7622	1.7844	1.7872	1.7852	1.7821	1.7789	1.7760	1.7733	1.7708	1.7621	1.7569	1.7509	1.7477	1.7457	1.7429	1.7414
7	1.5732	1.7010	1.7169	1.7157	1.7111	1.7059	1.7011	1.6969	1.6931	1.6898	1.6781	1.6712	1.6635	1.6593	1.6567	1.6530	1.6511
8	1.5384	1.6569	1.6683	1.6642	1.6575	1.6508	1.6448	1.6396	1.6350	1.6310	1.6170	1.6088	1.5996	1.5945	1.5914	1.5870	1.5848
9	1.5121	1.6236	1.6315	1.6253	1.6170	1.6091	1.6022	1.5961	1.5909	1.5863	1.5705	1.5611	1.5506	1.5449	1.5414	1.5364	1.5338
10	1.4915	1.5975	1.6028	1.5949	1.5853	1.5765	1.5688	1.5621	1.5563	1.5513	1.5338	1.5235	1.5119	1.5056	1.5017	1.4962	1.4933

$$\bar{x} - z_h \frac{\sigma}{\sqrt{n}} \leq \mu \leq \bar{x} - z_l \frac{\sigma}{\sqrt{n}} \quad (3.21)$$

(Equation (3.21) is obtained by rearranging Equation (3.20), which follows from applying Equation (3.17) to the standard normal variable z .) If, for instance, the confidence interval is chosen to be symmetric about μ (as is usually done), z_h is normally written as $z_{\alpha/2}$ to denote that $\alpha/2$ percentage points fall above z_h . Symmetry would also provide $z_l = -z_h = z_{\alpha/2}$. The following example illustrates the process of determining the confidence interval for a population mean.

Example 3.14

For a filtration experiment, the variance of the solids collection rate is known to be $\sigma^2 = 4.50$. After three experimental runs, the collection rate was determined to have a sample mean $\bar{x} = 25.50$. Determine the two-sided confidence interval of the population mean μ for a confidence level of 95%.

Solution

1. With a two-sided confidence interval, 2.5% of the distribution is above and 2.5% is below the upper and lower bounds, respectively. Therefore, $\alpha = 0.05$.
2. Using Table 3.2, the z value is 1.96 and -1.96 for the upper and lower bounds, because $F(z \leq 1.96) = 0.975$. Because the normal distribution is symmetric, the lower bound is $z_l = -1.96$. (One could confirm this by showing that $F(z \leq -1.96) = 0.025$.)
3. Using Equation (3.7),

$$-1.96 \leq \frac{25.5 - \mu}{\sqrt{4.5} / \sqrt{3}} \leq 1.96$$

4. The 95% confidence interval for μ is calculated as

$$23.1 \leq \mu \leq 27.9$$

Since the confidence interval depends on $1/\sqrt{n}$, it becomes narrower as n increases, as the next example shows.

Example 3.15

When seven additional experimental runs are completed, n increases from 3 to 10, and the sample mean becomes $\bar{x} = 25.76$. In this case, σ , z_l , and z_h are unchanged. Determine the new 95% confidence interval for μ .

Solution

One can proceed directly to step 3. Entering $\bar{x} = 25.76$ and $n = 10$ into Equation (3.20),

$$-1.96 \leq \frac{25.76 - \mu}{\sqrt{4.5} / \sqrt{10}} \leq 1.96$$

Solving yields a slightly smaller interval:

$$24.5 \leq \mu \leq 27.1$$

Example 3.16

For a confidence level of 80% ($\alpha = 0.2$) and with $\bar{x} = 25.76$ and $n = 10$, determine the confidence interval for μ .

3. Equation (3.22) becomes

$$-4.303 \leq \frac{25.5 - \mu}{\sqrt{4.8} / \sqrt{3}} \leq 4.303$$

4. The 95% confidence interval for μ is, then,

$$20.06 \leq \mu \leq 30.94$$

This interval is larger when defined by a t statistic. Some difference is due to the sample variance being slightly larger than the population variance in the previous example, but the major difference is due to the t distribution being much wider than the standard normal distribution when the sample size is small. The following example demonstrates the effect of sample size on confidence intervals.

Example 3.18

If the sample size for the solids collection experiment had been increased to $n = 10$, but the sample mean and sample variance were unchanged, what would be the 95% confidence interval for μ ?

Solution

The lower and upper t values are $t_{0.975,9} = -2.262$ and $t_{0.025,9} = 2.262$ (as listed in Table 3.3). Entering the parameters into Equation (3.23), as shown below, there is a smaller interval as compared with the case of three samples:

$$25.50 - 2.262 \frac{\sqrt{4.8}}{\sqrt{10}} \leq \mu \leq 25.50 + 2.262 \frac{\sqrt{4.8}}{\sqrt{10}}$$

and the 95% confidence interval is, then,

$$23.93 \leq \mu \leq 27.07$$

3.3.3 CONFIDENCE INTERVAL OF THE DIFFERENCE OF TWO MEANS

Occasionally, an experiment should determine if two populations have different population means. For example, following process modification, has the product's specification(s) changed? Measuring the confidence interval for the difference in the population means is a statistical test that can be employed. The t distribution is widely used in this case [2]. Table 3.10 shows the equations to be used. Because the population variances of the two samples may differ, two sets of equations are necessary.

The variables \bar{x}_i , s_i^2 , and n_i in Table 3.10 are the sample mean, sample variance, and number of data points of the i th sample, respectively. In the calculation of v in the case of unequal population variances, the result should be rounded to the nearest integer. The t distribution can approximate the difference of sample means for populations with unequal population. The t variable is obtained via Table 3.3. Table 3.10 is also important; one should not assume that the population variances are identical without evidence. When in doubt, assume that the populations have differing variances, as this may provide a wider confidence interval (and a larger margin of error in drawing conclusions).

The most important conclusion is to determine whether there is any difference in population means. Depending on the chosen confidence level, the resulting confidence interval may contain the value zero. For such a case, at the given level of confidence, the populations do not have statistically different means, despite any difference in the sample means or variances. Conversely, if zero is not contained in the confidence interval, then the population means differ at that confidence level.

4. Entering known values and rearranging,

$$0.0922 \text{ s} \leq \mu_1 - \mu_2 \leq 7.71 \text{ s}$$

Since zero is not included in the confidence interval, the mean assembly time of procedure 2 is less than that of procedure 1.

Example 3.20

Repeat Example 3.19 if it is not known whether the populations have equal variances.

Solution

Since the population variances are not equal, the degrees of freedom are calculated using the appropriate equation from the right side of Table 3.10 as follows:

$$v = \frac{\left(\frac{s_1^2}{n_1} + \frac{s_2^2}{n_2} \right)^2}{\frac{(s_1^2/n_1)^2}{n_1 - 1} + \frac{(s_2^2/n_2)^2}{n_2 - 1}} = \frac{\left(\frac{4.91^2}{11} + \frac{2.54^2}{9} \right)^2}{\frac{(4.91^2/11)^2}{11 - 1} + \frac{(2.54^2/9)^2}{9 - 1}} = 15.53 \approx 16$$

(Note that v is rounded to the nearest integer, as noninteger degrees of freedom are not sensible.) The upper and lower t values (from Table 3.3) are 2.1120 and -2.1120 , respectively. Entering the t variable in the right side of Table 3.10 into Equation (3.17), the interval is defined by

$$t_{0.975,16} \leq \frac{(x_1 - x_2) - (\mu_1 - \mu_2)}{\sqrt{\frac{s_1^2}{n_1} + \frac{s_2^2}{n_2}}} \leq t_{0.025,16}$$

Entering the known values into the above equation yields

$$0.285 \text{ s} \leq \mu_1 - \mu_2 \leq 7.52 \text{ s}$$

Once again, zero is not included in the interval and, as such, the two procedures have differing mean assembly times. Interestingly, the interval generated without the assumption of equal population variances is smaller than the previous case, owing mainly to the large difference between the two sample standard deviations.

3.3.4 CONFIDENCE INTERVAL FOR THE VARIANCE

As discussed in Section 3.2.6, the variance of a sample can be calculated using the chi-square distribution. Computing the confidence interval for the population variance from the sample statistic is straightforward using the procedure laid out in Section 3.3 with the chi-square test statistic shown in Equation (3.14). Since the chi-square distribution is not symmetric, the upper and lower bounds are not simply opposite in sign, as they are in the normal or t distributions.

Example 3.21

For the solids collection experiment in Examples 3.17 and 3.18, the variance of the collection rate of a sample of size $n = 10$ was stated to be 4.8. Determine the 90% confidence interval of the population variance.

$$\frac{s_1^2 / s_2^2}{F_{\alpha/2, v_1, v_2}} \leq \frac{\sigma_1^2}{\sigma_2^2} \leq \frac{s_1^2 / s_2^2}{F_{1-\alpha/2, v_1, v_2}}$$

$$0.870 \leq \frac{\sigma_1^2}{\sigma_2^2} \leq 14.4$$

Hence, the ratio of population variances falls between 0.870 and 14.4. Since this interval contains unity, the ratio may be unity at a 95% confidence level and, hence, the two population variances do not differ based on this test.

3.3.6 SUMMARY OF CONFIDENCE INTERVALS

The confidence intervals discussed in this subsection are shown in Table 3.11 [2] in two-sided form. These intervals can be converted to one-sided form by removing the appropriate inequality and replacing the remaining $(1 - \alpha/2)$ or $\alpha/2$ term with $(1 - \alpha)$ or α . For example, the generic two-sided confidence interval $y_{\alpha/2} \leq y \leq y_{1-\alpha/2}$ is replaced with $y \leq y_{1-\alpha}$ to define a one-sided interval with an upper bound.

TABLE 3.11
Summary of Several Two-Sided Confidence Intervals

Interval Type	Sample Parameter	Two-Sided Interval with Confidence Level $100(1 - \alpha)\%$
Population mean (μ), variance (σ^2) known	\bar{x}	$\bar{x} - z_{\alpha/2} \frac{\sigma}{\sqrt{n}} \leq \mu \leq \bar{x} + z_{1-\alpha/2} \frac{\sigma}{\sqrt{n}}$
Population mean (μ), variance (σ^2) unknown	\bar{x}	$\bar{x} - t_{\alpha/2, n-1} \frac{s}{\sqrt{n}} \leq \mu \leq \bar{x} + t_{1-\alpha/2, n-1} \frac{s}{\sqrt{n}}$
Difference between population means ($\mu_1 - \mu_2$) for $\sigma_1^2 = \sigma_2^2$	$\bar{x}_1 - \bar{x}_2$	$\bar{x}_1 - \bar{x}_2 - t_{\alpha/2, n_1+n_2-2} s_p \sqrt{\frac{1}{n_1} + \frac{1}{n_2}} \leq \mu_1 - \mu_2 \leq \bar{x}_1 - \bar{x}_2 + t_{1-\alpha/2, n_1+n_2-2} s_p \sqrt{\frac{1}{n_1} + \frac{1}{n_2}}$ <p>where $s_p = \sqrt{\frac{(n_1-1)s_1^2 + (n_2-1)s_2^2}{n_1 + n_2 - 2}}$</p>
Difference between population means ($\mu_1 - \mu_2$) for $\sigma_1^2 \neq \sigma_2^2$	$\bar{x}_1 - \bar{x}_2$	$\bar{x}_1 - \bar{x}_2 - t_{\alpha/2, v} \sqrt{\frac{s_1^2}{n_1} + \frac{s_2^2}{n_2}} \leq \mu_1 - \mu_2 \leq \bar{x}_1 - \bar{x}_2 + t_{1-\alpha/2, v} \sqrt{\frac{s_1^2}{n_1} + \frac{s_2^2}{n_2}}$ <p>where $v = \frac{\left(\frac{s_1^2}{n_1} + \frac{s_2^2}{n_2}\right)^2}{\frac{(s_1^2/n_1)^2}{n_1-1} + \frac{(s_2^2/n_2)^2}{n_2-1}}$</p>
Population variance (σ^2)	s^2	$\frac{(n-1)s^2}{\chi_{\alpha/2, n-1}^2} \leq \sigma^2 \leq \frac{(n-1)s^2}{\chi_{1-\alpha/2, n-1}^2}$
Ratio of population variances (σ_1^2/σ_2^2)	s_1^2/s_2^2	$\frac{s_1^2 / s_2^2}{F_{\alpha/2, n_1-1, n_2-1}} \leq \frac{\sigma_1^2}{\sigma_2^2} \leq \frac{s_1^2 / s_2^2}{F_{1-\alpha/2, n_1-1, n_2-1}}$

Source: Montgomery, Douglas C., and Runger, George C., *Applied Statistics and Probability for Engineers*, 3rd ed., John Wiley & Sons, New York (2003).

Solution

We must determine whether 0.530 s^{-1} is an acceptable value for the rate constant.

1. The value of interest is the mean value of the rate constant. For this example, the mean value will be denoted μ and is equal to 0.530 h^{-1} . The estimate of this mean is denoted \bar{x} and is given by the measured value, 0.503 h^{-1} . The standard error, $SE(\bar{x})$, is 0.022 h^{-1} .
2. The two hypotheses:
 $H_0: k = 0.530 \text{ h}^{-1}$ (the given value is correct).
 $H_1: k \neq 0.530 \text{ h}^{-1}$ (the given value is incorrect).
3. Since the stated confidence level is to be 95%, the significance level is $\alpha = 0.05$.
4. For a mean with unknown population variance, the proper test statistic is the t variable, defined for this case [2] as

$$t = \frac{\bar{x} - \mu}{SE(\bar{x})}$$

5. For a linear regression, the number of degrees of freedom is $v = n - 2$ because two degrees of freedom are taken by the fitting parameters (see Section 3.5). Thus, $v = 9$. The critical region will be the upper and lower tails of the t distribution that have cumulative probability of 0.025 each. Thus, reading from Table 3.3, the lower t value is $t_{11,0.975} = -2.26$ and the upper t value is $t_{11,0.025} = 2.26$. Thus, the critical region is defined by

$$t < -2.26 \quad \text{and} \quad t > 2.26$$

Since this hypothesis test is two sided, there are two regions in which the null hypothesis could be rejected.

6. The t variable is

$$t = \frac{\bar{x} - \mu}{SE(\bar{x})} = \frac{0.503 \text{ h}^{-1} - 0.530 \text{ h}^{-1}}{0.022 \text{ h}^{-1}} = -1.23$$

Since the t variable is neither greater than 2.26 nor less than -2.26 , and therefore, falls outside the critical region, the null hypothesis should be accepted. The alternative hypothesis is rejected. At a confidence level of 95%, one may state that the mean rate constant k is 0.530 s^{-1} .

Example 3.24

During a polymerization reaction, the viscosity of a reactor effluent is measured periodically to determine the reaction progress. The measurement is repeated so that $n = 6$. If the true variance exceeds 0.8 cSt^2 ($\text{cSt} = \text{centistokes}$), the measurements are repeated to achieve better precision. For this sample, the mean viscosity was determined to be 106.4 cSt with variance 1.9 cSt^2 . At a confidence level of 95%, does the variance exceed the desired variability?

Solution

1. The value of interest is the population variance σ^2 , which is estimated for this sample of $n = 6$ with sample variance $s^2 = 1.9 \text{ cSt}^2$.
2. The hypotheses are
 $H_0: \sigma^2 \leq 0.8 \text{ cSt}^2$.
 $H_1: \sigma^2 > 0.8 \text{ cSt}^2$.
3. For a 95% confidence level, the significance level is $\alpha = 0.05$.

For both regression types, one begins with a set of independent variables \mathbf{X}_i (bold denoting vector notation); a measured, dependent response y_i ; and a regression function $\hat{y}(\mathbf{X}_i)$ with adjustable parameters $\{\beta_j\}$. Each response may be assumed to be distributed normally with variance σ_i^2 . If one makes the assumption that each measurement is independent, then the joint probability of the set of n data points [2] is

$$P = \prod_{i=1}^n \left[\frac{1}{\sqrt{2\sigma_i^2}} \exp \left(\frac{-[y_i - \hat{y}(\mathbf{X}_i)]^2}{2\sigma_i^2} \right) \right] \quad (3.25)$$

The parameters that produce the best model maximize P . One can alternatively maximize $\ln P$ instead of P and still arrive at the maximum probability. Therefore, Equation (3.25) is transformed to

$$\ln P = \ln \left(\prod_{i=1}^n \frac{1}{\sqrt{2\sigma_i^2}} \right) - \frac{1}{2} \sum_{i=1}^n \frac{[y_i - \hat{y}(\mathbf{X}_i)]^2}{\sigma_i^2} \quad (3.26)$$

Since the first term on the right-hand side does not depend on the adjustable parameters, maximizing P is equivalent to minimizing the summation in Equation (3.26). The optimal solution occurs when, for all β_j ,

$$\frac{\partial}{\partial \beta_j} \left(\sum_{i=1}^n \frac{[y_i - \hat{y}(\mathbf{X}_i)]^2}{\sigma_i^2} \right) = 0 \quad (3.27)$$

One usually does not have values or reliable estimates of σ_i^2 . Hence, the assumption that the variance of each y_i is uniform, i.e., $\sigma_i = \sigma$, is made so that Equation (3.27) reduces to

$$\frac{\partial}{\partial \beta_j} \left(\sum_{i=1}^n [y_i - \hat{y}(\mathbf{X}_i)]^2 \right) = 0 \quad (3.28)$$

When reliable σ_i are available, the adjustable parameters may be obtained from Equation (3.27), but the derivation is more involved than the simpler case of uniform variance. More information regarding the full derivation is provided by Press et al. [10]. The remainder of this section focuses on regression analyses with the assumption of constant variance, with separate discussions of simple linear, generalized multiple linear, and nonlinear regression.

3.5.1 SIMPLE LINEAR LEAST SQUARES REGRESSION

Linear least squares regression is the most common method of fitting a response that is a function of a single independent variable. Many nonlinear functions may be transformed to simple linear functions, extending the capabilities of the simplest regression algorithm.

3.5.1.1 Basic Algorithm

For linear least squares, the following model is entered into the equations of the previous subsection:

$$\hat{y}(x) = \beta_0 + \beta_1 x \quad (3.29)$$

the rate of reaction at constant volume and temperature follows a first-order exponential decay given by

$$C_A(t) = C_{A0} \exp(-kt)$$

and the variables are as identified in Example 3.25. The table below lists C_A as a function of t that was measured experimentally. Determine k via a linear regression.

t (h)	$C_A(t)$ (mol/l)	$y_i = \ln C_A(t)$
0.0	7.96	2.07
1.0	4.95	1.60
2.0	3.67	1.30
3.0	2.10	0.742
4.0	1.73	0.548
5.0	0.637	-0.451
6.0	0.566	-0.569
7.0	0.224	-1.50
8.0	0.202	-1.60
9.0	0.0688	-2.68
10.0	0.0670	-2.70

Solution

The above equation is identical in form to Equation (3.35). Therefore, its intrinsically linear form is

$$\ln C_A(t) = \ln C_{A0} - kt$$

As in Example 3.25, let $y = C_A$ and $x = t$. Again, $\beta_0 = \ln C_{A0}$ and $\beta_1 = -k$. The new y values are listed in the table, and the x values are identical to those in the t column. First, the average values of x and y are $\bar{x} = 5.0$ h and $\bar{y} = -0.273$ and $n = 11$. Then, following Equations (3.30)–(3.32), the sums of squares are

$$SS_{xx} = \sum_{i=1}^n x_i^2 - n \cdot \bar{x}^2 = 110 \text{ h}^2$$

$$SS_{yy} = \sum_{i=1}^n y_i^2 - n \cdot \bar{y}^2 = 28.2$$

$$SS_{xy} = \sum_{i=1}^n x_i y_i - n \cdot \bar{x} \cdot \bar{y} = -55.3 \text{ h}$$

The regression coefficients, following Equations (3.33) and (3.34), are

$$\beta_1 = \frac{SS_{xy}}{SS_{xx}} = -0.503 \text{ h}^{-1}$$

In terms of this estimated variance and the previously defined terms, the standard errors of the adjustable parameters [2] are

$$SE(\beta_0) = \sqrt{s^2 \left(\frac{1}{n} + \frac{\bar{x}^2}{SS_{xx}} \right)} \quad (3.39)$$

$$SE(\beta_1) = \sqrt{\frac{s^2}{SS_{xx}}} \quad (3.40)$$

These standard error estimates determine confidence intervals for the adjustable parameters. Another measure of uncertainty is that of calculations from the resultant model (i.e., the uncertainty of $\hat{y}(x)$). This uncertainty is estimated in terms of the variance of the model calculations [2], given by

$$V(\hat{y}(x_0)) = s^2 \left(\frac{1}{n} + \frac{(x_0 - \bar{x})^2}{SS_{xx}} \right) \quad (3.41)$$

where x_0 is the value of the dependent variable at which the model prediction and associated variance are calculated. Note that this variance depends on the distance between x_0 from the mean \bar{x} value. The variance is wider for points far from the mean \bar{x} . This variance allows for the determination of a confidence interval of the true value of y in terms of the model parameters [2]

$$\beta_0 + \beta_1 x_0 - t_{\alpha/2, n-2} \sqrt{s^2 \left(\frac{1}{n} + \frac{(x_0 - \bar{x})^2}{SS_{xx}} \right)} \leq y \leq \beta_0 + \beta_1 x_0 + t_{\alpha/2, n-2} \sqrt{s^2 \left(\frac{1}{n} + \frac{(x_0 - \bar{x})^2}{SS_{xx}} \right)} \quad (3.42)$$

where α denotes the significance level.

The accuracy of the regression is often measured by the coefficient of determination (R^2) defined [2] as follows:

$$R^2 = 1 - \frac{\sum_{i=1}^n e_i^2}{SS_{yy}} \quad (3.43)$$

Mathematically, R^2 measures the proportion of the error in $\hat{y}(x)$ arising from the regression. When R^2 is nearly equal to unity, the model predicts the experimental data points well. It does not, however, mean that the model represents the true data trend. To evaluate the model, examine the plot comparing the predicted and experimental values.

Example 3.27

For the concentration-versus-time data given in Example 3.26, determine the standard errors of the regression parameters β_0 and β_1 and the R^2 value. Plot the 95% confidence intervals for calculations from the model.

Solution

Entering the known values from Example 3.25 into Equations (3.38)–(3.40) and (3.43),

3.5.2.1 Basic Algorithm

The model consists of a single measured response y_i and k independent variables \mathbf{x}_i [2]. The independent variables may be any chosen independent variable or any linear function of the independent variables. For example, if pressure and temperature are independent variables P and T , respectively, then the set of independent variables \mathbf{x}_i may be a combination of P , T , $P \cdot T$, P^2 , T^2 , etc. The model for y_i may be

$$\hat{y}(\mathbf{x}_i) = \beta_0 + \beta_1 x_{i1} + \beta_2 x_{i2} + \dots + \beta_k x_{ik} \quad (3.44)$$

with $\{\beta_j\}$ being the set of $(k + 1)$ adjustable parameters. (The $(k + 1)$ th parameter is the constant term in the model.) Solving for an optimal $\{\beta_j\}$ is accomplished more easily using a vector-matrix technique. The following vectors and matrix are defined:

$$\hat{\mathbf{y}} = \begin{bmatrix} \hat{y}(\mathbf{x}_1) \\ \hat{y}(\mathbf{x}_2) \\ \vdots \\ \hat{y}(\mathbf{x}_n) \end{bmatrix} \quad \mathbf{X} = \begin{bmatrix} 1 & x_{11} & x_{12} & \cdots & x_{1k} \\ 1 & x_{21} & x_{22} & \cdots & x_{2k} \\ \vdots & \vdots & \vdots & \ddots & \vdots \\ 1 & x_{n1} & x_{n2} & \cdots & x_{nk} \end{bmatrix} \quad \boldsymbol{\beta} = \begin{bmatrix} \beta_0 \\ \beta_1 \\ \vdots \\ \beta_k \end{bmatrix} \quad \mathbf{y} = \begin{bmatrix} y_1 \\ y_2 \\ \vdots \\ y_n \end{bmatrix} \quad \mathbf{x}_i = \begin{bmatrix} 1 \\ x_{i1} \\ x_{i2} \\ \vdots \\ x_{ik} \end{bmatrix} \quad (3.45)$$

For n data points, Equation (3.44) may be rewritten as

$$\hat{\mathbf{y}} = \mathbf{X}\boldsymbol{\beta} \quad (3.46)$$

The residual vector is written as

$$\mathbf{e} = \mathbf{y} - \hat{\mathbf{y}} \quad (3.47)$$

Tedious manipulation indicates that the square error, $|\mathbf{e}|^2$, is minimized when the set of adjustable parameters [2] is as follows:

$$\boldsymbol{\beta} = (\mathbf{X}^T \mathbf{X})^{-1} \mathbf{X}^T \mathbf{y} \quad (3.48)$$

where the superscript T denotes the transpose vector or matrix and the superscript -1 indicates the inverse matrix.

Example 3.28

For specific heat (C_p)-vs.-temperature (T) data, the following model is often employed:

$$\hat{C}_p(T) = \beta_0 + \beta_1 T + \beta_2 T^2$$

Determine its coefficients for the data in the following table:

T (K)	C_p (J/mol · K)
200	34.96
300	35.94
400	37.32
500	38.21
600	39.46

$$\text{cov}(\beta_i, \beta_j) = s^2 C_{ij} \quad i \neq j \quad (3.52)$$

Predictions from the model [2] have variance

$$V(\hat{y}(\mathbf{x}_0)) = s^2 \mathbf{x}_0^T \mathbf{C} \mathbf{x}_0 \quad (3.53)$$

The confidence interval for predictions from the model is

$$\hat{y}(\mathbf{x}_0) - t_{\alpha/2, n-k-1} \sqrt{s^2 \mathbf{x}_0^T \mathbf{C} \mathbf{x}_0} \leq y \leq \hat{y}(\mathbf{x}_0) + t_{\alpha/2, n-k-1} \sqrt{s^2 \mathbf{x}_0^T \mathbf{C} \mathbf{x}_0} \quad (3.54)$$

Model adequacy may again be measured using R^2 (coefficient of determination), which is given by Equation (3.43). The interpretation of R^2 for multiple linear regression is identical to that used in the simple linear version of least squares.

Example 3.29

Referring to Example 3.28, where C_p was fit to a polynomial function of T , determine the standard error of each regressor β_j and the variance of the model's prediction for $T = 200$ K.

Solution

To determine the standard error of each β_j , one first needs the covariance matrix and s^2 . Entering the \mathbf{X} matrix determined in Example 3.28 into Equation (3.50), the covariance matrix \mathbf{C} is

$$\mathbf{C} = (\mathbf{X}^T \mathbf{X})^{-1} = \begin{bmatrix} 15.8 & -8.40 \times 10^{-2} \text{ K}^{-1} & 1.00 \times 10^{-4} \text{ K}^{-2} \\ -8.40 \times 10^{-2} \text{ K}^{-1} & 4.67 \times 10^{-4} \text{ K}^{-2} & -5.71 \times 10^{-7} \text{ K}^{-3} \\ 1.00 \times 10^{-4} \text{ K}^{-2} & -5.71 \times 10^{-7} \text{ K}^{-3} & 7.14 \times 10^{-10} \text{ K}^{-4} \end{bmatrix}$$

Following Equation (3.49), the variance estimator is

$$s^2 = \frac{\mathbf{y}^T \mathbf{y} - \beta^T \mathbf{X}^T \mathbf{y}}{n - k - 1} = \frac{0.0434 \left(\frac{\text{J}}{\text{mol} \cdot \text{K}} \right)^2}{5 - 2 - 1} = 0.0217 \left(\frac{\text{J}}{\text{mol} \cdot \text{K}} \right)^2$$

Therefore, via Equation (3.51), the standard errors of the adjustable parameters are

$$\begin{aligned} SE(\beta_0) &= \sqrt{s^2 C_{00}} = 0.586 \frac{\text{J}}{\text{mol} \cdot \text{K}} \\ SE(\beta_1) &= \sqrt{s^2 C_{11}} = 3.18 \times 10^{-3} \frac{\text{J}}{\text{mol} \cdot \text{K}^2} \\ SE(\beta_2) &= \sqrt{s^2 C_{22}} = 3.94 \times 10^{-6} \frac{\text{J}}{\text{mol} \cdot \text{K}^3} \end{aligned}$$

For the data at $T = 200$ K, the \mathbf{x}_0 vector (a column vector identical to the first row of \mathbf{X} ; see Equation (3.45)) is

TABLE 3.12
Table Form Summary of ANOVA Procedure

Source of Variance	Degrees of Freedom	Sum of Squares	Mean Square	F_0	P
Regression	k	SS_R	$MS_R = SS_R/k$	MS_R/MS_E	$P(F > F_0)$
Error	$n - k - 1$	SS_E	$MS_E = SS_E/(n - k - 1)$
Total	$n - 1$	SS_T

Source: Montgomery, Douglas C., and Runger, George C., *Applied Statistics and Probability for Engineers*, 3rd ed., John Wiley & Sons, New York (2003).

denoted P) is smaller than the significance level α , the regression is significant. The ANOVA procedure is usually presented as a table, such as the summary given in Table 3.12.

Example 3.30

With a significance level of $\alpha = 0.05$ (95% confidence level), use an ANOVA table to determine whether the multiple linear regression model determined in Example 3.28 is significant.

Solution

For the multiple linear regression in Example 3.28, there were five data points and three regressors for $n = 5$ and $k = 2$. From the model and basis data in that example, the following sums of squares were computed via Equations (3.55 through 3.57):

For example,

$$SS_T = \mathbf{y}^T \mathbf{y} - n(\bar{y})^2 = \begin{bmatrix} 34.96 & 35.94 & 37.32 & 38.21 & 39.46 \end{bmatrix} \begin{bmatrix} 34.96 \\ 35.94 \\ 37.32 \\ 38.21 \\ 39.46 \end{bmatrix} \left(\frac{\text{J}}{\text{mol} \cdot \text{K}} \right)^2$$

$$- 5 \left(\frac{34.96 + 35.94 + 37.32 + 38.21 + 39.46}{5} \frac{\text{J}}{\text{mol} \cdot \text{K}} \right)^2 = 12.744 \left(\frac{\text{J}}{\text{mol} \cdot \text{K}} \right)^2$$

Then,

$$SS_T = 12.744 \left(\frac{\text{J}}{\text{mol} \cdot \text{K}} \right)^2$$

$$SS_R = 12.701 \left(\frac{\text{J}}{\text{mol} \cdot \text{K}} \right)^2$$

$$SS_E = 0.043 \left(\frac{\text{J}}{\text{mol} \cdot \text{K}} \right)^2$$

$$\sigma^2(y) = \sum_{i=1}^n a_i^2 \sigma^2(x_i) + 2 \sum_{i=1}^n \sum_{j=i+1}^n a_i a_j \text{Cov}(x_i, x_j) \quad (3.61)$$

where $\sigma^2(x_i)$ is the variance of the i th measured variable, and $\text{Cov}(x_i, x_j)$ is the covariance of the i - j pair of measurements. The covariance term in Equation (3.61) allows for the measured variables (x_1, x_2, \dots, x_n) to be correlated. The measured variables are often uncorrelated, which allows for removing the second summation term in Equation (3.61). If the measured variables are indeed correlated, the covariance relationship between two variables may be unknown, seemingly leaving Equation (3.61) useless. One may, however, simplify the problem by assuming that the covariance terms are zero, reducing Equation (3.61) to

$$\sigma^2(y) = \sum_{i=1}^n a_i^2 \sigma^2(x_i) \quad (3.62)$$

Thus, for a computed value that is linearly dependent on all measured variables, the variance of the computed value can be predicted in a straightforward fashion from the variance of the individual measured variables.

Since the relationship between a computed quantity and measured variables is often nonlinear, an approximate method is needed to calculate the variance of the computed quantity. Suppose that a quantity y is given by a nonlinear function and that the individual measured quantities (x_1, x_2, \dots, x_n) are independent. (The assumption of independence removes the need for covariance terms.) Then the variance of y may be approximated [15] as

$$\begin{aligned} \sigma^2(y) &= \left(\left. \frac{\partial y}{\partial x_1} \right|_{\{x_j\}} \right)^2 \sigma^2(x_1) + \left(\left. \frac{\partial y}{\partial x_2} \right|_{\{x_j\}} \right)^2 \sigma^2(x_2) + \dots + \\ &\left(\left. \frac{\partial y}{\partial x_n} \right|_{\{x_j\}} \right)^2 \sigma^2(x_n) = \sum_{i=1}^n \left(\left. \frac{\partial y}{\partial x_i} \right|_{\{x_j\}} \right)^2 \sigma^2(x_i) \end{aligned} \quad (3.63)$$

where $\{x_j\}$ indicates that the partial derivatives of y are evaluated at the current set of measured variables (x_1, x_2, \dots, x_n). (Equation (3.63) reduces to Equation (3.62) for the case of a linear function. Despite this similarity, Equation (3.63) is still an approximation [15].)

With Equations (3.62) and (3.63), one can determine estimates of the variance of a calculated value from the variance of measured variables. The individual variance terms, $\sigma^2(x_i)$, might not be known, however, and one must make estimates. Through repeated experiments, $\sigma^2(x_i)$ could be estimated by $s^2(x_i)$, the sample variance of variable x_i . If one has information about the sensitivity of a measuring device, this previous knowledge could be input as a variance term.

Example 3.31

For a fully developed laminar flow in a pipe, the Hagen-Poiseuille equation is used to calculate the pressure drop per unit length ($\Delta P/L$) at a given volumetric flow rate \dot{V} , pipe diameter D , and fluid viscosity μ :

$$\left(\frac{\Delta P}{L} \right) = \frac{\pi D^4}{128 \mu \dot{V}} \quad (3.64)$$

If the design matrix is in a coded form (i.e., the values of the x_j terms are scaled or changed to a simpler number), the coding equations must be designated.

3.7.2 DESIGN FOR ONE-FACTOR EXPERIMENT

The preferred choice of conditions for experiments depends on the model. Some designs for several simple models are discussed next. The experiments are hopefully conducted to minimize the random error of the response, and σ^2 is therefore estimated by s^2 .

3.7.2.1 $\hat{y} = \beta_0 = \bar{y}$

For this constant-value model, the only consideration is how many times to replicate, since the conditions are constant. The selection of n can be logically determined from the confidence interval equation. The width of this interval is proportional to $t_{\alpha/2, v}$ (the t variable for chosen confidence level and number of runs) and s / \sqrt{n} , the standard error of the average. More runs reduce the confidence interval in two ways. Increasing n decreases the standard error, since it is inversely proportional to the square root of n . Also, the value of $t_{\alpha/2, v}$ decreases with increasing n as the number of degrees of freedom, $v = n - 1$, increases. After selecting n to obtain a desired confidence interval, it is a trial-and-error calculation, since $t_{\alpha/2, v}$ depends upon n and is obtained from Table 3.3. Of course, an estimate of the experimental error is needed. An estimate is normally based on knowledge of the process to obtain a preliminary value. After a few runs are completed, an experimental value of s^2 is calculated, and a revised value can be determined.

3.7.2.2 $\hat{y} = \beta_1 x$

For this proportionality model, first determine the confidence interval of the slope, which is a fixed value that is calculated by

$$V(\beta_1) \propto \frac{1}{\sum_{i=1}^n x^2} \quad (3.65)$$

since the matrix \mathbf{C} is 1×1 for this case. Sufficient runs are made to obtain reliable values to minimize the confidence interval. At $x = 1$, the confidence interval on the response is equal to the confidence interval on β_1 .

3.7.2.3 $\hat{y} = \beta_0 + \beta_1 x$

The general straight-line model is often used as a starting point for model development. The confidence interval often widens at the ends (see Section 3.5). More levels of the factor act to reduce the confidence interval. Equally spaced levels are often tested. The number of levels depends on the complexity of the model or on the number of additional terms to be considered. Enough levels should be provided for left-out terms. The number of levels should exceed the number of parameters expected. Even if a straight line is likely, more than three levels should be considered, plus some replication.

3.7.3 DESIGN FOR SEVERAL FACTORS

With several factors to study, the size of the experimental design becomes large, time consuming, and expensive. Two levels are often selected for an exploratory design.

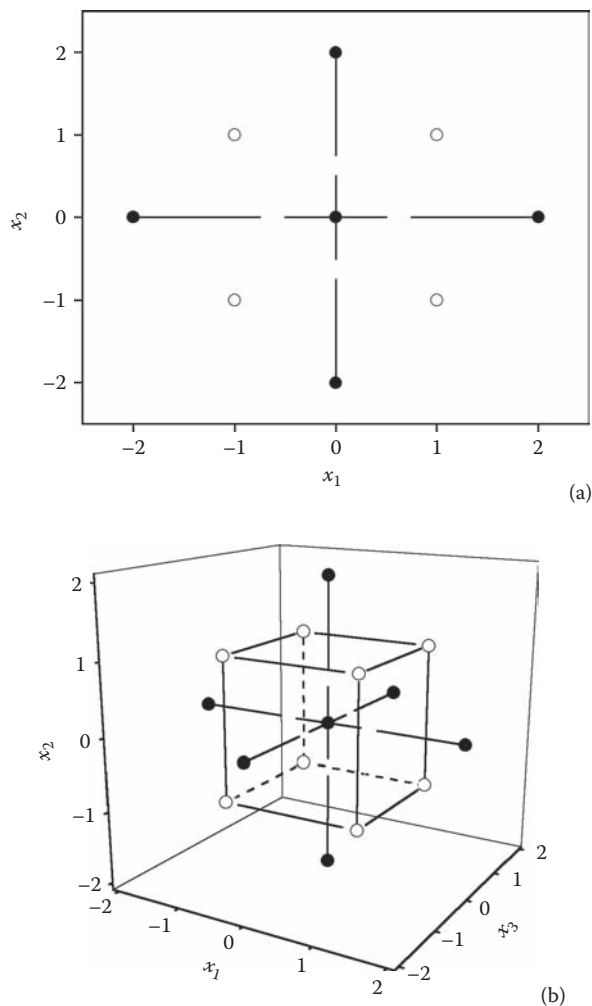


FIGURE 3.3 Composite designs, two-level factorial plus star design, for (a) two factors and (b) three factors.

3.7.5 BLOCKS AND NEW DUPLICATES

Sometimes a block of runs is performed to estimate reproducibility. For example, one block (or group) of runs is made with one feedstock or one reactor system. In these cases, partial factorial runs may act as different blocks, or replicates are performed.

3.7.6 COMPUTER-AIDED EXPERIMENTAL DESIGN

Several computer software packages are helpful in designing experiments. A current commonly used software is JMP, produced by SAS [17]. Typically, design-of-experiments software will ask the user to input the number of factors and levels and the size of the design, e.g., 1/2 or 1/4 factorials or even smaller. Afterward, the software self-selects those terms to alias and then will usually display the model appropriate to the factorial design. The software may also randomize the order of experiments or enter the experiments into blocks if the user desires. JMP is particularly useful, as it contains both the experimental-design software and multiple linear regression algorithms, and both are designed to work in tandem, providing a platform for experimental design and follow-up mathematical modeling.

- c. Comparisons: Two Processes
- d. Comparisons: Three + Processes
- 8. Assessing Product Reliability
 - a. Introduction
 - b. Assumptions/Prerequisites
 - c. Reliability Data Collection
 - d. Reliability Data Analysis

ACKNOWLEDGMENT

The author is grateful to the late Robert Eckert for notes that assisted in the compilation of this handbook chapter.

REFERENCES

1. National Institute of Standards and Testing, Gaithersburg, MD, *NIST/SEMATECH e-Handbook of Statistical Methods*; available online at <http://www.itl.nist.gov/div898/handbook/index.htm>; accessed 22 May 2007.
2. Montgomery, Douglas C., and Runger, George C. 2003. *Applied Statistics and Probability for Engineers*, 3rd ed. New York: John Wiley & Sons.
3. Metcalfe, Andrew V. 1994. *Statistics in Engineering*. London: Chapman & Hall.
4. Fraser, D.A.S. 1976. *Probability and Statistics: Theory and Applications*. North Scituate, MA: Duxbury Press.
5. Microsoft Excel electronic help files 2007.
6. Microsoft Excel online assistance; available online at <http://office.microsoft.com/en-us/assistance/CH790018021033.aspx>; accessed 22 May 2007.
7. Mathematica electronic help files 2007.
8. MATLAB electronic help files 2007.
9. Gosset, William S., "The Probable Error of a Mean," *Biometrika*, 6: 1–25 (1908).
10. Press, William H., Flannery, Brian P., Teukolsky, Saul A., and Vetterling, William T. 1992. *Numerical Recipes in FORTRAN*, 2nd ed. Cambridge: Cambridge University Press.
11. Amundson, Neal R. 1966. *Mathematical Methods in Chemical Engineering*. Englewood Cliffs, NJ: Prentice-Hall.
12. Frazer, Robert A., Duncan, William J., and Collar, Arthur R. 1960. *Elementary Matrices and Some Applications to Dynamics and Differential Equations*. New York: Cambridge University Press.
13. Lay, David C. 2005. *Linear Algebra and Its Applications*. Reading, MA: Addison Wesley.
14. Barry, Austin B. 1978. *Errors in Practical Measurement in Science, Engineering, and Technology*. New York: John Wiley & Sons.
15. Bragg, Gordon M. 1974. *Principles of Experimentation and Measurement*. Englewood Cliffs, NJ: Prentice-Hall.
16. Hougen, Olaf A., and Watson, Kenneth. M. 1947. *Chemical Process Principles*, vol. 3, 943–58. New York: John Wiley & Sons.
17. SAS JMP™ electronic help files 2007.

4.3	Liquid Solutions	325
4.3.1	Ideal and Real Solutions	325
4.3.2	Ideal and Excess Solution Properties	328
4.3.3	Activity-Coefficient Models	329
4.3.3.1	Redlich–Kister Equation	330
4.3.3.2	Van Laar Equation	330
4.3.3.3	Regular Solutions	332
4.3.3.4	Flory–Huggins Equation	334
4.3.3.5	Wilson's Local-Composition Equation	336
4.3.3.6	Nonrandom Two-Liquids (NRTL) Equation	338
4.3.3.7	The Complete Local-Composition Equation	339
4.3.3.8	UNIQUAC Equation	341
4.3.4	Group Contribution Methods	343
4.3.4.1	Four Postulates of Group Solution	343
4.3.4.2	Analytical Solution of Groups	345
4.3.5	Gibbs Energy Models of Liquid Solutions	347
References	350
4.4	Fluid-Phase Equilibria	351
4.4.1	Vapor-Liquid Equilibrium in a Single-Component Fluid	351
4.4.2	Vapor-Liquid Equilibrium of Ideal Mixtures	355
4.4.3	Vapor-Liquid Equilibrium by γ - ϕ Models	358
4.4.3.1	Low-Pressure Models	358
4.4.3.2	A High-Pressure Model	362
4.4.4	Vapor-Liquid Equilibrium by ϕ - ϕ Models	364
4.4.4.1	ϕ - ϕ Models— ϕ from vdW Mixing Rules	364
4.4.4.2	Free-Energy-Matching Mixing Rules	367
4.4.5	Liquid-Liquid Equilibrium Models	367
4.4.6	Gas-Solid Equilibrium Models	372
References	374
4.5	Chemical Reaction Equilibria	375
4.5.1	Chemical Reaction Equilibrium	375
4.5.2	Equilibrium Constants	376
4.5.3	Phase Rule for Chemically Reacting Species	384
4.5.4	Open Systems with Reaction	385
4.5.5	Stoichiometric Formulation	388
References	391
Data References	392

4.1 PRINCIPLES OF THERMODYNAMICS

4.1.1 INTRODUCTION

Thermodynamics has played an increasingly important role over the years in the engineering analysis and synthesis of chemical processes. There has been an expansion of this role with the success of vapor-pressure-fitted van der Waals equations of state and group contribution methods. By far the major part of computer time in chemical process design is now devoted to thermodynamic calculations. This chapter presents the thermodynamic methods needed to perform the analysis and synthesis, to start from basic principles, to describe the phenomena, to develop the methods, and to illustrate applications.

In a brief review of the terminology of thermodynamics, the portion of the universe that is studied is called a *system*. The rest of the universe that interacts with the system is the *surroundings*.

object to be determined; form the pV products and extrapolate to determine a zero-pressure limiting value; call it β . Repeat this experiment at the steam point to determine a benchmark value β_s . Repeat again at the ice point to determine another benchmark value β_i . The temperature of the object on the ideal-gas temperature scale in kelvins, K , is given by

$$T = 100\beta / (\beta_s - \beta_i) \quad (4.1)$$

In Equation (4.1), the steam-point temperature and the ice-point temperature are defined to differ by $100^\circ K$. The ideal-gas temperature is independent of the species and quantity of gas and of the apparatus used for the measurement. Substituting β_i for β in Equation (4.1), the ice point has been found to be 273.15° and, similarly, the steam point to be $373.15^\circ K$.

In terms of ideal-gas temperature, it follows from Equation (4.1) that all gases are described by

$$\lim_{p \rightarrow 0} pv = \kappa T \quad (4.2)$$

where κ is a constant in the equation but depends on the quantity of gas. The quantity assumes a universal constant value for 1 mole of gas by Avogadro's law, which states that equal volumes of gas of any chemical species measured at the same temperature and pressure contain equal numbers of molecules at ideal-gas conditions,

$$\lim_{p \rightarrow 0} pv = RT \quad (4.3)$$

where v denotes molar volume and R is a universal constant determined to be $8.314510 \text{ J}/(\text{mol}\cdot K)$.

For real gases, the pV product attains the limiting value RT at zero pressure, where intermolecular potential energy vanishes. The extrapolation to zero pressure frees the pV product from the effect of intermolecular forces. An ideal gas is defined as one that is free of intermolecular potential energy at finite pressures. For the ideal gas, the pV product equals RT at all pressures, and is called the ideal-gas equation,

$$pv = RT \quad (4.4)$$

This equation is an approximation of real gas behavior at high temperatures or low pressures. The approximation remains good at lower temperatures at progressively lower pressures. Where the degree of approximation is acceptable, the equation is in common use for its simplicity.

A real gas or real liquid is said to be in the ideal-gas state when its intermolecular potential is ignored. The properties of the fluid in the ideal-gas state can be calculated with ease using Equation (4.4). One simple universal equation applies to all substances, requiring no substance-specific parameters. However, for most real states, the ideal-gas equation is inadequate, and real-fluid properties are obtained by adding to the ideal-gas equation the contribution of intermolecular potential in the form of deviation functions, also called residual functions. A major objective of Section 4.2 is to derive the deviation functions from the equation of state of the substance. Because the ideal-gas properties are known, to find the deviation function is as good as finding the state function of a real substance. In this way the ideal-gas equation is used universally in all equation-of-state calculations of thermodynamic functions.

4.1.3 FIRST LAW OF THERMODYNAMICS AND INTERNAL ENERGY

The first law of thermodynamics states that energy can be converted from one form to another or transported from one system to another, but the sum of the energies involved—kinetic energy,

potential energy of the molecules is the only form of molecular energy that is volume dependent, the internal energy of the ideal gas is independent of pressure or density, but is a function of temperature only:

$$(\partial U / \partial p)_T = 0 \quad (4.9)$$

$$(\partial U / \partial \rho)_T = 0 \quad (4.10)$$

While the intermolecular forces are absent, the internal structure of the molecule and the attendant energies remain unaltered from the real gas. The internal energy, heat capacity, and related functions retain their specific values for each substance in the ideal-gas state.

For the phenomena addressed in this chapter, changes in the mechanical energy of a substance are insignificant compared with changes in the internal energy; mechanical energy contents will not be included in the first law equation in the rest of the chapter. We will simply write

$$dU = \delta Q + \delta W \quad (4.11)$$

A change of volume is always associated with the phenomena addressed in this chapter; we will consider volume change as the only means by which work is exchanged with the surroundings, $\delta W = -pdV$, the sign convention being for the work to be positive when done on the system. Thus

$$dU = \delta Q - pdV \quad (4.12)$$

As a state function, how does U change with state? Let us express dU in terms of the state variables and V ,

$$dU = (\partial U / \partial V)_T dV + (\partial U / \partial T)_V dT \quad (4.13)$$

Combining the two equations, we express the heat exchange in terms of changes of state,

$$\delta Q = [(\partial U / \partial V)_T + p]dV + (\partial U / \partial T)_V dT \quad (4.14)$$

Let C_V denote heat capacity at constant volume defined by

$$(\delta Q = C_V dT)_V \quad (4.15)$$

Comparison of Equation (4.14) and Equation (4.15) shows that

$$C_V = (\partial U / \partial T)_V \quad (4.16)$$

At constant volume, the change of U with a change of from state 1 to 2 is given by

$$U_2 - U_1 = \int_1^2 C_V dT \quad (4.17)$$

Example 4.1: Throttle

A throttle is a device (such as a partly closed valve or porous plug) that reduces the pressure of a flowing fluid without any shaft work or significant acceleration of the fluid (i.e., no appreciable change in the kinetic energy of the fluid). With a single inlet and outlet stream, and assuming that these streams and the heat transfer are negligible, Equation (4.22) reduces to

$$h_{out} = h_{in} \quad (4.23)$$

A throttle does not change the enthalpy of the fluid; throttling is an isenthalpic process. For a given input state and a specified outlet pressure, one finds the outlet temperature by conducting a one-dimensional search for a temperature at which the enthalpy is equal to the input enthalpy. An enthalpy chart provides a convenient means for the search. Another method of solution is to apply the Joule-Thompson coefficient, μ_{JT} , defined by

$$\mu_{JT} = \left(\frac{\partial T}{\partial P} \right)_h \quad (4.24)$$

The sign of the above partial derivative determines whether a fluid expanded through a throttle experiences a temperature drop. For an ideal gas, $\mu_{JT} = 0$, so that there is no change for a given pressure drop. For real gases, at high enough temperatures (depending upon the substance of interest), $\mu_{JT} < 0$, so that the temperature of the gas increases upon expansion. Below some inversion temperature, μ_{JT} becomes positive, so that the gas now cools upon expansion through a throttle. For example, this inversion temperature is about 1319 for CO_2 and about 40 for He. Typically, another inversion temperature exists at even lower temperatures, where μ_{JT} again becomes negative. Also, there is usually a single inversion pressure, where above that pressure μ_{JT} is always negative. For example, this inversion pressure is 884 bar for CO_2 and around 27.5 bar for He. Typically, a throttle is used to cool a gas upon expansion. If the temperature drop is large enough, the gas can be partially liquefied.

Example 4.2: Heat Exchangers

Consider a heat exchanger operating with two streams, A and B, with steady flow rates of \dot{n}_A and \dot{n}_B . Since the volume of the heat exchanger is constant and no shaft work is performed, $\dot{W} = 0$. Also, assuming that all transfer of heat occurs between the two streams inside the heat exchanger, so that no heat is lost to the surroundings, then $\dot{Q} = 0$. With kinetic and potential energy changes being small, the energy balance reduces to

$$\Delta h_A \dot{n}_A + \Delta h_B \dot{n}_B = 0 \quad (4.25)$$

where $\Delta h_i = h_{i,out} - h_{i,in}$. If the incoming and outgoing pressure of a stream is the same, then Δh_i can be calculated from

$$\Delta h_i = \int_{T_{i,in}}^{T_{i,out}} C_{p,i} dT$$

Example 4.3: Venting of an Insulated Tank

Consider a rigid (constant-volume), well-insulated (adiabatic) tank containing a gas at some initial high pressure. Then a valve is opened and the gas is slowly vented through a pipe. Assuming that the changes in kinetic energy are small (as compared with the enthalpy fluxes and internal energy changes of the system), Equation (4.20) reduces to

where we have also made use of the mass balance equation. In this example $dN > 0$. Since the enthalpy of the incoming stream, h_{in} , is constant, we may integrate both sides of the above equation to obtain

$$U_f - U_i = h_{in}(N_f - N_i)$$

Because $N_i = 0$, $U_i = 0$, so that the above reduces to

$$U_f = N_f u_f = h_{in} N_f$$

or

$$u_f = h_{in} = u_{in} + p_{in} v_{in} \quad (4.29)$$

The first term on the far right side represents the molar internal energy that entered the tank, while the second term represents the work done by the incoming stream as it enters the tank.

For an ideal gas, $p v = R T$ and $du = c_v dT$, so that Equation (4.29) becomes (by using an average heat capacity)

$$u_f - u_{in} = c_v (T_f - T_{in}) = p_{in} v_{in} = R T_{in}$$

or

$$T_f = \frac{c_p}{c_v} T_{in} \quad (4.30)$$

Because $C_p > C_v$, then $T_f > T_{in}$. This problem clearly illustrates one of the differences between open and closed systems and of the importance of the work due to flow (which, in this example, is responsible for the increase of the final temperature above that of the external source). As an example, air, modeled as a pure-component ideal gas, is well represented by $c_v = (5/2)R$ and $c_p = (7/2)R$, so that $T_f = (7/5)T_{in}$, a 40% temperature rise above T_{in} .

4.1.4 SECOND LAW OF THERMODYNAMICS AND ENTROPY

The second law according to Planck is widely cited: *It is impossible to construct a machine operating in cycles that will convert heat into work without producing any other changes in the surroundings.* Another form of the second law is: *It is impossible to operate any process solely to transfer heat from a lower temperature to a higher one.* It can be shown that both are equivalent and both are deducible from the following statement:

There exists an extensive state function called entropy S that is defined by

$$dS = \delta Q / \theta \quad (4.31)$$

where δQ is the differential heat absorbed reversibly from the surroundings and θ is the thermodynamic temperature of the system. The thermodynamic temperature is an absolute temperature that can never be less than zero, and is otherwise unspecified. It will be shown shortly that it is identical to the ideal-gas temperature.

Since entropy is a state function, its change is also zero. Adding up the entropy changes for all four steps of the cycle,

$$Q_1/\theta_1 + Q_2/\theta_2 = 0 \quad (4.38)$$

The cycle is characterized by the absorption of heat at only one temperature and by the rejection of heat at only one temperature, such that the effect of temperature on the quantity of heat absorbed or rejected can be revealed. By Equation (4.38), the effect is a simple proportionality,

$$Q_1/\theta_1 = -Q_2/\theta_2 \quad (4.39)$$

The efficiency of the cycle is defined to be the fraction of the heat absorbed at the high temperature that is converted into work, $(-W)/Q_1$. By combining Equation (4.37) and Equation (4.38), the efficiency of the Carnot cycle is obtained,

$$(-W)/Q_1 = (\theta_1 - \theta_2)/\theta_1 \quad (4.40)$$

The theoretical efficiency of the ideal reversible cycle is seen to depend only on the temperatures of the heat source and sink, and is independent of the working fluid confined in the piston-cylinder device.

Let us use an ideal gas in a Carnot cycle and find the efficiency of the cycle by using ideal-gas properties in enumerating the changes in the four steps of the cycle. Let us designate the initial state of step 1 with the subscript A, the initial state of step 2 with B, and so on. The high temperature at step 1, which is θ_1 on the thermodynamic temperature scale, will be T_1 on the ideal-gas temperature scale. The low temperature of step 3 will be T_2 , corresponding to θ_2 . The work and heat terms of a step will be designated with subscripts 1, 2, 3, or 4.

1. Isothermal expansion at a high temperature T_1 :

$$U_B - U_A = 0$$

$$W_1 = -\int p dV = -nRT_1 \ln (V_B/V_A)$$

$$Q_1 = -W_1$$

2. Adiabatic expansion to cool down from T_1 to T_2 :

$$Q_2 = 0$$

$$U_C - U_B = W_2$$

3. Isothermal compression at a low temperature T_2 :

$$U_D - U_C = 0$$

$$W_3 = -\int p dV = -nRT_2 \ln (V_D/V_C)$$

$$Q_3 = -W_3$$

between the same high temperature T_1 and low temperature T_2 , it *absorbs* heat Q_2 at T_2 and *rejects* heat Q_1 at T_1 while *consuming* work W . The ratio W/Q_1 remains the same as before. Suppose an irreversible machine exists that has a higher efficiency than the Carnot cycle. Let it absorb heat Q_1' at T_1 and produce the same work W as consumed by the reversed Carnot. Then, as supposed,

$$W/Q_1' > W/Q_1 \quad (4.50)$$

$$Q_1' < Q_1 \quad (4.51)$$

If the reversed Carnot cycle were coupled to the irreversible machine and driven by it, there would be a net amount of heat $Q_1 - Q_1' > 0$ flowing into the reservoir from this coupled machine. There being no net work production, this amount of heat is obtained from the low-temperature reservoir at T_2 . The coupled machine would be pumping heat from a lower temperature to a higher temperature while producing no other changes in the surroundings. But such a result is impossible by the second law.

The efficiencies of all reversible machines are equal. For, if any one should have a different efficiency, the machine with the higher efficiency can be operated to drive the one with lower efficiency in reverse. The combined machine would be capable of pumping heat from a lower temperature to a higher temperature without producing any other changes in the surroundings, hence violating the second law.

The Carnot cycle reveals a fundamental difference of heat from mechanical energies. Whereas the conversion of mechanical energy to heat can be readily completed, the conversion of heat to work is incomplete, even under ideal conditions. Only part of the heat can be converted, and the rest has to be rejected to a lower temperature sink. In thermodynamics, work denotes all forms of energy that are interconvertible without any theoretical limit on the degree of convertibility. Thus potential energy, kinetic energy, electrical energy, surface energy, etc., belong to the category of work.

4.1.5 EQUILIBRIUM ENERGY FUNCTIONS

Consider the change of entropy of a system that is isolated and cannot exchange heat or work with the surroundings. Not being able to exchange work means a constant volume, $dV = 0$. Following from the further restriction of no heat exchange, the first law requires no change of internal energy, $dU = 0$. By the second law, there can be no entropy change due to heat exchange with the surroundings. But entropy can increase due to irreversible processes within the system,

$$(dS > 0)_{U,V} \quad (4.52)$$

The increase persists as long as irreversible processes take place until entropy reaches a maximum

$$(dS = 0)_{U,V} \quad (4.53)$$

and the system attains an equilibrium state. Equilibrium criteria are described in the following subsections.

4.1.5.1 Equilibrium Criterion I

At fixed U and V , a system seeks equilibrium by increasing its entropy until equilibrium is attained as S attains a maximum.

Figure 4.1 shows an S - V - U space. The equilibrium states are represented by a surface in this space. The space on the concave side of the equilibrium surface is taken up by nonequilibrium

Subsequent to landing on the equilibrium surface, movement on the surface is achieved by varying S or V , or both, according to Equation (4.54) with the equal sign,

$$dU = T dS - p dV \quad (4.57)$$

The coefficients of the differentials of the independent variables are given by the geometry of the $U(S,V)$ surface. Thus

$$T = (\partial U / \partial S)_v \quad (4.58)$$

and

$$p = -(\partial U / \partial V)_s \quad (4.59)$$

where S and V are used as state variables to describe a process, and U is the state function that expresses the changes in the system in a most useful way. To illustrate, the work that can be extracted from a fluid will be found for a reversible adiabatic nonflow process. The differential work done by a fluid in a nonflow process is given by

$$-\delta W = p dV \quad (4.60)$$

In a reversible adiabatic process, $\delta Q = 0$ and $dS = 0$; the process is isentropic. Comparison with Equation (4.57) shows

$$(\delta U = dW)_s \quad (4.61)$$

Integration gives

$$(-\Delta U = -W)_s \quad (4.62)$$

The decrease in U is the measure of reversible nonflow work that can be extracted from a fluid upon isentropic expansion. The state function U , upon being measured or calculated for various states, becomes useful for engineering design of work-production processes that expand the fluid from one state to another that are tabulated or calculated.

Equation (4.57) indicates the fundamental differential relation of equilibrium U to the variables S and V . The simplicity and directness of the relation indicate that U is best suited for the exploration of phenomena expressed in the independent variables $[S,V]$. Equilibrium U is said to be the natural, or canonical, energy function of its natural variables S and V . We set out to find energy functions that are natural to other variables. The variables of greatest general usefulness are the sets $[S,V]$, $[S,P]$, $[T,V]$, and $[T,p]$. Having had the fundamental differential equation and natural energy function for the first set of variables $[S,V]$, our method is to change variables one at a time, starting from the known, to successively find new ones.

Switching to the variables $[S,P]$, we find enthalpy to be just the natural energy function. Enthalpy has been defined in Equation (4.19) as

$$H = U + pV \quad (4.63)$$

The differential of H is

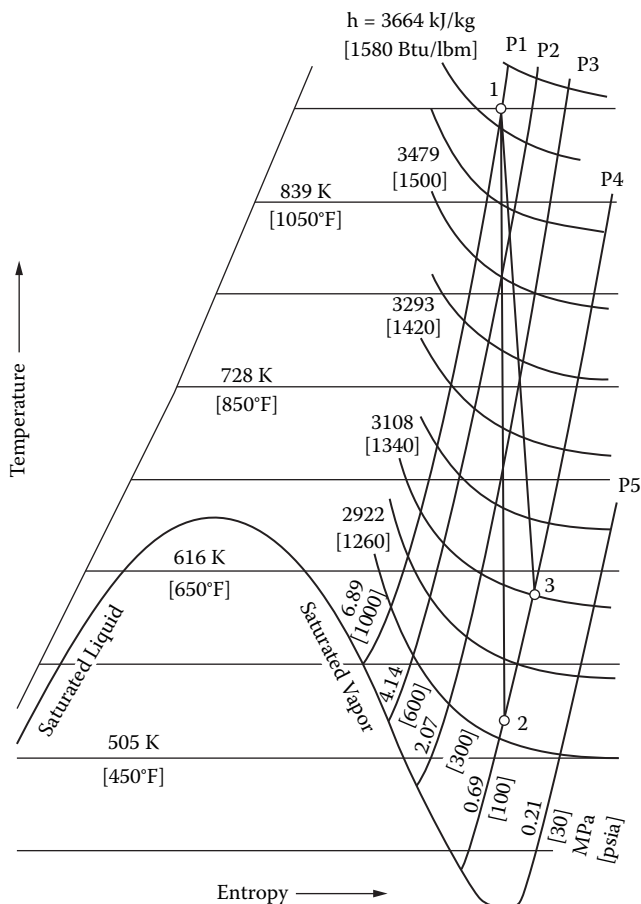


FIGURE 4.2 T-S chart for steam. (From Keenan, J. H., Keyes, F. G., Hill, P. G., and Moore, J. G. *Steam Table, Thermodynamic Properties of Water, Including Vapor, Liquid, and Solid Phases*. New York: John Wiley, 1969. With permission.)

$$(-\Delta H = -W)_s \quad (4.72)$$

The decrease of enthalpy is the measure of reversible work that can be extracted from a flowing fluid upon expansion.

Example 4.5: Work of Expansion of Steam

Steam at 6.89 MPa and 849° (1150°F) is expanded adiabatically to 0.69 MPa in a turbine. How much reversible flow work can be extracted from 1 kg of steam?

Solution

The reversible adiabatic flow work done by the steam is given by $(H_1 - H_2)$. From Figure 4.2, $H_1 = 3687$ kJ/kg and $H_2 = 2961$ kJ/kg. Therefore, $-W = 3687 - 2961 = 726$ kJ/kg.

If the expansion is adiabatic and irreversible, entropy increases during the expansion. Point 3 shows a possible final state. The enthalpy of the final state would be greater than the H_2 given above, and the work produced, being equal to the decrease in H , would be reduced.

Example 4.6: Enthalpy as a Measure of Heat Effect

Enthalpy is useful as a measure of the heat effect of constant-pressure processes. By the first law, $dU = \delta q - p dV$ when pV work is the only work term. At a condition of constant pressure, $p dV =$

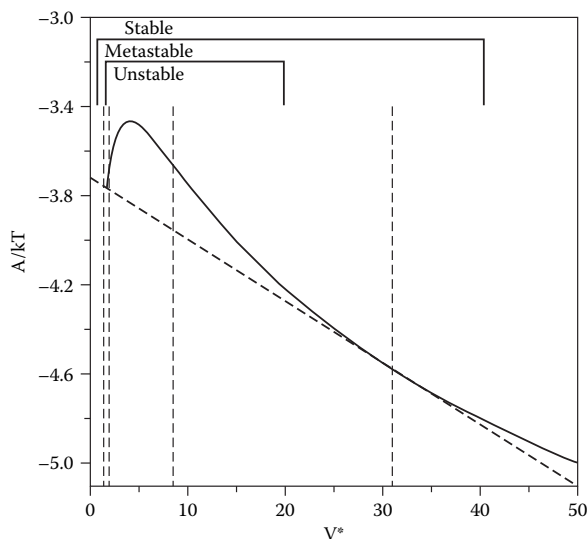


FIGURE 4.3 Helmholtz energy of the Lennard-Jones fluid at a condensation temperature $T^* = 1$ (From Watson, B. S., and Chao, K. C. *J. Chem. Phys.* 96: 9046, 1992. With permission.).

Figure 4.3 shows the molar Helmholtz energy of a fluid at a constant T in the condensation range. The curve represents the A of equilibrium states as a function of volume. A point above the curve represents a nonequilibrium state. The natural tendency is for the point to move down until it settles on the curve.

Example 4.7: Mechanical Instability

An equilibrium state of a homogeneous phase system is not stable if its Helmholtz energy is lowered by separating into two equilibrium phases of different densities. Thus in Figure 4.3 the equilibrium state at point a splits into two phases d and e , the saturation states. Points b and c show a possible intermediate state in separation. Line $d-e$ is tangent to the equilibrium curve at both d and e . The Helmholtz energy reaches a minimum at point f on the line $d-e$ at the conclusion of the separation. The slope of the tangent is the vapor pressure.

The Helmholtz energy isotherm of a sub-critical fluid is made up of five regions: (1) Unstable region in which

$$(\partial^2 A / \partial V^2)_T < 0 \quad (4.82)$$

Unstable states do not exist in practice. No homogeneous fluid phase can be found in this density range. (2) Meta-stable region—There are two meta stable regions, one on either side of the unstable region. The second derivative is greater than zero in the metastable region. The meta-stable region is bounded on one side by the spinodal point where the second derivative of A is zero, and by the saturation point on the other side. Because its equilibrium A stands above the common tangent $d-e$. A metastable state naturally decomposes into saturated states like d and e , but can be obtained experimentally with care to exclude nucleation. Super-heated liquid and super-saturated vapor are metastable. (3) Stable region—The second derivative of A with respect to v is positive in this region. There are two stable regions; each is bounded by a saturation point. Vapor phase exists at densities below the saturation value, and liquid at densities above.

Finally, we look for the natural energy function for the variables T and p . The Helmholtz energy of the natural variables T and V offers a starting point. We define the state function Gibbs free energy G by

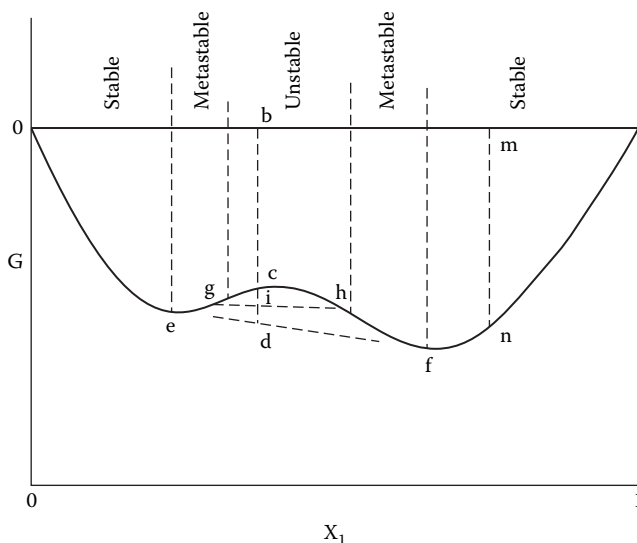


FIGURE 4.4 Gibbs energy of a partially miscible solution at a constant $[T, p]$.

should a small difference in composition develop in any small part of the fluid due to molecular diffusional fluctuation, the difference will be promoted by a decrease in G . The difference grows, and two parts of the solution will be formed to become more and more different until they eventually separate into two phases e and f . Points g and h show an intermediate stage of the separation process. The Gibbs energies of g and h add up to a total G of the system at i , which is lowered from c . The separated phases come to a stop at e and f , yielding a minimal total G at d . Points e and f are the two immiscible mixtures at equilibrium.

The sufficient condition of diffusional instability is

$$(\partial^2 G / \partial x^2)_{T,p} < 0 \quad (4.91)$$

The equation applies to the equilibrium states in the unstable region of x . To the outside of e and f , we find the stable states for which the second derivative of G with respect to x is greater than 0. The states between the unstable region and e or f , despite having a positive value for the second derivative of G with respect to x , seek to decompose into the two phases at e and f to lower their Gibbs energy. These states are metastable.

The state variables T and p are particularly suited for systems at heterogeneous phase equilibrium because equilibrium phases coexist at uniform T and p . As the natural energy function of $[T, p]$, the Gibbs energy and derived functions will be used to describe phase equilibrium.

The state functions U , H , A , and G are called energy functions. Each is associated with a pair of natural variables. To map the energy functions of a substance over a range of states by experimental measurement, by correlation of data, or by theoretical calculations, it is advantageous to develop *one* energy function as a function of its natural variables. Then all other energy functions can be obtained by elementary mathematical operations. The procedure is illustrated in the following, with Helmholtz free energy A having been worked out as a function of $[T, V]$. From the defining differential equation of A , Equation (4.79), the partial derivatives have been identified in Equation (4.80) and Equation (4.81): $S = -(\partial A / \partial T)_V$, $p = -(\partial A / \partial V)_T$. Substitution in the defining equations of the energy functions leads successively to

$$G = A + pV = A[T, V] - V(\partial A / \partial V)_T \quad (4.92)$$

Differentiation of Equation (4.101) and combination with Equation (4.99) gives

$$dU = T dS - p dV + \sum_i \mu_i dn_i \quad (4.102)$$

$$dH = T dS + V dp + \sum_i \mu_i dn_i \quad (4.103)$$

$$dA = -S dT - p dV + \sum_i \mu_i dn_i \quad (4.104)$$

$$dG = -S dT + V dp + \sum_i \mu_i dn_i \quad (4.105)$$

These four equations complete the Gibbs fundamental forms. It follows from these equations that μ_i is also the partial mole number derivative of U , H , or A in addition to that of G ,

$$\mu_i = (\partial U / \partial n_i)_{S,V,n_j} = (\partial H / \partial n_i)_{S,p,n_j} = (\partial A / \partial n_i)_{T,V,n_j} \quad (4.106)$$

However, the partial differentiations here are not at constant T and p ; consequently, μ_i is not partial molar U , nor partial molar H , nor partial molar A . The conditions of the partial differentiation for U and H cannot be physically interpreted, making the partial derivatives of U and H of little interest for the description of real systems. But the partial differentiation of A is at a physically meaningful condition that makes the partial derivative useful for the calculation of chemical potential.

Chemical potential plays a fundamental role in phase and chemical equilibria. Consider a heterogeneous system at a constant T and p consisting of a number of phases that are open and are at equilibrium with respect to one another. The chemical potential, like any intensive property, must assume a uniform value in any phase because each phase is at equilibrium. The chemical potential is the same value in different phases at equilibrium, so that diffusional mass transfer does not take place between the phases. Consider the transport of dn_i , moles of i from phase α of higher μ_i to phase β of lower μ_i . The change of G is

$$dG = [(\partial G_\beta / \partial n_i)_{T,p,n_j} - (\partial G_\alpha / \partial n_i)_{T,p,n_j}] dn_i \quad (4.107)$$

$$= [\mu_{\beta,i} - \mu_{\alpha,i}] dn_i \quad (4.108)$$

showing that $dG < 0$. By equilibrium criterion V, a system at constant T and p seeks equilibrium by decreasing G . Mass transfer then occurs, and the system is not at equilibrium. For the phases to be at equilibrium, $dG = 0$, it is necessary that $\mu_{\alpha,i} = \mu_{\beta,i}$. Therefore, the condition of phase equilibrium is expressed by

$$T_\alpha = T_\beta = \dots \quad \text{for all phases} \quad (4.109)$$

$$p_\alpha = p_\beta = \dots \quad \text{for all phases} \quad (4.110)$$

$$\sum_i \mu_i \nu_i = 0 \quad (4.119)$$

Hence the sum of chemical potentials of the reactants must balance the sum of the products.

By considering the reaction system at constant T and p , and equilibrium criterion V, $dG = 0$, one arrives at the same conclusion that Equation (4.119) is the condition of chemical reaction equilibrium.

Equation (4.119) is the fundamental equation of chemical equilibrium. To make progress toward a useful description of chemical equilibrium, efforts are required in two stages:

1. Replace chemical potential with fugacity and find out how fugacity depends on the species and the state of the mixture. This is the subject of Sections 4.2 and 4.3.
2. Search for the state at which the fugacities satisfy the criterion of chemical equilibrium while meeting the specified conditions of temperature, pressure, moles, enthalpy, or other factors. This is the subject of Section 4.5.

4.1.7 PARTIAL MOLAR QUANTITIES AND THE GIBBS-DUHEM RELATION

The fundamental differential form for Gibbs energy can be integrated to express Gibbs energy as a sum of contributions by the components. From Equation (4.99),

$$dG = -SdT + Vdp + \sum_i (\partial G / \partial n_i)_{T,p,n_j} dn_i \quad (4.120)$$

upon integration at constant T , p , and composition, and thus constant μ_i ,

$$G = \sum_i (\partial G / \partial n_i)_{T,p,n_j} n_i = \sum_i \mu_i n_i \quad (4.121)$$

By Equation (4.121), the partial molar Gibbs energy of component i represents the contribution of i to the total Gibbs energy of the mixture.

An extensive property Y in general can be similarly represented in terms of contributions by the components. Let Y be a state function of T , p , and the mole numbers n_i : $Y(T, p, n_1, n_2, \dots)$, where n_i denotes a mole number. The differential of Y at constant p is

$$dY = \sum_i (\partial Y / \partial n_i)_{T,p,n_j} dn_i \quad (4.122)$$

This equation is integrated at constant T , p , and composition, and thus at constant $(\partial Y / \partial n_i)_{T,p,n_j}$, in a homogeneous phase to give

$$Y = \sum_i (\partial Y / \partial n_i)_{T,p,n_j} n_i = \sum_i Y_i n_i \quad (4.123)$$

where $Y_i = (\partial Y / \partial n_i)_{T,p,n_j}$ stands for the partial molar Y of i in a homogeneous phase. Thus, for a phase,

$$\sum_i n_i dH_i = 0 \quad (4.133)$$

The method of derivation for H is generally useful for extensive properties to relate the effect of intensive properties on partial molar properties.

Example 4.9: Heat Generated by Adding a Stream to a Tank

In a batch-feed operation, 100 mol of pure liquid is added at the rate of 2 mol/min to a tank of liquid solution initially containing 100 mol of pure A. The tank is stirred, and its contents are assumed to be thoroughly mixed and uniform in composition at all times. The tank is jacketed to provide for heat removal to keep the tank contents at a constant temperature of 300°K. The pressure is constant at 1 atm.

Find the rate of evolution of heat of dilution as a function of time from $t = 0$ to $t = 50$ min in units of kJ/min. Find the total heat evolved.

Given:

Partial Molar Enthalpy at 300

Mol % of	H_B , kJ/mol
0	-6,240
10	-17,556
20	-25,916
30	-31,768
40	-38,038
50	-43,890
60	-46,816
100	-56,430

No information is given about the partial enthalpy of A.

Solution

For the mixing process at constant pressure, the heat release is equal to the decrease in enthalpy upon mixing according to Example I.E-2. We need to find the enthalpy change of mixing. For the addition of dn moles of into the body of mixture containing n_A moles of A and n_B moles of B, the initial state enthalpy is

$$H_i = (n_A H_A + n_B H_B) + H_B^0 dn_B$$

where the superscript 0 denotes pure liquid and subscripts A or B denote a partial molar quantity of A or B, respectively. The final state enthalpy is

$$H_f = (n_A H_A + n_B H_B) + d(n_A H_A + n_B H_B)$$

The differential change of enthalpy upon mixing is

$$\begin{aligned} dH &= H_f - H_i = d(n_A H_A + n_B H_B) - H_B^0 dn_B \\ &= (H_A dn_A + n_A dH_A + n_B dH_B + H_B dn_B) - H_B^0 dn_B \end{aligned}$$

Thus the integral is verified to agree with the total enthalpy calculation. Although only H_B is used in the integral method of calculation, information about H_A and the molar of the mixture are implied in H_B and can be explicitly revealed by integrating H_B to yield H_A , and subsequently adding the two partials to obtain the molar of the mixture.

For 1 mole of a binary mixture, in general, by the Gibbs-Duhem equation at constant and p ,

$$x_A dH_A + x_B dH_B = 0$$

Transporting the second term to the other side and integrating,

$$H_A - H_A^0 = - \int_0^1 (x_B / x_A)(dH_B / dx_B) dx_B$$

Having found H_A , the total mixture is obtained by summing,

$$= x_A H_A + x_B H_B$$

The enthalpy of the mixture becomes completely known as soon as the partial molar enthalpy of one component is determined.

4.2 VOLUMETRIC AND THERMODYNAMIC PROPERTIES

4.2.1 PRESSURE–VOLUME–TEMPERATURE RELATIONSHIP

A substance can exist as a gas, liquid, or solid. The gas state exists at low pressure. Within a range of temperature, depending on the substance, as the pressure is increased at a constant temperature, the gas condenses into a liquid. At temperatures above the range, the gas stays unchanged in phase state to very high pressures. At temperatures below the range, the gas condenses upon compression directly into a solid.

Figure 4.5 shows the pressure variation with volume at various constant temperatures for a typical substance. The isotherms are ordered: the higher the temperature, the higher is the isotherm; the isotherms do not intersect. At T_1 , the highest temperature shown, the substance is a gas at all pressures, and the ideal-gas law is often a good approximation. This isotherm approximates a hyperbola.

At a lower temperature T_2 , the gas state exists at low pressures. As the pressure is increased to point 5 in Figure 4.5, the vapor becomes saturated and begins to condense. With further reduction of volume, more condensation occurs while the pressure stays unchanged. The intensive properties of the vapor and liquid phases remain constant until condensation is complete at point 6. At higher pressures, a compressed liquid is found that changes volume only slightly upon further compression.

At temperature T_3 lower than T_2 , the low-pressure gas becomes condensed as it is compressed, just like at T_2 . Upon being sufficiently compressed, the liquid begins to solidify at point 9. The pressure stays constant as volume is reduced while solidification progresses along the line segment 9 to 10 until solidification is complete at point 10. Only solid exists at higher pressure in the p – V space beyond the line f–g–h.

At temperature T_4 lower than T_3 , the low-pressure gas condenses directly into a solid at a usually low pressure called the *sublimation pressure*. The condensation proceeds as volume is reduced at constant pressure until the condensation is complete at point 12. Further reduction of volume of the solid requires application of high pressure. The gas states are found in the area marked G, generally at low pressure and high temperature. Liquids are found in the area marked L, and solid states in S.

Below the critical temperature, the liquid state and gas state are clearly separated in the L+G region. The transition from one state to the other must go through a phase change, but at temperature above the critical, only one fluid state exists. A gas can become a liquid without going through a phase transition when heated to a supercritical temperature, compressed, and cooled to a subcritical temperature. Conversely, a liquid can become a gas without going through a phase change by following the reverse route. The solid state separates from the fluid states, either gas or liquid, by a phase transition. The solidification line f-g-h extends to the highest pressure that has been observed.

For a state to be mechanically stable, by Equation (4.82),

$$\left(\frac{\partial^2 A}{\partial V^2} \right)_T \geq 0 \quad (4.136)$$

By Equation (4.79), $dA = -SdT - pdV$. The coefficient of the last differential in this equation is identified as

$$\left(\frac{\partial A}{\partial V} \right)_T = -p \quad (4.137)$$

Differentiating with respect to V ,

$$\left(\frac{\partial^2 A}{\partial V^2} \right)_T = - \left(\frac{\partial p}{\partial V} \right)_T \quad (4.138)$$

Comparing Equation (4.127) and Equation (4.138) shows that mechanical stability requires

$$\left(\frac{\partial p}{\partial V} \right)_T \leq 0 \quad (4.139)$$

The isotherms must have a negative or zero slope. In Figure 4.5 the slope is negative for single-phase states and zero for the two-phase states.

Figure 4.6 shows the pVT relationship in the pT plane with lines of constant volume called isochores. The isochore v_1 is a high-density line; it starts from the two-phase coexistence line of the S+L regions to enter into the liquid region, rapidly gaining pressure as temperature is increased. The isochores v_2 and v_3 are at successively larger volume or lower density; both start from the two-phase coexistence line of L+G, which is the *vapor pressure curve*, to enter into the liquid region. The slope of the isochore drops successively from v_1 to v_3 . The isochores v_4 and v_5 , with successively larger volume and both being larger than the critical, likewise start from the L+G coexistence line, but go into the gas region. The isochore v_6 , starting from the two-phase line S+G, becomes a sublimed vapor as p and T increase; its volume is the largest shown.

Isochores with $v < v_c$ are above the L+G two-phase coexistence line; isochores with $v > v_c$ are below the line. The isochore with $v = v_c$ coincides with the L+G coexistence line over the entire range from the triple point t to the critical point c . Beyond the critical point it is a continuous extension of the coexistence line. The isochores are remarkable by their near linearity. The curvature, generally small, is the largest at states close to the two-phase line.

The S+G two-phase coexistence line, or the *sublimation pressure curve*, $f-t$, starts from the triple-point t to proceed downward toward the left. The S+L two-phase coexistence line, $t-h$, is the *melting point curve*. Typically the melting temperature is higher at elevated pressure, as shown in

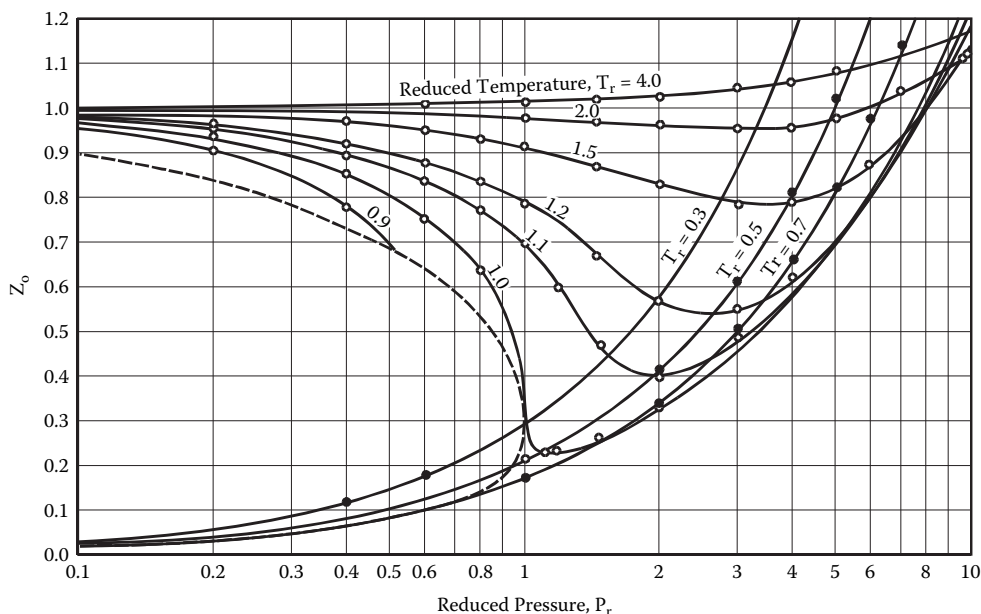


FIGURE 4.7 z_0 for simple fluids. (From Lee, B. I., and Kesler, M. *AIChE J.* 21: 510–527, 1975. With permission.)

decreases, the isotherms become lower. At the Boyle point, the isotherm becomes horizontal at $p_r = 0$, which defines the Boyle point. Below the Boyle point, the isotherms approach $p_r = 0$ with a negative slope. Until the temperature is lowered to $T_r = 1$, the isotherms are continuous from $p_r = 0$ to high pressure. Below $T_r = 1$, the isotherms extend smoothly from $p_r = 0$ only to the point of saturation of the vapor, where it descends vertically at a constant pressure until it reaches the saturated liquid state. Increase of pressure beyond the vapor pressure sends the isotherm up steadily due to the small compressibility of the liquid, eventually to large values of z .

To extend the PCS correlation to fluids other than the simple fluids, it is observed that deviation from the PCS correlation of the simple fluids occurs in a systematic way, depending on the shape, size, and chemical nature of the molecule. A prominent example is the reduced vapor pressure p_{rs} as a function of the reduced temperature T_r . Although it is almost exactly the same function for the three simple fluids, the reduced-vapor-pressure lines of other substances are lower with more elongated or more polar molecules. Pitzer and Brewer [1] adopt the lowering of the reduced-vapor-pressure curve of a substance from that of the simple fluids as the basis for defining a parameter to extend the PCS correlation to substances other than simple fluids. At the reduced temperature of 0.7, the reduced vapor pressure of simple fluids equals 0.1 and $-\log p_{rs} = 1$. Taking the difference at $T_r = 0.7$ between the $(-\log p_{rs})$ of a substance and that of the simple fluids, Pitzer and Brewer defined the acentric factor

$$\omega \equiv (-\log p_{rs}) - 1 \quad (4.143)$$

The minus value of $\log p_{rs}$ is used to make it a positive number. The lower the reduced-vapor-pressure curve of a substance, the larger is the positive value $-\log p_{rs}$ and, hence, the larger ω for the substance. The acentric factor is zero for the simple fluids and increases as the molecules are more nonspherical or more polar.

With the use of ω as the third parameter (in addition to T_c and p_c), the pVT relationship of nonpolar and weakly polar substances, called normal fluids, is correlated on the basis of PCS by extending the z correlation of simple fluids according to

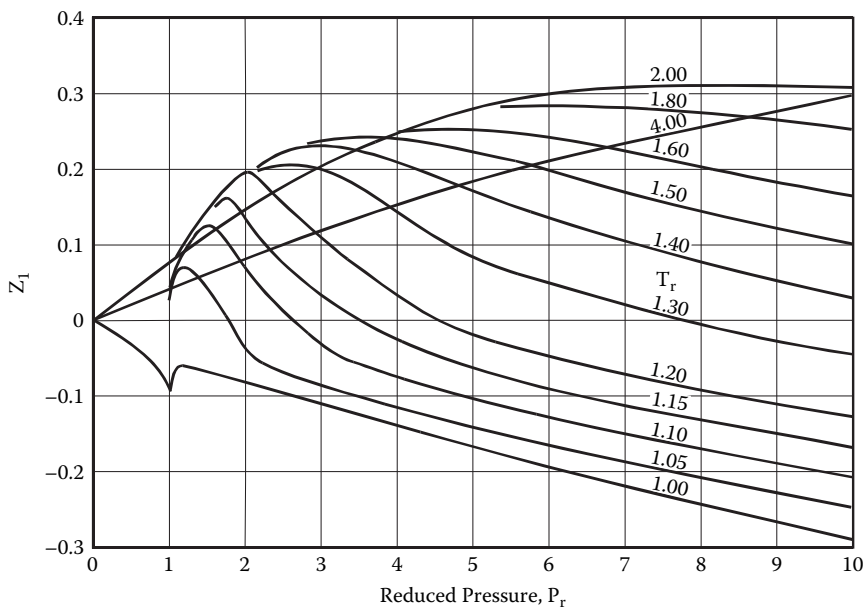


FIGURE 4.9 z_1 for normal fluids at $p_r > 1$. (From Lee, B. I., and Kesler, M. *AIChE J.* 21: 510–527, 1975. With permission..

$$v = zRT/p = (0.892)(82.0)(300)/68 = 323 \text{ cm}^3/\text{mol} = 20.2 \text{ cm}^3/\text{gm}$$

For methane, ω is small, and the correction from z_0 is small.

4.2.3 PHASE RULE

The phase rule due to J. Willard Gibbs gives the number of intensive variables that can be specified to completely fix the intensive state of a system at heterogeneous phase equilibrium. The number of intensive variables that can be specified is called the degree of freedom F . Experience tells us that for a given material existing as a one-phase gas, liquid, or solid, it requires two intensive variables to be specified, for example T and p , or T and ρ , to fix the intensive state of the system; thus $F = 2$. But for a pure substance, for instance steam and liquid water, to coexist in two equilibrium phases, only one intensive variable can be specified, for example T or p . By fixing the temperature, the pressure is fixed at the vapor pressure, and all intensive properties of the coexisting vapor or liquid, such as the density of the vapor, density of the liquid, etc., are all fixed; thus $F = 1$.

To find the degree of freedom in general for a system consisting of C components coexisting in P phases, Gibbs considered the conditions of the phases in coexistence, Equations (4.145) to (4.147). There are in total $(2 + C)(P - 1)$ equations. For each phase there are $2 + (C - 1)$ independent variables, e.g., p , and $(C - 1)$ compositions variables, adding up for the P phases to a total number of $P(2 + C - 1)$. How many independent variables can be specified for the equations to have a solution? The answer is: the number of variables minus the number of equations,

$$F = P(2 + C - 1) - (2 + C)(P - 1) \quad (4.145)$$

or

$$F = C - P + 2 \quad (4.146)$$

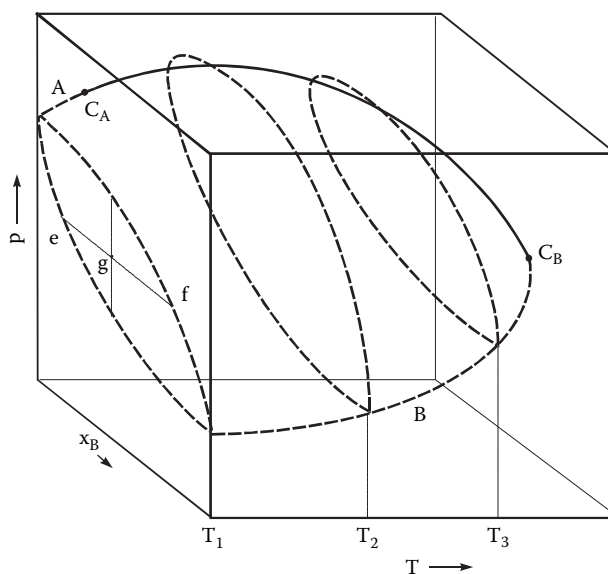


FIGURE 4.10 Gas-liquid equilibria of a binary system.

up of a phase at e and another phase at f , both phases being at different compositions. The total composition of the two phases is represented by g .

More than one phase border loop exists at one temperature for some mixtures of components of greater disparity. Figure 4.11 shows the isothermal gle of *n*-heptane + ethanol at 313° and 333°K. Two connected loops occur at each temperature. Both branches of the lower curves are dew-point states; the upper curve, bubble-point states. The dew state and bubble state on the same branch of the saturation loop and at the same T and p are at phase equilibrium. To illustrate, two phases are at equilibrium at 313°K and 20 kPa and also at 333° and 50 kPa. All four pairs are shown with dashed line segments.

At the connection point of the two saturation loops, the gas and the liquid at equilibrium are of the same composition but different densities. The mixture of equal gas and liquid composition is called an azeotrope. The azeotrope composition changes with p and T . It is a minimum boiling azeotrope when boiling occurs at a temperature less than those of the two components. Maximum boiling azeotropes are also found, though not as often.

To examine gle at elevated pressures we return to Figure 4.10. At T_1 , which is below the critical temperature of both A and B, the bubble- and dew-point curves both start at the low-pressure end at the vapor pressure of B, which is the less volatile component. At higher pressure, the two curves diverge and finally both end at the vapor pressure of A, the more volatile component. At T_2 , which is between the critical temperatures of A and B, the bubble- and dew-point curves at the low-pressure end still start at the vapor pressure of B, but at the higher-pressure side they meet at the mixture critical state. The critical points of mixtures of varying composition form the *mixture critical loci*, a space curve that connects the critical states of A and B.

Unusual behavior is observed even for simple mixtures in the near critical region. Depending on the relative location of the critical state, the vaporization-condensation process in the near critical region known as *retrograde condensation* occurs, and two dew points are found on the constant-pressure line. Between the dew points is a point of maximum condensation. Thus heating the fluid causes a liquid to appear, to increase to a maximum, then to decrease, and finally to disappear. Cooling the fluid along the same line produces the opposite sequence of events. The phenomenon is also often observed upon expanding or compressing the fluid at a constant temperature; it is called *retrograde condensation of the first kind*. In contrast, *retrograde condensation of the second*

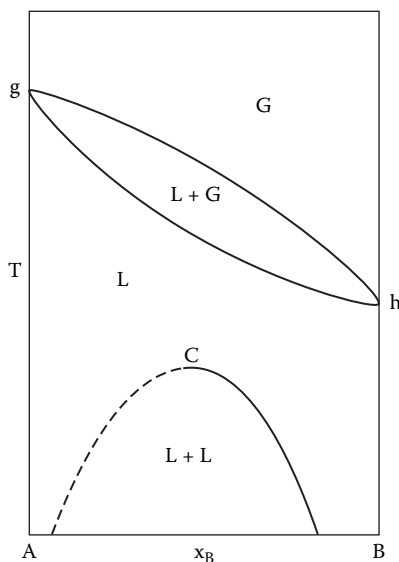


FIGURE 4.12 T-X diagram of an lle and gle system at a low pressure.

L+L area at P_2 is evolved from the L_A+L_B area at P_1 . While the L+G areas and the L+L area are contiguous in P_1 , the L+G and L+L areas are separated at P_2 . Since the L+G area at P_2 touches both coordinates $x = 0$ and $x = 1$, P_2 is below the critical pressures of both A and B. At P_2 , T_g is the boiling point of A and T_h is that of B. A liquid-liquid critical point appears at P_2 , located at the peak of the L+L region. Since the two-phase region is located below it, this critical temperature is called an upper critical solution temperature, UCST. This temperature changes with T , p , and x to form a curve similar to the gl critical loci. The vapor pressure curves of A and B are similar to the gl critical loci. These curves terminate at the critical points at high p and T ; the gle space is bounded by the critical loci. For some systems, even solidification of the heavier component occurs. As an example, Figure 4.13 shows such solidification and the formation of a quaternary point for mixtures of methane and n-heptane at high pressures.

4.2.4.3 Gas-Gas Equilibrium

Gas-gas equilibrium refers to the fluid-phase equilibrium that exists at high temperature and very high pressures above the critical points of the components and that persists to ever higher temperature and pressure apparently without limit. The occurrence of gge in mixtures follows the breakup of the gle critical locus and the merging of one branch of the broken gle critical loci with the UCST. The other branch of the critical locus, unhinged from the critical point of the light component, becomes free to move up to ever higher temperature and pressure. As an example, helium-nitrogen mixtures show such behavior. These are two branches of the saturation loop that intersect on the vapor-pressure curve of nitrogen. Above the T_c of helium, there is no intersection on the other composition axis. At a higher temperature T_2 , the loop develops a pinch, indicating a maximum mutual solubility at the pinch pressure. The pinch tightens with increasing temperature until at T_3 the pinch is complete, and the saturation loop divides into two branches with a critical state located on each. The locus of critical states at the lower branches is connected to the critical point of nitrogen. The upper branch with its critical state proceeds to ever higher temperatures. The saturation loops of the upper branch are all open-ended at the top and remain open to the highest pressures explored. The openness is displayed by many systems of weak interaction between the unlike components, notably water + hydrocarbons.

$$p = \frac{RT}{v - b} - \frac{a}{v^2} \quad (4.148)$$

Pressure is expressed as the difference between a repulsive pressure (the first term on the right-hand side) and an attractive pressure (the second term). The repulsive pressure is due to the forces of molecules that resist overlapping of volumes of different molecules. The volume open and free for molecular motion, called free volume, is reduced from the bulk fluid volume. In the vdW eos, the free volume is expressed by $(v - b)$, where b is the "excluded volume" representing the volume that is unavailable to molecular motion due to the molecular hard cores. For the collision between two molecules assumed to be spherical, the excluded volume is a sphere at the center of either of the colliding molecules and of a radius equal to the sum of the radii of both molecules in contact, i.e., the diameter of the molecules D . There being only one excluded spherical volume for each two molecules in collision, the total excluded volume of a fluid of N molecules is $(N/2)(4/3)(\pi D)^3$. The volume of the hard cores of the molecules v_b is $N(4/3)\pi R^3$, where R is the radius of a molecule. Therefore, the excluded volume is four times the hard core volume of the molecules:

$$b = 4v_b \quad (4.149)$$

In the vdW eos, the excluded volume is a constant independent of density. Taking out the excluded volume as being unavailable for molecular motion, the volume in the ideal-gas equation is replaced by the free volume to form the repulsive pressure $RT/(v - b)$ of Equation (4.148). The attractive pressure $-a/v^2$ in the vdW eos arises from the attraction between molecules in proximity. Since the frequency of encounter of molecules in pairs is proportional to the concentration of molecules squared, the attractive pressure is given by the inverse of the volume squared. The negative sign indicates that the attractive force contributes to a reduction of pressure.

In the vdW eos, two parameters a and b are specific for each substance. These are determined by fitting the equation to experimental data, including the critical state. Upon applying the critical conditions, Equation (4.134) and Equation (4.135), to the eos and solving for a and b from the two resulting equations, we obtain

$$a = 27R^2T_c^2 / (64p_c) \quad (4.150)$$

$$b = RT_c / (8p_c) \quad (4.151)$$

The vdW eos is reducible to a dimensionless form when Equation (4.150) and Equation (4.151) are substituted into Equation (4.149). The reduction gives

$$p_r = \frac{8T_r}{3v_r - 1} - \frac{3}{v_r^2} \quad (4.152)$$

The vdW eos is the first to describe the phenomena of condensation/vaporization, vapor pressure, and critical state. Although only qualitative, it often gives more reliable answers than many complex equations.

With mixtures, the parameters a and b need to represent the effect of molecular encounters, two molecules at a time. For pure fluids, encounters are between molecules of the same kind. In a mixture, the probability of finding a molecule i at a position is x_i ; the probability of finding a molecule j at the proximity is x_j . The probability of finding both i and j in the proximity is the product of the two independent probabilities, $x_i x_j$, assuming no correlation. This is the probability

The fundamental assumption of the vdW eos is that the intermolecular force is separated into repulsive and attractive pressures. The separate representation of the repulsive and attractive forces is maintained in the vdW-type eos and the perturbation equations, but is dropped in the virial equations and the extended virial equations.

Redlich and Kwong (RK) [6] changed the vdW eos as follows:

$$p = \frac{RT}{v-b} - \frac{a}{T^{0.5}v(v+b)} \quad (4.159)$$

When the constants a and b are fitted to the critical temperature and pressure, they are given by

$$a = 0.42747R \ 2T_c^{2.5} / p_c \quad (4.160)$$

$$b = 0.08664 RT_c / p_c \quad (4.161)$$

One change made by RK is to introduce the factor $1/T^{0.5}$ into the attractive pressure, in essence making the vdW attractive-pressure parameter α a decreasing function of temperature. The second change is to replace the v^2 with $v(v+b)$, opening the possibility of replacing v^2 with a second-degree polynomial of v . The repulsive pressure is left unchanged. Thus the RK equation gives improved representation of the gas state, including the second virial coefficient, the fugacity of vapors up to the vapor pressure, and fugacity of gases up to high pressures. But it is of no help for liquid states.

Wilson [7] correlated the vapor pressure of normal fluids to obtain a modified RK eos as follows:

$$p = \frac{RT}{v-b} - \alpha \frac{a_c}{v(v+b)} \quad (4.162)$$

where a_c and b are constants determined at the critical state. The new factor is introduced as a function of reduced temperature,

$$\alpha = T_r[1 - (1.57 + 1.62\omega)(1/T_r - 1)] \quad (4.163)$$

where ω is Pitzer's acentric factor, as defined in Equation (4.143). Equation (4.163) is obtained by fitting α to vapor pressure of various substances at various temperatures and correlating the fitted values. Although Wilson's equation does not accurately fit vapor pressure, it is the key to the success of eos for the accurate representation of the chemical potential of liquids and, in consequence, other energy functions of liquids and vapor-liquid equilibrium.

Soave [8] retained the form of the Wilson eos, Equation (4.162), but developed a new function to fit vapor pressure,

$$\alpha = [1 + (0.480 + 1.574\omega - 0.176\omega^2)(1 - T_r^{0.5})]^2 \quad (4.164)$$

The equation, referred as the SRK eos, gives quantitative fitting of vapor pressure, good representation of the fugacity of liquid, and improved representation of the energy functions of liquid for normal fluids, although liquid density is not well represented. The equation was the first to be widely used for both the gas and liquid phases and, hence, for gas-liquid equilibrium in engineering calculations.

TABLE 4.1
PRSV Equation-of-State Parameters

	κ_1	ω	P_s % deviation
Inorganic			
Carbon dioxide	0.04285	0.225	0.544
Ammonia	0.001	0.2517	0.12
Water	-0.06635	0.3438	0.29
Hydrocarbons			
Methane	-0.00159	0.01045	0.458
Ethane	0.02669	0.09781	0.472
Propane	0.03136	0.15416	0.782
n-Butane	0.03443	0.20096	0.545
n-Pentane	0.03946	0.25143	0.783
n-Hexane	0.05104	0.30075	1.106
n-Heptane	0.04648	0.35022	0.885
n-Octane	0.04464	0.39822	0.546
n-Decane	0.0451	0.49052	0.99
Cyclonexane	0.07023	0.20877	0.363
Benzene	0.07019	0.20929	0.541
Toluene	0.03849	0.26323	0.363
Ethylbenzene	0.03994	0.3027	0.4
p-Xylene	0.01277	0.32141	0.584
Other organics			
Methanol	-0.16816	0.56533	0.915
Ethanol	-0.03374	0.64439	0.949
1-Propanol	0.21419	0.62013	0.196
Acetone	-0.00888	0.30667	0.435
Butanone	0.05717	0.18909	0.72
Dimethyl ether	0.05717	0.18909	0.72
Acetonitrile	-0.13991	0.3371	5.632
Acetic acid	-0.19724	0.4594	0.379
Furfural	-0.03471	0.39983	3.067

pressure, hard-sphere-chain pressure, pressures of fluids of various hard bodies, square-well attractive pressure, Lennard-Jones attractive pressure, intramolecular pressure, rotational pressure, association pressure, etc. The appropriate pressures are summed to form the equation of state of the fluid.

A commonly used reference fluid is the hard-sphere fluid expressed by the Carnahan-Starling (CS) equation of state:

$$z = \frac{1 + \eta + \eta^2 - \eta^3}{(1 - \eta)^3} \quad (4.172)$$

where z denotes the compressibility factor pV/RT ; $\eta = \pi\rho\sigma^3/6$ is a reduced dimensionless density, also referred to as the packing fraction, expressing the fraction of volume that is packed by the spheres; ρ is the density of molecules n/V ; and σ is the diameter of the hard sphere. This equation is based on the fluid structure derived from correlation theory and is verified by molecular simulation. It takes the place of the repulsive pressure $RT/(v - b)$ of the vdW eos, which is an oversimplification in counting excluded volume as due to all molecules in binary collisions. In

of Equation (4.172) in light of the increased degrees of freedom of the chain of spheres from that of the single sphere. Let the number of external degrees of freedom of a chain molecule be denoted by $3c$. These are transformed from the $3r$ degrees of translational motion of the r spheres that make up the chain. In general, $3c$ is smaller than $3r$ but larger than 3 and consists in the three translational modes and some rotational modes. Any vibrational modes are of high energy and independent of the density of the fluid; they are not included in the $3c$ degrees of external motion. The rotational modes are of lower energy. Though not fully free, some are density dependent. They need to be addressed in equations of state of polyatomic molecular fluids. Prigogine [16] expressed these rotational modes as equivalent translational degrees of freedom. Flory et al. [17] constructed a cell theory for the equivalent translational modes that is widely used in polymer equations of state and polymer solution theory. Beret and Prausnitz [14] and Donohue and Prausnitz [15] reinterpreted the terms in the numerator of the CS equation in light of the added equivalent translational degrees of freedom of the chain molecule. The result is the new terms in the numerator of Equation (4.178). These terms revert to their forms in Equation (4.172) upon setting $3c = 3$.

The attractive pressure of the chain-of-spheres model is the sum of the double-series attractive pressures of the c external degrees of freedom,

$$z = -c \sum_n \sum_m \frac{mA_{nm}}{\tilde{v}^m \tau^n} \quad (4.179)$$

where the reduced variables are $\tau = ckT/(q)$ and $\tilde{v} = v\sqrt{2}/(Nr\sigma^3)$ and the variable ε is the characteristic intermolecular potential energy of a molecule per unit surface area, εq is the surface area of a molecule, and q is the characteristic attractive energy of a molecule. The constants A_{nm} have been adjusted to fit data for alkanes.

The PHCT pressure is the sum of the hard-sphere-chain pressure of Equation (4.172) and the attractive pressure of the chain of spheres of Equation (4.179),

$$z_{\text{PHCT}} = z_{\text{R}} + z_{\text{att}} \quad (4.180)$$

Three adjustable parameters are specific for each substance: εq , $r\sigma^3$, and c . The parameters are fitted to pVT and vapor pressure data. The PHCT is applicable to a very wide domain: for simple molecules where $c \rightarrow 1$, it reduces to the perturbed Carnahan-Starling eos; at low density, it gives a reasonable second virial coefficient and approaches ideal gas at very low density; for high densities, PHCT is essentially equal to the Prigogine–Flory–Patterson theory of polymer liquids.

In the chain-of-rotators (COR) equation proposed by Chien, Greenkorn, and Chao [17], a chain molecule is modeled as joined spheres in which adjacent covalent bonds can rotate. Rotation takes place because the chain is not straight; any two adjacent bonds are joined at an angle like the radials from the center of a pyramid to the four corners. Chien et al. found the pressure of rotation by comparing the pressure of Boublik and Nezbeda's hard dumbbell fluid [18] with the pressure of Carnahan and Starling's hard spheres. The rotational pressure found is

$$z_{\text{rot}} = c \left(\frac{e-1}{2} \right) \left(\frac{3\eta + 3e\eta^2 - (e+1)\eta^3}{(1-\eta)^3} \right) \quad (4.181)$$

where η is a reduced density defined to be v_h/v , also referred to as the packing fraction; v_h is the hard core volume; c is the rotational degrees of freedom of a molecule; and e is the eccentricity parameter of the model dumbbell rotator, defined by

groups of the molecule. Once the group parameters are determined, properties of the molecular fluids can be calculated. Since many molecules are composed of a relatively small number of groups, the group contribution method can be used for many molecular fluids.

To make it suitable for group contribution, Pults et al. [19] simplified the COR eos by replacing the double-series attractive pressure with the Redlich-Kwong attractive pressure in Equation (4.159). The COR group contribution (CORGC) eos is

$$z = \frac{1 + \eta + \eta^2 - \eta^3}{(1 - \eta)^3} + c \left(\frac{e - 1}{2} \right) \left(\frac{3\eta + 3e\eta^2 - (e + 1)\eta^3}{(1 - \eta)^3} \right) - \frac{a(T)}{RT[v + b(T)]} \quad (4.184)$$

where y is the reduced density equal to $b(T)/(4v)$; $b(T)$ is the covolume, a function of T ; c is the degree of rotational freedom; e is a constant = 1.078; and $a(T)$ is a T -dependent attractive-pressure parameter.

The eos parameters a , b , and c are made up of group contributions according to the following equations:

$$a(T) = \sum_i^{N_c} \sum_j^{N_c} x_i x_j \sum_m^{N_i} \sum_n^{N_j} v_{im} v_{jn} q_m q_n q_{mn}(T) \quad (4.185)$$

$$b_i(T) = \sum_m^{N_i} v_{im} b_m(T) \quad (4.186)$$

$$b(T) = \sum_i^{N_c} x_i b_i(T) \quad (4.187)$$

$$c_i = \sum_m^{N_i} v_{im} c_m \quad (4.188)$$

$$c = \sum_i^{N_c} x_i c_i \quad (4.189)$$

In these equations, v_{im} is the number of groups m in molecule i . The index N_i is the number of group species in molecule i , and N_c represents the number of components in the mixture. The coordination number q_m is a normalized surface area of group m based on a value of $q_m = 10$ for methane.

Equation (4.185) combines the interactions of groups to give the total interaction of the fluid. It is a generalization of the van der Waals mixing rule to include groups (or atoms) as well as molecules as entities that interact. To count the interaction of groups is in accord with the nature of polyatomic molecules. Equations (4.185) to (4.189) are given in their general forms for pure fluids and mixtures. For pure fluids, set $i = j = 1$, $N_i = N_j = 1$, and $x_i = x_j = 1$. The equations simplify to van der Waals mixing rule for a mixture of monatomic molecules, with $v_{im} = 1$ for all i and all n .

Equation (4.186) sums up the excluded volume of the constituent groups to form the excluded volume of the molecule. The linear sum is justified because the excluded volume of a group is defined as $(4v_h)$, where v_h stands for the hard core volume. Equation (4.187) linearly combines the

To apply to high polymers, Sy-Siong-Kiao, Caruthers, and Chao [21] extend the COR eos to obtain the polymer chain-of-rotator (PCOR) equation,

$$\frac{pv_m}{RT} = c_m \left(\frac{e-1}{2} \right) \frac{3\eta + 3e\eta^2 - (e+1)\eta^3}{(1-\eta)^3} - \frac{a_{mm}}{RT(v_m + b_m)} \quad (4.192)$$

The equation addresses the molar volume of a segment of the polymer v_m , the subscript m indicating a segmental molar quantity. The parameters of the equation are segmental parameters: thus b_m is the excluded volume of a segment; $\eta = b_m/(4v_m)$ is the density of the fluid expressed in a reduced dimensionless form, also called the packing fraction; and a_{mm} is the attractive-pressure parameter of the segment. The eccentricity parameter of the rotators is e , equal to 1.078 for the model rotator. Results of data reduction indicate the attractive parameter a_{mm} to vary weakly and linearly with temperature,

$$a_m = a_{m0} + a_{m1}T \quad (4.193)$$

The parameter b_m does not change with temperature, being a constant value for each polymer. The temperature independence of b_m in the range of temperature of the data indicates low kinetic energy of the giant polymer molecules.

Comparing the PCOR with the COR eos, Equation (4.183), the translational pressure in the COR eos is missing in the PCOR eos. The long-chain polymer molecules are so entangled and entwined that the molecules make only translational rotations.

The PCOR eos describes only a liquid state. In agreement with experimental observation, a high polymer does not vaporize or exert a vapor pressure as pressure approaches zero. The equation does give an accurate quantitative representation of the pVT relationship of high-polymer melts. Average absolute deviation of the equation from the experimental specific volumes is 0.1% or less for the complete range of the experimental data covering a pressure range of 0 to 100 or 200 MPa for all polymers studied.

By generalizing Flory's dimer theory, Hall and coworkers [22, 23] obtained the GF-D equation of state, which is as follows:

$$Z_m = Z_1 + \frac{v_{e,m} - v_{e,1}}{v_{e,2} - v_{e,1}} (Z_2 - Z_1) \quad (4.194)$$

where the compressibility factor of the chain molecule is expressed as an extrapolation of the monomer and dimer values linearly with respect to the excluded volume. The chain molecule is modeled as an m -mer of tangential hard spheres with an attractive potential. The incremental compressibility factor with the addition of a sphere to the chain is a constant equal to the increment at the formation of the dimer from the monomer. The compressibility factor for the monomer or dimer fluid is given by

$$Z_i = Z_i^{rep} + Z_i^{att} \quad i = 1 \text{ or } 2 \quad (4.195)$$

For the hard core reference fluids, the following monomer and dimer equations apply:

$$Z_1^{rep} = \frac{1 + \eta + \eta^2 - \eta^3}{(1 - \eta)^3} \quad (4.196)$$

$$v^0 = v^{00} + 0.005T \quad (4.207)$$

$$\varepsilon / k = \varepsilon^0 / k - 0.004T \quad (4.208)$$

The temperature dependences of v^0 and ε/k do not apply to alkanols and water; these quantities are kept constant independent of T .

The statistical-associated fluid theory (SAFT) of Chapman et al. [25, 26] is based on the perturbation theory of Wertheim [27]. The model molecule is a chain of hard spheres that is perturbed with a dispersion attractive potential and association potential. The residual Helmholtz energy a^R of the fluid is given by the sum of the Helmholtz energies of: the initially free hard spheres; bonding the hard spheres to form a chain; the dispersion attractive potential; and the association potential,

$$a^R = a_{hs} + a_{chain} + a_{disp} + a_{assoc} \quad (4.209)$$

Wertheim found a_{chain} and a_{assoc} in his perturbation theory. Upon differentiating the Helmholtz energy with respect to volume, the equation of state is obtained,

$$z = z^{id} + z_{hs} + z_{chain} + z_{disp} + z_{assoc} \quad (4.210)$$

where the ideal-gas $z^{id} = 1$, and

$$z_{hs} = r \frac{4\eta - 2\eta^2}{(1 - \eta)^3} \quad (4.211)$$

$$z_{chain} = (1 - r) \frac{5\eta - 2\eta^2}{(1 - \eta)(2 - \eta)} \quad (4.212)$$

$$z_{disp} = r \sum_n \sum_m m D_{nm} \left(\frac{u}{kT} \right)^n \left(\frac{\eta}{\eta_{cp}} \right)^m \quad (4.213)$$

$$z_{assoc} = \rho \sum_S \left(\frac{1}{X^S} - \frac{1}{2} \right) \left(\frac{\partial X^S}{\partial \rho} \right) \quad (4.214)$$

where r is the number of spheres in a chain; η is the packing fraction $= r\rho_A(\pi/6)d^3$; ρ is the molar density of the chain molecules; d is the temperature-dependent diameter of the spheres given by Equation (4.176) in terms of the 0°K value σ , which is related to the eos parameter v_0 , the closest packed volume of the spheres at 0°K, $N_A\sigma^3 = \sqrt{2} v_0$; and $\eta_{cp} = \pi\sqrt{2}/6$. By Chen and Kreglewski, the energy well depth u is temperature dependent and is given by Equation (4.177).

Associating molecules are bonded at association sites. There can be a number of association sites on a molecule. In Equation (4.214), X^S denotes the mole fraction of site S that is not bonded and is given by

$$X^S = \left\{ 1 + N_A \sum_Y \rho X^Y \frac{2 - \eta}{2(1 - \eta)^3} \left[\exp \left(\frac{\varepsilon^{SY}}{kT} \right) - 1 \right] \right\}^{-1} \quad (4.215)$$

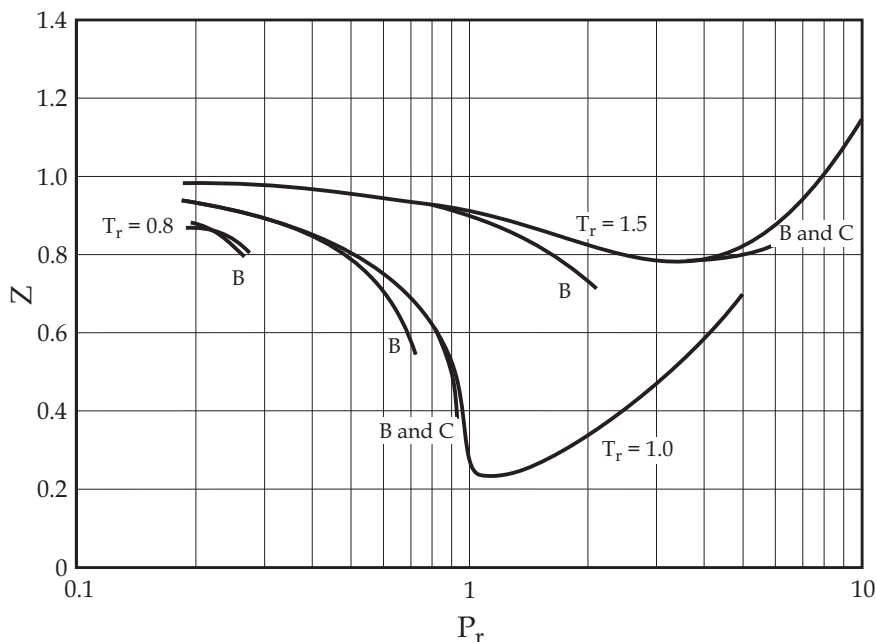


FIGURE 4.14 Comparison of virial equation with a generalized correlation.

the critical pressure. Enhanced by its simple form, and availability of the second virial coefficient, the B -virial equation is convenient and widely used for the vapor phase in low pressure and medium pressure vapor-liquid equilibrium work.

For vapor-liquid equilibrium calculations up to moderate pressures, the B equation is suitable and convenient for the vapor phase for its applicability and simple form. Formulas have been derived from statistical theory for the calculation of virial coefficients, including B , from intermolecular potential energy functions, but intermolecular energy functions are hardly known quantitatively for real molecules. B is found for practical calculations by correlating experimental B values. Pitzer [1] correlated B of normal fluids in a generalized form with acentric factor ω as the third parameter,

$$\frac{Bp_c}{RT_c} = B_0[T_r] + \omega B_1[T_r] \quad (4.219)$$

where $T_r \equiv T/T_c$ and where B_0 (of simple fluids) and B_1 generalize the correlation to normal fluids. Tsionopoulos [29] revised Pitzer's correlation and extended the correlation to polar and hydrogen-bonded fluids using B_0 and B_1 functions as follows:

$$\frac{Bp_c}{RT_c} = B_0[T_r] + \bar{\omega} B_1[T_r] + B_2[T_r] \quad (4.220)$$

$$B_0 = 0.1445 - 0.330/T_r - 0.1385/T_r^2 - 0.0121/T_r^3 - 0.000607/T_r^8 \quad (4.221)$$

$$B_1 = 0.0637 + 0.331/T_r^2 - 0.423/T_r^3 - 0.008/T_r^8 \quad (4.222)$$

$$p_{cij} = z_{cij} RT_{cij} / v_{cij} \quad (4.233)$$

For the polar and hydrogen-bond interaction terms, the following rules are suggested: polar-polar interaction can be approximated with the geometric mean; two hydrogen bonds interact with full force; hydrogen bond interacts with dipoles with reduced force; and nonpolar molecules do not interact with poles or hydrogen bonds.

4.2.5.4 Extended Virial Equations

The extended virial equations are made up of a truncated virial series followed by a closure term or terms. In the Benedict-Webb-Rubin (BWR) Equation (4.177), the closure term is an exponential,

$$P = RT\rho + (B_0RT - A_0 - C_0/T^2)\rho^2 + (bRT - a)\rho^3 + \alpha a\rho^6 + c\rho^3(1 + \gamma\rho^2)(1/T^2)\exp(-\gamma\rho^2) \quad (4.234)$$

The eight constants required have been reported for numerous hydrocarbons.

The Lee-Kesler eos [2] is an extended BWR equation in reduced variables, as follows:

$$z = 1 + \frac{B}{v_r} + \frac{C}{v_r^2} + \frac{D}{v_r^5} + \left(\frac{c_4}{T_r^3 v_r^2} \right) (\beta + \tilde{a}/v_r^2) \exp(-\tilde{a}/v_r^2) \quad (4.235)$$

$$B = b_1 - \frac{b_2}{T_r} - \frac{b_3}{T_r^2} - \frac{b_4}{T_r^3} \quad (4.236)$$

$$C = c_1 - \frac{c_2}{T_r} + \frac{c_3}{T_r^3} \quad (4.237)$$

$$D = d_1 + \frac{d_2}{T_r} \quad (4.238)$$

where $v_r = p_c v / (RT_c)$ and $T_r = T/T_c$.

Using this equation, Lee and Kesler developed a generalized correlation of the pVT relationship of normal fluids in the following form:

$$z = z_0 + (\omega / \omega_r)(z_0 - z_r) \quad (4.239)$$

The subscript 0 denotes simple fluids with acentric factor $\omega = 0$, and subscript r denotes a reference fluid with acentric factor $\omega_r = 0.3978$ from its origin in *n*-octane. The Lee-Kesler equation constants for z_0 and z_r are presented in Table 4.4. The compressibility factors in Equation (4.239)— z , z_0 , z_r —are at the same $[T_r, p_r]$. This correlation is a three-parameter generalized correlation that improves the Pitzer correlation to a wider range of states. The lower temperature bound of the correlation is extended from $T_r = 0.8$ to 0.3.

Extended virial equations of many terms and constants have been developed for the highly accurate representation of experimental data. Some are developed specifically for standard tables of density and derived thermodynamic functions such as entropy and enthalpy. Bender [31] extended the virial equation to a 20-constant equation to represent argon, oxygen, methane, hydrogen, ethene,

$$H^* = H^*[T] \quad (4.244)$$

The ideal-gas enthalpy can be found in standard references for a large number of chemical substances.

Ideal-gas free energies A and G are, however, p or V dependent. Consider Helmholtz energy first. From the fundamental differential Equation (4.79),

$$dA = -SdT - pdV \quad (4.245)$$

At constant T , $dT = 0$, we substitute Equation (4.240) into Equation (4.245) and integrate from the volume V^0 at the standard pressure p^0 of either 1 atm or 1 bar to the system volume V ,

$$A^* - A_0 = nRT \ln(V_0/V) \quad (4.246)$$

Replacing the standard-state volume in Equation (4.246) with $(RT/1)$ we obtain

$$A^* = A^0 + nRT \ln \frac{RT}{V(1)} \quad (4.247)$$

The factor 1 standing for the standard pressure is often left out of the equation, but is kept here as a reminder that the units of the other factors in RT/V must be consistent with the units of the standard pressure. The ideal-gas A^0 or G^0 is tabulated in standard references.

To find the Gibbs energy of an ideal gas, start from the fundamental differential Equation (4.88):

$$dG = -SdT + Vdp \quad (4.248)$$

At constant T ($dT = 0$), substitute Equation (4.240) into Equation (4.248) and integrate from a standard pressure $p^0 = 1$ atm or 1 bar to p to obtain

$$G^* - G_0 = nRT \ln(p/p_0) \quad (4.249)$$

If pressure is in units of atmospheres or bars in Equation (4.249), to agree with the units of the standard state, p^0 can be omitted from the equation, leaving

$$G^* = G_0 + nRT \ln p \quad (4.250)$$

The ideal-gas standard-state G^0 can be looked up from standard references for a large number of substances.

To find the entropy of an ideal gas, we combine the enthalpy of Equation (4.244) with the Gibbs energy of Equation (4.250),

$$S^* = (H^* - G^*)/T \quad (4.251)$$

$$= S^0 - nR \ln p \quad (4.252)$$

To find the energy functions of ideal-gas mixtures, we start with the ideal-gas equation of state, Equation (4.240), recognizing that the number of moles n in the equation includes the moles of all species in the mixture, i.e., $n = n_1 + n_2 + \dots$. To show the mole numbers of the various species, we write the ideal-gas eos as follows:

The Helmholtz energy of an ideal-gas mixture is, following the principle of independent action,

$$a^*[T, p] = \sum y_i a_i^*[T, p_i] \quad (4.263)$$

It is often useful to relate the mixture a^* to the standard value a_i^0 of the components at the standard pressure of 1 atm or 1 bar so it can be looked up in standard references. By substituting $p_i = py_i$ and making use of Equation (4.247), we obtain

$$a_i^*[T, p_i] = a_i^0 + RT \ln y_i + RT \ln p \quad (4.264)$$

Substituting into Equation (4.263) gives

$$a^*[T, p] = \sum y_i a_i^0 + RT \sum y_i \ln y_i + RT \ln p \quad (4.265)$$

Relating the mixture to the pure components all at the same p , we rewrite Equation (4.265) as follows:

$$a^*[T, p] = \sum y_i a_i^*[T, p] + RT \sum y_i \ln y_i \quad (4.266)$$

The Gibbs energy of an ideal-gas mixture is obtained by adding RT to the Helmholtz energy equations. Employing standard values of the pure components and Equation (4.265),

$$g^*[T, p] = \sum y_i g_i^0 + RT \ln p + RT \sum y_i \ln y_i \quad (4.267)$$

To relate the mixture g to the pure-component values at the same pressure, we have from Equation (4.266)

$$g^*[T, p] = \sum y_i g_i^0[T, p] + RT \sum y_i \ln y_i \quad (4.268)$$

The entropy of an ideal-gas mixture is obtained by combining the internal energy of Equation (4.261) and the Helmholtz energy of Equation (4.265):

$$s^* = (u^* - a^*)/T \quad (4.269)$$

$$= \sum y_i s_i^0 - R \ln p - R \sum y_i \ln y_i \quad (4.270)$$

Equation (4.270) is rewritten upon referring to Equation (4.252) to relate the mixture entropy to the pure gases at the same pressure,

$$s^* = \sum y_i s_i^* - R \sum y_i \ln y_i \quad (4.271)$$

Example 4.11

Find the Helmholtz Energy of Peng-Robinson eos

Solution

The PR eos is Equation (4.165),

$$p = \frac{RT}{v-b} - \frac{\alpha a_c}{v(v+b) + b(v-b)} \quad (4.278)$$

where α is a function of T , and a_c and b are constants.

Substituting Equation (4.278) into Equation (4.275) and then integrating gives the residual Helmholtz energy by the PR eos,

$$a - a^* = RT \ln \frac{v}{v-b} + \frac{\alpha a_c}{2\sqrt{2}b} \ln \frac{v + (1-\sqrt{2})b}{v + (1+\sqrt{2})b} \quad (4.279)$$

Replacing a^* with a^0 by using Equation (4.276), we obtain the Helmholtz energy,

$$a = RT \ln \frac{RT}{v-b} + \frac{\alpha a_c}{2\sqrt{2}b} \ln \frac{v + (1-\sqrt{2})b}{v + (1+\sqrt{2})b} + a^0 \quad (4.280)$$

4.2.7.2 Gibbs Energy

To obtain Gibbs energy from eos, we begin by forming the residual function

$$g - g^* = (a - a^*) + pv - RT \quad (4.281)$$

Expressing $(a - a^*)$ in terms of an eos by Equation (4.275), we obtain

$$g - g^* = \int_{\infty}^v \left(-p + \frac{RT}{v} \right) dv + pv - RT \quad (4.282)$$

Using Equation (4.250) to replace g^* with g^0 ,

$$g = \int_{\infty}^v \left(-p + \frac{RT}{v} \right) dv + pv - RT + RT \ln + \frac{RT}{v} + g^0 \quad (4.283)$$

Example 4.12: Gibbs Energy by PR eos

The integral in Equation (4.282) for the PR eos will be taken from Equation (4.279). The pv term in Equation (4.282) will be formed by using the PR eos presented in Equation (4.278). It follows that

$$\begin{aligned} g - g^* = & RT \ln \frac{v}{v-b} + \frac{\alpha a_c}{2\sqrt{2}b} \ln \frac{v + (1-\sqrt{2})b}{v + (1+\sqrt{2})b} \\ & + \frac{RT_v}{v-b} - \frac{\alpha a_c v}{v(v+b) + b(v-b)} - RT \end{aligned} \quad (4.284)$$

$$\left(\frac{\partial p}{\partial T}\right)_v = \frac{R}{v-b} - \frac{a_c \alpha'}{v^2 + 2bv - b^2} \quad (4.292)$$

where α' stands for $\alpha d/dT$ obtained from Equation (4.162),

$$\alpha' = -2[1 + (0.37465 + 1.5422\omega - 0.26992\omega)(1 - T_r^{0.5})] \\ (0.37464 + 1.5422\omega - 0.26992\omega^2) / (T_r^{0.5} T_c) \quad (4.293)$$

Substituting p of Equation (4.159) and its derivative Equation (4.292) into Equation (4.291) and integrating, we obtain internal energy by PR eos,

$$u = \frac{a_c(\alpha - T\alpha')}{2\sqrt{2}b} \ln \frac{v + (1 - \sqrt{2})b}{v + (1 + \sqrt{2})b} + u^0 \quad (4.294)$$

The internal energy deviation from ideal gas ($u - u^0$) given in this equation is entirely due to the attractive-force term of the eos. The hard core makes no contribution to the internal energy, as the hard core pressure vanishes in the combination $T(\partial p/\partial T)_v - p$. The hard core in a van der Waals-type eos does not contribute to internal energy. However, in some van der Waals-type eos's, the hard core has a slight temperature dependence, and that does make a weak contribution to internal energy.

4.2.7.5 Enthalpy

To obtain enthalpy from eos we add pv to the internal energy. From Equation (4.290), we obtain the general formula for residual enthalpy from eos,

$$h - h^* = \int_{\infty}^v \left[T \left(\frac{\partial p}{\partial T} \right)_v - p \right] dv + pv - RT \quad (4.295)$$

For an ideal gas, enthalpy is independent of v but is a function of T only, and $h^* = h^0$. Equation (4.295) is rewritten to give h itself,

$$h = \int_{\infty}^v \left[T \left(\frac{\partial p}{\partial T} \right)_v - p \right] dv + pv - RT + h^0 \quad (4.296)$$

Example 4.14: Enthalpy by Peng-Robinson eos

By adding $(pv - RT)$ to Equation (4.294), we obtain enthalpy by PR eos,

$$h = \frac{a_c(\alpha - T\alpha')}{2\sqrt{2}b} \ln \frac{v + (1 - \sqrt{2})b}{v + (1 + \sqrt{2})b} + \frac{RTb}{v-b} - \frac{v\alpha a_c}{v^2 + 2bv - b^2} + h^0 \quad (4.297)$$

4.2.7.6 Some General Comments

The independent variables in the formulas for thermodynamic functions derived from eos are $[T, v]$. To use the formula for a state specified in $[T, p]$, the volume at the given state must first be found

The factor 1 in the equation is the standard-state pressure of 1 atm or 1 bar, and will be left out in subsequent equations for simplicity, with the understanding that f has the dimension of pressure in units of either atmospheres or bars, depending on the convention for g_i^0 . It follows from the two equations above that, for an ideal-gas mixture, $f_i = p_i$, reducing for a pure ideal gas to $f = p$.

Upon substitution of μ_i from the defining equation of fugacity, Equation (4.302), in the phase-equilibrium equation, Equation (4.111) et seq., canceling out g_i^0 and RT , and exponentiating, we obtain the fugacity equality condition of heterogeneous phase equilibrium,

$$f_{\alpha i} = f_{\beta i} \quad (4.303)$$

for all components i and all phases α and β . The fugacity of any component must assume the same value in all phases in a heterogeneous system at equilibrium. These equations will be used in calculations in place of the chemical potential equality conditions of Equation (4.111) et seq. in the following sections of this chapter.

Why is fugacity so convenient that it is to be used in place of chemical potential in calculations? The reasons are:

1. Fugacity is freed from the ideal-gas standard state g^0 . It is completely determined by the properties of the fluid at the temperature of interest.
2. Low-pressure gas states can be conveniently represented by f , for $f_i = p_i$, for an ideal gas. It follows for a real gas at a low or moderate pressure that $f_i \approx p_i$. The fugacity of a dilute component in a liquid is equal to the fugacity of the component at a small partial pressure in a gas mixture at equilibrium with the liquid, again $f_i \approx p_i$. Since the partial pressure of a gas is a well-behaved mathematical quantity, the fugacity is also well behaved at small partial pressures in a gas or at a small concentration in liquids. In contrast, for a dilute component, as its $p_i \rightarrow 0$ in an ideal-gas mixture, $\mu_i \rightarrow -\infty$ by Equation (4.301). It follows that $\mu_i \rightarrow -\infty$ for a dilute component in a real gas or in a liquid. The limit of $-\infty$ is ill-behaved and is avoided with the replacement of μ_i by f_i , which simply approaches zero.

To obtain a formula to calculate fugacity from an equation of state, we appeal to A , as its natural variables, T and V , are the independent variables of eos. We start with Equation (4.106) and carry out the indicated partial differentiation on Equation (4.276) to obtain

$$\mu_i = \int_{\infty}^v \left[\frac{RT}{v} - \left(\frac{\partial p}{\partial n_i} \right)_{T,V,n_j} \right] dv + RT \ln \frac{RT}{v} + RT \ln y_i + g_i^0 \quad (4.304)$$

Substitution of this μ_i into Equation (4.302) gives

$$RT \ln(f_i/1) = \int_{\infty}^v \left[\frac{RT}{v} - \left(\frac{\partial p}{\partial n_i} \right)_{T,V,n_j} \right] dv + RT \ln \frac{y_i RT}{v} \quad (4.305)$$

The ratio of fugacity to partial pressure, $f_i/(y_i p)$, called the *fugacity coefficient*, ϕ_i , is in common use as a measure of departure of a real fluid f_i from its ideal-gas value. For a pure fluid, the fugacity coefficient is simply $\phi \equiv f/p$. For an ideal-gas mixture, $\phi_i = 1$ for all i ; for a pure ideal gas, $\phi = 1$. For a real fluid, by rearranging Equation (4.305),

$$\ln \phi_k = \ln \frac{v}{v-b} + \frac{b_k}{v-b} - \frac{2 \sum_i y_i a_{ik}}{RTb} \ln \frac{v}{v-b} + \frac{ab_k}{RTb^2} \left(\ln \frac{v}{v+b} - \frac{v}{v+b} \right) - \ln z \quad (4.312)$$

REFERENCES

1. Pitzer, K. S., and Brewer, L. *Revision of Thermodynamics*, by G. N. Lewis and M. Randall. New York: McGraw-Hill, 1961.
2. Lee, B. I., and Kesler, M. *AIChE J.* 21: 510–527, 1975.
3. Walas, S. M. *Phase Equilibrium in Chemical Engineering*. Stoneham, MA: Butterworth, 1985, 3–102.
4. Sandler, S. I., Orbey, H., and Lee, B. I. In *Models for Thermodynamic and Phase Equilibria Calculations*. Edited by S. I. Sandler. New York: Marcel Dekker, 1994, 87–186.
5. Han, S. J., Lin, H. M., and Chao, K. C. *Chem. Eng. Sci.* 43: 2327–2367, 1988.
6. Redlich, O., and Kwong, J. N. S. *Chem. Rev.* 44: 233–244, 1949.
7. Wilson, G. M. *Adv. Cryogen. Eng.* 9: 168–174, 1964.
8. Soave, G. *Chem. Eng. Sci.* 27: 1197–1203, 1972.
9. Peng, D. Y., and Robinson, D. B. *Ind. Eng. Chem. Fund.* 15: 59–64, 1976.
10. Stryjek, R., and Vera, J. H. *Canadian J. Chem. Eng.* 64: 323–333, 1986.
11. Chen, S. S., and Kreglewski, A. *Ber. Bunsenges. Phys. Chem.* 81: 1049, 1977.
12. Boublik, T. *J. Chem. Phys.* 63: 4084, 1975.
13. Alder, B. J., Young, D. A., and Mark, M. A. *J. Chem. Phys.* 56: 3013, 1972.
14. Beret, S., and Prausnitz, J. M. *AIChE J.* 21: 1123, 1975.
15. Donohue, M. D., and Prausnitz, J. M. *AIChE J.* 24: 849, 1978.
16. Prigogine, I. *The Molecular Theory of Solutions*. New York: North Holland, 1957.
17. Chien, C. H., Greenkorn, R. A., and Chao, K. C. *AIChE J.* 29: 560–571, 1983.
18. Boublik, T., and Nezbeda, I. *Chem. Phys. Lett.* 46: 315, 1977.
19. Pults, J. D., Greenkorn, R. A., and Chao, K. C. *Chem. Eng. Sci.* 44: 2553, 1989.
20. Pults, J. D., Greenkorn, R. A., and Chao, K. C. *Fluid Phase Equilibria* 51: 147, 1989.
21. Sy-Siong-Kiao, R., Caruthers, J. M., and Chao, K. C. *Ind. Eng. Chem. Res.* 35: 1446–1455, 1996.
22. Honnell, K. G., and Hall, C. K. *J. Chem. Phys.* 90: 1841–1855, 1989.
23. Yithiraj, A., and Hall, C. K. *J. Chem. Phys.* 95: 8494–8506, 1991.
24. Wu, C. S., and Chen, Y. P. *Fluid Phase Equilibria* 101: 3–26, 1994.
25. Chapman, W. G., Gubbins, K. E., Jackson, G., and Radosz, M. *Fluid Phase Equilibria* 52: 31, 1989.
26. Chapman, W. G., Gubbins, K. E., Jackson, G., and Radosz, M. *Ind. Eng. Chem. Res.* 29: 1709, 1990.
27. Wertheim, M. S. *J. Chem. Phys.* 87: 127, 1987.
28. Huang, S. H., and Radosz, M. *Ind. Eng. Chem. Res.* 29: 2284, 1990; 30: 1944, 1991.
29. Tsonopoulos, C. *AIChE J.* 20: 263, 1974; 21: 827, 1975; 24: 1112, 1978.
30. Benedict, M., Webb, G. B., and Rubin, L. C. *J. Chem. Phys.* 8: 334, 1940.
31. Bender, E. *Cryogenics* 15: 667, 1975.
32. Jacobsen, R. T., and Stewart, R. *Br. J. Phys. Chem. Ref. Data* 2: 757, 1973.
33. Keenan, J. H., Keyes, F. G., Hill, P. G., and Moore, J. G. *Steam Table, Thermodynamic Properties of Water, Including Vapor, Liquid, and Solid Phases*. New York: John Wiley, 1969.

The activity coefficient is the ratio of the fugacity of a component in a real solution to its ideal-solution value,

$$\gamma_i = \frac{f_i}{x_i f_i^p} \quad (4.316)$$

For ideal solutions, $\gamma_i = 1$ for all i at all compositions. The more different γ is from 1, the more nonideal is the solution. According to Equation (4.316), the fugacity of a component in a real solution is given by

$$f_i = \gamma_i x_i f_i^p \quad (4.317)$$

The activity coefficient expresses the nonideal-solution behavior of fugacity. The formal development of models for the activity coefficient in solution thermodynamics follows.

Both the ideal-solution Equation (4.314) and the real-solution Equation (4.317) reveal the motivation to use vapor pressure as the basis to find fugacity of components in liquids. This method of using vapor pressure and activity coefficient was practically the sole method for the quantitative calculation of fugacities of liquid solutions until the 1970s. Then, van der Waals-type equations of state were employed to calculate liquid fugacities with good accuracy using Equation (4.307) to perform the integration across the condensation range. Subsequently, some extended virial equations and the perturbation equations were used. Different methods are suitable for various classes of solutions or in different pressure ranges. The activity-coefficient method is suitable for highly nonideal solutions at low pressure and is also suitable for high pressure when the activity coefficient is incorporated in an equation of state. The activity-coefficient method is not readily applied to liquid solutions of light gases.

The fugacities f_i or activity coefficients γ_i of a liquid solution are measured in vapor-liquid equilibrium experiments. In commonly employed methods, the liquid solution is brought in contact and kept in contact with a vapor mixture of the same components until equilibrium is attained between the phases. A sample of the vapor is then withdrawn and analyzed to determine its mole fractions y_i , $i = 1, 2, \dots$. Similarly for the liquid sample, the mole fractions $x_i = 1, 2, \dots$ are determined. Together with the measured p , an experimental point of vapor-liquid equilibrium is given by

$$T, p, x_i (i = 1, 2, \dots) \quad \text{and} \quad y_i (i = 1, 2, \dots)$$

The fugacities in the gas mixtures are obtained from the gas-phase data: using an equation of state, one can calculate the fugacity coefficient ϕ_i from the experimental y_i and p and then form the product to give

$$f_{iv} = p y_i \phi_i \quad (4.318)$$

A simple equation of state is sufficient to find ϕ_i for the present purposes because the gas phase is usually at a low pressure. The virial equation truncated after B is useful, and correlation of B is found in Section 4.2.5.

By Equation (4.303), the fugacity of a component in the liquid is equal to that of the component in the equilibrium vapor. In light of Equation (4.318), the experimental fugacities of the components in the liquid are determined as

$$f_{iL} = p y_i \phi_i \quad (4.319)$$

ideal solution. In a dilute solution, where the solute follows Henry's law, the solvent follows the ideal-solution law.

4.3.2 IDEAL AND EXCESS SOLUTION PROPERTIES

Activity coefficient is a function of the state of a mixture. An activity-coefficient equation is required to calculate the fugacities of real solutions. The interrelationship of the activity coefficients through the Gibbs-Duhem equation implies that the activity-coefficient equations of all components are derivatives of a common thermodynamic function. Since the activity coefficient is an expression of the nonideal behavior of a component, a thermodynamic function is needed to express the nonideality of the total solution and then to obtain from it the activity-coefficient equation.

With the fugacity equation of a real solution, Equation (4.317), taking the logarithm of the equation and multiplying by RT gives

$$RT \ln f_i = RT \ln f_i^P + RT \ln x_i + RT \ln \gamma_i \quad (4.324)$$

Transforming the fugacities f_i , and f_i^P into chemical potentials by using Equation (4.302) gives

$$\mu_i = g_i^P + RT \ln x_i + RT \ln \gamma_i \quad (4.325)$$

where g_i^P is the molar Gibbs energy of pure liquid i at the $[T, p]$ of the solution.

Forming the molar Gibbs energy from the partial values of Equation (4.325),

$$g = \sum_i x_i g_i^P + RT \sum_i x_i \ln x_i + RT \sum_i x_i \ln \gamma_i \quad (4.326)$$

The molar Gibbs energy of an ideal solution is obtained by setting $\gamma_i = 1$ for all i in Equation (4.326),

$$g^{ld} = \sum_i x_i g_i^P + RT \sum_i x_i \ln x_i \quad (4.327)$$

Even for an ideal solution, the Gibbs energy is not equal to the sum of the pure-liquid constituents.

The change of Gibbs energy upon mixing is the difference between the Gibbs energy of solution and the sum of its pure-liquid constituents at the same $[T, p]$. For 1 mole of solution,

$$g^M \equiv g - \sum_i x_i g_i^P \quad (4.328)$$

Thus, according to Equation (4.326),

$$g^M = RT \sum_i x_i \ln x_i + RT \sum_i x_i \ln \gamma_i \quad (4.329)$$

This is the change in Gibbs energy when the pure liquids are mixed to form 1 mole of solution. For the formation of 1 mole of ideal solution with $\gamma_i = 1$, Equation (4.329) simplifies to

Experience has shown that the binary interaction equations are at least as good as any larger cluster interaction equation in fitting data; usually they are superior. Their convenience and economy can be over-riding. The binary interaction equations have become the preferred equations to use. The other types of equations are included in this section only because they are still in the literature.

4.3.3.1 Redlich–Kister Equation

Redlich and Kister (RK) [1] employ a parabola $B_{12}x_1x_2$ as the basic form for the g^E of a binary solution. A power series in $(x_1 - x_2)$ is added to to express the asymmetry, if any, of the g^E function,

$$\frac{g_{12}^E}{RT} = x_1x_2[B_{12} + C_{12}(x_1 - x_2) + D_{12}(x_1 - x_2)^2] \quad (4.335)$$

Binary parameters B , C , and D are to be determined by fitting activity-coefficient data. Progressively more parameters are used, depending on the complexity of the function, but D is generally the highest employed. Differentiation of Equation (4.335) gives the activity coefficients

$$\begin{aligned} \ln \gamma_1 &= (B + 3C + 5D)x_2^2 - 4(C + 4D)x_2^3 + 12Dx_2^4 \\ \ln \gamma_2 &= (B - 3C + 5D)x_1^2 + 4(C - 4D)x_1^3 + 12Dx_1^4 \end{aligned} \quad (4.336)$$

The RK equation is strictly data fitting with a power series. The judiciously selected function gives a good representation of experimental data for many nonpolar, polar, and associated systems with activity coefficients either greater than or smaller than 1. It is easy to use. But for three-component and higher solutions, the RK equation becomes complex and unwieldy; they are not presented here.

4.3.3.2 Van Laar Equation

Van Laar [2] developed an activity-coefficient equation for liquid solutions based on the vdW eos. This equation has found wide use. Based on the observation that strongly nonideal solutions were associated with large heats of mixing, it was conjectured that nonideality was due to heat of mixing only. Neglecting s^E ,

$$g^E = h^E \quad (4.337)$$

For liquids, pv^E is small, and excess enthalpy is assumed equal to u^E ,

$$g^E = u^E \quad (4.338)$$

Van Laar [2] modified the van der Waals (vdW) equation to reduce the internal energy by Equation (4.291):

$$u = -\frac{a}{v} + u^0 \quad (4.339)$$

Forming u^E from the energies of the liquids, and setting the u^E to be g^E ,

$$A_{21} = b_2 \left(\frac{\sqrt{a_2}}{b_2} - \frac{\sqrt{a_1}}{b_1} \right)^2 \quad (4.348)$$

Equations (4.345) and (4.346) are the van Laar activity-coefficient equations that are used for fitting data by adjusting the parameters A_{21} and A_{12} . Although these parameters are derived from pure-component parameters, as shown in Equations (4.347) and (4.348), they are, nevertheless, considered mixture-specific binary interaction parameters and are thus indicated with subscripts because they are determined by fitting binary mixture data. Equations (4.347) and (4.348), while showing the source of derivation of the parameters, are not used for their determination.

From the assumed $s^E = 0$, the van Laar equation gives $(RT \ln \gamma)$ as a constant, independent of temperature. The van Laar equation gives a good representation of the activity coefficient of many mixtures, including highly nonideal solutions. However, because it always gives activity coefficient greater than 1, it is not to be used for negatively deviating solutions with $g^E < 0$ and $\gamma < 1$.

By following the same procedure, the activity coefficient in a ternary solution is obtained,

$$RT \ln \gamma_1 = \left[x_2^2 A_{12} \left(\frac{A_{21}}{A_{12}} \right)^2 + x_3^2 A_{13} \left(\frac{A_{31}}{A_{13}} \right)^2 + x_2 x_3 \frac{A_{21} A_{31}}{A_{12} A_{13}} \left(A_{12} + A_{13} - A_{32} \frac{A_{13}}{A_{31}} \right) \right] / \left(x_1 x_2 \frac{A_{21}}{A_{12}} + x_3 \frac{A_{31}}{A_{13}} \right)^2 \quad (4.349)$$

To obtain the activity coefficient of component 2 or 3, the subscripts are shifted in the order 1-2-3-1.

The three-component equation is complex, and the complexity increases rapidly with the number of components of the solution. Hence, the van Laar equation is rarely used for solutions containing more than two components.

4.3.3.3 Regular Solutions

Hildebrand et al. [3] define a regular solution as one with negligible excess entropy that is composed of nonpolar or slightly polar compounds that do not chemically associate or hydrogen bond. Like van Laar's solutions, the nonideality of regular solutions is an energy effect. Study of solubility data led to the observation that the energy effect is more precisely an energy density effect. The energy density is defined for a pure liquid by

$$a = \frac{u^* - u}{v} \quad (4.350)$$

The residual energy or the molecular interaction energy $(u^* - u)$ is obtained from the heat of vaporization minus RT and plus any vapor nonideality correction.

Scatchard [4] suggests that the molar energy of a solution be given by

$$(u^* - u)_m = v_m \sum_i \sum_j \phi_i \phi_j a_{ij} \quad (4.351)$$

where ϕ denotes a volume fraction defined by

$$RT \ln \gamma_A = v_A \phi_B^2 (\delta_B - \delta_A)^2 \quad (4.360)$$

$$RT \ln \gamma_B = v_B \phi_A^2 (\delta_A - \delta_B)^2 \quad (4.361)$$

The v and δ are pure-component properties. There are no mixture parameters to adjust for data fitting in Equation (4.357), Equation (4.360), and Equation (4.361). The regular solution equation is predictive based on pure-component liquid properties. It is generally useful for a first-order estimate for nonpolar, nonassociating, nonhydrogen bonding solutions. $RT \ln \gamma_k$ of a regular solution by Equation (4.357) is not dependent on T ,

$$\left(\frac{\partial g^E}{\partial T} \right)_{p,x} = -s^E = 0 \quad (4.362)$$

The regular solution equation is useful for solutions of normal fluids encountered in the petroleum and gas industries up to high pressure. The regular solution equation is useful for the calculation of solubility of gases. Since the temperature of usual interest is greatly above the critical temperature of the light gases, a hypothetical standard state has to be determined for the regular solution equation to be useful for the light gases. This and other topics related to gas solubility will be found in Section 4.4.

4.3.3.4 Flory–Huggins Equation

The dissolution of polymers into a solvent produces little heat effect for polymers and solvent of similar chemical structure. However, the solvents in these solutions are much less volatile than in an ideal solution with activity coefficients much lower than 1.

Solutions with no heat of mixing are called athermal, and $h^E = 0$. The nonideality of an athermal solution is due to excess entropy. Flory and Huggins independently found the excess entropy of polymer solutions by counting the number of ways by which space is occupied by molecules of different sizes. The more ways to occupy space, the greater is the entropy. According to statistical mechanics, entropy is determined by the number of micromolecular states, $S = k \ln \Omega$, where k is the Boltzmann constant equal to the universal ideal-gas constant per molecule R/N_A ; and for molecular solutions, Ω is the number of states for the molecules to occupy space. For the purpose of counting the states, the elemental segments of the polymer molecular chain are assumed to be located on a regular lattice structure like that of a crystal, with each segment taking up one lattice point. Suppose the polymer molecules are placed on the lattice structure one at a time so that the elemental segments of the molecule take up contiguous sites. The number of ways to place the i th polymer molecule on the lattice, ω_i , is $(M_0 - M_{i-1})[z(1 - M_{i-1}/M_0)]^{m-1}$, where the factors are:

$(M_0 - M_{i-1})$ is the number of ways to place the first segment of the i th molecule on the lattice, with M_0 being the total number of lattice sites and M_{i-1} being the number of lattice sites that are occupied after $i - 1$ molecules have been placed.

z is the coordination number of the lattice, i.e., the number of closest neighbors of a site. For face-centered and hexagonal close-packed lattices, $z = 12$, and for body-centered packing, $z = 8$. Thus a number from 8 to 10 would be a reasonable value to assign to the hypothetical lattice of a liquid. Although used in the counting, the value of z does not make a difference to the entropy.

$$\ln a_2 = \ln \phi_2 + (1-r)\phi_1 \quad (4.369)$$

where a_i is the activity $\equiv x_i \gamma_i \equiv f_i / f_i^P$. The equations are, in fact, asymmetric with respect to solvent and polymer.

It is remarkable that no empirical mixture parameters and no experimental data are required to use the equation. The only parameters in the Flory-Huggins equation are the hard core volumes v_i , which are a pure-component property, and the atomic or group contribution values are found in standard compilations. Since the v_i 's are significant in the FH equation only in terms of their ratios, pure-liquid molar volumes are often used for v_i in place of hard core volumes. For solutions of polymers of the same chemical formula, molecular masses are legitimate substitutes for v_i , for the same reason. Thus the volume fractions ϕ_i can be substituted by mass fractions w_i . Either volume fraction or mass fraction is directly related to laboratory data. To avoid mole fractions, the activity a_i from Equations (4.368) and (4.369) can be used to calculate f_i by $f_i \equiv a_i f_i^P$.

A surprisingly simple but elegant statistical mechanical result is represented by Equations (4.367), (4.368), and (4.369). Though originally developed for polymer solutions, it is also applicable to solutions of small molecules to account for molecular size differences. It has been made part of some activity-coefficient equations, as will be discussed in the following.

Polymer solutions are not athermal when the solvent and the polymer are of different chemical structure. To account for the effect of energy of mixing, Flory suggested, from counting the change of contacts of the different molecular species upon mixing, an explanation for the excess energy as follows:

$$u^E = RT \frac{v_m}{v_1} \chi \phi_1 \phi_2 \quad (4.370)$$

where v is molar liquid volume and (v_m/v_1) is a measure of the total molecular contacts. The exchange energy, $\chi \equiv \chi_{12} - (\chi_{11} + \chi_{22})/2$, expressing the energy of formation of a 1–2 contact at the expense of a 1–1 contact and a 2–2 contact, is a mixture-energy parameter for each solvent-polymer combination at a fixed temperature, and is a constant independent of molecular mass for homopolymers. This constant is zero for solutions of a polymer in its monomer.

By adding the u^E of Equation (4.370) with the s^E of Equation (4.365) to form g^E , and by differentiating the g^E , the activity coefficient is obtained,

$$\ln a_1 = \chi \phi_2^2 + \ln \phi_1 + \left(1 - \frac{1}{r}\right) \phi_2 \quad (4.371)$$

$$\ln a_2 = r \chi_1^2 + \ln \phi_2 + (1-r)\phi_1 \quad (4.372)$$

where subscript 1 denotes solvent and 2 is a polymer. These are Flory's χ equations, in which the χ parameter is adjusted for data fitting. Although supposed to be constant, χ has been found to vary with concentration and with polymer molecular mass to varying extent, depending on the mixture system. The χ equation is not as generally useful as the Flory-Huggins equation.

4.3.3.5 Wilson's Local-Composition Equation

Wilson [7] postulated that the nonideality of a solution is caused by a realignment of molecules at the microscopic neighborhood due to the different attractive energies of the various species. Certain molecules are strongly attracted to the central molecule preferentially. The local composition about

The activity coefficient is obtained by taking partial molar derivatives of g^E ,

$$\ln \gamma_i = 1 - \ln \left(\sum_j x_j \ln \Lambda_{ij} \right) - \sum_k \left(\frac{x_k \Lambda_{ki}}{\sum_j x_j \Lambda_{kj}} \right) \quad (4.379)$$

For a binary solution, Equation (4.379) reduces to

$$\ln \gamma_1 = -\ln(x_1 + \Lambda_{12}x_2) + x_2 \left(\frac{\Lambda_{12}}{x_1 + \Lambda_{12}x_2} - \frac{\Lambda_{21}}{\Lambda_{21}x_1 + x_2} \right) \quad (4.380)$$

$$\ln \gamma_2 = -\ln(x_2 + \Lambda_{21}x_1) - x_1 \left(\frac{\Lambda_{12}}{x_1 + \Lambda_{12}x_2} - \frac{\Lambda_{21}}{\Lambda_{21}x_1 + x_2} \right) \quad (4.381)$$

Two adjustable parameters, Λ_{12} and Λ_{21} , need to be determined by fitting binary-solution data to Equation (4.380) and Equation (4.381). Parameters obtained from binary solutions are useful and sufficient in Equation (4.379) for multicomponent solutions, since no higher interaction parameters are required in the multicomponent equation.

The Wilson equation is widely used for many nonpolar, polar, and associated solutions in vapor-liquid equilibrium systems. It is often best for hydrogen-bonded substances. For multicomponent solutions, it makes effective use of binary-solution parameters to give good results, but it cannot predict the liquid immiscibility phenomena.

4.3.3.6 Nonrandom Two-Liquids (NRTL) Equation

To extend the activity-coefficient equation to partially miscible solutions, Renon and Prausnitz [8] introduced a factor to the exponential energy term in Wilson's equation. With $\alpha < 1$, the effect is to suppress the preferential attraction of molecules to the central molecule. The local mole fraction of component 2 about component 1 in a binary solution is given by

$$x_{21} = \frac{x_2 \exp[-\alpha_{12}(g_{21} - g_{11})/RT]}{x_1 + x_2 \exp[-\alpha_{12}(g_{21} - g_{11})/RT]} \quad (4.382)$$

and the local mole fraction of 1 about 1 is

$$x_{11} = \frac{x_1}{x_1 + x_2 \exp[-\alpha_{12}(g_{21} - g_{11})/RT]} \quad (4.383)$$

The factor α is assumed to be a constant for a binary system, $\alpha_{11} = \alpha_{22} = \alpha_{12} = \alpha_{21}$. The partial contribution of component 1 to the excess Gibbs energy of the solution is assumed to be $g^{(1)} - g_p^1$, where

$$g^{(1)} = x_{11}g_{11} + x_{21}g_{21} \quad (4.384)$$

and g_p^1 is the g of 1 in the pure-liquid state, set to be g_{11} . Renon and Prausnitz [8] changed Wilson's g , which is energy to Gibbs energy. Summing the contributions of both 1 and 2,

$$u^E = \frac{1}{2} \sum_i x_i \sum_j z x_{ji} (g_{ji} - g_{ii}) \quad (4.392)$$

where g is energy as in Wilson's equation, and z is the coordination number, i.e., the number of closest neighbor molecules.

Adding Equation (4.392) to Wilson's $-Ts^E$ gives the complete g^E ,

$$g^E = \frac{z}{2} \sum_i x_i \sum_j x_{ji} (g_{ji} - g_{ii}) + RT \sum_i x_i \ln(\phi_{ii} / x_i) \quad (4.393)$$

The activity coefficient obtained from Equation (4.393) is

$$\begin{aligned} \ln \gamma_i = \frac{1}{RT} \left(\frac{z}{2} \right) & \left[\sum_j x_{ji} (g_{ji} - g_{ii}) + \sum_j x_j \sum_k x_{kj} \left(\frac{x_{ij}}{x_i} \right) (g_{ij} - g_{kj}) \right] \\ & + 1 - \ln \left(\sum_j x_j \Lambda_{ij} \right) - \sum_k \left(\frac{x_k \Lambda_{ki}}{\sum_j x_j \Lambda_{kj}} \right) \end{aligned} \quad (4.394)$$

where Λ_{ij} is defined as

$$\Lambda_{ij} = \frac{v_j}{v_i} \exp \frac{-(g_{ji} - g_{ii})}{RT} \quad (4.395)$$

For binary mixtures, Equation (4.394) simplifies to

$$\ln \gamma_1 = \frac{1}{RT} \left(\frac{z}{2} \right) \left[x_{21}^2 (g_{21} - g_{11}) + x_2 x_{22} \frac{x_{12}}{x_1} (g_{21} - g_{22}) \right] \quad (4.396)$$

$$- \ln(x_1 + \Lambda_{12} x_2) + x_2 \left(\frac{\Lambda_{12}}{x_1 + x_2 \Lambda_{12}} - \frac{\Lambda_{21}}{x_2 + x_1 \Lambda_{21}} \right)$$

$$\ln \gamma_2 = \frac{1}{RT} \left(\frac{z}{2} \right) \left[x_{21}^2 (g_{12} - g_{22}) + x_1 x_{11} \frac{x_{21}}{x_2} (g_{21} - g_{11}) \right] \quad (4.397)$$

$$- \ln(x_2 + \Lambda_{21} x_1) + x_1 \left(\frac{\Lambda_{12}}{x_1 + x_2 \Lambda_{12}} - \frac{\Lambda_{21}}{x_2 + x_1 \Lambda_{21}} \right)$$

The effective volume v is generally set to be the pure-liquid molar volume. The coordination number z has been found to be 6 by fitting the equation to a number of solutions. Two adjustable parameters ($g_{21}-g_{11}$) and ($g_{12}-g_{22}$) are to be determined by fitting experimental data on the binary solution. The binary-solution parameters are useful for multicomponent solutions in Equation (4.394).

where z , the coordination number, is set equal to 10. The segment fraction ϕ^* and area fractions θ and θ' are given by

$$\phi_i^* = \frac{r_i x_i}{\sum_j r_j x_j} \quad (4.404)$$

$$\theta_i = \frac{q_i x_i}{\sum_j q_j x_j} \quad (4.405)$$

$$\theta'_i = \frac{q'_i x_i}{\sum_j q'_j x_j} \quad (4.406)$$

Parameter r measures the number of segments of a molecule for the term v in the Flory-Huggins equation. Parameters q_i and q' are surface areas that are interchangeable for all except strongly hydrogen-bonded water and alcohols. Parameters r , q , and q' are pure-component molecular structure parameters. The combinatorial g^E is dependent only on pure-component parameters. The residual g^E depends additionally on binary interaction parameters τ_{ij} and τ_{ji} ,

$$\tau_{ij} = \exp\left(-\frac{a_{ij}}{T}\right) \quad (4.407)$$

$$\tau_{ji} = \exp\left(-\frac{a_{ji}}{T}\right) \quad (4.408)$$

where $a_{ij} = \Delta u_{ij}/R$ is an energy of interaction expressed in Kelvins. The terms a_{ij} and a_{ji} are the adjustable parameters for fitting binary-solution data.

The UNIQUAC activity-coefficient equation is given by

$$\begin{aligned} \ln \gamma_i = & \ln \frac{\phi_i^*}{x_i} + \frac{z}{2} q_i \ln \frac{\theta_i}{\phi_i^*} + \ell_i - \frac{\phi_i^*}{x_i} \sum_j x_j \ell_j - q'_i \ln \left(\sum_j \theta'_j \tau_{ji} \right) \\ & + q'_i - q'_i \sum_j \frac{\theta'_j \tau_{ij}}{\sum_k \theta'_k \tau_{kj}} \end{aligned} \quad (4.409)$$

where

$$\ell_j = \frac{z}{2} (r_j - q_j) - (r_j - 1) \quad (4.410)$$

1. The partial molar G^E , or simply $\ln \gamma_i$, of a molecular species is made up of two parts: one due to the size differences, called $\ln \gamma_i^s$, and the other due to interaction of the groups, called $\ln \gamma_i^g$,

$$\ln \gamma_i = \ln \gamma_i^s + \ln \gamma_i^g \quad (4.413)$$

The subscript i denotes a molecule.

2. The contribution due to size differences of the molecules is given by the Flory-Huggins athermal solution equation. The constituent atoms (other than hydrogen) m_i are used as a measure of molecular size:

$$\ln \gamma_i^s = \ln \frac{m_i}{\sum_j x_j m_j} + 1 - \frac{m_i}{\sum_j x_j m_j} \quad (4.414)$$

3. A group i has an activity coefficient Γ_i that is a function of group fractions X_k , $k = 1, 2, \dots, v$, and temperature. The group fraction is the mole fraction of the group in the group solution that is converted from the mole fraction x of the molecules that make up the solution:

$$X_k = \frac{\sum_j v_{kj} x_j}{\sum_l \sum_j v_{lj} x_j} \quad (4.415)$$

where X_k is the group fraction of group k , x_j is the mole fraction of molecules j , and v_{kj} is the number of k groups in a j molecule. The activity of a group can be represented by a function F :

$$\ln \Gamma_k = F_k(X_1, X_2, X_3, \dots; T) \quad (4.416)$$

where F can be one of the activity-coefficient equations such as the Wilson equation or the UNIQUAC equation.

4. The group interaction contribution to the activity coefficient of molecule j , $\ln \gamma_j^g$, is the sum of $\ln(\Gamma_k / \Gamma_{kj}^*)$ of all groups k in molecule j ,

$$\ln \gamma_j^g = \sum_k v_{kj} (\ln \Gamma_k - \ln \Gamma_{kj}^*) \quad (4.417)$$

where Γ_k is given by Equation (4.416) and Γ_{kj}^* is the activity coefficient of group k in pure liquid j , and is given by the same function F of Equation (4.416):

$$\ln \Gamma_{kj}^* = F_k(X_{1,j}^*, X_{2,j}^*, \dots; T) \quad (4.418)$$

The group fraction $X_{1,j}^*$ is that of group 1 in pure liquid j , and similarly for the other groups. The subtraction of $\Gamma_{1,j}^*$ in Equation (4.417) ensures that the standard state of the pure liquid is satisfied; γ_j^g always approaches 1 as $x_j \rightarrow 1$ in any solution.

The core volume r_i is given by

$$r_i = \sum_k v_{ki} R_k \quad (4.423)$$

with v_{ki} being the number of group k in molecule i , and R_k being the volume of group k .

The surface area θ_i is given by

$$\theta_i = x_i q_i / \sum_j x_j q_j \quad (4.424)$$

The surface area fraction q_i is the sum of the group values:

$$q_i = \sum_k v_{ki} Q_k \quad (4.425)$$

where Q_k is the surface area of group k .

The residual activity coefficient is the sum of group activity coefficients Γ_k ,

$$\ln \gamma_i^R = \sum_k v_{ki} \ln \Gamma_k - \ln \Gamma_k^{(i)} \quad (4.426)$$

where the summation of all groups in molecule i and $\Gamma_k^{(i)}$ is the Γ_k in a group solution that is purely molecules of i .

The group Γ_k is given by the UNIQUAC equation applied to the groups,

$$\ln \Gamma_k = Q_k \left[1 - \ln \left(\sum_m \theta_m \Psi_{mk} \right) - \sum_m \left(\theta_m \Psi_{mk} / \sum_n \theta_n \Psi_{nm} \right) \right] \quad (4.427)$$

$$\Psi_{nm} = \exp(-a_{nm} / T) \quad (4.428)$$

$$\theta_m = Q_m X_m / \sum_n Q_n X_n \quad (4.429)$$

The group fraction X is given by

$$X_m = \frac{\sum_j v_{mj} x_j}{\sum_j \sum_n v_{nj} x_j} \quad (4.430)$$

The $\Gamma_k^{(i)}$ in Equation (4.426) is determined from Equation (4.427) at group fractions $X_k^{(i)}$ of the group solution that is purely molecules of i .

Group volume R and surface area Q are presented for 50 groups by Hansen et al. [17]. While the group volume R and surface area Q are obtained from analysis of pure substance data, the group-interaction parameters are obtained from correlation of mixture vapor-liquid equilibrium data.

$$\begin{aligned} \frac{g_{\text{eos}}^E}{RT} = & \frac{1}{2\sqrt{2}RT} \ln \left(\frac{k+1-\sqrt{2}}{k+1+\sqrt{2}} \right) \left[\frac{a}{b} - \sum_i x_i \left(\frac{a_i}{b_i} \right) \right] \\ & + \frac{pk}{RT} \left(b - \sum_i x_i b_i \right) - \ln b + \sum_i x_i \ln b_i \end{aligned} \quad (4.435)$$

where $k = 1.15$ for the PR eos.

Upon adopting the additive mixing rule for b ,

$$b = \sum_i x_i b_i \quad (4.436)$$

The middle term of Equation (4.435) can be eliminated, and Equation (4.435) becomes

$$\begin{aligned} \frac{g_{\text{eos}}^E}{RT} = & \frac{1}{2\sqrt{2}RT} \ln \left(\frac{k+1-\sqrt{2}}{k+1+\sqrt{2}} \right) \left[\frac{a}{b} - \sum_i x_i \left(\frac{a_i}{b_i} \right) \right] \\ & - \ln b + \sum_i x_i \ln b_i \end{aligned} \quad (4.437)$$

Upon setting the g_{eos}^E of Equation (4.437) to be equal to g_{sm}^E of the solution model, we solve for a/b to obtain

$$\frac{a}{b} = \frac{2\sqrt{2}RT}{\ln \left(\frac{k+1-\sqrt{2}}{k+1+\sqrt{2}} \right)} \left(\frac{g_{\text{sm}}^E}{RT} + \ln b - \sum_i x_i \ln b_i \right) - \sum_i x_i \left(\frac{a_i}{b_i} \right) \quad (4.438)$$

Equation (4.436) and Equation (4.438) make a set of mixing rules for a and b . The fugacity coefficient obtained from the mixing rules is

$$\begin{aligned} \ln \phi_i = & -\ln \left[\frac{p(v-b)}{RT} \right] + \frac{b_i}{b} (z-1) \\ & + \frac{a}{2\sqrt{2}bRT} \left[\frac{1}{na} \left(\frac{\partial n^2 a}{\partial n_i} \right) - \frac{b_i}{b} \right] \ln \left[\frac{v+b(1-\sqrt{2})}{v+b(1+\sqrt{2})} \right] \end{aligned} \quad (4.439)$$

with

$$\frac{1}{na} \left(\frac{\partial n^2 a}{\partial n_i} \right) = \frac{b_i}{b} + \frac{b}{a} \left\{ K \left[-\ln \gamma_i + \ln \left(\frac{b_i}{b} \right) + 1 - \frac{b_i}{b} \right] + \frac{a_i}{b_i} \right\} \quad (4.440)$$

and

$$K = \frac{-2\sqrt{2}RT}{\ln \left(\frac{k+1-\sqrt{2}}{k+1+\sqrt{2}} \right)} \quad (4.441)$$

to b , so that the mixing state is at infinite pressure. As a result, the eos does not fit experimental low-pressure data, unless the solution-model parameters in the incorporated eos are refitted to the data. Huron-Vidal's method cannot utilize the wealth of correlated low-pressure g_{sm}^E and γ , including correlations such as ASOG and UNIFAC. By setting the mixing at a low-pressure liquid state, the method of Novenario et al. [19] succeeded in making use of liquid-solution models with parameters fitted to low-pressure data.

In the method of Wong and Sandler [20, 21], mixing rules are developed for a and b to satisfy two conditions:

1. To equate the excess Helmholtz energy of the eos at infinite pressure to that of a solution model at a low pressure
2. To impart a quadratic composition dependence to the second virial coefficient of the eos

To achieve the first condition, it is found that

$$g^E(T, p = 1 \text{ bar}) \approx a^E(T, p = 1 \text{ bar}) \approx a^E(T, \text{high pressure}) \approx a^E(T, p)$$

Using the Peng-Robinson eos for illustration, the excess Helmholtz energy is found by combining the Helmholtz energy given by Equation (4.280). Upon setting $v = b$ in the excess function to attain infinite pressure,

$$a_{\text{eos}}^E = -\frac{a}{b} + \sum_i x_i \frac{a_i}{b_i} \quad (4.447)$$

where the un-subscripted a and b refer to the mixture. Setting this excess function to be equal to the g_{sm}^E of a solution model and solving for the a/b of the eos,

$$\frac{a}{b} = -g_{sm}^E + \sum_i x_i \frac{a_i}{b_i} \quad (3.448)$$

This is one of the two equations that are to be solved to give the combining rules for a and b . We turn to the second virial coefficient to find the other equation to be solved for a and b .

$$b = \frac{\sum_i \sum_j x_i x_j \left(b - \frac{a}{RT} \right)_{ij}}{1 + \frac{g_{sm}^E}{RT} - \sum_i x_i \left(\frac{a_i}{b_i RT} \right)} \quad (4.448)$$

Equation (4.447) and Equation (4.448) together make the mixing rules for a and b .

The free-energy-matching method of Wong et al. [20, 21] has been found to have good accuracy with experimental value data for ethanol-water mixtures and for acetone-water mixtures.

REFERENCES

1. Redlich, O., and Kister, A. T. *J. Am. Chem. Soc.* 71: 505, 1949.
2. van Laar, J. J. Z. *Phys. Chem.* 72: 723, 1929.

$$\frac{dp}{dT} = \frac{\Delta_v s}{\Delta_v v} \quad (4.452)$$

The symbol Δ_v denotes the change with vaporization. The change of entropy with vaporization is equal to the heat of vaporization divided by T , therefore:

$$\frac{dp}{dT} = \frac{\Delta_v h}{T \Delta_v v} \quad (4.453)$$

This is the Clapeyron equation, the differential equation for vapor pressure as a function of T .

To integrate the equation at low pressure, we assume: the vapor volume to be given by the ideal-gas equation; the liquid volume to be negligible; and the heat of vaporization to be unchanging with T . We obtain from Equation (4.453) the Clausius-Clapeyron equation,

$$d \ln p = \frac{\Delta_v h}{RT^2} dT \quad (4.454)$$

Integration gives

$$\ln p = A - \frac{\Delta_v h}{RT} \quad (4.455)$$

where A is an integration constant. Lumping the parameters, we have the vapor pressure equation

$$\ln p = A - B/T \quad (4.456)$$

which contains two parameters to be adjusted to fit the data. This equation gives good fitting of data in a moderate temperature range, but becomes only approximate when extended to a large temperature range. By fitting the equation to the critical state and the normal boiling point, we obtain a quick approximation at the interpolation range. The deviation grows quite large at extrapolated temperatures below the normal boiling point.

$$\ln p = \frac{\ln p_c - \ln 1.0}{1/T_b - 1/T_c} \left(\frac{1}{T_b} - \frac{1}{T} \right) \quad (4.457)$$

Here pressure is atmospheric, and T is absolute temperature. Subscript b denotes boiling point, and c denotes the critical point.

Another approximate equation is obtained by interpolation between the critical point and $T_r = 0.7$ by employing the acentric factor,

$$\log P_r = \frac{7}{3} \left(\frac{1}{0.7} - \frac{1}{T_r} \right) (\omega + 2) - (1 - \omega) \quad (4.458)$$

A common logarithm is used in this equation. Both Equation (4.456) and Equation (4.458) are useful for making an initial estimate of either T or p in iterative computer calculations for vapor-liquid equilibrium calculations.

$$p^S = \frac{1}{v_V - v_L} \int_{v_L}^{v_V} p dv \quad (4.466)$$

This is the implicit vapor pressure equation. It is solved by repeated substitution. Beginning with an estimated p^S , v_V and v_L are calculated at a given T until they converge adequately.

Example 4.16

Find the implicit vapor pressure equation of the Redlich-Kwong eos. The RK eos, Equation (4.153), will be written in a simplified form,

$$p = \frac{RT}{v-b} - \frac{a_T}{v(v+b)} \quad (4.467)$$

where a_T is a function of T and is given as $a/T^{0.5}$ for the RK eos. Substituting Equation (4.159) into Equation (4.465) and integrating gives

$$p^S = \frac{1}{v_V - v_L} \left[RT \ln \frac{v_V}{v_L} - \frac{a_T}{b} \ln \frac{v_V(v_L+b)}{v_V(v_V+b)} \right] \quad (4.468)$$

The saturated volumes v_V and v_L in Equation (4.468) are solved in the RK eos, Equation (4.467), at the vapor pressure, which makes the equation implicit. The equation can be readily solved for the saturated pressure by repeated substitution. Agreement with vapor pressure is qualitative at best.

Many eos's also provide only a qualitative representation of vapor pressure data due in part to the fact that vapor pressure by eos is determined by the integral $\int p dv$ of the eos in Equation (4.466) in the condensation range from v_L to v_V . The eos is either unstable or metastable in this range. No experimental data exist for the unstable states. Only scarce data exist for some metastable states. It is impossible to fit the eos to the pv isotherm in this range, as the isotherm hardly exists in the range of interest.

Yet it is desired that the eos give an accurate representation of vapor pressure. The key to achieving this goal is in Equation (4.468), which shows that the p^S by the RK eos is dependent on the attractive-pressure parameter a . By solving Equation (4.468) for a and letting p^S be the experimental vapor pressure, we obtain

$$a_T = \frac{RT \frac{v_V - b}{v_L - b} - p^S(v_V - v_L)}{\frac{1}{b} \ln \frac{v_V(v_L+b)}{v_L(v_V+b)}} \quad (4.469)$$

This equation is implicit in a_T , inasmuch as the saturated volumes are dependent on a_T , but the equation can be readily solved, for instance, by the method of repeated substitution. By using the solved value of a_T in the eos, Equation (4.162), the vapor pressure calculated by the eos simply reproduces the experimental vapor pressure data. Wilson correlated the a_T 's that are fitted to vapor pressure data of a number of normal fluids to obtain Equation (4.157), the Wilson eos. Vapor pressure calculated by the Wilson eos is improved over that of the RK eos, but the accuracy still leaves something to be desired. Soave correlated the vapor pressure, fitting a_T with Equation (4.164). Even better, the Soave eos is useful for the quantitative calculation of vapor pressure. In addition, the Peng-Robinson and the chain-of-rotators eos's provide quantitative calculations of vapor pressure.

The K values in an ideal mixture are given, according to Equation (4.472), by

$$K_i^{\text{Id}} = f_i^{\text{PL}} / f_i^{\text{PV}} \quad (4.474)$$

The pure-component fugacity is a substance-specific function of $[T, p]$. It follows from Equation (4.474) that ideal K values are substance-specific functions of $[T, p]$, but they are also independent of the composition of the mixture. Ideal K values provide an approximate description of mixtures of isomers, mixtures of near-neighbor homologues, and mixtures of isomers of near-neighbor homologues.

K values are useful for vapor-liquid equilibrium (vle) calculations. Five vle calculations are basic in applications:

1. Bubble-point temperature
Given: liquid composition and pressure
To find: vapor composition and temperature
2. Bubble-point pressure
Given: liquid composition and temperature
To find: vapor composition and pressure
3. Dew-point temperature
Given: vapor composition and pressure
To find: liquid composition temperature
4. Dew-point pressure
Given: vapor composition and temperature
To find: liquid composition and pressure
5. Flash
Given: T, p , and overall composition of feed mixture
To find: fraction of liquid formed, and composition and fraction of vapor formed and composition

The solution of the bubble- and dew-point problems using K values will be illustrated with the bubble-point temperature determination: Start by making an initial estimate of the bubble-point temperature. Using a chosen K -value chart, read K_i for the components of the mixture at the given pressure and the estimated temperature. Calculate the mole fractions of the incipient vapor by using the K values and the given x_i : $y_i = K_i x_i$ for all i . Sum the y_i 's and check if the sum is equal to 1,

$$\sum_i K_i x_i = 1 \quad (4.475)$$

If the equation is not satisfied to within a specified small tolerance, the summation is repeated using a new estimated temperature until convergence is obtained. The converged T is the bubble-point temperature. The method is a one-dimensional temperature search.

To find the bubble-point pressure, begin by making an estimate of the bubble pressure and carry out a one-dimensional search for the pressure at which $\sum_i K_i x_i = 1$ is satisfied to within a tolerance. Make a new chart reading for new K values at each new pressure. The converged pressure is the sought bubble pressure, and the converged $y_i = K_i x_i$ is the mole fraction of the vapor.

The dew-point problems are similarly one-dimensional searches, but the criterion to satisfy becomes the formation of an incipient dew expressed by the equation

$$\sum_i \frac{z_i}{n_L + (1 - n_L)K_i} - \sum_i \frac{K_i z_i}{n_L + (1 - n_L)K_i} = 0 \quad (4.484)$$

The necessary and sufficient condition for the search for an n_L to succeed is that $\sum_i K_i z_i > 1$ and $\sum_i z_i/K_i > 1$ so as to ascertain that the specified $[T, p]$ is bracketed by the dew point and the bubble point. When the conditions are satisfied, numerous one-dimensional search procedures can be used. Upon finding n_L and n_v , the x_i 's follow from Equation (4.480) and the y_i 's from Equation (4.482).

Calculation of vapor-liquid equilibrium states using K values is particularly convenient for ideal mixtures for which the K values are independent of composition, changing only with temperature or pressure or both. While convenient, the K -value method does satisfy all the equilibrium conditions: the component fugacities are equal in both phases for all components in the mixture, and temperature and pressure are equal in both phases. It follows that the K -value method can be used in general for nonideal mixtures as well. The composition dependence of the K values of nonideal mixtures is addressed next.

4.4.3 VAPOR-LIQUID EQUILIBRIUM BY γ - ϕ MODELS

Most mixtures are not ideal. An activity coefficient is then introduced in the liquid solution and a fugacity coefficient in the vapor of the mixture. A γ - ϕ model is made up of a selected activity-coefficient equation for the liquid and a selected equation of state for the vapor plus the associated standard-state equations and parameters.

4.4.3.1 Low-Pressure Models

Low pressure is generally meant to be less than 5 bar. The departure of a low-pressure gas mixture from ideal-gas mixture behavior is generally minor, and a simple equation of state is commonly employed to calculate the ϕ_i . The γ - ϕ model primarily counts on the activity-coefficient model to describe the vle phenomenon.

4.4.3.1.1 Fugacities of the Liquid Components

The fugacities in the liquid are given by

$$f_{iL} = x_i \gamma_i f_{iL}^P \quad i = 1, 2, \dots, v \quad (4.485)$$

An activity-coefficient equation is to be selected which, to a large extent, defines the character of the model. Examples will be given later of models of various activity-coefficient equations.

The required standard-state fugacity f_{iL}^P in Equation (4.485) is given by

$$f_{iL}^P = p^S \phi^S \exp \left[\frac{v_L^S (p - p^S)}{RT} \right] \quad (4.486)$$

The subscript i is left out of Equation (4.486) to address the pure component. Of the three factors on the right-hand side of the equation that make up the standard fugacity, the first one, p^S , is the primary factor. For a nonpolar component at a low pressure, a good approximation ignores the other two factors, thereby simplifying the standard fugacity to be just the vapor pressure. Such a simplification may introduce an overestimate of the standard fugacity by $\approx 1\%$ for a nonpolar liquid at its normal boiling point. The next higher approximation is to ignore only the exponential factor that accounts for the pressure effect on the liquid fugacity. This factor generally does not differ significantly from 1. For the difference $(p - p^S)$ as much as 5 atm, the exponential factor does not

$$z = 1 + \frac{1}{v} \sum_i \sum_j y_i y_j B_{ij} \quad (4.493)$$

at the specified $[T, p]$. A correlation of second virial coefficient is found in Section 4.2.5

4.4.3.1.3 Equilibrium Equations and Calculations

Equilibrium between the gas and liquid phases requires the fugacities of component i in both phases to be equal,

$$x_i \gamma_i f_{iL}^P = p y_i \phi_i, \quad i = 1, 2, \dots, v \quad (4.494)$$

These are the equilibrium equations of the γ - ϕ model that are to be solved for the unknown variables among T , p , x , y , n_L , or n_v from the known variables simultaneously with the mass balances and/or other applicable constraint equations. A common method of solution of the simultaneous equations is to use K values. From Equation (4.494) the K values are formed,

$$K_i \equiv y_i / x_i = \gamma_i f_{iL}^P / (p \phi_i) \quad i = 1, 2, \dots, v \quad (4.495)$$

As described in Section 4.4.2, the K values are useful for the calculation of the bubble, dew, or flash states. However, the method of calculation described in Section 4.4.2 needs to be modified because the K values formed by Equation (4.495) are not constant at a specified $[T, p]$ but change with composition. The method of repeated substitution is suited to the use of composition-dependent K values: One begins by making an initial estimate for the variables that are being sought, be it p , T , x_i , y_i , n_v , or n_L , while using specified values of the specified variables. The K_i 's are computed by Equation (4.495). The bubble, dew, or flash calculations are made as described in Section 4.4.2 to obtain values of the sought variables, be it T , p , x_i , y_i , n_v , or n_L . The calculated variables are generally not the same as the initial estimates. Use the calculated values as the new estimates and repeat the equilibrium calculation until adequate convergence occurs.

The equilibrium calculations are straightforward without iteration if the gas phase is an ideal-gas mixture, as it may be assumed at low pressures for normal fluids. Consider the bubble-point pressure problem: given T and x_i , find p and y_i . From Equation (4.487),

$$y_i p = x_i \gamma_i f_{iL}^P / \phi_i \quad (4.496)$$

Summing over i and setting $\sum y_i$ equal to 1 at the bubble pressure, we obtain the bubble pressure

$$p = \sum_i X_i \gamma_i f_{iL}^P / \phi_i \quad (4.497)$$

The vapor composition is obtained by dividing Equation (4.496) by Equation (4.497),

$$y_i = (x_i \gamma_i f_{iL}^P / \phi_i) / \left(\sum_j x_j \gamma_j f_{jL}^P / \phi_j \right) \quad (4.498)$$

The two equations are the complete solutions of the bubble-point problem, but the equations are implicit because the ϕ_i 's are functions of y_i and p , and f_{iL}^P and f_{jL}^P are functions of p . Repeated

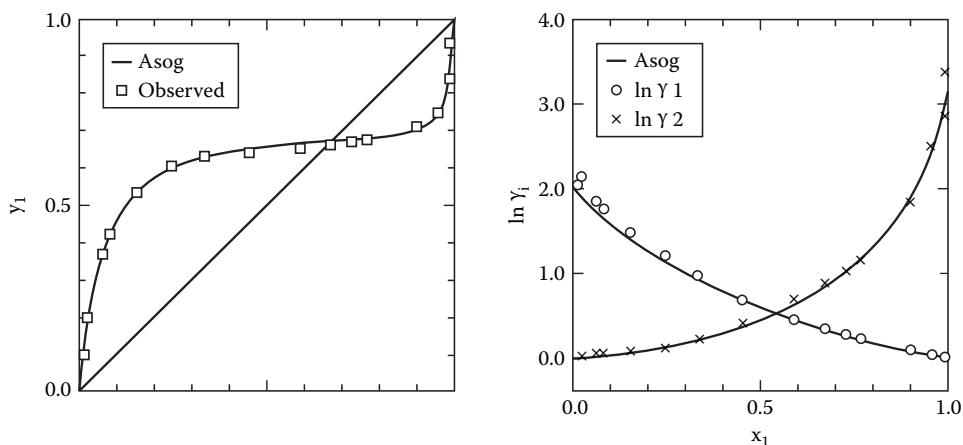


FIGURE 4.17 x-y and $\ln \gamma$ -x diagram for n-hexane (1) + ethanol (2) mixtures at 1 atm calculated from ASOG compared with data. (From Kojima, K., and Tochiji, K. *Prediction of Vapor-Liquid Equilibria by the ASOG Method*, New York: Elsevier Scientific Publishing, 1979. With permission.)

4.4.3.2 A High-Pressure Model

The Chao-Seader correlation [8] is applicable up to high pressures for normal fluids, including hydrocarbons (paraffins, olefins, aromatics, and naphthenes) and inert gases (methane and hydrogen). The correlation is a combination of three parts: (a) pure-liquid fugacity coefficient v_i , (b) liquid-solution activity coefficient γ_i , and (c) gas mixture fugacity coefficient ϕ_i . From these parts, the liquid fugacities and vapor fugacities are obtained:

$$\text{Liquid fugacities:} \quad f_{iL} = x_i \gamma_i v_i p \quad i = 1, 2 \dots v \quad (4.499)$$

$$\text{Vapor fugacities:} \quad f_{iV} = y_i p \phi_i \quad i = 1, 2 \dots v \quad (4.500)$$

The vle equations are obtained by setting the liquid and gas fugacities equal for each component,

$$x_i \gamma_i v_i p = y_i p \phi_i \quad i = 1, 2 \dots, v \quad (4.501)$$

Rearranging x_i and y_i , to the left side and the other variables to the right gives

$$y_i / x_i = v_i \gamma_i / \phi_i \quad i = 1, 2, \dots, v \quad (4.502)$$

Upon setting $K_i \equiv y_i/x_i$ in Equation (4.502), it follows that

$$K_i = v_i \gamma_i / \phi_i \quad i = 1, 2, \dots, v \quad (4.503)$$

The three factors— v_i , γ_i , and ϕ_i —that make up the K value in Equation (4.503) are described in the following subsections.

4.4.3.2.1 Pure-Liquid Fugacity Coefficient

The liquid fugacity coefficient plays the part of an ideal K value. Indeed, it is the K value if the liquid solution is ideal $\gamma_i = 1$ and the gas phase is an ideal-gas mixture $\phi_i = 1$. Equations (4.487)

$$p = \frac{RT}{v-b} - \frac{a}{T^{0.5}v(v+b)} \quad (4.508)$$

The resulting Chao-Seader correlation predicts K values of both methane/n-heptane mixtures and propane/isopentane mixtures down to at least $T_r = 0.5$.

4.4.4 VAPOR-LIQUID EQUILIBRIUM BY ϕ - ϕ MODELS

In a ϕ - ϕ model, one equation of state is used to obtain both the gas-phase fugacity coefficients ϕ_{iV} and the liquid-phase fugacity coefficients ϕ_{iL} . Upon setting the gas and liquid fugacities of a component i to be equal and canceling the pressure on both sides of the equation, we obtain

$$\phi_{iV}y_i = \phi_{iL}x_i \quad (4.509)$$

The K value, defined to be the ratio y_i/x_i , is obtained by rearranging Equation (4.509) as the ratio of the fugacity coefficients,

$$K_i = \phi_{iL} / \phi_{iV} \quad (4.510)$$

While the same eos-derived ϕ equation is used for both ϕ_{iL} and ϕ_{iV} , the input variables to the equation are different: for ϕ_{iL} , the liquid mol fractions x_i and liquid molar volume v_L are the input; for ϕ_{iV} , the gas mol fractions y_i and gas molar volume v_V are the input. Find the liquid volume v_L by solving the eos at specified $[x_i, p,]$ and pick the small root; find the vapor volume v_V by solving the eos at specified, $[y_i, p,]$ and pick the large root. The vapor-liquid equilibrium calculations using K values are much the same as in the use of γ - ϕ K values.

4.4.4.1 ϕ - ϕ Models— ϕ from vdW Mixing Rules

In this subsection, we present examples of ϕ - ϕ models in which ϕ is derived from vdW mixing rules by which the parameters a and b of mixtures are combinations of the parameters of the components according to

$$a = \sum_i \sum_j jx_i x_j a_{ij} \quad (4.511)$$

$$b = \sum_i \sum_j jx_i x_j b_{ij} \quad (4.512)$$

The identical double subscripts refer to a pure component, thus $a_{ii} \equiv a_i$ and $a_{ii} \equiv b_i$. The cross interaction a_{ij} is conventionally expressed as an adjusted geometric mean of the pure-component a 's:

$$a_{ij} = (1 - k_{ij}) \sqrt{a_i a_j} \quad (4.513)$$

The parameter k_{ij} is obtained by fitting experimental data on binary mixtures of i and j . It is common practice to estimate b_{ij} as the arithmetic mean,

$$b_{ij} = b_i + b_j / 2 \quad (4.514)$$

The vle phase results for methane and propane mixtures at 213.71°K were calculated using an interaction parameter to 12 of 0.0114; excellent agreement was found with experimental dew points and bubble points at pressures up to the initial point. Similar calculations (with good agreement with experimental data) have also been made for mixtures of methane and haptane and of carbon dioxide and n-butane.

Han et al. [10] made many comparisons of the Peng-Robinson eos K values ϕ_{iL}/ϕ_{iV} calculated with experimental K values y_i/x_i . For the eos K -value calculations, a cross-interaction coefficient k is determined for each binary system. For 20 symmetric binary systems for which the experimental temperature is below the critical of both components, the average absolute deviation (AAD) of the calculated from the experimental was found to be $\approx 2.5\%$. The AAD for the individual systems fall in the range from the smallest value of $\approx 1.0\%$ for ethylene + propylene to the largest value of $\approx 4.3\%$ for propylene + isobutene.

The PR eos gives excellent quantitative representations of the vle of normal fluids, including hydrocarbons and nonpolar and slightly polar light gases, using van der Waals mixing rules. The representation of liquid density is fairly good, making vle results expressed in volume fractions readily useful. The PR eos is widely used in engineering design applications.

Example 4.19: vle Chain-of-Rotators eos

The chain-of-rotators (COR) eos has been presented in Equation (4.183). For mixtures, using van der Waals mixing rules for a and b and linear additive rule for c ,

$$c = \sum_i x_i c_i \quad (4.518)$$

and following the method of Equation (4.306) leads to the fugacity coefficient equation

$$\begin{aligned} \ln \phi_i = & \frac{y(4-3y)}{(1-y)^2} + \frac{c_i}{2}(\alpha-1) \left[\frac{(\alpha+4)y-3y^2}{(1-y)^2} + (\alpha+1)\ln(1-y) \right] \\ & - \frac{\ln(1+4y)}{RT} \left[-b_i \left(\frac{a}{b^2} \right) + \frac{2}{b} \left(\sum_j x_j a_{ij} \right) \right] + \frac{b_i}{b}(z-1) - \ln z \end{aligned} \quad (4.519)$$

The parameters a and b in this COR eos are functions of T as follows:

$$a = a_1 \exp(-a_2 T) \quad (4.520)$$

$$b = b_1 \exp(-b_2 T^{1.5}) \quad (4.521)$$

Five parameters— a_1 , a_2 , b_1 , b_2 , and c —are required to be known for the eos to apply to a substance. The parameter values have been reported in the literature for numerous substances. For 11 hydrocarbon mixtures, the average AAD was 2.3% (ranging from 0.5 to 5.65%). For 12 methane-containing mixtures, the AAD was 3.92% (ranging from 1.32 to 8.16%). The five parameters required for each substance are a drawback to convenient application. The eos is superior in its representation of density of liquid and compressed fluid states—to within 1% up to the highest pressures.

The chain-of-rotators eos often predicts vle information for ternary systems except near the critical point; a good example is the mixture of methane, n-butane, and decane.

Han et al. [10] compared the COR eos K values ϕ_{iL}/ϕ_{iV} calculated with experimental K values y_i/x_i . For the eos calculations, a cross-interaction coefficient k is determined for each binary by

TABLE 4.5
Find Liquid-Liquid Equilibrium Phase Compositions in a Three-Component Mixture

1. Initialization: Assign a value for x_1 . Make initial estimate of mol fractions of all components in both phases other than x_1 .
2. $x_{2\alpha} = x_{2\beta}\gamma_{2\beta}/\gamma_{2\alpha}$
3. $x_{3\alpha} = x_{3\beta}\gamma_{3\beta}/\gamma_{3\alpha}$
4. $x_{2\alpha} = x_{2\alpha}(1 - x_{1\alpha})/(x_{2\alpha} + x_{3\alpha})$
5. $x_{3\alpha} = x_{3\alpha}(1 - x_{1\alpha})/(x_{2\alpha} + x_{3\alpha})$
6. $x_{1\beta} = x_{1\alpha}\gamma_{1\alpha}/\gamma_{1\beta}$
7. $x_{2\beta} = x_{2\alpha}\gamma_{2\alpha}/\gamma_{2\beta}$
8. $x_{3\beta} = x_{3\alpha}\gamma_{3\alpha}/\gamma_{3\beta}$
9. $x_{1\beta} = x_{1\beta}/(x_{1\beta} + x_{2\beta} + x_{3\beta})$
10. $x_{2\beta} = x_{2\beta}/(x_{1\beta} + x_{2\beta} + x_{3\beta})$
11. $x_{3\beta} = x_{3\beta}/(x_{1\beta} + x_{2\beta} + x_{3\beta})$
12. Check convergence: Are all mol fractions unchanged within a specified tolerance from the preceding iteration values?
 If unchanged, calculation is successfully completed. If changed, repeat iteration by going to step 2.

Source: Adapted from data provided by Sandler, S. I. *Chemical and Engineering Thermodynamics*, 3rd ed., New York: John Wiley & Sons, 1999.

$$c_i = \gamma_{i\alpha} / \gamma_{i\beta} \quad (4.525)$$

from the chosen activity-coefficient model at the phase compositions of either the initial estimate or the current iteration. Using c_i in place of K_i , perform a flash calculation on an estimated total feed composition in between the estimated equilibrium phase compositions. Since the c_i 's are composition dependent, it is necessary to iterate until convergence. The flash calculation is repeated with the obtained phase compositions to recalculate the activity coefficients; by Equation (4.525) obtain c_i ; then perform a flash calculation to obtain phase compositions and check convergence. Flash calculation is a relatively robust method for lle calculations, but it is still not as robust as it is for vle calculations. Initial estimated compositions are particularly important for success.

Another method to calculate equilibrium-phase compositions makes use of repeated substitutions in the fugacity equality conditions, Equation (4.523), while disregarding any mass balances required in the flash calculations. Suppose T and p are given. The variables are $2v$ mol fractions. There are v equilibrium equations and two equations expressing the sum of x being equal to 1 in either phase, totaling $(v + 2)$ equations. The degree of freedom is the number of variables $2v$ minus the number of equations $(v + 2)$; $F = v - 2$. The method will be illustrated with a three-component mixture, $v = 3$ and $F = 1$. One degree of freedom must be specified; let it be $x_{1\alpha}$. Table 4.5 shows a flow sheet of the method.

Besides being expressed in terms of activity coefficients, the fugacities of a liquid solution can also be calculated from equations of state in the form of a fugacity coefficient ϕ_i . The equality of fugacities of two liquid phases at equilibrium becomes expressed by

$$\phi_{i\alpha} p x_{i\alpha} / \phi_{i\beta} p x_{i\beta} \quad (4.526)$$

Canceling p from both sides of the equation,

$$\phi_{i\alpha} x_{i\alpha} = \phi_{i\beta} x_{i\beta} \quad (4.527)$$

For the calculation of the equilibrium phase compositions, it is convenient to use the distribution coefficient c_i ($\equiv x_{i\alpha}/x_{i\beta}$) to perform a flash calculation. The distribution coefficient for the flash calculation is now formed according to Equation (4.527) by

TABLE 4.6
UNIFAC LLE Group-Interaction Parameters

	1 CH	2 C=C	3 ACH	4 ACCH	5 OH	6 HO	7 ACOH	8 CH CO	9 CHO	10 COOH	11 COOC	12 CH O
1 CH	0	74.54	-114.8	-115.7	644.6	1300	2255	472.6	158.1	139.4	972.4	662.1
2 C=C	292.3	0	340.7	4102	724.4	896	...	343.7	-214.7	1647	-577.5	289.3
3 ACH	156.5	-94.78	0	167	703.9	859.4	1649	593.7	362.3	461.8	6	32.14
4 ACCH	104.4	-269.7	-146.8	0	4000	5695	292.6	916.7	1218	339.1	5688	213.1
5 OH	328.2	470.7	-9.21	1.27	0	28.73	-195.5	67.07	1409	-104	195.6	262.5
6 H O	342.4	220.6	372.8	203.7	-122.4	0	344.5	-171.8	-349.9	-465.7	-6.32	64.42
7 ACOH	-159.8		-473.2	-470.4	-63.15	-595.9	0	-825.7	-898.3	...
8 CH CO	66.56	306.1	-78.31	-73.87	216	634.8	-568	0	-37.36	1247	258.7	5.202
9 CHO	146.1	517	-75.3	223.2	-431.3	623.7	...	128	0	0.75	-245.8	...
10 COOH	1744	-48.32	75.49	147.3	118.4	652.3	...	-101.3	1051	0	-117.6	-96.62
11 COOC	-320.1	485.6	114.8	-170	180.6	385.9	337.3	58.84	1090	1417	0	-235.7
12 CH O	1571	76.44	52.13	65.69	137.1	212.8	...	52.38	...	1402	461.3	0

concentration. For the combination of benzene–n-heptane–acetonitrile, the model predicts well even at high concentrations. Such predictions can be used in liquid-liquid extractions.

Example 4.27: Comparison of lle by SAFT, Peng-Robinson, and UNIFAC

You and Chen [13] have compared these three eos's for calculating lle. They employed data for 5 binary mixtures of methanol + an aliphatic hydrocarbon, 6 binaries of phenol + an aliphatic hydrocarbon, 12 binaries of water + an aliphatic or a hydrocarbon, 7 binaries of water + an ester, 5 binaries of acetic acid + an aliphatic or a naphthenic hydrocarbon, and 6 binaries of aniline + an aliphatic or a naphthenic hydrocarbon. Temperature was in the range of 273–343°K, with one exception at 236°K.

Predictions of calculated versus experimental data were in the following order of absolute average duration (aad) of X_1 : SAFT of 1.90×10^{-2} , PR eos of 3.7×10^{-2} ; UNIFAC with Magnussen et al. [12] parameters of 3.5×10^{-2} , and UNIFAC with Larsen parameters of 5.4×10^{-2} . SAFT was also best for extrapolation of both lle and solubility. SAFT also predicted the ternary systems that tested best.

4.4.6 GAS-SOLID EQUILIBRIUM MODELS

Gas-solid equilibrium for a single-component system is commonly referred to as sublimation equilibrium. Sublimation pressure, the vapor pressure of a solid, is basic to the modeling of solid-gas equilibrium. Sublimation pressure changes with temperature by an equation similar to that of the vapor pressure of a liquid, Equation (4.453),

$$\frac{dp}{dT} = \frac{\Delta h}{T \Delta v} \quad (4.529)$$

where the Δ sign designates change upon sublimation. Since sublimation pressure is usually not large, the Antoine equation (4.459) gives useful representation for the entire range of temperature of common interest for many solids,

$$\ln p = A - B/(T + C) \quad (4.530)$$

The fugacity of the pure saturated vapor is given by the sublimation pressure times the fugacity coefficient,

$$f_v = p^S \phi^S \quad (4.531)$$

The superscript S denotes a saturated state. The fugacity coefficient ϕ can be calculated from an eos or a correlation of a second virial coefficient, but is often assumed to be 1 at the low vapor pressure of many solids.

The fugacity of the solid at sublimation equilibrium is equal to the fugacity of the pure saturated vapor and is therefore also given by Equation (4.531),

$$f_s = p^S \phi^S \quad (4.532)$$

Mixture gas-solid equilibrium is basic to supercritical extraction, the extraction of a solid component from a mixture of solids with a compressed gas at a state above and about its critical point. Another example is deposition of solid carbon dioxide, hydrogen sulfide, or heavy

Example 4.28: Supercritical Extraction

In supercritical extraction, a compressed gas at a temperature above and near its critical temperature is used as a solvent to dissolve a solid component. At near-critical states, molecular clusters are formed in abundance; the formation of clusters of small solvent molecules about a large solute molecule effectively contributes to the solvent power of the compressed gas. The fugacity coefficient ϕ_i is reduced, and the solubility y is raised.

An attractive application is the extraction of heat-sensitive biological materials using light gases such as carbon dioxide, ethane, and ethylene as the solvent gas. Their critical temperatures are 304, 305, and 282°K, respectively. Hence, they are often good solvents for supercritical extractions near room temperature. Expansion of the saturated gas from the extractor precipitates the extract for recovery, and the gas is ready to be recycled by compression to the extractor for reuse. Heating and cooling requirements are minimal. Meanwhile, the extract is not exposed to any high-temperature or low-temperature conditions, a vital consideration for heat-sensitive materials, such as many biological products.

In the food industry, supercritical carbon dioxide is used for the decaffeination of coffee, deodorization of plant oils, and extraction of hops and spices. In the tobacco industry, supercritical carbon dioxide is utilized in denicotinizing tobacco. Studies have also been made for the refining of coal by supercritical extraction.

As a general rule, extraction is best when the density of the compressed gas approaches that of the liquid. Often there is a large increase of solubility as the pressure increases at pressures just above the critical pressure. Further increased pressure then results in little increased solubility.

Haselow [14] has compared predictions made with seven eos's for binary mixtures. The four best sets of predictions as expressed as absolute average deviations of 31 binary mixtures four are as follows: Redlich-Kwong, 34; cubic chain-of-rotators, 37; Hans-Coy-Bono-Kwolz-Harling, 38; and Heyen, 40. The other three showed much larger deviations. It can be concluded that predictions involving supercritical fluids are not easy to make with high accuracy because of the high uncertainty in predicting critical properties. Such properties had to be estimated in several systems by group-contribution methods. Furthermore, several eos's, otherwise considered reliable, are not suitable for predicting supercritical information or for solid solutes.

Some success has, however, been obtained in predicting data involving solid phase, e.g., solubility of solid carbon dioxide in compressed air at 143°K (using a truncated second virial eos at pressures up to 40 atm). Good predictions were also realized for existence of solid carbon dioxide in liquid and gaseous mixtures of methane and carbon dioxide. The Peng-Robinson eos was used with success.

REFERENCES

1. Frost, A. A., and Kalkwarf, D. R. *J. Chem. Phys.* 21: 264, 1953.
2. Pasek, G., and Thodos, G. *J. Chem. Eng. Data* 7: 21, 1962.
3. Reynes, E. G., and Thodos, G. *Ind. Eng. Chem. Fund.* 1: 127, 1962.
4. Harlacher, E. A., and Braun, W. G. *Ind. Eng. Chem. Proc. Des. Dev.* 9: 479, 1970.
5. Lee, B. I., and Kesler, M. G. *AIChE J.* 21: 510, 1975.
6. Curl, R. F., and Pitzer, K. S. *Ind. Eng. Chem.* 50: 265, 1958.
7. Lydersen, A. L., Greenkorn, R. A., and Hougen, O. A. Engineering Experimental Station Report no.4, Madison: University of Wisconsin, October 1955.
8. Chao, K. C., and Seader, J. D. *AIChE J.* 7: 598, 1961.
9. Jin, Z. L., Greenkorn, R. A., and Chao, K. C. *AIChE J.* 41: 1602, 1995.
10. Han, S. J., Lin, H. M., and Chao, K. C. *Chem. Eng. Sci.* 43: 2327–2367, 1988.
11. Renon, H., and Prausnitz, J. M. *AIChE J.* 14: 143, 1968.
12. Magnussen, T., Rasmussen, P., and Fredenslund, A. *Ind. Eng. Chem. Proc. Des. Dev.* 20: 331–339, 1981.

Even if the actual chemical reaction pathways are not known, a set of linear independent reactions can be generated from some given set of components, thereby allowing Equation (4.541). This approach is known as the stoichiometric formulation and is considered in some detail in Section 4.5.5. We must emphasize that the independent reactions generated by this method do not necessarily describe the actual chemical reactions that occur in the system. These independent reactions relate the mole changes of each species in each reaction to changes in the extent of reaction via a stoichiometric coefficient, i.e., Equation (4.540). Since the final equilibrium state will be independent of the particular pathway taken, the final equilibrium compositions of the given species will still be correctly described by Equation (4.541).

4.5.2 EQUILIBRIUM CONSTANTS

To begin with, consider a system in which only one independent reaction occurs. The chemical potential of each species i in the mixture can be represented as follows (see Section 4.2.8):

$$\mu_i = g_i^0 + RT \ln \frac{f_i}{f_i^{P,0}} \quad (4.542)$$

where g_i^0 is the molar Gibbs free energy of pure i in its standard state (denoted by the superscript 0) at the given temperature and reference pressure p^0 (typically chosen to be unity in the units of pressure that are chosen, such as 1 bar), f_i is the fugacity of species i in the mixture at the given temperature and pressure p of the mixture, and $f_i^{P,0}$ is the fugacity of pure i in its standard state at and p^0 . Combining Equation (4.541) with Equation (4.541) yields

$$\sum_i \nu_i \left(g_i^0 + RT \ln \frac{f_i}{f_i^{P,0}} \right) = 0 \quad (4.543)$$

or

$$\prod_i \left(\frac{f_i}{f_i^{P,0}} \right)^{\nu_i} = \exp \left[- \left(\sum_i \nu_i g_i^0 / RT \right) \right] \quad (4.544)$$

The equilibrium compositions of all components participating in the reaction are determined from Equation (4.544).

By convention, the standard-state Gibbs energy change upon reaction, Δg_{rx}^0 , is written as

$$\Delta g_{rx}^0 = \sum_i \nu_i g_i^0 \quad (4.545)$$

with all the components being in their respective standard states. The equilibrium constant, K_a , for the reaction is defined as

$$K_a \equiv \prod_i \left(\frac{f_i}{f_i^{P,0}} \right)^{\nu_i} \quad (4.546)$$

so that

$$\Delta C_p^0 = \sum_i \nu_i C_{p,i}^0 \quad (4.552)$$

in which $C_{p,i}^0$ is the isobaric heat capacity of pure i in its standard state at the reference pressure p^0 .

Equation (4.550) also allows one to determine how the equilibrium constant varies with temperature. With Equation (4.547), Equation (4.550) implies that

$$\frac{d \ln K_a}{dT} = - \frac{d(\Delta g_{rx}^0 / RT)}{dT} = \frac{\Delta h_{rx}^0}{RT^2} \quad (4.553)$$

If the reaction is exothermic, or $\Delta h_{rx}^0 < 0$, then K_a decreases with an increase in temperature. Conversely, K_a increases with an increase in temperature when the reaction is endothermic, or $\Delta h_{rx}^0 > 0$.

Substitution of Equation (4.551) into Equation (4.553) yields, upon an integration by parts, the following expression for the standard-state Gibbs energy change upon reaction:

$$\frac{\Delta g_{rx}^0(T)}{RT} = \frac{\Delta g_{rx}^0(T_0) - \Delta h_{rx}^0(T_0)}{RT_0} + \frac{\Delta h_{rx}^0(T_0)}{RT} + \frac{1}{T_0} \int_{T_0}^T \frac{\Delta C_p^0}{R} dT - \int_{T_0}^T \frac{\Delta C_p^0}{RT} dT \quad (4.554)$$

which then can be used to determine K_a at a given temperature. Often, Δh_{rx}^0 does not vary appreciably with temperature. Thus, Equation (4.551) can be integrated with a constant Δh_{rx}^0 to yield

$$\ln K_a(T) = \ln K_a(T_0) = - \frac{\Delta h_{rx}^0}{R} \left(\frac{1}{T} - \frac{1}{T_0} \right) \quad (4.555)$$

implying that $\ln K_a$ is a linear function of $1/T$. Equation (4.555) provides a useful means of correlating equilibrium constants with temperature. In general, over small temperature changes, $\ln K_a$ is nearly linear to $1/T$ in plots.

The determination of both Δg_{rx}^0 and Δh_{rx}^0 requires that the reference state, or standard state, be known. In general, the choice of the standard state varies. For gases, both real and ideal, the standard state is chosen as the pure materials in an ideal-gas unit fugacity state (that is, at a pressure p^0 , which is unity for whatever choice of pressure units is desired; hence, f_i must also be expressed in the same pressure units). Thus, in this case, Δg_{rx}^0 and Δh_{rx}^0 represent changes for the components if they were ideal gases, and not the corresponding changes for the real gases (likewise, in Equations (4.551 and 4.552), $C_{p,i}^0$ represents the isobaric heat capacity of pure i as an ideal gas). With this choice of standard state, the reference fugacities, $f_i^{p,0}$, are always chosen to be unity fugacities, so that, in effect, Δg_{rx}^0 and Δh_{rx}^0 are functions of temperature only. Consequently, K_a is only a function of temperature.

Some tables list the Gibbs energies of formation for states that are different from the ideal-gas unity fugacity state. For example, for substances that are typically solutes, properties at two or more standard states may be given. One standard state is the solute as a pure solid (in the crystalline state) and the other is for the solute in solution at a specified concentration.

In the cases discussed above, most of the standard states are chosen at a fixed reference pressure. Hence, neither K_a nor Δg_{rx}^0 is a function pressure. Yet, if one or more of the standard states for any of the components were chosen to be at the system pressure, p , then both K_a and Δg_{rx}^0 would become

The pressure correction for each $f_i^p / f_i^{p,0}$ can, however, be readily evaluated. If the liquid solution is ideal (so that $\gamma_i = 1$), a further simplification results:

$$K_a = K_x \quad (\text{ideal solution; pressure correction neglected}) \quad (4.561)$$

For an equilibrium constant of a heterogeneous chemical reaction where the components are present in separate phases, the standard states of each component may be different. Let there be a reaction between a pure solid, say component 1, and additional components all present in the vapor phase. The equilibrium constant is now expressed as

$$K_a \left(\frac{f_1^p}{f_1^{p,0}} \right)^{v_1} \prod_{i \neq 1} f_i^{v_i}$$

where, in the gas phase, the standard-state fugacities are taken as unit fugacity. With the standard state of the pure solid chosen to be a pressure of 1 bar or the solid's vapor pressure at the given temperature, $f_1^p / f_1^{p,0}$ is often taken as being approximately equal to unity. Hence, the equilibrium constant reduces to

$$K_a = \prod_i f_i^{v_i} \quad (\text{pressure correction of the solid neglected}) \quad (4.562)$$

Further simplification would result if the gaseous components were assumed to behave as an ideal-gas mixture (see Equation [4.558]).

Example 4.29

Calculate the equilibrium mole fractions for the decomposition of nitrogen tetroxide as a result of the reaction $\text{N}_2\text{O}_4(\text{g}) = 2 \text{NO}_2(\text{g})$ at 25°C and 1 bar. Assume the components form an ideal-gas mixture. Initially there is only 1 mol of N_2O_4 .

Solution

The equilibrium relation is given by Equation (4.557), in which

$$K_a = \prod_i f_i^{v_i} = \left(\prod_i \phi_i^{v_i} \right) \left(\prod_i y_i^{v_i} \right) P^{v_t} = \frac{y^2 \text{NO}_2}{y \text{N}_2\text{O}_4} = \exp[-\Delta g_{rx}^0(T = 25^\circ\text{C}, P = 1 \text{ bar}) / RT]$$

where the fugacity coefficients are all unity, since the components form an ideal-gas mixture and the standard-state fugacities were chosen as 1 bar. The pressure also cancels out of the equation, since $P = 1$ bar. Using the table provided at the end of this chapter for the Gibbs energy of formation for each component, then, with Equation (4.548),

$$\Delta g_{rx}^0(T = 25^\circ\text{C}, P = 1 \text{ bar}) = 2\Delta g_{f,\text{NO}_2}^0 - \Delta g_{f,\text{N}_2\text{O}_4}^0 = 4.7 \text{ kJ/mol}$$

so that $K_a = 0.15$.

If ξ moles of N_2O_4 react, there will be $1 - \xi$ moles of N_2O_4 remaining. In addition, 2ξ moles of NO_2 would have been produced. Therefore, there will be $(1 - \xi) + (2\xi) = 1 + \xi$ total moles at equilibrium. Hence, the equilibrium mole fractions of each species will be given by

$$K_a = \prod_i f_i^{v_i} = \left(\prod_i \phi_i^{v_i} \right) \left(\prod_i y_i^{v_i} \right) P^v = K_\phi K_y P^v$$

but the above relation cannot be further simplified. With $P = 1$ bar, we have that

$$0.15 = \frac{y_{\text{NO}_2}^2}{y_{\text{N}_2\text{O}_4}} \frac{\phi_{\text{NO}_2}^2}{\phi_{\text{N}_2\text{O}_4}}$$

whereas before

$$y_{\text{N}_2\text{O}_4} - \frac{1-\xi}{2+\xi} \quad y_{\text{NO}_2} = \frac{2\xi}{2+\xi} \quad y_{\text{N}_2} = \frac{1}{2+\xi}$$

In this nonideal example, the fugacity coefficients are also functions of temperature, pressure (which is 1 bar), and mole fractions. Numerical solution is required for this case, in addition to an expression for the fugacity coefficients of the components of the mixture (see Section 4.2.8).

Example 4.30

Now consider the following two gas-phase reactions with the given equilibrium constants:



The reactions occur at 2 bar, and initially there are 2 moles of A, 1 mole of B, and 3 moles of D. Assume the components form an ideal-gas mixture.

Solution

Begin by defining two extents of reaction, ξ_1 and ξ_2 . At equilibrium, there will be $2\xi_1$ moles of A, $1\xi_1$ moles of B, $\xi_1 - \xi_2$ moles of C, $3 - \xi_2$ moles of D, and $2\xi_2$ moles of E. Thus, the total number of moles of all species at equilibrium will be $6 - \xi_1$ moles. Therefore,

$$K_{a1} = \frac{y_{\text{C}}}{y_{\text{A}} y_{\text{B}} P} \quad \text{or} \quad 1.5 = \frac{(\xi_1 - \xi_2)(6 - \xi_1)}{2(2 - \xi_1)(1 - \xi_1)}$$

$$K_{a2} = \frac{y_{\text{E}}^2}{y_{\text{C}} y_{\text{D}}} \quad \text{or} \quad 2.5 = \frac{4\xi_2^2}{(\xi_1 - \xi_2)(3 - \xi_2)}$$

Numerical solution of the above two expressions yields $\xi_1 = 0.73$ moles and $\xi_2 = 0.54$ moles. Hence, at equilibrium

$$y_{\text{A}} = 0.24 \quad y_{\text{B}} = 0.050 \quad y_{\text{C}} = 0.036 \quad y_{\text{D}} = 0.47 \quad y_{\text{E}} = 0.21$$

to the reactor is 1 mole, the above equation also describes the fraction of methane that has reacted (as well as providing the number of moles of solid carbon that was produced by the reaction).

4.5.3 PHASE RULE FOR CHEMICALLY REACTING SPECIES

The Gibbs phase rule is modified in the following way when both phase and chemical equilibria need to be satisfied:

$$F = n - 2 - \pi - r$$

where n is the number of components, π is the number of phases, and r is the number of independent reactions. Each reaction (via Equation (4.541)) provides another constraint on the chemical potentials of the species participating in the reaction, serving to decrease the number of independently variable intensive properties of the system.

As an example of the application of the phase rule with reaction, consider a mixture of four components in which only two participate in a reaction. If all components are present in the gas phase, then $F = 4 + 2 - 1 - 1 = 4$. Hence, only four intensive variables are independently variable (e.g., T , P , y_1 , and y_2 ; or P , y_1 , y_2 , and y_3) if the vapor is ideal. For example, the independent reaction yields the following form of the equilibrium constant:

$$K_a(T) = \frac{y_2}{y_1}$$

and not all sets of four intensive variables can be chosen to describe the system. The above reaction-equilibrium relation reveals that T , y_1 , and y_2 are not independently variable. Once any two of these three variables are chosen, the value of the other is fixed by the reaction-equilibrium relation. Thus, from the set of four intensive variables denoting the degrees of freedom of the system, T , y_1 , and y_2 cannot all be chosen. At least two others, such as p and y_3 , must be chosen to generate a complete set of four intensive variables (e.g., T , y_1 , P , and y_3).

If the gas phase is not ideal, the restriction on T , y_1 , and y_2 is removed. Fugacity coefficients would now appear in the reaction-equilibrium relations, which themselves are functions of T , p , and the mole fractions of the components (say y_1 , y_2 , and y_3). Hence, the reaction-equilibrium relation no longer provides a constraint on just T , y_1 , and y_2 , although it still provides a constraint on p , and all the $(n - 1)$ mole fractions. T , y_1 , and y_2 can again be chosen, in addition to a fourth intensive variable (such as p or y_3), to generate a set of four intensive variables denoting the degrees of freedom of the system.

As another example, consider the heterogeneous reaction $A(g) + B(g) = C(s)$. The phase rule states that $F = 3 + 2 - 2 - 1 = 2$, so that only two intensive variables are independently variable. Since C is present as a pure solid, one of those independent variables cannot be a mole fraction of C . Only the mole fraction of A , or B , in the vapor phase is relevant. The appropriate reaction-equilibrium relationship is

$$K_a(T) = \frac{f_C^P / f_C^{P,o}}{(f_A / f_A^{P,o})(f_B / f_B^{P,o})}$$

Now, the left-hand side of the above expression is only a function of T (the standard state of the pure solid is chosen as $P = 1$ bar or the vapor pressure, and so is only a function of T), while the right-hand side is only a function of T , p , and y_A (or y_B). With the degrees of freedom set at two, any two of these intensive variables can be chosen without overspecifying the system.

$$\dot{n}_{out} = \sum_i \dot{n}_{out,i} = \dot{n}_{in} + \xi \sum_i v_i \quad (4.567)$$

with the energy balance being rewritten as

$$H_{in} \dot{n}_{in} = \dot{n}_{in} \sum_i y_{in,i} \bar{H}_{in,i} = \dot{n}_{out} \sum_i y_{out,i} \bar{H}_{out,i} = H_{out} \dot{n}_{out} \quad (4.568)$$

which yields, in combination with the mole balance, Equation (4.567), the following upon rearrangement:

$$\sum_i \dot{n}_{in,i} (\bar{H}_{out,i} - \bar{H}_{in,i}) = -\xi \sum_i v_i \bar{H}_{out,i} = -\xi \Delta \bar{H}_{rxn,out} \quad (4.569)$$

where $\Delta \bar{H}_{rxn,out}$ is the heat of reaction based on the outlet conditions and is calculated not from the enthalpies of the pure components, but from their partial molar enthalpies (so that enthalpy of mixing effects are included in this term).

Equation (4.569) is a general result for the steady-state adiabatic reactor with a single inlet and outlet stream. For convenience, let us assume that we have an ideal-gas mixture, so that $\bar{H}_i = H_i(T)$, where H_i is the pure-component molar enthalpy of species i . Therefore, Equation (4.569) becomes

$$\sum_i \dot{n}_{in,i} (H_i(T_{out}) - H_i(T_{in})) = -\xi \Delta h_{rxn}(T_{out}) \quad (4.570)$$

where $\Delta h_{rxn}(T_{out})$ is now the heat of reaction (as defined by Equation (4.549)) at the exiting temperature T_{out} . The left side of Equation (4.570) can be rewritten as an integral over the pure-component isobaric heat capacities from T_{in} to T_{out} , while the heat of reaction, if known at some reference temperature T_0 , can be rewritten using Equation (4.551), so that

$$\sum_i \dot{n}_{in,i} \int_{T_{in}}^{T_{out}} C_{p,i} dT = -\xi \Delta h_{rxn}^0(T_0) - \xi \sum_i v_i \int_{T_0}^{T_{out}} C_{p,i} dT \quad (4.571)$$

or

$$\xi = \frac{-\sum_i \dot{n}_{in,i} \int_{T_{in}}^{T_{out}} C_{p,i} dT}{\Delta h_{rxn}^0(T_0) - \sum_i v_i \int_{T_0}^{T_{out}} C_{p,i} dT} \quad (4.572)$$

with T_{in} known, and ξ is just a function of T_{out} .

Since the exiting stream is at chemical equilibrium, we are able to use the equilibrium relations discussed in Section 4.5.2. With the exiting temperature equal to T_{out} , the equilibrium constant for the ideal-gas mixture at the outlet is equal to

$$\xi = 1 - \sqrt{\frac{1}{1 + \Gamma(T_{out})}}$$

where

$$\Gamma(T_{out}) = \frac{P_{out} \sqrt{27 H_a(T_{out})}}{4}$$

The value of K_a at T_{out} can be determined from Equation (4.554). For $T_0 = 298.15^\circ$ and a unit ideal-gas fugacity of $P = 1$ bar, $\Delta g_{f,N_2}^0 = 0$, $\Delta g_{f,H_2}^0 = 0$, and $\Delta g_{f,NH_3}^0 = -16.5$ kJ/mol, so that $\Delta g_{rx}^0(T_0) = -33$ kJ/mol, and $\Delta h_{f,N_2}^0 = 0$, $\Delta h_{f,H_2}^0 = 0$, and $\Delta h_{f,NH_3}^0 = -46.1$ kJ/mol, so that $\Delta h_{rx}^0(T_0) = -92.2$ kJ/mol. (These values were taken from Table 4.7.) Therefore, $\ln K_a(T = 298.15 \text{ K}) = 13.3$. Isobaric heat capacities of the components are found in Smith et al. (2001).

Using the given data, one finds from Equation (4.554) that, for example, $\ln K_a(T = 800^\circ\text{K}) = -11.6$. Since the heat of reaction is negative, K_a decreases with an increase in T_{out} . Thus, Equation (4.575) indicates that ξ decreases with an increase in T_{out} . For $P_{out} = 300$ bar, ξ ranges from $\xi = 0.998$ mol/s at $T_{out} = 298.15$ to $\xi = 0.0955$ mol/s at $T_{out} = 1000^\circ\text{K}$.

Now, ξ is also related to T_{out} via the energy balance relation, Equation (4.572). Since the heat of reaction is negative and the reactor is adiabatic, Equation (4.572) reveals that an increase in ξ results in an increase in T_{out} . For example, with $T_{in} = 298.15^\circ = 25^\circ\text{C}$, $T_{out} = 300^\circ$ corresponds to $\xi = 0.00232$ mol/s, while $T_{out} = 800^\circ$ corresponds to $\xi = 0.753$ mol/s.

When plotted as ξ versus T_{out} , Equation (4.572) shows ξ increasing with an increase in T_{out} , while Equation (4.573) shows ξ decreasing with an increase in T_{out} . The point at which Equation (4.572) and Equation (4.575) intersect determines the adiabatic outlet temperature and the extent of reaction. For $T_{in} = 298.15$, we find that $T_{out} = 688$ and $\xi = 0.563$ mol/s. Thus, the outlet compositions are equal to $y_{out,N_2} = 0.152$, $y_{out,H_2} = 0.456$, and $y_{out,NH_3} = 0.392$.

4.5.5 STOICHIOMETRIC FORMULATION

As stated in Section 4.5.1, even if the actual chemical reaction pathways are not known, linear independent reactions can be generated from the given components, thereby allowing one to determine equilibrium compositions via Equation (4.541). This approach, known as the stoichiometric formulation, is discussed below. Although the independent reactions generated by this method do not necessarily describe the chemical reactions that occur in the system, they enable one, however, to relate the mole changes of each species in each reaction to changes in the extent of reaction via a stoichiometric coefficient. Since the final equilibrium state is independent of the particular pathway taken, the final equilibrium compositions of the given species are still correctly described by the chemical equilibrium condition in Equation (4.541).

The stoichiometric formulation begins with the introduction of a matrix **D** in which each element d_{ij} denotes the number of atoms of type i in component j . Each row of the matrix therefore represents an element found in each component, while the columns represent a given component present in the system. Let there be m total elements and n' total components. Note that components found in two or more phases, e.g., $\text{H}_2\text{O}(\text{l})$ and $\text{H}_2\text{O}(\text{g})$, are counted as distinct components. Thus, if there are up to n components in each of p phases, then $n \leq n' \leq np$.

Example 4.33

Given CO_2 , H_2 , C , and H_2O in the gaseous phase and H_2O in a separate liquid phase, generate the corresponding matrix **D**.

the number of components given as n' , the number of independent reactions is equal to $n' - c$. The stoichiometric coefficient for component j participating in reaction r ($r = 1, \dots, n' - c$) can be obtained from the following vector equation:

$$\mathbf{D}\mathbf{v}_r = 0 \quad (4.576)$$

where \mathbf{v}_r is a column vector of stoichiometric coefficients $v_{j,r}$, in which the stoichiometric coefficient of component j in the independent reaction r is $v_{j,r}$, where $r = 1, \dots, n' - c$.

Example 4.34

Determine the number of independent reactions, and suggest some possible reaction pathways for CO_2 , H_2 , C , CO , and H_2O .

Solution

The matrix \mathbf{D} is given by

$$\mathbf{D} = \begin{array}{c|ccccc} & \text{CO}_2 & \text{H}_2 & \text{C} & \text{CO} & \text{H}_2\text{O} \\ \hline \text{C} & 1 & 0 & 1 & 0 & 0 \\ \text{H} & 0 & 2 & 0 & 0 & 2 \\ \text{O} & 2 & 0 & 0 & 1 & 1 \end{array}$$

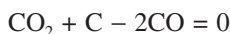
When the matrix is reduced to echelon form by Gauss-Jordan elimination, the rank of the matrix can be shown to be equal to 3. With $n' = 5$, the number of independent reactions is $5 - 3 = 2$. Equation (4.575) requires that, for each of the two independent reactions,

$$\begin{pmatrix} d_{11} & d_{12} & d_{13} & d_{14} & d_{15} \\ d_{21} & d_{22} & d_{23} & d_{24} & d_{25} \\ d_{31} & d_{32} & d_{33} & d_{34} & d_{35} \end{pmatrix} \times \begin{pmatrix} v_1 \\ v_2 \\ v_3 \\ v_4 \\ v_5 \end{pmatrix} = \begin{pmatrix} 0 \\ 0 \\ 0 \end{pmatrix}$$

With the given elements of the matrix \mathbf{D} , the above vector equation reduces to

$$\begin{array}{rclclcl} v_1 & & +v_3 & +v_4 & & = & 0 \\ & +2v_2 & & & +2v_5 & = & 0 \\ 2v_1 & & & +v_4 & +v_5 & = & 0 \end{array}$$

These relations describe a set of three equations with five unknowns. Hence, we are free to choose the values of any two coefficients. For example, let us choose $v_1 = 1$ and $v_2 = 0$. Therefore, $v_3 = 1$, $v_4 = -2$, and $v_5 = 0$. Thus, one independent reaction would be



when $v_1 = 0$ and $v_2 = 1$, so that $v_3 = -1$, $v_4 = 1$, and $v_5 = -1$, and the second independent reaction would be



Smith, J. M., Van Ness, H. C., and Abbott, M. M. *Introduction to Chemical Engineering Thermodynamics*, 6th ed., New York: McGraw-Hill, 2001.

Tester, J. W., and Modell, M. *Thermodynamics and Its Applications*, 3rd ed., Upper Saddle River, NJ: Prentice Hall, 1997.

DATA REFERENCES

Where to find thermophysical property data?

See Chapter 1 of this handbook plus several of the books listed in the references for this chapter for comprehensive tables of energies of formation. Two other widely referenced sources from which enthalpies and free energies of formation have been compiled are:

“TRC Thermodynamic Tables—Hydrocarbons,” Thermodynamic Research Center, Texas A&M Univ. System, College Station, TX.

“The NBS Tables of Chemical Thermodynamic Properties,” *Physical and Chemical Reference Data* 11 (suppl. 2): 1982.

When thermodynamic property data cannot be found, one may use group-contribution methods to estimate the enthalpy and Gibbs energy of formation. These methods are discussed in detail in

Reid, R. C., Prausnitz, J. M., and Poling, B. E., *The Properties of Gases and Liquids*, 4th ed., New York: McGraw-Hill, 1987.

5.5.9	Noncircular Conduits.....	435
5.5.10	Turbulent Drag Reduction.....	437
5.5.11	Compressible Flows	438
5.5.11.1	Isothermal Pipe Flow	440
5.5.11.2	Adiabatic Flow	441
5.5.11.3	Choked Flow	441
5.5.11.4	Isentropic Nozzle Flow	442
5.5.11.5	Supersonic Flow	442
5.6	Pumps and Compressors	443
5.6.1	Pump Types	443
5.6.2	Centrifugal Pump Characteristics.....	444
5.6.2.1	Required Head.....	446
5.6.2.2	Composite Curves	446
5.6.2.3	Cavitation and NPSH.....	447
5.6.2.4	Specific Speed.....	449
5.6.3	Compressors	449
5.6.3.1	Isothermal, Isentropic, and Polytropic Operations	451
5.6.3.2	Staged Operation.....	452
5.7	Flow Measurement and Control.....	453
5.7.1	Pitot Tube.....	453
5.7.2	Venturi and Nozzle	454
5.7.3	Orifice Meter	455
5.7.3.1	Incompressible Flow	455
5.7.3.2	Compressible Flow.....	460
5.7.3.3	Loss Coefficient	462
5.7.3.4	Applications.....	462
5.8	Control Valves	462
5.8.1	Valve Characteristics	464
5.8.2	Valve Sizing Equations—Incompressible Flows	464
5.8.2.1	Matching Valve Trim and System Characteristics	465
5.8.3	Compressible Flows	468
5.8.4	Viscosity Correction	473
	References	476

5.1 INTRODUCTION

The flow behavior of fluids is crucial to virtually every aspect of the chemical process and related industries. The most common application involves the transportation of fluids through piping systems containing fittings, valves, etc., by means of a driving force such as that provided by a pump, static elevation change, or some other source of pressure. While this is indeed important, an understanding of fluid flow is the key to various other operations such as packed and fluidized beds, fluid-solid separations, safety relief systems, flow metering and control, etc. These flows may be either laminar or turbulent, and the fluids may be either incompressible Newtonian or non-Newtonian liquids, compressible gases, or complex two-phase flows involving gas-liquid, solid-liquid, or solid-gas combinations. Various aspects of each of these will be considered in this chapter.

5.2 FLUID PROPERTIES

The properties of a fluid that influence flow behavior are its density and viscosity. Fluids may be classified as incompressible or compressible, depending upon whether the density is constant or a

$$\tau_{yx} = G\gamma_{yx} \quad (5.5)$$

where G is the *shear modulus*, and is constant. When the stress is removed, the strain also goes to zero, representing a material with a “perfect memory.” However, a material that exhibits a “memory,” but for which the displacement is a nonlinear function of the applied force, is a *nonlinear (non-Hookean) elastic solid*:

$$G = \tau_{yx} / \gamma_{yx} = fn(\tau \text{ or } \gamma) \quad (5.6)$$

G is still the shear modulus, but it is no longer a constant; it is a *function* of the displacement gradient (strain) (γ_{yx}), or of the magnitude of the applied stress (τ_{yx}), i.e., $G(\gamma)$ or $G(\tau)$. The particular form of the function depends upon the specific nature (i.e., constitution) of the material.

If the material is a fluid with negligible resistance to deformation (e.g., a low-pressure gas), the governing equation is

$$\tau_{yx} = 0 \quad (5.7)$$

This is called an *inviscid (Pascalian) fluid*. However, if the fluid molecules exhibit a significant attraction, and the resistance to flow is directly proportional to the relative motion, the material is a *Newtonian fluid*:

$$\tau_{yx} = \mu \dot{\gamma}_{yx} \quad (5.8)$$

where $\dot{\gamma}_{yx}$ is the *rate of shear strain* or, for short, *shear rate*:

$$\dot{\gamma}_{yx} = \frac{d\gamma_{yx}}{dt} = \frac{dv_x}{dy} = \frac{V_x}{h_y} \quad (5.9)$$

Here μ is the fluid *viscosity*, defined as $\mu = d\tau_{yx}/d\dot{\gamma}_{yx}$. If the shear stress and shear rate are not proportional, the fluid is *non-Newtonian*, in which case the viscosity is not constant but is a *function* of either the shear rate or shear stress:

$$\eta = \frac{\tau_{yx}}{\dot{\gamma}_{yx}} = fn(\tau \text{ or } \dot{\gamma}) \quad (5.10)$$

Most common fluids of simple structure are Newtonian (i.e., water, air, glycerine, oils, etc.). However, fluids with complex structures (i.e., high polymer melts or solutions, suspensions, emulsions, foams, etc.) are generally non-Newtonian. Examples of non-Newtonian behavior include mud, paint, ink, mayonnaise, shaving cream, polymer melts and solutions, toothpaste, etc. Many “two-phase” systems (e.g., suspensions, emulsions, foams, etc.) are purely viscous fluids and do not exhibit significant elastic or “memory” properties. However, many high polymer fluids (e.g., melts and solutions) are *viscoelastic* and exhibit both elastic (memory) as well as nonlinear viscous (flow) properties. A classification of material behavior is summarized in Table 5.1 (in which the subscripts have been omitted for simplicity). Only purely viscous Newtonian and non-Newtonian fluids are considered here. The properties and flow behavior of viscoelastic fluids are the subject of numerous books and papers (e.g., Darby, 1976; Bird et al., 1987).

5.2.2 MEASUREMENT OF VISCOSITY

Two common methods for measuring viscosity are the cup and bob (Couette) and the tube flow (Poiseuille) viscometers.

5.2.2.1 Cup and Bob (Couette) Viscometer

This viscometer consists of two concentric cylinders, the outer "cup" and the inner "bob," with the test fluid in the annular gap. The radius of the bob is R_i , that of the cup is R_o , and the length of surface in contact with the sample is L . One of the cylinders (preferably the cup) is rotated at various controlled angular velocities (Ω), and the resulting torque (T) is measured. The shear stress is

$$\tau_{r\theta} = \frac{T}{2\pi r^2 L} = \tau \quad (5.11)$$

Setting $r = R_i$ gives the stress on the bob surface, and $r = R_o$ gives the stress on the cup. If the gap is small (i.e., $(R_o - R_i)/R_i \leq 0.02$), the average shear stress is evaluated at $(R_i + R_o)/2$, and the corresponding average shear rate is given by

$$\dot{\gamma}_{yx} = \frac{dv_\theta}{dr} = \frac{\Omega}{1 - \beta} = \dot{\gamma} \quad (5.12)$$

where $\beta = R_i/R_o$. If the gap is not small, the shear rate at the bob is given by

$$\dot{\gamma} = \frac{2\Omega}{n'(1 - \beta^{2/n'})} \quad (5.13)$$

which is accurate to 1–2% in most cases, with an extreme error of about 5% in the worst case, for any size gap and any type of fluid (e.g., Darby, 1985). Here n' is the point slope of the log-log plot of T versus Ω :

$$n' = \frac{d(\log T)}{d(\log \Omega)} \quad (5.14)$$

A series of data points of T versus Ω must be obtained in order to determine n' at each point. The viscosity at each shear rate (or shear stress) is then determined by dividing the shear stress at the bob by the shear rate at the bob for each data point.

5.2.2.2 Tube Flow (Poiseuille) Viscometer

Viscosity can also be determined by measuring the total pressure drop ($\Delta\Phi = \Delta P + \rho g \Delta z$) and flow rate (Q) in steady laminar flow through a uniform circular tube of length L and diameter D (this is called *Poiseuille flow*). The shear stress at the tube wall (τ_w) is determined from the measured pressure drop:

$$\tau_w = -\frac{\Delta\Phi}{4L/D} \quad (5.15)$$

and the shear rate at the tube wall ($\dot{\gamma}_w$) is given by

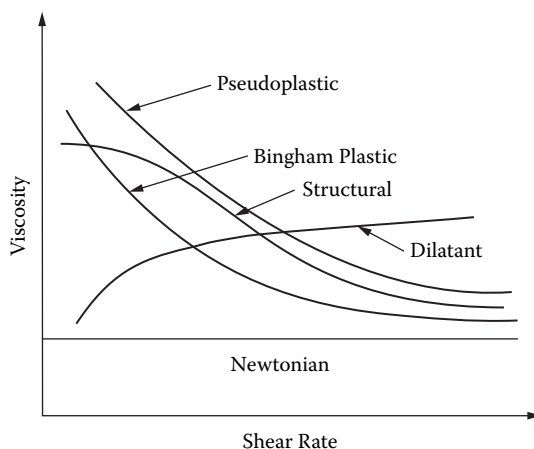


FIGURE 5.3 Viscosity versus. shear rate for fluids in Figure 5.4.

The two rheological properties required—the *yield stress*, τ_o , and the *high-shear-limiting (or plastic) viscosity*, μ_∞ —determine the flow behavior of a Bingham plastic. The viscosity function for the Bingham plastic is

$$\eta(\dot{\gamma}) = \frac{\tau_o}{\dot{\gamma}} + \mu_\infty \quad (5.21)$$

or

$$\eta(\tau) = \frac{\mu_\infty}{1 - \tau/\tau_o} \quad (5.22)$$

Since this material will not “flow” unless the shear stress exceeds the yield stress, these equations apply only when $|\tau| > \tau_o$. For smaller values of the shear stress, the material behaves as a rigid solid, i.e.,

$$\text{for } |\tau| < \tau_o \quad \dot{\gamma} = 0 \quad (5.23)$$

The Bingham plastic is *shear thinning*, i.e., the higher the shear stress or shear rate, the lower is the viscosity. This behavior is typical of many concentrated slurries and suspensions, such as muds, paints, foams, emulsions (e.g., mayonnaise), ketchup, blood, etc.

If the data (either shear stress or viscosity) exhibit a straight line on a log-log plot, the fluid follows the *power law* (or Ostwald deWaele) model:

$$\text{Power Law: } \tau = m\dot{\gamma}^n \quad (5.24)$$

The viscosity parameters are the *consistency coefficient* (m) and the *flow index* (n). The apparent viscosity function for the power law model can be expressed in terms of either the shear rate or the shear stress:

of p in the Sisko model is set equal to $1/2$, the result is equivalent to the *Bingham plastic* model:

$$\text{Bingham: } \eta(\dot{\gamma}) = \eta_{\infty} + \frac{\eta_o}{\lambda \dot{\gamma}} \quad (5.29)$$

where the yield stress τ_o corresponds to η_o/λ , and η_{∞} is the (high shear) limiting viscosity.

3. *Intermediate shear rate*: For $\eta_{\infty} \ll \eta \ll \eta_o$ and $(\lambda \dot{\gamma})^2 \gg 1$, the Carreau model reduces to the *power law model*:

$$\text{Power Law: } \eta(\dot{\gamma}) = \frac{\eta_o}{(\lambda \dot{\gamma})^{2p}} \quad (5.30)$$

where the power law parameters m and n are equivalent to the following combination of Carreau parameters:

$$m = \frac{\eta_o}{\lambda^{2p}}, \quad n = 1 - 2p \quad (5.31)$$

Other models have been proposed to provide a more accurate fit of some detailed viscosity data. Two of these are the *Meter model*, a stress-dependent viscosity model that has the same general characteristics as the Carreau model:

$$\text{Meter: } \eta(\dot{\gamma}) = \eta_{\infty} + \frac{\eta_o - \eta_{\infty}}{[1 + (\tau / \sigma)^{2a}]} \quad (5.32)$$

where σ is a characteristic stress parameter and a is the shear-thinning index, and the *Yashuda model*. The Yashuda model (1981) is also similar to the Carreau model, but with one additional parameter (a total of five parameters):

$$\text{Yashuda: } \eta = \eta_{\infty} + \frac{(\eta_o - \eta_{\infty})}{[1 + (\lambda \dot{\gamma})^{2a}]^{p/a}} \quad (5.33)$$

which reduces to the Carreau model for $a = 1$. (This is also sometimes called the *Carreau-Yashuda* model.) This model is particularly useful for representing polymer melt data for broad-molecular-weight polymers for which the zero-shear viscosity is approached very gradually. Each of these last three models reduces to Newtonian behavior at very low and very high shear rates, and to power law behavior at intermediate shear rates.

It should be stressed that the specific model that best represents a given non-Newtonian, and the values of the parameters defined by the model, cannot be predicted accurately from first principles or from more basic information. The specific function and the values of the parameters must be determined from laboratory viscosity measurements.

Example 5.1

The following data were taken in a cup and bob viscometer, having a bob radius of 2.5 cm, a cup radius of 2.75 cm, and a bob length of 6.5 cm. Determine the viscosity of the sample and the nature of the shear dependence of this viscosity.

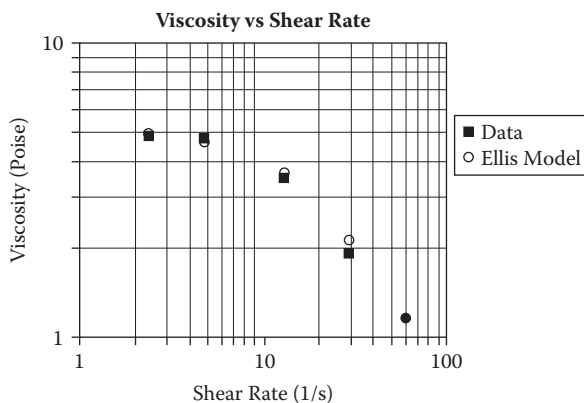


FIGURE 5.5 Viscosity vs. shear rate.

5.3 CONSERVATION PRINCIPLES

The flow behavior of fluids is governed by the basic laws for conservation of mass, energy, and momentum coupled with appropriate expressions for the irreversible rate processes (e.g., friction loss) as a function of fluid properties, flow conditions, geometry, etc. These conservation laws can be expressed in terms of “microscopic” or point values of the variables, or in terms of “macroscopic” or integrated average values of these quantities. In principle, the macroscopic balances can be derived by integration of the microscopic balances. However, unless the “local” microscopic details of the flow field are required, it is often easier and more convenient to start with the macroscopic balance equations.

5.3.1 CONSERVATION OF MASS

The macroscopic conservation of mass, or continuity, equation for any system is

$$\sum_{in} \dot{m}_i - \sum_{out} \dot{m}_o = \frac{dm_s}{dt} \quad (5.34)$$

where \dot{m}_i and \dot{m}_o are the rate of mass entering with streams (i) and leaving with streams (o), respectively, and m_s is the mass of the system. For a flow system at steady state,

$$\sum_{in} \dot{m}_i = \sum_{out} \dot{m}_o \quad (5.35)$$

or

$$\sum_{in} (\rho VA)_i = \sum_{out} (\rho VA)_o \quad (5.36)$$

For only one inlet and one outlet stream, this becomes

$$\dot{m}_i = \dot{m}_o \quad (5.37)$$

“velocity head.” For gases, if the pressure change is less than about 20%, the incompressible equation can be applied with reasonable accuracy by assuming the fluid density to be constant at a value equal to the average density in the system.

The α factors in the kinetic energy (or velocity head) term represent a correction factor to account for the deviation from plug flow through the conduit. For a Newtonian fluid in laminar flow in a circular tube, the profile is parabolic and the value of α is 2. For a highly turbulent flow, the profile is much flatter and $\alpha \approx 1.06$ (depending on the Reynolds number), although for practical purposes it is usually assumed that $\alpha = 1$ for turbulent flow.

Example 5.2

The mass flow rate of a hot coal-oil slurry can be determined by injecting a small sidestream of cool oil at a controlled rate and measuring the change in temperature downstream of the injection point. Calculate the flow rate of a slurry that is initially at 146.9°C (300°F) and has a density of 1200 kg/m³ and a specific heat of 0.7 kcal/kg°C (Btu/lb_m°F), if a sidestream of oil is injected at a rate of 0.454 kg/s (1 lb_m/s). The temperature of the sidestream is 15.6°C (60°F), and it has a density of 800 kg/m³ and a specific heat of 0.6 kcal/kg°C (Btu/lb_m°F). The temperature of the slurry downstream of the injection point is 147.8°C (298°F) with no sidestream injected, and 146.1°C (295°F) with the stream injected.

Solution

The steady-state energy balance applied to the slurry and sidestreams, excluding any pump in the line, is

$$\sum_{in} (h + gz + V^2/2)_i \dot{m}_i - \sum_{out} (h + gz + V^2/2)_o \dot{m}_o + \dot{Q} = 0$$

Assuming negligible change in elevation and kinetic energy, this becomes

$$h_{s1} \dot{m}_s + h_o \dot{m}_o - h_{s2} \dot{m}_s - h_{o2} \dot{m}_o + \dot{Q} = 0$$

where the subscripts s = slurry, o = oil, 1 = point upstream of injection point, and 2 = point downstream of injection point. \dot{Q} is the rate of heat lost from the pipe between point 1 and point 2. Assuming $\Delta h = c_p \Delta T$ (i.e., negligible pressure drop), this becomes

$$\dot{m}_s c_{ps} (T_1 - T_2) + \dot{m}_o c_{po} (T_o - T_1) + \dot{Q} = 0$$

For no sidestream injection, $T_2 = T'_2 = 147.8^\circ\text{C}$ (298°F):

$$\dot{Q} = \dot{m}_s c_{ps} (T'_2 - T_1)$$

Inserting this into the previous equation and solving for \dot{m}_s ,

$$\dot{m}_s = \frac{\dot{m}_o c_{po} (T_2 - T_o)}{c_{ps} (T'_2 - T_2)} = \frac{(0.454 \text{ kg/s})(0.6 \text{ kcal/kgC})(146.1 - 15.6)^\circ\text{C}}{(0.7 \text{ kcal/kgC})(147.8 - 146.1)^\circ\text{C}} = 29.9 \text{ kg/s}$$

Solution

The system is the fluid between the tank exit (at 791 kPa) and the valve exit (at 101 kPa). The loss coefficient relates the friction loss in the valve to the velocity leaving the valve, $e_f = K_f V_2^2/2$. Since the tank is much larger than the valve discharge, the velocity (and kinetic energy) in the tank can be neglected, and the flow is highly turbulent (which can be verified), so that $\alpha = 1$. The exit velocity (V_2) is then determined from the Bernoulli equation:

$$V_2 = \left[\frac{2(P_1 - P_2)}{\rho(1 + K_f)} \right]^{1/2} = \left[\frac{2(690 \times 10^3 \text{ Pa})}{(1000 \text{ kg/m}^3)(1 + 3)} \right]^{1/2} = 18.6 \text{ m/s}$$

and the mass flow rate through the valve is determined from the continuity equation:

$$\dot{m} = \rho V_2 A_2 = (1000 \text{ kg/m}^3)(18.6 \text{ m/s}) \frac{\pi}{4} (0.1524 \text{ m})^2 = 339 \text{ kg/s}$$

The x and y components of the force on the valve are determined from the corresponding components of the momentum balance equation:

$$\sum_{\text{On Fluid}} F_x = -(F_x)_{\text{On Valve}} = \dot{m}(V_{x2} - V_{x1}) = (339 \text{ kg/s})(18.6 \text{ m/s}) = 6305 \text{ N}$$

$$\sum_{\text{On Fluid}} F_y = -(F_y)_{\text{On Valve}} + P_1 A_1 = \dot{m}(V_{2y} + V_{1y}) = 0$$

$$(F_y)_{\text{On Valve}} = (791 \times 10^3 \text{ Pa}) \frac{\pi}{4} (0.1016 \text{ m})^2 = 6413 \text{ N}$$

$$\theta = \tan^{-1}(F_y / F_x) = 45.5^\circ$$

Thus there is a force component in the $-x$ direction of 6300 N and in the $+y$ direction of 5600 N. The net force is $|F| = \sqrt{F_x^2 + F_y^2} = 9000 \text{ N}$, and it acts in a direction up and to the left at an angle of 45.5° from the horizontal.

5.4 FLUID STATICS

5.4.1 THE BASIC EQUATION OF FLUID STATICS

If there is no *relative* motion within the fluid, the differential form of the energy balance (Bernoulli equation) reduces to

$$\frac{dP}{dz} = -\rho g \quad (5.45)$$

Integration of this equation gives the pressure as a function of elevation (z) if the variations of g and ρ are known. Various special cases follow.

5.4.1.1 Constant Density

For a constant-density “isochoric” (or incompressible) fluid, under constant gravity,

5.4.1.3 The Standard Atmosphere

The “standard atmosphere” is based on a representative observed average of the temperature distribution in the atmosphere, averaged over the entire earth and over all seasons:

$$\text{For } 0 < z < 11 \text{ km: } \frac{dT}{dz} = -6.5^\circ/\text{km} = -G \quad (5.54)$$

$$\text{For } z > 11 \text{ km: } T = -56.5^\circ\text{C}$$

where the average temperature at sea level ($z = 0$) is taken to be 15°C (285 K). Using this expression along with the ideal gas law gives the pressure as a function of elevation:

$$P_2 = P_1 \left[1 - \frac{G\Delta z}{T_0 - Gz_1} \right]^{Mg/RG} \quad (5.55)$$

where $T_0 = 285 \text{ K}$.

5.4.2 MOVING SYSTEMS

The basic equation of statics also applies to fluids in motion, as long as there are no *relative* motion or velocity *gradients* that give rise to shear stresses. If the motion involves a uniform acceleration, an additional component of the pressure gradient results, as illustrated.

If the fluid accelerates upward with an acceleration of a_z , this is equivalent to an increase in the gravitational acceleration, i.e.,

$$\frac{dP}{dz} = -\rho(g + a_z) \quad (5.56)$$

Likewise, an acceleration in any direction, such as the i direction, will result in a pressure gradient within the fluid in the $-i$ direction of magnitude ρa_i :

$$\frac{\partial P}{\partial x_i} = -\rho a_i \quad (5.57)$$

Example 5.4

Determine the shape of the free surface in an open container that is rotating uniformly at an angular velocity of ω (see Figure 5.7).

Solution

The uniform rotation results in an (inward) radial acceleration equal to $\omega^2 r$. This gives rise to a radial pressure gradient in the fluid, which is in addition to the vertical pressure gradient due to gravity. The total pressure differential within the fluid is thus

$$dP = \left(\frac{\partial P}{\partial z} \right) dz + \left(\frac{\partial P}{\partial r} \right) dr = \rho(-g dz + \omega^2 r dr)$$

TABLE 5.2
Standard Steel Pipe Dimensions and Capacities

TABLE 5.2 Standard Steel Pipe Dimensions and Capacities											
Nominal Pipe Size, in.	Outside Diameter, in.	Schedule No.	Wall Thickness, in.	Inside Diameter, in.	Cross-Sectional Area		Circumference, ft, or Surface, ft ² /ft of Length		Capacity at 1-ft/s Velocity		Weight of Plain-End Pipe, lb/ft
					Metal, in. ²	Flow ft ²	Outside	Inside	U.S. gal/ min	lb/h Water	
1/4	0.405	10S	.049	.307	.055	.00051	.106	.0804	.231	115.5	.19
		40ST, 40S	.068	.269	.072	.00040	.106	.0705	.179	89.5	.24
		80XS, 80S	.095	.215	.093	.00025	.106	.0563	.113	56.5	.31
1/4	0.540	10S	.065	.410	.097	.00092	.141	.107	.412	206.5	.33
		40ST, 40S	.088	.364	.125	.00072	.141	.095	.323	161.5	.42
		80XS, 80S	.119	.302	.157	.00050	.141	.079	.224	112.0	.54
3/8	0.675	10S	.065	.545	.125	.00162	.177	.143	.727	363.5	.42
		40ST, 40S	.091	.493	.167	.00133	.177	.129	.596	298.0	.57
		80XS, 80S	.126	.423	.217	.00098	.177	.111	.440	220.0	.74
1/2	0.840	5S	.065	.710	.158	.00275	.220	.186	1.234	617.0	.54
		10S	.083	.674	.197	.00248	.220	.176	1.112	556.0	.67
		40ST, 40S	.109	.622	.250	.00211	.220	.163	0.945	472.0	.85
3/4	1.050	80XS, 80S	.147	.546	.320	.00163	.220	.143	0.730	365.0	1.09
		160	.188	.464	.385	.00117	.220	.122	0.527	263.5	1.31
		XX	.294	.252	.504	.00035	.220	.066	0.155	77.5	1.71
1	1.315	5S	.065	.920	.201	.00461	.275	.241	2.072	1036.0	0.69
		10S	.083	.884	.252	.00426	.275	.231	1.903	951.5	0.86
		40ST, 40S	.113	.824	.333	.00371	.275	.216	1.665	832.5	1.13
1	1.315	80XS, 80S	.154	.742	.433	.00300	.275	.194	1.345	672.5	1.47
		160	.219	.612	.572	.00204	.275	.160	0.917	458.5	1.94
		XX	.308	.434	.718	.00103	.275	.114	0.461	230.5	2.44
1	1.315	5S	.065	1.185	.255	.00768	.344	.310	3.449	1725	0.87
		10S	.109	1.097	.413	.00656	.344	.287	2.946	1473	1.40
		40ST 40S	.133	1.049	.494	.00600	.344	.275	2.690	1345	1.68
1	1.315	80XS, 80S	.179	0.957	.639	.00499	.344	.250	2.240	1120	2.17
		160	.250	0.815	.836	.00362	.344	.213	1.625	812.5	2.84
		XX	.358	0.599	1.076	.00196	.344	.157	0.878	439.0	3.66

TABLE 5.2 (Continued)
Standard Steel Pipe Dimensions and Capacities

TABLE 5.2 (Continued) Standard Steel Pipe Dimensions and Capacities											
Nominal Pipe Size, in.	Outside Diameter, in.	Schedule No.	Wall Thickness, in.	Inside Diameter, in.	Cross-Sectional Area		Circumference, ft, or Surface, ft ² /ft of Length		Capacity at 1-ft/s Velocity		Weight of Plain-End Pipe, lb/ft
					Metal, in. ²	Flow ft ²	Outside	Inside	U.S. gal/ min	lb/h Water	
4	4.5	5S	.083	4.334	1.152	.10245	1.178	1.135	46.0	23,000	3.92
		10S	.120	4.260	1.651	.09898	1.178	1.115	44.4	22,200	5.61
		40ST, 40S	.237	4.026	3.17	.08840	1.178	1.054	39.6	19,800	10.79
		80XS, 80S	.337	3.826	4.41	.07986	1.178	1.002	35.8	17,900	14.98
		120	.438	3.624	5.58	.07170	1.178	0.949	32.2	16,100	19.00
		160	.531	3.438	6.62	.06647	1.178	0.900	28.9	14,450	22.51
5	5.563	XX	.674	3.152	8.10	.05419	1.178	0.825	24.3	12,150	27.54
		5S	.109	5.345	1.87	.1558	1.456	1.399	69.9	34,950	6.36
		10S	.134	5.295	2.29	.1529	1.456	1.386	68.6	34,300	7.77
		40ST, 40S	.258	5.047	4.30	.1390	1.456	1.321	62.3	31,150	14.62
		80XS, 80S	.375	4.813	6.11	.1263	1.456	1.260	57.7	28,850	20.76
		120	.500	4.563	7.95	.1136	1.456	1.195	51.0	25,500	27.01
6	6.625	160	.625	4.313	9.70	.1015	1.456	1.129	45.5	22,750	32.96
		XX	.750	4.063	11.34	.0900	1.456	1.064	40.4	20,200	38.55
		5S	.109	6.407	2.23	.2239	1.734	1.677	100.5	50,250	7.60
		10S	.134	6.357	2.73	.2204	1.734	1.664	98.9	49,450	9.29
		40ST, 40S	.280	6.065	5.58	.2006	1.734	1.588	90.0	45,000	18.97
		80XS, 80S	.432	5.761	8.40	.1810	1.734	1.508	81.1	40,550	28.57
8	8.625	120	.562	5.501	10.70	.1650	1.734	1.440	73.9	36,950	36.39
		160	.719	5.187	13.34	.1467	1.734	1.358	65.9	32,950	45.34
		XX	.864	4.897	15.64	.1308	1.734	1.282	58.7	29,350	53.16
		5S	.109	8.407	2.915	.3855	2.258	2.201	173.0	86,500	9.93
		10S	.148	8.329	3.941	.3784	2.258	2.180	169.8	84,900	13.40
		20	.250	8.125	6.578	.3601	2.258	2.127	161.5	80,750	22.36
40ST, 40S	30	.277	8.071	7.265	.3553	2.258	2.113	159.4	79,700	24.70	
	40ST, 40S	.322	7.981	8.399	.3474	2.258	2.089	155.7	77,850	28.55	
	60	.406	7.813	10.48	.3329	2.258	2.045	149.4	74,700	35.64	

TABLE 5.2 (Continued)
Standard Steel Pipe Dimensions and Capacities

Nominal Pipe Size, in.	Outside Diameter, in.	Schedule No.	Wall Thickness, in.	Inside Diameter, in.	Cross-Sectional Area		Circumference, ft, or Surface, ft ² /ft of Length		Capacity at 1-ft/s Velocity		Weight of Plain-End Pipe, lb/ft
					Metal, in. ²	Flow ft ²	Outside	Inside	U.S. gal/ min	lb/h Water	
16		40	0.438	13.124	18.66	0.9397	3.665	3.44	422	211,000	63.44
		XS	0.500	13.000	21.21	0.9218	3.665	3.40	414	207,000	72.09
		60	0.594	12.812	25.02	0.8957	3.665	3.35	402	201,000	85.05
		80	0.750	12.500	31.22	0.8522	3.665	3.27	382	191,000	106.13
		100	0.938	12.124	38.49	0.8017	3.665	3.17	360	180,000	130.85
		120	1.094	11.812	44.36	0.7610	3.665	3.09	342	171,000	150.79
		140	1.250	11.500	50.07	0.7213	3.665	3.01	324	162,000	170.21
		160	1.406	11.188	55.63	0.6827	3.665	2.93	306	153,000	189.11
	16	5S	0.165	15.670	8.21	1.3393	4.189	4.10	601	300,500	27.90
		10S	0.188	15.624	9.34	1.3314	4.189	4.09	598	299,000	31.75
		10	0.250	15.500	12.37	1.3104	4.189	4.06	587	293,500	42.05
		20	0.312	15.376	15.38	1.2985	4.189	4.03	578	289,000	52.27
		30, ST	0.375	15.250	18.41	1.2680	4.189	3.99	568	284,000	62.58
		40, XS	0.500	15.000	24.35	1.2272	4.189	3.93	550	275,000	82.77
		60	0.656	14.688	31.62	1.1766	4.189	3.85	528	264,000	107.50
		80	0.844	14.312	40.19	1.1171	4.189	3.75	501	250,500	136.61
		100	1.031	13.938	48.48	1.0596	4.189	3.65	474	237,000	164.82
		120	1.219	13.562	56.61	1.0032	4.189	3.55	450	225,000	192.43
		140	1.438	13.124	65.79	0.9394	4.189	3.44	422	211,000	223.64
		160	1.594	12.812	72.14	0.8953	4.189	3.35	402	201,000	245.25
18	18	5S	0.165	17.670	9.25	1.7029	4.712	4.63	764	382,000	31.43
		10S	0.188	17.624	10.52	1.6941	4.712	4.61	760	379,400	35.76
		10	0.250	17.500	13.94	1.6703	4.712	4.58	750	375,000	47.39
		20	0.312	17.376	17.34	1.6468	4.712	4.55	739	369,500	58.94
		ST	0.375	17.250	20.76	1.6230	4.712	4.52	728	364,000	70.59

TABLE 5.2 (Continued)
Standard Steel Pipe Dimensions and Capacities

TABLE 5.2 (Continued) Standard Steel Pipe Dimensions and Capacities											
Nominal Pipe Size, in.	Outside Diameter, in.	Schedule No.	Wall Thickness, in.	Inside Diameter, in.	Cross-Sectional Area		Circumference, ft, or Surface, ft ² /ft of Length		Capacity at 1-ft/s Velocity		Weight of Plain-End Pipe, lb/ft
					Metal, in. ²	Flow ft ²	Outside	Inside	U.S. gal/ min	lb/h Water	
30	30	5S	0.250	29.500	23.37	4.746	7.854	7.72	2130	1,065,000	79.43
		10, 10S	0.312	29.376	29.10	4.707	7.854	7.69	2110	1,055,000	98.93
		ST	0.375	29.250	34.90	4.666	7.854	7.66	2094	1,048,000	118.65
		20, XS	0.500	29.000	46.34	4.587	7.854	7.59	2055	1,027,500	157.53
		30	0.625	28.750	57.68	4.508	7.854	7.53	2020	1,010,000	196.08
<i>Note:</i> 5S, 10S, and 40S are extracted from Stainless Steel Pipe, ANSI B36.19–1976, with permission of the publisher, the American Society of Mechanical Engineers, New York. ST = standard wall, XS = extra strong wall, XX = double extra strong wall, and Schedules 10 through 160 are extracted from Wrought-Steel and Wrought-Iron Pipe, ANSI B36.10–1975, with permission of the same publisher. Decimal thicknesses for respective pipe sizes represent their nominal or average wall dimensions. Mill tolerances as high as ±12 1/2% are permitted.											
Plan-end pipe is produced by a square cut. Pipe is also shipped from the mills threaded, with a threaded coupling on one end, or with the ends beveled for welding, or grooved or sized for patented couplings. Weights per foot for threaded and coupled pipe are slightly greater because of the weight of the coupling, but it is not available larger than 12 in or lighter than Schedule 30 sizes 8 through 12 in, or Schedule 40 sizes 6 in. and smaller.											
To convert inches to millimeters, multiply by 25.4; to convert square inches to square millimeters, multiply by 645; to convert feet to meters, multiply by 0.3048; to convert square feet to square meters, multiply by 0.0929; to convert pounds per foot to kilograms per meter, multiply by 1.49; to convert gallons to cubic meters, multiply by 3.7854 × 10 ⁻³ ; and to convert pounds to kilograms, multiply by 0.4536.											

Note: 5S, 10S, and 40S are extracted from Stainless Steel Pipe, ANSI B36.19–1976, with permission of the publisher, the American Society of Mechanical Engineers, New York. ST = standard wall, XS = extra strong wall, XX = double extra strong wall, and Schedules 10 through 160 are extracted from Wrought-Steel and Wrought-iron Pipe, ANSI B36.10–1975, with permission of the same publisher. Decimal thicknesses for respective pipe sizes represent their nominal or average wall dimensions. Mill tolerances as high as $\pm 12\ 1/2\%$ are permitted.

Plan-end pipe is produced by a square cut. Pipe is also shipped from the mills threaded, with a threaded coupling on one end, or with the ends beveled for welding, or grooved or sized for patented couplings. Weights per foot for threaded and coupled pipe are slightly greater because of the weight of the coupling, but it is not available larger than 12 in or lighter than Schedule 30 sizes 8 through 12 in, or Schedule 40 sizes 6 in. and smaller.

To convert inches to millimeters, multiply by 25.4; to convert square inches to square millimeters, multiply by 645; to convert feet to meters, multiply by 0.3048; to convert square feet to square meters, multiply by 0.0929; to convert pounds per foot to kilograms per meter, multiply by 1.49; to convert gallons to cubic meters, multiply by 3.7854×10^{-3} ; and to convert pounds to kilograms, multiply by 0.4536.

5.5.3.2 Turbulent Flow

For smooth pipe for Reynolds numbers from 4000 to 10^6 , the *von Karman* equation provides an implicit relation between the friction factor and the Reynolds number:

$$\frac{1}{\sqrt{f}} = 4.0 \log(N_{\text{Re}} \sqrt{f}) - 0.04 \quad (5.66)$$

where $N_{\text{Re}} \sqrt{f}$ is

$$N_{\text{Re}} \sqrt{f} = \left(\frac{e_f D^3 \rho^2}{2 L \mu^2} \right)^{1/2} \quad (5.67)$$

which is independent of flow rate.

5.5.3.3 Rough Pipe

Colebrook extended the *von Karman* equation to account for tube wall roughness (ϵ/D) as follows:

$$\frac{1}{\sqrt{f}} = -4 \log \left[\frac{\epsilon/D}{3.7} + \frac{1.255}{N_{\text{Re}} \sqrt{f}} \right] \quad (5.68)$$

The *Colebrook* equation is convenient for determining the flow rate from the allowable friction loss (e.g., driving force), tube size, and fluid properties. Published plots of f vs. N_{Re} and ϵ/D (i.e., the *Moody* diagram) are usually generated from the *Colebrook* equation.

The actual size of the roughness elements on any surface will vary with the material, age and usage, deposits, dirt, scale, rust, etc. Typical values for various materials are given in Table 5.3. The most common pipe material—clean, new, commercial steel—has an effective roughness of about 0.0018 in. (0.045 mm). Other surfaces, such as concrete, may vary as much as several orders of magnitude, depending upon the nature of the surface finish.

5.5.3.4 All Flow Regimes

The expressions for the friction factor in both laminar and turbulent flows were combined into a single expression by *Churchill* (1977) as follows:

$$f = 2 \left[\left(\frac{8}{N_{\text{Re}}} \right)^{12} + \frac{1}{(A + B)^{3/2}} \right]^{1/12} \quad (5.69)$$

where

$$A = \left[2.457 \ln \left(\frac{1}{\left(\frac{7}{N_{\text{Re}}} \right)^{0.9} + \frac{0.27\epsilon}{D}} \right) \right]^{16} \quad (5.70)$$

Solution

At this temperature, the viscosity of water is 1 cP and the density is 1 g/cc. The actual ID of the sch 40 pipe is 154.1 mm (6.065 in.), and it is assumed to have a roughness of 0.045 mm (0.0018 in.). The power is the work done by the pump per unit mass of fluid ($-w$) times the mass flow rate, \dot{m} . From the Bernoulli equation for no change in pressure or elevation, this is

$$-w\dot{m} = e_f\dot{m} = \left(\frac{4fL}{D} \right) \left(\frac{V^2}{2} \right) \rho Q = \frac{32fLQ^3}{\pi^2 D^5}$$

The friction factor (f) depends on the Reynolds number ($N_{\text{Re}} = 4Q\rho/\pi D\mu = 2.61 \times 10^5$) and the relative roughness ($\epsilon/D = 2.97 \times 10^{-4}$). From the Churchill equation (or the Colebrook equation, by iteration), $f = 0.00432$. Using this value in the above equation gives $-w\dot{m} = 81.3 \text{ kW}$ (109 hp).

5.5.3.5 Water in Sch 40 Pipe

For the special case of water at 60°F in sch 40 steel ($\epsilon = 0.045 \text{ mm}$ or 0.0018 in.) pipe, the relation between flow rate, velocity, pressure drop, and pipe size is tabulated in Table 5.4. The range of values tabulated covers most of the range that would be expected in practice. Note that the friction loss is tabulated as “pressure drop” in psi per 100 ft of pipe, which is equivalent to $(100 \rho e_f/L)$ in English engineering units.

5.5.4 POWER LAW FLUIDS

The power law model is very popular for representing the viscosity of a wide variety of non-Newtonian fluids because of its simplicity and versatility. However, care should be exercised in its application; for reliable results, the range of shear stress (or shear rate) expected in the application should not extend beyond the range of the rheological data used to evaluate the model parameters. Both laminar and turbulent pipe flow of highly loaded slurries of fine particles, for example, can often be adequately represented by either of these two models, as shown by Darby et al. (1992).

5.5.4.1 Laminar Flow

The form of the power law model that applies to tube flow is

$$\tau_{rx} = -m \left(-\frac{dv_x}{dr} \right)^n \quad (5.72)$$

since the velocity gradient (shear rate) and shear stress are negative. This can be integrated to give the flow rate:

$$Q = \pi \left(\frac{\tau_w}{mR} \right)^{1/n} \left(\frac{n}{3n+1} \right) R^{(3n+1)/n} \quad (5.73)$$

which is the power law fluid equivalent of the Hagen-Poiseuille equation. The dimensionless form of this equation is

$$fN_{\text{RePL}} = 16 \quad (5.74)$$

where

$$N_{\text{RePL}} = \frac{8D^n V^{2-n} \rho}{m[2(3n+1)/n]^n} \quad (5.75)$$

is the power law Reynolds number.

5.5.4.2 All Flow Regimes

There are insufficient data in the literature to provide a reliable estimate of the effect of roughness on friction loss for non-Newtonian fluids in turbulent flow. However, the influence of roughness is normally neglected, since the laminar boundary layer thickness for such fluids is typically much larger than for Newtonian fluids (i.e., the flow conditions most often fall in the “hydraulically smooth” range for common pipe materials). An expression by Darby et al. (1992) for f for the power law fluid, which applies to both laminar and turbulent flow, is

$$f = (1 - \alpha)f_L + \frac{\alpha}{[f_T^{-8} + f_{Tr}^{-8}]^{1/8}} \quad (5.76)$$

where

$$f_L = \frac{16}{N_{\text{RePL}}} \quad (5.77)$$

$$f_T = \frac{0.0682n^{-1/2}}{N_{\text{RePL}}^{1/(1.87+2.39n)}} \quad (5.78)$$

$$f_{Tr} = 1.79 \times 10^{-4} \exp(-5.24n) N_{\text{RePL}}^{(0.414+0.757n)} \quad (5.79)$$

and the parameter α is given by

$$\alpha = \frac{1}{(1 + 4^{-\Delta})} \quad (5.80)$$

where

$$\Delta = N_{\text{RePL}} - N_{\text{RePLc}} \quad (5.81)$$

and the “critical” Reynolds number that corresponds to the onset of turbulence is given by

$$N_{\text{RePLc}} = 2100 + 875(1 - n) \quad (5.82)$$

5.5.5 BINGHAM PLASTIC FLUIDS

The Bingham plastic model usually provides a good representation for the viscosity of concentrated slurries, suspensions, sediments, emulsions, foams, etc. Such materials often exhibit a yield stress,

Buckingham-Reiner equation is implicit in f , so it must be solved by iteration for known values of N_{Re} and N_{He} .

5.5.5.2 All Flow Regimes

For the Bingham plastic fluid, there is no abrupt transition from laminar to turbulent flow, as is observed for Newtonian fluids. Instead, a gradual deviation from purely laminar flow to fully turbulent flow occurs. For turbulent flow, the friction factor can be represented by the empirical expression of Darby and Melson (1982) (as modified by Darby et al., 1992):

$$f_T = \frac{10^a}{N_{\text{Re}}^{0.193}} \quad (5.89)$$

where

$$a = -1.41[1 + 0.146 \exp(-2.9 \times 10^{-5} N_{\text{He}})] \quad (5.90)$$

For all values of N_{Re} and N_{He} , f is given by

$$f = (f_L^m + f_T^m)^{1/m} \quad (5.91)$$

where

$$m = 1.7 + \frac{40,000}{N_{\text{Re}}} \quad (5.92)$$

and f_L is given by the Buckingham-Reiner equation (5.86).

Example 5.6

Calculate the power required to pump a coal slurry that is 50% (by weight) solids at a rate of 315.5 m³/s (500 gpm) through a 6-in. sch 40 pipeline (ID = 154.1 mm) that is 16.1 km (10 mi) long. The slurry behaves as a Bingham plastic, with a yield stress of 1.16 Pa, a limiting viscosity of 40.6 × 10⁻³ Pa·s, and a density of 1162 kg/m³.

Solution

The same general equation used in Example 5.5 applies, i.e.,

$$-w\dot{m} = e_f \dot{m} = \left(\frac{4fL}{D} \right) \left(\frac{V^2}{2} \right) \rho Q = \frac{32fL\rho Q^3}{\pi^2 D^5}$$

where now the friction factor depends on both the Reynolds number ($N_{\text{Re}} = 4Q\rho/\pi D\mu_\infty = 6.42 \times 10^3$) and the Hedstrom number ($N_{\text{He}} = D^2\rho\tau_0/\mu_\infty = 7.78 \times 10^3$). Using Equations (5.90) to (5.93), we find: $a = -1.574$, $m = 7.93$, $f_L = 0.2045$, $f_T = 0.00491$, $f = 0.205$. Thus, the above equation gives $-w\dot{m} = 3860$ kW (5170 hp).

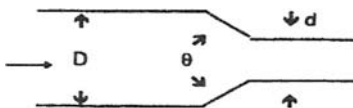
5.5.6 FITTING LOSSES

The loss coefficient for pipe is related to the Fanning friction factor by

TABLE 5.5
Loss Coefficients for Expansions and Contractions

K_i to be used with upstream velocity head, $V_1^2/2$. $\beta = d/D$

Contraction



$\theta < 45^\circ$

$N_{Re,1} < 2500$:

$$K_i = 1.6 \left[1.2 + \frac{160}{N_{Re,1}} \right] \left[\frac{1}{\beta^4} - 1 \right] \sin \frac{\theta}{2}$$

$N_{Re,1} > 2500$:

$$K_i = 1.6 [0.6 + 1.92 f_i] \left[\frac{1 - \beta^2}{\beta^4} \right] \sin \frac{\theta}{2}$$

$\theta > 45^\circ$

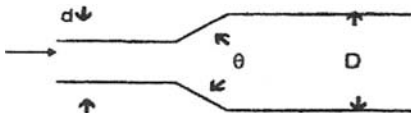
$N_{Re,1} < 2500$:

$$K_i = \left[1.2 + \frac{160}{N_{Re,1}} \right] \left[\frac{1}{\beta^4} - 1 \right] \left[\sin \frac{\theta}{2} \right]^{1/2}$$

$N_{Re,1} > 2500$:

$$K_i = [0.6 + 1.92 f_i] \left[\frac{1 - \beta^2}{\beta^4} \right] \left[\sin \frac{\theta}{2} \right]^{1/2}$$

Expansion



$\theta < 45^\circ$

$N_{Re,1} < 4000$:

$$K_i = 5.2(1 - \beta^4) \sin \frac{\theta}{2}$$

$N_{Re,1} > 4000$:

$$K_i = 2.6(1 + 3.2 f_i)(1 - \beta^2)^2 \sin \frac{\theta}{2}$$

$\theta > 45^\circ$

$N_{Re,1} < 4000$:

$$K_i = 2(1 - \beta^4)$$

$N_{Re,1} > 4000$:

$$K_{i1} = (1 + 3.2 f_i)(1 - \beta^2)^2$$

Source: Hooper, W. B., "Calculate Head Loss Caused by Change in Pipe Size,"
Chem. Eng., p. 89, Nov. 7 (1988).

fluids if the (Newtonian) Reynolds number is replaced by a single corresponding dimensionless group that adequately characterizes the influence of the non-Newtonian properties. For the power law model, the appropriate Reynolds number was derived for pipe flow:

$$N_{RePL} = \frac{2^{7-3n} \rho Q^{2-n}}{m \pi^{2-n} D^{4-5n}} \left[\frac{n}{3n+1} \right]^n \quad (5.96)$$

For the Bingham plastic, a corresponding expression for the Reynolds number based on the ratio of inertial to viscous momentum flux is

TABLE 5.7
3-*K* Constants for Loss Coefficients for Valves and Fittings

$$K_f = K_1/N_{Re} + K_i(1 + K_d/D_{in}^{0.3})$$

Fitting				$(L/D)_{eq}$	K_1	K_i	K_d
Elbows	90°	threaded, standard	$(r/D = 1)$	30	800	0.14	4.0
			$(r/D = 1.5)$	16	800	0.071	4.2
			$(r/D = 1)$	20	800	0.091	4.0
		flanged, welded, bends	$(r/D = 2)$	12	800	0.056	3.9
			$(r/D = 4)$	14	800	0.066	3.9
			$(r/D = 6)$	17	800	0.075	4.2
	45°	mitered	1 weld (90°)	60	1000	0.27	4.0
			2 welds (45°)	15	800	0.068	4.1
			3 welds (30°)	8	800	0.035	4.2
		threaded standard	$(r/D = 1)$	16	500	0.071	4.2
			long radius $(r/D = 1.5)$		500	0.052	4.0
			mitered				
	180°	threaded, close-return bend	1 weld (45°)	15	500	0.086	4.0
			2 welds (22.5°)	6	500	0.052	4.0
		flanged	$(r/D = 1)$	50	1000	0.23	4.0
			$(r/D = 1)$		1000	0.12	4.0
			all $(r/D = 1.5)$		1000	0.10	4.0
Tees	Through-branch (as elbow)	threaded	$(r/D = 1)$	60	500	0.274	4.0
			$(r/D = 1.5)$		800	0.14	4.0
		flanged	$(r/D = 1)$	20	800	0.28	4.0
			stub-in branch		1000	0.34	4.0
	Run-through	threaded	$(r/D = 1)$	20	200	0.091	4.0
		flanged	$(r/D = 1)$		150	0.05	4.0
		stub-in branch			100	0	0
Valves	Angle valve	45°	full line size, $\beta = 1$	55	950	0.25	4.0
		90°	full line size, $\beta = 1$	150	1000	0.69	4.0
	Globe valve	standard, $\beta = 1$		340	1500	1.70	3.6
	Plug valve	branch flow		90	500	0.41	4.0
		straight through		18	300	0.084	3.9
		three-way (flow through)		30	300	0.14	4.0
	Gate valve	standard, $\beta = 1$		8	300	0.037	3.9
	Ball valve	standard, $\beta = 1$		3	300	0.017	3.5
	Diaphragm	dam type			1000	0.69	4.9
	Swing check	$V_{min} = 35[\rho \text{ (lb}_m/\text{ft}^3)]^{-1/2}$		100	1500	0.46	4.0
	Lift check	$V_{min} = 40[\rho \text{ (lb}_m/\text{ft}^3)]^{-1/2}$		600	2000	2.85	3.8

Source: Darby, R., *Chemical Engineering Fluid Mechanics*, 2nd ed., Marcel Dekker, New York (2001).

is the net “driving force” for moving the fluid, and

$$\sum_i e_{fi} = \frac{1}{2} \sum_i (V^2 K_f)_i = \frac{8Q^2}{\pi^2} \sum_i \left(\frac{K_f}{D^4} \right)_i \quad (5.100)$$

where the summation is over each fitting and segment of pipe (of diameter D_i) in the system. The loss coefficients for the pipe and fittings are given by the Fanning friction factor in the 3- K formula:

TABLE 5.8
Cost of Pipe (1980 \$)

Pipe Grade ^a	Pipe Cost Correlation Parameters ^b				
	ANSI 300#	ANSI 400#	ANSI 600#	ANSI 900#	ANSI 1500#
<i>a</i>	23.1	23.9	30.0	38.1	55.3
<i>p</i>	1.16	1.22	1.31	1.35	1.39

^a ANSI grades correspond roughly to Schedules 20, 30, 40, 80, and 120, respectively.

^b Pipe cost: \$/ft = $a(ID_p)^p$, \$/m = $3.28 \times a(0.3048 ID_m)^p$

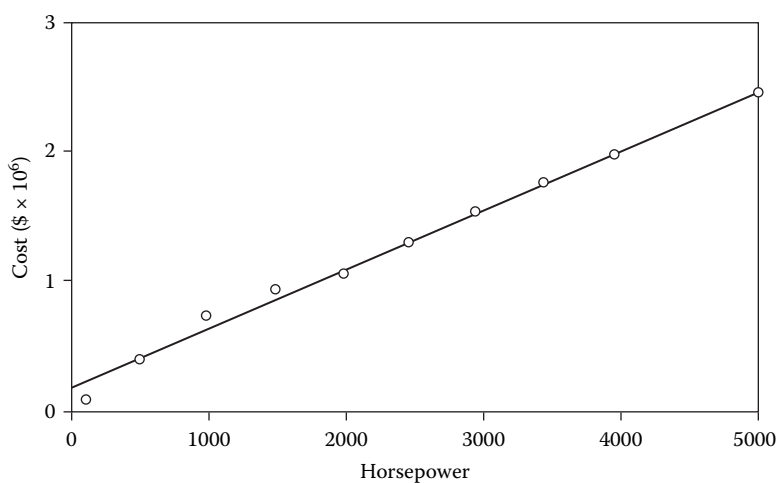


FIGURE 5.8 Cost of pump stations (1980 \$).

$$CCPS = A + BHP / \eta_e \quad (5.105)$$

where $A = \$172,800$, $B = \$605/\text{kW}$ (\$450.8/hp) (in 1980 \$), and HP/η_e is the power rating of the pump.

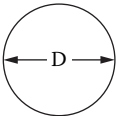
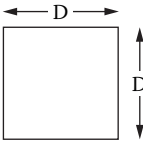
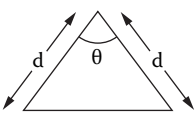
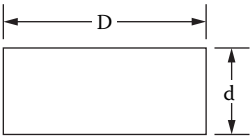
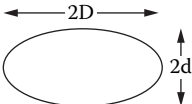
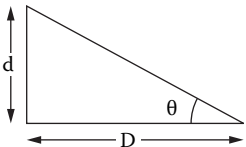
The energy cost is determined from the pumping power requirement, as calculated from the Bernoulli equation:

$$HP = -w\dot{m} \left[\frac{2fLV^2}{D} + \frac{\Delta\Phi}{\rho} \right] = \frac{32fL\dot{m}^3}{\pi^2\rho^2D^5} + \dot{m} \frac{\Delta\Phi}{\rho} \quad (5.106)$$

and the total energy cost per year is

$$EC = \frac{CHP}{\eta_e} \quad (5.107)$$

TABLE 5.9
Laminar Flow Factors for Noncircular Conduits

 Circle	$A = \pi D^2/4$ $D_h = D$	$fN_{\text{Reh}} = 16$																
 Square	$A = D^2$ $D_h = D$	$fN_{\text{Reh}} = 14.2$																
 Isosceles Triangle	$A = 1/2 (d^2 \sin \theta)$ $D_h = ((d \sin \theta)/(1 + \sin(\theta/2)))$	<table><tr><th>θ (deg)</th><th>fN_{Reh}</th></tr><tr><td>10</td><td>12.5</td></tr><tr><td>30</td><td>13.1</td></tr><tr><td>45</td><td>13.3</td></tr><tr><td>60</td><td>13.3</td></tr><tr><td>90</td><td>13.2</td></tr><tr><td>120</td><td>12.7</td></tr><tr><td>150</td><td>12.5</td></tr></table>	θ (deg)	fN_{Reh}	10	12.5	30	13.1	45	13.3	60	13.3	90	13.2	120	12.7	150	12.5
θ (deg)	fN_{Reh}																	
10	12.5																	
30	13.1																	
45	13.3																	
60	13.3																	
90	13.2																	
120	12.7																	
150	12.5																	
 Rectangle	$A = Dd$ $D_h = 2Dd/(D + d)$ $fN_{\text{Reh}} = 16/[2/3 + (11/24)(d/D)(2 - d/D)]$	<table><tr><th>D/d</th><th>fN_{Reh}</th></tr><tr><td>1</td><td>14.2</td></tr><tr><td>2</td><td>15.8</td></tr><tr><td>5</td><td>19.2</td></tr><tr><td>10</td><td>21.1</td></tr></table>	D/d	fN_{Reh}	1	14.2	2	15.8	5	19.2	10	21.1						
D/d	fN_{Reh}																	
1	14.2																	
2	15.8																	
5	19.2																	
10	21.1																	
 Ellipse	$A = \pi dD$ $fN_{\text{Reh}} = 2D_h^2(D^2 + d^2)/(D^2d^2)$ $D_h = [4dD(64 - 16c^2)]/[(d + D)(64 - 3c^4)]$ $c = (D - d)/(D + d)$ (for $0.1 < D/d < 10$)																	
 Right Triangle	$A = dD/2$ $D_h = 2dD/[d + D + (d^2 + D^2)^{1/2}]$ $\theta = \tan^{-1} (d/D)$	<table><tr><th>θ</th><th>fN_{Reh}</th></tr><tr><td>10</td><td>12.5</td></tr><tr><td>30</td><td>13.0</td></tr><tr><td>45</td><td>13.2</td></tr><tr><td>60</td><td>13.0</td></tr><tr><td>70</td><td>12.8</td></tr><tr><td>90</td><td>12.0</td></tr></table>	θ	fN_{Reh}	10	12.5	30	13.0	45	13.2	60	13.0	70	12.8	90	12.0		
θ	fN_{Reh}																	
10	12.5																	
30	13.0																	
45	13.2																	
60	13.0																	
70	12.8																	
90	12.0																	

important to note that the proper definitions of the fanning friction factor (f) and the hydraulic Reynolds number be used in these expressions, i.e.,

$$f = \frac{e_f}{(4L/D_h)(V^2/2)} \quad (5.112)$$

TABLE 5.10
Parameters for k_1 and k_2 for Various Polymer Solutions

Polymer	Conc. (mg/kg)	Diam. (cm)	k_1	k_2 (s ^{k₁})	Reference
Guar gum (Jaguar A-20-D)	20	1.27	0.05	0.009	Wang (1972)
	50		0.06	0.014	
	200		0.07	0.022	
	500		0.10	0.029	
	1000		0.16	0.028	
Guar gum	30		0.05	0.008	White (1966)
	60		0.06	0.010	
	240		0.08	0.016	
	480		0.11	0.018	
Polyacrylamide (Separan AP-30)	100	0.176	0.093	0.0342	Darby (1991)
	250	to	0.095	0.0293	
	Fresh	500	1.021	0.105	
	(Separan AP-30)	100		0.088	
	Degraded	250		0.095	
	500			0.103	
(AP-273)	10	1.090		0.12	White (1975)
(PAM E198)	10	0.945	0.21	0.0074	Virk (1970)
				0.0078	
(PAA)	300	2.0 & 3.0	0.40	0.0050	Hoffmann (1975)
	700		0.53	0.0049	
(ET-597)	125	0.69,	0.47	0.00037	Astarita (1969)
	250	1.1, &	0.39	0.0013	
	500	2.05	0.30	0.0061	
Hydroxyethyl cellulose (OP-100M)	100	2.54	0.10	0.0074	Wang (1972)
	200		0.16	0.0072	
	500		0.24	0.0068	
	1000		0.35	0.0063	
(HEC)	2860	4.8, 1.1 &	0.02	0.0310	Savins (1969)
		2.05			
Polyethylene oxide (WSR 301)	10	5.08	0.22	0.017	Goren (1967)
	20		0.21	0.016	
	50		0.19	0.014	
(W205)	10	0.945	0.31	0.0022	Virk (1970)
	105		0.26	0.0080	
Xanthan gum (Rhodopol 23)	1000	0.52	0.02	0.046	Bewersdorff (1988)

Source: Darby, R., and Pivsa-Art, S., *Canad. J. Chem. Eng.*, 69, 1395 (1991).

$$f_p = \frac{0.41}{[\ln(N_{Res} / 7)]^2} \frac{1}{(1 + N_{De}^2)^{1/2}} \quad (5.116)$$

5.5.11 COMPRESSIBLE FLOWS

For gases, the dependence of density upon pressure and temperature has a significant effect on the flow behavior when the change in pressure is significant (e.g., 20% or more) relative to the absolute pressure in the system. At low velocities (relative to the speed of sound), the relative change in pressure and associated effects are often small, and the assumption of constant density (evaluated

TABLE 5.11
Properties of Gases

Name of Gas	Chemical Formula or Symbol	Approx. Molecular Weight (M)	Weight Density, Pounds per Cubic Foot (π)	Specific Gravity Relative to Air (S_g)	Individual Gas Constant (R)	Specific Heat at Room Temperature (Btu/Lb °F)		Heat Capacity per Cubic Foot		k Equal to C_p/C_v
						C_p^a	C_v^b	C_p	C_v	
Acetylene (ethyne)	C ₂ H ₂	26.0	.0682	0.907	59.4	0.350	0.269	.0239	.0184	1.30
Air	—	29.0	.0752	1.000	53.3	0.241	0.172	.0181	.0129	1.40
Ammonia	NH ₃	17.0	.0448	0.596	91.0	0.523	0.396	.0234	.0178	1.32
Argon	A	39.9	.1037	1.379	38.7	0.124	0.074	.0129	.0077	1.67
Butane	C ₄ H ₁₀	58.1	.1554	2.067	26.5	0.395	0.356	.0614	.0553	1.11
Carbon dioxide	CO ₂	44.0	.1150	1.529	35.1	0.205	0.158	.0236	.0181	1.30
Carbon monoxide	CO	28.0	.0727	0.967	55.2	0.243	0.173	.0177	.0126	1.40
Chlorine	Cl ₂	70.9	.1869	2.486	21.8	0.115	0.086	.0215	.0162	1.33
Ethane	C ₂ H ₆	30.0	.0789	1.049	51.5	0.386	0.316	.0305	.0250	1.22
Ethylene	C ₂ H ₄	28.0	.0733	0.975	55.1	0.400	0.329	.0293	.0240	1.22
Helium	He	4.0	.01039	0.1381	386.3	1.250	0.754	.0130	.0078	1.66
Hydrogen chloride	HCl	36.5	.0954	1.268	42.4	0.191	0.135	.0182	.0129	1.41
Hydrogen	H ₂	2.0	.00523	0.0695	766.8	3.420	2.426	.0179	.0127	1.41
Hydrogen sulphide	H ₂ S	34.1	.0895	1.190	45.2	0.243	0.187	.0217	.0167	1.30
Methane	CH ₄	16.0	.0417	0.554	96.4	0.593	0.449	.0247	.0187	1.32
Methyl chloride	CH ₃ Cl	50.5	.1342	1.785	30.6	0.240	0.200	.0322	.0268	1.20
Natural gas	—	19.5	.0502	0.667	79.1	0.560	0.441	.0281	.0221	1.27
Nitric oxide	NO	30.0	.0780	1.037	51.5	0.231	0.165	.0180	.0129	1.40
Nitrogen	N ₂	28.0	.0727	0.967	55.2	0.247	0.176	.0180	.0127	1.41
Nitrous oxide	N ₂ O	44.0	.1151	1.530	35.1	0.221	0.169	.0254	.0194	1.31
Oxygen	O ₂	32.0	.0831	1.105	48.3	0.217	0.155	.0180	.0129	1.40
Propane	C ₃ H ₈	44.1	.1175	1.562	35.0	0.393	0.342	.0462	.0402	1.15
Propene (propylene)	C ₃ H ₆	42.1	.1091	1.451	36.8	0.358	0.314	.0391	.0343	1.14
Sulphur dioxide	SO ₂	64.1	.1703	2.264	24.0	0.154	0.122	.0262	.0208	1.26

Note: Weight density values were obtained by multiplying density of air by specific gravity of gas. For values at 60°F, multiply by 1.0154.

Natural gas values are representative only. Exact characteristics require knowledge of specific constituents.

^a C_p = Specific heat at constant pressure.

^b C_v = Specific heat at constant volume.

Source: Molecular weight, specific gravity, individual gas constant, and specific heat values were abstracted from, or based on, data in Table 24 of Mark's *Standard Handbook for Mechanical Engineers* (7th edition)

5.5.11.1 Isothermal Pipe Flow

For isothermal flow in a pipe, the mass flux ($G = \dot{m}/A$) can be determined by integrating the differential form of the Bernoulli to give

$$G = \sqrt{P_1 \rho_1} \left[\frac{(1 - P_2^2 / P_1^2)}{4 f L / D - 2 \ln(P_2 / P_1)} \right]^{1/2} \quad (5.123)$$

Neglecting the logarithmic term in the denominator (which comes from the change in kinetic energy of the gas) gives the *Weymouth equation*. Furthermore, if the average density of the gas is used in the Weymouth equation, i.e.,

and P_2^* is determined from

$$\Sigma K_f = \left(\frac{P_1}{P_2^*} \right)^2 - 2 \ln \left(\frac{P_1}{P_2^*} \right) - 1 \quad (5.130)$$

The pressure at the (inside of the) end of the pipe at which the flow becomes sonic (P_2^*) is a unique function of the upstream pressure (P_1) and the sum of the loss coefficients in the system (K_f). The equation is implicit for P_2^* and can be solved by iteration for given values of K_f and P_1 . For adiabatic flow, the corresponding expressions are

$$G^* = \sqrt{P_1 \rho_1} \left[k \left(\frac{P_2^*}{P_1} \right)^{(k+1)/k} \right]^{1/2} \quad (5.131)$$

and

$$\Sigma K_f = \frac{2}{(k+1)} \left[\left(\frac{P_1}{P_2^*} \right)^{(k+1)/k} - 1 \right] - \frac{2}{k} \ln \left(\frac{P_1}{P_2^*} \right) \quad (5.132)$$

5.5.11.4 Isentropic Nozzle Flow

The mass flux for the adiabatic flow of an ideal gas flowing through a frictionless conduit or a constriction (such as an orifice, valve, etc.) for which $A_1 \gg A_2$ (i.e., $V_1 \ll V_2$) is given by

$$G = \sqrt{P_1 \rho_1} \left[\left(\frac{2k}{k-1} \right) \left(\frac{P_2}{P_1} \right)^{2/k} \left\{ 1 - \left(\frac{P_2}{P_1} \right)^{(k-1)/k} \right\} \right]^{1/2} \quad (5.133)$$

The mass flow is a maximum when

$$\frac{P_2}{P_1} = \frac{P_2^*}{P_1} = \left(\frac{2}{k+1} \right)^{k/(k-1)} \quad (5.134)$$

which, for $k = 1.4$ (e.g., air), has a value of 0.528. Thus, if the downstream pressure is approximately one-half or less of the upstream pressure, the flow will be choked. The mass flow rate under adiabatic conditions is always somewhat greater than that under isothermal conditions, but the difference is normally <20%. In fact, for long piping systems ($L/D > 1000$), the difference is usually less than 5% (e.g., Holland, 1973).

5.5.11.5 Supersonic Flow

The conservation of mass, energy, and momentum equations can be written for the adiabatic flow of an ideal gas, and, when arranged in dimensionless form,

$$G^* = \sqrt{P_1 \rho_1} \left(\frac{P_2^*}{P_1} \right)^{1/2} \quad (5.135)$$

pressure requirements, very viscous fluids, and applications where precisely controlled or metered flow rate is required.

Centrifugal pumps operate by the transfer of energy (or angular momentum) from a rotating impeller to the fluid, normally inside a casing. The kinetic energy of the fluid is increased by the angular momentum imparted by the high-speed impeller, and is then converted to pressure energy (or head) in a diverging (volute) area. The developed head depends upon the pump design and the size, shape, and speed of the impeller, and the flow rate is determined by the fluid resistance of the system in which the pump is installed. Centrifugal pumps operate at approximately constant head over a wide range of flow rates (within limits). They can be operated in a "closed off" condition (i.e., closed discharge line), since the liquid will recirculate within the pump without causing damage. However, this condition should be avoided, because energy dissipation within the pump can result in excessive heating of the fluid or the pump, and cavitation or unstable operation could occur with adverse consequences. Centrifugal pumps are appropriate for "ordinary" liquids (i.e., low to moderate viscosity) and low to moderate pressures over a wide variety of flow conditions.

5.6.2 CENTRIFUGAL PUMP CHARACTERISTICS

The hydraulic work ($-w$) delivered per unit mass of fluid, the pressure (ΔP) developed by the pump, and the pump head (H_p) are related by

$$-w = \frac{\Delta P}{\rho} = gH_p \quad (5.135)$$

The pump efficiency, η_e , is the hydraulic work delivered to the fluid divided by the work delivered to the pump by the motor ($-w_m$):

$$\eta_e = \frac{-w}{-w_m} \quad (5.136)$$

The efficiency of a pump depends upon the pump and impeller design, the size and speed of the impeller, and the operating flow rate, and it is measured by the pump manufacturer.

When selecting a pump for a particular application, the flow capacity and required pump head must be specified. Although a variety of different pumps might satisfy the given specifications, the best pump is generally the one that requires the least power to operate at the specified conditions. The horsepower required for the pump-driving motor is determined by

$$HP = -w_m \dot{m} = \frac{\Delta P Q}{\eta_e} = \frac{\rho g H_p Q}{\eta_e} \quad (5.137)$$

The motor power is also related to the motor torque (Γ) and speed (ω) by

$$HP = \Gamma \omega = \frac{\rho g H_p Q}{\eta_e} \quad (5.138)$$

The angular momentum balance provides a relation for the required motor torque:

$$\Gamma = \dot{m} \omega R_i^2 = \rho Q \omega R_i^2 \quad (5.139)$$

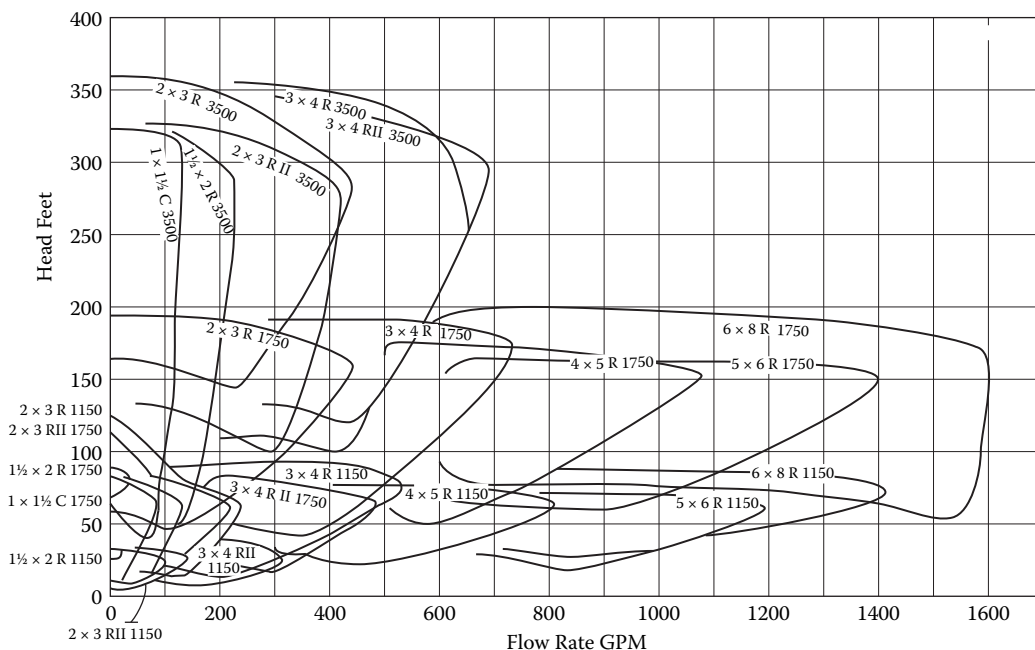


FIGURE 5.10 Typical centrifugal pump composite curves. (From TRW Mission Pump Brochure [manufacturer's catalog].)

5.6.2.1 Required Head

A typical application involves specifying a pump for a specified flow rate and given fluid properties. The piping system with the necessary valves, fittings, etc., should be sized for the most economical pipe size. Application of the energy balance (Bernoulli equation) to the pipeline determines the required pump head:

$$H_p = \frac{P_2 - P_1}{\rho g} + (z_2 - z_1) + \frac{8Q^2}{g\pi^2} \sum_i \left(\frac{K_f}{D^4} \right)_i \quad (5.141)$$

For highly turbulent flow (i.e., constant K_f 's), the required pump head H_p is a quadratic function of the flow rate Q . This relation, which is superimposed on the pump characteristic curves (see line S1 in Figure 5.9), is the *operating line* for the system. The actual pump head and the resulting flow rate are determined by the intersection of the operating line and the pump impeller characteristic curve. For the specified flow rate, the best (least cost) pump/impeller/motor combination that will provide this flow rate should be selected.

5.6.2.2 Composite Curves

Composite curves such as those shown in Figure 5.10 are provided by most pump manufacturers, and can be used to quickly identify the operating range of various pumps. Once a pump that can deliver the specified head and flow rate is identified, the individual pump characteristic curves for that pump should then be consulted and the impeller diameter selected that will produce the required head or greater. This can be repeated for various pump, impeller, and speed combinations to determine the combination that results in the least power requirement.

determine: (a) the required pump head (in meters); (b) the proper impeller diameter to use; (c) the pump efficiency and NPSH at the operating point; (d) the power of the motor required to drive the pump; and (e) the maximum height above the pond that the pump can be located without cavitating. Fluid properties: $\rho = 996 \text{ kg/m}^3$, $\mu = 0.798 \text{ cP}$, $P_v = 31.824 \text{ mm Hg}$.

Solution

The required pump head is calculated from Equation (5.141), with $P_1 = P_2$:

$$H_p = (z_2 - z_1) + \frac{8Q^2}{g\pi^2} \sum_i \left(\frac{K_f}{D^4} \right)_i$$

where

$$\sum_i K_f = 4K_{el} + \left(\frac{4fL}{D} \right)_{\text{pipe}}$$

and K_{el} is determined from the 3- K correlation:

$$K_{el} = \frac{800}{N_{Re}} + 0.091 \left(1 + \frac{4.0}{D_{n,in}^{0.3}} \right)$$

The Reynolds number is

$$N_{Re} = \frac{4Q\rho}{\pi D\mu} = \frac{4(0.0126 \text{ m}^3/\text{s})(996 \text{ kg/m}^3)}{\pi(0.07793 \text{ m})(0.000798 \text{ Pa s})} = 2.57 \times 10^5$$

so that $K_{el} = 0.353$ ($4 K_{el} = 1.41$). From the Churchill equation, $f = 0.00475$, which gives

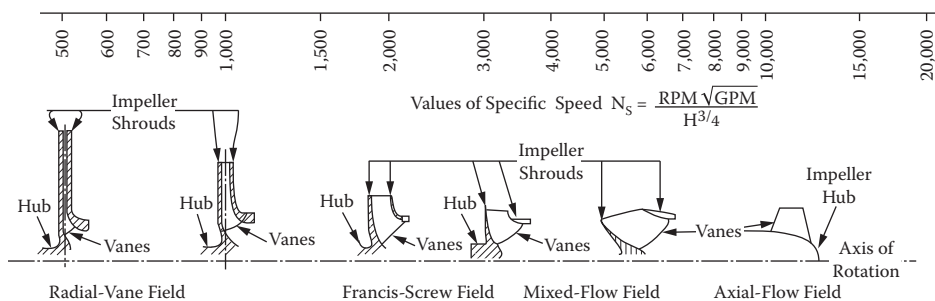
$$K_{\text{pipe}} = \frac{4fL}{D} = \frac{4(0.00475)(67 \text{ m})(1000 \text{ mm/m})}{77.93 \text{ mm}} = 16.36$$

Inserting these values into the Bernoulli equation [Equation (5.141)] results in $H_p = 67.3 \text{ m}$ (221 ft). Referring to Figure 5.9, this pump will deliver a head of 220 ft (67.1 m) (which is close enough) at a flow rate of 200 gpm (0.0126 m³/s) using an impeller with a diameter of 7-1/4 in. (184 mm). (Note that if the desired operating head and flow rate intersect at a point between the curves for available impeller diameters, the next larger impeller must be used, which will result in a pump head somewhat higher than necessary. This will result in a flow rate higher than desired, unless a valve is included in the line that can be adjusted to take the excess head as friction loss.)

From Figure 5.9 at the operating point, read $\eta_e = 0.42$ and NPSH = 11 ft (3.35 m). The required motor power is then given by

$$HP = \frac{\rho Q g H_p}{\eta_e} = \frac{(996 \text{ kg/m}^3)(0.0126 \text{ m}^3/\text{s})(9.81 \text{ m/s}^2)(67.3 \text{ m})}{0.42} = 19.8 \text{ kw (26.6 hp)}$$

The maximum suction lift for the pump that can be achieved without cavitation is given by Equation (5.144) as



Variation in Impeller Profiles with Specific Speed and Approximate Range of Specific Speed for the Various Types.



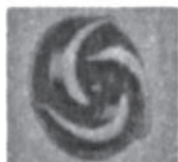
Straight-Vane, Single-Suction Closed Impeller.
(Worthington Pump, Inc.)



Open Mixed-Flow Impeller.
(Worthington Pump, Inc.)



Axial-Flow Impeller.
(Worthington Pump, Inc.)



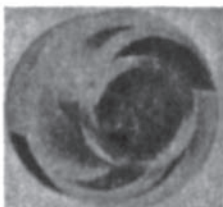
Semiopen Impeller.
(Worthington Pump, Inc.)



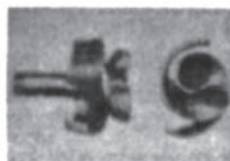
Open Impeller. Notice that the Impellers at Left and Right Are Strengthened by a Partial Shroud.
(Worthington Pump, Inc.)



Open Impeller with a Partial Shroud.



Phantom View of a Radial-Vane Nonclogging Impeller.
(Worthington Pump, Inc.)



Paper-Pulp Impeller.
(Worthington Pump, Inc.)

FIGURE 5.11 Impeller designs and specific speed characteristics. (From Karassik et al., 1976.)

For an ideal gas under adiabatic frictionless (i.e., isentropic) conditions,

$$\frac{P}{\rho^k} = \text{const}, \quad \text{where } k = \frac{c_p}{c_v} \text{ and } c_p = c_v + R/M \quad (5.148)$$

(Note that setting $k = 1$ reduces the isentropic state to the isothermal state). For isentropic compression,

$$-w = \frac{RT_1 k (r^{(k-1)/k} - 1)}{M(k-1)} \quad (5.149)$$

As ($k \rightarrow 1$), this expression reduces to Equation (5.148). For a given compression ratio, the isothermal work is always less than the isentropic work. However, most compressors operate under more nearly adiabatic conditions because of the relatively short residence time of the gas in the compressor. The temperature rise during an isentropic compression is

$$\frac{T_2}{T_1} = \left(\frac{P_2}{P_1} \right)^{(k-1)/k} = r^{k-1/k} \quad (5.150)$$

In reality, many compressor conditions are neither purely isothermal nor isentropic, but somewhere in between. This can be taken into account by using the isentropic Equation (5.149) and replacing the isentropic exponent k by a “polytropic” constant γ (where $1 < \gamma < k$), which is a function of the compressor design as well as the properties of the gas.

5.6.3.2 Staged Operation

Multiple compressor stages can be arranged in series to increase the overall compression ratio. To increase the overall efficiency, the gas is cooled between stages by “interstage coolers.” As the number of stages increases, the total compression work for isentropic compression with interstage cooling to the initial temperature (T_1) approaches that of isothermal compression at T_1 . The optimum compression ratio for each stage that minimizes the total compression work for any number of stages (n) with interstage cooling to the initial temperature is

$$r = \frac{P_2}{P_1} = \frac{P_3}{P_2} = \dots = \frac{P_{n+1}}{P_n} = \left(\frac{P_{n+1}}{P_1} \right)^{1/n} \quad (5.151)$$

If there is no interstage cooling, or for interstage cooling to a temperature other than T_1 , the optimum compression ratio for each stage (i) is related to the temperature entering that stage (T_i) by

$$T_i \left(\frac{P_{i+1}}{P_i} \right)^{(k-1)/k} = T_i t_i^{(k-1)/k} = \text{constant } t \quad (5.152)$$

The above relations apply to ideal (frictionless) compressors. To account for friction losses, the ideal computed work is divided by the compressor efficiency, η_c , to get the total work that must be supplied to the compressor:

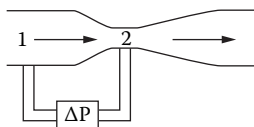


FIGURE 5.14 Venturi meter.

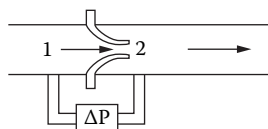


FIGURE 5.15 Nozzle.

the presence of the probe and the stem inserted into the flow are minimized if the probe length is 14 times the probe diameter, and the static pressure holes are six probe diameters from the end of the probe. Also, axial alignment of the probe is important for accurate measurement, and the probe should be located no closer than 100 pipe diameters from any bend or flow constriction. The total flow rate (Q) through the conduit can be determined by measuring a sufficient number of radial points across the conduit to enable accurate evaluation of the integral in Equation (5.155).

The pitot tube requires considerable effort and time to obtain an accurate value of the total flow rate. However, the probe offers minimal resistance to the flow and hence is very efficient from the standpoint of the resulting permanent pressure drop due to friction. It is also the only practical means for determining the flow rate in very large conduits (e.g., smokestacks). Errors increase as the ratio of the probe diameter to pipe diameter increases, and for accurate readings the probe diameter should be no larger than 2% of the tube diameter. This limits accurate application to pipes of about 40-cm diameter or larger.

5.7.2 VENTURI AND NOZZLE

Other devices can be used to determine the flow rate from a single measurement. These are sometimes referred to as *obstruction meters*, since the basic principle involves introducing an “obstruction” (e.g., a constriction) into the flow channel and then measuring the pressure drop across this obstruction, which depends on the flow rate. Two such devices, the venturi meter and the nozzle, are illustrated in Figures 5.14 and 5.15, respectively. In both cases, the pressure drop from a point upstream of the meter to a point in a plane with the minimum flow area (A_2) is related to the velocity V_2 by the Bernoulli equation:

$$V_2 = C_v \sqrt{\frac{-2\Delta P}{\rho(1-\beta^4)}} \quad (5.157)$$

where C_v is the discharge coefficient for the venturi, which is a function of the conduit Reynolds number, as shown in Figure 5.16. The coefficient accounts for deviation from plug flow as well as irreversible effects. However, since the coefficient is not greatly different from 1.0 at high Reynolds numbers (having a value of about 0.985 at [pipe] Reynolds numbers, N_{ReD} , above about 2×10^5), this indicates that these nonidealities are small. According to Miller (1983), for $N_{ReD} > 4000$, the discharge coefficient for the venturi, as well as for the nozzle and orifice, can be described as a function of N_{ReD} and β by the general equation

$$C = C_\infty + \frac{b}{N_{ReD}^n} \quad (5.158)$$

where the parameters C_∞ , b , and n are given in Table 5.12 as a function of β (the ratio of the throat diameter to the pipe diameter). The range over which this equation applies and its approximate accuracy are given in Table 5.13. The pressure recovery in the venturi is relatively large, so that the net friction loss across the entire meter is a relatively small fraction of the measured pressure drop, as indicated in Figure 5.17.

TABLE 5.12
Values of Parameters for Meter Discharge Coefficients

Primary Device	Discharge Coefficient C_∞ at Infinite Reynolds Number	Reynolds Number Term	
		Coefficient b	Exponent n
Venturi			
Machined inlet	0.995	0	0
Rough cast inlet	0.984	0	0
Rough welded sheet-iron inlet	0.985	0	0
Universal Venturi Tube ^b	0.9797	0	0
Lo-Loss tube ^c	$1.005 - 0.471\beta + 0.564\beta^2 - 0.514\beta^3$	0	0
Nozzle:			
ASME long radius	0.9975	$-6.53\beta^{0.5}$	0.5
ISA	$0.9900 - 0.2262\beta^{4.1}$	$1708 - 8936\beta + 19,779\beta^{4.7}$	1.15
Orifice:			
Venturi nozzle (ISA inlet)	$0.9858 - 0.196\beta^{4.5}$	0	0
Corner taps	$0.5959 + 0.0312\beta^{2.1} - 0.184\beta^6$	$91.71\beta^{2.5}$	0.75
Flange taps (D in inches)			
$D \geq 2.3$	$0.5959 + 0.0312\beta^{2.1} - 0.184\beta^6 + 0.09 \frac{\beta^4}{D^*(1-\beta^4)} - 0.0337 \frac{\beta^3}{D}$	$91.71\beta^{2.5}$	0.75
$2 \leq D \leq 2.3^4$	$0.5959 + 0.0312\beta^{2.1} - 0.184\beta^6 + 0.039 \frac{\beta^4}{1-\beta^4} - 0.0337 \frac{\beta^3}{D}$	$91.71\beta^{2.5}$	0.75
Flange taps (D^* in millimeters)			
$D^* \geq 58.4$	$0.5959 + 0.0312\beta^{2.1} - 0.184\beta^6 + 2.286 \frac{\beta^4}{D^*(1-\beta_4)-\beta^4} - 0.856 \frac{\beta^3}{D^*}$	$91.71\beta^{2.5}$	0.75
$50.8 \leq D^* \leq 58.4^d$	$0.5959 + 0.0312\beta^{2.1} - 0.184\beta^6 + 0.039 \frac{\beta^4}{1-\beta^4} - 0.856 \frac{\beta^3}{D^*}$	$91.71\beta^{2.5}$	0.75
D and $D/2$ taps	$0.5959 + 0.0312\beta^{2.1} - 0.184\beta^6 + 0.039 \frac{\beta^4}{1-\beta^4} - 0.0158\beta^3$	$91.71\beta^{2.5}$	0.75
$2 \frac{1}{2} D$ and $8D$ taps	$0.5959 + 0.461\beta^{2.1} + 0.48\beta^6 + 0.039 \frac{\beta^4}{1-\beta^4}$	$91.71\beta^{2.5}$	0.75

^a Detailed Reynolds number, line size, beta ratio, and other limitations are given in Table 5.13.

^b From BIF CALC-440/441; the manufacturer should be consulted for exact coefficient information.

^c Derived from the Badger Meter, Inc. Lo-Loss tube coefficient curve; the manufacturer should be consulted for exact coefficient information.

^d For $1/2 \leq D \leq 1 \frac{1}{2}$ in. ($12 \leq D^* \leq 40$ mm), use flow coefficient equation (10.1) or Equation (10.2) given in Chapter 10, (Miller), with $C = \sqrt{1-\beta^4} K$.

^e Source: Stolz (1978).

Source: Miller, R. W., *Flow Measurement Engineering Handbook*, McGraw-Hill, New York (1983).

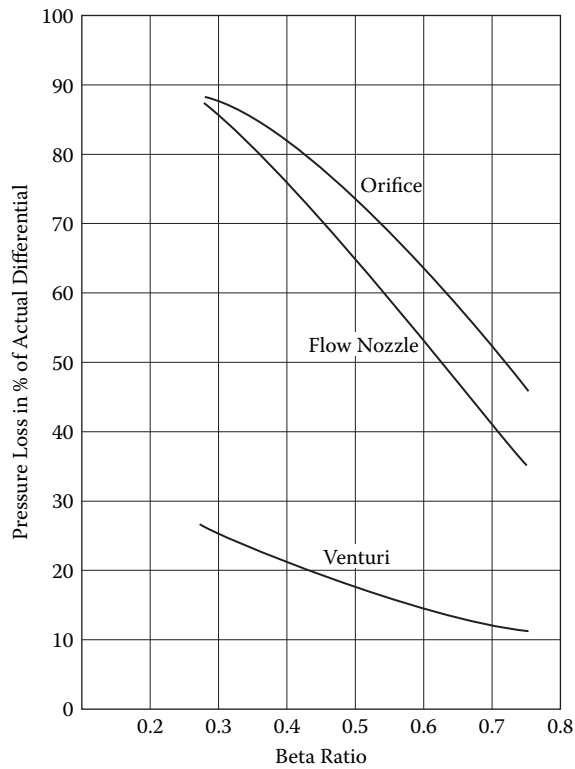


FIGURE 5.17 Unrecovered pressure loss in various meters. (From Miller, R. W., *Flow Measurement Engineering Handbook*, McGraw-Hill, New York (1983).)

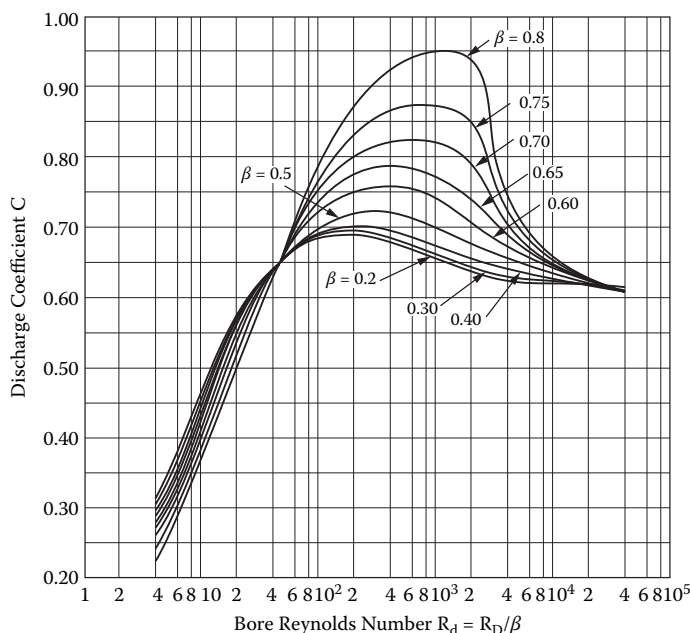


FIGURE 5.20 Orifice discharge coefficient for square-edged orifice and flange, corner, or radius tap. (From Miller, R. W., *Flow Measurement Engineering Handbook*, McGraw-Hill, New York (1983).)

additional taps through the pipe. Pipe taps measure essentially the total unrecovered pressure drop (friction loss), which is considerably lower than the maximum pressure drop across the orifice plate. Vena contracta taps are sometimes specified, with the upstream tap 1 D from the plate and the downstream tap at the vena contracta location, although the latter varies with the Reynolds number and beta ratio, and thus is not a fixed position (radius taps approximate this condition). The orifice coefficient shown in Figure 5.20 is valid to within 2–5% (depending upon the Reynolds number and β) for all pressure tap locations except pipe and vena contracta taps. More accurate values can be calculated from Equation (5.160) for high Reynolds numbers, with the parameter expressions given in Table 5.12 for the specific orifice and pressure tap arrangements.

5.7.3.2 Compressible Flow

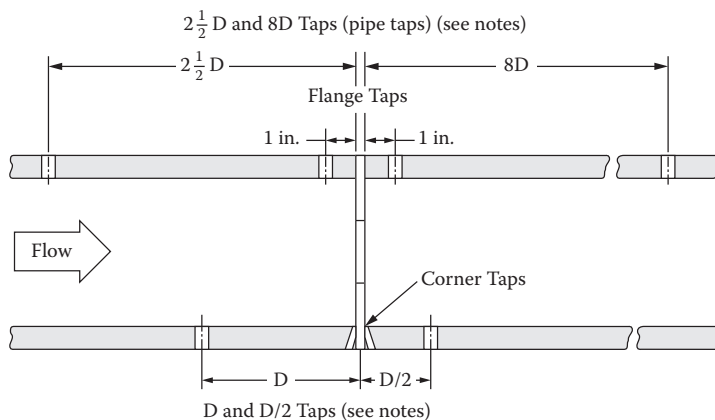
For an ideal gas flowing through an orifice under adiabatic conditions, the flow equation is

$$\dot{m} = C_o A_o \sqrt{\frac{P_1 \rho_1}{1 - \beta^4}} \left\{ \frac{2k}{k-1} \left(\frac{P_2}{P_1} \right)^{2/k} \left[\left(\frac{P_1}{P_2} \right)^{(k-1)/k} - 1 \right] \right\}^{1/2} \quad (5.160)$$

where the value of C_o is assumed to be the same as for an incompressible flow. The ratio of this equation to the incompressible equation is called the *expansion factor* Y . Thus,

$$\dot{m} = C_o A_o Y \sqrt{\frac{2 \rho_1 \Delta P}{(1 - \beta^4)}} \quad (5.161)$$

where the density ρ_1 is evaluated at the upstream pressure (P_1). Values of Y are shown as a function of $\Delta P/P_1$ and β for a square-edged orifice, nozzles, and venturi meters for values of $k = c_p/c_v$ of



Notes:

- (1) $2\frac{1}{2}D$ and $8D$ Pipe Taps Are Not Recommended in ISO 5167 or ASME Fluid Meters.
- (2) D and $D/2$ Taps Are Now Used in Place of Vena Contract Taps.

FIGURE 5.22 Orifice pressure tap locations. (From Miller, R. W., *Flow Measurement Engineering Handbook*, McGraw-Hill, New York (1983).)

5.7.3.3 Loss Coefficient

The total unrecovered pressure drop, i.e., the friction loss, $(P_1 - P_3)$, in an orifice meter is characterized by the loss coefficient, K_f :

$$K_f = \frac{(1 - \beta^4)(1 - \beta^2)}{C_o^2 \beta^4} \quad (5.164)$$

which is to be used with the pipe velocity (V_1). If K_f is based upon the velocity through the orifice (V_o) instead of the pipe velocity, the β^4 term in the denominator should be omitted.

5.7.3.4 Applications

Determining the flow rate for a given pipe/orifice geometry and known pressure drop from Equation (5.162) requires an iterative procedure, since the orifice coefficient C_o depends on the Reynolds number (e.g., Figure 5.20), which cannot be found until the flow rate is known. This procedure is usually simplified by initially assuming $C_o = 0.61$.

If the orifice diameter is to be determined for a specified value or range of flow rate and pressure drop in a given pipe, it is more convenient to rearrange Equation (5.162) for β as follows:

$$\beta = \left[\frac{X}{1 + X} \right]^{1/4} \quad \text{where } X = \frac{8}{\rho_1 \Delta P} \left[\frac{\dot{m}}{\pi D^2 Y C_o} \right] \quad (5.165)$$

An iterative procedure for C_o is still required, since $C_o = f(\beta)$, and this can be simplified as above by initially assuming $C_o = 0.61$.

5.8 CONTROL VALVES

A control valve is a specially designed globe valve that acts as a “variable resistance” in the line to control the flow rate. Closing down on the valve decreases the area between the plug and the

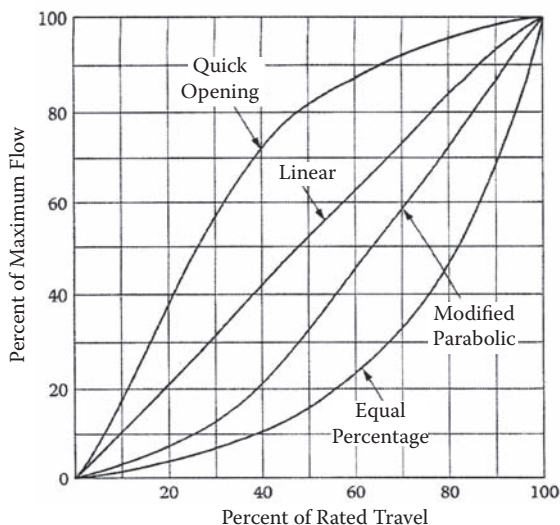


FIGURE 5.24 Control valve trim characteristics. (From Fisher Controls, Catalog 10, chap. 2, Fisher Controls, Marshalltown, IA (1987). With permission.)

seat, which increases the valve flow resistance (i.e., the K_f). The relation between the valve stem or plug position (which is the manipulated variable) and the flow rate through the valve (which is the controlled variable) is normally nonlinear to compensate for the nonlinear pressure-flow characteristics of the piping system, pump, etc., and is determined by the valve characteristic or “trim,” i.e., the shape and design of the valve plug and the flow channel through the valve.

5.8.1 VALVE CHARACTERISTICS

Different shaped valve plugs or cages are available for a given valve that determine the valve response or trim characteristic as a function of the valve stem position. The valve trim is chosen to match the dynamic response of the piping system to give the desired response relation. Figure 5.24 illustrates typical trim characteristics (Fisher, 1987). The “quick opening” characteristic provides the maximum change in flow rate at low opening or stem travel, with a fairly linear relationship. As the valve approaches wide open, the change in flow with travel approaches zero. This is best suited for on-off control, but is also appropriate where a linear valve is desired. The “linear” flow characteristic has a constant “valve gain,” i.e., the incremental change in flow rate with change in valve plug position is the same at all flow rates. This is a commonly desired property, particularly for liquid level control. The “equal percentage” flow trim provides the same percentage change in flow for equal increments of valve plug position. This characteristic is often used in pressure control applications and where a relatively small pressure drop across the valve is required relative to that in the rest of the system. The modified parabolic characteristic is intermediate to the linear and equal-percentage characteristics and can be substituted for equal-percentage valve plugs in many applications, with some loss in performance. However, the actual flow response to changes in stem position depends on the characteristics of the piping system as well as the valve, as described below.

5.8.2 VALVE SIZING EQUATIONS—INCOMPRESSIBLE FLOWS

For incompressible fluids, Bernoulli's equation relates the pressure drop across a valve and the flow rate through the valve in terms of the loss coefficient, K_f :

TABLE 5.14
Example Flow Coefficient Values for a Linear Control Valve

Linear												Linear Characteristic
Coeffi- cients	Body Size, Inch	Port Diameter, Inch	Total Travel, Inch	Valve Opening, Percent of Total Travel								$K_m^{(1)}$ and C_1
				10	20	30	40	50	60	70	80	
C_v (Liquid)	2 & 3 x 2	1-7/8	1-1/2	1.69	8.45	21.9	33.4	42.7	50.0	55.6	59.6	72
	3 & 4 x 3	2-7/8	2	3.41	25.4	52.6	76.0	96.4	114	127	133	91
	4 & 6 x 4	3-5/8	2	6.69	25.1	50.1	77.9	106	134	157	175	86
	6 & 8 x 6	5-3/8	3	9.40	63.8	138	212	282	339	373	389	61
C_g (Gas)	2 & 3 x 2	1-7/8	1-1/2	60.8	326	729	1110	1400	1600	1710	1780	28.0
	3 & 4 x 3	2-7/8	2	142	839	1760	2540	3240	3880	4490	4540	33.6
	4 & 6 x 4	3-5/8	2	229	791	1530	2350	3250	4190	5090	5850	35.0
	6 & 8 x 6	5-3/8	3	287	1910	4060	6160	8400	10,600	12,300	13,300	34.8
C_s (Steam)	2 & 3 x 2	1-7/8	1-1/2	3.04	16.3	36.5	55.5	70.0	80.0	85.5	89.0	28.9
	3 & 4 x 3	2-7/8	2	7.10	42.0	88.0	127	162	194	216	225	33.6
	4 & 6 x 4	3-5/8	2	11.5	39.6	76.5	118	163	210	255	293	35.0
	6 & 8 x 6	5-3/8	3	14.4	95.5	203	308	420	530	615	665	34.8
Equal Percentage												Equal Percentage Characteristic
C_v (Liquid)	2 & 3 x 2	1-7/8	1-1/8	1.04	1.59	3.52	6.99	12.1	19.7	30.5	40.9	79
	3 & 4 x 3	2-7/8	1-1/2	2.56	5.17	10.80	18.2	28.9	44.9	62.6	82.9	91
	4 & 6 x 4	3-5/8	1-1/2	3.44	7.12	13.1	21.8	34.8	54.0	80.4	109	71
	6 & 8 x 6	5-3/8	2-1/2	5.27	13.0	22.1	35.3	57	93	141	194	64
C_g (Gas)	2 & 3 x 2	1-7/8	1-1/8	41.5	61.2	123	233	401	653	996	1320	31.4
	3 & 4 x 3	2-7/8	1-1/2	88.9	175	381	638	985	1530	2190	2890	34.2
	4 & 6 x 4	3-5/8	1-1/2	134	240	430	700	1080	1650	2460	3440	33.4
	6 & 8 x 6	5-3/8	2-1/2	152	422	673	1020	1710	2730	3990	5490	29.9
C_s (Steam)	2 & 3 x 2	1-7/8	1-1/8	2.08	3.06	6.15	11.7	20.1	32.7	49.8	66.0	79.5
	3 & 4 x 3	2-7/8	1-1/2	4.45	8.75	19.1	31.9	49.3	76.5	110	145	200
	4 & 6 x 4	3-5/8	1-1/2	6.70	12.0	21.5	35.0	54.0	82.5	124	172	257
	6 & 8 x 6	5-3/8	2-1/2	7.60	21.1	33.7	51.0	65.5	137	200	275	32.9
Modified Equal Percentage												Equal Percentage Characteristic
C_v (Liquid)	2 & 3 x 2	1-7/8	1-1/2	1.07	2.65	6.87	15.1	28.6	38.3	47.6	53.7	73
	3 & 4 x 3	2-7/8	2	3.08	8.63	18.5	34.3	57.8	84.5	108	123	88
	4 & 6 x 4	3-5/8	2	4.49	10.7	21.8	41.2	71.0	107	141	166	85
	6 & 8 x 6	5-3/8	3	6.67	16.4	29.3	52.0	92.5	151	217	280	75
C_g (Gas)	2 & 3 x 2	1-7/8	1-1/2	43.0	95.9	230	493	874	1280	1530	1660	29.8
	3 & 4 x 3	2-7/8	2	105	295	635	1140	1930	2890	3720	4250	33.6
	4 & 6 x 4	3-5/8	2	172	337	663	1280	2240	3380	4470	5480	34.6
	6 & 8 x 6	5-3/8	3	200	298	694	1520	2620	4330	6270	8210	32.9
C_s (Steam)	2 & 3 x 2	1-7/8	1-1/2	2.15	4.80	11.5	24.7	43.7	63.0	76.5	83.0	90.0
	3 & 4 x 3	2-7/8	2	5.25	14.8	31.8	57.0	96.5	145	186	213	227
	4 & 6 x 4	3-5/8	2	8.60	16.9	33.2	64.0	112	169	224	274	323
	6 & 8 x 6	5-3/8	3	10.0	24.9	44.7	76.0	131	217	314	411	535

This table lists The K_m values for the C_v coefficients and the C_1 values for the C_g and C_s coefficients at 100% total travel.

A typical pump and system curve is illustrated in Figure 5.25. The effect on the system curve of partially closing the valve is shown. Closing down on the valve (reducing X) decreases the valve C_v and increases the head loss through the valve, h_v . This shifts the system curve upward by an amount h_v at a given flow rate (h_v depends on flow rate). The range of possible flow rates (i.e., the "turndown" ratio) lies between the intersection on the pump curve of the system curve with a "fully open" valve (Q_{\max} , corresponding to $C_{v,\max}$) and the intersection of the system curve with the (partly) closed valve. The desired operating point should be as close as practical to Q_{\max} , since this corresponds to an open valve with minimum flow resistance and is the most efficient region on the pump curve. Thus the flow is controlled by closing down on the valve (i.e., reducing X and C_v , and thus raising h_v). The minimum operating flow rate (Q_{\min}) is established by the turndown ratio required for proper control. These limits set the size of the valve (e.g., the required $C_{v,\max}$), and the head-flow-rate behavior of the system over the desired flow range determines the proper trim for the valve. The system curve is shifted by the amount h_v in response to closing the valve (i.e., reducing X), where

valve with equal-percentages trim (with flow coefficients given in Table 5.14). The pressure in the upstream tank is 170 kPa (10 psig) and is atmospheric in the downstream tank, and the elevation of the downstream tank is 1.52 m (5 ft) lower than that in the upstream tank. Determine the flow rate of the water in the system if the valve position (X) is (a) fully open and (b) half-open.

Solution

The Bernoulli equation for the piping system can be solved for the flow rate (Q) to give

$$Q = \frac{\pi D^2}{2\sqrt{2}} \left[\frac{DF}{\sum K_f} \right]^{1/2}$$

where $\sum K_f$ includes all losses in the pipe, fittings, and the control valve as well as all entrance and exit losses. Although the loss coefficients for the pipe and fittings are dependent upon the Reynolds number (hence on Q), a first estimate can be obtained by assuming fully turbulent flow. In this case, the fitting loss coefficients are determined by the 3- K correlation by omitting the K_m term. This gives ($4 K_{el}$) = 1.41 and ($2 K_{bv}$) = 0.132. For pipe in fully turbulent flow:

$$f = \frac{0.0625}{\left[\log \left(\frac{3.7D}{\epsilon} \right) \right]^2} = 0.00433$$

so that $K_{pipe} = 4fL/D = 6.77$. From Equation (5.167), the loss coefficient for the control valve is related to the valve flow coefficient by

$$(K_f)_{CV} = 1.732 \frac{2A^2}{C_v^2 \rho_w}$$

where A is the pipe cross-section area. The factor 1.732 includes the conversion factors required for C_v in $\text{gpm}/(\text{psi})^{1/2}$ (Table 5.14), A in mm^2 , and ρ_w in kg/m^3 . From Table 5.14, the value of C_v is 28.9 for the valve half-open, and 117 when fully open, giving $(K_f)_{cv}$ of 5.75 and 94.2, respectively. Setting $K_{entr} = 0.5$ and $K_{exit} = 1.0$ gives $\sum K_f = 15.6$ for the fully open valve and 104.2 for the half-open valve. Inserting these values into the equation for Q gives $Q = 0.0156 \text{ m}^3/\text{s}$ (248 gpm) for the open valve and $0.00606 \text{ m}^3/\text{s}$ (96 gpm) for the half-open valve.

5.8.3 COMPRESSIBLE FLOWS

The minimum pressure in the valve (P_{vc}) generally occurs at the vena contracta, just downstream of the flow orifice. The pressure then rises downstream to P_2 , with the amount of pressure recovery depending upon the valve design. If P_{vc} is less than the fluid vapor pressure (P_v), the liquid will partially vaporize, forming bubbles. If the pressure recovers to a value greater than P_v , these bubbles may collapse suddenly, setting up local shock waves, which can result in considerable damage. The result is *cavitation*, as opposed to *flashing*, which occurs if the recovered pressure remains below P_v and the bubbles do not collapse. After the first vapor cavities form, the flow rate will no longer be proportional to the square root of the pressure difference across the valve due to the decreasing density of the mixture. If sufficient vapor forms, the flow can become choked, at which point the flow rate will be independent of the downstream pressure as long as P_1 remains constant. The critical pressure ratio ($r_c = P_{2c}/P_v$) at which choking will occur is shown in Figure 5.26 for

TABLE 5.15
Critical Pressures for Various Fluids

Ammonia	1636
Argon	705.6
Butane	550.4
Carbon Dioxide	1071.6
Carbon Monoxide	507.5
Chlorine	1118.7
Dowtherm A	465
Ethane	708
Ethylene	735
Fluorine	808.5
Helium	33.2
Hydrogen	188.2
Hydrogen Chloride	1198
Isobutane	529.2
Isobutylene	580
Methane	673.3
Nitrogen	492.4
Nitrous Oxide	1047.6
Oxygen	736.5
Phosgene	823.2
Propane	617.4
Propylene	670.3
Refrigerant 11	635
Refrigerant 12	596.9
Refrigerant 22	716
Water	3206.2

Source: Fisher Controls, Catalog 10, chap. 2, Fisher Controls, Marshalltown, IA (1987).

$$K_m = \frac{P_1 - P_2}{P_1 - P_{vc}} \quad (5.178)$$

Values of K_m for the Fisher Controls Example valve are given in the last column of Table 5.14, and representative values for other valves at the fully open condition are given in Table 5.16. If $\Delta P > \Delta P_c$, the value of ΔP_c is used as the pressure drop in the standard liquid sizing equation to determine Q ; otherwise, the value of $(P_1 - P_2)$ is used:

$$Q = C_v \sqrt{\Delta P_c / SG} \quad (5.179)$$

The notation used here is that from the Fisher Controls literature (e.g., Fisher Controls, 1990). The ANSI/ISAS 75.01 standard for control valves (e.g., Baumann, 1991; Hutchison, 1971) gives the same equations with the notation $F_L = (K_m)^{1/2}$ and $F_F = r_c$ in place of the factors K_m and r_c .

For relatively low pressure drops, the effect of compressibility is negligible, and the general flow equation (Equation (5.167)) applies. Including conversion factors for flow rate in *scfh* and the density of air at standard conditions (1 atm, 520°R), this equation is

$$Q_{scfh} = 1362 C_v P_1 \sqrt{\frac{\Delta P}{P_1 (SG) T_1}} \quad (5.180)$$

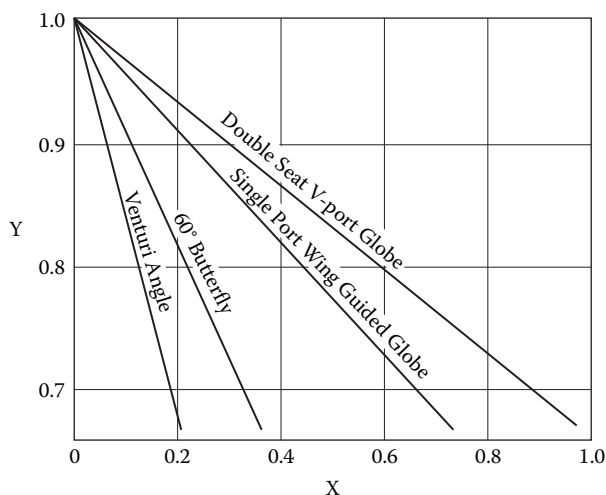


FIGURE 5.28 Expansion factor (Y) as a function of pressure drop ratio (X) for four different types of control valves. (From Hutchison, J. W., *ISA Handbook of Control Valves*, Instrument Society of America, Research Triangle Park, NC (1971).)

pressure ratio across the valve at which choking occurs, and any further increase in X (e.g., ΔP) due to lowering P_2 can have no effect on the flow rate.

The flow coefficient C_v is determined by calibration with water, and it is not entirely satisfactory for predicting the flow rate of compressible fluids under choked flow conditions. This has to do with the fact that different valves exhibit different pressure recovery characteristics with gases and hence will choke at different pressure ratios, which is not significant for liquid flows. For this reason, another flow coefficient, C_g , is often determined by calibration with air under critical flow conditions (Fisher Controls, 1977). The corresponding flow equation for gas flow is

$$Q_{critical} = C_g P_1 \left(\frac{520}{SGT} \right)^{1/2} \quad (5.184)$$

Equation (5.181), which applies at low pressure drops, and Equation (5.185), which applies to critical (choked) flow, have been combined into one general “universal” empirical equation by Fisher (1977), by using a sine function to represent the transition between the limits of both of these states:

$$Q_{scfh} = C_g \sqrt{\frac{520}{(SG)T_1}} P_1 \sin \left[\frac{3417}{C_1} \sqrt{\frac{\Delta P}{P_1}} \right]_{degrees} \quad (5.185)$$

Here, $C_1 = C_g/C_v$ and is determined by measurements on air. Values of C_1 are listed in the last column in Table 5.14 for the valve illustrated. C_1 is also approximately equal to $40\sqrt{X_T}$ (Hutchison, 1971). For steam or vapor at any pressure, a corresponding equation is

$$Q_{lb/hr} = 1.06 C_g \sqrt{P_1 \rho_1} \sin \left[\frac{3417}{C_1} \sqrt{\frac{\Delta P}{P_1}} \right]_{degrees} \quad (5.186)$$

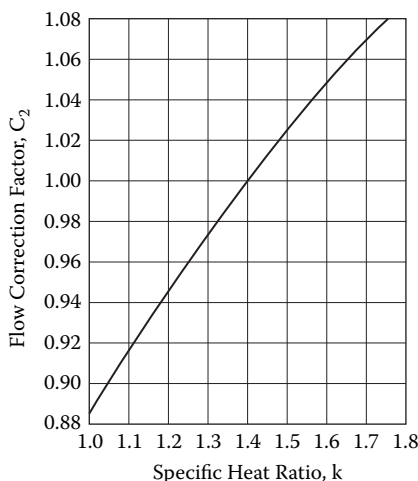


FIGURE 5.29 Correction factor for gas properties.

Then determine the Reynolds number for the valve from

$$N_{\text{Re}} = \frac{17250Q}{\sqrt{C_v v_{cs}}} \quad (5.192)$$

where Q is in gpm, ΔP is in psi, and v_{cs} is the fluid kinematic viscosity (μ/ρ) in centistokes. The viscosity correction factor, F_v , is then read from the middle line on Figure 5.30 and used to calculate a corrected value of C_v as follows:

$$C_{vc} = C_v F_v \quad (5.193)$$

The proper valve size and percent opening are then found from the table for the valve flow coefficient (e.g., Table 5.14) at the point where the coefficient is equal to or higher than this corrected value.

To predict flow rate for a given valve (i.e., a given C_v) and given ΔP , the maximum flow rate (Q_{max}) is determined as

$$Q_{\text{max}} = C_v \sqrt{\Delta P / SG} \quad (5.194)$$

The Reynolds number is then calculated from Equation (5.192), and the viscosity correction factor, F_v , is read from the bottom curve in Figure 5.30. The corrected flow rate is then

$$Q_c = \frac{Q_{\text{max}}}{F_v} \quad (5.195)$$

To predict pressure drop for a given valve (C_v) and given flow rate (Q), calculate the Reynolds number as above and read the viscosity correction factor, F_v , from the top line of Figure 5.30. The predicted pressure drop across the valve is then

$$\Delta P = SG \left(\frac{QF_v}{C_v} \right)^2 \quad (5.196)$$

REFERENCES

- Astarita, G., G. Greco Jr., and L. Nicodemo, *AIChE J.*, 15, 564 (1969).
- Barnes, H. A., J. F. Hutton, and K. Walters, *An Introduction to Rheology*, Elsevier, New York, 1989.
- Baumann, H. D., *Control Valve Primer*, Instrument Society of America, Research Triangle Park, NC, 1991.
- Bewersdorff, H. W., and N. S. Berman, *Rheol. Acta*, 27, 130 (1988).
- Bird, R. B., R. C. Armstrong, and O. Hassager, *Dynamics of Polymeric Liquids*, vol. 1, *Fluid Mechanics*, Wiley, New York, 1988.
- Cheremisinoff, N. P., and P. N. Cheremisinoff, *Instrumentation for Process Flow Engineering*, Technomic Publishing Co., Lancaster, PA, 1987.
- Christy, J. R. E., "On Selecting Appropriate Control Valves for Pipework Systems," *Chemical Engineering Education*, winter, 54–57 (1996).
- Churchill, S. W., *Chem. Eng.*, p. 91, Nov. 7 (1977).
- Crane Co., "Flow of Fluids through Valves, Fittings, and Pipe," Technical Manual 410, Crane Co., New York (1978).
- Crane Co., "Flow of Fluids through Valves, Fittings, and Pipe," Technical Paper 410, Crane Co., New York, (1991).
- Darby, R., *Viscoelastic Fluids*, Marcel Dekker, New York (1976).
- Darby, R., and J. Melson, *Chem. Eng.*, p. 59, Dec. 28 (1981).
- Darby, R., and J. Melson, *J. Pipelines*, 2, 11 (1982).
- Darby, R., and H. D. Chang, *AIChE J.*, 30, 274 (1984).
- Darby, R., *J. Rheology*, 29, 359 (1985).
- Darby, R., and S. Pivsa-Art, *Canad. J. Chem. Eng.*, 69, 1395 (1991).
- Darby, R., R. Mun, and D. V. Boger, *Chem. Eng.*, p. 116, Sept. (1992).
- Darby, R., Matching Control Valve Trim to the System, *Chem. Eng.*, 104 (6), 147 (1997).
- Darby, R., *Chem. Eng.*, July, 101 (1999).
- Darby, R., *Chemical Engineering Fluid Mechanics*, vol. 2, Marcel Dekker, New York, 2001.
- Darby, R., "Correlate Pressure Drops through Fittings," *Chem. Eng.*, 108 (4), 127 (2001).
- Dodge, D. W., and A. B. Metzner, *AIChE J.*, 5, 189 (1959).
- Fisher Controls, *Control Valve Handbook*, 2nd ed., Fisher Controls, Marshalltown, IA, 1977.
- Fisher Controls, Catalog 10, chapter 2, Fisher Controls, Marshalltown, IA, 1987.
- Fisher Controls, *Control Valve Source Book*, Fisher Controls, Intl., Marshalltown, IA, 1990.
- Goren, Y., and J. F. Norbury, *ASME J. Basic Eng.*, 89, 816, 1967.
- Hall, N. A., *Thermodynamics of Fluid Flow*, Prentice-Hall, New York, 1951.
- Hoffmann, L., and P. Schummer, *Rheol. Acta*, 17, 98, 1978.
- Holland, F. A., *Fluid Flow for Chemical Engineers*, Chemical Publishing Co., New York, 1973.
- Hooper, W. B., "The 2-K Method Predicts Head Losses in Pipe Fittings," *Chem. Eng.*, p. 97, Aug. 24 (1981).
- Hooper, W. B., "Calculate Head Loss Caused by Change in Pipe Size," *Chem. Eng.*, p. 89, Nov. 7 (1988).
- Hutchison, J. W., *ISA Handbook of Control Valves*, Instrument Society of America, Research Triangle Park, NC, (1971).
- Krassik, I. J., W. C. Krutzsch, W. H. Frazer, and J. P. Messina, *Pump Handbook*, McGraw-Hill, New York, 1976.
- Miller, R. W., *Flow Measurement Engineering Handbook*, McGraw-Hill, New York, 1983.
- Murdock, J. W., *Fluid Mechanics and Its Applications*, Houghton Mifflin Co., Boston, 1976.
- Olson, R. M., *Essentials of Engineering Fluid Mechanics*, 4th ed., Harper & Row, New York, 1980.
- Perry, R. H., and D. W. Green, *Perry's Chemical Engineers' Handbook*, 7th ed., McGraw-Hill, New York, 1997.
- Savins, J. G., in *Viscous Drag Reduction*, C. S. Wells, Ed., p. 183, Plenum Press, New York, 1969.
- Shapiro, A. H., *The Dynamics and Thermodynamics of Compressible Fluid Flow*, vol. 1, The Ronald Press, New York, 1953.
- Virk, P. S., and H. Baher, *Chem. Eng. Sci.*, 25, 1183 (1970).

6.3.5.4	Natural Convection between Two Horizontal Parallel Plates	523
6.3.5.5	Other Geometries	523
6.4	Condensation and Vaporization Heat Transfer	523
6.4.1	Mechanisms of Condensation	523
6.4.2	Design Equations for Filmwise Condensation	524
6.4.2.1	Condensation on Vertical Plane and Tubular Surfaces	524
6.4.2.2	Condensation inside a Horizontal Tube.....	528
6.4.2.3	Condensation outside Horizontal Tubes and Tube Banks.....	529
6.4.3	Special Cases in Condensation	530
6.4.3.1	Enhanced Surfaces in Condensation.....	530
6.4.3.2	Condensation in the Presence of a Noncondensable Gas	530
6.4.3.3	Condensation of a Multicomponent Vapor	530
6.4.3.4	Condensation of Superheated Vapor.....	530
6.4.4	Mechanisms of Vaporization	531
6.4.5	Boiling Heat-Transfer Correlations.....	532
6.4.5.1	Nucleate Boiling	532
6.4.5.2	Critical Heat Flux in Pool Boiling	533
6.4.5.3	Natural and Forced Convection Vaporization.....	533
6.4.6	Special Cases in Vaporization	535
6.4.6.1	Boiling Outside Tube Bundles.....	535
6.4.6.2	Enhanced Surfaces in Boiling.....	536
6.4.6.3	Subcooled Boiling.....	536
6.5	Heat Exchangers.....	536
6.5.1	Introduction.....	536
6.5.2	Types of Heat Exchangers and Their Selection.....	537
6.5.2.1	Criteria for Heat-Exchanger Selection	537
6.5.2.2	Double-Pipe Heat Exchangers	537
6.5.2.3	Shell-and-Tube Heat Exchangers	538
6.5.2.4	Multitube ("Hairpin") Heat Exchangers.....	545
6.5.2.5	Gasketed-Plate Heat Exchanger and Related Partially Welded Variants	545
6.5.2.6	Plate-Fin (Matrix) Heat Exchangers.....	547
6.5.2.7	Air-Cooled Heat Exchangers	547
6.5.2.8	Mechanically Aided Heat Exchangers.....	549
6.5.3	Principles of Heat-Exchanger Design	550
6.5.3.1	Heat Transfer between Two Fluids Separated by a Wall	550
6.5.3.2	The Basic Design Integral	552
6.5.3.3	The Mean Temperature Difference Concept	552
6.5.4	Logic of the Heat-Exchanger Design Process	560
6.5.5	Fouling	562
References	563

6.1 INTRODUCTION

This chapter deals with the transfer of heat in systems likely to be of interest to chemical engineers. These situations include transfer within a single phase (especially between two surfaces of a solid), between a solid surface and a fluid, between fluids separated by a solid surface, and between surfaces of neighboring bodies. The basic heat-transfer processes discussed include conduction, single-phase convection, vaporization, and condensation. These processes are described physically, and representative equations are given for calculating the rate at which heat is transferred.

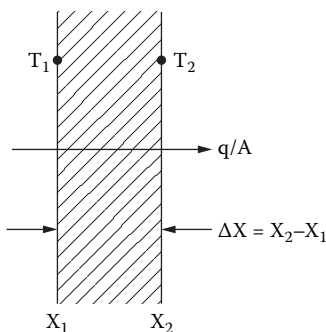


FIGURE 6.1 Conduction through a plane wall.

Equation (6.1) can be generalized to apply to three-dimensional, transient conduction with internal heat sources or sinks, but most chemical engineering applications can be treated as one- or two-dimensional, steady-state cases as described below. More advanced treatments are given in the literature [1–3].

6.2.2 ONE-DIMENSIONAL STEADY-STATE CONDUCTION

Equation (6.1) can be readily integrated for several important cases of one-dimensional steady-state conduction, including the following:

1. Plane slab of thickness Δx , with uniform temperatures on each surface (Figure 6.1). Integrating Equation (6.1) with $T = T_1$ on one surface (at $x = x_1$) and $T = T_2$ on the other surface (at $x = x_2$) gives

$$\frac{\dot{q}}{A} = \frac{k|(T_1 - T_2)|}{(x_2 - x_1)} = \frac{k|(T_1 - T_2)|}{\Delta x} \quad (6.2)$$

The vertical bars on the temperature difference indicate that the absolute value is to be used. It is assumed that the face dimensions Δy and Δz (where $\Delta y \Delta z = A$) either are large compared with Δx , or that the edges of the slab are well-insulated (adiabatic).

2. Multiple plane slabs in series with uniform temperatures on each surface (Figure 6.2). For two slabs of thicknesses Δx_1 and Δx_2 with thermal conductivities k_1 and k_2 , and with $T = T_1$ on the front face of the first slab and $T = T_2$ on the rear face of the second slab, Equation (6.2) gives

$$\frac{\dot{q}}{A} = \frac{k_1|(T_1 - T^*)|}{\Delta x_1} = \frac{k_2|(T^* - T_2)|}{\Delta x_2} \quad (6.3)$$

where T^* is the temperature of the contact surface between the two slabs. This assumes no contact resistance between the two slabs; contact resistance is discussed in Section 6.2.3. T^* can be eliminated from Equation (6.3) to give

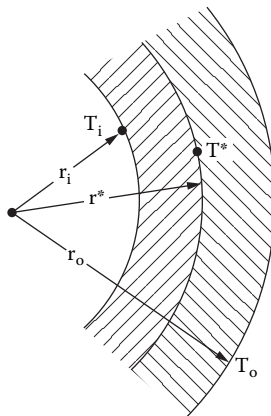


FIGURE 6.4 Conduction through a composite tube wall.

$$\frac{\dot{q}}{L} = \frac{2\pi k |T_i - T_o|}{\ln\left(\frac{r_o}{r_i}\right)} \quad (6.6)$$

The diametral ratio (D_o / D_i) can be used in the logarithmic term.

The heat flux, i.e., the heat-flow rate per unit area of heat-transfer surface, may be found from

$$\frac{\dot{q}}{A_i} = \frac{\dot{q}}{2\pi r_i L} = \frac{k |T_i - T_o|}{r_i \ln(r_o / r_i)} \quad (6.7)$$

for the inside surface area of the tube, and from

$$\frac{\dot{q}}{A_o} = \frac{\dot{q}}{2\pi r_o L} = \frac{k |T_i - T_o|}{r_o \ln(r_o / r_i)} \quad (6.8)$$

for the outside surface area. It is necessary to specify the area involved whenever a heat flux is given.

4. Multiple concentric cylinders with uniform temperatures on inside and outside surfaces (Figure 6.4), with zero contact resistance at the interface. Applying Equation (6.6) to each cylinder gives

$$\frac{\dot{q}}{L} = \frac{2\pi k_i |T_i - T^*|}{\ln\left(\frac{r^*}{r_i}\right)} = \frac{2\pi k_o |T^* - T_o|}{\ln\left(\frac{r_o}{r^*}\right)} \quad (6.9)$$

where k_i and k_o are the thermal conductivities of the inner and outer cylinders, respectively. Eliminating T^* gives

$$\frac{\dot{q}}{A_o} = \frac{\dot{q}}{\pi D_o L} = \frac{6.34 \times 10^4}{\pi(0.0315)} = 6.41 \times 10^5 \text{ W/m}^2 (= 2.03 \times 10^5 \text{ Btu/hr ft}^2)$$

for the outside surface of the tube.

6.2.3 THERMAL CONTACT RESISTANCE

When two solid surfaces, even finely machined ones, are placed in physical contact, there are still gaps between the two surfaces due to the inherent irregularities—roughness—of each surface. These gaps are usually filled with the ambient atmosphere, which usually has a lower effective thermal conductivity than the materials in contact. Heat transfer from one surface to another thus tends to be concentrated at those areas where the surfaces are in direct physical contact, which are also the areas on which the pressure forces act to keep the two surfaces in static equilibrium. The concentration of the heat-flow paths on only a part of the adjoining surfaces increases the local temperature gradients and in effect creates an additional resistance to heat transfer at the interface. This is termed the *thermal contact resistance*, and its possible effect in reducing the rate of heat transfer through composite materials (such as the bimetallic tube described above) must be considered.

Several factors determine the magnitude of the resistance, including

1. The roughnesses of the surfaces (height of surface irregularities)
2. The topology of the surfaces, e.g., whether the surfaces are grooved or randomly bumpy (grainy roughness), etc.
3. Hardness of the surface materials
4. Pressure exerted by one surface on the other
5. Thermal conductivities of the surface materials and the interstitial fluid
6. Other possible thermal transport mechanisms between the two surfaces, including radiation, natural convection, and free molecule transport at low pressures

The most generally applicable predictive method for contact resistance is ascribed to Irvine and Tabor in Section 2.4.6 of the *Heat Exchanger Design Handbook* [1]. Their method requires numerical values of the above properties, which usually do not have high accuracy, and the authors estimate about 25% mean error, with an error spread of a factor of 2 about the actual value. A typical thermal contact resistance is on the order of

$$1 - 2 \times 10^{-4} \frac{\text{m}^2\text{K}}{\text{W}} (6 - 12 \times 10^{-4} \text{ hr ft}^2 \text{ }^\circ\text{F/Btu})$$

The contact resistance is also affected by differential thermal expansion when the surfaces are at elevated temperatures or with large temperature differences in the two materials. The problem is aggravated by thermal cycling, especially if one material is heated above its elastic behavior range, and must be considered with finned tubes in air-cooled heat exchangers.

Example 6.2

Recalculate the results of Example 6.1 assuming a thermal contact resistance of $2 \times 10^{-4} \text{ m}^2\cdot\text{K/W}$ at the interface between the low-carbon and stainless steels. Assume that the dimensions are unchanged.

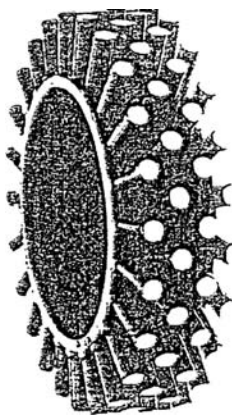


FIGURE 6.7 Studs or pin fins on a tube.

6.2.4.2 Convective Heat Transfer

Convection is the transfer of heat to or from, and within, flowing fluids. Section 6.3 of this chapter provides a more extensive treatment of convective heat transfer. For the analysis of heat-transfer fins, the rate of heat transfer to/from the fin surface from/to the ambient fluid is given by the equation

$$(\dot{q}/A)_{fin} = h_{fluid} |T_{fluid} - T_{fin}| \quad (6.11)$$

where $(\dot{q}/A)_{fin}$ is the heat flux (W/m^2 or $\text{Btu}/\text{h}\cdot\text{ft}^2$) to or from the fin, T_{fluid} is the bulk (mixed mean) temperature of the ambient fluid (K or $^{\circ}\text{C}$ or $^{\circ}\text{F}$), and T_{fin} is the surface temperature of the fin (K or $^{\circ}\text{C}$ or $^{\circ}\text{F}$). The film heat-transfer coefficient, h_{fluid} ($\text{W}/\text{m}^2\cdot\text{K}$ or $\text{Btu}/\text{h}\cdot\text{ft}^2\cdot^{\circ}\text{F}$), is the constant of proportionality between the heat flux to/from the ambient fluid and the temperature differential for heat transfer to/from the fluid. The value of h_{fluid} depends upon the geometry of the system and the velocity and physical properties of the fluid. The relationship among the variables is in the form of empirical correlations, which are given in Sections 6.3 and 6.4 of this chapter.

6.2.4.3 Heat Transfer in Fins of Constant Cross Section

Fins such as those shown in Figures 6.5 and 6.7 usually have a constant cross-sectional area for conduction and are usually several times as high as they are thick. This allows the use of the one-dimensional conduction equation to calculate the temperature profile in the fin (Figure 6.8). It is also usually assumed that the film heat-transfer coefficient is uniform over the surface (nonconservative) and that the fin tip is adiabatic (i.e., no heat transfer, which is a slightly conservative assumption).

The temperature distribution is given by

$$\frac{T_{fin} - T_{fluid}}{T_{fin,b} - T_{fluid}} = \frac{\cosh N(X - x)}{\cosh N X} \quad (6.12)$$

where

$$N = \sqrt{\frac{2h_{fluid}}{Yk_{fin}}} \quad (6.13)$$

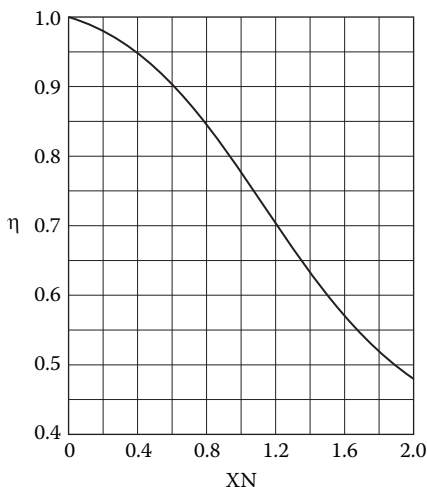


FIGURE 6.9 Fin efficiency for longitudinal and stud fins of constant cross-sectional area.

$$A_{eff} = A_{prime} + A_{fin}\eta_{fin} \quad (6.17)$$

In using the fin efficiency, the seemingly precise analytical solutions actually are premised upon several assumptions of unknown validity. Therefore, the resulting numerical values must be used cautiously and conservatively. And it must be remembered that, when using convective heat-transfer correlations for finned surfaces, the experimental data underlying these correlations were reduced using computed fin efficiencies.

Example 6.3

Twelve longitudinal low-carbon steel fins, each 15.8 mm (0.625 in.) high and 3.18 mm (0.125 in.) thick, are uniformly spaced around the outside surface of a 2-in. Schedule 40 (outside diameter = 6.033 cm = 2.375 in.) low-carbon steel pipe. The outside pipe wall temperature is 150°C (302°F), and it is cooled by a viscous oil flowing along the pipe at an average bulk temperature of 40°C (104°F). The oil has a film heat-transfer coefficient of 120 W/m²·K (21.1 Btu/h·ft²·°F), which is assumed constant over the outside surface of the pipe and the fins. The thermal conductivity of the steel is assumed constant at 49.1 W/m·K (28.4 Btu/h·ft·°F). Find the rate of heat transfer from the finned pipe per unit length and compare this with the heat transfer from the same length of unfinned pipe.

Solution

The heat-transfer area of the fins per meter of finned pipe (neglecting the fin tips) is

$$\frac{A_{fin}}{L} = 12(2)(15.8 \times 10^{-3}) = 0.379 \text{ m}^2/\text{m} (= 1.25 \text{ ft}^2/\text{ft})$$

The outside surface area of the pipe, excluding the area covered by the bases of the fins, A_{prime} , is

$$\begin{aligned} \frac{A_{prime}}{L} &= \pi(6.033 \times 10^{-2}) - 12(3.18 \times 10^{-3}) \\ &= 0.1514 \text{ m}^2/\text{m} (= 0.497 \text{ ft}^2/\text{ft}) \end{aligned}$$

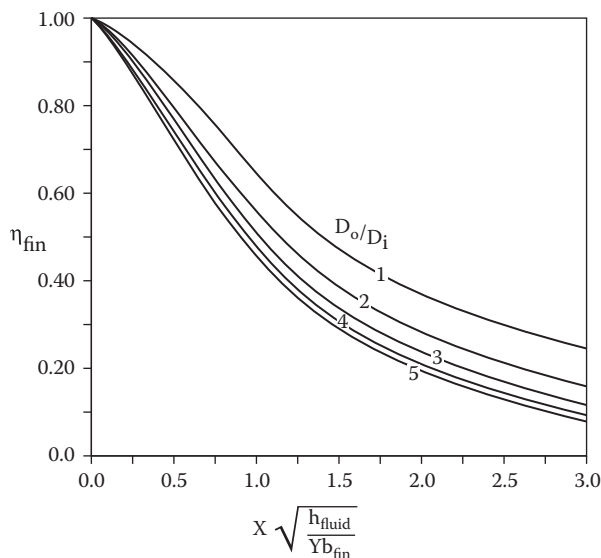


FIGURE 6.10 Fin efficiency for radial fins of constant thickness.

of the tube and fins. Assume negligible contact resistance. The thermal conductivity of Alloy 1100 is 218 W/m·K (126 Btu/h·ft·°F).

Calculate the heat-transfer rate per unit length of tube and compare that result with the unfinned tube under the same conditions.

Solution

The total fin area per unit length of tube is

$$\begin{aligned}\frac{A_{fin}}{L} &= \frac{\pi}{4} (D_{fin}^2 - D_{root}^2) (2) (400) \\ &= \frac{\pi}{4} [(0.0570)^2 - (0.0254)^2] (2) (400) \\ &= 1.636 \text{ m}^2/\text{m} (= 5.38 \text{ ft}^2/\text{ft})\end{aligned}$$

The prime tube outside area (that area not covered by the fin bases) is

$$\begin{aligned}\frac{A_{prime}}{L} &= \pi (0.0254) [1 - 400 (0.483 \times 10^{-3})] \\ &= 6.44 \times 10^{-2} \text{ m}^2/\text{m} (= 0.211 \text{ ft}^2/\text{ft})\end{aligned}$$

The fin efficiency is found from

$$X \sqrt{\frac{h_{fluid}}{Y k_{fin}}} = 15.8 \times 10^{-3} \sqrt{\frac{70}{(0.483 \times 10^{-3})(218)}} = 0.407$$

$$S = \frac{\dot{q}}{k\Delta T} \quad (6.18)$$

where \dot{q} is the rate of heat flow (W or Btu/h), k is the thermal conductivity of the conducting medium, and ΔT is the temperature difference between the heat source and the heat sink (both of which are assumed to be isothermal).

The shape factor may be found by one of two primary methods: analytical solution of the fundamental equations, or numerical solution in generalized dimensions presented in simple empirical equations to a sufficient degree of accuracy.

A solution of useful shape factors is given in Figure 6.11, taken from Parker et al. [8].

Example 6.5

A rectangular steel cold box with 4.76 mm (3/16 in.) thick walls has interior dimensions of 1.0 m by 1.25 m by 2.0 m (3.28 ft by 4.10 ft by 6.56 ft). It is insulated on all sides by a 10 cm (3.94 in.) thick layer of rock wool with a thermal conductivity of 0.040 W/m·K (0.023 Btu/h·ft·°F). The interior wall temperature is -20°C (-4°F), and the exterior surface of the insulation is at 40°C (104°F).

Calculate the heat-transfer rate from the surrounding atmosphere to the interior of the box.

Solution

The thermal resistance of the steel wall is negligible compared with that of the insulation. Assume zero contact resistance between the wall and the insulation.

Refer to the last diagram in Figure 6.11:

$$\sum L = 4(1.0) + 4(1.25) + 4(2.0) = 17.0 \text{ m} (= 55.8 \text{ ft})$$

$$\Delta X = 0.10 \text{ m} (= 0.328 \text{ ft})$$

$$A = 2(1.0)(1.25) + 2(1.0)(2) + 2(1.25 \times 2.0) = 11.5 \text{ m}^2 (= 124 \text{ ft}^2)$$

$$S = \frac{11.5}{0.10} + 0.54(17.0) + 1.2(0.1) = 124.3 \text{ m} (= 408 \text{ ft})$$

$$\dot{q} = (124.3 \text{ m}) \left(0.040 \frac{\text{W}}{\text{m} \cdot \text{K}} \right) (40 - (-20))^{\circ}\text{C}$$

$$\dot{q} = 298 \text{ W} (= 1020 \text{ Btu/hr})$$

Note that this calculation does not consider the convective heat transfer on either side of the insulated surface. An average temperature difference between the outside atmosphere and the outer surface could be obtained by using

$$\dot{q} = \bar{h}A_{\text{outside}}(T_{\text{atm}} - T_{\text{surface}})$$

where \bar{h} is an appropriate film heat-transfer coefficient (Section 6.3), A_{outside} is the outside area of the box, and T_{atm} and T_{surface} are the temperatures of the atmosphere and the outside surface of the box, respectively. This assumes that the entire outside area of the box is exposed to the atmosphere and that \bar{h} is constant and uniform.

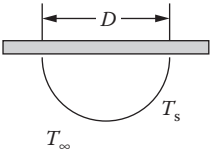
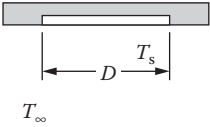
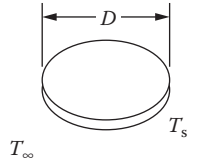
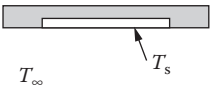
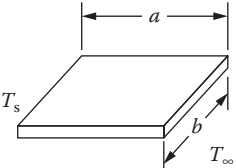
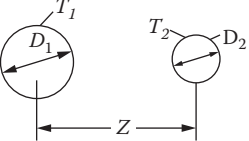
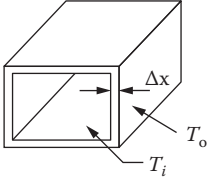
Shape	Diagram	$S = \frac{\dot{q}}{k \Delta T}$
Half-sphere submerged into the surface of a semi-infinite medium with otherwise adiabatic surface and temperature T_∞ at a large distance.		πD
Disk placed on surface of semi-infinite medium with otherwise adiabatic surface and temperature T_∞ at a large distance.		$2D$
Thin disk in infinite medium having temperature T_∞ at a large distance.		$4D$
Rectangular plate on surface of semi-infinite medium with otherwise adiabatic surface and temperature T_∞ at a large distance. Plate has dimensions $a \times b$.		$\frac{\pi a}{\ln \frac{4a}{b}}$ $a > b$
Thin rectangular plate of dimensions $a \times b$ buried in infinite medium having temperature T_∞ at large distance		$\frac{2 \pi a}{\ln \frac{4a}{b}}$ $a > b$
Conduction between cylinders of length L a distance Z apart, located in an infinite medium. No heat loss from cylinders to medium is considered.		$\frac{2\pi L}{\cosh^{-1} \left(\frac{4Z^2 - D_1^2 - D_2^2}{2D_1 D_2} \right)}$
Conduction between inside and outside surfaces of a rectangular box having uniform inside and outside surface temperatures. Wall thickness Δx is less than any inside dimensions.		$\frac{A}{\Delta x} + 0.54 \Sigma L + 1.2 \Delta x$ ΣL = Sum of all inside lengths, Δx = Thickness of walls, A = Inside surface area.

FIGURE 6.11 Continued.

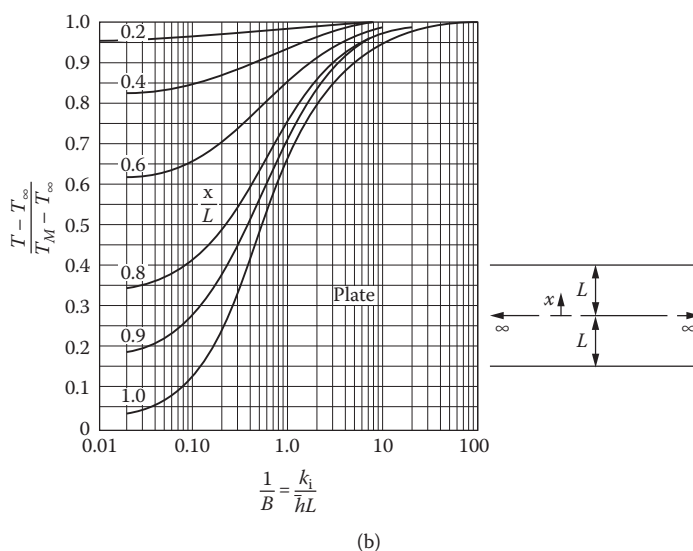
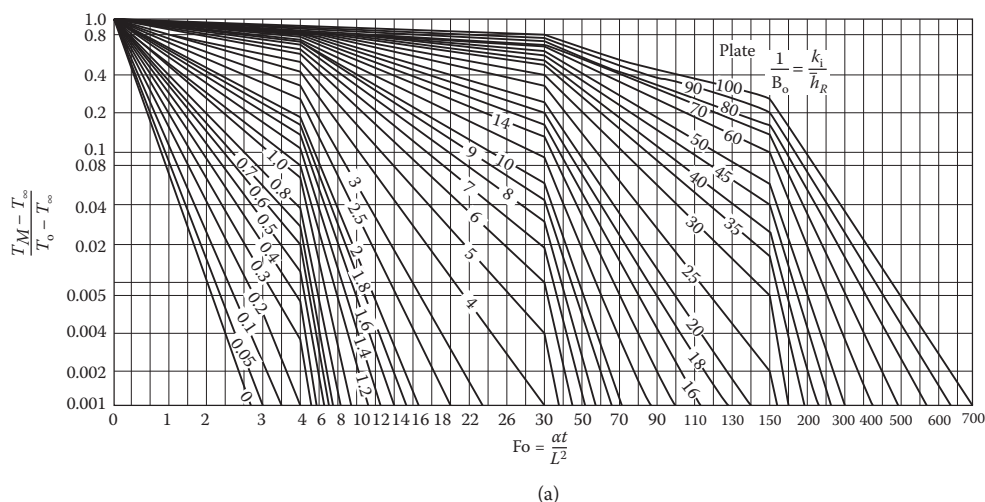


FIGURE 6.12 (a) Variation of the midplane temperature of a plane solid with dimensionless time. (b) Variation of temperature in a plane solid as a function of position.

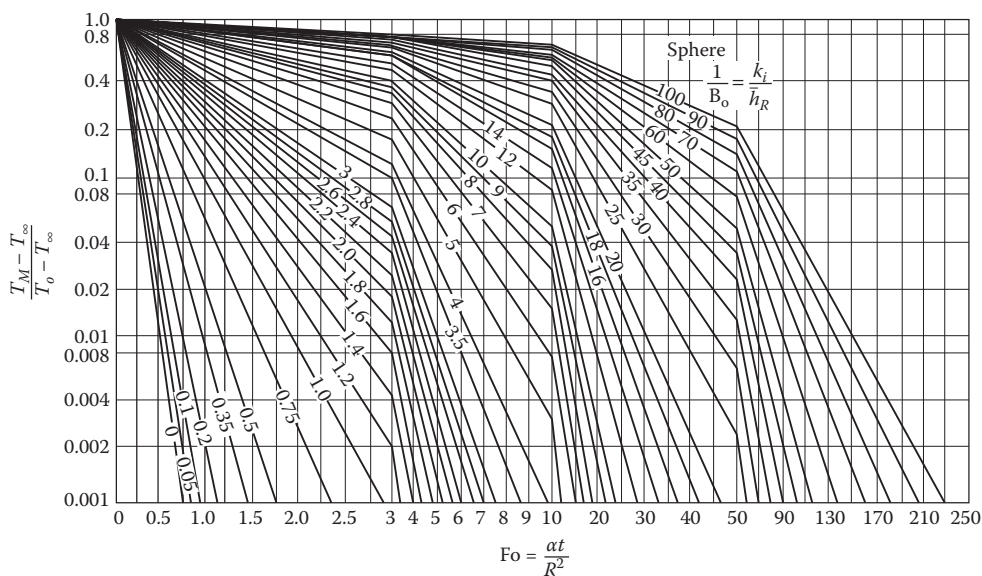
The second chart in each pair (Figures 6.12b, 6.13b, and 6.14b) relates the temperature at any position in the solid to the temperature at the center at any given time, using as parameters $1/B_0$ and the relative position in the solid between the center and the surface.

A property of these solutions is that they may be combined to give the solution to additional cases. For example, consider the case of a rectangular solid having dimensions X , Y , Z . The temperature at a given position within that solid at a given time $T(x,y,z,t)$ is given by

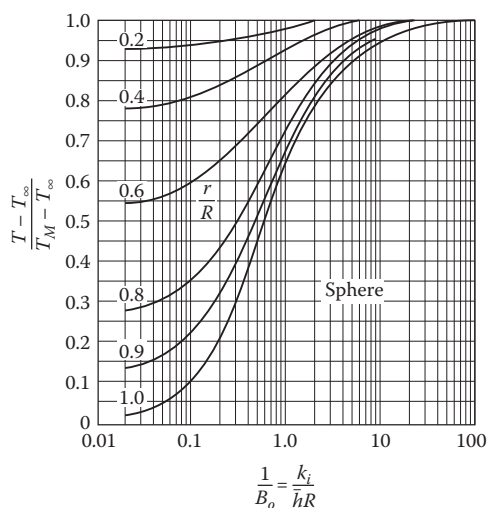
$$T(x,y,z,t) = T(x,t)T(y,t)T(z,t) \quad (6.25)$$

where $T(x,t)$ is the solution found for position x at time t assuming Y and Z to be infinite, $T(y,t)$ the solution for position y at time t assuming X and Z to be infinite, and $T(z,t)$ the solution for position z at time t assuming X and Y to be infinite.

The case for a short cylinder is illustrated in the following example.



(a)



(b)

FIGURE 6.14 (a) Variation of the center temperature of a sphere with dimensionless time. (b) Variation of temperature in a sphere as a function of position.

Solution

The small cylinder can be modeled as an infinitely long cylinder of radius 3.0 mm, intersected by plane surfaces of 12.5 mm half-thickness perpendicular to the cylinder axis. (See Figure 6.15.)

The thermal diffusivity is

$$\alpha = \frac{0.194}{1,186(1,520)} = 1.076 \times 10^{-7} \frac{\text{m}^2}{\text{sec}} \left(= 4.15 \times 10^{-3} \frac{\text{ft}^2}{\text{hr}} \right)$$

$$\left(\frac{T_m - T_\infty}{T_o - T_\infty}\right)_{\text{pellet}, t=t^*} = \left(\frac{T_m - T_\infty}{T_o - T_\infty}\right)_{\text{cylinder}, t=t^*} \times \left(\frac{T_m - T_\infty}{T_o - T_\infty}\right)_{\text{plane}, t=t^*}$$

This is a trial-and-error solution, but an initial upper bound can be found by neglecting the relatively minor effect of the plane ends. Therefore, from Figure 6.13a, for

$$\frac{T_m - T_\infty}{T_o - T_\infty} = 0.111 \quad \text{at} \quad \frac{1}{Bo} = 1.29$$

Fo is found to be about 1.8 and t is found from

$$t = \frac{1.8}{1.196 \times 10^{-2}} = 151 \text{ s}$$

For a second estimate, try $t = 120$ s, with $Fo = 1.44$ for the cylinder and $Fo = 0.083$ for the plane from Figure 6.12a. For the cylinder,

$$\left(\frac{T_m - T_\infty}{T_o - T_\infty}\right)_{\text{cylinder}} = 0.17$$

and for the plane,

$$\left(\frac{T_m - T_\infty}{T_o - T_\infty}\right)_{\text{plane}} = 0.92$$

giving an estimate for

$$\left(\frac{T_m - T_\infty}{T_o - T_\infty}\right)_{\text{pellet}} = 0.156$$

A third estimate of $t = 135$ s gives $Fo = 1.61$ for the cylinder, $Fo = 0.093$ for the plane,

$$\left(\frac{T_m - T_\infty}{T_o - T_\infty}\right)_{\text{cylinder}} = 0.14, \quad \left(\frac{T_m - T_\infty}{T_o - T_\infty}\right)_{\text{plane}} = 0.88, \quad \text{and} \quad \left(\frac{T_m - T_\infty}{T_o - T_\infty}\right)_{\text{pellet}} = 0.12$$

This is as close as the charts can be read, and probably as close as the normal uncertainties and approximations in such problems justify, so the required heating time is 135 s.

The temperature on the outside surface of the pellet at the lengthwise center can be found from Figure 6.13b. Reading at

$$\frac{r}{R} = 1.0 \quad \text{and} \quad \frac{1}{Bo} = 1.29$$

gives

is calculated from a heat balance. The difference between the wall, bulk, and centerline temperatures must be considered when dealing with a temperature-sensitive fluid.

These heat-transfer mechanisms have been modeled both analytically and numerically for many flow geometries. Most numerical methods require a computer to obtain an analytical answer, and because of the simplifications and assumptions required to obtain a solution, they are usually more accurate than the empirical methods discussed in this chapter. Good introductions to these methods are provided by Hewitt [1], Patankar [10], and Shah and London [11].

6.3.2 FILM COEFFICIENT OF HEAT TRANSFER

For the majority of convective heat-transfer cases, the heat flux (\dot{q}/A) between the surface and the fluid is nearly proportional to the temperature difference between the bulk fluid and the wall ($T - T_w$). A constant of proportionality h or α is termed the *film coefficient* of heat transfer and is defined by

$$\dot{q}/A = h|(T - T_w)| \quad (6.26)$$

where the bars denote that the absolute value of temperature difference is to be used. The area A used in the equation is usually (but not necessarily; see Section 6.3.3) the surface area across which the heat actually flows; this area should always be carefully defined to avoid confusion. For example, for heat transfer to a fluid inside a plain cylindrical tube, the heat-transfer area is $A_i = \pi d_i L$, where d_i is the inside diameter, L is the tube length over which heat transfer occurs, and h_i is defined as the film heat-transfer coefficient based on (or referenced to) the inside heat-transfer surface of the tube.

The value of h is found from correlations specific to the flow geometry (e.g., inside a tube or across a bank of tubes) and also depends upon the fluid velocity and physical properties. These correlations come primarily from experimental data and are usually expressed as functions of dimensionless numbers to generalize them. The form of the correlation may arise from theory or mechanistic models. In a very few instances, dimensional equations may be the only forms available; they must be used with data given in the stated dimensions and are usually of very limited generality.

Certain heat-transfer processes, notably nucleate boiling, do not follow the proportionality described above. Nevertheless, the concept of a film heat-transfer coefficient is so convenient for practical computation that it is often used in these cases. Special care is required to ensure that the heat flux, the temperature difference, and the coefficient are consistent.

Because the film coefficient correlations are based on experimental data, the calculated coefficients are not more accurate than those data. Further, the conditions in the experiments are often different from those in practical applications. The result is that the best correlations (e.g., the Petukhov-Popov correlation for turbulent flow [17] in long plain round tubes) have an uncertainty of about $\pm 10\%$, and correlations for more complex cases are significantly less accurate. The consequences of these uncertainties must be considered when applying the calculated results to the design of equipment or interpretation of equipment performance.

6.3.3 DIMENSIONLESS NUMBERS

Heat-transfer-coefficient correlations are usually presented in terms of dimensionless numbers, which are groups of variables that have no net dimensions when evaluated in any consistent system of units. The most important dimensionless numbers for heat transfer are defined next.

6.3.3.1 Reynolds Number, Re

The Reynolds number is defined as

6.3.3.3 Stanton Number, St

An alternative way to represent the heat-transfer coefficient is by the Stanton number, defined as

$$St = \frac{h}{V\rho c_p} \quad (6.29)$$

where c_p is the specific heat of the fluid at constant pressure. The Stanton number is the ratio of the heat-transfer rate to the heat transported in the stream.

6.3.3.4 Colburn j -Factor for Heat Transfer, j_H

The Colburn j -factor is another representation of the heat-transfer coefficient and arises from a boundary layer theory model. It is defined as

$$j_H = St \text{Pr}^{2/3} \left(\frac{\mu_w}{\mu} \right)^{0.14} \quad (6.30)$$

where St is the Stanton number defined in Section 6.3.3.3, Pr is the Prandtl number defined in Section 6.3.3.5, and $(\mu_w/\mu)^{0.14}$ is the Sieder-Tate term described in Section 6.3.3.9.

6.3.3.5 Prandtl Number, Pr

The Prandtl number is defined as

$$\text{Pr} = \frac{c_p \mu}{k} \quad (6.31)$$

where c_p is the specific heat at constant pressure, μ is the absolute viscosity, and k is the thermal conductivity of the fluid. The Prandtl number is the ratio of the momentum diffusivity (μ/ρ) to the thermal diffusivity ($k/\rho c_p$) of the fluid.

6.3.3.6 Graetz Number, Gz

The Graetz number is defined as

$$Gz = \frac{D}{L} \cdot \frac{V\rho c_p D}{k} \quad (6.32)$$

where L is the distance from the start of heating (for heat transfer at a given point) or length of heat-transfer surface (for total amount of heat transferred). The Graetz number is primarily of interest for laminar flow heat transfer with a developing temperature profile.

6.3.3.7 Peclet Number, Pe

The Peclet number is defined as

$$Pe = \frac{V\rho c_p D}{k} \quad (6.33)$$

of them assume constant physical properties and hence fail to show the effect of natural convection induced by the density change due to heating or cooling. One well-known analytical solution is the so-called Graetz-Nusselt problem (parabolic velocity profile) for fully developed laminar flow in a plain round tube (described by Shah and London [11] and Sieder and Tate [12]). The exact solution is unwieldy and is usually represented by the Hausen Equation (15):

$$\frac{\bar{h}_i D_i}{k} = \left[3.65 + \frac{0.0668 \text{Re} \text{Pr}(D_i / L)}{1 + 0.04[\text{Re} \text{Pr}(D_i / L)]^{2/3}} \right] \left(\frac{\mu}{\mu_w} \right)^{0.14} \quad (6.37)$$

where \bar{h}_i is the average heat-transfer coefficient over the heat-transfer length of the tube L . The Sieder-Tate term has been added. This equation does not include natural convection effects. The Palen-Taborek equation [16] does consider natural convection:

$$\frac{\bar{h}_i D_i}{k} = 2.5 + 4.55(\text{Re}^\circ)^{0.37} (d_i / L)^{0.37} \text{Pr}^{0.17} \left(\frac{\mu}{\mu_w} \right)^{0.14} \quad (6.38)$$

where

$$\text{Re}^\circ = \text{Re} + 0.8 \text{Gr}^{0.5} \exp(-0.42 / \text{Gr}^2) \quad (6.39)$$

The temperature difference ΔT used in the Grashof number is the average temperature difference between the bulk fluid and the wall over the heat-transfer length. This equation applies only to horizontal tubes.

For vertical tubes, the natural convection effect depends upon both the flow direction and whether the fluid is being heated or cooled. This problem is examined in the work of Jakob [14] and in Section 2.5.10 of the *Heat Exchanger Design Handbook* [1].

$$6.3.4.1.2 \quad \text{Turbulent Flow, } \text{Re} = \frac{D_i \rho V_i}{\mu} > 7000$$

The Sieder-Tate equation [12],

$$\frac{h_i D_i}{k} = 0.023 \text{Re}^{0.8} \text{Pr}^{1/3} \left(\frac{\mu}{\mu_w} \right)^{0.14} \quad (6.40)$$

is convenient and reliable for Reynolds numbers above about 7000. The Petukhov-Popov equation [17] is generally regarded as the best available for this case:

$$\frac{h_i D_i}{k} = \frac{(f_F / 2) \text{Re} \text{Pr}}{1.07 + 12.7(f_F / 2)^{1/2} (\text{Pr}^{2/3} - 1)} \left(\frac{\mu}{\mu_w} \right)^{0.14} \quad (6.41)$$

where

$$f_F = (3.64 \log_{10} \text{Re} - 3.28)^{-2} \quad (6.42)$$

and Equation (6.41) gives

$$Nu = \frac{h_i D_i}{k} = \frac{(0.00494 / 2)(64,400)(4.21)}{1.07 + 12.7 \left(\frac{0.00494}{2} \right)^{1/2} [(4.21)^{2/3} - 1]} (1.048) = 337$$

Then

$$h_i = 337 \left(\frac{0.631 \text{ W/mK}}{21.2 \times 10^{-3} \text{ m}} \right) = 10,020 \text{ W/m}^2\text{K (or } 10,020 \text{ W/m}^2\text{K), or } 1,760 \text{ Btu/hr ft}^2\text{°F}$$

The coefficients are based on the inside-tube heat-transfer surface. The corresponding fluxes are

$$q / A_i = (10,020 \text{ W/m}^2\text{C})(60 - 40)\text{C} = 200,400 \text{ W/m}^2, \text{ or } 63,400 \text{ Btu/hr ft}^2$$

The agreement between the two correlations in this case is within about 20%, which is an example of the possible differences in two different but accepted correlations.

6.3.4.1.3 Transition Flow, $2100 < Re < 7000$

Prediction of the heat-transfer coefficient in the transition flow regime is uncertain due to the strong effects of entrance conditions and instability of the flow pattern. Gnielinski [18] modified the Petukhov-Popov equation to accommodate the transition region and extend it into the turbulent flow range:

$$\frac{h_i D_i}{k} = \frac{(f_F / 2)(Re - 1000)Pr}{1 + 12.7(f_F / 2)^{1/2}(Pr^{2/3} - 1)} \left[1 + \frac{D_i}{L} \right]^{2/3} \left(\frac{\mu}{\mu_w} \right)^{0.14} \quad (6.43)$$

Again, f_F is given by Equation (6.42). The Sieder-Tate term has been added to the equation.

6.3.4.2 Internally Enhanced Tubes

Many techniques—straight, spiraled, and circular fins; twisted tape and wire inserts; and various corrugations—improve the heat-transfer coefficient or increase the heat-transfer area inside tubes. There is always an increased pressure drop as well as increased cost associated with these enhancements. There may also be a change in the fouling characteristics, which may be either a positive or negative factor, depending upon the circumstances. These tubes are ordinarily considered in cases where the inside-tube heat-transfer coefficient is substantially lower than the outside coefficient, since the use of enhanced tubes can only be justified if increased cost and possible operational complications are offset by a savings in the overall size and cost of the heat exchanger. Webb [7] provides an excellent overview of enhanced heat transfer for a wide variety of geometries and operational conditions.

6.3.4.3 Inside Annular Channels

An annular channel is the space between two concentric cylindrical tubes, shown in Figure 6.16. This geometry is used in double-pipe heat exchangers, as described later. The primary interest is on heat transfer on the outside surface of the inner tube. In evaluating the Reynolds, Nusselt, and

6.3.4.4 Flow across a Circular Cylinder

Heat transfer in flow across a circular cylinder occurs in many situations over a wide range of conditions. The dominant flow mechanisms change gradually from creeping laminar at very low Re to a fully developed turbulent boundary layer on the forward surface of the cylinder with a strongly eddied wake region at high Re . A combination of flow modeling and extensive experimental data have suggested the following correlations (modified from Eckert and Drake [21]):

For $1 \leq Re \leq 1000$:

$$Nu = (0.43 + 0.50 Re^{0.5}) Pr^{0.38} \left(\frac{\mu}{\mu_w} \right)^{0.25} \quad (6.46)$$

For $1000 \leq Re \leq 2 \times 10^5$:

$$Nu = 0.25 Re^{0.6} Pr^{0.38} \left(\frac{\mu}{\mu_w} \right)^{0.25} \quad (6.47)$$

In these equations, the cylinder diameter D_o is used in Nu and Re , and the undisturbed approach velocity is used in Re .

Example 6.9

Calculate the rate of heat loss by convection from the outer surface of an uninsulated 4-in. Schedule 40 pipe ($D_o = 4.500$ in. = 0.114 m) exposed to wind blowing at 8.0 m/s (26.3 ft/s) perpendicular to the pipe. The air is at -23°C (-9.4°F), and the pipe surface is at 27°C (80.6°F).

Solution

Air properties at -23°C and 1 atm abs are

Density, $\rho = 1.41 \text{ kg/m}^3$ (0.088 lb_m/ft³)

Viscosity, $\mu = 1.49 \times 10^{-5} \text{ kg/m}\cdot\text{s}$ (0.0360 lb_m/ft·h)

Thermal conductivity, $k = 0.0223 \text{ W/m}\cdot\text{K}$ (0.0127 Btu/h·ft·°F)

Specific heat, $c_p = 1.00 \times 10^3 \text{ Ws/kgK}$ (0.24 Btu/lb_m·°F)

The air viscosity at the surface of the pipe (at 27°C) is $\mu_w = 1.98 \times 10^{-5} \text{ kg/m}\cdot\text{s}$ (0.0478 lb_m/ft·h).

$$Re = \frac{D_o \rho V}{\mu} = \frac{(0.114 \text{ m})(1.41 \text{ kg/m}^3)(8.0 \text{ m/s})}{(1.49 \times 10^{-5} \text{ kg/ms})} = 86,300$$

$$Pr = \frac{c_p \mu}{k} = \frac{(1.00 \times 10^3 \text{ Ws/kg K})(1.49 \times 10^{-5} \text{ kg/ms})}{0.0223 \text{ W/m K}} = 0.668$$

From Equation (6.47),

$$\frac{h D_o}{k} = 0.25(86,300)^{0.6} (0.668)^{0.38} \left(\frac{1.49 \times 10^{-5}}{1.98 \times 10^{-5}} \right)^{0.25} = 183$$

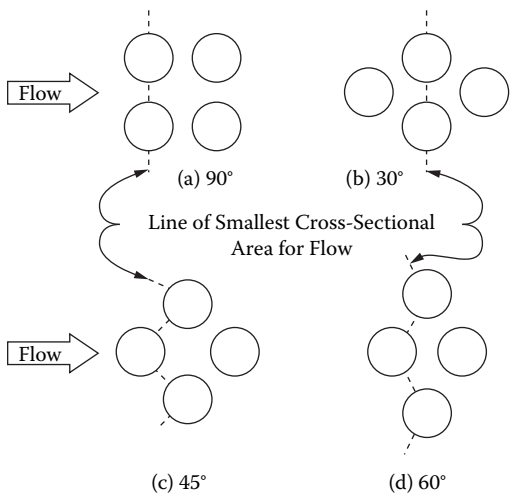


FIGURE 6.17 Typical tube layouts used in shell-and-tube heat exchangers.

ratio, the greater the surface area per unit volume; practical construction considerations set the minimum pitch ratio to about 1.25. As the pitch ratio is increased, the pressure drop for a given flow rate decreases much faster than the heat-transfer coefficient, but requires a relatively modest increase in heat-exchanger size. For handling liquids, the pitch ratio is usually chosen between 1.25 and 1.5; for gases and in vacuum service (including condensing and vaporizing), pitch ratios of 2 or even greater can be considered.

Generalized transfer and pressure-drop correlations for several commonly used ideal (no bypass or leakage flows) tube banks are shown in Figures 6.18, 6.19a, and 6.19b over the usual Reynolds number range. Figure 6.20 gives more specialized and accurate curves over a narrower but critical range.

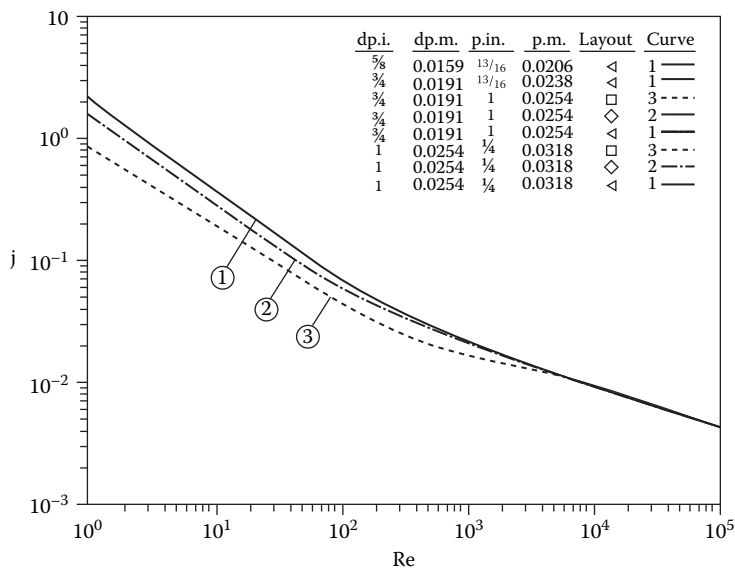


FIGURE 6.18 Correlation of Colburn j -factors for ideal tube banks.

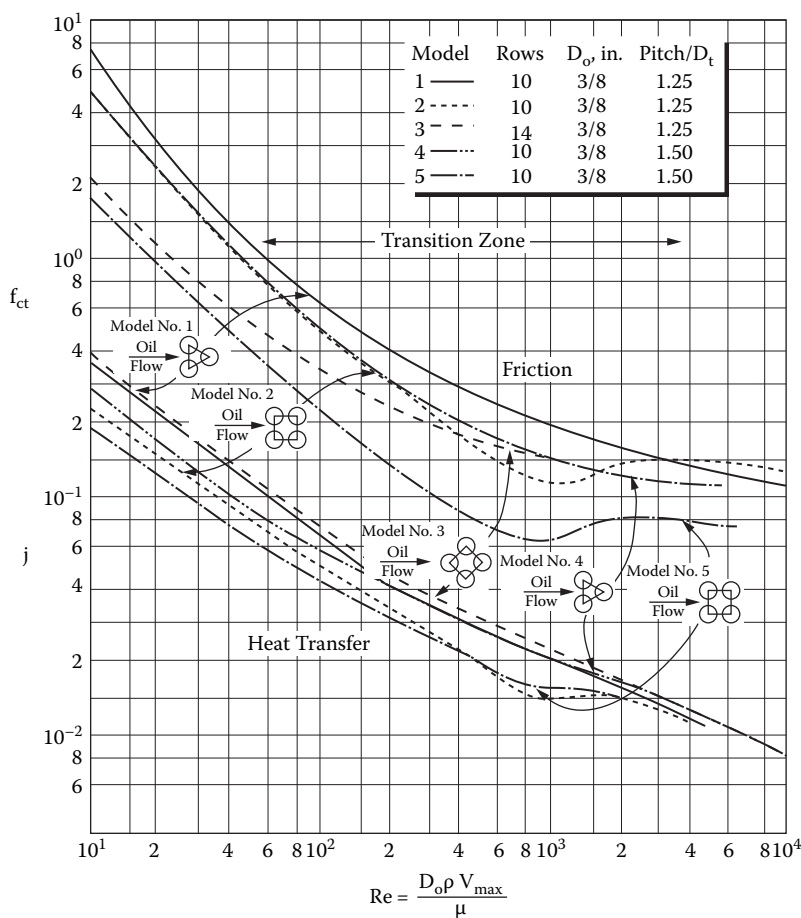


FIGURE 6.20 Summary of Delaware ideal tube-bank friction factor and Colburn j -factor data.

$$f_{ct} = \frac{2\Delta p g_c}{4\rho V_{\max}^2 N} \left(\frac{\mu}{\mu_w} \right)^{0.14} \quad (6.50)$$

In this equation, N is the number of major restrictions in the tube bank (i.e., the number of times the flow reaches its maximum velocity in flowing through the tube bank). In the 30° and 90° arrangements, N is equal to the number of tube rows crossed in the bank; for the 45° and 60° layouts, N is one less than the number of rows crossed. The term Δp is the frictional pressure drop across the tube bank.

Example 6.10

Calculate the heat-transfer coefficient and frictional pressure loss for the following case: Water at an average temperature of 20°C (68°F) is flowing at the rate of 50 kg/s ($110\text{ lb}_m/\text{s}$) across a tube bank composed of 274 tubes, each 25.4 mm (1.00 in.) in diameter and 1 m long in a 30° layout with a 1.25 pitch ratio, as shown in Figure 6.21.

There are 7 rows with 20 tubes per row and 6 rows with 19 tubes per row. The heat-transfer and pressure-drop characteristics are represented by curve 1 in Figures 6.18 and 6.19a and by model 1 in Figure 6.20. The tube surface temperature is 60°C (140°F).

$$\Delta p = \frac{4(0.12)(1.001 \times 10^3 \text{ kg/m}^3)(0.361 \text{ m/s})^2(13)}{2(1)} \left(\frac{4.71 \times 10^{-4}}{1.007 \times 10^{-3}} \right)^{0.14}$$

$$= 366 \frac{\text{kg}}{\text{m} \cdot \text{s}^2} = 366 \text{ N/m}^2 = 366 \text{ Pa} = 5.3 \times 10^{-2} \text{ lb}_f/\text{in.}^2$$

The heat-transfer coefficient is obtained from Equation (6.48), where

$$\text{Pr} = \frac{(4.183 \times 10^3 \text{ Ws/kg K})(1.007 \times 10^{-3} \text{ kg/ms})}{(0.597 \text{ W/m K})} = 7.06$$

and

$$h = \frac{0.0090(4.183 \times 10^3 \text{ Ws/kg K})(1.001 \times 10^3 \text{ kg/m}^3)(0.361 \text{ m/s})}{(7.06)^{2/3} \left(\frac{4.71 \times 10^{-4}}{1.007 \times 10^{-3}} \right)^{0.14}}$$

$$= 4.11 \times 10^3 \text{ W/m}^2\text{K} (= 724 \text{ Btu/h} \cdot \text{ft}^2 \cdot ^\circ\text{F})$$

6.3.4.5.2 Banks of Low-Finned Tubes

The limited experimental results of Williams and Katz [25] and Briggs et al. [26] can be used to modify the results for plain tubes to apply to cross flow in banks of low-finned tubes commonly used in shell-and-tube heat exchangers.

The plain-tube j -factor curves can be used for the corresponding low-finned tubes for Reynolds numbers above 1000. At lower Re, the retardation of the flow between the fins reduces the j -factor. It is necessary to calculate V_{\max} , taking into account the flow area between the fins. The root diameter of the tube (i.e., the tube diameter at the base of the fins) is used in the Reynolds number. The coefficient thus calculated is based on the entire external tube area including fins, but a fin efficiency (calculated by the method of Section 6.2.4.3) must be applied to the fin area.

For calculating pressure drop, the friction factors given in Figures 6.19a, 6.19b, and 6.20 should be multiplied by a factor of 1.5.

6.3.4.5.3 Banks of High-Finned Tubes

The experimentally based correlation of Briggs and Young [27] is recommended for this case:

$$\frac{h_o D_r}{R} = 0.134 \text{Re}^{0.68} \text{Pr}^{1/3} \left(\frac{H}{s} \right)^{-0.2} \left(\frac{Y}{s} \right)^{-0.12} \quad (6.51)$$

The heat-transfer coefficient h_o is referenced to the entire outside tube surface, including fins, and the fin efficiency is found from Section 6.2.4.3. D_r is the root diameter of the tube (to the base of the fins), H is the fin height, Y is the fin thickness, and s is the face-to-face spacing between the fins. The Reynolds number Re is defined as

$$\text{Re} = \frac{D_r \rho V_{\max}}{\mu} \quad (6.52)$$

$$\Psi = \frac{V_{total} - V_s}{V_{total}} \quad (6.61)$$

In these equations, D_{sphere} is the diameter of the spheres; V_{free} is the fluid velocity in the cross section of the empty vessel; ρ and μ are, respectively, the density and absolute (dynamic) viscosity of the fluid; and V_{total} and V_s are, respectively, the volume of the empty vessel and the total volume of the spheres respectively.

The corresponding pressure drop can be estimated by the Ergun Equation [27]:

$$\frac{\Delta p}{L} \frac{D_p}{\rho V_s^2} \left(\frac{\epsilon^3}{1-\epsilon} \right) = 150 \left(\frac{D_p \rho V_s}{\mu} \right) + 1.75 \quad (6.62)$$

where L is the height of the bed and ϵ is the porosity.

Fluidized beds are widely used in chemical processing, but the heat-transfer and fluid-flow characteristics are too complex to be adequately treated here. Martin (in [1], Section 2.8.4) gives an excellent overview.

6.3.5 SINGLE-PHASE HEAT TRANSFER IN NATURAL CONVECTION

In natural convection heat transfer, fluid motion is induced by the density difference between the fluid in contact with the solid heat-transfer surface and the bulk fluid. The density difference is related to the temperature difference between wall and bulk by

$$\Delta \rho = \rho_{wall} - \rho_{bulk} = \beta \bar{\rho} (T_{bulk} - T_{wall}) \quad (6.63)$$

where β is the thermal expansion coefficient of the fluid at constant pressure, defined by

$$\beta = -\frac{1}{\bar{\rho}} \left(\frac{\partial \rho}{\partial T} \right)_p \quad (6.64)$$

and $\bar{\rho}$ is the mean density,

$$\bar{\rho} = \frac{1}{2} (\rho_{wall} + \rho_{bulk}) \quad (6.65)$$

For small density differences, β can be assumed constant. The value of β can be found from a table of density vs. temperature (at constant pressure) over the temperature range of interest.

The resulting induced flow may be laminar (usually at small temperature differences and/or viscous fluids) or turbulent, or often in a transition or mixed laminar and turbulent regime. Correlations may be based on analytical or experimental studies, and numerical methods are now available. A major limitation to analytical solutions is that constant viscosity is generally assumed, whereas the variation of viscosity with temperature is likely to have a major effect upon the velocity gradient and the dominant flow regime near the heat-transfer surface.

Other factors that need to be considered in any natural convection calculation include the geometry of the container (if any), flows generated from (or limited by) other surfaces in the vicinity, the interaction with forced flows, and possible radiative heat-transfer interactions. Because natural

where

$$f_2(\text{Pr}) = \left[1 + \left(\frac{0.437}{\text{Pr}} \right)^{9/16} \right]^{-4/9} \quad (6.72)$$

The average coefficient from $x = 0$ to $x = x$ ($x \leq L$) is

$$\overline{\text{Nu}}_x = 0.67 \text{Ra}_x^{1/4} f_2(\text{Pr}) \quad (6.73)$$

where ΔT in Ra_x is based on the wall temperature at $x/2$.

3. Turbulent flow, $\text{Ra}_x > 10^9$:

The heat-transfer coefficient for a turbulent boundary layer is

$$\overline{\text{Nu}}_x = \frac{\bar{h}_x x}{k} = 0.15 \text{Ra}_x^{1/3} f_3(\text{Pr}) \quad (6.74)$$

where

$$f_3(\text{Pr}) = \left[1 + \left(\frac{0.492}{\text{Pr}} \right) \right]^{-16/27}$$

4. Combined laminar and turbulent flow:

These equations can be combined to give an average coefficient over a vertical length L :

$$\overline{\text{Nu}}_L = 0.68 + 0.67 \text{Ra}_L^{1/4} [f_1(\text{Pr})] [1 + 1.6 \times 10^{-8} \text{Ra}_L [f_1(\text{Pr})]^4]^{1/2} \quad (6.75)$$

6.3.5.2 Natural Convection from Horizontal Plates

Heat transfer in this case depends upon the dimensions of the surface and which surface (upper or lower) is heated or cooled. Hewitt et al. [30] recommend the following equations:

1. Upper surface of heated plate or lower surface of cooled plate:

$$\overline{\text{Nu}}_L = \frac{\bar{h}L}{k} = 0.54 \text{Ra}_L^{1/4} \quad \text{for } (10^4 \leq \text{Ra}_L \leq 10^7) \quad (6.76)$$

$$\overline{\text{Nu}}_L = \frac{\bar{h}L}{k} = 0.15 \text{Ra}_L^{1/3} \quad \text{for } (10^7 \leq \text{Ra}_L \leq 10^{11}) \quad (6.77)$$

2. Lower surface of heated plate or upper surface of cooled plate:

$$\overline{\text{Nu}}_L = 0.27 \text{Ra}_L^{1/4} \quad \text{for } (10^5 \leq \text{Ra}_L \leq 10^{10}) \quad (6.78)$$

The characteristic length L used in the Rayleigh and Grashof numbers is defined as

have proven operationally impractical. However, care must be taken when starting up new equipment with condensing steam as a heating medium because the initial high heat-transfer rate can lead to high surface temperatures and excessive fouling rates on the other stream.

When the condensing surface is completely wetted, the condensate film flows under the influence of gravity and vapor shear, and its heat-transfer characteristics can be reasonably predicted from hydrodynamic principles. This is the usual design mode for condensation and is developed in detail in the next section.

Direct-contact condensation occurs when a subcooled liquid is sprayed into the vapor or allowed to flow down a structural surface in a vapor space. Condensation occurs directly on the surface of the coolant. Heat-transfer rates for this equipment (such as barometric condensers) are strongly dependent upon the sprayer characteristics and/or the particular structured surface, and must be obtained from the vendor.

If a body of vapor can be sufficiently subcooled without contact with a surface (by radiation, for example), theory predicts that a liquid phase can form spontaneously. This process is termed *homogenous condensation*, and fog formation is often cited as an example. However, the subcooling required is so great that it is unlikely to occur in any process situation. Fog formation *does* occur in process condensers, but the probable mechanism is condensation on tiny droplets carried over from a previous processing step (a distillation column, for example, where bubble collapse produces large numbers of submicroscopic droplets).

The present discussion is limited to filmwise condensation on a few common geometries. There are several comprehensive and specialized references that can be consulted: the *Heat Exchanger Design Handbook* [1] covers an especially wide range of theory and application, while Hewitt et al. [30] and Incropera and DeWitt [31] present good summaries. Collier and Thome [34] cover convective condensation processes.

6.4.2 DESIGN EQUATIONS FOR FILMWISE CONDENSATION

For condensation of a pure vapor, the basic assumptions are that (a) the latent heat of condensation is released at the interface between the vapor and the liquid condensate film and (b) the interface temperature is equal to the saturation temperature of the vapor at the existing pressure. The heat-transfer rate through the condensate film depends upon the thickness and heat-transfer mechanisms of the film, which in turn depend upon the geometry of the condensing surface and the flow regime of the condensate (laminar or turbulent, gravity driven or vapor-shear driven). The presentation and discussion of the correlations is organized in the following sections according to the basic geometry.

6.4.2.1 Condensation on Vertical-Plane and Tubular Surfaces

6.4.2.1.1 Gravity Driven

In the absence of a strong vapor flow, the condensate film on a vertical surface drains under the influence of gravity only. At low flow rates, the flow is laminar, and a theoretical analysis by Nusselt [35] is applicable. The local value of the coefficient at a distance x from the start of condensation is

$$h_x = \left[\frac{k_\ell^3 \rho_\ell (\rho_\ell - \rho_v) \lambda g}{4 \mu_\ell (T_{sat} - T_w) x} \right]^{1/4} \quad (6.82)$$

where k_ℓ , ρ_ℓ , and μ_ℓ are the thermal conductivity, density, and viscosity of the condensate, respectively; ρ_v is the vapor density; λ is the latent heat of condensation; g is the gravitational acceleration (usually 9.81 m/s^2 or 32.2 ft/s^2); and T_{sat} and T_w are the vapor saturation temperature and wall temperature, respectively.

heat-transfer rate, most strongly when gravity and vapor flow are collinear but even when the forces are opposed. Boyko and Kruzhilin [37] developed an equation for fully developed vapor-shear controlled condensation and validated it experimentally for flow in horizontal tubes. However, it is also applicable to vertical flows:

$$\frac{h_c D_i}{k_\ell} = 0.024 \left(\frac{D_i G_T}{\mu_\ell} \right)^{0.8} (\text{Pr}_\ell)^{0.43} \left[\frac{\sqrt{(\rho/\rho_m)_i} + \sqrt{(\rho/\rho_m)_o}}{2} \right] \quad (6.86a)$$

where

$$(\rho/\rho_m)_i = 1 + \left(\frac{\rho_\ell - \rho_v}{\rho_v} \right) x_i \quad (6.86b)$$

and

$$(\rho/\rho_m)_o = 1 + \left(\frac{\rho_\ell - \rho_v}{\rho_v} \right) x_o \quad (6.86c)$$

The term h_c is the effective mean heat-transfer coefficient for condensing a stream from an inlet quality (mass fraction vapor) x_i to an outlet quality x_o . For the usual case of totally condensing a saturated vapor stream ($x_i = 1$; $x_o = 0$), the bracketed term in Equation (6.86a) becomes

$$\left[\frac{1 + \sqrt{\rho_\ell / \rho_v}}{2} \right] \quad (6.86d)$$

G_T is the mass velocity (mass flux) of the entering fluid, defined as the mass flow rate in kg/s (lb_m/h) divided by the cross-sectional area of the tube or the flow channel. The subscript ℓ refers to the physical properties of the condensate and v to the vapor. Equation (6.86a) may be used to calculate the local condensing heat-transfer coefficient at any quality x by replacing the bracketed term by

$$\left[\sqrt{1 + \left(\frac{\rho_\ell - \rho_v}{\rho_v} \right) x} \right] \quad (6.86e)$$

6.4.2.1.3 Selection of a Condensing Correlation

Four possibilities for a condensing film on a vertical surface exist: laminar, transition, turbulent gravity driven, and turbulent vapor-shear driven. How does one select the correct one? Consideration of the problem reveals that the flow situation that most likely exists in a given case is also the one that gives the highest coefficient. Therefore, the recommended procedure is to find the coefficients given, respectively, by Equation (6.82), Figure 6.22, and Equation (6.86a, b, c, d, e), and choose the highest one. Caution, however, should be taken because all of the correlations have uncertainties of at least 10–20%.

Example 6.11

Saturated propane vapor at 55°C (131°F) and 1900 kPa abs (275 lb_f/in^2 abs) is flowing downward at a rate of 25 kg/h (55.1 lb_m/h) through a vertical 1-in. 14 BWG tube (inside diameter of 0.834

In this case, the condensation process that gives the highest coefficient is gravity-driven, turbulent film, and the proper coefficient to use is $h_c = 4,450 \text{ W/m}^2\text{K}$.

The total heat duty to be removed should include the relatively small contribution of subcooling the condensate from the saturation temperature to the mean film temperature of about 47.5°C :

$$q = (25 \text{ kg/hr}) \left[(271 \text{ kJ/kg}) + \left(3.07 \frac{\text{kJ}}{\text{kg K}} \right) (7.5 \text{ K}) \right]$$

$$= 7.35 \times 10^3 \text{ kJ/h} = 2.04 \text{ kW} (= 6.97 \times 10^3 \text{ Btu/h})$$

The tube inside surface area required is

$$A_i = \frac{\dot{q}}{h_c \Delta T} = \frac{2.04 \times 10^3 \text{ W}}{(4,450 \text{ W/m}^2 \text{ K})(15 \text{ K})} = 0.0306 \text{ m}^2 (= 0.328 \text{ ft}^2)$$

and the length L required is

$$L = \frac{0.0306 \text{ m}^2}{\pi(21.2 \times 10^{-3} \text{ m})} = 0.459 \text{ m} (= 1.51 \text{ ft})$$

6.4.2.2 Condensation inside a Horizontal Tube

6.4.2.2.1 Gravity Driven

At low flow rates, a vapor may be condensed inside a horizontal or nearly horizontal tube under the condition that the condensate film drains down the inside surface of the tube by gravity and in laminar flow into the liquid pool at the bottom of the tube and then out the tube outlet. Kern [38] proposed a simple modification of the Nusselt equation for condensation outside horizontal tubes (see next section) that can be used for this case:

$$h_c = 0.761 \left[\frac{k_\ell^3 \rho_\ell (\rho_\ell - \rho_v) g L}{m_c \mu_\ell} \right]^{1/3} \quad (6.87)$$

where m_c is the mass flow rate of the condensate formed in the tube.

6.4.2.2.2 Vapor-Shear Driven

At sufficiently high vapor flow rates, vapor shear causes the condensate film to become turbulent and drain from the tube more rapidly. The Boyko-Kruzhilin equation (6.86a, b, c, d, e) was validated by condensing steam data.

6.4.2.2.3 Selection of a Correlation

Similar to the case for vertical tubes, the correlation (either Equation (6.87) or Equation (6.86a, b, c, d, e)) giving the higher coefficient for a given case most likely represents the actual controlling flow situation. There is a transition region between the two correlations, where the actual coefficient may be 20–30% higher than the prediction of either correlation. In designing for condensing inside “horizontal” tubes, it is important to ensure that the tube is actually slightly inclined downward toward the exit; 1/4 to 1/2 in. per foot of length is usually sufficient for good drainage.

a bundle of horizontal tubes (as in a shell-and-tube heat exchanger) is uncertain. An acceptable procedure for most purposes is to ignore both the row-number effect and the vapor-shear enhancement and use the single-horizontal-tube equations (6.88), (6.89), (6.90a), and (6.90b) for the entire tube bundle.

6.4.3 SPECIAL CASES IN CONDENSATION

6.4.3.1. Enhanced Surfaces in Condensation

Enhanced surfaces can often significantly increase the effective heat-transfer coefficient in condensation, especially if the condensing heat-transfer coefficient is the limiting factor in the overall heat-transfer-coefficient equation. Such enhancements include low fins on horizontal tubes, which increase the heat-transfer area, and fluting on vertical tubes and plane surfaces, which thins the condensate film over part of the surface by surface-tension effects. However, these improvements are limited by condensate retention between the fins and flooding of the drainage paths [7, 34].

6.4.3.2 Condensation in the Presence of a Noncondensable Gas

Condensing vapors often contain a gas that is noncondensable and effectively insoluble in the condensate, such as a small concentration of air in steam. The condensation process may be little affected by the presence of noncondensables at the start of condensation. As the condensation proceeds, the concentration of the noncondensable increases, the dew point decreases (decreasing the temperature difference for heat transfer), and the mass-transfer resistance to the vapor diffusing to the condensing surface increases and may eventually control the rate of condensation. This process was first seriously studied by Colburn and Hougen [40] and more recently by Mueller [41]. A fundamentally sound design procedure requires commercially available computer-based design methods, but a reasonable estimate can be made using the method described next.

6.4.3.3 Condensation of a Multicomponent Vapor

Condensation of a multicomponent vapor, often including noncondensable gases, is a common design problem in the process industries and in energy-producing cycles and air-conditioning and refrigeration systems using mixed working fluids or refrigerants. As the less-volatile components preferentially condense, the dew point continuously falls, and the rate of condensation is controlled by the diffusion and counterdiffusion of the various components to and away from the condensing surface. It is usually assumed that the remaining vapor and the condensate are in thermodynamic equilibrium at every point in the process, but this is only approximately true, even if care is taken to keep the total vapor and condensate streams in intimate contact throughout the condenser. If the condensate is allowed to fall out of contact with the remaining vapor, the condenser acts as a poor fractionator, and the condensing capability is sharply reduced.

The basic fluid dynamics and heat- and mass-transfer processes for multicomponent condensation are poorly understood, and the computation is difficult; available design methods are both heuristic and feasible only for computer solution. The basic model was developed by Silver [42] and put in more general form by Bell and Ghaly [43]. Computer-based design methods that have been validated against experimental data are commercially available.

6.4.3.4 Condensation of Superheated Vapor

A superheated vapor may be condensed directly from the vapor state by contact with a surface that is below the saturation temperature or the dew point of the vapor. The heat-transfer coefficient is predicted by the equations in this section if the saturation temperature (*not* the superheat temperature) is used as the effective temperature for heat transfer, i.e., a desuperheater/condenser may be

At temperature differences below about 3–5°K (5–9°F), the heat transfer is by natural convection to the liquid; the slightly superheated liquid rises quiescently to the free-liquid surface and vaporizes with no obvious evidence of boiling action. At temperature differences above about 5°K (9°F), vapor bubbles begin to form at specific nucleation sites on the surface, grow, detach, and rise to the free surface, while the process repeats itself regularly. Nucleation sites are usually microscopic pits, scratches, grain boundaries, or other surface irregularities where gas or vapor is trapped to initiate the bubble growth. The smoother the surface, the greater is the superheat required to initiate nucleation and nucleate boiling. Surfaces such as glass may be so devoid of nucleation sites that the liquid may be highly superheated before a random piece of dust sets off a sudden nucleation, desuperheating, and burst of vapor generation. Rough surfaces may nucleate at very small superheats.

Once stable nucleate boiling is established, the heat flux and vapor generation rate are strong functions of the temperature difference. As the surface temperature increases, more nucleation sites are activated, and the bubble generation rate increases at already active sites. Each surface has its own characteristics, and those can change with time as a result of corrosion, fouling, mechanical damage, or even how the equipment was shut down. Consequently, any estimate of nucleate boiling heat-transfer coefficients is approximate.

However, there is an upper limit on the heat flux that can be sustained in nucleate boiling. As the heat flux, and therefore the vapor generation, rises, it is increasingly difficult for sufficient liquid to reach the surface to maintain the vapor generation. At the peak nucleate boiling heat flux, the liquid reaching the surface is equal to the vapor generation rate. This condition, termed the “peak” or “critical” heat flux, can be estimated using equations given in the next section.

If the peak heat flux is exceeded even momentarily and/or locally, a portion of the surface dries out and usually further heats up, and becomes essentially useless for heat transfer. The dry-out process will usually spread over more surface and result in a pronounced decrease in the heat-transfer rate. This is termed the *transition boiling regime*, and extended operation in this regime may result in rapidly increasing fouling and loss of heat-transfer capability, until the next cleaning. Once the transition boiling regime has been entered, only a sharp reduction in the surface temperature, or even complete shutdown, can restore the nucleate boiling regime. If the heat source is hot enough, the surface temperature rises until the surface is covered by a continuous film of vapor and the heat-transfer rate reaches a minimum. This condition is termed the *Leidenfrost point* and marks the beginning of the “film boiling regime.”

In film boiling, all heat is transferred by conduction/convection through the vapor and by radiation from the hot surface to the liquid interface. Further increases in surface temperature result in a slow increase in the heat transfer. However, heat transfer in film boiling is poor and may result in severe fouling and even thermal decomposition of the boiling fluid. If the heat source is a constant-flux device, such as an electrical resistance heater, the surface temperature may rise to the melting point and the equipment may be permanently damaged. Film boiling should be avoided. When starting up boiling equipment, it is important to introduce the cold liquid first to prevent initial overheating of the surface into the film boiling regime.

In convective vaporization, the same boiling regimes are encountered, but modified by the net motion of the two-phase fluid past the surface. At low velocities or high heat fluxes, the convection effect is small, and nucleate boiling dominates. At higher velocities, the heat-transfer rate is dominated by the two-phase mixture sweeping across the surface. It is still important to avoid transition and film boiling, but the onset of these phenomena is complicated by many factors. (See [1, 34].)

6.4.5 BOILING HEAT-TRANSFER CORRELATIONS

6.4.5.1 Nucleate Boiling

Prediction of nucleate-boiling heat transfer is complicated by the strong dependence of bubble nucleation on boiling surface characteristics that are hard to quantify or even identify and measure.

$$h_c = h_{\ell 0} F_{TP} \quad (6.95b)$$

where $h_{\ell 0}$ is calculated from Equations (6.41) and (6.42), treating the entire mass flow rate as liquid. The two-phase flow correction factor F_{TP} is given by

$$F_{TP} = [(1-x)^{1.5} + 1.9x^{0.6}(\rho_\ell / \rho_v)^{0.35}]^{1.1} \quad (6.95c)$$

Example 6.12

A two-phase mixture of steam and water is flowing upward in a 1-in. OD (25.4 mm) 14 BWG tube (ID = 0.834 in. [21.2 mm]) at 185°C (366°F) and 11.225 bar abs (165 psig). The total mass flow rate is 0.284 kg/s (0.626 lb_m/s). The local quality (mass fraction vapor) is 0.05, and the local heat flux is 250 kW/m² (79,250 Btu/h·ft²). Calculate the local heat-transfer coefficient and the local inside tube wall temperature.

Solution

The thermophysical properties required are

Liquid density, ρ_ℓ : 881.67 kg/m³ (54.99 lb_m/ft³)

Vapor density, ρ_v : 5.745 kg/m³ (0.3634 lb_m/ft³)

Liquid viscosity, μ_ℓ : 145.2×10^{-6} kg/m·s (0.351 lb_m/ft·h)

Liquid thermal conductivity, k_ℓ : 671.1×10^{-3} (0.388 Btu/h·ft·°F)

Liquid Prandtl number, Pr_ℓ : 0.957

Critical pressure, p_{crit} : 220.55 bar abs (3206 lb_f/in.² abs)

Reduced pressure, p_R : 11.225 bar/220.55 bar = 0.0509

First, evaluate h_{TP} from Equation (6.95a), utilizing Equation (6.92a) to calculate h_{NB} , and using Equations (6.41), (6.42), (6.95c), and (6.95b) to calculate h_o , F_{TP} , and h_c , respectively.

Calculation of h_{NB} :

$$\begin{aligned} h_{NB} &= 0.1011(220.55)^{0.69}(250,000)^{0.7} \times [1.8(0.0509)^{0.17} + 4(0.0509)^{1.2} + 10(0.0509)^{10}] \\ &= 30,100 \text{ W/m}^2 \text{ K} (= 5300 \text{ Btu/hr ft}^2 \text{ °F}) \end{aligned}$$

(Note: This is a dimensional equation, so the units are not “calculable” in the usual sense.)

Calculation of h_o :

$$Re = \frac{D_i \rho_\ell v_{\ell 0}}{\mu_\ell}$$

$$v_{\ell 0} = \frac{0.284 \text{ kg/s}}{\left(881.67 \frac{\text{kg}}{\text{m}^3}\right) \frac{\pi}{4} (21.2 \times 10^{-3} \text{ m})^2} = 0.913 \text{ m/s} (= 2.99 \text{ ft/s})$$

$$Re = \frac{(21.2 \times 10^{-3} \text{ m})(881.67 \text{ kg/m}^3)(0.913 \text{ m/s})}{(145.2 \times 10^{-6} \text{ kg/m s})} = 118,000$$

6.4.6.2 Enhanced Surfaces in Boiling

A variety of enhancements to the boiling process are commercially available. Low-finned tubes are commonly used with many organic liquids (which tend to give low boiling coefficients) to increase the heat-transfer area available. Other surfaces are designed to increase the availability of nucleation sites or increase the circulation rate of the boiling liquid past the heat-transfer surface by natural convection. These surfaces are particularly effective in initiating and improving the boiling performance at very low temperature differences. However, they generally do little or nothing to increase the critical heat flux. Manufacturers' data and recommended design practices are necessary to fully utilize the advantages of these special surfaces.

6.4.6.3 Subcooled Boiling

Boiling also will occur with a liquid that is below its saturation temperature if the hot surface temperature is sufficiently above the nucleation temperature for the surface. The bubbles thus formed collapse quickly when they move from the surface into the bulk subcooled liquid, resulting in high heat-transfer rates. Moderate subcooling at the entrance to a vaporizer can be assumed to be heated by heat transfer at the same rates as for the saturated boiling process, if the saturation temperature of the fluid at the existing pressure is used in the temperature difference.

6.5 HEAT EXCHANGERS

6.5.1 INTRODUCTION

Heat exchangers vary in heat-transfer surface area from less than 1 m² (10 ft²) to over 10,000 m² (100,000 ft²), in service temperatures from near absolute zero to over 1400°C (2500°F), and in pressures from near full vacuum to over 600 bar (atmospheres). The smaller ones used for routine duties like jacket water and lube oil cooling can often be ordered quickly from standardized designs or assembled from off-the-shelf components. The larger exchangers and those used for process stream heating, cooling, or phase change are usually custom-designed, implying among other things specialized design and fabrication personnel and facilities, and longer delivery times. Those intended for extreme conditions are always custom designs.

This section describes the major types of heat exchangers used in the process industries, their major construction features and options, and their most common applications. Next is a subsection devoted to the basic equations of heat-exchanger design, including the concept of an overall heat-transfer coefficient, the basic design equation (used mainly in computer-based design methods), and the mean temperature difference formulation (used primarily with hand-based design methods). The next subsection describes the basic logic of heat-exchanger design methods, whether by hand or by computer. The last subsection introduces fouling mechanisms and techniques for amelioration.

The *Heat Exchanger Design Handbook* [1] is the most comprehensive reference, but Shah and Sekulic [51] and Kakac and Liu [52] are more handy and cover most areas. Hewitt et al. [30] includes much information on heat exchangers. Qualitative factors in design and application are discussed by Bell [53]. Other, more specialized references are given with the descriptions of the various types.

Most heat exchangers for the process industries are designed by computer programs. There are commercially available design programs for most common heat-exchanger types. Many manufacturers employ their own programs. Many have proprietary programs for their equipment, which vary in accuracy and reliability. All design programs are to some degree heuristic in that they incorporate correlations that have not been tested over the full range of possible process variables. All make assumptions (such as the uniformity of flow distribution among a multitude of parallel tubes, for example) that are not exactly achievable and may be seriously compromised in some situations. The input data are always to some degree uncertain, especially

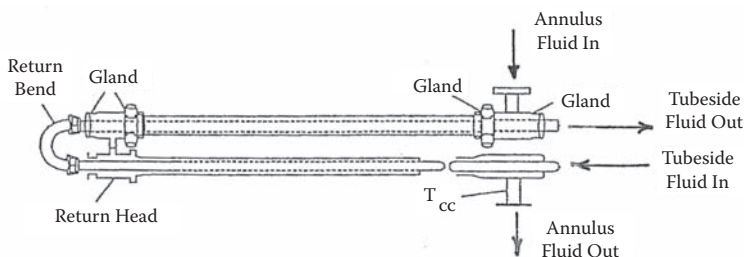


FIGURE 6.24 Basic double-pipe heat exchanger, with arrows showing countercurrent flow.

provided to meet pressure-drop limits. Pure countercurrent, pure cocurrent, and various series- or parallel-flow arrangements may be used.

Double-pipe exchangers are comparatively bulky, heavy, and expensive per unit heat-transfer area and hence are usually limited to units of less than 50 m² (500 ft²), though there is no absolute limit. The advantages of the double-pipe exchanger lie in the flexibility of application and piping arrangement. They can be quickly assembled by plant maintenance crews and are usually cleanable on either side. Uniform and stable flow distribution in each channel of a double-pipe heat exchanger is assured by providing a pump for each parallel section; this can be of particular importance in cooling viscous liquids.

6.5.2.3 Shell-and-Tube Heat Exchangers

Shell-and-tube heat exchangers are the workhorses of the process industries and other applications. The basic configuration, flow across/along a bank of cylindrical tubes, is mechanically strong, provides high heat-transfer surface per unit volume, and allows the use of a variety of special design features to meet many unusual and extreme conditions of chemical processing. The cost per unit area is relatively low, especially in low-carbon steel. The major disadvantage is that they are inflexible once they are constructed, and an exchanger that does not perform satisfactorily in service is usually difficult to modify. Sometimes, performance can be upgraded by replacing the tubes with externally or internally enhanced tubes (e.g., low-finned tubes, twisted wire or tape inserts, etc.).

Most shell-and-tube exchangers are built to the standards of the Tubular Exchanger Manufacturers Association—TEMA Standards [54]—which cover nomenclature, manufacturing standards, recommended good practices, and much else, but do not include thermal design methods. These exchangers generally must conform to the ASME Boiler and Pressure Vessel Code [55] or comparable standards in other countries. Most refinery and chemical process exchangers also satisfy API Standard 660 [56], and power plant exchangers are covered under the various standards of the Heat Exchange Institute [57]. Singh and Soler [58] present mechanical design procedures, and Yokell [59] gives a comprehensive survey of exchanger nomenclature, components, manufacturing techniques, inspection procedures, and maintenance.

The TEMA standards identify three classes of exchanger construction: Class R covers exchangers for the generally severe requirements of the refinery and related processing industries. Class C meets the moderate requirements of commercial and general process applications. Class B meets the special requirements of chemical process service, mainly addressed to the use of special alloys for corrosion resistance. There is relatively little difference between the requirements, and most process-plant exchangers are built to Class R standards.

Figure 6.25 is a schematic diagram of a typical shell-and-tube heat exchanger. The tubes are the basic component of the shell-and-tube exchanger, providing the heat-transfer surface between one fluid flowing inside the tubes and another fluid flowing across the outside of the tubes. The tubes are generally drawn or extruded seamless metal, or welded. Low-carbon or alloy steel, stainless steel, copper, Admiralty, cupronickel, Inconel, aluminum, or titanium tubes are common; other materials may be specified for special applications.

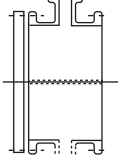
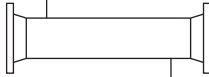
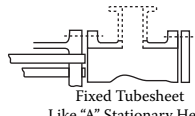
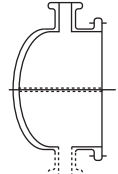
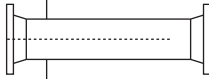
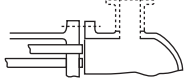
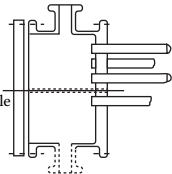


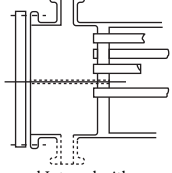
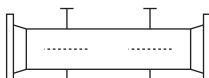

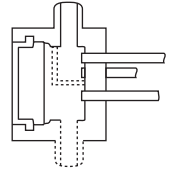
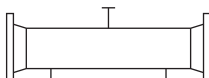
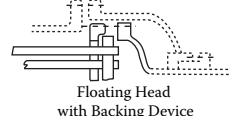
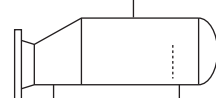
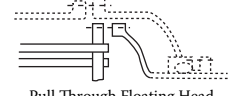
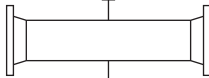
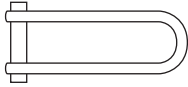

	Front End Stationary Head Type		Shell Types		Rear End Head Types
A	 Channel and Removable Cover	E	 One Pass Shell	L	 Fixed Tubesheet Like "A" Stationary Head
B	 Bonnet (Integral Cover)	F	 Two Pass Shell with Longitudinal Baffle	M	 Fixed Tubesheet Like "S" Stationary Head
C	 Removable Tube Bundle Only Channel Integral with Tubesheet and Removable Cover	G	 Split Flow	N	 Fixed Tubesheet Like "N" Stationary Head
N	 Channel Integral with Tubesheet and Removable Cover	H	 Double Split Flow	P	 Outside Packed Floating Head
D	 Special High Pressure Closure	J	 Divided Flow	S	 Floating Head with Backing Device
		K	 Kettle Type Reboiler	T	 Pull Through Floating Head
		X	 Cross Flow	U	 U-Tube Bundle
				W	 Externally Sealed Floating Tubesheet

FIGURE 6.26 TEMA shell-and-tube heat exchanger nomenclature. (Reprinted with permission from *Standards of Tubular Exchanger Manufacturers Association*, 9th ed., Tarrytown, NY (2007).)

across the longitudinal baffles is less serious in this case than for the F shell; the baffles should fit closely in the shell and be secured against vibration, but need not be welded to the shell.

The J shell is mainly used for condensation of low-pressure vapor because it splits the flow, reducing velocities and resulting in lower pressure drops. It is also sometimes used for single-phase flow. The J shell can also be used with the two nozzles on top, and two J shells can be mounted nozzle to nozzle in series for long-condensing-range vapors.

The K shell is used for boiling on the shell side ("kettle reboiler") with steam or hot fluid inside a bundle of U-tubes; less commonly, a floating head may be used with straight tubes. The large-diameter shell allows for disengagement of most of the entrained liquid from the vapor; further drying of the vapor can be achieved with mesh demister pads or centrifugal vane separators at the outlet shell-side nozzle. The liquid level is ordinarily maintained at the top of the tube bundle by a weir (as shown in the drawing) or an external liquid-level control device.

They do allow single-tube pass design if fitted with a rear head tube-side nozzle and flexible piping. Individual tube replacement is possible.

The floating head with backing device (also termed “split-ring floating head”) and pull-through floating-head designs, TEMA S and T, provide more positive sealing of the shell-side fluid, with the T design used for the most critical cases. While Figure 6.26 indicates (by the dashed lines) that a rear-head packed tube-side nozzle (and hence single tube-side pass) is possible, this increases the possibility of shell-side fluid leakage and is rarely used.

All of the floating-head designs require elimination of some of the peripheral tubes (compared with the same diameter fixed tubesheet design) in order to accommodate the tubesheet flange or skirt. Omission of these tubes also creates bypass flow paths around the tube bundle, reducing the flow rate and heat-transfer coefficient across the tubes and reducing the effective temperature difference for heat transfer. These bypass lanes can be partially blocked and the thermal effectiveness largely restored by inserting sealing strips—metal strips that are about as wide as the clearance between the shell and the tube bundle and run the length of the exchanger through slots cut into the baffles. The strips are installed symmetrically on both sides of the tube bundle and both sides of the central plane—one pair about every six tube rows in the direction of flow is suggested. Tie rods and spacers located in the bypass lanes also help block the flow but are not as effective as sealing strips.

The essential purpose of the shell-side baffles (item G in Figure 6.25) is to support the tubes against sagging and vibration. A secondary role is to guide the shell-side flow across and through the tube bundle to achieve maximum thermal effectiveness for the allowable pressure drop. The most common configuration is the single segmental baffle, shown in Figure 6.28a. The baffle cut and spacing are design variables chosen (within the limits set by the TEMA standards) to best meet these requirements. Typically, the baffle cut is 15–25% of the shell inside diameter for liquids and 40–45% for gases. Spacing and cut will usually be selected so that the baffle window free-flow area is about 50–100% of the tube bundle free cross-flow area. A tube vibration analysis is used in all questionable cases to verify that damaging levels of vibration will not occur. TEMA also specifies the diametral clearances between tube and baffle hole and between baffle and shell inside diameter; these clearances are necessary for bundle assembly and removal and for tube replacement.

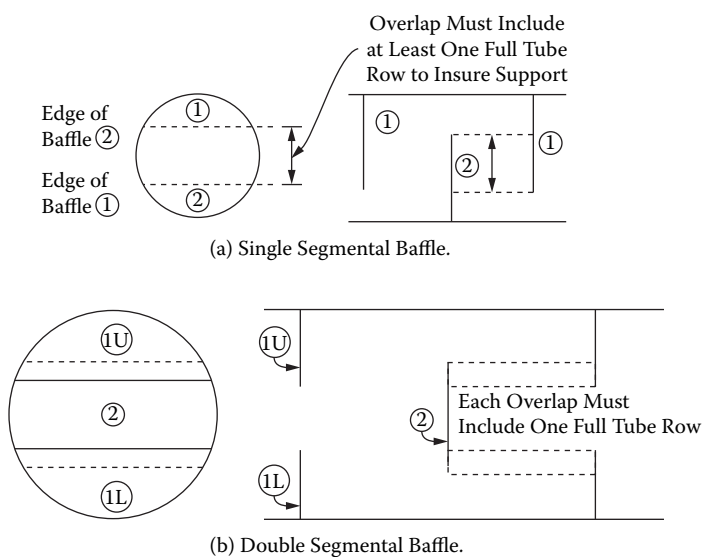


FIGURE 6.28 (a) Single-segmental baffle configuration. (b) Double-segmental baffle configuration.

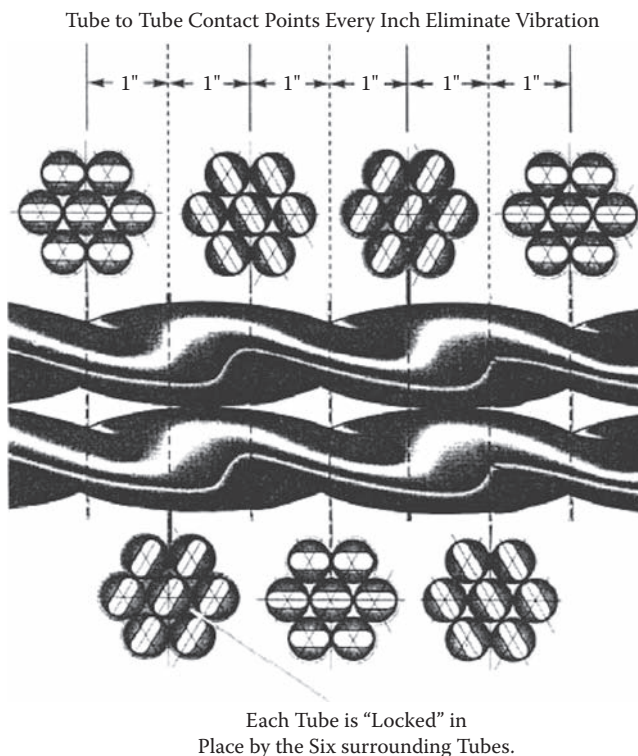


FIGURE 6.32 Diagram of two Twisted Tubes®, showing how tubes are mutually self-supporting. (Courtesy of Koch Heat Transfer Company LP.)

required, to provide support and rigidity, and each tube is supported on all four sides in each set. The sets are held together by welded tie rods. Tube vibration is effectively eliminated, and the nearly longitudinal flow gives significantly reduced pressure drop and a somewhat reduced heat-transfer coefficient than the corresponding conventionally baffled exchanger. Annular distributors (see below) are often specified for RODbaffle exchangers to minimize pressure drop and ensure good distribution.

Helically baffled heat exchangers, illustrated in Figure 6.31, are a recent development. The spiral path through the shell side eliminates or reduces eddy regions and bypass flows, resulting in improved heat transfer for a given pressure drop [61].

Twisted Tube™ construction (Figure 6.32) eliminates the need for baffles altogether, since the tubes can be oriented ("tuned") to contact surrounding tubes periodically along the exchanger. The shell-side flow is longitudinal, and special correlations have been developed for both heat transfer and pressure drop on both sides of the surface. Laminar flow inside the tube is enhanced by the secondary flow induced by the twisted flow path.

Impingement plates are another shell-side construction feature that may be required to prevent tube vibration or erosion. The impingement plate is placed under the shell-side inlet nozzle and should be larger than the nozzle opening, with an escape area off the edges of the plate that is twice the flow area of the nozzle. The impingement plate is attached to the shell or the tie rods. TEMA standards specify the conditions under which an impingement plate is required.

An alternative to the impingement plate is the annular distributor (Figure 6.33), which, through the use of a partial double shell, absorbs the impact of the inlet fluid jet and distributes the fluid more uniformly into the tube bundle. An annular distributor is designed to require a low-pressure

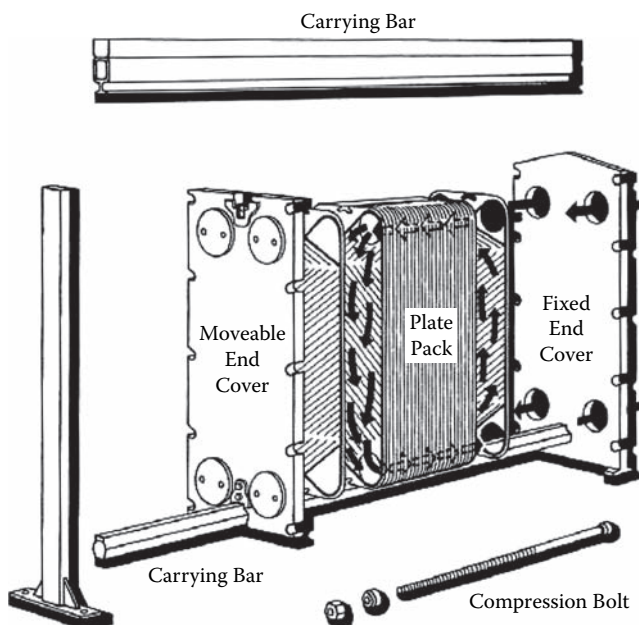


FIGURE 6.35 Exploded diagram of a gasketed-plate heat exchanger. (Reproduced with permission of Alfa Laval Inc.)

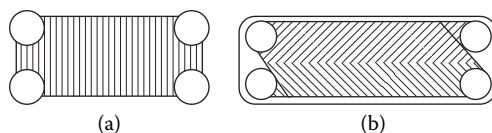


FIGURE 6.36 Two types of plates for the gasketed-plate heat exchanger: (a) parallel-corrugated plate; (b) cross-corrugated plate ("herringbone" or "chevron" pattern).

The gaskets are made from a variety of elastomers; they are confined in grooves around the plate edges and ports, and must be firmly and uniformly compressed to provide an effective seal. These gasket sets can generally be reused, allowing plate exchangers to be regularly disassembled for cleaning or sterilization. The gasket material and construction limit the temperature range and pressures of the application. Small plates can be used up to about 20–25 bar (300–375 psig) at temperatures below about 100°C (210°F), whereas large plates are limited to about 8 bar (120 psig). Maximum temperatures are about 150°C (300°F) with reusable gaskets. Jacketed asbestos gaskets can be used to about 250°C (480°F), but cannot be reused. Limits vary among manufacturers and with the specific designs. Designs with pairs of plates welded together have been manufactured. These designs allow higher pressure operation on the welded channel side, but sacrifice some of the flexibility of disassembly and reassembly. A diffusion-bonded Monobloc™ construction is also available for very high pressure operation, but it cannot be disassembled.

Major manufacturers have design and rating programs that reflect the pressure-drop and heat-transfer characteristics of their specific plates, which can vary widely and are generally proprietary. API [62] provides standards for gasketed-plate exchangers. Where higher alloy construction is required, gasketed-plate exchangers generally have a lower capital cost and are more compact than shell-and-tube exchangers of comparable thermal capacity. Fouling is generally less severe (though fluids containing larger solid particles or fibrous materials tend to plug the fine channels) due to the high turbulence and shear stress developed, and most designs can be disassembled easily for cleaning. Reassembly without leaks can be more difficult unless maintenance crews are specially

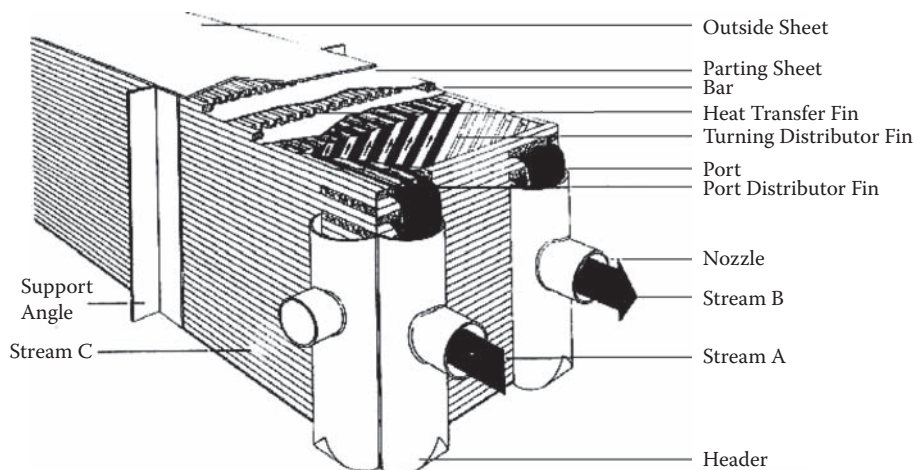


FIGURE 6.38 Cutaway view of a brazed aluminum plate fin (or matrix) heat exchanger configured for three streams. (Courtesy Chart Energy and Chemicals, Inc., La Crosse, WI, a wholly owned subsidiary of Chart Industries, Cleveland, OH.)

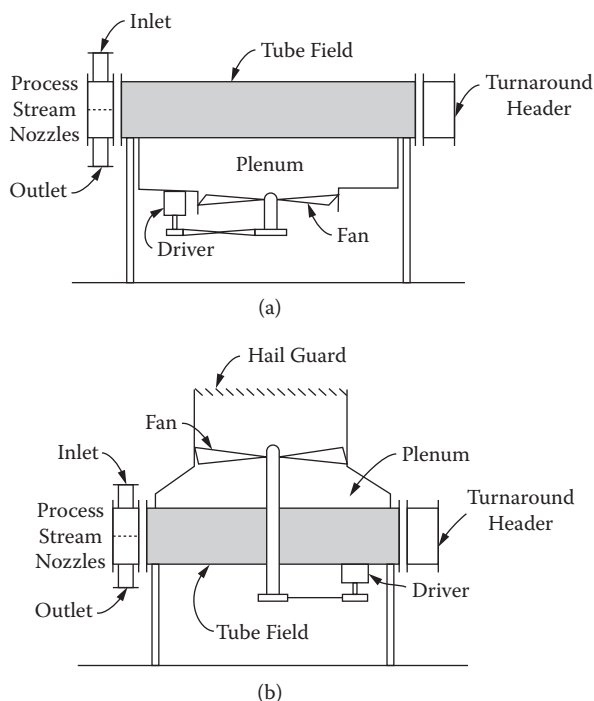


FIGURE 6.39 Schematic diagrams of air-cooled heat exchangers: (a) forced draft, (b) induced draft.

properties of air. The low density of atmospheric air and its low specific heat require the moving of large volumes of air, requiring large single-stage axial flow fans. These fans can only achieve low pressure rises; a typical design pressure drop for the air side is 3/4 in. of water (0.027 psi, or 0.19 kPa). Consequently, the air is limited to low velocities—a face velocity of about 10 ft/s (3 m/s) for a six-row tube bank is typical. The low velocity and low thermal conductivity result in low heat-transfer coefficients and require the use of high-finned tubes (Section 6.3.4.5.3).

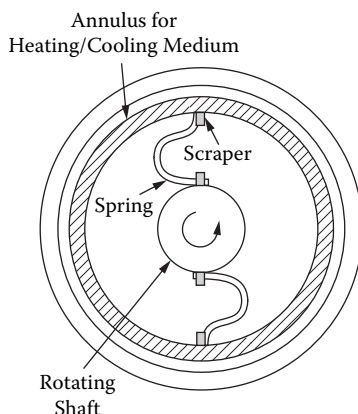


FIGURE 6.40 Cross-sectional view of a scraped-surface heat exchanger with spring-loaded blades.

mounted on a jointed arm, with the blade free to swing outward by centrifugal force as the shaft rotates; the force acting on the scraped surface is thus controlled by the rotational speed.

6.5.3 PRINCIPLES OF HEAT-EXCHANGER DESIGN

6.5.3.1 Heat Transfer between Two Fluids Separated by a Wall

Figure 6.41 shows a cross section of a typical heat-exchanger tube with a hot fluid inside at temperature T and a cold fluid outside at t . (The following argument applies to hot fluid outside and cold inside with appropriate change of sign. It applies whether the respective heat-transfer processes are single-phase convection, or condensation or vaporization, always noting that heat flows from the hot fluid to the cold.) The figure also shows fouling films on both surfaces, which is almost always the practical situation; fouling is discussed in more detail in Section 6.5.5.

Under the reasonable assumptions that the heat-transfer process is at near-steady state (i.e., conditions at any given point do not vary rapidly with time) and that the longitudinal heat-transfer rates along the tube are negligible compared with those radially through the tube wall, the heat-transfer rate, Q (watts or Btu/h), for a tube of length L (m or ft) is given by the following equations:

$$Q = h_i A_i (T - T_{fi}) \quad (6.96a)$$

$$Q = \frac{A_i (T_{fi} - t_{wi})}{R_{fi}} \quad (6.96b)$$

$$Q = \frac{(2\pi L) k_w (t_{wi} - t_{wo})}{\ln(r_o / r_i)} \quad (6.96c)$$

$$Q = \frac{A_o (t_{wo} - t_{fo})}{R_{fo}} \quad (6.96d)$$

$$Q = h_o A_o (t_{fo} - t) \quad (6.96e)$$

Any other convenient, well-defined area, such as the inside heat-transfer area A_i , can be used as the reference area. For a typical low-finned tube, the effective outside area of the tube, A_{eff} , must include the fin efficiency, η_{fin} , from Figure 6.10.

$$A_{eff} = A_{prime} + \eta_{fin} A_{fin} \quad (6.101)$$

where A_{prime} is the outside surface area of the tube between the bases of the fins and A_{fin} is the total surface area of all the fins.

The relationship between area and overall heat-transfer coefficient is

$$U^* A^* = U_o A_o = U_i A_i = \dots \quad (6.102)$$

Because the values of the heat-transfer coefficients are referenced to the area upon which they are based, care must be taken to always identify the reference area in any situation where there is any possibility of confusion or misunderstanding.

6.5.3.2 The Basic Design Integral

The above equations relate the heat-transfer rate to the local temperature difference ($T - t$) and the heat-transfer area A through the overall heat-transfer coefficient U . In almost all practical situations, one or both temperatures will vary along the length of the heat exchanger. The change in temperature of each stream is calculated from the enthalpy balance on that stream. To apply Equation (6.98) to the design of a heat exchanger in which the temperature difference is not constant, the equation needs to be written in differential form:

$$dA^* = \frac{dQ}{U^*(T - t)} \quad (6.103)$$

which can then be formally integrated over the entire heat duty of the heat exchanger, Q_T :

$$A^* = \int_0^{Q_T} \frac{dQ_T}{U^*(T - t)} \quad (6.104)$$

This is the basic design equation for heat exchangers having two fluids exchanging heat across a well-defined solid surface. The local fluid temperatures are calculated as a function of the entering temperatures and the amount of heat exchanged up to a given point in the heat exchanger. The individual film heat-transfer coefficients, and hence the overall coefficient, may also be functions of the amount exchanged, especially in condensing and vaporizing services, as discussed in Section 6.4.

Most large heat exchangers are designed using commercially available computer programs to evaluate Equation (6.104) numerically. However, if certain assumptions are made, the equation can be analytically solved to give a simple algebraic solution. This procedure is discussed in the next section.

6.5.3.3 The Mean Temperature Difference Concept

If certain assumptions are made, Equation (6.104) can be analytically integrated for a number of important heat-exchanger configurations and applications. The following set of assumptions is reasonably valid for many cases:

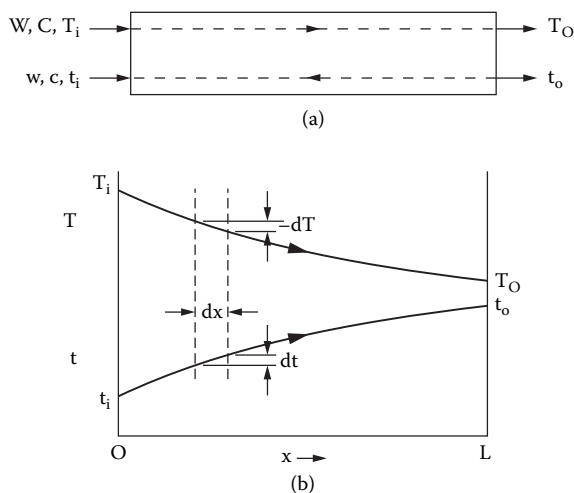


FIGURE 6.42 (a) Cocurrent flow pattern through a heat exchanger. (b) Typical temperature profiles through a cocurrent heat exchanger.

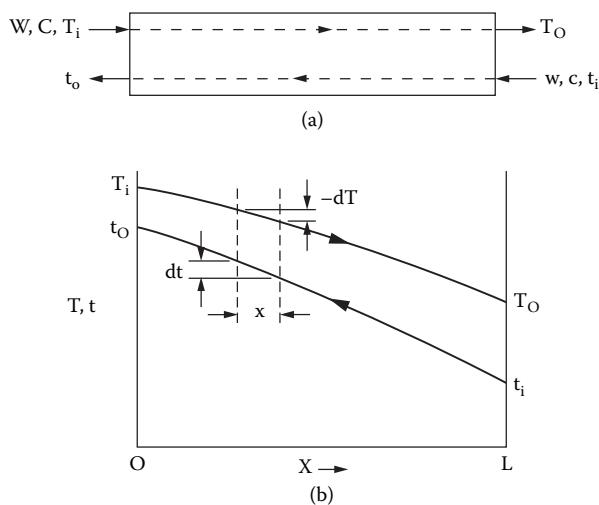


FIGURE 6.43 (a) Countercurrent flow pattern through a heat exchanger. (b) Typical temperature profiles through a countercurrent heat exchanger.

6.44b. Similarly, air-cooled exchangers as described in Section 6.5.2.7 have the air in cross flow to the tubes.

If certain additional assumptions are made, many of these cases can be handled by a modification of Equation (6.105):

$$A^* = \frac{Q_r}{U^*(MTD)} \quad (6.108a)$$

where

$$(MTD) = F(LMTD)_{\text{counter current}} \quad (6.108b)$$

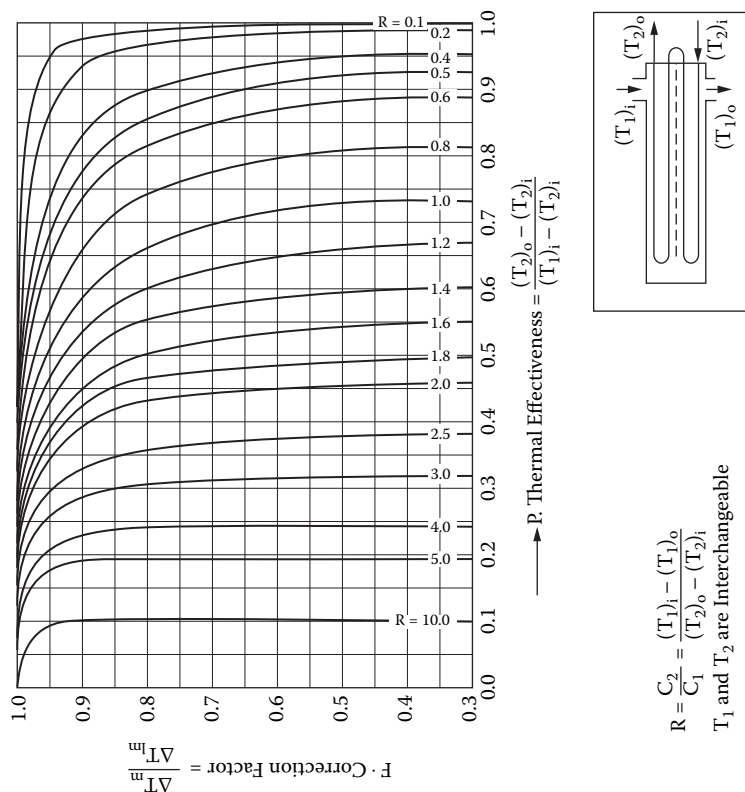


FIGURE 6.45 F chart for one E shell with any even number of tube passes. (Adapted from Hewitt, G. F., Ed., *Heat Exchanger Design Handbook*—1998, Begell House, New York (1998).)

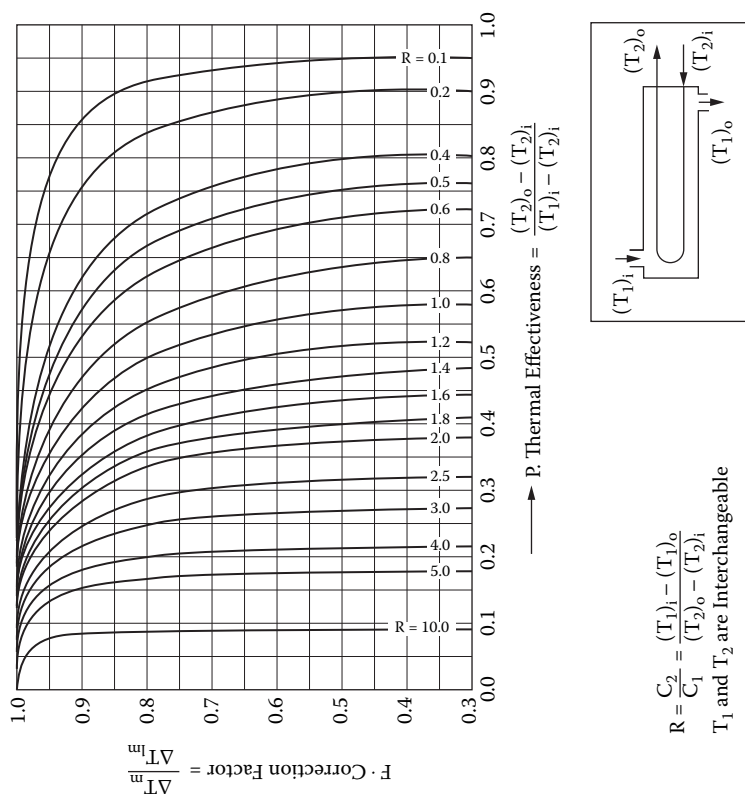


FIGURE 6.46 F chart for two E shells in series with any even number of tube passes or an F shell with four, eight, etc., tube passes. (Adapted from Hewitt, G. F., Ed., *Heat Exchanger Design Handbook*—1998, Begell House, New York (1998).)

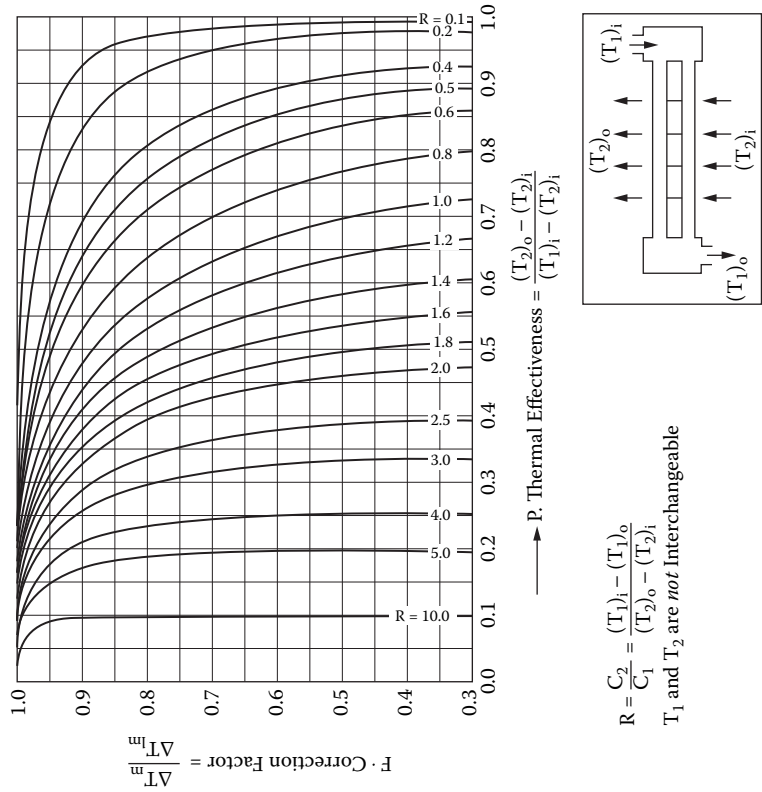


FIGURE 6.50 F chart for a cross-flow exchanger, two-tube rows, one pass, unmixed. (Adapted from Hewitt, G. F., Ed., *Heat Exchanger Design Handbook*—1998, Begell House, New York (1998).)

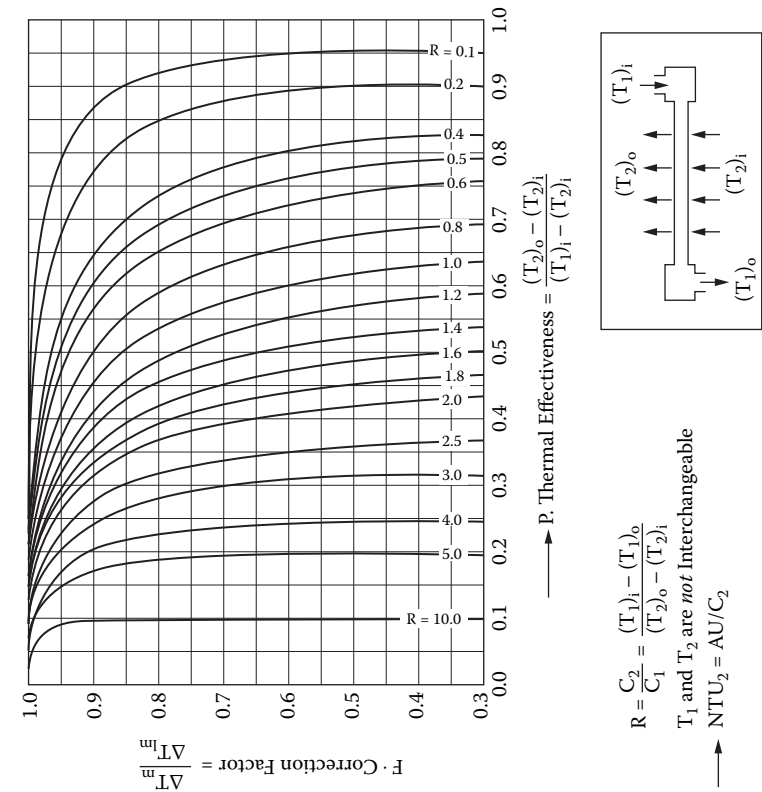


FIGURE 6.49 F chart for a cross-flow exchanger, one-tube row, unmixed. (Adapted from Hewitt, G. F., Ed., *Heat Exchanger Design Handbook*—1998, Begell House, New York (1998).)

the outlet of the hot stream. This is inefficient—part of the heat-transfer surface is transferring heat in the wrong direction—and this condition is seldom designed for. However, this condition may occur when starting up a clean exchanger, when flow rates are reduced, or for an oversurfaced heat exchanger. It also makes it difficult to obtain valid performance data on a clean heat exchanger. As a general rule, design of any exchanger with $F < 0.8$ or where F is read from the steep part of the curve should be considered carefully—it is probably inefficient, and even small departures from the ideal assumptions of the MTD method may render the exchanger thermodynamically incapable of achieving the design conditions.

When it is necessary to transfer heat between two fluids over wide overlapping temperature ranges with multiple tube pass exchangers, two or more exchangers may be connected in series, with the overall flows countercurrent, as shown in Figures 6.46 and 6.47. F increases rapidly as the number of exchangers in series increases, the only limit being the allowable pressure drops.

6.5.4 LOGIC OF THE HEAT-EXCHANGER DESIGN PROCESS

Figure 6.53 diagrams the logical structure of the heat-exchanger design process, whether done by computer or by hand. If there is a validated computer design program available, the computer is faster and more precise, though not necessarily more accurate. But the human mind offers advantages, such as the ability to perceive problems and opportunities during the calculation, which may lead to solutions beyond the ken of the design logic built into the program. The combination of a good program and an experienced designer working interactively is best of all.

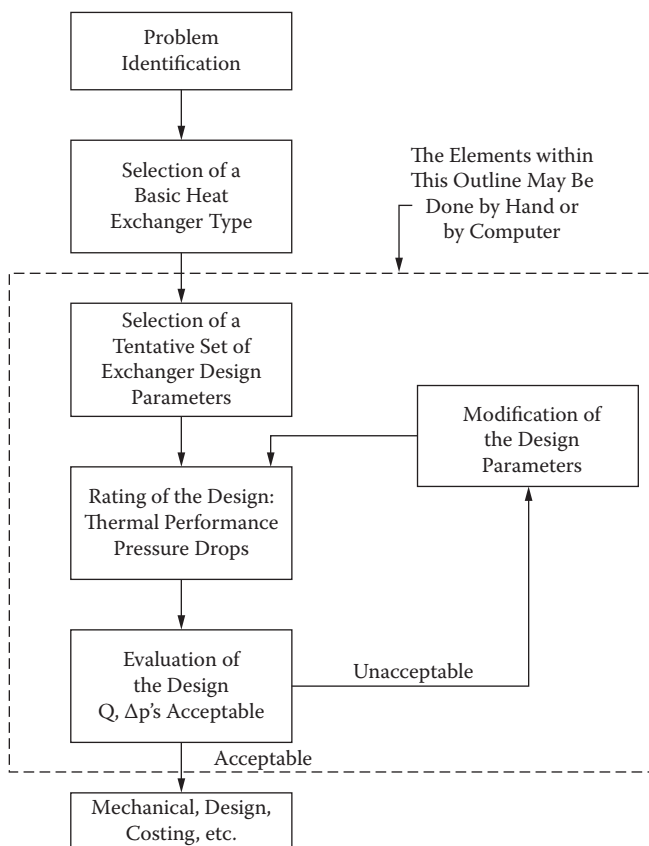


FIGURE 6.53 Logical structure of the process heat-exchanger design procedure.

larger predicted pressure than the “allowable” but with superior qualifications in other respects should be accepted.

If any of the rating output is deemed “unacceptable” by the program, the “Design Modification” program takes over, following a very detailed sequence of evaluating what is acceptable and what needs to be changed in the design. The objective function is usually to minimize the surface area required within the pressure-drop limitations, since this usually leads to the minimum first cost. The changes made must satisfy applicable codes and standards, as well as accepting only feasible construction features and commercially available components, e.g., tubes. The number of logical paths through such a program is enormous, and it can never be completely checked out. Writing such a program requires the very highest knowledge and skill. Even so, illogical or suboptimal results may ensue, and the output must be carefully evaluated every time. The prudent designer will consider whether rerunning the program with a different set of input specifications (e.g., changing the TEMA type or the tube layout) may not produce a superior design.

6.5.5 FOULING

Fouling is any unwanted deposit on the heat-transfer surface of a heat exchanger or any deposit that interferes with the desired flow pattern in the heat exchanger. In the first case, fouling increases the resistance to heat transfer, resulting in reduced thermal capability or requiring higher temperature differences or increased velocities to maintain thermal performance. In the second case, pressure drop increases at the same throughput, and a higher fraction of the flow may be forced into bypass areas.

Fouling is the greatest unsolved problem in heat-exchanger design. The most comprehensive book on fouling is by Bott [66], and there are many individual papers, but there are few quantitative and generalizable principles. TEMA Standards [54] provides tables of suggested values of the fouling resistance for a wide variety of services, but the mechanisms are so complex and dependent upon the specifics of each stream, exchanger design, and operating conditions that predictions are very uncertain.

Fouling processes are time dependent, starting at or near zero in new or freshly cleaned exchangers, increasing in time, sometimes to an asymptotic limit and other times increasing without limit until the exchanger is shut down and cleaned. Fouling deposits are often due to a combination of mechanisms, which complicates both the choice of a fouling resistance and the recommended amelioration technique.

There are several fouling mechanisms:

1. **Sedimentation:** Deposition of silt or other suspended material in the fluid on the heat-transfer surface. These deposits are generally weak and can be reduced or eliminated by increasing the velocity. The fouling resistance often reaches a constant value as long as conditions are unchanged. In this case, additional surface can be provided through a fouling resistance, R_f , in the overall heat-transfer coefficient equation. Cleaning can usually be effected by the use of high-velocity water sprays, though mechanical scraping may be required for heavy deposits.
2. **Corrosion of the surface:** Rust on low-carbon steel or other deposits formed by chemical attack on the heat-transfer surface by the process fluid form quickly and are generally adherent. Transient behavior depends upon whether or not the deposit acts to protect the surface from further attack. Where available and cost effective, selection of a different metal or a higher alloy is the best preventive. Coating a base metal with a chemically resistant polymer has not been generally satisfactory and introduces a significant resistance to heat transfer. Extreme cases can be handled with all-polymer exchangers, but these have poor heat-transfer characteristics and low strength and temperature limits. Heavy corrosion layers can usually be removed by appropriate chemical treatment or by water jets or mechanical scraping, but this only exposes the cleaned surface to renewed attack.

4. Gardner, K. A., "Efficiency of Extended Surfaces," *Trans. ASME* 67, 621–631 (Nov. 1945).
5. Kern, D. Q., and Kraus, A. D., *Extended Surface Heat Transfer*, McGraw-Hill, New York, 1972.
6. Kraus, A. D., Azziz, A., Welty, J. R., and Aziz, A., *Extended Surface Heat Transfer*, McGraw-Hill, New York, 2000.
7. Webb, R. L., *Principles of Enhanced Heat Transfer*, John Wiley, New York, 1994.
8. Parker, J. D., Boggs, S. H., and Blick, E. F., *Introduction to Fluid Mechanics and Heat Transfer*, Addison-Wesley, Reading, MA, 1969.
9. Heisler, M. P., "Temperature Charts for Induction and Constant Temperature Heating," *Trans. ASME* 69, 227–236, (1947).
10. Patankar, S. V., *Numerical Heat Transfer and Fluid Flow*, Taylor and Francis, Philadelphia, PA, 1980.
11. Shah, R. K., and London, A. L., *Laminar Flow Forced Convection in Ducts, Advances in Heat Transfer*, supp. 1, Academic Press, New York, 1978.
12. Sieder, E. W., and Tate, G. E., "Heat Transfer and Pressure Drop of Liquids in Tubes," *Ind. Eng. Chem.* 28, 1429 (1936).
13. Kakac, S., Shah, R. K., and Aung, W., *Handbook of Single Phase Convective Heat Transfer*, John W. Wiley and Sons, New York, 1987.
14. Jakob, M., *Heat Transfer*, vol. 1, John W. Wiley and Sons, New York, 1949.
15. Hausen, H., "VDIZ. Beih." *Verfahrenstech.* 4, 91 (1943).
16. Palen, J. W., and Taborek, J., "An Improved Heat Transfer Correlation for Laminar Flow of High Prandtl Number Liquids in Horizontal Tubes," *AIChE Symposium Series* 81 (245), 90–96 (1985).
17. Petukhov, B. S., "Heat Transfer and Friction in Turbulent Pipe Flow with Variable Liquid Properties," *Advances in Heat Transfer*, vol. 6, Hartnett, J. P., and Irvine, T. F., Jr., Eds., pp. 504–561, Academic Press, New York, 1970.
18. Gnielinski, V., "New Equations for Heat and Mass Transfer in Turbulent Pipe and Channel Flow," *Int. Chem. Eng.* 16, 359–368 (1976).
19. Martin, H., in Ref. 1, citing Gauler, K., "Wärme- und Stoffübertragung an eine mit bewegte ebene Grenzfläche bei Grenzschichtströmung," Dr.-Ing., University of Karlsruhe, Germany (1972).
20. Petukhov B. S., and Roizen, L. I., "An Experimental Investigation of Heat Transfer in a Turbulent Flow of Gas in Tubes of Annular Section," *High Temperature (USSR)* 1, 373–380 (1963).
21. Eckert, E. R. G., and Drake, R. M., Jr., *Analysis of Heat and Mass Transfer*, p. 406, McGraw-Hill, New York, 1972.
22. Bell, K. J., "Process Heat Transfer Notes," Oklahoma State University, Stillwater, OK, 1972.
23. Bergelin, O. P., Brown, G. A., and Doberstein, S. C., *Trans. ASME* 74, 953 (1952).
24. Zukauskas, A., Skrinksa, A., Zingzda, J., and Gnielinski, V., "Banks of Plain and Finned Tubes," in *Heat Exchanger Design Handbook—1998*, Hewitt, G. F., Ed., Section 2.5.3, Begell House, New York, 1998.
25. Williams, R. B., and Katz, D. L., "Performance of Finned Tubes in Shell and Tube Heat Exchangers," *Trans. ASME* 74, 1307–1320 (1952).
26. Briggs, D. E., Katz, D. L., and Young, E. H., "How to Design Finned Tube Heat Exchangers," *Chem. Eng. Prog.* 59 (11), 49–59 (1963).
27. Briggs, D. E., and Young, E. H., "Heat Transfer—Houston," *Chem. Eng. Prog. Symposium Series No. 41*, 59, 1 (1963).
28. Robinson, K. K., and Briggs, D. E., "Heat Transfer—Los Angeles," *Chem. Eng. Prog. Symposium Series No. 64*, 62, 177 (1965).
29. Gnielinski, V., "Equations for the Calculation of Heat and Mass Transfer during Flow through Stationary Spherical Packings at Moderate and High Peclet Numbers," *Int. Chem. Eng.* 21, 378–383 (1981).
30. Hewitt, G. F., Shires, G. L., and Bott, T. R., *Process Heat Transfer*, CRC Press, Boca Raton, FL, 1994.
31. Incropera, F. P., and DeWitt, D. P., *Fundamentals of Heat and Mass Transfer*, 4th ed., John Wiley and Sons, New York, 1996.
32. Churchill, S. W., and Chu, H. H. S., "Correlating Equations for Laminar and Turbulent Free Convection from a Horizontal Cylinder," *Int. J. Heat Mass Transfer* 18, 1049 (1975).
33. Globe, S., and Dropkin, D., "Natural Convection Heat Transfer in Liquids Confined between Two Horizontal Plates," *J. Heat Transfer* 81C, 24, (1959).
34. Collier, J. G., and Thome, J. R., *Convective Boiling and Condensation*, 3rd ed., Clarendon Press, Oxford, U.K., 1994.

64. Kays, W. M., and London, A. L., *Compact Heat Exchangers*, 3rd ed., Krieger Publishing, Malabar, FL, 1998.
65. American Petroleum Institute, API Standard 661, "Air-Cooled Heat Exchangers for General Refinery Service," API, Washington, DC, 2002.
66. Bott, T. R., *Fouling of Heat Exchangers*, Elsevier Science, Amsterdam, 1995.

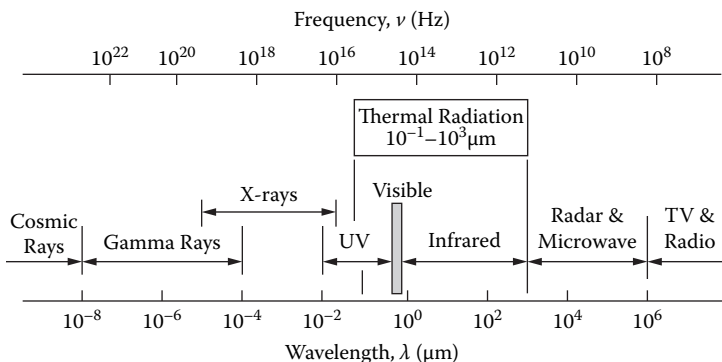


FIGURE 7.1 Thermal radiation: a region of the electromagnetic-wave spectrum.

as electromagnetic waves. In the *particle theory*, the energy of an individual photon is proportional to its frequency,

$$E_{\text{photon}} = h\nu \quad (7.1)$$

where $h = 6.6261 \times 10^{-34}$ J·s is Planck's constant, and ν is the frequency [Hz]. The momentum of each photon is $h\nu/c$. The particle theory is important in deriving the spectral distribution of thermal radiation and in the study of gas emission and absorption. The *wave theory* treats radiation as electromagnetic waves. One of the most important characteristics of a wave is its wavelength λ , which is related to its frequency and the speed of light by

$$\lambda\nu = c \quad (7.2)$$

The frequency is independent of the medium in which radiation propagates, but the speed of light and the wavelength are inversely proportional to the refractive index (n) of the medium. This is to say, $\lambda = \lambda_0 / n$ and $c = c_0 / n$. The refractive index of air is about 0.03% greater than 1 (the refractive index of vacuum), and therefore it is often approximated as 1.

Radiation at a single wavelength (or within a very narrow spectral band) is called monochromatic radiation (examples are lasers and high-temperature gas emission), whereas radiation in a broad wavelength region is called polychromatic or broadband radiation (such as that emitted from the sun). The visible spectrum covers the wavelength region from about 0.4 to 0.7 μm , a small region within the very broad electromagnetic spectrum shown in Figure 7.1. Thermal radiation, which is pertinent to heat transfer, refers to the spectral region from approximately 0.1 to 1000 μm , where the emission depends on temperature. It includes part of the ultraviolet region and the entire visible and infrared regions.

7.2 SURFACE EMISSION

7.2.1 INTENSITY, EMISSIVE POWER, AND IRRADIATION

As illustrated in Figure 7.2, the *spectral intensity* of radiation emitted by an element surface dA in the direction (θ, ϕ) is defined as the rate of emitted energy (radiant power) dq per unit wavelength interval about λ , per unit solid angle about this direction, and per unit area of dA projected to the direction (θ, ϕ) :

it reaches a maximum, and then decreases to zero as $\lambda \rightarrow \infty$. The wavelength corresponding to the maximum emissive power λ_{\max} can be determined by differentiating Equation (7.5) with respect to λ and setting the result to zero. The result is known as Wien's displacement law:

$$\lambda_{\max} = c_3 / T \quad (7.6)$$

where $c_3 = 2897.8 \mu\text{m}\cdot\text{K}$ is sometimes called the third radiation constant. The fraction of emitted energy in the wavelength region from λ_1 to λ_2 is referred to as the blackbody band fraction and has the form

$$F_{\lambda_1-\lambda_2} = \frac{1}{\sigma T^4} \int_{\lambda_1}^{\lambda_2} E_{\lambda,b} d\lambda = \int_{\lambda_1 T}^{\lambda_2 T} \frac{c_1}{\sigma(\lambda T)^5 (e^{c_2/\lambda T} - 1)} d(\lambda T) \quad (7.7)$$

Figure 7.3a represents the Planck distribution for blackbody spectral emissive power with $E_{\lambda,b} / \sigma T^5$ as a function of λT . The band fraction of emitted energy in the region from 0 to λT is equal to the shaded area, which is expressed as $F_{0 \rightarrow \lambda T}$ and shown in Figure 7.3b. About a quarter of the emitted energy is at wavelengths shorter than λ_{\max} , and nearly 95% of the emitted energy is distributed between $0.6\lambda_{\max}$ and $6\lambda_{\max}$. The spectral distribution of solar radiation can be approximated as a blackbody at 5800 K. Therefore, $\lambda_{\max} \approx 0.5 \mu\text{m}$, and the spectral region (95%) important for solar radiation is between 0.3 and 3 μm . For radiation from objects near room temperature, $\lambda_{\max} \approx 10 \mu\text{m}$ and the spectral region of importance (95%) is between 6 and 60 μm .

If $\lambda T \ll c_2$, the RHS of Equation (7.5) can be approximated as $c_1 \lambda^{-5} e^{-c_2/\lambda T}$; this is known as Wien's approximate formula, which yields a relative error of less than 0.7% up to λ_{\max} . If $\lambda T \gg c_2$, the RHS of Equation (7.5) is approximately equal to $c_1 T / c_2 \lambda^4$, which is known as the Rayleigh-Jeans formula and is applicable only for very long wavelengths.

Blackbody radiation is achieved in an isothermal enclosure or cavity under thermodynamic equilibrium, as shown in Figure 7.4a. A uniform and isotropic radiation field is formed inside the enclosure. The total or spectral irradiation on any surface inside the enclosure is diffuse and identical to that of the blackbody emissive power. The spectral intensity is the same in all directions and is a function of λ and T given by Planck's law. If there is an aperture with an area much smaller compared with that of the cavity (see Figure 7.4b), λ the radiation field may be assumed unchanged and the outgoing radiation approximates that of blackbody emission. All radiation incident on the aperture is completely absorbed as a consequence of reflection within the enclosure. Blackbody cavities are used for measurements of radiant power and radiative properties, and for calibration of radiation thermometers (RTs) traceable to the International Temperature Scale of 1990 (ITS-90) [5].

7.3 RADIATIVE PROPERTIES OF SOLIDS

7.3.1 EMISSIVITY

The ratio of the spectral emissive power of an object to that of a blackbody at the same temperature defines the spectral emissivity:

$$\epsilon_\lambda(\lambda, T) \equiv \frac{E_\lambda(\lambda, T)}{E_{\lambda,b}(\lambda, T)} \quad (7.8)$$

The total emissivity is defined as and related to ϵ_λ by

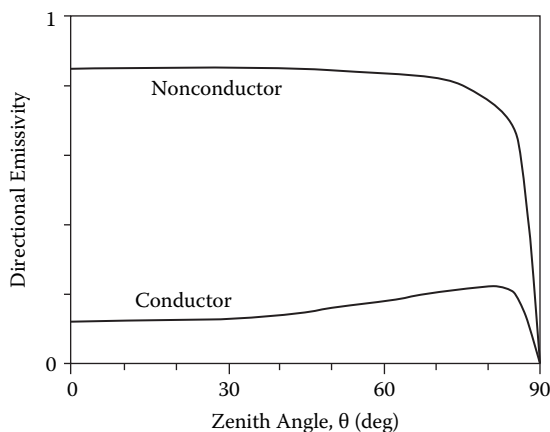


FIGURE 7.5 Directional distributions of the total directional emissivity for conductors (metals) and nonconductors (dielectrics).

$$\epsilon(T) \equiv \frac{E(T)}{E_b(T)} = \frac{1}{\sigma T^4} \int_0^\infty \epsilon_\lambda E_{\lambda,b} d\lambda \quad (7.9)$$

The ϵ_λ and ϵ defined above are hemispherical emissivities. The directional emissivities may be defined based on the ratio of the emitted (spectral or total) intensity to the blackbody (spectral or total) intensity. For a diffuse emitter, the emissivity is independent of the direction. For a *gray surface*, the emissivity is independent of wavelength, $\epsilon = \epsilon_\lambda$. In practice, the surface may be considered gray if the emissivity is independent of the wavelength over the spectral regions of irradiation and emission.

Many industrial materials have *spectrally selective* surfaces for which the emissivity is a complicated function of temperature, wavelength, and the direction of emission, and depends on the surface conditions. For perfectly smooth surfaces, the emissivity can be predicted from the electromagnetic wave theory [2–4]. Typical directional distributions of the total, directional emissivity are shown in Figure 7.5. For conductors (metallic materials), the emissivity is nearly constant for $\theta \leq 40^\circ$, increases to a maximum near 80° , and finally drops to zero. For nonconductors, the emissivity is nearly constant for $\theta \leq 70^\circ$ and decreases sharply to zero. The hemispherical emissivity is slightly higher ($\leq 30\%$) than the normal emissivity for conductors and slightly lower ($\leq 5\%$) than the normal emissivity for nonconductors. Diffuse emission is a good first-order approximation in many engineering applications, and the hemispherical emissivity may be assumed equal to the normal emissivity. The range of the total normal emissivities for a variety of materials near room temperature is listed in Table 7.1. The variation is mainly caused by the different types of materials and surface conditions. It can be seen that pure metals usually have a very low emissivity. Some spectrally selective materials that are highly reflecting in the visible may have a high emissivity (such as white paint and paper). The spectral and total normal emissivities for selected materials are shown in Figures 7.6 and 7.7 [1, 6]. The nature of surface finishing and coating can greatly affect the emissivity. A comprehensive compilation of radiative properties of solids is given by Touloukian and DeWitt [6].

Example 7.1

Assuming that ϵ_λ of stainless steel shown in Figure 7.6 is independent of temperature, how will its total emissivity ϵ change as the surface temperature increases?

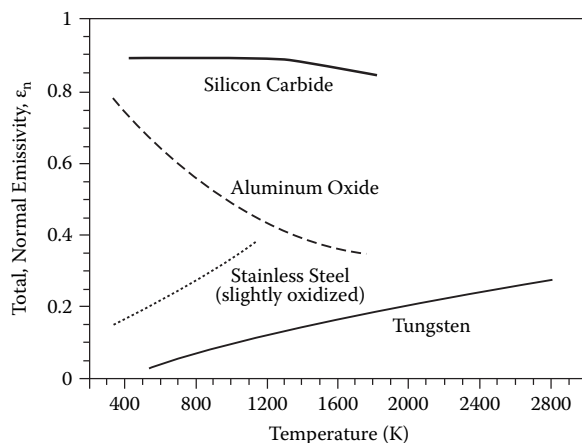


FIGURE 7.7 Temperature dependence of the total normal emissivity of selected materials. (Adapted from Incropera, F. P., and D. P. DeWitt, *Fundamentals of Heat and Mass Transfer*, 4th ed., Wiley, New York, 1996; and from Touloukian, Y. S., and D. P. DeWitt, *Thermal Radiative Properties*, vols. 7, 8, and 9, in *Thermophysical Properties of Matter*, TPRC Data Series, Y. S. Touloukian and C. Y. Ho, eds., IFI Plenum, New York, 1970–1972.)

mittance τ are defined, respectively, as the fraction of irradiation that is absorbed, reflected, or transmitted by the object. The radiative energy balance on the irradiated surface yields

$$\alpha + \rho + \tau = 1 \quad (7.10)$$

For an opaque object ($\tau = 0$), the reflectance and absorptance are also referred to as reflectivity and absorptivity in some literature. The subscript λ may be added to specify spectral properties. The total absorptance α is related to the spectral absorptance α_λ by

$$\alpha = \int_0^\infty \alpha_\lambda G_\lambda(\lambda) d\lambda \bigg/ \int_0^\infty G_\lambda(\lambda) d\lambda \quad (7.11)$$

where $G_\lambda(\lambda)$ represents the spectral distribution of the irradiation. In general, the value of α depends on the spectral and directional distributions of the incident radiation (the radiative environment to which the surface is exposed) and the spectral absorptance. Equation (7.11) also holds for the reflectance or transmittance when α is replaced by ρ or τ .

Sometimes it is important to consider the direction of reflected irradiation exitent from a surface. A property called the bidirectional reflectance distribution function (BRDF) is used to specify the directional distribution of the reflected intensity for a specified direction of incident radiation [2–4]. A specular surface is a mirrorlike surface for which the incidence angle is equal to the reflection angle. For a diffusely reflecting surface, the reflected intensity is the same in all directions, and if perfectly reflective, the BRDF is $1/\pi \text{ sr}^{-1}$.

7.3.3 KIRCHHOFF'S LAW

Consider an object in a blackbody enclosure. Under thermodynamic equilibrium, the emitted radiant power $\epsilon A_s E_b$ must equal the absorbed power $\alpha A_s G$, where A_s is the area of the surface. Because $G = E_b$, it follows that

$$\epsilon = \alpha \quad (7.12)$$

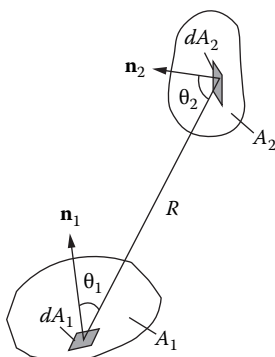


FIGURE 7.9 Definition of the view factor.

surface. The *total* radiosity is $J = \rho G + E$, and the *spectral* radiosity is $J_\lambda = \rho_\lambda G_\lambda + E_\lambda$. Radiosity is a useful concept in calculating radiation exchange between surfaces. Like E and G , J is also a hemispherical property.

7.4.2 THE VIEW FACTOR

Radiative exchange between diffuse-gray and opaque surfaces, including blackbodies, have many engineering applications. In the simplest case, the medium between the surfaces can be assumed *nonparticipating* (no absorption, emission, or scattering during propagation). The *view factor* (also called the configuration factor or shape factor) F_{ij} is defined as the fraction of radiation leaving surface i that is intercepted by surface j . For diffuse-gray surfaces with uniform radiosity, the view factor from A_1 to A_2 (see Figure 7.9) is

$$F_{12} = \frac{1}{A_1} \iint_{A_2 A_1} \frac{\cos \theta_1 \cos \theta_2}{\pi R^2} dA_1 dA_2 \quad (7.13)$$

The view factor depends only upon the geometric arrangement of the surfaces, and satisfies the *reciprocity relation* $A_i F_{ij} = A_j F_{ji}$. The view factor must be between 0 and 1. In an enclosure consisting of N surfaces, the *summation rule* gives

$$\sum_{j=1}^N F_{ij} = 1$$

The term F_{ij} refers to the fraction of radiation that leaves surface i and is directly intercepted by surface j . For flat or convex surfaces, $F_{ii} = 0$; and for concave surfaces, F_{ii} is nonzero. Table 7.2 provides equations for calculating the view factors for some common configurations often encountered in practical applications [1, 2, 8]. The view factors for more complicated geometries can be found in [2].

7.4.3 RADIATION EXCHANGE BETWEEN BLACKBODY SURFACES

If all surfaces are blackbodies, the net radiative heat-transfer rate from surface i to j is

$$q_{ij} = E_{bi} A_i F_{ij} - E_{bj} A_j F_{ji} = A_i F_{ij} (\sigma T_i^4 - \sigma T_j^4) \quad (7.14)$$

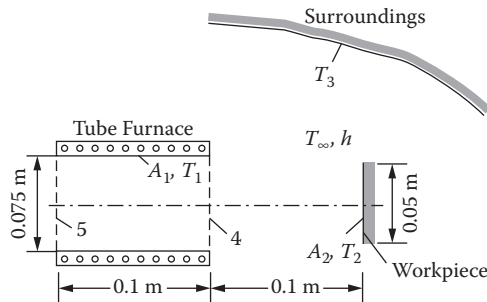


FIGURE 7.10 Example 7.3: tube furnace (1), workpiece (2), and surroundings (3) form a three-black-surface enclosure.

In an enclosure of N blackbody surfaces, the net radiative heat-transfer rate from surface i is

$$q_i = \sum_{j=1}^N q_{ij} = \sum_{j=1}^N A_i F_{ij} (\sigma T_i^4 - \sigma T_j^4), \quad i = 1, 2, \dots, N \quad (7.15)$$

Given the geometry of the enclosure, if the temperatures of all the surfaces are known, Equation (7.15) can be used to determine the net radiative transfer from each surface. If the temperatures of k ($1 \leq k \leq N$) surfaces and the net heat transfer from the remaining $(N - k)$ surfaces are known, Equation (7.15) may be solved to obtain the unknown temperatures and the net heat-transfer rates.

Example 7.3

An electrically heated tubular furnace with a black inner surface of uniform temperature $T_1 = 1200$ K irradiates a coaxial thin disk workpiece, as shown in Figure 7.10. The surface of the disk facing the furnace is painted black and the back side is well insulated. The furnace heater and the workpiece are placed in a large room with a uniform wall temperature T_3 (isothermal surroundings) of 300 K and air temperature $T_\infty = 293$ K. Determine the temperature of the disk, T_2 , by (a) neglecting convective heat transfer and (b) including convective heat transfer, assuming the convective heat-transfer coefficient between the disk and the air is $h = 10$ W/m²·K.

Solution

- (a) The black surface of the furnace (1), workpiece (2) and surroundings (3) form a three-surface enclosure. Performing a radiative energy balance on the workpiece, $q_{1-2} - q_{2-3} = 0$, and using the reciprocity relation $A_1 F_{12} = A_2 F_{21}$, find $A_2 F_{21} \sigma (T_1^4 - T_2^4) - A_2 F_{23} \sigma (T_2^4 - T_3^4) = 0$. The view factor F_{21} may be calculated using the relation between two concentric disks (Table 7.2), $F_{21} = F_{24} - F_{25} = 0.086$, where 4 and 5 are the hypothetical circular disks at the right end and left end of the heating tube, respectively. Also, $F_{23} = 1 - F_{21}$. The result is $T_2 = 655.6$ K.

- (b) The energy balance for surface 2 including convection is $q_{1-2} - q_{2-3} - q_{conv} = 0$, or

$$A_2 F_{21} (\sigma T_1^4 - \sigma T_2^4) - A_2 F_{23} (\sigma T_2^4 - \sigma T_3^4) - A_2 h (T_2 - T_\infty) = 0$$

Solving by iteration, find $T_2 = 601$ K. Although convective heat loss is only about half of the radiative heat loss, it should not be neglected.

The N -linear algebraic equations given above can be solved for the spectral intensities $I_{\lambda,i}$. The foregoing treatment, the net-radiation method, is limited to opaque, diffuse-gray surfaces, which can be extended to include some specular surfaces using the *imaging method*. If the irradiation is not uniform, the *integration method* using differential surfaces is often used. In addition, the *Monte Carlo method*, which is a statistical method, can also be used to determine the radiative heat transfer between enclosure surfaces. Detailed discussions of these more complicated can be found in the literature [2–4, 7, 8].

7.4.5 THE NETWORK REPRESENTATION

The radiative energy balances of Equations (7.16) and (7.17) can be represented in a network. Compared with an electric network, E_b and J_i are analogous to the potential, q_i and q_{ij} are analogous to the current, and $(1 - \epsilon_i)/A_i \epsilon_i$ and $1/A_i F_{ij}$ are analogous to the resistances. The network analogy provides a useful way for visualizing radiation exchange in an enclosure and is a convenient tool for calculating the radiative exchange in an enclosure consisting of two or three surfaces. For an enclosure of two surfaces, using the *network method* as shown in Figure 7.11,

$$q_1 = -q_2 = q_{12} = \frac{\sigma T_1^4 - \sigma T_2^4}{\frac{1 - \epsilon_1}{\epsilon_1 A_1} + \frac{1}{A_1 F_{12}} + \frac{1 - \epsilon_2}{\epsilon_2 A_2}} \quad (7.20)$$

If surface 1 is a plane wall exposed to isothermal surroundings as shown in Figure 7.12a, then $F_{12} = 1$ and $A_1/A_2 \ll 1$. The net radiative heat-transfer rate from A_1 to its surroundings is

$$q_{\text{rad}} = q_1 = A_1 \epsilon_1 \sigma (T_1^4 - T_{\text{sur}}^4) \quad (7.21)$$

Radiative heat transfer is often coupled with convective heat transfer to form the boundary conditions for conduction problems. A *radiation heat transfer coefficient* may be defined by $q_{\text{rad}} = A_1 h_{\text{rad}} (T_1 - T_{\text{sur}})$, where $h_{\text{rad}} = \epsilon_1 \sigma (T_1^2 + T_{\text{sur}}^2)(T_1 + T_{\text{sur}})$ is a strong function of the temperatures and emissivity. As a first-order estimate, h_{rad} may be compared with the convection heat transfer

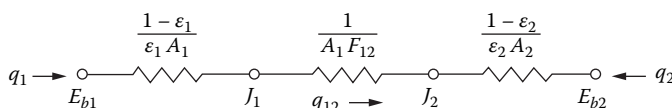


FIGURE 7.11 The radiation network for a two-surface enclosure.

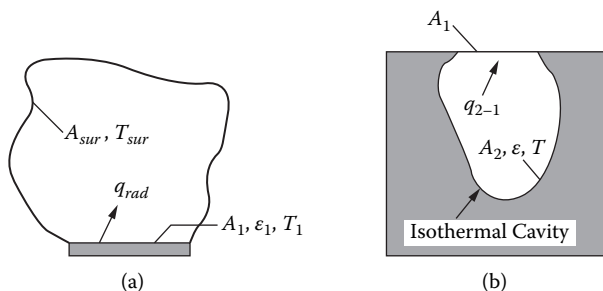


FIGURE 7.12 Applications of net radiation exchange between two surfaces: (a) a small, convex surface and large, isothermal surroundings; (b) an isothermal cavity radiating into cold, black surroundings.

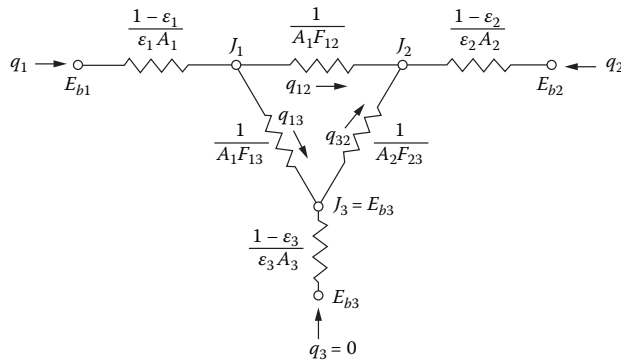


FIGURE 7.14 Network representation for a three-surface enclosure.

The view factor between the tube bank and each plate can be approximated by subtracting the view factor between two tubes from 0.5:

$$F_{21} = F_{23} = \frac{1}{2} - \frac{1}{\pi} \left[\sin^{-1} \frac{D}{s} + \sqrt{\left(\frac{s}{D} \right)^2 - 1} - \frac{s}{D} \right] = 0.4186$$

Therefore, $F_{12} = \frac{A_2}{A_1} F_{12} = 0.6576$ and $F_{13} = 1 - F_{12} = 0.3424$.

$$\begin{aligned} \text{(a)} \quad q_1 = q_{12} = -q_2 &= \frac{\sigma(T_1^4 - T_2^4)}{\frac{1-\epsilon_1}{A_1\epsilon_1} + \left(A_1F_{12} + \frac{1}{1/A_1F_{13} + 1/A_2F_{23}} \right)^{-1} + \frac{1-\epsilon_2}{A_2\epsilon_2}} \\ &= \frac{5.67 \times 10^{-8} (1200^4 - 600^4)}{\frac{1-0.7}{0.7} + \left(0.6576 + \frac{1}{1/0.3424 + 1/(1.57 \times 0.4186)} \right)^{-1} + \frac{1-0.5}{1.57 \times 0.5}} \\ &= 50.14 \text{ kW/m}^2 \end{aligned}$$

$$\text{(b)} \quad J_1 = E_{b1} - q_1 \left(\frac{1-\epsilon_1}{A_1\epsilon_1} \right) = 96.08 \text{ kW/m}^2, \quad J_2 = E_{b2} - q_2 \left(\frac{1-\epsilon_2}{A_2\epsilon_2} \right) = 39.29 \text{ kW/m}^2$$

$$A_1F_{13}(J_1 - E_{b3}) = A_2F_{23}(E_{b3} - J_2)$$

yields $E_{b3} = 58.74 \text{ kW/m}^2$ and $T_3 = 1009 \text{ K}$.

- (c) Because q_{12} and all the geometric parameters and emissivities have not changed, we have $T_1^4 - T_2^4 = T_1'^4 - T_2'^4$, which can be solved to obtain $T_1' = 1238.6 \text{ K}$. That is to say, for the same heat transfer rate, only a 40 K temperature increase in T_1 will increase the tube temperature by 200 K.

Note that the emissivity value of the reradiating surface does not affect the results. If surfaces A_1 and A_2 are treated as blackbodies, $\epsilon_1 = \epsilon_2 = 1$, then the predicted net radiative heat transfer rate q_{12} would be 97.3 kW/m^2 , which is almost twice the value calculated in part (a).

$$\frac{dI_\lambda}{d\zeta_\lambda} + I_\lambda = (1 - \Omega_\lambda)I_{\lambda,b} + \frac{\Omega_\lambda}{4\pi} \int_{4\pi} I_\lambda(\zeta_\lambda, \omega') \Phi_\lambda(\omega', \omega) d\omega' \quad (7.24)$$

This is an integro-differential equation, and its RHS is called the source function. The boundary conditions also need to be specified. The integration of the spectral intensity over all wavelengths and all directions gives the radiative heat flux. Unless the temperature field is prescribed, Equation (7.24) is generally coupled with the thermal diffusion equation in a macroscopically stationary medium and with the energy conservation equation in a fluid with bulk movement. Under radiation equilibrium (steady state with no heat generation and without conduction or convection), the governing equation (energy equation) prescribes that the divergence of the radiative heat flux is zero.

Analytical solutions of the RTE rarely exist for applications with multidimensional and non-homogeneous media. Approximate models have been developed to deal with special types of problems, including Hottel's *zonal method* [8], the *differential and moment methods* (often using the spherical harmonic approximation), and the *discrete ordinates method*. The statistical model using the Monte Carlo method is often used for complicated geometries and radiative properties. Detailed discussions of these solution methods can be found in the literature [2–4, 7, 8] and are beyond the scope of this chapter. For an isothermal medium without scattering, integrating the RTE yields

$$I_\lambda(\zeta_\lambda) = I_\lambda(0)e^{-\zeta_\lambda} + I_{\lambda,b}(1 - e^{-\zeta_\lambda}) \quad (7.25)$$

where $e^{-\zeta_\lambda}$ and $(1 - e^{-\zeta_\lambda})$ may be regarded, respectively, as the transmissivity and emissivity of the gas along the path length 0 to s . Optically thin and optically thick limits refer to the cases when $\zeta_\lambda \ll 1$ (essentially transparent) and $\zeta_\lambda \gg 1$ (essentially opaque).

As an example, consider a sphere of radius R with a black wall of temperature T_w filled with an isothermal gas at T_g , as shown in Figure 7.16. Neglect scattering and assume that the gas has a refractive index of 1 and an absorption coefficient κ that is independent of the wavelength (gray assumption). The spectral intensity at the wall is a function of angle θ . From Equation (7.25), we have $I_\lambda(\theta) = I_{\lambda,b}(T_w)e^{-2\kappa R \cos \theta} + I_{\lambda,b}(T_g)(1 - e^{-2\kappa R \cos \theta})$. Since κ is not a function of the wavelength, a similar expression can be written for the total intensity by omitting the subscript λ . The heat flux on the wall can be obtained by integrating the intensity over the hemisphere:

$$q'' = \int_{\phi=0}^{2\pi} \int_{\theta=0}^{\pi/2} I(\theta) \cos \theta \sin \theta d\theta d\phi.$$

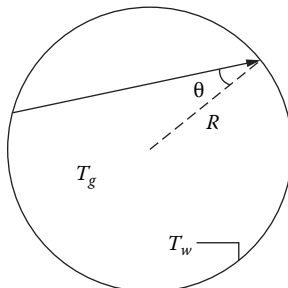


FIGURE 7.16 Example 7.5: an isothermal gas in a sphere.

and the total emissivities should be added and then subtracted by the contribution of the overlapping bands; hence,

$$\epsilon_{a+b} = \epsilon_a + \epsilon_b - \Delta\epsilon_{ab} \quad (7.26)$$

where subscripts a and b represent two different gases, typically H_2O and CO_2 , and $\Delta\epsilon_{ab}$ is the contribution due to overlapping bands (which is about $2.7 \mu\text{m}$ for H_2O and CO_2). A similar expression can be obtained for the total absorptance. However, the integration must be weighted over the Planck distribution at the wall temperature. Notice that the total emissivity is a function of the gas temperature, pressure, partial pressure, and path length; and the total absorptivity is also a function of the wall temperature. Most heat transfer textbooks present the total emissivity and absorptivity of H_2O and CO_2 in charts [1, 2], an approach first introduced by Hottel [8]. New charts and equations have also been proposed. A summary can be found in the textbook by Modest [4]. For nonisothermal gases, the zonal method is widely employed for calculating radiative heat transfer in combustion chambers [2, 8].

Small particles are important for radiative transfer in atmosphere and combustion chambers [2–4]. Soot particles ranging from 5 to 100 nm in size are formed during a combustion process and emit thermal radiation (often stronger than the emission from combustion gases) in a continuous spectrum over the infrared and some visible regions. In pulverized-coal combustion furnaces, coal, char, and fly ash particles are important, as are soot particles. Particles can also scatter electromagnetic waves or photons, causing a change in the direction of propagation. In the early 20th century, Mie developed a theory for a spherical particle based on Maxwell's electromagnetic wave equations, known as the *Mie scattering theory*, which can be used to predict the scattering-phase function. In the case when the particle sizes are small compared with the wavelength (Rayleigh limit), the formulation reduces to the simple expression obtained earlier by Rayleigh. In the Rayleigh limit, the scattering efficiency is inversely proportional to the wavelength to the fourth power. This factor explains why the sky is blue and why the sun appears red at sunset. The absorption efficiency, on the other hand, is proportional to the inverse of the wavelength. The scattering phase function is symmetric as far as forward and backward scattering is concerned, and is nearly isotropic [2–4]. Soot particles generally fall in the Rayleigh limit. For spheres whose diameters are much greater than the wavelength, diffraction theory and geometric optics based on specular surface or diffuse surface can be applied [4]. If the scattering by one particle is affected by the presence of other particles, the scattering is called dependent scattering and requires more complicated treatments. Detailed discussions of particle properties and scattering theory can be found from [2–4] and references therein.

7.6 RADIATION THERMOMETRY

Radiation thermometry (or pyrometry) is a subject that involves determining the temperature of an object from measurement of its exitent intensity. A radiation thermometer (RT) is a radiometer calibrated to indicate the temperature of a blackbody, as shown in Figure 7.17a. RTs have been used in high-temperature furnaces, glass processing, steel processing, crystal growth, aluminum manufacturing, and thermal imaging [10]. The application of RTs to high-temperature furnaces is addressed in [11]. A more recent review on surface temperature measurements using optical techniques is given by Zhang [5]. When an RT is used to measure the temperature of a real surface, as shown in Figure 7.17b, two issues arise. The first is the unknown emissivity of the surface and the second is the influence of the surrounding radiation. Various methods have been developed to deal with these problems, including the creation of a blackbody cavity on the surface, the two-color method, and the use of a controlled reference source [5, 10, 11]. The development of optical

In practice, the choice of operating wavelength also depends on the surrounding radiation. Therefore, it is an important issue to select the operating wavelength.

Example 7.5

For a surface at $T = 1800$ K with an emissivity of 0.6, what are the radiance temperatures at $\lambda = 0.65$ μm and 1.5 μm ? If a conical hole is formed with a half-cone angle of 15° , what is the effective emissivity and the radiance temperature at $\lambda = 0.65$ μm ?

Solution

From Equation (7.30), $T_\lambda \approx 1728$ K at $\lambda = 0.65$ μm and 1643 K at $\lambda = 1.5$ μm . If the emissivity is not taken into consideration, the error would be $1800 - 1728 = 72$ K, or 4% for a radiation thermometer at $\lambda = 0.65$ μm , and 157 K or 8.7% for an RT at $\lambda = 1.5$ μm . If a cavity is formed, assuming that the surface is diffuse, the effective emissivity can be approximated by Equation (7.22). Because the half-cone angle is 15° , $A_1/A_2 = \sin 15^\circ$ and $\epsilon_{\text{eff}} = 0.853$. The radiance temperature based on the effective emissivity is $T_{\lambda=0.65 \mu\text{m}} \approx 1777$ K. The error in RT will be reduced to 23 K or 1.3%. The effective emissivity for a specular surface would be even larger in this case, which would result in a smaller difference between T_λ and T .

If the target is not a blackbody and the surrounding radiation is not negligible, $L_{\lambda, \text{ex}}(\lambda)$ is the sum of the emitted and reflected spectral radiances:

$$L_{\lambda, \text{ex}}(\lambda) = L_{\lambda, \text{e}}(\lambda, T) + L_{\lambda, \text{r}}(\lambda) \quad (7.31)$$

The reflected spectral radiance depends on the distribution of the surrounding radiation incident on the target and the bidirectional reflectance distribution function of the target, and except for well-controlled environments or in some limited cases, $L_{\lambda, \text{r}}(\lambda)$ is difficult to determine.

For flame or gas temperature measurements, the exitent radiance is proportional to $L_{\lambda, \text{b}}(1 - e^{-\zeta_\lambda})$, where ζ_λ is the optical thickness. The emission from the surface may transmit through the gas and needs to be taken into consideration [11]. Although RTs can be used to measure temperatures for high-temperature surfaces and flames with uncertainties ranging from a few kelvin to a few tens of kelvin, great care must be taken in the calibration and operation of RTs. Calibration is usually done with high-temperature blackbody furnaces. In the measurement, the field of view and the angle of incidence need to be correctly chosen. The alignment needs to be carefully performed. Background radiation and other radiation sources should be avoided.

REFERENCES

1. Incropera, F. P., and D. P. DeWitt, *Fundamentals of Heat and Mass Transfer*, 4th ed., Wiley, New York, 1996.
2. Siegel, R., and J. R. Howell, *Thermal Radiation Heat Transfer*, 3rd ed., Hemisphere, Washington, 1992.
3. Brewster, M. Q., *Thermal Radiative Transfer and Properties*, Wiley, New York, 1992.
4. Modest, M. F., *Radiative Heat Transfer*, McGraw-Hill, New York, 1993.
5. Zhang, Z. M., in *Annual Review of Heat Transfer*, vol. 11, C. L. Tien, ed., 351–411, Begell House, New York, 2000.
6. Touloukian, Y. S., and D. P. DeWitt, *Thermal Radiative Properties*, vols. 7, 8, and 9, in *Thermophysical Properties of Matter*, TPRC Data Series, Y. S. Touloukian and C. Y. Ho, eds., IFI Plenum, New York, 1970–1972.
7. Sparrow, E. M., and R. D. Cess, *Radiation Heat Transfer*, augmented ed., Hemisphere, Washington, 1981.
8. Hottel, H. C., and A. F. Sarofim, *Radiative Transfer*, McGraw-Hill, New York, 1967.

C_i = concentration of species i , g-moles/cm³

Z = distance, cm

D_i = a proportionality constant, called the *diffusion coefficient* for species i , cm²/s

Equation (8.1) is basic and states that the rate of diffusion of a molecule, in mixture with others, moves at a rate directly proportional to its concentration gradient and the cross section through which it diffuses, and is inversely proportional to the distance through which it must travel. It implies steady-state diffusion.* The negative sign in Equation (8.1) is simply to make the flux positive, since the concentration gradient is negative. Variations of Equation (8.1) can be used to allow concentration expressed in mole fraction or mass fraction, for example,

$$J_i = -C_m D_i \frac{\partial y_i}{\partial z} \quad (8.1a)$$

where

J_i = molar mass flux of species i , g-moles/(s·cm²)

C_m = average total concentration, total g-moles/cm³

z = distance, cm

y_i = mole fraction of species i (g-moles i /total g-moles)

D_i = proportionality constant, the *diffusion coefficient* for species i , cm²/s

The value of D depends upon the conditions of transport. For the often-used case of diffusion under nonturbulent conditions, *molecular diffusion* prevails, and D is a *molecular diffusion coefficient*.† As such, its value depends on temperature, pressure, relative size of molecules involved, and in some cases, whether all molecules, including i , are polar. If turbulent conditions prevail, we have an *eddy diffusion coefficient*, usually designated by the symbol ϵ . The models used in this chapter do not involve the turbulent case, largely because it lacks a firm basis for estimation, i.e., degrees of turbulence are not easily evaluated.

Equation (8.1) has its counterparts for heat flux (Fourier's equation) and momentum flux. Evaluation of D_i is relatively simple for binary systems, i.e., species i moving through, say, species j . If i is moving through several components that can be grouped as a single pseudo component, evaluation of D_i is straightforward. However, if all species in the mixture are diffusing at different rates (and in different directions), one must use the Maxwell-Stefan relationships, which are beyond the coverage of the present chapter. Taylor and Krishna [1] provide extensive coverage of multi-component diffusion.

8.2 MOLECULAR DIFFUSION COEFFICIENTS

8.2.1 GASES—BINARY MIXTURES

Diffusion coefficients for some binary gas mixtures have been measured and are reported in various compendia, such as *Perry's Handbook* [2]. Of concern here are the models available for *estimating* the coefficients, or for extrapolating the values of measured coefficients. A number of predictive models have been presented for the case of binary gas mixtures. The models are based on experimental data, where the movement of one component is measured under carefully controlled laminar conditions. A model combining both accuracy and ease of use is due to Fuller et al. [3]:

* Fick's second law deals with transient diffusion, not covered in this chapter.

† The terms *diffusion coefficient* and *diffusivity* are synonymous. The former will be used here.

Example 8.1

Estimate the gaseous diffusion coefficient for methanol diffusing through water vapor at 25°C and 1.0 atm pressure.

Solution

Equation (8.2) is used, with the following values:

$$\begin{aligned}T &= 298^\circ\text{K} \\M_i &= 32.0 \text{ (methanol)} \\M_j &= 18.1 \text{ (water)} \\P &= 1.0 \text{ atm} \\\Sigma v_i &= 16.5 + 4(1.98) + 5.48 = 29.9 \text{ (Table 8.1)} \\\Sigma v_j &= 12.7 \text{ (Table 8.1)}\end{aligned}$$

By Equation (8.2),

$$D_{ij} = \frac{1.0(10)^{-3} (298)^{1.75}}{1.0 \left[(29.9)^{1/3} + (12.7)^{1/3} \right]^2} \left(\frac{1}{32.0} + \frac{1}{18.1} \right)^{0.5} = 0.213 \text{ cm}^2/\text{s}$$

8.2.2 LIQUIDS—BINARY MIXTURES

The liquid phase is less predictable than the gas phase, and methods for predicting diffusion coefficients do not have the support that gases have from the kinetic theory of gases. The Stokes-Einstein relationship forms the basis for modeling:

$$D_{ij}^L = \frac{kT}{4\pi r_i \mu_j} \quad (8.3)$$

Wilke and Chang [7] modified this relationship to develop a *dimensional* relationship for the dilute case, i.e., low concentrations of *i* in *j*:

$$D_{ij}^{LO} = \frac{7.4(10^{-8})(\phi_j M_j)^{1/2} T}{V_i^{0.6} \mu_j} \quad (8.4)$$

where

D_{ij}^{LO} = liquid diffusion coefficient for dilute solute *i* in solvent *j*, cm²/s

ϕ_j = correction factor for associated liquid solvent; $\phi = 1.0$ for nonassociated liquids, = 2.4 for water, 1.9 for methanol, and 1.5 for ethanol

M_j = molecular weight of solvent *j*

T = absolute temperature, °K

μ_j = viscosity of solvent, mPa·s (centipoise)

V_i = molar volume of solution at normal boiling point, cm³/g-mole

Values of V_i may be estimated by means of the LeBas parameters given in Table 8.2.

For non-ideal liquid mixtures, the Vignes [8] relationship should be used:

$$D_{ij}^L = (D_{ij}^{LO})^{x_j} (D_{ji}^{LO})^{x_i} \left(1 + x_i \frac{d \ln \gamma_i}{d x_i} \right) \quad (8.6)$$

For an ideal-liquid mixture, this equation shows a linear plot of $\ln D$ vs. molar concentration. The term γ_i is the liquid-phase activity coefficient, and the term $d \ln \gamma_i / dx_i$ is the slope of the conventional plot of the logarithm of the activity coefficient versus mole fraction (see Figures 12.7 and 12.9 in Chapter 12, or see Chapter 4). Thus, for the value of the liquid diffusion coefficient of a concentrated binary mixture i - j , Equations (8.5) or (8.6) should be used, depending on ideality of the solution.

When water is the solute, diffusing at very low concentration through a solvent, the dimensional relationship by Sitaraman et al. [9] gives a somewhat better fit than Equation (8.4):

$$D_{ij}^{LO} = 16.8(10^{-10}) \left(\frac{M_j^{0.5} \lambda_j^{0.333} T}{\mu_j V_i^{0.5} \lambda_i^{0.3}} \right)^{0.93} \quad (8.7)$$

where

λ_i and λ_j = latent heats of vaporization of the solute and solvent, respectively, at their normal boiling points, J/kg

μ_j = viscosity of the solute, cP

and other terms are the same as for Equation (8.4). Special relationships apply when an organic is diffusing through an ionic solution; for such a case, consult Hirschfelder et al. [4] or Reid et al. [6]

Example 8.2

For a liquid solution of 10 mole-% methanol in water, calculate the diffusion coefficients for each component. Temperature is 25°C, pressure is 1.0 atm, viscosity of the methanol is 0.55 cP, and viscosity of water is 0.95 cP.

Solution

Let i be methanol and j be water. The infinite-dilution coefficient for methanol in water is computed using Equation (8.4). Values of terms are

Association parameters $\phi = 2.6$ for water and 1.9 for methanol

Molecular weights $M = 18.1$ for water and 32.0 for methanol

Molecular volumes (Table 8.2): for methanol = $14.8 + 4(3.7) + 7.4 = 37.0$; for water = 18.9

1. Methanol in water

$$D_{ij}^{LO} = \frac{7.40(10)^{-8} [(2.6)(18.1)]^{1/2} (298)}{(37)^{0.6} (0.95)} = 1.824(10)^{-5} \text{ cm}^2/\text{s}$$

2. Water in methanol

8.2.4 LIQUIDS—MULTICOMPONENT MIXTURES

If the mixture is ideal, or nearly so, a modification of the Vignes equation (8.6) may be used, considering the mixture j,k,l,\dots as a pseudo component. Thus, for a ternary ideal mixture i,j,k ,

$$D_{i\text{-mixture}}^{LO} \mu_{ijk} = \left(D_{ij}^{LO} \mu_j \right)^{x_j} \left(D_{ik}^{LO} \right)^{x_k} \quad (8.9)$$

For, say, a ternary non-ideal mixture, activity-coefficient data must be available. In such a case, the result of Equation (8.9) can be multiplied by $(1 + x_i(\partial \ln \gamma_i / \partial x_i))$ as in the Vignes equation (8.6). One should recognize, however, that activity-coefficient data for mixtures with more than two components are scarce; the best source for such data is the Gmehling series [11].

8.2.5 DIFFUSION THROUGH POROUS SOLIDS

For a gas diffusing through the very small pores of an adsorbent or solid catalyst, a form of Fick's equation (Equation (8.1)), called the slab equation, may be used:

$$J_i = - \frac{D_{ki}}{z_o} (C_{i2} - C_{i1}) = \frac{D_{ki}}{RT} \left(\frac{(p_1 - p_2)_i}{z_o} \right) \quad (8.10)$$

where

z_o = length of pore traveled, cm

R = gas constant, 82.057 (atm·cm³)/(g·moles·°K)

T = absolute temperature, °K

p_i = partial pressure of i , obtained from concentration using the gas law:

$$C_i = \frac{n_i}{V} = \frac{p_i}{RT} \quad (8.11)$$

and D_{ki} is the *Knudsen diffusion coefficient* for species i , so called because, in the very small and crooked pores, the molecules collide more frequently with the pore wall than with each other. Thus, the value of this coefficient depends more on the pore geometry than on the diffusing species:

$$D_{ki} = D_k = 2 / 3 r_e \left(\frac{8 RT}{\pi M_i} \right)^{0.5} = 9700 r_e \sqrt{\frac{T}{M_i}} \text{ cm}^2/\text{s} \quad (8.12)$$

with r_e being the effective pore radius, cm.

The pore size may be known, or it can be estimated:

$$r_e = \frac{2 \epsilon}{S \rho_p} \quad (8.13)$$

where

ϵ = fraction voids in solid particle

S = total surface area of solid, cm²/g

ρ_p = particle density, g/cm³

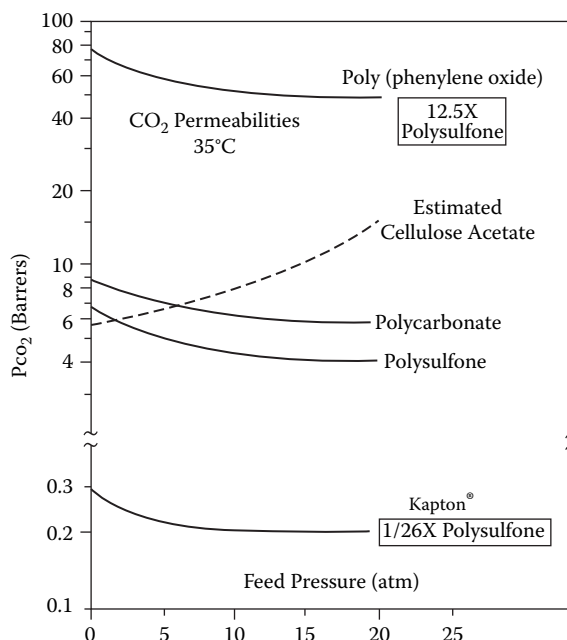


FIGURE 8.1 Permeabilities for carbon dioxide passing through several membrane materials. (From Fair, J. R. *Chem. Proc.* 52 (10): 81 (1989). With permission.)

8.2.6 GASES—DIFFUSION THROUGH MEMBRANES

Again, Fick's law is used, with the length term equal to the membrane thickness. The diffusion coefficient is usually called a *permeability* and is measured by observing the flux J_i for a given membrane material coupled with a known pressure difference on either side of the membrane. For a semipermeable membrane, the permeability P is a function of both a mobility term and a solubility term, i.e., $P = DS$. Because the separating power of a membrane is based on different values of P for each component, it follows that the selectivity term α_{ij} is

$$\alpha_{ij} = \frac{P_i}{P_j} = \frac{D_i}{D_j} \frac{S_i}{S_j} = \left(\frac{\text{mobility}}{\text{selectivity}} \right) \left(\frac{\text{solubility}}{\text{selectivity}} \right) \quad (8.16)$$

To indicate the influence of the membrane material on a diffusing species, Figure 8.1 shows permeabilities for carbon dioxide moving through different membranes under the influence of a pressure-driving force [13]. The permeability is calculated from measured flux:

$$P_{CO_2} = \frac{\text{Std. cm}^3 \text{ diffusing}}{\text{s} - \text{cm}^2 - \text{cm Hg driving force}}$$

Researchers in membrane technology have adopted the special permeability unit called the Barrer:

$$1.0 \text{ Barrer} = \frac{10^{10} (\text{cm}^3 @ \text{STP})(\text{cm})}{\text{cm}^2 (\text{sec})(\text{cm Hg})}$$

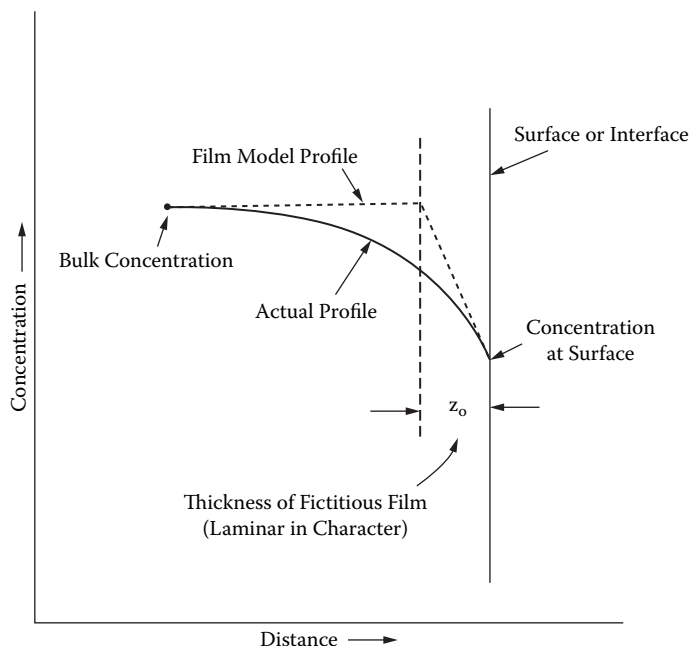


FIGURE 8.2 Elements of the film theory.

8.3.1 STAGNANT-FILM MODEL

This model, developed by Whitman [16] in 1923, is still used. The assumption is that adjacent to the interface there exists a thin film that is laminar in character and through which transfer is by molecular diffusion only. In this film, the entire concentration driving force exists, i.e., outside the film, in the bulk fluid, the concentration is constant at some steady state. Flow outside the film may be laminar or turbulent, but inside the film, flow conditions are completely laminar. Figure 8.2 shows the elements of the theory.

It is possible in some cases to measure the thickness of the film, which is akin to the boundary layer in turbulent flow. In most cases, however, this is not practical, if indeed possible. Accordingly, the quotient D/z_0 is simply called a *mass transfer coefficient*. Equations for the different mass transfer coefficients are shown in Table 8.3.

The coefficient is subject to certain variables, not all quantifiable:

1. The coefficient increases or decreases according to the variables affecting the diffusion coefficient, Equations (8.2) or (8.4).
2. The film is subject to the fluid mechanics of the bulk mixture. For example, high bulk fluid velocities can thin the film and thus increase the value of the coefficient.

Even if the flow of the bulk fluid is laminar, there is still considered to be a separate film at the interface.

One must be very careful about the units used. Those shown in Table 8.3 are typical, but many other combinations can be used.

8.3.2 PENETRATION MODEL

In searching for a more realistic model than one containing a “fictitious film,” Higbie [17] proposed the elimination of the film idea and replacing it with an unsteady-state model that permits turbulent conditions adjacent to the interface. Sometimes called the “Higbie model,” it contains the following elements:

time, let alone a range of exposure times, just as there is little experimental support for the stagnant film of finite thickness.

8.3.3 SURFACE RENEWAL MODEL

This model, proposed originally by Danckwerts [18], is an extension of the penetration model. Whereas Higbie assumed that all exposure times were the same, Danckwerts provided for a range of times, based on probability theory. After a given exposure, the surface (interface) was renewed, leading to the name of the theory. The elements of the model are

- There are no films.
- Eddies bring packets to the interface, remaining there for a variety of times.
- The surface (interface) is renewed on the basis of fluid flow and geometry.
- Mass transfer occurs only during exposure.

The flux equation by this model is

$$J_i = (C_{iB} - C_{i,int}) \sqrt{S D_{ij}} \quad (8.20)$$

where S is the fractional surface renewal rate, s^{-1} ; and the mass transfer coefficient is $\sqrt{S D_{ij}}$, cm/s. In reality, the difference between the penetration and surface-renewal models is the factor of 2 in the flux equation. The models are used interchangeably, with little attempt to predict the range of exposure times. Use of these models is described in the following section.

8.4 MASS TRANSFER ACROSS A PHASE BOUNDARY

The practical applications provided here all involve two phases, with molecules transferring between them. Thus, there are two resistances to transfer, plus possibly a third resistance at the interface itself. We have just discussed transfer within a phase and ending at a phase boundary, such as an interface. It is necessary to couple individual phase resistances to characterize the overall transfer process. The first attempt at this, and indeed a lasting one, was presented by Lewis and Whitman [19] as the *two-film theory*. More recently it has been called simply the *two-resistance theory*, eliminating the requirement that transport in each phase be handled by the film concept.

8.4.1 TWO-FILM MODEL

To describe this model, let us assume that a species is transferring from a gas phase to a liquid phase, as in gas absorption. Figure 8.3 diagrams the process. If the transfer flux is based on a unit area of interface, we may write the total flux equation as follows:

$$J_i = k_{y,i} (y_{ib} - y_{i,int}) = k_{x,i} (x_{i,int} - x_{ib}) \quad (8.21)$$

[gas] [liquid]

where

- J_i = mass flux of i , g-moles/s·cm² interfacial area
- k_x, k_y = mass transfer coefficients for gas and liquid, respectively, defined in Table 8.3
- y_{ib} = mole fraction of i in the bulk gas phase
- $y_{i,int}$ = mole fraction of i in the gas, at the interface
- $x_{i,int}$ = mole fraction of i in the liquid, at the interface

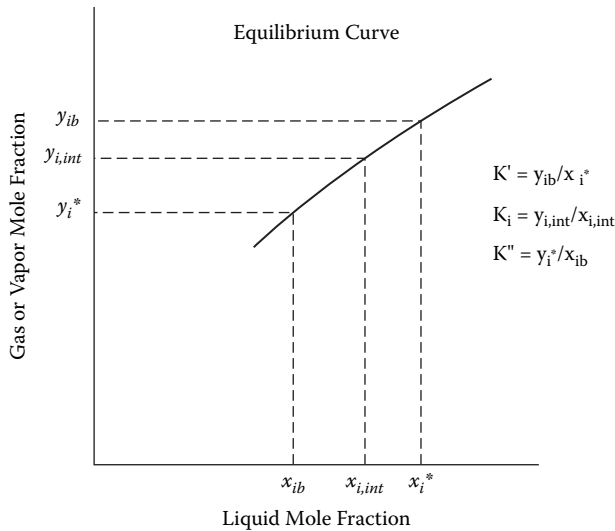


FIGURE 8.4 Variation of K values for interphase transfer, binary system.

measure or to predict. However, they do not deal with the individual mass transfer characteristics of the individual phases. For most engineering calculations, knowledge of the contributions of the phases to mass transfer are needed, obtainable from the following relationship for transferring species i :

$$\frac{1}{K_{ox}} = \frac{1}{K_i k_y} + \frac{1}{k_x} \quad (8.23)$$

$$\frac{1}{K_{oy}} = \frac{1}{k_y} + \frac{K_i}{k_x} \quad (8.24)$$

Equations (8.23) and (8.24) are equivalent and represent a series resistance expression:

$$R_{\text{total}} = R_{\text{gas}} + R_{\text{liquid}}$$

When essentially all of the resistance is on the gas side of the interface, $k_x \gg k_y$, and $K_{oy} \approx k_y$ or $K_{ox} \approx k_y K_i$. A well-known example of pure gas-phase resistance is the humidification of dry air with pure water. Because there is no concentration gradient in the liquid, the interface concentration equals the vapor pressure of water at the temperature under consideration. Thus the only driving force is $p^{\text{vap}} - p_b$, where p_b = partial pressure of water in the air, equivalent to the humidity. Many distillation separations have most of the resistance in the vapor phase.

Conversely, when essentially all of the resistance is on the liquid side, $K_{oy} \approx k_g/K_i$ or $K_{ox} \approx k_x$. For test work, this situation is simulated by the stripping of oxygen from water by air. Because of the limited solubility of oxygen in water, the value of K_i is very high, and the first term on the right-hand side of Equation (8.23) is essentially zero. This is the situation for many strippers, where the solute is relatively insoluble in the solvent.

Equations (8.22)–(8.24) and their associated discussion refer to a single diffusing component. Further, they are based only on one set of symbols from those given in Table 8.3. Equations with other symbols are included in Table 8.4.

$$\frac{1}{K_{ox}a} = \frac{1}{K_i k_y a} + \frac{1}{k_x a} \quad (8.25)$$

$$\frac{1}{K_{oy}a} = \frac{1}{k_y a} + \frac{K_i}{k_x a} \quad (8.26)$$

where a is the interfacial area per unit volume.

For design purposes, representative expressions for total transfer, considering resistance of both phases, are

Absorption, gas to liquid:

$$N_i = K_{oy,i} a (y_i - y_i^*) = K_{ox,i} a (x_i^* - x_i) \quad (8.27)$$

Stripping, liquid to gas:

$$N_i = K_{oy,i} a (y_i^* - y_i) = K_{ox,i} a (x_i - x_i^*) \quad (8.28)$$

In Equations (8.27 and 8.28), N_i is the total moles/time of i transferred, and a is the effective interfacial area at the phase boundary. Individual phase resistances are handled by Equations (8.25) or (8.26).

Distillation, equimolar counterdiffusion:

$$N_i = K'_i a (y_i - y_i^*) \quad (8.29)$$

By convention, distillation calculations are based on the gas (vapor) phase, since usually most of the resistance is in that phase. Note also that since components are diffusing in both directions, the coefficient has a slightly different definition (see Table 8.3 for the individual mass transfer coefficients, which are primed). Further, the equilibrium ratio is replaced by the slope of the equilibrium curve, m . The overall coefficient is, then,

$$K'_{oy} a = \frac{1}{\frac{1}{k'_{oy} a} + \frac{m}{k'_x a}} \quad (8.30)$$

For a binary mixture, a typical y^*, x graph is shown in Figure 8.5. It is clear that with a change in location within the distillation column, the slope varies, being relatively large at the bottom. The liquid-side resistance to mass transfer is thus greater at the bottom than at the top, since the $m/k'_x a$ term represents the liquid-phase resistance.

8.4.4 VOLUMETRIC COEFFICIENTS, LIQUID-LIQUID

For two immiscible liquids in contact, a phase boundary occurs, and it is possible to transfer a solute I between them. The analogy between liquid-liquid and gas-liquid systems is apparent, and the equations for gas-liquid mass transfer apply. The phase with the lower density is called the

In Equations (8.33) and (8.34), the term $K_{L/H,i}$ is called an equilibrium *distribution coefficient*, and is often carried in terms other than mole fractions. (See Chapter 10 on liquid-liquid extraction.) The point to be made here is that the analogy between gas-liquid and liquid-liquid systems applies. However, one must be very careful in converting between sets of units (concentrations or mass fractions versus mole fractions) as well as in phase designations. Many designers call the y phase the solvent (or extract) phase, with transfer from the x phase to the y phase, with the stripping analogy in gas-liquid contacting. However, the solvent phase is often the light phase.

Designers of extraction equipment often use mass concentration units, which requires that the equilibrium ratio be expressed in the same units. An equivalent of Equations (8.31) and (8.32), using movement from continuous to dispersed phases, is

$$M_{i,c \rightarrow d} = K_{OL,cont} a (C'_{i,cont} - C'^*_{i,cont}) \quad (8.35)$$

where

M = g/(s-cm³) transferred

a = interfacial area, cm²/cm³

$K_{OL,cont}$ = overall coefficient for the diffusing species (i.e., solute), cm/s

C' = mass concentration in bulk continuous phase, g/cm³

C'^* = continuous phase concentration in equilibrium with bulk dispersed phase, i.e., $C'^* = m_{cd} C'_{disp}$

m_{cd} = equilibrium distribution coefficient, g/g

Example 8.4 has been included to help clarify the extraction adaptation of the gas-liquid relationships.

Example 8.4

Acetone is being removed from water by contacting with toluene in a packed extraction column. Water is the continuous [heavy] phase, and toluene is the dispersed [light] phase. Calculate the overall mass transfer coefficient for this process.

Data:

Continuous phase: density = 0.994 g/cm³, viscosity = 0.92 cP, molecular weight \approx 18 (lean solution)

Dispersed phase: density = 0.860 g/cm³, viscosity = 0.54 cP, molecular weight \approx 92 (lean solution)

Molecular weight of solute = 58

Distribution coefficient (equivalent to equilibrium ratio) = $C_{disp}/C_{cont} = 0.67$

Solution

Seibert and Fair [20] have found, for the system in question and for the particular packing type and flow rates, effective interfacial area = $a = 1.46$ cm²/cm³, and the following phase mass transfer coefficients:

$$k_{L,cont} = 4.20 \times 10^{-3} \text{ cm/s}$$

$$k_{L,disp} = 9.81 \times 10^{-3} \text{ cm/s}$$

Because concentrations are used, the equilibrium ratio is also in terms of concentrations. Thus,

Data:

Toluene mol. wt. = 92, and its vapor pressure = 40 mm Hg, or 0.053 atm.

Solution

By Equation (8.39),

$$J_i = \frac{0.67(0.5)^{0.78} (18/92)^{1/3} 0.053}{(82.057 \times 305.2)} = 4.79 \times (10^{-7}) \frac{\text{gm-moles}}{\text{s-cm}^2}$$

For $3 \times 10^4 \text{ cm}^2$ and converting to familiar units, rate of evaporation = 0.175 lb/min.

8.5 SUMMARY

This chapter deals with the diffusional transfer of mass to and across a phase boundary. In particular, gas-liquid, gas-solid, and liquid-liquid phase combinations have been considered. Process applications include absorption, stripping, distillation, extraction, adsorption, and the diffusional aspects of chemical reactions on a solid surface. For steady-state transfer operations, the rates of mass transfer can be correlated by variations of Fick's first law, which states that the rate is directly proportional to the concentration driving force and the extent of interfacial area, and inversely proportional to the distance of movement of the mass to the interface.

To make Fick's law tractable for engineering calculations, several theories, or models, have been discussed. Their application usually introduces some empiricism, since distance of diffusion and extent of interfacial area are usually indeterminate. For most calculations, the time-tested film model is appropriate, not because it represents with validity the physical situation, but rather because it is supported by a wealth of experience as well as the ready availability of data, particularly molecular diffusion coefficients. The penetration and surface-renewal models have specialized applications and also depend on empirically derived parameters.

Not all possible applications of mass transfer theory have been discussed, and multicomponent systems have been treated as pseudo binary or ternary systems. To delve deeper, the reader should consult specialized books, some of which are listed in the References section.

NOMENCLATURE

a	interfacial area, s^{-1}
c_m	mean concentration, g-moles/cm^3
C	concentration, g-moles/cm^3
C_m	average total concentration, g-moles/cm^3
D	molecular diffusion coefficient of gas, cm^2/s
D^L	molecular diffusion coefficient, liquid phase, cm^2/s
D^{LO}	molecular diffusion coefficient of liquid at infinite dilution, cm^2/s
H	Henry's law coefficient, p/x or y/C
i	diffusing species i
j	diffusing species j
J	diffusion flux for unidirectional transfer, g-moles/s-cm^2
k	diffusing species k
k	Boltzmann constant, Equation (8.3)
K	overall mass transfer coefficient

REFERENCES

1. Taylor, R., and Krishna, R. *Multicomponent Mass Transfer*. New York: John Wiley, 1993.
2. Perry, R. H., and Green, D. W. *Perry's Chemical Engineers' Handbook*, 7th ed., 328–332. New York: McGraw-Hill, 1997.
3. Fuller, E. N., Schettler, P. D., and Giddings, J. C. *Ind. Eng. Chem.* 58 (1996): (5) 19.
4. Hirschfelder, J. O., Bird, R. B., and Spotz, E. L. *Chem. Rev.* 44 (1949): 205.
5. Brokaw, R. S. *Ind. Eng. Chem. Proc. Des. Devel.* 8 (1969): 240.
6. Reid, R. C., Prausnitz, J. M., and Sherwood, T. K., *The Properties of Gases and Liquids*, 3rd ed., 554. New York: McGraw-Hill, 1977.
7. Wilke, C. R., and Chang, P. *AIChE J.* 1 (1955): 264.
8. Vignes, A. *Ind. Eng. Chem. Fundam.* 5 (1966): 189.
9. Sitaraman, R., Ibrahim, S. H., and Kuloor, N. R. *J. Chem. Eng. Data* 8 (1963): 198.
10. Wilke, C. R. *Chem. Eng. Prog.* 45 (1949): 218.
11. Gmehling, J., Onken, U., and Arlt, W. *Vapor-Liquid Equilibrium Data Collection*. Frankfurt/Main, Germany: Dechema, 1977.
12. Alvarez-Trevit, J. A. "Steam Regeneration of Activated Carbon Adsorbents," Ph.D. diss., The University of Texas at Austin, 1995.
13. Fair, J. R. *Chem. Proc.* 52 (1989): (10) 81.
14. Sherwood, T. K., Pigford, R. L., and Wilke, C. R. *Mass Transfer*. New York: McGraw-Hill, 1975.
15. Hines, A. L., and Maddox, R. N. *Mass Transfer—Fundamentals and Applications*, 20–25. Englewood Cliffs, NJ: Prentice-Hall, 1985.
16. Whitman, W. G., *Chem. Met. Eng.* 29 (1923): 146.
17. Higbie, R., *Trans. AIChE* 31 (1935): 365.
18. Danckwerts, P. V. *Ind. Eng. Chem.* 43 (1951): 1460.
19. Lewis, W. K., and Whitman, W. G. *Ind. Eng. Chem.* 16 (1924): 1215.
20. Seibert, A. F., and Fair, J. R. *Ind. Eng. Chem. Res.* 27 (1988): 470.
21. Mackay, D., and Matsu, R. S. *Can. J. Chem. Eng.* 51(1973): 433.
22. Peress, J. *Chem. Eng. Prog.* 99 (2003): (4) 32.

9.6	Solid-Liquid Mixing	653
9.6.1	Introduction	653
9.6.2	Settling Solids	653
9.6.3	Particle Suspension in Stirred Vessels	655
9.6.4	Just-Suspended Conditions	656
9.6.5	Floating Solids.....	657
9.6.6	Uniform Solids Concentrations.....	657
9.6.7	Power Requirements.....	659
9.6.8	Equipment.....	659
9.6.9	Solids Suspension by Jet Mixing.....	660
9.7	Gas-Liquid Mixing	660
9.7.1	Introduction and Scope	660
9.7.2	Mass Transfer—General	661
9.7.3	Equipment and Its Function.....	662
9.7.4	Impeller Characteristics in Gas-Liquid Mixing.....	663
9.7.5	Mass Transfer and Gas Holdup	666
9.7.6	Gas Residence Time.....	668
9.7.7	Scale-Up	669
9.8	Immiscible Liquid-Liquid Mixing	671
9.8.1	Introduction	671
9.8.2	Characterization of Immiscible Liquid-Liquid Systems	671
9.8.3	Drop Sizes	672
9.8.4	Dispersion of Drops, Laminar Flow, and Low Viscosity.....	673
9.8.5	Dispersion of Low-Viscosity (Inviscid) Drops ($\mu < 0.020$ Pa·s) Turbulent Flow	674
9.8.6	Dispersion of Higher-Viscosity Drops ($\mu > 0.02$ Pa·s) Turbulent Flow	676
9.8.7	Time for Dispersion	677
9.8.8	Coalescence of Suspended Drops	677
9.8.9	Population-Balance Methods	678
9.8.10	Creating a Dispersion—Maintaining Drop Suspension	678
9.8.11	Simultaneous Suspension, Dispersion, and Coalescence	680
9.8.12	Equipment Used for Liquid-Liquid Mixing	681
9.8.13	Processes.....	681
9.9	Static In-Line Mixers	682
9.9.1	Introduction to In-Line Static Mixers.....	682
9.9.2	Hydrodynamics and Other Characteristics of Mixing in Static Mixers.....	683
9.9.3	Static Mixer Selection and Design Issues	684
9.9.4	Reynolds Number and Flow Regime.....	685
9.9.5	Component Flow and Viscosity Ratios.....	686
9.9.6	Variation Coefficient in Blending Applications.....	687
9.9.7	Dispersed-Phase Size Distribution in Liquid-Liquid and Gas-Liquid Systems.....	688
9.9.8	Interfacial Areas for Gas-Liquid Systems	690
9.9.9	Mass-Transfer Coefficients for Gas-Liquid Dispersions	690
9.9.10	Heat-Transfer Enhancement in Laminar Flow Applications.....	691
9.9.11	Pressure Drop and Power Requirements	691
9.9.12	Mixing Efficiency.....	692
9.9.13	Injection Considerations and Designs	693
9.9.14	Pump Selection and Flow Control.....	693
9.10	Jet Mixing.....	694
9.10.1	Introduction	694
9.10.2	Principles	694

to an improved performance. In cases where reaction rates are very fast, such as in reaction injection molding (RIM), impinging jet mixers create the rapid mixing needed for producing high-quality products. Mixing helps promote desirable rates of polymer chain growth for polymerizations. Many exothermic reactions, such as nitration and emulsion polymerization reactions, are operated by continuous reagent/feed addition. Such processes require rapid mixing to avoid local segregation that could lead to undesirable side reactions. Neutralization reactions often form solid precipitates. Conditions of locally high supersaturation, due to inadequate mixing, lead to the formation of hard-to-filter fine particles. This can be prevented by introducing reagents to the impeller region, where local mixing rates are fast.

For two-phase systems, mixing promotes faster mass transfer by creating higher interfacial area due to smaller bubbles or drops. Turbulence also helps reduce the boundary-layer resistance around drop or bubble surfaces, leading to faster mass transfer.

For solid-liquid systems, agitation provides solids suspension, either by maintaining movement at the bottom of a vessel, or by maintaining a desired level of uniformity throughout the vessel.

Agitation is required for blending, where the process objective is to promote homogenization of a fluid to a desired degree of uniformity, often in a specified time. The rate of approach to uniformity is an exponential process. Complete uniformity takes a very long time. In practice, one sets specifications to typically 95 or 99% uniformity, based on the process requirements.

The subjects discussed in this chapter are described more fully in the *Handbook of Industrial Mixing* [1].

9.1.3 EQUIPMENT AND DESIGN

It is important to match mixing equipment capabilities with process requirements. While it is desirable to have an optimum design and operating conditions for every step in the process sequence, it is seldom practical to do so. For example, specialty and pharmaceutical processes require the use of multipurpose reactors. An important consideration is to understand how less-than-ideal equipment will function in all stages of operation.

Documenting mixing performance data is vital to future troubleshooting. During the life of the equipment, modifications of both processes and equipment are common. For example, increased production requirements could lead to higher process concentrations and viscosity. Under such conditions, mixing may become inadequate, leading to regions of stagnation. Documented performance conditions for the original process are useful for diagnosing how the process responds to new conditions. A simple design or operational change can often meet the new challenge.

Mixing intensities vary greatly throughout a stirred vessel. While turbulent mixing can exist in the impeller region, transitional or laminar-flow conditions can exist elsewhere. Energy dissipation near the impeller is 40–50 times greater than in other regions (see Zhou and Kresta [2]). Common practice introduces feed to the surface of the liquid. While this avoids plugging problems and feed-pipe stagnation, it places the feed in a weakly mixed region.

Computational fluid dynamics or CFD (also known as computational fluid mixing, CFM) was introduced to the chemical process industries in the late 1980s. CFD/CFM is a numerical technique for solving fluid relationships such as conservation, transport, and the Navier-Stokes equations. Commercial CFD software enables one to predict the effects that geometry, feed location, physical properties, and operating conditions have on conditions in the vessel. Typical results predict velocity profiles, rates of energy dissipation, concentrations, and flow streamlines as they would occur in the vessel. This tool enables one to appreciate the good and bad features for each considered design. CFD simulations are based on assumptions. Some are low risk, but some impose high risk. Experimental validation is important particularly for nontrivial applications. Validation is advisable. Published velocity profile data can often help to validate results. At the time of this writing, CFD is weak in its ability to model large-scale turbulence and multiphase flow.

9.2.2 COMMON DIMENSIONLESS GROUPS USED IN MIXING CORRELATIONS

Name	Symbols	Significance
Reynolds number	$Re = D^2 N \rho / \mu$	Ratio of inertial to viscous stress; defines turbulent, transitional, and laminar-flow regimes; a correlating parameter for flow-sensitive terms in mixing
Power number	$Np = P / \rho N^3 D^5$	A function of the impeller Reynolds number and impeller type; Np is constant at $Re > 10^4$; increases with decreasing Re in the laminar region
Flow number	$Nq = Q / ND^3$	Ratio of actual impeller flow to an idealized flow
Fourier number	$Fo = \mu \theta / \rho T^2$	Used to correlate mixing times; also referred to as the vessel Reynolds number
Gas flow number	$Fl_G = Q / ND^3$	Ratio of gas to idealized liquid flow
Dämköhler number	$Da = \tau_M / \tau_R$ $Da = k_2 c_{BO} / E$	Ratio of mixing time to reaction time Half life of a reaction to the rate of engulfment
Capillary number	$Ca = \tau \cdot r_D / \sigma$	Ratio of fluid stress on a drop to its interfacial resistance
Froude number	$Fr = N^2 D / g$	Ratio of centrifugal to gravity forces; used for vortex definition and in gas-liquid mixing correlations
Nusselt number	$Nu = hD / k$	Used with Re and Pr to correlate heat-transfer data
Prandtl number	$Pr = c_p \mu / k$	Ratio of convective to conductive heat transfer
Weber number	$We = N^2 D^3 \rho / \sigma$	Ratio of inertia to surface/interfacial forces for gas-liquid and immiscible L-L systems; used to correlate bubble/drop size

9.2.3 SIGNIFICANCE OF COMMONLY USED MIXING TERMS

Power Number, Np : The power number, Np , sometimes referred to as Po , is a measure of the relative drag of the impeller. Streamline curved blades, like hydrofoils and retreat-curve impellers, have less drag than flat blades; consequently, their power numbers are lower than those for flat-blade impellers. Power numbers of some of the more popular impellers are given in Table 9.1. The calculation of power from impeller diameter, speed, and liquid density is given by Equation (9.1).

Flow Number, Nq : The magnitude of the flow number is a measure of an impeller's ability to produce flow. The larger the flow number, the greater is the flow. The total impeller flow consists of the direct discharge flow plus entrained flow. Most reported flow numbers include both flows. Equation (9.3) shows the use of Nq in calculating the total discharge flow.

Mixing time, θ_M : Mixing time, θ_M , is the time it takes to mix initially segregated materials to a specified degree of uniformity. For example, it takes 60% longer to mix to 99% uniformity than to mix to only 95%. Mixing times can be calculated from the methods described in Section 9.4. For certain reactions, it is important to have mixing times shorter than reaction times. The Dämköhler number, Da , is the ratio of mixing to reaction times and is further described in Section 9.5.

Impeller Reynolds number, Re , N_{Re} , and vessel Reynolds number, Re : The impeller and vessel Reynolds numbers are the ratios of inertia to viscous forces. They are indicators of flow conditions: turbulent, laminar, or transitional. They are used to correlate other quantities such as the power number, Figure 9.1, and the inside heat-transfer coefficients shown by Equation (9.85).

Micro-Mixing: Micro-mixing is the smallest scale of mixing. In terms of dimensions, it is at or below the Kolmogoroff microscale that can be calculated by Equation (9.9). Micro-

TABLE 9.1 (Continued)
Characteristics of Commonly Used Impellers

Model	Flow Pattern	No. of Blades	Features	Np	Nq	Supplier
R-500	Weak radial	many	Very high shear, effective in dissolving polymers, forming solutions; removes boundary-layer resistance	0.17–0.3	...	Lightnin
Curved Blade turbine	Highly radial	6	Lower shear rate than straight blade; not commonly used today	3.91	0.82	Various
Propeller 1.5/1.0 Pitch	Strong axial	3	Efficient, costly, heavy compared with HE-3 and A-310	0.87/0.35	0.77/0.44	Various
Curved Blade Turbine	Radial	4	Good pumping due to broad blades; a glassed steel impeller	1.7–1.4	0.54	Pfaudler
Retreat-curve impeller (RCI)	Radial	3	Used with glass-lined equipment; usually at bottom of vessel and with large D/T ratios; effective general-purpose impeller; can be used for limited gas dispersion, with good baffling	0.5–0.3	0.24	Pfaudler
Vertical-blade turbine	Radial	2 + 2	Similar to vertical pitch flat-blade design; glassed steel, overlapping hub design	2.7	0.65	DeDietrich Tycon Pfaudler
Turbofoil	Axial	4	A glassed hydrofoil, similar to HE-3 or A-310, except has four blades	0.4–0.3	0.48	Pfaudler

9.3.2 POWER

Figure 9.1 is a log-log plot of the power number, N_p , vs. the Reynolds number for several impellers in a fully baffled vessel. A few important features are noted here:

- In the laminar region ($1 \leq Re \leq 10$), the power number decreases linearly with increasing Reynolds number.
- In the transition region ($10 \leq Re \leq 10,000$), the power number decreases more gradually, and for some impellers, it then begins to increase, while for others, it continues to decrease with increasing Reynolds number.
- In the fully turbulent region ($Re \geq 10,000$), power numbers are constant, but design dependent.

There is a different power number for each impeller, reflecting its unique shape and drag-producing characteristics. The power number values given in Table 9.1 are only applicable for turbulent flow. Manufacturers offer a variety of impellers, the characteristics of which are given in Table 9.1.

The power requirement for a single impeller operating in a baffled vessel can be calculated from

$$P = N_p \cdot \rho \cdot N^3 D^5 \quad (9.1)$$

In English units, Equation (9.1) becomes

$$HP = P_o \cdot \rho \left(lb \cdot ft^{-3} \right) \cdot N^3 \left(s^{-1} \right) \cdot D \left(ft \right) / 32.2 \left(ft \cdot s^{-2} \right) \cdot 550 \left(ft \cdot lb \cdot hr^{-1} \right) \quad (9.1a)$$

In metric units, Equation (9.1) becomes

$$kW = N_p \cdot \rho \left(kg \cdot m^{-3} \right) \cdot N^3 \left(s^{-1} \right) \cdot D^5 \left(m \right) / 1,000 \quad (9.1b)$$

In practice, the Reynolds number must first be determined to obtain the power number. The impeller Reynolds number is defined for stirred vessels and given by

$$Re = \frac{D^2 N \rho}{\mu} \quad (9.2)$$

Example 9.1

Determine the power needed to agitate a fluid using a Rushton impeller, given the specific gravity of the liquid is 1.0, the tank diameter is 3.0 m, the height of liquid is 3.0 m, the impeller diameter is 1.0 m, the speed is 1.0 s^{-1} , and the liquid viscosity is 1.0 cP .

Solution

Substituting the Reynolds number in Equation (9.2), $Re = (1.0^2)(1)(1,000)/0.001 = 10^6$. Flow is therefore fully turbulent. The power number for a Rushton impeller, the top curve in Figure 9.1, is $N_p = 5.0$. The density = 1000 kg/m^3 , and the power is

$$P_{\text{Rushton}} = 5.0(1000)(1.0^3)(1.0^5)/1000 = 5.0 \text{ kW}$$

9.3.4 FLOW DISCHARGE

The discharge flow rate from most impellers is expressed in terms of the flow number N_q . Values are given in Table 9.1. The flow number, Nq , is defined by

$$Nq = \frac{Q}{ND^3} \quad (9.3)$$

where Q represents the total flow (direct + entrained) in m^3/s (ft^3/s), N is the speed in s^{-1} , and D is the impeller diameter in m (ft).

Flow rate calculations can be used to estimate the mean circulation time, τ_c , of fluid in the vessel. It is the liquid volume divided by the impeller flow rate. A rule of thumb is that the approximate mixing time, τ_M , is three to four times the mean circulation time, τ_c .

The flow rate resulting from complementing dual impellers is not significantly greater than for a single impeller. The performance improvement comes from better flow distribution. The mean circulation time is the time a particle takes to complete a circuit in the vessel. Every vessel has a distribution of circulation times. Multiple impellers reduce the circulation time distribution (see Section 9.4).

Figure 9.3 shows many of the impellers listed in Table 9.1.

9.3.5 BAFFLES

Baffles are used to convert tangential to axial flow and are required for all stirred-tank turbulent-flow applications. They are optional for transitional-flow conditions ($10 \leq \text{Re} \leq 10,000$) and should never be used for laminar-flow applications. Within the transitional-flow range, a good rule of thumb is to use some baffling for $300 \leq \text{Re} \leq 1000$ but not below 300. Baffles are required for most low-viscosity, multiphase applications.

The standard fully baffled vessel consists of four equally spaced vertical plates, T/12 to T/10 wide, and set away from the wall a distance of T/72 to T/90. Baffle lengths extend from near the liquid surface to the bottom of the straight wall. Baffles reaching the surface create eddies, which are helpful for engulfing addition streams or floating solids. Surface eddies also lead to incorporation of headspace gases, which sometimes need to be prevented. Short baffles located in the impeller region can substitute for full-length designs. Baffles used with glass-lined equipment include the beavertail, finger, "h," "d," and fin baffles. These are shown in Figure 9.4. One or two of these baffles are normally suspended from top openings on the vessel. Care must be taken to avoid excessive drag and fluctuating loads that could damage the glass lining of the support nozzle.

The demand for instrumentation, feed inlets, vent lines, relief systems, and inspection ports places a heavy demand on nozzle availability for baffles. Baffling often becomes secondary to these other process needs. While two baffles generally improve mixing rates by as much as 20% over single baffles, surprisingly good mixing can be achieved with one "h," "d," or fin-type baffle. The baffles shown in Figure 9.4 usually come equipped with temperature-sensing provisions. The degree of baffling can be varied by changing the baffle angle relative to flow, thus creating a variable flow resistance. Less conventional baffle designs include 90° angle-shaped baffles welded to the vessel walls.

Short top-entering baffles located at a distance $2/3R$ and extending to mid-depth convert angular to axial momentum; their submergence affects mixing. The optimum depth for suspended baffles is from $1/3$ to $2/3$ of the total liquid depth. Deeper penetration suppresses overall momentum and results in poorer mixing. Shallower penetration fails to convert enough tangential to axial momentum. Applications requiring changing liquid levels or operation at low liquid levels are often equipped with one deep and one shallow baffle. Similar arguments also hold for wall-attached baffles.

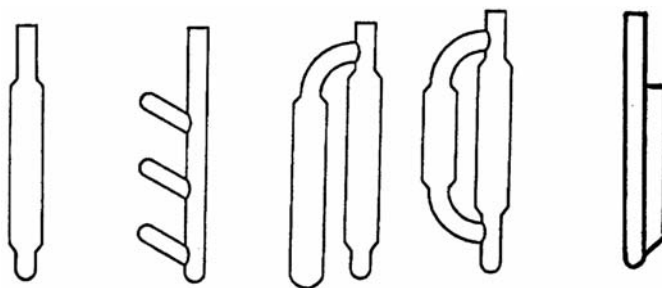


FIGURE 9.4 Baffles used in glass steel vessels (L-R): flattened pipe (Beavertail), finger, “h,” “d,” and fin.

9.3.6 VESSEL SHAPE

The optimal vessel design is a dish-bottom tank having an H/T of approximately 1.2. Flat-bottom tanks, particularly larger storage vessels, can be used for simple mixing applications, but the flat-bottom tank is prone to develop dead zones in the corners. Also, the flat bottom is not conducive to redirecting the flow upward. Similarly, cone-bottom tanks should be avoided except for certain solids applications. Tall, slender vessels are used to increase gas residence time and to reduce wall thickness of pressure vessels. A major disadvantage is that tall vessels require long shafts requiring larger shaft diameters or use of steady bearings. Good circulation can be a problem for these designs. Draft tubes can promote good circulation, but require a constant level in the tank. Single impellers can be effectively used, coupled with optimum baffling, to provide good mixing in tanks up to 2:1 H/T . Harvey [4] shows that multiple different-size 45° PBTs can be optimized to improve mixing in transitional flow fluid applications.

9.3.7 MECHANICAL CONSIDERATIONS

The torque required of a mixer is

$$\text{torque} (N \cdot m) = \frac{P (kW) \cdot 10^3}{2\pi N (s^{-1})} \quad (9.4a)$$

$$\text{torque} (in \cdot lb) = \frac{63,000 \cdot (HP)}{N (min^{-1})} \quad (9.4b)$$

The head developed by an impeller is

$$\text{head} \propto \frac{P}{Q} \quad (9.5)$$

where the head is in N/m^2 (lb/ft^2), P is in $N \cdot m/s$ ($ft \cdot lb/min$), and Q (the impeller discharge flow) is in m^3/s (ft^3/min).

Impeller size (D/T ratio) influences whether flow or turbulence governs the process of mixing. Oldshue [5] shows, for equal process results, that impeller diameter affects power and torque characteristics, as shown in Figure 9.5. The values for power and torque are normalized to the values for an impeller with $D/T = 0.333$.

D/T ratios can be in the range of 0.2 to 0.7, but commonly they are 0.3 to 0.5. At equal power, large impellers rotate more slowly and require large gearboxes compared with smaller impellers.

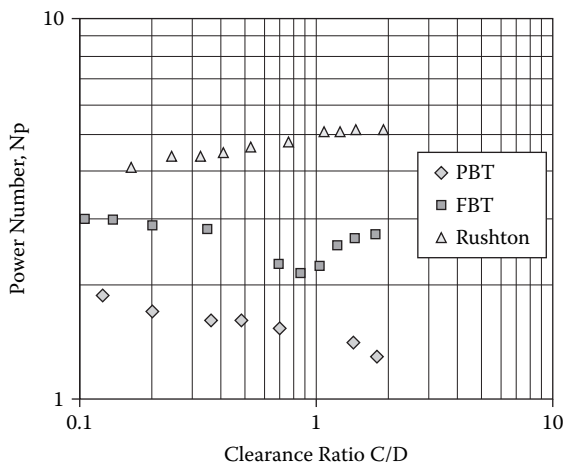


FIGURE 9.6 Effect of clearance on power. (From Bates et al., 1963).

9.4 BLENDING

9.4.1 INTRODUCTION AND SCOPE

Blending is the mixing of different, but miscible, fluids. The topics that are discussed in this section include: fluid properties (rheology), mixing mechanisms, equipment used, and the energy required to mix to a certain degree of uniformity in a given time. This section emphasizes the stirred tank, but blending is also done in static mixers and by jet mixing. These topics are discussed in Sections 9.9 and 9.10 in this chapter. The kinetics of blending is discussed as well as how blend time is related to design, impeller selection, and operation.

The fluid viscosity is one of the primary considerations when selecting an impeller. Turbine-type impellers are used for fluid viscosity of up to 50,000 cP. Smaller diameter turbines are used for low-viscosity fluids; larger ones for higher viscosity applications. Beyond 50,000 cP, the helical ribbon impeller, screw/draft tube designs, gate types, paddles, and anchors are used. While gates, paddles, and anchors are considerably less expensive than the helical ribbon or screw/draft tube designs, they are less able to produce good top-to-bottom flow, essential for good mixing.

9.4.2 TURBULENT, TRANSITIONAL, AND LAMINAR FLOW BLENDING

Blending is all about creating a specified degree of homogeneity from initially segregated materials in a given time. The *degree of mixing* is a term used to describe the quality of the result. For example, θ_{95} refers to the time it takes to reach 95% uniformity, and θ_{99} the time to reach 99% uniformity. Higher degrees of uniformity require longer mixing times. An example is given later in this section.

Turbulent and laminar mixing are quite different. Turbulent mixing takes place by three mechanisms: turbulent eddy motion, bulk or convective flow, and molecular diffusion. Laminar flow has no eddies to assist in mixing. Laminar mixing first depends on creating very thin layers between initially unmixed components, followed by molecular diffusion.

Efficient laminar mixing requires that very thin layers of fluid be well distributed throughout the vessel. Laminar mixing is slow and can take orders of magnitude longer to reach an equivalent state of uniformity than turbulent mixing.

In designing blending systems, it is important to establish whether conditions will be turbulent, transitional, or laminar. Turbulent mixing occurs at impeller Reynolds numbers greater than 10^4 .

TABLE 9.2
Constants in the Metzner-Otto Equation

Impeller Type	Mean Shear Rate Constant, K
Propeller	10
Rushton turbine	12
Flat-blade turbine	12
Pitch-blade turbine	12
Anchor	25
Helical ribbon	30

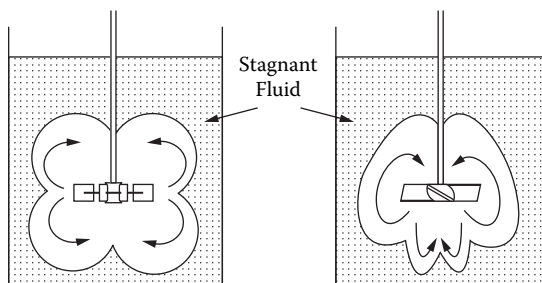


FIGURE 9.8 Shape of cavity in a shear-thinning suspension. (From Wichterle et al., 1981.)

Recent advances in commercial CFD software have enabled this problem to be modeled. The diameter and height of caverns have been correlated:

$$\left(\frac{D_c}{D}\right)^3 = N_p \cdot \left(\frac{\rho \cdot N^2 D^2}{\tau_y \pi^2 \left(1/3 + H_c/D_c\right)}\right) \quad (9.8)$$

where D_c and H_c are the cavern diameter and height and τ_y is the yield stress. The value of H_c/D_c for a Rushton turbine was found to be 0.4 [9].

Example 9.2

Calculate the impeller Reynolds number for a power-law fluid with $k = 1.5$ poise, $n = 0.7$, and density = 1000 kg/m³. Assume the vessel diameter is 2 m, and the impeller, a 45° PBT, is 0.7 m in diameter. The operating speed is 90 rpm. Determine the nature of flow.

Solution

The mean shear rate constant K , for a 45° PBT, from Table 9.2 is 12. The mean shear rate at 90 rpm is $12 (90/60) = 18 \text{ s}^{-1}$. The viscosity is defined as the shear stress/shear rate and is $\mu = k\gamma^{(n-1)}$ for a power-law fluid. For the problem at hand, this becomes $1.5 (18)^{-0.3} = 0.630$ poise (0.063 kg/m·s). The Reynolds number is $0.7^2 (90/60) 1000/0.063 = 11,666$. The flow is fully turbulent in this example.

9.4.3 THE NATURE OF TURBULENT FLOW

Large eddies are produced when an impeller passes through a low-viscosity liquid. These eddies are close to the impeller tip and are similar in size to the blade width. Figure 9.9 shows the energy $E(k)$ as a continuous function of wave number (k), along with terms commonly used in turbulent mixing. Large eddies depend on how the turbulence is generated. Smaller eddies do not. Eddy size,

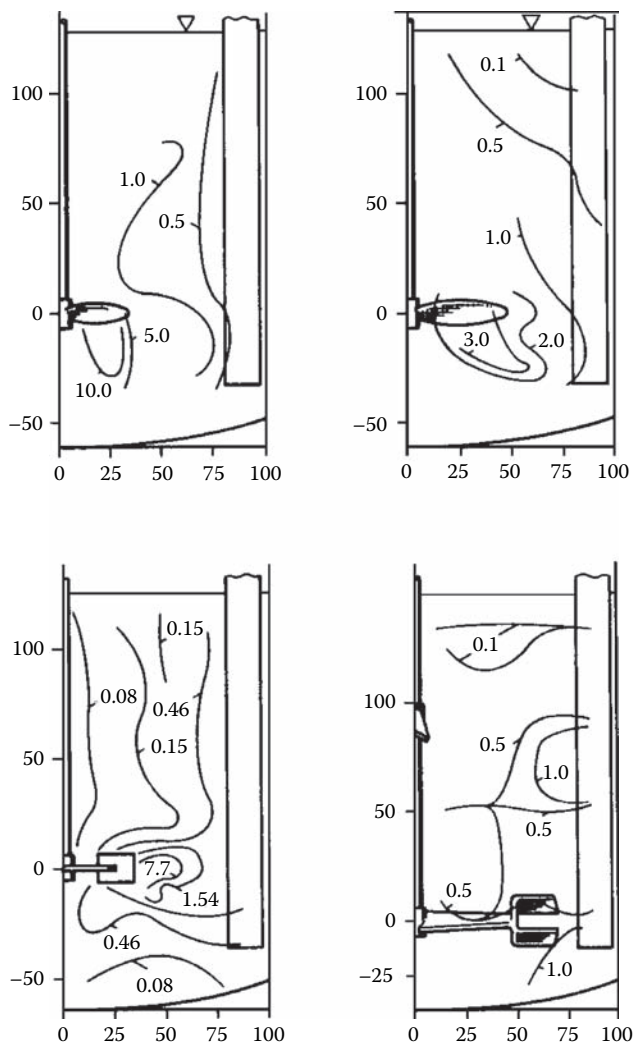


FIGURE 9.10 Energy contours for different impellers (L-R): (top) small propeller, large propeller; (bottom): Rushton turbine, Ekato-MIG. (From Todtenhaupt et al., 1991.)

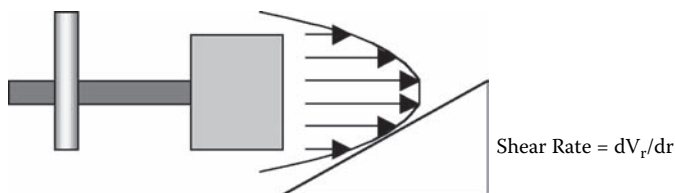


FIGURE 9.11 Typical velocity profile of the discharge flow from a disc turbine.

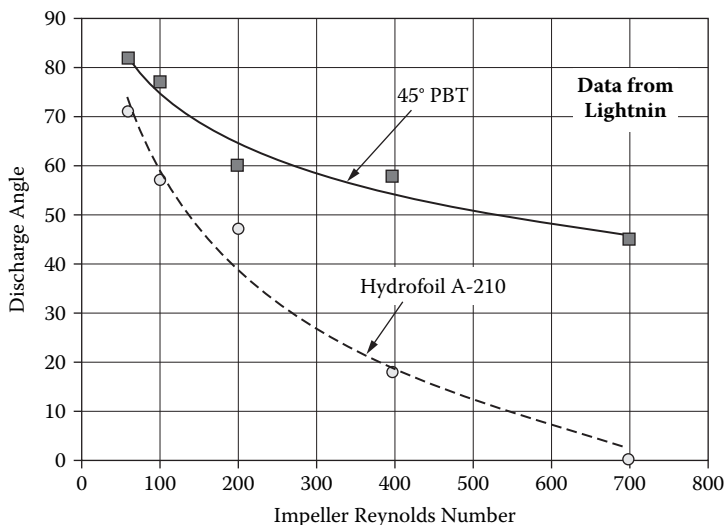


FIGURE 9.13 Flow discharge angles for two Lightnin viscous flow impellers.

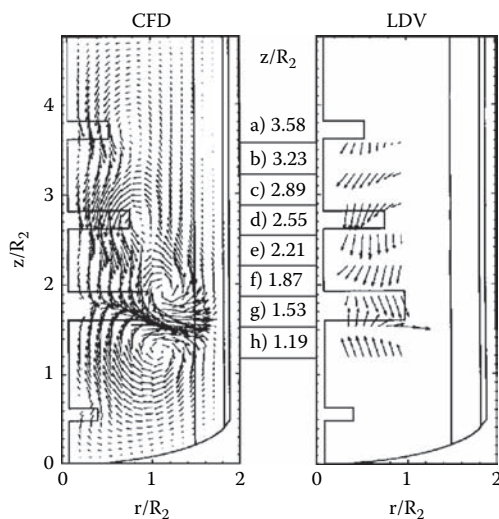


FIGURE 9.14 Experimental and CFD modeling of a series of 45° PBTs for fluids in the transition region. (From Harvey et al., 1997.)

details are usually lacking. For example, the effects of multiple impellers, clearance, spacing, and baffle design on mixing time are not well known, but the effects of speed, impeller diameter, and impeller type are better understood.

Many investigators have found that, under turbulent conditions, mixing is complete after three to four turnovers. This is shown schematically in Figure 9.15.

The mean circulation time (assuming the turbulent flow discharge, Q , from an impeller is $Q = N_q N D^3$, the tank shape is $T = H$, its volume is V_R , and D/T is constant) is

$$\theta_c = \frac{V_R}{Q} \propto \frac{T^3}{N_q N D^3} \quad (9.10)$$

These equations enable one to calculate θ_{95} , or the time to mix to 95% completion. If more uniformity is desired, for example, 99% complete, it will require 1.6 times longer, as shown by

$$\frac{\theta_{99}}{\theta_{95}} = \frac{\ln(0.01)}{\ln(0.05)} = 1.6 \quad (9.16)$$

There are some interesting conclusions from this work. At equal power input and impeller diameter D , mixing time is impeller independent. Impellers with a low power number, such as A-310 or HE-3, must operate at higher speeds to attain comparable power to a higher-power-number impeller. Higher speeds mean lower torque and a smaller, less costly design.

Example 9.3

Addition polymerization requires that monomer groups be added to a core polymer containing reactive ends. If the chain ends see low monomer concentration, end groups will be short; but if locally high concentrations are encountered, end groups will be long. Quality considerations demand uniformity of chain length of the end groups. Rapid monomer mixing is essential. Kinetic studies showed the half-life of the addition reaction to be ≈ 5.0 minutes. The pre-polymer is dissolved in a solvent, the viscosity at the operating conditions is 1000 cP, and fluid behavior is Newtonian. The reactor is 6 ft in diameter \times 8 ft high, with top and bottom elliptical heads. The active average volume is 1160 gal. The viscosity remains constant during end-group addition. Design a mixing system to give 99% complete mixing in 1.0 min, or at 20% of the reaction half-life.

Solution

Equations (9.11) to (9.13) must be solved iteratively. An equation solver (or spreadsheet) provides a convenient way to do this. First, a Lightnin A-320 impeller is selected. (A 45° PBT could also have been a reasonable first choice.) Choose $D = 28$ in. so that $D/T \approx 0.4$. The height of liquid is 72 in. and the volume including the elliptical head is 1162 USG. A single impeller is selected, since the H/T is 1.0. Assume a speed; determine the Re and the crossover point for transitional flow (Equation (9.15)) and the mixing time θ_{99} . The trial-and-error solution using a spreadsheet is shown in Table 9.3.

We are mainly interested in numbers in the last (eighth) column. A speed of 145 rpm was selected to give a 99% mixing time (valid for the transitional region) in just under a minute. Had the Reynolds number been higher than values in the sixth column, the correlation for turbulent flow (column 7) would have been used. The power requirement is 2.58 hp. The volumetric based power is 2.22 hp/1000 gal.

TABLE 9.3
Solution to Problem 3

Speed (rpm)	HP	HP/1000 gal	Re	Re Trans	θ_{95} (min) Turb	θ_{95} (min) Trans	θ_{99} (min) Trans
100	0.85	0.73	843	6719	0.38	1.26	2.01
110	1.13	0.97	927	6736	0.34	1.05	1.67
120	1.46	1.26	1011	6782	0.32	0.88	1.41
130	1.86	1.60	1095	6764	0.29	0.76	1.21
140	2.32	2.00	1180	6776	0.27	0.65	1.05
145	2.58	2.22	1222	6781	0.26	0.61	0.98

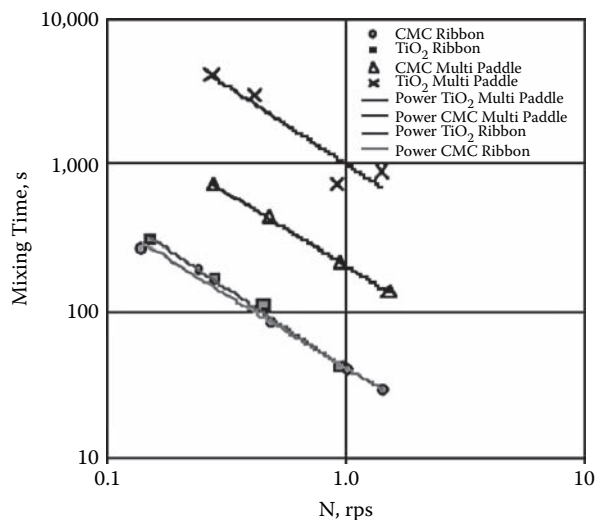


FIGURE 9.16 Comparison of the mixing time for ribbon and multistage paddle in non-Newtonian liquids. (From Nagata, 1975.)

9.5.1 INTRODUCTION

The challenges of mixing of fluids during reaction are important for fast reactions in homogeneous systems as well as for all multiphase systems. There are two issues involved: degree of segregation and timing. The degree of segregation refers to whether mixing occurs on the microscopic level (mixing at the molecular level in the limit) or the macroscopic level (mixing of clumps or globs of fluid). The second issue refers to how fast or slow is the change in the degree of segregation from the initial (feed) state to the final (exit) state, i.e., whether the macrofluid (glob of fluid) reaches its ultimate size early or late as it flows through the reactor. Since both macro-mixing and micro-mixing vary with reactor size, the following three undesirable effects are typically observed upon scale-up of mixing sensitive reaction systems:

1. Reduced reaction rates and conversion
2. Reduced selectivity
3. Reduced product quality (increased impurity levels)

Since mixing is very efficient on a laboratory scale, the detrimental effects of mixing observed on larger scales generally come as an unwanted surprise.

9.5.2 FUNDAMENTAL CONCEPTS IN REACTIVE MIXING

When two miscible reactant fluids A and B are mixed, it is normally assumed that the two streams first form a homogeneous mixture that then reacts. This is true if, and only if, the chemical reaction is slower (say requiring more than 100–400 s) than the mixing time (typically 0.1 s to 50 s in a well-designed turbulent reactor). Mixing time is strongly dependent on scale. When the half-lives of the two processes are similar in magnitude, or when mixing is slower than reaction, mixing and reaction proceed simultaneously, not consecutively. Reaction occurs in localized zones. As the intrinsic reaction rate increases, the sizes of the reaction zones shrink to a plane. Only a small part of the reactor volume is used for reaction. For example, in any proton transfer reactions in aqueous phase (half-life of less than a millionth of a second), the reaction takes place in a very small volume,

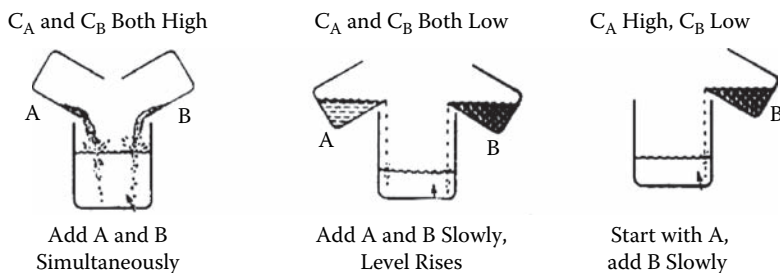


FIGURE 9.17 Contacting patterns for various combinations of high and low concentrations of reactants in noncontinuous operations. (From Levenspiel, 1972.)

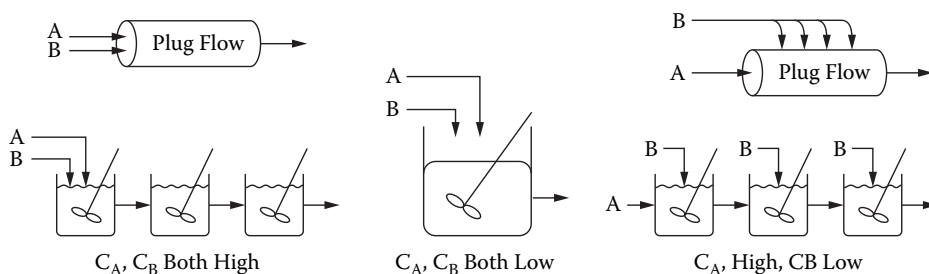


FIGURE 9.18 Contacting patterns for various combinations of high and low concentration of reactants in continuous flow operations. (From Levenspiel, 1972.)

a semi-batch mode of operation. At other times, safety considerations may require very little buildup of a potentially dangerous intermediate.

If kinetics are known for all the reactions (a rare occasion in practice), it is possible to predict the yield and selectivity in ideal reactors or their combinations. Please refer to any reaction engineering textbook for more information on this subject.

9.5.3 MACRO-MIXING AND MICRO-MIXING

Turbulence can be conceptualized as the transfer of kinetic energy from large eddies (on the order of the size of the impeller blade width) to successively smaller eddies. The smaller eddies originally in the inertial sub-range disintegrate further into the viscous sub-range, and eventually all energy is dissipated into heat. This subject is dealt with more fully in the discussion on blending in Section 9.4.

Macro-mixing is mixing that is associated with the length scales larger than the viscous sub-range. Macro-mixing is visible, a result of flow rate, fluid motion, and convection. Flow patterns, circulation cells, and back-mixing regions are macro-mixing phenomena. The residence-time distribution (RTD) is related to macro-mixing.

Micro-mixing is mixing associated at length scales in the viscous sub-range or smaller. Molecular diffusion and turbulence intensity are important micro-mixing parameters. In reality, there is no sharp distinction between these two types of mixing. The names macro- and micro-mixing are conceptualizations of processes that take place simultaneously, and on all scales. Intense micro-mixing without macro-mixing (or vice versa) does not lead to an effective mixing process.

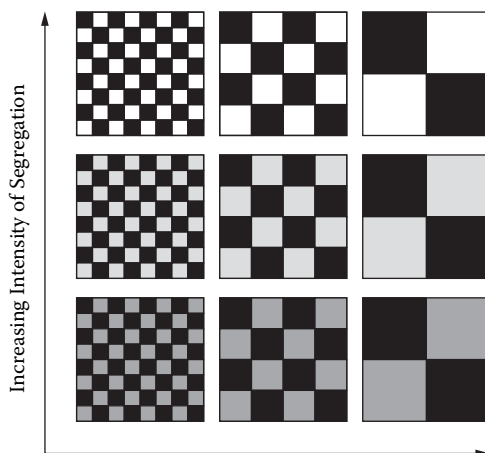


FIGURE 9.19 Scale and intensity of segregation.

9.5.5 MICRO-MIXING AND SEGREGATION

Each feed stream to a reactor usually contains only one reactant, and the large portions of fluid thus introduced must be broken down rapidly so that each reactant can be dispersed to encounter the others and react. The large turbulent eddies break down the fluid elements to successively smaller sizes until a size is reached when the inertial forces are unlikely to reduce it further, and the energy decays due to viscous action. Based on work presented in the literature [16–20], it is possible to make an estimate of the size of agglomerates.

For example, Kolmogoroff's length scale, λ_k , represents the eddy size that is associated with the boundary between the inertial and viscous subranges and is defined by

$$\lambda_k = \left(\frac{v^3}{\epsilon_T} \right)^{1/4} \quad (9.19)$$

where ϵ_T is the local energy dissipation rate expressed as power per unit mass, and v is the kinematic viscosity.

For a typical power input of 1 kW/m³ ($P/V = 5$ hp/1000 gal) with a waterlike fluid (v of 0.009 cm²/s) in a stirred reactor, λ_k is 30 μ m. Note that this is the scale at which molecular diffusion dominates, and a 30- μ m (micron) diameter sphere still contains 4×10^{14} molecules of water!

The *scale of segregation* effectively measures the size of unmixed regions. As mixing proceeds, the scale of segregation is reduced, due to liquid motion.

The *intensity of segregation* measures the concentration variations in the mixture. As mixing proceeds, the intensity of segregation is reduced, due to diffusion (Figure 9.19).

Consider two limiting cases to help explain the effect of segregation on a single reaction: Feed streams containing reactants A and B are available, each first as a micro-fluid (free to mix) and then as a macro-fluid (segregation maintained) [15]. Micro-fluids A and B behave in the expected manner and reaction occurs. However, upon mixing of macro-fluids, no reaction takes place because molecules of A cannot contact molecules of B (except at the interface, which has a zero volume in this idealization). These two situations are illustrated in Figure 9.20.

9.5.6 MICRO-MIXING AND SELECTIVITY

If only a single fast (or instantaneous) reaction is involved, relatively slow mixing and state of segregation may cause a change in the apparent reaction rate (reduction in plant capacity), but no

Considering the agglomerate size to be on the order of the Kolmogoroff scale (or some other appropriate length scale), the micro-mixing time for molecular diffusion is given by

$$T_m = \lambda_k^2/D \quad (9.21)$$

where D is the molecular diffusivity. For typical waterlike fluid, the micro-mixing time falls in the range of 1 to 20 ms.

Equation (9.22) can be used to determine the reaction time for the second reaction, forming an undesirable product:

$$T_r = \frac{1}{(k_2^* B_o)} \quad (9.22)$$

where B_o is the initial or local concentration of B . It is important to remember that the local reaction rate is not given by the bulk concentration, but by the feed or local concentration.

The ratio of time constants for mixing and reaction defines the Dämköhler number or the micro-mixing modulus, a dimensionless number shown in

$$Da = \frac{k_2 \lambda_k^2 B_o}{D} \quad (9.23)$$

The dependence of X_s on the micro-mixing modulus is given in Figure 9.21 at various ratios of the two kinetics constants. The S-shaped curve for high ratio of k_1/k_2 (practically relevant for reasons stated earlier) shows that the selectivity is sensitive to micro-mixing, especially if the Dämköhler number is around 1 or greater.

Bourne and coworkers [21–23] have developed the mathematics and applied their model to predict the effects of stoichiometric ratio, startup of a semi-batch reactor, effect of volumetric feed ratio, batch vs. continuous operation, etc. They have also experimentally demonstrated the use of reaction systems with well-characterized kinetics to determine the level of micro-mixing. Thus chemical reactions can be considered as molecular probes to be used to study segregation. Other

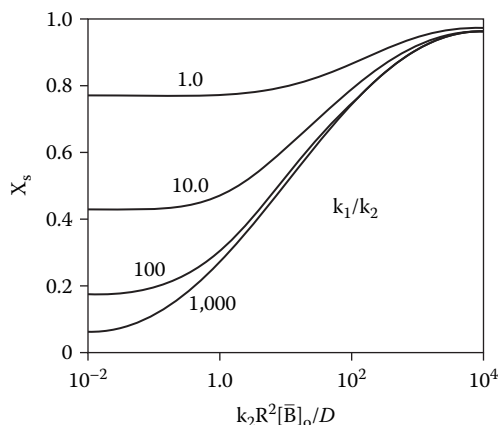


FIGURE 9.21 Influence of k_1/k_2 on product distribution from CSTR; parameter: k_1/k_2 ($a = 1$; $N_{AO} = N_{BO}$; $\tau = 100 \tau_E$). (From Baldyga et al., 1984.)

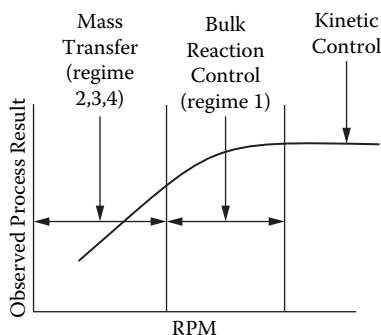


FIGURE 9.22 Effect of agitation speed on observed process rate.

the observed rate of reaction increases. However, a condition may be reached when the observed rate does not increase with increasing the rpm or mixing intensity, indicating the overall process is bulk-reaction controlled (regime 1). For the exact mathematical conditions for the various regimes, please refer to the illustrative example and the reference book [29]. Design speed should be at the minimum required to keep reaction conditions in regime 1.

Certain fast or instantaneous reactions (for example, proton transfer reactions) are always mass-transfer controlled. The enhancement factor, I , accounts for the effect of chemical reactions on mass transfer and is defined as the ratio of the process rate over the mass-transfer rate in absence of a chemical reaction.

- In regime 2, the reaction is fast enough to keep the bulk liquid phase concentration of the gaseous reactant essentially zero but not fast enough to occur substantially in the liquid film. There is no enhancement of mass transfer due to reaction. Diffusion and reaction take place in series fashion.
- In regime 3, the reaction is sufficiently fast to completely consume the gaseous reactant in the liquid film. Diffusion and reaction are occurring simultaneously in a parallel fashion in the liquid film. The true liquid-side mass-transfer coefficient has no effect on the overall process rate.
- In regime 4, the reaction is so fast (virtually instantaneous) that the gaseous reactant (A) and the liquid-phase reactant (B) cannot coexist. Diffusion of A from the interface and diffusion of B from the bulk liquid toward the reaction plane control the overall process.

There are systems that could fall between these regimes, and the division between them is not always clear-cut.

It is important to determine the regime of a particular reaction system, since the equipment choice and the effect of design and operating variables on the process performance depend on the regime. A lack of this fundamental understanding leads to many apparent discrepancies between different scales of operations and sometimes to scale-up failures. For instance, in the lab, the process may be operating in regime 1, while in production scale it could operate in regime 2. In this specific case, on the lab scale, the increasing concentration of the liquid-phase reactant increases the process rate, while on the production scale, there would be an essentially no effect. Alternatively, one may design equipment for minimal mass-transfer requirements based on the confirmation of regime 1 on lab scale only to find much lower process rates. There would be a negligible effect of partial pressure of A if the process operates in regime 4. The effect of temperature is minimal if the system is in regimes 2 and 4. It is substantial in regime 3 (apparent activation energy is half of the true activation energy) and maximum in regime 1 (apparent activation energy is equal to the true activation energy).

The feed should be introduced to the suction of the impeller, as shown in Figure 9.23 [31], to take full advantage of maximum energy dissipation to promote rapid blending of the feed. Unfortunately, it is the worst possible location for getting back-mixing into the feed pipe with potential subsequent reactions under milder turbulent conditions leading to plugging problems.

To minimize back-mixing into feed pipe and to prevent the feed jet from penetrating through the impeller zone, Fasano and Penney [31] recommend:

- For feed location above impeller: $0.09 V_t < V_f < 0.12 V_t$
- For feeding in the plane of impeller: $V_t < V_f < 40 \text{ ft/s}$

where V_t = impeller tip speed, and V_f = feed jet velocity.

Other devices are used to conduct reactive mixing. Reaction injection-molding systems (RIM) use high-energy opposing jets, each delivering a reactive component such as for polyurethane parts. Reaction rates are fast relative to diffusion. High-velocity impinging jets ensure intensive mixing for RIM applications. A typical micro-mixing Kolmogoroff scale (referred to as striation thickness in reaction injection mixing, RIM, literature) is 10 to 50 μm . Reactive mixing can also be carried out in other types of equipment, such as static mixers, coaxial pipes, tee-mixers, dynamic propeller driven in-line mixers, and rotor-stator mixers.

Static mixers (see Section 9.9) can be used for fast and instantaneous reactions involving low-viscosity fluids when high turbulence intensity and short residence time are needed. The turbulence encountered by the fluid is more uniform in static mixers than in an agitated tank. Static mixers give very good radial mixing, and the flow pattern is close to plug flow. All the fluid elements leaving the static mixer have similar residence times and have encountered essentially the identical environment (neighbor elements). The absence of back-mixing is very advantageous for consecutive competitive reaction schemes. Hence a small, well-designed static mixer can replace a large agitated tank with improved yield, lower capital costs, and lower operating costs.

The turbulent energy dissipation rate in static mixers typically varies between 100 to 1000 kW/m^3 (20 to 200 hp/1000 gal) for waterlike fluids at room temperature. Values of volumetric mass-transfer coefficients ($k_1 a$) for gas-liquid systems obtained in static mixers are 10 to 100 times higher than those obtained in agitated tanks [32, 33]. In the design of static mixers as reactors, the main variables are (a) standard mixer diameter, (b) element lengths, (c) mixer voidage, and (d) pressure drop. Turbulence intensity and hence mixer performance are strongly dependent on diameter for a fixed throughput. For example, a 25% increase in diameter decreases the energy dissipation rate by a factor of five.

If plugging is apt to be a potential problem, a static mixer with more open area (higher voidage) should be selected. The absence of back-mixing requires very precise, controlled metering of feed streams into static mixers. Any variations in the feed flows and concentrations could lead to uncorrectable and wrong stoichiometric ratios of reactants, eliminating the selectivity and yield improvements that static mixers have over agitated tanks.

In stirred vessels, with some reaction systems such as nitrations and sulfonations, unmixed zones can form in the reactor either due to density differences in the case of homogeneous systems or phase separation in the case of heterogeneous systems. Unmixed zones can result from poor design, agitator failure, low-impact initial addition, or feed interruption in a continuous reactor. If unmixed fluids are suddenly mixed, violent exothermic reactions can occur, leading to a major disaster. This possibility should be carefully considered in the design of equipment and operating procedures involving fast exothermic reactions.

For highly exothermic reactions, consider semi-batch operation instead of a batch operation. The semi-batch operation allows for a better control of temperature and heat removal by limiting the feed rate of the reactants.

If the reaction intermediates are potentially hazardous, their concentration levels should be kept minimal in the reactors. For continuous processes, consider a plug-flow operation instead of a

TABLE 9.5
Constants for Use with Equation (9.24)

Impeller	α	β	X
HE-3	0.77	1.0	0.0
Square-pitch marine propeller	0.83	0.442	0.06
45° PBT-4	1.00	0.327	0.52
FBT-4	1.035	0.270	0.63
Disc: R-100, D-6	1.06	0.250	0.50

As discussed earlier, micro-mixing depends upon how the local energy dissipation affects the glob size at the feed point, and how long it takes for the glob (position of feed in the circulation loop) to reach the impeller zone (where the glob size could be reduced to its ultimate size). If the ingredients are added at the point of maximum energy dissipation, as suggested earlier, the scale-up could be based on the local power per unit volume as long as the reactions are extremely fast, i.e., virtually instantaneously. If reactions are not completed by the time the “fresh reactants” leave the region of high turbulence intensity, the constant local power per unit volume may not be adequate. To complete the reaction, macro-mixing becomes important, and the blend time could become the limiting scale-up criterion.

The chemical kinetics are usually not known for many industrial reactions and are often quite difficult to determine. While CFD holds the most promising approach for homogeneous systems when the kinetics are fully known, some experimental work with verification of CFD predictions is required for a successful scale-up. Most frequently, there is no luxury of determining detailed kinetics and doing CFD computations and verification. Hence, the following procedure (modified from Fasano [31]) is recommended:

- Conduct experiments to determine yield, (X_s), varying N , D/T , feed location, and feed time or feed rate. If possible, this should be done at two scales (for example, 1-gal and 25-gal reactors).
- Plot the yield data vs. mixing time, power per unit volume, local power per unit volume, etc., and determine the appropriate scale-up criterion.
- If blend time is the appropriate criterion, use Figure 9.24 to determine the feasibility of using an agitated vessel without a pump-around loop.
- If blend time is excessive on a large scale without requiring impractical power input, use a circulation loop containing static mixers.
- If local power per unit volume (micro-mixing) is the criterion, generally there should be no scale-up difficulty in terms of design. Make sure that macro-mixing does not become limiting upon scale-up.

9.5.11 SOME PRACTICAL GUIDELINES FOR SMALL-SCALE (LAB) EXPERIMENTATION

To set process conditions successfully in industrial design, it is useful to first determine the optimal conditions and design on a model scale. When applied properly, upscaling and downscaling have immense advantages. One of the important, but often ignored, functions of small-scale research is to learn from “blunders.”

The lab reactor should be geometrically similar to a full-scale reactor, with the proper impeller and baffles as appropriate, not round-bottom flasks with magnetic stirrers. The latter ones are not useful to gather scale-up data.

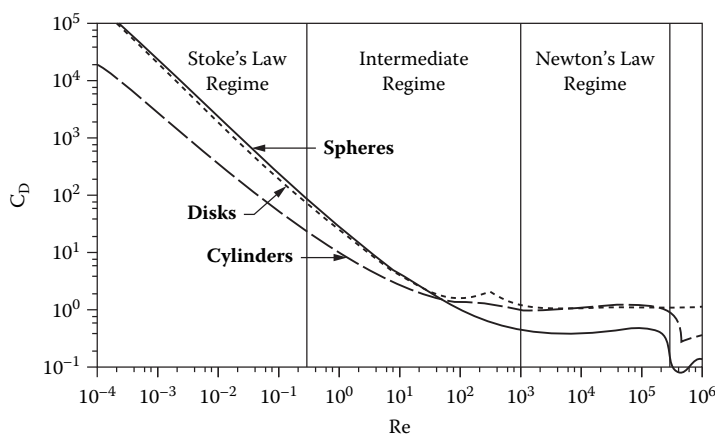


FIGURE 9.25 Dependence of drag coefficient on Reynolds number for spheres, cylinders, and discs.

TABLE 9.6
Expressions for C_D for Spheres in Different
Flow Regimes

Region	Reynolds Number	Expression for C_D
Stokes law regime	$Re \leq 0.3$	$C_D = 24/Re_p$
Intermediate regime	$0.3 \leq Re_p \leq 1000$	$C_D = 18.5/Re_p^{3/5}$
Newton's law regime	$1000 \leq Re_p \leq 3.5 \cdot 10^5$	$C_D = 0.445$

$$Re_{\text{particle}} = \frac{d_p V_t \rho_l}{\mu_l} \quad (9.25)$$

where d_p is the particle diameter, V_t is the terminal settling velocity, and ρ_l and μ_l are the density and viscosity of the suspending phase. Stokes's law applies when the particle Reynolds number is less than 0.3.

Figure 9.25 shows the effect of particle shape on the drag coefficient over a range of Reynolds numbers.

The following equation enables one to calculate the free settling velocity of a particle:

$$V_t = \left(\frac{4g_c d_p (\rho_s - \rho_l)}{3C_D \rho_l} \right)^{1/2} \quad (9.26)$$

The drag coefficient C_D is a variable depending on the flow conditions represented by the particle Reynolds number and is given in Table 9.6 or Figure 9.25.

Equation (9.27) is the corresponding terminal settling velocity expression for the laminar regime or Stokes's law given in Table 9.6:

$$V_t = \frac{g_c d_p (\rho_s - \rho_l)}{18 \mu} \quad (9.27)$$

TABLE 9.7
Power Numbers and s Values (Zwietering
Equation) for Different Impellers,
Clearances (C/T), and Impeller Sizes (D/T)

Impeller Type	C/T	D/T	Po	s
4–45°-PBT, downflow	1/5	1/3	1.4	5.7
	1/4	1/3		6.2
	1/4	1/2		5.8
	1/4	1/4		7.1
6–45°-PBT, downflow	1/4	1/2	1.6	5.7
	1/4	1/2		6.4
A-310, downflow	1/5	1/3	0.25	7.6
	1/4	1/3		7.9
	1/4	1/3		7.8
	1/4	1/2		6.0
HE-3, downflow	1/4	1/2	0.25	6.2
	1/4	1/3		7.2
Intermig (2 off)	1/6/2/3	7/10	0.7	7.4
6–45°-PBT, upflow	1/4	1/2	1.6	6.9

9.6.4 JUST-SUSPENDED CONDITIONS

The determination of the just-suspended speed, N_{js} , for off-the-bottom suspension has been extensively studied [37, 38], most recently by the British Hydrodynamics Group (BHRG). All studies support the Zwietering equation given by

$$N_{js} = sv^{0.1} \left[\frac{g\Delta\rho}{\rho_l} \right]^{0.45} X^{0.13} d_p^{0.20} D^{-0.85} \quad (9.30)$$

where N_{js} = speed in rps to just-suspended particles, $\Delta\rho$ = difference in density between the solid and liquid phases, ρ_l the density of the liquid phase in kg/m³, X = mass ratio of solids to liquid, v = kinematic liquid viscosity in m²/s, $g = 9.8$ m/s², d_p = average particle size in m, D = impeller diameter in m, and s is the geometry factor given below in Table 9.7.

The speed for just suspension can be calculated by means of Equation (9.30) using s values given in Table 9.7. Note that s varies with impeller type, clearance, and D/T . Additional values for s may be found in the *Handbook of Industrial Mixing* (chapter 10, 560) [1].

For purposes of scale-up, the Zwietering equation predicts for equal systems that

$$ND^{0.85} = \text{const} \quad (9.31)$$

Equation (9.31) would represent scale-up conditions for off-the-bottom suspension. Lacking precise process information, vendors sometimes recommend the value of 0.75 for the scale-up exponent for conditions where $Re > 10^4$ and vessels are geometrically similar. This is an intermediate value between 0.85, the Zwietering value, and 0.67, the value required for scaling solids uniformity.

These relationships are for a single impeller installation. The use of a second impeller has little effect on N_{js} , but does provide for better solids uniformity.

where C_m is the overall mean concentration, n is the number of sample points, and C_{ij} is the concentration of the i th position, j th speed.

Low values of the RSD mean better uniformity. Dual impellers help establish better uniformity by effectively distributing flow, hence solids, throughout the vessel. Recent CFD studies have shown reasonably good agreement between measured and calculated solids concentration profiles.

Design recommendations for obtaining good solids uniformity include using:

- Dish-shaped bottom heads
- Four baffles $T/12$ wide, placed $T/72$ away from the wall, and extending from the lower tangent line to the surface of the liquid
- Impellers: 45° PBT, hydrofoil (HE-3, A-310), or a bottom-located RCI
- A second impeller, if solids uniformity is essential, and $H/T > 1.2$

Mak [41] has shown that at three different scales, the RSD scales up using constant P/V . This is shown in Figure 9.27. Increasing the power (increasing N^3D^2) reduces the relative standard deviation (RSD). The data for three widely different scales were originally plotted against various different scaling criteria; the one shown in Figure 9.27 is for constant P/V . The close agreement for the three scales validates the P/V scaling assumption. This agreement for large-scale vessels is important. It implies that model suspension experiments can safely be conducted in fairly small equipment. At the Dow Chemical Company, the author determined the power needed to form completely uniform suspension of fast-settling solids. Studies were done in three bench-scale vessels of 0.3 m, 0.457 m, and 0.61 m in diameter using process materials. Equivalent solids suspension at different sizes was found at $P/V = \text{constant}$. This result was applied to a (20-ft diameter) 50,000-gal slurry reactor. Sampling at different positions showed solids uniformity had been reached.

A useful rule of thumb for solids suspension is to relate the solids settling velocity to the calculated suspension velocity created by the impeller. When the flow velocity exceeds the solids settling velocity by a factor of 1.5 to 2.0, usually good performance can be expected. As an example, we calculate the speed to completely suspend solids in a 3.05-m (10-ft) vessel equipped with a 1.22-m (4-ft) HE-3 impeller. The solids settling velocity is 3.05 m/min (10 ft/min). Furthermore, it is assumed that downflow occurs in an area of $1.2 D$ and that the circulation pattern is single loop. The annular upflow area becomes $(\pi/4)(3.048^2 - 1.52^2) = 5.48 \text{ m}^2$. The velocity in this region must

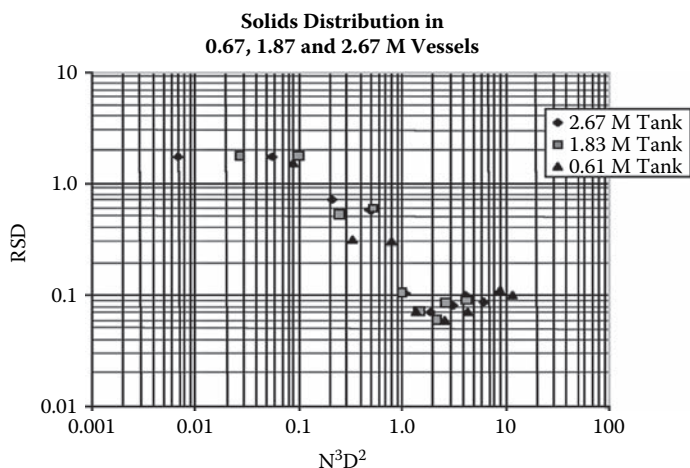


FIGURE 9.27 Power per unit volume as the scale-up criterion for solids distribution. (From Mak et al., 1990.)

Solids $X = 0.30$

$D = 0.51 \text{ m}$

$d_p = 10^{-4} \text{ m}$

$\nu = 10^{-6} \text{ m}^2/\text{s}$

$(g \Delta \rho / \rho) = 9.81 \times 2.34 \text{ m/s}^2$

$s = 3.9$ (for flat-blade turbines, taken to be equivalent to the glassed impeller)

Solution

The basis for the calculation is the Zwietering Equation (Equation (9.29)). Substituting, we get

$$N_{JS} = 3.9 \cdot (10^{-6})^{0.1} [9.81 \cdot 2.34]^{0.45} 0.30^{0.13} (10^{-4})^{0.2} 0.51^{-0.85} = 1.92 \text{ rps}$$

Given that the impeller is a glass-coated retreat-curve type, the approximate calculation for the minimum suspension speed is 115 rpm. A recommended design speed would be 130–150 rpm. This would guarantee more than minimum suspension conditions. The power at 150 rpm based on a power number of 0.6 would be 0.323 kW ($\approx 0.5 \text{ hp}$).

9.6.9 SOLIDS SUSPENSION BY JET MIXING

Liquid jets can be used to suspend solids. There are both simple nozzle designs and proprietary designs such as the Aerocleve-Pentech. In the latter, multiple jets radiate outward from the central feeder. Jets function in a similar fashion to impeller streams, so that many of the terms used in the Zwietering equation apply to solids suspended by jets. Effective suspension is created when the jet is centrally placed at a height of about $T/6$ to $T/10$ above the bottom of the floor of the tank. Jet solid suspension is designed on the basis of the V_{JS} , the jet velocity required to just suspend particles. Particle movement is the same as defined for the case of the agitated vessel. Research at BHRG for the FMP consortium has developed extensive technology on jet solid suspension for its members. For more information on jet mixing, see Section 9.10.

9.7 GAS-LIQUID MIXING

9.7.1 INTRODUCTION AND SCOPE

Gas-liquid mixing is one of the most frequently used operations in the process industries, being involved with waste treatment, fermentation, hydrogenation, oxidation, chlorination, and gas stripping. Throughout this section, liquid is the continuous phase and gas is the dispersed phase. The purpose of gas-liquid mixing is to introduce soluble gases into the liquid phase, where reactions can take place. Mixing affects how quickly this process occurs by creating an interfacial bubble surface area and a suitable bubble distribution throughout the vessel. If the interfacial area controls the rate of a reaction, reactions are referred to as being mass-transfer-controlled. If chemistry is slow and mass transfer is not limiting, reactions are referred to as being kinetically limiting.

Energy provided by agitation creates an interfacial area by dispersing bubbles. High-shear impellers (four- or six-blade flat-blade disc designs) are often used, since they can deliver more power (at a given speed and diameter) to the fluid than other impeller designs. The disc, shown in Figure 9.3, helps collect gas and direct it to the blades, where dispersion occurs. While disc turbines are most commonly used for gas dispersion, any impeller capable of delivering energy to the liquid can be used to disperse gas. This includes the 45° or 60° PBT, the FBT, hydrofoils, and even retreat-curve impellers.

Cavitation commonly occurs in g-l mixing operations, and this reduces the impeller function. Cavitation, shown in Figure 9.28, is a condition where large pockets of gas collect and cling to the

The mass-transfer coefficient $k_L a$ is often correlated by equations such as

$$k_L a = c \cdot \left(\frac{P_g}{V} \right)^\alpha \cdot v_{sg}^\beta \cdot \left(\frac{\mu^*}{\mu_{ref}} \right)^\gamma \quad (9.37)$$

where V_{sg} is the superficial gas velocity, P_g/V is the gassed power per unit volume, C is a constant, and μ^* is the viscosity at process conditions relative to μ_{ref} at reference conditions.

9.7.3 EQUIPMENT AND ITS FUNCTION

A conventional stirred vessel used for gas-liquid mixing is shown in Figure 9.29. A very common configuration for gas-liquid mixing includes a drive unit, four sidewall baffles, a sparger, a lower gas-dispersing impeller, and an upper axial-flow-type impeller. Some operations place the gas-dispersing turbine as the upper one and the axial-flow turbine as the lower one. In this case, the axial-flow turbine is up-pumping. Advantages for this configuration are that it greatly reduces fluctuating loading on the drive, and it reduces cavitation. On the negative side, gas holdup is more difficult to achieve. Various vessel shapes can be used for gas-liquid mixing. Tall vessels, e.g., $H/T = 4/1$ containing multiple impellers, have the advantage of providing longer gas residence times, but it is more difficult for these to provide good turnover. The minimum H/T should be at least 1:1. A common impeller-to-tank diameter ratio for gas dispersion is $D/T = 0.4$, but this can vary from 0.33 to 0.50. The energy input for gas dispersion is high and can vary from 0.5 to 6.0 kW/m³ (2.5 to 30 hp/1000 gal). Many applications fall into 1–2 kW/m³ (5–10 hp/1000 gal) based on gassed conditions. Because of this high energy, other aspects such as uniformity are usually met with ease.

Effective gas dispersion occurs in stages. First, large bubbles form from a sparger or inlet pipe. These are entrained by flow to the impeller blades, where the second stage of dispersion takes place. Smaller bubbles form here. Ring spargers, shown in Figure 9.29, are commonly used for introducing gas to the impeller. They are described more fully later in this section. Pipes can also be used to introduce gas. These can be single or multiple dip-pipe arrangements. Because of their large openings, pipes deliver larger bubbles than ring spargers. These bubbles can bypass the impeller. In pipe sparging, entering gas is sheared away from the tip, creating bubbles by a shedding mechanism.

Direct loading is a term used to describe gas bubbles passing directly from the point of entry to the impeller. *Indirect loading* refers to the condition where bubbles first pass up the tank, then get redirected by entrainment to the impeller for dispersion.

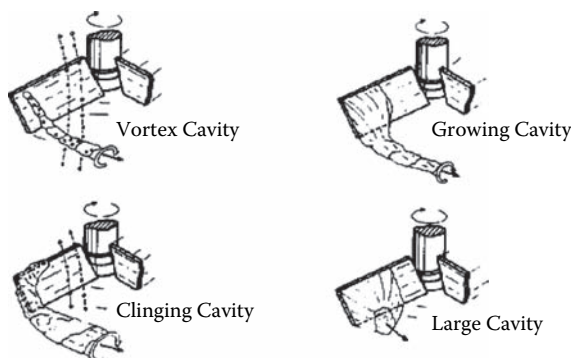


FIGURE 9.29 Development of cavity formation on a 45° PBT.

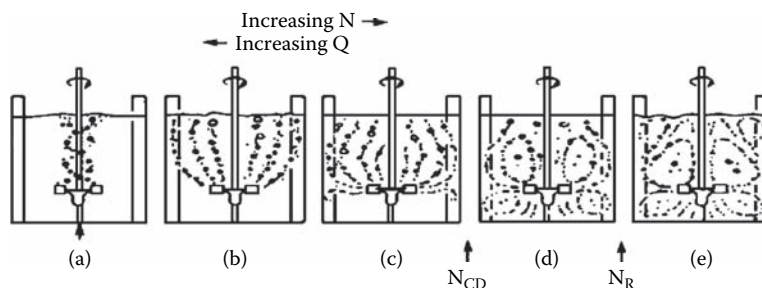


FIGURE 9.30 Changing vessel performance with agitation and gassing rates. (From Nienow et al., 1977.)

size at constant conditions. The sweeping motion of the blades first collects gas bubbles. There they impinge on the blades, creating large cavities (bottom right) because of coalescence. Gas leaves the cavities by shedding from the vortex tip. (See upper right picture in Figure 9.28.)

Figure 9.30 shows the changing bubble distribution patterns in the vessel as gassing and agitation rates change. Figure 9.30(a) shows a flooded impeller. Gas, instead of being dispersed by the impeller, passes centrally up the middle of the tank to the surface. As the agitation rate increases, N_{CD} is reached (shown by Figure 9.30(d)), and a condition known as “complete” dispersion is reached. At still higher speeds, N_R , gas bubbles are entrained back to the impeller. This condition (Figure 9.30(e)) represents excellent circulation and bubble distribution throughout the vessel. Figures 9.30(a–e) show the effects of decreased gas flow at a given rate of agitation. At Figure 9.30(a), while agitation is strong, the gas flow is high, and the impeller cavitates, resulting in gas bypassing the impeller.

The conditions shown by Figure 9.30(a–e) are represented schematically in a regime map, Figure 9.31, where the Froude number is shown as a function of the gas flow number. The Froude number, Fr , is N^2D/g , and the gas flow number, Fl_g , is Q/ND^3 . These numbers are calculated for a design and its operation; the values are then placed on the regime map to determine if the design is workable. Such a procedure can help avoid costly scale-up mistakes.

The following are design guidelines for good gas-liquid mixing. Conditions shown by Figure 9.30(a, b) exist for $Fr < 0.05$. This condition must be avoided. Regime I represents conditions shown by Figure 9.30(e). While dispersion and mixing are excellent, power may be excessive for most applications. Regime II is a practical compromise between performance and energy cost. Most industrial gas-liquid applications will fall into regime II. Regime III is reached by high gassing rates or by low-speed conditions. Regime III is equivalent to conditions shown by Figure 9.30(c). The bubble distribution is not uniform, and holdup is decreased. In some cases, operation in regime III is acceptable, provided that liquid circulation below the impeller is good. The actual location of all lines is a function of the impeller selection. It is essential to determine into which region the system falls, both from a standpoint of design and for troubleshooting. Some suppliers provide charts similar to Figure 9.31 with their literature and proposals.

The following applies to Rushton (D-6) turbines having $(D/T) = 0.40$ [44]:

- Flooding occurs when $Fl_g > \approx 1.2 Fr$ (Figure 9.30(a) and the lower-sloped line in Figure 9.31).
- Gas recirculation begins when $Fr > \approx 2.75 Fl_g^{1/2}$ (Figure 9.30(e) and the upper line in Figure 9.31).
- Vortex and large cavities on upper impellers (multiple impeller systems) develop when $Fl_g Fr \times 0.2$ (Figure 9.30(c))

TABLE 9.9
Parameters for Use in Equation (9.38) Based on
Air/Water

Impeller	a	b	c	d	Avg. % error
D-6	-7.15×10^{-4}	0.723	24.54	0.25	7.09
CD-6	-1.15×10^{-4}	0.440	12.08	0.37	5.20

9.7.5 MASS TRANSFER AND GAS HOLDUP

The general features of mass transfer were previously given in Section 9.7.1. The mass-transfer coefficient, $k_L a$, and gas fraction holdup, Φ , are closely related and depend on the same variables. Equation (9.36) relates area, holdup, and mean bubble size, and the main variables affected by agitation is d_{32} and a . Bubble rise time and thus escaping tendency are a function of the bubble size, and this affects holdup. The fundamental expression for mass transport includes the $k_L a$, and the driving force and is given by

$$N_i = k_L a (C_{Li}^* - C_{Li}) \quad (9.35)$$

Agitation mainly affects the a in $k_L a$, since it represents the total interfacial area per unit volume of gas plus liquid. It therefore has units of length^{-1} . The units of $k_L a$ are usually expressed in s^{-1} or min^{-1} . Typical $k_L a$ values for agitated vessels lie between 0.05 to 0.4 s^{-1} . The mass-transfer coefficient k_L , is one of the resistances to transport of species (i) from the gas phase inside the bubble to the bulk fluid outside the bubble. The overall resistance $1/K_L$ is the sum of the inside and outside resistances shown in Equation (9.39), where E is the equilibrium constant. In the great majority of cases, $k_L \approx K_L$. This implies that k_G is small compared with k_L and means that the liquid film resistance outside the bubble is controlling:

$$\frac{1}{K_L} = \frac{1}{Ek_G} + \frac{1}{k_L} \quad (9.39)$$

The gas film resistance, k_G , for small bubbles is controlled by diffusion, D_G , as shown by

$$k_G = \frac{2\pi^2 D_G}{3d_{32}} = 6.6 \frac{D_G}{d_{32}} \quad (9.40)$$

The liquid-side mass-transfer coefficient, $k_L a$ (s^{-1}), is related to the superficial gas velocity, V_{SG} (m/s), and the gassed power per unit volume of liquid, P_G/V , (kW/m^3). The viscosity term μ^*/μ accounts for the effect of process viscosity on the mass-transfer coefficient relative to standard conditions, typically water at 20°C :

$$k_L a = C \cdot \left(\frac{P_g}{V} \right)^\alpha \cdot (V_{SG})^\beta \cdot \left(\frac{\mu^*}{\mu_{ref}} \right)^\gamma \quad (9.37)$$

TABLE 9.11
Constants for Gas Holdup Equation (9.43)

Author	System	Type	D/T	K	α	β
Kar [46]	Air/water	CD-6	0.4	2.92	0.19	0.88
Kar [46]	Air/water	CD-6	0.5	3.93	0.25	0.92
Kar [46]	Air/water	D-6	0.4	1.15	0.3	0.64
Kar [46]	Air/water	D-6	0.5	2.58	0.39	0.81
Parthasarathy [50]	Air/NaCl/water	D-6	0.4	1.01	0.24	0.67

TABLE 9.12
Constants for Gas Holdup Equation (9.43)

Configuration	Impellers	Deionized Water			Na ₂ SO ₄ (28 g/l)			PVP (7.4 mPa·s)		
		K	α	β	K	α	β	K	α	β
Rushton	1	0.222	0.215	0.684	0.0069	0.664	0.523	0.0096	0.699	0.483
	2	0.223	0.264	0.699	0.0179	0.520	0.415	0.0361	0.518	0.479
	3	0.278	0.217	0.662	0.0651	0.435	0.548	0.0586	0.536	0.654
A-315	1	1.13	0.231	0.781	0.0481	0.429	0.580	0.206	0.454	0.804
	2	0.321	0.195	0.695	0.114	0.385	0.649	0.312	0.379	0.782
	3	0.328	0.216	0.691	0.130	0.355	0.619	0.286	0.390	0.769
A-310 + R-100	1 R	0.222	0.215	0.684	0.0069	0.664	0.523	0.0096	0.699	0.483
	1 A-310 + 1 R-100	0.151	0.244	0.566	0.0660	0.392	0.514	0.0705	0.425	0.521
	2 A-310 + 1 R-100	0.256	0.244	0.636	0.103	0.403	0.587	0.0832	0.491	0.590

Source: Pinelli, D., M. Nocentini, and F. Magelli, "Hold-Up in Low Viscosity Gas-Liquid Systems Stirred with Multiple Impellers: Comparison of Different Agitators Types and Sets," I. C. Engrs., Eighth European Conference on Mixing, University of Cambridge (*I. Chem. E.* 136, 81–88 [1994]).

Gas holdup studies in tall vessels including three impeller configurations were reported by Pinelli [51] for (a) three equally spaced Rushton turbines, (b) three A-315 turbines, and (c) one Rushton (bottom) and two A-315 turbines. Holdup was correlated using Equation (9.43), with constants shown in Table 9.12. The units for P_G/V are in W/m^3 , V in m/s , and holdup in volume fraction gas.

For the case of equally spaced Rushton turbines in deionized water (fast coalescence), all constants are virtually the same. Power was additive, suggesting that the turbines functioned independently. While there is some variation in K for other configurations, values of α and β are nearly constant. The gas flow constant dominates over power. This is not the case for noncoalescing polyvinylpyrrolidone (PVP) and salt-containing solutions. Experiments included one impeller with $H/T = 1.0$, two impellers with $H/T = 2.0$, and three impellers with $H/T = 3$. All impellers were equally spaced.

Holdup and bubble size can be rough indications of the quality and intensity of mixing, but less information is revealed than for $k_L a$.

9.7.6 GAS RESIDENCE TIME

The gas residence time becomes important for sparingly soluble gases and cases where a high gas conversion is desired. The gas residence time depends on viscosity, flow rate, bubble size, and the height of liquid in the vessel. In Figures 9.30(a–c), bubble rise time and liquid height are dominant factors, but in Figures 9.30(d–e), entrained flow is also important. Actually, very little has been

1. Keep the vvm (volume of gas per volume of liquid per minute) constant. This leads to an increase in V_g and results in higher gas holdup and $k_L a$ values. If the gas is a reagent, constant vvm maintains reaction stoichiometry.
2. Maintain both V_{SG} and $[P_G/V]$ constant. This preserves both $k_L a$ and holdup, but leads to reduced rates of reaction.

Example 9.5

Batch fermentation is being used to produce an antibiotic. The broth is assumed to be Newtonian. Examination of the operating data suggests that insufficient oxygen is available at certain times. The viscosity reaches a maximum of 300 cP during fermentation.

Examine the design and make recommendations for improvements. The volume of the fermenter is 80 m³. Its critical vessel and impeller dimensions are $T = 3.66$ m, $H = 5.1$ m, $D_L = 1.4$ m, and $D_U = 1.65$ m. The vessel has four conventional baffles, and a 1.3-m ring sparger is located below the lower impeller. The lower impeller is a Rushton (R-100, D-6) type, and the upper impeller is a hydrofoil of A-310, HE-3 type. The speed is 60 rpm. The air flow rate is 1.0 vvm.

Solution

At the maximum viscosity, the impeller Reynolds number for the lower impeller is 6500, which indicates that the flow is in the transitional regime, but close to fully developed turbulent flow. At ungassed conditions, the Rushton impeller ($D = 1.4$ m, $N_p = 5.75$) consumes 30.5 kW (40.98 hp). The upper impeller ($D = 1.65$ m, $N_p = 0.3$) consumes 3.68 kW (4.93 hp). The combined power is 34.2 kW (45.91 hp). The quiescent volume at a height of 5.1 m (200 in.), including the dished head, is 50.5 m³ (13,333 gal). This makes the P/V for the lower R-100 impeller = 0.61 kW/m³ (3.1 hp/1000 gal). The gas flow at 1.0 vvm is 50.5 m³/min (13,333 gal/min), 0.841 m³/s (46.5 ft³/s). The superficial gas velocity, V_{SG} , is 0.125 m/s (0.41 ft/s). The Froude number, $N^2 D/g$, is 0.1423 and the gas flow number, Fl_g , (i.e., Q_g/ND^3), is 0.482.

1. Determine the gassed power input using Equation (9.38). Substituting values, P_G/P_{UG} is 0.688. So $P_G/V = 0.419$ kW/m³ (2.13 hp/1000) gal.
2. Determine bubble dynamics in the vessel. Flooding occurs when $Fl_g > 1.2$ Fr. In this case, 1.2 Fr = 0.171. From this, we conclude that the impeller is flooded. The Froude number is greater than 0.05, so operations (with reference to Figure 9.31) are in regime III, and gas will not reach the lower portions of the vessel. Conditions represented by Figure 9.30(a) or 9.30(b) probably exist. The best option is to increase the speed and then consider increasing the gas flow rate (first the speed).
3. Solving $Fl_g > 1.2$ Fr for N , at $Q = 1.317$ m³/s (46.5 ft³/s), using $D = 1.397$ m (55 in), gives $N > 85$ rpm. This speed would result in a 41% increase in shear rate, which might be unacceptable to the microorganisms. Maintaining the same impellers operating at 85 rpm results in a power draw of 91.44 kW or a P/V of 1.69 kW/m³ (10 hp/1000 gal).
4. If a CD-6 having an $N_p = 3.67$ were selected, the combined impeller power draw at ungassed conditions would be 60.0 kW (80.44 hp). The corresponding Froude number = 0.28, and the gas flow number is 0.341. Thus 1.2 Fr = 0.342, so conditions are just at the onset of flooding. Increasing the gas flow by 20% results in $Q = 1.58$ m³/s (55.8 ft³/s), which would make $Fl_g = 0.409$. This condition would place operations solidly in region II, a more desirable condition.
5. Calculate gassed power, $k_L a$, and holdup at these new conditions. $P_G/P_{UG} = 0.745$, and $P_G = 55.47(0.745) = 41.32 + 4.55 = 45.87$ kW. (For $k_L a$, use only the power draw for the lower turbine.) Use Kar's constants found in Table 9.10, $A = 0.78$, $\alpha = 0.48$, $\beta = 0.57$, and $\gamma = -0.77$. The input variables are $P_G/V = 0.756$ kW/m³ and $V_{SG} = 0.15$ m/s. The calculation for $k_L a$ using Equation (9.37) is 0.00286 s⁻¹. The high viscosity causes this value to be low. At 1 cP, the $k_L a$ would be 0.231 s⁻¹, an acceptable value. Calculations

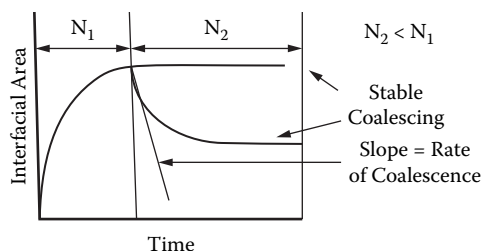


FIGURE 9.34 Dynamic test for coalescence.

TABLE 9.14
Dispersions Classified by Drop Size

Drop Size	Comments	Equipment, Agents Used
$<0.5\ \mu\text{m}$	Stabilized by Brownian motion	Emulsifiers, ultrasonic devices, rotor-stator mixers, impingement mixers, etc.
$0.5 \geq d \geq 3.0\ \mu\text{m}$	Marginally stable, can cream and separate	Rotor-stator, impingement mixers, static mixers, emulsifiers
$>3.0\ \mu\text{m}$	Often unstable	Static mixers, in-line mixers, stirred vessels

A more accurate dynamic test for relative drop stability uses agitation and an optical transmission probe. First, a dispersion is created using vigorous mixing, N_1 . Agitation is then decreased to N_2 . If the interfacial area (indicated by a decrease in optical transmission) decreases, it is due to either coalescence or settling. If settling is the cause, choose a higher value for N_2 . If the transmission remains constant after speed change, it suggests that the system is noncoalescing. The probe reading is constant under dynamic equilibrium between dispersion and coalescence. If the system coalesces, the optical transmission will increase, indicating a loss of interfacial area. The probe used is similar to that described by Rodger [55]. The output is schematically illustrated in Figure 9.34. If the optical transmission is recorded and the probe calibrated (e.g., with glass beads), the initial slope of the curve gives the coalescence rate. Another way to classify liquid-liquid systems is by drop size, as shown by Table 9.14. This section focuses on drops larger than $\approx 5.0\ \mu\text{m}$.

Initially, dispersion occurs throughout the vessel, but with time, the dispersion region shrinks to that close to the impeller. Experimental data and computational fluid dynamics (CFD) have confirmed that energy dissipation close to the impeller can be ≈ 40 times greater than the mean for the vessel. Coalescence rates are fastest in regions of gentle flow, where drop contact/rest times are longer. Under stagnant conditions, drops settle, touch each other, and can coalesce to form a condensed layer. Under gentle dynamic conditions, drops collide and remain in contact so that, if sufficient film thinning takes place, coalescence occurs. If the contact time is brief, so that insufficient drainage occurs, drops will separate and no coalescence occurs. Coalescence also results from drop collisions with impeller blades, baffles, and vessel walls.

9.8.3 DROP SIZES

The Sauter mean drop diameter, d_{SM} or d_{32} , defined by Equation (9.45), is most commonly used to characterize drop size because it relates to the volume fraction of the dispersed phase, Φ , and the interfacial area, a . The Sauter mean drop diameter is also known as the volume-to-surface average drop diameter. The interfacial area, a , in Equation (9.45) is also used to deal with mass transfer, such as $k_L a$. Other commonly used terms are d_{50} , d_{90} , and d_{max} . They represent the midsize, the 90th percentile, and the largest size in the drop size distribution, respectively, on a volume basis. The

for a loop impeller of diameter D and a circular cross-sectional diameter D_c is given by Equation (9.47). A loop impeller consists of rectangular-shaped arms made from pipe. The diameter is usually $D/T = 0.67$, and the height is nearly equal to the depth of liquid in the vessel. The number of arms is commonly two, but four arms have been used successfully. The ratio of $V_{\text{tan}}/V_{\text{tip}}$ at the tip of the impeller determines the value of k , where V_{tan} is the tangential velocity component at the impeller tip.

$$d_{\text{max}} = \text{Const} \cdot \gamma \cdot \left(\frac{D_c}{\mu_c \rho_c} \right)^{0.5} \cdot [ND(1-k)]^{-1.5} \left(\frac{P+1}{1.19P+1} \right) f(P) \quad (9.47)$$

Equation (9.48) gives the expression for a flat paddle:

$$d_{\text{max}} = \text{Const} \cdot \gamma \cdot \left(\frac{1}{\mu_c \rho_c} \right)^{0.5} \left[N^{-1.5} D^{-1} (1-k^2)^{-0.75} \right] \cdot \left(\frac{P+1}{1.19P+1} \right) \cdot f(P) \quad (9.48)$$

Equation (9.48) was tested commercially for scale-up using geometrically similar vessels and for drop sizes ranging from 300 to 1200 μm . Noncoalescing suspension polymerization experiments enabled sizes to be determined for finished beads using screen-analysis measurements. Equation (9.48) was confirmed for dimensionally similar vessels from 8.2 to 15,000 liters. Long dispersion times were used to ensure that complete dispersion had occurred.

9.8.5 DISPERSION OF LOW-VISCOSITY (INVISCID) DROPS ($\mu < 0.020 \text{ Pa}\cdot\text{s}$) TURBULENT FLOW

The maximum drop size is determined by equating the surface energy, E_s , associated with a drop of diameter d with the equivalent turbulent energy, E_T , associated with a spherical volume of fluid of diameter d shown by Equation (9.49).

$$E_T \geq E_s \quad (9.49)$$

The turbulent energy is determined by integrating the energy spectrum over wave numbers from $1/d$ to ∞ . Assuming isotropic turbulence, the function can be integrated upon substitution of the Kolmogoroff hypothesis relationship for $E(k)$. This procedure leads to Equation (9.50) [60].

$$\frac{d_{\text{max}}}{D} = \text{Const} \cdot \text{We}^{-0.6} = \text{Const} \cdot \left(\frac{D^3 N^2 \rho}{\gamma} \right)^{-0.6} \quad (9.50)$$

Chen [60], using data for 14 inviscid organic/water systems, determined the proportionality constant to be 0.053–0.057. Different-size disc turbines were used, and the L-L systems had interfacial tensions from 0.0047 to 0.048 N/m (4.7 to 48 dyne/cm). Figure 9.36 shows the data. The slope of the statistical correlation of the data is -0.57 , which is in close agreement with the -0.6 indicated by Equation (9.50).

Ample literature data show that drop diameters depend on the Weber number. However, much early data were erroneous due to unreported effects of coalescence, the presence of contaminants, and nonsteady-state operating conditions.

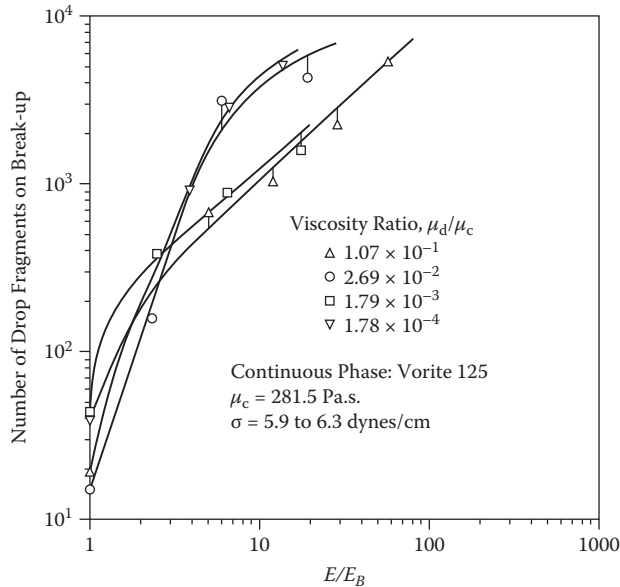


FIGURE 9.37 Drop fragmentation as a function of excess energy ratio E/E_B . (From Grace, 1982.)

Drop size distribution will be addressed briefly. When a drop breaks, there can be few or many fragments. The breadth of the distribution of daughter drops depends on the level of energy intensity at the time of breakage. Figure 9.37 shows that a large number of drops can form from a single drop at high energy. E/E_B is the ratio of local energy E to minimum bursting energy E_B for the drop. The viscosity ratio also affects drop breakage. More fragments form when μ_d/μ_c is small. In applications where the breadth of the size distribution must be minimized, such as in suspension polymerization, it is essential to provide uniform energy distribution.

9.8.6 DISPERSION OF HIGHER-VISCOSITY DROPS ($\mu > 0.02$ PA·S) TURBULENT FLOW

Calabrese et al. [60] and Wang et al. [63] show that the breakage condition in Equation (9.49) should include a term E_v for dealing with drop viscosity. Equations (9.54) and (9.55) show the result:

$$E_T \geq E_S + E_v \quad (9.54)$$

Equation (9.55) by Calabrese et al. [62] includes viscous terms:

$$\frac{\rho_c \epsilon^{-2/3} d_{\max}^{5/3}}{\gamma} = C_5 \left[1 + C_6 \left(\frac{\rho_c}{\rho_d} \right)^{1/2} \frac{\mu_d \epsilon^{-1/3} D_{\max}^{1/3}}{\gamma} \right] \quad (9.55)$$

When interfacial tension is the main resistance ($E_s \geq E_v$), Equation (9.52) reduces to Equation (9.56), which is equivalent to Equation (9.50):

$$d_{\max} = \text{const} \cdot \left(\frac{\gamma^{0.6}}{\rho_c^{0.6} \epsilon^{0.4}} \right) \quad (9.56)$$

Upon integration and substitution of the initial and final conditions, $h = h_0$ at $t = 0$, and $h = h_c$ at time t , Equation (9.58) becomes

$$\Delta t = t - t_0 = \frac{3\pi\eta R^4}{4F} \left(\frac{1}{h^2} - \frac{1}{h_0^2} \right) \quad (9.59)$$

The initial distance h_0 is large compared with h , the thickness of the film at time t . The change in time, Δt , is the time it takes to reach a critical thickness for film rupture. Several versions of this equation exist that include internal circulation within the drop, rigid yet deformable interfaces, and complete interface mobility [64, 65].

This relationship has practical implications:

- If Δt , the total drainage, is sufficient such that the critical separation thickness is reached during the contact interval, the drops will coalesce.
- If insufficient drainage occurs during the contact interval, Δt , the drops will not coalesce.
- A low interfacial tension leads to greater flattening of the approaching drop surfaces. This produces a larger disc and makes the thinning process slower. Surfactants lower the interfacial tension, γ , and reduce the likelihood of coalescence. The surfactant may also reduce interfacial mobility, leading to further retardation of drainage rates.
- A higher impact force, F might increase the likelihood of coalescence, but it also creates larger discs, trapping more liquid and making drainage more difficult. Centrifuges and electrostatic coalescers are examples of force-amplification devices; decanters, on the other hand, depend on gravitational force.
- A higher continuous-phase viscosity reduces drainage rates and coalescence probability. For this reason, if two similar volumes of immiscible liquids are dispersed, the fluid with the higher viscosity will normally become the continuous phase.

The presence of solids at the interface usually retards film drainage rates, thereby reducing the probability of coalescence. A few suspension-polymerization processes use solid particles as suspending agents.

9.8.9 POPULATION-BALANCE METHODS

Population-balance analysis has been adapted to both coalescence and dispersion of drops in numerous papers by Calabrese, Ramkrishna, and Tavlarides. The analyses with these tools have led to a considerably better understanding of breakage kernels, breakage rates, coalescence efficiency, and collision rates. However, the description and use of these tools goes beyond the scope of this chapter. For a detailed understanding, see Ramkrishna [66].

9.8.10 CREATING A DISPERSION—MAINTAINING DROP SUSPENSION

This subsection deals with creating a dispersion from two settled phases of different density, obtaining uniformity, and then determining the minimum speed to accomplish a dispersion.

The minimum speed, N_m , to form dispersions from two settled phases of different densities is expressed in terms of dimensionless variables. Differences in constant C reflect the effect of impeller clearance. Similarities can be seen between N_{js} for solids suspension and N_{min} for

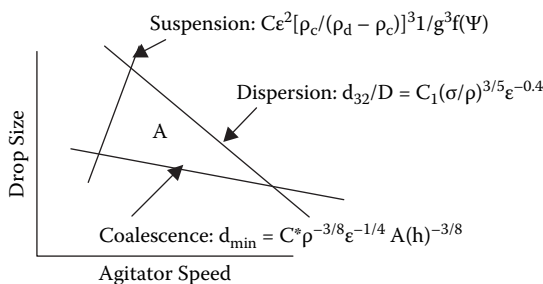


FIGURE 9.39 Dispersion, coalescence, and suspension. (From Church et al., 1961.)

9.8.11 SIMULTANEOUS SUSPENSION, DISPERSION, AND COALESCENCE

Church [69] describes the simultaneous processes taking place in a stirred vessel. Figure 9.39 shows the result of three processes that form a bounded region. Within this region, equilibrium stability exists. For example, a drop within the region bounded by the three lines can grow by coalescence until it reaches the upper dispersion line. At this point it is dispersed by the local energy. Smaller drops below the coalescence line grow by coalescence until they reach the coalescence line. A drop located to the left of the suspension line will separate. The expressions that describe the lines in Figure 9.39 are given as Equations (9.61 to 9.63).

Dispersion:

$$d_{32}/D = C_1 \cdot (We)^{-0.6} = \left(\frac{\sigma^{3/5}}{\rho_c^{3/5} \cdot \bar{\epsilon}^{2/5}} \right) \quad (9.61)$$

Coalescence:

$$d_{32} = C_2 N^{-0.75} D^{-0.5} \rho^{-0.375} A(h)^{0.375} \quad (9.62)$$

where $A(h)$ is the adhesive or attractive force and is a function of the separation distance, h .

Suspension:

$$d_{\max} = C_3 D^4 N^6 \left(\frac{\Delta \rho}{\rho_c} \right)^3 \left(\frac{1}{g} \right)^3 f(\Psi) \quad (9.63)$$

Regions around the impeller are usually dominated by high turbulence that causes dispersion. Elsewhere in the vessel, turbulence is much lower, and this promotes coalescence. Church [69] refers to this ongoing process as an agitation-stabilized system. This is fine, but the problem comes when one is scaling up a coalescing system. In a small vessel, circulation times are short and the turbulence zones dominate. The reverse is true for a large vessel. Simply keeping P/V constant and the geometry similar does not guarantee comparable drop size with scale-up. As mentioned earlier, an added complication for noncoalescing systems is the time to reach comparable stages of dispersion in different scales. Strongly coalescing systems reach steady state much more quickly than noncoalescing systems.

Dispersion, suspension, and heat removal must be simultaneously controlled in dealing with suspension polymerization. In Figure 9.39, the intersection of suspension and dispersion lines represents the largest maximum drop size that can be produced under existing conditions. Selection of different impellers can affect the position of this intersection. In continuous extraction applications, the goal is to create a large interfacial area, yet not make the drops so small that they are difficult to coalesce.

Other types of equipment such as static (motionless) mixers, rotor-stator mixers, and impingement mixers are used to create dispersions (see Section 9.9).

Example 6

In this example, solvent extraction is to be used to recover a product from a fermentation process. Processing information includes: broth viscosity $\mu = 0.3 \text{ Pa}\cdot\text{s}$ (300 cP), interfacial tension $\sigma = 0.003 \text{ N/m}$ (3.0 dynes/cm), bulk density $\rho_C = 1000 \text{ kg/m}^3$ (1.0 g/cm³), vessel volume = 3.54 m³ (750 gal), vessel diameter = 1.524 m (5.0 ft), and $D/T = 0.4$. Laboratory studies showed that acceptable extraction efficiency was obtained with mean drop sizes of 50 μm . Determine the power and speed required to produce 50- μm drops in the 750-gal extractor.

Solution

The solvent will disperse in the broth phase and will be slow to coalesce, since the broth has high viscosity. Equation (9.51) from Chen [60], $d_{\max}/D = 0.053(D^3N^2\rho/\sigma)^{-0.6}$, will be used. Substituting $d_{32} = 0.005 \text{ cm}$, $D = 61 \text{ cm}$, $\sigma = 3.0 \text{ dyne/cm}$, and $\rho = 1.0 \text{ g/cm}^3$, then solving for N gives $N = 48 \text{ rpm}$ (0.8 rps).

The Reynolds number, $\text{Re} = D^2N\bar{\rho}/\mu$, is 7700 using a volume average viscosity of 38.6 cP. Flow is transitional but nearly turbulent. The power requirement using $\text{Np} = 5.0$, a mean density of 1.0, and impeller speed of 48 rpm, gives

$$\text{hp} = \text{Np} \bar{\rho} N^3 D^5 / 17,719 = 0.3$$

9.9 STATIC IN-LINE MIXERS

9.9.1 INTRODUCTION TO IN-LINE STATIC MIXERS

A static mixer, also known as a motionless mixer, is a mixing device without any moving parts. It is also known as a pipeline mixer. It creates mixing as fluids pass through stationary geometric elements located inside the pipe. Static mixing elements vary in geometry from ordinary pipe internals such as orifices and baffles to specially designed complex structures. Turbulent pipe flow will ordinarily achieve a reasonably high degree of radial mixing in a length of roughly 100 pipe diameters. Static mixers achieve the same mixing in lengths of three to five pipe diameters.

There are over 30 different designs of static mixer elements. The more popular commercial ones and their suppliers include:

- Chemineer Kenics: KM series and HEV, Figure 9.40(a)
- Sulzer Chemtech: (or Koch) SMX, SMXL, SMV, SMVL, Figure 9.40(b)
- Ross: LPD, LLPD, Figure 9.40(c); ISG, Figure 9.40(d)
- Komax mixer

Static mixers are readily available in a wide variety of materials, including metals, alloys, and plastics in sizes from 1/2 to 24 inches in diameter.

Static mixers are widely used in situations where continuous in-line or pipeline mixing is required. Table 9.17 shows that applications span the entire spectrum from laminar to turbulent flow regimes, and they cover a wide variety of mixing processes involving the blending of gas-gas

TABLE 9.17
Selected Static Mixers and Mixing Applications

Mixer	Laminar Mixing		Turbulent Mixing		
	L-L Blending	S-L Blending	G-G or L-L Blending	L-L Dispersion	G-L Dispersion
Kenics KM	x	...	x	x	x
Kenics HEV	x
Sulzer or Koch SMX	x	x	x	x	x
Sulzer or Koch SMXL	x	x
Sulzer or Koch SMV	x	x	x
Ross LPD or LLPD	x	x	x
Ross ISG	x	x
Komax mixer	x	x	x
Komax ultramixer	x

anticlockwise, induce jets or turbulence eddies that interact with one another, etc., as the fluids move down the pipe. The specific hydrodynamic environment depends on the flow regime, laminar or turbulent. It is also different for different mixer designs, but the end result is good transverse or radial mixing with little or no axial back-mixing. The energy for mixing is the additional pressure drop due to the elements. Energy for mixing is supplied by feed pumps.

The manufacturer provides scale-up rules and correlations. These include the estimation of pressure drop and the number of elements required for a desired process result. These are reliable and may be used with confidence.

Static mixers offer certain advantages over dynamic in-line mixers and continuous stirred tanks. Table 9.18 is a summary of the characteristics of a static mixer compared with a conventional mechanically stirred vessel.

The hydrodynamic environment in a static mixer is characterized by a more uniform distribution of energy and shear rates than in a conventional agitated tank. Thus, for dispersion processes, a static mixer can produce a narrower drop or bubble size distribution. Also, the narrower residence-time distribution in a static mixer makes it the preferred mixing device for processes involving fast reactions or polymerizations requiring no back-mixing.

The static mixer produces an outlet concentration profile nearly as sharp as a step-change input in a plug-flow device.

Limitations of static mixers include the following:

- Provide little or no axial mixing (but excellent radial mixing)
- Cannot compensate for temporal variations in concentration or flow
- Pressure drop increases with the number of elements
- Certain slurries are prone to plug
- Low residence time and holdup are limitations for many reactions
- Performance is flow sensitive in turbulent applications
- Not easy to adapt to unexpected performance requirements

9.9.3 STATIC MIXER SELECTION AND DESIGN ISSUES

The proper selection or design of a static mixer starts with a clear understanding of process objectives and limitations. Table 9.19 gives design information for blending and dispersion applications. The following steps are recommended:

TABLE 9.19
Key Information for Blending and Dispersion in a Static Mixer

Key Information	Blending Applications: Miscible Fluids	Dispersion Applications: Immiscible Fluids
Process information	Number of component flows Component flow rates Component phases Component flow viscosity Component flow density Combined flow rate Combined flow viscosity Combined flow density Allowable pressure drop in mixer Heat transfer: Yes/No Reacting flows: Yes/No	Number of component flows Component flow rates Component phases Component flow viscosity Component flow density Combined flow rate Combined flow viscosity Combined flow density Interfacial tension Allowable pressure drop in mixer Heat transfer: Yes/No Reacting flows: Yes/No Inter-phase mass transfer: Yes/No
Static mixing process parameters	Reynolds No. Component flow ratios Component viscosity ratios	Reynolds No. Component flow ratios Component viscosity ratios Weber No.
Desired process result	Concentration/temperature homogeneity Variation coefficient Heat-transfer rate	Concentration/temperature homogeneity Drop size and distribution Interfacial area Mass-transfer coefficient Heat-transfer coefficient
Mixer selection and design information	Number of mixers Mixer design Feed arrangements Injector design Mixer diameter Mixer length or number of elements Mixer pressure drop Mixing efficiency	Number of mixers Mixer design Feed arrangements Injector design Mixer diameter Mixer length or number of elements Mixer pressure drop Mixing efficiency

$$\text{Re}' = \frac{\rho V D_h}{\mu} \quad (9.64)$$

where Re' is a dimensionless correlating parameter for static mixer design, and D_h is the hydraulic diameter. The transition from laminar to turbulent flow for pipes occurs at $\text{Re} = 2100$, but in static mixers, the transition point may be as low as 100. Blending under turbulent flow usually requires fewer than five elements. Laminar blending requires many more, depending on the desired uniformity.

9.9.5 COMPONENT FLOW AND VISCOSITY RATIOS

These determine the difficulty of the mixing application, as illustrated in Figure 9.41. The wider the viscosity difference between the component streams, the more difficult is the blending application. The most difficult application is the addition of a small, low-viscosity stream into a large, high-viscosity stream in laminar flow. For example, Tables 9.20(a) and 9.20(b) show effects

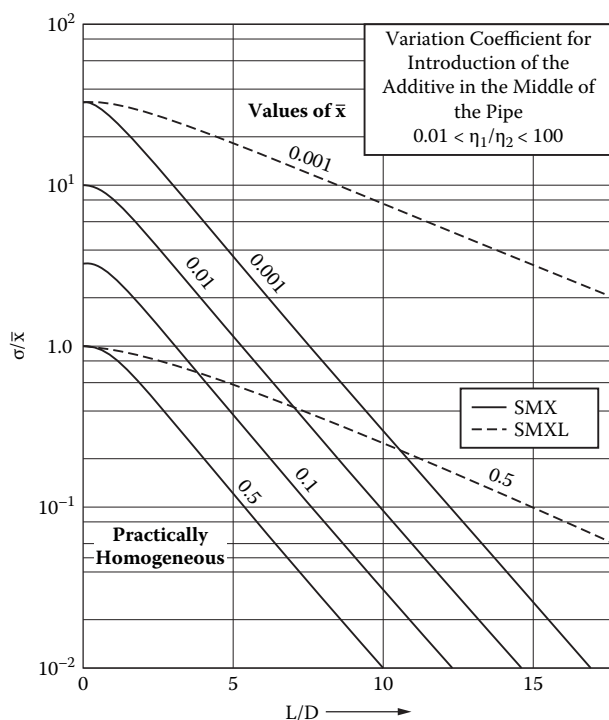


FIGURE 9.42 Variation coefficient as a function of mixer length for Koch SMX and SMXL mixers.

the center of the main flow under laminar conditions in the static mixers. The parameter, the arithmetic mean value, \bar{x} , represents the fraction of the additive in the total flow.

Key points in Figure 9.42 are

- Longer mixer lengths are required to reduce the variation coefficient.
- Shorter lengths are required for the SMX than for the SMXL.
- Longer mixers are required as the ratio of the additive decreases; it is easier to blend 50/50 than 99/1.
- The length required is insensitive to the viscosity ratio over a range of $0.01 < \mu_1/\mu_2 < 100$.

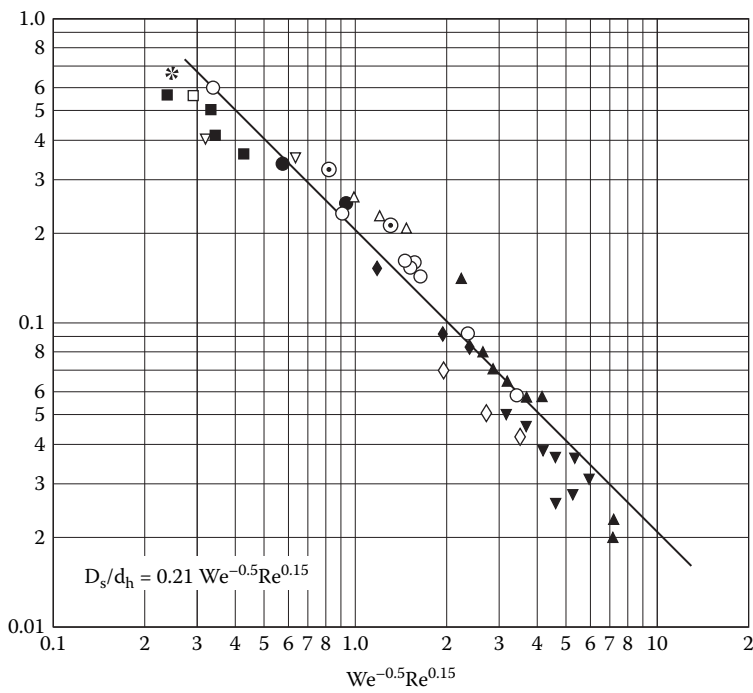
Key points in Figure 9.43 are

- In laminar flow, there are big differences in performance between different mixers.
- The top line represents an open pipe.
- Mixing efficiency does not necessarily follow Figure 9.44. Pressure drop needs to be considered.

A coefficient of variation, σ/\bar{x} , of 0.05 is considered to be a normal level of homogeneity. Less homogeneity may be acceptable if further processing will be done. More homogeneity may be required for critical reactions, particularly when dealing with fast competing chemical reactions.

9.9.7 DISPERSED-PHASE SIZE DISTRIBUTION IN LIQUID-LIQUID AND GAS-LIQUID SYSTEMS

The static mixer creates a hydrodynamic environment where critical viscous shear stresses deform drops, causing them to break. The dispersion process decreases the drop sizes and increases the



Continuous Phase	Dispersed Phase	$\sigma(10^{-3} \text{ N/m})$	$d_h \text{ (mm)}$					
			2	4	8	17	32	64
Water	Benzene	25.5	⊙	●	○			
	Toluene	25			■			
	Cyclohexane	46			*			
	Kerosene	34.7			□			
	Air	74.4			▽	△	◆	◇
Kerosine	Water	24.7			▲	▼		

FIGURE 9.45 Sauter mean drop diameter as a function of Weber and Reynolds numbers for Sulzer SMV mixer.

9.9.8 INTERFACIAL AREAS FOR GAS-LIQUID SYSTEMS

The interfacial mass transfer area, a , is related to the superficial gas velocity, V_G , and gas holdup, Φ_G , for a Sulzer SMV [73], as shown in Figure 9.46. The plot shows that

$$a \propto V_G^{0.85} \Phi_G^{0.15} \tag{9.66}$$

where the proportionality constant varies with the mixer geometry.

9.9.9 MASS-TRANSFER COEFFICIENTS FOR GAS-LIQUID DISPERSIONS

In the same study of gas-liquid mixing in SMV [73], the mass-transfer coefficient, k_L , was found to increase with the average liquid velocity, V_L , as

$$k_L \propto V_L^{1.22} \tag{9.67}$$

TABLE 9.22
Laminar-Flow Pressure Drop in
Static Mixers

Mixer Type	$C = 2fR_e$	$\Delta P_{SM}/\Delta P = K$
Empty pipe	32	1
Kenics KM	184–220	7
Koch-Sulzer SMX	1200–1240	37.5
Koch-Sulzer SMXL	245–250	8.98
Koch-Sulzer SMV	1440	45
Ross LPD	...	8
Ross LLPD	...	3.7
Ross ISG	7300–9600	228
Komax	592–620	25

Note: f is the Fanning friction factor. The Darcy friction factor is $4f$.

TABLE 9.23
Turbulent Flow Friction Factors

Mixer Type	Darcy's Friction Factor
Empty pipe	0.02
Kenics HEV	0.43
Kenics KM	2–3
Sulzer SMXL	3
Sulzer SMV	6–12
Sulzer SMX	12

TABLE 9.24
Measured Laminar Mixing Efficiency for Selected Static Mixers

Mixer Type	$P_{SM}/P(L/D) @ \sigma/\bar{X} = 0.05$	$(L/D) @ \sigma/\bar{X} = 0.05$	$P_{SM}/P = K$
Sulzer SMXL	130–200	17–26	8
Kenics KM	180–200	25–29	7
Sulzer SMX	320–350	9	39
Komax	730	29–38	25
Sulzer SMV	800	18	45
Ross ISG	1700–3000	6–10	300

$$Power = Q\Delta P_{SM} \quad (9.71)$$

where Q is the total flow rate through the static mixer.

9.9.12 MIXING EFFICIENCY

The mixing efficiency, ϵ , of a static mixer has been defined as a normalized product of the pressure drop and the mixing length required to achieve a specified variation coefficient of 0.05:

Plugging potential is related to the complexity of the design. Mixers having streamlined shape elements, such as the Kenics or the simple two-blade design of the Ross LLPD and LPD, are less apt to plug than the more complex Koch or Sulzer SMX and SMXL mixers. Removable mixer elements are preferred over welded-in-place designs for ease of cleaning or modification.

9.10 JET MIXING

9.10.1 INTRODUCTION

Liquid jets, as opposed to impellers/drives, can provide effective mixing in vessels. A typical configuration is to place a pipe/nozzle at the bottom corner of a vessel and directed upward toward the liquid surface on the opposite side. Mixing effectiveness depends on creating flow. This flow is comprised of direct pumped jet flow plus the entrained flow. The jet stream must be free in order to entrain large quantities of surrounding liquid as it moves toward the upper surface. The longer the path of the jet, the more is the liquid that becomes entrained. Jets in tanks provide effective low-viscosity blending when longer mixing times are acceptable. They can be adapted to various vessel shapes, including rail cars, highway transporters, and flat-bottomed storage tanks. Jets can also be used for light-duty solids suspension, as noted in Section 9.6. Jets should not be used for dispersing immiscible liquids, blending viscous fluids, or for any application requiring rapid mixing. Frequently, a transfer pump can serve double duty as a means to provide jet mixing. Mixing times for jet mixers are given by expressions shown in Section 9.10.4. Jet mixing is similar in many ways to mixing using side-entering, wall-mounted propeller mixers.

9.10.2 PRINCIPLES

A free jet moving diagonally through a vessel entrains approximately 15 to 20 times its pumped flow rate. As a first approximation, estimates of mixing times (95%) can be made assuming five turnovers and a 20:1 entrainment ratio. This gives

$$\theta_{approx} = 5V / 20 \cdot (\text{pumping rate}) \quad (9.73)$$

where V is the volume of liquid in the vessel.

While maximizing jet length is important for flow entrainment, applications requiring changing levels sometimes force compromises to be made. It is advisable to aim the jet at the corner representing the lowest expected operating level. This avoids the jet shooting out from the surface when lower levels are reached. At very low liquid levels, the jet must be aimed horizontally across the floor of the vessel. For this case, entrained flows are a half, due to floor effects, and mixing times will be twice that suggested by Equation (9.73).

It is important to create an efficient flow pattern in the vessel. A typical pattern is shown in Figure 9.49. When the jet is aimed diagonally across the tank, in the top view the pattern is symmetrical, and in both top and front views, two symmetrical flow patterns develop.

9.10.3 EQUIPMENT

Figure 9.49 shows the most common arrangement for a jet-stirred vessel. The jet stream expands at an angle of 15° to 25° due to entrainment and decrease in fluid velocity. The jet velocity at the centerline decreases with distance from the nozzle according to

$$V_z = 6 \cdot \left(\frac{d_j}{z} \right) V_j \quad (9.74)$$

TABLE 9.25
Fossett's Values for K in Equation (9.80)

Density Difference (%)	K in Equation (9.80)
1.0	23
2.0	18
6.0	15

$$P = \frac{\rho v_J^2}{2} \left(\frac{\pi \cdot v_J d_J^2}{4} \right) = \frac{\pi}{8} \rho v^3 d_J^2 \quad (9.79)$$

where ρ is in kg/m^3 , d_J is in m, and v_J is in m/s.

An important reference for jet mixing is the work of Fossett [75]. He studied the blending of tetraethyl lead in gasoline stored in very large tanks. Fossett's work included liquids of different densities, ρ_1 and ρ_2 . The jet was submerged a distance S from the surface and was aimed at an angle of α (measured from the horizontal). Equation (9.80) gives a relationship for h , the excess head needed by the jet to overcome the density differences:

$$h = \frac{KS}{\sin^2 \alpha} \left(\frac{\rho_2 - \rho_1}{\rho_2} \right) \quad (9.80)$$

Values of K are experimental and are given in Table 9.25.

Equation (9.81) gives Fossett's equation for mixing time for liquids of equal density:

$$\theta_M = \frac{8T^2}{(Qv_J)^{1/2}} = \frac{0.144T^2}{G^{1/3}h^{1/4}} \quad (9.81)$$

where G is in gallons per minute, T is in ft, h is the excess head given by Equation (9.80), and θ_M is in hours.

Example 9.7

A 3.658-m (12 ft) diameter by 4.572-m (15 ft) tall tank is to be mixed using a 0.3785- m^3/min (100 gpm) pump. The liquid level in the vessel is constant at 3.658m (12 ft), and fluids have equal densities. Determine the mixing time for 95% homogeneity.

Solution

The tank contains 38.44 m^3 (10,152 gal) of liquid.

1. As a first approximation, use Equation (9.73) to estimate the mixing time. Direct substitution in Equation (9.73) gives $\theta_M = 25$ min.
2. Using Equation (9.76), first calculate d_J for a velocity of 9.14 m/s (30 ft/s):

$$d_J = \left(\frac{4Q}{\pi v_J} \right)^{1/2} = \left(\frac{4 \cdot 0.3785}{60 \cdot \pi \cdot 9.14} \right)^{1/2} = 0.0296 \text{ m} = 1.17 \text{ in}$$

An agitated vessel may be operated in either a continuous, batch, or semi-batch mode. In continuous operations, the typical heat-transfer requirement is to maintain a set process temperature by either adding or removing heat, depending on the chemical reaction involved. In batch operations, the heat-transfer process can have a number of different functions at different stages of the operation. Examples include the:

- Establishment of initial reaction temperature
- Maintenance of a set temperature
- Cooling of a product to a final desired temperature

The heat-transfer coefficient on both the “process” (agitated) and “service” (jacket) side may change dramatically during the course of processing, usually as a result of physical property or chemical changes.

Heat transfer seldom dictates equipment design. Process mixing requirements dictate design for the majority of agitated tank systems. Heat transfer is then a necessary adjunct, and the design objective is to accommodate a suitable means of matching the heat-transfer requirements to other process requirements.

Surface area for process heat transfer is made available by means of jackets, coils, baffles, and plates. When these fail to adequately meet process requirements, pumps and external heat exchangers are commonly used. Under certain conditions, condensers can be designed to remove process heat through the refluxing of a solvent or reactant.

9.11.2 IMPORTANT HEAT-TRANSFER CONSIDERATIONS

The following are some of the key issues to consider for designing a new system or to troubleshoot an existing one:

Process characteristics:

- Is the process continuous, semi-batch, or batch?
- Is an exothermic reaction involved?
- Is the heat of reaction known? What is the magnitude of heat release?
- Is there a wall temperature limitation? (reactivity, purity, fouling)
- Are internal surface area devices acceptable?
- Is temperature control important?
- Can desirable heat-transfer rates be maintained by controlling the reaction?
- Is corrosivity a problem?
- Are gases evolved from processing? If so, can gas release rates be controlled?

Batch operations:

- What is the minimum level that will be maintained and its level relative to the agitator?
- Is heat-transfer surface area available at all stages of processing?
- How do the physical properties change during the course of processing?

Fouling:

- Can any undesirable reactions occur in the vapor space of the vessel that may deposit on the upper surface?
- Will controlling the wall temperatures prevent fouling?
- Will the process foul the surface of the vessel or any internals?
- Are solids formed upon cooling or in the course of reaction?
- Is the design suitable for cleaning?

Safety:

- Is the heat release due to mixing?

9.11.4 HEAT-TRANSFER SURFACES AND EFFECTIVE AREA

Jackets, internal helical pipe coils, tube baffles, and plate coil baffles are used to provide heat-transfer surface area. The only surface area effective for heat transfer is that portion that is wetted by both service and process fluids. The effective heat-transfer area for some items may be determined as follows:

- Use the total wetted area for plain or spirally baffled jackets.
- The area between the half-pipes is not totally effective for heat transfer when using half-pipe coil jackets, usually fabricated from 2-, 3-, or 4-in. pipes with typical 3/4-in. spacing.
- The total outside wetted area is effective for internal helical coils:

$$A_{co} = \pi d_{co} H_c n \left(\pi d_c^2 + n^{-2} \right)^{0.6} \quad (9.84)$$

where n = number of coil turns per foot of coil height = $1/p$; H_c = total height of coil, ft; and d_c = centerline diameter of coil helix, ft.

9.11.5 JACKETS AND OTHER APPLIED DEVICES

Jackets form what amounts to a double wall on the mixing vessel. Several varieties are possible, as illustrated in Figure 9.52. The plain jacket is the simplest construction and therefore the lowest initial cost. It is suitable for condensing heating fluids such as steam, but results in very poor performance using sensible heat-transfer fluids. Large passage areas limit the ability to create good wall velocities.

Installation of “agitating” nozzles is recommended if sensible liquid heating or cooling is to be used with plain jackets. Nozzles produce liquid jets directing the inlet jacket fluid in a spiral fashion into the jacket. This increases the effective velocity and turbulence level. Vendors have information dealing with their performance and installation.

Spiral-baffled jacket: The spiral-plate baffle consists of a spiral strip welded edgewise to the shell. This forms a channel that raises the velocity next to the wall. The largest drawback to this baffle is that there will inherently be some clearance between the edge of the baffle and the tank wall, allowing fluids to bypass the spiral passageway.

Half-pipe jacket: This type of jacket consists of a half-pipe section welded to the vessel wall. This construction is quite good if high jacket pressures are required, but it is also an expensive method, because each course requires two long welds along each edge of the cut pipe. It is suitable for sensible heating/cooling but not for condensing/vaporizing fluids. Heat-transfer predictability is well defined, since the geometry is known and no bypassing is possible.

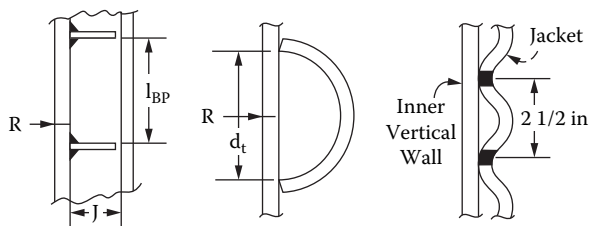


FIGURE 9.52 Jacket designs: spiral, half pipe, dimpled.

- A standard condenser
- A reflux (or knock-back) condenser
- A sensible heat exchanger through which the vessel contents are circulated

These external auxiliary devices are only required when the heat-transfer requirements cannot be met by use of jackets or internal devices.

9.11.9 PROCESS-SIDE HEAT-TRANSFER CORRELATIONS

Heat-transfer coefficients on the agitated side are determined by the same principles as for any other heat-transfer process. Correlations have been developed for each of the major impeller types. These are all basically of the same form, but differ only in the pre-proportionality constant and values of the exponents.

The general form of the correlating equation is

$$Nu = \frac{h_o T}{k} = K \cdot \text{Re}^a \cdot \text{Pr}^b \cdot \left(\frac{\mu}{\mu_w} \right)^c \quad (9.85)$$

where K accounts for geometry variations.

Note that Equation (9.85) is basically the same general form as the familiar Dittus-Boelter equation for heat transfer in tubes. The basic heat-transfer mechanism is identical. It is dependent on the flow of fluid next to the heat-transfer surfaces, whether these are the vessel walls or some internals. Differences in the correlations are therefore mainly due to the differences in flow characteristics generated by the different impellers relative to the surface under consideration. This is reflected in the value of K .

These correlations are all of an overall nature and do not take variation in flow due to the flow pattern into account, nor do they consider any local variation in fluid bulk temperature in the vessel. If these things are critical to the application being considered, either experimentation, CFD modeling, or consultation with a vendor will be required.

The process-side heat-transfer coefficient (for flat-blade turbines) for heat transfer to a jacket is based on the work of Brooks [78]. The recommended correlation is

$$Nu = \frac{h_o T}{k} = 0.74 \cdot \text{Re}^{0.66} \cdot \text{Pr}^{0.33} \cdot \left(\frac{\mu}{\mu_w} \right)^{0.14} \quad (9.86)$$

where Re = impeller Reynolds number; h_o = heat-transfer coefficient at the vessel wall; k = thermal conductivity of the process fluid, $\text{W/m} \cdot ^\circ\text{K}$ ($\text{Btu/h} \cdot \text{ft} \cdot ^\circ\text{F}$); T = tank diameter, m (ft); Nu = Nusselt number; Pr = Prandtl number; Re = Reynolds number; μ = viscosity of the process fluid, $\text{Pa} \cdot \text{s}$ (cP); and μ_w = viscosity of the process fluid at the vessel wall, $\text{Pa} \cdot \text{s}$ (cP).

Other authors have extended the basic correlations to include more details of the impeller geometry, such as blade width, pitch, and number of blades. As long as the process is in the turbulent regime, most of these geometrical variables have little impact on heat transfer, and their use is not recommended until details of an agitation system are selected or in place.

Ackley [79] suggests use of Equation (9.87) for unbaffled retreat-curve (blade) impellers typically used in glass-lined vessels:

$$Nu = \frac{h_o T}{k} = 0.68 \cdot \text{Re}^{0.67} \cdot \text{Pr}^{0.33} \cdot \left(\frac{\mu}{\mu_w} \right)^{0.14} \quad (9.87)$$

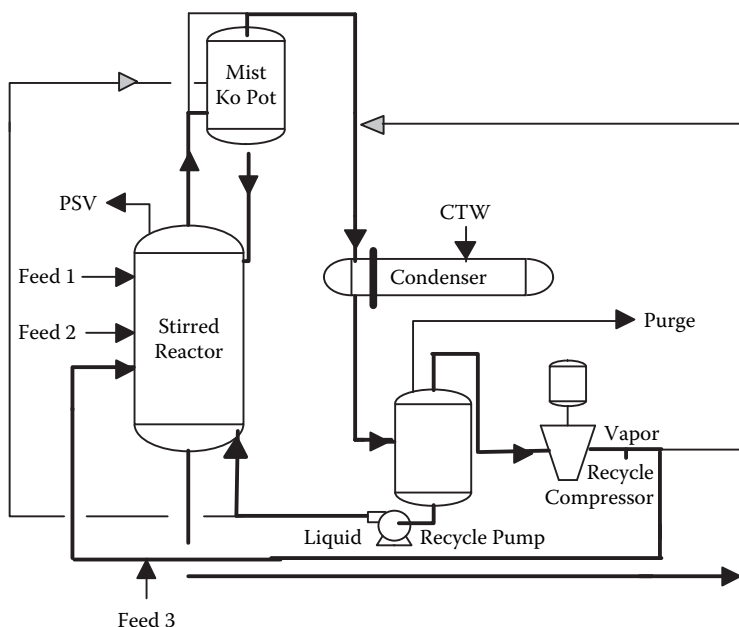


FIGURE 9.54 Reactor system schematic.

These equations require the use of the equivalent diameter, D_e , of the jacket. This is calculated by

$$D_e = \left(\frac{D_{jo}^2 - D_{ji}^2}{D_{ji}} \right)$$

and flow area A_x , by

$$A_x = \pi \cdot \left(\frac{D_{jo}^2 - D_{ji}^2}{4} \right)$$

The flow area is used to calculate the velocity, V , in the Reynolds number term.

Example 9.8

A reactor is operated according to the system schematic shown in Figure 9.54. Boiling of the carrier that is condensed out of the vapor provides most cooling, and both condensate and uncondensed gas are recycled to the reactor. This reactor has a dimpled jacket. Calculate the heat duty of the jacket under the given conditions.

The following system engineering data are provided.

Reactor: 12-ft diameter, 24-ft straight side height, 12-ft liquid level

Impeller: 5-ft diameter flat-blade turbine @ 37 rpm

Production: 10,000 lb/h

Heat of reaction: 1500 Btu/lb

Operating temp.: 85°C (176°F)

4. Harvey, A. D., S. P. Wood, and D. E. Leng, *Chem. Eng. Sci.* 52: 1479 (1997).
5. Oldshue, J. Y., *Fluid Mixing Technology*, M.-H. Publications, Chemical Engineering, New York, 1983.
6. King, R., in *Mixing in the Process Industries*, N. Harnby, M. F. Edwards, and A.W. Nienow, eds., 414, Butterworth Heinemann, Oxford, 1992.
7. Ulbricht, J. J., and J. J. Patterson, *Mixing of Liquids by Mechanical Agitation*, J. J. Ulbricht, ed., vol. of *Chemical Engineering: Concepts and Reviews*, Gordon and Breach Science Publishers, New York, London, Paris, Montreux, Tokyo, (1986).
8. Metzner, A. B., and R. E. Otto, *AIChE J.* 3: 3 (1957).
9. Wichterle, K., and O. Wein, *Int. Chem. Eng.* 21: 116 (1981).
10. Elson, T. P., D. J. Cheesman, and A. W. Nienow, *Chem. Eng. Sci.* 41: 2555 (1986).
11. Todtenhaupt, P., E. Todtenhaupt, and W. Muller, *Handbook of Mixing Technology*, EKATO Ruhr-und Mischtechnik. Schopfheim, Germany GmbH, 1991.
12. Grenville, R. K., S. Ruszkowski, and E. Garred, "Blending of Miscible Liquids in the Turbulent and Transitional Regimes," NAMF Mixing XV, Banff, Canada, 1995.
13. Tatterson, G. B., *Fluid Mixing and Gas Dispersion in Agitated Tanks*, McGraw-Hill, New York, 1991.
14. Nagata, S., *Mixing Principles and Applications*, Halstead Press, a division of John Wiley and Sons, New York, 1975.
15. Levenspiel, O., *Chemical Reaction Engineering*, John Wiley, New York, 1972.
16. Kolmogoroff, A. N., *Compt. Rend. Acad. Sci. URSS* 30: 301 (1941).
17. Kolmogoroff, A. N., *Compt. Rend. Acad. Sci. URSS* 32: 16 (1941).
18. Rosensweig, R. E., *AIChE J.* 10: 92 (1964).
19. Batchelor, G. K. J., *Fluid Mech.* 5: 113 (1959).
20. Corrsin, S., *AIChE J.* 10: 87 (1964).
21. Baldyga, J., and J. R. Bourne, *Chem. Eng. Commun.* 28: 231 (1984).
22. Baldyga, J., and J. R. Bourne, *Chem. Eng. Commun.* 28: 243 (1984).
23. Baldyga, J., and J. R. Bourne, *Chem. Eng. Commun.* 28: 259 (1984).
24. Baldyga, J., and J. R. Bourne, *Chem. Eng. J.* 42: 83 (1989).
25. Baldyga, J., and J. R. Bourne, *Chem. Eng. J.* 42: 93 (1989).
26. Baldyga, J., and J. R. Bourne, *Chem. Eng. J.* 45: 25 (1990).
27. David, R., and J. Villermaux, *Chem. Eng. Comm.* 54: 333 (1987).
28. Tosun, G., "An Experimental Study of the Effect of Mixing in BaSO₄ Precipitation Reaction," Sixth European Conference on Mixing, Pavia, Italy, 1988.
29. Doraiswamy, L. K., and M. M. Sharma, *Heterogeneous Reactions*, vols. 1 and 2, Wiley Interscience, New York, 1984.
30. Danckwerts, P. V., *Gas-Liquid Reactions*, McGraw-Hill, New York, 1970.
31. Fasano, J. B., and W. R. Penney, *Chem. Eng. Prog.* 87: 46 (1991).
32. Paul, E., *Chem. Ind.* 21: 320 (1990).
33. Paul, E., *Chem. Eng. Sci.* 43: 1773 (1988).
34. Middleton, J. C., "Motionless Mixers as Gas-Liquid Contacting Devices," AIChE 71 Annual Meeting, Miami, 1978.
35. Leng, D. E., *Chem. Eng. Prog.* 87: 23 (1991).
36. Maude, A. D., and R. L. Whitmore, *Br. J. Appl. Phys.* 9: 477 (1958).
37. Zwietering, T. N., *Chem. Eng. Sci.* 8: 244 (1958).
38. Nienow, A. W., *Chem. Eng. Sci.* 23: 1453 (1968).
39. Joosten, G. E. H., J. G. M. Schilder, and A. M. Broere, *Trans. Instn. Chem. Engrs.* 55: 220 (1977).
40. Mak, A. T. C., S. Yang, and G. Ozcan-Taskin, "The Effect of Scale on the Suspension and Distribution of Solids in Stirred Vessels," G.F.d.G.d. Procides, Mixing IX, Paris, 1997.
41. Mak, A. T. C., and S. W. Ruszkowski, "Scaling-Up of Solids Distribution in Stirred Vessels," I. Chem.E., Mixing IV, University of Bradford (*I. Chem. E.* 121: 379 1990).
42. Oldshue, J. Y., and N. R. Herbst, *A Guide to Fluid Mixing*, Lightnin, Rochester, NY, 1992.
43. Armenante, P. M., H. Yu-Tsang, and L. I. Tong, *Chem. Eng. Sci.* 47: 2865 (1992).
44. Nienow, A.W., D. J. Wilson, and J. C. Middleton, Proc. 2nd European Conf. on Mixing, Cambridge, England, 1977.
45. Middleton, J. C., in *Mixing in the Process Industries*, E. A. N. Harnby, ed., 322, Butterworth Heinemann, Oxford, 1995.

4. Since the amount of transfer (or separation) in a single stage (or single contact) is generally inadequate, multiple contacts are often employed in industrial processes. Generally, countercurrent flow of the two liquids is employed in the overall separation process. With multiple stages, most of the desired component often can be extracted.
5. Frequently, the extract is processed to recover the solute in a more or less pure form. This latter step is sometimes one of the following: distillation, evaporation, freeze drying, crystallization or precipitation, and filtration.

When solvent extraction is employed, two largely immiscible liquids (e.g., an aqueous feed and an organic solvent) are mixed together, allowed to settle, and then separated. During these steps, one or more species that are initially dissolved in the feed liquid transfer to the other liquid phase to form an extract. The feed liquid residual, or raffinate, is thus partly depleted of the solutes, and the original solvent becomes enriched in them. In this way, LLE can be used to separate and purify solutes.

Thermodynamic equilibrium between the two liquids determines the direction of mass transfer and the theoretical amount of compound(s) transferred in a given step. The rate of transfer depends on the level of agitation provided to the dispersion and the interfacial areas between the phases. After the extraction step is completed, separation of phases is (hopefully) rapid. As already indicated, the separated phases are often then sent countercurrent to another extraction unit [2]. Countercurrent cascades of mixers and settlers generally provide the most efficient use of solvent.

Two liquid phases may be contacted in different ways to achieve separation. In the laboratory, the simplest example of LLE involves the use of a separatory funnel where a feed mixture, perhaps an aqueous phase from a reactor, is contacted with several washes of solvent (say, diethyl ether) to extract a solute. If the same aqueous phase is contacted repeatedly with fresh amounts of extracting solvent, such a process is said to be *crosscurrent*.

Industrial applications usually are based on the most efficient methods that involve the countercurrent flow of two liquids across multiple stages. A variety of mechanical devices are available that can be used to achieve such mixing and separate the resulting extract and raffinate and so achieve the desired separation. Once the extraction is complete, almost always both the extract and raffinate need to be treated to recover solvent residuals as well as the desired products.

Liquid-liquid extraction is often advantageous if the solute is heat sensitive and can be recovered by LLE at ambient conditions. It is also advantageous whenever direct separation (e.g., distillation) is too expensive. LLE tends to be advantageous whenever the solvent has a high affinity for the solute and is highly selective for the solute, and the solute is present in very low concentrations and cannot be easily removed by direct separation techniques. Under the right conditions, it can provide high recovery and concentration factors to enable the economic purification of resource materials even when they are found in dilute forms. It is often used to reduce energy consumption by enabling preconcentration of a resource with minimal energy expenditures.

The disadvantages of solvent extraction usually revolve around the solvent cost. Since high solvent losses can easily make an extraction process uneconomical, considerable effort is usually expended to find solvents that are economical and can be easily recovered and recycled.

There are usually many candidate solvents for any particular application. Important factors to consider are (1) the affinity of the solute for the solvent (i.e., its distribution coefficient should be large); (2) the affinity of other species in the mixture for the solvent (i.e., their distribution coefficients should be small); (3) solvent safety considerations (e.g., flammability and toxicity); (4) solvent handling properties such as density, viscosity, and vapor pressure; (5) solvent solubility in the raffinate phase (high solubilities may translate into high solvent losses unless steps are taken to prevent such losses); and (6) solvent cost. In addition, liquid-liquid interfacial tension affects the interfacial area and the rate of mass transfer between the phases.

Safety and health are also often issues for extraction, particularly whenever the potential of fire from using highly flammable solvents is high. On the other hand, LLE is favored in the nuclear

substantially as new, environmentally acceptable techniques are developed and applied to solve separation problems.

Supercritical or near-critical fluids can be used both for extraction and chromatography. Many chemicals, primarily organic species, can be separated and analyzed using this approach [6], which is particularly useful in the food industry. Substances that are useful as supercritical fluids include carbon dioxide, water, ethane, ethene, propane, xenon, ammonia, nitrous oxide, and a fluoroform. Carbon dioxide is most commonly used, typically at a pressure near 100 bar. The required operating pressure ranges from about 43 bar for propane to 221 bar for water. Sometimes a solvent modifier is added (also called an *entrainer* or *cosolvent*), particularly when carbon dioxide is used.

On a laboratory scale, supercritical fluids may be contacted with a substrate on a once-through basis. Typically, the pressurized fluid is heated and passed through a chamber containing a solid or liquid sample. The desired solute selectively dissolves in the pressurized fluid and is transported out of the chamber and through a throttle into a container where the pressurized fluid evaporates at atmospheric pressure, leaving a solute residue in the container.

Small-scale supercritical extractions may be either dynamic or static. If the fluid is pumped through the sample chamber continuously, then the method is dynamic. If the sample container is filled batchwise with pressurized fluid, then the method is static. In the latter case, the sample container is charged, equilibrated statically, and then discharged through a throttle to collect the residue as before. In either case, the pressurized fluid or solvent is not recycled, and this feature limits the applicability to industrial use, because solvent costs, even with recycle, often determine whether or not extraction is economical.

More important solvent extraction references include the *Handbook of Solvent Extraction*, edited by Lo, Baird, and Hanson [7]. International Solvent Extraction Conferences (ISECs) have been held, and the proceedings, usually two or three volumes from each conference, provide considerable information, particularly of ongoing studies. Akell and King [8] have edited a volume of selected papers taken from ISEC '83, including papers of significant chemical engineering content and which focus on developments in solvent extraction equipment design. Schügerl [4] has written a monograph on the use of LLE in biotechnology, primarily to recover metabolites. Kulov [9] has edited a book focusing on the kinetics of LLE. This last book also includes chapters on gas-liquid kinetics, which is appropriate since many of our kinetic models for LLE are derived from analogy with gaseous diffusion. Blumberg [10] also provides a book on LLE that may prove helpful. Marcus and Kertes [11] and Marcus, Kertes, and Yanir [12] provide extensive data on extraction systems that are based on solvation and ion exchange reactions.

10.2 DISPERSION, MASS TRANSFER, AND COALESCENCE

Quantitative and (hopefully, at least) qualitative considerations are helpful in characterizing a liquid-liquid system for a potential extraction application. Batch shakeout tests are frequently the easiest way to determine basic feasibility by simply measuring the primary and secondary break times and by analyses to measure the compositions of the equilibrated phases. Such tests are readily conducted by mixing small volumes of each phase in a vial, which is then vigorously agitated and placed on a lab bench to settle. The resulting behavior of the liquid-liquid mixture depends on physical properties and system characteristics. The greater the density difference and interfacial tension between the two liquid phases, for example, the more rapidly the phases tend to separate. More viscous systems separate more slowly.

The primary break time is that length of time required to form a clearly defined interface between the two phases, although both phases may still remain hazy. The physical properties of the liquid-liquid system and the vigor of mixing are of critical importance and usually provide qualitative information that permits rapid screening of large numbers of solvents with minimal effort. The resulting primary break time should be on the order of 1 or 2 min; Treybal [13] suggests

inert diluent and an active extractant that reacts with the inorganic species. The extractant solvates the solutes so that they transfer into the organic layer. Chemical reactions may be characterized either as solvation reactions or those involving ion exchange. Solute mass transfer in this instance is from the aqueous to the oily solvent phase.

Similarly, chemical reactions may be used to convert a lipophilic chemical into a hydrophilic, water-seeking species. Solute mass transfer then occurs from the oily solvent phase into the aqueous phase. Pure fluids or mixtures of species that form hydrogen bonds or contain polar moieties are usually highly nonideal. In pure fluids, strong attractive interactions between like molecules may cause molecular aggregation through dipole-dipole and other interactions. In mixtures, specific interactions can occur between molecules of the same species (self-association) or between molecules of different species (solvation).

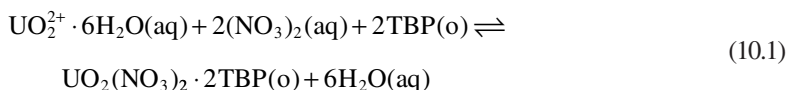
10.3.1 LIGNIN EXTRACTION

Relatively large, complex lignin molecules can be extracted by complexation, solvation, and coordination with the correct solvents. The black liquor produced by the Kraft pulping process is an alkaline mixture of lignin-bearing micelles. It is essentially opaque and darkly colored, hence its name. When acidified with dilute sulfuric or hydrochloric acid, the micelles are acidified, and the oily lignin is liberated. It floats to the top of the aqueous phase to form an interfacial precipitate.

A solvent mixture can form an effective solvation system for lignin obtained from black liquor, whereas individual components in the solvent mix are ineffective. Acetone alone is miscible with black liquor, so it cannot be used as a solvent by itself, since it doesn't form a second liquid phase when mixed with water. The solvent 2-ethylhexanol is immiscible with water but does not extract lignin from acidified black liquor. On the other hand, a one-to-one by volume mixture of 2-ethylhexanol and acetone extracts much of the acidified lignin and about half of the total dissolved solids. The resulting aqueous phase is water-white after acidification and extraction by this solvent mixture. The resulting organic layer is ruby red. Presumably, acetone displaces sufficient waters of hydration around lignin to enable the resulting acetone-lignin complex to coordinate with 2-ethylhexanol and transfer into the organic layer. This system dramatically illustrates the power of extraction by solvation and coordination.

10.3.2 SIMPLIFIED TBP REACTION MODELS

As used in the tri-*n*-butyl phosphate (TBP), or PUREX, process to recover uranium (U) and plutonium (Pu), the solvent is typically a blend of about 30 vol% TBP and 70 vol% of an aliphatic diluent, say C-12 to C-15 branched paraffins. Spent nuclear fuel⁵ is dissolved in nitric acid and then contacted with this TBP solvent. Actinide elements, primarily uranium and plutonium, are coextracted into the organic layer by coordination and solvation with TBP. The extraction of uranium, for example, is thought to occur by the following reaction [14–21]:



indicating that uranyl nitrate hexahydrate in the aqueous phase coordinates with two molecules of TBP in the organic phase to form an anhydrous uranyl nitrate solvate with TBP in the organic phase and leaves six waters of hydration behind in the aqueous phase when it transfers.

The extraction of water by TBP requires a more rigorous model, but the extraction of U and HNO₃ by TBP can be modeled fairly accurately using simplified models based on equilibrium constants and the law of mass action. At least one reaction must be assumed for each species that extracts. In the case of uranium and nitric acid, the following simplified reactions [5] can be assumed:

that are incompatible with normal PUREX operations. While TBP strips well in the presence of dilute acid, say around 0.01 M HNO_3 or less, DBP and MBP are acidic extractants that complex actinides strongly under these same conditions. For this reason, it becomes difficult, if not impossible, to remove actinides from TBP extract using a dilute acid scrub after MBP and DBP have grown into it as radiolysis products. To maintain solvent viability, it must first be treated with aqueous sodium carbonate wash to remove the degradation products, after which it can be recycled to extract more U and Pu.

Like lignin in alkaline NaOH, DBP and MBP can be removed from TBP solvent by forming micellar structures in alkaline sodium carbonate wash solutions. Actinides that were originally complexed by DBP and MBP in the TBP organic phase prior to carbonate wash are also transferred from the solvent and are loosely incorporated into the micellar structure of the wash, the aqueous raffinate.

Reactive solvent extraction can then be used to recover the actinides from such scrub solutions, not by extracting the actinides but rather by extracting the degradation products [22] into an alcohol solvent layer. Acidification of carbonate scrub washes with nitric acid destroys the carbonate and forms an interfacial crud that floats to the top of the aqueous phase. This crud is similar in behavior to that formed by acidified lignin.

If the same acidification is performed while the scrub solution is actively mixed with 2-ethylhexanol, then a different result is achieved. In this latter case, the degradation products extract into the organic phase rather than forming an interfacial crud. When properly extracted, the resulting aqueous phase is then suitable for recycle back to the PUREX process and subsequent actinide recovery using conventional PUREX chemistry. The 2-ethylhexanol containing the degradation products can be treated using caustic wash to remove them and to enable 2-ethylhexanol solvent recycle.

10.4 DISTRIBUTION COEFFICIENTS

The initial solvent and feed concentrations, the desired final concentrations, and equilibrium behavior determine the direction of mass transfer, the minimum solvent-to-feed ratio, and the minimum theoretical tray requirements. These theoretical trays (or stages) are analogous in many respects to theoretical plates of a distillation column, and absorption (or stripping) columns discussed by Fair in another chapter. For any particular solvent-to-feed ratio, equilibrium relationships and the operating line determine theoretical stage requirements.

Experimental equilibrium data are almost always essential. While theoretical models are available to predict such data, and are very helpful in preliminary design, pilot studies and scaleup should be based on confirmed experimental measurements. Many nomographs providing data are available. Wisniak and Tamir [23–26], Sorensen and Arlt [27–29], and Macedo and Rasmussen [30] provide useful compilations of LLE data. Tiegs [31] provides activity coefficient data at infinite dilution. Although these data are generally quite good, users are advised to at least spot check them for accuracy.

10.4.1 THERMODYNAMIC MODELS

Thermodynamic models predict phase equilibrium. They can be based on solubility considerations alone or on chemical reactions between the two liquid phases.

10.4.2 NONREACTIVE SYSTEMS

When two liquid phases are thoroughly mixed in a closed system at constant temperature and pressure,* the mixture reaches thermodynamic equilibrium. At equilibrium, the fugacities of each species in each liquid phase are equal, and

* The pressure dependence is weak except near the critical point.

10.4.3 REACTIVE SYSTEMS

As mentioned above, chemical theory has been applied in many instances to explain nonideal behavior [36, 37]. Dolezalek [38] was one of the first to assume that hydrogen bonding forms new chemical species in mixtures. Since then, chemical theory has been applied to a wide range of thermodynamic problems [39–42].

Using chemical theory, one must hypothesize reactions to form specific aggregates (i.e., the “true” species) by complexation. This is a disadvantage for at least two reasons. First, there are usually many plausible aggregates. Second, each hypothesized aggregate introduces additional adjustable parameters. Thus, significant experimental data are needed to fit model parameters and to distinguish between alternative equilibria. On the other hand, chemical models can be highly effective while still relatively simple (e.g., the TBP model above), and they can give insight into the nature of the solvent extraction process and the best ways to exploit chemical behavior.

Lattice theories [37] enable one to consider nonspecific physical forces (e.g., molecular dipole moments, induction effects, and London dispersion forces) and have been applied successfully to model nonideality in a wide range of mixtures. Guggenheim [43] was the first to develop a quasichemical theory using lattice models. Wilson [44], Renon and Prausnitz [45], Abrams and Prausnitz [46], and Vera et al. [47] modified it for nonrandom mixtures. Panayiotou and Vera [48, 49] developed expressions for estimating local surfaces and compositions based on quasichemical theory. Kumar et al. [50] revised the equations for multicomponent mixtures. Martinez [51] applied lattice theory to clustering and dissociation. Sayegh and Vera [52] provide a review.

Tri-*n*-butyl phosphate (TBP) is a reactive extractant that has been widely used in the processing of heavy metal ores and spent fuel elements [53]. It is often mixed with a diluent to improve solvent properties (e.g., to reduce viscosity or to control its extraction power). Such diluents include paraffins such as Amsco 125-82 and *n*-heptane, benzene, and, to a lesser extent, chloroform and carbon tetrachloride.

Tributyl phosphate extracts metals by solvation and can be considered a reactive solvent, but experimental evidence suggests that it may also dimerize [54]. Of course, adding paraffinic diluents to TBP decreases the degree of TBP self-association by mass action, and diluents such as chloroform or 1-butanol may also form TBP solvates [55]. Phosphorus NMR shift in the system *n*-heptane and TBP suggests that diluent mass action and TBP dissociation in the dilute TBP range affect phosphorus chemical shift [54–56]. Rytting et al. [57] arrived at a similar conclusion from studying TBP and carbon tetrachloride mixtures in the dilute TBP range. Extraction studies often suggest the existence of complexes of the TBP monomer and dimer in the presence of diluents [58, 59], but virtually all of these investigators have assumed that solvation and association reactions form ideal mixtures in the TBP-diluent phase rather than attempting to evaluate activities.

A more realistic approach attempts to describe each equilibrium in terms of its thermodynamic equilibrium constant, molar volumes of specific aggregates, and a heat of reaction to estimate the chemical contribution to excess enthalpy H_{chem}^E . The first two parameters contribute to the excess Gibbs energy g^E model.

A more general reaction model considers both chemical (specific) and physical (nonspecific) contributions to excess Gibbs energy. Using TBP as an example, one first begins by assuming that the physical and chemical contributions are separable so that

$$g^E = g_{chem}^E + g_{phys}^E \quad (10.13)$$

Then the chemical contribution can be computed from the estimated “true” mole fractions. With the assumption that the mixture is ideal, chemical activities simply equal the true mole fractions of monomeric species, and Prigogine and Defay [60] have shown that, regardless of the solvation or association reactions that may occur, in an ideal true mixture with $g_{phys}^E = 0$,

$$g_{phys}^E = g_{ms}^E + g_{sd}^E + g_{rs}^E \quad (10.18)$$

By equating activities for the stoichiometric species with those for the monomers, one eventually obtains an expression for the stoichiometric activity coefficient:

$$\gamma_{i,s} = \frac{\gamma_i z_{i1}}{x_{i,s} \gamma_i^o z_{i1}^o} \quad (10.19)$$

in terms of monomeric mole fractions in the true mixture and reference states, the stoichiometric mole fraction, and activity coefficients in the true mixture and reference states.

Additional details describing these models can be found elsewhere [61–63]. Such models describe extraction and enthalpic behavior, and measured shifts in nuclear magnetic resonance.

10.4.4 EMPIRICAL DISTRIBUTION MODELS

In preliminary design work, it is convenient to correlate distribution coefficients on a mass-fraction basis. An empirical correlation technique that is simple to use and often highly effective is

$$\ln D_i = \beta_0 + \sum_{i=1}^n \beta_i X_i + \beta_{n+1} V_m + \beta_{n+2} / T \quad (10.20)$$

where the β_i are empirical parameters; X_i are mass fractions at equilibrium in the mixture; V_m is the stoichiometric volume fraction of the active extractant, which is a solvent blend; and T is the temperature in either K or R. The variable n is the number of components in the mixture. While it is true that D_i may exhibit a composition dependence on any of the species in a mixture (i.e., $\beta_i \neq 0$, $i = 1, 2, \dots, n$), it is also commonly true that only a few of the β_i parameters inside the summation term on the right-hand side of Equation (10.20) are statistically nonzero. In fact, the strongest dependence may simply be on the solute mass fraction, while other species can be ignored. In any event, the appropriateness of Equation (10.20) is easily determined by fitting experimental data.

Equation (10.20) is often sufficient to model a liquid-liquid extraction system, especially in the early stages of design. Its simplicity is advantageous, but it has no theoretical basis. As a consequence, users should be careful not to extrapolate it to untested compositions. An additional limitation is the fact that Equation (10.20) does not predict the locus of the mutual solubility curve, and, for $\beta_i > 0$, one might be tempted by this equation to extrapolate to conditions that are actually outside the two-phase region (see Figure 10.1).

Many useful solvents are actually blends of a diluent and a modifier. These blends are often formulated on a volume basis (e.g., 30 vol% TBP in Isopar-M), and for such systems the V_m variable is helpful if the solvent blend can be designed and optimized.

The key feature of Equation (10.20) that makes it particularly useful is the fact that D_i often exhibits a weaker composition dependence than K_{D_i} , which is based on the ratio of mole fractions as shown in Equation (10.11).

10.5 DESIGN OF EXTRACTION SYSTEMS

Liquid-liquid extraction columns may be designed in three different ways: (1) as a collection of equilibrium stages, (2) as a continuous differential contactor with mass transfer, or (3) using purely kinetic models. The first two methods are more commonly used (particularly the first) and, when correctly and carefully performed, they give essentially the same results. The latter method, design

TABLE 10.1
Liquid-Liquid Equilibrium Data Obtained at 25°C
and 1 atm [64]

LLE Data for Acetic Acid (A), Water(W), and Isopropyl Ether (E)

Water-Rich Layer			Ether-Rich Layer		
Wt% A	Wt% W	Wt% E	Wt% A	Wt% W	Wt% E
1.41	97.1	1.49	0.37	0.73	98.9
2.89	95.5	1.61	0.79	0.81	98.4
6.42	91.7	1.88	1.93	0.97	97.1
13.30	84.4	2.3	4.82	1.88	93.3
25.50	71.1	3.4	11.4	3.9	84.7
36.70	58.9	4.4	21.6	6.9	71.5
45.30	45.1	9.6	31.1	10.8	58.1
46.40	37.1	16.5	36.2	15.1	48.7

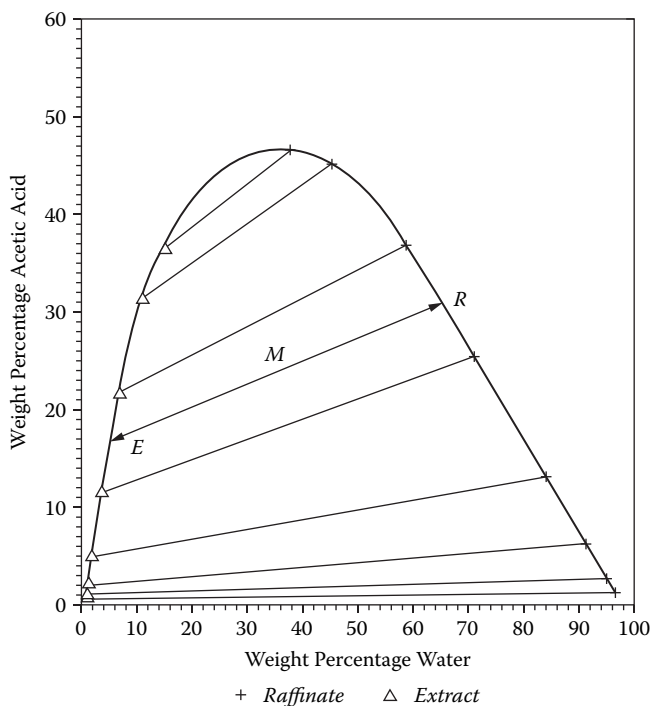


FIGURE 10.2 Liquid-liquid data for the system water, acetic acid, and isopropyl ether. Since mixture M falls inside the mutual solubility curve, it separates into extract and raffinate phases with compositions E and R , respectively. The equilibrium data are at 25°C and 1 atm.

where R and E are the masses of raffinate and extract, respectively, and x_{ij} are mass fractions, with $i = \{w, a\}$ referring to either with water or acetic acid mass fractions and $j = \{e, m, r\}$ referring to either point E , M , or R .

The point M is also known as the mix point, and it defines the overall stoichiometric composition of the mixture (i.e., the composition if only a single phase was formed by mixing), while the extract and raffinate compositions E and R are found from constructing a line parallel to the nearest tie line that also intersects the mix points and the mutual solubility curve.

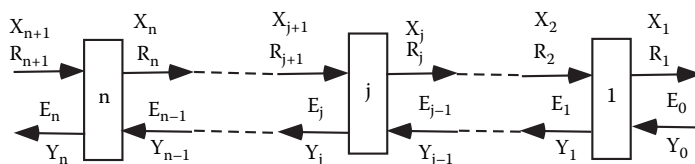


FIGURE 10.4 Stages in a countercurrent cascade. R_{n+1} is the aqueous feed. E_0 is the fresh solvent.

$$M = E_0 + R_{n+1} = E_n + R_1 \quad (10.23)$$

which can be rearranged to give the difference point D ,

$$D = E_0 - R_1 = E_n - R_{n+1} \quad (10.24)$$

As shown in Figure 10.5, the line $E_0 - R_1$ intersects the line $E_n - R_{n+1}$ at the D -point. Graphically, all lines that intersect the D -point and a raffinate composition on the mutual solubility curve between R_1 and R_{n+1} , say R_{j+1} , also intersect the extract composition, E_j , on the solvent-rich side of the mutual solubility curve. So each line intersecting the D -point and a raffinate composition, R_{j+1} , also intersects the extract, E_j , which is passing that raffinate on the j th stage. If the extract E_j and raffinate R_j leaving the j th stage are assumed to be at equilibrium, then a graphical method can be used to step off theoretical stages, as shown in Figure 10.6.

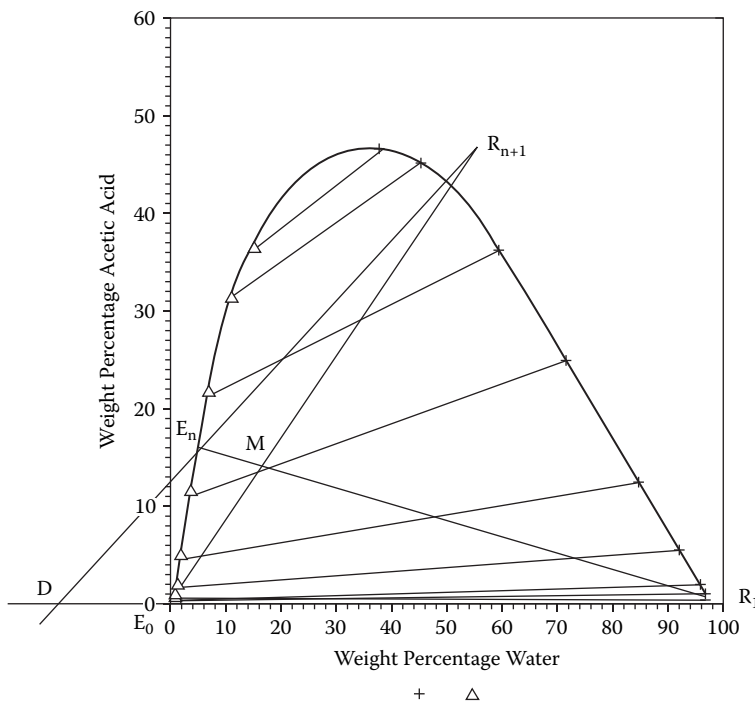


FIGURE 10.5 Liquid-liquid data at 25°C for the system water, acetic acid, and isopropyl ether. Mixing liquids with compositions R_{n+1} and E_0 results in mix point M . Specification of R_1 yields E_n , since the same line also intersects M . The equilibrium data are at 25°C and 1 atm.

$$\phi_E = \frac{E_e - 1}{E_e^{N+1} - 1} \quad (10.26)$$

where ϕ_E is the solute fraction in the entering feed that is not extracted, N is the required number of theoretical (or equilibrium) stages to extract $1 - \phi_E$ fraction of the feed, and E_e is the extraction factor, which is constant.

Example: 10.1

A countercurrent LLE cascade is needed to remove 99% of solute species A from an aqueous phase. The aqueous feed rate is 100 kg/h, and the feed contains 5 mass% species A. The distribution coefficient, on a mass ratio basis, is nearly constant, and D_i equals 1.4 kg water/kg solvent. How many theoretical stages are needed if pure solvent can be provided to the cascade at a rate of 90 kg/h?

Solution

$E_e = D_i E/R = 1.4(90)/100 = 1.26$, and the fraction not extracted is $\phi_E = 0.01$. Rearranging Equation (10.26) gives

$$N + 1 = \ln[(E_e + \phi_E - 1)/\phi_E] / \ln(E_e) = \ln(27) / \ln(1.26) = 14.26$$

$N = 13.26$ theoretical stages.

10.6 INDUSTRIAL EXTRACTION EQUIPMENT

In-depth treatment of extraction equipment can be found in several books. Godfrey and Slater [67] provide more current details, but the treatments provided by Lo, Baird, and Hanson [7] and Skelland and Tedder [68] are also useful.

10.6.1 MIXER SETTLERS

Mixer-settlers are simply tanks configured to permit mixing in one followed by decantation in a second. Each stage consists of a mixer and settler pair (i.e., two tanks). When several mixer-settler stages are configured countercurrently, they constitute a cascade as indicated in Figure 10.4.

The advantages of mixer settlers are (1) simple maintenance and operation, (2) high tolerance for undissolved solids (e.g., as often occurs in the mining industry), (3) high tolerance for interfacial precipitates, (4) simple adjustment of mixing from stage to stage, and (5) easy measurement of concentration profiles throughout the cascade. The disadvantages of mixer-settlers are (1) potentially high inventory and (2) longer residence times than with other types of contactors. This latter disadvantage can be particularly serious if one is processing materials that degrade the solvent (e.g., fission products with a high radiation field).

Mixer-settlers are widely used, particularly in the mining industry. Vendors are available, and they are easily designed. In the laboratory, small-scale, mini-mixer-settlers are available that offer as many as 16 countercurrent stages and are capable of achieving steady state using 500 mL of feed or less.

10.6.2 RECIPROCATING PLATE COLUMNS

In reciprocating plate columns, the height equivalent to a theoretical stage (*HETS*) is a strong function of the reciprocating speed, Af , the product of the reciprocation amplitude and frequency. Karr columns actually exhibit optimal values for Af where the (*HETS*) is clearly minimized. These

Rearranging Equation (10.27) gives the following dependencies:

$$HETS \propto D^{0.385} \sigma^{0.525} (Af)^{-1.15} U_T^{0.235} \rho_c^{-0.465} (\Delta \rho g)^{-0.146} \quad (10.30)$$

for $(Af) < (Af)_{opt}$. Similarly, rearrangement of Equation (10.28) gives these dependencies:

$$HETS \propto D^{0.892} \sigma^{-0.776} (Af)^{+1.99} U_T^{1.30} \rho_c^{+1.65} (\Delta \rho g)^{-0.872} \quad (10.31)$$

for $(Af) < (Af)_{opt}$. Analysis of these dependencies can be helpful when comparing these correlations with those developed by other investigators.

The minimum ($HETS$) for a column can be estimated from an estimate of $(Af)_{opt}$. The latter quantity may be obtained by differentiating Equation (10.29) and setting $\partial HETS / \partial (Af) = 0$:

$$\begin{aligned} (Af)_{opt} &= \left\{ \frac{\Gamma_U}{\Gamma_L} (Af)^{-3.15} \right\}^{-1/3.15} \\ (Af)_{opt} &= \left\{ 1.24 D^{0.515} \sigma^{-1.30} U_T^{1.06} \rho_c^{2.12} (\Delta \rho g)^{-0.8} \mu_c^{0.015} \left(\frac{U_c}{U_d} \right)^{0.794} \right\}^{-1/3.15} \end{aligned} \quad (10.32)$$

which predicts $(Af)_{opt} \pm 6\%$.

Example: 10.2

Estimate the minimum $HETS$ for a 2-in diameter reciprocating plate column. The liquid-liquid interfacial tension is 30 dyne/cm. The solvent phase density and viscosity are 0.82 g/cm³ and 1.3 cP, respectively. The aqueous phase density and viscosity are 1 g/cm³ and 1.129 cP, respectively. Water is the continuous phase, and its linear velocity down the column is $U_c = 0.40$ cm/s. The velocity of the dispersed solvent phase is $U_d = 0.12$ cm/s.

Solution

$$U_T = U_c + U_d = 0.40 + 0.12 = 0.52 \text{ cm/s}$$

$$\Delta \rho = |\rho_d - \rho_c| = |0.82 - 1.0| = 0.18 \text{ g/cm}^3$$

Substituting into Equation (10.32) gives $(Af)_{opt} = 10$ cm/s. Substitution of $(Af)_{opt}$ and the other properties into Equations (10.27) through (10.29) gives

$$C_{dt} = D \Delta \rho g / \rho_c U_T^2 = 5.08(0.18)980.66 / [1(0.52^2)] = 3316$$

$$C_{dr} = D \Delta \rho g / (Af)^2 \rho_c = 5.08(0.18)980.66 / [(10^2)1] = 8.967$$

$$N_{Re} = \rho_c U_T D / \mu_c = 1.0(0.52)(5.08) / [1.129(10^{-2})] = 234$$

$$N_{We} = D U_T^2 \rho_c / g_c \sigma = 5.08(0.52^2)1.0 / [1.0(30)] = 0.046$$

TABLE 10.3
Correlations for Estimating fob Purchased Costs for Internals
(e.g., Distillation Trays, Absorber Packings, Solvent Extraction
Columns, and Others. Referenced to Mid-1968 Dollars with
(M&S = 273.1). Correlated Using Information from Guthrie [71]

Item	Correlation
Sieve Trays, 24-in spacing, shop installed ^{a,b}	$E_i = C_4(HT - 10) \left(\frac{M \& S}{273.1} \right)$ $C_4 = \begin{cases} 8.665D - 1.218 & D < 4 \text{ ft} \\ 16.67D - 33.35 & 4 \leq D \leq 6 \text{ ft} \\ 23.33D - 73.31 & 6 < D \leq 7 \text{ ft} \\ 25D - 75 & 7 \leq D \leq 10 \text{ ft} \end{cases}$ $D = \text{nominal column diameter, ft}$ $HT = \text{nominal column height, ft, actual trays plus 10 ft}$
Sieve Trays, 24-in spacing, field installed ^c	$E_i = C_4(HT - 10) \left(\frac{M \& S}{273.1} \right)$ $C_4 = 20D - 60 \quad D > 10 \text{ ft}$ $D = \text{nominal column diameter, ft}$ $HT = \text{nominal column height, ft, actual trays plus 10 ft}$

^a Add 0.08 E_i as indirects for freight, taxes, and insurance.
^b Add 0.05 E_i to estimate shop labor for installation.
^c Add 0.58 E_i for field labor and 0.75 E_i for indirects.

Example: 10.3

Estimate the fob purchased cost of a stainless steel pulse column when the Marshall & Swift (M&S) index is 1200. The column is 30 ft high and 2 ft in diameter. Internals are estimated as sieve trays with 1.5-ft spacing.

Solution

From the column dimensions, the bare module cost for the internals, if they are constructed of carbon steel and have 24-in spacing, would be

$$C_4 = 8.665(2) - 1.218 = 16.112$$

$$E_i = 16.112(20)(1200/273.1) = \$1,416 \text{ for the internals.}$$

Since the internals have 1.5-ft spacing and are of stainless steel,

$$E'_i = \$1,416(1.4 + 1.7) = \$4,390 \text{ fob.}$$

For the column, we have $C_3 = 33.143/30 + 0.127 = 1.23177$:

$$E = 2000(2.0/1.23177)^{1.047}(1200/273.1) = \$14,598 \text{ if the column is of carbon steel.}$$

K_{z_j}	= product of true mole fractions for complex j
K_{ϕ_j}	= product of true volume fractions for complex j
K_{γ_j}	= product of true volume fraction-based activity coefficients for complex j
K_{γ_j}	= product of true mole fraction-based activity coefficients for complex j
m_j	= diluent coordination number in j th complex
n_j	= solute coordination number in j th complex
N_{Bo}	= a Bond number
N_{RE}	= $\rho_c U_T D / \mu_c$, a Reynolds number
N_{Sl}	= Af / U_T , a Strouhal number
N_{We}	= $DU_T^2 \rho_c / g_c \sigma$, a Weber number
P_i^{sat}	= pure component vapor pressure for species i , mm H _g
R	= universal gas constant, J/mol-K
T	= temperature, K
U_c	= the continuous phase superficial velocity in cm/s
U_d	= the dispersed phase superficial velocity in cm/s
U_T	= net superficial velocity of phases = $U_d + U_c$, cm/s
V_i	= molar liquid volume for species i assuming $V^E = 0$
$\chi_{i,s}$	= stoichiometric mole fraction of species i
z_i	= true mole fraction of species i
z_{i1}	= true mole fraction of i th monomer
β_j	= empirical parameter
$\Delta\rho$	= $ \rho_d - \rho_c $, g/ml
Γ_L	= suboptimal <i>HETS/D</i> correlations for $(Af) < (Af)_{opt}$
Γ_U	= the superoptimal <i>HETS/D</i> correlation for $(Af) > (Af)_{opt}$
γ_j	= true mole fraction-based activity coefficient for species j
$\gamma_{i,s}$	= stoichiometric activity coefficient for species i
μ_c	= viscosity of the continuous phase, cP
$\phi_{i,s}$	= stoichiometric volume fraction of species i
ϕ_i	= volume fraction of species i if $V^E = 0$
ρ_e	= density of the continuous phase, g/ml
ρ_d	= density of the dispersed phase, g/ml
ρ_d	= interfacial tension, d/cm

REFERENCES

1. A. W. Francis, *Handbook for Components in Solvent Extraction*. New York: Gordon & Breach, Science Publishers, 1972.
2. E. J. Henley and J. D. Seader, *Equilibrium-Stage Separation Operations in Chemical Engineering*. New York: John Wiley & Sons, 1981.
3. J. T. Long, *Engineering for Nuclear Fuel Reprocessing*, 2nd ed. La Grange, IL: American Nuclear Society, 1978.
4. K. Schügerl, *Solvent Extraction in Biotechnology*. New York: Springer-Verlag, 1994.
5. M. Benedict, T. H. Pigford, and H. W. Levi, *Nuclear Chemical Engineering*, 2nd ed. New York: McGraw-Hill, 1981.
6. J. R. Williams and A. A. Clifford, eds., *Supercritical Fluid Methods and Protocols*, vol. 13 of *Methods in Biotechnology*. Totowa, NJ: Humana Press, 2000.
7. T. C. Lo, M. H. I. Baird, and C. Hanson, eds., *Handbook of Solvent Extraction*. New York: John Wiley & Sons, 1983.
8. R. B. Akell and C. J. King, eds., *New Developments in Liquid-Liquid Extractors: Selected Papers from ISEC '83*, vol. 80 (238) of *AIChE Symposium Series*. New York: American Institute of Chemical Engineers, 1984.

34. C. J. King, Acetic acid extraction, in T. C. Lo, M. H. I. Baird, and C. Hanson, eds., *Handbook of Solvent Extraction*. New York: John Wiley & Sons, Inc., 1983, 567–573.
35. Y. Marcus, Principles of solubility and solutions, in J. Rydberg, C. Musikas, and G. R. Choppin, eds., *Principles and Practices of Solvent Extraction*, chap. 2. New York: Marcel Dekker, 1992, 21–70.
36. W. E. Acree, *Thermodynamic Properties of Nonelectrolyte Solutions*. New York: Academic Press, 1984.
37. J. M. Prausnitz, R. N. Lichtenthaler, and E. G. de Avzevedo, *Molecular Thermodynamics of Fluid-Phase Equilibria*, 2nd ed. Englewood Cliffs, NJ: Prentice Hall, 1986.
38. F. Dolezalek. 1908. Zur Theorie der Binaren Gemische und Korzentrierten Loungen, *Z. Phys. Chem.* 64: 727.
39. Ioannis G. Economou and Marc D. Donohue. December 1991. Chemical, quasi-chemical and perturbation theories for associating fluids. *AIChE J.*, 37 (12): 1875–1894.
40. M. M. Abbott and H. C. Van Ness. September 15, 1992. Thermodynamics of solutions containing reactive species. A guide to fundamentals and applications. *Fluid Phase Equilib.* 77: 53–119.
41. H. R. Rabie and J. H. Vera. April 4, 1995. Chemical theory for ion distribution equilibria in reverse micellar systems. New experimental data for aerosol-OT-isooctane-water-salt systems. *Langmuir* 11: 1162–1169.
42. Scott W. Campbell. November 1994. Chemical theory for mixtures containing any number of alcohols. *Fluid Phase Equilib.* 102: 61–84.
43. E. A. Guggenheim, *Mixtures*. Oxford, UK: Clarendon, 1952.
44. G. M. Wilson. January 1964. Vapor-liquid equilibrium. XI. a new expression for the excess free energy of mixing. *J. Am. Chem. Soc.* 86: 127–130.
45. H. Renon and J. M. Prausnitz. 1968. Local compositions in thermodynamic excess functions for liquid mixtures. *AIChE J.* 14: 135.
46. D. S. Abrams and J. M. Prausnitz. 1975. Statistical thermodynamics of liquid mixtures: A new expression for the excess Gibbs energy of partly or completely miscible systems. *AIChE J.* 21 (1): 116–128.
47. J. H. Vera, S. G. Sayegh, and G. A. Ratcliff. 1977. A quasi lattice-local composition model for the excess Gibbs free energy of liquid mixtures. *Fluid Phase Equilib.* 1: 113.
48. C. Panayiotou and J. H. Vera. 1980. The quasi-chemical approach for nonrandomness in liquid mixtures: Expression for local surfaces and local compositions with an applications to polymer solutions. *Fluid Phase Equilib.* 5: 55.
49. C. Panayiotou and J. H. Vera. 1982. Statistical thermodynamics of γ -mer fluids and their mixtures. *Polymer J.* 14: 681.
50. S. K. Kumar, U. W. Suter, and R. C. Reid. 1987. A statistical mechanics based lattice model equation of state. *Ind. Eng. Chem. Res.* 26: 2532.
51. Gregory M. Martinez. August 1994. Lattice statistics for size, clustering and dissociation with example applications in vapor-liquid equilibria. *Chem. Eng. Sci.* 49 (15): 2423–2435.
52. S. G. Sayegh and J. H. Vera. 1980. Lattice-model expressions for the combinatorial entropy of liquid mixtures: A critical discussion. *Chem. Eng. J.* 19: 1.
53. W. W. Schulz and J. D. Navratil, eds., *Science and Technology of Tri-n-Butyl Phosphate*, vol. 3. Boca Raton, FL: CRC Press, 1986a.
54. K. Choi and D. W. Tedder. 1995. Nuclear magnetic resonances of TBP-diluent mixtures. *Spectrochimica Acta part A* 51: 2301–2305.
55. W. W. Schulz and J. D. Navratil, eds., *Science and Technology of Tri-n-Butyl Phosphate*, vol. 4. Boca Raton, FL: CRC Press, 1986b.
56. K. Choi, *Molecular Interactions in Polar Solvents*. Ph.D. thesis, Atlanta, GA: School of Mechanical Engineering, Georgia Institute of Technology, 1995.
57. J. H. Rytting, A. Goldkamp, and S. Lindenbaum. 1975. Heats of dilution of trialkyl phosphates in isooctane and carbon tetrachloride: Interpretation in terms of self-association. *J. Solution Chem.* 4: 1005.
58. C. R. Blaylock and D. W. Tedder. 1989. Competitive equilibria in the system: Water, nitric acid, tri-n-butyl phosphate and Amsco 125-82. *Sol. Ext. & Ion Exch.* 7 (2): 249–271.
59. A. M. Rozen, L. P. Khorhorina, V. G. Yurkin, and N. M. Novikova. 1963. The reaction of tributyl phosphate (TBP) and TBP-solvate with diluents. *Proc. Acad. Sci. USSR (transl.)* 153: 1387.
60. I. Prigogine and R. Defay, *Chemical Thermodynamics*. London: Longmans Green & Co., 1954.

11.4	Classification of Reactors and Their Description	799
11.4.1	Introduction.....	799
11.4.2	Pressure Energy	800
11.4.2.1	Gas-Liquid Reactors.....	800
11.4.2.2	Liquid-Liquid Reactors	812
11.4.2.3	Solid-Liquid Reactors	812
11.4.2.4	Gas-Solid Catalytic Fixed-Bed Reactors	813
11.4.2.5	Gas-Solid Catalytic Fluidized-Bed Reactors	821
11.4.2.6	Gas-Solid Noncatalytic Reactors	835
11.4.3	Kinetic Energy (Stirred Tank Reactors).....	839
11.4.3.1	Introduction	839
11.4.3.2	Blending	841
11.4.3.3	Gas Dispersion	841
11.4.3.4	Solid Suspension	843
11.4.3.5	Heat Transfer.....	844
11.4.3.6	Blending in Gas-Liquid Systems	844
11.4.3.7	Blending in Solid-Liquid Systems.....	845
11.4.3.8	Suspension in Gas-Liquid-Solid Systems.....	845
11.4.3.9	Heat Transfer in Gas-Liquid Systems	846
11.4.3.10	Dead End Systems	846
11.4.4	Potential Energy (Film Contactors)	849
11.4.5	Comparison of Gas-Liquid Reactors	849
11.5	Case Studies	849
11.5.1	Introduction.....	849
Case Study 11.1	Homogeneous Liquid Phase Simple Reaction: $A \rightarrow R$	852
Case Study 11.2	Homogeneous Gas-Phase Complex Reaction: Oxidation of NO Using Ozone	869
Case Study 11.3	Gas-Solid (Catalytic) Reaction: Modeling of a Complex Reaction on a Deactivating Catalyst (a Model Scheme).....	870
Case Study 11.4	Gas-Solid (Catalytic) Reaction in Fixed-Bed NINA and Adiabatic Reactors: Reduction of Nitrobenzene to Aniline	878
Case Study 11.5	Comparison of Selected Fluid-Bed Models for the Catalytic Reduction (by Hydrogen) of Nitrobenzene to Aniline	883
Case Study 11.6	Gas-Solid Noncatalytic Reaction: Development of a Solid Sorbent for Cleaning Coal Gas Followed by Modeling of the Reaction and a Conceptual Reactor Design.....	893
Case Study 11.7	Gas-Liquid Reaction: Air Oxidation of Sodium Sulfide (a Simple Reaction with Typical Problems of Gas-Liquid Reactions).....	900
Case Study 11.8	Gas-Liquid Reaction: Absorption of NO_x Gases for the Manufacture of Nitric Acid (a System with Multiple Complexities)	917
Case Study 11.9	Gas-Liquid-Solid (Noncatalytic) Reaction: Oxydesulfurization of Coal in a Slurry Reactor.....	919
Case Study 11.10	Gas-Liquid-Solid (Noncatalytic) Reaction: Carbonation of Lime	925
Case Study 11.11	Gas-Liquid-Solid (Catalytic) Reaction: Hydrogenation of an Organic Compound	934
Case Study 11.12	Solid Reaction Followed by a Gas-Solid Reaction: Manufacture of Methylchlorosilanes	943
Postscript	954
Acknowledgments	956
Nomenclature	956
References	961

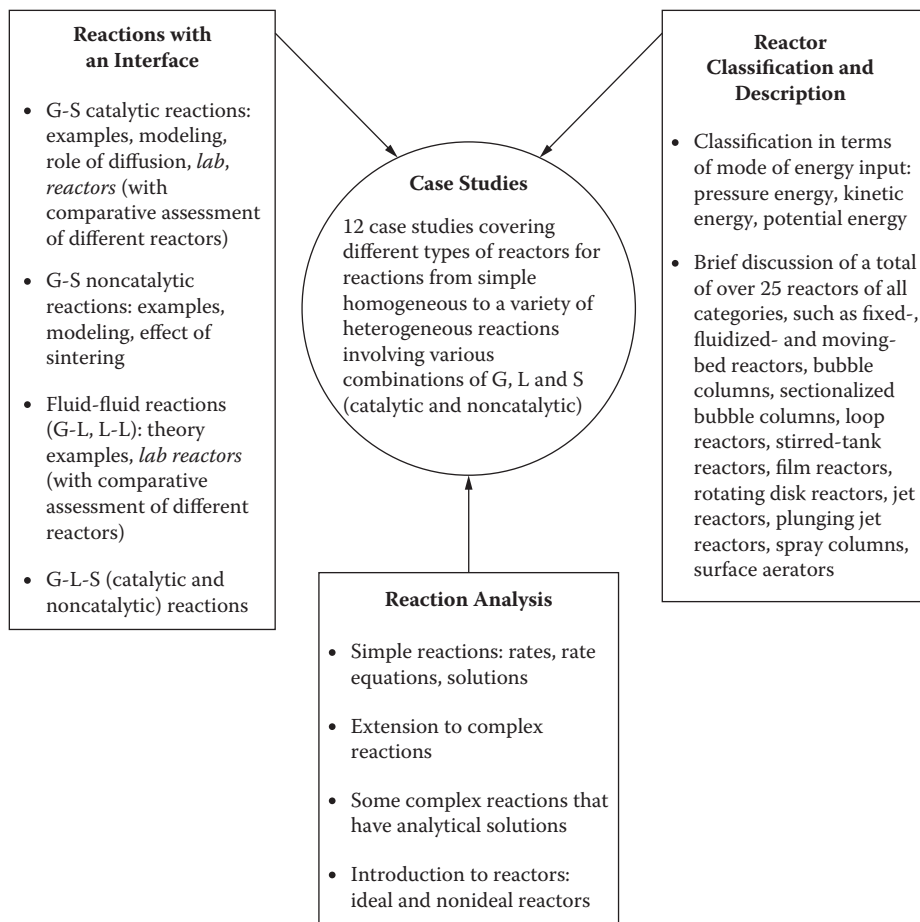


FIGURE 11.1 Scope and format of the chapter.

optimization. A special feature of the present chapter is its treatment of reactors in terms of rigorous case studies following a qualitative description of numerous reactors commonly used in industry.

Sometimes reaction rates can be enhanced by using multifunctional reactors, i.e., reactors in which more than one function (or operation) can be performed. Examples of reactors with such multifunctional capability, or *combo* reactors, are distillation column reactors in which one of the products of a reversible reaction is continuously removed by distillation thus driving the reaction forward; extractive reaction; biphasing; membrane reactors in which separation is accomplished by using a reactor with membrane walls; and simulated moving-bed (SMB) reactors in which reaction is combined with adsorption. Typical industrial applications of multifunctional reactors are esterification of acetic acid to methyl acetate in a distillation column reactor, synthesis of methyl-*ter*-butyl ether (MTBE) in a similar reactor, vitamin K synthesis in a membrane reactor, oxidative coupling of methane to produce ethane and ethylene in a similar reactor, and esterification of acetic acid to ethyl acetate in an SMB reactor. These specialized reactors are increasingly used in industry, mainly because of the obvious reduction in the number of equipment. These reactors are considered by Fair in Chapter 12.

Aspects of CRE not covered in this chapter include computational fluid dynamics (CFD). Total integration of CRE and CFD will generate much more reliable and theoretically sound procedures for reactor design but may not happen for the next 15 to 20 years. Meanwhile, incremental infusions of CFD in CRE will add increasing rigor to existing design procedures and methods for combining

from the engineering point of view, the overall “single step” represented by R11.1 is adequate. Its mechanistic evolution is largely irrelevant. The rate at which this reaction proceeds is given by

$$\text{rate} = (\text{constant}) [A] \quad (11.1)$$

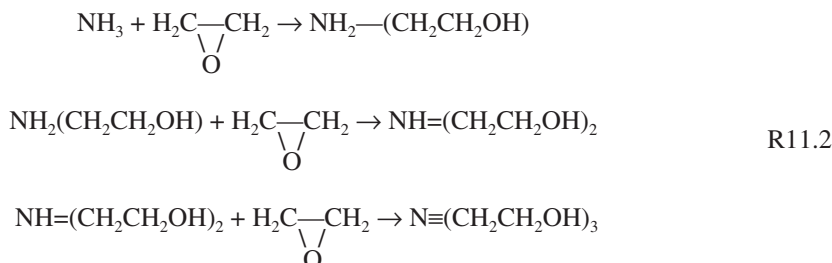
The concentration of A is raised to a power equal to the stoichiometric coefficient of A in the reaction (unity in this case). We refer to such reactions as *stoichiometric* reactions. If experimental data conform to the empirical form

$$\text{rate} = (\text{constant}) [A]^n \quad (11.2)$$

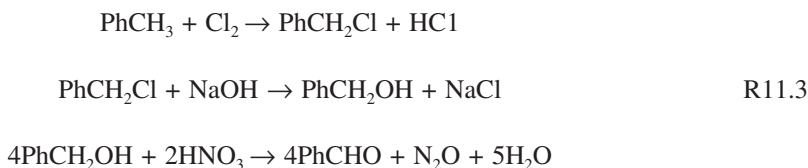
where n is some constant not equal to the stoichiometric coefficient, then the reaction is considered to be nonstoichiometric. The exponent on the concentration term, whether stoichiometric or nonstoichiometric, is called the *reaction order*. The proportionality constant is typically called the *rate constant*. However, because it is a function of temperature and pressure, the term “constant” is misleading and “coefficient” is a more correct choice (like, for example, mass or heat transfer coefficient and diffusion coefficient). However, “rate constant” is accepted.

11.2.3 COMPLEX (MULTIPLE AND MULTISTEP) REACTIONS

Let us now consider the following reaction in which several ethanolamines (mono-, di-, and tri-) are formed and referred to as a *multiple reaction*:



These intermediates are experimentally detectable. The literature refers to such a reaction as a *multistep reaction*. We prefer the term “multiple” and reserve “multistep” to a reaction scheme in which a number of steps, each requiring a different set of operating conditions, are employed to synthesize a compound starting from a given set of raw materials. Thus, the following scheme for synthesizing benzaldehyde (PhCHO) starting from toluene (PhCH_3) is a *multistep reaction*:

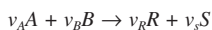
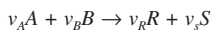


In this chapter, both simple and multiple reactions are considered.

11.2.4 STOICHIOMETRY

Reaction rates (as we shall see later) are always expressed in terms of concentrations of the reacting species or their partial pressures. It is usually convenient to express the concentrations of the various

TABLE 11.1
Concentration Equations in Terms of X_A
for the General Reaction



i = B, R, or S

(+ for product, – for reactant)

Batch

$$[i] = \frac{N_i}{V}$$

$$\begin{aligned} V &= V_0 \left(\frac{N_T}{N_{T0}} \right) \left(\frac{P_0}{P} \right) \left(\frac{T}{T_0} \right) \\ &= V_0 (1 + \epsilon_A X_A) \left(\frac{P_0}{P} \right) \left(\frac{T}{T_0} \right) \\ &= V_0 \text{ for constant volume} \end{aligned}$$

Flow

$$[i] = \frac{F_i}{Q}$$

$$\begin{aligned} Q &= Q_0 \left(\frac{F_T}{F_{T0}} \right) \left(\frac{P_0}{P} \right) \left(\frac{T}{T_0} \right) \\ &= Q_0 (1 + \epsilon_A X_A) \left(\frac{P_0}{P} \right) \left(\frac{T}{T_0} \right) \\ &= Q_0 \text{ for constant volume} \end{aligned}$$

$$\delta_A = \frac{\nu_S + \nu_R - \nu_B - \nu_A}{\nu_A}$$

$$\epsilon_A = y_{A0} \delta_A = \frac{V_{X_A=1} - V_{X_A=0}}{V_{X_A=0}}$$

$$[i] = \frac{y_{i0} P_0}{R_g T_0}, \quad [A] = \frac{y_{A0} P_0}{R_g T_0}$$

$$[A] = \frac{[A]_0 (1 - X_A)}{1 + \epsilon_A X_A}$$

$$[i] = \left\{ \frac{[A]_0 \left(\psi_i \pm \frac{\nu_i}{\nu_A} X_A \right)}{1 + \epsilon_A X_A} \right\} \left(\frac{P}{P_0} \right) \left(\frac{T_0}{T} \right)$$

$$\psi'_i = \frac{[i]_0}{[A]_0} = \frac{F_{i0}}{F_{A0}} = \frac{y_{i0}}{y_{A0}}$$

Note: When there is no volume change, $\epsilon_A = 0$ and when the system is isothermal and isobaric, $P = P_0$ and $T = T_0$.

TABLE 11.3

Analytical Solutions (Design Equations) for Simple Reactions in a Batch Reactor (Also Valid for PFR with t Replaced by \bar{t})

Reaction	Rate Equation	Analytical Solution ^a
1. $A \rightarrow R$	$-r_A = k[A]$	$kt = \ln\left(\frac{1}{1-X_A}\right), \frac{[A]}{[A]_0} = e^{-kt}$
2. $2A \rightarrow R$	$-r_A = k[A]^2$	$k[A]_0 t = \left[\frac{X_A}{1-X_A}\right], \frac{[A]}{[A]_0} = \frac{1}{1+k[A]_0 t}$
3. $3A \rightarrow R$	$-r_A = k[A]^3$	$k[A]_0^2 t = \frac{1}{2}\left[\frac{1}{(1-X_A)^2} - 1\right], 2kt = \frac{1}{[A]^2} - \frac{1}{[A]_0^2}$
4. $A \rightarrow R$	$-r_A = k[A]^n$	$k[A]_0^{n-1} t = \frac{1}{(n-1)}\left[(1-X_A)^{1-n} - 1\right], n \neq 1$
5. $A + B \rightarrow R \ \psi_B = 1$	$-r_A = k[A][B]$	$k[A]_0 t = \left[\frac{X_A}{(1-X_A)}\right], t = \frac{1}{k}\left(\frac{1}{[A]} - \frac{1}{[A]_0}\right)$
6. $A + B \rightarrow R \ \psi_B \neq 1$	$-r_A = k[A][B]$	$k[A]_0 t = \frac{1}{(\psi_B - 1)} \ln\left[\frac{\psi_B - X_A}{\psi_B(1-X_A)}\right]$
7. $\nu_A A + \nu_B B \rightarrow R \ \psi_B = \nu_B / \nu_A$	$-r_A = k[A][B]$	$k[A]_0 t = \frac{1}{\psi_B} \left[\frac{X_A}{1-X_A}\right]$
8. $A + 2B \rightarrow R \ \psi_B = 2$	$-r_A = k[A][B]^2$	$k[A]_0^2 t = \frac{1}{8}\left[\frac{1}{(1-X_A)^2} - 1\right]$
9. $A + B \rightarrow R \ \psi_B = 1$	$-r_A = k[A][B]^2$	$k[A]_0^2 t = \frac{1}{2}\left[\frac{1}{(1-X_A)^2} - 1\right]$
10. $A + 2B \rightarrow R \ \psi_B \neq 2$	$-r_A = k[A][B]^2$	$k[A]_0^2 t = \frac{1}{(2-\psi_B)^2} \left[\ln \frac{\psi_B - 2X_A}{\psi_B(1-X_A)} + \frac{2X_A(2-\psi_B)}{\psi_B(\psi_B - 2X_A)}\right]$
11. $\nu_A A + \nu_B B \rightarrow R \ \psi_B \neq \nu_B / \nu_A$	$-r_A = k[A][B]$	$k[A]_0 t = \frac{1}{\left[\psi_B - \left(\frac{\nu_B}{\nu_A}\right)\right]} \ln\left[\frac{\psi_B - \left(\frac{\nu_B}{\nu_A}\right)X_A}{\psi_B(1-X_A)}\right]$
12. $\nu_A A + \nu_B B \rightarrow R \ \psi_B = \nu_B / \nu_A$	$-r_A = k[A]^n[B]^m$	$k[A]_0^{m+n-1} t = \frac{1}{\psi_B(m+n-1)} \left[\frac{1}{(1-X_A)^{m+n-1}} - 1\right]$

^a LHS = $k[A]_0^{n-1}t$, where k has the units of an n th [or $(m+n)$]-order reaction, $\left(\frac{\text{m}^3}{\text{mol}}\right)^{n-1} \frac{1}{s}$; $\psi_B = \frac{[B]_0}{[A]_0}$.

TABLE 11.4
Rate Equation in Terms of Partial Pressures for
an Illustrative Reaction $A \rightarrow R + 2S$, and Its
Use in Extracting Kinetic Parameters

Reaction:^a



Rate equation:

$$-r_A = -\frac{d[A]}{dt} = k[A]^n \quad (1)$$

For isothermal constant-volume operation, Table 11.1 gives

$$V = V_0 \left(1 + \epsilon_A X_A\right) \left(\frac{P_0}{P}\right) \left(\frac{T}{T_0}\right), \text{ or}$$

$$X_A = \frac{1}{y_{A0} \delta_A P_0} (P - P_0) \quad (2)$$

$$= \frac{1}{P_{A0} \delta_A} (P - P_0)$$

Expressed in concentration units,

$$[A] = [A]_0 (1 - X_A) \quad (3)$$

Combining Equations (2) and (3),

$$[A] = \frac{P_{A0} - [(P - P_0)/\delta_A]}{R_g T} \quad (4)$$

Now, $\delta_A = 2$, and $p_{A0} = P_0$ (if pure A is used), thus

$$[A] = \frac{3P_0 - P}{2R_g T} \quad (5)$$

Combining Equations (1) and (5),

$$\frac{dP}{dt} = \tilde{k} (3P_0 - P)^n \quad (6)$$

where

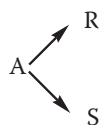
$$\tilde{k} = k (2R_g T)^{1-n} \quad (7)$$

Integration of Equation (6) for $n = 1$ gives

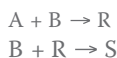
$$\ln \frac{2P_0}{3P_0 - P} = \tilde{k} t \quad (8)$$

Thus, if the reaction is first order, either the differential method [Equation (6)] or the integral method [Equation (8)] can be used. If $n \neq 1$, only the differential method can be used.

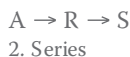
^a Classical example: gas-phase decomposition of di-*t*-butyl peroxide (Peters and Skorpinski, 1965; see also Fogler, 1999; Doraiswamy, 2001).



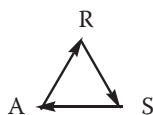
1. Parallel



4. Series-Parallel



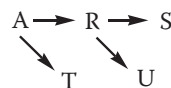
2. Series



5. Triangular



3. Independent



6. Denbigh

R11.7

Analytical solutions can often be found (see, e.g., Levenspiel 1999; Doraiswamy 2001). These are for batch reactors (also applicable to plug-flow reactors). Solutions for mixed-flow reactors (see Section 11.2.7.2) will be different.

11.2.7 IDEAL REACTORS

11.2.7.1 Batch Reactor

The material balance for any reactor can be written as

$$\text{Input} - \text{output} = \text{accumulation} + \text{disappearance (or formation)} \quad (11.12)$$

For a batch reactor, the input and output terms are absent, and we have for reactant A

$$-r_A = \frac{dN_A}{dt} \frac{1}{V} \quad (11.13)$$

Integration with no volume change, with $N_A = N_{A0}(1 - X_A)$, gives the following:

*n*th order

$$k[A]_0^2 t = \frac{1}{n-1} (1 - X_A)^{1-n}, \quad n \neq 1 \quad (11.14)$$

First order

$$kt = \ln \left(\frac{1}{1 - X_A} \right) \quad (11.15)$$

The corresponding general equation for a reaction with volume change is

$$t = [A]_0 \int_0^{X_A} \frac{dX_A}{(-r_A)(1 + \epsilon_A X_A)} \quad (11.16)$$

sufficiently large number) is identical to plug flow. The degree of mixing in the two partially mixed reactors can be controlled by the recycle ratio (R) in one case and the number of tanks (N) in the other. Yet another nonideal reactor is the variable volume reactor, in which only a fraction of the batch reactor contents is emptied. In other words, V^* ($= V/V_M$, where V_M is the maximum volume) is fixed at a value between 1 (when the reactor functions as an MFR) and 0 (when it functions as a batch reactor). The relationship between the principal parameters of the three reactors is given by

$$V^* = \frac{R}{1 + R} = \frac{1}{N} \quad (11.23)$$

11.2.7.3 The Role of Mixing

The concept of mixing is inherent in the recycle and tanks-in-series reactors, since deviations from plug or fully mixed flow are expressed in terms of R and N . Rigorous accounting of mixing must, however, be based on more fundamental concepts of mixing. In many situations, not all elements of a fluid flowing through a reactor leave the reactor at the same time. That is, the residence times for different elements vary. The residence time distribution (RTD) is denoted by a curve that represents the amount of fluid with times between t and $t + dt$ flowing out in the exit stream. When normalized with respect to the total flow (i.e., expressed as fraction of the total flow), this RTD satisfies the condition

$$\int_0^\infty \delta(t) dt = 1 \quad (11.24)$$

where $\delta(t)$ is the distribution function. The mean residence time is then given by

$$\bar{t} = \int_0^\infty t \delta(t) dt \quad (11.25)$$

For the two ideal cases referred to earlier, those corresponding to plug flow and fully mixed flow, the distribution functions take the following forms:

Plug flow (Dirac delta function):

$$\delta(t) = g(\bar{t}) \quad (11.26)$$

which shows $\delta(t) = 0$ at all times except at $t = \bar{t}$.

Mixed flow (exponential distribution):

$$\delta(t) = \frac{1}{\bar{t}} \exp\left(-\frac{t}{\bar{t}}\right) \quad (11.27)$$

The two distributions are explained in Figure 11.3.

In the equations presented above, the term “fully mixed” represents mixing at the molecular level. There is another mixing condition in which clumps or aggregates of molecules enter the reactor and flow through it without interacting with one another. Within each clump, however, there is complete mixing of molecules, and the residence time of each molecule is the same as that of

TABLE 11.5**Some Examples of Industrially Important Catalytic Reactions/Reactors**

Desulfurization of petroleum feedstock (FBR), catalytic cracking (MBR or FI BR), hydrodewaxing (FBR), steam reforming of methane or naphtha (FBR), water-gas shift (CO conversion) reaction (FBR-A), ammonia synthesis (FBR-A), methanol from synthesis gas (FBR), oxidation of sulfur dioxide (FBR-A), isomerization of xylenes (FBR-A), catalytic reforming of naphtha (FBR-A), reduction of nitrobenzene to aniline (FBR), butadiene from n-butanes (FBR-A), ethylbenzene by alkylation of benzene (FBR), dehydrogenation of ethylbenzene to styrene (FBR), methyl ethyl ketone from sec-butyl alcohol (by dehydrogenation) (FBR), formaldehyde from methanol (FBR), disproportionation of toluene (FBR-A), dehydration of ethanol (FBR-A), dimethylaniline from aniline and methanol (FBR), vinyl chloride from acetone (FBR), vinyl acetate from acetylene and acetic acid (FBR), phosgene from carbon monoxide (FBR), dichloroethane by oxichlorination of ethylene (FBR), oxidation of ethylene to ethylene oxide (FBR), oxidation of benzene to maleic anhydride (FBR), oxidation of toluene to benzaldehyde (FBR), phthalic anhydride from o-xylene (FBR), furane from butadiene (FBR), acrylonitrile by ammoxidation of propylene (FI BR)

Note: FBR = fixed-bed reactor (usually multitubular), FBR-A = adiabatic fixed-bed reactor, FI BR = fluidized bed reactor, MBR = moving-bed reactor.

Adapted from Doraiswamy, 2001.

Table 11.6 adapted from Doraiswamy (2001) provides a partial list of these categories. The main features and applications of these two categories of catalysts are discussed in more detail by Doraiswamy (2001). Of these zeolites, TS-1 catalysts and homogeneous catalysts immobilized on solid supports deserve special mention.

Zeolites were first employed in the petroleum industry and then the petrochemicals industry through Mobil's ZSM-5 catalysts. They are crystalline aluminosilicates possessing characteristic pore and cage structures. Chemical transformations have three restrictions imposed by the lattice structure, collectively referred to as *shape selectivity*:

1. Reactant selectivity (where only certain reactant molecules can enter the pores)
2. Product selectivity (where only certain product molecules can leave the pores)
3. Transition state selectivity (where only certain transition state dimensions are viable)

Zeolites function as Brönsted or Lewis acid catalysts or (less frequently) as basic catalysts. Examples of the former are alkylation and isomerization of aromatics, such as the isomerization of xylenes; an example of the latter is the use of cesium zeolite in the synthesis of the key intermediate, 4-methylthiazole, used in the preparation of the anthelmintic, thiabendazole.

TS-1 catalysts are zeolites containing titanium silicate used in the oxidation of organic substrates by hydrogen peroxide. Only those cations that meet certain specific steric requirements can fit into the tetrahedral positions of the zeolite lattice. One such cation is titanium. TS-1 catalysts are very powerful and selective oxidizing catalysts and are potentially among the most useful catalysts developed. For example, phenol can be oxidized to catechol and hydroquinone.

Because homogeneous catalysts lend themselves to *a priori* design (although much still must be done in this direction) and solid catalysts do not, "bottling" of a homogeneous catalyst within a solid provides a good practical means of combining the advantages of the two types of catalysts. There are four classes of such immobilized, bottled, or "heterogenized" homogeneous catalysts, as shown in Table 11.7 (Doraiswamy, 2001) along with important subcategories of each. These catalysts find wide application in the case of enzymes. A particularly important class of heterogenized catalysts is the supported aqueous phase (SAP) catalyst. This is a distinctive class, since here the catalyst is first solubilized in the aqueous phase (which in itself is an important advance), in contrast to the common case where it is soluble in the organic phase and is then heterogenized

TABLE 11.7
Classification of Methods for Immobilizing (or Heterogenizing) Homogeneous Catalysts

Heterogenized Homogeneous Catalysts			
Supported liquid-phase catalysts (SLPC)	Organic solid (polymer)-bound catalysts	Inorganic solid-bound catalysts	Synthesis within porous structure (zeolites)
Supported organic-phase (SOP) catalysts	Modification of preformed polymers	Copolymerization with inorganic monomers	
Supported aqueous-phase (SAP) catalysts	Polymerization of functionalized monomers	Surface bonding with organic oxides	
		Anchoring on functionalized oxides	

Source: Doraiswamy, L. K., 1991; *Organic Synthesis Engineering*, New York: Oxford, 2001.

[supported organic phase (SOP) catalyst]. Water-soluble homogeneous catalysts often have the advantage that the product is returned to the organic phase while the catalyst remains in the aqueous phase, thus minimizing separation problems. This advantage continues in the supported version. A useful application of SAP catalysts is the use of water-soluble homogeneous catalyst (SAP-Ru-BINAP-4SO₃Na) supported on controlled pore glass in the enantioselective hydrogenation of 2-(6'-methoxy-2'-naphthyl) acrylic acid to naproxen (Wan and Davis, 1993a, b).

This brief overview of solid catalysts addresses only the nature, class, and catalytic properties of a variety of catalysts. Modeling the kinetics of a reaction occurring on a solid surface is a challenging task and is firmly rooted in the principles of surface science. As this is still an evolving area, empirical shortcuts are often invoked. Furthermore, for solid catalysts, the reactant(s) must first diffuse into the solid, and product(s) must diffuse out of it. Also, the heat evolved or required must be transported between the solid and the fluid bulk. Hence, diffusion accompanied by reaction becomes a major consideration. These *microenvironmental* aspects of solid catalysts are briefly described below.

11.3.1.2 Kinetics of Reactions on Solid Surfaces

In formulating rate equations for homogeneous reactions, concentrations were used to represent the qualitative presence of different components. What is important in catalytic reactions is the "surface concentration" or fractional coverage of the surface by the adsorbed species. Because there is no easy way of directly measuring surface coverage, theoretical equations are used to relate the fractional surface coverage to the corresponding concentration or partial pressure in the homogeneous phase from where the molecules strike the surface and are adsorbed on it. These equations are known as *isotherms*, the most common being the Langmuir isotherm. This isotherm is based on the assumption that the surface behaves ideally. An ideal surface is one in which

1. All active centers on the surface, i.e., centers on which catalysis can occur, are equally active, and the heat of adsorption is independent of surface coverage by previously adsorbed molecules, and
2. There is no interaction between the adsorbed molecules.

For the case of a single molecular species *A*, the equation is

$$\theta_A = \frac{K_A p_A}{(1 + K_A p_A)} \quad (11.29)$$

and for a number of competitively adsorbing species, *A*, *B*, *C*, ...,

$$-r_A = k\theta_A \quad (11.34)$$

Incorporating the Langmuir expression for θ_A ,

$$-r_A = \frac{kK_A p_A}{(1 + K_A p_A + K_R p_R)} \quad (11.35)$$

where the units of k are the units of the rate. This is a typical so-called Langmuir–Hinshelwood–Hougen–Watson (LHHW) model.

For the reaction



again assume that surface reaction is controlling, but note that two product molecules are formed. Thus, a vacant site must be available next to the one on which A is adsorbed, to accommodate the second molecule. This leads to the equation

$$-r_A = k\theta_A\theta_v \quad (11.36)$$

Substituting for θ_A and θ_v , we get

$$-r_A = \frac{k K_A p_A}{(1 + K_A p_A + K_R p_R + K_S p_S)^2} \quad (11.37)$$

For the reaction



the rate equation (for surface reaction control) is

$$-r_A = \frac{k K_A K_B p_A p_B}{(1 + K_A p_A + K_B p_B + K_R p_R + K_S p_S)^2} \quad (11.38)$$

Where one of the molecules, say A , is dissociated, it can be shown that $K_A P_A$ should be substituted by $\sqrt{K_A p_A}$.

All LHHW equations can be written in a general consolidated form as

$$\text{Rate} = \frac{(\text{kinetic term})(\text{potential term})}{(\text{adsorption term})^n} \quad (11.39)$$

where n is the number of sites involved. Yang and Hougen (1950) have tabulated expressions for each of the three terms for four major types of reactions. In addition to surface reaction control models, they have also considered adsorption and desorption control models. When one of the reactants is not adsorbed, say B in R11.10, then θ_B is replaced simply by p_B and Equation (11.38) is suitably modified. These are the Eley–Rideal models. Selected equations involving different rate-controlling steps, as formulated from Yang and Hougen's tables, were listed by Doraiswamy (2001).

$$\phi_{s1} = R \sqrt{\frac{k_v}{D_{eA}}} \quad (11.42)$$

Equation (11.41) can be solved for the boundary conditions

$$\begin{aligned} \left[\hat{A} \right] &= 1 && \text{Surface} \\ \frac{d \left[\hat{A} \right]}{d \hat{R}} &= 0 && \text{Center} \end{aligned} \quad (11.43)$$

to give

$$\left[\hat{A} \right] = \frac{\sinh(\phi_{s1} \hat{R})}{\hat{R} \sinh \phi_{s1}} \quad (11.44)$$

An effectiveness factor is now defined as

$$\epsilon = \frac{\text{actual rate based on average concentration within the pellet}}{\text{rate based on surface concentration throughout the pellet}} \quad (11.45)$$

leading to

$$\begin{aligned} \epsilon &= \frac{3}{\phi_{s1}} \left(\frac{1}{\tanh \phi_{s1}} - \frac{1}{\phi_{s1}} \right) \\ &= \frac{3}{\phi_{s1}^2} (\phi_{s1} \coth \phi_{s1} - 1) \end{aligned} \quad (11.46)$$

Similar equations can be derived for a flat plate and a cylinder. Instead of writing different equations for different shapes, the following single continuity equation can be written for a first-order reaction by defining a generalized reduced length parameter ξ (r/R for a sphere or a cylinder and ℓ/L for a flat plate):

$$\frac{d^2 [\hat{A}]}{d\xi^2} + \frac{\beta}{\xi} \frac{d[\hat{A}]}{d\xi} = \phi_1^2 [\hat{A}] \quad (11.47)$$

where β is a shape factor with values of 2 for a sphere, 1 for a cylinder, and 0 for a flat plate. The Thiele modulus ϕ_1 (with the shape suffix s removed) is a generalized modulus for all shapes for a first-order reaction given by

$$\phi_1 = s \sqrt{\frac{k_v}{D_{eA}}} \quad (11.48)$$

where now s is a new length parameter (sometimes also called the *shape factor*) defined as (Aris 1957)

of transition from chemical to diffusion control is a practically useful value, since it represents a pellet of optimal dimension. A larger pellet would attract diffusional resistance, whereas a smaller one would involve a higher pressure drop in the reactor. The various regions are clearly marked in the figures. The effectiveness factor concept developed here is based on power law models for the reaction rate. Attempts to extend the analysis to LHHW kinetics (e.g., Roberts and Satterfield, 1965, 1966; Aris, 1975; Satterfield, 1991; Doraiswamy and Sharma, 1984; Doraiswamy, 1991) are not discussed here.

11.3.1.3.2 Nonisothermal Effectiveness Factors

The equations developed above can be extended to nonisothermal situations, i.e., to reactions for which the heat effects cannot be neglected for highly exothermic reactions. The basic equation used here is the mass-energy balance:

$$\left(\begin{array}{c} \text{Heat generated by reaction of} \\ A \text{ in the pellet} \end{array} \right) = \left(\begin{array}{c} \text{Heat transferred from} \\ \text{the pellet to the surface} \end{array} \right)$$

$$\mathbf{D}_{eA}([A]_s - [A])(-\Delta H_r) = k_{T,er}(T - T_s) \quad (11.52)$$

In dimensionless form, this becomes

$$\hat{T} = \frac{T}{T_s} = 1 + \beta_m \left(1 - [\hat{A}] \right) \quad (11.53)$$

where

$$\beta_m = \frac{(-\Delta H_r) \mathbf{D}_{eA} [A]_s}{k_{T,er} T_s} \quad (11.54)$$

The parameter β_m is a measure of the heat evolved (or absorbed), being close to zero for athermal reactions. The nondimensional continuity equation follows:

$$\frac{d^2[\hat{A}]}{d\xi^2} + \frac{\beta}{\xi} \frac{d[\hat{A}]}{d\xi} + \phi^2 [A]^n \left[\alpha_s \beta_m \frac{1 - [\hat{A}]}{1 + \beta_m (1 - [\hat{A}])} \right] \quad (11.55)$$

In deriving this equation, the rate constant (appearing in ϕ) is written at surface conditions:

$$k_v = k_{vs} \exp \left[\alpha_s \left(1 - \frac{1}{\hat{T}} \right) \right] \quad (11.56)$$

where

$$\alpha_s = \frac{E}{R_g T_s} \quad (11.57)$$

number (for mass properties) and the Nusselt number (for heat transfer) to the Prandtl number (for thermal properties) and the Reynolds number (see Wen and Fan, 1975; Doraiswamy and Sharma, 1984).

Using the Sherwood number for the mass transfer coefficient for bulk-to-surface transfer, the following expression can be developed for a flat plate:

$$\varepsilon = \frac{\tan \phi_{p1}}{\phi_{p1} \left(1 + \frac{\phi_{p1} \tanh \phi_{p1}}{Bi_m} \right)} \quad (11.58)$$

A practical way of plotting this equation is to use the observed quantity $\phi_a = \varepsilon \phi_1^2$, where ϕ_1 is independent of shape. Such a plot (with Bi_m as parameter) has been presented by Carberry (1976).

11.3.1.5 Relative Roles of Internal and External Diffusion

The following observations can be made regarding the relative roles of heat and mass transfer in internal and external diffusion (Carberry, 1976). These roles depend on the state of the bulk fluid, gas, or liquid.

Gas-solid (catalytic) reactions. Mass transfer is likely to be more important within the pellet than in the external film, and heat transfer more important in the film than within the pellet. In other words, intraphase mass transfer and interphase heat transfer would normally be the dominant transport processes. Thus the pellet can reasonably be assumed to be isothermal.

Liquid-solid (catalytic) reactions. Heat transfer is likely to be more important within the pellet than in the surrounding film, and mass transport more important in the film than within the pellet. In other words, intraphase heat transfer and interphase mass transfer would normally be the dominant transport processes.

11.3.1.6 Effects of Various Factors on Catalyst Effectiveness

The equations and plots presented in the foregoing sections largely pertain to the diffusion of a single component followed by reaction. There are several other situations of industrial importance on which considerable information is available. They include biomolecular reactions in which the diffusion-reaction problem must be extended to two molecular species, reactions in the liquid phase, reactions in zeolites, reactions in immobilized catalysts, and extension to complex reactions (see Aris, 1975; Doraiswamy, 2001). Several factors influence the effectiveness factor, such as pore shape and constriction, particle size distribution, micro-macro pore structure, flow regime (bulk or Knudsen), transverse diffusion, gross external surface area of catalyst (as distinct from the total pore area), and volume change upon reaction. Table 11.8 lists the major effects of all these situations and factors.

11.3.1.6.1 Practical Effects of Diffusion in Complex Reactions

The analysis of complex reactions was briefly reviewed in Section 11.2.2. Diffusion can also greatly influence such complex reactions. In fact, an understanding of the role of diffusion can be incorporated in the design of the reactor system to increase or decrease the rate of certain steps and thus enhance the selectivity of the desired product. Some salient features of the effect of diffusion on some selected complex schemes are outlined in Table 11.9.

11.3.1.6.2 Criteria Based on Measurable Quantities for Eliminating Transport Disguises

In determining the true kinetic parameters of a reaction, all mass and heat transfer effects (or *disguises*, as they are sometimes called) must be eliminated. Several criteria (based on measurable

TABLE 11.9
Effect of Diffusion on Some Industrially Important Classes of Complex Reactions

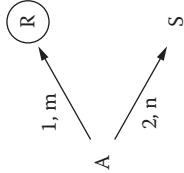
Reaction ^a	Pore Structure	Intrinsic Selectivity, Yield	Actual Selectivity, Yield	Main Features
1. Independent <div>$A \xrightarrow{1} R$ $B \xrightarrow{2} S$</div>	Monodispersed	$s = \frac{k_{v1}}{k_{v2}}$	$s_a = \left(\frac{s}{-D} \right)$	Greater diffusional resistance for reaction 2 enhances y_{Ra}
2. Parallel <div></div>	Monodispersed	$s = \frac{k_{v1}}{k_{v2}}$ $Y_R = \frac{1}{1 + p_{im}}$ where $p_{im} = \frac{k_{v2}}{k_{v1}} [A]_s^{m-1}$	$s_a = s^{1/2}$ $\frac{Y_{Ra}}{Y_R} = \frac{n+1}{1m-n+1}$ (Roberts 1972; Pawlawski 1961)	Y_{Ra} / Y_R decreases as p_{im} and ϕ increase

TABLE 11.10
Criteria for the Absence of Mass and Heat Transfer Effects in Gas-Solid Catalytic Reactions (Doraiswamy, 2001)*

Interphase	Intraparticle	Interphase and Intraparticle
Mass transfer	Isothermal	Isothermal
1. $\eta = 1 - \frac{k_a d_p^{1.5}}{11\sqrt{D_b}u}$	1. $\frac{d_p^2 r_a}{4D_{eA}[A]_s} < 1, n = 1$	1. $\alpha_b \beta_{mb} + 0.3n\alpha_b \left(\frac{(-\Delta H)_r r_a d_p}{2h_{fp}T_b} \right) \leq 0.05n$
Ruthven (1968)	Weisz and Prater (1954); Weisz (1957)	Mears (1971a); see also Guha and Narsimhan (1972)
2. $\frac{r_a d_p}{2[A]_b k_G} < \frac{0.15}{n}$	2. $\frac{d_p^2 r_a}{4D_{eA}[A]_s} < n , n \neq 0$	Nonisothermal
	Stewart and Villadsen (1969); Mears (1971a)	2. $\frac{r_a d_p^2}{4[A]_b D_{eA}} < \frac{1 + 0.33\alpha_b \frac{(-\Delta H)_r (-r_a) d_p}{2h_{fp}T_b}}{ n - \alpha_b \beta_{mb} \left(1 + 0.33n \left(\frac{r_a d_p}{2[A]_b k_G} \right) \right)}$
		Mears (1971a)

* r_a = observed rate (mol/m³ cat s); k_a = observed rate constant (1/s); $\alpha_b = \alpha$ at bulk conditions; ($\beta_{mb} = \beta_m$ at bulk conditions; η = external effectiveness factor; θ = volume change parameter given by $(v_B - 1)y_{As}$, where v_B is the stoichiometric coefficient in the reaction $A \rightarrow v_B B$ and y_{As} is the mole fraction of A at the catalyst surface. See Mears (1971b, 1976) for interparticle criteria (i.e., criteria for the reactor as a whole) such as that for the absence of axial diffusion.

man (1974) and in a more general way by Doraiswamy and Tajbl (1974), Doraiswamy and Sharma (1984), Hofmann (1986), Pratt (1987), and most recently by Doraiswamy (2001).

The internal diffusional effect can be avoided by performing experiments with catalysts of different sizes under otherwise identical conditions and determining that size above which there is a lowering of conversion due to internal diffusional resistance. The external mass transfer effect can be examined by operating the reactor at different feed velocities but at the same residence time (i.e., keeping W/F constant). The velocity beyond which the conversion levels off should be noted and used as the minimum velocity at which to operate an integral reactor. The same method holds for a fully mixed reactor, in which the agitation parameter is the extent of stirring.

Several reactors normally used to obtain kinetic data for a nondecaying catalyst under diffusion-free conditions (as established by tests just described) are shown in Figure 11.7. The integral reactor (operated under plug-flow conditions) is the simplest, but the conversion-residence time data obtained must be differentiated to get the rates (see Figure 11.2). The differential reactor consists of a very small amount of catalyst giving conversions of 1 to 2%. This enables direct determination of the rate corresponding to the average component partial pressures in the bed. Clearly, the analytical methods used for determining the compositions of the inlet and outlet streams must be accurate. Also, since the differential element used corresponds to a small axial section of the integral reactor, it is necessary to use synthetic feeds that will contain all the components of the process stream, including impurities. The main advantage is that the measurements give the rates directly. This advantage can be retained in a CSTR with the additional advantage that integral level conversions (usually in excess of 10%) can be obtained under "differential conditions." In other words, there is no need for differentiating integral conversion data (as in a typical integral reactor). The fully mixed condition can be realized in many ways, most importantly by placing the catalyst in baskets attached to the stirrer (the Carberry reactor), by attaching the catalyst to the pot provided with a suitable internal recirculation system (the Berty reactor), or by attaching the catalyst to the

stirrer as in the Carberry reactor but rotating the pot provided with suitable baffles (the Choudhary–Doraiswamy reactor). In another design (Borman et al., 1994), perfect mixing is achieved by circulating the gas in the reactor using an axial flow impeller in a well streamlined enclosure. A batch reactor can also be used, but since this reactor is the batch equivalent of the continuous integral (plug-flow) reactor, the conversion-time data (as against the conversion-residence time data in the integral reactor) must be differentiated to extract the rates. Pulsed reactors can also be used in which a reactant pulse is passed through a catalyst bed and the rates extracted from a theoretical analysis of the data (see, e.g., Yushchenko et al. 1968; Luckner and Wills 1973; Doraiswamy and Sharma 1984). Since, in this case, a carrier gas is used to introduce the feed into the reactor, the velocities are usually high enough to eliminate external mass transfer effects.

All mixed and differential reactors operate essentially isothermally. Another way to accomplish isothermality and the fully mixed condition is to provide a recirculation loop to a PFR.

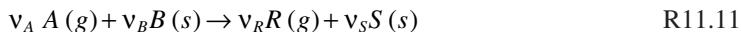
If the catalyst decays rapidly with time, then these reactors must be used with caution: the data should be obtained before decay occurs and vitiates the results. If this cannot be done, transport reactors should be used. In such a reactor, a suspension of the catalyst in the fluid is passed through a tube placed in a fluidizing bath for approaching isothermality. The main difficulties are ensuring uniformity of suspension in the feed stream and the need to separate the catalyst from fluid immediately after sampling to prevent further reaction. Gullett et al. (1990) slid a catalyst bed into a process gas stream and then automatically retracted it after a preset exposure time (which can be as low as 0.3 s). In all the reactors mentioned so far, it is assumed that the catalyst surface is equally accessible at all points. This is true only for special hydrodynamic situations, e.g., the stagnation region of a circular cylinder. Balaraman et al. (1980) proposed a reactor in which the catalyst is placed in this zone. The single-pellet reactor proposed by Hegedus and Petersen (1973a–c, 1974) is particularly useful for studying catalyst deactivation and the role of internal diffusion, but it is generally not recommended for routine kinetic studies.

Many of the reactors mentioned are available commercially, particularly the Berty reactor. They can be operated with a software and appropriate interfacing that can set and implement the experiments for each of a series of sequential runs (Mandler et al., 1983), resulting in the emergence of the most acceptable model for a reaction.

The main features of these reactors and their ratings, along with comments and selected references, are outlined in Table 11.11. They are based on the authors' conclusions and the rating scale [good (G), fair (F), and poor (P)] of Weekman (1974).

11.3.2 GAS-SOLID NONCATALYTIC REACTIONS

Reactions between gases and solids include combustion of solid fuels, environmental control (pollution abatement), energy generation, mineral processing, chemical vapor deposition, and catalyst manufacture and regeneration. Representing the solid by s and gas by g , several categories are listed in Table 11.12 along with selected examples of each. The analysis and modeling of these reactions obviously depend on the specific category at hand, but common principles can be identified by considering the most general case,



Thus our presentation will largely be confined to this class of reactions, although brief references will also be made to other classes, notably $A(g) + B(s) \rightarrow R(g)$, represented by the gasification of coal.

11.3.2.1 Modeling of Gas-Solid Reactions

The first model, the shrinking core model (SCM) or the sharp interface model (SIM), was proposed about half a century ago. Other models also describe the behavior of the solid as it undergoes

TABLE 11.11 (Continued)
Laboratory Reactors for Gas-Solid Catalytic Reactions: Their Principal Features and Ratings

	Main Features	Isothermality	Diffusion-Free Operation	Contact Time Determination	Rate Measurement	Comments	Selected References
4. Stirred batch reactor	A batch of fluid and catalyst is placed in a stirred reactor and the progress of reaction is followed as a function of time.	G	G	G	I ^d	Generally not recommended for gas-solid reactions	
5. Pulse reactor	A microreactor in which a pulse of feed is introduced; can be integral or differential	G	G	P	I ^e	Good for a rapidly deactivating catalyst; far removed from the "real world"	Galiski and Hightower (1970) Richardson and Friedrich (1975)
6. Single-pellet reactor	Used specifically to study deactivation and internal diffusion in a catalyst pellet (Hegedus-Petersen reactor)	F-G	NA	G	D	Good mainly for studying role of deactivation; can also be used for kinetic studies but not recommended	Hegedus and Petersen (1973a,b,c; 1974)
7. Reactor with well-defined hydrodynamics	The forward stagnation zone of a circular cylinder used for obtaining an equiaccessible surface which allows accurate accounting of mass transfer (Balaraman-Mashelkar-Doraiswamy reactor)	F-G	NA	F-G	I ^e	Precise accounting of mass transfer effect possible if present	Balaraman et al. (1980)
8. Nonisothermal reactor (including adiabatic reactor)	Reactor operated without any effort to make it isothermal; can also be operated adiabatically	NA	F	F	I ^e	Industrial conditions are best simulated; adiabatic operation requires only temperature profile measurement and no chemical analysis as in all other reactors.	Doraiswamy and Tajbl (1974) Doraiswamy and Sharma (1984) Froment and Bischoff (1990)

*G = good, F = fair, D = direct, I = indirect, a = in general, b = for highly exothermic or endothermic reactions, c = with bed dilution, d = refer Figure 11.2, e = see reference(s), NA = not applicable.

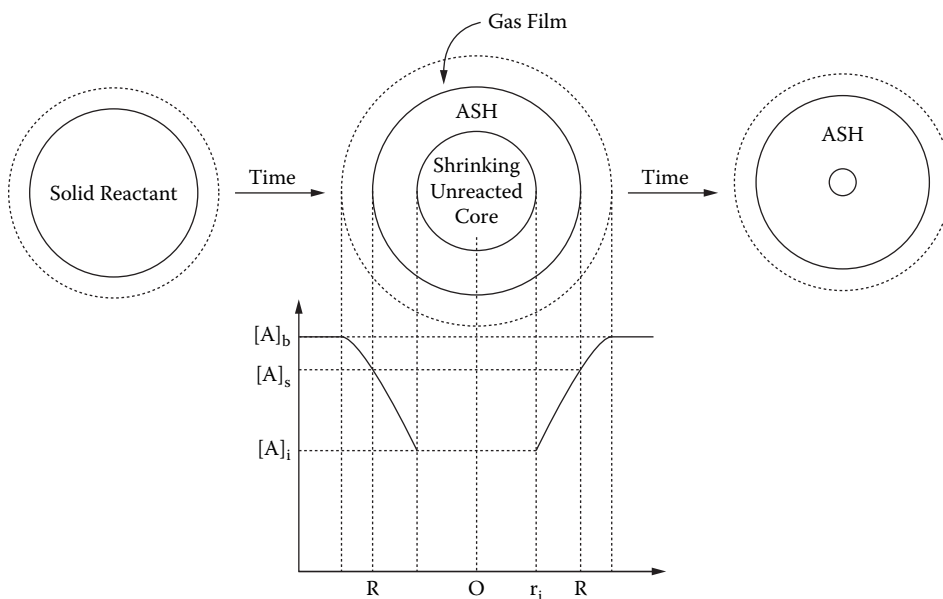


FIGURE 11.8 The shrinking core model (SCM) for gas-solid noncatalytic reactions.

11.3.2.1.1 Shrinking Core Model (SCM)

Figure 11.8 illustrates the basic features of SCM. The gas first diffuses through the film surrounding the pellet and reacts at the interface. As the reaction progresses, the interface moves inward, leaving behind a shell of the exhausted solid (called ash). In effect, the unreacted core shrinks until the entire solid has reacted. This behavior is possible only if the solid is nonporous. Otherwise, the gas will diffuse below the surface, and the reaction will no longer be confined to the interface.

The mathematical analysis of this model is facilitated by the pseudo-steady-state (PSS) assumption, i.e., the interface remains stationary while the mass flux equations are written. This is generally satisfied for gas-solid reactions. The following equations for makers of A diffusing per unit time for a single pellet, R_A can be written:

Diffusion through gas film:

$$R_A = 4\pi R^2 k_G \quad (11.59)$$

Diffusion through ash layer:

$$R_A = \frac{4\pi R r_i D_{e,As}}{R - r_i} \quad (11.60)$$

Chemical reaction at the interface:

$$R_A = 4\pi r_i^2 k_s \quad (11.61)$$

Noting that conversion in a spherical pellet is related to the ratio of the initial and interface radii by the equation

TABLE 11.13
Time-Conversion Relationships for SIM for Different Particle Geometries^a

Controlling Regime	Functional forms for			τ
	Flat Plate	Cylinder	Sphere	
Film diffusion, $f_1(X_B)$	X_B	X_B	X_B	$\frac{\rho_B R}{v k_g [A]_b}$
Ash diffusion, $f_2(X_B)$	X_B^2	$X_B + (1 - X_B) \ln(1 - X_B)$	$1 - (1 - X_B)^{2/3} + 2(1 - X_B)$	$\frac{\rho_B R^2}{2v D_{e,As} [A]_b}$
Reaction, $f_3(X_B)$	X_B	$1(1 - X_B)^{1/2}$	$1 - (1 - X_B)^{1/3}$	$\frac{\rho_B R}{v k_s [A]_b^n}$

^a Conversion $X_B = 1 - (r/R)^s$, where $s = 1, 2$, and 3 for flat plate, cylinder, and sphere, respectively.

$$\varepsilon = \left[1 + \hat{R}_i Da \left(\frac{1}{Sh} + \frac{1 - \hat{R}_i}{\hat{R}_i} \right) \right]^{-1} \quad (11.67)$$

where Sh (same as Bi_m) = $k_G R / D_{e,As}$ and $Da = k_s R [A]_b^{m-1} / D_{e,As}$ (with $m = 1$). The equation takes an implicit form for nonfirst-order reactions.

SCM is a phenomenological model that predicts the total conversion of a solid in a finite time and is well suited for many practical systems. However, it cannot account for such features as the leveling off of conversion at a value lower than the total conversion. Most importantly, it is not suitable for porous solids.

11.3.2.1.2 Volume Reaction Model

When the solid is porous, the reaction occurs throughout the pellet, with no sharp interface. If diffusion is assumed to be fast, the gas concentration will be uniform throughout the pellet, leading to the so-called homogeneous model. The rate of reaction can then be simply written as

$$r_A = k_v [A]^m [B]^n \quad (11.68)$$

The general conservation equations for the solid and reactant species for the volume reaction model in dimensionless form are as follows:

$$\nabla^2 [\hat{A}] = \phi^2 [\hat{A}]^m [\hat{B}]^n \quad (11.69)$$

$$-\frac{d[\hat{B}]}{dt} = [\hat{A}]^m [\hat{B}]^n \quad (11.70)$$

where

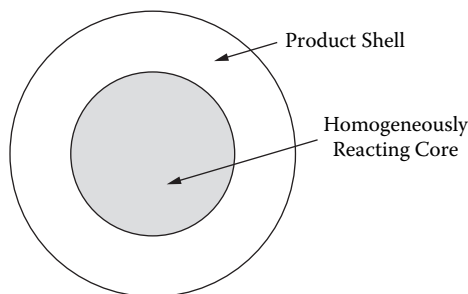


FIGURE 11.9 The two-zone model for gas-solid noncatalytic reactions.

The importance of reaction orders m and n has been examined at length (see, e.g., Doraiswamy and Sharma, 1984). The case of $m = 1$, $n = 0$ (i.e., zero order with respect to the solid reactant) is particularly important, since the gas concentration can drop to zero within the pellet, depending on the value of ϕ . In fact, a critical value given by

$$\phi_{cr} = \frac{6}{2/Sh + 1} \quad (11.78)$$

exists beyond which the concentration of A can fall to zero at some point within the pellet. For $\phi < \phi_{cr}$, the concentration would be finite at all points in the pellet, and Equation (11.75) describes the conversion-time behavior.

11.3.2.1.3 The Zone Models

The homogeneous model behaves in part as a shrinking core model when the reaction-diffusion interaction is such that the outer layers become exhausted, leading to the formation of an ash layer as in SIM. The difference, however, is that the reaction is not topochemical; i.e., it is not confined to the interface but occurs throughout the reactant matrix (core) as in the homogeneous model (Figure 11.9). Ishida and Wen (1968) have derived equations for this so-called two-zone model. A more general model is, however, one in which a reaction zone is sandwiched between the ash layer and the unreacted core (Bowen and Cheng, 1969). The model, sketched in Figure 11.10, is characterized by three stages (Mantri et al., 1976): (1) zone formation starting from the pellet surface until it has reached a thickness determined by the reaction-diffusion interaction for the system, (2) zone travel to the interior leaving a layer of ash as the shell, and (3) zone collapse as it merges with the core (thus becoming a two-zone model), the reaction continuing in the core until the entire solid is exhausted. The experimental results of Prasannan and Doraiswamy (1982) on the oxidation of zinc sulfide reveal three stages of the reaction. The zone width is clearly a function of the Thiele modulus. Their model reveals that, when the zone thickness is zero, it reduces to SIM, and when it is of the pellet dimension, it reduces to the homogeneous model. In an extension of this model to reversible reactions, Khan (1999) postulates two reaction zones.

11.3.2.1.4 The Particle-Pellet or Grain Models

Although such models are based on the granular structure of the pellet, the first version did not account for changes in the grain size. Hence, they can broadly be considered as spanning the macroscopic models in which pore evolution is ignored and the structural models in which the progress of reaction is explicitly related to pore evolution with time (i.e., to structural changes). The basic feature of these models, sketched in Figure 11.11, is that the grains constituting a pellet are spherical and of the same size, that each grain reacts according to SIM, and that the size of the grain does not change with reaction (thereby implying no voidage change with reaction and hence no pore evolution).

The mathematical formulation of the model requires consideration of the rate processes within an individual grain, and the overall mass balance for the gaseous reactant in the pellet and its stoichiometric relationship with the extent of solid consumed. As far as the individual grain is concerned, the rates of diffusion through the reacted portion of the grain and of reaction at the interface can be obtained in analogy with Equations (11.60) and (11.61) as

$$\mathbf{R}_{GA} = \frac{4\pi \mathbf{D}_{eG} r_{Gi} r_{G0}}{r_{Gi} - r_{G0}} ([A]_S - [A]_i) \quad (11.79)$$

$$\mathbf{R}_{GA} = 4\pi r_{Gi}^2 k_s [A]_i \quad (11.80)$$

Eliminating the unknown concentration $[A]_i$ at the interface, we obtain the overall rate per unit grain as

$$\mathbf{R}_{GA} = \frac{4\pi r_{Gi}^2 k_s [A]}{(1 + r_{Gi} k_s / \mathbf{D}_{eG})(1 - r_{Gi} / r_{G0})} \quad (11.81)$$

Once the rate of reaction for the individual grain is known, the overall pellet equation can be written:

$$\nabla^2 [A] = \mathbf{R}_{GA} \frac{3(1 - \epsilon_p)}{4\pi r_{G0}^3} \quad (11.82)$$

where the term in parentheses refers to the grains in the pellet volume. The term \mathbf{R}_{GA} involves a knowledge of the interfacial position r_{Gi} within each grain, which is a function of both the time and position within the pellet. To evaluate this, a stoichiometric balance on the solid reactant B can be written for an individual grain in analogy with Equation (11.65) as

$$-\frac{d}{dt} \left[\frac{4}{3} \pi r_{Gi}^3 \frac{\rho_B}{M_B} \right] = \mathbf{R}_{GA} \quad (11.83)$$

The term $[A]$ appearing in \mathbf{R}_{GA} [Equation (11.82)] in this equation fixes the position of the individual grain in the pellet.

The appropriate boundary conditions to the problem are

$$\begin{aligned} r = R: \quad \mathbf{D}_{eAs} \frac{d[A]}{dr} &= k_G ([A]_b - [A]_S) \\ r = 0: \quad \frac{d[A]}{dr} &= 0 \\ r = 0: \quad r_{Gi} &= r_{G0} \end{aligned} \quad (11.84)$$

In general, these equations require numerical solution.

Considering the physical features of the model, two parameters are involved: τ_G , the time required for complete conversion of the grain in the $[A]$ environment; and τ_p , the time for complete conversion of the particle by diffusion if the grain conversion process is extremely fast. In the limiting case of grain diffusion controlling, the simple homogeneous model is recovered. The

Goring, 1965) and nondimensionalized to incorporate the effect through a dimensionless quantity for volume change. The final asymptotic solution (Sohn and Sohn, 1980) obtained is

$$\frac{\ln(1+\theta)}{\theta} \frac{\hat{t}}{\phi^2} = 1 - \frac{(\beta+1)(1-X_B)^{2/(\beta+1)} - 2(1-X_B)}{(\beta-1)} = f(X_B) \quad (11.86)$$

where β is the shape factor and ϕ and θ are, respectively, the Thiele modulus and a volume change modulus defined as

$$\phi = \frac{sV_p}{A_p} \sqrt{\frac{k_V}{2\mathbf{D}_{e,As}}} \quad (11.87)$$

$$\theta = \left(\frac{v_R}{v_A} - 1 \right) X_A$$

Clearly, $\theta = 0$ for a reaction with no volume change.

These equations are, however, not applicable to nonisothermal reactions. SIM equations are based on the applicability of the PSS assumption, which is not applicable to nonisothermal reactions.

11.3.2.2.2 Effect of Nonisothermicity

Although SIM generally cannot be applied to analyze a nonisothermal reaction, it is well suited for certain decomposition reactions (Narsimhan, 1961; Hills, 1968; Campbell et al., 1970), such as



The phase rule suggests one degree of freedom. Each temperature, therefore, has a fixed value of partial pressure of the product gas S . Once this value is reached, the reaction starts, and the front moves inside. The process typically yields SIM behavior and is controlled either by heat or gas diffusion through the product layer. For heat transfer through the product layer controlling, the interface stays isothermal, and the equation for SIM with $\mathbf{D}_{e,As}$ replaced by the corresponding heat transfer parameters in the definition of represents the conversion-time behavior. Where gas diffusion is controlling, the variation of $\mathbf{D}_{e,As}$ with temperature should be accounted for. This variation usually takes the form $\mathbf{D}_{e,As} = T^{1.5-2.0}$ in the bulk diffusion regime with $D_{e,As} = T^{0.5}$ in the Knudsen regime. Luss and Amundson (1969) have provided a more rigorous analysis that incorporates the transient heat accumulation term and gives the interface temperature as a function of the interfacial position r_i .

11.3.2.3 Models That Account for Structural Variations

The main structural changes that occur in a solid are those due to reaction and sintering.

11.3.2.3.1 Effect of Reaction

The reaction effect is mainly the result of the difference in molal volumes of the product and reactant solids, leading to voidage and therefore diffusivity changes as the reaction progresses. To incorporate these effects in any model, it is necessary to relate the overall solids conversion to voidage and diffusivity. An important feature of the structural effect is that when the porosity at the surface of the solid becomes zero (pore closure), the governing equations predict incomplete conversion, so often observed in gas-solid reactions (and not predicted by the basic models).

One way to account for structural changes is to allow for changes in the grain size in the particle-pellet model (Garza-Garza and Dudukovic, 1982a, b). A more useful way is to incorporate

$$S_p^*(X_B) = [1 + (Z_v - 1)X_B]^g \quad (11.91)$$

where g is the grain shape factor (2/3 for the sphere, 1/2 for the cylinder, and 0 for the flat plate).

For the random pore model,

$$S^*(X_B) = (1 - X_B) \sqrt{1 - \psi' \ln(1 - X_B)} \quad (11.92)$$

$$S_p^*(X_B) = [1 + (Z_v - 1)X_B] \sqrt{1 - \psi' \ln[1 + (Z_v - 1)X_B]} \quad (11.93)$$

where ψ' is a structural parameter defined by

$$\psi' = \frac{1}{\ln\left(\frac{1}{1 - \epsilon_0}\right)} \quad (11.94)$$

for uniform pore radius. The equation becomes complicated for a nonuniform radius (see Bhatia and Perlmutter, 1983). Substituting the expressions for any of these models in Equation (11.88) and integrating leads to the desired conversion-time relationship. Although the random pore model appears more realistic, the predictions of the grain model are surprisingly close to those of this model. Several improvements, many marginal, have been suggested (see Bhatia and Gupta, 1993).

11.3.2.3.2 Effect of Sintering

The use of high temperatures in certain reactions, such as those in gas cleaning using lime-based adsorbents or exothermic reactions with generation of large amounts of heat, leads to sintering of the solid. It becomes more severe at higher temperatures (usually over 800 K), causing a decrease in the effective diffusivity of the solid or an increase in grain size leading to a lower specific area. Also, there could be a decrease in porosity and an increase in the tortuosity factor, both leading to a lowering of the effective diffusivity. Empirical models have been used for sintering, such as exponential decay for diffusivity and first-order decay for surface area (Ranade and Harrison, 1979, 1981). The combined effects of the two have been considered by Kim and Smith (1974), Chan and Smith (1976), and Ramachandran and Smith (1977b). The following is recommended:

$$\mathbf{D}_e = \frac{1}{F(f_p)} \left[1 - (1 - \epsilon_0) \left(\frac{r_{Gi}}{r_{G0}} \right)^3 \right]^2 (1 - f_p) \quad (11.95)$$

where f_p is the fraction of pores removed and is given by

$$\frac{df_p}{dt} = k_p (1 - f_p) \quad (11.96)$$

where k_p is the rate constant for pore removal.

TABLE 11.15
Examples of Industrially Important Gas-Liquid Reactions

Regime 1: Very slow reaction

Air oxidation of a variety of aliphatic and alkyl aromatic compounds; air oxidation of *p*-nitrotoluene sulfuric acid; substitution chlorination of a variety of organic compounds; reaction between isobutylene and acetic acid; oxidation of ethylene to acetaldehyde (Wacker processes); hydrochlorination of olefins; absorption of phosphine in an aqueous solution of formaldehyde and hydrochloric acid; acetic acid from the carbonylation of methanol; oxidation of tri-alkyl phosphine; dimerization of olefins.

Regime 2: Slow reaction

Absorption of CO₂ in carbonate solution; absorption of O₂ in aqueous acid solutions of CuCl at concentrations less than 1×10^{-4} mol/cm³; oxidation of organic compounds; preparation of the C-13 isotope.

Regime between 1 and 2

Absorption of CO₂ in carbonate buffer solutions in packed columns; oxidation of black liquor in the paper and pulp industry; absorption of CO₂ in carbonate solution; wet air oxidation of soluble compounds in waste water.

Regime 3: Fast reaction

Absorption of CO₂ and COS in aqueous solutions of amines and alkalies; absorption of oxygen in aqueous acidic and neutral solutions of cuprous chloride, and in cuprous and cobaltous amine complexes in aqueous and polar solutions; absorption of oxygen in aqueous alkaline solutions of sodium dithionite (hydrosulfite); absorption of oxygen in aqueous sodium sulfite; absorption of NO/NO₂/N₂O₄ in water and aqueous solutions containing reactive species; reaction between dissolved NO and O₂; absorption of oxygen and ozone in aldehydes; absorption of isobutylene, 2-butene, and 2-methyl-2-butene in aqueous solutions of sulfuric acid; absorption of isobutylene in aqueous solutions containing thallium (III) ions; absorption of lean phosphine in aqueous solutions of sodium hypochlorite and concentrated sulfuric acid; absorption of ozone in aqueous and non-aqueous solutions, with or without dissolved organic chemicals; oxidation of cyanide ions in aqueous alkaline solutions and organic media containing olefinic substances; waste water treatment; oxidation of organometallic compounds; hydrogenation of unsaturated compounds with homogeneous catalysts; absorption of Cl₂ in aqueous solutions containing phenolic substances and aromatic nitro and sulfuric compounds; absorption of Cl₂ in aqueous and non-aqueous solutions of ketones.

Regime 4: Instantaneous reaction

Absorption of CO₂ in aqueous solutions of MEA; absorption of H₂S and mercaptans in aqueous solutions of alkanolamines and caustic soda; absorption of carbon monoxide in aqueous cuprous ammonium chloride solutions; absorption of lower olefins in aqueous solutions of cuprous ammonium compounds; absorption of pure chlorine in aqueous solutions of sodium carbonate or sodium hydroxide; conversion of dithiocarbamates to thiuram disulfides; sulfonation of aromatic compounds with lean SO₃; recovery of bromine from lean aqueous solutions of bromides; reactions of importance in pyrometallurgy; absorption of CO₂ in aqueous solutions of caustic alkalies and amine; absorption of O₂ in aqueous solutions of sodium dithionite; absorption of O₂ in aqueous sodium sulfite solutions; absorption of O₂ in alkaline solutions containing the sodium salt of 1,4-naphthaquinone-2-sulfonic acid (NQSA); special case: role of diffusion in the absorption of gases in blood in the human body.

Representative lists for gas-liquid and liquid-liquid reactions are given in Tables 11.15 and 11.16, respectively. Doraiswamy and Sharma (1984) have covered in detail the theory of mass transfer with simple and complex reactions. A summary of simple irreversible reactions is given below.

11.3.3.1 Theory of Mass Transfer Accompanied by Irreversible Chemical Reaction

The gas phase contains *A* and the liquid phase contains reactive species *B*. *A* is sparingly soluble in the *B* phase, and the reaction occurs exclusively in the *B* phase. The overall reaction involves two steps.

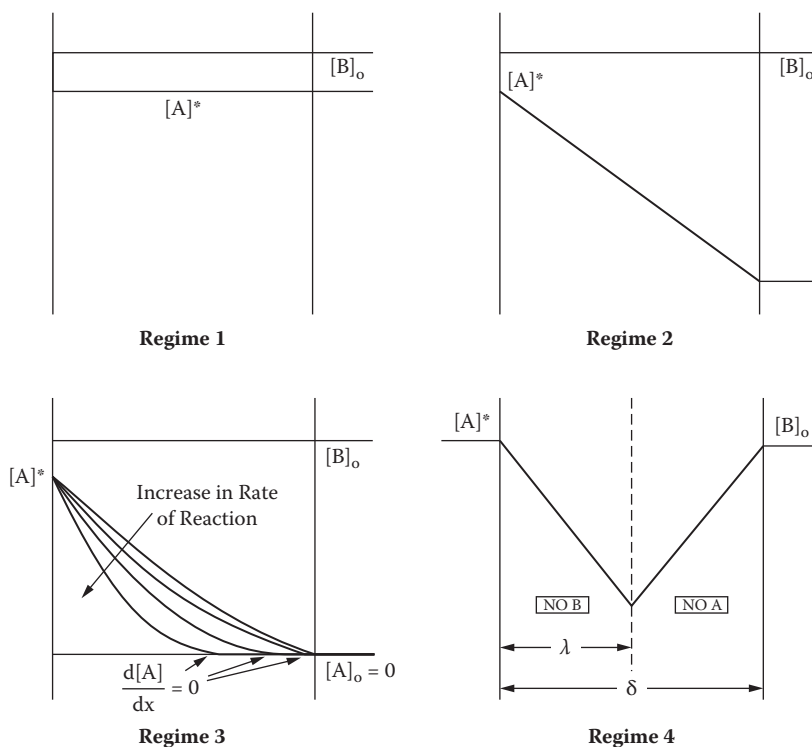


FIGURE 11.13 The different operating regimes in gas-liquid reactions.

A enters the bulk liquid. Furthermore, it can be seen from Figure 11.13 that the concentration profile of *B* is flat in the first three regimes. This means that the rate of diffusion of *B* is faster than the chemical reaction in the film. In regime 4, the reaction between *A* and *B* is instantaneous and occurs as soon as they meet at the reaction plane. The overall rate is controlled by the diffusion of *A* and *B* to the reaction plane.

Doraiswamy and Sharma (1984) have given detailed derivations for the overall rates of reaction and the conditions to be satisfied in each regime of operation. The final equations and conditions are summarized in Table 11.17. It is likely that a reaction falls in the intermediate range or more than one regime. For these cases, expressions for the overall rates are given in Table 11.18. Recently, Doraiswamy (2001) has given similar tables for some complex reactions.

11.3.3.2 Laboratory Reactors for Fluid-Fluid Reactions

For designing fluid-fluid reactors (described in Section 11.4), there are two basic requirements: (1) the flow behavior in reactors that governs the distribution of concentrations (including partial pressures) and temperature along the length and transverse directions and in all the phases, and (2) knowledge of overall rates at a given point in the reactor (with known concentrations and temperature). For the examples of industrial importance indicated in Tables 11.15 and 11.16, the equations for overall rates are given in Tables 11.17 and 11.18. For the estimation of overall rates of reaction, three types of information are needed: (1) physical properties of the system such as diffusivity, solubility, density, viscosity, and so on; (2) hydrodynamic parameters such as effective interfacial area, a , and true mass transfer coefficient $k_L a$; and (3) kinetic parameters such as rate constants, orders with respect to different reactants, and activation energy. The chapter by Harvey in this book suggests how to obtain the desired data. The work by Reid et al. (1977) is also helpful. The hydrodynamic parameters a and $k_L a$ depend on the type of reactor, flow rates of various phases,

TABLE 11.18**Overall Rates of Reaction for Overlapping Regimes**

1. Regime 1 and 2,
- $m = 1$
- ,
- $n = 1$

$$R_A a = \frac{[A]^*}{\left[\frac{1}{k_L a} \right] + \frac{1}{\varepsilon_L k_{mn} [A]^{*m-1} [B]_0^n}}$$

2. Regime 2 and 3

$$R_A a = a [A]^* \sqrt{\frac{2}{m+1} \mathbf{D}_A k_{mn} [A]^{*m-1} [B]_0^n + k_L^2}$$

or

3. Regime 1, 2 and 3 (
- $m = 1$
- ,
- $n = 1$
-)

$$R_A a = \frac{k_L a [A]^* \sqrt{M}}{\tanh \sqrt{M}}$$

$$R_A a = \frac{a [A]^*}{\frac{1}{\sqrt{\mathbf{D}_A k_2 [B]_0 + k_L^2}} + \frac{a}{\varepsilon_L k_2 [B]_0}}$$

4. Regime 3 and 4

$$R_A a = \Phi k_L a [A]^*$$

where

$$\Phi = \sqrt{M} \left[\frac{(\phi_a - \phi)}{(\phi_a - 1)} \right]^{0.5}$$

$$\Phi_a = 1 + \frac{[B]_0}{Z[A]^*} \sqrt{\frac{D_B}{D_A}}$$

5. Regime 1, 2, 3 and 4 together with gas side resistance (
- $m = 1$
- ,
- $n = 1$
-)

$$R_A a = \Phi_L a [A]^*$$

where

$$\Phi_a = \sqrt{\frac{M^2}{4(\phi_a - 1)} + \frac{M\phi_a}{\phi_a - 1} + 1} - \frac{M}{2(\phi_a - 1)}$$

$$M = \frac{\mathbf{D}_A k_2 [B]_0}{k_L^2}$$

$$\phi_a = - + \sqrt{\beta^2 + \gamma}$$

$$\beta = 0.5(1 + f_1 / f_3) + \sqrt{M} / f_3 - \sqrt{M}$$

$$\gamma = \sqrt{M} (1 + f_1 / f_3)$$

$$f_1 = k_G / H_A k_L$$

$$f_2 = \frac{\mathbf{D}_B [B]_0}{Z \mathbf{D}_A [A]_0}$$

$$f_3 = f_1 / f_2$$

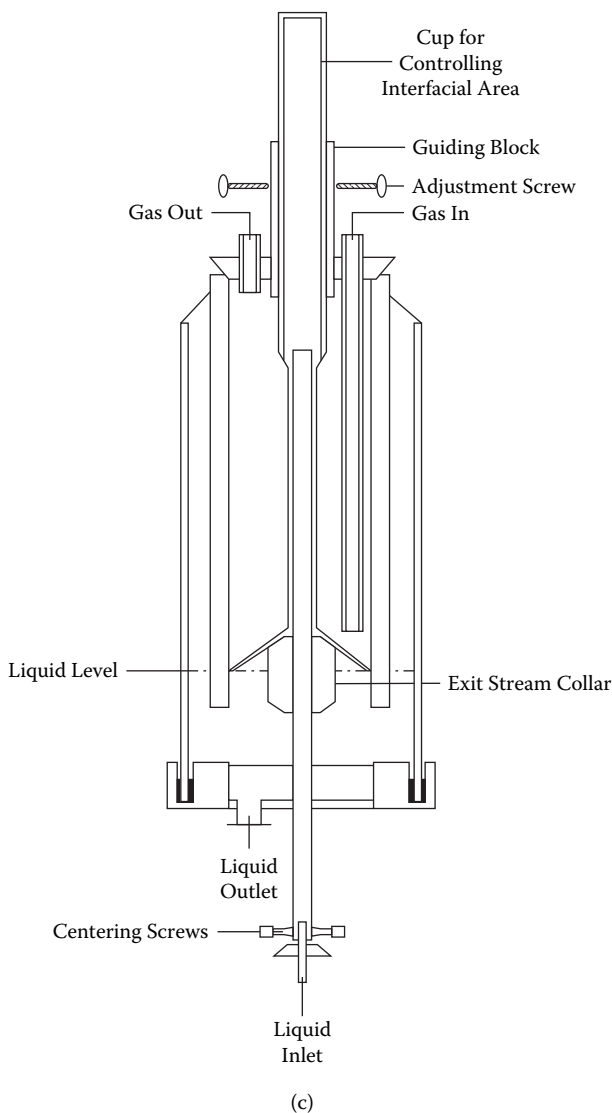


FIGURE 11.14 *Continued.*

gas-phase impeller speed. The rate of reaction is estimated by following the liquid-phase concentration.

From Table 11.17, it can be seen that the kinetic parameters are included in the rate equations for regimes 1 and 3, whereas the rate equations for regime 2 and 4 represent completely mass transfer-controlled operations. Therefore, for obtaining the kinetic parameters, it is important that the experiments in a stirred cell satisfy the conditions of either regime 1 or regime 3. A given stirred cell is characterized by vessel diameter (T), impeller diameter (D), and impeller design and location from the gas-liquid interface.

A typical stirred cell may have $T = 100$ mm, $D = 90$ mm, and a two-bladed paddle with $W/D = 0.1$ located 10 mm below the interface. The gas-phase impeller may be powered by a motor as shown in Figure 11.14a. A stepwise procedure for obtaining the kinetic parameters is outlined as follows:

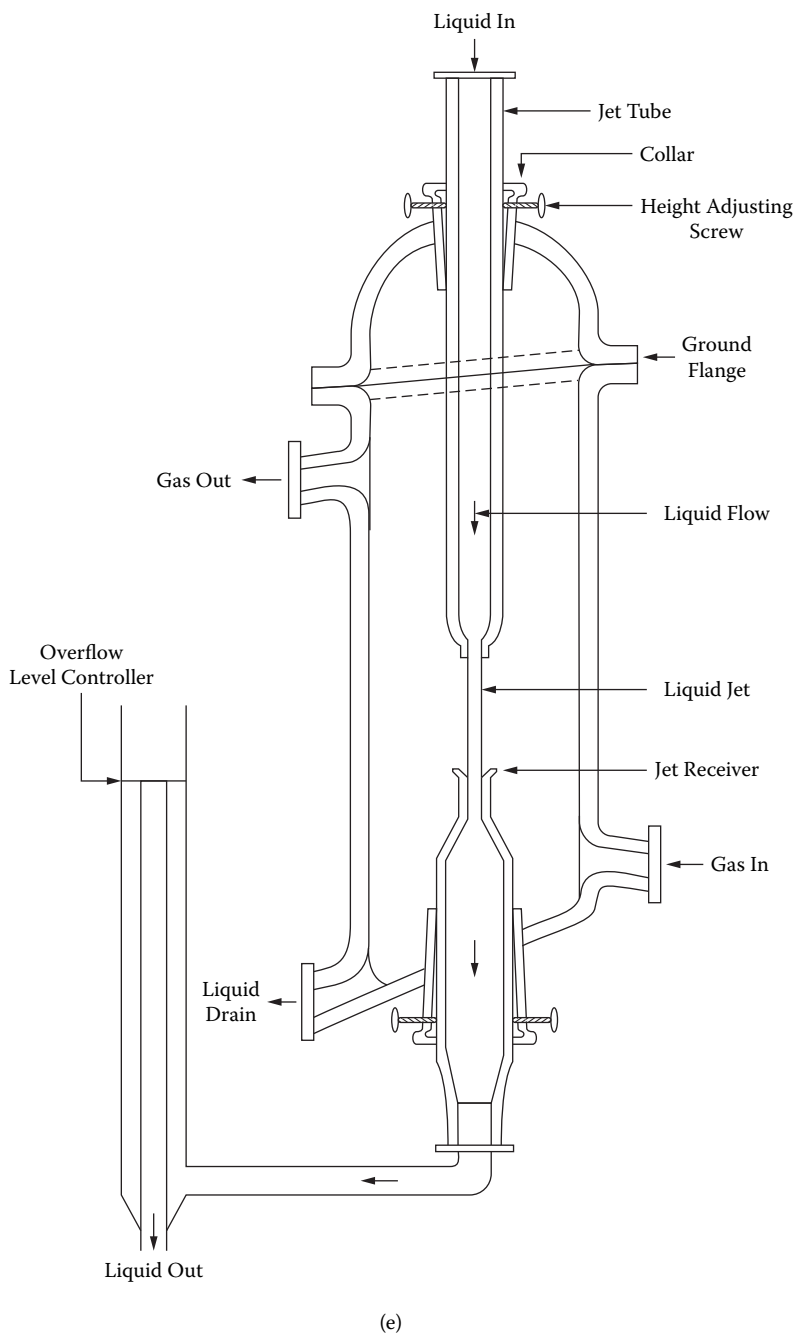


FIGURE 11.14 Continued.

$$\eta = \frac{R_A}{k_L [A]^*} \quad (11.102)$$

5. If $\eta < 1$, the absorption occurs between regimes 1 and 2. To achieve the conditions of regime 1, the impeller speed is increased such that R_A becomes independent of it, or ϕ becomes much less than 1. In regime 1, the overall rate of absorption (Table 11.17) is

TABLE 11.19
Dependence of Stirred Cell Performance (Rate of Absorption per Unit Volume) on Operating Parameters in All the Four Regimes

Regime	Impeller Speed (N)	k_L	A	D_A	$[A^*]$	$[B]_0$	Volume of Liquid
1	No	No	No	No	$\propto [A^*]^m$	$\propto [B]_0$	Yes
2	Yes	$\propto k_L$	$\propto a$	$\propto \sqrt{D_A}$	$\propto [A^*]$	No	No
3	No	No	$\propto a$	$\sqrt{D_A}$	$\propto [A^*]^{\frac{m+1}{2}}$	$\propto [B]_0^{n/2}$	No
4	Yes	$\propto k_L$	$\propto a$	$\propto \frac{D_A}{D_B}$	No	$\propto [B]_0$	No

The variation of $[A^*]$ and $[B]_0$ over a wide range gives the values of m , n , and k_{mn} . The activation energy is also estimated.

The experimentally observed orders are $(m + 1)/2$ and $n/2$ in regime 3, whereas they are m and n in regime 1, although in both cases the operation is chemical reaction controlled. Obviously, the regime of operation should be known. It was mentioned earlier that, in regime 1, $\phi \ll 1$, whereas in regime 3, $\phi > 3$. In addition, another condition can be obtained from the equations for the overall rate of reaction given in Table 11.17. The overall rate is expressed per unit volume of total reactor, which includes all the phases. Thus, for a stirred cell, the rate is expressed per unit of total cell volume including liquid and gas phases. From the rate equation for regime 1, the rate is proportional to the liquid fraction (ϵ_L) or the liquid volume taken for the reaction. Since the values of the effective interfacial area (cross-sectional area divided by total cell volume) and k_L are independent of liquid volume, the overall rate does not depend on the liquid volume in regimes 2, 3, and 4. These observations are listed in Table 11.19. Furthermore, the reaction-controlled regime 1 does not show any dependence on k_L (and hence impeller speed) and interfacial area. In regimes 2 and 4, the rate is proportional to k_L (and hence impeller speed), and in regimes 2, 3, and 4, the rate is proportional to a . All these dependencies are summarized in Table 11.19. The dependencies on $[A^*]$ and $[B]_0$ can be determined from the rate equations given in Table 11.19.

In addition to the stirred cell, other laboratory reactors commonly used include rotating drum contactor, wetted wall column, wetted sphere column, laminar jet, and stirred contactor. These equipments are shown schematically in Figures 11.14b–f. All have several common features, the principal one being a well defined gas-liquid interfacial area and the ability to vary the area per unit reactor volume (a). In the stirred cell, it is achieved by varying the liquid height. As an alternative way, a solid circular baffle is placed at the gas-liquid interface. Holes are drilled on the baffle plate so that the hole opening area becomes the interfacial area. For varying a , baffle plates are made with different free (hole) areas.

In the rotating drum contactor (Figure 11.14b), the value of a is adjusted by sliding the gas-tight screen, thus permitting the opening over a wide range from fully closed (no interfacial area) to fully open where half the cylinder is exposed to the gas. In the wetted wall column (Figure 11.14c), a film is formed over a certain height of the rod, below which a tight collar removes the liquid and discharges it into the liquid pool at the bottom. The interfacial area is varied by changing the film height by positioning the collar. In the wetted sphere column (Figure 11.14d), a is varied by changing the number of spheres (Pigford and Pyle, 1951). In the four

TABLE 11.20
Laboratory Reactors for Fluid-Fluid Reactions: Their Principal Features and Ratings^a

	Residence Time	Surface Renewal Time	Effective Interfacial Area m ² /m ³	Interfacial Area per Unit Liquid Volume m ² /m ³	Range of $k_L \times 10^5$ m/s	Ease of Operation	Accuracy of Liquid Phase Residence Time/Liquid Phase Mixing	Ease of Sampling and Accuracy of Measurement	Construction Difficulties and Cost
1. Stirred cell	Wide range possible	0.05 to 4	4 to 25	10 to 40	1 to 20	G	F to P/G	G	G
2. Stirred contactor	Wide range possible	0.005–0.1	40 to 300	50 to 400	20 to 50	F to G	F to P/G	G	F to G
3. Cylindrical wetted wall	0.05 to 4	0.05 to 4	10 to 50	300 to 6000	1 to 20	F	G	F to G	F to G
4. Spherical wetted wall	0.03 to 5	0.03 to 5	10 to 50	300 to 6000	1 to 20	F	G	F to G	F to G
5. Rotating drum	0.002 to 0.5	0.002 to 0.5	10 to 50	300 to 3000	5 to 70	F	F to P	F to G	F
6. Laminar Jet	0.001 to 0.1	0.001 to 0.1	40 to 500	1000 to 10,000	10 to 100	F to P	G	F to G	F

^a F = fair, G = good, P = poor.

columns, plate extraction columns, static mixers, and so on. Similar equipments are widely used in gas-liquid-solid, gas-liquid-liquid, and gas-liquid-liquid-solid contactors.

In multiphase contactors, the dispersed phase is either bubbles, drops, particles, or combinations thereof. The continuous phase is either liquid or gas. The governing features of the dispersed phase are its size and velocity distributions, both of which have a major impact on the performance of these equipments. The other governing parameters include column diameter, column height, sparger design, and internal design. Furthermore, in class 1 equipment, the energy is supplied through the introduction of phases. For instance, in the case of bubble columns and gas-fluidized beds, the gas is supplied against the static pressure of the multiphase dispersion, and the energy input rate is given by the following equation:

$$E_i = Q_G \bar{\rho}_D H_D g \quad (11.104)$$

where $\bar{\rho}_D$ is the average density of the dispersion, and E_i is the pressure energy. Class 1 equipments, therefore, are classified under pressure energy.

Class 2 equipments include mainly stirred-tank reactors, in which impellers supply energy to the reactant(s). The fluid leaving the impeller has kinetic energy. The energy is used for a variety of objectives such as producing liquid-liquid, gas-liquid, solid-liquid, and higher-order dispersions. Stirred reactors, in which one or more impellers generate the desired flow and mixing, are among the most widely used reactors. Stirred reactors offer unmatched flexibility and control over the transport processes in the reactor. The performance of a stirred reactor can be optimized by appropriate adjustments of the reactor hardware and the operating parameters (reactor and impeller shapes; number, type, location and size of impellers; degree of baffling; control the performance of stirred reactors; and so on).

In class 3 equipments, the energy supplied is in the form of potential energy associated with the liquid. For instance, in the conventional packed column (used for either distillation or absorption), the liquid is pumped to the top of the column and distributed over the packing. If the gas is introduced at the bottom, the gas phase has the pressure energy; however, it is usually negligible as compared with the potential energy of the liquid. Even if the gas and liquid phases flow cocurrent downward, the major contribution to the energy is by the liquid phase. Since the liquid flows as films, these equipments (class 3) may also be termed *film contactors*. Other equipments in this category include trickle-bed reactors and falling-film reactors/evaporators. In packed columns, a variety of packing shapes (and of course sizes and materials of construction) are used in practice; these include Raschig rings (in old installations), Berl saddles, partition rings, intelox saddles, Pall rings, hipack rings, and structured packing. Equally important is the uniformity of liquid distribution. The more important ones (under each class) are described below. Table 11.23 presents a list of reactors under each category.

11.4.2 PRESSURE ENERGY

11.4.2.1 Gas-Liquid Reactors

11.4.2.1.1 Bubble Columns

The bubble column used as a reactor consists of a vertical cylindrical vessel with height-to-diameter ratio in the range of 1 to 20 (often 3 to 10). Gas is introduced at the bottom via a sparger. Spargers include sieve plate, ring, spider, radial sparger, ejector, injector, and so on. Schematic diagrams of a bubble column and spargers are shown in Figures 11.15 and 11.16, respectively. The column top is expanded to facilitate foam breakage and to reduce the entrainment of liquid in the exit gas. The bubble column is operated either in a semicontinuous mode (gas, continuous; liquid, batch) or in a continuous mode (gas and liquid both continuous). In the latter case, the liquid phase may flow either cocurrent or countercurrent to the gas.

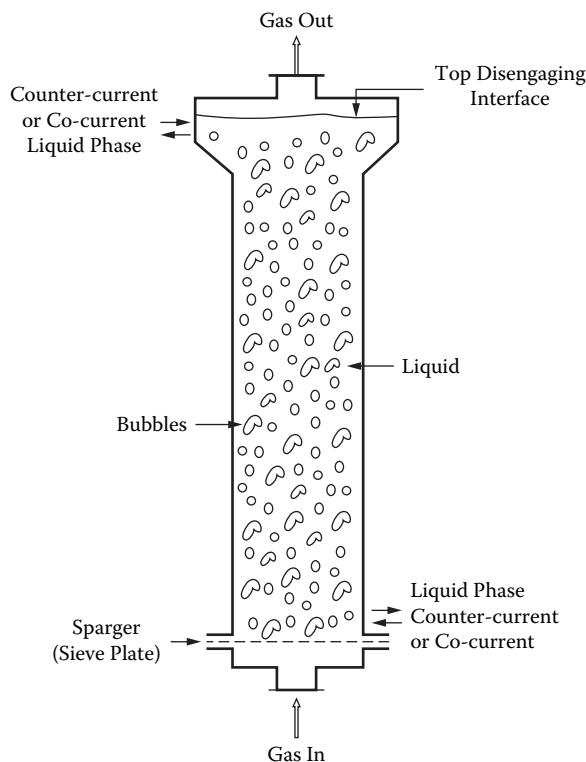


FIGURE 11.15 Schematic diagram of bubble column.

effect, however, depends on the regime of dispersion in bubble columns: homogeneous or heterogeneous. The homogeneous regime is characterized by almost uniform sized bubbles. Furthermore, the concentration of bubbles is also uniform, particularly in the transverse direction (Figure 11.17a). If the gas is sparged uniformly into the bottom of the column, it remains uniformly distributed across the column. All bubbles rise virtually vertically with only minor transverse and axial oscillations plus little coalescence or redispersion. Hence, the size of the bubbles in the homogeneous regime is governed mainly by the design of the sparger and the physical properties of the system.

In contrast, the heterogeneous regime is characterized by nonuniform bubble concentration (Figure 11.17b). The ϵ_G profile is usually parabolic and results in pressure profiles as shown in Figure 11.18a. These profiles cause upward liquid circulation in the central region and downward near the column wall (Figure 11.18b). In such a recirculatory flow, turbulence is much higher as compared to the homogeneous regime, where the recirculation is absent. In the heterogeneous regime, the bubbles retain their identity only over a small distance from the sparger, and this region is called the *sparger region*. In the bulk region, the bubble size is governed by the coalescence and redispersion phenomena. A wide bubble size distribution occurs in the bulk, and the average bubble size (which is called the *secondary bubble size*, d_{bs}) is decided by the balance between the breaking (viscous and turbulent shear stress), the retaining (surface tension) forces, and the coalescing nature of the liquid phase. The value of d_{bs} decreases with a decrease in surface tension and an increase in the power consumption per unit volume (P/V). Furthermore, for a given value of P/V , the average bubble size is smaller in noncoalescing liquids than in coalescing liquids. It is known that the coalescing nature increases with an increase in liquid viscosity and a decrease in gas density. Pure liquids usually show coalescing behavior. However, a mixture of two liquids gives some noncoalescing properties (Bach and Pilhofer, 1978). For example, water and aliphatic alcohol are individually of the coalescing type. The addition of small quantities of aliphatic alcohol to water makes

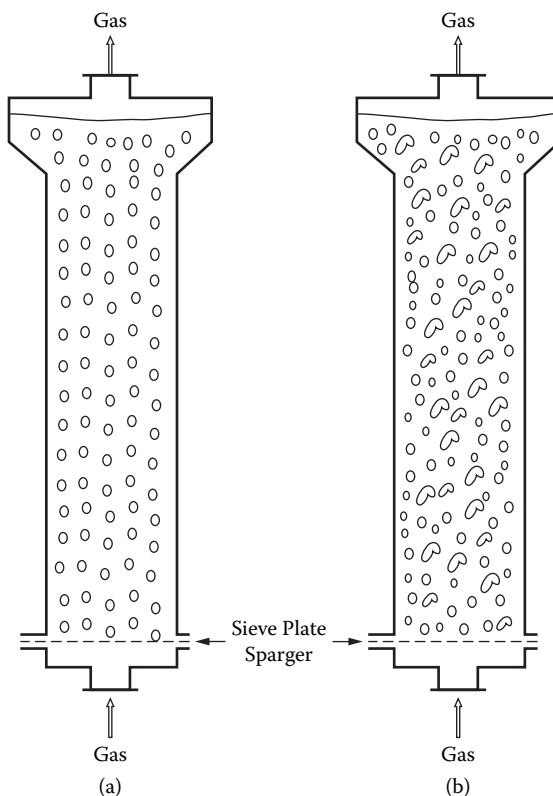


FIGURE 11.17 (a) Schematic representation of the homogeneous regime: uniform concentration and size distributions of bubbles in the transverse direction. (b) Schematic representation of the heterogeneous regime: nonuniform concentration and bubble size distributions in the transverse direction. (From Bhole, M. R. and Joshi, J. B. Stability analysis of bubble columns: Predictions for regime transition. *Chem. Engr. Sci.*, 4493–4507 (2005).)

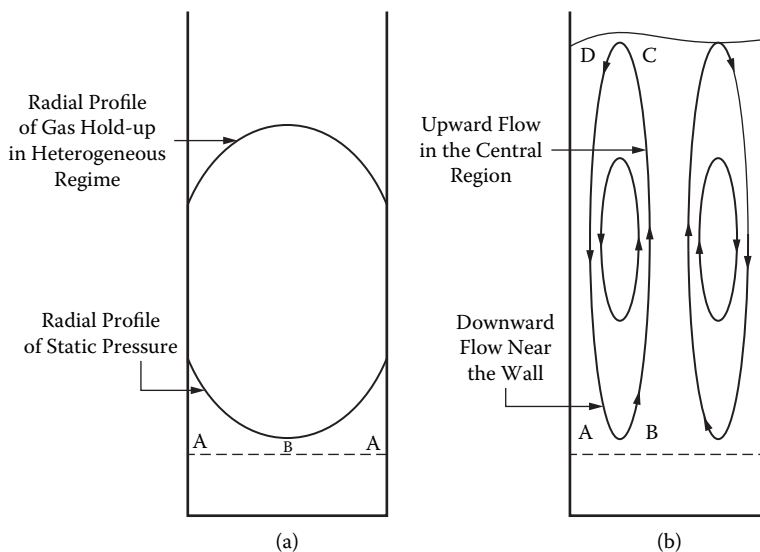


FIGURE 11.18 Some aspects of the heterogeneous regime: (a) radial profiles of gas holdup and static pressure, (b) schematic of liquid circulation pattern.

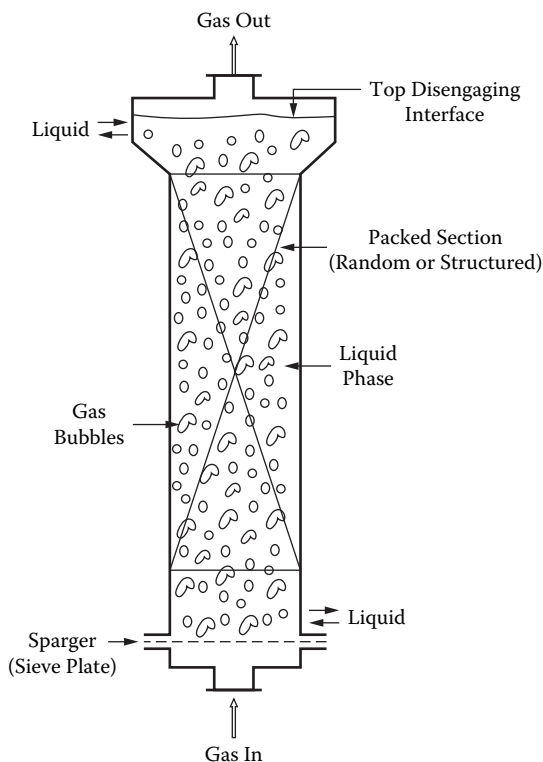


FIGURE 11.20 Packed bubble column.

in non-Newtonian behavior and an increase in viscosity beyond 100 mPa. Further details pertaining to bubble columns are reported by Deckwer (1992) and Joshi et al. (1998).

Bubble columns are simple in construction and operation, providing sufficient flexibility for the liquid-phase residence time. Also, they provide some flexibility even for the gas-phase residence time. However, the bubble columns have two limitations: back-mixing in the liquid phase and high pressure drop for the gas phase. To minimize these limitations, modified bubble columns are often used, as next reported.

11.4.2.1.2 Packed Bubble Columns

A bubble column filled with packings reduces liquid circulation (Figure 11.20). The extent of reduction depends on the resistance provided by the packings, which in turn depends on the voidage and packing factor. The packings may be random, wire mesh, or structured. Pandit and Joshi (1983) have reported that backmixing in packed bubble columns is three to five times lower than that in unpacked bubble columns. For a given duty, the volume of a packed bubble column is less than that of a bubble column, but the cost of the packed bubble column per unit volume is much higher. Therefore, the total equipment cost should be calculated before making any decision.

Packed bubble columns are also used as catalytic reactors where the packings are catalyst particles in the form of extrudates or tablets. These particles have a dual role: one as a catalyst and the second to reduce backmixing. In this case, there is the need to optimize column diameter, height, particle size, and shape.

11.4.2.1.3 Sectionalized Bubble Columns and Plate Columns

Liquid circulation is reduced by baffles. Figure 11.21 shows radial baffles with central openings. Figures 11.21a and b show flat and conical baffles, respectively (conical shape is preferable for a solid suspension). These baffles minimize liquid circulation. The resulting flow pattern is shown

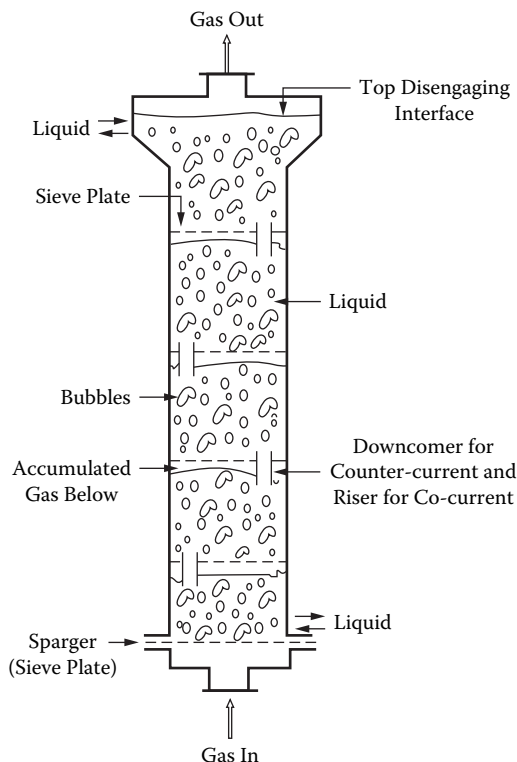


FIGURE 11.22 Sectionalized bubble column with sieve plate.

11.4.2.1.4 Air-Lift Reactors

The bubble column reactor suffers from two major limitations: (1) complete backmixing in the liquid phase and (2) high pressure drop. To overcome the first limitation, suitable modifications were described in previous sections. Now, let us consider the air-lift reactor, which offers the advantage of low pressure drop. Air-lift reactors are of two types: external-loop (Figures 11.23a and b) and internal-loop (Figure 11.24). An external-loop air-lift reactor (EL-ALR) consists of two columns that are connected at the bottom by a U-type connection as shown in Figure 11.23. At the top, a gas disengagement tank is provided. To start the operation of an air-lift reactor, gas is first introduced through the riser sparger. The gas phase ascends in the form of bubbles in the riser section and finally disengages at the top liquid surface in the disengagement tank. The gas bubbles are maintained on the riser side by a vertical baffle, which is located between the riser and downcomer sections. The downcomer section is kept bubble free during the startup. Since the gas-liquid dispersion is present only in the riser section, the average fluid density ($\epsilon_L \rho_L + \epsilon_G \rho_G$) is less in the riser section. Therefore, the static pressure at the bottom of the riser (point C in Figure 11.23a) is low as compared to that at the corresponding location (point D) in the riser. The resulting pressure generates flow from D to C, which further ascends in the riser, overflows the top baffle, and flows downward in the downcomer. As a consequence, well-directed circulation is established. The average liquid circulation can be calculated, as a first approximation, by equating the pressure driving head with the velocity head:

$$P_C = (\epsilon_{LR} \rho_L + \epsilon_{GR} \rho_g) g H_d \quad (11.106)$$

$$P_D = \rho_L g H_D \quad (11.107)$$

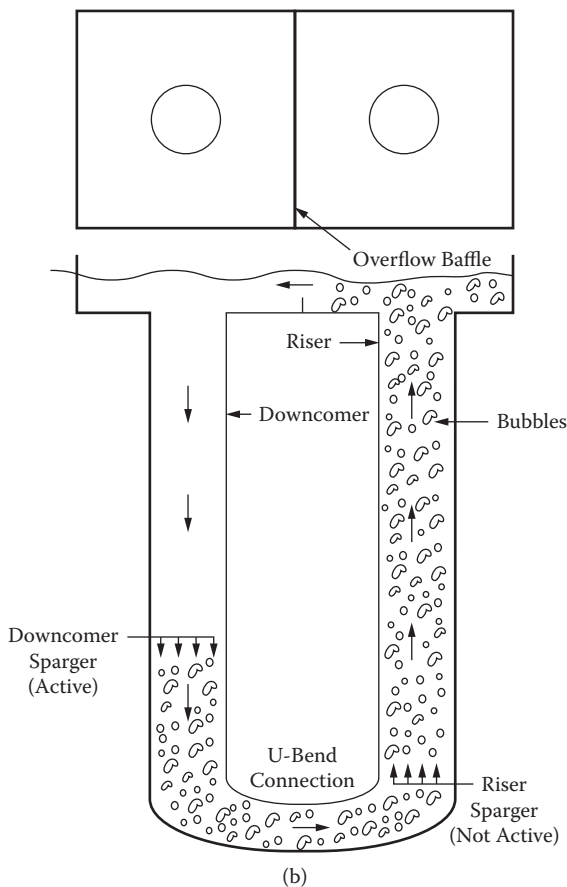


FIGURE 11.23 Continued.

where H_{sd} is the sparger location on the downcomer side and P_C is given by Equation (11.106). Now, the average liquid circulation velocity is given by

$$u = \sqrt{2(\epsilon_{GR}gH_D - \epsilon_{GD}gH_{SD})} \quad (11.111)$$

The liquid circulation continues until the value of u is higher than the bubble rise velocity. This is true even if the riser sparger is stopped (of course, after the circulation pattern is well developed). Furthermore, from Equation (11.111), it can be seen that the circulation velocity decreases with an increase in H_{sd} . At a critical location of $H_{sd}(H_C)$, u equals the bubble rise velocity. In reality, H_{sd} has to be lower than H_C . As a factor of safety, typically, H_{sd} is up to 40% of H .

The gas phase (Figure 11.23b) is introduced downward through the downcomer sparger, takes a U turn at the bottom, ascends in the riser, and leaves the column through the disengagement tank. Thus the gas phase need not be introduced at the bottom as in the conventional bubble column, and hence the pressure drop can be reduced up to 40% since sparger location is permissible at a higher level where the static pressure is obviously lower. Since the gas phase passes through the bottom section, high pressure in the bottom section results in a high saturation concentration of the solute gas.

In addition to low pressure drop, external-loop air-lift reactors have several advantages over bubble-column reactors. The former offer much flexibility in design in terms of height-to-diameter ratio, area ratio of downcomer to riser, sparger locations, and so on. Conditions can be manipulated

and (e) mist flow. Regime maps for horizontal and vertical flows have been discussed in detail in various books (Green and Perry 2007). Such reference books also give the present status on the estimation procedures for two-phase pressure drop and fractional phase holdup.

11.4.2.2 Liquid-Liquid Reactors

Liquid-liquid reactors are similar to gas-liquid reactors. In the former case, the dispersed phase is in the form of droplets as against bubbles in the latter. The motion of bubbles and drops can be described using a unified approach. A spray column (or a drop column) is the equivalent of a bubble column but with one difference. The dispersed gas phase is always lighter than the continuous liquid phase ($\rho_G < \rho_L$). However, the dispersed liquid phase in spray columns may be lighter or heavier than the continuous immiscible liquid phase. Nevertheless, spray columns can be easily described similar to bubble columns. Furthermore, packed bubble columns and sectionalized bubble columns can be considered equivalent to packed extraction columns and plate extraction columns. External-loop and internal-loop reactors are also possible (for equivalent gas-liquid reactors, refer to Section 11.4.2.1.4).

11.4.2.3 Solid-Liquid Reactors

The upward flow of a fluid through a fixed bed of particles results in rather low flow rates. However, when the superficial fluid velocity is sufficiently high, the particles become supported in the liquid, resulting in a fluidized bed. If the flow rate of fluid is increased beyond the minimum required to produce a fluidized bed, either of two possibilities occurs: (1) the bed continues to expand so that the average distance between the particles becomes greater with no holdup gradients in the radial direction, or (2) the excess fluid passes through the bed in the form of bubbles, resulting in holdup gradients. These types of fluidization are usually termed as *particulate* and *aggregative*, respectively. In general, particulate (or homogeneous) fluidization occurs with solid-liquid systems. For solid-gas systems, homogeneous fluidization occurs when the particle settling velocity is low (fine particles or/and high operating pressure) and is limited to a relatively small range of velocities. Heterogeneous fluidization occurs with all other solid-gas systems, and sometimes with solid-liquid systems as well when the particles are of high density or/and size. Particulate/aggregative fluidization has been discussed in detail by Joshi et al. (2001).

If a liquid is passed vertically upward through a bed of uniform particles, the pressure drop, ΔP , increases with an increase in the superficial liquid velocity, u_L . The relation between pressure drop and velocity is the same as for a fixed bed, as indicated by the following equation (Ergun, 1952):

$$\Delta P = \frac{150\mu_L u_L L}{d_p^2} \frac{\epsilon_s^2}{\epsilon_L^3} + 1.75 \frac{\rho_L u_L^2 L}{d_p} \frac{\epsilon_s}{\epsilon_L} \quad (11.112)$$

For a given bed of particles, ρ_L and d_p , a log-log plot of ΔP vs. u_L (line LM in Figure 11.25) is linear. When the velocity reaches such a value that the frictional force on a particle equals the force due to the gravity minus the buoyancy, the particles become freely supported. At this stage (point M in Figure 11.25) the frictional pressure drop equals the buoyant weight of particles per unit bed cross-sectional area, and the bed is just fluidized and is said to be at the *point of incipient fluidization*. The superficial liquid velocity at this point is called the *minimum fluidization velocity*, u_{mf} . As the liquid velocity is further increased, the pressure drop across the bed remains constant (line MN in Figure 11.25) because the buoyant weight of solids remains constant. The wall pressure drop is usually negligible as compared with the frictional pressure drop at the particle-liquid interface.

The pressure drop in a fixed and fluidized bed can be given by the following single generalized equation (Pandit and Joshi, 1998):

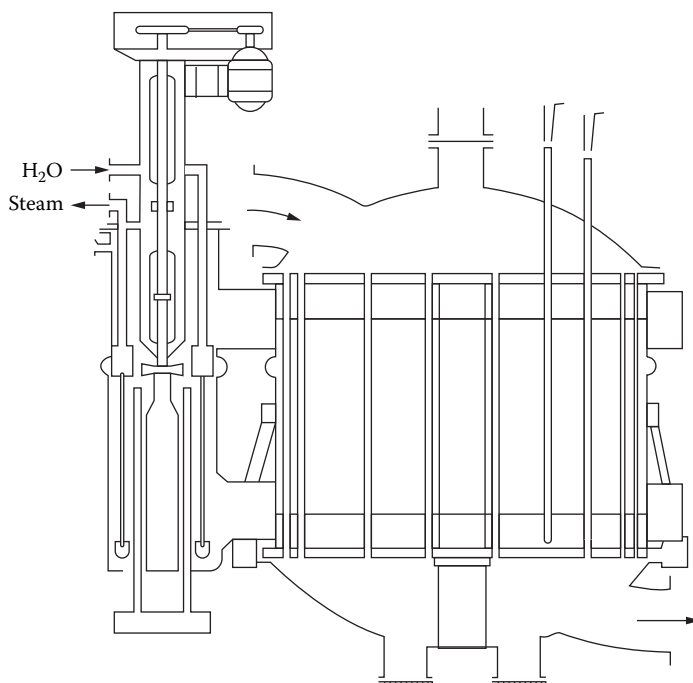


FIGURE 11.26 A typical NINA-FBR design: reactor for SO_2 oxidation (Suter, 1972).

radial and axial concentrations, and temperature profiles, the diameter and height are recalculated for optimum performance.

The approach to the design of an A-FBR is, however, quite different. There is no heat transfer in this reactor; radial transport of heat is absent, and that of mass can usually be neglected. Hence, the reactor diameter can be quite large, thus dispensing with the need for using small-diameter tubes as in the NINA-FBR. A single, large-diameter reactor should, in principle, be all that is needed. In practice, more than one stage may be needed to cool or heat the process fluid between stages. The design here calls for optimizing the inlet and outlet conditions (and therefore the stage height for a given diameter) for each stage to obtain the desired conversion/selectivity at the end of the final stage. The recommended method for optimizing is dynamic programming. A brief summary is presented below of the design procedures for both NINA-FBR and A-FBR units. An illustration of the use of the more important methods is provided in Case Study 11.4.

11.4.2.4.1 Fixed-Bed Reactors: Design of NINA-FBR

From the desired production rate and the allowable velocity in each tube, the number of tubes is obtained. Calculations are made to determine the height of the tube to obtain the required conversion. Since the tubes usually have ($L/D \gg 50$), plug flow can usually be assumed. However, this assumption may not always be valid, because radial gradients often exist. Axial diffusion can also be present, thus modifying the conversion gradient that would normally exist due to flow as the reaction progresses from inlet to outlet. These gradients can cause severe deviations from the values corresponding to plug flow. To account for all these gradients and other possible nonidealities, several models have been proposed. Four are sketched in the Figure 11.27. Of these, the continuum model is the most common. Here, the solid-fluid system is considered as a single pseudohomogeneous phase with properties of its own. These properties (e.g., diffusivity, thermal conductivity, and heat transfer coefficient) depend on the properties of the gas and solid components of the pseudo phase. They are anisotropic; i.e., they have different values in the radial and axial directions.

TABLE 11.24
Classification of Models for Nonisothermal
Nonadiabatic Fixed-Bed Reactors (NINA-FBR)
(Doraiswamy, 2001)

Nonisothermal Nonadiabatic	
A	B
Pseudohomogeneous	Heterogeneous
A1	B1
One-dimensional	One-dimensional
A1-a	B1-a
PFR (basic model)	No axial mixing
A1-b	B1-b
Axial mixing	Axial mixing
A2	B2
Two-dimensional	Two-dimensional
A2-a	B2-a
PFR (basic model)	No axial mixing
A2-b	B2-b
Axial mixing	Axial mixing
	Internal transport
	B1-a-I
	B1-b-I
	B2-a-I
	B2-b-I
	External transport
	B1-a-E
	B1-b-E
	B2-a-E
	B2-b-E
	Internal and external transport
	B1-a-IE
	B1-b- IE
	B2-a-IE
	B2-b-IE

Source: Doraiswamy, L. K., 1991; *Organic Synthesis Engineering*, New York: Oxford, 2001.)

$$u \frac{d[A]}{d\ell} + (-r_A) = 0 \quad (11.115)$$

$$u\rho \frac{dT}{d\ell} = \frac{4U}{d_T} (T - T_w) - (-\Delta H_r)(-r_A) = 0 \quad (11.116)$$

with the initial conditions

$$\left. \begin{array}{l} [A] = [A]_0 \\ T = T_0 \end{array} \right\} \text{at } \ell = 0 \quad (11.117)$$

These equations can be recast in dimensionless form as

blown out until the tube becomes almost empty. Such a situation can be avoided by making incremental additions (say, in 10% lots) of catalyst and measuring the pressure drop in each tube after each addition. The tubes must be tapped or vibrated between additions to ensure uniform pressure drop at each height. Another strategy is to provide for a much larger pressure drop at the tube entrance than that created by the catalyst bed itself, so that any fluctuations in the latter will not affect the flow distribution. This can be accomplished by using a tube sheet with a single nozzle at the bottom of each tube, with a high pressure drop across it. This practice is, however, not generally followed, since tackling the problem at the source, as described earlier, is a much better alternative. The problem of fluid distribution is not critical except in the headers whose diameter corresponds to the shell diameter, which is very much larger than that of the tubes.

11.4.2.4.2 Fixed-Bed Reactors: Design of A-FBR

As already mentioned, the design of an A-FBR is quite different from that for a NINA-FBR. If it becomes necessary to limit the height of each stage in this reactor to avoid excessive temperature rise or fall, then a large number of stages with interstage cooling or heating are required to achieve the desired conversion (Figure 11.28). Two decisions must be taken for each stage: the inlet temperature and the outlet conversion to be achieved in it. Thus, if there are N beds, $2N$ decision variables must be simultaneously varied to optimize reactor operation to maximize profit. This almost always involves prohibitive calculations. A practical method of reducing the amount of computation is

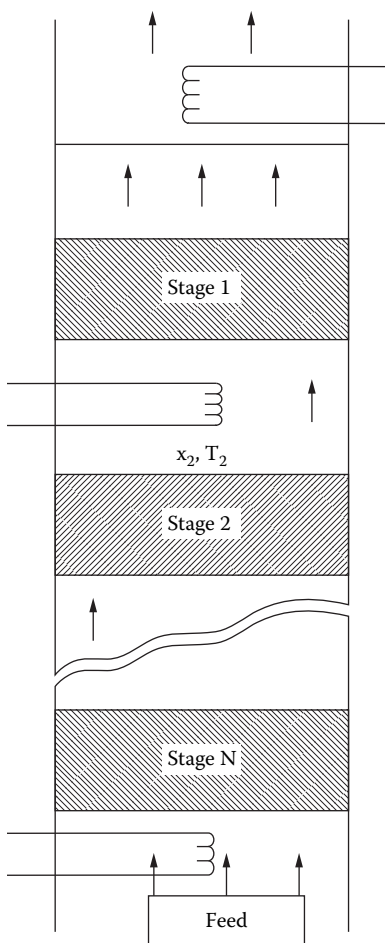


FIGURE 11.28 An interstage heat transfer scheme for A-FBR design.

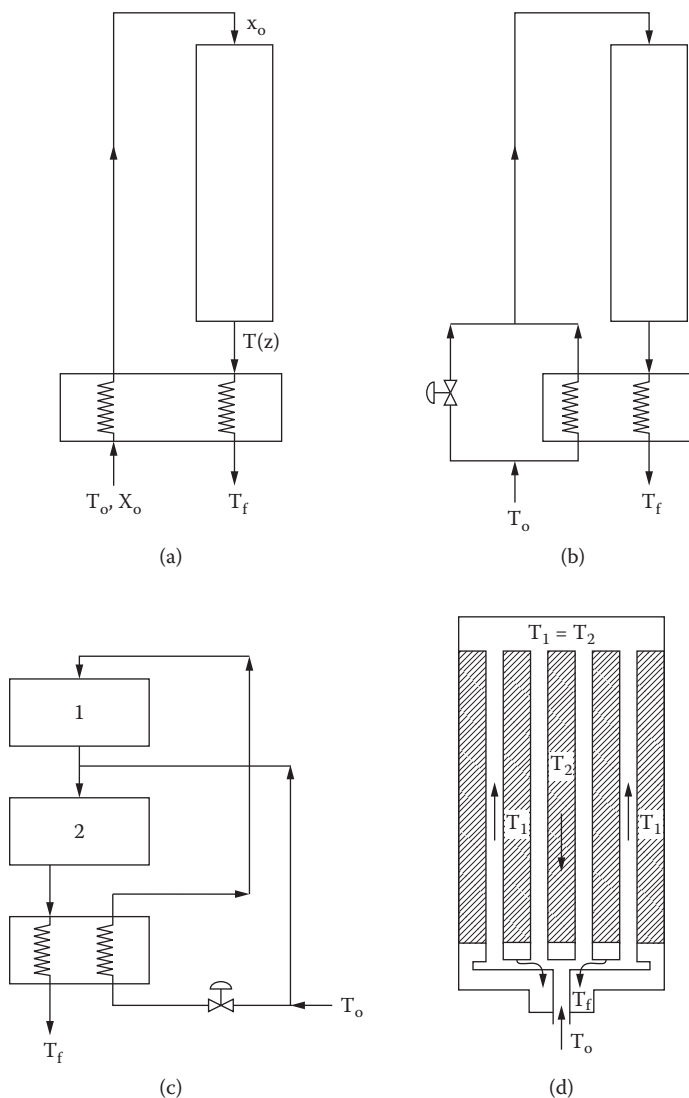


FIGURE 11.29 Typical heat exchange schemes for adiabatic operation.

2. For reactions with no volume change, outward flow of gas yields a higher conversion than inward flow for positive-order kinetics, whereas inward flow is superior for negative-order kinetics.
3. For a first-order reaction with increase in volume, outward flow gives higher conversions, whereas for a reaction with decrease in volume, inward flow is superior.
4. For ideal plug flow, the direction of flow is inconsequential. The difference in behavior between the two directions of flow is therefore due entirely to the dispersion effect. For example, for the ammonia reactor, which satisfies the plug-flow criterion given by Equation (11.126), the change of direction makes no difference.

11.4.2.4.3.2 Catalytic Wire-Gauze Reactors

In certain reactions involving precious metals like platinum, rhodium, or silver as catalyst, the catalyst is used in the form of wire gauze or filament. Examples of reactions that use wire-gauze

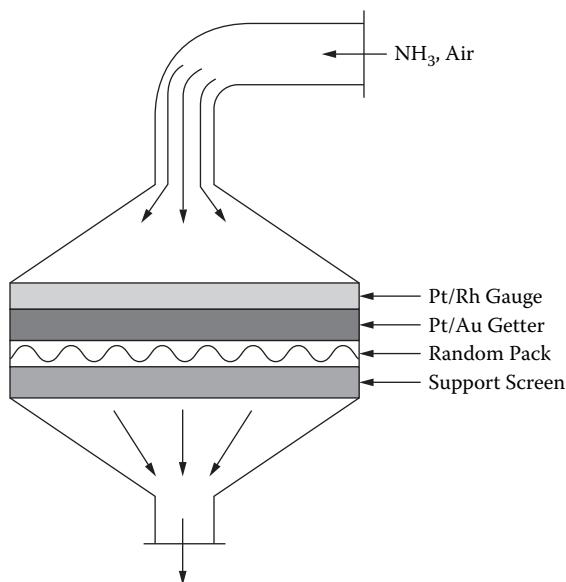


FIGURE 11.31 A typical catalytic wire-gauze reactor.

$$(Fr_{mf})(Re'_{mf})\left(\frac{\rho_s - \rho_G}{g}\right)\left(\frac{L_{mf}}{d_T}\right) < 100, \text{ particulate} \quad (11.127)$$

$$> 100, \text{ aggregative}$$

where $Fr_{mf} = u_{mf}^2/gd_p$ (Froude group at minimum fluidization), and $Re'_{mf} = d_p u_{mf} \rho_G / \mu$ (Reynolds number at minimum fluidization).

Although several studies over many years have added to the understanding of fluidization, six developments stand out as significant—providing the basic structure of fluid-bed reactor analysis and design:

1. Davidson's fluid dynamic approach to fluid-bed reactor design (see Davidson and Harrison, 1963)
2. Geldart's classification (1973) of solids in terms of their fluidization behavior
3. Grace's explicit recognition (1986) of different regimes of fluidization (drawing from other similar previous studies, e.g., Yerushelmi and Cankurt, 1978; Werther, 1980; Li and Kwauk, 1980; Squires et al., 1985; Horio et al., 1986), through a comprehensive map that demarcates the different regimes
4. Kunii and Levenspiel's modification (see their book, 1991, for original references) of the Davidson model and formulation of reactor design procedures for the different categories of Geldart's particles
5. The finding by Lewis and Gilliland (see Kunii and Levenspiel, 1991) that solids circulation between two fluidized beds (usually a reactor and a regenerator) and in the transport lines connecting them can occur stably
6. The finding that a fluidized-bed reactor can operate at more than one steady state (Elnashaie and Cresswell, 1973; Bukur and Amundson, 1975a, b; Furusaki et al., 1978; de Lasa et al., 1980), in particular the Kulkarni–Ramachandran–Doraiswamy criterion in 1980 for multiple solutions for a first-order reaction

11.4.2.5.3 Classification of Fluidized-Bed Reactors

Several categories of fluidized-bed reactors are possible, depending on the mode of operation. The chief features of these reactors are summarized in Table 11.25 and sketched in Figure 11.33. As can be seen from this table, bed behavior (and category) is essentially determined by the fluidizing gas (reactant) velocity and particle size. This transition from fixed to pneumatic bed is usually depicted in terms of a *fluidization map* (e.g., Atipovi et al., 1978; van Deemter, 1980; Werther, 1980; Squires et al., 1985; Horio et al., 1986; Grace, 1986). The latest version, as consolidated by Kunii and Levenspiel (1991), is reproduced in Figure 11.34. Our main concern is with the bubbling bed, although the turbulent bed is only qualitatively different from it.

TABLE 11.25
Principal Features of Different Types (Regimes) of Fluidized-Bed Reactors

Type (Regime) of Fluidization	Main Features	Examples
1. Incipiently fluidized bed (stationary)	Upward flow of gas at about u_{mf} for A and B particles; no solids mixing; gas mostly in plug flow; solids mixing by a stirrer is sometimes useful; $u_o \leq 1.2 u_{mf}$ with no bubbles; $\epsilon_s \approx 0.5$ –0.6 throughout bed	Methylchlorosilanes
2. Bubbling fluidized bed (stationary)	Upward flow of gas through a wide range of A and B particles; onset of bubbling depends on particle size, ranging roughly from $u_b = 40 u_{mf}$ to $70 u_t$ for small particles to a very narrow range ($u_{mf} < u_b \leq 2 u_{mf}$) for large particles; $\epsilon_s \approx 0.6$ (bottom)–0.4 (top)	Polymerization of ethylene to LD polyethylene, ethylene dichloride, vinyl acetate
3. Turbulent bed* (stationary)	Starts gradually at $u_o \gg u_t$ for small particles and $u_p \gg 0.5 u_t$ for large particles, and merges smoothly into fast fluidized-bed region at higher velocities in each case; as u_o is not very high, internal cyclone is usually adequate; solids entrainment is usually high and, instead of bubbles, clusters of solids and voids of gas move through the bed; $\epsilon_s \approx 0.3$ –0.4 (bottom) to 0.2–0.3 (top); the void lifetime is short so that, overall, the bed looks more uniform than in regime 2.	Phthalic anhydride, <i>o</i> -cresol and 2–6 xyleneol, acrylonitrile, chloromethanes
4. Fast fluidized bed* (circulating)	Continuous feed of both gas and solids; sufficiently high solids velocity—in excess of the upper limit for regime 5; the transition point (from the reverse direction) causes <i>choking</i> at the entry and collapse of the lean dispersion of that regime into the fluidized mass of regime 4; suitable gas distributor is used to ensure high density at bottom that merges smoothly with the low-density region at the top (corresponding roughly to the freeboard region of the bubbling bed); $\epsilon_s \approx 0.5$ –0.2 (bottom) to 0.05–0.01 (top); essentially a circulating bed with plug flow of gas accompanied by slugs of emulsion; bed even more uniform than in regime 3.	Fischer-Tropsch synthesis of hydrocarbons
5. Pneumatic or transport bed (circulating)	Upflow of gas with a low continuous feed of solids and no distributor plate; $u_o/u_s \approx 20$, $u_o \approx 20 u_t$; gas in plug flow with $\sigma_s \approx 0.02$ throughout; is essentially a lean upflowing dispersed gas-solids mixture (with no bubbles)	FCC units for petroleum cracking

* The distinction between bubbling-bed and turbulent-bed reactors is not always clear. Hence, the classification of reactions under these categories is uncertain.

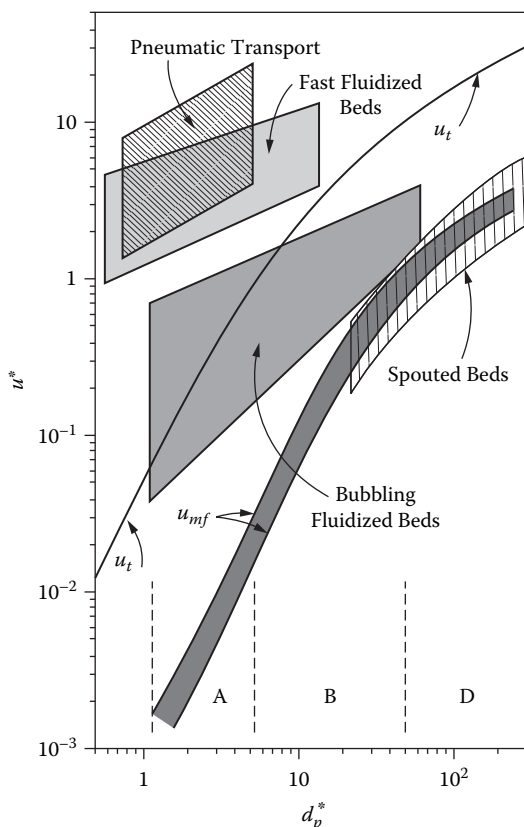


FIGURE 11.34 Fluidization map (from Grace, 1986, as modified by Kunii and Levenspiel, 1991). The

parameters are $u^* = u \left[\frac{(\rho_s - \rho_G)_g}{\mu^2} \right]^{1/3}$, $d_p^* = \left[\frac{\rho_G^2}{\mu(\rho_s - \rho_G)} \right]^{1/3}$.

11.4.2.5.4 Design of Various Types of Reactors

From Table 11.25, four different (but somewhat overlapping) categories of fluidized-bed reactors can be recognized: bubbling-bed, turbulent- (or fluid-) bed, fast-bed, and pneumatic- (or transport-) bed. Occasionally, reactor operation at velocities close to u_{mf} has been attempted.

A fluidized-bed reactor can generally be divided into three zones of operation, as shown in Figure 11.35 (Doraiswamy, 2001). The lower jet zone is relevant only for cases with very high velocities (100 m/s) through the nozzles and is usually not important. Salient features of its design have been described by Behie et al. (1971, 1976) and Behie and Kehoe (1973).

11.4.2.5.4.1 Bubbling-Bed Reactor

Details of the bubbling-bed reactor are explained in Case Study 11.5 along with a comparison and discussion of alternative models with varying degrees of complexity. The Miyanchi–Marooka model for the freeboard region (or the dilute phase) is among the models considered. Kunii and Levenspiel (1991) have also proposed a freeboard model in continuation of their bubbling-bed model.

11.4.2.5.4.2 Turbulent-Bed Reactor

Due to the higher gas velocities (which make the bubble-bed reactor more suitable for high-throughput reactions), there is greater turbulence at the interface, leading to more violent bursting of bubbles and splashing of emulsion clusters. Otherwise, it is not much different from the bubbling-bed reactor, despite the fact that the bubble and emulsion phases are not as clearly demarcated.

or back into the same reactor. Hence, although the bubbling or turbulent regime may be involved within the reactor or regenerator, the transport line (or the riser) operates in the pneumatic regime. In the main reactor, bubbling does not commence immediately after u_{mf} is reached, and the turbulent regime sets in far beyond u_r . In this regime, bubble short-circuiting is much less prevalent, and hence the conversions are higher. On the other hand, the regenerator operates in the bubbling regime even though the velocities involved (0.6 m/s) correspond to the turbulent regime. This is because of the absence of fines. As indicated in Section 11.4.2.5.7, the presence of fines plays an important role (see Yadav et al., 1994).

11.4.2.5.4.5 Staged Reactors

Vertical staging of the catalyst can sometimes be advantageous because the gas flow often approximates plug flow. The region between two consecutive beds is obviously the freeboard region of the lower bed. The holes in the grid plates of these beds must be carefully designed to balance the upward and downward flows of solids from each bed. Thus, the holes in the plate of a given stage should be large enough to allow particles from the lower freeboard region to flow into this stage (thus preventing their accumulation at the bottom of the plate) but small enough to prevent particles from the bed to leak into this freeboard region and then into the lower stage. There is, however, always a through flow of solids, downward or upward. For countercurrent contacting of gas and solid, downflow of solids is necessary, as in fluidized-bed reduction of metal ores. For details of particle interchange at perforated plates and factors influencing particle leakage in staged reactors, see Briens et al. (1978).

11.4.2.5.5 Circulation Systems

In Table 11.25, we saw that certain types of fluidization (fast and pneumatic) involve solids recirculation. Figure 11.36 indicates that the solids are circulating between two fluidized beds A and B. They are connected through the two curves of a U-tube in such a way that the difference in static pressures drives the solids from one bed to the other. The use of a second U-tube completes the circulation between the beds. As there is a frictional resistance associated with solids flow (increasing with increasing flow rate), the rate of circulation is controlled by a balance between the frictional resistance and the static pressure difference mentioned earlier. The frictional resistance can be controlled by varying the average densities of the flowing gas-solid mixtures in the various sections of the circulation loop.

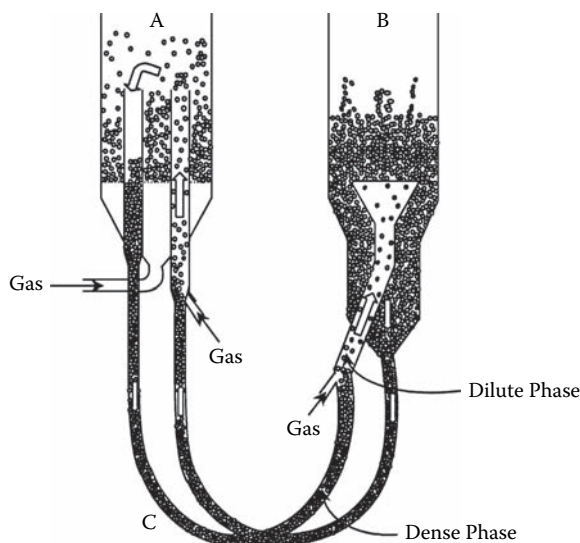


FIGURE 11.36 The main features of solids circulation in fluidized-bed reactors.

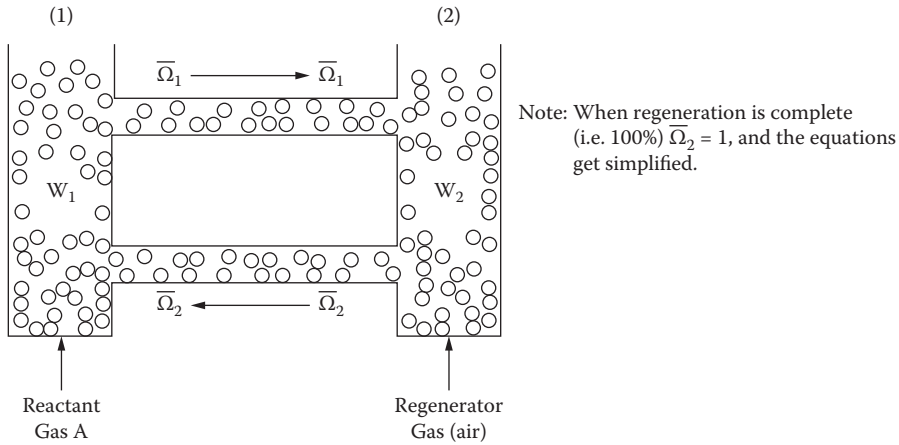


FIGURE 11.38 Fluidized-bed circulation system for catalyst deactivation control.

$$\text{Deactivation: } -\frac{d\Omega}{dt} = k_d \Omega \quad (11.130)$$

$$\text{Regeneration: } \frac{d\Omega}{dt} = k_a (1 - \Omega) \quad (11.131)$$

It is reasonable to assume that the solids flow is fully backmixed with an exponential distribution of residence times. Based on this assumption and by writing an expression for the average activity of the leaving catalyst stream (which contains particles of all ages with their corresponding activities), the following equations are derived:

$$\text{Reactor: } k_d \bar{t}_1 = \frac{\bar{\Omega}_2 - \bar{\Omega}_1}{\bar{\Omega}_1} \quad (11.132)$$

$$\text{Regenerator: } k_a \bar{t}_2 = \frac{\bar{\Omega}_2 - \bar{\Omega}_1}{1 - \bar{\Omega}_1} \quad (11.133)$$

where

$$\bar{t}_1 = \frac{W_1}{F_S}, \quad \bar{t}_2 = \frac{W_2}{F_S}$$

Eliminating $\bar{\Omega}_2$ from Equations (11.132) and (11.133),

$$\bar{\Omega}_1 = \frac{k_a \bar{t}_2}{k_d \bar{t}_1 + k_d k_a \bar{t}_2 + k_a \bar{t}_2} \quad (11.134)$$

This equation for average catalyst activity is then combined with the rate constant, k_v , to give $\bar{\Omega}k_v$ in the usual reactor equations that would normally use simply k_v . For the three gas flows, we obtain

problem of reactor design and choice for a deactivating catalyst in general. An important parameter in considering the role of catalyst deactivation is the production or on-stream time (which is also the catalyst decay time). This is the time t_p for which the reactor is run before subjecting the catalyst to regeneration. The total decay time for a given level of decay is t_{p1} . Assuming that reactant A is passing through a decaying bed of catalyst under diffusion-free conditions and is undergoing a simple reaction, the first step in the analysis is to write the continuity equation for the reactor. Then, by introducing appropriate dimensionless groups, the following equations can be derived for the fixed-, fluidized-, and moving-bed reactors by assuming exponential decay of the catalyst, i.e.,

$$k_v(t_p) = k_{v0} \exp(-d_c t_p) \quad (4.36)$$

where d_c is the decay constant and k_{v0} is the rate constant for the fresh catalyst. The final equations obtained are the following.

Fixed-bed reactor:

$$\frac{dy_A}{dZ} = -B' \exp(-\lambda \hat{t}) y_A^m \quad (11.140)$$

where

$$\left. \begin{aligned} \hat{t} &= \frac{t_p}{t_{p1}}, \quad \lambda = d_c t_{p1} \\ B' &= \frac{M}{\rho_A S_{v,A}} (1 - \varepsilon_B) k_{v0} \\ Z &= \text{reduced length} \end{aligned} \right\} \quad (11.141)$$

When a decaying catalyst is used, the average conversion over a given period of time is determined from

$$\bar{X}_A = 1 - \bar{y}_A = 1 - \int_0^1 y_A d\hat{t} \quad (11.142)$$

Fluidized-bed reactor:

If the solids are fully mixed, we have

$$\frac{dy_A}{dZ} = \left(\frac{B'}{\lambda + 1} \right) y_A^m \quad (11.143)$$

Since this is a steady-state operation, the conversion is simply

$$X_A = 1 - y_A \quad (11.144)$$

11.4.2.5.7.2 *Defluidization of Bed*

During the operation of a fluid-bed reactor, there should be no sudden increase in pressure due to malfunctioning of valves or choking in downcomers by solid particles. If it does occur, the mass velocity for minimum fluidization will increase at the same total flow rate, and a stage may be reached at which the minimum fluidization velocity might actually exceed the gas velocity, leading to defluidization. Defluidization can also occur due to an increase in temperature or coke deposition of catalyst particles (leading to increased u_{mf}). Another reason is the switch from an inert fluidizing gas used at startup to the actual gas.

11.4.2.5.7.3 *Gulf Streaming*

The phenomenon of gulf streaming arises from the formation of violent circulating currents induced by bubbles. These currents may become especially significant in large commercial beds (especially shallow beds). Davidson and Harrison (1971) have shown that circulation velocities of 200 mm/s can exist in large beds. As a result, the bubble residence time is smaller, leading to lower conversions. No simple way has yet been found to overcome this problem; thus, a pilot plot of appropriate size seems almost unavoidable.

11.4.2.5.7.4 *Effects of Fines*

A size distribution of particles is always desired rather than a single size in a fluidized bed. The two-phase theory of fluidized-bed operation is suspect when a bed contains appreciable fines, and models based on uniform particles should be used with caution. The dense phase in such cases should really be regarded as consisting of two phases: emulsion and clusters of fines ($d_p < 40 \mu\text{m}$). Indeed, the results of Yadav et al. (1994) on commercial propylene ammoxidation catalyst clearly show that the fines agglomerate. A critical level of fines (30%) was found in terms of bed expansion, aeratability, and cluster size at which fluid-bed behavior is optimum. They proposed a model that takes the two dense phase components (emulsion and cluster) into account. Adding fines widens the limits of operable gas velocities and minimizes the segregation of particles.

11.4.2.5.7.5 *Start-Up*

The start-up of a fluidized bed requires an initial burst of pressure to lift the solids and initiates fluidization. This can severely damage the bed internals, and indeed the entire structural framework. It is therefore essential to begin the operation with an empty reactor (by removing the solids after each shutdown) and progressively increase the gas velocity and introduce the solids incrementally at the same time.

Other practical considerations are attrition of particles; caking of catalyst from malfunctioning of the reactor due to formation of tarry products (resulting sometimes in "cakes" as large as the reactor diameter); and the need to avoid premixing of reactants (particularly when they can form explosive mixtures) and fix their relative locations within the bed (e.g., in the chlorination of methane and ammoxidation of propylene). Refer to Doraiswamy and Sharma (1984) for further details.

11.4.2.5.8 *Fluidized-Bed vs. Fixed-Bed Reactors*

Following their first major success in 1942 in the refining/petrochemical industries, fluidized-bed reactors were hailed as the panacea for most reactor evils. This optimism was clearly too hasty in view of many spectacular failures. But more recently there has been a better understanding of fluid-bed behavior in general. The main advantages are a prevalence of near-isothermal conditions in the entire bed due to solids movement (and therefore the absence of hot spots, a key drawback of fixed-bed reactors), less danger of explosions and temperature excursions, better operational flexibility, and higher heat and mass transfer rates compared to other modes of fluid-solids contacting (often leading to smaller sized heat exchangers). The fixed-bed reactors are less frequently chosen, in spite of their many advantages, namely relatively easy scale-up, minimum catalyst loss due to attrition, and the theoretical possibility of imposing an optimum temperature profile (taking advantage of the inherent nonisothermicity of the bed).

conforming to pellet reaction control. Their use is especially appropriate for the following reasons. As brought out in Section 11.3.4, the controlling regime in a reactive pellet changes as the reaction progresses. For example, in the case of SIM, the reaction usually starts with reaction control but eventually becomes diffusion controlled, making it necessary to consider individual pellets in the reactor. Often, recourse to one- or two-dimensional heterogeneous models becomes necessary. In such cases, the choice of the gas-solid reaction model has an important bearing on reactor simulation (Sotirchos and Zarkanitis, 1989). Mutasher et al. (1989) have simulated a fixed-bed reactor using the zone model. The particle-pellet model used here has greater generality.

Consider a typical reaction,



As pointed out in Section 11.3.4, it can be assumed that the pellet itself is isothermal, even for reactions involving large heat effects. One can also reasonably assume that axial diffusion effects are absent (particularly for long beds), and hence the one-dimensional model can be used. We shall also assume that the heat generated by reaction is lost through the sensible heat carried by the gas leaving the system and by convection at the outside surface of the reactor wall. The nonisothermicity of the reaction greatly affects the linear velocity and density of gas along the reactor, and these effects should be considered. However, in our relatively simple approach, we ignore them.

Derivation of the model equation is reported by Evans and Song (1974). The following equations are written: material and energy balances for the gas phase and the rate equations for the pellet assuming any one of the models described in Section 11.3.4. As mentioned earlier, we use the particle-pellet model. Appropriate initial and boundary conditions are also written. Assuming isothermal behavior, the material balance equation is

$$-G_A \frac{\partial c}{\partial t} = \frac{(1 - \epsilon_p)(1 - \epsilon_b) \rho_{Bm}}{v} \frac{dX^x}{dt} + (\epsilon_p + \epsilon_b) [\bar{A}] \frac{\partial c}{\partial t} \quad (11.146)$$

where $[\bar{A}]$ is the external field concentration at some point in the bed, and c is the dimensionless external field concentration. The changing value of the concentration $[\bar{A}]$ with position allows for a more realistic simulation of the reactor.

Here the reactor equation is general and independent of the rate equation, which depends on the gas-solid reaction model used. It can also be adapted to other reactors with appropriate modifications. However, these involve unacceptable assumptions for the fluid-bed model.

The particle-pellet equation is written in terms of a generalized effectiveness factors defined as

$$\epsilon = \frac{\int_0^1 \xi^{s-1} g \eta^{g-1} [\hat{A}]_p d\xi}{\int_0^1 \xi^{s-1} d\xi} \quad (11.147)$$

where s and g are, respectively, the shape factors for the pellet and grain [3 for the sphere, 2 for the cylinder, and 1 for the flat plate, based on Equation (11.49)], and ξ and η are the dimensionless positions in the pellet and grain, respectively. We use this in the material balance Equation (11.146) recast in dimensionless form to give

$$-\frac{\partial c}{\partial Z^*} = \frac{dX^*}{dt^*} = c\epsilon \quad (11.148)$$

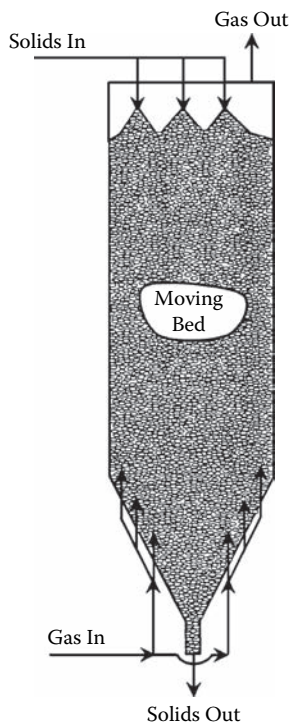


FIGURE 11.42 A typical moving-bed reactor.

plug flow and complete mixing of the solids. The following are based on the more likely plug-flow behavior.

The equations for the gas and solid phases are

$$\text{Gas: } \frac{dc}{dZ^*} = -c\epsilon \quad (11.155)$$

$$\text{Solid: } \frac{dX^*}{dZ^*} = v \left(\frac{G_A}{G_B} \right) c\epsilon = R'c\epsilon \quad (11.156)$$

The boundary conditions are

$$c = 1, Z^* = 0 \quad (11.157)$$

and

$$\text{for cocurrent flow, } X^* = 0, Z^* = 0$$

$$\text{for countercurrent flow, } X^* = 0, Z^* = L^* \quad (11.158)$$

where L^* is a dimensionless reactor length defined for concurrent flow, defined as

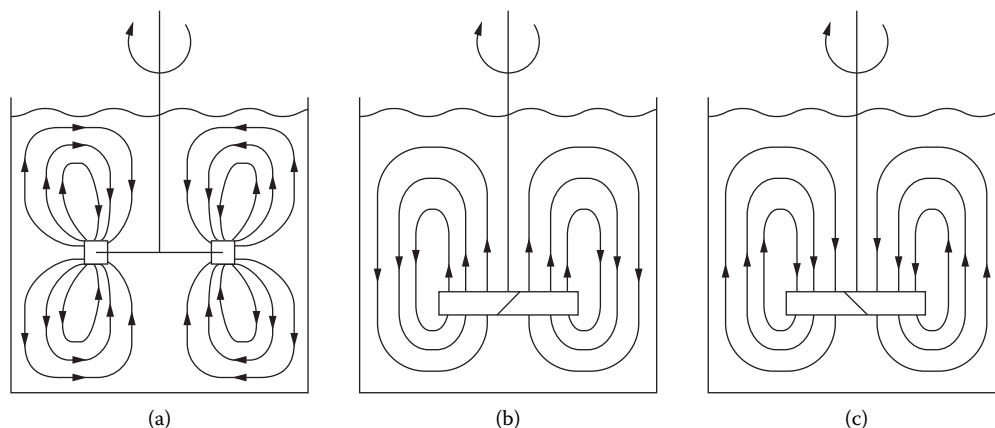


FIGURE 11.43 Flow patterns in a stirred tank reactor: (a), radial flow, (b) axial upflow, (c) axial downflow.

ethoxylation, alkylation), it may be necessary to maintain a uniform concentration in the reactor; in such cases, mixing is of importance. If the gas is sparingly soluble, its concentration in the liquid phase is fairly small, and the overall reaction may become mass transfer controlled. In many gas-liquid/gas-liquid-solid reacting systems, conversion of gas per pass is low. If it is undesirable (because of toxicity, explosion, or cost considerations) to vent this unreacted gas, then the unreacted gas has to be recycled back into the reactor. Hydrogenation, chlorination, alkylation, oxidation with pure oxygen, ozonolysis, hydrochlorination, and others are in this category. Recycling of the unreacted gas can be achieved with what is called a *dead-end reactor* in which the unreacted gas is not vented. These systems employ gas-inducing impellers, surface aerators, rotating disc contactors, jet-loop reactors, and plunging jet reactors to recontact the gas with the liquid phase.

All the above-mentioned processes require external energy input. In the stirred reactor, energy is supplied by the impeller. The fluid leaving the impeller receives mean and turbulent kinetic energy resulting from the impeller motion. The presence of a second or third phase may also introduce additional energy. The impeller designs are generally classified into two types: (1) radial flow impellers and (2) axial flow impellers. Rushton turbine, straight-blade turbines, curved-blade turbines, Brumagins, and so on belong to the radial flow category. The flow field generated by them is radially outward (Figure 11.43a), toward the wall. At the wall, this flow divides into two parts, one going above the impeller and the other going below. Both flows then return to the impeller near the vessel centerline. Axial flow impellers can be operated in either the "pumping-up" mode (Figure 11.43b) or "pumping-down" mode (Figure 11.43c). Marine propellers, pitched-blade turbines, hydrofoil impellers, and so forth fall under this category. In the pumping-down mode, the impeller generates a downward flow, which hits the vessel bottom, turns radially, and is ultimately converted to upflow before returning to the impeller. The mean flow generated causes bulk motion of the constituents, whereas the turbulence generated is responsible for eddy diffusion of momentum, heat, and mass. The size, shape, and number of impellers; vessel geometry such as number, location, and size of baffles; vessel diameter; liquid level; impeller clearance; and system properties all have a profound impact on the flow field, thus affecting the performance of the stirred vessel.

To design/select impellers on a rational basis, an understanding of two aspects is essential: (1) the relation between impeller design, vessel geometry, and the flow field produced; and (2) the relation between the flow field and design objectives such as mixing, heat transfer, solid suspension, gas dispersion, and others. From 1950 to 1970, impeller design was investigated mainly empirically. For this purpose, the investigators fabricated several different shapes and used them in laboratory-scale equipment. The performances of the various impellers in terms of a design objective (e.g.,

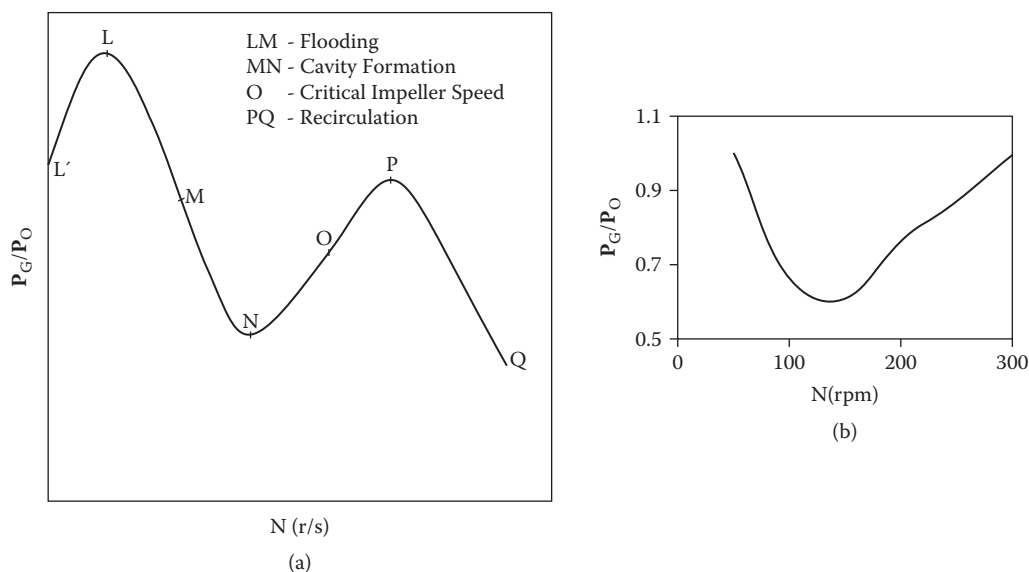


FIGURE 11.44 Regimes of operation in a stirred tank reactor: (a) with a pitched-blade downflow turbine with sparger below the impeller; (b) with upflow impeller.

this point, the gas becomes dispersed in the radial direction. As the impeller speed increases further, the gas is distributed radially from the impeller, i.e., loading occurs. Then the gas starts forming cavities behind the impeller blades (MN in figure). The size of the cavities increases with a higher impeller speed, and therefore P_G/P_O falls. At still higher speeds, the impeller-generated flows are dominant and overcome the upward flow generated by the bubbles. Under these conditions, the impeller disperses gas even below the impeller. This is referred to as complete dispersion. Beyond this point (point N in figure), the shear forces become strong enough to break the cavities, and the cavity size reduces. This leads to an increase in the P_G/P_O ratio (point O in the figure), and the so-called critical impeller speed is reached. At very high speeds, the impeller-dispersed gas phase is recirculated by the impeller-generated flow called recirculation (beyond point P in the figure). The gas holdup in the impeller region and therefore the average density in the impeller region start reducing; as a result, the P_G/P_O ratio again starts reducing. To obtain efficient gas-liquid dispersion, the impeller should be operated at a speed above the critical speed required for complete dispersion.

For the upflow impeller, the P_G/P_O vs. impeller speed curve is shown in Figure 11.44b. The flow generated by this impeller and the gas flow are complementary to each other, and thus formation of large cavities is prevented (Bujalski et al., 1988). Mhetras et al. (1994) have correlated the critical impeller speed for complete dispersion with the gas flow number as

$$Fr = aF_l^b \quad (11.164)$$

Values of the constants a and b have been reported for many impeller designs.

Ideally, an impeller should have a P_G/P_O ratio of unity. Efforts to reach this have resulted in the development of axial-flow impellers (up-pumping or down-pumping) with a high solidity ratio, as well as radial-flow impellers with convex-shaped blades. The power drawn by these impellers is practically constant, even at high gas flow rates. These are therefore called *gas-foil impellers*. When compared on the basis of equal power consumption per unit mass, gas-foil impellers show a larger gas holdup (that is, better gas dispersion) than conventional Rushton turbines (McFarlane and Nienow, 1996). Mhetras et al. (1994) found that axial-flow impellers give higher gas holdups

$$N_{CS} = 1.15 \frac{u_{S\infty}^{0.28} X^{0.1}}{D^{0.85}} (\mathbf{D}/T)^{0.8} \quad (11.166)$$

For other impellers, see Zwietering (1958) and Chapman et al. (1983).

11.4.3.5 Heat Transfer

To operate isothermally, it is generally necessary to remove heat from, or supply heat to, the reactor. This can be achieved by using jacketed reactors or helical coils inside the reactor. The heat transfer area provided by jackets per unit volume of the reactor is equal to $4/d_T$, where d_T is the reactor diameter. Thus, upon scale-up, the heat transfer surface area per unit volume of reactor decreases. Helical coils provide larger heat transfer area per unit volume and are generally preferred. Under certain conditions, especially for low-viscosity applications, it may be necessary to consider the heat transfer coefficient on the reactor side as well as the jacket/coil side and then determine the overall heat transfer coefficient. When only one impeller is to be used, it is desirable to keep the impeller centrally located to obtain good heat transfer coefficients over the entire length of the jacket/coil. The reactor-side heat transfer coefficients for a jacketed vessel have been correlated as follows for a wide range of impeller designs (Uhl and Gray, 1966); they also report values of the exponents:

$$\frac{h D}{k_T} = a \left(\frac{N \mathbf{T}^2 \rho}{\mu} \right)^b \left(\frac{c_P \mu}{k_T} \right)^c \left(\frac{\mu_w}{\mu} \right)^d \quad (11.167)$$

The values of b range from 0.66 to 0.75, those of c to from 0.25 to 0.50, and of d to from -0.14 to -0.25 . The values of the constant a vary dramatically from 0.17 to 0.75. Since the heat transfer coefficient is typically proportional to $N^{0.67}$, it can be considered to be proportional to $(power)^{0.22}$ (Oldshue, 1983). Oldshue also provides a general correlation for the heat transfer coefficient for an immersed tube as

$$\frac{h \mathbf{T}}{k_T} = 0.17 \left(\frac{N D^2 \rho}{\mu} \right)^{0.67} \left(\frac{c_P \mu}{k_T} \right)^{0.37} \left(\frac{D}{\mathbf{T}} \right)^{0.1} \left(\frac{d}{D} \right)^{0.5} \left(\frac{\mu}{\mu_s} \right)^m \quad (11.168)$$

where m is a function as defined by Oldshue. Fasano et al. (1991) compared the heat transfer coefficients for a pitched-blade turbine and HE-3 impeller. At the same \mathbf{T}/D and C/D ratios and at equal impeller Reynolds numbers, the heat transfer coefficient of the Rushton turbine was marginally smaller than that for the four-bladed pitched-blade turbine. Since the power number of the Rushton turbine is three times that of the four-bladed pitched-blade turbine (used in their work), this would mean that at equal power, the pitched blade turbine would give a roughly 35% higher heat transfer coefficient. The six-bladed pitched-turbine resulted in an even larger heat transfer coefficient. Oldshue (1983) had also previously recommended axial-flow impellers for efficient heat transfer.

11.4.3.6 Blending in Gas-Liquid Systems

Gas in a stirred reactor alters the flow pattern dramatically, depending on the regime of operation (flooding, loading, complete dispersion, and so on). Rewatkar and Joshi (1991b) systematically investigated the mixing characteristics in various regimes of operation. The mixing time in the presence of gas is larger than that in its absence. However, the relative increase depends on the

(Rewatkar et al., 1991). N_{SG} increased with an increase in the superficial gas velocity, particle size, and solid loading. Their correlation is recommended for design:

$$N_{SG} - N_{CS} = 132.7 u_{SG\infty}^{0.5} T^{-1.67} Du_G \quad (11.173)$$

Chapman et al. (1983) provide a similar correlation.

11.4.3.9 Heat Transfer in Gas-Liquid Systems

Heat transfer coefficients in gas-liquid systems are generally lower than those in the liquid alone (Karcz, 1999), a result of the reduction in power consumption in the presence of gas. The heat transfer coefficient is approximately proportional to $(power)^{0.22}$.

11.4.3.10 Dead End Systems

11.4.3.10.1 Gas-Inducing Impellers

A gas-inducing impeller generates a high velocity in the impeller region. The local pressure decreases sufficiently to overcome the hydrostatic head; gas is hence induced from the head space (Figure 11.45a). Many designs of these impellers have been reported in the published literature and are divided into three categories: hollow-pipe impellers, hollow pipes with dispersers, and stator-rotor systems. Saravanan and Joshi (1995, 1996) and Saravanan et al. (1996, 1997) investigated single- as well as multiple-impeller stator-rotor systems. When a single gas-inducing impeller is located close to the top liquid surface for maintaining a high rate of gas induction, the following drawbacks occur: poor dispersion of the induced gas, poor solid suspension ability, and so on. They arise from the fact that the liquid flow and turbulence characteristics are feeble in a major portion below the gas-inducing impeller. These drawbacks become more serious with a large-scale operation. These limitations have been overcome by using a second impeller below the gas-inducing impeller. The gas-inducing impeller can be positioned near the top liquid surface (about 100 to 200 mm below the liquid surface), irrespective of the scale of operation, to ensure a high gas induction rate. For performing gas dispersion (distribution of the induced gas throughout the equipment), solid suspension, heat transfer, mixing, and so forth, a second impeller is often used. The flow patterns for multiple-impeller combinations are depicted in Figures 11.45b and c. The design of the lower impeller was further optimized for different duties such as gas holdup, solid suspension

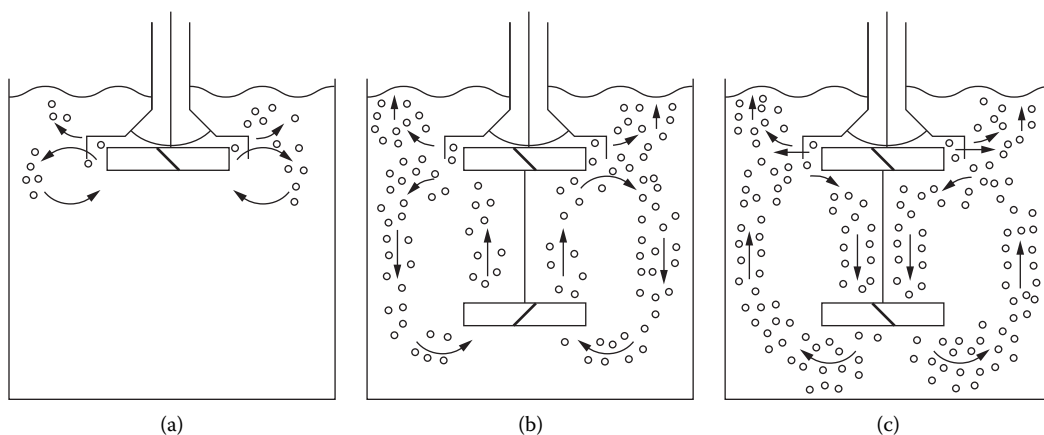


FIGURE 11.45 Gas-inducing reactors: (a) single inducing impeller, (b) inducing impeller together with upflow lower impeller, and (c) inducing impeller together with downflow lower impeller. (From Patwardhan, A. W. and Joshi, J. B., 1998.)

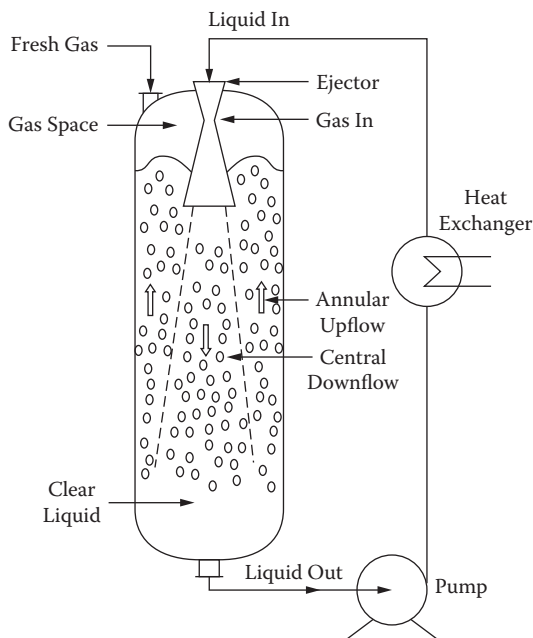


FIGURE 11.47 Jet-flow reactor.

dispersion is created in the mixing tube. The diffuser section at the end of the mixing tube helps in pressure recovery and compresses the gas-liquid mixture to the discharge pressure. The entire assembly (nozzle, mixing tube, and diffuser) is collectively called the *ejector*. The gas-liquid dispersion issuing from the ejector is sent to a separator, a reactor vessel, or a holding tank, which provides additional gas-liquid contact. The liquid jet performs two functions: it provides the momentum necessary for circulation of the vessel contents to ensure good mixing, and it disperses the entrained gas into small bubbles producing a large interfacial area. The unreacted gas escapes back into the head space, which can again be entrained into the ejector. Bhutada and Pangarkar (1987, 1989) investigated the effects of nozzle and ejector geometry, operating conditions, and physico-chemical properties on the rate of gas entrainment and fractional gas holdup. These were found to be independent of the shape of the entry section of the nozzle. With a decrease in the mixing tube length, the rate of gas entrainment increases, whereas the fractional gas holdup is almost independent of the length. A pressure recovery diffuser section improves the rate of gas induction and the fractional gas holdup. The effects of geometrical parameters on the mass transfer characteristics need to be investigated systematically and related to the gas holdup and rate of gas entrainment.

11.4.3.10.4 Rotating Biological Contactors (RBC)

An RBC consists of a number of plastic disks mounted on a rotating horizontal shaft, and it is placed in a concrete tank containing the liquid to be treated. During rotation, the disk surface withdraws a thin film of liquid from the tank and transfers it through the gas space (i.e., air). This thin liquid film on the disk surface absorbs oxygen from the air, thereby providing gas-liquid contact. A pictorial representation of this reactor is shown in Figure 11.48. The RBC system provides high interfacial area per unit volume of contractor, resulting in efficient aeration. Vaidya and Pangarkar (1985) solved the simplified Navier–Stokes equation for a Newtonian fluid, assuming a half-immersed disk vertically withdrawn from a pool of liquid; various radial points on the disk had different linear speeds ($r\omega$) and hence different film thicknesses. Using computed profiles, the conservation equation for the gas phase was solved in addition to the mass transfer coefficient.

TABLE 11.26
Comparative Performances of Gas-Liquid Reactors

Equipment	Capacity	Turndown Ratio (L/G)	Liquid Phase Residence Time	Axial Mixing		Gas-Side Pressure Drop	Mass Transfer Coefficient	G/L Interfacial Area	Heat Transfer Coefficient	No. of Theoretical Stages
				Liquid	Gas					
Bubble Column	5	2,3,4	3,4,5	1,2	3,4,5	1	3,4	3,4,5	3,4	1
Packed Bubble Column	3	2,3,4	3,4,5	3	4,5	1	4	3,4,5	3,4	2
Sectionalized Bubble Column	5	2,3,4	3,4,5	4,5	5	1	4	3,4,5	3,4	4,5
Plate Column	3,4	1,2	2,3	5	5	2,3	4	4,5	3,4	5
External-Loop Airlift Reactor	5	2,3,4	4,5	2,3	4,5	2	4	4,5	4,5	2,3
Internal-Loop Airlift Reactor	5	2,3	3	1,2	3,4,5	1,2	4	3,4	3,4	1
Spray Column	5 (GP)	1,2	1	4	1,2	5	1,2	1,2	0	1
Pipeline Reactor	1,2	2,3	1	4,5	5	3,4	2	1,2	1,2	1
Static Mixer	1,2	2,3	1	4,5	5	3,4	5	2,3,4	3,4	1
Stirred Reactor Single Stage	2,3,4	4,5	3,4	1	1,2	2,3	4,5	3,4,5	4	1
Stirred Reactor Multistage	1,2,3	4,5		2,3	2,3,4	1,2	4,5	3,4,5	4	2,3
Packed Column	4	1,2	1,2	4,5	4,5	4,5	2,3	2,3	0	2,3,4
Falling Film Reactor	2,3	1,2	1	5	4,5	5	2	2	2	2
Rotating Disc Contactor	2,3	4,5	3,4	1,2	3,4	5	2	2,3,4	0	1,2
Jet-Loop Reactor	2,3	4,5	2,3	1,2	3,4	5	5	3,4	5	1,2

1: poor, 5: excellent; GP: gas phase.

For sound process design, we need values of numerous design parameters such as fractional phase holdups, pressure drop, dispersion coefficients (the extent of axial mixing) of all the compounds, heat and mass transfer coefficients across a variety of fluid-fluid and fluid-solid interfaces depending on the type of multiphase system, type of reactor, and the rate-controlling steps. To clarify the scope of the case studies selected, their salient features are next listed.

Examples of several classes of industrially important multiphase reactions were given in Section 11.3. The case studies are chosen to represent different classes of reactions. Thus, we cover reactions ranging from simple homogeneous to quite complex multiphase reactions.

The rate-determining step is particularly important when a choice has to be made between competing mechanisms for a given reaction. One case study illustrates a rigorous statistical procedure.

In available texts, emphasis is often on the design of a single (often arbitrarily selected) reactor for a given reaction. In some case studies presented here, several reactor configurations are considered for a single reaction, and an optimum configuration (along with appropriate geometrical details) is recommended. Such a study can nontrivially alter reactor choice and performance.

Several models are sometimes available for the design of the reactor. Thus, in one case study, designs are made using several models, and a comparative assessment is presented.

Capital and operating costs are central to reactor selection. This aspect of design is illustrated in two case studies.

It is theoretically possible to include all considerations mentioned above in just two or three case studies. This has the disadvantage of severely restricting their breadth. Therefore, we decided to spread these considerations over 12 carefully selected case studies.

At the end of each case study, general remarks are given that bring out the lessons learned. Furthermore, at the end of the case studies we give our recommendations (morphology) for the selection and design of reactors.

CASE STUDY 11.1 HOMOGENEOUS LIQUID-PHASE SIMPLE REACTION: $A \rightarrow R$

Nomenclature for Case Study 11.1

A	reactant
A_A	available area of heat transfer available (m^2)
A_H	area of heat transfer (m^2)
$[A]$	concentration of reactant A
$[A]_0$	inlet concentration of A
$[A]_e$	exit concentration of A (mol/m^3)
A_S	shell area (m^2)
a_S	cross-sectional area for shell-side flow (m^2)
B	baffle spacing (m)
C	clearance (m)
C_{PC}	heat capacity of coolant ($\text{kcal}/\text{kg K}$)
D	diameter of tube (m)
D_C	diameter of coil helix (m)
Do	outer diameter of tube (m)
D_S	shell diameter (m)
D	dispersion coefficient (m^2/s)
d_E	equivalent diameter of the shell (m)
f	friction factor (—)
f_C	friction factor for a coil (—)
f_P	permissible stress for steel (N/m^2)
f_S	friction factor on shell side (—)
G_S	shell-side mass velocity ($\text{kg}/\text{m}^2/\text{s}$)
H	height (m)
ΔH	heat of reaction (kcal/kmol)

Subscripts

<i>C</i>	coil/coolant
<i>E</i>	equivalent
<i>e</i>	outlet
<i>o</i>	inlet
<i>S</i>	shell side
<i>T</i>	tube side

The Problem

A continuous reactor is to be designed for a homogeneous liquid-phase reaction $A \rightarrow R$. The reaction is first order with respect to A , and the rate is given by

$$-r_A = k_1[A] \quad (\text{CS1.1})$$

where $k_1 = 0.00167 \text{ s}^{-1}$. The heat of exothermic reaction is -209 kJ/gmol . The flow rate of the reactant is $0.01 \text{ m}^3/\text{s}$. The concentration of A at the inlet of the reactor is 1 kmol/m^3 , and a conversion of 99% is desired. Find the volume of the reactor if the same reaction is to be performed in a (1) backmixed reactor and (2) plug-flow reactor (PFR). Calculate the optimum length-to-diameter ratio for a plug-flow reactor. Also examine the alternative configurations, i.e., (3) a coil reactor and (4) a shell-and-tube heat exchanger type reactor.

Data

Density (ρ) = 1000 kg/m^3 ; specific heat (C_p) = 4180 J/kg K ; viscosity (μ) = $1 \times 10^{-3} \text{ Pa}\cdot\text{s}$; Prandtl number (Pr) = 5; number of working hours per year = 8000; cost of electric power = $0.03 \text{ \$/kWh}$; cost of mild steel = $0.4 \text{ \$/kg}$; density of steel = 8000 kg/m^3 ; permissible stress for steel (f_p) = $8.5 \times 10^7 \text{ N/m}^2$; design pressure of the reactor = $0.5 \times 10^6 \text{ N/m}^2$.

Solution

1. Completely Backmixed Reactor

Assumption: isothermal operation

Data: $[A]_0 = 1 \text{ kmol/m}^3$, $x = 0.99$, $F = 0.01 \text{ m}^3/\text{s}$, outlet concentration,

$$\begin{aligned} [A]_e &= [A]_0(1 - X) \\ &= 0.01 \text{ kmol/m}^3 \end{aligned} \quad (\text{CS1.2})$$

For a backmixed reactor, the residence time is given by the following equation:

$$\begin{aligned} \bar{t} &= V/Q = ([A]_0 - [A]_e) / k_1[A]_e \\ &= 59281 \text{ s} \end{aligned} \quad (\text{CS1.3})$$

Therefore, the reactor volume, $V = \bar{t} \times Q = 59400 \times 0.01 = 593 \text{ m}^3$

2. Plug-Flow Reactor: Pipeline Reactor

The operation is assumed to be isothermal. To start with, we assume plug flow, a condition that is validated later. For a plug-flow reactor, the residence time is given by

Friction factor,

$$\begin{aligned} f &= 0.08 \operatorname{Re}^{-0.25} \\ &= 0.0057 \end{aligned} \quad (\text{CS1.11})$$

Dispersion coefficient $D = 5.05 uD(f/2)^{0.5} = 0.0104 \text{ m}^2/\text{s}$

Peclet number $Pe = uL_T/D = 3742$

Peclet number is very high (>50), which confirms the assumption of plug flow.

Pressure drop,

$$\begin{aligned} \Delta P &= 2 f L_T u^2 \rho / D \\ \Delta P &= 161 \text{ N/m}^2 \end{aligned} \quad (\text{CS1.12})$$

$$\begin{aligned} \text{Power} &= Q \times \Delta P \\ &= .01 \times 160 = 1.61 \text{ W} \end{aligned} \quad (\text{CS1.13})$$

Annual electric energy required = $(1.6 \text{ W}/1000) \times (8000 \text{ h/year}) = 12.8 \text{ kWh}$

Annual operating cost = $12.8 \text{ kWh} \times 0.03 \text{ \$/kWh} = \$0.4$

Estimating the fixed cost of the reactor:

Thickness,

$$\begin{aligned} t_T &= PD / 2 f_P \eta \\ &= 0.5 \times 10^6 \times 0.327 \left[2 \times 8.5 \times 10^7 \times 0.9 \right] \end{aligned} \quad (\text{CS1.14})$$

$t_T = 0.0011 \text{ m} \sim 1.1 \text{ mm}$, which is very low. In addition, we need to have some corrosion allowance:

Assuming a minimum thickness of 4 mm, $t_T = 0.004 \text{ m}$

Weight of the material required,

$$\begin{aligned} W_R &= \pi D L_T t_T \rho_s \\ &= 3.142 \times 0.327 \times 327 \times 0.004 \times 8000 = 10750 \text{ kg} \end{aligned} \quad (\text{CS1.15})$$

Cost of reactor = $W_R \times \text{unit cost of material} = 10750 \text{ kg} \times 0.4 \text{ \$/kg}$, i.e.,

Fixed cost = \$4300

Considering 20% of the fixed cost as the annualized cost (depreciation cost),

Total annualized cost = operating cost + 20% of fixed cost = $0.4 + 0.2 \times 4300 = \$860/\text{year}$

TABLE CS1.1
Sensitivity Analysis of Length-to-Diameter Ratio for the Pipeline Reactor

L_T/D	D m	L_T m	A_H m^2	u m/s	Re	f	ΔP N/ m^2	Power W	Annual Electric Energy Cost \$	Final Tube Thickness m	Weight kg	Fixed Cost \$	Annualized Cost \$	h_T W/ m^2 K	ΔT $^{\circ}C$
1	3.28	3.28	33.68	0.001	3890	0.010	0.000	0.000	6.86E-08	0.011	2884	1154	231	7.44	6120.3
5	1.92	9.58	57.59	0.003	6651	0.009	0.001	0.000	2.56E-06	0.006	2884	1154	231	19.53	1362.7
10	1.52	15.20	72.56	0.006	8380	0.008	0.005	0.000	1.22E-05	0.005	2884	1154	231	29.60	713.6
50	0.89	44.45	124.08	0.016	14330	0.007	0.190	0.002	4.56E-04	0.004	3970	1588	318	77.75	158.9
100	0.71	70.56	156.33	0.026	18054	0.007	0.904	0.009	2.17E-03	0.004	5002	2001	400	117.84	83.2
500	0.41	206.32	267.32	0.075	30872	0.006	33.78	0.338	8.11E-02	0.004	8554	3422	684	309.52	18.5
1000	0.33	327.51	336.80	0.119	38896	0.006	160.70	1.607	3.86E-01	0.004	10778	4311	863	469.14	9.7
5000	0.19	957.63	575.92	0.347	66512	0.005	6007.67	60.08	1.44E+01	0.004	18429	7372	1489	1232.21	2.2
10000	0.15	1520.15	725.61	0.551	83800	0.005	28577.46	285.77	6.86E+01	0.004	23219	9288	1926	1867.68	1.1

From Table CS1.2, fixed cost = \$3422

$$\text{Total annualized cost} = 0.13 + \$3422 \times 0.2 = \$684.53$$

However, there is an enhancement in the heat transfer, too, compared to the pipeline reactor (Kern, 1950):

$$\begin{aligned} h_C / h_T &= (1 + 3.5 D / D_C) \\ h_C / h_T &= 1.35 \end{aligned} \quad (\text{CS1.21})$$

Therefore, the $(\Delta T)_{LM}$ requirement is reduced to $25.00 \times h_T / h_C = 18.52^\circ\text{C}$ or a lower L_T/D ratio may be selected.

4. Multitubular Reactor

The same reaction can be performed in a multitubular reactor (with a shell-and-tube heat exchanger configuration). Two possibilities exist: the reactant is on the tube side or on the shell side. Both are considered below.

REACTANT ON THE TUBE SIDE

Tube-Side Calculations

Number of tubes:

Besides the diameter of the tube, the number of tubes, N_T , is also assumed and, correspondingly, the length required is

$$L_T = V / [(\pi/4) D^2 N_T] \quad (\text{CS1.22})$$

If we consider 25 tubes with an inner diameter of 0.154 m and an outer diameter of 0.168 m, the length of the tube becomes $L_T = 27.63 / [(\pi/4) \times 0.154^2 \times 25] = 59.3$ m.

Such a long tube needs many 1-1 shell-and-tube exchangers in series or a multipass exchanger with many passes on the tube side. A 1-1 type heat exchanger is considered here for simplicity.

Pressure Drop:

$$S = (\pi/4) \times 0.154^2 = 0.0186 \text{ m}^2 \quad (\text{CS1.23})$$

$$u = Q / S N_T$$

$$u = [0.01 \text{ m}^3/\text{s}] / [0.0186 \text{ m}^2 \times 25] = 0.021 \text{ m/s}$$

$$\text{Reynolds number } Re = Du\rho/\mu = 3306$$

$$\text{Friction factor } f = 0.08 Re^{-0.25} = 0.011$$

$$\text{Dispersion coefficient } D = 5.05 u D (f/2)^{0.5} = 0.00121 \text{ m}^2/\text{s}$$

Peclet number $Pe = u L_T / D = 1028 (>>50)$, which confirms our assumption of plug flow

$$\text{Pressure drop } \Delta P = 2 f L_T u^2 \rho / D = 3.7 \text{ N/m}^2$$

$$\text{Power} = Q \times \Delta P = 0.01 \times 3.7 = 0.037 \text{ W}$$

Heat Transfer Coefficient:

The tube-side Reynolds number is in the transition regime between laminar and turbulent flows ($2100 < Re < 4000$): using the Sieder–Tate equation for laminar flow ($Re < 2100$),

$$\left(\frac{h_T D}{k_T} \right) = 1.86 \left(Re Pr \frac{D}{L_T} \right)^{1/3} \left(\frac{\mu}{\mu_w} \right)^{0.14} \quad (\text{CS1.24})$$

At $Re = 2100$, substituting the values of Re , Pr , D , and L_T in Equation (CS1.24), the Nusselt number for laminar flow is 5.6. At the other extreme, for turbulent flow, the Nusselt number is given by

$$\left(\frac{h_T D}{k_T} \right) = 0.023 Re^{0.8} Pr^{1/3} \left(\frac{\mu}{\mu_w} \right)^{0.14} \quad (\text{CS1.25})$$

Assuming the value of $(\mu/\mu_w)^{0.14} \sim 1$, $Re = 4000$, and $Pr = 5$, the Nusselt number is 29.8. Using interpolation of the log-log relation of the Nusselt number and Reynolds number in the transition regime ($2100 < Re < 4000$),

$$\frac{\ln(h_T D / k_T) - \ln(5.6)}{\ln(29.8) - \ln(5.6)} = \frac{\ln(Re) - \ln(2100)}{\ln(4000) - \ln(2100)} \quad (\text{CS1.26})$$

At $Re = 3306$, $Nu = 18.18$. Substituting for D and k_T in the Nusselt number ($h_T D / k_T$), the heat transfer coefficient, $h_T = 99 \text{ W/m}^2 \text{ K}$.

Shell-Side Calculations

Flow Rate of the Cooling Medium:

Assume the cooling medium to be chilled water with an inlet temperature $T_{C0} = 7^\circ\text{C}$, density (ρ_C) = 1000 kg/m^3 , specific heat (C_{PC}) = 4180 J/kg K , viscosity (μ_C) = $1 \times 10^{-3} \text{ Pa}\cdot\text{s}$, Prandtl number (Pr_C) = 5.

Assuming an outlet temperature (T_{Ce}) of 27°C ,

$$Q_H = M_C C_{PC} (T_{Ce} - T_{C0}) \quad (\text{CS1.27})$$

Mass flow rate of the chilled water required is $M_C = Q_H / \{C_{PC}(T_{Ce} - T_{C0})\} = 26.1 \text{ kg/s}$

$$\text{Chilled water volumetric flow rate } V_C = M_C / \rho_C = 0.026 \text{ m}^3/\text{s}$$

Shell Diameter:

Assuming a triangular pitch of the tubes, with a pitch of $P_T = 1.33 \times D_O$

$$P_T = 1.33 \times 0.168 = 0.224 \text{ m}$$

$$d_E = 4 \frac{\frac{1}{2} P_T 0.86 P_T - \frac{1}{2} \frac{\pi D_o^2}{4}}{\frac{1}{2} \pi D_o} \quad (\text{CS1.35})$$

$G_S = 65.1 \text{ kg/m}^2/\text{s}$, and the equivalent diameter (d_E) of the shell is given by

$$d_E = 0.158 \text{ m}$$

Reynolds number,

$$\begin{aligned} \text{Re}_S &= d_E G_S / \mu c \\ &= 10263 \end{aligned} \quad (\text{CS1.36})$$

Friction factor, $f_S = 0.08 \text{ Re}^{-0.25} = 0.008$:

$$\Delta P_S = \frac{f_S G_S^2 D_S \frac{L_T}{B}}{2 \rho_C d_E} \quad (\text{CS1.37})$$

Pressure drop on the shell side ΔP_S is given by

$$\Delta P_S = 8 \text{ N/m}^2$$

$$\text{Power} = Q_C \times \Delta P_S = 0.207 \text{ W}$$

$$\left(\frac{h_S D}{k_T} \right) = 0.36 \text{ Re}^{0.55} \text{ Pr}^{1/3} \left(\frac{\mu}{\mu_W} \right)^{0.14} \quad (\text{CS1.38})$$

Shell-Side Heat Transfer Coefficient:

Assuming $(\mu/\mu_W)^{0.14} \sim 1$ and substituting the values of Re, Pr, D , and k_T in the above equation, the calculated value of the shell-side heat transfer coefficient $h_S = 524 \text{ W/m}^2 \text{ K}$.

Overall Heat Transfer Coefficient (U):

For simplicity, considering only the shell- and tube-side resistances (neglecting dirt factors), the overall heat transfer coefficient U is given by

$$\frac{1}{U} = \frac{1}{h_T} + \frac{1}{h_S D_o / D} \quad (\text{CS1.39})$$

$$U = 88 \text{ W/m}^2 \text{ K}$$

Check for Adequacy of Heat Transfer Area:

Initially it was assumed that the chilled water outlet temperature is 27°C . The log mean temperature difference is given by

TABLE CS1.3
Sensitivity Analysis of Length-to-Diameter Ratio for the Multitubular Reactor

TABLE CS1.3 Sensitivity Analysis of Length-to-Diameter Ratio for the Multitubular Reactor																						
No.	Shell id	T _e °C	L _T /D	D m	D _o m	N _T	L _T m	M _c kg/s	t _s m	B m	Reactant on the Tube Side			Power		Power W	Annual Electrical Energy Cost \$	Weight kg	Fixed Cost \$	Annual Cost \$	U _T W/m ² K	LMTD ^a °C
											Re (Tube Side)	W	(Shell Side)	W	W							
1	1.34	27	413	0.15	0.16	23	63.7	26.1	0.0074	1.08	3549	0.05	0.24	0.29	0.069	56603	22641	4528.06	91.4	31.5		
2	1.38	20	383	0.15	0.16	25	59	41.3	0.0075	1.11	3287	0.04	0.7	0.74	0.17	56151	22461	4528.17	80.8	35.7		
3	1.38	27	386	0.15	0.16	25	59.4	25.1	0.0075	1.11	3063	0.04	0.2	0.24	0.058	56172	22469	4494.05	84.7	32		
4	1.41	15	364	0.15	0.16	26	56.1	70.7	0.0076	1.12	3127	0.03	2.83	2.86	0.69	55870	22348	4469.69	75.1	38.4		
5	1.25	27	375	0.20	0.22	11	76.7	26.1	0.0071	1	5671	0.05	0.28	0.33	0.08	48920	19568	3913.08	121.1	31.6		
6	1.37	20	293	0.20	0.22	14	59.9	41.3	0.0075	1.09	4433	0.03	0.56	0.58	0.14	47368	18947	3790.14	107.3	35.7		
7	1.43	15	265	0.20	0.22	16	54.2	70.7	0.0077	1.15	4005	0.02	1.85	1.87	0.45	46799	18719	3744.40	99.5	38.4		
Reactant on the Shell Side																						
8	1.07	25	216	0.20	0.22	7	44.1	29.1	0.0065	0.21	24818	1.18	0.88	2.06	0.49	19956	7982	1596.48	305.1	32.8		
9	1.5	20	123	0.20	0.22	18	25.1	41.3	0.0079	0.3	14419	0.37	0.15	0.52	0.12	24328	9731	1946.12	203.1	35.7		
10	2.15	15	200	0.20	0.22	42	13.5	70.7	0.01	0.44	10493	0.2	0.02	0.22	0.05	28835	11534	2307.05	147.7	38.4		
11	1.7	25	135	0.15	0.17	43	20.9	29.1	0.0086	0.34	5662	0.1	0.11	0.21	0.05	31899	12759	2252.03	147.8	32.8		
12	2.25	20	83	0.15	0.17	82	12.9	41.3	0.0104	0.44	4150	0.05	0.03	0.08	0.02	36621	14648	2930.02	113.5	35.7		
13	2.97	15	51	0.15	0.17	154	7.9	70.7	0.0127	0.61	3802	0.05	0.01	0.05	0.01	40937	16375	3275.10	91.7	38.4		

^a LMTD = log mean temperature difference.

^a LMTD = log mean temperature difference.

4. Assume chilled water (coolant) inlet temperature $T_{C0} = 7^\circ\text{C}$ and outlet temperature $T_{Ce} = 25^\circ\text{C}$.
5. Mass flow rate of the chilled water required is $M_C = Q_H / \{C_{PC} (T_{Ce} - T_{C0})\} = 29.1 \text{ kg/s}$.
6. Tube-side pressure drop and heat transfer coefficient:

$$Re_T = 5662, \text{ pressure drop} = 3.4 \text{ N/m}^2, \text{ heat transfer coefficient } h_T = 213 \text{ W/m}^2 \text{ K}$$

7. Shell-side pressure drop and heat transfer coefficient: Since the reactant is on the shell side, assume low baffle spacing so that the flow may be assumed to be plug.
 Assume baffle spacing of $0.2 \times D_S = 0.34 \text{ m}$
 Shell-side pressure drop $= 11 \text{ N/m}^2$
 Heat transfer coefficient $h_S = 525 \text{ W/m}^2 \text{ K}$
8. Overall heat transfer coefficient and log mean temperature difference:
 For simplicity, considering only the shell- and tube-side resistances (neglecting the dirt factor),

$$U = 148 \text{ W/m}^2 \text{ K}$$

Log mean temperature difference is given by Equation (CS1.40), where T_0 and T_e are the inlet and outlet temperatures of the reaction mixture (process fluid), respectively. Assuming the tube side to be isothermal, $T_0 = T_e = 50^\circ\text{C}$, $(\Delta T)_{LM} = 32.77^\circ\text{C}$.

$$A_H = \frac{Q_H}{U \Delta T_{LM}} = 427.27 \text{ m}^2$$

9. Required heat transfer area is calculated from the actual area available A_A of the shell-and-tube exchanger as $A_A = N_T \pi D L_T = 427 \text{ m}^2$.
10. $A_A/A_H = 0.999 \sim 1$. This is a good match. If the value of A_A/A_H was found to be very different from 1, then the number and/or diameter of tubes would need to be varied and the whole procedure repeated to finally obtain a value of 1.
11. Annual operating cost:
 Shell-side power required $= Q \times \Delta P_S = 0.01 \times 11 = 0.11 \text{ W}$
 Tube-side power required $= Q_C \times \Delta P_T = 0.029 \times 3.4 = 0.1 \text{ W}$
 Power (shell side + tube side) $= 0.21 \text{ W}$
 Annual electric energy required $= (0.21 \text{ W}/1000) \times (8000 \text{ hr/year}) = 1.68 \text{ kWh}$
 Annual operating cost $= 1.68 \text{ kWh} \times 0.03 \text{ \$/kWh} = \$0.05$

Fixed cost of reactor:

Shell thickness, $t_S = PD_S/2f_P\eta = (0.5 \times 10^6) \times 1.7/[2 \times (8.5 \times 10^7) \times 0.9] = 0.0056 \text{ m} \sim 5.6 \text{ mm}$.
 In addition, since we need to have some corrosion allowance, say 3 mm, thickness $t_S = 0.0086 \text{ m}$.
 Weight of the material of construction required $= \pi D_S L_T t_S \rho_S = 7698 \text{ kg}$.
 Weight of tubes $= N_T \pi D L_T t_T \rho_S = 24409 \text{ kg}$. For simplicity, we consider only the cost of the shell and tubes. In reality, however, one also has to consider the tube sheets, head, nozzles, baffles, and cost of fabrication.

$$\text{Cost of reactor} = \text{Total weight} \times \text{unit cost of material} = (7698 + 24409) \text{ kg} \times 0.4 \text{ \$/kg} = \$12842.$$

$$\text{Fixed cost} = \$12842.$$

+ ozone) is as follows: NO- 389 ppm, NO₂- 39 ppm, HNO₂- 6 ppm, N₂O₅- 0 ppm, HNO₃- 1 ppm, O₃- 663 ppm, O₂- 6.5297 mol%, SO₂- 1944 ppm, CO- 0 ppm, CO₂- 11.9815 mol%, SO₃- 0 ppm, CO- 0 ppm, HNO₃- 1 ppm, O₃- 663 ppm, H₂O- 6.9974 mol%, N₂- rest. The theoretical requirement has been estimated on the basis of NO and NO₂ conversion.

Solution

The following assumptions are made: (1) Ozone and flue gas are thoroughly mixed in a short distance using a proper distributor. (2) Gas moves in plug flow. (3) Gas follows ideal gas law. (4) There are no radial gradients of temperature, concentration, and density. (5) The reactor is operating at steady state.

Component balances across a differential length can be established for O₃, O₂, NO, NO₂, N₂O₅, HNO₃, H₂O, SO₂, CO, and SO₃, and ten first-order ordinary differential equations are written. For the solution of this set of simultaneous differential equations, the Runge-Kutta fourth-order method was employed. The integration along the volume of the reactor was performed using the feed composition as the inlet boundary condition. The outlet boundary condition was specified to be 99% conversion of the total inlet NO_x to N₂O₅.

The level of ozone affects the reactor volume. The rate of ozonation of NO being fast, NO is consumed almost instantaneously, forming NO₂. NO₂ concentration decreases due to the formation of N₂O₅. The residence time required for 99% conversion is 7.4 s. The effect of percentage excess of ozone on reactor performance for 99% conversion of total inlet NO_x (NO and NO₂) can be easily calculated.

Lesson

The abatement of NO_x pollution is an important environmental problem that has alternative technologies. This case study focuses on technology that won the McGraw-Hill 2001 Kirkpatrick Award. The main reaction involves the ozonation of NO_x to give N₂O₅, followed by absorption in water/Ca(OH)₂. While Case Study 11.1 illustrates a detailed procedure for determining the geometric specifications for a simple reaction, the present study outlines a design methodology for a complex system and tells us that such a study is not only relevant but almost inescapable. Because this case study pertains to the treatment of exhaust gases, it demands very low pressure drops, even at high volumetric gas flow rates. Although not considered in this case study, the injection methodology of ozone in flue gases using a distributor should be such that the length required for mixing of ozone (in flue gases) is negligible compared to the length of the reactor.

CASE STUDY 11.3 GAS-SOLID (CATALYTIC) REACTION: MODELING OF A COMPLEX REACTION ON A DEACTIVATING CATALYST (A MODEL SCHEME)

Nomenclature for Case Study 11.3

(Some symbols are defined in the text; some are self-evident statistical terms.)

A_1, A_2, A_3	chemical species
f_1, f_2, f_3, f_4	functions
h	proportionality constant defined by Equation (CS3.13)
I_r	$(r \times r)$ identity matrix
K, K_1, K_3	vectors of rate constants, equilibrium constants, etc.
m	total number of models
n	total number of experiments at any stage
P	fouling complex
$P_{n+1,v}$	posterior probability of the v th model
$P_{n,v}$	prior probability of the v th model
p	total number of parameters

TABLE CS3.1
Experimental Rate Data

Sr. No.	Space Time g h/g mol	Decay Time h	Mol Fraction of A ₁	Mol Fraction of A ₂	Reaction Rate of A ₁ mol/g h × 10 ²	Reaction rate of A ₂ mol/g h × 10 ²
		<i>t</i>	<i>y</i> ₁	<i>y</i> ₂	<i>r</i> ₁	<i>r</i> ₂
1	15	0	0.871	0.120	-0.819	0.833
2	30	0	0.757	0.242	-0.697	0.707
3	45	0	0.661	0.337	-0.591	0.563
4	75	0	0.499	0.482	-0.511	0.439
5	105	0	0.363	0.599	-0.321	0.258
6	15	1	0.871	0.127	-0.776	0.728
7	30	1	0.766	0.229	-0.659	0.643
8	75	1	0.515	0.475	-0.495	0.370
9	90	1	0.443	0.520	-0.460	0.242
10	60	2	0.598	0.406	-0.531	0.483
11	30	3	0.784	0.216	-0.606	0.600
12	15	5	0.890	0.109	-0.715	0.668
13	90	5	0.478	0.496	-0.476	0.430
14	60	6	0.632	0.352	-0.518	0.450
15	15	9	0.903	0.095	-0.585	0.524
16	105	9	0.505	0.451	-0.303	0.320

Doraiswamy (1974) on a particular variety of silica gel in a fixed-bed reactor. The role of catalyst deactivation was studied by obtaining kinetic data at various times. Fortunately, by-products were negligible. This case study describes the reaction-deactivation kinetics and proposes a complete model using appropriate statistical methods. The emphasis will be on the use of a suitable algorithm for sequential updating of the models until one of them emerges as the “best.”

Procedure

For model discrimination to be accomplished sequentially, leading to the selection of the “best” model, the following data/techniques are essential:

1. Experimental rate data in a suitable form.
2. A set of plausible models containing the true model.
3. An efficient method of parameter estimation.
4. A good sequential design strategy.
5. A powerful discriminatory criterion.

Experimental Data

For the reaction under consideration, values of the reaction rate as a function of concentration and catalyst decay time may be obtained by numerical differentiation of the experimental data obtained by Prasad and Doraiswamy (1974) at various space velocities and catalyst decay times in a fixed-bed reactor. The bed length was maintained small enough to give isothermal conditions to within 2°C. It was also ensured that the feed velocity was high enough, and the particle size small enough, to eliminate external and internal diffusion effects, respectively. The kinetic parameters, including decay time, will vary with the type of silica gel used. The data obtained for the silica gel used are summarized in Table CS3.1.

Models

Vapor-phase catalytic chlorination of A₁ on activated silica gel at 200°C is accompanied by slow deactivation of the catalyst. A₁ is successively chlorinated to A₂ and A₃. Trace quantities of by-

TABLE CS3.2
The Rival Models

Model No.	Fouling Reactions	Expressions for f_3 in Equation (CS3.2)	Model Equations for	
			\mathcal{E}_1	\mathcal{E}_2
1.	$A_1 \rightarrow P$	$-\mathbf{K}_3 y_1$	$-\mathbf{K}_1 y_1 \exp[-\mathbf{K}_3 y_1 t]$	$[\mathbf{K}_1 y_1 - \mathbf{K}_2 y_2] \exp[-\mathbf{K}_3 y_1 t]$
2.	$A_2 \rightarrow P$	$-\mathbf{K}_3 y_2$	$-\mathbf{K}_1 y_1 \exp[-\mathbf{K}_3 y_2 t]$	$[\mathbf{K}_1 y_1 - \mathbf{K}_2 y_2] \exp[-\mathbf{K}_3 y_2 t]$
3.	$A_3 \rightarrow P$	$-\mathbf{K}_3 [1 - y_1 - y_2]$	$-\mathbf{K}_1 y_1 \exp[-\mathbf{K}_3 (1 - y_1 - y_2) t]$	$[\mathbf{K}_1 y_1 - \mathbf{K}_2 y_2] \exp[-\mathbf{K}_3 (1 - y_1 - y_2) t]$
4.	$A_1 + A_2 \rightarrow P$	$-\mathbf{K}_3 y_1 y_2$	$-\mathbf{K}_3 y_1 \exp[-\mathbf{K}_3 y_1 y_2 t]$	$[\mathbf{K}_1 y_1 - \mathbf{K}_2 y_2] \exp[-\mathbf{K}_3 y_1 y_2 t]$
5.	$A_1 + A_3 \rightarrow P$	$-\mathbf{K}_3 y_1 [1 - y_1 - y_2]$	$-\mathbf{K}_1 y_1 \exp[-\mathbf{K}_3 y_1 (1 - y_1 - y_2) t]$	$[\mathbf{K}_1 y_1 - \mathbf{K}_2 y_2] \exp[-\mathbf{K}_3 y_1 (1 - y_1 - y_2) t]$
6.	$A_2 + A_3 \rightarrow P$	$-\mathbf{K}_3 y_2 [1 - y_1 - y_2]$	$-\mathbf{K}_1 y_1 \exp[-\mathbf{K}_3 y_2 (1 - y_1 - y_2) t]$	$[\mathbf{K}_1 y_1 - \mathbf{K}_2 y_2] \exp[-\mathbf{K}_3 y_2 (1 - y_1 - y_2) t]$
7.	$A_1 + A_2 + A_3 \rightarrow P$	$-\mathbf{K}_3 y_1 y_2 [1 - y_1 - y_2]$	$-\mathbf{K}_1 y_1 \exp[-\mathbf{K}_3 y_1 y_2 (1 - y_1 - y_2) t]$	$[\mathbf{K}_1 y_1 - \mathbf{K}_2 y_2] \exp[-\mathbf{K}_3 y_1 y_2 (1 - y_1 - y_2) t]$
8.	$A_1 \rightarrow P$ $A_2 \rightarrow P$	$-\mathbf{K}_3 [y_1 + y_2]$	$-\mathbf{K}_1 y_1 \exp[-\mathbf{K}_3 (y_1 + y_2) t]$	$[\mathbf{K}_1 y_1 - \mathbf{K}_2 y_2] \exp[-\mathbf{K}_3 (y_1 + y_2) t]$
9.	$A_1 \rightarrow P$ $A_3 \rightarrow P$	$-\mathbf{K}_3 [1 - y_2]$	$-\mathbf{K}_1 y_1 \exp[-\mathbf{K}_3 (1 - y_2) t]$	$[\mathbf{K}_1 y_1 - \mathbf{K}_2 y_2] \exp[-\mathbf{K}_3 (1 - y_2) t]$
10.	$A_2 \rightarrow P$ $A_3 \rightarrow P$	$-\mathbf{K}_3 [1 - y_1]$	$-\mathbf{K}_1 y_1 \exp[-\mathbf{K}_3 (1 - y_1) t]$	$[\mathbf{K}_1 y_1 - \mathbf{K}_2 y_2] \exp[-\mathbf{K}_3 (1 - y_1) t]$
11.	$A_1 \rightarrow P$ $A_2 \rightarrow P$ $A_3 \rightarrow P$	$-\mathbf{K}_3 [y_1 + y_2 + (1 - y_1 - y_2)]$ $= -\mathbf{K}_3$	$-\mathbf{K}_1 y_1 \exp[-\mathbf{K}_3 t]$	$[\mathbf{K}_1 y_1 - \mathbf{K}_2 y_2] \exp[-\mathbf{K}_3 t]$

Main reaction is $A_1 \rightarrow A_2 \rightarrow A_3$

squares but, for the present two-response system, the resulting equations are quite involved. Hence, the following least squares objective function may be minimized using the "complex" method of Box (1965):

$$S = \det \begin{bmatrix} s^{11} & s^{12} \\ s^{12} & s^{22} \end{bmatrix} \quad (\text{CS3.7})$$

where s^{ij} is the sum of cross products of residuals of the i th and j th responses.

A Good Sequential Design Strategy

Basic Equations

Any experimental program involving r dependent and s independent variables and p parameters in the k th experiment may be described by algebraic equations,

$$y_k^i = \eta_k^i(\mathbf{x}_k, \mathbf{K}) + \varepsilon_k^i, \quad i = 1, 2, \dots, r \quad (\text{CS3.8})$$

where \mathbf{x}_k is an $(s \times 1)$ vector of independent variables for the k th experiment, is a $(p \times 1)$ vector of model parameters, η_k^i is the true value of the i th response for the k th experimental settings \mathbf{X}_k , y_k^i is the observed value of the i th response, and ε_k^i is the experimental error for the i th response, also for the k th experiment. The u th model for all the responses may be written in vector form as

$$\mathbf{y}_k = \boldsymbol{\eta}_k(\mathbf{x}_k, \mathbf{K}) + \boldsymbol{\varepsilon}_k^i \quad (\text{CS3.9})$$

If the i th component of the $(r \times 1)$ vector of nonlinear functions η_k is expanded in Taylor's series about an estimate $\hat{\mathbf{K}}_u$ of the parameters and truncated after the first partial derivatives, Equation (CS3.8) may be written for the $(n + 1)$ th experiment as

where $\mathbf{Z}_{n+1,v}$ is the $(r \times p)$ matrix of partial derivatives whose (i, ℓ) th element is given by Equation (CS3.11), \mathbf{M}_v^{-1} is the $(p \times p)$ precision matrix of parameters of the v th model, and \mathbf{V} is the precision matrix. \mathbf{M}_v is given by

$$\mathbf{M}_v = \sum_{i=1}^r \sum_{j=1}^r \alpha^{ij} \mathbf{X}_v^{iT} \mathbf{X}_v^j, \quad v = 1, 2, \dots, m \quad (\text{CS3.16})$$

where α^{ij} is the (i, j) th component of \mathbf{V}^{-1} and \mathbf{X}_v^i is the $(n \times p)$ matrix of partial derivatives of the i th response for the v th model whose (k, ℓ) th element is obtained from Equation (CS3.11) by replacing subscript $(n + 1)$ with k . Since Equation (CS3.12) is basic to the Bayesian procedure, the probabilities of all the models are sequentially updated by collecting additional data until one model emerges with the highest probability.

A Powerful Discriminatory Criterion

Often, no single model emerges as the most probable. In such a case, the next experiment should be performed at a setting of independent variables that maximizes the divergence between competing candidates. This is done by using a discriminatory design criterion, which is some suitably defined function of the vector of independent variables \mathbf{x}_k , called the *utility function* $U(\mathbf{x}_k)$. Several criteria have been proposed (Reilly and Blau, 1974). The Box–Hill (1967) criterion is perhaps the most commonly used and is given by

$$U(\mathbf{x}_k) = \frac{1}{2} \sum_{u=1}^m \sum_{v=u+1}^m P_{n,u} P_{n,v} \left[\text{Tr}(\boldsymbol{\Phi}_u \boldsymbol{\Phi}_v^{-1} + \boldsymbol{\Phi}_v \boldsymbol{\Phi}_u^{-1} - 2I_r) + (\boldsymbol{\eta}_u - \boldsymbol{\eta}_v)^T (\boldsymbol{\Phi}_u^{-1} + \boldsymbol{\Phi}_v^{-1}) (\boldsymbol{\eta}_u - \boldsymbol{\eta}_v) \right] \quad (\text{CS3.17})$$

where $U(\mathbf{x}_k)$ is the utility function for the k th set of independent variables \mathbf{x}_k , $P_{n,u}$ is the posterior probability of the u th model after n experiments, $\boldsymbol{\Phi}_u$ is the $(r \times r)$ precision matrix for the predictions made by the u th model after n experiments, and $\boldsymbol{\eta}_u$ is the $q \times 1$ vector of predicted responses for the u th model using the k th set of independent variables \mathbf{x}_k . This criterion weighs the divergences over the inverse of the precision matrix so that large divergences due to imprecisely known parameters do not contribute significantly to the utility function. The object is to find the $\max_k U(\mathbf{x}_k)$ that determines the next best experiment to be performed to maximize divergence between rival models. Hence, several new sets of \mathbf{x}_k can be randomly generated to evaluate U_{\max} .

A Sequential Discrimination Algorithm

A computational algorithm for sequential discrimination among rival models is presented in Figure CS3.1.

Choice of Model for the Present System (see Prasad and Rao, 1977)

The eleven models given in Table CS3.2 can be compared taking an initial probability of 1/11 or 0.0909 for each and with an initial set of six experiments taken at random from Table CS3.1. Ten sequential experiments (total of 16 experiments) were performed (Table CS3.3), at the end of which one of the models (model 9) attained a probability of 0.912, compared to 0.088 for the nearest rival (model 1). The probabilities of the other models are negligibly small, even after the first discriminatory experiment.

The computations show that the given system represents an example of series-parallel deactivation:



with the rate equations

$$r_1 = -K_1 y_1 \exp[-K_3(1 - y_2)t] \quad (\text{CS3.18})$$

$$r_2 = (K_1 y_1 - K_2 y_2) \exp[-K_3(1 - y_2)t] \quad (\text{CS3.19})$$

where y_1 , y_2 are the mole fractions of A_1 and A_2 in the product mixture. The values of the parameters K_1 , K_2 , and K_3 are

$$K_1 = 0.933 \text{ h}^{-1}$$

$$K_2 = 0.136 \text{ h}^{-1}$$

$$K_3 = 0.549 \text{ h}^{-1}$$

Lesson

This case study describes a statistical method for modeling a complex reaction. A model reaction occurring on a deactivating catalyst, in which the fouling reactions generate the complexity, is chosen for illustration, but the procedure is equally applicable to any complex reaction scheme with or without fouling, catalytic or noncatalytic. While a great reliance on statistics is not always needed, this study tells us that the statistical method can identify the controlling step. On the other hand, it does not consider the possibility that the true rate-determining mechanism may have been omitted from the list of candidates. Thus, any statistical procedure of this kind, so common in chemical engineering, is no more than one of convergence to the “best” and not a direct postulation of a model from first principles and validated by experiments.

When this procedure is applied to LHHW models, caution should be exercised in claiming a model to be the “best.” The need for this increases with the number of unknown parameters, since several models may then show almost equal convergence. In general, it is advisable to confine the methods to models with no more than three or four unknown parameters. Furthermore, it should be ensured that all data points are of equal precision.

CASE STUDY 11.4 GAS-SOLID (CATALYTIC) REACTION IN FIXED-BED NINA AND ADIABATIC REACTORS: REDUCTION OF NITROBENZENE TO ANILINE

Nomenclature for Case Study 11.4

A	nitrobenzene
$[A]$	concentration of A (kmol/m ³)
B	hydrogen
$[B]$	concentration of B (kmol/m ³)
C_p	heat capacity [kcal/kg (reactant gases)°C]
C_{pm}	molar heat capacity (kcal/kg °C)

where

$$k_w = k_w^o \exp\left(-\frac{E}{R_g T}\right), \text{ cm}^3/\text{g cat s} \quad (\text{CS4.2})$$

$$K_B = K_B^o \exp\left(\frac{E_{ad}}{R_g T}\right), \text{ cm}^3/\text{mol} \quad (\text{CS4.3})$$

Assuming a pseudohomogeneous two-dimensional reactor model with plug flow of fluid and constant properties, calculate the axial concentration and temperature profiles at several radial positions along the axis of a single tube. Use the following property/parameter values (Doraiswamy, 2001):

$[A]_0 = 7.1 \times 10^{-4} \text{ mol/L}$, $(-\Delta H_r) = 180 \text{ kcal/mol}$, $\rho_s = 2.18 \text{ g/cm}^3$, $\varepsilon_B = 0.312$, $C_p = 0.49 \text{ cal/g (reactant gases) } ^\circ\text{C}$ at 200°C , $k_{T,er} = 1.4 \text{ cal/m } ^\circ\text{C s}$, $h_w = 9.5 \times 10^{-4} \text{ cal/cm}^2 ^\circ\text{C s}$, $\mathbf{D}_{A,er} = 4.74 \times 10^{-4} \text{ cm}^2/\text{s}$, $\rho = 0.0944 \text{ g/L}$, $u = 40 \text{ cm/s}$, $k_w^o = 9.46 \times 10^{-3} \text{ L/g catalyst s}$, $E = 2631 \text{ cal/mol}$, $K_B^o = 10.7 \text{ cm}^3/\text{mol}$, $E_{ad} = 8039 \text{ cal/mol}$. $T_0 = 160^\circ\text{C}$, $T_w = 100^\circ\text{C}$.

Solution

Before proceeding with the solution, it is instructive to list the governing equations for a number of simple and complex situations. These situations have already been described in Section 11.4, and Table 12.2 of Doraiswamy and Sharma (1984) lists the more important equations. Case A2-a of this table is the so-called basic model that incorporates enough complexity to make the design sufficiently realistic and yet is relatively easy. The homogeneous nonisothermal nonadiabatic (NINA) model allows one to compute temperature and concentration profiles within the reactor tube. The equations for this model are

$$\mathbf{D}_{A,er} \left(\frac{\partial^2 [A]}{\partial r^2} + \frac{1}{r} \frac{\partial [A]}{\partial r} \right) - u \frac{\partial [A]}{\partial z} - (-r_A) = 0 \quad (\text{CS4.4})$$

$$-k_{T,er} \left(\frac{\partial^2 T}{\partial r^2} + \frac{1}{r} \frac{\partial T}{\partial r} \right) - u \rho C_p \frac{\partial T}{\partial z} + (-\Delta H_r)(-r_A) = 0 \quad (\text{CS4.5})$$

with boundary conditions

$$\begin{aligned} \frac{\partial [A]}{\partial r} &= 0 \quad \text{at } r = 0, z > 0 \\ [A] &= [A]_0 \quad \text{at } r > 0, z = 0 \\ \frac{\partial T}{\partial r} &= 0 \quad \text{at } r = 0, z > 0 \\ -k_{T,er} \frac{\partial T}{\partial r} &= h_w (T - T_w) \quad \text{at } r = 0, z = 0 \end{aligned} \quad (\text{CS4.6})$$

$$-r_{wA} = \frac{k_w^o \exp(-E/2T) \left(\frac{1-X_A}{61-X_A} \right)}{\left[1 + K_B^o \exp(E_{ad}/2T) \left(\frac{X_A}{61-X_A} \right) \right]^2} \quad (\text{CS4.10})$$

A material balance on A gives

$$F_{A0} dX_A = (-r_{wA}) dW \quad (\text{CS4.11})$$

or

$$F_{A0} dX_A = (-r_{wA}) \rho_b (l - \varepsilon_b) S dz \quad (\text{CS4.12})$$

and an energy balance gives

$$F_{A0} (-\Delta H_r) dX_A = F_{t0} C_{pm} dT \quad (\text{CS4.13})$$

where F_{t0} is the total flow rate of the inlet gases. In view of the large excess of hydrogen, F_{t0} can be assumed constant.

From Equations (CS4.12) and (CS4.13), we can write

$$dX_A = \left[\frac{\rho_b (1 - \varepsilon_b) S (-r_{wA})}{F_{A0}} \right] dz \quad (\text{CS4.14})$$

$$dT = \left[\frac{(-\Delta H_r) \rho_b (1 - \varepsilon_b) S (-r_{wA})}{F_{t0} C_{pm}} \right] dz \quad (\text{CS4.15})$$

or

$$dX_A = \alpha dz \quad (\text{CS4.16})$$

$$dT = \beta dz \quad (\text{CS4.17})$$

Equations (CS4.16) and (CS4.17) are coupled ordinary differential equations in conversion and temperature. They can be solved for the initial conditions

$$z = 0, \quad X_A = 0, \quad T_0 = 473 \text{ K}$$

using the Runge-Kutta fourth-order method for different tube diameters and ratios [note that Equation (CS4.10) will be slightly different for different ratios].

The results (not given here) show that (1) conversion and temperature decrease with the reactor length with an increase in $\text{H}_2\text{-C}_6\text{H}_5\text{NO}_2$ ratio, and (2) for a given ratio, conversion and temperature rise throughout the reactor length with an increase in reactor diameter. Hence, in general, larger diameters and lower ratios are favored.

q	flow rate between the bubble and emulsion phases induced by circulation (m^3/s)
r	radius (m)
s_{bb}	solids fraction in bubble, Equation (CS5.9)
s_{cb}	solids fraction in cloud, Equation (CS5.10)
s_{ce}	solids fraction in emulsion, Equation (CS5.11)
s_{wb}	fraction of solids in wake, Equation (CS5.12)
U	fluidization group defined by Equation (CS5.2)
u_{br}	slip velocity (m/s)
u_b	real bubble velocity
u_f	fluidization velocity (m/s)
u_{mf}	velocity at minimum fluidization (m/s)
V_b	bubble volume (m^3)
X_A	conversion of A (—)
Y	mass exchange group defined by Equation (CS5.2)
Z	dimensionless height of fluidized bed, L/L_f (—)
Z_t	total dimensionless height of fluidized bed including the dilute bed region, L_t/L_f

Greek

α	ratio u_{br}/u_f
δ	volume fraction of bubbles in bed
ϵ_b	static bed voidage
ϵ_{mf}	bed voidage at minimum fluidization
ρ_c	density of catalyst (kg/m^3)

Subscripts

b	bubble
c	cloud
e	emulsion
f	fluidization
mf	minimum fluidization

The Problem

Aniline is produced by the hydrogenation of nitrobenzene on a solid catalyst as was shown in CS4.R1 (Case Study 11.4). Kinetic data for this reaction using a copper-based catalyst were obtained during pilot plant studies at the National Chemical Laboratory. Although an LHHW model was proposed, it was also possible to fit a simpler, power law equation to the data, with a rate constant of 1.2 s^{-1} . The purpose of the present case study is to calculate the conversions obtained for this reaction in a fluid-bed reactor using several available models. Although more rigorous models have been proposed that account for bubble size distribution, volume change, and other complicating features of a fluidized bed, simpler models are usually quite adequate. In this study, we compare the predictions of the following five models: Davidson, Kunii–Levenspiel, Miyauchi, Fryer–Potter, and Jayaraman–Kulkarni–Doraiswamy. As the catalyst maintains its initial activity for over a year, a batch fluidized bed is used, and the catalyst is replaced after it begins to lose its activity.

To put the five models in perspective, and to understand the complications that may arise in more rigorous modeling, we conclude this case study with a brief discussion of a few complex models.

Data

The following data (calculated, assumed, or experimentally obtained) will be used:

Minimum fluidization velocity $u_{mf} = 2 \text{ cm/s}$, feed velocity at inlet $u_0 = 30 \text{ cm/s}$, bubble diameter $d_b = 10 \text{ cm}$, initial (fixed-bed) height $L_0 = 1.4 \text{ m}$, reaction rate constant $k_v = 1.2 \text{ s}^{-1}$, bed voidage

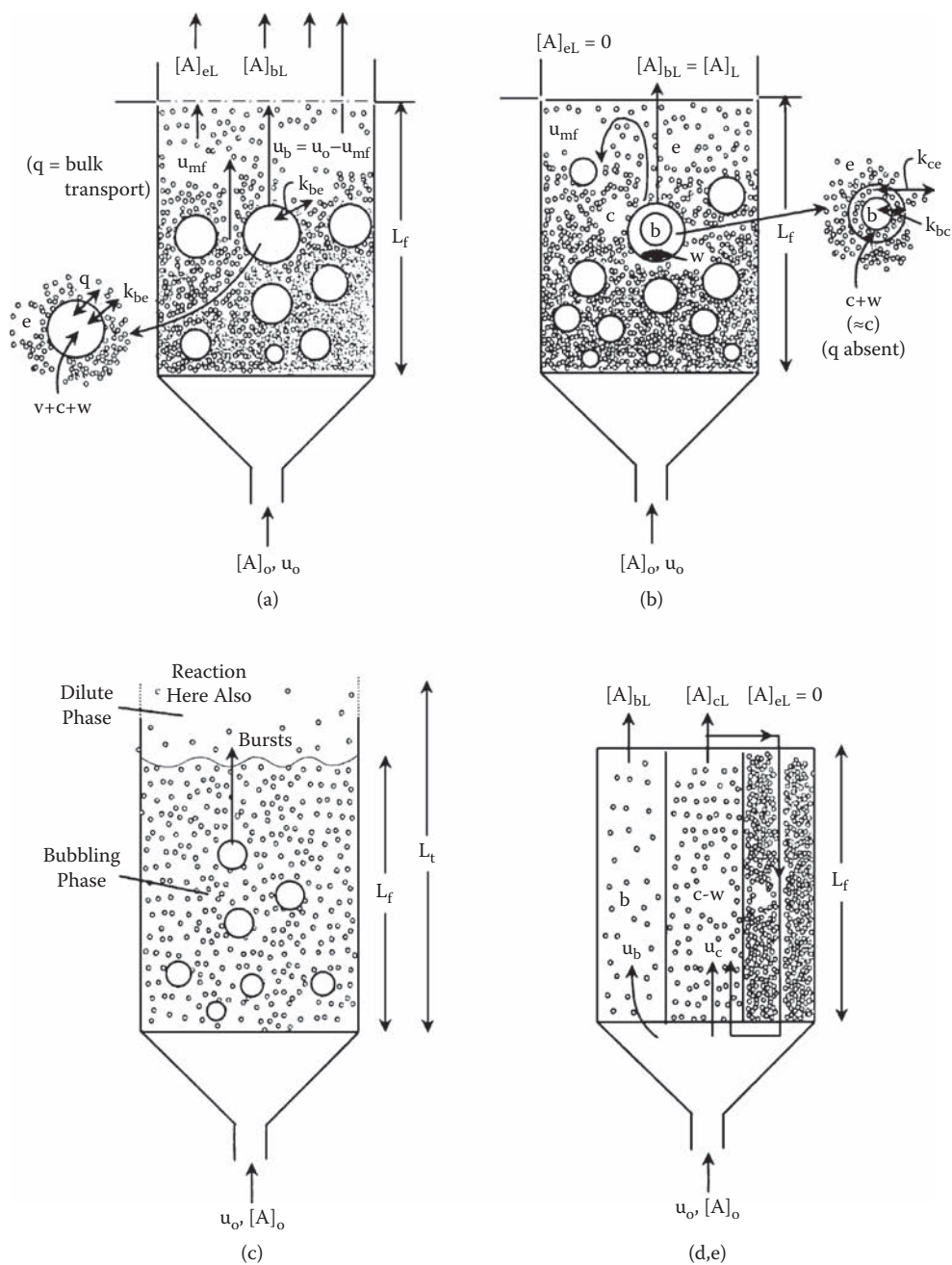


FIGURE CS5.1 Schematics of several fluidized-bed reactor models: (a) Davidson model, (b) Kunii-Levenspiel model, (c) Miyauchi model, (d), (e) Fryer-Potter and Jayaraman-Kulkarni-Doraiswamy models.

greater than the emulsion gas velocity. The thickness of the cloud is a function of the bubble velocity, which in turn depends on the size of the bubbles and of the fluidizing particles. In a bed of small particles with large bubbles (with corresponding high velocities), a cloud of thickness calculated as

$$\frac{r_c - r_b}{r_b} \cong \frac{u_f}{u_{br}} = \frac{1}{\alpha} \quad (\text{CS5.8})$$

$$\frac{r_c}{r_b} = \left(\frac{\alpha + 2}{\alpha - 1} \right)^{1/3} \quad (\text{more rigorous})$$

develops around each bubble. The bubble gas does not circulate through the rest of the bed. The gas exchange is by diffusive transfer with no bulk circulation (unlike in the Davidson model, which has both). Furthermore, as already mentioned in Section 11.4.2.5.1, as the bubble moves upward, suction is created at the bottom of the bubble; solid particles are drawn into that region and lodged there. This is known as the *wake* and, for purposes of mass transfer, it is assumed to be fully mixed with the cloud-phase components. Because there are now two operative phases in the bubble-cloud-wake unit (bubble and cloud/wake), mass transfer between the emulsion and this unit occurs by two consecutive steps (unlike in the Davidson model, where only one step is involved): between emulsion and cloud, and between cloud and bubble/cloud/wake. For simplicity, the gas and solid particles are assumed to be fully mixed in each of the phases, cloud/wake and bubble. Reaction occurs in all three phases, and the extent of reaction in each phase depends on the solids fraction in that phase. These solid fractions are defined as

$$s_{bb} = \frac{\text{volume of solids in bubbles}}{\text{volume of bubbles}} \quad (\text{CS5.9})$$

$$s_{cb} = \frac{\text{volume of solids in clouds/wake}}{\text{volume of bubbles}} \quad (\text{CS5.10})$$

$$s_{eb} = \frac{\text{volume of solids in emulsion}}{\text{volume of bubbles}} \quad (\text{CS5.11})$$

$$s_{wb} = \frac{\text{volume of solids in wake}}{\text{volume of bubbles}} \quad (\text{CS5.12})$$

Hence, several reaction and mass transfer steps occur in the overall scheme as shown in Figure CS5.2. Assuming that only the bubble gas exists in the bed (the emulsion gas is assumed to circulate within the bed), mass balances can be written as shown in the figure. All these equations can be algebraically combined and rearranged to give the following design equation:

$$1 - X_A = e^{-K_f} \quad (\text{CS5.13})$$

where K_f represents a composite constant given by

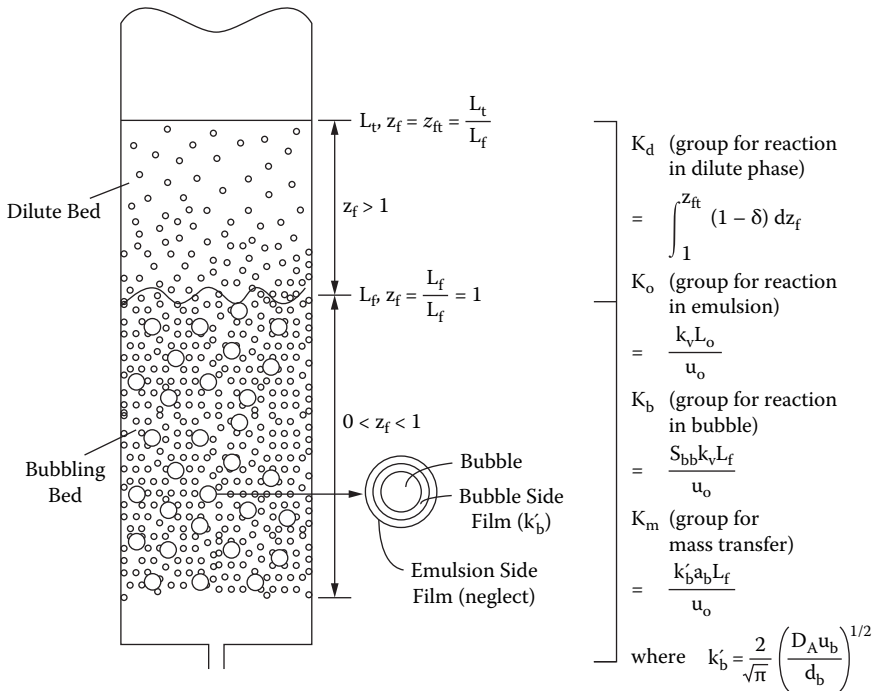


FIGURE CS5.3 Parameters of the Miyauchi model. (From Doraiswamy, L. K., 1991.)

immediately above the bed. This region is characterized by higher voidage and by an increase of this voidage with height (Lewis et al., 1962; Fan et al., 1962). The final equation is developed in terms of four dimensionless groups: for reaction in the emulsion phase (K_o), for reaction in the bubble phase (K_b), for mass transfer (K_m), and for reaction in the dilute phase above the bubbling bed (K_d) based on experimental voidage distribution data. K_m and K_o are combined into a single group K' . The various groups and their definitions are given in Figure CS5.3 (Doraiswamy, 2001), and the final equation may be written as

$$(1 - X_A) = \exp[-(K' + K_b + K_d)] \quad (\text{CS5.19})$$

where

$$\frac{1}{K'} = \frac{1}{K_m} + \frac{1}{K_o} \quad (\text{CS5.20})$$

Assigning numerical values,

$$K_m = k_{ob} a_b L_f / u_o \quad (\text{CS5.21})$$

The value of k_{ob} (the overall coefficient at the bubble-emulsion interface) can be calculated by an elaborate method described by Miyauchi and Marooka (1969) (see also Doraiswamy and Sharma, 1984), giving a value of 0.819 cm/s. Thus,

$$K_m = 4.7502$$

it is fully mixed, the Fryer–Potter model converts from a boundary value problem to an initial value problem (Jayaraman et al., 1981). This leads to considerable simplification in the calculations. All equations other than the emulsion phase equation remain unchanged. All mass balance equations can be readily written and solved (see Jayaraman et al., 1981). The conversion obtained is 88.98%.

Summary of Results

Model	Conversion, %
1. Davidson	88.10
2. Kunii–Levenspiel	77.90
3. Miyauchi	92.35
4. Fryer–Potter	92.35
5. Jayaraman–Kulkarni–Doraiswamy	88.98
Mean	87.93

Other Models: A Brief Discussion

The five models used in the design just presented do not differ greatly in predicting the exit conversion. The average deviation is 2.41% and the maximum is 4.57%. These deviations are not greatly significant, considering the many simplifying assumptions made. The assumption of a single effective bubble size is the most limiting. The values of the wake fraction used and the assumption of complete mixing or plug flow of gas are other serious drawbacks. It is likely that the gas is only partially mixed, which is difficult to accommodate in any design. The assumption of isothermicity is questionable for highly exothermic or endothermic reactions and is inconsistent with the plug-flow assumption, notwithstanding the role of solids mixing in eliminating temperature variations.

Models have been proposed that eliminate the constant bubble size assumption and allow for variation in size. Features of the major models now available have been summarized by Doraiswamy and Sharma, Table 14.3 (1984).

The assumptions discussed above are obvious. Many others are less so and are inherent in almost all fluid-bed models. The most important is with respect to particle size range. Most models do not account for this explicitly, except the K–L model, which gives different equations for fine, intermediate, and coarse particles (Kunii and Levenspiel, 1991). Our calculations for all the five models are for mainly Geldart B class particles and should generally be valid for the so-called fine and intermediate size particles. With the inherent uncertainties of prediction in all the models now available, a finer distinction is not warranted between these two classes of particles.

Except the Miyauchi model, the models considered do not account for conversion in the dilute phase. For really fast reactions with high velocities through the grid plate nozzles, conversion in the jetting region immediately above the grid plate should also be considered (see Figure 11.35). It has to be calculated separately, and it becomes the conversion used as the inlet to the bubbling bed region of any of the models now available. On the other hand, the conversion in the dilute phase is part of the overall calculation in the Miyauchi model considered in our calculations. Kunii and Levenspiel (1991) also suggest a procedure by which this can be included in their model.

An Overall Strategy

Several factors have to be considered in the design of a fluidized-bed reactor. The designs just considered did not include all factors as required for a more rigorous design (see Doraiswamy and Sharma, 1984; Doraiswamy, 2001; and Kunii and Levenspiel, 1999).

Lesson

Fluidized-bed reactor modeling has attracted considerable attention over the years, but there also has been an increasing realization that so many “unpredictables” are involved in the modeling that a realistic design from first principles is difficult. This case study examines five important available models. The chief lesson from this study is that, for a complicated reactor system like the fluidized-

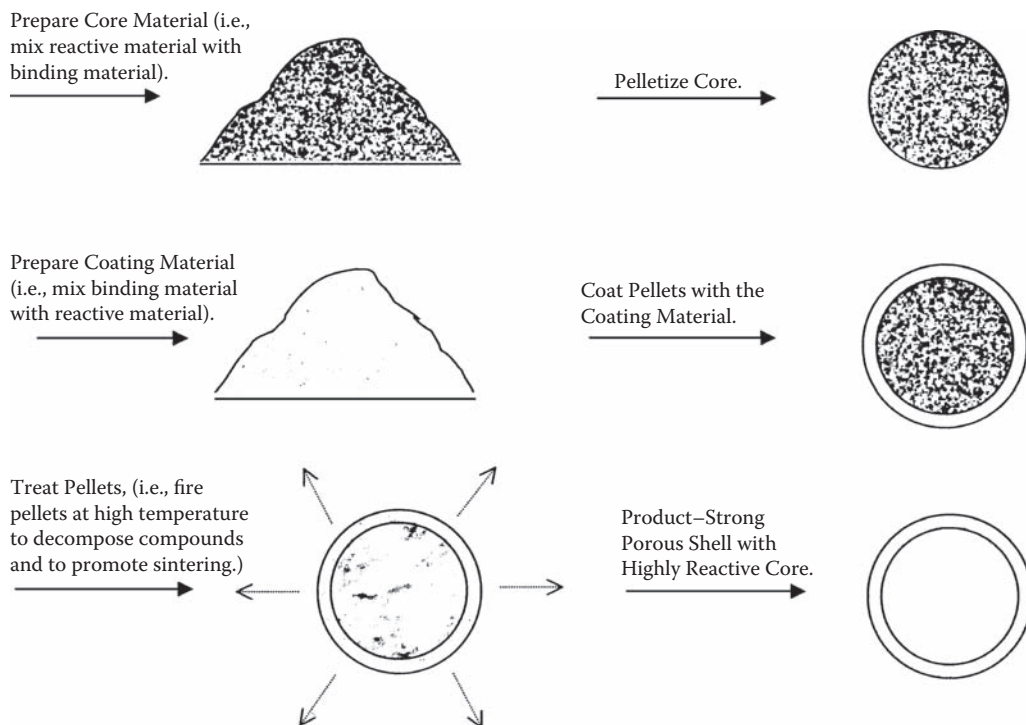
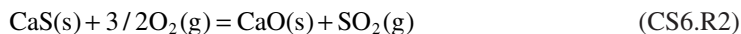


FIGURE CS6.1 A practical protocol for preparing core-in-shell pellets.

of larger entities into the required pellets at the expense of the smaller ones that get crushed). Based on these steps, a protocol for preparing CIS pellets is illustrated in Figure CS6.1.

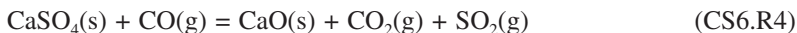
As mentioned earlier, a viable procedure for pellet regeneration is an integral part of pellet development. Several procedures have been suggested (e.g., Yoo and Steinberg, 1983; Chou and Li, 1984a, b; Illerup et al., 1993; van der Ham et al., 1996; Jagtap and Wheelock, 1996; Wheelock, 1997, 2000). The recommended procedure (Jagtap and Wheelock, 1996; Wheelock, 1997, 2000, 2004) essentially involves a cyclic operation alternating between oxidizing and reducing atmospheres in the reactor. During the oxidation process, CaS is converted to CaO according to the reaction



However, under the conditions of high temperature (650 to 1000 K) and excess oxygen existing in the reactor, the following reaction also occurs:



which is unfortunately the favored reaction, both thermodynamically and kinetically. The larger volume of the CaSO₄ causes pore plugging, eventually leading to an impenetrable layer around the reactive solid (CaO). However, the CaSO₄ can be converted back to CaO by treatment with CO according to the reaction



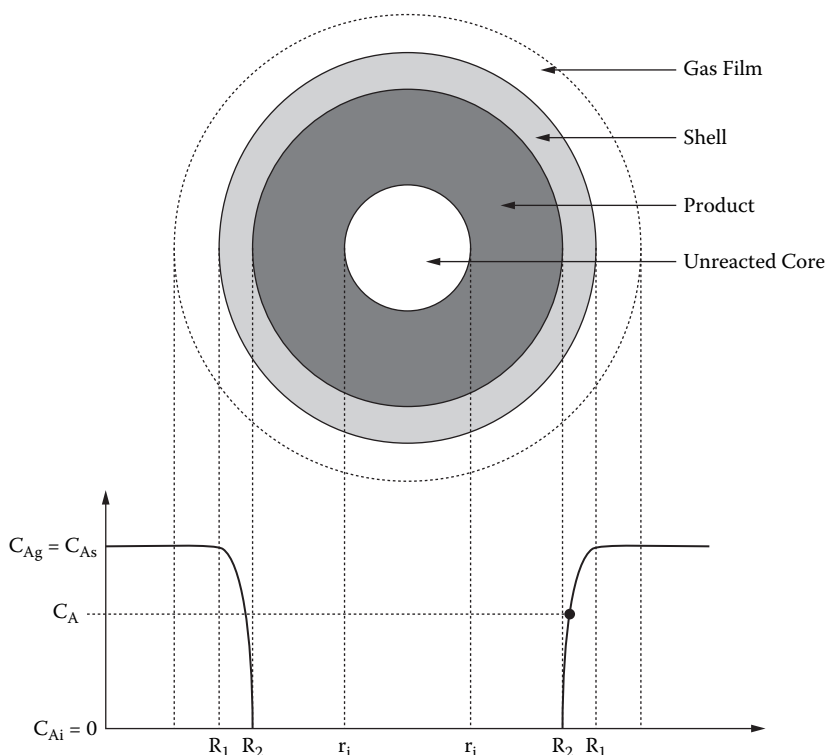


FIGURE CS6.4 A model for reaction in a CIS pellet assuming the shell acts as a separate phase offering pure mass transfer resistance.

design. A model can also be developed for the CIS pellet, but we use the simpler SIM (Akiti, 2001; Hasler et al., 2003).

Two simple extensions of SCM can be used to describe CIS behavior. The external shell is treated as a separate phase surrounding the pellet (Figure CS6.4) that offers one more step of pure mass transfer resistance with no reaction in addition to the fluid film. Akiti. (2001) used such a model to obtain an approximate fit of the data.

More recent studies by Hasler et al. (2003) showed, however, that the lime in the shell (see Figure CS6.2) reacts to the extent of 25% to 40%. The photograph shown in Figure CS6.5 suggests that one of the zone models described in Section 11.3.2.1.3 better describes the observed behavior. Since the zone thickness exhibits rapidly decreasing product density toward the core, one can, as a first approximation, assume SCM behavior with the ash and shell layers treated as separate layers as proposed by Akiti (2001). The outer shell acts as a “solid film.” Although this shell contains some lime that undergoes reaction, the amount is so small relative to that in the core that it can be neglected. Diffusion through the two layers (ash and shell) is the controlling resistance, with a small contribution from the fluid film surrounding the pellet. Further studies are needed, however, to verify the zone model (or the particle-pellet model).

Reactor Design

In Section 11.4.2, we discussed the three main categories of reactors that can be used for gas-solid reactions. Since the present system uses pellets of reasonable size, fluid-bed reactors can be ruled out. We shall therefore consider fixed- and moving-bed reactors. Two features of this system should first be noted:

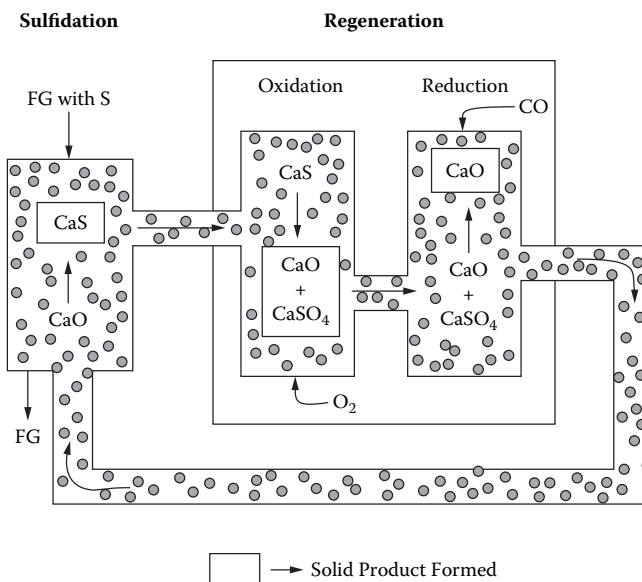


FIGURE CS6.6 A reaction-regeneration cycle into which a secondary regeneration cycle is embedded consisting of alternate cycles of oxidation and reduction.

be the best basis for designing the sulfidation reactor. A modification of the Westinghouse design was proposed by Colver et al. (2002), in which the gas and solids move countercurrently (as against the cocurrent flow in the original Westinghouse design); this modification is recommended here. This reactor differs from the conventional moving-bed reactor mainly with respect to the details of design, as brought out in Figures CS6.7a and b. The design equations given in Section 11.4.2.5.2

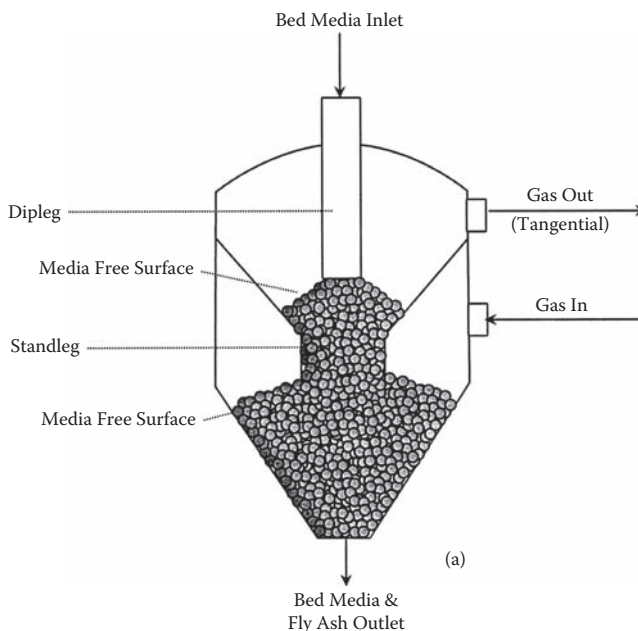


FIGURE CS6.7 Moving-bed reactor designs for the system at hand: (a) conventional design; and (b) a special design proposed by Colver et al. (2002). *Continued.*

encased in a hard outer shell (the so-called core-in-shell pellet). As in all kinetic analyses involving solid catalysts, the kinetic parameters determined experimentally hold only for that catalyst and for the feed of specified purity used; these parameters hold only for the sorbent developed for a particular coal. However, it must be noted that, in the preparation of the sorbent, any chloride compound should be avoided, since the released HCl would be harmful to the sorbent's life. CaO-based sorbents stabilize after 16 to 18 regenerations, with the value falling to about 60% of the original. Even so, it is quite economical to use this sorbent. The type of coal, including the maceral impurities, is of minor importance. The composition of the sorbent is the determining factor and works for many coals, provided compounds like chlorides are avoided. Hence, preliminary testing is always recommended.

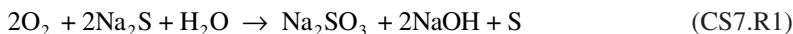
The kind of pellet developed in this study has implications outside the limits of its present use in coal gas cleaning. The core-in-shell concept a priori can be extended to reversible reactions where one of the products of reaction can be "adsorbed out" by the inner core while the reaction continues in the catalytic shell, thus increasing the conversion. The lesson is that novel solutions can be found for challenging problems and, equally important, they can often find applications in a variety of other situations, if only one keeps looking for possibilities.

CASE STUDY 11.7 GAS-LIQUID REACTION: AIR OXIDATION OF SODIUM SULFIDE (A SIMPLE REACTION WITH TYPICAL PROBLEMS OF GAS-LIQUID REACTIONS)

Nomenclature for Case Study 11.7

$[A]$	bulk concentration of solute gas (kmol/m ³)
$[A^*]$	saturation concentration of solute gas (kmol/m ³)
$[B]$	concentration of liquid phase reactant (kmol/m ³)
C_1	constant in Equation (CS7.38) (1/kmol)
C_p, C_v	heat capacities (kJ/kg °C)
D_A	diffusivity of component A (m ² /s)
D	column diameter (m)
D_D	diameter of downcomer (m)
D_R	diameter of riser (m)
d_N	nozzle diameter (m)
f_G	friction factor for gas flow in a pipe (—)
G	molar flow rate of gas (kmol/s)
g	acceleration due to gravity (m/s ²)
H	column height (m)
H_C	location of the downcomer sparger from the bottom (m)
H_D	height of dispersion (m)
H_W	Henry's coefficient for aqueous Na ₂ S solution (kmol/m ³ Pa)
h	height coordinate (m)
k_i	rate constant, $i = 1, 2, \dots$ (conc ¹⁻ⁿ /time)
k_L	true liquid-side mass transfer coefficient (m/s)
$k_L a$	volumetric liquid-side mass transfer coefficient (1/s)
L	volumetric liquid flow rate (m ³ /s)
L_c	length of the contactor (m)
N_N	number of nozzles
P	power consumption (W)
p_{O_2}	oxygen partial pressure (Pa)
P	pressure (Pa)
\bar{P}_T	average pressure in the column (Pa)
R_A	specific rate of absorption of A (kmol/m ² s)
$(Re)_G$	gas-phase Reynolds number (—)
$(Re)_L$	liquid-phase Reynolds number (—)
r_A	volumetric rate of absorption of A (kmol/m ³ s)

uously are to be considered: (1) bubble column, (2) sectionalized bubble column, (3) external loop air-lift reactor, (4) horizontal sparged contactor, (5) pipeline contactor, and (6) packed column. The operating conditions for each contactor are given at the appropriate places. The black liquor contains additional dissolved solids, which consume O_2 . Its properties are significantly different from those of an aqueous sodium sulfide solution. However, for illustration, we shall consider the oxidation of an aqueous sodium sulfide solution according to the following stoichiometric equation:



Data

The reaction is first order in both oxygen and sodium sulfide, rate constant k_2 at $75^\circ C = 4.64 \text{ m}^3/\text{kmol s}$ (there is some doubt about this constant, as it is dependent on several metal impurities; however, for the sake of illustration, this value is reasonably reliable), Henry's constant for O_2 in water at $75^\circ C = 7.2 \times 10^{-9} \text{ kmol/m}^3\text{Pa}$, Henry's constant for O_2 in Na_2S solution $H_w = 6.42 \times 10^{-9} \text{ kmol/m}^3\text{Pa}$ (at the average concentration), density of the solution $\rho_L = 1000 \text{ kg/m}^3$, vapor pressure of water at $75^\circ C = 3.87 \times 10^4 \text{ Pa}$ (290 mm Hg), diffusivity of O_2 in Na_2S solution at $75^\circ C = 6.8 \times 10^{-9} \text{ m}^2/\text{s}$.

1. Bubble Column (BC) (Countercurrent Operation)

Assumptions

The liquid phase is completely backmixed, and the gas phase moves in plug flow. The superficial velocity of the gas at the top of the column will be fixed at $5 \times 10^{-2} \text{ m/s}$. It may be further assumed that the value of $k_L a$ in the column is 0.04 s^{-1} and that of k_L is $2 \times 10^{-4} \text{ m/s}$. Fractional liquid holdup in the bubble column = 0.8. The values of ϵ_L , k_L , and a actually depend on superficial gas velocity (u_G), column diameter (D), column height (H), sparger design, the nature of the gas-liquid system, and operating pressure and temperature. At relatively low pressures ($<0.5 \text{ MPa}$), it is known (Deckwer, 1992; Joshi et al., 1998) that the values of ϵ_L , k_L , and a are independent of column diameter when D exceeds 0.15 (refer to Section 11.4.2.1.1). Furthermore, these are independent of column height and sparger design when H/D exceeds a certain critical value (3 for highly coalescing to 10 for highly noncoalescing systems). However, quantification of the nature of the gas-liquid system (and its variation with temperature and pressure) is not currently possible. Therefore, it is desirable to measure k_L and a in a small-scale bubble column ($D > 150 \text{ mm}$, $10 > H/D > 3$) using the same system and operating conditions (T and P). Such measurements are preferably made at least at four levels of u_G and three of T and P in the vicinity of the proposed operating conditions. In the present case study, it is assumed that the experiments were performed as indicated above and that, at the operating condition of u_G , T , and P under consideration, the values of ϵ_L , k_L , and a are 0.8, $2 \times 10^{-4} \text{ m/s}$, and $200 \text{ m}^2/\text{m}^3$, respectively.

Solution

The rate of oxygen absorption in aqueous Na_2S is assumed to be

$$R_A a = k_L a ([A]^* - [A]_b) \quad (CS7.1)$$

The conditions to be satisfied are

$$k_L a \approx \epsilon_L k_2 [B]_b \quad (CS7.2)$$

$$\sqrt{\frac{D_A k_2 [B]_b}{k_L}} \ll 1 \quad (CS7.3)$$

$$\begin{aligned}
 & y_0 \exp \left[-\frac{\beta}{2\psi} (1 + \psi H_D)^2 \right] - y_e \exp \left[-\frac{\beta}{2\psi} \right] \\
 & + \frac{v}{H_D} \sqrt{\frac{\pi}{2\beta\psi}} \left[\operatorname{erf} \left(\sqrt{\frac{\beta}{2\psi}} (1 + \psi H_D) \right) - \operatorname{erf} \left(\sqrt{\frac{\beta}{2\psi}} \right) \right] = 0
 \end{aligned}
 \tag{CS7.13}$$

Here we have $L = 2.32 \times 10^{-3} \text{ m}^3/\text{sec}$, $[B]_0 = 0.154 \text{ kmol/m}^3$, and $[B]_e = 6.4 \times 10^{-3} \text{ kmol/m}^3$.

The amount of oxygen provided is 200% in excess of the stoichiometric requirement. We also assume that G remains constant. Therefore, $y_e = 2/3 \times 0.21 = 0.14$.

The overall material balance can be written as

$$G(y_0 - y_e) = \frac{L}{Z} ([B]_0 - [B]_e) \tag{CS7.14}$$

Substituting the relevant values, we determine $G = 4.89 \times 10^{-3} \text{ kmol/s}$. From the values

$$\epsilon_L k_2 [B]_e = 0.0238 \text{ s}^{-1}, \quad k_L a = 0.04 \text{ s}^{-1}, \quad \text{and} \quad \sqrt{\frac{\mathbf{D}_A k_2 [B]_e}{k_L}} = 0.071$$

we note that the condition given by Equations (CS7.2) and (CS7.3) is satisfied. The superficial gas velocity at the top of the column $= 5 \times 10^{-2} \text{ m/s}$.

The gas phase also contains water vapor. It is assumed that relatively small amounts of Na_2S do not alter the vapor pressure characteristics of water. Furthermore, the increase in the concentration of Na_2S due to the evaporation of water may be neglected, as the rate of evaporation of water is about 1.75% of the liquid flow rate.

Therefore, the overall volumetric gas flow rate at the outlet is given by

$$4.89 \times (760/470) \times (348/273) \times 22400 = 22.59 \times 10^4 \text{ cm}^3/\text{s} = 0.2259 \text{ m}^3/\text{s}$$

Hence, the cross-sectional area of the bubble column, $S = (0.2259/5 \times 10^{-2}) = 4.52 \text{ m}^2$. Therefore, $D = 2.4 \text{ m}$.

We thus have

$$P_T = \frac{760 - 290}{760} = 0.618 \text{ atm} = 6.26 \times 10^4 \text{ Pa}, \quad \beta = \frac{k_L a H_w P_T S}{G} = 1.49 \times 10^{-2}$$

$$\psi = \frac{\epsilon_L \rho_L g}{P_T} = 0.125, \quad v = \frac{k_L a (y_0 - y_e)}{\epsilon_L k_2 [B]_e} = 0.118$$

After substituting the relevant values, Equation (CS7.13) was solved by trial and error to give $H_D = 29.1 \text{ m}$.

Due to the foaming nature of the black liquor, the value of $k_L a$ is likely to be higher than 0.04 s^{-1} at a u_G of $5 \times 10^{-2} \text{ m/s}$. The problem is reworked for a value of $k_L a$ equal to 0.12 s^{-1} at $u_G = 5 \times 10^2 \text{ m/s}$ and the value of H_D found to be 30.0 m . The height of the column changes little with such a large correction of $k_L a$. When $H_D = 29.1 \text{ m}$, $\epsilon_L = 0.8$, and $\rho_L = 1000 \text{ kg/m}^3$, the total pressure at the bottom (P_B) is $2.28 \times 10^5 \text{ Pa}$. As a result, the oxygen partial pressure at the bottom ($p_{\text{O}_2}_B$) =

liquor usually contains considerable suspended impurities). The sectionalized bubble column is shown schematically in Figure 11.21c.

For the n th section of the sectionalized bubble column, the relationship between y_n and y_{n+1} can be obtained from Equation (CS7.13) as

$$y_{n+1} \exp \left[-\frac{\beta}{2\psi} (1 + \psi H_D)^2 \right] - y_n \exp \left(-\frac{\beta}{2\psi} \right) + \Gamma \left(\frac{y_{n+1} - y_n}{[B]_{b_n}} \right) = 0 \quad (\text{CS7.15})$$

where

$$\Gamma = \frac{k_L a}{\varepsilon_L k_2 H_D} \sqrt{\frac{\pi}{2\beta\psi}} \left[\operatorname{erf} \left(\sqrt{\frac{\beta}{2\psi}} (1 + \psi H_D) \right) - \operatorname{erf} \left(\sqrt{\frac{\beta}{2\psi}} \right) \right] \quad (\text{CS7.16})$$

Material balance for the n th section gives

$$y_{n+1} - y_n = \frac{L}{zG} ([B]_{b_{n-1}} - [B]_{b_n}) \quad (\text{CS7.17})$$

Substitution of y_{n+1} from Equation (CS7.17) into Equation (CS7.15) and subsequent rearrangement gives

$$\lambda_1 [B]_{b_n}^2 - [B]_{b_n} (\lambda_1 [B]_{b_{n-1}} + \lambda_2 y_n - 1) - [B]_{b_{n-1}} = 0 \quad (\text{CS7.18})$$

where

$$\lambda_1 = \frac{1}{\Gamma} \exp \left(-\frac{\beta}{2\psi} (1 + \psi H_D)^2 \right) \quad (\text{CS7.19})$$

$$\lambda_2 = \frac{zG}{L\Gamma} \left(\exp \left[-\frac{\beta}{2\psi} (1 + \psi H_D)^2 \right] - \exp \left(-\frac{\beta}{2\psi} \right) \right) \quad (\text{CS7.20})$$

Equation (CS7.18) can be solved for $[B]_{b_n}$ to give

$$[B]_{b_n} = \frac{(\lambda_1 [B]_{b_{n-1}} + \lambda_2 y_n - 1) + \sqrt{(\lambda_1 [B]_{b_{n-1}} + \lambda_2 y_n - 1)^2 + 4\lambda_1 [B]_{b_{n-1}}}}{2\lambda_1} \quad (\text{CS7.21})$$

Procedure for the Design of a Sectionalized Bubble Column

1. Calculate the area of cross section of the column from a consideration of superficial gas velocity.
2. Choose a suitable height for the section.

$$u_L = [2(\epsilon_{GR}H_D - \epsilon_{GD}H_C)g]^{0.5} \quad (\text{CS7.24})$$

Solving the above equations simultaneously yields the values of fractional gas holdup for the riser as well as the downcomer, the liquid velocity, and the height of critical location of the sparger from the bottom. The downcomer sparger is located 5.4 m from the bottom. Since $H_D = 15.3$ m, the diameter of the downcomer and riser ($D_D = D_R$ assumed) was found in such a way that the total gas volume in EL-ALR equals that in the bubble column of case 2 in Table CS7.3. As a result, we get $D_R = D_D = 1.88$ m. It may be noted that the procedure has been considerably simplified. For rigorous calculations, see Lele and Joshi (1993).

4. Horizontal Sparged Contactor (HSC)

For all other contactors considered previously, we have used 200% excess oxygen. Hence, the gas utilization efficiency in these contactors is low. Let us consider a horizontal sparged contactor, which has the advantage of low pressure drops. The following assumptions are made: the liquid phase is completely backmixed, and the average pressures can be used (since the pressure drop is small).

The following dimensions may be considered: diameter of the contactor = 5 m, liquid submergence = 4 m, nozzle spacing = 0.5 m, distance of the nozzle tips from the bottom of the contactor = 0.2 m.

The material balance for oxygen can be written as

$$Gdy = k_L a ([A]^* - [A]_b) dV_D \quad (\text{CS7.25})$$

$$= k_L a (H_w \bar{P}_T y - [A]_b) dV_D \quad (\text{CS7.26})$$

The direction of V_D has been taken as the direction of increasing y . Integration of Equation (CS7.26) gives

$$V_D = \frac{G}{k_L a H_w \bar{P}_T} \ln \left[\frac{H_w \bar{P}_T y_0 - [A]_b}{H_w \bar{P}_T y_e - [A]_b} \right] \quad (\text{CS7.27})$$

$[A]_b$ can be obtained from an overall material balance as

$$G(y_0 - y_e) = \frac{L}{Z} ([B]_0 - [B]_e) = V_D \epsilon_L k_2 [A]_b [B]_e \quad (\text{CS7.28})$$

Eliminating $[A]_b$ between Equations (CS7.27) and (CS7.28) gives

$$V_D = \frac{G}{k_L a H_w \bar{P}_T} \ln \left[\frac{y_0 - \frac{\delta}{V_D} ([B]_0 - [B]_e)}{y_e - \frac{\delta}{V_D} ([B]_0 - [B]_e)} \right] \quad (\text{CS7.29})$$

where

$$\delta = L / (\epsilon_L Z k_2 H_w \bar{P}_T [B]_e)$$

5. Pipeline Contactor (PC)

Data

Pure oxygen, 20% in excess over the theoretical requirement; operating pressure = 3.04×10^5 Pa, absolute; liquid-side Reynolds number = 40,000 (to keep the two-phase flow patterns as froth); liquid-side mass transfer coefficient at the entrance ($u_G = 0.127$ m/s, $u_L = 0.077$ m/s); $k_L a = 0.12$ s⁻¹.

Assumptions

The two-phase flow pattern (in this case, froth) does not change along the length of the pipeline. The liquid-side mass transfer coefficient varies linearly with the superficial gas velocity at a constant liquid flow rate. As indicated later, the pressure drop can be neglected.

The fractional liquid holdup can be calculated by the procedure proposed by Lockhart and Martinelli (1949). The values of fractional liquid holdup are calculated to be 0.5 at the inlet ($u_G = 0.127$ m/s, $u_L = 0.077$ m/s) and 0.7 at the outlet ($u_G = 0.0212$ m/s, $u_L = 0.077$ m/s). The following correlation is assumed to hold for ϵ_L :

$$\epsilon_L = -585G + 0.74 \quad (\text{CS7.32})$$

Overall material balance between the inlet and the location where oxygen flow rate is G gives

$$G_0 - G = \frac{L}{Z}([B]_0 - [B]) \quad (\text{CS7.33})$$

or

$$[B] = [B]_0 - \frac{Z}{L}(G_0 - G) \quad (\text{CS7.34})$$

The material balance for a differential length dz , z cm away from the entrance, gives

$$-dG = R_A a S dz \quad (\text{CS7.35})$$

The values of $k_L a$ and $\epsilon_L k_2 [B]$ are comparable at the entrance and at the exit, as shown below.

	$k_L a$ (s ⁻¹)	$\epsilon_L k_2 [B]$ (s ⁻¹)
Entrance	0.12	0.357
Exit	0.02	0.0208

Under these conditions, the rate of absorption of oxygen is calculated by the following equation:

$$R_A a = [A]^* \left[\frac{1}{\frac{1}{k_L a} + \frac{1}{\epsilon_L k_2 [B]}} \right] \quad (\text{CS7.36})$$

Substitution of Equation (CS7.36) in Equation (CS7.35) gives

The oxygen supplied is 20% in excess of the theoretical requirement. Therefore,

$$G_o = 0.41 \times 10^{-3} \text{ kmol/s and } G_e = (0.41 - 0.342) \times 10^{-3} = 0.068 \times 10^{-3} \text{ kmol/s}$$

It is given that the Reynolds number of the liquid = 40,000 and the viscosity of the solution at 75°C = 0.38×10^{-3} Pa·s.

Therefore, diameter of pipeline = 0.197 m; cross-sectional area, $S = 0.031 \text{ m}^2$. At the entrance, $k_L a = C_1 G_o = 0.12 \text{ s}^{-1}$, $G_o = 0.41 \times 10^{-3}$; therefore $C_1 = 293.68$, and

$$\begin{aligned}\delta' &= L \left([B]_0 - \frac{ZG_0}{L} \right) \\ &= -5.27 \times 10^{-5}\end{aligned}$$

$$\begin{aligned}[A]^* &= (P - P_{\text{H}_2\text{O}}) H_w \\ &= 1.703 \times 10^{-3} \text{ kmol/m}^3 \\ v' &= L / [k_2 (0.74 + 585\delta')] \\ &= 0.705 \times 10^{-3}\end{aligned}$$

Substitution of the relevant values in Equation (CS7.43) gives

$$z_t = 170 \text{ m}$$

In the above case of a pipeline contactor, pure oxygen is used instead of air. The excess of unreacted oxygen, which comes out of the pipeline contactor, can be compressed and reused with the fresh oxygen feed.

Let us consider the use of a large excess of oxygen to reduce the length of the contactor. The above problem is reworked for the case of 250% excess oxygen over the theoretical requirement:

$$G_0 = 1.197 \times 10^{-3} \text{ kmol/s, } G_e = 0.855 \times 10^{-3} \text{ kmol/s}$$

The values of fractional liquid holdup, ϵ_L , at the inlet and exit are found to be 0.37 and 0.43, respectively. For this case, ϵ_L can be assumed to be constant and equal to the average value of 0.4.

Following the same procedure as per Equations (CS7.35) through (CS7.44), the length of the contactor can be obtained from the following equation:

$$z_t = \frac{1}{S[A]^*} \ln \left[\left(\frac{G_0}{G_e} \right)^{\frac{1}{C_1}} \left(\frac{\delta' + G_0}{\delta' + G_e} \right)^{v''} \right] \quad (\text{CS7.45})$$

where

$$\begin{aligned}v'' &= L / (\epsilon_L k_2) = 1.25 \times 10^{-3}, \quad C_1 = 292.68 \\ \delta' &= L \{ [B]_0 - (ZG_0 / L) \} = -0.84 \times 10^{-3}\end{aligned}$$

$$\gamma = y_e + \alpha'[B]_0 \quad (\text{CS7.49})$$

Material balance across a differential height dh of the column gives:

$$\frac{L}{Z} d[B] = R_A a S dH \quad (\text{CS7.50})$$

At the top of the column,

$$\epsilon_L k_2 [B]_0 = 0.0715 \text{ s}^{-1}; \quad k_L a = 0.005 \text{ s}^{-1} \quad \text{and} \quad \sqrt{M} = 1.39; \quad \epsilon_L = 0.1$$

where

$$\sqrt{M} \text{ is } \sqrt{\mathbf{D}_A k_2 [B]_0} / k_L$$

From the above values, it can be seen that

$$k_L a \ll \epsilon_L k_2 [B]_0 \quad (\text{CS7.51})$$

and

$$\sqrt{M} = 1 \quad (\text{CS7.52})$$

At the bottom of the column,

$$\epsilon_L k_2 [B]_e = 2.98 \times 10^{-3} \text{ s}^{-1}, \quad k_L a = 0.005 \text{ s}^{-1}, \quad \sqrt{M} = 0.284$$

Therefore,

$$k_L a = \epsilon_L k_2 [B]_0, \quad \sqrt{M} \ll 1 \quad (\text{CS7.53})$$

Based on Equations (CS7.51) and (CS7.52) at the top of the column, the reaction falls in between regimes 1, 2, and 3. From Equation (CS7.53), at the bottom of the column, the reaction falls in between regimes 1 and 2. Thus, the following equation holds for $R_A a$ in the entire column:

$$R_A a = a[A]^* \left[\frac{1}{\frac{1}{\sqrt{\mathbf{D}_A k_2 [B] + k_L^2}} + \frac{a}{\epsilon_L k_2 [B]}} \right] \quad (\text{CS7.54})$$

Substituting $R_A a$ from Equation (CS7.54) into Equation (CS7.50) and using Henry's law ($[A^*] = H_w P_A$), we get

Hence, $S = 3.652 \text{ m}^2$, and $D = 2.16 \text{ m}$.

$$\alpha' = L/(ZG) = 0.293, \quad \gamma = y_e + \alpha'[B]_0 = 0.1319$$

$$\beta^* = \left[ZaSH_w Pr \sqrt{D_A k_2} \right] / L = 9.85 \times 10^{-3}$$

$$\delta_1 = k_L / \left(\sqrt{D_A k_2} \right) = 0.281$$

$$\delta = \left(a \sqrt{D_A k_2} \right) / (\epsilon_L k_2) = 0.038$$

Substituting the relevant values in Equation (CS7.59), H can be calculated and is found to be 469 m, i.e., an abnormally large packed column. Such a column provides very low liquid holdup (0.03 to 0.1), and the present oxidation reaction occurs in the liquid phase. Therefore, a packed column should be rejected.

A comparison of all the equipment is presented in Table CS7.3. For all the cases, the reactor volume and power consumption are given. The former indicates the capital cost, whereas the latter indicates the operating cost. A preliminary comparison reveals that SBC and EL-ALR are comparable but superior to the conventional BC. The volume of HSR is approximately 5.4 to 5.8 times higher than SBC or EL-ALR. However, the power consumption is low (0.25 and 0.362 times lower, respectively). Although the power consumption of the PC is very low, the capital cost of the packed volume would be prohibitive.

Lesson

This case study on oxidation of sodium sulfide illustrates the design of a variety of gas-liquid reactors and compares their performances. Bubble column reactors are particularly attractive, as they offer advantages such as simplicity of construction and operation, but they suffer from such drawbacks as high pressure drop and backmixing in the liquid phase. To reduce the pressure drop, two modifications have been considered: an external-loop air-lift reactor and a horizontal sparger reactor. Both result in substantial energy savings (because of low ΔP) under similar conditions of capacity and conversions in the gas and liquid phases.

The other limitation of liquid-phase backmixing has been addressed through the modification of sectionalization. In this manner, near plug-flow behavior is achieved, and the column height is reduced to as much as 60%. The reduction in height reduces the equivalent pressure drop and hence the energy consumption for air compression.

The case study demonstrates yet another peculiar behavior of bubble columns: steep reduction in oxygen partial pressure from bottom to top, mainly a result of the change in total pressure due to hydrostatic head. Such a situation results in column underutilization. To overcome this problem, guidelines have been given, with detailed calculations indicating substantial savings.

The effects of a few other important parameters have also been considered, but the study should be extended to include investigation of all of them. Cost considerations in selecting parameters such as temperature, pressure, excess oxygen, height-to-diameter ratio, and so forth play an important role in final selection. Cost implications in the design and selection of downstream equipment also constitute a major factor. The philosophy and details of design outlined above for bubble columns should be extended to include other gas-liquid reactors. For instance, for packed columns, the type, size, and cost of different packings (offered by different vendors) should be examined by careful selection of liquid distributors, redistributors, and packing supports.

A practically useful table, presented in Section 11.4 (Table 11.26), provides valuable guidelines for the selection of gas-liquid reactors. Other reactor configurations should be considered and a table similar to Table 11.26 prepared.

temperatures requiring significant refrigeration. The rate of heat removal due to vaporization of a liquid refrigerant (often ammonia) can be used advantageously in the top section, where the rate of oxidation is very low. Most heat is usually removed in the bottom section of the column by the ambient water. Hence, the operating temperature is decided by the ambient temperature, and the optimum heights for empty section and submergence section can be selected rather directly. However, the optimum temperature and pressure depend on the geographical location of the nitric acid plant and the cost of power. The costs will be considered in the optimum design strategy.

Optimum Design

The total cost (\$/day) was estimated at two levels of outlet NO_x concentration, 700 and 150 ppm. The sensitivity of fixed cost was studied by assuming stainless steel prices at two levels: \$3.52/kg and \$7.04/kg. The results are in Tables 9A and 9B for different combinations of weir and empty section heights at five levels of total pressure, 0.4, 0.71, 1.01, 1.31, and 2.02 MPa. As indicated, pressure is a major parameter governing the fixed cost. To understand the overall effect of fixed and operating costs, the daily contribution was estimated on the basis of 25 and 45% of the fixed cost as the yearly (300 days) expenditure. For this case, 95% of the compressor energy was assumed to be recoverable, i.e., 5% of the cost of compression was included in the operating cost. The analysis was performed at a height of 0.025 m, with empty section height as parameter. The results are shown in Figures 6A and 6B for 700-ppm, and in Figures 6C and 6D for 150-ppm, outlet concentration. The following observations can be noted: (1) For empty heights of 0.4 and 0.7 m, the total cost decreases monotonically with increase in pressure. The reduction is sharp up to 1 MPa and thereafter minimal. (2) For empty heights of 1.5, 4, and 10 m, the total cost curves show minima. The curve for 1.5 m is shallow, whereas it is deep for 10 m and in between for 4 m. The optimum pressure decreases with an increase in empty height. However, it must be emphasized that the optimum costs (at minima) for 4- and 10-m empty heights are higher than those for 0.4-, 0.7-, and 1.5-m empty heights. (3) The total costs for three empty heights (0.4, 0.7, and 1.5 m) are comparable-being in the range 0.7 to 1.0 MPa. (4) The optimum plate spacing depends on the fixed cost components. For instance (from Figures 6E and 6F of the original reference), at 0.4 MPa pressure, the total cost is minimum for 4-m empty height. With an increase in pressure, the optimum height decreases. Thus, the optimum heights are 1.5, 0.7, and 0.4 m at pressures of 0.7, 1.0, and 1.3 MPa, respectively. Suchak and Joshi (1994) and Pradhan et al. (1997) have examined the effects of mass transfer characteristic and residence time on the designs of packed and plate column.

Lesson

Examples of simple reactions (such as considered in Case Study 11.7) are not hard to find in industry, but those of complex reactions are more widespread. One can envisage systems with increasing complexities such as the manufacture of nitric acid. The complexities include the following: (1) multiple (parallel) reactions by the same reactant, (2) reactions in series, (3) multiple reactions among multiple reactants, (4) reversible reactions, (5) reactions in multiple phases, and (6) simultaneous mass transfer with chemical reactions. These complex problems can be tackled if sufficient details of the following are provided: (1) reaction chemistry, (2) rate expressions, (3) rate constants, and (4) diffusivities and solubilities in the case of multiphase systems. The kinetics of each reaction can be determined in the laboratory by (1) ensuring conditions that make the desired step rate controlling and (2) minimizing/suppressing the other reactions. In some cases, lumped parameters such as $H\sqrt{kD}$ can be obtained and used directly.

Although one can progressively account for one additional complexity at a time, it is also possible to take a direct leap to a problem with a combination of complexities, as illustrated in this case study on NO_x absorption in the manufacture of nitric acid. The NO_x absorption system may contribute about 40% of the total equipment cost. Hence, optimal design of the NO_x absorption tower is important; major cost-determining factors should be identified and selectively addressed with greater rigor.

Data

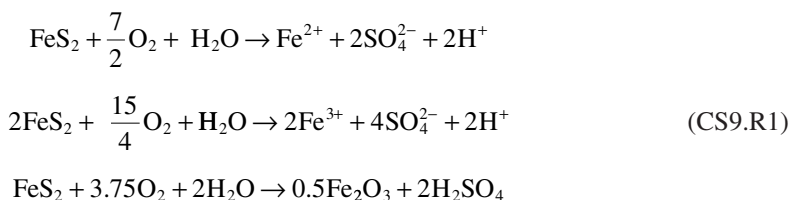
The reaction temperature and the water vapor pressure are 466 K and 1.36 MPa, respectively. The coal particle size is 100 μ m. At the operating temperature of 460 K and in the range of H₂SO₄ concentrations encountered in oxydesulfurization, the vapor pressure of sulfuric acid is below 1×10^{-2} Pa. The operating pressure is in the range of 2 to 7 MPa, and thus most of the sulfuric acid will remain in the liquid phase. For simplicity, all the sulfur is assumed to be in the form of FeS₂ (content = 2.7 wt% of coal). The bulk density of coal is 889 kg/m³ and of water for making the slurry is 1000 kg/m³. The slurry concentration is 26 wt%.

Determination of the Rate-Controlling Step

The steps during the process of oxydesulfurization are as follows:

1. Transfer of oxygen through the gas-liquid film
2. Transfer of oxygen through the liquid-solid film
3. Diffusion of oxygen through the ash layer
4. Chemical reaction between the dissolved oxygen and FeS₂ at the solid surface

The mechanism of oxydesulfurization of coal has been extensively investigated by Vracar et al. (1970), Friedman and Warzinski (1977), Vetter (1967), and Joshi et al. (1982). The dissolution of sulfide minerals can be interpreted as an electrochemical surface reaction similar to the corrosion of metals. Oxygen is reduced at cathodic areas, and sulfides are dissolved liberating electrons to complete the couple.



To determine the rate-controlling step, it is necessary to study all of the four possibilities by experiments over a wide range of particle sizes, temperatures, pressures, and impeller speeds.

The overall reaction may be represented by the shrinking core model (SCM). Laboratory-scale experiments were carried out in a 1-L vessel in the temperature range of 428 to 488 K and total air pressure range of 3.44 to 7.88 MPa. Coal particles of practically uniform size were used for the experiments, and coal loading was varied over a range of 0.025 to 0.22 kg/L of water. The experiments were carried out by changing the stirrer speed, and it was observed that, above a certain critical speed (N_c), the rate was independent of the speed. Therefore, the gas-liquid and liquid-solid mass transfer resistances can be considered to be negligible when the stirrer speed is higher than N_c . Thus, the process becomes either ash diffusion controlled or chemical reaction controlled. The experiments over the temperature range mentioned enabled the estimation of the energy of activation, which was found to be 46.5×10^6 J/kmol. The value of activation energy indicates that the overall operation is reaction controlled. The reaction order with respect to oxygen was found to be 0.7 (for reasons reported by Joshi et al., 1981).

To get supporting evidence for the earlier conclusion of the reaction-controlled operation, the fractional conversion of FeS₂ (in coal) with time was studied, and the time required for complete conversion was also obtained. The following SCM relationships were used (see Section 11.3.2.1.1) to determine the controlling mechanism. For ash diffusion control,

The residence time distribution is obtained by solving the following material balance equation for a tracer:

$$\frac{\partial c}{\partial \theta} = \frac{1}{Pe} \frac{\partial^2 c}{\partial Z^2} - \frac{\partial c}{\partial Z} \quad (\text{CS9.5})$$

where c is the dimensionless concentration, and other dimensionless parameters are

$$Z = z/L, \quad e = \frac{L u_{SL}}{(1 - \epsilon_G) D_s}, \quad \theta = \frac{t u_{SL}}{L(1 - \epsilon_G)} \quad (\text{CS9.6})$$

The boundary conditions are

$$\begin{aligned} c_0 = c|_{0^-} &= c|_{0^+} - \frac{1}{Pe} \frac{\partial c}{\partial Z} \Big|_{0^+} \text{ at } Z = 0 \quad \text{for all } \theta \\ \frac{\partial c}{\partial Z} &= 0 \text{ at } Z = 1, \quad \text{for all } \theta \\ c &= 0 \text{ at } \theta = 0, \quad \text{for all } Z \end{aligned} \quad (\text{CS9.7})$$

The parameters are

$$\int_0^\infty c dt = \int_0^\infty (C/Q) dt = 1 \quad (\text{CS9.8})$$

and

$$Q = \int_0^\infty C dt \quad (\text{CS9.9})$$

where C is the actual concentration at the exit, and Q is the amount of pulse tracer. When solved in dimensionless form, the exit age distribution is given as

$$E(\theta) = 2 \exp(Pe/2) \sum (-1)^{r+1} \exp(T_r, \theta) \frac{b_r^2}{\frac{4}{Pe} + 1 + b_r^2} \quad (\text{CS9.10})$$

where b_r is the root of

$$b_r = \tan \left(r \frac{\pi}{2} - \frac{Pe b_r}{4} \right) \quad \text{and} \quad T_r = \left(-\frac{Pe}{4} \right) (1 + b_r^2)$$

For the case of continuous feed of particles to a bubble column slurry reactor, with an exit age distribution of particles $E(\theta)$, a mass balance gives

2. For obtaining the time required for the desired fractional conversion (99%), Figure CS9.1 can be used over a range of Pe numbers. For example, for $Pe = 0.3$, the ratio of residence time to the time required for complete conversion can be seen to be 6.75.
3. Since $\tau = 1160$ s, the average residence time (\bar{t}) becomes 7830 s. The reactor volume is obtained by taking the product of the average residence time and the average flow rate ($0.00458 \text{ m}^3/\text{s}$) and is 35.88 m^3 . This is a slurry volume. If the fractional gas holdup is 5%, and the gas space (over the dispersion) is 20%, the reactor volume is 45.2 m^3 .
4. The volumetric gas flow rate is $8.66 \times 10^{-3} \text{ m}^3/\text{s}$. If we select a superficial gas velocity of 5 mm/s, the cross-sectional area is 1.766 m^2 , and $D = 1.5$ m. For the reactor volume of 45.33 m^3 , total height (H) = 25.6 m, and the height of dispersion (H_D) = 21.33 m, which leaves 20% for the gas space. The superficial slurry velocity is obtained from

$$u_{SL} = H(1 - \epsilon_G) / \bar{t} = 0.00259 \text{ m/s} \quad (\text{CS9.12})$$

5. For given superficial gas and liquid velocities as well as temperature and pressure, the fractional gas holdup (and also other design parameters) depends on the nature of the gas-liquid systems. Fortunately, the value of ϵ_G is independent of column diameter if the operating regime remains unchanged. For the ranges of u_G , u_L , P , and T under consideration, the regime of operation is homogeneous (for further details, refer to Deckwer, 1992; Joshi et al., 1998). Therefore, it is usually recommended that a few experiments be performed in a small-scale column (at least 150 mm I.D.) in the ranges of interest of u_G , u_L , P , and T as used for large-scale columns. For the present values of these variables, let ϵ_G be 0.05 and the slip velocity 0.1 m/s.
6. Similar to ϵ_G , the dispersion coefficient also depends on the nature of the gas-liquid system. Therefore, it is recommended that the dispersion coefficient be estimated in a small-diameter column. Furthermore, the literature correlation is accepted except for the proportionality constant, which is estimated using the results from 150-mm I.D. column and for the system under consideration.

Let the resulting correlation be

$$\mathbf{D}_s = 326 \left[\frac{DS_{wb}\epsilon_G u_s}{1 - \epsilon_G - S_{wb}\epsilon_G} \right]^{1.7} \quad (\text{CS9.13})$$

where S_{wb} is the ratio of wake to bubble volumes. Kumar and Kuloor (1970) have recommended $S_{wb} = 11/16$. For $\epsilon_G = 0.05$ and $u_s = 0.1$ m/s, \mathbf{D}_s works out to be $0.0489 \text{ m}^2/\text{s}$.

7. The estimated values of the dispersion coefficient can be used to calculate the Peclet number as

$$Pe = \frac{H_D u_{SL}}{(1 - \epsilon_G) \mathbf{D}_s} = \frac{21.39 \times 0.00259}{0.95 \times 0.0489} = 1.19 \quad (\text{CS9.14})$$

8. From Figure CS9.1, it can be seen that, for an overall average conversion of 99% at $Pe = 1.19$, \bar{t}/τ is 3.18. Therefore, $\bar{t} = 3683$ s and slurry volume = 16.87 m^3 and the reactor volume is 45.29 m^3 . Let us select, $D = 1.5$ m, $H = 25.63$ m, $H_D = 21.36$ m. Substitution of these values in Equation (CS9.14) gives $Pe = 1.19$ which is different from the starting

N_{JSG}	critical speed for solid suspension in presence of gas (rps)
N_{\max}	maximum operating speed (rps)
n	moles of CO_2 required (kmoles)
P	total pressure (N/m^2)
p_x	partial pressure of component x (N/m^2)
PDN	production (kg)
\mathbf{P}_O	power number (–)
\mathbf{P}_G	power consumption in presence of gas (W)
\mathbf{P}_L	power consumption in absence of gas (W)
Q	volumetric flow rate of gas (m^3/s)
R_A	specific rate of absorption of A ($\text{kmol/m}^2 \text{ s}$)
Re_p	particle Reynolds number (–)
R_g	universal gas constant ($\text{J}/(\text{kgmol K})$)
r_A	rate of reaction ($\text{kmol/m}^3 \text{ s}$)
S	cross-section of reactor (m^2)
Sc	Schmidt number, $\mu_L/\rho_L \mathbf{D}_B$ (–)
Sh	Sherwood number, $k_{SL}d_p/D_{AB}$ (–)
T	temperature (K)
\mathbf{T}	reactor diameter (m)
u	superficial velocity (m/s)
u_c	circulation velocity (m/s)
u_G	superficial gas velocity (cm/s)
u_{G0}	superficial gas velocity at the inlet (m/s)
$u_{S\infty}$	terminal settling velocity of particle (m/s)
V_D	volume of dispersion (m^3)
V_S	volume of solids (m^3)
W	blade width (m)
X_S	percentage solid loading (%)
x	mol CO_2 /mol inerts (–)
x_1	mole of CO_2 /mole of inerts at the inlet (–)
Z	stoichiometric coefficient (–)

Greek

α	constant defined in Equation (CS10.4) (–)
α_1	constant defined in Equation (CS10.3) (–)
β	term defined in Equation (CS10.12) (–)
β_1	constant defined in Equation (CS10.3) (–)
ϵ_G	gas holdup (–)
ϵ_L	liquid holdup (–)
ϵ_S	solid holdup (–)
ϵ_{S0}	initial solids holdup (–)
γ_P	number of particles per unit volume ($1/\text{m}^3$)
η	enhancement factor defined by Equation (CS10.11) (–)
μ_L	viscosity of liquid (kg/m s)
$\bar{\rho}$	average density of the medium (kg/m^3)
ρ_S	density of solid (kg/m^3)
ρ_L	density of liquid (kg/m^3)

Subscripts

D	dispersion
f	final
G	gas

product = $5100/100 = 51$ kmoles. Stoichiometric Ca(OH)_2 required = 51 kmoles, stoichiometric CO_2 required = 51 kmoles. An estimation of the operating parameters is given below.

Gas Flow Rate

CO_2 is available from another plant as a 20 mol% stream (remaining 80% inerts, N_2). Assuming 5% excess CO_2 , the gas stream required = $(51/0.2) \times (105/100) = 267.75$ kmoles. Since the reactor can handle up to $2 \times 10^5 \text{ N/m}^2$ maximum process pressure, choose a lower operating pressure of $1.8 \times 10^5 \text{ N/m}^2$. Choose room-temperature operation, $T = 30^\circ\text{C} = 303.16 \text{ K}$. Initial gas volume = $nR_g T/P = (267.75 \times 8314 \times 303.16)/1.8 \times 10^5 = 3749 \text{ m}^3$. Since this volume is very high compared to the reactor volume of 10 m^3 , choose semibatch mode of operation with continuous supply of feed gas and removal of residual gas to maintain the reactor pressure. In view of this, a slurry of Ca(OH)_2 in water is prepared and CO_2 is bubbled through it for 4 h. The mother liquid phase will be initially saturated with Ca(OH)_2 . As the reaction proceeds, CaCO_3 precipitates out. The mother liquor can be separated from the solid CaCO_3 precipitate by filtration. For ease of operation and control, assume constant gas flow rate.

$$\text{Inlet gas flow rate} = Q = 3749 \text{ m}^3/(4 \text{ h} \times 3600) = 0.26 \text{ m}^3/\text{s}$$

$$\text{Reactor inner diameter } T = 2.19 \text{ m, height } H = 2.64 \text{ m}$$

$$\text{Area of cross section of the reactor } S = (\pi/4)T^2 = 3.767 \text{ m}^2$$

$$\text{Superficial gas velocity at the inlet, } u_{G0} = Q/S = 0.069 \text{ m/s}$$

$$F_1, \text{ kmol/s of inert} = 267.75/(4 \times 3600) \times \text{mol fraction of inerts}$$

$$= \{267.75/(4 \times 3600)\} \times (1 - 0.2) = 0.0149 \text{ kmol/s}$$

$$x \text{ at the outlet} = 0.012$$

Initial solids holdup ϵ_{s0} :

Of the reactor volume of 10 m^3 , assume 20% head space.

$$\text{Volume of the dispersion} = 10 \times [1 - (20/100)] = 8 \text{ m}^3.$$

Stoichiometric quantity of CO_2 required for the reaction = 51 kmol/s

$$\text{Initial weight of } \text{Ca(OH)}_2 = 51 \times 74 = 3774 \text{ kg.}$$

$$\text{Density of solid } \text{Ca(OH)}_2, \rho_s = 2080 \text{ kg/m}^3.$$

$$\text{Volume of solids } V_s = 3774/2080 = 1.814 \text{ m}^3.$$

Initial holdup of solids, ϵ_{s0}

$$\epsilon_{s0} = V_s/V_D = 0.2268.$$

Gas holdup ϵ_G :

Assume an impeller speed (N) of 3.82 rps. The gas holdup is calculated using the following correlation (Rewatkar et al. 1993):

$$\epsilon_G = 3.54 \left(\frac{D}{T} \right)^{2.08} \left(\frac{N^2 D}{g} \right)^{0.51} \left(\frac{Q}{(N)D^3} \right)^{0.43} = 0.233 \quad (\text{CS10.1})$$

Liquid holdup ϵ_L :

$$\epsilon_L = 1 - \epsilon_G - \epsilon_{s0} = 0.54$$

Power consumption:

To calculate the power consumption in the absence of gas (P_L),

$$\text{Average density, } \bar{\rho} = \rho_L (1 - \epsilon_{s0}) + \rho_s \epsilon_{s0}$$

Bubble diameter d_b :

$$d_b = 6\epsilon_G/a = 2 \times 10^{-3} \text{ m}$$

Interfacial area for solid liquid mass-transfer a_{p0} :

Initial particle surface area $a_{p0} = 6\epsilon_{s0}/d_{p0} = 6 \times 0.2268/0.0001 = 13608.2 \text{ m}^2/\text{m}^3$. As the particle dissolves and reacts, the particle size diminishes until it vanishes.

Schmidt number Sc :

$$Sc = \left(\frac{\mu_L}{\rho_L \mathbf{D}_B} \right) = 288.02, \text{ where } B \text{ denotes } \text{OH}^- \text{ ion}$$

As soon as $\text{Ca}(\text{OH})_2$ dissolves into the aqueous phase, it ionizes almost completely, being a strong base.

Gas-liquid mass transfer coefficient $k_L a$:

The value of $k_L a$ is estimated using the following correlation (Chandrasekharan and Calderbank, 1981):

$$k_L a = \frac{0.0248}{D^4} \left(\frac{\mathbf{P}_G}{V_D \epsilon_L} \right)^{0.55} Q^{0.551/\sqrt{D}} = 2.28 \quad (\text{CS10.7})$$

In the presense of fine particles $k_L a$ decreases and has been assumed to be 0.49 sec^{-1} .

$$k_L = (k_L a) / a = 6.86 \times 10^{-4} \text{ m/s}$$

Solid-liquid mass transfer coefficient k_{SL} :

The value of k_{SL} is estimated using the following correlation (Rowe et al., 1965):

$$Sh = 2.0 + 0.72 (\text{Re}_P)^{0.5} Sc^{0.333} \quad (\text{CS10.8})$$

where

$$\text{Re}_P = \frac{d_P u_{s\infty} \rho_L}{\mu_L} = 0.59, \quad Sh = \frac{k_{SL} d_P}{\mathbf{D}_B} = 5.6$$

$$k_{SL} = 1.96 \times 10^{-4} \text{ m/s}$$

Estimation of batch time for the reaction:

It is assumed that the gas is completely backmixed. Gas-side resistance for mass transfer is neglected. The reaction is performed under isothermal conditions. Initially, a slurry of $\text{Ca}(\text{OH})_2$ in water is prepared and the liquid is saturated with $\text{Ca}(\text{OH})_2$. Then CO_2 gas is sparged to the reactor. It is assumed that the number of reacting $\text{Ca}(\text{OH})_2$ particles per unit volume of the reactor is constant (no breakage or agglomeration) until the particles are completely consumed. The instantaneous rate of reaction is integrated with respect to time until all the $\text{Ca}(\text{OH})_2$ is consumed. Thus, the batch time is obtained:

$$R_A a = k_L a H_{\text{CO}_2} P \left(\frac{x}{1+x} \right) \eta \quad (\text{CS10.15})$$

where $x = \text{kmol CO}_2/\text{kmol inerts}$ at the outlet and has the same value throughout the backmixed vessel. The above equation is solved for x at any time t and the rate of CaCO_3 production (kg/s) is calculated from

$$\frac{d}{dt} (PDN)_{\text{CaCO}_3} = R_A a V_D M_{\text{wCaCO}_3} \quad (\text{CS10.16})$$

As the Ca(OH)_2 is consumed, its particle size decreases:

$$-\frac{d}{dt} \left[\gamma_P \left(\frac{\pi}{6} d_P^3 \right) \rho_s V_D \right] = R_A a V_D M_{\text{wCa(OH)}_2} \quad (\text{CS10.17})$$

$$-\frac{d}{dt} (d_P) = \frac{2 R_A a V_D M_{\text{wCa(OH)}_2}}{\pi \gamma_P \rho_s V_D d_P^2} \quad (\text{CS10.18})$$

where γ_P = number of Ca(OH)_2 particles per unit volume of dispersion.

In the final stages of the reaction, when the particle size is very small, the rate of solid dissolution is very low as compared to the rate of CO_2 absorption with reaction. The bulk concentration of OH^- ,

$$\frac{k_{SL} a_P [B]_S}{Z} \ll k_L a [A]^* \eta \quad (\text{CS10.19})$$

$$[B]_0 = 0$$

Thus, the overall rate is governed by the supply of OH^- ions. In this phase, the production rate of CaCO_3 is given by

$$\frac{d}{dt} (PDN)_{\text{CaCO}_3} = \frac{1}{2} k_{SL} (\gamma_P \pi d_P^2) [B]_S V_D (M_{\text{wCaCO}_3}) \quad (\text{CS10.20})$$

As the Ca(OH)_2 is consumed, there is a corresponding decrease in the particle size:

$$-\frac{d}{dt} \left[\gamma_P \left(\frac{\pi}{6} d_P^3 \right) \rho_s V_D \right] = \frac{1}{2} k_{SL} (\gamma_P \pi d_P^2) [B]_S V_D M_{\text{wCa(OH)}_2} \quad (\text{CS10.21})$$

$$-\frac{d}{dt} (d_P) = \frac{k_{SL} [B]_S M_{\text{wCa(OH)}_2}}{\rho_s} \quad (\text{CS10.22})$$

The rates of production and decrease in particle diameter are integrated with time until the particle vanishes. In this way, the batch time is calculated and is 4.09 h, which is close to the desired batch time for the reaction.

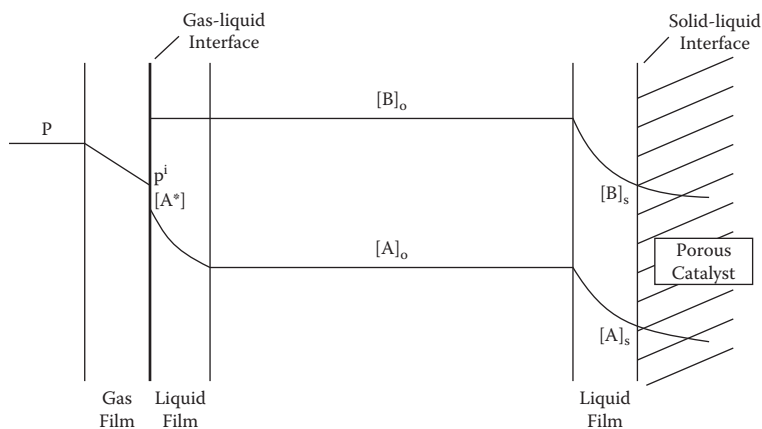
Lesson

This case study is an example of how a common reaction can provide the basis for modeling a novel reaction system: a gas-liquid-solid reaction performed in the batch mode; the solid in this case is first dissolved followed by chemical reaction with a product of the reactive absorption of the solute gas. Unlike Case Study 11.9, where all steps were in series, here some steps occur in parallel. Moreover, the rate-controlling mechanisms often change with time and process conditions. These facets of the problem are dealt with to determine the maximum production capacity of a reactor, which can often be a cost-determining issue. The lesson here is that maximizing the use of an existing reactor is sometimes preferable to designing a new one.

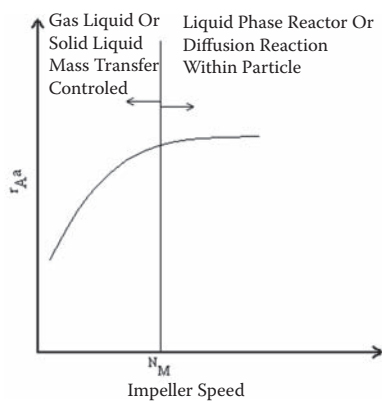
CASE STUDY 11.11 GAS-LIQUID-SOLID (CATALYTIC) REACTION: HYDROGENATION OF AN ORGANIC COMPOUND

Nomenclature for Case Study 11.11

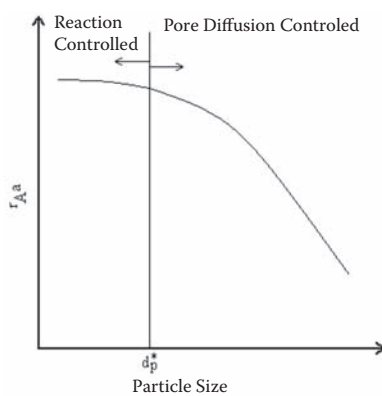
A	constant in Equation (CS11.7) (–)
$[A]_b$	bulk concentration of solute gas A (kmol/cm ³)
$[A]^*$	saturation concentration of gas A (kmol/cm ³)
$[A]_s$	surface concentration of gas A (kmol/cm ³)
a_1, b_1, c_1	constants in Equation (CS11.9) (–)
A	effective gas-liquid interfacial area per unit volume (m ² /m ³)
a_p	area of the catalyst particle per unit volume (m ² /m ³)
$[B]_b$	concentration of the liquid phase reactant (gmol/cm ³)
$[B]_s$	surface concentration of B (kmol/cm ³)
C_3	constant in Equation (CS11.6) (–)
D	impeller diameter (m)
D_0	diffusivity (m ² /s)
d_b	bubble diameter (m)
d_p	diameter of catalyst particle (m)
d_p^*	critical particle size of diffusion control operation (m)
Fl	flow number, Q_G/ND^3 (–)
Fr	Froude number, u^2/gd_p (–)
g	gravitational constant (m/s ²)
k_i	rate constant, $i = 1, 2, \dots$ (conc ¹⁻ⁿ /time)
k_{SL}	solid-liquid mass transfer coefficient (m/s)
k_L	mass transfer coefficient (m/s)
L	characteristic length of the catalyst particle (–)
\sqrt{M}	enhancement factor (–)
N	impeller speed (rps)
N_{CG}	critical impeller speed for gas induction (rps)
N_M	impeller speed at which mass transfer resistance is eliminated (rps)
P_0	power consumption in absence of gas (W)
P_G	power consumption in presence of gas (W)
Q_G	gas induction rate (m ³ /s)
Q_{GS}	rate of gas induction in presence of sparging (m ³ /s)
Q_{UG}	net rate of escape of the unreacted gas into the head space (m ³ /s)
R	impeller radius (m)
R_A	rate of reaction of A (kmol/m ² s)
Re	Reynolds number, $d_p u_{GO} \rho / \mu$ (–)
r_A	overall rate of reaction of component A (kmol/(m ³ s))
S	impeller submergence (m)
T	tank diameter (m)
u_{GO}	superficial gas velocity at the inlet (m/s)
u_t	impeller tip speed in Equation (CS11.7) (m/s)
V_L	liquid volume (m ³)
W	solid loading (kg/m ³)



(a)



(b)



(c)

FIGURE CS11.1 The three-phase catalytic reactor: (a) concentration profiles of gas and liquid phase components; (b) effect of impeller speed on overall rate of reaction; and (c) effect of particle size on overall rate of reaction at stirrer speeds higher than N_M . (From Patwardham, A. W. and Joshi, J. B., 1998.)

TABLE CS 11.1
Effect of Variable Parameters on the Rate of Reaction

Effect of Increase in Values of Variables on the Overall Rate of Reaction								
Rate controlling step	$[A^*]$	$[A]_b$	$[A]_s$	$[B]_0$	$[B]_s$	ε_s	d_p	N
Gas-liquid mass transfer	$\propto [A^*]$	$\propto [A^*] - [A]_b$	$[A]_s = [A]_b$	No effect	No effect	No effect	No effect	increases
Solid-liquid mass transfer	$[A^*] = [A]_0$	$\propto [A]_b$	$\propto [A]_b - [A]_s$	No effect	No effect	$\propto \varepsilon_s$	$\propto (1/d_p)$	increases
Pore diffusion	$[A^*] = [A]_s$	$[A]_b = [A]_s$	$\propto [A]_s$	No effect	No effect	No effect	$\propto (1/d_p)$	No effect
Chemical reaction	$[A^*] = [A]_s$	$[A]_b = [A]_s$	$\propto [A]_s^m$	$[B]_b = [B]_s$	$\propto [B]_s^n$	$\propto \varepsilon_s$	No effect	No effect

the second term on the right-hand side of Equation (CS11.3) is affected. If the rate of reaction varies linearly with the solid loading, then it can be concluded that the overall reaction is solid-liquid mass transfer controlled. However, if the rate of reaction is unaffected by the solid loading, then gas-liquid mass transfer is the rate-controlling step.

Whenever heat effects are important, a proper energy balance has to be established. The rate at which heat is generated inside the reactor and the rate at which heat is transferred to and from the heat transfer media need to be quantified to determine whether the rate of heat transfer is the controlling step. Table CS11.1 summarizes the effect of various parameters such as $[A^*]$, $[A]_s$, $[B]_b$, d_p , ε_s , impeller speed, and so forth on the overall rate of reaction for different rate-controlling steps. For the geometry under consideration, the values of $k_L a$ and $k_{SL} a_p$ can be estimated from available correlations. Using these values and the estimated kinetic parameters, it is possible to determine the rate-controlling step. During the course of the reaction, one or more operating conditions often change. For example, reactant concentration, operating temperature, pressure, and other conditions may change. Then the rate-controlling step itself may change with time or location in the vessel. In such cases, the rate-controlling step has to be determined as a function of time/location in the reactor. Once the rate-controlling step is known, the overall rate of reaction can be written. This overall rate of reaction can then be integrated with respect to space or time to determine the throughput of the reactor.

Solved Example

Hydrogenation of an organic compound is a typical example of such reactions. The gas and liquid phase reactants are denoted by A and B , respectively. For the purpose of illustration, it will be assumed that the overall reaction is mass transfer controlled. It is desirable to perform such a reaction in a gas-including contractor along with a sparger. The lower impeller is a pitched blade up-flow turbine (PBTU), and a large ring sparger will be assumed. Let u_{G0} be the superficial velocity of the sparged gas. A part of this sparged gas reacts in the vessel, and the remainder escapes into the head space. Simultaneously, the gas is recycled into the liquid using a gas-inducing impeller. Part of the entrained/induced gas also reacts, and the remainder escapes into the head space. For an overall material balance, the maximum permissible superficial gas velocity (u_{G0}) should be such that the rate of gas sparging equals the rate of reaction of the gas. This ensures that the head space pressure remains unchanged with time. Alternatively, if an overall material balance is written for the head space, then it is clear that the net rate of escape of the unreacted gas into the head space (Q_{UG}) must be equal to the rate of gas induction.

Figure CS11.2a shows a comparison of fractional gas holdup under sparging conditions, with and without the use of a gas-inducing impeller. In the absence of a gas-inducing impeller, such a system behaves like a conventional mechanically agitated contactor (MAC). The comparison is made in terms of gas holdup as a function of power consumption per unit volume for different superficial velocities of sparged gas ($u_{G0} = 0, 6, 18$, and 29 mm/s). It can be seen that the fractional

3. A particular superficial gas velocity, u_{Gi} , is chosen.
4. For this value of superficial gas velocity, the gas induction rate (Q_G), fractional gas holdup (ϵ_G), and power consumption (\mathbf{P}_G) are calculated, both in the presence of a gas-inducing impeller and in its absence. Hydrodynamic characteristics and the mass transfer coefficient are estimated using the correlations of Patwardhan and Joshi (1998).
5. Based on these hydrodynamic characteristics, the volumetric mass transfer coefficient ($k_L a$) is calculated. Alternatively, the value of $k_L a$ could also be measured in a small-scale experimental reactor (at least 0.5 m dia.) under the actual conditions prevailing (temperature, pressure, physicochemical properties, and so forth).
6. From the value of $k_L a$, the rate at which the sparged and the induced gas react is estimated.
7. The net rate at which the sparged gas accumulates (Q_{UG}) into the head space is calculated as the difference between the rate of sparging and the rate of reaction of the sparged gas.
8. If Q_G is lower than Q_{UG} , pressure builds up in the head space, and the u_{Gi} is unacceptable, or if Q_G is higher than Q_{UG} , head space pressure decreases and, again, the u_{Gi} is unacceptable. Thus, a new value of u_{Go} is chosen, and the procedure is repeated from step 3 onward until $Q_{UG} = Q_G$. Thus, this procedure yields a value of u_{Gi} that is acceptable for a given geometry of the system (step 2).
9. The procedure is repeated by choosing different operating conditions (e.g., impeller speed) so that different values of $u_{Go} - \mathbf{P}_G$ are generated.
10. The entire procedure can be repeated if there is an enhancement in the rate of mass transfer due to chemical reaction. The results of the above procedure are given in Figures CS11.2b through d. The following correlations were used for the calculations:

$$N_{CG} \text{ in absence of sparging, } N_{CG} = \frac{1}{2\pi R} \sqrt{\frac{2gS}{\Psi}} \quad (\text{CS11.5})$$

$$\text{Change in } N_{CG} \text{ due to sparging, } \frac{(\Delta N_{CG})^2 \pi^2 D^2 \Psi}{2gS} = \alpha_1 (C_3 / D)^{\alpha_2} u_G^{\alpha_3} (S / \mathbf{T})^{\alpha_4} \quad (\text{CS11.6})$$

Gas induction rate in absence of sparging,

$$Q_G = \lambda^* N R^2 \left(1 - \frac{2gS}{\Psi u_i^2} \right) + \alpha^* N R^3 \left(1 - A \left(\frac{2gS}{\Psi u_i^2} \right)^{3/2} \right) \quad (\text{CS11.7})$$

$$\text{Change in gas induction rate due to sparging, } 1 - \frac{Q_{GS}}{Q_G} = \beta_1 F_1^{\beta_2} (C_3 / D)^{\beta_3} \quad (\text{CS11.8})$$

$$\text{Fractional gas holdup, } \epsilon_G = a_1 (D / \mathbf{T})^{b_1} (\text{Re } FrFl)^{c_1} \quad (\text{CS11.9})$$

Power consumption,

$$\frac{\mathbf{P}_G}{\mathbf{P}_O} = 0.1 \left(\frac{N V_L}{Q_G} \right)^{1/4} \left(\frac{N^2 D^4}{W V_L^{2/3} g} \right)^{-1/5} \quad (\text{CS11.10})$$

$$\mathbf{P}_O = N_P \rho_L N^3 D^5$$

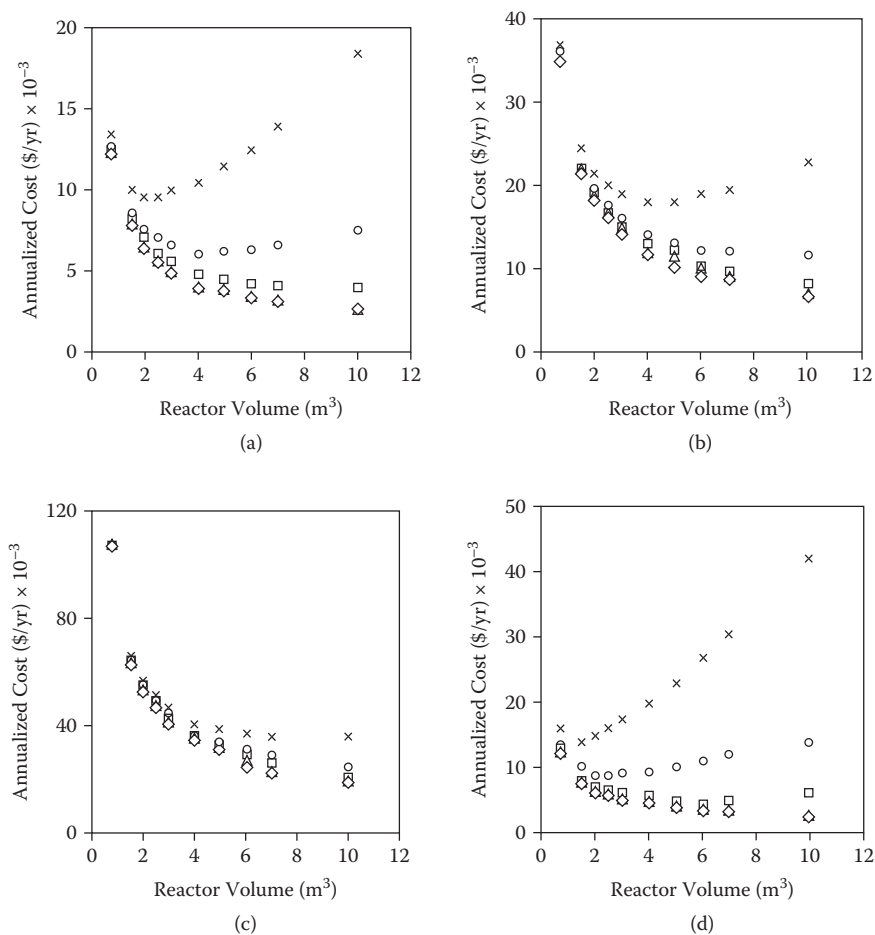


Figure	Electricity Cost \$/ (kW.hr)	Annualized Capital Cost \$/ (kg yr)				
		◆	△	□	○	x
(a)	0.035					
(b)	0.01	0.144	0.48	1.44	0.48	14.4
(c)	0.3					
(d)	0.035	0.36	1.2	3.6	12.0	36.0

FIGURE CS11.3 Optimization of hydrogenation reactor on the basis of annualized cost. (From Patwardnam, A. W. and Joshi, J. B., 1998.)

the fabrication cost was considered as 60% of the material cost. The operating cost was calculated as the product of power consumption and the electricity cost. The optimum reactor size was determined based on the annualized cost (capital + operating).

Figure CS11.3 shows the annualized cost for various combinations of fixed and operating cost. The principal operating cost includes electricity, and this has been considered at four levels: 0.035, 0.01, 0.3, and 0.035 \$/kWh in Figures CS11.3a through d. For every figure, the annualized capital cost consists of two parts:

1. Cost of material of construction
2. Level of depreciation, interest, maintenance, etc.

F_{se}	quantity of solids elutriated (kg/s)
f_{eff}	fraction defined by Equation (CS12.1)
G	methyl chloride
I	integral defined by Equation (CS12.42)
k	general notation for rate constant (appropriate units)
k_1	constant given by Equation (CS12.9)
k_2	constant given by Equation (CS12.9) (1/s)
k_{ac}	rate constant for the autocatalytic step ($\text{m}^3/\text{mol s}$)
k_{hom}	rate constant for homogeneous reaction ($\text{m}^3/\text{mol s}$)
\dot{k}	rate of change of pore radius (constant) given by Equation (CS12.30) (m/s)
N	total number of particles in the feed (—)
N_B^o	total number of particles of A and B surrounding one central B particle
P	reaction product (SiCl_4)
Q	reaction product (Cu^*)
$[Q]$	concentration of Q (kmol/m^3)
R	radius of solid or cylindrical coordinate (m)
R_0	initial radius (m)
R_A, R_B	radii of solids A and B (m)
R_{st}	smallest feed size for a growing particle or largest size for a shrinking particle (m)
$r(R)$	rate of change of particle size (m/s)
r_A	rate of reaction of A ($\text{mol}/\text{m}^3 \text{ s}$)
r_{hom}	rate of homogeneous reaction ($\text{mol}/\text{m}^3 \text{ s}$)
r_t	sum of rates ($r_{hom} + r_{ac}$) ($\text{mol}/\text{m}^3 \text{ s}$)
$r_{t,max}$	r_t at $X_{A,max}$
s	shape factor (—)
t	time (s)
\bar{t}	residence time (s)
t_i	induction period for the reaction (s)
W	weight of solids (kg)
W_A, W_B	weights of solids A and B (kg)
w	weight ratio, W_A/W_B
x_i	conversion of i (—)
\bar{X}_A	residence time averaged conversion (—)
$\bar{\bar{X}}_A$	residence time and particle size averaged conversion (—)

Greek

α	group defined by Equation (CS12.2)
δ	bubble fraction in a fluidized bed
ϕ	size distributions function
ϕ_0, ϕ_1, ϕ_e	size distributions in the feed, outflow and elutriation streams, respectively
η	η phase (Cu_3Si)
ρ_A, ρ_B	densities of solids A and B (kg/m^3)
τ	time for complete conversion as defined in Table 11.13

Defining the Systems

Methylchlorosilanes are used in the manufacture of a variety of resins, elastomers, and silicone oils. They are produced as a mixture of chlorosilanes, mainly dimethyldichlorosilane, by the reaction between silicon and methyl chloride by a direct route discovered independently by Rochow (1945) and Muller (1950). In this route, metallic copper, with or without promoters, is used to accelerate the reactions. The form of copper is important and depends on its preparation and association with the silicon phase. The whole system of solids comprising silicon metal, copper

$$f_{\text{eff}} = \frac{N(A/B)}{N_B^o} = \left(\frac{\alpha w}{1 + \alpha w} \right)^m \quad (\text{CS12.1})$$

Here, α is given by

$$\alpha = \frac{R_B^3 \rho_B}{R_A^3 \rho_A} \quad (\text{CS12.2})$$

where R_A and R_B are the radii of A and B , respectively, ρ_A and ρ_B their densities, N_B^o is the total number of particles of A and B surrounding one central B particle, and w is the weight ratio of the components (W_A/W_B). The hypothetical particle with this surface area will be completely in contact with the other component (A). This analysis has the merit of bringing it in line with that for gas-solid reactions, and it is generally very useful.

Where the solids are present as pellets, the analysis becomes far more complicated. Factors such as the formation of a product zone between the two reactant solids, the change in contact area with reaction progress (from a point contact for spheres) to a flat surface, formation of a “neck” between the reacting solids, self-diffusion of reactants as well as their diffusion into the product, and sintering come into play. Models have been proposed to account for these; see, e.g., Arrowsmith and Smith (1966) and Tamhankar and Doraiswamy (1978) for the role of diffusion, and Ristic (1979) for the role of sintering. In the present problem, we shall not be concerned with the analysis of pellet behavior. Furthermore, in view of the general applicability of models based on order of reaction, we use this concept in formulating the kinetics of formation of the η -phase.

Experimental data (Tamhankar et al., 1981) on the formation of the η -phase are plotted in Figure CS12.1 as conversion-time curves. The shape of the curves clearly suggests autocatalytic behavior. In this respect, the η -phase formation reaction is unique, for it is perhaps the only instance

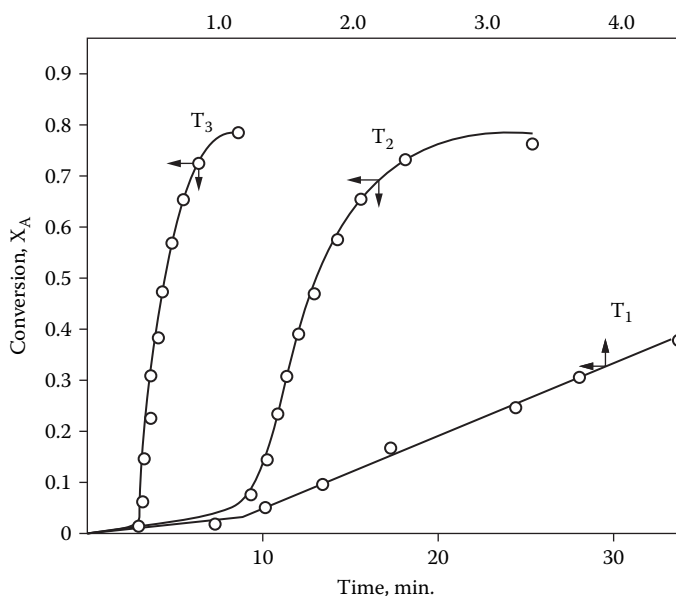


FIGURE CS12.1 Fractional removal of CuCl as a function of time (redrawn from the data of Tamhankar et al., 1981).

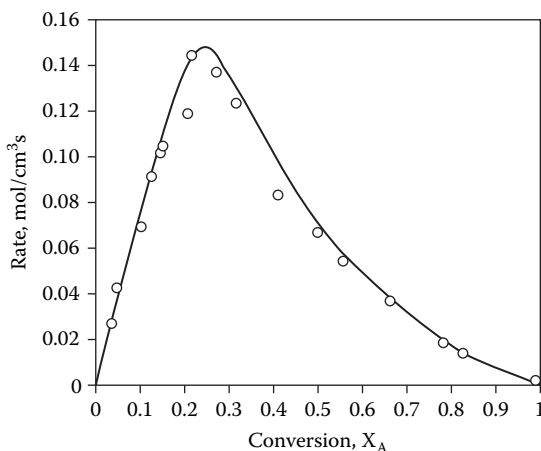


FIGURE CS12.2 Rate as a function of conversion for run T2 of Figure CS12.1 (redrawn from the data of Tamhankar et al., 1981).

$$k_1 = k_{\text{hom}} / [A]_0 k_{ac} \quad (\text{CS12.9})$$

$$k_2 = k_{\text{hom}} + [A]_0 k_{ac} \quad (\text{CS12.10})$$

t_i = induction period for the reaction

A plot of LHS vs. $(t - t_i)$ should give k_2 if k_1 is known (but it is not).

To get k_1 , we differentiate the S-shaped X_A vs. t curves (Figure CS12.1). Because of the nature of autocatalysis, the resulting rate curves (see Figure CS12.2) show a maximum. Thus, at

$$X_A = X_{Am} \quad (\text{CS12.11})$$

$$\frac{d(dX_A / dt)}{dX_A} = \frac{dr_t}{dt} = [A]_0^2 k_{ac} - k_{\text{hom}} [A]_0 - 2[A]_0^2 k_{ac} X_{Am} = 0$$

giving

$$k_{\text{hom}} / [A]_0 k_{ac} = k_1 = (1 - 2X_{Am}) \quad (\text{CS12.12})$$

where $X_{Am} = X_A$ at $r_{t,\text{max}}$.

Using k_1 for getting the LHS in plotting Equation (CS12.8), k_2 can be obtained. Finally,

$$\left. \begin{aligned} k_{\text{hom}} &= \frac{k_1 k_2}{(k_1 + 1)} \\ k_{ac} &= \frac{k_2}{[A]_0 (k_1 + 1)} \end{aligned} \right\} \quad (\text{CS12.13})$$

The actual values obtained are (Tamhankar et al., 1981):

With complete backmixing of the solid, the size distribution of the outflow stream also represents that of the solids within the bed. This equation can be written as

$$\begin{aligned}
 F_{s,0}\check{\phi}_0(R) - F_{s,1}\check{\phi}_1(R) - WE^*(R)\check{\phi}_1(R) \\
 - W \frac{d}{dR} \left[r(R)\check{\phi}_1(R) \right] \\
 + \frac{sW}{R} r(R)\check{\phi}_1(R) = 0
 \end{aligned} \tag{CS12.15}$$

The term $E^*(R)$ represents the elutriation constant defined by the equation

$$\left(\begin{array}{c} \text{rate of removal} \\ \text{of solids of size } R_j \end{array} \right) = E^* \left(\begin{array}{c} \text{weight of that} \\ \text{size of solids} \\ \text{in the bed} \end{array} \right) \tag{CS12.16}$$

and s and $r(R)$ represent, respectively, the shape factor of the particle (3 for a sphere, 2 for a cylinder and 1 for a flat plate) and the rate of change of particle size. Equation (CS12.15), valid for a particular size range, can be supplemented by an overall balance equation over all sizes to give

$$F_{s,e} + F_{s,1} - F_{s,0} = sW \int_{\text{all } R} \frac{\check{\phi}_1(R)r(R)}{R} dR \tag{CS12.17}$$

This equation assumes positive or negative values depending on whether the particle grows or shrinks. For shrinking particles, Equations (CS12.15) and (CS12.17) can be rearranged to give the following expression for $W/F_{s,0}$:

$$\frac{W}{F_{s,0}} = \int_{R_f \rightarrow \infty}^{R_M} \frac{R^3}{r(R)} I \left[\int_{R_0=R}^{R_0=R_M} \frac{\check{\phi}_0(R) dR_0}{R_0^3 I} \right] dR \tag{CS12.18}$$

The corresponding outflow size distribution is given by

$$\check{\phi}_1(R) = \frac{F_{s,0} R^3}{Wr(R)} I \left[\int_{R_0=R}^{R_0=R_M} \frac{\check{\phi}_0(R) dR_0}{R_0^3 I} \right] \tag{CS12.19}$$

For growing particles, the integration limits are reversed. In these equations, R_M represents the smallest feed size for a growing particle or the largest size for a shrinking particle, and I is an integral defined as

$$I = \exp \left[\int_R^{R_0} \frac{(F_{s,1}/W) + E^*(R)}{r(R)} dR \right] \tag{CS12.20}$$

TABLE CS12.1
Conversion Equations for Gas-Solid Reactions at Specified Reactor Conditions

State of Solids Feed	Flow Pattern of Solids	Gas Composition	Conversion Equations	Remarks
1 Single size particles	Plug flow	Uniform	Same as those given in Table 11.13 for all the three controlling steps	Equations give X_B directly; no averaging of any kind is involved since all particles spend equal times in the reactor in a PFR
2 Mixture of different sizes	Plug flow	Uniform	$1 - \bar{X}_B = \sum_{R(t=\tau)}^{R_M} \left[1 - X_B(R_i) \right] \frac{F_{s,0}(R_i)}{F_{s,0}}$	Averaging over size range required; for each size in the equation, the expression for the controlling step involved is used (from Table 3.9)
3 Single size particles	Mixed flow	Uniform	Film resistance control: $1 - \bar{X}_B = \frac{1}{2} \left(\frac{\tau}{t} \right) - \frac{1}{3!} \left(\frac{\tau}{t} \right)^2 + \frac{1}{4!} \left(\frac{\tau}{t} \right)^3$ Ash diffusion control: $1 - \bar{X}_B = \frac{1}{5} \left(\frac{\tau}{t} \right) - \frac{19}{4 \cdot 20} \left(\frac{\tau}{t} \right)^2 + \frac{41}{4620} \left(\frac{\tau}{t} \right)^3 - 0.000149 \left(\frac{\tau}{t} \right)^5 + \dots$ Chemical reaction control: $X_B = 3 \frac{\tau}{t} - 6 \left(\frac{\tau}{t} \right)^2 + 6 \left(\frac{\tau}{t} \right)^3 \left[1 - \exp(\tau/t) \right]$	Since the particles spend different times in the reactor, characterized by exponential distribution in a perfectly mixed reactor, averaging of conversions in particles of all residence times is involved.

have to be incorporated into the model, and separate equations for the bubble and cloud-wake phases are necessary.

During the course of reaction, the solid reactant in the particles is increasingly displaced by the solid product formed. The volume and specific density of the product formed may not be the same as those of the reactant. For a realistic representation of the bed, it is therefore necessary to account for variations in both size and density of the particles.

Thus, the modeling of the gas-solid noncatalytic reactor is far more complex than that of its catalytic counterpart. Even so, simplified models have been used to get a qualitative (and to some extent, quantitative) feel for the performance of the reactor. Thus, the two-phase model of Davidson and Harrison (1963) has been used by Campbell and Davidson (1975) to analyze the data on the combustion of carbon particles for short periods of combustion in a batch reactor. The model has also been used and considerably extended by Amundson (see Bukur et al., 1977). Tigrel and Pyle (1971) have used this model for the not-too-different problem of catalyst deactivation. Kunii and Levenspiel (1969) and Kato and Wen (1969) have extended their models to gas-solid noncatalytic systems. A particularly useful model that takes account of some of the complexities in practical systems has been suggested by Chen and Saxena (1978).

Comments

In this case, no specific problem in quantitative terms has been posed and solved. For the first step, which is a solid-solid reaction, experimental details have been given because it is a unique solid-solid reaction, perhaps the only known autocatalytic one. Having clearly established this fact, general procedures are described for the two reactors involved, since no experimental data are available for attempting a specific design. The thrust here is the description of a procedure for calculating the outlet solid size distribution given the inlet size distribution. This is an important factor in solid-phase reactions.

Lesson

Silicon reacts with copper chloride catalytically to form a solid product known as η -phase, which then catalyzes the reaction between silicon and methyl chloride to form methyl chlorosilanes. The formation of the η -phase is a unique example of an autocatalytic solid-solid reaction (we are not aware of any other example of such a reaction). Procedures for determining the kinetics of this reaction and the size distribution of the final products of the second reaction are described in this case study. The most important feature of the study is the unexpected discovery of autocatalysis in a solid-solid reaction, which leads us to the important lesson that one should vigorously pursue any such observation that falls outside the "comfort zone" of research, for that is where true discoveries lie. This advice is particularly relevant to engineers, since they generally do not accept the unexpected and would prefer to tread on safer ground.

POSTSCRIPT

The case studies presented in this chapter illustrate reactor design procedures for a carefully selected set of reacting systems wherein the physical dimensions of the reactor (diameter, height) and fixed and operating parameters (catalyst loading, superficial velocity, impeller speed, and other) were calculated. As a postscript to these studies, we would like to consolidate and emphasize certain fundamental and practical considerations in reactor selection and design.

- For a given system, the necessary requirements for any proposed reactor design are that the desired capacity, selectivity, and purity be achieved. The exercise should also include pertinent aspects of environmental load and safety.
- Although the engineer may be required to design for a given capacity, it is advisable to provide for additional capacity (in case, this is inexpensive and not the cost-controlling

- For highly exothermic reactions such as polymerization, it is advisable to include a means for quenching the reaction (e.g., by providing for addition of an inhibitor) in the event of a runaway situation.
- Not only should hazardous conditions be avoided during normal operation, but any such possibility during startup or shutdown should also be foreseen.
- In the case of reactions carried out in mechanically agitated reactors where heat transfer is crucial, provision must be made for adequate heat transfer. During power failure, agitation may stop. Emergency power must be provided to the crucial drives, and provision must be made to drain/flare the contents during an emergency.
- In the case of catalytic packed-bed reactors, provision of extra volume should be considered to accommodate additional catalyst in case of selectivity/activity loss over time.
- In some heat transfer-controlled reactions, it may be possible to partly evaporate the solvent itself, condense it in a reflux condenser, and send the solvent back to the reactor.
- The thermal sensitivities of all the species in the reactor must be known. Some compounds may decompose dangerously at certain conditions, and suitably lower temperatures must be chosen for operation.
- Some reactions may produce solid products that degrade within the reactor and deposit on the cooling coils, and so forth, and drastically affect the heat transfer and product quality. This possibility must be envisaged and accounted for in the design.
- Where handling of solid reactants is involved, the equipment must be designed to prevent clogging and choking.
- The reactor must be able to perform with different feedstocks (especially of petrochemical origin), and, expectedly, operating conditions for each of them must be specified.

ACKNOWLEDGMENTS

In writing this chapter, particularly the case studies, we have been greatly helped by our students, present and former. We particularly thank Amol Kulkarni, Anand Kulkarni, Ashwin Patwardhan, Dharmesh Ranjan, K. Ekambara, Indraneel Chatterjee, Janaki Patwardhan, T. Kumaresan, Mahesh Dhotre, Rajesh Ghadge, Sanjay Danao, and Swarnendu Roy of the University Institute of Chemical Technology, Mumbai. Our thanks are also due to K. B. S. Prasad of the Indian Institute of Chemical Technology, Hyderabad, for his valuable help and to several graduate students at the Department of Chemical Engineering, Iowa State University, Ames, Iowa. We (particularly L. K. D.) thank Linda Edson for her exquisite typing and for coordinating the staggering list of exchanges between the two authors, incorporating repeated additions, corrections, and revisions. L. K. D. also thanks C. E. Glatz, chair of the Department of Chemical Engineering, for his continued support, even in the author's "retirement."

Nomenclature

A	chemical species (–)
A_p	area of pellet (m^2)
$[A]_p$	concentration of A within a pellet (kmol/m^3)
$[A]_s$	concentration of A at catalyst or any solid surface (kmol/m^3)
\bar{A}	average concentration of A (kmol/m^3); external field concentration at some point in a bed (kmol/m^3)
$[A]_0$	entrance concentration of A (kmol/m^3)
$[A]_e$	exit or effluent concentration of A (kmol/m^3)
$[A]_f$	final concentration (in time) of A (kmol/m^3)
$[A]_i$	initial concentration of A (kmol/m^3)
\hat{A}	dimensionless concentration of A within a pellet, $[A]_p/[A]_s$ (–)
a	interfacial area (m^2/m^3); any exponent (–)
B	chemical species (–)

K_m	rate constant for an m th-order reaction $[(\text{m}^3/\text{kmol})^{m-1}(\text{s})]$
k_p	rate constant for pore removal (1/s)
k_S	rate constant $[(\text{kmol}/\text{m}^2 \text{ cat}) (\text{m}^3/\text{kmol})^m (\text{s})]$
k_v	rate constant $[(\text{m}^3 \text{ reactor}/\text{kmol})^{m-1} (\text{s})]$
k_v	rate constant $[(\text{m}^3 \text{ cat}/\text{kmol})^{m-1} (\text{s})]$
k_{v0}	rate constant for fresh catalyst (1/s)
k_{vs}	rate constant at surface conditions, conforming to any set of units of k_v
k_w	rate constant $[(\text{mol}/\text{kg cat}) (\text{m}^3/\text{mol})^m (\text{s})]$
k^o	Arrhenius pre-exponential factor (units of the corresponding rate constant)
L	reactor length (m)
L_{mf}	reactor length at minimum fluidization (m)
L^*	dimensionless reactor length defined by Equation (11.162) (–)
M	number of reactions; the “space factor” (appropriate units)
\sqrt{M}	ratio of reaction in film to that in bulk, $\sqrt{D_A k[B]_b / k_L}$
M_i	molecular weight of species i (kg/kmol)
m	reaction order; any exponent (–)
N	number of components; number of kmoles (–); speed (rps)
N_{cs}, N_{CM}	see text
N_{SG}	see text
N_{C50}	see text
N_{C70}	see text
N_i	number of kmoles of component i (–)
N_p	number of particles
N_{QS}	secondary flow number (–)
N_t	total number of kmoles (–)
Nu	Nusselt number (–)
n	reaction order (–)
P	pressure (atm or Pa)
P	power (W)
Pe_{hr}	radial Peclet number for heat transfer, $d_p u C_p \rho / k_{per}$ (–)
Pe_{ma}	axial Peclet number for mass transfer, $d_p u / D_{ed}$ (–)
P_i	partial pressure of i (atm or Pa)
P_{nm}	parameter defined in Table 11.9 (–)
Q	volumetric flow rate (m^3/s)
Q_S	solids circulation rate (m^3/s)
R	chemical species (–); radius (m)
R'	group $\sum u_A / u_B$
R_A	specific rate of absorption (reaction) ($\text{kmol}/\text{m}^2/\text{s}$)
R_A	reaction rate per pellet (kmol/s)
R_{GA}	reaction rate of A in a grain (kmol/s)
R_g	ideal gas law constant (kcal/kmol K)
\hat{R}	dimensionless radius, r/R (–)
Re_p	particle Reynolds number ($d_p u_g \rho / \mu$) (–)
Re'_{mf}	Reynolds number at minimum fluidization, $u_{mf} d_p \rho / \mu$ (–)
r	general notation for reaction rate (appropriate units); radial coordinate (m)
r	vector ($M \times 1$ matrix) of reaction rates (–)
r_A, r_{VA}	reaction rate of A ($\text{kmol}/\text{m}^3 \text{ reactor s}$)
R_{Go}	initial grain radius (m)
r_{Gi}	interface radius in a grain (m)
r_i	radial position at the core-shell interface in SIM (m)
r_j	reaction rate of the j th reaction (appropriate units)
r_{SA}, r_A'	reaction rate of A ($\text{kmol}/\text{m}^2 \text{ cat s}$)
r_{vA}	reaction rate of A ($\text{kmol}/\text{m}^3 \text{ cat s}$)
r_{wA}	reaction rate of A ($\text{kmol}/\text{kg cat s}$)
S	selectivity term defined variously as in Table 11.9

ε_b	bulk or bed porosity (voidage) (–)
$\bar{\varepsilon}_G$	average gas holdup (–)
ε_{gr}	riser gas holdup (–)
ε_{LD}	downcomer liquid holdup (–)
ε_{lr}	riser liquid holdup (–)
ε_i	change in total volume upon reaction per kmole of i reacting (m^3/kmol)
ϕ	generalized Thiele modulus independent of pellet shape and reaction order defined by Equation (11.50); also general notation for Thiele modulus; modulus defined by Equations (11.71) and (11.87) (–)
ϕ_a	actual or Weisz modulus defined by Equation (11.51) (–)
ϕ_c	a critical value of the Thiele modulus given by Equation (11.78) (–)
ϕ_n	shape generalized Thiele modulus for an n order reaction (–)
ϕ_{pn}	Thiele modulus for an n th-order reaction in a flat plate
ϕ_{sn}	Thiele modulus for an n th-order reaction in a spherical pellet (–)
η	dimensionless position in grain (–); viscosity (Pa·s); enhancement factor (–)
λ	group defined by Equation (11.141)
v	ratio of stoichiometric coefficients, v_B/v_A (–)
v_i	stoichiometric coefficient of species i (–)
v_{ij}	stoichiometric coefficient of A_i in the j th reaction (–)
\mathbf{v}	$(N \times M)$ matrix of stoichiometric coefficients (–)
θ	volume change modulus defined by Equation (11.87) (–)
θ_i	fraction of active sites occupied by species i (–)
θ_v	fraction of vacant active sites (–)
ρ	density (kg/m^3)
ρ_B	density of B (kg/m^3)
ρ_{Bm}	Molar density of B (mol/m^3)
ρ_b	bulk density (kg/m^3)
ρ_i	density of i (kg/m^3)
$\bar{\rho}_D$	average density of dispersion (kg/m^3)
σ	reaction modulus defined by Equation (11.153) (–); surface tension (dynes/m)
τ	total time given by Equation (11.66) (–)
τ'	dimensionless temperature in a reactor, T/T_0 (–)
τ_p, τ_a, τ_c	times for complete conversion of a solid if film transfer, ash diffusion, or reaction alone were controlling (s)
τ_G	time required for complete conversion of a grain (s)
τ_p	reaction or on stream time (s); time required for complete conversion of a pellet(s)
ω	dimensionless radial position in a reactor, r/R (–)
ξ	dimensionless position in a catalyst pellet or reacting solid (–)
ξ_i	dimensionless position of unreacted core, r_i/R (–)
ξ_j	molecularity of reaction j (i.e., number of kmoles reacting according to reaction j) (–)
Ψ	ratio y_{i0}/y_{A0} , F_{i0}/F_{A0} or $[i]/[i]_0$; cumulative gas concentration given by Equation (11.75) (–)
Ψ'	structural parameter (–)
Ψ_B	initial concentrations ratio, $[B]_0/[A]_0$ (–)
Ω	catalyst activity (–)
$\bar{\Omega}$	average catalyst activity (–)
ℓ	length coordinate (m)
\mathfrak{N}_m	mass transfer group, $d_p/u[A]_0$ ($\text{m}^3\text{s}/\text{kmol}$)
\mathfrak{N}_H	heat transfer group, $(-)_p d_p/uC_p T_0$ ($\text{m}^3\text{s}/\text{kmol}$)

Subscripts

b	bulk
bp	bubble generated at the sparger
bs	secondary bubble
CS	critical speed for solid suspension in the absence of gas
C	catalyst

- Behie, L. A., Bergougnou, M. A. and Baker, C. G. J., in *Fluidization Technology*, vol. 1, Keairns, D. L., ed. Washington, DC: Hemisphere, 1976.
- Behie, L. A., Bergougnou, M. A., Baker, C. G. J. and Base, T. E. 1971. *Can. J. Chem. Eng.* 49: 557.
- Bellman, R., *Dynamic Programming*. Princeton, NJ: Princeton University Press, 1957.
- Bellman, R. and Dryfus, S. E., *Applied Dynamic Programming*. Princeton, NJ: Princeton University Press, 1962.
- Berty, J. M. 1973. Paper presented at AIChE 66th Annual Meeting, Philadelphia.
- Beveridge, G. S. G. and Goldie, P. J. 1968. *Chem. Eng. Sci.* 23: 912.
- Bhatia, S. and Gupta, J. S. 1993. *Rev. Chem. Eng.* 8: 177.
- Bhatia, S. K. and Perlmutter, D. D. 1980. *AIChE J.* 26: 379; 1981a. *AIChE J.* 27: 226; 1981b. *AIChE J.*, 27: 247; 1983. *AIChE J.* 29: 287.
- Bhutada, S. R. and Pangarkar, V. G. 1987. *Chem. Eng. Commun.* 61(1–6): 23; 1989. *Chem. Eng. Sci.* 44: 2384.
- Bischoff, K. B. 1965. *AIChE J.* 11: 351; 1968. *Chem. Eng. Sci.* 23: 451.
- Borman, P. C., Boss, A. N. R. and Westerterp, K. R. 1994. *AIChE J.* 40: 862.
- Boudart, M. and Djeja Mariadasseau, G., *Kinetics of Heterogeneous Catalytic Reactions*. Princeton, NJ: Princeton University Press, 1984.
- Bowen, J. H. and Cheng, C. K. 1969. *Chem. Eng. Sci.* 24: 1829.
- Box, G. E. P. 1965. *Computer J.* 8: 42.
- Box, G. E. P. and Hill, W. J. 1967. *Technometrics* 4: 30.
- Briens, C. L., Bergougnou, M. A. and Baker, C. G. J. 1978. *2nd Fluid Proc. Eng. Found. Conf.*: 38.
- Briggs, R. A. and Sacco, A., Jr. 1991. *J. Mater. Res.* 6: 574.
- Buchholtz, R., Sepentoinides, T., Stienmann, J. and Onken, U. 1983. *Ger. Chem. Eng.* 6: 105.
- Bujalski, W., Konno, M. and Nienow, A. W. 1988. *Proc. 6th Eur. Conf. Mixing* 24–26 May, BHRA, Leeuwenhorst, Pavia, Italy.
- Bukur, B. D. and Amundson, N. R. 1975a. *Chem. Eng. Sci.* 30: 847; 1975b. *ibid.* 30: 1159.
- Bukur, D. V., Caram, H. S. and Amundson, N. R., in *Chemical Reactor Theory—A Review*, Lapidus, L. and Amundson, N. R., eds., Englewood Cliffs, NJ: Prentice-Hall, 1977.
- Butt, J. B., *Reaction Kinetics and Reactor Design*, 2nd ed. Englewood Cliffs, NJ: Prentice Hall, 1999.
- Butt, J. B., Bliss, H. and Walker, C. A. 1962. *AIChE J.* 8: 42.
- Calo, J. M. 1978. *ACS Symp. Ser.* 65: 550.
- Campbell, E. K. and Davidson, J. F., in *Fluidization Technology*, vol. 2, Keairns, D. F., ed. Washington, DC: Hemisphere, 1975.
- Campbell, R. R., Hills, A. W. D. and Paulin, A. 1970. *Chem. Eng. Sci.* 25: 929.
- Carberry, J. J. 1962. *Chem. Eng. Sci.* 17: 675; 1964. *Ind. Eng. Chem.* 56: 39; *Chemical and Catalytic Reactor Engineering*. New York: McGraw-Hill, 1976.
- Carberry, J. J. and Kulkarni, A. A. 1973. *J. Catal.* 31: 41.
- Carberry, J. J. and Wendel, M. 1963. *AIChE J.* 9: 129.
- Catipovic, N. and Levenspiel, O. 1979. *Ind. Eng. Chem. Process Des. Dev.* 18: 558.
- Chakrabarti, A. and Sharma, M. M. 1993. *Reactive Polym.* 20: 1.
- Chan, O. T. and Rinker, R. G. 1978. *Chem. Eng. Sci.* 33: 1201.
- Chan, S. F. and Smith, J. M. 1976. *Indian Chem. Eng.* 18: 42.
- Chandrasekharan, K. and Calderbank, P. H. 1981. *Chem. Eng. Sci.* 36: 819.
- Chandrashekar, B. C. and Vortmeyer, D. 1979. *Warme-Stoff.* 12: 105.
- Chang, C. C., Fan, L. T. and Rong, S. X. 1982. *Can. J. Chem. Eng.* 60: 272.
- Chapman, C., Nienow, A. W., Cooke, M. and Middleton, J. C. 1983. *Chem. Eng. Res. Des.* 61: 82.
- Chen, T. P. and Saxena, S. C. 1978. *AIChE Symp. Ser.*, no. 176, 74: 149.
- Chou, C. L. and Li, K. 1984a. *Chem. Eng. Com.* 29: 153; 1984b. *ibid.*, 181.
- Choudhary, V. R. and Doraiswamy, L. K. 1972. *Ind. Eng. Chem. Proc. Des. Dev.* 11: 420; 1975. *ibid* 14: 227.
- Chrostowski, J. W. and Georgakis, C. 1978. *ACS Symp. Ser.* 65 (*Chem. React. Eng.*), Houston, TX: 225.
- Chuang, K. C., Young G. W. and Benslay R. M., *Advanced Fluid Catalytic Cracking Technology*. New York: AIChE, 1992.
- Chudacek, M. W. 1982. *Proc. 4th Eur. Conf. on Mixing*, 27–29 April, BHRA, Leeuwenhorst, Netherlands.
- Clark, J. H., Kybett, A. P. and Macquarrie, D. J., *Supported Reagents: Preparation, Analysis, and Applications*. Weinheim, Germany: VCH, 1992.

- Green, D. W. and Perry, R. H. *Perry's Chemical Engineers' Handbook*, 8th ed. New York: McGraw-Hill, 2007.
- Guha, B. K. and Narasimhan, G. N. 1972. *Chem. Eng. Sci.* 27: 703.
- Gullett, B. K., Bruce, K. R. and Machilek, R. M. 1990. *Rev. Sci. Instrum.* 61(2): 904.
- Harnby, N., Edwards, M. F. and Nienow, A. W., *Mixing in the Process Industries*, 2nd ed. Oxford, UK: Butterworth-Heinemann, 1992.
- Hartig, F. and Keil, F. J. 1993. *Ind. Eng. Chem. Res.* 32: 424.
- Hasler, D. J. L., Doraiswamy, L. K. and Wheelock, T. D. *Ind. Eng. Chem. Res.* 42: 2003.
- Heesink, A. B. M. and van Swaaij, W. P. M. 1995. *Chem. Eng. Sci.* 50: 2983.
- Hegedus, L. L. and Petersen, E. E. 1973a. *Chem. Eng. Sci.* 28: 69; 1973b. 345; 1973c. *J. Catal.* 28: 150; 1974. *Catal. Rev., Sci. Eng.* 9: 245.
- Heijnen, J. J. and van't Riet, K. 1984. *Chem. Eng. J.* 28: B21.
- Hill, W. J. 1966. Thesis, University of Wisconsin, Madison, WI.
- Hills, A. W. D. 1968. *Chem. Eng. Sci.* 23: 297.
- Hlavacek, V. 1970. *Ind. Eng. Chem.* 62: 8.
- Hlavacek, V. and Kubicek, M. A. 1972. *Chem. Eng. Sci.* 25: 1537.
- Hlavacek, V. and Votruba, J., in *Chemical Reactor Theory—A Review*, Lapidus, L. and Amundson, N. R., eds. Englewood Cliffs, NJ: Prentice Hall, 1977.
- Hlavacek, V., Marek, M. and John, T. M. 1969. *Coll. Czech. Chem. Commun.* 34: 3868.
- Hoelderich, W. F. and van Bekkum, H. 1991. In *Introduction to Zeolite Science and Practice*, van Bekkum, H., Flanigen, E. M. and Jansen, J. C., eds. *Stud. Surf. Sci. Catal.* 58: 631.
- Hofmann, H., in *Chemical Reactor Design and Technology: Overview of the New Development of Energy and Petrochemical Reactor Technologies*, de Lasa, H. I., ed. *Proceedings of the NATO Advanced Study Institute on Chemical Reactor Design and Technology*, London, Ontario, Canada, 2–12 June, 1985, Kluwer Academic, Dordrecht, Netherlands, 1986.
- Horio, M., Nonaka, A., Hoshiba, M. L., Morisita, K., Kobukai, Y., Naito, J., Tashibana, O., Watanabe, K. and Yoshida, N., in *Circulating Fluidized Bed Technology*, Basu, P., ed. New York: Pergamon, 1986.
- Hughes, C. C. and Mann, R. 1978. *ACS Symp. Ser.* 65: 201.
- Illerup, J. B., Dam-Johansen, K. and Johnsson, J. E. 1993. *Gas Clean High Temp. [Pap. Int. Symp.]* 2: 492.
- Ishida, M. and Wen, C. Y. 1968. *AIChE J.* 14: 311.
- Jagtap, S. B. and Wheelock, T. D. 1996. *Energy & Fuels* 10: 821.
- Jayaraman, V. K., Kulkarni, B. D. and Doraiswamy, L. K. 1981. *Am. Chem. Soc. Symp. Ser.* 168: 19.
- Joglekar, H. S.; Samant, S. D. and Joshi, J. B. 1991. *Water Res.* 25: 135.
- Johnstone, R. A. W., Wilby, A. H. and Entwistle, I. D. 1985. *Chem. Rev.* 85: 129.
- Jorgensen, K. A. 1989. *Chem. Rev.* 89: 431.
- Joshi, J. B. 1983. *Trans. Inst. Chem. Eng.* 61: 143.
- Joshi, J. B. and Sharma, M. M. 1979. *Trans. Inst. Chem. Eng.* 57: 244.
- Joshi, J. B., Abichandani, J. S., Shah, Y. T., Ruether, J. A. and Ritz, H. J. 1981. *AIChE J.* 27: 937.
- Joshi, J. B., Dinkar, M., Deshpande, N. S. and Phanikumar, D. V. 2001. *Adv. Chem. Eng.* 28: 1.
- Joshi, J. B., Mahajani, V. V. and Juvekar, V. A. 1985. *Chem. Eng. Commun.* 33: 1.
- Joshi, J. B., Parasu Veera, U., Prasad, Ch. V., Phanikumar, D. V., Deshpande, N. S., Thakre, S. S. and Thorat B. N. 1998. *PINSA-A.* 64: 441.
- Joshi, J. B., Patil, T. A., Ranade, V. V. and Shah, Y. T. 1990a. *Rev. Chem. Eng.* 6: 73.
- Joshi, J. B., Ranade, V. V., Gharat, S. D. and Lele, S. S. 1990b. *Can. J. Chem. Eng.* 68: 705.
- Joshi, J. B., Shah, Y. T., Albal, R. S., Ritz, H. J. 1982. *Ind. Eng. Chem. Process Des. Dev.* 21: 594.
- Juvekar, V. A. 1976. Ph.D. thesis, University of Mumbai, Mumbai, India.
- Kammermeyer, K. A. and Rutz, L. O. 1959. *Chem. Eng. Prog. Symp. Ser.* 55 (24): 163.
- Karcz, J. 1999. *Chem. Eng. J.* 72 (3): 217.
- Kato, K. and Wen, C. Y. 1969. *Chem. Eng. Sci.* 24: 1351.
- Kern, D. Q., *Process Heat Transfer*. Tokyo, Japan: McGraw-Hill Kogakusha, 1950.
- Khan, A. R. 1999. *Chem. Eng. Res. Des.* 77: 11.
- Khare, G. P., Delzer, G. A., Kubicek, D. H. and Greenwood, G. J. 1995. *Environ. Prog.* 14: 146.
- Kijenski, S., Gliniski, M. and Reinhercs, J., in *Heterogeneous Catalysis and Fine Chemicals*, Guisnet, M., Barbier, J., Barrault, J., Bouchoule, C., Dupez, D., Montassier, C., and Pérot, G. eds. Amsterdam: Elsevier, 1988.
- Kim, K. K. and Smith, J. M. 1974. *AIChE J.* 20: 670.

- Olah, G. A., Iyer, P. S. and Prakash, G. K. S. 1986. *Synthesis*: 513.
- Oldshue, J. Y., *Fluid Mixing Technology*. New York: McGraw-Hill, 1983.
- Oroskar, A. and Stem, S. A. 1979. *AIChE J.* 25: 903.
- Otani, S., Wakao, N. and Smith, J. M. 1965. *AIChE J.* 11: 466.
- Pandit, A. B. and Joshi, J. B. 1983. *Chem. Eng. Sci.* 38: 1189; 1984. *Rev. Chem. Eng.* 2: 1; 1998. *Rev. Chem. Eng.* 14: 321.
- Pansing, W. F. and Malloy, J. B. 1962. *Chem. Eng. Prog.* 58: 12, 53.
- Parulekar, S. J., Joshi, J. B. and Shertukde, P. V. 1988. *Chem. Eng. Sci.* 44: 543.
- Patwardhan, A. W. and Joshi, J. B. 1998. *Can. J. Chem. Eng.* 76: 339; 1999a. *Ind. Eng. Chem. Res.* 38: 3131; 1999b. *ibid*, 49.
- Pawalski, J. 1961. *Chem. Eng. Tech.* 33: 492.
- Perkins, T. K. and Rase, H. F. 1958. *AIChE J.* 4: 351.
- Pérot, G. and Guisnet, M. 1990. *J. Mol. Catal.* 61: 173.
- Peters, M. S. and Skorpinski, E. J. 1965. *J. Chem. Educ.* 42: 329.
- Pigford, R. L. and Pyle, C. 1951. *Ind. Eng. Chem.* 43: 1649.
- Pilling, M. J. and Seakins, P. W., *Reaction Kinetics*. Oxford, UK: Oxford Science Publications, 1995.
- Powell, R. 1969. Nitric Acid Technology, Recent Developments. *Chem. Proc. Rev.* 30.
- Pradhan, M. P., Suchak, N. J., Walse, P. R. and Joshi, J. B. 1997. *Chem. Eng. Sci.* 52: 4569.
- Prasad, K. B. S. and Doraiswamy, L. K. 1974. *J. Catal.* 32: 384.
- Prasad, K. B. S. and Rao, M. S. 1977. *Chem. Eng. Sci.* 32: 1411.
- Prasannan, P. C. and Doraiswamy, L. K. 1982. *Chem. Eng. Sci.* 37: 925.
- Prasannan, P. C., Ramachandran, P. A. and Doraiswamy, L. K. 1986. *Chem. Eng. J.* 33: 19.
- Pratt, K. C., in *Catalysis: Science and Technology*, vol. 8, Anderson, J. R. and Boudart, M., eds. Netherlands: Springer-Verlag, 1987.
- Raab, C. G., Englisch, M., Marenelli, T. B. L. W. and Lercher, J. A. 1993. *Stud. Surf. Sci. Catal.* 78: 211.
- Radar, C. G. and Weller, S. W. 1974. *AIChE J.* 20: 515.
- Raghav Rao, K. S. M. S., Rewatkar, V. B. and Joshi, J. B. 1988. *AIChE J.* 34: 1332.
- Rajadhyaksha, R. A. and Joshi, G. W., in *Heterogeneous Catalysis and Fine Chemicals*, Guisnet, M., Barbier, J., Barrault, J., Bouchoule, C., Dupez, D., Montassier, C. and Pérot, G., eds. Amsterdam: Elsevier, 1991.
- Rajadhyaksha, R. A., Vasudeva, K. and Doraiswamy, L. K. 1975. *Chem. Eng. Sci.* 20: 25; 1976. *J. Catal.* 41: 61.
- Rajagopalan, K. and Luss, D. 1979. *Ind. Eng. Chem. Proc. Des. Dev.* 18: 459.
- Ramachandran, P. A. and Doraiswamy, L. K. 1982. *AIChE J.* 28: 881.
- Ramachandran, P. A. and Kulkarni, B. D. 1980. *Ind. Eng. Chem. Proc. Des. Dev.* 19: 717.
- Ramachandran, P. A. and Smith, J. M. 1977a. *Chem. Eng. J.* 4: 137; 1977b. *AIChE J.* 23: 353.
- Ranade, P. V. and Harrison, D. P. 1979. *Chem. Eng. Sci.* 34: 427; 1981. *Chem. Eng. Sci.* 36: 1079.
- Rao, Y. K. 1979. *Met. Trans. B.* 10: 243.
- Raskin, A., Ja, et al. 1968a. *Theoret. Found. Chem. Tech.* 2: 220; 1968b. *Chim. Ind. (Milan)* 44: 199.
- Reid, R. C., Prausnitz, J. M. and Sherwood, T. K., *The Properties of Gases and Liquids*. New York: McGraw-Hill, 1977.
- Reilly, P. M. and Blau, G. E. 1974. *Can. J. Chem. Eng.* 52: 289.
- Rewatkar, V. B. and Joshi, J. B. 1991a. *Chem. Eng. Commun.* 102: 1; 1991b. *Chem. Eng. Technol.* 14: 333; 1991c. *Chem. Eng. Technol.* 14: 386; 1991d. *Ind. Eng. Chem. Res.* 30: 1784.
- Rewatkar, V. B., Deshpande, A. J., Pandit, A. B. and Joshi, J. B. 1993. *Can. J. Chem. Eng.* 71: 226.
- Richardson, J. F. and Zaki, W. N. 1954. *Trans. Inst. Chem. Eng.* 32: 35.
- Richardson, J. T. and Friedrich, H. 1975. *J. Catal.* 37: 8.
- Ristic, M. M., *Sintering: "New Developments"* in *Proc. 4th Intl. Round Table Conf. on Sintering* (Durbronic, Poland). Amsterdam: Elsevier, 1979.
- Roberts, G. W. 1972. *Chem. Eng. Sci.* 27: 1409.
- Roberts, G. W. and Satterfield, C. N. 1965. *Ind. Eng. Chem. Fundam.* 4: 288; 1966. 5, 317.
- Roberts, M. W. and McKee, C. S., *Chemistry of the Metal-Gas Interface*. New York: Oxford University Press, 1979.
- Roberts, S. M., *Dynamic Programming in Chemical Engineering and Process Control*. New York: Academic Press, 1964.
- Rochow, E. G. 1945. *J. Am. Chem. Soc.* 67: 963; 1945. U.S. Patents 2,380,995 and 2,380,996.

- Torok, B., Molnar, A., Borszeki, K., Toth-Kadar, E. and Bakonyi, I., in *Heterogeneous Catalysis and Fine Chemicals*, Guisnet, M., Barbier, J., Barrault, J., Bouchoule, C., Dupez, D., Montassier, C. and Pérot, G., eds. Amsterdam: Elsevier, 1993.
- Treybal, R. E., *Mass-Transfer Operations*. 3rd ed. New York: McGraw-Hill, 1980.
- Uhl, V. W. and Gray, J. B., *Mixing: Theory and Practice*, vol. 1, Orlando: Academic Press, 1966.
- Ulrichson, D. L. and Mahoney, D. J. 1980. *Chem. Eng. Sci.* 35: 567.
- Uner, D. O., Pruski, M., Gerstein, B. C. and King, T. S. 1994. *J. Catal.* 146: 530.
- Usyal, B. Z., Aksahin, I. and Yusel, H. 1988. *Ind. Eng. Chem. Res.* 27: 434.
- Vaidya, R. N. and Pangarkar, V. G. 1985. *Chem. Eng. Commun.* 39: 337.
- van Deemter, J. J., in *Fluidization III*, Grace, J. R. and Matsen, J. M., eds. New York: Plenum, 1980.
- van den Bleek, C. M. Van der Wiele, K. and Van den Berg, P. J. 1969. *Chem. Eng. Sci.* 24: 681.
- van der Ham, A. G. J., Heesink, A. B. M., Prins, W. and van Swaaij, W. P. M. 1996. *Ind. Eng. Chem. Res.* 35: 1487.
- van Welsenaere, R. J. and Froment, G. F. 1970. *Chem. Eng. Sci.* 25: 1503.
- van't Riet, K. and Smith J. M. 1973. *Chem. Eng. Sci.* 28: 1031.
- Varghese, P. and Wolfe, E. E. 1980. *AIChE J.* 26: 55.
- Varghese, P., Varma, A. and Carberry, J. J. 1978. *Ind. Eng. Chem. Fundam.* 17: 195.
- Vetter, K. J., *Electrochemical Kinetics, Theoretical and Experimental Aspects*. New York: Academic Press, 1967.
- Villa, L. T. and Quiroga, O. D. 1989. *Chem. Eng. Res. Des.* 67: 76.
- Vracar, R., Vucurovic, D., Rudarstvo, I. 1970. *Metallurgija*.
- Wan, K. and Davis, M. E. 1993a. *J. Chem. Soc. Chem. Commun.* 1262; 1993b. *Tetrahedron: Asymmetry* 4(12), 2461.
- Warmoeskerken, M. C. G. and Smith, J. M. 1985. *Chem. Eng. Sci.* 40: 2063.
- Weekman, V. W., Jr. 1968. *Ind. Eng. Chem. Proc. Des. Dev.* 7: 90; 1974. *AIChE J.* 20: 833.
- Weekman, W. W., Jr. and Gorring, R. L. 1965. *J. Catal.* 4: 260.
- Weisz, P. B. 1957. *Physik. Chem.* (Frankfurt) 11: 1.
- Weisz, P. B. and Hicks, J. S. 1962. *Chem. Eng. Sci.* 17: 265.
- Weisz, P. B. and Prater, C. D. 1954. *Adv. Catal.* 6: 143.
- Wen, C. Y. and Fan, L. T., *Models for Flow Systems and Chemical Reactors*. New York: Marcel Dekker, 1975.
- Werther, J. 1980. *Intl. Chem. Eng.* 20: 529.
- Westmoreland, P. R. and Harrison, D. P. 1976. *Environ. Sci. and Technol.* 10: 659.
- Wheelock, T. D. 1997. U.S. patent 5,653,955; 2000. U.S. patent 6,083,862.
- Wheelock, T. D. and Akiti, T. T., Jr. Filed January 27, 2000, U.S. patent pending.
- Yadav, N. K., Kulkarni, B. D. and Doraiswamy, L. K. 1994. *Ind. Eng. Chem. Res.* 33: 2412.
- Yang, K. H. and Hougen, O. A. 1950. *Chem. Eng. Prog.* 46: 146.
- Yang, W. C., Newby, R. A., Lippert, T. E., Keairns, D. L., and Cicero, D. C. 1992. Fluidization VII. *Proc. 7th Eng. Found. Conf. on Fluidization*, Brisbane, Australia, May 2–8, Potter, O. E. and Nicklin, D. J., eds.
- Yerushelmi, J. and Cankurt, N. T., in *Fluidization*, Davidson, J. F. and Keairns, D., eds. London and New York: Cambridge University Press, 1978.
- Yoo, H. J. and Steinberg, M. 1983. Final Report DOE/CH00016–1494.
- Yrjas, K. P., Cornelis, A. P. and Hupa, M. M. 1996. *Ind. Eng. Chem. Res.* 35: 176.
- Yushchenko, V. V. Korneichirk, G. P., Usha-Kova, Stasevich, V. P. and Semenyuk, Yu. V. 1968. *Kinet. Katal.* 4: 154.
- Zahradnik, J., Fialova, M., Linek, V., Sinkule, J., Reznickova, J. and Kastanek, F. 1997. *Chem. Eng. Sci.* 52: 4499.
- Zevenhoven, C. A. P., Yrjas, K. P. and Hupa, M. M. 1996. *Ind. Eng. Chem. Res.* 35: 943.
- Zwietering, T. N. 1958. *Chem. Eng. Sci.* 8: 244.

12.7	Packed Column Hydraulics	1029
12.7.1	Packing Characteristics.....	1030
12.7.1.1	Maximum Vapor–Liquid Capacity	1033
12.7.1.2	Pressure Drop	1037
12.7.1.3	Liquid Distribution	1038
12.7.1.5	Liquid Distributors	1039
12.7.1.6	Liquid Redistribution	1040
12.7.1.7	Vapor Distribution	1041
12.7.1.8	Turndown	1041
12.8	Mass Transfer Efficiency	1041
12.8.1	General Mass Transfer Relationships	1042
12.8.2	Tray Column Efficiency	1043
12.8.2.1	Regimes on Trays.....	1043
12.8.2.2	Tray Efficiency Definitions	1044
12.8.2.3	Point Efficiency	1045
12.8.2.4	Tray (Murphree) Efficiency	1046
12.8.2.5	Overall Column Efficiency E_{oc}	1046
12.8.2.6	Efficiency from Performance Data	1047
12.8.2.7	Empirical Efficiency Methods.....	1048
12.8.2.8	Efficiency from Laboratory Experiments	1049
12.8.2.9	Efficiency from Mass Transfer Models	1050
12.8.2.10	Conversion of Point Efficiency to Tray Efficiency.....	1052
12.8.2.11	Entrainment Effects on Efficiency	1052
12.8.2.12	Overall Column Efficiency.....	1054
12.8.2.13	Multicomponent Systems.....	1054
12.8.3	Packed Column Efficiency	1055
12.8.3.1	Random Packings	1056
12.8.3.2	Structured Packings.....	1057
12.8.3.3	Mechanistic Model for Structured Packings	1059
12.8.3.4	Scale-Up of Structured Packing Efficiency	1061
12.8.3.5	Structured Packing Performance.....	1062
12.8.4	Packings versus Crossflow Trays	1063
12.8.4.1	Counterflow Trays	1065
12.9	Troubleshooting	1065
12.9.1	Inadequate Vapor Capacity	1066
12.9.2	Liquid Flow Capacity	1066
12.9.3	Pressure Drop	1066
12.9.4	Separation Efficiency	1066
12.9.5	Stability.....	1066
12.10	Nomenclature	1066
	References	1069

Distillation is a physical process for separating a liquid mixture into its constituents. When such a mixture is partially vaporized, the vapor normally has a composition different from that of the residual liquid. Implied in the method is the condensation of the vapor to form a product liquid, called the *distillate*. The residual liquid product is often called the *bottoms*.

Distillation in crude form was practiced over 2000 years ago, usually for the concentration of alcoholic spirits. The first formalized documentation of distillation appears to be the treatise by Brunschwig in 1500.¹ Distillation has since emerged as the key method for separating liquid

- the separation. In many cases, computer-aided design packages predict physical properties such as equilibria, densities, viscosities, surface tensions, and diffusion coefficients.
4. Calculate the appropriate index of separability (usually *theoretical stages* but sometimes numbers of *transfer units*) for the separation required.
 5. Specify the equipment needed for the process. Although the emphasis may be on the distillation column, heat exchangers, pumps, control systems, and so forth must also be included. This step includes determining the actual stages as some function of theoretical stages, or the height of the contacting zone as some function of transfer units.

12.1 BASIC MODELS

12.1.1 PHASE EQUILIBRIUM

The fundamental basis of distillation is the physical equilibrium between the liquid and vapor phases of a system. Equilibrium is the condition reached after an infinite time of contact between the phases. In practice, liquid-vapor systems normally reach a state close to equilibrium in a comparatively short time of contact. At equilibrium, the composition in the vapor phase is usually different from that in the liquid. (If this is not the case, then an *azeotrope* is present, as discussed later.) The relationship of equilibrium concentrations of a component between phases is described by the *equilibrium ratio*. Other terms used for this ratio can include *distribution coefficient*, *equilibrium constant*, *K-constant*, or simply *volatility*.

The equilibrium ratio for a component i is defined as

$$K_i = y_i^* / x_i \quad \text{or} \quad y_i^* = K_i x_i \quad (12.1)$$

where

K_i = equilibrium ratio for component i
 y_i^* = mole fraction of i in vapor at equilibrium
 x_i = mole fraction of i in liquid

For example, if at equilibrium the liquid contains 0.1 mol fraction isobutane (iC_4), and if the equilibrium ratio of iC_4 under the system conditions is 2.5, then 0.25 mol fraction iC_4 is in the vapor. The equilibrium ratio is some function of temperature, pressure, and the composition of the liquid, which may be expressed as

$$K_i = f(T, P, x) \quad (12.2)$$

where

T = system temperature
 P = system pressure
 x = vector (set) of liquid molar concentrations for all components

The equilibrium ratios of two components in the system may be compared at the same conditions by means of the *relative volatility*, defined as

$$\alpha_{ij} = K_i / K_j \quad (12.3)$$

where α_{ij} = relative volatility of i with respect to j .

TABLE 12.1
Effect of Relative Volatility on Required Stages
for a Typical Separation

Relative Volatility, α_{ij}	Required Equilibrium Stages, N
10	10
5	14
2	33
1.5	57
1.2	126
1.1	241
1.0	∞

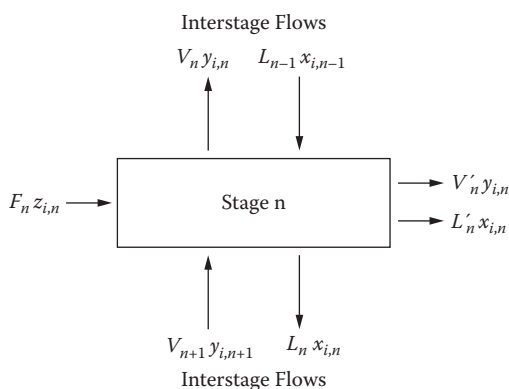


FIGURE 12.2 Component mass flows on a contacting stage.

conversion obtained on the stage at its temperature and pressure conditions. For the hypothetical *theoretical stage*, the exit streams of liquid and vapor must be in equilibrium with each other.

A mass balance may be written around stage n as follows:

$$F_n z_{i,n} + L_{n-1} x_{i,n-1} + V_{n+1} y_{i,n+1} = (V_n + V'_n) y_{i,n} + (L_n + L'_n) x_{i,n} \quad (12.7)$$

An energy balance can be written around the contacting stage using the enthalpies of all vapor and liquid streams (Figure 12.3):

$$F_n H_{F,n} + L_{n-1} h_{n-1} + V_{n+1} H + Q_n = (V_n + V'_n) H_n + (L_n + L'_n) h_n \quad (12.8)$$

where Q_n represents the heat added, removed, or generated within the stage either by a heat exchanger or an exothermic or endothermic reaction. In these balances, the stages are numbered downward from the top of the column.

The enthalpies of the vapor and liquid streams are functions of temperature, pressure, and composition:

$$H = f(T, P, y) \quad (12.9)$$

$$h = f(T, P, x) \quad (12.10)$$

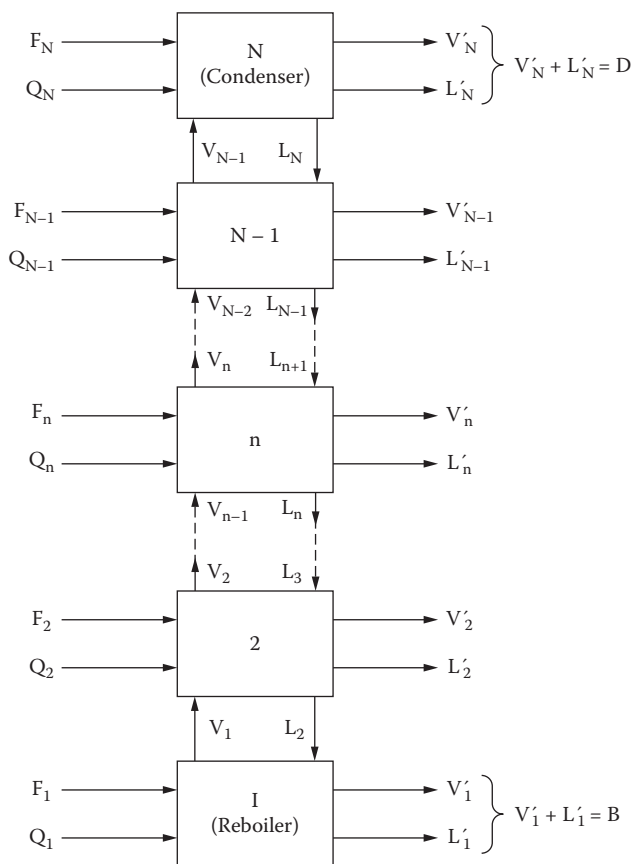


FIGURE 12.4 Cascaded stages in a distillation column.

where the vapor pressure p_i^{sat} is a function of temperature normally represented by the Antoine equation:

$$\ln p_i^{sat} = A + B/(T + C) \quad (12.13)$$

where constants A , B , and C have been evaluated for many elements and compounds.

If Dalton's law applies,

$$y_i^* = p_i/P \quad (12.14)$$

Combining Equations (12.1), (12.12), and (12.14) gives

$$K_i = \frac{y_i^*}{x_i} = \frac{p_i/P}{p_i/P_i^*} = \frac{P_i^*}{P} \quad (12.15)$$

The relative volatility between the two components i and j [Equation (12.3)] is

$$\alpha_{ij} = K_i/K_j \quad (12.16)$$

For the binary system, since $x_j = 1 - x_i$ and $y_j^* = 1 - y_i^*$,

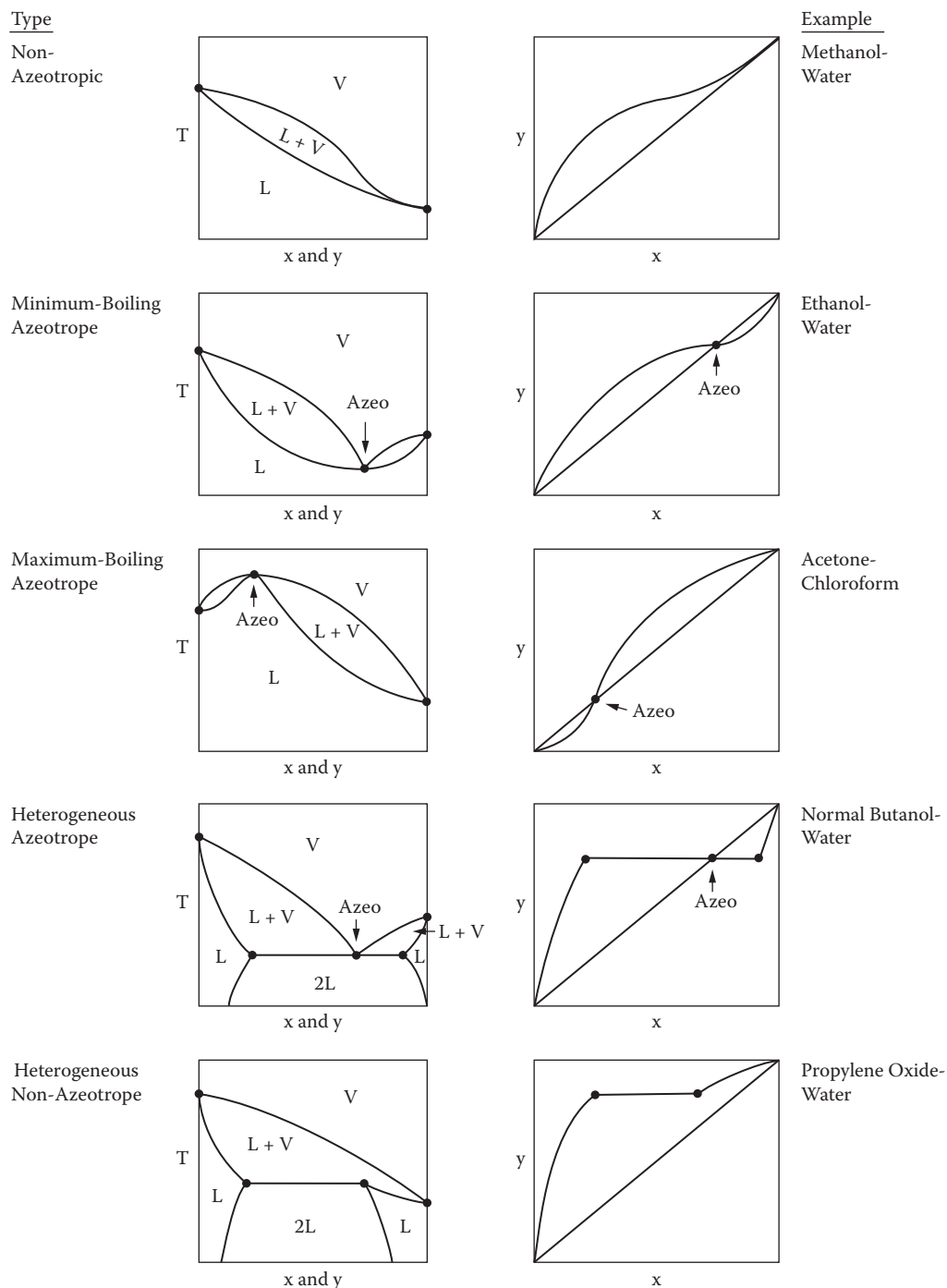
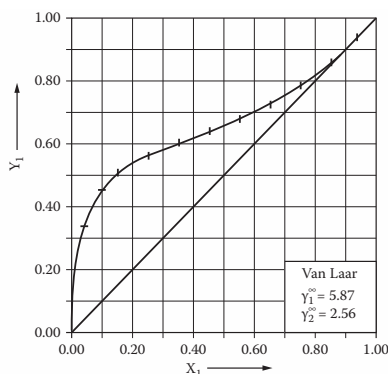


FIGURE 12.6 Common types of binary systems. (W. L. Bolles; J. R. Fair, 1982. *Encyclopedia of Chemical Processing and Design* 16: 51. Courtesy of Routledge/Taylor & Francis Group, © 1982.)

(1) ETHANOL						C2H6O	
-----						-----	
(2) WATER						H2O	
-----						-----	
+++++ ANTOINE CONSTANTS			REGION			+++++	
(1)	8.11228	1592.864	226.184	28-	93 C	METHOD 1	+
(2)	8.87131	1738.638	233.426	1-	108 C	METHOD 2	+
PRESSURE= 760.00 MM HG (1.013 BAR)							
LIT: KOJIMA K., TOCHIGI K., SEKI H., WATASE K.							
KAGAKU KOGAKU 32,149 (1968) .							
CONSTANTS:		A12	A21	ALPHA12			
MARGULES		1.6252	0.8618				
VAN LAAR		1.7693	0.9489				
WILSON		464.2336	926.2759				
NRTL	-114.8438	1376.3536	0.2983				
UNIQUAC	-6.5974	319.8115					



EXPERIMENTAL DATA			MARGULES		VAN LAAR		WILSON		NRTL		UNIQUAC	
T, DEG C	X1	Y1	DIFF T	DIFF Y1	DIFF T	DIFF Y1	DIFF T	DIFF Y1	DIFF T	DIFF Y1	DIFF T	DIFF Y1
100.00	0.000	0.0	0.0	0.0	0.0	0.0	0.0	0.0	0.0	0.0	0.0	0.0
90.00	0.0500	0.3372	-0.65	0.0141	-0.03	-0.0006	0.23	-0.0051	-0.28	0.0036	-0.07	0.0006
85.93	0.1000	0.4521	-0.38	0.0039	-0.09	0.0007	-0.21	0.0073	-0.11	0.0009	-0.10	0.0013
83.97	0.1500	0.5056	-0.08	-0.0064	-0.02	-0.0012	-0.32	0.0098	0.02	-0.0021	-0.03	-0.0005
82.90	0.2000	0.5359	0.38	-0.0138	0.09	-0.0041	-0.24	0.0071	0.16	-0.0050	0.08	-0.0033
82.14	0.2500	0.5589	0.41	-0.0158	0.12	-0.0047	-0.16	0.0046	0.18	-0.0051	0.11	-0.0037
81.52	0.3000	0.5794	0.38	-0.0138	0.09	-0.0034	-0.11	0.0032	0.14	-0.0031	0.08	-0.0024
80.99	0.3500	0.5987	0.30	-0.0100	0.04	-0.0016	-0.08	0.0021	0.08	-0.0006	0.04	-0.0006
80.52	0.4000	0.6177	0.20	-0.0054	0.0	0.0001	-0.05	0.0013	0.02	0.0016	0.0	0.0010
80.10	0.4500	0.6371	0.10	-0.0009	-0.03	0.0015	-0.03	0.0006	-0.01	0.0035	-0.03	0.0024
79.75	0.5000	0.6558	0.06	0.0015	-0.02	0.0008	0.02	-0.0014	-0.01	0.0031	-0.02	0.0017
79.42	0.5500	0.6765	0.01	0.0038	-0.02	0.0005	0.06	-0.0026	-0.01	0.0028	-0.01	0.0012
79.13	0.6000	0.6986	-0.01	0.0047	-0.01	-0.0006	0.09	-0.0038	-0.00	0.0017	0.00	0.0001
78.85	0.6500	0.7258	-0.05	0.0066	-0.02	0.0003	0.09	-0.0025	-0.02	0.0024	-0.01	0.0009
78.60	0.7000	0.7558	-0.10	0.0083	-0.03	0.0020	0.08	0.0008	-0.04	0.0038	-0.02	0.0025
78.42	0.7500	0.7848	-0.11	0.0050	-0.02	-0.0002	0.10	-0.0011	-0.03	0.0011	-0.01	0.0002
78.30	0.8000	0.8167	-0.11	0.0011	-0.00	-0.0021	0.12	-0.0018	-0.01	-0.0014	0.01	-0.0018
78.22	0.8500	0.8591	-0.11	0.0028	0.01	0.0019	0.12	0.0034	-0.01	0.0021	0.01	0.0022
78.20	0.9000	0.8959	-0.10	-0.0052	0.02	-0.0039	0.11	-0.0018	0.0	-0.0041	0.02	-0.0037
78.24	0.9500	0.9474	-0.06	-0.0019	0.02	0.0002	0.08	0.0021	0.01	-0.0000	0.02	0.0003
78.33	1.0000	1.0000	-0.00	0.0	-0.00	0.0	-0.00	0.0	-0.00	0.0	-0.00	0.0
MEAN DEVIATION:			0.18	0.0066	0.04	0.0016	0.12	0.0032	0.06	0.0025	0.04	0.0016
MAX. DEVIATION:			0.65	0.0158	0.12	0.0047	0.32	0.0098	0.20	0.0051	0.11	0.0037
THE FOLLOWING ANTOINE CONSTANT(S) A WERE USED FOR FITTING THE DATA:								COMPONENT 1		A= 8.11165		
								COMPONENT 2		A= 8.07126		

FIGURE 12.8 Example tabulation of equilibrium data from the Chemistry Data Series. [J. Gmehling et al., 1979. *Vapor-Liquid Equilibrium Collection*, Chemistry Data Series (continuing series), DECHEMA, Frankfurt, Germany.]

Equation (12.19) applies primarily to lower pressures (below 2 to 3 atmospheres), where the equilibrium vapor mixes ideally and also behaves ideally according to the perfect gas law. The rigorous thermodynamic expression for the K value, taking all conditions into account, is

$$K_i = \left(\frac{Y_i^L}{Y_i^V} \right) \left(\frac{P_i^*}{P} \right) \exp \left[\frac{1}{RT} \int_{P_i^*}^P (v_i^L dP) \right] \exp \left[\frac{1}{RT} \int_P^{P_i^*} \left(v_i^V - \frac{RT}{P} \right) dP \right] \quad (12.21)$$

The modeling of activity coefficients in multicomponent systems and the application of the general model [Equation (12.21)] are discussed in detail by Walas² and Reid et al.³

12.2.1 ESTIMATION AND MEASUREMENT OF ACTIVITY COEFFICIENTS

When equilibrium data can be found, as for example in the Gmehling compilations,⁵ they should, of course, be checked for thermodynamic consistency and viewed critically. They may not cover all possible temperature, pressure, and composition conditions, thus they should be incorporated into a model such as described above. Then they can be extrapolated with some measure of reliability. Many distillation simulators have VLE built into them.

TABLE 12.2
Procedure for Estimating VLE for Distillation Conditions

Steps	Comments
Obtain vapor pressure data for the components present in the mixture.	Antoine constants, thermo data, handbooks, etc.
Check vapor phase for departure from ideal gas, i.e., obtain fugacities.	Thermo data, eq. of state, generalized correlations.
View mixture for possible deviations from Raoult's law.	Homologs? Polar/non-polar mixtures? Azeotropes?
For hydrocarbon mixtures, K values may suffice at this point, with small departures from liquid phase idealities taken up by the convergence pressure.	K values from company files, API data book, GPSA data book, etc.
Find whether the mixture has been studied elsewhere (binary pairs).	Consult Hala et al., Gmehling et al., DIPPR data.
Find whether the mixture (total or by pairs) is in the Gmehling compilation.	Be careful about temperature and pressure variations.
If binary pair data are available from Gmehling or other sources, use appropriate model.	VanLaar, Wilson, NRTL, Uniquac, etc.
If still no data, check for azeotropes and calculate parameters for activity coefficient models	Consult Horsley or the new, extensive compilation by Gmehling and coworkers.
Failing the above, make estimates of activity coefficients:	
<ul style="list-style-type: none"> • Use UNIFAC structural contribution method. 	Readily available on computer diskette (e.g., Sandler, S.I. <i>Chem. and Eng. Thermo.</i> , 2nd ed., Wiley, NY, 1989).
<ul style="list-style-type: none"> • As a variation for hydrocarbon mixtures, consider the Chao-Seader version of regular solution theory. 	Occasionally the basic Scott-Hildebrand regular solution model might be useful for non-hydrocarbon mixtures.
<ul style="list-style-type: none"> • For critical cases where small errors could result in large costs, have experiments made to confirm estimated VLE. 	Outside laboratories are available for this work if it is not feasible to do it in-house.
<ul style="list-style-type: none"> • Finally, recognize the importance of variations in composition, temperature, and pressure on the values of the K values used for design. 	

Note: Process simulators can aid in some of the steps listed above.

If the pressure is high, corrections for departure from ideal gas behavior must be taken into account; equations of state or generalized compressibility charts are usually sufficient.

Mixtures with nonsimilar molecular structures, and in particular mixtures containing water, generally exhibit nonideal behavior. When this situation prevails, recourse must be made to published experimental data or correlations of liquid phase activity coefficients. With a minimum of experimental data, some very good models are available to provide activity coefficients over a broad range of conditions. If no experimental data are available, and there is no azeotrope, then approximate results can be obtained from the UNIFAC model. But it is better to make some experiments.

A procedure for approaching the problem of liquid phase nonideality through the use of activity coefficients is given in Table 12.2.

Problem 12.1

At 1.0 atm, ethanol and water form an azeotrope at 78.17°C and 0.9037 mole fraction ethanol. From this information, calculate the $\gamma^L - x$ relationships for ethanol (*i*) and water (*j*), and compare the results with the experimental data shown in Figure 12.8. Make a comparison also with curves generated by the UNIFAC method.

At 78.17°C and use of the Antoine constants in Figure 12.8,

12.3 STAGE CALCULATIONS

As noted earlier, distillation columns may be designed as a series of contacting stages, with each stage having a finite approach to an equilibrium stage. (An alternative approach, to be discussed later, is needed when the column does not contain discrete stages or plates.) Calculations for multistage columns are based on the assumption that equilibrium is attained, and correction is made later to account for the failure to reach equilibrium. Stage calculations are made to evaluate the parameters required for the column to meet the separation specifications. These parameters are commonly the number of stages, reflux ratio, distillate:feed ratio, and feed location. More details on stage calculations may be found in references 9 and 10.

12.3.1 SEPARATION SPECIFICATIONS

These specifications define the desired degree of separation. For a simple distillation process (separation of a single feed into two products, distillate and bottoms), the specifications consist of one (and only one) variable related to the distillate quality and one (and only one) variable related to the bottoms quality. For example, consider a feed of 60 mole-% benzene and 40% toluene, benzene being the more volatile. One specification might be that the distillate contain no more than 1.0 mole-% toluene and the bottoms no more than 1.0 mole-% benzene. This would fix the overall material balance and show that over 99% of the entering benzene is recovered in the distillate. Alternatively, one could specify that 95% of the benzene in the feed be recovered in the distillate at 99.0% purity. This would fix the material balance.

12.3.2 SINGLE-STAGE PROCESS

In some cases, a single stage is sufficient to effect the desired degree of separation between feed components. The single-stage process may be either *continuous* (steady state) or *differential* (batch). The continuous process is frequently referred to as flash vaporization, because one way of carrying out this process is to superheat the liquid feed and “flash” it across a valve to a vessel operating at a lower pressure, where the single-stage equilibrium between vapor and liquid is achieved.

The principal design and operating variables in the single-stage process are pressure, temperature, and L/V (liquid/vapor) ratio. Application of Gibbs' phase rule shows that these three variables are not entirely independent: fixing two of them automatically fixes the third. Ordinarily, two of the variables are specified, and computations are employed to determine the value of the third variable as well as the compositions of the vapor and liquid products.

There are two limiting cases. One is the *dew point*, where $L/V = 0$ and the product is entirely vapor but at the threshold of condensation. The relationship between pressure and temperature at the dew point is obtained by a summation of mole fractions:

$$\sum x_i = 1 \quad (12.22)$$

where

$$x_i = z_{iF} / K_i \quad (12.23)$$

The other limit is the bubble point, where $L/V = \infty$, and the product is entirely liquid at the threshold of vaporization:

$$\sum y_i = 1.0 \quad (24)$$

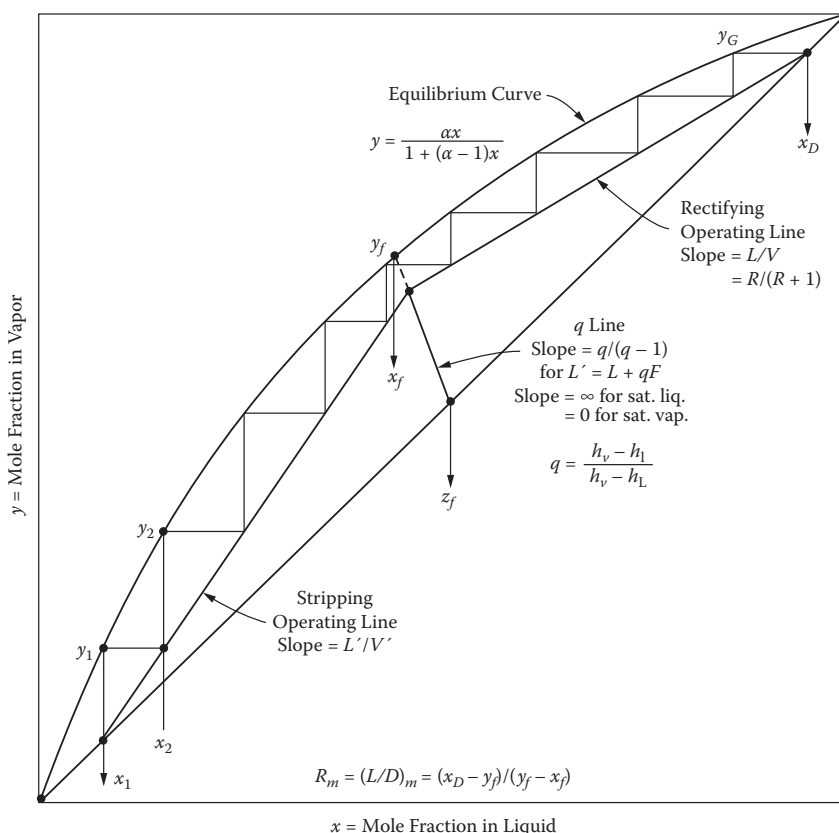


FIGURE 12.10 McCabe–Thiele diagram for a binary system.

McCabe and Thiele⁸ as summarized in Figure 12.10. First, equilibrium mole fraction coordinates are plotted to obtain the y - x curve. Then the feed, distillate, and bottoms compositions are located on the diagonal. Next, the q -line is drawn from the feed point with a slope as determined by its enthalpy as noted on the graph. (For a saturated liquid feed, the line is vertical, and for a saturated vapor feed, the line is horizontal.) Then the *rectification operating line* is drawn from the distillate composition point with a slope determined from the *reflux ratio*. Next, the *stripping operating line* is drawn from the bottoms composition point up to the intersection of the q -line and the rectification operating line. (These lines will be straight if the molal latent heats of vaporization of the pure components are equal; if these heats are unequal, then the lines will be curved and can be located only by running intermediate heat balances.) Finally, the equilibrium stages are stepped off as indicated in Figure 12.10 to give the required number of equilibrium stages. Nine equilibrium stages are shown in Figure 12.10. Details on the construction and use of McCabe–Thiele diagrams (Figure 12.10) are found in standard texts.^{4,9,10}

In the above procedure, the reflux ratio is specified and the required stages calculated. Alternatively, the number of stages is specified and the required reflux ratio calculated. This implies a fitting procedure on the chart, with the operating lines adjusted to give the correct number of stages. Such a procedure is useful when conditions are changed in an operating column; e.g., the feed composition changes and the proper reflux ratio adjustment can be predicted. The McCabe–Thiele approach can also be used to determine the minimum number of stages at total reflux and the minimum reflux ratio corresponding to an infinite number of stages.

The McCabe–Thiele approach is applicable to any binary system, even if nonideal, as will be evidenced by an unusual shape of the equilibrium curve. As normally used, the procedure requires

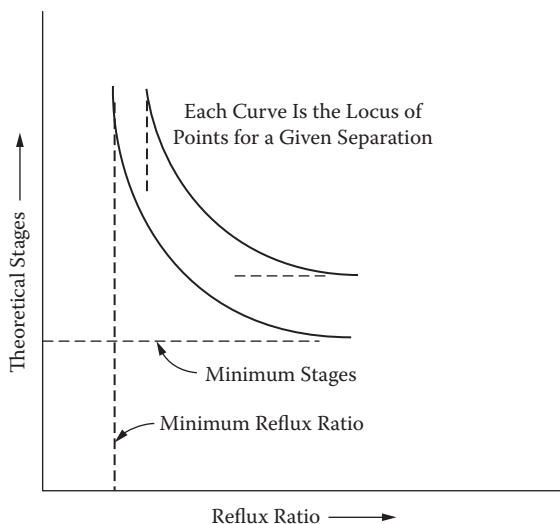


FIGURE 12.12 Representative plot of theoretical stages vs. reflux ratio for a given separation. Note the limiting conditions of minimum reflux and minimum stages.

For the limiting case of total reflux (Figure 12.12), the minimum number of stages may be determined by the Fenske¹³ equation:

$$N_m = \frac{\ln \left[\frac{(x_i / x_j)_D}{(x_i / x_j)_B} \right]}{\ln \alpha_{ij}} = \frac{\ln \left[\frac{(x_D / x_B)_i}{(x_D / x_B)_j} \right]}{\ln \alpha_{ij}} \quad (12.32)$$

where i and j are usually the light and heavy key components. The Fenske method is rigorous if the relative volatility is constant throughout the section of the column being considered. It can be used for binary systems to obviate the need for the McCabe–Thiele graphics if the relative volatility is constant, i.e., the y - x curve is uniform.

The other limiting parameter, minimum reflux ratio at infinite stages, may be calculated by means of the Underwood¹⁴ equations:

$$R_m = \sum_i \left[\frac{\alpha_i x_{iD}}{\alpha_i - \theta} \right] - 1 \quad (12.33)$$

where θ is the root of

$$\sum_i \frac{\alpha_i x_{iF}}{\alpha_i - \theta} = 1 - q \quad (12.34)$$

and q is computed as in the McCabe–Thiele method (see Figure 12.9).

The relationship between stages and reflux ratio was quantified empirically by Gilliland¹⁵ and presented graphically in Figure 12.13a. Numerous authors have published mathematical fits to the Gilliland curve, a representative fit being that of Rusche:¹⁶

$$Y = 1.0 - 0.1256X - 0.8744X^{0.2910} \quad (12.35)$$

where

$$Y = \frac{N_t - N_m}{N_t + 1} \quad (12.36)$$

$$X = \frac{R - R_m}{R + 1} \quad (12.37)$$

The relationship shown in Figure 12.13a is equivalent to that shown in Figure 12.12, with the separation parameters absorbed in the values of N_m and R_m .

As Figure 12.12 indicates, many combinations of reflux ratio and stage number can be used to obtain a required separation. The question is: what is the optimum combination? This is a classical problem in chemical engineering economics: a greater number of stages makes the column higher and more expensive, and this is balanced against the savings of utilities at the lower reflux ratio. Thus it is a matter of balancing capital and operating costs in some rational fashion. The usual approach is to express the optimum condition in terms of an optimum ratio of R to R_m .

12.3.7 OPTIMUM REFLUX

A popular rule of thumb is to use a ratio R/R_m of about 1.2. Fair and Bolles¹⁷ made a detailed study of this ratio, and three cases of their work are shown in Figure 12.13b. The cases represent different levels of coolant ranging from -85°C (requiring expensive two-level refrigeration) to $+30^\circ\text{C}$ (cooling water). The shapes of the curves are strikingly similar, with an optimum R/R_m of about 1.05. However, the computation of minimum reflux R_m is imprecise, especially for multicomponent systems, owing to inaccuracies of phase equilibrium and stage model execution. To avoid the danger of an impossible design, optimum R/R_m values in the range of 1.15 to 1.25 should be used. The curves are fairly flat at higher R/R_m values, so the selection of the design value has flexibility and may very well be influenced by such practical concerns as maximum allowable diameter, plant limitations on maximum height, and so on.

Figure 12.13a or Equation (12.35) may be used to obtain an approximate number of theoretical stages from the simple Fenske equation for minimum stages. Equations (12.36) and (12.37) may be modified to

$$Y = \frac{N_t/N_m - 1}{N_t/N_m + 1/N_m} \quad (12.36)$$

$$X = \frac{R/R_m - 1}{R/R_m + 1/R_m} \quad (12.37)$$

For example, if $N_m = 5$ and $R_m = 0.70$ (from Fenske and Underwood relationships), and optimum $R/R_m = 1.15$, $X = 0.058$ and, from Figure 12.13a, $Y = 0.57$. Solving, $N_t/N_m = 2.59$. While this ratio will vary with conditions, the heuristic of $N_t/N_m = 2.5$, given in Section 12.1.1, is often used.

12.3.8 DESIGN PROCEDURE

First, the minimum number of stages is computed by the Fenske method. Then, the minimum reflux ratio is computed by the Underwood method. Next, the design (operating) reflux ratio is chosen as some multiple of the minimum reflux ratio, e.g., $1.15 \times R_m$. (The optimum multiple is in the

calculations proceed from the ends of the column toward the feed [or from one end to the other, taking into account the addition of the feed(s)]. In each stage, four criteria must be satisfied: material balance, equilibrium between phases, summation of phase mole fractions to 1.00, and heat balance.

From the first letters, the familiar MESH equations are identified. These equations must be solved rigorously at each stage before moving to the next. When the traverse of the column is completed, there must be a match between the computed and assumed overall material balance. If not, another trial is necessary. Especially onerous are the points of addition of components not present in both distillate and bottoms streams. While the Lewis–Matheson method is straightforward (although extremely laborious) for hand calculations, it was the standard method before large computers became available. With large computers, it often presents serious programming problems with respect to the convergence algorithm—particularly the assumptions of splits of nonkey components.

The *rating method* for rigorous stage calculations was developed by Thiele and Geddes.¹⁹ Their approach is a “rating” method in that it starts with a specified number of stages and reflux ratio and then rates the separation possible with that combination. The method is more amenable to computer implementation and now is the standard. The Thiele–Geddes derivation begins with a component mass balance on the general contacting stage, counting downward from the top of the column:

$$V y_{n+1,i} + L x_{n-1,i} - V y_{n,i} - L x_{n,i} + F z_{n,i} = 0 \quad (12.38)$$

Equation (12.38) may be rewritten in terms of the molar flow rates of a specific component:

$$v_{n+1,i} + l_{n-1,i} - v_{n,i} - l_{n,i} + f_{n,i} = 0 \quad (12.39)$$

The phase equilibrium relationship is defined by

$$y_{i,n} = K_{i,n} x_{i,n} \quad (12.40)$$

which may be rewritten as

$$\frac{v_{n,i}}{V} = K_{i,n} \frac{l_{n,i}}{L} \quad (12.41)$$

from which

$$l_{n,i} = \left(\frac{L}{K_{i,n} V} \right) v_{n,i} \quad (12.42)$$

Introducing the “absorption factor” A_n , defined as

$$A_{n,i} = L/K_{i,n} V \quad (12.43)$$

Equation (12.42) becomes

$$l_{n,i} = A_{n,i} v_{n,i} \quad (12.44)$$

TABLE 12.4
Computer Solution for Problem 12.3 Six-Component Deethanizer

Part 1							
Reflux ratio, mol/mol	1.722						
Reflux rate, lb-mol/h	65.160						
Column duties, Btu/h:							
Condenser	494,790						
Reboiler	573,407						
External stream data	Top liquid	Bottom liquid	Feed 1				
Theoretical stage number	15	0	7				
Flow rate, lb-mol/h	37.840	62.160	100.000				
Mole ratio to Feed 1	0.378	0.622	1.000				
Mean molecular weight	28.70	48.46	40.99				
Flow rate, lb/h	1086.088	3012.558	4098.645				
Temperature, °F	−10.92	174.84	90.38				
Pressure, lb/in. ²	400.000	402.400	401.700				
Vapor, mol%	0.0	0.0	0.0				
Enthalpy, Btu/lb-mol	−960.167	3838.231	1236.349				
Composition, mol%							
Methane	13.2129	0.0004	5.0000				
Ethane	82.9823	5.7907	35.0000				
Propylene	2.4010	22.6697	15.0000				
Propane	1.3986	31.3236	20.0000				
<i>i</i> -Butane	0.0043	16.0849	10.0000				
<i>n</i> -Butane	0.0009	24.1307	15.0000				
Composition, mass%							
Methane	7.3839	0.0001	1.9567				
Ethane	86.9371	3.5928	25.6779				
Propylene	3.5201	19.6832	15.4002				
Propane	2.1485	28.4962	21.5144				
<i>i</i> -Butane	0.0087	19.2894	14.1803				
<i>n</i> -Butane	0.0018	28.9382	21.2704				
Recovery, %							
1. Methane	99.9950	0.0050					
2. Ethane	89.7158	10.2842					
3. Propylene	6.0569	93.9341					
4. Propane	2.6462	97.3538					
5. <i>i</i> -Butane	0.0162	99.9838					
6. <i>n</i> -Butane	0.0022	99.9978					
Part 2							
Stage	Temperature (°F)	Pressure (lb/in. ²)	Liquid flow (lb-mol/h)	Vapor flow (lb-mol/h)	Molecular weight		Murphree % Efficiency
					Liquid	Vapor	
15	−10.92	400.00	65.16	0.0	28.70	22.53	100.0
14	42.11	401.00	69.23	103.00	30.99	28.70	100.0
13	55.27	401.10	67.53	107.07	32.32	30.18	100.0
12	64.57	401.20	65.18	105.37	33.66	31.02	100.0
11	73.62	401.30	63.14	103.02	35.00	31.84	100.0

TABLE 12.4 (Continued)

Computer Solution for Problem 12.3 Six-Component Deethanizer

Part 3						
Stage Liquid Compositions, mol%						
Stage	Methane	Ethane	Propylene	Propane	<i>i</i> -Butane	<i>n</i> -Butane
15	13.2129	82.9824	2.4010	1.3986	0.0043	0.0009
14	2.9845	86.6237	6.2324	4.1270	0.0255	0.0069
13	1.4660	79.6127	10.8481	7.9536	0.0892	0.0304
12	1.2486	70.0240	15.6894	12.6693	0.2572	0.1115
11	1.2266	60.5271	19.7462	17.5037	0.6421	0.3543
10	1.2311	52.5229	22.2506	21.5755	1.4232	0.9967
9	1.2376	46.3140	22.8969	24.1831	2.8463	2.5220
8	1.2450	41.4649	21.6470	24.7590	5.1421	5.7419
7	1.2552	37.3540	18.6561	22.9094	8.2599	11.5654
6	0.4215	34.8887	20.1297	24.4285	8.4259	11.7057
5	0.1395	30.9766	21.8767	26.3576	8.6912	11.9583
4	0.0457	26.0987	23.7688	28.6531	9.0898	12.3439
3	0.0148	20.6871	25.4766	31.0782	9.7342	13.0092
2	0.0047	15.2175	26.4363	33.0905	10.8664	14.3846
1	0.0014	10.1366	25.8269	33.6826	12.8729	17.4795
0	0.0004	5.7907	22.6697	31.3236	16.0849	24.1307
Stage Vapor Compositions, mol%						
Stage	Methane	Ethane	Propylene	Propane	<i>i</i> -Butane	<i>n</i> -Butane
15	54.2878	45.0709	0.4272	0.2137	0.0003	0.0000
14	13.2122	82.9828	2.4011	1.3987	0.0043	0.0009
13	6.5986	85.3369	4.8787	3.1630	0.0180	0.0047
12	5.6835	80.8223	7.8155	5.6003	0.0587	0.0198
11	5.6424	74.7827	10.8093	8.5304	0.1643	0.0709
10	5.7174	68.9399	13.2477	11.4699	0.4031	0.2219
9	5.7973	64.1303	14.6862	13.8865	0.8825	0.6172
8	5.8823	60.5355	14.9477	15.3463	1.7440	1.5442
7	5.9905	57.9268	14.0158	15.4965	3.1049	3.4655
6	2.0280	56.7902	16.1847	17.7282	3.4413	3.8277
5	0.6758	52.4624	18.5958	20.2643	3.8003	4.2016
4	0.2228	46.0511	21.4021	23.3853	4.2659	4.6728
3	0.0725	38.1634	24.4218	27.0665	4.9342	5.3416
2	0.0232	29.4659	27.1308	30.9334	5.9916	6.4551
1	0.0072	20.7356	28.6410	34.1247	7.8117	8.6798
0	0.0020	12.6775	27.6728	35.0618	10.9949	13.5909

The occurrence of a minimum or maximum on the temperature vs. composition surface is caused by positive or negative deviations from Raoult's law [see Equation (12.19)]; a system is *positive* if the logarithm of the activity coefficient γ_i^L is greater than zero, and *negative* if the logarithm is less than zero. Deviation from Raoult's law is not sufficient to cause the occurrence of an azeotrope; the boiling points of the pure components must also be sufficiently close to permit a minimum or maximum temperature to occur. Close-boiling components with small deviations from ideality may form an azeotrope. On the other hand, compounds that form very nonideal liquid mixtures may not exhibit an azeotrope because of a wide difference in their boiling points. Azeotropes seldom occur between compounds whose boiling points differ by more than 30°C.

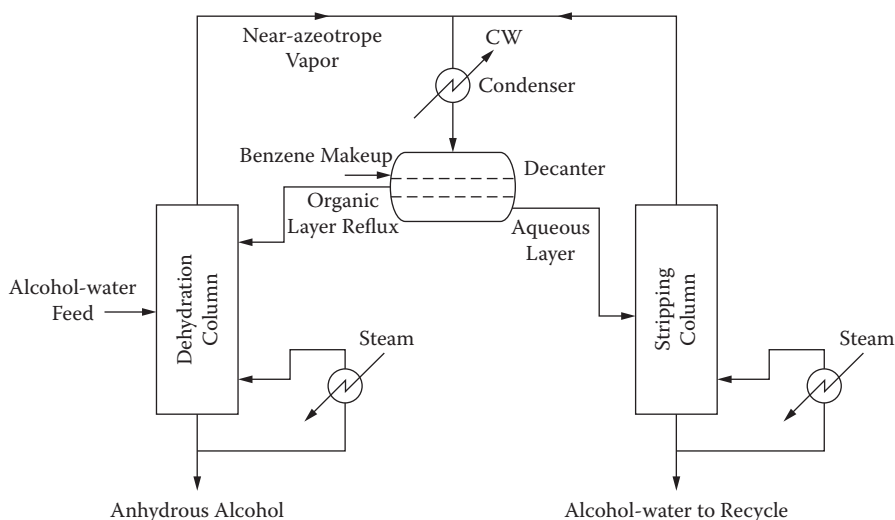


FIGURE 12.15 Flow diagram of azeotropic distillation system to obtain anhydrous ethanol.

alcohol azeotrope. Figure 12.15 shows a flow diagram of the entire process, starting with the water-ethanol azeotrope as feed. Thus, in the total process, the following could be involved:

	B.P., °C at 1 atm	Comp., wt-%
Benzene–alcohol–water azeotrope	64.86	H ₂ O 7.4, EtOH 74.1, C ₆ H ₆ 74.1
Benzene–alcohol azeotrope	68.3	EtOH 32.0
Benzene–water azeotrope	69.0	H ₂ O 8.8
Alcohol–water azeotrope	78.2	H ₂ O 4.0
Alcohol	78.3	
Benzene	80.1	
Water	100	

If alcohol is to be produced in high purity as a bottoms stream, then the water and benzene must be tied up in lower-boiling azeotropes and pure compounds and distilled overhead.

For approximate calculations, the azeotropes may be considered pseudocomponents with their individual vapor pressures, as indicated in Figure 12.16. The vapor pressure of the pseudocomponent (butanol–water azeotrope) roughly parallels the lines for *n*-butanol and water, and relative volatilities between the three components could be established.

Problem 12.4

Consider producing anhydrous ethanol from a feed stream containing 85 mole-% C₂H₅OH and the remainder water. Since this system exhibits a minimum-boiling azeotrope at 78.1°C containing 89.43 mole-% C₂H₅OH (at 1 atm), the separation is impossible by ordinary distillation.

However, the addition of benzene as an entrainer results in a minimum-boiling heterogeneous ternary azeotrope at 64.86°C (1 atm) of the following molar composition:

Ethanol	22.8%
Benzene	53.9%
Water	23.3%
	<hr/> 100.0%

is affected to a degree different from that of the other component. Horsley²¹ and Gmehling et al.²² discuss methods for estimating the azeotropic composition and temperature for numerous systems.

One of the mechanisms for identifying possible entrainers is hydrogen bonding. Ewell et al.^{23a} have classified liquids into five groups according to their hydrogen bonding characteristics. For example, the following are considered strong and weak in their hydrogen bonding:

Strong	Weak
O → HO	N → HN
N → HO	O → HCCl ₃
O → HN	HCCl-CCl
	N → HCNO ₂
	HCCN

The hydrogen bonding grouping provides insight for screening suitable entrainers in the development of a feasible azeotropic distillation process. Selected entrainers are then tested experimentally for their quantitative effect on VLE.

12.4.2 EXTRACTIVE DISTILLATION

In extractive distillation, an *extractive agent* is added to the mixture to be distilled for the purpose of modifying the relative volatility of the key components without forming an azeotrope. Extractive distillation is usually employed to improve the separability between close-boiling components for which ordinary distillation would not be economically feasible.

Like azeotropic distillation, extractive distillation involves highly nonideal phase equilibria as well as the addition of an agent, often called a *solvent*, that modifies and improves the phase equilibria among the system components. However, extractive distillation is different in that no azeotropes are involved, and the agent added is essentially nonvolatile and introduces no new azeotropes.

Extractive distillation is a simpler process than azeotropic distillation. Because of its low volatility, the solvent always leaves the column with the bottoms product, and thus an additional distillation step is required to separate the solvent for recycle. To maintain the solvent throughout the column, the solvent must be introduced with or above the fresh feed. It is customary to employ a rectification section with reflux, above the solvent feed point, so as to prevent loss of solvent with the distillate.

Methods of analysis based on simple distillation may often be used on a solvent-free basis. The relative volatility between key components, *i* and *j*, is based on the simple relationship

$$\alpha_{ij} = \frac{p_i^*}{p_j^*} \left(\frac{\gamma_i^L}{\gamma_j^L} \right)_{\text{solvent}} \quad (12.47)$$

When the vapor pressures are very close, searches for effective solvents involve simple measurement of the activity coefficient ratio. The searching process is easier than that for azeotropic distillation. The usual approach is to select a solvent that is similar in structure to the heavy key component. Since the light key component is of a different structure (as it must be, or simple distillation could be employed), the solvent serves to increase the volatility of the light key relative to the heavy key.

An example of an extractive distillation process is the separation of methylcyclohexane (MCH) from toluene using a phenol solvent, as shown in Figure 12.17. Since MCH boils at 101.0°C and toluene boils at 110.7°C (1 atm), their separation by ordinary distillation is very difficult even though they do not form an azeotrope. Phenol is an effective solvent, since it has a structure more similar to the aromatic than to MCH (a naphthene), and it is relatively nonvolatile. The rectification

approximation to the true boiling point as a function of the percent of feed distilled. The TBP curve was traditionally obtained by subjecting the feed to distillation in a batch column with several hundred equilibrium stages operated at a reflux ratio of 100:1 or higher. A precision chromatograph is currently used to obtain the TBP curve.

Figure 12.18 shows how a complex system differs from a multicomponent system. The complex system exhibits a smooth TBP curve, because even the high separating power of the TBP apparatus cannot resolve all the many close-boiling constituents. The multicomponent system, on the other hand, is easily resolved by the powerful TBP apparatus, although any azeotropes will be distilled over as though they were pure (pseudo) components.

To design complex distillation columns, multicomponent methods are used. The true boiling curve is replaced by an approximate stepwise representation as shown in Figure 12.18. Each step represents a pseudocomponent with a boiling point as indicated and a fraction of the total feed mixture based on the length of the horizontal portion of the step.

12.4.4 STEAM DISTILLATION

A steam distillation is simply a distillation in which steam is involved as a process component. Steam (water) is inexpensive and immiscible with many chemical compounds (e.g., hydrocarbons and many organic chemicals) and hence is a special case of azeotropic distillation. In the usual application, very little of the steam condenses in the liquid phase, and thus problems of handling two liquid phases in the contacting equipment are avoided.

If an organic compound is essentially immiscible with water in the liquid phase, then vapor pressures are additive to make up the system total pressure:

$$p_{org}^{sat} + p_{water}^{sat} = P \quad (12.48)$$

This simple equation is based on very little miscibility such that the activity coefficients for each phase are essentially unity.

Application of Equation (12.48) with the Antoine equation [Equation (12.13)] shows that steam distillation can be used to distill an organic compound at much lower temperatures than would otherwise be possible. Considering the system pressure P as constant, then the more steam introduced, the lower will be the partial and vapor pressures of the organic and thus the lower its boiling point. The other key element of the choice of water as the entrainer is that it is easily separated from the product (organic) by simple condensation followed by decanting.

Thus, steam distillation finds application in the purification of heat-sensitive materials as an alternative to vacuum distillation, since the dilution effect of steam enables lower effective boiling points of the materials.

12.4.5 BATCH DISTILLATION

Batch distillation is performed on a fixed charge quantity—the batch. The original charge is replenished by another charge at the end of each cycle.

This process is used extensively in the laboratory and in small production units where the same equipment can serve different applications. Between each batch operation, the equipment can be cleaned as necessary. When the charge is a multicomponent mixture, batch distillation in a single column can separate all constituents, whereas continuous distillation would require several columns.

For a binary system with a single equilibrium stage, i.e., a reboiled stillpot with no rectification column, the mass balance is given by the Rayleigh equation:

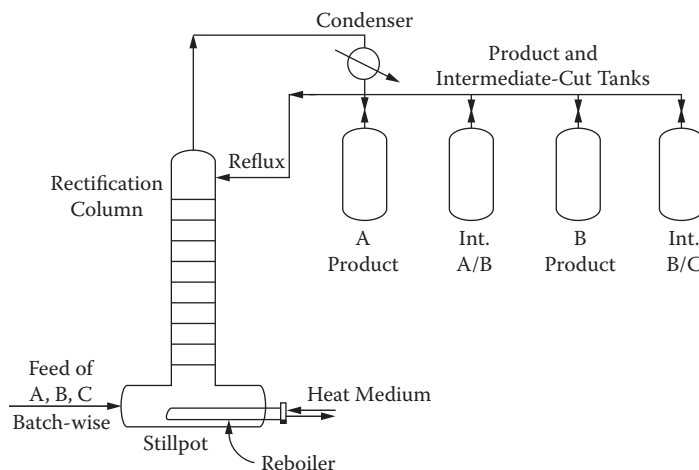


FIGURE 12.19 Typical batch distillation system.

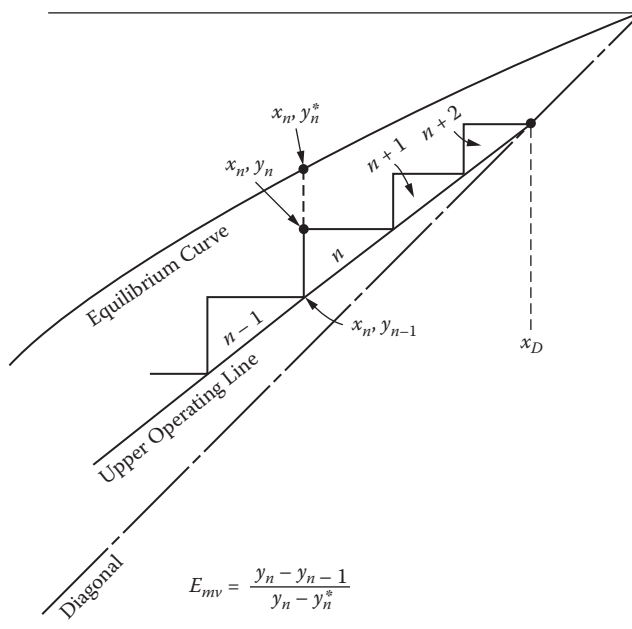


FIGURE 12.20 Upper quadrant of a McCabe–Thiele diagram for batch distillation at constant reflux. Four theoretical stages shown.

the column affects the concentration gradients in the column. The equation for the effect of holdup on the mass balance around a general batch contacting stage n is

$$J_n \left(\frac{dx_{i,n}}{dt} \right) = L_{n-1} x_{i,n-1} + V_{n+1} y_{i,n+1} - L_n x_{i,n} - V_n y_{i,n} \quad (12.52)$$

where J_n is the stage molar holdup, and dx/dt is the rate of change of liquid concentration with respect to time.

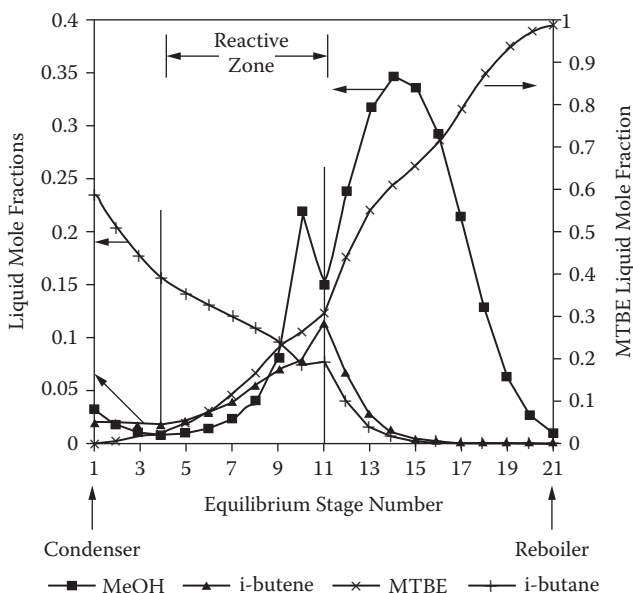


FIGURE 12.22 Computed composition profiles in an MTBE reactive column. Composition of the diluent, *n*-butane, may be obtained by difference. (H. E. Subawalla, 1997. Ph.D. dissertation, Univ. of Texas at Austin.)

- Is there an advantage in shifting the chemical equilibrium? A reaction with a highly favorable equilibrium is not likely to be a candidate.
- The reaction product must boil in an appropriate range and be separable by distillation. If the boiling point of the desired product instead falls within a range of other products, more distillation columns will be needed.
- The optimum temperature and pressure conditions for the reaction must be the same as those required for separation.
- Only one liquid phase should be present. A second liquid phase can introduce problems in the hydraulic design of the distillation column. In some cases, this problem can be avoided through the use of a separate cosolvent, which then must be separated for recycle.
- If the catalyst is a solid, it must create neither excessive pressure drop nor an excessively large column. An optimal arrangement of solid catalysts in the column is needed.
- A suitable model must be available for determining concentration profiles throughout the column and judging needs for reflux and boilup. This implies knowledge of the reaction kinetics, likely obtained separately in laboratory equipment.

A representative profile for a column in which methanol and *i*-butene are reacted to form methyl tert-butyl ether (MTBE) is shown in Figure 12.22. Note that an inert *n*-butane, is not shown. The reactants are fed at different stages, and the desired product, MTBE, is removed from the bottom of the column in high purity.

Many patents and publications relating to reactive distillation have been published. A paper on the heuristics of reactive distillation column design contains many references.²⁹

12.5 DISTILLATION COLUMNS

As noted earlier, distillations are performed in vertical, cylindrical columns when more than a single contacting stage is required, as indicated in Figure 12.23.

TABLE 12.5
Criteria for Selecting a Distillation Column Device

Vapor-handling capacity	Entrainment flooding. At incipient flooding, the minimum column diameter is fixed.
Liquid-handling capacity	Fixes the size of downcomers. Downcomer backup can also lead to flooding.
Mass transfer efficiency	Sets the required height, for a given number of theoretical stages. The efficiency can be a function of column diameter.
Flexibility	Is a concern when the column must be operated under a wide range of feed rates, or when future capacity needs must be considered in the initial design.
Pressure drop	Low pressure drop is critical for vacuum columns, especially when there are needs to maintain a low bottoms temperature.
Cost	The total cost of the system must be considered, including auxiliary equipment. A more expensive device might lead to lower operating costs.
Design limitations	The device should have been proven commercially. Also, the user needs to understand how the device was designed (if by a vendor)
Special concerns	Fouling, corrosion Ease of installation or removal Potential foaming problems Adequate residence time for reactions Special heat transfer needs

the effects of the geometry of the column have been taken into consideration. (This is the *rating approach*, common in chemical engineering practice, where a device geometry is contrived and then rated for capability to perform the needed service.) Thus, as a result of earlier studies, the following information will be at hand: actual stages (or packed height), vapor flow rate, liquid flow rate, vapor and liquid compositions, temperatures, and pressures.

Ideally, this information will be available for a number of points in the column. As a bare minimum, it must be available at the top, bottom, and center (above and below the feed point for a single column). Some approximations may be in order, e.g., assumed: pressure profile, equal molal downflow and upflow, and constant efficiency throughout the column. Normally, these assumptions will in turn be verified or modified.

The general objective of equipment process design is to establish specifications for the optimum fractionating system hardware. (Alternatively, an objective could be to gain an understanding of an existing system under analysis.) For the column only, criteria for selection of the internal contacting devices are given in Table 12.5. Each of these criteria should be considered carefully.

The function of the device is to bring vapor and liquid into intimate contact. Many devices have been developed through the years.³⁰ Three important tray-type devices are shown in Figure 12.24, and several packings are shown in Figure 12.25. All devices vary in their ability to provide intimate contacting, effect sharp separations, realize low pressure drops, and handle liquids that might foul or plug the system.

An enormous amount of study has been made to evaluate the performance of many contacting devices, using a variety of test mixtures. Only a portion of the results have been published in the open literature, on a random basis with unification through handbooks, texts, and review papers. Fractionation Research, Inc. (FRI), an industry-sponsored organization for conducting commercial-scale tests of devices under carefully controlled experimental distillation or absorption conditions, has been a leader, performing thousands of experiments.^{31,32} An updated state-of-the-art review of equipment types and characteristics has been published by FRI and collaborators.³³

Devices for effecting contact of vapor and liquid may be classified as shown in Table 12.6. Recently, there has been a trend away from the conventional crossflow devices, in the direction of counterflow devices, mostly packings. Still, an enormous number of older columns are operating with trays, and thus the technology of tray design and analysis is important.

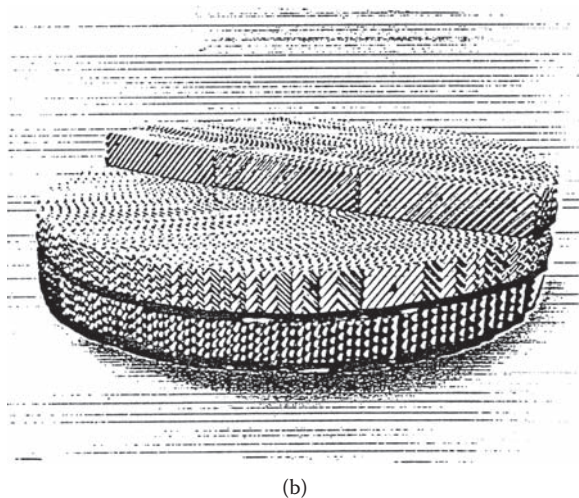
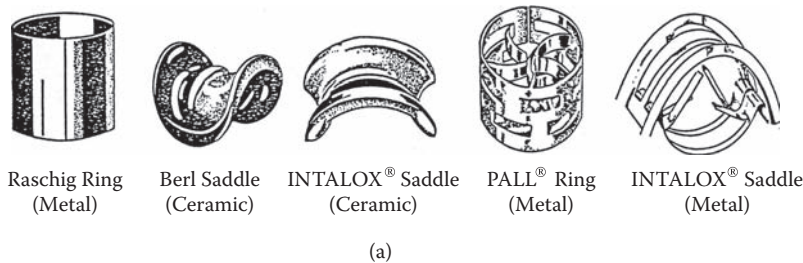


FIGURE 12.25 Views of representative packing elements. (a) Random. (b) Structured.

TABLE 12.6
Classification of Contacting Devices

Crossflow trays	Bubble-cap	
	Sieve	
	Valve	
Counterflow Packings	Random	Rings
		Saddles
		Other
	Ordered	Structured
		Mesh
		Grid
Counterflow Trays	Dualflow	
	Multiple downcomer	
	Baffle trays (splash decks)	
Special devices	Sprays	
	CoFlo	
	Moving internals	

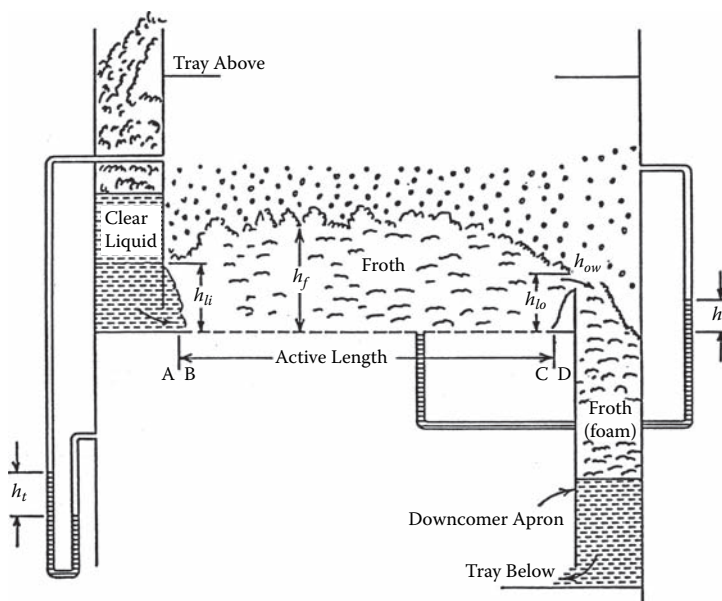


FIGURE 12.28 Schematic diagram of a crossflow sieve tray. Valve trays and bubble-cap trays have equivalent diagrams.

low liquid-to-vapor volumetric flow ratios such as occur in high-vacuum distillations. Liquid is distributed to the tray by flow under the downcomer apron; additional distribution can be obtained from an inlet weir (not shown). The active length BC normally includes the total distance from downcomer apron (or inlet weir) to outlet weir, i.e., A and D lengths are effectively zero.

The droplets carried above the froth may return to the froth or, for very small droplets, are entrained to the tray above. When the froth level approaches the tray above, as at high rates of vapor flow, even the large droplets cannot complete their trajectories and thus impact the tray above, possibly moving through the perforations as entrained liquid. Such a phenomenon drastically reduces tray efficiency.

Allowable flows of vapor through the froth are correlated on the basis of liquid entrainment. Balancing of the drag force of the vapor on a representative drop of liquid against the gravitation force on the drop has led to the relationship,

$$U_N = C_{sb} \left(\frac{\rho_L - \rho_v}{\rho_v} \right)^{0.5} \quad (12.54)$$

where U_N is the superficial vapor velocity based on A_N (Figure 12.27) and C_{sb} is a correlating term called the Souders–Brown capacity parameter.

Values of C_{sb} may be obtained from Figure 12.29 and are based on tray spacing, surface tension, vapor velocity through the perforations, and liquid flow rate. The abscissa group, $L / G \sqrt{\rho_v / \rho_L}$, is an important correlating term called the *flow parameter* and represents a ratio of kinetic energies of liquid to gas. It is used for several correlations involving vapor-liquid ratios. Figure 12.29 represents experimental data, including recent FRI work, and should be used for design purposes.³⁵ It has the following restrictions: (1) low- to nonfoaming system, (2) weir height less than 15% of tray spacing, (3) hole diameter 0.5 in. (12.7 mm) or less (sieve trays), and (4) hole (or riser) area 10% or more of the active (bubbling) area. Smaller hole areas tend to produce jetting because of high hole velocities, and corrections are as follows:

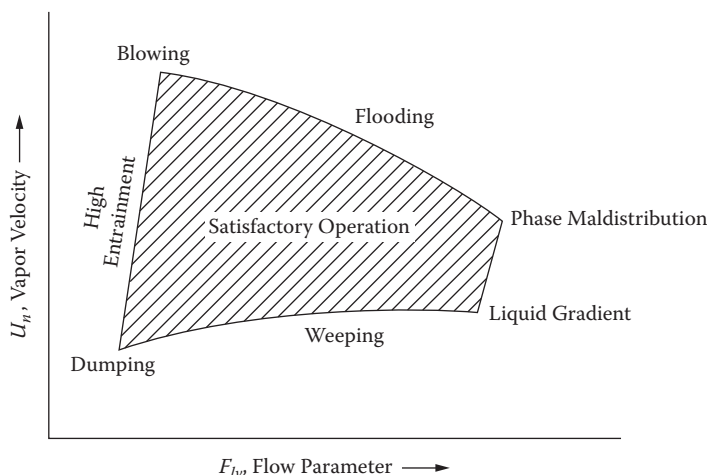


FIGURE 12.30 Generalized plot showing operating zones of a crossflow tray.

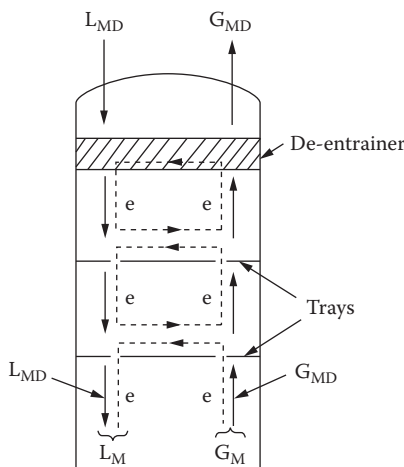


FIGURE 12.31 Diagram showing the recirculation effect of liquid entrainment, and the definition of terms used in design Equation (12.55).

12.6.1.2.2 Pressure Drop

The decrease in pressure, as the vapor flows upward through a tray, is the sum of the pressure drop through the perforations and the residual drop through the froth or spray:

$$h_t = h_d + h_L \quad (12.56)$$

where pressure drop is expressed in terms of head of clear liquid on the tray. For flow through the perforations, the simplified orifice equation is used (assuming uniform flow through all the holes):

$$h_d = \frac{50.8}{C_v^2} \frac{\rho_v}{\rho_L} U_h^2 \quad (12.57)$$

The discharge coefficient C_v may be obtained from Figure 12.33³⁹ or from the relationship

$$C_v = 0.74(A_t/A_a) + \exp[0.29(t_t/d_h) - 0.56] \quad (12.58)$$

where t/d_h is the tray thickness/hole diameter ratio. Equation (12.58) and Figure 12.33 predict pressure drops that check well with observations of commercial scale sieve tray columns.

For pressure drop through the froth or spray,

$$h_L = h_t - h_d \quad (12.59)$$

where h_L is simply regarded as a residual term and is correlated on the basis of dry tray pressure drop measurements, standardizing on Equation (12.58) for the orifice coefficients when actual data are not available, along with overall tray pressure drop measurements (usually available in operating columns). Values of h_L are determined as a function of vapor hole velocity and liquid flow rate as shown in Equations (12.60) and (12.61):

$$\beta = h_L/(h_w + h_{ow}) \quad (12.60)$$

$$\beta = 0.19 \log_{10} L_w - 0.62 \log_{10} F_{vh} + 1.679 \quad (12.61)$$

where

β = dimensionless aeration factor

h_w and h_{ow} = weir height and weir crest (clear liquid basis), mm

L_w = flow rate of liquid over the outlet weir, m³/s-m weir length

F_{vh} = vapor "F-factor" based on hole velocity, $F_{vh} = U_h(\rho_v)^{0.5}$

The value of the weir crest h_{ow} in Equation (12.60) employs the classic Francis weir equation:

$$h_{ow} = 664 L_w^{0.667} \quad (12.62)$$

Even though froth actually flows over the weir (unless calming zones are used), h_{ow} is expressed on an equivalent clear liquid basis, assuming that the Francis relationship also represents froth flow.

Later, in connection with mass transfer in tray froths, we will discuss a relative froth density:

$$\phi_f = \rho_f/\rho_L \quad (12.63)$$

This is a ratio of the average density of the two-phase mixture to the liquid density (it approaches unity for lightly aerated liquids). Equation (12.62) may thus be modified by Equation (12.63) to give

$$h_{ow} = 664 \phi_f^{1/3} L_w^{2/3} \quad (12.64)$$

This area of sieve tray froth hydraulics has been the subject of considerable study. While the relationships thus far presented are not completely fundamental, they are simple to apply and are sufficiently reliable for most engineering purposes.

12.6.1.1.3 Liquid-Handling Capacity

The downcomer serves to transfer the downflowing liquid between the trays in a column and can become a bottleneck under high liquid flow conditions (as in high-pressure absorbers and fractionators). Downcomers are normally sized such that they do not fill completely with the combination of clear liquid and froth (Figure 12.28). Overloaded downcomers lead to a flood condition in the entire column. Thus, we distinguish between "entrainment flood" and "downcomer flood" but recognize that one often leads to the other.

TABLE 12.7
Capacity Discount Factors for Foaming Systems

Nonfoaming systems	1.00
Moderate foaming, as in oil absorbers, amine, and glycol regenerators	0.85
Heavy foaming, as in amine and glycol absorbers	0.73
Severe foaming, as in MEK units	0.60
Foam-stable systems, as in caustic regenerators	0.15

When the liquid has foaming tendencies, additional residence time must be allowed for phase disengagement. System discount factors, recommended by Koch–Glitsch, Inc. on the basis of field experience, are shown in Table 12.7. As an example, the “maximum allowable velocity” of 0.1 m/s would be multiplied by the discount factor so as to provide adequate downcomer volume.

12.5.1.1.4 Minimum Vapor Rate

As shown previously in Figure 12.25, the performance of tray devices drops off at low velocity because of weeping and/or poor vapor dispersion. Weeping is usually associated with sieve trays or fixed valve trays, which have no built-in protection against liquid flow through the openings at low vapor velocities. Movable valve trays can also weep, since the valve units are designed not to close completely at zero vapor rate. In theory, at steady state and with equal vapor velocity through all of the holes, there will be no weeping on a sieve tray when

$$(h_d + h_\sigma) > h_L \quad (12.68)$$

Then the pressure drop through the hole plus the head of liquid necessary to overcome surface tension can act against the liquid head above the hole to prevent liquid from entering the hole. The term h_σ in Equation (12.68) may be estimated from the following *dimensional* equation:

$$h_\sigma = 409 \left(\frac{\sigma}{\rho_L d_h} \right), \text{ mm liquid} \quad (12.69)$$

where

σ = surface tension, mN/m

d_h = hole diameter, mm

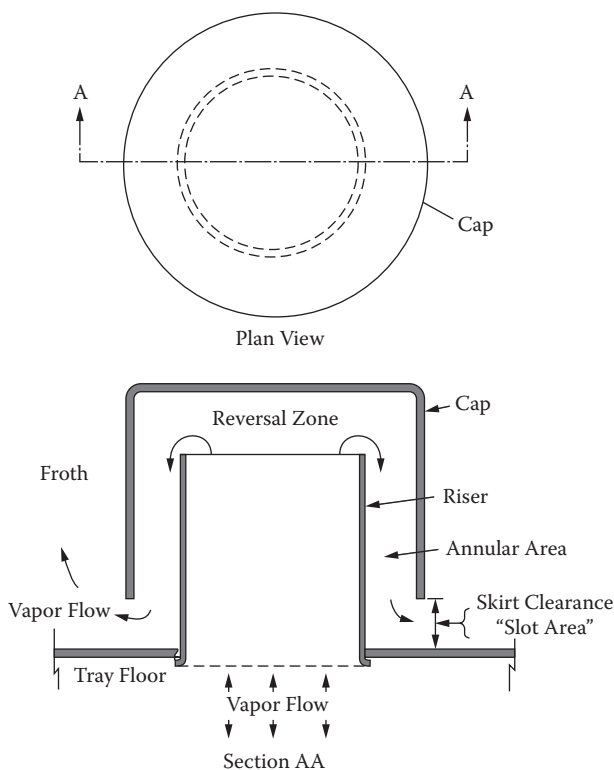
ρ_L = liquid density, kg/m³

Equation (12.68) applies only to a steady-state condition, and this rarely happens. Some holes pass neither vapor nor liquid. There is considerable sloshing, froth pounding, oscillation, and so on. A modified Equation (12.68) is shown in Figure 12.35. The lines of the figure may be approximated by

$$h_d + h_\sigma = 0.036(h_w + h_{ow}) + 0.25 \text{ (20\% open)} \quad (12.70)$$

$$h_d + h_\sigma = 0.013(h_w + h_{ow}) + 0.25 \text{ (6–14\% open)} \quad (12.70a)$$

While weeping may occur over a broad range of operating rates, it does not necessarily detract from the mass transfer capability of the tray, so long as loadings are reasonably high. At some very low vapor rate, efficiency plunges, and the flow condition is often called the *dump point*. Figure



Note: Riser & Cap Held in Place by Suitable Clips and Spacers

FIGURE 12.36 Diagram of a typical bubble cap.

12.6.1.2.2 Movable Valve Trays

These contacting devices can extend the operating range of a crossflow sieve tray, as indicated by Figure 12.26, which shows that the sieve tray under observation loses efficiency at an F-factor of about $1.0 \text{ m/s}(\text{kg/m}^3)^{0.5}$, whereas the addition of valves permits operation down to an F-factor of 0.6 or below. A movable valve is shown in Figure 12.37 alongside a fixed valve counterpart. Note that valves can have various shapes, often circular (see Figure 12.24).

Manufacturers of valve trays, such as Koch–Glitsch, Inc., of Wichita, Kansas (Ballast trays and Flexitrays), and Sulzer–Chemtech (formerly Nutter Engineering Co.), of Tulsa, Oklahoma (Float Valve Trays), have prepared proprietary design manuals. Hence, only limited discussion will be given here. As for bubble-cap trays, design methods follow those for sieve trays. The vapor capacity chart (Figure 12.29) covers valve trays, as does the alternate method of Kister and Haas.³⁶ Information on liquid entrainment is proprietary, but measurements have been made by Fractionation Research, Inc.³¹ Because of the vapor flow reversal, one would not expect entrainment from valve trays to be greater than that from sieve trays. Liquid capacity considerations follow exactly those for sieve trays.

Pressure drop prediction follows the same approach as for sieve trays, with the primary difference being in the determination of dry tray pressure drop. Values of dry drop for fully open and fully closed valves may be estimated from relationships such as those of Klein⁴³:

$$\text{Closed: } h_d = K_c \frac{\rho_v}{\rho_L} U_c^2 \quad (12.71)$$

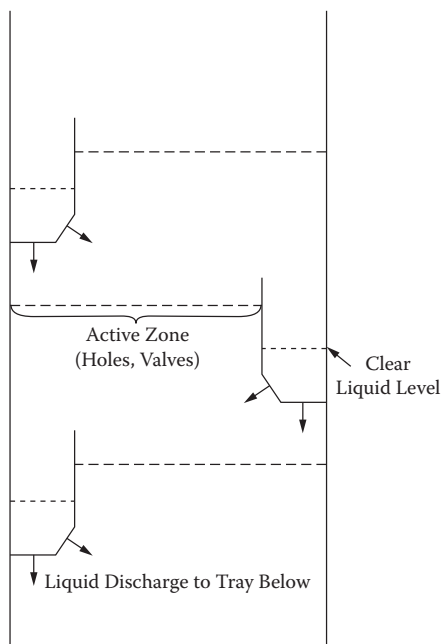


FIGURE 12.38 Hanging downcomer tray. Note that the part of the tray floor normally used as the bottom of the downcomer is converted to bubbling (active) area.

capacity has not always been achieved, however, and the design of the downcomer is critical, because too big of an opening at its bottom can allow vapor to bypass the contacting zone.

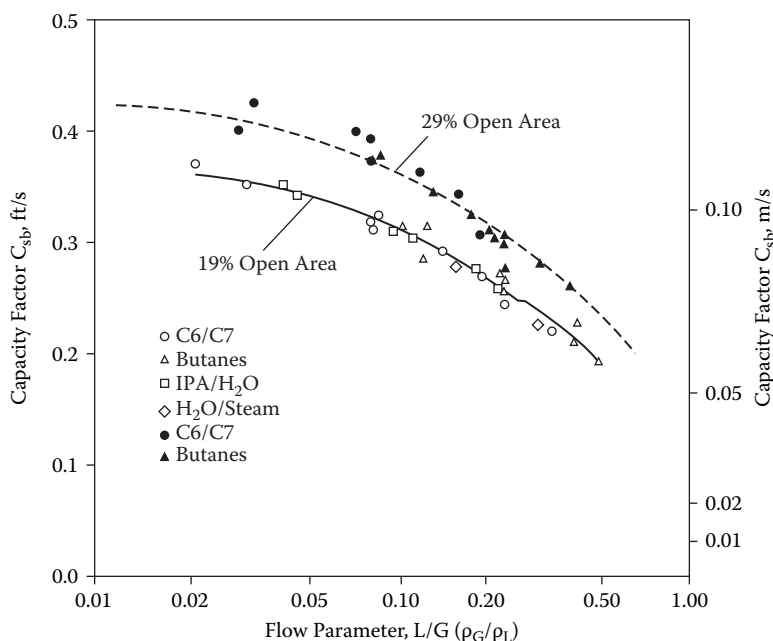
12.6.2 COUNTERFLOW PERFORATED TRAYS

These trays, often called *dualflow trays*, are perforated and occupy the entire column cross section. Similar devices are known as *turbogrid trays* and *ripple trays*. Their simplicity is evident from the view in Figure 12.39. Since there are no downcomers, liquid must compete with vapor for passage through the perforations, and this complicates the hydraulic analysis of the device. Observations show that a given perforation passes either vapor or liquid, but not both at the same time. Furthermore, the phase flowing through the perforation shifts with time in a random way. This alternative flow is believed to be the reason why trays of this type can often handle systems that foul conventional trays and packings.

Extensive commercial-scale performance data on counterflow devices were released by FRI in 2000. Detailed information on tray performance and modeling was reported.⁴⁷ Figure 12.40, from reference 48, shows the influence of open area on efficiency and also makes clear the sensitivity of efficiency to loading. The figure is quite revealing: One can obtain increased capacity at the expense of efficiency by going to larger open areas. The figure also shows that the counterflow device has a characteristically narrow operating range.

Geometric variables for design are few: perforation type and size, open area, and tray spacing. The perforations are usually round and in the range of 12.7- to 25.4-mm diameter. Open areas run from 15 to 25%. Vapor flow capacity (entrainment limitation) is correlated in a fashion similar to that for crossflow trays, as shown in Figure 12.41, from reference 47. The figure is based on FRI data taken in a 1.2-m diameter column.

Zuiderweg and coworkers⁴⁹ identified a segregation effect on turbogrid trays and found that towers in the range of 3- to 4-m diameter have 80% or less of the efficiency of a small (0.5 m) tower, because of phase segregation and channeling.



Note: Data normalized to 610 mm (24-in) Tray Spacing and 12.7 mm (0.5-in) Holes.
 Factor = 0.81 for 304 mm (12-in) Spacing, 1.16 for 914 mm (36-in) Spacing.
 Factor = 1.06 for 25.4 mm (1.0-in) Holes

FIGURE 12.41 Flooding capacity of dualflow trays, based on FRI data. Column diameter = 1.2 m. (J. A. Garcia; J. R. Fair, 2002. *Ind. Eng. Chem. Res.* 41: 1632.)

12.6.3 BAFFLE TRAYS

As in the case of counterflow trays, baffle trays are often used for fouling services, e.g., handling slurries that would plug conventional crossflow trays. Their simplistic design does not lead to mass transfer efficiencies as high as those for counterflow trays, but their pressure drop and capacity can have advantages over the conventional devices.

The internals for these columns have also been called “splash decks” or “shower decks,” descriptive terms to indicate the type of phase contacting expected. Vapor (or gas) flows upward through the baffle openings and there contacts the liquid showering down from one baffle to the next. Figure 12.42 shows a representative baffle tray column containing segmental baffles.

Geometric design variables for baffle tray columns are simple and few. The horizontal opening for gas flow is known as the *window area*. The vertical opening through which gas passes in a more horizontal direction is the *curtain area*. Much of the vapor-liquid contacting occurs within a zone bounded by the curtain area. Excessive constrictions in either area can cause higher pressure drop and flooding. Normally, it is desirable to make the two areas about equal in size.

A recent paper⁵⁰ provides a most complete analysis of design methodology for baffle columns. Figure 12.43 provides flooding prediction and uses the same parameters as the charts for crossflow trays (Figure 12.29) and counterflow perforated trays (Figure 12.41). The data points on Figure 12.43 include results from Fractionation Research, Inc. (FRI) for total reflux tests with the several systems indicated.^{50a} These tests were run in a 1.2-m diameter column, and some variation in baffle geometry was employed. The term “cut” is the percentage of open area for phase flows.

Pressure drop through baffle columns is primarily a function of vapor flow rate, with about two velocity heads per opening being a good rule of thumb. For high liquid rates, this estimate must be increased. FRI tests indicate that the efficiency of a baffle column will be about half that for a

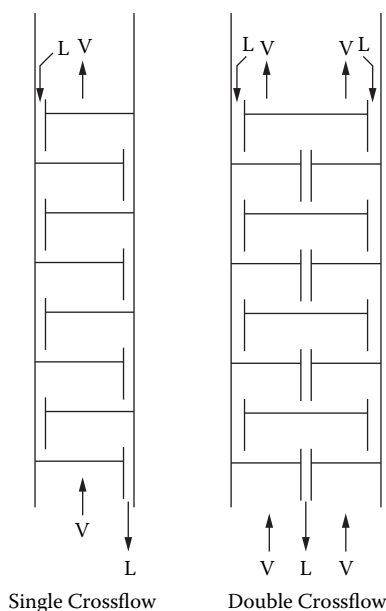


FIGURE 12.44 Multipass liquid flow arrangements for crossflow tray columns.

crossflow tray column under the same loading conditions. Hence, it may be better to estimate mass transfer rates from heat transfer rates using the mass transfer–heat transfer analogy. This is covered in some detail by Fair.⁵¹

12.6.4 MULTIPLE DOWNCOMER TRAYS

These devices are suitable for high liquid flow services (e.g., high-pressure fractionation), and their operating characteristics are described by Delnicki and Wagner.⁵² Multiple downcomer trays (MD trays) have several small downcomers spread over the tray area, each downcomer being the hanging type. The vapor is normally dispersed through sieve-type holes. In general, their hydraulic behavior resembles that of crossflow trays, even though they exhibit some characteristics of counterflow trays. Their design is normally handled by the proprietor of the tray technology.

12.6.5 GENERAL COMMENTS ON TRAY-TYPE COLUMNS

For high liquid flow cases, it may be necessary to split the flow into two or more passes. This creates separate contacting zones, as shown in Figure 12.44. For the *two-pass tray* shown, liquid flows side to center and center to side on successive trays; this means that the effective weir crests differ because of differing weir lengths. The center weir is about the same length as the column diameter, whereas the side weir may be only 70% or so of the diameter.

The downcomer aprons can be sloped to give a larger cross section of downcomer at the top than at the bottom. Although this can aid in vapor disengagement from the downcomer liquid, the larger area can detract from the available vapor flow area, and this must be taken into account in estimating the approach to flood. Because of changing vapor and liquid flows throughout the column, hydraulic studies should include, as a minimum, conditions at top and bottom, and above and below the feed tray. This variation in flow is particularly pronounced in high-vacuum columns, where the vapor density can change twofold or more in a single column. With a feed stream that is partially vaporized, volume must be provided to allow adequate phase separation.

Relative volatility, EB/SM = α = 1.40		
Vapor density	0.030 lb/ft ³	0.481 kg/m ³
Liquid density	52.2 lb/ft ³	837 kg/m ³
Surface tension	25 dyn/cm	25 mN/m

The flow conditions are

Vapor	126,000 lb/hr = 1,200 lb-moles/hr = 1,167 ft ³ /s 15.88 kg/s = 33.0 m ³ /s
Liquid	108,000 lb/hr = 1,028 lb-moles/hr = 0.57 ft ³ /s 13.61 kg/s = 1.162 (10 ⁻²) m ³ /s

Develop dimensions of a crossflow sieve tray for these conditions, plus these specified parameters:

Tray spacing	24 in.	0.61 m
Weir height	1.0 in.	25.4 mm
Hole diameter	0.1875 in	4.8 mm
Tray metal thickness	0.078 in	2.0 mm
Downcomer area = 5% of total cross section	Hole area = 14% of active (bubbling) area	
Weir length	79.2 in.	2012 mm
Downcomer clearance	0.75 in.	19 mm

Solution:

Column Diameter: First, the abscissa value for Figure 12.29 is calculated: $13.61/15.88 \sqrt{0.481/837} = 0.021$. From that figure, for 0.61 m spacing, $C_{sbf} = 0.37$ ft/s = 0.11 m/s, based on net area, which is 95% of the total cross section. This gives a flooding vapor velocity (corrected for surface tension) = 4.91 m/s through the net area. Thus, minimum net area = $33.0/4.91 = 6.72$ m².

Use 80% of flood for design; therefore, design vapor velocity = $0.8(4.91) = 3.93$ m/s through net area. This gives a required net area = $6.72/0.80 = 8.40$ m² and a required total cross section of $8.40/0.95 = 8.85$ m². *Required column diameter = 3.36 m (11.0 ft).*

For this geometry, several useful parameters emerge:

Active area $A_a = 7.98$ m ²	Active area vapor velocity $U_a = 33.0/7.98 = 4.14$ m/s
F-factor for active area	$F_{wa} = 2.87$ m/s(kg/m ³) ^{0.5}
F-factor for hole area	$F_{wh} = 2.87/0.14 = 20.5$ m/s(kg/m ³) ^{0.5}

Pressure Drop: From Figure 12.33, for $A_h/A_a = 0.14$ and tray thickness/hole diameter of $2/4.8 = 0.42$, the orifice coefficient is 0.76. Then, by Equation (12.5),

$$h_d = \frac{50.8}{(0.76)^2} \frac{0.481}{837} \left(\frac{33.0}{1.12} \right)^2 = 43.9 \text{ mm liquid}$$

By Equation (12.62), $h_{ow} = 664 L_w^{0.667}$, and $L_w = 1.615(10^{-2})/(2.012)$

$$\therefore h_{ow} = 26.6 \text{ mm}$$

From Equation (12.61), $\beta = 0.47$

$$\therefore h_t = h_d + \beta(h_w + h_{ow}) = 43.9 + 0.47(25.4 + 26.6) = 68.3 \text{ mm total drop/tray}$$

from which $h_L = 24.4$ mm liquid

of random packings are *ordered* or *structured packings*, which are relatively large, fabricated to close dimensional tolerances, and carefully positioned in the column. Random packings and ordered packings are usually competitive for a given problem, and the designer must know the characteristics of each, as discussed separately below.

12.7.1 PACKING CHARACTERISTICS

Representative random packings were shown in Figure 12.25; properties of important packings of the class are given in Table 12.9. The first three packings listed are the “through-flow” type in which the phases can flow freely through the elements with reduced form drag. The others listed are of the “around flow” type, with increased form drag and therefore higher pressure drop.

TABLE 12.9
Characteristics of Random Packings

Name	Material	Nominal Size, mm	Surface Area m ² /m ³	% Voids	Packing Factor, m ⁻¹	Vendor
Intalox saddles* “IMTP”	M	(No. 25)		97	135	Koch-Glitsch, LP
		(No. 40)		97	24	Wichita, KN
		(No. 50)		98	59	
Pall rings*	M	16	—	92	266	(Generic)
		25	205	94	184	
		38	130	95	131	
		50	115	96	88	
		90	92	97	59	
Pall rings*	P	16	340	87	310	(Generic)
		25	205	90	180	
		50	130	91	131	
		90	100	92	85	
Berl saddles	C	13	465	62	790	(Generic)
		25	250	68	360	
		38	150	71	215	
Intalox saddles	C	13	625	78	660	Koch-Glitsch, LP
		25	255	77	197	Wichita, KN
		50	118	79	98	
		75	92	80	70	
Intalox saddles	P	25	206	91	131	Koch-Glitsch, LP
		50	108	93	92	Wichita, KN
		75	88	94	59	
Raschig rings	C	13	370	64	1900	(Generic)
		25	190	74	587	
		38	120	68	305	
		50	92	74	213	
		75	62	75	121	
Raschig rings	M	19	245	80	730	(Generic)
		25	185	86	470	
		38	130	90	270	
		50	95	92	187	
		75	66	95	105	

Note: Materials of construction: C = ceramic; M = metal; P = plastic (usually polypropylene).

* Through-flow packing.

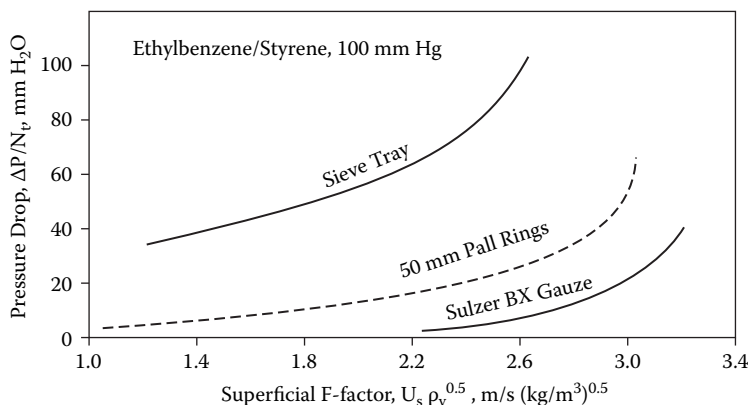


FIGURE 12.47 Comparison of devices for vacuum service, pressure drop/theoretical stage.

Most structured packings are of the corrugated sheet type. In these packings, crimped, corrugated sheets of metal or metal gauze are positioned to create flow channels for the gas and promote distribution. Some details of their fabrication and assembly are shown in Figure 12.48. (Less common types of ordered packings, involving meshes and grids, are not discussed here.) Structured packings can also be made from a variety of materials; the choice of material depends not only on corrosion resistance and cost but also on the wettability of the surface by the liquid being used. For example, water does not wet clean metals well but spreads almost completely on many ceramic surfaces. Aspects of packing wetting will be discussed below, in the “Mass Transfer Efficiency” section.

As in the case of trays, the important hydraulic considerations for packings are pressure drop and flooding. To a lesser extent, liquid holdup is also important. The hydraulics affect the performance profile for a given separation in a specific packing. A typical profile for efficiency and pressure drop is shown in Figure 12.49.⁵⁴ The equivalence to the tray profile is evident (see Figure 12.26). The ordinate is given in theoretical stages per unit of bed height, but a more common description of efficiency is the inverse of this, the *height equivalent to a theoretical plate (HETP)*. A generalized profile for a packed column is shown in Figure 12.50, which shows the importance of having uniform liquid distribution to the bed. (The distributor for the tests shown in Figure 12.49 was of exceptionally high quality.)

Some random packings correct a poor initial distribution of liquid, whereas others (especially the high-void, low-form-drag packings) must always be fed a uniformly distributed liquid at the top of the bed if they are to perform efficiently. Still other packings exhibit a deterioration of a good distribution with bed depth, making the use of *redistributors* mandatory at depths beyond around 3 to 6 m.

Liquid and vapor flow countercurrently through openings between and within packing elements. At low vapor rates, there is relatively little disturbance of liquid by the vapor, and mass transfer proceeds in a fashion similar to that in a wetted wall column. At higher rates, there is considerable interaction between the phases, with vapor flow causing increases in liquid turbulence and holdup. In the so-called “loading zone,” there is an enhancement of mass transfer but, as rates are increased further, flooding occurs.

The loading/flooding phenomena are best understood through a study of pressure drop curves such as those shown schematically in Figure 12.51. For a dry packing (with no liquid irrigation), pressure drop follows a traditional friction factor, orifice-type relationship. When there is irrigation at a constant liquid rate, increasing the gas rate leads to a change in the slope of the pressure drop curve, indicating the onset of loading. Further gas rate increase leads to a rapid and continuing increase in pressure drop, indicating flooding. Flooding can also be reached by increasing the liquid rate at

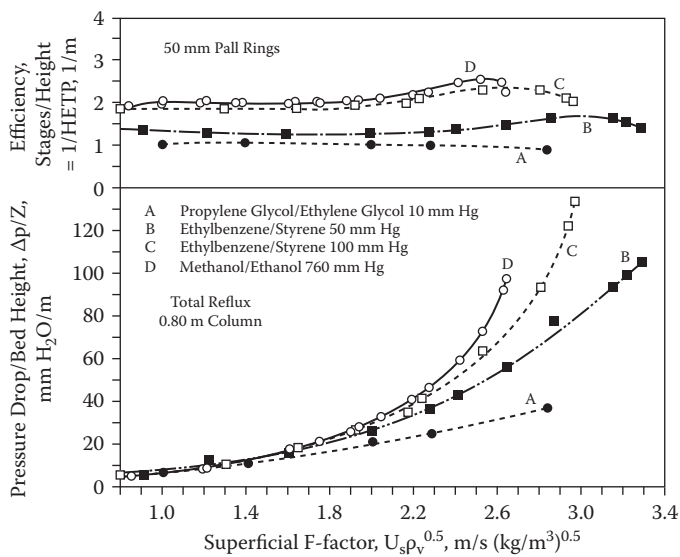


FIGURE 12.49 Performance of 50-mm Pall rings, various services. (R. Billet, 1969. *ICHEME Symp. Ser. 32*, 5: 111.)

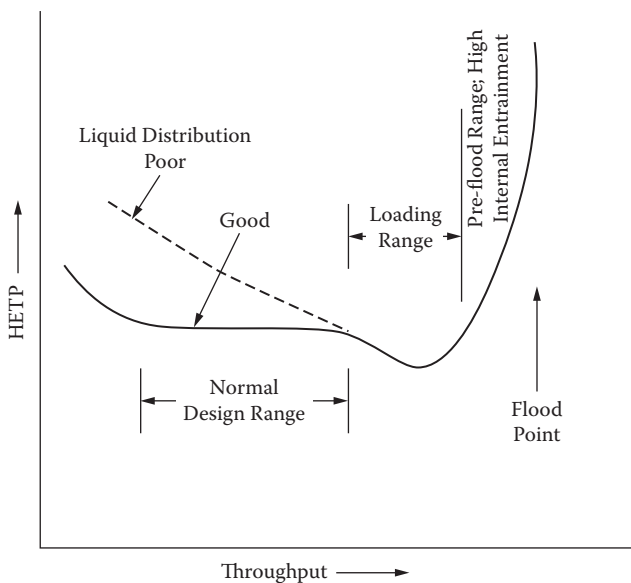


FIGURE 12.50 Generalized efficiency profile for a packed column.

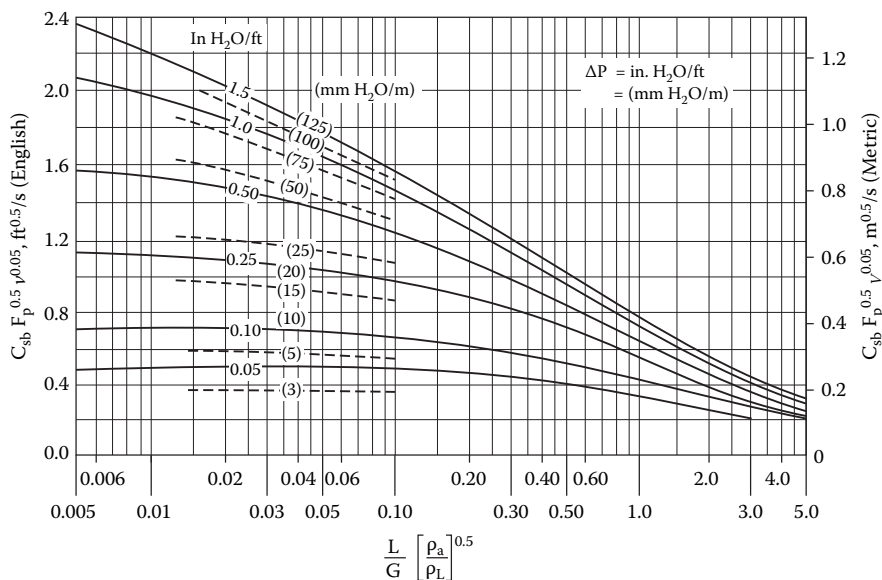


FIGURE 12.53 Generalized chart for estimating pressure drop and maximum capacity of packings. (R. F. Strigle, 1994. *Packed Tower Design and Applications*, 2nd ed., Houston: Gulf Publ. Co.)

small increase in flow rate of either phase. Methods for estimating maximum hydraulic capacity for a packing provide a basis for design (optimum approach to flood). Such methods employ one of three separate approaches:

- Generalized pressure drop correlation (GPDC)^{56,57}
- Empirical flow parameter versus capacity parameter plots
- Friction factor–dry pressure drop correction methods

The first approach has been modified several times in use for a longer period of time, and several updates and modification have been made over the years. The modification by Strigle⁵⁸ is described here. Two other approaches are described elsewhere;^{59,60} the graph of Strigle is shown in Figure 12.53.

The Strigle diagram provides both limiting capacity and pressure drop predictions. Packing size and type effects merge through the use of a *packing factor* that is presumed to be constant for a given packing size and type. Packing factors are included in Tables 12.10 and 12.11.

For flooding, an estimate can be made from Figure 12.53, although manufacturers often like to omit the flood line from the chart. Maximum throughput is assumed to occur at the top curve (125 mm H₂O/m), although slightly more capacity is sometimes available. The presumption that flooding occurs at a constant value of pressure drop is not necessarily correct, since the more open-type packings flood at lower pressure drops. Also, flooding occurs at lower pressure drops under high liquid loadings and gas densities for a given packing.

The ordinate value of the Strigle chart is, in fact, a capacity parameter, with a slight correction for liquid viscosity,

$$\text{ordinate} = C_s F_p^{0.5} v^{0.05} \text{ which has units of } \text{ft}^{0.5}/\text{sec} \text{ or } \text{m}^{0.5}/\text{s}$$

where

$$C_s = U_s [\rho_v/(\rho_L - \rho_v)]^{0.5}, \text{ft/sec or m/s}$$

$$v = \text{liquid kinematic viscosity} = \text{centistokes (centipoises/density, g/ml)}$$

$$F_p = \text{packing factor, 1/ft or 1/m (Tables 12.9 and 12.10)}$$

$$F_s = U_s \rho_v^{0.5} = 5.10 (0.480)^{0.5} = 3.50$$

(a) Flood F-factor = 3.50 m/s (kg/m³)^{0.5}

Note that performance curve *C* of Figure 12.49 indicates flooding at $F \sim 3.0 \text{ m/s}(\text{kg/m}^3)^{0.5}$.

(b) For pressure drop at $F = 2.4$, convert to $C_{sb} = F_s/\rho_L^{0.5} = 2.4/(837)^{0.5} = 0.0830$.

$C_{sb} = 0.0830 \text{ m/s}$. Then, ord. of Figure 12.53 = $0.0830 (88)^{0.5} (0.46)^{0.05}$.

ord = 0.748 m0.5/s for which, at $FP = 0.021$, $\Delta P = 40 \text{ mm H}_2\text{O/m}$.

The experimental value was about 50 mm H₂O/m.

12.7.1.3 Liquid Distribution

Good liquid distribution is essential to the effective performance of packed columns. While there are no quantitative measures for "good distribution," experience leads to the following guidelines: for dumped packings, the ratio of column diameter to packing element diameter should be 8 or greater, and the liquid distributor should produce at least 10 inlet streams, evenly distributed, per square foot (100 per square meter) of cross section. The "around flow" bluff body packings (e.g., Raschig rings) may require fewer inlet liquid streams.

Problem 12.8

Problem 12.6 deals with the dimensioning of a large ethylbenzene/styrene tray-type fractionator. Because high pressure drop in this separation leads to increased tar production, a packing (instead of trays) is to be considered. The conditions are the same as for Problem 12.6. For 80% flood, determine the required column diameter and associated pressure drop for a 50-mm Pall ring random packing.

Solution. For both capacity and pressure drop, Figure 12.53 will be used. For the mixture, the absolute viscosity is 0.38 cP, giving a kinematic viscosity of 0.45 cSt. From Table 12.8, the packing factor F_p for 50-mm metal Pall rings is 88 m⁻¹ or 26.8 ft⁻¹. The abscissa for the figure (the flow parameter) is the same as before: $FP = 0.021$. For Figure 12.53, the ordinate term is

$$C_{sb} F_p^{0.5} \nu^{0.02} = C_{sb} (5.18) (0.45^{0.02}) = 5.10 C_{sb} \text{ ft/s}$$

At the highest curve of Figure 12.53 (assumed equivalent to flooding), the ordinate value is 2.05, from which $C_{sb} = 0.40 \text{ ft/s}$. At 80%, the ordinate value is $2.05(0.80) = 1.64$, and the pressure drop is 55 mm H₂O/m (0.66 in H₂O/ft) or 66 mm liquid/m.

The column diameter is based on $C_{sb} = 0.80$, $C_{sb} = 0.32 \text{ ft/s} = 0.98 \text{ m/s}$. For a vapor flow of 33.0 m³/s, the required diameter is 3.21 m or 10.5 ft.

Comparison with Trays. The pressure drop for a tray with 0.61-m spacing was found to be 58.4 mm liquid. The comparative packing pressure drop is $66(0.61) = 40.3 \text{ mm liquid}$. The diameter for the packed column is 3.21 m vs. 3.36 m for the trays. If a lower approach to flood for the packing is used, to make the column diameter 3.36 m, the packing pressure drop becomes less than half that of the trays.

Once the liquid has been introduced to the top of the bed, the question arises as to whether the initial distribution is maintained throughout the bed. Silvey and Keller⁶³ used internal bed liquid samplers and total reflux, and found that bluff body packings such as ceramic Raschig rings correct an inadequate initial liquid distribution and also maintain a good distribution throughout the bed. But the "through-flow" random packings and the structured packings cannot correct an initial problem. Potthoff⁶⁴ elucidated in-bed distribution effects, and representative plots of his findings are shown in Figure 12.54. The difference between a single-point distributor (the worst possible case) and a multipoint distributor is dramatic. The effect of bed height on efficiency is discussed in the next section.

In any event, the optimum number of pour points per unit of tower cross section depends on the type and size of packing selected, and also on the practical limits of distributor design and

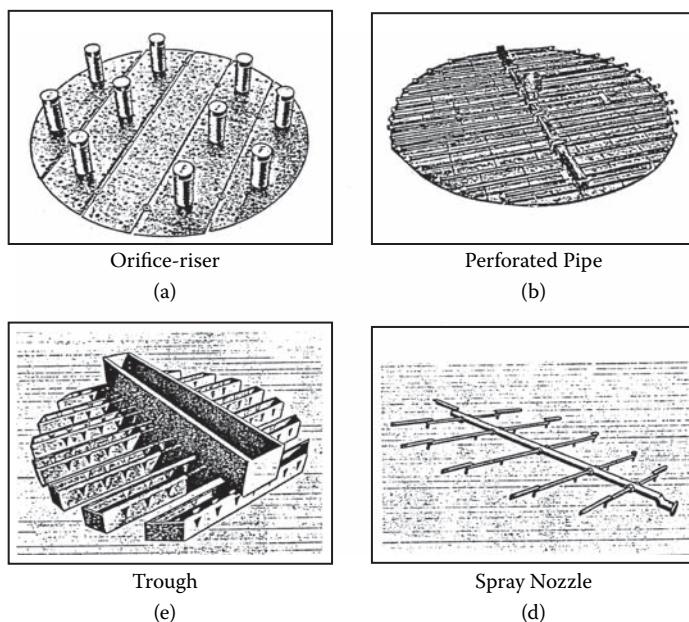


FIGURE 12.55 Examples of liquid distributors.

u_{Lh} = liquid velocity through the distributor holes, m/s

U_r = vapor velocity through the risers, m/s

Thus, liquid backup can be attributed to both orifice area and riser area.

For distribution-sensitive packings, some pour points are needed near the wall (to within 2 cm). For larger-diameter columns, and for low liquid rates, the distributor must be level within ± 5 mm for a 3-m diameter column. In addition, the risers must be high enough to accommodate backup for high liquid and vapor flow rates.

The *drip tube/riser distributor* is a variation of the orifice/riser device, with tubes added to the orifices to ensure close contact with the packing (not shown in Figure 12.55). When it is necessary that all tubes discharge evenly, a double tubesheet affair can be used with liquid under pressure; pressure drop through the orifices and tubes must be estimated carefully for this arrangement.

The *perforated pipe distributor* has a central feed sump with pipes that branch out to provide the liquid discharge. The level in the sump varies with liquid total flow rate, and the size of the lateral pipes and their orifices must be dimensioned carefully to ensure that the ends of the pipes are not starved for liquid. The orifice sizes are typically 0.125 to 0.25 in. (3 to 6 mm) in diameter and can plug if foreign matter is present. The pipes must be leveled carefully, especially in large-diameter columns.

The *spray nozzle* is not widely used. If more than one nozzle is used, it is difficult to obtain a uniform spray pattern because of overlap and underlap of the patterns. Also, liquid entrainment from the sprays is a problem. Spray distributors are sometimes used in petroleum refinery vacuum columns.⁶⁵ The full cone nozzle is normally used, singly or in banks.

12.7.1.6 Liquid Redistribution

For bed heights greater than 6 to 8 m, the total bed is subdivided. This is because of natural deterioration of mass transfer efficiency with height. Since each bed must have good initial distribution, it is necessary to collect the liquid flowing from a bed (which may have become maldis-

$$E_{oc} = N_t / N_a \quad (12.64)$$

where the theoretical tray count *for the column* (not including theoretical stages for reboiler and partial condenser) is N_a , and the actual number of column trays needed is N_t . The number of trays actually specified for the column may be greater than N_a if allowance is made for column upsets or for alternate operating conditions (e.g., different feed composition or different separation).

For packed columns, mass transfer efficiency is related to transfer rates in counterflow vapor-liquid contacting. A *height equivalent to a theoretical plate* is often used:

$$HETP = Z / N_t \quad (12.65)$$

where Z is the height of packing required to achieve a separation equivalent to that of N_t theoretical stages. As in the case of trays, $HETP$ often should be adjusted to allow for upsets or alternative separating conditions.

Thus, the total height of contacting zone is determined as follows:

$$\text{Tray columns: } Z = \frac{N_t}{E_{oc}} TS \quad (TS = \text{tray spacing}) \quad (12.66)$$

$$\text{Packed columns: } Z = N_t HETP \text{ or } Z = N_{og} H_{og} \quad (12.67)$$

12.8.1 GENERAL MASS TRANSFER RELATIONSHIPS

Mass transfer relationships in a distillation column are based on the basic interphase transfer model for a differential slice of the cross section, as shown in Figure 12.57. The slice is taken from the packed bed or from the tray froth. For component i ,

$$Ldx_i + x_i dL = Vdy_i + y_i dV \quad (12.68)$$

For equimolar counterdiffusion (approximately the case for distillation), $dV = dL$, and for net transfer of i from bulk vapor to bulk liquid,

$$Vdy_i = K_g a_i (y_i - y_i^*) dZ \quad (12.69)$$

where y_i is the mole fraction of i in the vapor, and y_i^* is the mole fraction of i in the vapor that would be in equilibrium with bulk liquid composition x_i . Note that y_i^* is not a real composition but rather a calculated term from the equilibrium expression $y_i^* = K_i x_i$.

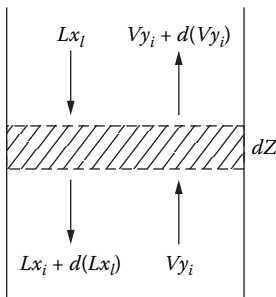


FIGURE 12.57 Flows in a differential section of a countercurrent contactor.

$$F_{lv} = \left(\frac{L}{G} \right) \left(\frac{\rho_G}{\rho_L} \right)^{1/2} \quad (12.72)$$

This parameter represents a ratio of liquid-to-vapor kinetic energies, and approximate ranges for the regimes are

$$F_{lv} < 0.01 \text{ spray (vapor continuous)}$$

$$0.01 < F_{lv} < 0.10 \text{ froth (liquid continuous)}$$

$$F_{lv} > 0.10 \text{ emulsion or free bubbling}$$

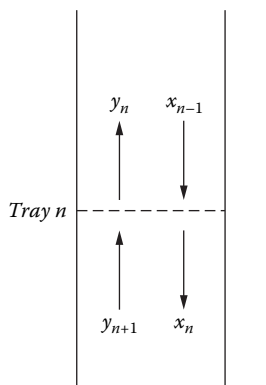
The transition between spray and froth regimes is usually detected by light-scattering techniques. Mass transfer models discussed later are based on the froth regime, the one that normally prevails.

12.8.2.2 Tray Efficiency Definitions

The mass transfer efficiency of contacting trays is often expressed in several ways, but here only two efficiencies will be used: point efficiency and tray efficiency. The former deals with the approach to equilibrium at some point on the tray and cannot be greater than 1.0 (100%). Clearly, the equilibrium can vary across the tray as liquid composition varies; thus, there are a number of different values of point efficiency when the tray liquid is not completely mixed (the normal case).

The overall tray efficiency E_{MV} (often called “Murphree efficiency”) takes into account concentration gradients on the tray. It has an arbitrary definition based on the average total vapor composition leaving the froth and the specific liquid composition *leaving* the tray [not the *average* composition on the tray (see Figure 12.58)]. Because of this arbitrariness, the overall tray efficiency value can exceed 1.0. When there are no composition gradients on the tray, $E_{og} = E_{MV}$.

The point efficiency is a fundamental criterion of mass transfer, whereas the overall tray efficiency is the value that can be measured, especially for larger distillation columns. Large-column



$$E_{mv} = \frac{y_n - y_{n+1}}{y_n^* - y_{n+1}} = \frac{y_n - y_{n+1}}{Kx_n - y_{n+1}}$$

Notes: y_n and y_{n+1} are Averaged Over the Cross Section

x_n Is Overflow Composition Only (which can differ from averaged x_n)

FIGURE 12.58 Compositions leading to the definition of overall tray efficiency, E_{MV} .

velocity of the gas. The number of overall transfer units [Equation (12.71)], based on gas concentrations, follows from the individual phase units:

$$\frac{1}{N_{OG}} = \frac{1}{N_G} + \frac{\lambda}{N_L} \quad (12.79)$$

where λ is the ratio of slopes, equilibrium line to operating line:

$$\lambda = \frac{m}{L/V} = \frac{mV}{L} \quad (12.80)$$

Thus, a continuous contacting approach (use of transfer units) is employed. The point efficiency is computed from the value of N_{OG} :

$$E_{OG} = 1 - \exp[-N_{OG}] \quad (12.81)$$

12.8.2.4 Tray (Murphree) Efficiency

For complete mixing, $E_{MV} = E_{og}$. For the *plug flow* of liquid,

$$E_{MV} = \frac{1}{\lambda} \left(\exp[\lambda E_{og}] - 1 \right) \quad (12.82)$$

The point and overall efficiencies are the same when the phases in the froth are completely mixed. This is more likely for small columns and for very high gas-to-liquid ratios for larger columns. When the liquid is in plug flow, $E_{MV} > E_{og}$. To deduce point efficiency values from measured overall efficiency values, a model involving mixing tendencies must be available, as discussed later.

12.8.2.5 Overall Column Efficiency E_{oc}

This is the efficiency most used and understood [see Equation (12.66)]. At total reflux, E_{oc} and E_{MV} are about equal. Otherwise,

$$E_{oc} = \frac{\ln[1 + E_{MV}(\lambda - 1)]}{\ln \lambda} \quad (12.83)$$

or

$$E_{MV} = \frac{(\lambda^{E_{oc}} - 1)}{(\lambda - 1)} \quad (12.83a)$$

where λ is defined by Equation (12.80).

The relationships between these efficiencies are shown in Figure 12.59. For design, the sequence is

$$E_{og} \rightarrow E_{MV} \rightarrow E_{oc}$$

with the reverse applying to the analysis of existing columns.

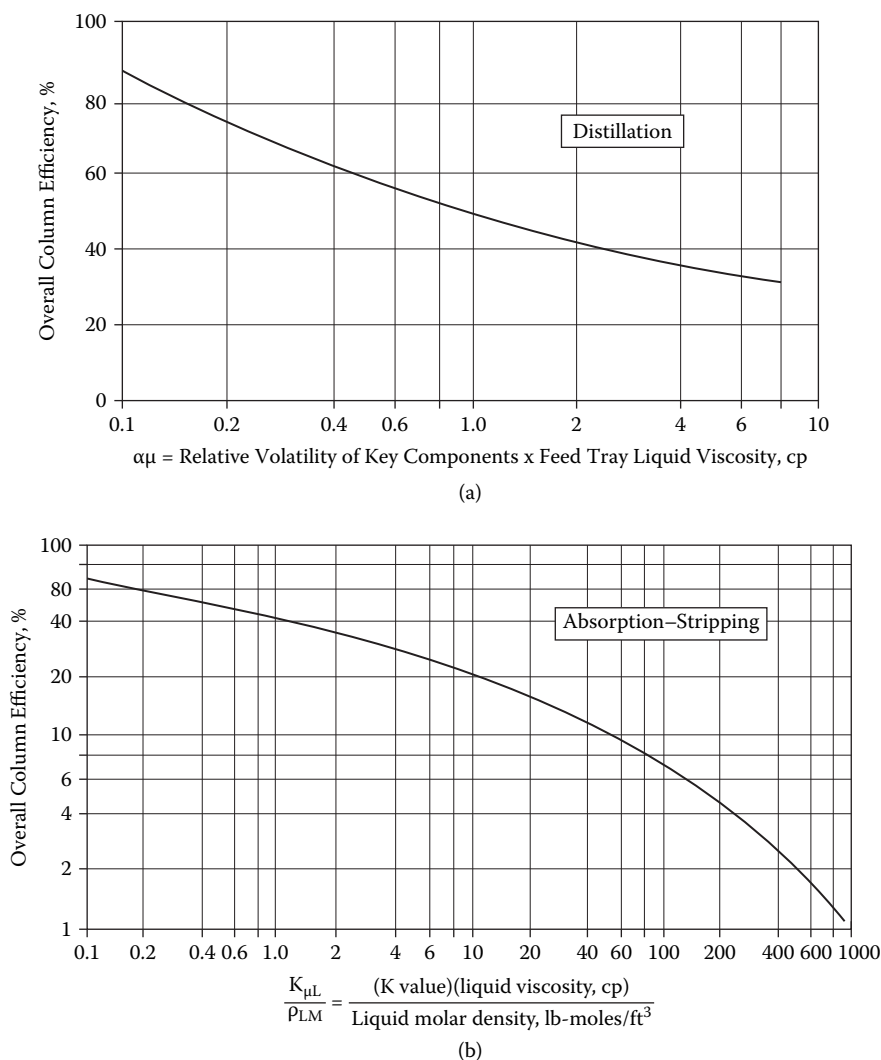


FIGURE 12.60 O'Connell method for estimating overall column efficiencies of distillation columns and absorbers. (H. E. O'Connell, 1946. *Trans AIChE* 42: 741.)

different? Is the loading about the same as for the existing system? Is the same contacting device to be used? Clearly, caution is needed, but it is the best basis to use. Those with access to Fractionation Research, Inc. (FRI) data can benefit from this approach if the system at hand is similar to a system studied by FRI. However, the same questions must be asked.

12.8.2.7 Empirical Efficiency Methods

The best known and most used empirical method is that of O'Connell⁶⁸ (Figure 12.60), for distillation columns and absorbers. The curves are based on plant data for several bubble-cap columns plus a few pilot-scale units. Efficiency is related to two properties of the feed mixture: liquid viscosity μ_L and relative volatility α . Higher values of the $\mu_L\alpha$ product indicate larger liquid-side mass transfer resistance and hence a lower efficiency. For a vapor feed or a mixed vapor-liquid feed, the correlating viscosity should be that of the feed tray liquid.

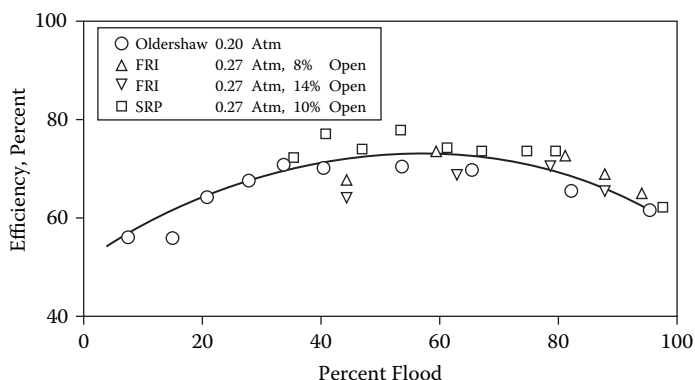


FIGURE 12.62 Comparison of tray point efficiencies for different column sizes. Cyclohexane/*n*-heptane system, 0.20–0.27 atm pressure, total reflux. (Separations Research Program, Univ. of Texas at Austin.)

TABLE 12.11
Conditions for Efficiency Comparisons in Figure 12.62

	Oldershaw ¹	SRP ²	FRI-1 ³	FRI-2 ⁴
Head pressure, atm	0.20	0.27	0.27	0.27
Column diameter, m	0.025	0.43	1.2	1.2
Tray spacing, m	0.025	0.46	0.61	0.61
Tray open area, % of active area	10.0	8.7	8.0	14.0
Weir height, mm	51	51	51	
Hole diameter, mm	0.89	4.8	12.7	12.7
Downcomer area, % of total area	8.2	7.2		

Notes: All runs with cyclohexane/*n*-heptane mixture at total reflux. The SRP column contained a splash baffle. FRI efficiencies are corrected from overall column to point.

Sources: ¹Fair, J. R.; Null, H. R.; Bolles, W.L. *Ind. Eng. Chem. Proc. Des. Devel.* 1983, 22, 53. ²Garcia, J. A., Ph.D. Dissertation, The Univ. of Texas at Austin, 1999. ³Sakata, M.; Yanagi, T. *ICHEME Symp. Ser. No. 56*, 1979, 3.2/21. ⁴Yanagi, T.; Sakata, M. *Ind. Eng. Chem. Proc. Des. Devel.* 1982, 21, 712.

12.8.2.9 Efficiency from Mass Transfer Models

The above relationships, coupled with experimental efficiency results, provide a semifundamental approach to modeling tray efficiency. Since the contacting process is not well understood, only an approximation of the efficiency can be expected. However, the application of mass transfer principles can aid the overall process of design by showing relative effects of variables.

The AIChE efficiency model⁷¹ was the first to use a rational approach to mass transfer efficiency. Equations (12.74) through (12.83) are used to predict point efficiency. The values of $k_G a_i'$, $k_L a_i'$, t_G , and t_L are deduced from laboratory measurements with small test trays containing bubble caps. No attempt is made to evaluate interfacial area a_i' . The detailed procedure is in reference 71.

An adaptation of the AIChE model was published by Chan and Fair,⁷² is specific to sieve trays, and is based on larger-scale sieve tray measurements. For the vapor phase,

However, the volume $A_a Z_f$ is not all effective for mass transfer; its upper zone provides relatively little area for mass transfer. Accordingly, some effective value of Z_f applies. Because this value is not easily determined, an alternative approach to estimating vapor residence time is used:

$$t_G = \frac{(1 - \phi_{ef}) h_L}{\phi_{fe} U_a} \quad (h_L \text{ in m}) \quad (12.86)$$

where an *effective froth density* ϕ_{fe} [see Equation (12.63)] is used, based on the work of Bennett et al.,⁷³ who provided the basis for estimating ϕ_{fe} :

$$\phi_{fe} = \exp \left[-12.55 (C'_{sb})^{0.91} \right] \quad (12.87)$$

with C'_{sb} based on the active area (rather than the net area), in m/s.

The number of liquid phase transfers is obtained from Equation (12.78), with the volumetric coefficient for *sieve trays*:

$$k_L a_i = (3.88 \cdot 10^8 D_L)(0.40 F_{va} + 0.17), \text{ sec}^{-1} \quad (12.88)$$

The residence time t_L is based on the volume of liquid flowing through the two-phase mixture on the tray:

$$t_L = \frac{\text{volume of liquid space in froth}}{\text{volumetric flow of liquid}} = \frac{A_a (1 - \epsilon) Z_f}{q_L} \quad (12.89)$$

which is also modified to eliminate the term Z_f :

$$t_L = \frac{h_L A_a}{q_L} \quad (12.90)$$

which implies that $Z_{f'} = h_L / \phi_{fe}$.

With a more mechanistic model for predicting tray point efficiency, Garcia and Fair⁷⁴ showed a better fit to a large database than did the older Chan–Fair model. A parity plot for the Garcia–Fair work is given in Figure 12.64. The newer method is more complex, however, and requires a fairly elaborate computer program.

12.8.2.10 Conversion of Point Efficiency to Tray Efficiency

The assumption of complete mixing on the tray leads to a conservative prediction of tray efficiency, i.e., E_{og} is assumed equal to E_{MV} , as discussed earlier. The other limiting case is where the liquid moves across the tray in pure plug flow and is represented by Equation (12.82). The partial mixing case between these two limits can be handled by available models, and the paper by Bennett and Grimm⁷⁵ provides predictive models based on diffusional-type backmixing of the liquid.

12.8.2.11 Entrainment Effects on Efficiency

The performance curve of a crossflow tray shows a lowering of efficiency as vapor velocity approaches a flooding value (Figure 12.27). This lowering results from liquid entrainment. Figure

$$\phi_{je} = \exp[-12.55(0.10)^{0.91}] = 0.21$$

$$t_G = [(1 - 0.21)0.0244]/[(0.21)(4.14)] = 0.022 \text{ sec [Equation (12.86)]}$$

From Equation (12.77), $N_G = 78.7(0.022) = 1.75$ transfer units.

By Equation (12.88), $k_L a_i = 3.88(10^8)(3.74)(10^{-9})[0.40(2.87) + 0.17] = 1.91 \text{ sec}^{-1}$.

By Equation (12.90), $t_L = 0.024(7.98)/0.01162 = 16.5 \text{ sec}$.

From which $N_L = 1.91(16.5) = 31.5$ transfer units.

The ratio of slopes, equilibrium/operating, will be taken for the rectifying section where slope $m = 1.005$. Then, $\lambda = m/(L/V) = 1.005/(1028/1200) = 1.17$.

Overall transfer units are calculated from Equation (12.79), combining N_G , N_L , and λ ; $N_{OG} = 1.64$.

Finally, the point efficiency is calculated from Equation (12.81), $E_{OG} = 0.81$ (81%).

Notes:

- The point efficiency may be enhanced by liquid crossflow effects and/or diminished by entrainment effects.
- The calculated efficiency is significantly greater than the estimate from the O'Connell method.

Commercial ethylbenzene/styrene fractionators show efficiencies in the range of 80 to 90%.

12.8.2.12 Overall Column Efficiency

As indicated by Figure 12.59, the final step is to convert E_{MV} (wet or dry) to the overall column efficiency E_{oc} . This is done using the Lewis⁷⁷ relationships:

$$E_{oc} = \frac{\ln[1 + E_{MV}(\lambda - 1)]}{\ln \lambda} \quad (12.92)$$

$$E_{MV} = \frac{\lambda^{E_{oc}} - 1}{\lambda - 1} \quad (12.93)$$

12.8.2.13 Multicomponent Systems

For binary systems, the efficiency for each component is the same and thus

$$(E_{og})_i = (E_{og})_j = (E_{og})_{i-j} \quad (12.94)$$

When more than two components are present, the efficiencies of each are not necessarily the same. The rigorous approach to handling multicomponent mixtures, outlined by Taylor and Krishna,⁷⁸ uses the Maxwell–Stefan diffusional equations. Chan and Fair⁷² used the rigorous approach to compare multicomponent system separations with those predicted by the use of the equivalent pseudobinary systems. They found that if the dominant pair of components present in the mixture is used to determine efficiency for all of the components, the separation determined is quite close to that resulting from rigorous multicomponent procedures.

General rules proposed by Toor and Burchard⁷⁹ for multicomponent systems are summarized as follows:

Equation (12.97) is strictly valid when the operating and equilibrium lines are straight. When the lines have equal slope, $N_{ov} = N_t$. The equation may be applied by dividing the column into sections where the equilibrium line can be considered straight.

For distillation,* the height of a transfer unit is defined as

$$H_{og} = \frac{V}{K_{og}a_i} \quad H_v = \frac{V}{k_g a_i} \quad H_L = \frac{L}{k_L a_i} \quad (12.98)$$

These relationships apply when the driving force for mass transfer is expressed as mole fractions. The overall mass transfer coefficient K_{og} is normally used in connection with

$$K_{og} = \frac{1}{\frac{1}{k_g} + \frac{m}{k_L}} \quad (12.99)$$

In these expressions, k and K have units of kg-moles/(s-m²-m.f.) or equivalent English units. Usually, the interfacial area a_i is not known and is not segregated from the mass transfer coefficient, giving volumetric coefficients $K_{og}a_i$, $k_g a_i$, and $k_L a_i$. These terms may be substituted in Equation (12.98).

The overall transfer unit height may be broken down into individual phase terms:

$$H_{oG} = \frac{V}{k_G a_i} + \lambda \frac{L}{k_L a_i} \quad (12.100)$$

or

$$H_{oG} = H_G + \lambda H_L \quad (12.100a)$$

from which

$$HETP = H_{oG} [\ln \lambda / (\lambda - 1)] \quad (12.100b)$$

12.8.3.1 Random Packings

Several methods have been proposed for predicting values of H_v and H_L as functions of system, flow conditions, and packing type.⁸⁰⁻⁸³ The model of Wagner et al.⁸² is directed specifically to the newer, open-style random packings. The Bolles-Fair⁸³ model has the broadest validation and will be used here and is summarized by the following equations:

$$H_G = \frac{\psi' Sc_G^{0.5} \left(Z_p / 3.05 \right)^{1/3} (3.28 D_c)^m}{3.28 (735 L' \Gamma)^m} \quad (12.101)$$

$$H_L = 0.305 \phi' C_F \left(Z_p / 3.05 \right)^{0.15} Sc_L^{0.5} \quad (12.102)$$

* For absorption and stripping, the equations are slightly different, in particular if concentrated solutions are being considered. See a mass transfer text, e.g., Hines and Maddox,⁶⁷ for a detailed discussion.

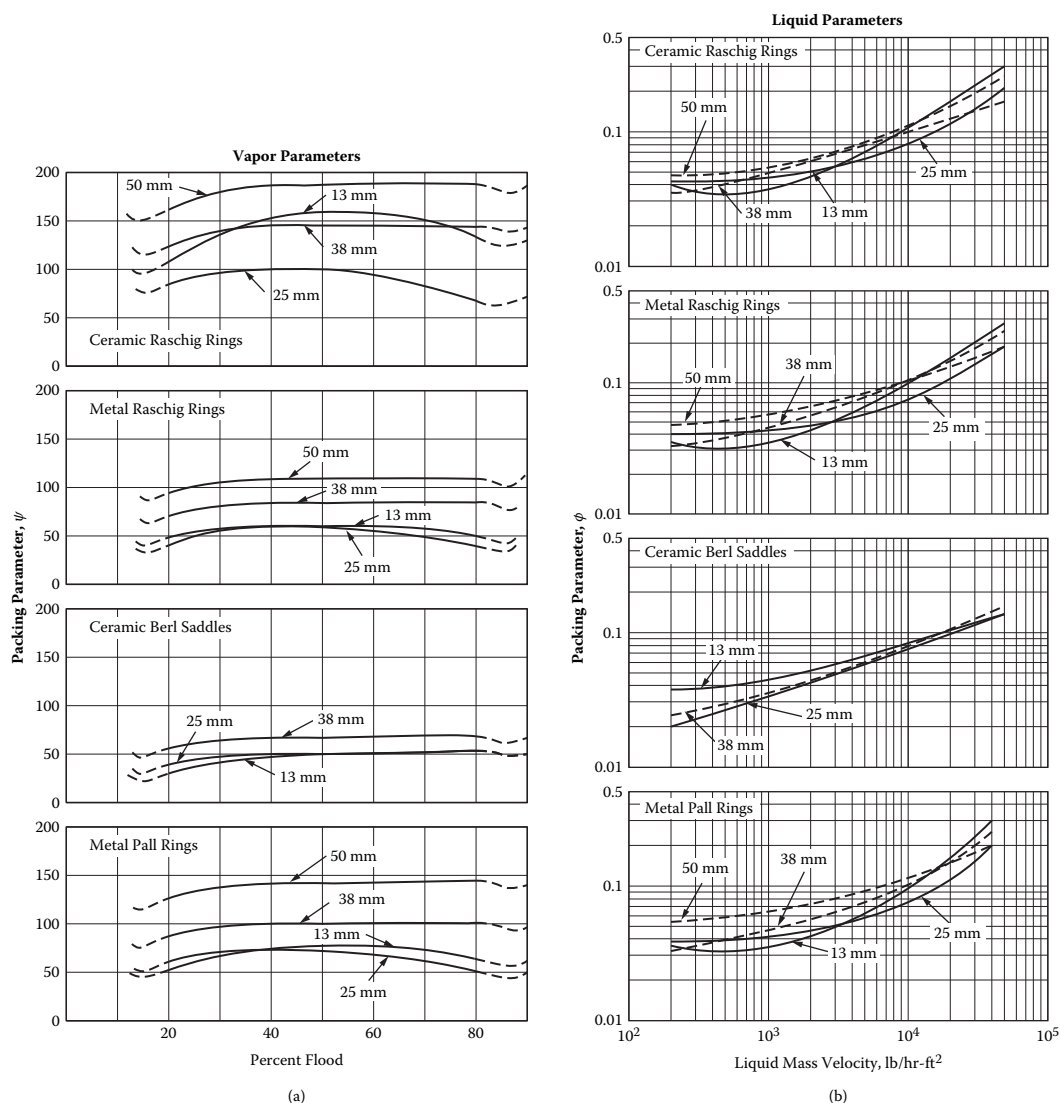


FIGURE 12.65 Packing parameters for random packing efficiency. (Bolles, W. L.; Fair, J. R. *Chem. Eng.* 1982, 89 (14) 109.

and *HETP* is in meters. The restriction of $\lambda = 1.0$ is not overly important, since many distillation columns have an average λ close to unity. Packings other than those listed may be used on an equivalent surface basis. Lockett suggests another useful approximation,

$$HETP = \frac{2450F_{vs,80}}{a_p^{0.5}} \quad (12.105)$$

that allows the use of whatever packing surface is to be specified (Table 12.10). Equations (12.104) and (12.105) require a value of the flooding velocity, obtainable from the vendor or from the generalized methods given earlier.

For the liquid side [Equation (12.105)],

$$H_L = 0.305(0.065)(0.60)(6.0/3.05)^{0.15} (122)^{0.5} = 0.15 \text{ m}$$

The height of an overall transfer unit is obtained from Equation (12.100a):

$$H_{oG} = H_G + \lambda H_L = 0.91 + 1.17(0.15) = 1.09 \text{ m}$$

This value can be converted to HETP for the case of $\lambda = 1.17$, by Equation (12.100b):

$$HETP = H_{oG} [\ln 1.17/(1.17 - 1)] = 1.09 [0.157/0.17] = 1.01 \text{ m (3.30 ft)}$$

Bravo et al. found that earlier data by Gilliland and Sherwood⁸⁷ and Johnstone and Pigford,⁸⁸ for countercurrent flow in vertical, round wetted-wall columns, agreed well with the results from structured packing experiments. The agreement confirmed that the gauze surface is essentially completely wetted, enabling the interfacial area to be equated to the specific surface area of the packing. The final model for the gas phase mass transfer coefficient is

$$Sh_v = 0.0338(Re_v)0.8(Sc_v)^{0.333} \quad (12.106)$$

where

$$Sh_v = \text{Sherwood number} = (k_v d_{eq}/D_v) \quad (12.107)$$

$$Re_g = \text{Reynolds number} = (d_{eq} \rho_g / \mu_g)(U_{g,eff} + U_{L,eff}) \quad (12.108)$$

$$Sc_g = \text{Schmidt number} = (\mu_g / \rho_v D_v) \quad (12.109)$$

The effective gas and liquid rates, $U_{g,eff}$ and $U_{L,eff}$, take into account the flow angles, void fractions, and film thicknesses that derive from gross flow rates and packing geometry. The equivalent diameter basis is shown in Figure 12.48.

For the liquid phase, a penetration model is used, with the exposure time based on flow across the corrugation side of the packing. Thus,

$$k_L = 2 \sqrt{\frac{D_L U_{L,eff}}{\pi S}} \quad (12.110)$$

where S is the length of a side of a corrugation.

Heights of transfer units for the individual phases are obtained from Equation (12.98), and Equation (12.100) provides the height of an overall transfer unit. For the gauze packings, with spreading aided by capillary action, interfacial area $a_i = a_p$ (specific surface area from Table 12.10). For sheet metal packings, which do not promote as much liquid spreading, an empirical correction factor was proposed by Fair and Bravo⁸⁹:

$$a_i = \beta a_p \quad (12.111)$$

where the discount factor β is some function of liquid rate and surface wettability. For poorly wetted surfaces, where rivulet flow dominates, β is quite low—in the range of 0.1 to 0.3, even at high liquid rates. On the other hand, for well wetted surfaces, β can range up to 1.0 or higher. For very approximate estimates, the designer can use the relationship for well wetted metal surfaces:

$$\beta = 0.50 + 0.0058 (\% \text{ flood}) \quad (12.112)$$

TABLE 12.12
Values of Parameters for Equations (12.114) through
(12.117)

	a_p (m ² /m ³)	F_{SE} (–)	ε (–)	S (m)	θ (deg)
Flexipac 2	233	0.350	0.95	0.018	45
Gempak 2A	223	0.344	0.95	45	
Intalox 1T	315	0.415	0.95	0.0152	45
Intalox 2T	213	0.415	0.95	0.0221	45
Jaeger Maxpak	229	0.364	0.95	0.0175	45
Mellapak 250Y	250	0.350	0.95	45	
Mellapak 500Y	500	0.350	0.91	45	
Sulzer BX	492	0.90	0.0090	60	

scale-up studies. Scaled-down versions of some of the packings are available in sizes of about 25 and 50 mm diameter.

Hufton et al.⁹² used a 23-mm diameter Sulzer BX laboratory packing and found that the original Bravo et al. model [Equation (12.106)] worked well at the small scale so long as the actual geometric dimensions of the laboratory packing were used.

12.8.3.5 Structured Packing Performance

The most common structured packing has a specific surface area in the range of 225 to 250 m²/m³, has a corrugation angle of 45°, and is fabricated from thin-gauge sheet metal; this is often called a “no. 2 packing.” The metal may have a textured surface to promote liquid spreading and may have perforations to equalize pressure (and promote spreading). Performance tests are usually run at total reflux with several standard test mixtures. Figure 12.67 shows how the performance of a no. 2 packing compares with that of two random packings (50-mm Pall rings and no. 40 IMTP) and that of a structured packing with twice the surface and fabricated from metal gauze (Sulzer BX). The structured packings are more efficient (lower HETP values) than the random packings.

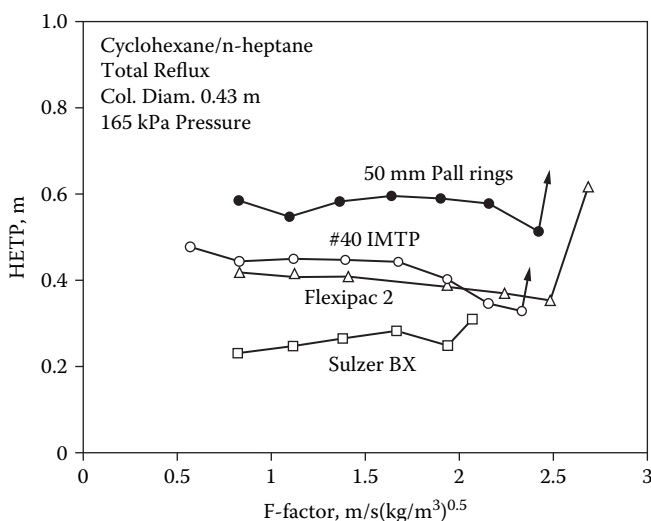


FIGURE 12.67 Efficiency comparison of several packings, cyclohexane/*n*-heptane test mixture. Total reflux, 0.43 m column, 165 kPa. (Z. Olujic et al., 2000. *Chem. Eng. Proc.* 39: 335.)

TABLE 12.13
Advantages-Crossflow Trays versus
High-Efficiency (Random or
Structured) Packings

Vapor capacity	Packings – lower pressure Trays – higher pressure
Liquid capacity	Trays – higher pressure Standoff – lower pressure
Pressure drop	Packings
Efficiency	Packings
Efficiency modeling	Packings
Foaming	Packings
Fouling	Trays
Chemical reactions	Trays
Control	Trays
Ultra-pure products	Trays
Designer comfort	Trays – hydraulics Packings – efficiency
Scaleup	Trays
Cost	Depends on situation

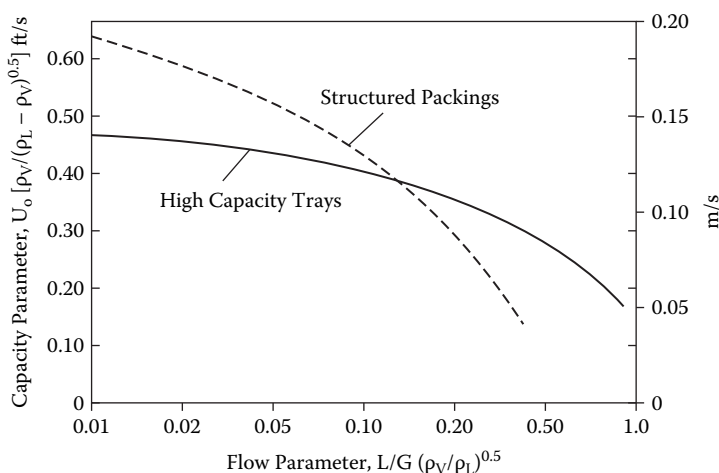


FIGURE 12.70 Generalized comparison of capacities, structured packings vs. high-capacity trays. [J. L. Bravo, 1998. *Chem. Eng.* 105 (2): 77.]

encountered in vacuum distillations; at high parameters, typical of high-pressure distillations, trays can handle the larger liquid flows.

Problem 12.11

Structured packing is now considered for the ethylbenzene/styrene separation. In Problem 12.10, 50-mm Pall rings were used in a 3.20-m column to give an HETP of 1.01 m. For the present case, a 3.05-m column will be used (i.e., rated) along with Mellapak 250Y (see Table 12.12). This is a sheet metal structured packing with about 250 m²/m³ surface and a corrugation angle of 45°, with the horizontal. For pressure drop and efficiency, the method of Rocha et al. [Equations (12.114)–(117)] is used.

12.9.1 INADEQUATE VAPOR CAPACITY

The criterion here is usually a capacity correlation such as given in Figures 12.29, 12.41, 12.43, and 12.53, depending on the type of contacting device. If the capacity falls short of prediction, there are several possibilities: the correlation was not used properly, too much was expected of the correlation, there is unexpected foaming, or the column internals are not arranged according to specification or are disarranged as a result of an internal vapor surge.

A gamma-ray scan of the column can generally pinpoint problem areas or zones. The rays penetrate the column metal, and their absorption depends on the amount of fluids or solids in their paths. Several commercial organizations specialize in scanning, and they are capable of traversing the entire column, with rays emitted in several different directions.

12.9.2 LIQUID FLOW CAPACITY

For tray columns, liquid flow constrictions are normally found in the tray downcomers. Example causes are lack of adequate froth collapse time, excessive pressure drop for flow under the downcomer baffle, and foreign materials being left in the downcomer by construction people. For packed columns, clogged support plates, broken packings, or growth of fouling deposits can cause liquid flow restrictions.

12.9.3 PRESSURE DROP

The usual problem is excessive pressure drop. It can be caused by flow constrictions/plugging, a bad predictive model, faulty internals, flow rates higher than design, entrainment, and weeping.

12.9.4 SEPARATION EFFICIENCY

Possible explanations for this shortcoming are faulty equilibrium data (relative volatility different from design), use of an improper stage model, wrong material balance (e.g., trace impurities), an erroneous scaleup model, or column internals being less efficient than anticipated.

In the previous sections, the comment was made that the process engineer should make certain that all possible components of the feed are identified. The comment should be extended to a concern about whether "hidden" azeotropes might be present.

12.9.5 STABILITY

Unstable operation often results from control system problems, improper design of the reboiler, or very low flow rates of liquid (leading to pulsing). Some devices, such as dualflow trays (with no downcomers), tend toward oscillating flows. The most common cause of stability is the control system.

12.10 NOMENCLATURE

a_i	= interfacial area for mass transfer, m^2/m^3
a_i'	= effective interfacial area for mass transfer, m^2/m^3
a_p	= total surface area of packing, m^2/m^3
A	= areas of trays, m^2
A_a	= active area of tray
A_d	= downcomer area
A_{da}	= area under downcomer baffle
A_h	= hole area
A_n	= net area

K	= vapor-liquid equilibrium ratio ("K value")
L	= molar liquid rate, lb-moles/hr-ft ²
l_w	= weir length, in
L, L_M	= liquid molar flow rate, kg-moles/s
L'	= liquid flow rate, kg-/s-m ²
L/G	= liquid to vapor mass flow rate ratio
L_w	= liquid flow rate over the tray weir, ft ³ /s-m
m	= slope of equilibrium curve
m_1	= exponent in Equation (12.101)
M_L	= molecular weight of liquid
n_1	= exponent in Equation (12.101)
N	= number of trays or stages
N_a	= actual stages or trays
N_m	= minimum stages
N_t	= total trays
N	= number of transfer units (also NTU)
N_L	= number of liquid phase transfer units
N_{ov}	= number of overall transfer units, liquid basis
N_v	= number of vapor phase transfer units
N_A	= molar flux, species A
p	= partial pressure, atm or bar
p^{sat}	= vapor pressure, atm or bar
P	= total pressure, atm or bar
q	= liquid flow rate, m ³ /s
Q	= vapor flow rate, m ³ /s
R	= reflux ratio
R_m	= minimum reflux ratio
Re	= Reynolds number, dimensionless [Equation (12.108)]
S	= length of a side of corrugation, structured packing, m
Sc	= Schmidt number, dimensionless [Equation (12.109)]
Sh	= Sherwood number, dimensionless [Equation (12.109)]
t	= residence time, s
T	= absolute temperature
u_a	= liquid velocity to active area of tray (q/A_a), m/s
u_{Lh}	= liquid velocity through distributor holes, m/s
U	= vapor or gas velocity, m/s
U_a	= vapor velocity through active area of tray (Q_v/A_a), m/s
U_g	= actual vapor velocity in structured packing, m/s
U_L	= actual liquid velocity on structured packing surface (film flow), m/s
v	= vapor or gas flow for an individual component, m/s
V	= vapor or gas flow rate, kg-moles/s
V'	= vapor sidestream flow, kg-moles/s
W	= length of flow travel on tray, m
x	= liquid mole fraction x^* = equilibrium value
y	= vapor mole fraction y^* = equilibrium value
z	= mole fraction in feed
Z	= height of packing, m
Z_f	= height of froth on tray, m

4. Van Laar Z. *Physik. Chem.* 1910, 72, 723; 1913, 83, 599.
5. Gmehling, J., Onken, U., and Arlt, W. *Vapor-Liquid Equilibrium Collection*, Chemistry Data Series (continuing series). Frankfurt, Germany: DECHEMA, 1979–.
6. Fredenslund, A., Gmehling, J., and Rasmussen, P. *Vapor-Liquid Equilibria Using UNIFAC*. Amsterdam: Elsevier, 1977.
7. Hala, E., Pick, J., Fried, V., and Vilim, O. *Vapor-Liquid Equilibrium*, 2nd ed., Oxford, U.K.: Pergamon, 1967.
8. McCabe, W. L. and Thiele, E. 1925. *Ind. Eng. Chem.* 17: 605.
9. Seader, J. D. and Henley, E. J. *Separation Process Principles*. New York: John Wiley & Sons, 1998.
10. Stichlmair, J. and Fair, J. R. *Distillation—Principles and Practices*. New York: Wiley-VCH, 1998.
11. Ponchon, M. 1921. *Tech. Mod.* 13 (20): 55.
12. Savarit, R. 1922. *Arts Metiers*, 65, 142, 178, 241, 266, 307.
13. Fenske, M. R. 1932. *Ind. Eng. Chem.* 24: 482.
14. Underwood, A. J. V. 1948. *Chem. Eng. Prog.* 44: 603.
15. Gilliland, E. R., 1940. *Ind. Eng. Chem.* 32: 1220.
16. Rusche, F. A. 1999. *Hydrocarb. Proc.* 78 (12): 41.
17. Fair, J. R. and Bolles, W. L. 1968. *Chem. Eng.* 75 (9): 156.
18. Lewis, W. K. and Matheson, G. L. 1932. *Ind. Eng. Chem.* 24: 494.
19. Thiele, E. and Geddes, R. L. 1933. *Ind. Eng. Chem.* 25: 289.
20. Stichlmair, J., Fair, J. R., and Bravo, J. L. 1989. *Chem. Eng. Prog.* 85 (1): 63.
21. Horsley, L. H. *Azeotropic Data—III*. Advances in Chemistry Series No. 116. Washington, DC: American Chemical Society, 1973.
22. Gmehling, J., Menke, J., Kraczyk, J., and Fischer, K. *Azeotropic Data*. New York/Weinheim: VCH Publishers, 1994.
23. Frank, T. 1997. *Chem. Eng. Prog.* 93: 52–63.
- 23a. Ewell, R. H., Harrison, J. M., and Berg, L. 1944. *Ind. Eng. Chem.* 36: 871.
24. Barton, P. and Roche, E. C. Batch Distillation, Section 1.3 in *Handbook of Separation Techniques*, P. A. Schweitzer, ed. New York: McGraw-Hill, 1997.
25. Diwekar, U. M. *Batch Distillation: Simulation, Optimal Design and Control*. Washington, DC: Taylor and Francis, 1995.
26. Aspen Technology, Cambridge, MA, Program *Batchfrak*.
27. Agreda, V., Partin, L., and Heise, W. 1990. *Chem. Eng. Prog.* 86 (2): 40.
28. Fair, J. R. 1998. *Chem. Eng.* 105 (11): 158.
29. Subawalla, H. and Fair, J. R. 1999. *Ind. Eng. Chem. Res.* 38: 3696.
30. Fair, J. R. 1984. Historical Development of Distillation Equipment, *AIChE Symposium Series No.* 235, 79: 1.
31. Fractionation Research, Inc., P. O. Drawer F, Bartlesville, OK 74005. Website www.fri.com.
32. FRI reports are available from Oklahoma State Archives, Stillwater, OK 74078.
33. Kunesh, J. G., Kister, H. Z., Lockett, M. J., and Fair, J. R. 1995. *Chem. Eng. Prog.* 91 (10): 43.
34. Billet, R., Conrad, S., and Grubb, C. M. 1969. *ICHEME Symp. Ser.* 32, 5: 111.
35. Fair, J. R., 1997. *Perry's Chemical Engineers' Handbook*, 7th ed. R. H. Perry and D. Green, eds., New York: McGraw-Hill.
36. Kister, H. Z. and Haas, J. R., 1990. *Chem. Eng. Prog.* 86 (9): 69.
37. Silvey, F. C. and Keller, G. J. 1966. *Chem. Eng. Prog.* 67 (1): 69.
38. Fair, J. R. and Mathews, R. L. 1958. *Petrol. Refiner* 37 (4): 153–158; Fair, J. R. 1961. *Petro/Chem Eng.* 33 (10): 57–64.
39. Leibson, I., Kelley, R. E., and Bullington, L. A. 1957. *Pet. Refiner* 36 (2): 127.
40. Hoek, P. J. and Zuiderweg, F. J. 1982. *AIChE J.* 28: 535.
41. Bolles, W. L. 1963. *Design of Equilibrium Stage Processes*, ed. B. D. Smith, Chapter 14. New York: McGraw-Hill, 1963.
42. *Perry's Chemical Engineer's Handbook*, 5th ed., R. H. Perry and C. H. Chilton, eds. New York: McGraw-Hill, 1973, 18–10–18–12.
43. Klein, G. F. 1982. *Chem. Eng.* 89: 81 (May 3, 1982).
44. Bolles, W. L. 1976. *Chem. Eng. Prog.* 72 (9): 43.
45. Nutter, D. E. 1979. *ICHEME Symp. Ser.* 56, 3.2: 47.

93. Kister, H. Z. 2006. *Distillation-Troubleshooting*. New York: Wiley-Interscience.
94. Lieberman, N. P. 1983. *Process Design for Reliable Operations*. Houston: Gulf Publ. Co.
95. Saletan, D. 1994. *Creative Troubleshooting in the Chemical Process Industries*. New York/London: Chapman & Hall.

13.7 Summary.....	1114
13.8 Nomenclature.....	1114
13.8.1 Greek Letters	1115
13.8.2 Subscripts.....	1116
References	1116

13.1 INTRODUCTION

13.1.1 FUNCTIONS OF ABSORPTION AND STRIPPING

Absorption and stripping are counterpart processes used in the process industries for separating gas or liquid mixtures. Their functions are generally of two types: *recovering* one or more components from the mixture or *purifying* the mixture to meet specifications or standards. In absorption, a gas mixture is contacted with a suitable liquid *solvent* to remove preferentially one or more mixture components from the gas phase. Conversely, in stripping, a liquid mixture is contacted by a suitable *stripping gas* to remove preferentially one or more components from the liquid phase. In practice, absorption and stripping are often coupled processes, as shown later. Both processes involve gas-liquid contacting, generally in vertical, cylindrical towers called *absorbers* or *strippers*.

Processes of this type are distinguished between physical and chemical absorption or stripping. For physical processes, transfer of the solute between phases is by physical mechanisms without any chemical reactions. For chemical processes, the solute reacts with a component of the solvent, resulting in an increased capacity of the solvent for the solute. Conversely, stripping sometimes breaks the chemical bonds between solute and solvent.

13.1.2 COMMERCIAL APPLICATIONS

Absorption is often used to purify a gas stream; an alternate name of the operation is *scrubbing*. Contaminated air, for example, can be purified by scrubbing out the contaminants with a selective solvent. Another example is removing sulfur and carbon dioxide from natural gas using solvents such as alkanolamines. As the solutes are being removed from the gas, the solvent becomes richer in these materials. To purify the solvent for reuse, stripping is needed. The contaminants are removed from the liquid by the action of a stripping gas. The general flow diagram for this coupled operation is shown in Figure 13.1. Such a process is useful for reducing the level of gaseous pollutants. Representative commercial applications of physical and chemical absorption are shown in Table 13.1.

Not all absorptions and strippings are as straightforward as indicated in Figure 13.1. Absorption may be used to produce a product—for example, the absorption of nitrogen oxides in water to form nitric acid. Or absorption may be used to recover valuable products, such as propanes and butanes from natural gas. And stripping may be a once-through operation such as the removal of volatile organic compounds (VOCs) from groundwater using atmospheric air for the stripping medium.

Flow diagrams for representative absorption and stripping processes are shown in Figures 13.2 and 13.3. In Figure 13.2, acetone is scrubbed from air to meet an exit air specification. The acetone transfers to the water phase, and the rich solvent flows to a distillation column wherein the acetone is recovered in high purity and the water is recycled to the absorber. In Figure 13.3, trichloroethylene (TCE) is stripped from groundwater by air, with the discharge from the stripper flowing through a carbon bed in which the TCE is adsorbed.

Obviously, a solvent must be found that has an affinity for the constituent(s) to be absorbed, and the stripping medium must be such that the physical or chemical bond between solute and solvent can be easily broken. This affinity, or solubility, is a critical consideration in the design of absorption/stripping systems, as discussed next.

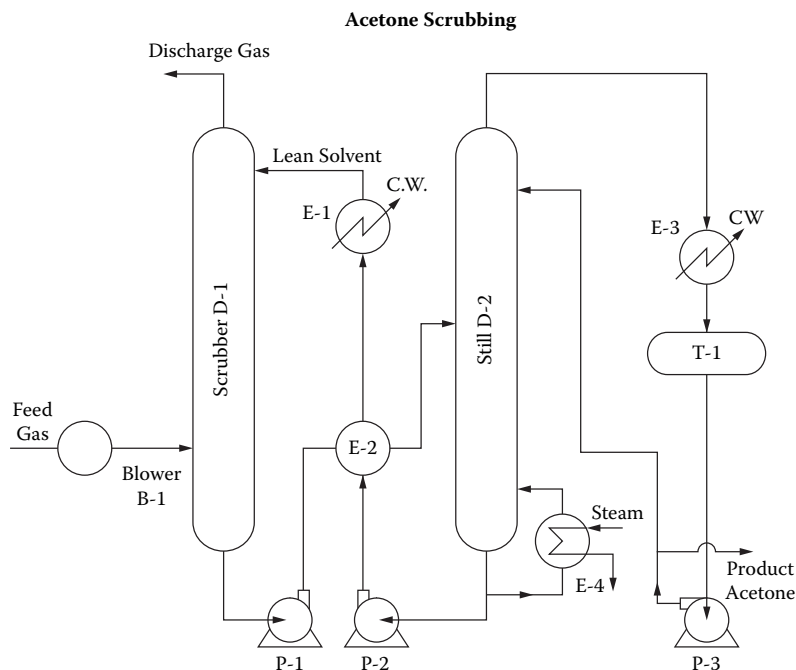


FIGURE 13.2 System for scrubbing acetone from air using a circulating solvent. Water or a non-volatile organic liquid can be used as the solvent.

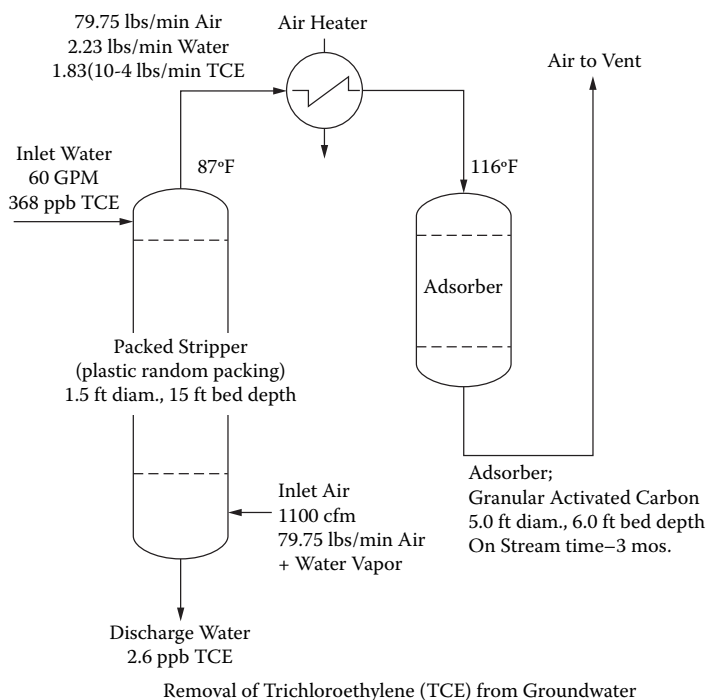


FIGURE 13.3 System for removing volatile organic compounds (VOCs) from groundwater, by stripping with atmospheric air. The exit gas contains the stripped VOCs and must be purified by flow through a bed of activated carbon.

data are for low-concentration conditions, the usual case for sparingly soluble organic compounds. For cases where experimental data do not exist, the predictive model UNIFAC,² discussed in Chapter 12 is recommended.

Problem 13.1

Acetone is to be scrubbed from dry air into water at 30°C and 1.0 atm. The acetone concentration is 2.60 vol-%. For the condition of thermodynamic equilibrium, calculate the following:

- The Henry's law coefficient
- The equilibrium ratio, K
- The liquid phase activity coefficient
- The Bunsen coefficient.

Data: molecular weights: acetone = 58, air = 29, water = 18

Vapor pressures at 30°C: acetone = 283 mm Hg, water = 31.8 mm Hg

According to the measurements of Othmer et al.,¹⁷ for a partial pressure of acetone = 760(0.025) = 19.0 mm Hg, the equilibrium acetone composition in the liquid is 0.010 mole-%. Thus,

- $H_i = 19/0.01 = 1900$ mm Hg/m.f. = 2.5 atm/m.f.
- K value = $0.025/0.010 = 2.50$ [$H_i = K_i P = 2.50(760) = 1900$ mm/m.f.]
- Since $K_i = \gamma_i p^{sat}/P$, then $\gamma_i = 2.5(760)/284 = 6.72$
- Bunsen coefficient [Equation (13.1)]. Basis 1.0 mole equil. liquid. Moles acetone = 0.025. Vol. acetone at STP = $22,400(0.025) = 560$ cm³. Vol. water = 18 (0.0975) = 1.755/1.00 = 1.755. Hence $\alpha_i = 560/(1.755 \times 19/760) = 12,760$ mm⁻¹ or 16.8 atm⁻¹

Yaws and coworkers³ have presented many compilations and correlations of solubility data, for example, hydrocarbons in water. Methods are available for estimating the solubility of gases in organic liquids.⁴⁻⁶ And special compendia include those in the Solubility Data Series,⁷ Seidell and coworkers,⁸⁻¹⁰ and Dack.¹¹ Extensive reviews have been provided by Markham and Kobe,¹² Long and McDevit,¹³ Battino and Clever,¹⁴ Wilhelm and Battino,¹⁵ and Wilhelm et al.,¹⁶ among others. Often data usually associated with vapor-liquid equilibrium in distillation can be used. Finally, various handbooks contain some useful solubility data.

13.1.3.2 Multicomponent Solubilities

The simplest case of absorption and stripping is the removal of a single component from the second component in a binary mixture. This means, however, that the solubility of the other component must also be considered. In Problem 13.1, the tacit assumption was made that air (the second component) is insoluble in water. For many situations, there is a mixture of varying solubilities to be removed in absorption, or varying effective vapor pressure to be stripped. Thus, *relative solubility* must be considered.

For dilute mixtures where the majority component is not being absorbed or stripped, the mixture components usually can be considered to behave as individual entities subject to their individual solubilities. Thus, for a mixture of 1000 ppm-vol trichloroethylene and 500 ppm-vol perchloroethylene, the solubility for each can be determined as if the other is absent. In general, for several components of varying solubility, the relative solubility is

$$\alpha'_{i,...n} = K_i/K_{j,...n} \quad (13.7)$$

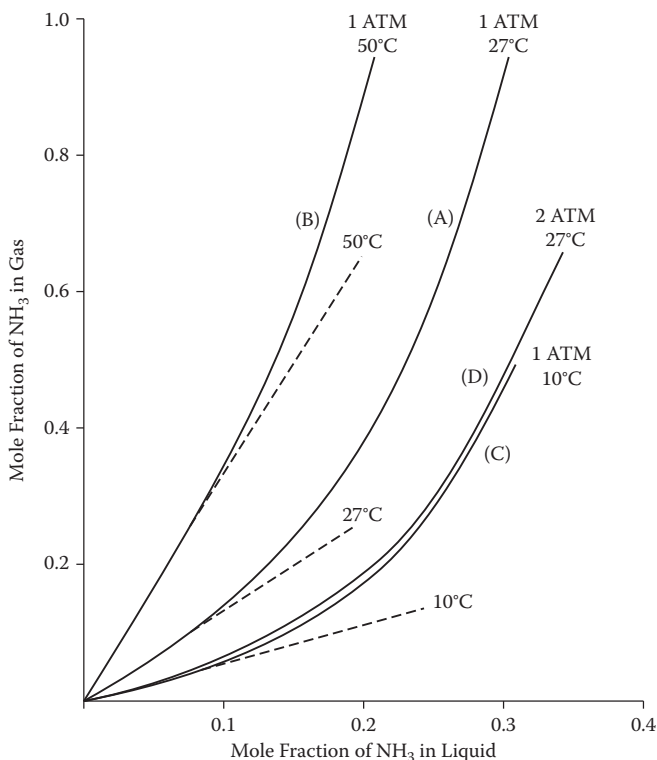


FIGURE 13.5 Solubility of ammonia in water from ammonia-air mixtures. The dashed lines indicate the slope of the lines near the origin. [Perry, R. H. (ed.), 1985. *Chemical Engineer's Handbook*, 5th ed., New York: McGraw-Hill.]

1. Availability and cost
2. Volatility (higher volatility can contaminate the absorber exit gas)
3. Stability, especially for recirculating systems
4. Corrosiveness
5. Ease of stripping
6. Convenience of disposal
7. Degree of hazard to humans and the environment

13.1.5 THEORETICAL STAGES/TRANSFER UNITS

In designing an absorber or stripper, one must ascertain some index of “difficulty of separation.” As in the case of distillation separations, this index is either the required *number of theoretical stages* or the required *number of transfer units*. These parameters are interchangeable, with stages often used for plate columns and transfer units for packed columns. Background on the parameters is provided in Chapter 12. For convenience in handling the associated hydraulics and mass transfer calculations, the remainder of this chapter is divided into three parts: “Plate Columns,” “Packed Columns,” and “Special Devices.”

13.2 PLATE COLUMNS

Plate columns are vertical vessels, usually circular in cross section, that contain a multiplicity of plates that bring gas and liquid into intimate contact. These columns are the same as those used

$$\text{Gas: } Y_i = \frac{y_i}{1 - y_i} = \frac{\text{moles solute}}{\text{mole solute free gas}} = \frac{\text{moles solute}}{\text{mole "carrier gas"}}$$
 (13.10)

$$\text{Liquid: } X_i = \frac{x_i}{1 - x_i} = \frac{\text{moles solute}}{\text{mole solute free solvent}} = \frac{\text{moles solute}}{\text{mole solvent}}$$
 (13.11)

Clearly, at very low concentrations, $y \sim Y$ and $x \sim X$, but as will be shown later, the modified relationships can be used for concentrated cases. When there is more than one solute, the denominators in Equations (13.10) and (13.11) do not change.

Consider a general-type absorber as diagrammed in Figure 13.6. Gas and liquid flow counter-currently through real or imagined stages. The usual specifications include (a) fraction of absorption of solute in the feed gas, (b) maximum allowable concentration of solute in the exit gas, and (c) optimal ratio of solvent to feed gas. Based on mass balances,

$$\text{Total: } G_{N+1} + L_o = G_1 + L_N$$
 (13.12)

$$\text{Solute } i: G_{N+1}Y_{N+1} + L_oX_o = G_1Y_1 + L_NX_N$$
 (13.13)

By definition, $G_{N+1} = G_1 = G$, and $L_o = L_N = L$

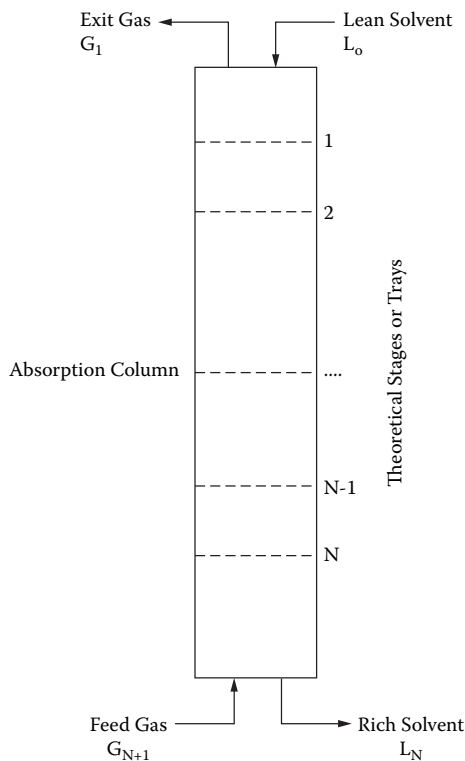


FIGURE 13.6 Arrangement and nomenclature for a plate-type absorber. Note that stages or trays are numbered from the top.

	Feed gas	Rich oil	Off gas	Entering solvent
Acetone	30	29.1	0.90	0
Air	70	0	70	0
Oil	0	244.4	0	244.4
	100	273.5	70.9	244.4

$$Y_{N+1} = 30/70 = 0.428 \quad X_N = 29.1/244.4 = 0.119 \quad Y_1 = 0.9/70 = 0.0129 \quad X_o = 0$$

The effective absorption efficiency is $(0.428 - 0.0129)/(0.428 - 0) = 0.970$.

For the modified coordinates, the K value is not constant at 1.8. The equilibrium line has a slight curvature, and its slope varies from 1.80 to 1.98. Use an average = 1.90. Then, the absorption factor is $244.4/(70 \times 1.90) = 1.84$.

Number of theoretical stages required [Equation (13.9)]:

$$N_t = \frac{\ln \left(\frac{0.97 - 1.84}{0.97 - 1} \right)}{\ln 1.84} - 1 = 4.52$$

The material balance for this case is

	Feed gas	Rich oil	Off gas	Entering solvent
Acetone	30	30.3	0.9	1.2
Air	70	0	70	0
Oil	0	244.4	0	244.4
	100	274.7	70.9	245.6

$$Y_{N+1} = 30/70 = 0.428 \quad X_N = 30.3/244.4 = 0.124 \quad Y_1 = 0.9/70 = 0.0129 \quad X_o = 1.2/244.4 = 0.005$$

Now the effective absorption efficiency is $(0.428 - 0.0129)/(0.428 - 0.005) = 0.981$.

The number of theoretical stages by Equation (13.9) = 5.04. The acetone in the entering oil increases the stage requirement from 4.52 to 5.04. The graphical treatment of case (c) is shown in Figure 13.8.

13.2.1.1 Multiple Solutes

Equation (13.8) can be used for multiple solute cases, since it can accommodate absorption factors A_i, A_j, A_k, \dots , each giving a different value of E_a . The liquid/gas ratio does not change, since it is based on overall flows. Thus, Equation (13.9) can give different values of N (theoretical stages). It is here that the key component enters into the picture. The required stages for that component are calculated, and then the same value of N is substituted back in Equation (13.8) to determine the relative absorption effectiveness of the other components.

The graphical counterpart of Equations (13.8) and (13.9) is shown in Figure 13.9 for the example of absorbing ethane, propane, butane, and pentane into absorption oil. Pentane is the key component, and its value of Y is reduced from 0.04 to essentially zero. The other components are restricted by the same operating line slope as required for pentane. Thus, butane is reduced from $Y = 0.08$ to $Y = 0.02$, propane is reduced from $Y = 0.08$ to 0.063, and ethane is reduced very little. The requirement for butane is about four stages. Ethane and propane fall into a "pinch" composition after one or two stages and then for the remaining stages have no change in composition. The absorption effectiveness values indicated in Figure 13.9 would also result from the use of Equations (13.8) and (13.9).

with the nomenclature the same as for Equation (13.8) (Figure 13.6) with the following additions:

$$A' = \frac{A_N(A_1 + 1)}{A_N + 1} \quad (13.16)$$

$$A_e = \sqrt{A_N(A_1 + 1) + 0.25} - 0.50 \quad (13.17)$$

$$A_N = \frac{L_N}{V_N K_N} \quad (13.18)$$

$$A_1 = \frac{L_1}{V_1 K_1} \quad (13.19)$$

$$V_N = V_{N+1} \left(\frac{V_1}{V_{N-1}} \right)^{1/N} \quad (13.20)$$

The Edmister approach makes corrections such that an average value A_e can be used in the Kremser-Brown relationship. The effect of solute in the entering solvent is accounted for by the first term on the right in Equation (13.15). For the same form to be used for stripping, tray numbering and other terms are amplified in Figure 13.10. The stripping equations will be given later.

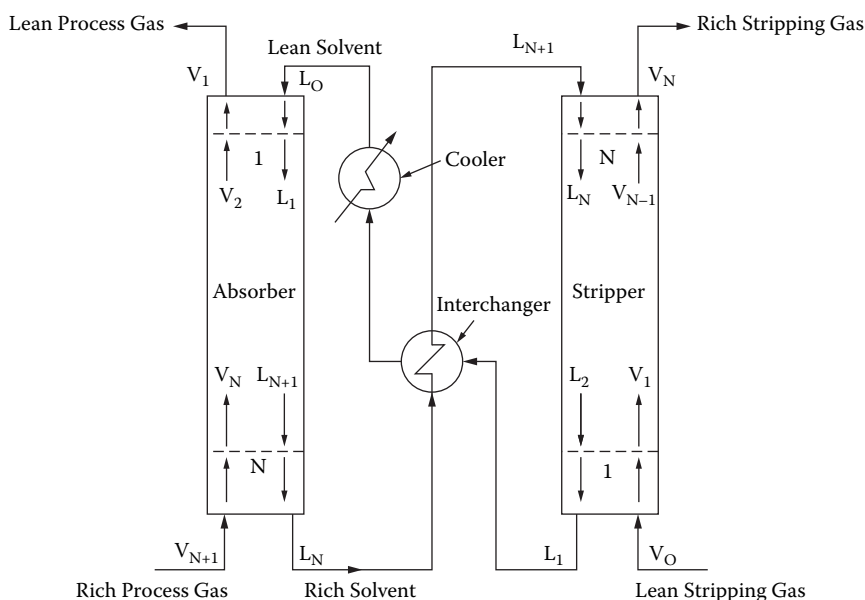


FIGURE 13.10 Nomenclature for use of the Edmister method for determining stages in absorbers and strippers. In order to maintain similarity of equations for absorption and stripping, the stages are numbered up from the bottom of the stripper.

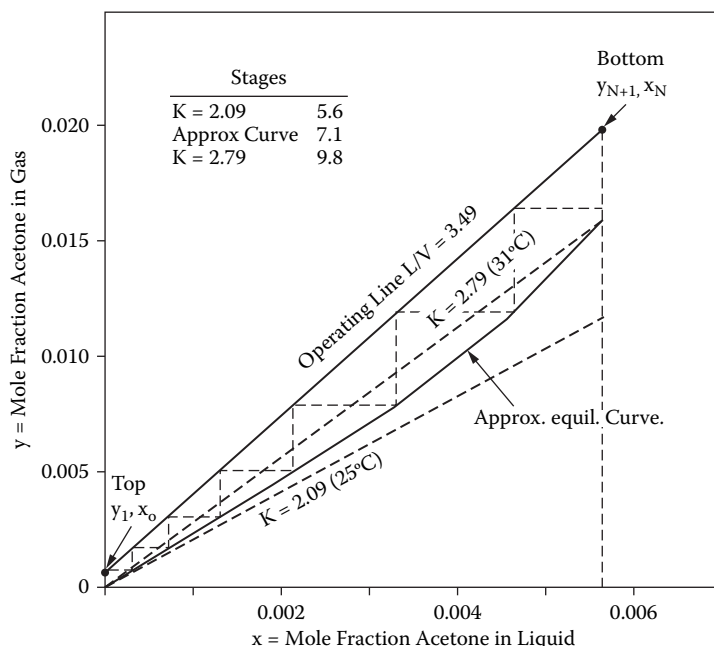


FIGURE 13.11 Diagram for Problem 13.3, showing effect of heat of absorption on required stages. Only the steps for the temperature-corrected equilibrium curve are shown.

Problem 13.3

Acetone is to be absorbed from wet air into pure water in a plate column. The laden air enters at 35°C, and the water solvent enters at 25°C. Pressure is atmospheric. The air contains 2.0 mole-% acetone and is 70% saturated with water vapor (4 vol-% water). The concentration of acetone in the air is to be reduced to 0.05 mole-% ($E_{ai} = 0.975$). The solvent rate is chosen such that the operating line has a slope of 3.49 on a mole fraction-plotting basis. How many stages are needed?

Solution

Based on an overall heat balance, with the exit air temperature closely approaching the inlet water temperature, the adiabatic temperature rise of the liquid is 6°C, giving an exit liquid temperature of 31°C. Isothermal K values ($= y/x$) are 2.09 at 25°C and 2.79 at 31°C. The exit water contains 0.57 mole-% acetone.

Figure 13.11 shows a y - x diagram with the isothermal equilibrium lines at 25 and 31°C. Also shown is the approximate actual equilibrium curve location, taking into account heat effects in the column. For the linear equilibrium line, stages are determined by Equation (13.9) or by stepping graphically. For the curved (approximate actual) line, stages are stepped off as shown in Figure 13.11:

1. For the straight line at 25°C: stages = 5.6
2. For the straight line at 31°C: stages = 9.8
3. For the actual curve: stages = 7.1

Clearly, the equilibrium line based on the outlet temperature (31°C) requires excessive stages—but neglecting heat effects is too optimistic. The design of 7.1 stages would be used.

The Kremser–Brown relationship [Equation (13.8)] can be modified for stripping:

$$V_N = V_{N-1} \left(\frac{V_N}{V_o} \right)^{1/N} \quad (13.28)$$

13.2.2.1 Minimum Stripping Gas Rate

An infinite number of stages will be required if the exit gas and the entering liquid approach equilibrium, i.e., $Y_N \sim K X_{N+1}$. It is recommended that a stripping gas rate of about twice the minimum be considered first. However, for once-through air strippers, where the stripping gas has no cost other than the energy needed to move it through the stripper, an optimum V/L ratio may depend on some trade-off of blower horsepower and height of contactor.

EQUIPMENT DESIGN

Plate columns for absorption and stripping are fairly standard in design, with the plates perforated to allow gas to pass upward and provisions for conveying liquid from a plate to the next plate below. Figure 13.12 shows an absorber of this type, which utilizes simple sieve trays for contacting. Only the rudiments of designing such a contactor will be given here; see Chapter 12 for more details. Predicting the performance of a plate absorber or stripper involves the following key elements:

- Capacity. This dictates the diameter of the needed column and is a function of the plate geometry, the vertical spacing of the plates, and the flow rates of liquid and gas.
- Pressure drop. This is a function of flow rates and plate geometry and is particularly important for large gas flows where blower horsepower may be an important element in the economics of system design.
- Efficiency. The foregoing discussions of absorption and stripping stages have led to a determination of theoretical stages or plates. For a practical design, a plate efficiency is needed to determine the number of *actual* plates needed in the column. The discussion on plate efficiency will follow.
- Liquid holdup. The amount of liquid present on the trays has implications for control system design; the more the holdup, the less responsive the column is to changes in control variables. It may be particularly important for chemical absorbers where a degree of residence time of the liquid is needed to complete the absorption/reaction. This is discussed further in a separate section on "Chemical Absorption/Stripping."

Problem 13.4

A contaminated groundwater stream contains 5 mg/L trichloroethylene (TCE) and 1.5 mg/L perchloroethylene (PCE) at 21°C. The stream is fed to the top of a tray column, where it is stripped with a countercurrent flow of air, also at 21°C.

- Calculate the minimum air rate needed (using infinite stages).
- For a molar feed-air ratio of 10.0, how many stages are needed to remove 99.8% of the TCE?
- What percentage of the PCE will be removed in the process?

Solubility data for TCE and PCE are given in Figure 13.4. Use $K = 6753$ for TCE and 61,790 for PCE.

Solution

The inlet composition of TCE may be converted to a mole fraction of $6.85(10^{-7})$. The equilibrium exit gas concentration is $6753(6.85)(10^{-7}) = 0.00463$ moles TCE per mole of air + TCE, or a

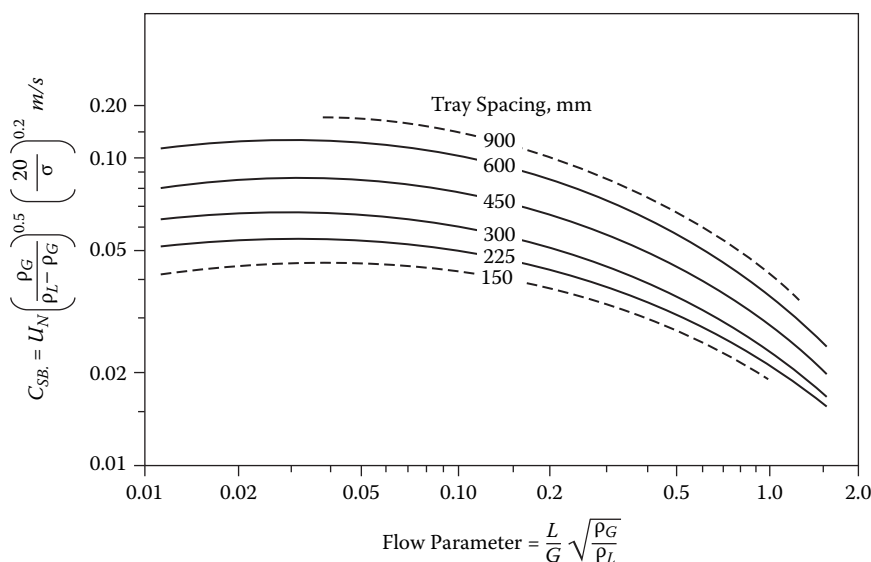


FIGURE 13.13 Capacity of plate-type absorbers and strippers. Curves denote the incipient flooding condition, and for design must be discounted. [Fair, J. R., 1961. *Petro/Chem. Engineer* 33 (9): 57.]

13.2.2.2 Capacity and Column Diameter

The maximum allowable capacity of a plate absorber or stripper is represented by an incipient flooding condition. The prudent operating capacity is based on about 85% of the predicted flooding condition. The first step is to calculate the dimensionless *flow parameter* for the point in the column being investigated:

$$FP = \frac{L}{G} \sqrt{\frac{\rho_G}{\rho_L}} \quad (13.29)$$

where L/G is the mass ratio of liquid to gas. This parameter is a high number for the typical high L/G ratios encountered in absorbers and strippers, but there are notable exceptions (e.g., the use of glycols to scrub water out of natural gas) where the L/G is extremely low. The allowable gas velocity for a given flow parameter is obtained from Figure 13.13,²¹ making use of the geometrical relationships shown in Figure 13.14.

The value of FP is obtained directly from the overall material balance. For a selected tray spacing (usually 18 in (457 mm) or 24 in (610 mm) and FP as the abscissa, a value of the ordinate is obtained. This is the capacity parameter C_{sbf} at the maximum (flood) capacity. The ordinate value is

$$C_{sbf} = U_N \left[\frac{\rho_G}{\rho_L - \rho_G} \right]^{0.5} \left[\frac{20}{\sigma} \right]^{0.2} \quad (13.30)$$

where U_N = linear gas velocity through the net area of the tray, i.e., through the cross section open to flow, considering the space blocked off by the downcomer(s), and σ = the surface tension of liquid in mN/m.

Since $U_N = U_s (A_T/A_N)$, the superficial gas velocity is calculated as

$$h_{total} = N_{act}(h_t) \quad (13.33)$$

where

h_{total} = drop through all the plates, in height of the flowing solvent

N_{act} = number of actual plates

h_t = pressure drop across a single plate

Equation (13.29) does not cover losses such as gas entrance, drop through a demister at the top of the column, and so on.

The pressure drop across the plate comprises two resistances in series, one for friction through the perforations and the other for head loss in flowing through the aerated liquid on the tray:

$$h_t = h_d + h_L, \text{ mm liquid} \quad (13.34)$$

For the perforations, the orifice equation applies:

$$h_d = \frac{50.8 \rho_G U_h^2}{C_v^2 \rho_L} \quad (13.35)$$

where

C_v = orifice coefficient, dimensionless

U_h = gas velocity through the holes

Typically, the area of the holes is 6 to 8% of the total cross-sectional area. The orifice coefficient is about 0.8, but for more precise work, consult Chapter 12, "Distillation." The drop through the aerated liquid depends on the loading of the plate, and Figure 13.15 enables an estimate of the height of the two-phase mixture (i.e., froth). This mixture is typically 80% gas by volume, so the froth height times 0.2 will give the equivalent height of clear liquid for use in Equation (13.30).

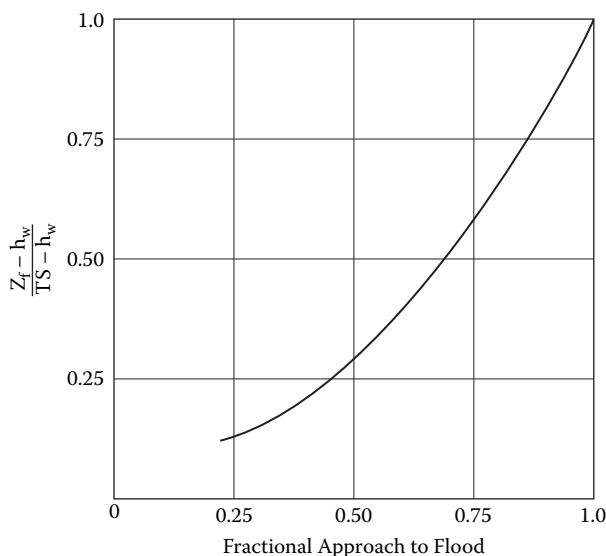


FIGURE 13.15 Chart for estimating the height of froth on a crossflow plate.

Diameter. From Figure 13.13, $C_{sbf} = 0.13$ m/s. At 85% of flood, $C_{sb} = 0.85(0.13) = 0.11$ m/s. Use downcomer area = 10% of the total cross section so that $A_T/A_N = 1.11$. From Equation (13.31),

$$U_s = \frac{0.11}{1.11 \sqrt{\frac{1.15}{1000 - 1.15} \left[\frac{20}{70} \right]^{0.2}}} = 3.75 \text{ m/s}$$

From Equation (13.32), diameter = $[1000/(60 \times 0.785 \times 3.75)]^{0.5} = 2.38 \text{ m} = 7.80 \text{ ft}$.

Efficiency. For Figure 13.16, the abscissa group at the bottom of the column is $(K\mu_L)/\rho_{LM}$, or $(2.8 \times 1.0)/(62.4/18) = 0.81$, for which $E_{oc} = 40\%$. Thus, $7.1/0.40 = 17.8$ —say 18 actual plates.

Pressure drop. For an open area $(A_H/A_A) = 0.14$ and 10% downcomers, the active area is $0.785(2.38)^2(0.80) = 3.56 \text{ m}^2$ and hole area = 0.498 m^2 . From Equation (13.35) and for one tray,

$$h_d = \frac{50.8(1.15) \left[\frac{1000}{60(0.498)} \right]^2}{(0.80)^2 (1000)} = 102.2 \text{ mm liquid} = 4.02 \text{ in liquid}$$

For pressure drop through the liquid at 85% flood, from Figure 13.15,

$$\text{Froth height} = Z_f = 0.75(610 - 50) + 50 = 470 \text{ mm}$$

At 20% liquid in froth, liquid head = $0.2(470) = 94 \text{ mm}$.

Total drop/tray = $102.2 + 94 = 196 \text{ mm liquid}$. For 18 plates, $3528 \text{ mm} = 3.528 \text{ m} = 5.0 \text{ lb/in}^2$.

13.3 PACKED COLUMNS

As in distillation columns, a packed column contains small packing elements dumped into the column in a random fashion, and these elements can provide the needed intimate contacting of the descending liquid and the rising gas or vapor. Packings of an ordered, or structured, form are rarely if ever used for absorption or stripping.

13.3.1 TRANSFER UNITS

Instead of stages or plates, *transfer units* are introduced to represent the separation requirement of a continuous, countercurrent contactor such as a packed column. As will be shown later, theoretical stages can be converted to transfer units for design purposes. Thus, only a summary of transfer unit theory will be given here, since it is usual practice to determine the required stages, as discussed in the previous section, and then convert them to transfer units. The conversion is in order because the mass transfer characteristics of packings are usually correlated in terms of heights of a transfer unit. Thus,

$$\text{Packed height} = Z = N_{og} H_{og} \quad (13.37)$$

where N_{og} = number of overall (both phases considered) transfer units and H_{og} = height of an overall transfer unit.

Overall transfer units may be expressed in terms of individual phase transfer units:

$$H_{og} = H_g + \lambda H_L \quad (13.38)$$

where

G_m = total gas flow, kg-moles/s-m²

k_{gi} = mass transfer coefficient, kg-moles/(s-m²-atm)

a_e = effective interfacial area, m²/m³

P = total pressure, atm

$$\text{Liquid: } H_{Li} = \frac{L_m}{k_{Li} a_e \rho_L (1 - x_i)} \quad (13.44)$$

where

L_m = total liquid flow, kg-moles/s-m²

k_{Li} = mass transfer coefficient, kg-moles/(s-m²-kg/m³)

ρ_L = average liquid density, kg/m³

In Equations (13.43) and (13.44), the units shown are representative; other consistent sets may be used.

13.3.4 HEIGHTS OF THEORETICAL STAGES

There are instances when it is preferable to convert from heights of transfer units to theoretical stages. The term *height equivalent to a theoretical plate (HETP)* is used. This is the height of a packed bed in which one theoretical stage of separation is achieved. The conversion is related to Equation (13.42):

$$HETP = H_{og} \left(\frac{\ln \lambda}{(\lambda - 1)} \right) \quad (13.45)$$

Thus, when $\lambda = 1.0$, $HETP = H_{og}$.

13.3.5 EQUIPMENT DESIGN

Packed columns for absorption and stripping are simple in design, if not in analysis. A vertical column is fitted with a packing support plate, filled with random packing, and equipped at the top with a suitable device to distribute the liquid to the bed. A screen or hold-down grid is usually placed on top of the bed to prevent movement of the packing, especially if the packing material has a low density (e.g., plastic) and the momentum of the gas is high. In a few cases, a special device at the bottom of the bed is used to ensure uniform gas distribution up through the bed. A representative packed absorber is illustrated in Figure 13.17; the liquid distributor is of the perforated pipe type, but other types, less subject to liquid fouling, can be used. See Chapter 12.

Problem 13.6

In Problem 13.3, theoretical stages were determined for a scrubber to remove acetone from air with a water solvent. For the same conditions, determine the required number of overall gas phase transfer units. The graphical work for the previous problem is shown in Figure 13.11.

Solution

Since this is a lean gas case, simplified expressions can be used. The number of gas phase transfer units can be obtained by integrating Equation (13.41), or from theoretical stages by Equation

condition). This can be done numerically or graphically. For the latter approach, values of $1/(y - y^*)$ are plotted on the Y scale against value of y on the X scale. The area under the plotted curve equals 8.2 (or 8.2 transfer units).

Since there is definite curvature of the equilibrium line, the value $N_{og} = 8.2$ should be used. It can be combined with a value of H_{og} for the packing device selected to provide the total packed height needed.

As in the case of tray absorbers and strippers, only the rudiments of design will be given here; more details are available in Chapter 12. Predicting the performance of a packed column involves four key criteria: capacity (column diameter), pressure drop (column diameter), efficiency (bed height), and liquid holdup (pressure drop and residence, as for chemical reactions). Each of these criteria depends strongly on the type and size of packing element selected. Thus, the first step is to choose a packing.

13.3.6 PACKING AND PACKED BED CHARACTERISTICS

Representative random packings are shown in Figure 12.25. Properties of important packings for absorption/stripping are given in Table 13.2. The first three packings listed are the “through-flow” type, in which the phases can flow freely through the elements with reduced form drag. The others listed are of the “around flow” type, with increased form drag and therefore higher pressure drop.

Random packings are fabricated from a wide variety of materials. Originally, most were made of ceramic and were popular for corrosive services despite their friability. Today, polypropylene is widely used to provide a bed that offers light weight, reasonable resistance to corrosion by many fluids, and low cost. Plastic random packings are often suitable where dissolved volatile organic compounds (VOCs) are to be removed from groundwaters.

Normally, liquid and gas flow countercurrently through the bed. At low gas rates, there is little disturbance of the downflowing liquid, but at higher gas rates the liquid is dragged by the vapor into a “loading” situation, and, if the gas flow is further increased, the packed bed begins to flood. Loading/flooding phenomena are shown schematically in Figure 12.51. While it may be optimum to operate a packed column in the loading zone, it is important not to operate too close to flooding. Thus, as a first consideration in design (or analysis of an operating column), the flood point is located as a function of gas and liquid flow rates, packing element geometry, and properties of the phases.

13.3.7 MAXIMUM GAS/LIQUID CAPACITY

The hydraulic flood point, as illustrated in Figure 12.51, is reached at a combination of counter-current gas and liquid rates such that the pressure drop exhibits a relatively large increase with a small increase in flow rate of either phase. Methods for estimating maximum hydraulic capacity for a packing provide a basis for design (optimum approach to flood). Although there are several approaches to predicting flooding, the most popular also provides a pressure drop estimating capability, most recently published by Strigle²³ as the diagram in Figure 12.53.

From Figure 12.53, both limiting capacity and pressure drop may be predicted. The abscissa term is the flow parameter [Equation (13.29)], used also for plate columns. The ordinate term is a capacity parameter CP , modified from the capacity parameter for plate columns [Equation (13.30)]:

$$CP = U_s \sqrt{\frac{\rho_G}{\rho_L - \rho_G}} F_p v^{0.05} = C_{sb} F_p v^{0.05} \quad (13.46)$$

where U_s = superficial gas velocity, m/s; v = kinematic viscosity, cs ; and F_p = packing factor, characteristic of the packing type and size. Packing factors are given in Table 13.2.

2" Pall Rings—Plastic

Column Diameter 30 Inches
 Packing Height 10 Feet
 Packing Factor25
 Liquid Rate lbs./ft.²/hr. as Parameter
 Gas Rate 500 lbs./ft.²/hr.
 Gas Concentration Ln Mean 1%
 Liquid Concentration 4% NaOH
 Liquid Temperature 75°F
 Carbonate Content25%
 Pressure Drop Inches Water/ft. Packing

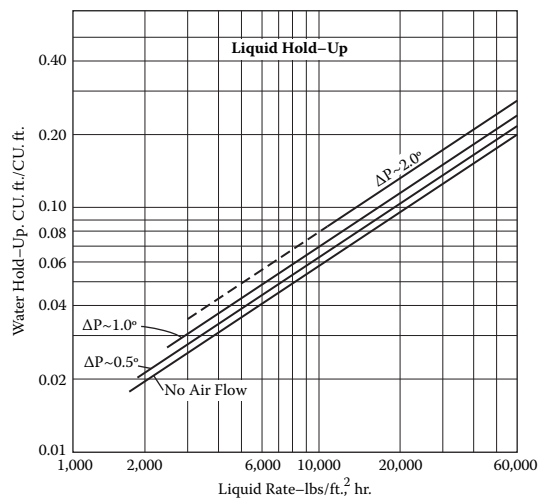
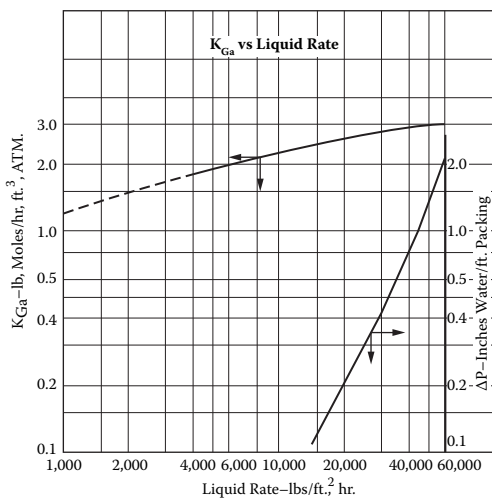
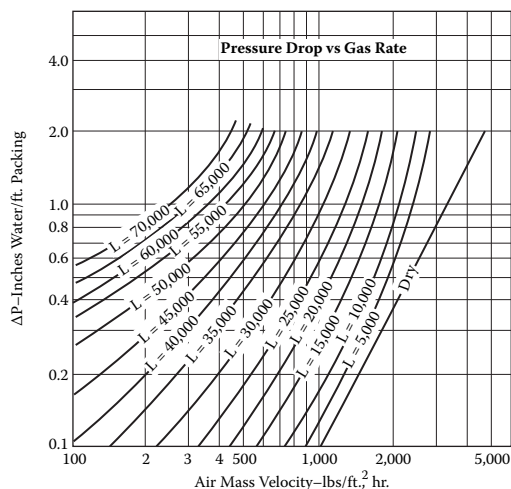


FIGURE 13.18 Representative vendor information on the characteristics of a random packing. Two-inch plastic Pall rings.

diameter can be expressed as the diameter of a sphere with the same surface area, i.e., $d_p = 6/a_p$. Values of packing surface area a_p may be obtained from Table 13.2 or equivalent listings.

For the liquid coefficient, Onda et al. departed from more usual formulations to obtain

$$k_L = 0.010 \left(\frac{g\mu_L}{\rho_L} \right)^{1/3} \left(\frac{L}{a_e \mu_L} \right)^{2/3} \left(\frac{\rho D}{\mu} \right)_L^{1/2} \quad (13.48)$$

where a_e is an effective interfacial area.

For absorption and stripping, Bravo and Fair^{29,30} found the effective area to be

$$a_e = 9.79 a_p \left(\frac{\sigma^{0.5}}{Z^{0.4}} \right) (Ca_L Re_G)^{0.1603} \quad (13.49)$$

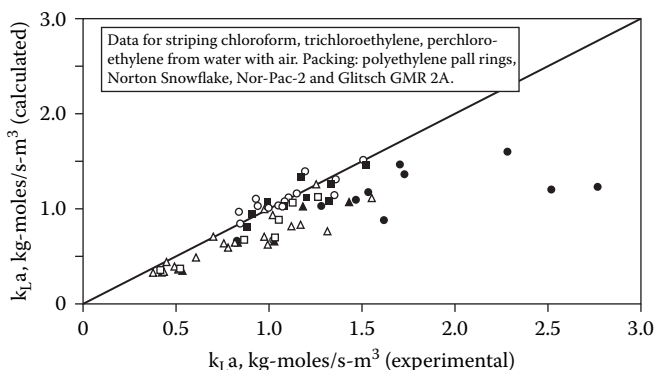


FIGURE 13.19 Parity plot for calculated vs. measured mass transfer coefficients, air-stripping of volatile organic compounds from water with air.

1. For the flow rates and properties, compute the effective area by Equation (13.49).
2. Calculate mass transfer coefficients k_G and k_L by Equations (13.47) and (13.48).
3. Compute heights of transfer units H_G and H_L by Equations (13.43) and (13.44), using volumetric mass transfer coefficients $k_g a_e$ and $k_L a_e$.
4. Compute overall H_{og} by Equation (13.38).
5. Multiply H_{og} by N_{og} to obtain required packed height, or
6. Convert H_{og} to HETP by Equation (13.45) and multiply by theoretical stages to obtain required packed height.

Problem 13.7 illustrates the procedure.

This model has been applied successfully to random packings of the ring and saddle type, in ceramic, steel, or plastic materials. A parity plot for tests of air-stripping of VOCs from water with air is shown in Figure 13.19, taken from reference 30. Several plastic packings were used. For details of the experiments, as well as use of the original Onda equations, see reference 31.

The Onda–Bravo approach has been found especially reliable for absorbers and strippers operating with lean mixtures, as is usually the case. For more concentrated cases (inlet gas > 5 vol-% solute for absorbers and inlet liquid > 5 vol-% solute for strippers), the Bolles/Fair²⁷ model is more appropriate.

13.4 OTHER DEVICES

While tray columns and packed columns are invariably the devices used for stripping, other devices are occasionally used for absorption or scrubbing. These are often proprietary, and the vendor does the design based on the specifications provided by the user and/or process designer. While the foregoing material is based on countercurrent contacting of gas and liquid, there may be some instances when cocurrent operation has advantages:

1. Throughput capacity is great, since flooding does not occur in the usual sense.
2. Pressure drop is lower than countercurrent.
3. Removal of solid particulates from the gas is favorable.

Problem 13.7

For Problem 13.4, a contaminated groundwater stream is used to illustrate the computation of theoretical stages. Now a stripping column is to be dimensioned based on the same removal of

(c) Transfer coefficients

[Equation (13.48)]

$$k_L = 0.0306 \left(\frac{9.81(1.02)(10^{-3})}{1000} \right)^{1/3} \left(\frac{31.57}{2.54(130)(1.02)(10^{-3})} \right)^{2/3} \left(\frac{1}{1150} \right)^{1/2} = 1.30(10^{-3}) \text{ m/s}$$

[Equation (13.47)]

$$k_G = \frac{0.145(130)(8.2)(10^{-6})}{(0.082)(294)} \left(\frac{2.00(10^5)}{(130)(1.75)} \right)^{0.7} (1.73)^{1/3} = 8.84(10^{-4}) \frac{\text{kg moles}}{\text{s-m}^2\text{-atm}}$$

[Equation (13.43)]

$$H_g = \frac{2.00}{(29)(8.84E-04)(215)(1.0)(1.0)} = 0.363 \text{ m}$$

[Equation (13.44)]

$$H_L = \frac{12.43}{18(1.30)(10^{-3})(215)(1000)(1.0)} = 2.47(10^{-3}) \text{ m} \quad \lambda = \frac{m}{L_m/V_m} = \frac{6753}{0.691/0.0690} = 675$$

$$H_{og} = H_g + \lambda H_L = 0.363 + 675(2.47(10^{-3})) = 0.363 + 1.667 = 2.03 \text{ m}$$

The stripping factor is 675 (same as λ). By Equation (13.22), 0.71 theoretical stages are needed.

By Equation (13.42), this translates to $N_{og} = 0.0066$, and $Z = N_{og}H_{og} = 0.013 \text{ m}$. Thus, for the relatively high gas/liquid ratio used, and for, say, 3.05 m bed height, the removal of TCE is far greater than 99%. In fact, it is greater than 99.999%. It is not unusual for a feed of, say, 20 parts per million to be purified to less than one part per billion by air stripping.

Figure 13.20 shows how a cocurrent absorber may be analyzed. Note the equilibrium limitation, which limits the degree of recovery of solute. Basic models for estimating hydraulics and mass transfer are based on countercurrent flow, which is normally more efficient, and must be adjusted if the gas flow direction is reversed.

Other contacting devices are shown in Figure 13.21 and discussed below.

13.4.1 SPRAY CHAMBER

This is the ultimate low-pressure drop device, since the energy for dispersion and contacting is pumped into the entering liquid. Spray contactors suffer from departure from countercurrent flow, due to the high degree of backmixing or circulation in the gas. Drop coalescence and migration of drops to the vessel wall compromise the effective area for mass transfer. The mass transfer rate is highest in the close vicinity of the spray nozzles. As shown in the figure, it is economical to use more than one level of spray nozzles, and for large diameter units, each level comprises a bank of nozzles. Heights of transfer units for commercial-scale spray chambers have been reported by Pigford and Pyle.³² More than two or three transfer units usually cannot be achieved in a spray contactor, but those units are achieved at very low pressure drop.

Spray chambers are frequently used for scrubbing sulfur dioxide and solid particulates from stack gases. The nozzles can be designed to handle slurries, e.g., lime slurry fed to the stack gas scrubber.

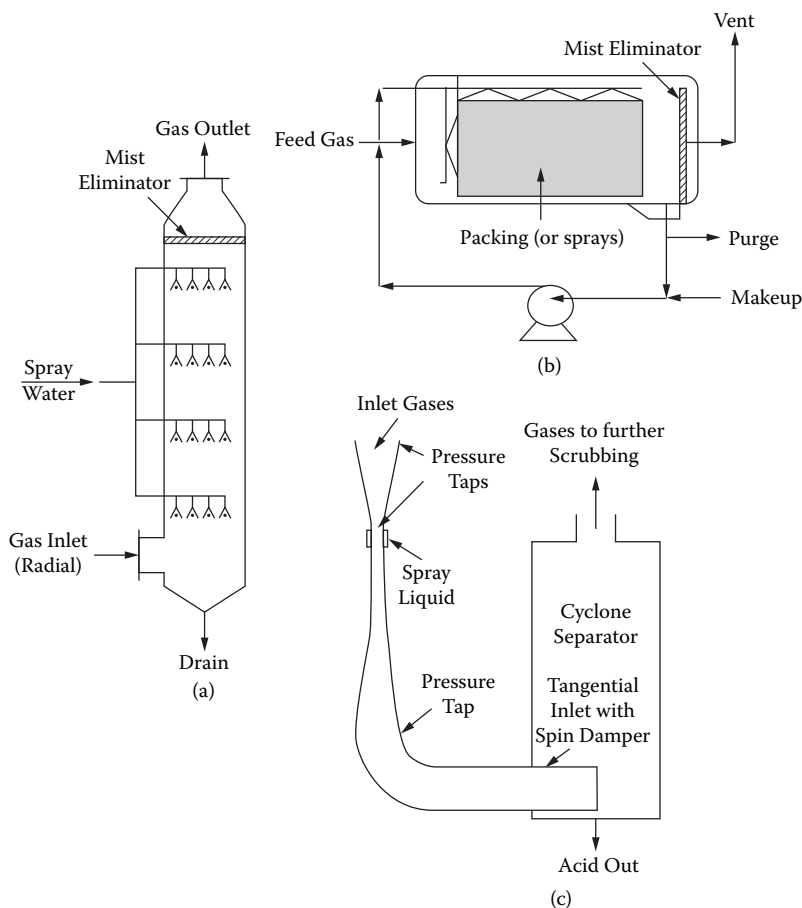


FIGURE 13.21 Representative vendor information on the characteristics of a random packing. Two-inch plastic Pall rings. [Courtesy of NorPro-St.Gobain Co., Akron, Ohio.]

Representative results from these studies are shown in Figure 13.23. The efficiencies tend to be low, and the liquid phase resistance dominates. Fair and Harvey³⁵ found that a slight modification of the Chan–Fair model³⁶ could be used for steam stripping (Figure 13.24).

While packed steam strippers are not widely used, there is no reason why they should not be. Performance data for such strippers are limited, however. Because of the temperature levels, metal pickings would normally be specified. Kolev et al.³⁷ studied chloroform stripping in a 0.40-m column using metal structured packing. Ortiz–Del Castillo et al.³⁸ studied toluene stripping in a 0.25-m column using metal structured and random packings. The latter group developed models for mass transfer based on air stripping experiences. The use of packing for commercial-scale steam stripping apparently has not been investigated.

The economics of vacuum steam stripping of volatile organic compounds have been reported by Rasquin et al.³⁹ The U.S. Environmental Protection Agency has favored steam stripping over air stripping, because the closed system prevents the stripped components from moving into the atmosphere.

Problem 13.8

A refinery aqueous stream flows at 600 gal/min and contains 15 lb/hr benzene. The benzene is to be removed at a stripping efficiency of 99.95%. A tray column is to be used. Consider two operating pressures, 2.0 psia and 14.7 psia. With no attempt at optimization, evaluate the parameters that should be considered for design. In keeping with refinery practice, use conventional English units.

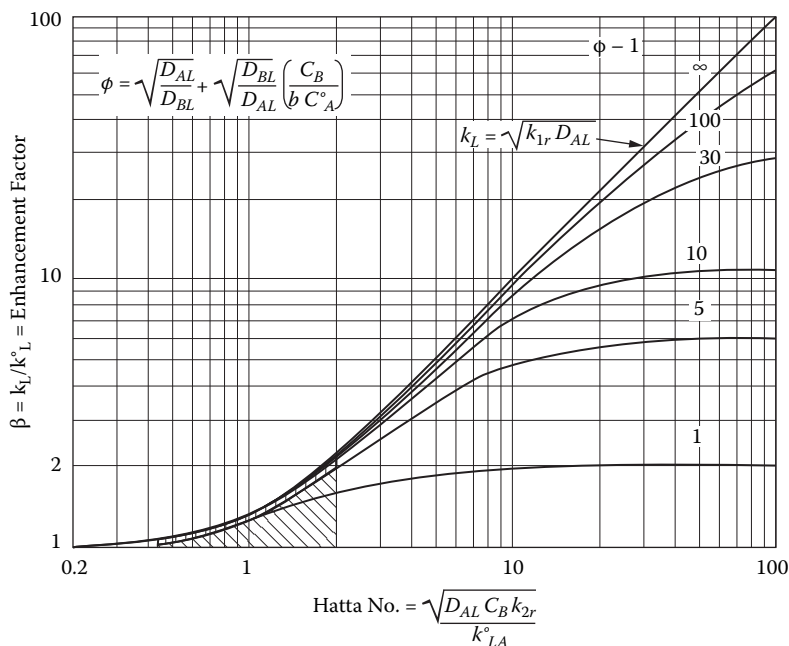


FIGURE 13.24 Enhancement factor as a function of Hatta number. Chemical absorption, irreversible reactions.

Properties:	2.0 psia	14.7 psia
Temperature, °F	126	212
Liquid density, lb/ft ³	61.6	59.8
Vapor density, lb/ft ³	0.0058	0.0373
Liquid viscosity, cp	0.56	0.27
K value	300	4300
Column feed flow rate, lb/hr	295,800	287,400
Column feed flow rate, lb-moles/hr	16,430	15,970
Entering benzene conc., ppmw	50.8	52.2
Entering benzene conc., ppmm	11.7	12.0

For the first try, use 2.0 psia and assume $S = K/(L/V) = 100$. Required stages [Equation (13.22)]:

$$N = \frac{\ln\left(\frac{E_s - S}{E_s - 1}\right)}{\ln S} - 1 = \frac{\ln\left(\frac{0.9995 - 100}{0.9995 - 1}\right)}{\ln 100} - 1 = 1.65 \quad \text{theo. stages}$$

The stage efficiency is obtained from Figure 13.16; the X-scale parameter is

$$K\mu_L/\rho_{LM} = \frac{(900)(0.56)}{(61.6/18)} = 147 \quad \text{from which, } E_{oc} = 0.060 = 6.0\%$$

$$\text{Actual plates required in column} = 1.65/0.060 = 28$$

$$\frac{p_i}{N_i} = \frac{1}{k_{gi} a_e} + \frac{H_i}{k_{Li} a_e} + \frac{H_i}{k_r a_e} \quad (13.53)$$

In other words, the total resistance to mass transfer is the sum of resistances of gas, liquid, and reaction:

$$R_t = R_g + R_L + R_r \quad (13.54)$$

where H_i is the Henry's law constant $= p_i^*/C_i$, and k_r is the specific velocity constant for the reaction. When the reaction is very rapid and complete, k_r is very high, and R_r drops out. If there is negligible gas resistance, R_g drops out, and

$$\frac{p_i}{N_i} = \frac{H_i}{k_L a_e}$$

or the equivalent of Equation (13.52), with $C_i \sim 0$. Usually, a bimolecular reaction is of interest, involving species A from the gas and B from the liquid,



We can define a dimensionless Hatta number,

$$Ha = \frac{\sqrt{D_{AL} C_B k_{2r}}}{k_{LA}^o} = \frac{\text{effective rate}}{\text{rate for diffusional transport only}} \quad (13.55)$$

where

D_{AL} = liquid diffusivity for A, m^2/s

C_B = bulk liquid concentration of B, $\text{kg-moles}/\text{m}^3$

k_{2r} = reaction velocity constant (second-order), $\text{m}^3/(\text{s-kg mole})$

k_{LA}^o = physical liquid phase mass transfer coefficient, $\text{kg mole}/(\text{s-m}^2\text{-kg mole}/\text{m}^3) = \text{m}/\text{s}$

When the Hatta number (Ha) is evaluated, the value of the enhancement factor may be determined from Figure 13.24, based on reference 43.

The parameters in Figure 13.24 are $\phi - 1$, where

$$\phi = \sqrt{\frac{D_{AL}}{D_{BL}}} + \sqrt{\frac{D_{BL}}{D_{AL}}} \left(\frac{C_B}{b C_A^*} \right) \quad (13.56)$$

The top curve in Figure 13.24 applies to first-order and pseudo-first-order irreversible reactions, and for $Ha > 3$,

$$k_L = \sqrt{k_{1r} D_{AL}} \quad (13.57)$$

The above treatment has dealt only with irreversible bimolecular reactions and, as a special case, first-order irreversible reactions. Although these cases predominate, others are certainly possible. The references cited are sources for additional situations.

From Figure 13.24, for Hatta No. = 32.0 and $\phi = 1171$, enhancement factor $\beta = 32$.

This converts to $K_{og}a_e = 2.18$ lb moles/(hr-ft³-atm), very close to the value of 2.20 measured by Eckert et al.⁴⁴ The absorption with reaction is about 32 times faster than for physical absorption alone.

13.7 SUMMARY

Absorption and stripping are counterpart processes, and the same general equations apply to both. Most applications of the processes deal with dilute mixtures, namely, absorbing small amounts of material from a large volume of gas or stripping small amounts of material from a large volume of liquid. When the dilute conditions prevail, the methodology for determining theoretical stages or transfer units is relatively simple. For concentrated mixtures, rigorous solutions normally are obtained from special computer programs. Approximate approaches to handling concentrated mixtures are given in this section.

Absorptions and strippings may be performed in conventional plate-type columns or counter-current packed columns. In a few cases, specialized equipment is used. The traditional approaches to plate and packed column design, used in distillation, apply also to absorption and stripping. Thus, readers of this chapter should also refer to Chapter 12 particularly for dimensioning the contacting equipment.

A significant number of commercial absorption processes involve a chemical reaction in the liquid phase. The effect of the reaction is to speed up the rate of mass transfer and, to some extent, make the determination of transfer units or stages simpler.

As for all separation processes, basic thermodynamic and physical property data must be available. For absorption and stripping, key data relate to solubility, and fortunately there are large databases available to support predictive methods.

13.8 NOMENCLATURE

a_e	= effective interfacial area, m ² /m ³
a_p	= specific surface area of packing, m ² /m ³
A	= area, m ²
A	= absorption factor, dimensionless [Equation (13.8)]
A_T	= total cross sectional area of column, m ²
A_N	= net area cross section, m ²
A'	= average absorption factor, dimensionless [Equation (13.16)]
C	= concentration, kg moles/m ³
C_v	= orifice coefficient, dimensionless
C_{sbf}	= capacity parameter, m/s [Equation (13.30)]
Ca	= dimensionless capillary number [Equation (13.49)]
CP	= capacity parameter [Equation (13.46)]
D	= diffusion coefficient (diffusivity), m ² /s
E_a	= absorption efficiency, fractional
E_{oc}	= overall column efficiency, fractional
E_s	= stripping efficiency, fractional
F_p	= pacing factor, 1/m (Table 13.1)
F_S	= gas F-factor = $U_s \rho_G^{0.5}$, m/s(kg/m ³) ^{0.5}
g	= gravitational constant, m/s ²
G	= gas flow, kg/s-m ²
G_m	= gas flow, kg moles/s-m ²
h	= pressure head, mm liquid
h_d	= head loss for flow through holes, mm liquid

β	= enhancement factor for chemical absorption [Equation (13.52)]
γ	= activity coefficient
λ	= ratio of slopes, equilibrium line/operating line
μ	= absolute viscosity, mPa-s (cp)
ν	= kinematic viscosity, cs
ρ	= density, kg/m ³
ρ_{LM}	= liquid molar density, kg moles/m ³
σ	= surface tension, mN/m (dynes/cm)
ϕ	= parameter for Figure 13.24

13.8.2 SUBSCRIPTS

1	= top plate in column for absorbers, bottom plate in column for strippers
A,B	= components A or B
g	= gas phase
i	= component i
L	= liquid phase
N	= bottom plate in column for absorbers, top plate in column for strippers

REFERENCES

1. Hwang, Y.-L.; Olson, J. D.; Keller, G. E. 1992. *Ind. Eng. Chem. Res.* 31: 1759.
2. Fredenslund, A.; Gmehling, J.; Rasmussen, P. 1977. *Vapor-Liquid Equilibria Using UNIFAC*, Amsterdam: Elsevier.
3. Yaws, C. L.; Pan, X.; Lin, X. 1993. *Chem. Eng.* 100 (2): 108.
4. Prausnitz, J. M.; Shair, F. H. 1961. *AIChE J.* 7: 682.
5. Yen, L. C.; McKetta, J. J. 1962. *AIChE J.* 8: 501.
6. Yaws, C. L.; Hopper, J. R.; Wang, X.; Rathinsamy, A. K. 1999, *Chem. Eng.* 106 (6): 102.
7. *Solubility Data Series* (continuing series). Elmsford, NY: Pergamon Press.
8. Seidell, A. 1952. *Solubilities of Inorganic and Organic Compounds*. New York: Van Nostrand.
9. Seidell, A. 1958. *Solubilities of Inorganic and Metal-Organic Compounds*. New York: Van Nostrand.
10. Linke, W. F.; Seidell, A., *Solubilities of Inorganic and Metal-Organic Compounds*, vol. 2. Washington, DC: American Chemical Soc., 1965.
11. Dack, M. J. R., ed. 1975. *Solutions and Solubilities*. New York: John Wiley & Sons.
12. Markham, A. E.; Kobe, K. A. 1941. *Chem. Rev.* 28: 519.
13. Long, F. A.; McDevit, W. F. 1952. *Chem. Rev.* 51: 119.
14. Battino, R.; Clever, H. L. 1966. *Chem. Rev.* 66: 395.
15. Wilhelm, E.; Battino, R. 1973. *Chem. Rev.*, 73: 1.
16. Wilhelm, E.; Battino, R.; Wilcock, R. J. 1977. *Chem. Rev.* 77: 219.
17. Othmer, D. F.; Kollman, R. C.; White, R. E. 1944. *Ind. Eng. Chem.* 36: 963.
18. Kremser, A. 1930. *Natl. Petroleum News*. 22 (21): 42; Souders, M.; Brown, G. G. 1932. *Ind. Eng. Chem.* 24: 519.
19. Edmister, W. C. 1943. *Ind. Eng. Chem.* 35: 837.
20. Fair, J. R., in *Perry's Chemical Engineers' Handbook*, 7th edition, R. H. Perry and D. W. Green, eds. New York: McGraw-Hill, 1997, 14–14, 14–15.
21. *Ibid.*, 14–27.
22. O'Connell, H. E. 1946. *Trans. AIChE* 42: 741.
- 22a. Hines, A. L.; Maddox, R. N. 1985. *Mass Transfer—Fundamentals and Applications*. Englewood Cliffs, NJ: Prentice Hall.
23. Strigle, R. F. 1994. *Packed Tower Design and Applications*. Houston: Gulf Publ. Co.
24. Stichlmair, J.; Bravo, J. L.; Fair, J. R. 1989. *Gas Sepn. Purif.* 3: 19.
25. Engel, V.; Stichlmair, J.; Geipel, W. A. "A New Correlation for Pressure Drop, Flooding and Holdup in Packed Columns." Presented at AIChE Meeting, Miami, FL, October 1998.

14.6.2 Displacement-Purge Cycle	1162
14.6.3 TSA Cycle	1162
Example 14.5 TSA Solvent Recovery	1162
14.6.4 PSA Cycle	1163
Bibliography	1170

14.1 INTRODUCTION

Adsorption is the phenomenon that selectively segregates atoms or molecules between a fluid and a solid. In some ways, it is like *absorption*, except the liquid-phase *absorbent* is replaced with a solid-phase *adsorbent*. Sometimes solids could be said to *absorb* or *adsorb* fluids, i.e., the distinction is blurred.* In this chapter, the focus is on selective uptake (and release) by porous solids, especially for process applications. Another subtle distinction occurs when vapor is adsorbed from a gas; it is like condensation, except that the driving force is subtle molecular forces rather than a temperature gradient.

When applied as a unit operation, adsorption can be used to split mixtures containing significant percentages of adsorbable components or purify streams containing trace amounts of contaminants. These separations, whether for gases or liquids, are accomplished by allowing the fluid and solid phases to interact under controlled conditions. Molecules that are selectively taken up are called *adsorbates*, and the solid surface that attracts the adsorbate is called the *adsorbent*. Jargon used in connection with adsorbents and adsorption, as well as some prominent definitions, are listed in Table 14.1. Fundamental causes and effects of adsorption are discussed in Section 14.3.

This chapter presents different facets of adsorption. Unfortunately, there is not sufficient space to provide case studies for any of the hundreds of unique applications of adsorption. On the other hand, most of the topics discussed here are the subject of dozens of technical papers each year, many of which appear in specialized journals, including (alphabetically) Adsorption, Carbon, Langmuir, Microporous and Mesoporous Materials (formerly Zeolites), Reactive Polymers, and other more general titles. Some subjects are also treated in much greater detail in books, many of which are listed in the bibliography that follows.

It is an understatement to say that adsorption is a diverse field. It impacts separation processes, materials science, catalysis, soil science, pharmaceutical products, environmental applications, and other widely different fields. A brief overview of those subjects, mainly oriented toward applications, is presented here.

Adsorption can perform many separations that are impossible or impractical by conventional techniques, such as distillation, absorption (gas–liquid), and even membrane-based systems. Adsorption has found recent applications in solving environmental problems and meeting stringent quality requirements. Important applications of adsorption fall in the category of purification, as cited by Yang (1987), but they represent only a small fraction of the uses of adsorption. The largest single application of adsorption is for water treatment. It employs nearly 100 million pounds of activated carbon annually in the U.S. alone, to remove compounds that could be toxic or merely pose problems of taste or odor. It was first used for municipal water treatment in powdered form in the late 1930s, and as granules in the 1960s. In addition, activated carbon has been used to decolorize sugar since the 1920s. Another widespread purification application is the pressure-swing air dryer found on heavy trucks and buses for their air-brake systems. Those would probably go unnoticed were it not for the abrupt, audible “blowdown” of these adsorbers, which sounds like a tire blowing out or a hydraulic system failure. A third, very widespread application is in the seal between thermopane windows. They employ 3A zeolite (as a powder mixed with caulk or as

* When a solid behaves like a sponge (i.e., by capturing a fluid via surface tension or by nonselective penetration), it could be called *absorbent* (e.g., granules used to pick up oil that has spilled on a floor). When a solid exhibits selective uptake, it should be called an *adsorbent* (e.g., granules contained in a column through which oil-laden water passed, selectively removing the oil).

TABLE 14.1 (Continued)
Definitions of Terms Used Commonly in Adsorption

Hysteresis	Divergence of uptake and release isotherm data due to the difference in mechanisms of pore filling vs. emptying, or other irreversible phenomena of uptake and release.
Iodine number	Amount of iodine adsorbed from an iodine/potassium iodide solution (0.02 N) per mass of activated carbon (mg/g). A measure of capacity of activated carbon for small molecules.
Ion exchange	Sorption using "fixed" acidic or basic functional groups, such as $-\text{SO}_3^-$, $-\text{NH}^+$, etc. Rates of uptake or release may be affected by reaction and/or diffusion.
Isobar	Plot of equilibrium data as amount adsorbed vs. temperature, holding partial pressure constant.
Isotherm	Set of equilibrium data: amount adsorbed (n_i^*) vs. concentration (c_i) or partial pressure (p_i), at constant temperature. See Figure 14.4 for classifications.
Constraints: (1) $\lim_{c_i \rightarrow 0} \frac{dn_i^*}{dc_i} < \infty$ (2) $\frac{dn_i^*}{dc_i} \geq 0$ Typical units: $n_i^* [=]$ $\frac{\text{moles } (i)}{\text{mass (adsorbent)}}$ or $\frac{\text{mass } (i)}{\text{mass (adsorbent)}}$ or $\frac{\text{std. vol. } (i)}{\text{vol. (adsorbent)}}$	
Macropores	$d_p > 500\text{\AA}$. (pigments, bacteria)
Mesopores	$d_p \in (20, 500)\text{\AA}$ (colloidal silica, viruses)
Micropores	$d_p < 20\text{\AA}$ (common molecules)
Mass transfer zone	Region of the axial composition profile in which the composition varies from that of the feed (toward the feed end) to that of the initially present fluid (toward the product end). Despite its name, the shape of this zone can depend on mass transfer resistances, dispersion, or equilibrium effects. For uptake with a favorable isotherm, the width remains essentially constant beyond a certain axial position, leading to the term <i>constant pattern front</i> . In that case, the effects are exclusively due to intraparticle- and/or film-diffusion resistances.
Methylene blue factor	Volume (cm^3) of 0.15% methylene blue solution decolorized by 100 g of adsorbent in 5 min.
Molasses number	Quantitative measure of decolorizing capacity based on the change in color of molasses; relates to adsorption of large molecules from a liquid.
Physisorption	Based on weak physical attraction: sensitive to temperature, nonspecific, rapid (no activation barrier), possibly multilayer $\Delta H_{\text{ADS}} < 3\Delta H_{\text{VAP}}$.
Proportional pattern	An axial composition profile (or breakthrough curve) having a shape that "relaxes" gradually as the front moves along the axis. This is characteristic of desorption for a system that has a favorable isotherm. Axial dispersion exhibits a similar effect but may affect uptake and release.
Sorption	Adsorption or desorption.
Structure	Described by densities, void fractions, porosity, pore-size distribution.
Unfavorable isotherm	Concave upward (also Type II; see Figure 14.4 and Section 14.3.2).
Working capacity	The effective change of loading of an adsorbent between the regenerated and exhausted states. May reflect either operating data or a theoretical limit based on isotherm data.

particles within an aluminum frame) to adsorb moisture in the air space, preventing it from fogging the internal glass surface.

Two types of *cyclic* adsorption technologies [pressure swing adsorption (PSA) and temperature swing adsorption (TSA)], developed since the mid-1960s, are widely used for industrial separations. Examples of PSA include air dryers (as mentioned previously), hydrogen from refinery off-gases (commercialized in the 1960s), oxygen from air (early 1970s), and nitrogen from air (late 1970s). Many TSA systems remove or recover VOCs from solvent-laden air, e.g., at polymer processing, painting, and pharmaceutical production sites. Those use steam, hot gases, or even electrical resistance heating for regeneration. In addition, simulated moving-bed (SMB) systems split xylene isomers, sugars, and pharmaceutical products.

Moving-bed systems are *continuous* and include vapor-phase recovery systems that employ staged fluidized beds in which the adsorbent circulates through a thermal regenerator. Generally, it is possible for the fluid phase and adsorbent to be contacted in a countercurrent flow pattern. An early version,

kieselguhr (or diatomaceous earth), and even sodium bicarbonate and limestone (for flue gas treatment). Some are used in an anhydrous state, whereas others are hydrated. Other inorganic adsorbents have been developed recently (e.g., pillared clays, aluminophosphates, and mesoporous adsorbents) that have not yet been commercialized. Those covered below are commercial products and are frequently encountered.

14.2.1 ADSORBENT SELECTION CRITERIA

Adsorbent selection criteria for any application generally include the following main attributes: capacity, selectivity, regenerability, kinetics, durability, and cost. These attributes represent combinations of properties that are strongly affected by the pertinent conditions. For example, the first four govern how much adsorbent is necessary for a particular application, and the last two affect the annual cost. Furthermore, the first three are tied to the equilibrium characteristics, about which much can be said (see Section 14.3). Likewise, kinetics is covered in more detail in Section 14.4. Both will be discussed briefly here, however. Finally, adsorbent cost obviously depends on both its price and lifetime, which can depend on its resistance to attrition, degradation, fouling, and so on.

Rarely will a single adsorbent be optimal in all of these respects. Frequently it will be possible to narrow the choice to one or two classes of adsorbents, leaving a vast array of possible particle sizes, shapes, pretreatment conditions, and so forth. Final decisions should always be based on data. To make budget estimates, however, a number of different approaches can be derived from rules of thumb to provide quick experimental feasibility tests. Potential sources of such information are adsorbent or equipment vendors, published or commercial databases, and in-house or external laboratories.

14.2.2 ADSORBENT CHARACTERISTICS

14.2.2.1 Capacity, Selectivity, and Regenerability

Adsorption capacity (or loading) is probably the most important characteristic of an adsorbent. More detail is provided in Section 14.3.2. The loading is the amount of adsorbate taken up by the adsorbent, per unit mass (or volume) of the adsorbent, and it depends on the fluid-phase concentration, the temperature, and other conditions (especially the initial condition of the adsorbent). Typically, adsorption capacity data are plotted as isotherms (loading of adsorbate on the adsorbent versus fluid-phase adsorbate concentration at constant temperature), isosteres, isobars, and others mentioned later. Examples are shown in Figures 14.1 through 14.3. Adsorption capacity is of paramount importance to the capital cost, because it sets the amount of adsorbent required and also the volume of the adsorber vessels; the costs of both are significant if not dominant. When comparing alternate adsorbents, it is fair to express their capacity on a per unit volume basis, since that fixes

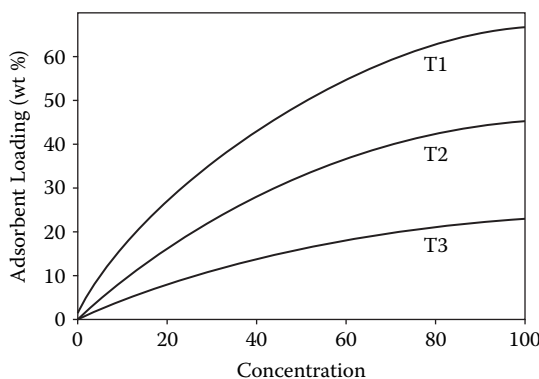


FIGURE 14.1 Typical Type I isotherms at increasing temperatures, $T_1 < T_2 < T_3$.

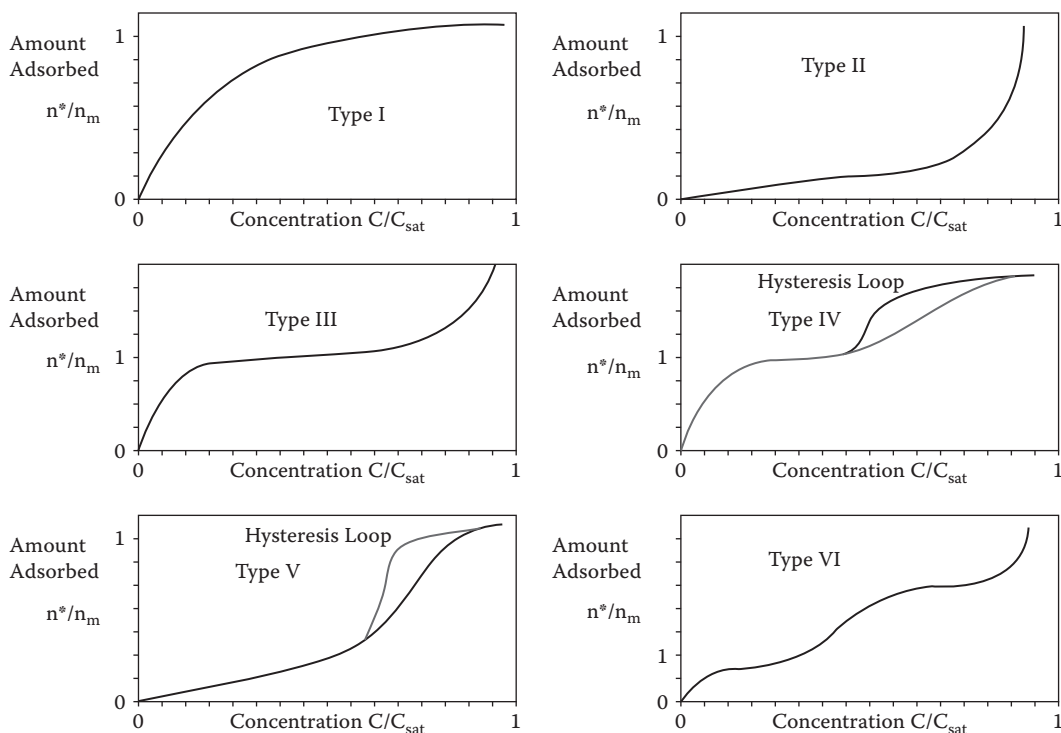


FIGURE 14.4 Isotherm classifications [Brunauer, Deming, Deming, and Teller (1940)].

(adsorptive or adsorbate) must be relatively weakly adsorbed (or physisorbed). The heat of adsorption provides a measure of the energy required for regeneration, and hence low values are desirable. Regeneration may be accomplished by a thermal swing, pressure swing, or chemical reaction (e.g., by displacement, elution, or supercritical extraction), or sometimes by a combination of those. Displacement would involve introducing a species that adsorbs more strongly than the adsorbate of interest, while elution would entail dissolving the adsorbed material by a solvent that is adsorbed weakly, if at all. Chemical methods require a separate separation operation that may be costly, plus the regenerated bed must be purged of the regenerant. In some cases, regeneration takes place by contacting the adsorbent with another fluid not used during loading. This requires draining or displacement, which might be time consuming and should be avoided whenever possible. The regenerability of an adsorbent affects the fraction of the original capacity that is retained for cyclic usage (sometimes called the *working capacity*) and the time, energy, and other requirements for regeneration.

14.2.2.2 Kinetics

Mass transfer kinetics is a catch-all term related to intraparticle mass transfer resistance. It is important because it controls the cycle time of a fixed-bed adsorption process. Fast kinetics provides a sharp breakthrough curve, while slow kinetics yields a distended breakthrough curve. The effect of a distended breakthrough curve can be overcome by increasing the amount of adsorbent and hence pressure drop in the bed. On the other hand, kinetics has been exploited as the basis of adsorptive separations. The most common example is the PSA process that splits nitrogen from air using a carbon molecular sieve, which relies on the relatively fast diffusion of oxygen compared with the much slower diffusion of nitrogen. In conventional adsorption processes, however, slow diffusion of any adsorbate is a disadvantage. To compensate for slow diffusion, it is also possible to use small particles, but there is a corresponding sacrifice resulting from the increased pressure

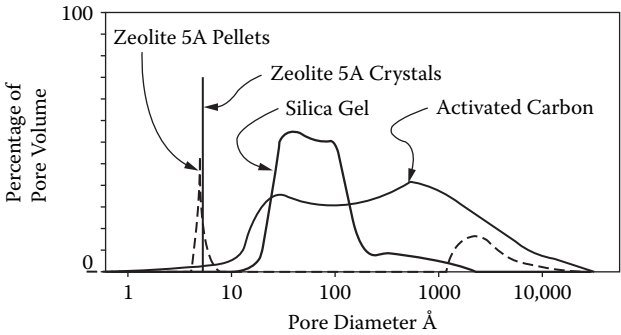


FIGURE 14.5 Differential pore size distribution for common adsorbents.

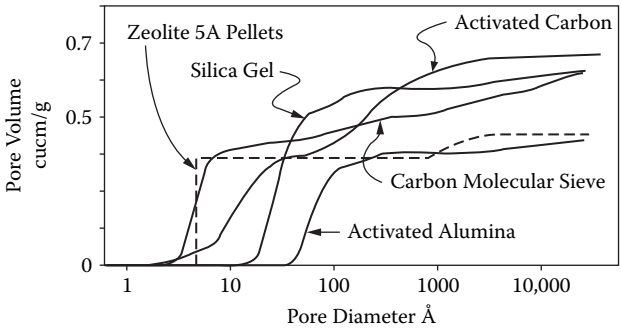


FIGURE 14.6 Cumulative pore size distribution for common adsorbents.

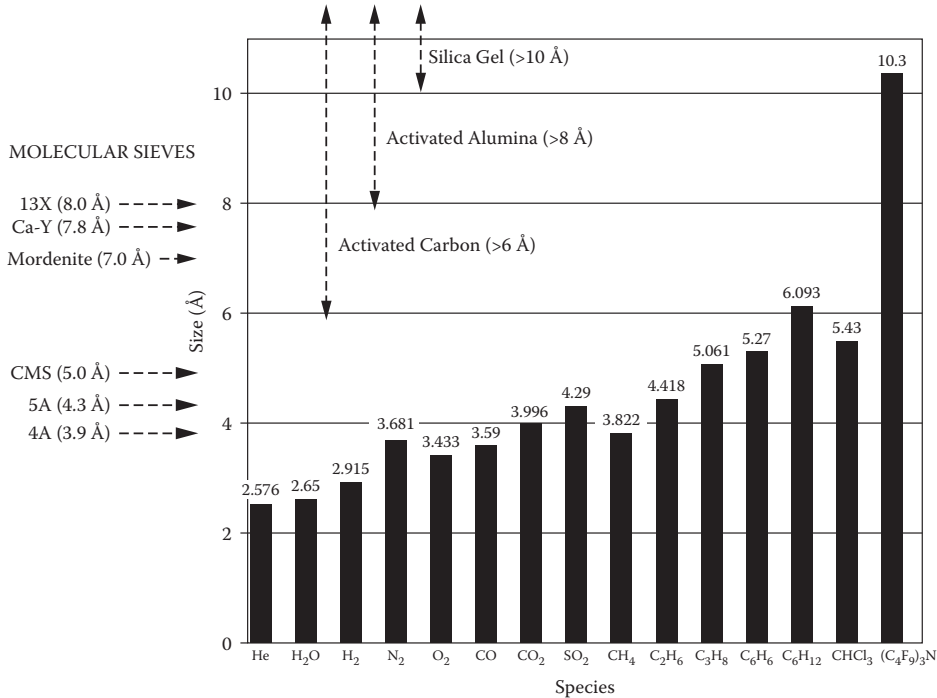


FIGURE 14.7 Molecular diameters and pore dimensions for common adsorbents.

14.2.3.1 Aluminas

Activated alumina is produced from hydrated alumina, $\text{Al}_2\text{O}_3 \cdot n \text{H}_2\text{O}$, where $n = 1$ or 3 , by dehydrating (calcining) under controlled conditions to get $n \approx 0.5$. This form, being hydroxylated, augments adsorption by hydrogen bonding. It is a white or tan opaque material that has a chalky appearance. Several grades are available from various manufacturers. The distinctions among products mostly are related to the specific crystal structures that alumina can exhibit. For example, stable crystalline forms are usually not thought of as adsorbents because of their low surface areas. Conversely, transitional forms, such as gamma and eta alumina, have defect spinel structures that lead to both higher concentrations of surface acid sites and effective surface areas from 200 to 400 m^2/g . Common forms are beads or balls 1 to 8 mm dia., granules, extrudates (pellets) 2 to 4 mm dia., and powder. Activated aluminas are widely used as catalysts (or catalyst supports) and as desiccants. Ancillary uses as an adsorbent are for removal of oxygenates and mercaptans from hydrocarbon feed streams, fluoride ions from water, HCl from hydrogen in catalytic reforming, and others. For most gas-phase applications, pretreatment requires heating to about 250°C .

14.2.3.2 Silicas

Silicas are also highly hydroxylated SiO_2 , so adsorption results, to a considerable extent, from hydrogen bonding. Most silica gels are transparent or translucent. Some silica gels are alloyed with a few percent alumina, which yields an opaque white or tan appearance. Several forms are available that encompass diverse types of silica gels, porous borosilicate glass, and aerogels. The last is a relatively new, exceedingly porous material currently with few commercial applications. Its unique characteristics make it an interesting prospect for the future. Silica gel and porous glass are both nondusting and resistant to attrition.

There are more than a dozen varieties of SiO_2 ; most adsorbent forms are rigid (but not crystalline) assemblages of spherical microparticles made of colloidal silica. Aerogels are a form of open-celled porous glass. Effective surface areas range from 300 to 900 m^2/g , depending on the density, with more dense materials having finer pores and larger surface areas. Common forms are beads 1 to 3 mm dia., granules, extrudates (pellets) 2 to 4 mm dia., and powder. The largest uses of silica gel and porous glass are as a desiccant. Other uses as an adsorbent are for separation of hydrocarbons, dewpoint reduction for natural gas, and drying of liquid hydrocarbons. Pretreatment for gas-phase applications (especially as a desiccant) requires heating to about 200°C .

14.2.3.3 Zeolites

In the mid-1700s, a Swedish mineralogist named Cronstedt discovered a mineral that appeared to boil when heated. He named it *zeolite*, from the Greek *zeo* (to boil) and *lithos* (stone). The observed boiling effect is caused by the expulsion of adsorbed water from inside the zeolite. The term zeolite now refers to a class of aluminosilicates that are stoichiometric blends of silica and alumina. They are generally opaque and white or tan in appearance. There are about 40 natural and 150 synthetic types having the general formula $M_{x/n}[(\text{AlO}_2)_x(\text{SiO}_2)_y] \cdot w \text{H}_2\text{O}$, where M represents a cation of valence n , w is the number of water molecules per "cage," and x/y is the Al-to-Si ratio. The sum $x + y$ is the number of tetrahedra per unit cell. Those that contain roughly equal amounts of silica and alumina are hydrophilic, whereas those that contain predominately silica (e.g., with Al-to-Si ratios > 10) are hydrophobic. Frequently, there is water of hydration within the crystals, and to balance the charges, cations are associated with the alumina. The presence of water is largely associated with field-dipole interactions, which can be large for zeolites.

Internally, zeolites are inherently crystalline and exhibit micropores within those crystals that have uniform dimensions, as depicted in the pore size distribution shown in Figures 14.5 and 14.6. The micropores are so small and uniform that they commonly can distinguish among nearly identically sized molecules. As a result they are frequently called "molecular sieves." That term,

tend to have rounded apertures, the carbon-based counterparts are more slit-like, as in the space between layers of graphite. To date, only one type of commercial separation employs this material: separation of nitrogen (at 97% to 99.99%) from air by PSA, which exploits the size difference between oxygen (3.43 Å) and nitrogen (3.68 Å).

14.2.3.5 Polymers

Polymeric adsorbents, including ion exchange resins, tend to be opaque spherical beads; most are white or tan, but some are brown, orange, or black. Some are inert, polystyrene-divinyl benzene, polymethacrylate, divinylbenzene/ethylvinylbenzene, or vinylpyridine beads, while others, which contain acidic or basic functional groups, are ion exchange resins. Internally, many of these polymer beads contain “microbeads” that are joined together at a few points each, creating a macropore structure. In addition, some polymeric adsorbents are activated via pyrolysis, in much the same way as carbon, yielding black materials.

Some polymeric adsorbents are sufficiently hydrophilic to be used as a desiccant, while others are quite hydrophobic. The effective surface area is usually smaller than for activated carbon, e.g., 5 to 800 m²/g. The corresponding pore diameters range from about 20 to 2000 Å, or from 3 to 2000 Å if activated. The available forms are generally limited to beads of 0.3 to 1 mm dia., usually in a relatively narrow range. Larger particles are not yet commercially available. A minor drawback of these materials is that they tend to shrink and swell with cyclic use. For gas-phase applications, they may require conditioning prior to use (e.g., washing with water and/or another solvent followed by drying).

The range of applications is somewhat restricted, since the cost of most polymeric adsorbents is typically about ten times more than that of other common adsorbents. In some instances, polymeric materials are the only choice. In other cases, they compensate for the cost differential by yielding much better performance, especially for high value-added uses. Current applications include recovery and purification of antibiotics and vitamins, decolorization, decaffeination, hemoperfusion, separation of halogenated light organics from water, and treatment of certain industrial wastes such as aqueous phenolics and VOC recovery from off-gases.

14.2.3.6 Biomass

Some adsorbents are organic materials that function as solid “absorbents” rather than adsorbents. Among these are cellulose (the most abundant biopolymer in nature), chitin (the second most abundant biopolymer in nature), collagen, wool, starch-polyacrylamide gels (which absorb many times their own weight of water at ambient temperature but release most of it by gentle heating), polysaccharides derived from corn, and miscellaneous forms of biomass (e.g., residue from crop harvests). The latter materials fall in the fuzzy gap between adsorbents and absorbents. Nevertheless, some of these may have niches, but none is a general-purpose adsorbent.

14.3 ADSORPTION THERMODYNAMICS

Adsorption relies mainly on the physisorption of molecules (and noble gases) and is analogous to condensation. Knaebel et al. (1999) indicated that two types of forces contribute to physisorption: *van der Waals* (or dispersion) forces and *electrostatic* forces. Van der Waals forces relate to polarizability, i.e., the ease with which an atom's or molecule's electron density can be distorted. That effect increases as atoms within a group in the periodic table become larger. The outcome is a favorable interaction energy that is significant for highly polarizable species. Similarly, electrostatic forces, which are relevant only if the surface is polar, are caused by polarization forces, field-dipole interactions, and field gradient-quadrupole interactions. In that vein, polarization forces are causative, while polarizability represents a latent tendency.

For sorbate, field-dipole interactions occur that exhibit a permanent dipole moment (e.g., H₂O), which interacts with the surface electric field to give an attractive energy. An example is hydrogen

Most fundamental equations have direct analogies to vapor–liquid equilibrium and simple gas laws. For example, an adsorbed component is frequently viewed as a two-dimensional fluid that exhibits a spreading pressure on the adsorbent, in contrast to its partial pressure in the gas phase. There is a corresponding empirical relationship between the spreading pressure, area covered per mole adsorbed, and temperature, analogous to the ideal gas law, but it is called the “ideal surface gas” equation. When applied to adsorption of mixtures, it is called the “ideal adsorbed solution” theory, developed by Myers and Prausnitz (1965). Equilibrium calculations mainly involve the interactions of one molecule (or atom) of adsorbate with the adsorbent surface; i.e., they neglect adsorbate–adsorbate interactions. This viewpoint is valid only in the most idealized conditions. Normally, the surface is irregular or heterogeneous (both energetically and geometrically), which can be taken into account by many theories, and the adsorbed molecules (or atoms) interact with each other via mutual repulsion (or sometimes attraction).

As mentioned above, equilibrium data can be presented and used in a variety of forms: isotherms (loading vs. concentration at constant temperature), isosteres [partial pressure (or dew-point, or some other form of concentration) vs. inverse absolute temperature at specific degrees of loading], and isobars [loading as a function of temperature for given partial pressures (or some other concentration)], listed in order of decreasing prevalence. The object of isosteres and isobars is to plot data on coordinates for which approximate linearity is expected, to make interpolation and extrapolation easier.

The heat of adsorption is a measure of the energy required for regeneration in gas- or vapor-phase applications, and low values are desirable. It also indicates the temperature rise that can be expected due to adsorption under adiabatic conditions. Again, there are several definitions: isosteric, differential, integral, and equilibrium, to name a few. The most relevant (because it applies to flow systems instead of batch systems) is the isosteric heat of adsorption, which is analogous to the heat of vaporization and is a weak function of temperature. The definition is

$$q_{st} = -R \left[\frac{\partial \ln p}{\partial (1/T)} \right]_{n^*} \quad (14.2)$$

where p and n^* , respectively, would be total pressure and loading for a pure gas or partial pressure and component loading for a mixture. Besides an indication of the energy required for regeneration, this term shows how the adsorbate interacts with the adsorbent. To illustrate, a plot of isosteric heat of adsorption vs. loading generally follows one of three trends (monotonically decreasing, increasing, or constant) as loading increases. The first case indicates that adsorption is strong at low concentrations, possibly due to a heterogeneous surface at which the “strong” sites are filled first. The net effect is that regeneration is likely to be difficult. The second case indicates the reverse, and regeneration is likely to be relatively easy, especially if the heat of adsorption is also low. The third case is neutral. Other, less utilitarian heats of adsorption are defined in Table 14.1.

14.3.2 SOURCES OF EQUILIBRIUM DATA

There are two types of sources of equilibrium data: literature and laboratory. In many ways, it is easier and cheaper to obtain data or correlations from the open literature. Unfortunately, there are not many compilations, so it may not be easy to find applicable data, even if they exist. A few that may prove useful are the *Adsorption Equilibrium Data Handbook* by Valenzuela and Myers (1989), *Carbon Adsorption Isotherms for Toxic Organics* by Dobbs and Cohen (1980), and *Adsorption-Capacity Data for 283 Organic Compounds* by Yaws, Bu, and Nijhawan (1995). Individual reports of equilibrium data are abundant and may be found in specialized journals such as *Adsorption*, *Adsorption Science and Technology*, *Journal of Colloid and Interface Science*, *Langmuir*, and *Separation Science and Technology*, as well as other more general journals such as *AIChE Journal*,

TABLE 14.2
Characteristics of Several Commercial Zeolites

Zeolite Type	Cationic Form	Nominal Pore Diameter (Å)	Si/Al
3A	K	3.0	1.0
4A	Na	3.9	1.0
5A	Ca	4.3	1.0
10X	Ca	7.8	1.2
13X	Na	8.0	1.2
Y	K	8.0	2.4
Mordenite	Na	7.0	5.0
ZSM-5	Na	6.0	31.0
Silicalite	—	6.0	∞

from adsorption, usually as a result of liquid filling pores in a certain way that is not the same as when they are emptied.

The following paragraphs describe the isotherms and explain the terms that are listed in Table 14.3. Most can accept any form of concentration, C , for the fluid phase (e.g., having units of mol/m³, lb/ft³, and so on) or a convenient variable (e.g., partial pressure, ppm, and so forth). Some, however, are restricted to relative saturation, i.e., expressed as a fraction. Generally, they can fit adsorbent loading, n^* , having units of mmol/g, lb/ft³, g/100 g, and others. Finally, the parameters A , B , and so forth are determined empirically.

The simplest equilibrium concept is that the extent of adsorption is proportional to the fluid-phase concentration, i.e., Henry's law [a in Table 14.3]. A principle of thermodynamic consistency is that isotherms should reduce to Henry's law at the limit of zero loading. If not, the equation (or data) is thermodynamically inconsistent and therefore fundamentally flawed. Conversely, there is pragmatic appeal to the premise that if an isotherm equation fits, one may use it, even though some scientific principle may be violated. The hazard of that approach arises if the data are flawed, causing an erroneous fit, which could lead to a defective design or mistaken predicted performance.

The Langmuir isotherm [b in Table 14.3] accounts for surface coverage by balancing the relative rates of uptake and release, the former being proportional to the fraction of the surface that is open, and the latter proportional to the fraction that is covered. The equilibrium constant for those rates is K , which also is the Henry's law coefficient. When the fluid concentration is very high, a monolayer forms on the adsorbent surface, having a loading of n_M . Those two parameters help us understand the nature of adsorption (although for some isotherms, n_M does not strictly refer to a monolayer but instead may denote a maximum). Hence, they are used directly in the equations when appropriate. When possible, the equivalent terms are listed in Table 14.2.

Freundlich recognized that, when data do not fit well on linear coordinates, the next logical step is to try log-log coordinates, and that led to the isotherm [c in Table 14.14. 3] bearing his name. It is probably the most commonly used isotherm equation, despite being "thermodynamically inconsistent."

The Brunauer–Emmett–Teller (B.E.T.) and B.D.D.T. isotherms [d and e in Table 14.3] account for pore filling via multiple layers instead of just a monolayer, and they use C/C_{sat} , that tends toward unity as the pores are completely filled. The B.D.D.T. isotherm includes the number of layers explicitly (m), as well as a heat of adsorption term (q). The B.E.T. isotherm is mostly used to estimate surface areas, not for process calculations [see Equation (14.10)].

The dual-mode isotherm is merely a combination of Henry's law and the Langmuir isotherm. Other isotherms, such as the Redlich–Peterson, Langmuir–Freundlich, Sips, and Toth [g, h, i, and j, respectively, in Table 14.3] versions extend the Langmuir isotherm by accounting for subtle

$$\varepsilon_i = RT \ln(f_i^* / f_i) \approx RT \ln(p_i^* / p_i) \approx RT \ln(C_i^* / C_i) \quad (14.3)$$

where the *pure* fluid fugacity and vapor pressure (or solute solubility limit) are f_i^* and p_i^* (or C_i^*), and the *equilibrium* fugacity and partial pressure (or solute concentration) are f_i and p_i or (C_i) , respectively, all at the temperature of interest, T . For vapors (neglecting fugacity coefficients), the adsorption potential is equivalent to the work required to compress the adsorbable component from its partial pressure to its vapor pressure. In addition, to apply this approach to liquids requires deducting a correction factor from ε_i to account for the displaced solvent.

Dubinin and coworkers showed that a specific adsorbent adsorbs nearly equal volumes of similar compounds when their adsorption potentials are equal. In this case, the adsorbed volume is estimated from the liquid density, usually at the same temperature. Their reasoning is that the adsorbed state closely resembles the liquid phase. They suggested a plot of volume adsorbed vs. adsorption potential would produce a “characteristic curve,” applicable to that group of compounds for the specific adsorbent. Most people who use this type of isotherm equation have adopted W as the symbol for loading, volume (of liquid) adsorbed per unit mass, or volume of adsorbent, but we will retain n^* and recognize that the units are specialized, as noted in Table 14.3. From the measured data (moles or mass adsorbed), one calculates the volume adsorbed using V_m , the molar volume of the saturated liquid evaluated at the adsorption pressure, but sometimes evaluated at the normal boiling point or another condition. Regardless, it should be consistent and clearly stated. It is then easy to extrapolate to other temperatures and other similar adsorbates for a given adsorbent. The main drawback is that the characteristic curve does not reduce to Henry's law at low coverage.

The isotherms developed by Dubinin and coworkers employ a power to which the adsorption potential is raised that indicates the prevalent type of pores. The Dubinin–Radushkevich equation [1 in Table 14.3] was intended for microporous adsorbents, since the exponent is 2. The Dubinin–Astakhov equation (m) allows the exponent B to vary, but a reasonable lower limit is unity (for macroporous adsorbents). The Dubinin–Stoeckli equation (n) allows a distribution of pore sizes, which is a feature of many adsorbents.

For this type of isotherm, n_0 represents the maximum loading, which correlates with pore volume among different adsorbents. The other isotherm parameters, k_0 and β_0 [no relation to the terms in Equations (14.4) or (14.5)], represent the *characteristic parameter* of the adsorbent and an *affinity coefficient* of the compound of interest, respectively. The characteristic parameter, k_0 , defines the shape of the n^* versus ε curve. The affinity coefficient, β_0 , adapts the compound of interest to the characteristic curve. It is a “fudge factor” that has been correlated to the ratio of molar volumes, parachors, or polarizabilities (via the Lorentz–Lorenz equation) of the compound of interest to that of a reference component (e.g., benzene or *n*-heptane). These three methods are roughly equivalent in accuracy. The molar volume version is $\varepsilon_i = \varepsilon_{ref} V_i / V_{ref}$. The only controversy is whether to use the actual temperature to estimate volumes or some other temperature such as the normal boiling point.

For given a set of data, which isotherm equation (or equations) fits best? And what is the impact of the quality of fit on predicted performance? Unfortunately, neither question can be answered fully. It is fair to say that the greater the number of parameters in an equation, the more likely it is to fit well; and the better it fits, the more valid will be subsequent process simulations. That should be balanced against the statistical significance of the parameters. Finally, the isotherm fit that best accommodates heat effects and multicomponent aspects, if any, will be superior. An example that illustrates different degrees of quality of fit of four equations to one set of data is provided in Section 14.5.4. Specialized programs are available that fit equations and plot the results.

The term *regenerability* was also referred to previously without giving an exact definition. To do so implies choosing the regeneration method. Regenerability would then revolve around the isotherm (or loading) under the process conditions vs. during regeneration. For a TSA cycle, this would mean looking at the appropriate isotherms for uptake and release and assessing the change of loading. Likewise, for chemical regeneration (e.g., by displacement or elution) or for a PSA

constant (at a given temperature), although it normally applies only at the limit of zero concentration. When discussing results, it is a good idea to clarify the definition of what is meant by selectivity or to speak of "good" or "bad" instead of "large" or "small."

There are five common means of dealing with mixtures rather than single adsorbable species. First and easiest, one may pretend that the mixture consists only of the major adsorbable component. That can be catastrophic. The second approach, treating the constituents independently, is useful and accurate when a nonadsorbing carrier contains very dilute contaminants. It is also very easy, since only pure component isotherms are required. Third, one may apply a method developed by Tien and coworkers (Jayaraj and Tien, 1984; Kage and Tien, 1987; Moon, Park, and Tien, 1991) called *species grouping*. The idea is to deal with a mixture of, say, ten components by identifying two or three (sometimes fictitious) components to represent the entire set. That reduces the complexity, saves time and money, and is fairly accurate if only an approximate answer is desired. It requires some pure component isotherm data to know how to group the species. The fourth method is to use one of several empirical isotherm equations that account for "competitive" adsorption of the relevant components. This method requires both pure component and mixture isotherm data. Depending on which equation is selected, the data analysis and fitting are more involved than for pure components, but not enormously so. In that case, the results are compact and relatively simple to use for design or simulation. Examples of the equations are listed in Table 14.4.

The fifth approach is more a field than a concise method, since it embodies so many theoretical concepts and associated methods. All are grouped together as "adsorbed mixture models." Basically, this involves treating the adsorbed mixture in the same manner that the liquid is treated when doing VLE calculations. The major distinction is that the adsorbed phase composition cannot be directly measured (i.e., it can only be inferred); hence, it is difficult to pursue experimentally. A *mixture model* is used to account for interactions, which may be as simple as Raoult's law or as involved as Wilson's equation. These correspond roughly to the Ideal Adsorbed Solution theory and Vacancy Solution model, respectively. Pure component and mixture equilibrium data are required. The unfortunate aspect is that they require iterative root-finding procedures and integration, which complicates adsorber simulation. They may be the only route to acceptably accurate answers, however. It would be nice if adsorbents could be selected to avoid both aspects, but adsorbate-adsorbate interactions may be nearly as important and as complicated as adsorbate-adsorbent interactions.

14.4 DYNAMICS OF ADSORPTION

14.4.1 OVERVIEW OF RATE PHENOMENA

To perform adsorber simulations or even to select an adsorbent, one must appreciate the impact of processing conditions, geometry, and transport constraints on performance. This might mean solving the governing partial differential equations or just gaining an awareness of the variables and parameters that affect transport phenomena, especially those regarding the adsorbent. At least two constraints of importance include intraparticle diffusion and pressure drop in the packed bed (see Do, 1998; Kärger and Ruthven, 1992; and Tien, 1994).

Film diffusion resistance, axial dispersion, and axial and radial temperature gradients (implying significant resistances to intraparticle heat transfer, as well as axial and radial conduction and convection) may all be relevant. Furthermore, the adsorbent itself, and internal fittings and devices (e.g., for bed retention or flow distribution), may affect flow behavior and pressure drop. Accordingly, these may affect performance, but accounting for them is not generally practical. Even if the equations could be written, determining the applicable coefficients would be very time consuming.

Mass transport in an adsorbent particle can be viewed as a combination of several mechanisms, as shown in Figure 14.8. Macropore and micropore diffusion are shown and could be considered as examples of intraparticle diffusion. Bulk flow or conveyance through the particle (e.g., via connected pores) is shown in that figure but, to be significant, requires high porosity or a large

Combining Equations (14.8) and (14.9) gives the overall effective diffusivity in the transition regime:

$$D_{eff}^* = \left[\frac{1}{D_{eff}} + \frac{1}{D_{K_{eff}}} \right]^{-1} \quad (14.11)$$

To understand how these parameters are involved in uptake or release rates, consider the fractional change, F , following a sudden change of composition. The expression is a solution of Fick's law. The *initial* response ($D_{eff}t/\ell^2 < 0.4$) and the *final* response ($D_{eff}t/\ell^2 > 0.4$) of a spherical particle, respectively, are approximated by

$$\begin{aligned} F \equiv \frac{C_t - C_0}{C_f - C_0} &\approx \frac{6}{\sqrt{\pi}} \left(\frac{D_{eff}t}{\ell^2} \right)^{1/2} - 3 \frac{D_{eff}t}{\ell^2} \Big|_{initial} \quad \text{or} \\ &\approx 1 - \frac{6}{\pi^2} e^{-\pi^2 D_{eff}t/\ell^2} \Big|_{final} \end{aligned} \quad (14.12)$$

where the C_0 , C_f and C_t represent the initial, final, and instantaneous values of concentration averaged over the particle. For a flow system, $t \approx \ell/v_i$, where $v_i = v_s/\epsilon_B$ = the interstitial velocity, and $v_s = Q/A_{cs}$ = the superficial velocity, where Q is the volumetric flow rate and A_{cs} is the cross-sectional area of the bed. From these approximations, we can see that when $D_{eff}t/\ell^2$ is less than 0.001, the adsorbent is not effective. Conversely, when it exceeds unity, adsorption is largely complete. Thus, when searching for an effective (fast) adsorbent, it is usually a safe bet to choose one having a large diffusivity or small diameter. Other concerns may overrule the selection of small particles, as mentioned later.

Interstitial mass transfer in fixed beds is frequently a significant factor in adsorption dynamics. Sherwood et al. (1975) developed an equation for both gases and liquids that employs the Colburn–Chilton j -factor:

$$j_D = 1.17 \text{ Re}^{-0.415} \quad [\text{for } 10 < \text{Re} < 2500] \quad (14.13)$$

where $j_D = (k_f/v_s)Sc^{0.667}$, the Reynolds number is $Re = \rho v_s d_p/\mu$, and the Schmidt number is $Sc = \mu/\rho D_{AB}$. We are primarily interested in the fluid-to-particle mass transfer coefficient, k_f . It is mostly governed by the fluid properties (density, ρ ; viscosity, μ ; and diffusivity, D_{AB}).

Yoshida et al. (1962) suggested another correlation for estimating the mass transfer coefficient:

$$j_D = 0.91 \text{ Re}'^{-0.51} \psi \quad [\text{for } \text{Re}' < 50] \quad (14.14)$$

where the modified Reynolds number is $\text{Re}' = \rho v_s/\mu a_p \psi$, in which $a_p = 6/d_p$ for beads; ψ = shape factor is 1.0 for spherical beads, 0.95 for granular adsorbents, 0.91 for cylindrical pellets, and about 0.86 for flakes; and $D_{A_{eff}} = D_{AB}/\mathcal{F}$, where \mathcal{F} is an apparent tortuosity factor that lumps the fluid phase resistance (film diffusion) with the intraparticle mass transfer resistance.

For practical purposes, these only depend on one adsorbent parameter, the particle diameter, d_p . As can be seen, $k_f \propto d_p^{-0.415}$ to $d_p^{-0.51}$, so for a given fluid and flow rate, a tenfold increase of the particle diameter would lead to a 60 to 70% decrease of the mass transfer coefficient. Conversely, a tenfold increase of the velocity often leads to a four- to threefold increase of the mass transfer coefficient. Generally, a large value of k_f is desired, although if achieved by employing high velocity, v_s , the associated pumping or compression costs will be high, and the time of exposure in Equation (14.12) will be short.

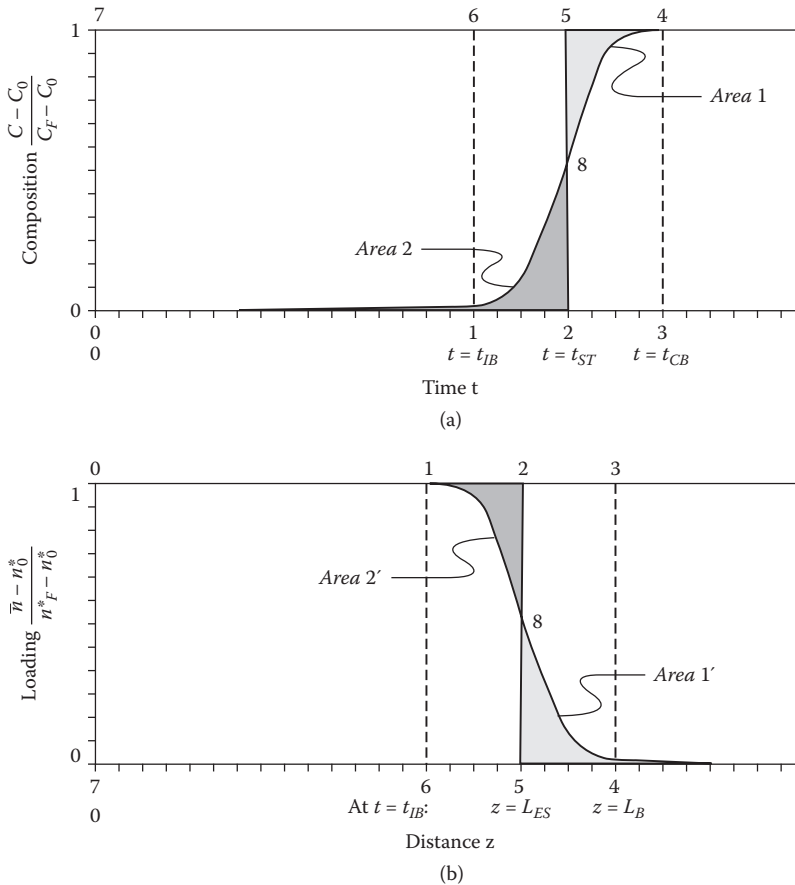


FIGURE 14.10 Breakthrough history (t) and profile (z). Times and positions are labeled to represent specific sets of conditions.

To determine the stoichiometric breakthrough time involves integration. Basically, the points 1 through 6 are chosen such that the area of the rectangle 1-2-5-6 equals that above (or below) the curve 1-8-4-6, and likewise the area of the rectangle 2-3-4-5 equals that below (or above) the curve 1-3-4-8. The result of those is that Area 1 = Area 2 and Area 1' = Area 2', and the time dividing them (at point 2) is by definition t_{ST} . If the curve is symmetric, point 8 will lie at the mid-point between the feed and initial concentrations, but that is only coincidental.

Before delving into specific mathematical models, it might be helpful to look at the basic mass conservation equation, because some terms that represent adsorbent properties appear in it. The material balance equation for solute A is

$$\epsilon_B \frac{\partial C_A}{\partial t} + (1 - \epsilon) \rho_p \frac{\partial \bar{n}_A}{\partial t} + \epsilon^v \frac{\partial C_A}{\partial z} = E_{ax} \frac{\partial^2 C_A}{\partial z^2} \quad (14.15)$$

where ϵ = bed void fraction, ρ_p = particle density, ρ_B = bulk density = $(1 - \epsilon_B)\rho_p$, C_A = solute concentration in fluid, \bar{n}_A = adsorbent loading (averaged), v = interstitial velocity (v_s = superficial velocity = ϵ^v), and E_{ax} = axial dispersion coefficient. If the column is well designed, the last term can be made negligible. Among these terms, the particle density and void fraction are inherent properties of the adsorbent. Of course, the adsorbent loading is, too, but it also depends on other operating conditions.

where Q is the volumetric flow rate and V_{ads} is the volume of the adsorbent bed ($= LA_{cs}$). This result applies to any favorable isotherm. It is restricted to isothermal plug flow with a constant fluid velocity. For uptake of a major gas component, allowance should be made for velocity variation.

14.4.2.2 Modified Wheeler and Robell Method

The Wheeler–Robell equation (1969) is an empirically adjusted local equilibrium model. It neglects axial dispersion but applies to any isotherm form:

$$\frac{C_A}{C_{AF}} = e^{k_w \left(\frac{C_{AF}}{\rho_B n_{Aeff}^*} t - \frac{A_{CS} L}{Q_F} \right)} \quad (14.21)$$

where k_w and n_{Aeff}^* are adjustable. Determining n_{Aeff}^* empirically along with k_w leads to discrepancies compared with true equilibrium values. Equation (14.21) can be altered by determining n_{Aeff}^* independently; e.g., by measuring or predicting it. In addition, the breakthrough time can be predicted via Equation (14.20) (the local equilibrium model) using isotherm data. Solving Equation (14.21) with $C_A/C_{AF} = 0.5$ leads to the following relation for the effective capacity of the adsorbent, n_{AF}^* :

$$n_{AF}^* = \frac{C_{AF} t_{BT} / \rho_B}{\theta - 0.693 / k_w} \quad (14.22)$$

where the superficial residence time is $\theta = A_{CS} L / Q_F$ in units consistent with k_w and t_{BT} .

Replacing t_{BT} with the local equilibrium model result $\approx \Delta t_{SH}$ gives a modified Wheeler equation:

$$\frac{C_A}{C_{AF}} = e^{\frac{k_w - 0.693/\theta}{\varepsilon_B + \rho_B n_{NF}^* / C_{AF}} t - k_w \theta} \quad (14.23)$$

The restrictions as written are to uptake in a clean bed of adsorbent, and only to $C_A/C_{AF} = 0.5$. They could be extended to arbitrary (but uniform) initial conditions, and they can be converted to symmetric breakthrough curve shapes.

14.4.2.3 Mass Transfer Resistances

Three main types of mass transfer resistances are recognized: *film diffusion* (which occurs at the external surface of the adsorbent), *intraparticle diffusion* (which occurs within the pores or amorphous structure of the adsorbent), and *adsorption/desorption kinetics* (which occurs at the internal surface of the adsorbent).

Film diffusion is expressed as a simple function, using the middle term of Equation (14.15):

$$(1 - \varepsilon_B) \rho_p \frac{\partial \bar{n}_A}{\partial t} = k_f a_p (C_A - C_A^*) \quad (14.24)$$

where k_f = film mass transfer coefficient and a_p = area (of surface) per unit volume.

Intraparticle diffusion is commonly expressed with Fick's law using terms of pore diffusion or surface diffusion (when adsorption loading is large):

$$\frac{\partial n_A}{\partial t} = \frac{D_{Aeff}}{r^2} \frac{\partial}{\partial r} \left(r^2 \frac{\partial C_A}{\partial r} \right) \quad \text{or} \quad \frac{D_{As}}{r^2} \frac{\partial}{\partial r} \left(r^2 \frac{\partial n_A}{\partial r} \right) \quad (14.25)$$

$$\bar{J} = (\zeta, \tau) \cong \frac{1}{2} [1 + \operatorname{erf}(\sqrt{\tau} - \sqrt{\zeta})] \quad (14.30)$$

Note that $\operatorname{erf}(-x) = -\operatorname{erf}(x)$, and that $\operatorname{erfc}(x) = 1 - \operatorname{erf}(x)$. An approximation for $\operatorname{erf}(x)$ is

$$\operatorname{erf}(x) \cong 1 - (A_1 t + A_2 t^2 + A_3 t^3) e^{-x^2} \quad (14.31)$$

where $t = (1 + A_4 x)^{-1}$, and the parameters are $A_1 = 0.34802$, $A_2 = -0.09588$, $A_3 = 0.7478556$, and $A_4 = 0.47047$. For example, $\operatorname{erf}(1) = 0.842701$, while the equation above predicts 0.842718.

Extensions of the Hougen–Marshall model, developed by Rosen (1954) account for mass transfer resistances in both the fluid and solid phases. However, it is seldom practical to conduct all the experiments necessary to determine values of both coefficients and their dependence on conditions.

14.4.3 HEAT TRANSFER

Adsorption from the gas or vapor phase is usually associated with significant heat release upon uptake, or cooling upon desorption. Three modes of operation are possible: isothermal, adiabatic, and intermediate (not quite either extreme). Isothermal operation can often be assumed for liquid-phase adsorption but generally not for gas- or vapor-phase systems. Temperature shifts affect adsorption capacity strongly but diffusivity to a lesser extent.

Following the form suggested by Equation (14.14), heat transfer to the fluid phase can be estimated by the Yoshida et al. (1962) correlations for particle to fluid heat transfer coefficients:

$$j_H = 0.91 \operatorname{Re}'^{-0.51} \psi \quad [\text{for } \operatorname{Re}' < 50] \quad (14.32)$$

$$j_H = 0.61 \operatorname{Re}'^{-0.41} \psi \quad [\text{for } \operatorname{Re}' > 50] \quad (14.33)$$

in which $j_H = (h/C_{pf} \rho v_s)(C_{pf} \mu / \lambda_f)^{2/3}$, in which the heat capacity, density, viscosity, and thermal conductivity of the fluid are C_p , ρ , μ , and λ , respectively, and the subscript f indicates “fluid phase and film temperature.” As in Equation (14.14), the particle shape factor is ψ . Likewise, the modified Reynolds number, Re' , is defined as before. An alternate for the previous equations is the Wakao and Funazkri correlation for the particle to the *gas* heat transfer coefficient:

$$Nu = 2.0 + 1.1 \operatorname{Pr}^{1/3} \operatorname{Re}^{0.6} \quad (14.34)$$

where $Nu = h_f d_p / \lambda_f$, in which the heat transfer coefficient is h_f and the gas phase thermal conductivity is λ_f .

Heat generation is frequently significant in adsorbents. Nevertheless, adsorbent particles are usually assumed to be at a uniform temperature. There are many reasons for this observation. Heats of adsorption (and desorption) are not sufficiently large to cause large temperature gradients within typical, small adsorbent particles, but the cumulative effects may generate swings of 10 to more than 50°C. The *thermicity* reveals the magnitude of temperature gradient expected in an adsorbent particle:

$$\beta = \frac{c_s (-\Delta H_{ads}) D_{eff}}{\lambda_s T_{ext}} \approx \frac{\Delta T_{max}}{T_{ext}} \quad (14.35)$$

in which c_s is the intraparticle concentration, ΔH_{ads} is the isosteric heat of adsorption, λ_s is the solid thermal conductivity, and T_{ext} is the external fluid temperature. For gas-phase systems, an order-of-

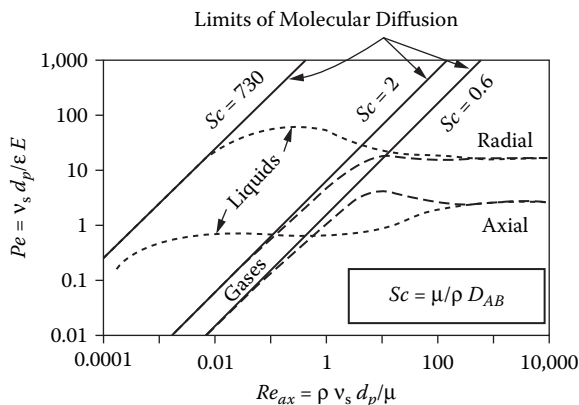


FIGURE 14.11 Axial and radial Peclet numbers for single-phase flow of a gas or liquid through a packed bed of spherical particles. The limits of molecular diffusion are shown by solid lines that represent $Pe = Re Sc \tau_B / \epsilon_B$, where τ_B = bed tortuosity = 1.4 and ϵ_B = bed voidage = 0.4 (Sherwood et al., 1975).

14.4.5 DISPERSION

The principal aspect that reflects flow distribution in fixed beds is dispersion. Flow through a packed bed is commonly represented by dispersed plug flow in which all mechanisms contributing to mixing are lumped together in effective dispersion coefficients, E_{ax} and E_r . A model analogous to Fick's law, as given by Equation (14.15), is applicable:

$$\frac{\partial c}{\partial t} + \frac{v_s}{\epsilon} \frac{\partial c}{\partial z} = \frac{E_r}{r} \frac{\partial}{\partial r} \left[r \frac{\partial c}{\partial r} \right] + E_{ax} \frac{\partial^2 c}{\partial z^2} \quad (14.41)$$

in which the terms for adsorption have been omitted, E_{ax} = the axial dispersion coefficient, and E_r = the radial dispersion coefficient. It is evident that there are two modes of dispersion: radial and axial. Axial dispersion always adversely affects adsorption performance. Despite that, axial dispersion can be offset by radial dispersion, meaning that radial dispersion promotes plug-flow behavior, which is always beneficial to adsorption performance. There are two main dispersive mechanisms: hindered molecular diffusion (corrected for tortuosity) and turbulent mixing arising from flow around the particles. Figure 14.11 indicates the limits of hindered molecular diffusion at low flow rates: $E_{ax} = E_r = D_{AB} / \tau_B$, where τ_B = bed tortuosity ≈ 1.4 (typical) for fixed beds.

The coefficient representing axial dispersion, E_{ax} , is measured using a tracer by pulse, sinusoidal, or step-change residence time distribution tests, or by measuring backflow. Sometimes the phenomenon is represented by a "cell" model, in which the number of well-mixed cells fits dispersion. The coefficient representing radial dispersion, E_r , is determined by measuring the radial spread of a tracer from the centerline toward the wall.

The Peclet number for dispersion is defined as $Pe = v_s d_p / \epsilon_B E$, which is dimensionless, and $v_s / \epsilon_B = v_i$ = the interstitial velocity. A convenient way to comprehend the data for fixed beds is via Figure 14.11, which shows the trends for gases and liquids in both axial and radial dispersions. A general correlating equation for gases is

$$\frac{1}{Pe_{ax}} = \frac{K_1}{Re Sc} + \frac{1}{Pe_{ax\infty}} \frac{1}{1 + K_2 / (Re Sc)} \quad (14.42)$$

where $Pe_{ax\infty} = 2.0$, the Reynolds number is $Re = \rho v_s d_p / \mu$, and the Schmidt number is $Sc = \mu / (\rho D_{AB})$. The product, $Re Sc = v_s d_p / D_{AB}$, is a Peclet number for ordinary diffusion. The coefficients K_1 and

14.5 DESIGN OF BATCH, FIXED-BED ADSORBERS

14.5.1 GENERAL OBJECTIVES

This section describes *batchwise* fixed-bed adsorbers in which the adsorbent is replaced with fresh material, or removed and regenerated after it is “exhausted,” then reinstalled. Commercial examples include columns used for chemical feedstock purification, decolorizing solutions, and wastewater treatment. The goal is generally to employ material balance and rate equations to predict adsorber performance, possibly to analyze experimental data (e.g., breakthrough curves and temperature histories), to diagnose problems, or to assess properties or conditions. Unfortunately, various conditions often result in nearly identical behavior, so diagnosing causes may be difficult.

Often there is an economy of scale, meaning that the cost to process material drops substantially as the size of the unit increases. Unfortunately, there are rather small economic advantages for larger adsorbers, because the cost of the adsorbent typically depends on the amount purchased with an exponent of 0.8 to 1.0. Depending on the pressure rating required, the length-to-diameter ratio (L/D) of a typical adsorber may range from 1 to 10, with larger values favored for high pressures. Flow is oriented vertically as a rule, since the adsorbent tends to settle, which would cause void space and bypassing at the top of a horizontal bed. Control is generally based on fixed time cycles, although effluent composition is preferred for performance reasons.

Factors affecting performance are the component isotherm(s), geometry, operating conditions, mass transfer resistances (including film diffusion, intraparticle diffusion, and dispersion), and thermal effects, especially for gases. How these are taken into account varies depending on the application, the tools available, and the situation. For many applications, established methods for simulation and design are readily available. The simplest approach is to estimate the volume of the adsorber, knowing only the adsorbent's capacity at the relevant concentration and temperature, and add a large safety factor.

For more detailed designs, the equations describing breakthrough behavior in the previous section, plus a modest safety factor, may be sufficient. With complex heat and/or mass transfer issues, multiple components, or unusual equipment geometry, a standard model is likely not suitable. In such cases, experimental tests may be required to develop a suitable mathematical model; the required effort might be up to a man-year.

14.5.2 EMPIRICAL VERSUS THEORETICAL APPROACHES

Model classifications are as follows:

Empirical. Experimental data and/or experience axes are needed; results are imprecise and prone to error, but this method is typically quick. Examples are the length of unused bed (LUB) and mass transfer zone (MTZ) methods, as discussed later.

Analytic. This is restricted to certain conditions (e.g., isothermal uptake with clean adsorbent) or no mass transfer resistances. Examples are the Hougen–Marshall and Thomas approaches, and the local equilibrium model. These approaches can be incorporated in a simple design procedure, as illustrated in the next section.

Rigorous. This involves solutions to numerous governing equations; they may include mass transfer resistances, heat effects, complex equilibria, pressure drop, axial dispersion, and others. The last can be time consuming; it lacks intuitive connections between performance and variables. Many applications require rigorous methods. An example is multicomponent adsorption of the type shown in Figure 14.13.

Beyond this, some methods and models do not fit these categories, because they have elements of two or all three, e.g., the modified Wheeler equation shown as Equation (14.23).

$$L_{ES} = v_s \Delta t_{SH} \left[\epsilon_B + \rho_B \frac{\Delta n_A^*}{\Delta C_A} \right]^{-1} \quad (14.45)$$

If the front moves at the idealized shock front velocity, v_{SH} , given by Equation (14.18), then $t_{ST} = t_{SH}$ and the times and positions of the front are related as

$$v_{SH} = \frac{L_{ES}}{t_{IB}} = \frac{L_B}{t_{ST}} \quad (14.46)$$

This equation allows a concise expression of L_{UB} :

$$L_{UB} = L_B - L_{ES} = v_{SH} (t_{ST} - t_{IB}) \quad (14.47)$$

Combining the previous two equations yields

$$L_{UB} = L_B (1 - t_{IB} / t_{ST}) \quad (14.48)$$

Equations (14.44) through (14.48) apply to a single flow rate and cross-sectional area (not to mention temperature, pressure, feed concentration, and other conditions). By analyzing breakthrough data from one column, it is easy to determine the relationships between bed length and time. For example, given the *actual* effluent concentration history, $C(t, L_{Ba})$, and bed length, L_B , for one system, it is straightforward to identify the *actual* times, t_{IBa} and t_{STa} . From those, the *actual* length of unused bed, L_{UBa} , can be found from Equation (14.47). Likewise, the *actual* length of the equilibrium section, L_{ESa} , can be found from Equation (14.45) or (14.46). A design situation could require choosing a bed with a different, “desired” length of unused bed, L_{UBd} , based on the *desired* and *actual* stoichiometric breakthrough times, t_{STd} and t_{STa} . Under those constraints, the length of the *desired* bed can be found from Equation (14.45), $L_{Bd} = L_{Ba} t_{STd} / t_{STa}$. Subsequently, Equation (14.46) can be used to estimate L_{ESd} for the *desired* bed, $L_{ESd} = L_{Bd} - L_{UBd}$.

To scale up by this technique, i.e., to accommodate other flow rates, Q , or bed geometries, masses should be used. They are found by using the cross-sectional area of the bed and the bulk density of the adsorbent. For a cylindrical bed,

$$W_B = \rho_B \pi d_B^2 L_B / 4 \quad (14.49)$$

where W_B is the mass of the bed, and by analogy W_{UB} and W_{ES} are the mass of the unused bed and mass of the equilibrium section, calculated from their lengths, respectively:

$$W_{ES} = \rho_B Q t_{ES} \left[\epsilon + \rho_B \frac{\Delta n_A^*}{\Delta C_A} \right]^{-1} \quad (14.50)$$

The relationship between W_B , W_{UB} , and W_{ES} ,

$$W_B = W_{ES} + W_{LUB} \quad (14.51)$$

The only problem occurs when $L_{UB} = f(Q)$, which must be determined empirically.

Example 14.1 Isotherm Fitting

Consider the following adsorption isotherm data for water vapor on silica gel at 25°C. Fit the data to the Langmuir, Freundlich, Redlich–Peterson, and B.D.D.T. equations.

Relative Humidity	Loading Mol/cm ³
0.0000	0.00000
0.0116	0.00173
0.0198	0.00223
0.0378	0.00353
0.0600	0.00484
0.1330	0.00868
0.1770	0.01120
0.1800	0.01182
0.2180	0.01367
0.2380	0.01526
0.2410	0.01559
0.2560	0.01708
0.2780	0.01740
0.2790	0.01794
0.2920	0.02003
0.3070	0.02043
0.3500	0.02345
0.3690	0.02528
0.5260	0.03097
0.5390	0.03204
0.6490	0.03303
0.6970	0.03332
0.7580	0.03387
0.8250	0.03411
0.8250	0.03415

Results

The data and isotherm fits are shown in Figure 14.14. The corresponding parameters and statistics are provided in Table 14.6. The average percentage deviations for those fits are 8.8, 12.0, 7.9, and 2.7%, respectively. The average errors for the Langmuir and Redlich–Peterson equations, in particular, seem high due to relatively large percentage deviations for the first few points. These deviations are exaggerated at low loadings. That is, if an adsorbent has a maximum loading of 1 kg/kg, a discrepancy of 0.01 kg/kg would be equivalent to a 100% deviation if it occurred at 1% of the maximum loading, but only a 1% deviation if it occurred at saturation. When, however, a weighted scale is used, in which the weights are simply proportional to loading, a discrepancy of 0.01 kg/kg amounts to a 1% deviation. Applying that for this example, the weighted percentage deviations are 3.9, 4.8, 1.9, and 1%, respectively.

The B.D.D.T. isotherm essentially provides an ideal fit at low, intermediate, and high concentrations. The parameter m indicates that 4.4 layers are adsorbed on the surface at saturation. This isotherm form also discerns the “real” Henry’s law coefficient, which is about four times larger than the value that the simpler equations estimate. The Redlich–Peterson equation fits the data well, although it incorrectly predicts a local maximum in loading. Hence, it is unreliable for extrapolations, and it underpredicts the loading at low concentrations (i.e., below 10% RH). The Langmuir isotherm predicts well at low concentrations but not near saturation. The Freundlich isotherm is least satisfactory in nearly every respect. It might be adequate for estimating overall life, but not for design purposes.

Multicomponent adsorption is complex (see Figure 14.13). Since this is a small application, delving into equilibria and column modeling is not justified. It is assumed that the lighter components are displaced by the heavier components. The feed, 10 cfm at 80°F, amounts to 9.1 scfm or 1.52 lb-mol/hr. Thus, the *loading rate* of each component that needs to be adsorbed is $0.0001 \times 1.52/MW$ (lb/h), where *MW* is its molecular weight. The time on line can be estimated by dividing the loading by the *loading rate*, assuming that they adsorb independently and completely (no premature breakthrough).

The best choice appears to be carbon *B*, since it offers a longer time on line than carbon *A* for the critical component, MEK, and the ratio (1.76) is greater than the cost ratio (1.5). If there were no MEK in the stream, the decision would be a tossup, since the respective carbons' loading ratios of those components are nearly identical to their cost ratios.

The final consideration is the type and cost of equipment. Modular units come packed with 150 to 500 lb of carbon. They can be installed and removed quickly and returned to the manufacturer on an exchange basis (possibly avoiding "hazardous waste" aspects). The smaller units would be packed with 4×6 mesh carbon and could handle up to 100 cfm, well within the range needed. For 50 lb per batch per contaminant, two parallel units would be needed to handle the MEK for 600 hr, allowing some excess to take care of rounding of the breakthrough curve. The cost would be in the range of \$600 each. Even at this low cost (\$17,520 per year, not including labor, shipping, and other costs), it might be possible to justify a small PSA unit that would recover concentrated vapor (for incineration) or a condensed product. Such systems are not yet available off the shelf, however.

Example 14.3 Dilute Liquid Solutions

Consider a feed of 0.3 mg/l (or 300 ppm) of diphenylamine in 100 gpm water, with a minimum on-line time of 500 hr.

Results

Dobbs and Cohen (mentioned earlier) reported that Filtrasorb-300 (Calgon Corp.) adsorbs 80 mg/g at this concentration. Thus, $\Delta n^*/\Delta C = 80$ (mg/g)/0.0003 (mg/cm³). $\rho_B = 31.2$ lb/ft³ (or 0.5 g/cm³), $\epsilon = 0.70$. They also noted that a fine powder (200 \times 400 mesh, or 0.05-mm diameter) required about 5 hr to equilibrate. Equation (14.12) suggests the time required to equilibrate a 0.5-mm diameter granule. Namely, the parameter $D_{eff}t/\ell^2$ would be constant, as would the effective diffusivity. Thus, $t_{3mm} = t_{0.05mm} (0.5 \text{ mm}/0.05 \text{ mm})^2$ or 500 hr! Granules will not exhibit a sharp breakthrough, so a large safety factor is needed. Accordingly, facilities often employ a slurry of powdered carbon with a downstream filter to remove the waste.

Equation (14.20) is used to estimate the bed volume, given the equilibrium breakthrough time. We find that the minimum volume of adsorbent is 112.5 gal = 15 ft³ or roughly 470 lb. To be conservative, a *safety factor* of 3 is recommended, but even that should be tested. Thus, the bed size would be about 45 ft³ (roughly 3 ft dia. \times 6.5 ft long), containing about 1400 lb of carbon. The length-to-diameter ratio, L_B/d_B , could be optimized. To obtain a large mass transfer coefficient, that ratio should be large, but to minimize pressure drop, that ratio should be small. Generally, the optimum ratio lies in the 1:1 to 5:1 range.

Example 14.4 Gaseous Emissions

Predict the breakthrough patterns for uptake of CO₂ from air by activated carbon under the following data, and compare with the breakthrough data (Note: the symbol [=] denotes "has units of"):

$$\begin{array}{lll} \rho_B = 0.360 \text{ g/cm}^3 & \epsilon_B = 0.345 & d_p = 0.5 \text{ mm} \\ d_B = 0.718 \text{ cm} & L_B = 72 \text{ cm} & p_{AF} = 0.1316 \text{ atm} \\ \dot{Q} = 1.85 \text{ std. cm}^3/\text{s} & T = 0^\circ\text{C} & P = 1 \text{ atm} \end{array}$$

$$n_A^* = \frac{0.0112 p_A}{1 + 7.258 p_A} [=] \frac{\text{mol (A)}}{\text{g (adsorbent)}}; \quad p_A [=] \text{ atm}$$

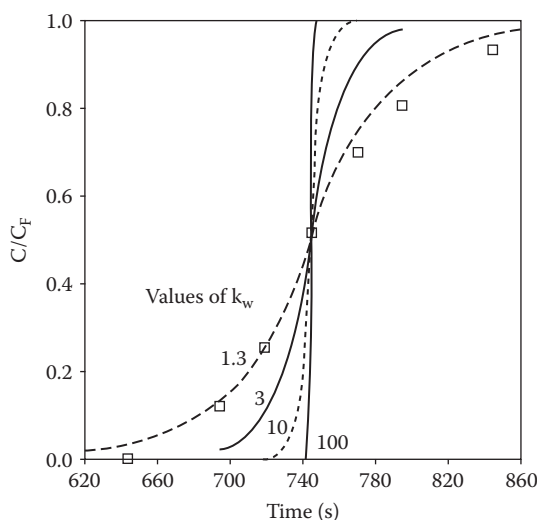


FIGURE 14.15 Comparison of breakthrough predictions for the Wheeler equation for $k_w = 1.3, 3, 10$, and 100 l/s. The data are shown as square symbols.

and are beyond the scope of this chapter. Nevertheless, it may be helpful to consider the features of typical continuous systems, since they may be transferred to other situations. Example flowsheets of three types of continuous process are given in Figures 14.16, 14.17, and 14.18. The first is a stirred system, which functions like a CSTR from the standpoint of the liquid. The adsorbent, however, undergoes a batchwise experience. The second flowsheet a continuous TSA system in which the adsorbent circulates through uptake and regeneration zones. The third flowsheet depicts a simulated moving-bed (SMB) system, in which the adsorbent is in a fixed bed and the feed, product, and regenerant entry and exit are shifted synchronously via valves such as in UOP's SorbexSM processes.

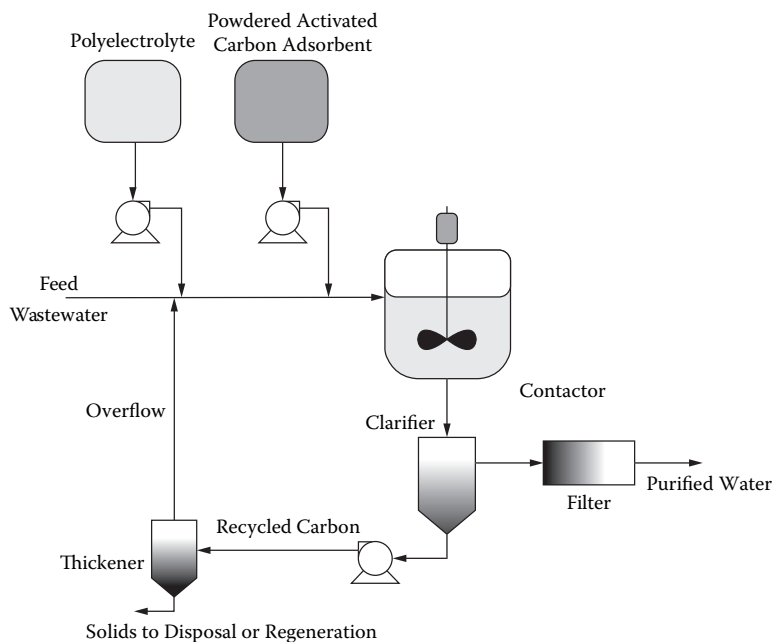


FIGURE 14.16 Powdered activated carbon system for cleanup of wastewater.

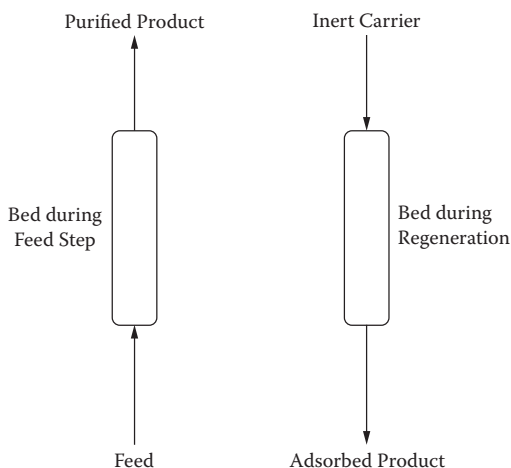


FIGURE 14.19 Simple two-column inert-purge adsorption system.

followed by regeneration with an inert fluid. It essentially transfers the adsorbed constituent from one stream to another, but in so doing it dilutes (instead of enriching) adsorbate. It also cools by desorption (i.e., the latent heat is taken up so as to achieve regeneration), and so it is advantageous to recover stored heat (which is released during uptake). The relevant breakthrough curves are shown in Figure 14.9.

14.6.2 DISPLACEMENT-PURGE CYCLE

Another relatively simple system is the *displacement-purge cycle*, shown in Figure 14.20. This is also a two-step process: adsorption in which the bed (being preloaded with a strongly adsorbed component, B), is gradually displaced by a weakly adsorbed component in the feed, A, followed by regeneration via the more strongly adsorbed component. The latter step desorbs A by selectively adsorbing B and enriches the desired adsorbate A.

14.6.3 TSA CYCLE

A third type of cycle is *temperature swing adsorption* (TSA). Typical TSA cycles comprise two or three steps of several minutes' to several days' duration. They are adsorption at low temperature, regeneration at high temperature, and cooling (which is optional) and may be done with solvent (or carrier) or a separate inert fluid. An illustration of how loading changes during a typical TSA cycle is shown in Figure 14.21.

TSA success usually depends on the regeneration step and the associated costs. To accomplish regeneration, one may use heated feed, hot solvent (or carrier), separate hot inert fluid, electrical current, microwaves, or steam. Steam, although widely used, usually accomplishes regeneration by conveyance rather than displacement, so the effluent composition profile is not sharp. Nevertheless, the adsorbate is enriched because the amount of fluid required for desorption is much less than that during uptake. The energy requirements of regeneration strongly affect overall cost. A typical cycle is shown in Figure 14.22.

EXAMPLE 14.5 TSA SOLVENT RECOVERY

Consider *n*-heptane-laden air at 5000 ppm, 1000 metric tons of solvent/yr (= 125 kg solvent/hr), operated 8000 hr/yr. The TSA cycle duration is 6 hr (half adsorption, half desorption), and the equipment consists of two parallel beds operating sequentially.

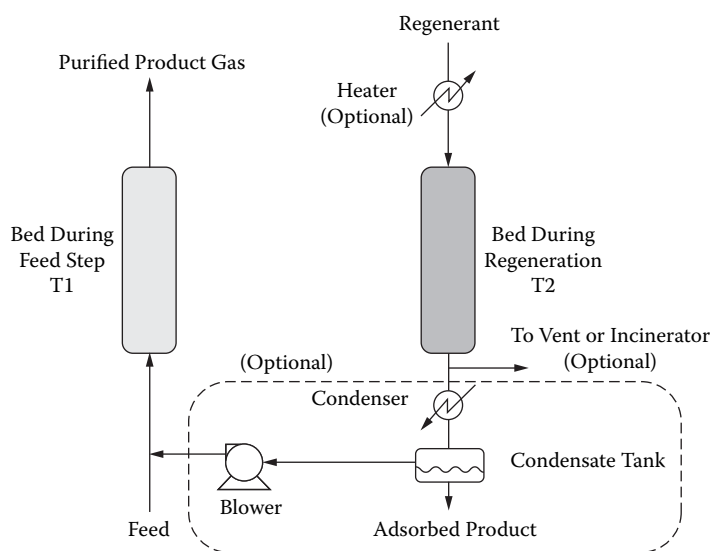


FIGURE 14.22 Typical two-column temperature swing adsorption system.

TABLE 14.7
Estimated Loadings and Service Times of Emitted Components (at 100 ppm each) for Activated Carbons A and B at 80°F

Component Name	Mol. Wt (g/mol)	Loading (lb/100 lb)		Loading Ratio B/A	Max. On Line (hr/100 lb)	
		Carbon A	Carbon B		A	B
Methyl ethyl ketone	72.10	7.5	13.2	1.76	683	1203
Toluene	92.14	19.6	28.8	1.47	1398	2054
<i>n</i> -Hexane	86.18	12.3	19.1	1.55	938	1456

TABLE 14.8
Comparison of Typical TSA Plants: 20 ppm Effluent Air, Adsorbent-Activated Carbon

	Inlet Concentration (ppm)	Working Capacity (wt% of bed)	Steam (kg/kg)
Methylene dichloride	10,000	17	1.4
Trichloroethylene	5,000	20	1.8
Tetrahydrofuran	5,000	9	2.3
Ethyl acetate	5,000	13	2.1
Methyl isobutyl ketone	2,000	9	3.5
<i>n</i> -Hexane	5,000	8	3.5
<i>n</i> -Heptane	5,000	6	4.3
Toluene	4,000	9	3.5

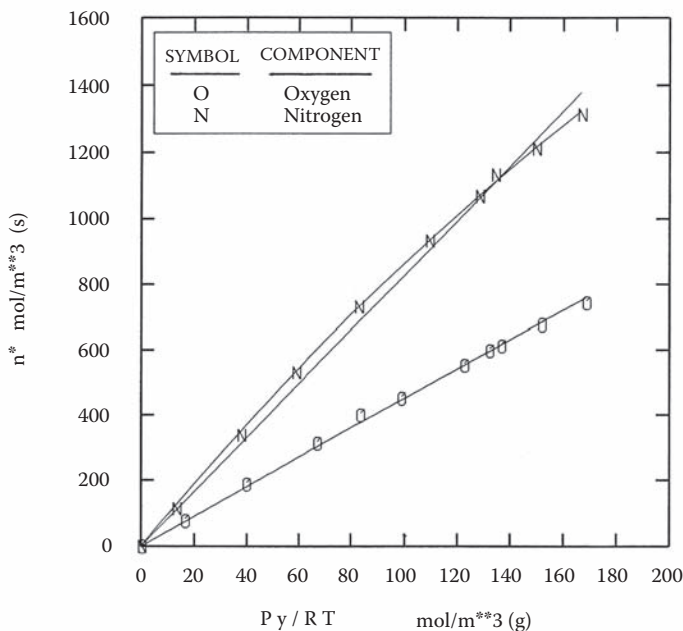


FIGURE 14.24 Isotherms of oxygen and nitrogen on zeolite 5A at 45°C.

as the fraction (or percentage) of the desired component in the product with respect to that in the feed. For example, the fractional recovery of the light component in the high-pressure product might be denoted $R_{HB} = y_{HB}\dot{Q}_{HB}/y_{FB}\dot{Q}_{FB}$, where the \dot{Q} 's represent molar flow rates. Adsorbent productivity is normally related to the space time and mass of adsorbent, as $P_{ads} = \dot{Q}_{HB}/M_{HB}m_{ads}$, where M_{HB} represents the mean molecular weight of the product, and m_{ads} is the mass of adsorbent. Occasionally, the units of productivity are expressed in terms of the volumetric ratio of flow to adsorbent rather than the mass ratio.

Common PSA cycles consist of 2 to 12 steps of a few seconds' to several minutes' duration. The most common steps are *pressurization* (with feed or purified light product), *feed* (at high pressure), *blowdown*, and *purge* (with purified product at low pressure). *Feed* involves a "wave" of the more adsorbable component moving toward the product end at high pressure. Flow stops when breakthrough is imminent and usually yields the less strongly adsorbed, or "light," product. Regeneration always occurs by *blowdown* or *depressurization*, which may be supplemented by *purging*, so it is ready for *pressurization*. Blowdown usually yields the more strongly adsorbed, or "heavy," by-product. Rinse (at high pressure) is optional, inserted after the feed step that permits adsorption of the "heavy" component, which allows the residual feed to be recovered. The heavy component can be subsequently recovered by depressurizing. Operating two beds in parallel, but 180° out of phase, generally permits continuous feeding and production.

Most cycles exploit *equilibrium selectivity* differences between species. Some exploit differences in *intraparticle diffusion rates*. These are becoming more prevalent with advances in adsorbent modification techniques. Efficient PSA cycles result from a good adsorbent, full exploitation of the input power, and careful control. The input power is exploited fully when a gas product or by-product is used to accomplish tasks as "reversibly" as possible. The shift in adsorbent loading may be 1 to 10 wt% for concentrated feeds. Generally, the energy requirements of regeneration most strongly affect overall cost.

The ratio of absolute pressures, \mathcal{P} , governs performance, since it governs performance and power consumption. Isotherm curvature, which becomes relevant as absolute pressure increases, leads to poorer performance at higher absolute pressures. Flow rates and step times are closely

be important, but it is generally simple and quick to implement. For equilibrium-based separations, the latter is in most ways adequate. For kinetics-based separations, the former is essential.

Fortunately, many applications can be predicted accurately via the simplest models. They ignore transport phenomena, mainly account for mass conservation, and are called equilibrium models. Though the concept is simple, such a model can account for a wide variety of effects, including flow, pressure, and composition variations, of course, as well as nonlinear isotherms and dispersive effects due to dead space, say, at the entrance or exit of the adsorbent bed.

The model considered here is the simplest equilibrium model that applies to many cases; it is very simple to use. The coefficients required for this model have already been introduced as β , β_A , and β_B . Furthermore, in tests conducted to date, the predictions have agreed with the detailed experimental observations. The theory usually reduces to simple performance equations that relate the operating conditions and design parameters. A fairly complete review of such models appears in the book by Ruthven et al. (1994). The model proposed by Knaebel and Hill (1985) is explained briefly here.

The inherent assumptions of this equilibrium theory are

1. Local equilibrium (i.e., at each axial location) is achieved instantaneously between the adsorbent and adsorbates.
2. The feed is a binary, ideal gas mixture.
3. Axial dispersion within and at the entrance and exit of the adsorbent bed is negligible.
4. Axial pressure gradients are negligible.
5. There are no radial velocity or composition gradients.
6. Temperature is constant.
7. One hundred percent of the adsorbent is utilized during the feed and purge steps.
8. Pressure is constant during the feed and purge steps.
9. The isotherms are linear and uncoupled.

The following individual component molar balance is similar to Equation (14.15). For a binary mixture, two equations are coupled in the gas-phase but are assumed independent in the adsorbed phase:

$$\epsilon \left(\frac{\partial P y_i}{\partial t} + \frac{\partial v P y_i}{\partial z} \right) + RT(1 - \epsilon) \frac{\partial n_i}{\partial t} = 0 \quad (14.55)$$

The general subscript i refers to component A or B . By convention, the more strongly adsorbed component is identified as component A . The linear isotherm equation gives the moles adsorbed per unit volume of adsorbent in terms of the gas-phase concentration in moles per unit open volume:

$$n_i = K'_i P y_i / RT \quad (14.56)$$

Combining Equations (14.55) and (14.56) yields

$$\frac{\partial P y_i}{\partial t} + \beta_i \frac{\partial v P y_i}{\partial z} = 0 \quad (14.57)$$

When pressure varies, and when one end is closed (e.g., during blowdown or pressurization), the overall material balance can be solved to find the interstitial velocity in the packed bed, as

$$v = \frac{-z}{\beta_B [1 + (\beta - 1) y_A]} \frac{1}{P} \frac{dP}{dt} \quad (14.58)$$

$$v_{SH} = \beta_A \frac{u_2 y_{A1} - u_1 y_{A1}}{y_{A2} - y_{A1}} \quad (14.64)$$

Propagation of this composition front or shock wave dominates the feed step and pressurization with feed.

By combining the equations for the various steps, expressions for product recovery can be obtained. Some examples are given here. The result for the light product recovery of the conventional four-step cycle is

$$R_B = (1 - \beta) \left[1 - \frac{1}{\rho y_{BF}} \right] \quad (14.65)$$

The light and heavy product recoveries from the five-step cycle including rinse are

$$R_B = 1 - \frac{1}{\rho y_{BF}} \quad (14.66)$$

$$R_A = 1 - \frac{1}{(1 - \beta) \rho y_{AF}} \quad (14.67)$$

Although many PSA applications exhibit some degradation of performance from that predicted by the equilibrium theory, only those that *rely* on differences in intraparticle diffusivities *require* detailed mathematical models. Carbon molecular sieves and special zeolitic molecular sieves have pore sizes tailored to admit compact molecules readily and to exclude marginally larger molecules. For example, splitting nitrogen from air by a carbon molecular sieve is reported to exhibit a ratio of effective diffusivities of oxygen to nitrogen of about 45. There happens to be essentially no equilibrium selectivity in that case. Similarly, for the same separation, a modified 4A zeolite exhibited an oxygen-to-nitrogen diffusion rate selectivity of about 50, but the equilibrium selectivity was about 2.0 in the reverse direction.

BIBLIOGRAPHY

- Basmadjian, D., 1997. *The Little Adsorption Book*. Boca Raton, FL: CRC Press.
- Brunauer, S., L. S. Deming, W. E. Deming, and E. Teller, 1940. On a Theory of the van der Waals Adsorption of Gases, *J. Am. Chem. Soc.* 62, 1723–1732.
- Breck, D. W., 1974. *Zeolite Molecular Sieves*. New York: John Wiley & Sons.
- Cheremisinoff, N. P. and P. N. Cheremisinoff, 1993. *Carbon Adsorption for Pollution Control*, Englewood Cliffs, NJ: Prentice Hall.
- Clark, R. M. and B. W. Lykins, 1991. *Granular Activated Carbon*. Chelsea, MI: Lewis Publishers.
- Collins, J. J., 1967. *Chem. Eng. Progress, Symp. Ser.* 63(74): 31.
- Cooney, D. O., 1999. *Adsorption Design for Wastewater Treatment*. Boca Raton, FL: CRC Press.
- Do, D. D., 1998. *Adsorption Analysis: Equilibria and Kinetics*. London: Imperial College Press.
- Dobbs, R. A. and J. M. Cohen, 1980. *Carbon Adsorption Isotherms for Toxic Organics*, EPA-600/8-80-023.
- Edwards, M. F. and J. F. Richardson, 1968. *Chem. Eng. Sci.* 23: 109.
- Ergun, S., 1952. *Chem. Eng. Prog.* 48, 89–94.
- Ganetsos, G. and P. E. Barker, eds., 1993. *Preparative and Production Scale Chromatography*, Chromatographic Sci. Ser., vol. 61. New York: Marcel Dekker.
- Gregg, S. J. and K. S. W. Sing, 1982. *Adsorption, Surface Area and Porosity*. London: Academic Press.
- Hougen, O. A. and W. R. Marshall, 1947. *Chem. Eng. Progress* 43: 197.

15.3.3.1	Proportional Action	1206
15.3.3.2	Integral Action	1206
15.3.3.3	Derivative Action	1207
15.3.4	Controller Design Issues	1208
15.3.4.1	P-Only Control	1208
15.3.4.2	PI Control	1208
15.3.4.3	PID Control	1208
15.3.5	Analysis of Typical Control Loops	1209
15.3.5.1	Flow Control Loop	1209
15.3.5.2	Level Control Loop	1210
15.3.5.3	Pressure Control Loop	1211
15.3.5.4	Temperature Control Loop	1211
15.3.5.5	Composition Control Loop	1212
15.4	PID Tuning	1213
15.4.1	Introduction	1213
15.4.2	Tuning Criteria and Performance Assessment	1213
15.4.2.1	Tuning Criteria	1213
15.4.3	Effect of Tuning Parameters on Dynamic Behavior	1214
15.4.3.1	PI Control	1214
15.4.3.2	PID Control	1216
15.4.3.3	Control Interval	1217
15.4.4	Recommended Approach to Controller Tuning	1218
15.4.5	Controller Reliability	1218
15.4.6	Selection of Tuning Criterion	1219
15.4.7	Tuning the Filter on Sensor Readings	1220
15.4.8	Fast-Response Loops	1221
15.4.9	Slow-Response Processes	1222
15.4.10	PID Tuning	1225
15.4.11	Level Controller Tuning	1225
15.5	Advanced PID Control	1227
15.5.1	Introduction	1227
15.5.2	Cascade Control	1227
15.5.3	Ratio Control	1229
15.5.4	Feedforward Control	1230
15.5.4.1	Tuning	1231
15.5.4.2	Overview	1232
15.5.5	Inferential Control	1233
15.5.5.1	Inferential Temperature Control for Distillation	1234
15.5.5.2	Inferential Reaction Conversion Control	1234
15.5.5.3	Inferential Measurement of the Molecular Weight of a Polymer	1235
15.5.5.4	Soft Sensors Based on Neural Networks	1235
15.5.6	Scheduling Controller Tuning	1236
15.5.6.1	Nonstationary Behavior	1237
15.5.7	Override/Select Control	1238
15.5.8	Computed Manipulated Variable Control	1239
15.5.9	Antiwindup Strategies	1240
15.5.10	Bumpless Transfer	1241
15.5.11	Split-Range Flow Control	1242
15.5.12	MIMO Process Control	1242
15.5.12.1	SISO Controllers and (c, y) Pairings	1242
15.5.12.2	Tuning Decentralized Controllers	1245

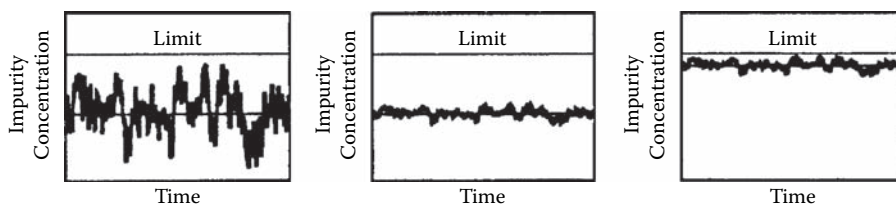


FIGURE 15.1 Comparison between impurity measurements and the upper limit on the impurity in a product for the original control system (case A), the improved control system with the original impurity setpoint (case B), and the improved control with new setpoint (case C).

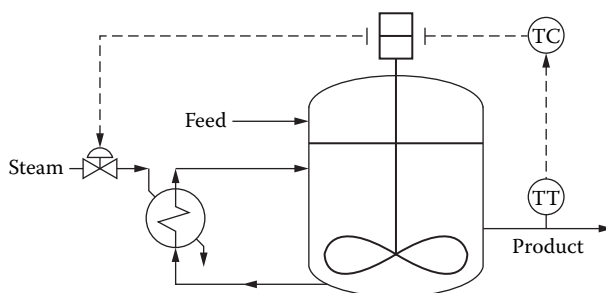


FIGURE 15.2 Schematic of an endothermic CSTR. TT = temperature sensor/transmitter, TC = temperature controller.

TABLE 15.1
Definition of Symbols for Control Diagrams

AC	– analyzer controller (i.e., composition controller)
AT	– analyzer transmitter (i.e., composition analyzer/transmitter)
DPC	– differential pressure controller
DPT	– differential pressure sensor/transmitter
HS	– high select (this element selects the larger of two or more inputs)
LC	– level controller
LS	– low select (this element selects the lower of two or more inputs)
LT	– level sensor/transmitter
PC	– pressure controller
pHC	– pH controller
pHT	– pH sensor/transmitter
PT	– pressure sensor/transmitter
RSP	– remote setpoint (i.e., the setpoint calculated by another controller)
TC	– temperature controller
TT	– temperature sensor/transmitter
⊗	– summation block (minus signs for an input compartment denote subtraction)
+	– addition function (i.e., two inputs are added to yield the output)
×	– multiplication function (i.e., two inputs are multiplied to yield the output)

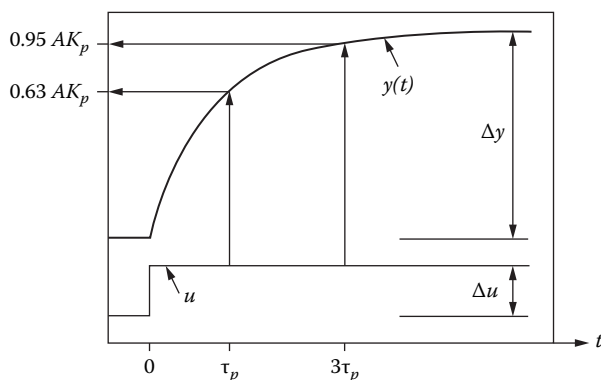


FIGURE 15.4 Dynamic response of a first-order process to a step input change.

The time constant for a well mixed vessel without chemical reaction is the volume of liquid in the vessel divided by the total volumetric feed rate, i.e., the residence time of the vessel.

Figure 15.5 shows the three general types of dynamic behavior of a second-order process, which can also be used to describe the dynamic behavior of feedback systems: overdamped, critically damped, and underdamped. Overdamped behavior is characterized by a monotonic approach to steady state. Underdamped behavior is characterized by an oscillatory approach to steady state. A critically damped response marks the boundary between overdamped and underdamped behavior.

Figure 15.6 shows the key features of an underdamped response. The rise time is the time required to first cross the final steady-state value. The response time or settling time is the time required for the response to settle to within $\pm 5\%$ of the steady-state change ($\pm 5\%$ D). The decay ratio is the ratio C/B , which indicates how fast the oscillations damp out.

Distillation, absorption, and extraction columns have a number of combined stages, which yield high-order dynamic behavior. Figure 15.7 shows the dynamic response of 3, 5, and 15 combined stages. Note that the more stages that are combined, the slower the response becomes; i.e., the process exhibits a sluggish response. For the case corresponding to 15 stages, it requires a relatively large amount of time before a significant change in the output, y , can be observed. The time after an input change before a significant change in the output variable can be observed is an indication of the process deadtime.

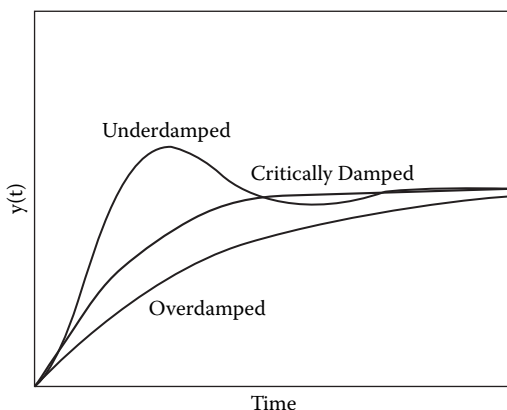


FIGURE 15.5 The three general types of dynamic behavior for a second-order process.

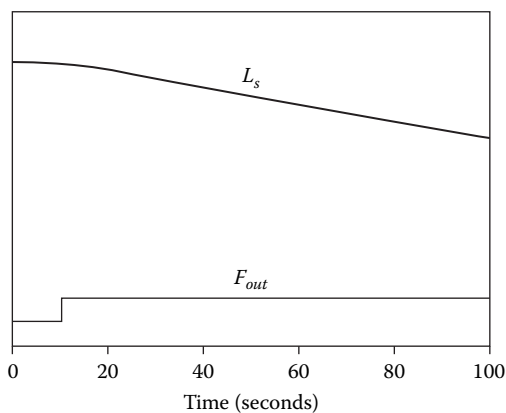


FIGURE 15.8 Dynamic response of a level in a tank to a change in the flow out of the tank.

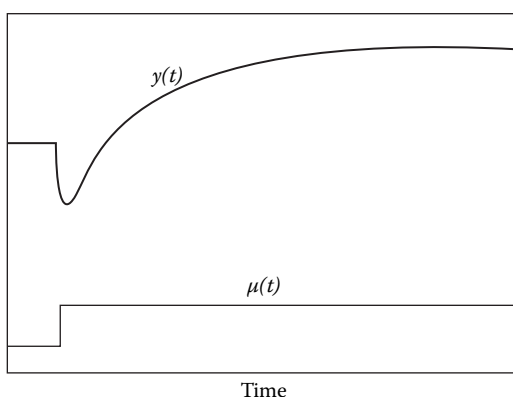


FIGURE 15.9 Dynamic response of an inverse-acting process.

state; i.e., the response time of the process is related to the time constant of the process. The deadtime indicates how soon after an input change has occurred that a noticeable change in y can be observed.

A step test (i.e., a step input change) in certain cases can be used to develop an FOPDT model. Figure 15.10 shows one such approach. First, identify the resulting change in y (i.e., Δy) and the step change in the input, Δu . Then, from the step response, identify the time required for one third of the total change in y to occur, $t_{1/3}$. Next, identify the time required for two thirds of the total change in y to occur, $t_{2/3}$. Then, the following estimates can be used:

$$\tau_p = \frac{t_{2/3} - t_{1/3}}{0.7}$$

$$\theta_p = t_{1/3} - 0.4\tau_p$$

$$K_p = \frac{\Delta y}{\Delta u}$$

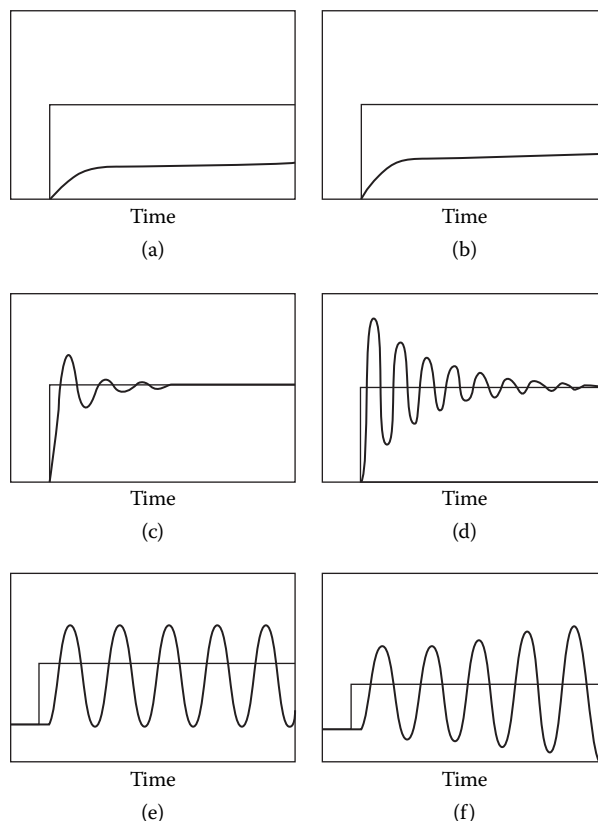


FIGURE 15.12 The general stages of dynamic behavior of a feedback system.

a small amount of feedback action is applied. As the aggressiveness of the controller is increased, the dynamic response becomes critically damped immediately before it becomes underdamped (exhibits oscillations). A further increase in the controller aggressiveness results in an increase in the rate of oscillations and a slower damping of the amplitude of the oscillations. As the controller aggressiveness is increased further, the amplitude of the oscillations eventually begins to increase, and unstable dynamic behavior results.

15.2 CONTROL LOOP HARDWARE AND TROUBLESHOOTING

15.2.1 INTRODUCTION

To apply control to a process, one measures the controlled variable and compares it to the setpoint and, based on this comparison, typically uses the actuator to make adjustments to the flow rate of the manipulated variable. The industrial practice of process control is highly dependent upon the performance of the actuator system (final control element) and the sensor system as well as the controller. If either the final control element or the sensor is not performing satisfactorily, it can drastically affect control performance regardless of controller action. Each of these systems (i.e., the actuator, sensor, and controller) is made up of several separate components; therefore, the improper design or application of these components, or an electrical or mechanical failure of one of them, can seriously affect the resulting performance of the entire control loop. The present description of these devices focuses on their control-relevant aspects. Later, troubleshooting approaches and control loop component failure modes are discussed.

erly and the thermowell is properly designed and located, the value of the analog signal corresponds closely to the temperature in the mixing tank. The thermocouple/thermowell/temperature transmitter makes up the sensor system for this process.

The 4–20 mA analog signal from the temperature transmitter is converted into a digital reading by the A/D converter. The output of the A/D converter is a digital measurement of the temperature that is used in the control calculations. The operator console shown in Figure 15.14 allows the operator or control engineer to observe the performance of the control loop and to change the setpoint, T_{sp} , and controller tuning parameters for this loop. The value of T_{sp} and the digital value of the measured mixer temperature are used by the control algorithm in the DCS (i.e., the control computer). The output from the controller is a digital signal that is converted into an analog signal by the D/A converter. The DCS, the D/A and A/D converters, and the operator consoles are typically located in a centralized control room, while the remaining equipment (i.e., the actuator and sensor system) resides in the field near the process equipment.

The analog signal from the D/A converter goes to the current-to-pressure (I/P) converter. The I/P converter uses a source of instrument air to change the air pressure applied to the control valve (3 to 15 psig). Changes of instrument air pressure change the opening of the control valve, which result in changes in the flow rate to the process. These changes in the flow rate to the process cause changes in the temperature of the mixer, which are measured by the sensor. This completes the feedback control loop. The final control element consists of the I/P converter, the instrument air system, and the control valve.

15.2.2 DISTRIBUTED CONTROL SYSTEM

15.2.2.1 Background

Based on technological breakthroughs in computers and associated systems in the 1970s, a new computer control architecture was developed and introduced by vendors in the latter part of the decade. It is based on using a number of local control units (LCUs), which have their own microprocessors and are connected together by shared communication lines (i.e., a data highway) as well as connected to operator/engineer consoles, a data acquisition system, and a general-purpose computer. This computer control architecture became known as a distributed control system (DCS) (Figure 15.15) since it involved a network with various control functions distributed for a variety of users.

The advantages of a DCS result from the use of microprocessors for the local control function. Even if a microprocessor fails, only the control loops serviced by that LCU are affected. A redundant microprocessor that performs the same calculations as the primary microprocessor (i.e., a hot backup) greatly increases the system's reliability. As a result, the probability that all the control loops will fail at the same time, or even that a major portion of the control loops will fail, is greatly reduced. In addition, the DCS is easy to expand. In comparing a DCS with electronic analog controllers, the application of conventional controls is generally equivalent, but implementing controllers is much easier and less expensive per loop using a DCS.

15.2.2.2 Structure of a DCS

A generalized schematic of a DCS is shown in Figure 15.15. A number of local control units (LCUs), which contain shared microprocessors, perform the control functions for the process in a distributed fashion. Each local control unit has several consoles attached to it. The consoles (video display units, VDUs), which utilize cathode ray tubes (CRTs), have video displays that show process schematics with current process measurements. Operators and control engineers use these displays to monitor the behavior of the process, set up control loops, and enter setpoints and tuning parameters. Normally, these consoles have touch screen capability so that, if operators want to make a change to a control loop, they touch the icon for the desired controller. Then a screen pops

time the control is executed. The time between subsequent calls to a controller applied by the DCS is called the *controller cycle time* or the *control interval*. The fastest cycle times for controller calls within a DCS are typically in the range of 0.2 s, while most loops are called only every 0.5 to 1.0 s. The regulatory control loops typically use control intervals in the range of 0.5 to 2.0 s, while supervisory control is typically applied with control intervals of 20 s up to several minutes. This controller cycle time does not present a limitation for slower control loops such as level, temperature, and composition control loops, but it does present a limitation for fast control loops such as flow controllers and some pressure controllers. A real-time control system for the DCS is used to enforce a priority ranking of control functions. That is, certain high-priority control loops are maintained at the expense of less-important loops.

Since DCSs are based on digital controller calculations, a wide variety of special control options are available in self-contained modular form. These can be easily selected by “click and drag” action on some DCSs. In this manner, complex control configurations can be conveniently assembled, interfaced, and implemented. In addition, a variety of signal-conditioning techniques can be applied to process measurements, including filtering and validity checks.

15.2.2.4 Programmable Logic Controllers

Programmable logic controllers (PLCs) are used primarily in the chemical process industries (CPI) for controlling batch processes and for sequencing of process startup and shutdown operations. PLCs are traditionally based on ladder logic, which allows the user to specify a series of discrete operations; e.g., start the flow of feed to the reactor until the level reaches a specified value, next start steam flow to the heat exchanger until the reactor temperature reaches a specified level, next start catalyst flow to the reactor, and so on. A small PLC can be responsible for monitoring 128 separate operations, while a large PLC can handle over 1000 operations. Today, the distinction between PLCs and DCSs has become less clear, as PLCs are being designed to implement conventional and advanced control algorithms, and DCSs are offered that provide control for sequenced operations. PLCs are typically attached to the data highway in a DCS (Figure 15.15) and provide sequenced control functions during startup, shutdown, and override of the normal controllers in the event of an unsafe operating condition.

15.2.2.5 Fieldbus Technology

The fieldbus approach to distributed control is shown in Figure 15.16. Control is distributed to intelligent field-mounted devices (i.e., sensors, valves, and controllers with onboard microproces-

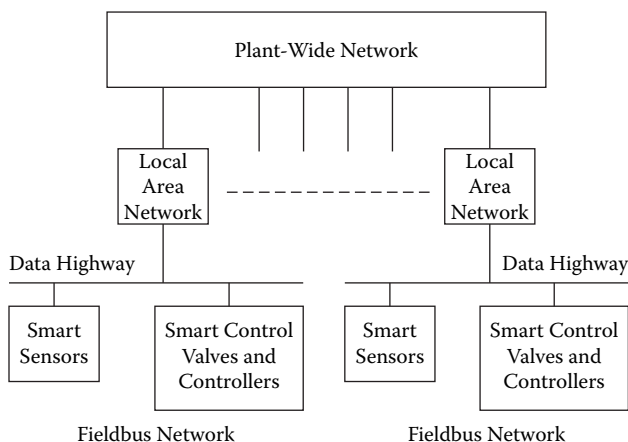


FIGURE 15.16 Schematic of the integration of the fieldbus with plant networks.

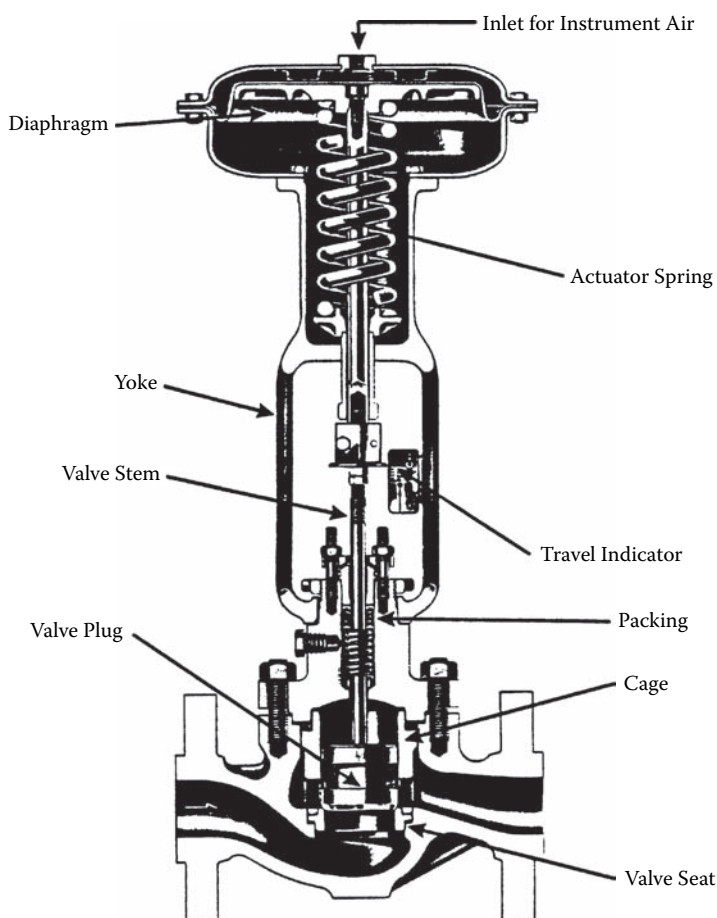


FIGURE 15.17 Cross section of a globe valve with an unbalanced plug. Courtesy of Fisher Controls.

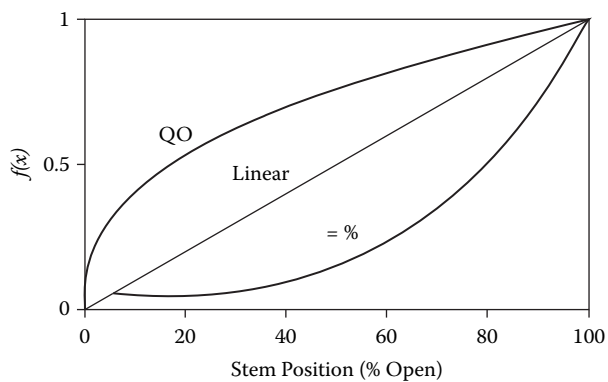


FIGURE 15.18 Inherent valve characteristics for a quick opening (QO), linear, and equal percentage valve (= %).

butterfly valves, which are generally less expensive than globe valves, are also used for flow control applications for which the line diameter is larger than 6 in. Butterfly valves have a significantly smaller range of valve position within which they perform well, compared with globe valves.

An important characteristic of a valve is the valve *deadband*, which is a measure of how precisely a control valve can control the flow rate. The deadband for a steering system on an automobile is the maximum positive and negative turn in the steering wheel that does not result in a noticeable change in direction of the automobile. For a control valve, deadband is the maximum positive or negative change, expressed in percent, in the signal to a control valve that does not produce a measurable change in the flow rate. Valve deadband is caused by the friction between the valve stem and valve packing and other forces on the valve stem. Typically, industrial control valves have a deadband of 10 to 25%. Generally, the larger and older the control valve is, the larger the deadband. A properly functioning valve with a valve positioner typically should have a deadband <0.5%.

Cavitation results when the liquid vaporizes and implodes inside the control valve. As a fluid flows through a control valve, the pressure drops sharply near the restriction between the valve plug and the valve seat because of high velocity in this region. As the fluid passes the valve restriction region and enters a region with a larger cross section, the pressure increases sharply (i.e., pressure recovery) as a result of the drop in the fluid velocity. Cavitation results in noise and vibration, reduced flow, and potentially rapid erosion of the body of the valve. It can be prevented by proper design using an increased downstream pressure.

15.2.3.2 Valve Actuators

The valve actuator provides the force necessary to move the valve stem position and alter the flow rate through the valve. The valve actuator must provide the force necessary to overcome pressure forces, flow forces, friction from the valve packing, and friction from the guide surfaces.

Figure 15.17 shows a cross section of a typical air-to-close actuator. The pressure of the instrument air acts on the diaphragm/spring system from the top, causing the valve to close as the air pressure supplied to the valve actuator is increased. An actuator with a control valve with an air-to-close valve actuator is also known as a *reverse-acting final control element*. For an air-to-open actuator, the instrument air enters below the diaphragm so that, as the air pressure is increased, the valve stem moves upward, opening the valve. An actuator with a control valve with an air-to-open valve actuator is also known as a *direct-acting final control element*. Valve actuators generally provide a fail-safe function.

15.2.3.3 I/P Transmitters

The I/P transmitter is an electromechanical device that converts the 4–20 mA signal from the controller to a 3–15 psig instrument air pressure to the valve actuator, which, in turn, affects the valve stem position.

15.2.3.4 Optional Equipment

Several devices are available for improving the overall performance of final control elements.

15.2.3.4.1 Valve Positioners

The valve positioner, which is usually contained in its own box and mounted on the side of the valve actuator, is designed to control the valve stem position at a prescribed position in spite of packing friction and other forces on the stem. The valve positioner itself is a feedback controller that compares the measured with the specified stem position and makes adjustments to the instrument air pressure to provide the proper stem position. In this case, the setpoint for the valve positioner can be a pneumatic signal coming from an I/P converter or the 4–20 mA analog signal coming directly from the controller. A valve with a deadband of 25% can provide flow rate precision

- *Accuracy* is the difference between the value of the measured variable indicated by the sensor and its true value. The true value is never known; therefore, accuracy is estimated by the difference between the sensor value and an accepted standard.
- *Repeatability* is related to the difference between sensor readings while the process conditions remain constant (see Figure 2.14).
- *Process measurement dynamics* indicate how quickly the sensor responds to changes in the value of the measured variable.
- *Calibration* involves the adjustment of the correlation between the sensor output and the predicted measurement so that the sensor reading agrees with a standard.

Smart sensors are available that have built-in microprocessor-based diagnostics. For example, smart pH sensors are available that can identify the buildup of coatings on the pH electrode surface and trigger a wash cycle to reduce the effect of the coatings. In general, smart sensors are moderately more expensive than conventional sensors, but, when they are properly selected and implemented, they can be an excellent investment in terms of greater sensor reliability and reduced maintenance. Best practice² for instrument selection, for instrument installation, and to reduce maintenance costs has been identified for the CPI.

A wide variety of sensors are available for measuring process variables.³ Choosing the proper sensor for a particular application depends on the controlled variable that is to be sensed, the properties of the process, accuracy and repeatability requirements, and costs, both initial and maintenance. The following is a coverage of the most commonly used sensors in the CPI that are used for feedback control.

15.2.4.1 Temperature Measurements

The two primary temperature-sensing devices used in the CPI are thermocouples (TCs) and resistance thermometer detectors (RTDs). Thermocouples are less expensive and more rugged than RTDs but are an order of magnitude less precise than RTDs. Typically, RTDs should be used for important temperature control points, such as on reactors and distillation columns.

15.2.4.2 Thermowells

Thermowells typically are cylindrical metal tubes that are capped on one end and protrude into a process line or vessel to bring the TC or RTD into thermal contact with the process fluid. Thermowells provide a rugged, corrosion-resistant barrier between the process fluid and the sensor that allows for removal of the sensor while the process is still in operation. Thermowells that are coated with polymer or another adhering material can significantly increase the lag associated with the temperature measurement, i.e., significantly increase the response time of the sensor.

15.2.4.3 Repeatability, Accuracy, and Dynamic Response

TCs typically have a repeatability of $\pm 1^\circ\text{C}$, whereas RTDs have a repeatability of $\pm 0.1^\circ\text{C}$. Accuracy is a much more complex issue. Errors in the temperature reading can result from heat loss along the length of the thermowell, electronic error, sensor error, error from nonlinearity, calibration errors, and other sources.⁴

The dynamic response time of a TC or RTD sensor within a thermowell can vary over a wide range and is a function of the type of process fluid (i.e., gas or liquid), the fluid velocity past the thermowell, the separation between the sensor and inside wall of the thermowell, and material filling the thermowell (e.g., air or oil). Typical well-designed applications result in time constants of 6 to 20 s for measuring the temperature of most liquids.

TABLE 15.2
Summary of Control-Relevant Aspects of Actuators and Sensors

	Time Constant (sec)	Valve Deadband or Sensor Repeatability	Turndown Ratio, Rangeability or Range
Control valve*	3–15	10–25%	9:1
Control valve w/valve positioner*	0.5–2	0.1–0.5%	9:1
Flow control loop w/valve positioner*	0.5–2	0.1–0.5%	9:1
TC w/thermowell	6–20	$\pm 1.0^{\circ}\text{C}$	–200 to 1300°C
RTD w/thermowell	6–20	$\pm 0.1^{\circ}\text{C}$	–200 to 800°C
Magnetic flow meter	<1	$\pm 0.1\%$	20:1
Vortex shedding meter	<0.1	$\pm 0.2\%$	15:1
Orifice flow meter	<0.2	$\pm 0.3\text{--}\pm 1\%$	3:1
Orifice meter w/smart transmitter	<0.2	$\pm 0.3\text{--}\pm 1\%$	10:1
Differential pressure level indicator	<1	$\pm 1\%$	9:1
Pressure sensor	<0.2	$\pm 0.1\%$	9:1

* Based on globe valves.

15.2.4.9 Transmitters

The transmitter converts the output from the sensor (i.e., a millivolt signal, a differential pressure, a displacement, and so forth) into a 4–20 mA analog signal that represents the measured value of the controlled variable. Consider a transmitter that is applied to a temperature sensor. Assume that the maximum temperature the transmitter is expected to handle is 200°C and that the minimum temperature is 50°C; then the span of the transmitter is 150°C and the zero of the transmitter is 50°C. Transmitters are typically designed with two knobs that allow for independent adjustment of the span and the zero of the transmitter. Properly functioning and implemented transmitters are so fast that they do not normally contribute to the dynamic lag of the process measurement. Modern transmitters have features that, if not applied properly, can reduce the effectiveness of the control loop. For example, excessive filtering of the measurement signal by the transmitter can add extra lag to the feedback loop, thus degrading control loop performance.

15.2.5 TROUBLESHOOTING CONTROL LOOPS

Control engineers spend a major portion of their time troubleshooting control loops. An operator may point out that a particular loop has been behaving erratically and ask the control engineer to improve its performance. The control engineer may discover that an important loop is under manual operation (open-loop operation). A final product may have excessive variability in its impurity levels, and the control engineer's job is to reduce the variability to an acceptable level. In this latter example, several control loops may require scrutiny. When one or more loops is not performing properly, troubleshooting is required to return them to the expected performance levels, or at least to identify the source of the problem. To effectively troubleshoot control loops, the control engineer must understand the proper design and expected performance of the hardware that compose a control loop.

Troubleshooting control loops involves identifying the source of the problem from an overwhelming number of possible causes. The size of this problem requires a systematic approach when troubleshooting. Control loop troubleshooting is too often treated as an afterthought and performed haphazardly. This section presents a general troubleshooting procedure as well as a detailed analysis of fault detection for the final control element, the sensor system, the control computer or DCS, and the process.

of the step change used in the block sine wave is initially small enough that consistent positive and negative changes in the measured value of the flow rate of the manipulated variable are not observed. The next block sine wave uses a larger-amplitude step change and, for this case, the measured manipulated variable can be seen to make both positive and negative changes corresponding to the positive and negative changes in the controller output. Therefore, the deadband of the actuator in this case is larger than the step size used in the first block sine wave and smaller than the one used in the second. The same block sine wave test can be used to estimate the time constant of the final control element. If the time between step changes used in the block sine wave is large enough, the settling time of the actuator can be estimated. Then, the time constant of the actuator is estimated as one quarter of the settling time.

Once the deadband and time constant of the actuator have been determined, the performance of the actuator can be assessed. The deadband for valves with positioners typically ranges from 0.1 to 0.5% of the flow rate for properly implemented systems and depends on the size of the valves, the pressure drop across the valve, the fluid properties, and other factors. The deadband for an industrial valve without a positioner typically ranges from 10 to 25%, and even higher for older valves that have not been maintained. The time constant of a properly functioning final control element is less than 2 s for a valve with a positioner or a control valve in a flow control loop. Otherwise, the actuator time constant is usually between 3 and 15 s.

If it has been determined that the actuator system is not functioning properly, one should first determine if the instrument air pressure system is operating properly. This can be done by observing that the instrument air pressure at the control valve after a step change in the signal to the final control element has been implemented in the DCS or in the control computer. If the instrument air pressure at the control valve increases sharply after the step test has been implemented, then the control valve is the source of the slow or erratic response. Another common problem is valve packing that is overtightened, which primarily increases the valve deadband. A valve that is operating below 10% or above 90% opening typically performs below standards. Another problem is an improperly tuned valve positioner. If the valve positioner is tuned too aggressively, oscillatory control performance results for the control valve, resulting in an increase in the actuator deadband. If the valve positioner is not tuned aggressively enough, the dynamic response of the actuator is slower than it should be. Table 15.3 lists a number of common problems with the components of the actuator system.

TABLE 15.3
Common Problems with the Final Control Element

- Excessive lag in the instrument air system
- Wrong type of instrument air connected to control valve. Some plants have high- and low-pressure instrument air
- Low instrument air pressure
- Wet or dirty instrument air
- Excessive deadband*
- Improperly sized control valve*
- Excessive resistance to movement of valve stem*
- Leak in diaphragm of control valve
- Debris is stuck in opening to control valve
- A plugged or obstructed instrument air line
- Plug/seat erosion in the control valve
- A bypass line open or leaking
- Flashing and cavitation
- Improperly tuned valve positioner*

* More frequently observed problems

TABLE 15.4
Commonly Encountered Problems with Components of a Sensor System

Sensor	Common Problems
Transmitter	Not calibrated correctly* Low resolution Excessive signal filtering* Slow sampling
Thermocouple/RTD	Off-calibration* Short in the electrical circuit/grounding problems Improperly located thermowell* Thermowell with excessive thermal resistance (e.g., stainless steel thermowells) Partially burned out thermocouple Interference from heat tracing
Pressure Indicators	Plugged line to pressure indicator* Confusion about absolute pressure readings, gauge pressure readings, and vacuum pressure readings Condensation in lines to pressure indicator*
Sampling System For GC	Excessive transport delay for an analyzer Sample drawn from wrong process point Plugged sample system* Sample system closed off
GC	Out of calibration Plugging in the GC column Failure of electrical components in GC Excessive noise on measurement Frozen signal Spiking due to inadequate flushing for GCs that run multiple samples
Flow Indicator	Square root compensation applied for non-differential pressure type flow indicator Square root compensation not applied for differential pressure type flow indicators Square root compensation applied twice, i.e., once in transmitter and once in DCS Orifice plate installed backwards Damaged orifice plate Plugged line to differential pressure sensor* Flashing of liquids as they flow through an orifice meter
Level Indicator	Plugged line from process to DP cell* Leak in line to DP cell or in DP cell itself Boiling of liquid in line to or from DP cell due to a steam leak in the steam tracing line Solidification of liquid in line to or from process to DP cell due to failure in steam tracing Formation of emulsions that can confound interface level measurements Leak in float type level indicators Formation of foams that can interfere with level measurements

* More frequently observed problems.

The performance of a closed-loop system can be assessed by the settling time, closed-loop deadband, and the variability of the controlled variable evaluated over an extended period of time. The settling time and the closed-loop deadband can be determined using a closed-loop block sine wave test. For a closed-loop block sine wave test, the setpoint for the control loop is applied in the form of a block sine wave, and the amplitude of the block sine wave is varied until the deadband is determined. During these tests, the settling time of the controller can also be estimated. An accurate determination of the variability of a controlled variable generally requires an extended period of operation. An evaluation of the variability based on a short period of time may not be representative of true system performance.

Consider a control system with an excessive lag (e.g., buildup of scale on the exterior of a thermowell) added to a control loop. The controller can be tuned for any tuning criterion (e.g., a decay ratio of 1/6 to critically damped); therefore, tuning a control loop to the desired tuning criterion is not, in itself, an indication of the performance of the control system. The settling time and the variability provide a measure of the performance of the control system. A process with the additional lag exhibits a longer settling time than a process without it. The average variability in the controlled variable over an extended period also shows that the system without the additional lag exhibits superior control performance. The variability is usually a direct measure of controller performance that generally can be related to the overall objectives of the process, but it requires a significant operating period (e.g., a week) to accurately determine. On the other hand, the settling time can be determined much more quickly and easily, but it provides only a relative measure of control performance. One can determine the relative change in controller performance by comparing the settling time before control loop troubleshooting was undertaken to it afterward.

The closed-loop deadband is an indication of the variability in the controlled variable that results from the combined effects of actuator deadband, sensor noise, and resolution of the A/D and D/A converters. The closed-loop settling time is an indication of the combined lags of the control loop components. The closed-loop performance assessment is a means of determining whether all the major problems within a control loop have been rectified.

Example 15.1 Troubleshooting Example

The following is a step-by-step troubleshooting process along with intermediate results for a temperature controller that was observed to result in sluggish closed-loop performance.

- Step 1. Determine the deadband of the final control element using a series of block sine wave tests. Result: the deadband of the final control element was less than 0.4%, and the dynamic response time of the final control element was 2 s; therefore, the final control element was found to be functioning properly.
- Step 2. Retune the temperature controller. Result: the controller settings did not change significantly; therefore, the controller tuning does not appear to be the problem.
- Step 3. Evaluate the sensor. Check the repeatability of the sensor by observing the temperature measurements during a steady-state or near steady-state period. Result: the repeatability was less than 0.1°C, which is good for an RTD. An independent measurement of the temperature is made and compared with the sensor reading. Result: the sensor reading is observed to have excessive lag, i.e., a dynamic response time for the sensor was estimated to be about 5 min. It was determined on further examination that there was an excessive air space between the RTD element and the surface of the thermowell. The position of the RTD in the thermowell was changed, and the dynamic lag of the sensor was found to be in the proper range. The controller was retuned, and control performance was significantly improved.

TABLE 15.6
Usual Convention for Selecting Direct- and
Reverse-Acting Controllers

Process Gain	Direct-Acting Actuator	Reverse-Acting Actuator
Positive	Use reverse-acting PID	Use direct-acting PID
Negative	Use direct-acting PID	Use reverse-acting PID

Now consider a heat exchanger in which the cooling water flow rate to the exchanger is manipulated to control the temperature of the process stream leaving it. Since an increase in cooling water flow rate to the heat exchanger results in a decrease in the controlled variable for this process, the process gain is negative. Also, consider a direct-acting final control element. Similar to the previous example, consider the case in which the controlled variable is below its setpoint. Under these conditions, a decrease in cooling water flow rate is required; therefore, a direct-acting controller should be used. Finally, if a reverse-acting final control element was substituted for the direct-acting one, a reverse-acting controller should be used. Table 15.6 summarizes these results. Obviously, these different combinations of positive and negative process gains and reverse- and direct-acting final control elements can occur in the implementation of industrial process control. As a result, the process control engineer needs a way to conveniently choose a direct-acting or a reverse-acting controller. On a modern control computer (i.e., DCS), when a control loop is set up, there is typically a box to check to select a direct- or reverse-acting controller. For analog controllers, there is a switch on the back that allows the user to select the proper form.

Another way to represent the controller gain is the proportional band (PB), which is an approach that was in more common use 10 to 15 years ago. Proportional band can be expressed (as a percent) in terms of K_c when K_c is in dimensionless form. For example, the controller output and the error from setpoint can be scaled 0 to 100%, yielding a dimensionless K_c :

$$PB = \frac{100\%}{K_c}$$

The proportional band is small when the controller gain is large, and PB is large when K_c is small.

When a setpoint change is made using the forms given by Equations (15.1) and (15.2), a spike in the calculated value of $de(t)/dt$ will occur, causing a spike in $c(t)$. This behavior is called *derivative kick* and can be eliminated by replacing $de(t)/dt$ with $-dy_s(t)/dt$, yielding

$$c(t) = c_0 - K_c \left[e(t) + \frac{1}{\tau_I} \int_0^t e(t) dt - \tau_D \frac{dy_s(t)}{dt} \right] \quad (15.3)$$

for a direct-acting controller. The derivative-on-measurement form of the PID algorithm is recommended because it is not susceptible to derivative kick.

Equation (15.3) is applied within a DCS by implementing it in a digital form using the following approximations:

$$\int_0^t e(t) dt \approx \sum_{i=1}^n e(i\Delta t) \Delta t$$

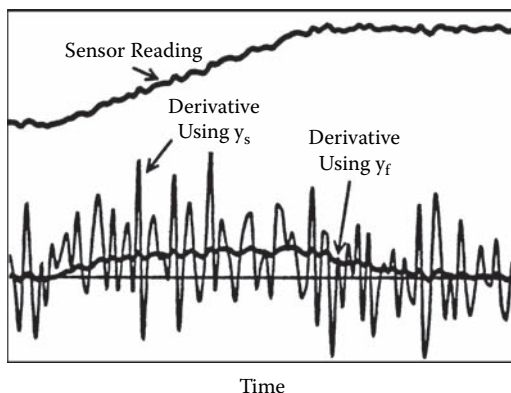


FIGURE 15.22 The instantaneous and filtered values for the derivative of a noisy sensor reading. Also shown is the value of the derivative calculated using filtered values of $y_s(t)$ with a filter factor of 0.08.

The advantage of this form of the PID controller is that it will not act as abruptly to setpoint changes as Equation (15.8). In fact, from Equation (15.8) it can be seen that only the integral action will move the process toward a new setpoint. This reduction in aggressive setpoint tracking has an effect that is similar to *bumpless transfer*, which is discussed later.

The position form of the PID algorithm calculates the absolute value of the output of the controller, whereas the velocity form calculates the change in the controller output that should be added to the current level of the controller output. The position and velocity modes are different forms of the same equation; therefore, they are generally equivalent. The velocity form is usually used industrially. In general, DCSs offer the velocity form of the PID controller in three versions: the velocity form in which P, I, and D are based on the error from setpoint [Equation (15.8)]; the form in which only P and I are based on the error from setpoint [Equation (15.6)]; and the form in which only integral action is based on the error from setpoint [Equation (15.9)].

When derivative action is applied to a process where there is significant noise on the sensor reading, erratic derivative action can result, since the difference between successive sensor readings can be dominated by the noise. Figure 15.22 shows a sensor reading with noise and the corresponding derivative value. A digital filter can be used to “smooth out” the noisy sensor reading:

$$y_f(t) = f y_s(t) + (1 - f) y_f(t - \Delta t) \quad (15.10)$$

where $y_f(t)$ is the sensor reading after a digital filter has been applied, $y_s(t)$ is the current sensor reading, and f is the filter constant, which is normally between 0.01 and 0.5. The digital filter provides a running average and tends to absorb short-term variations caused by the noise. In this manner, filtered values of the controlled variable can be used where the derivative is calculated in the PID control equation, i.e.,

$$c(t) = c_0 + K_c \left(e(t) + \frac{1}{\tau_i} \sum_{i=1}^m e(i\Delta t) \Delta t + \tau_d \frac{y_f(t) - y_f(t - \Delta t)}{\Delta t} \right) \quad (15.11)$$

When the ratio of noise to measured value of the controlled variable is large, the measured value of the controlled variable used for proportional action may also require filtering [Equation (15.11)]. Figure 15.23 shows the results of a PI controller with and without filtering on the measurement of the controlled variable. For the case without filtering, the noise on the measured

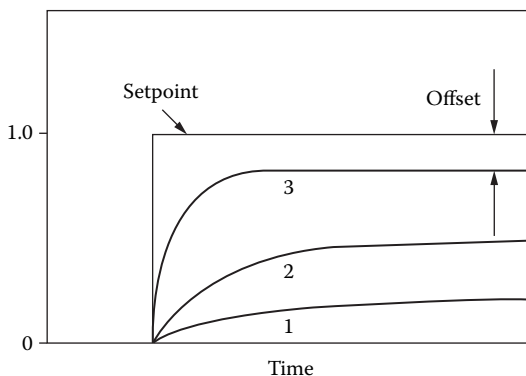


FIGURE 15.24 The effect of K_c on the response of a P-only controller for a first-order process to a setpoint change. Note that K_c is increased from 1 to 3.

noninteractive form of the PID controller. As a result, only the formulas for converting the settings from the interactive form to the noninteractive form are presented here.

15.3.3 ANALYSIS OF P, I, AND D ACTION

The results of a theoretical analysis of proportional-only, integral-only, and derivative-only controllers¹ are summarized as follows.

15.3.3.1 Proportional Action

The key characteristics of proportional action are summarized as follows:

1. In general, proportional action does not change the order of the process.
2. The closed-loop time constant is smaller than the open-loop time constant. That is, proportional action makes the closed-loop process respond faster than the open-loop process.
3. The steady-state gain is not equal to unity. Figure 15.24 shows setpoint changes for three different values of $K_c K_p$. The steady-state value differs from the setpoint value, which indicates offset. Offset is the error between the new setpoint and the new steady-state controlled variable value. Also note that as K_c increases, the offset is reduced.

Figure 15.25 shows the portion of the controller signal resulting from proportional action for a PI controller that is applying a setpoint change. The proportional control action is positive when y is below y_{sp} and negative when y is above y_{sp} ; its magnitude is directly proportional to the error from setpoint. Initially, the setpoint change causes a spike in proportional action, but as y moves toward the setpoint, the proportional action is reduced and eventually goes to zero as y settles at the setpoint.

15.3.3.2 Integral Action

The following are the fundamental characteristics of integral action:

1. All steady-state corrections for disturbances or setpoint changes must come from integral action.
2. There is no offset at steady state.

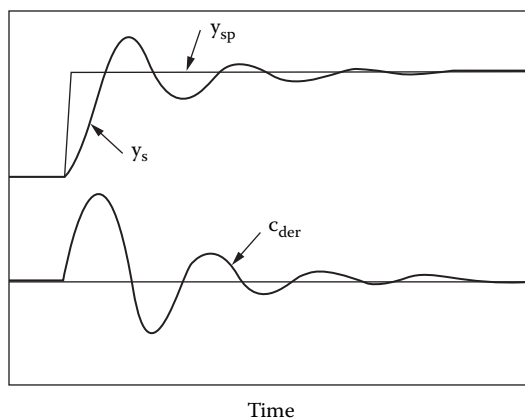


FIGURE 15.27 The portion of the manipulated variable level resulting from derivative action (c_{der}) for a setpoint change applied using a PID controller.

15.3.4 CONTROLLER DESIGN ISSUES

When choosing between P-only, PI, or PID controllers, one should consider the dynamics of the combined actuator/process/sensor system. For conventional control loops in the CPI, about 93% are PI controllers, 2% are P-only controllers, and 5% are PID controllers.² The following guidelines can be used to choose the proper controller mode based on process dynamics and control objectives.

15.3.4.1 P-Only Control

P-only control is used for processes that are not sluggish and for which some degree of offset is acceptable. A sluggish process is characterized as a process that does not respond quickly to changes in the manipulated variable (i.e., not a first-order-like response). Typical applications are level control and pressure control. Many control loops should use P-only controllers but instead use typical PI or PI with a relatively small amount of integral action, since most operators do not want offset from setpoint.

15.3.4.2 PI Control

PI controllers are used for processes that are not sluggish and for which it is necessary to have offset-free operation. Typical applications are flow control, level control, pressure control, temperature control, and composition control.

15.3.4.3 PID Control

PID controllers are useful for certain sluggish processes. Typical applications are temperature control and composition control. A sluggish process often has a tendency to cycle under PI control due to inertia; therefore, derivative action tends to reduce the tendency to cycling and allows more proportional action to be used, both of which contribute to improved control performance. A key issue here is to determine whether a process is sluggish enough to warrant a PID controller. Assume that an FOPDT model has been fit to an open-loop step test. If the resulting deadtime, θ_p , and time constant, τ_p , are such that

$$\frac{\theta_p}{\tau_p} < \frac{1}{2}$$

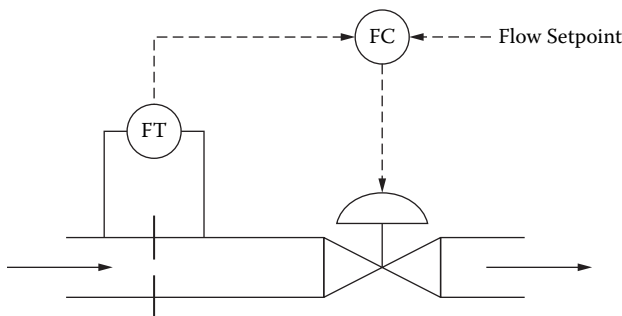


FIGURE 15.28 Schematic of a flow control loop.

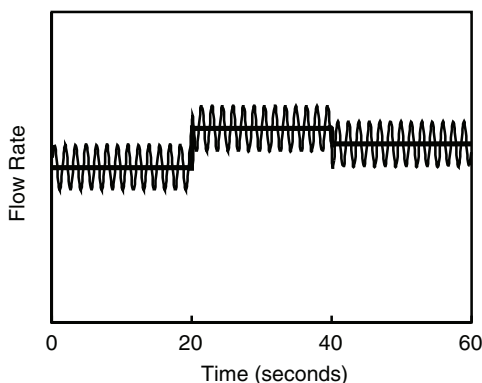


FIGURE 15.29 Measured flow rate and the specified average flow rate for a valve with a positioner. Thin line = measured flow rate, thick line = flow rate setpoint.

imprecise actuator is used. If a valve positioner is used, the valve positioner will provide the high-frequency feedback necessary to counteract the detrimental effects of the control valve deadband on the metering precision of the average flow rate. That is, the high-gain P-only controller applied by the valve positioner will open and close the valve in a manner similar to the results shown in Figure 15.29. A flow control loop applied to a control valve with a positioner will eliminate the offset that the positioner does not account for and absorb unmeasured disturbances such as changes in upstream and downstream pressures.

15.3.5.2 Level Control Loop

A schematic for a level control loop used to control the level in a tank is shown in Figure 15.30. A differential pressure sensor is used to measure the liquid level, and a flow control loop is used to control the flow rate from the tank. The output of the level controller is the setpoint for the flow controller on the line leaving the tank. Some level controllers send their outputs directly to the valve on the line, but most level controllers in the CPI are implemented as shown in Figure 15.30, using flow control loops. The objective of this loop is to maintain the level within a certain range—for example, from 30 to 40% of full level for changes in this feed rate to the tank and changes in operating conditions. On the other hand, many operators want levels controlled to specified setpoints and are not satisfied if, for example, the level is 32 or 38% when the setpoint is 35%.

The dynamics of the sensor are quite fast, and the dynamics of the flow control loop are usually fast compared with the dynamics of the process (i.e., percentage level change for change in flow

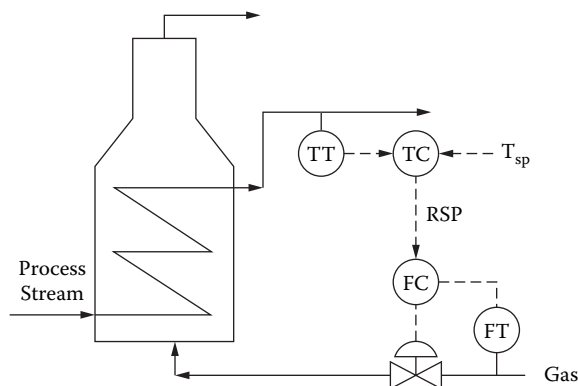


FIGURE 15.32 Schematic of a temperature controller for a gas-fired heater.

and the actuator is a flow control loop on the gas line to the heater. The objective of the temperature control loop is to maintain the temperature of the exiting process stream on setpoint in the face of changes in the temperature of the process stream entering the heater and changes in the heating value of the gas.

The dynamics of the flow control loop on the gas fuel are generally much faster than the dynamics of the process (i.e., change in outlet process temperature for a change in gas flow rate to the heater) and the sensor, which typically has a dynamic time constant between 6 and 20 s for a properly installed RTD. The process fluid entering the gas-fired heater flows by plug flow through the heat exchanger tubes that are exposed to high-temperature combusted gas. There is a thermal lag associated with changing the temperature of the metal of the heat exchanger tubes as well as transport delay caused by plug flow through the heater tubes. The transport delay and resulting overall process deadtime will increase as the feed rate of the process fluid is reduced. Since the heater is likely to behave as a sluggish process, a PID controller is generally the preferred choice in this example. Excessive sensor noise can make the use of derivative action ineffective. If this process were less sluggish, a PI controller would be preferable.

15.3.5.5 Composition Control Loop

Composition control loops are used to keep products produced by distillation columns on specification, to maintain constant conversion in a reactor, and to maintain oxygen levels in the flue gas of a boiler to eliminate carbon monoxide emissions. Figure 15.33 shows a schematic of a compo-

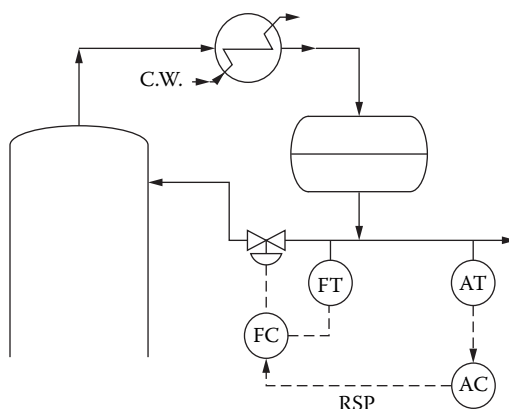


FIGURE 15.33 Schematic of a composition controller for the overhead of a distillation column.

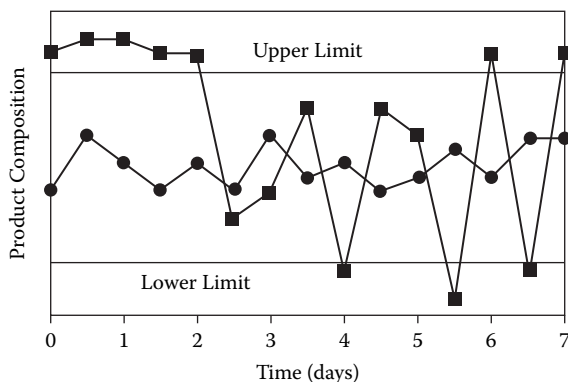


FIGURE 15.34 SPC chart based on a seven-day period of data for two different controllers on the same process.

Remember that the standard deviation is based on the error from the average value of a set of data, whereas this statistic is based on the error from setpoint.

Most companies keep statistical process control (SPC) charts that track the laboratory analysis of final products, which are typically sampled one to three times daily. Figure 15.34 is an example of an industrial SPC chart for two different controllers, for two different seven-day periods. It is easy to see which controller performed better.

15.4.3 EFFECT OF TUNING PARAMETERS ON DYNAMIC BEHAVIOR

For an open-loop overdamped process, the closed-loop dynamic behavior will go through the same stages as the controller aggressiveness is increased: overdamped, critically damped, underdamped, ringing, and unstable (see Figure 15.12). For a PID controller, controller aggressiveness is increased as K_c is increased or as τ_i is decreased.

15.4.3.1 PI Control

Figure 15.35 shows the dynamic behavior of a process for a setpoint change with different amounts of proportional action. Figure 15.35b shows the results for a PI controller tuned for quarter-amplitude damping (QAD, a decay ratio of 1/4). In addition, the QAD tuning was modified by increasing K_c (Figure 15.35c) while keeping τ_i constant and by decreasing K_c (Figure 15.35a) while keeping τ_i constant. Note that the increase in K_c resulted in ringing, while the decrease in K_c resulted in sluggish behavior. In addition, larger controller gains result in longer settling times. Figure 15.36 shows similar results for the effect of variations of τ_i . Figure 15.36b shows the results for QAD tuning and is the same result as shown in Figure 15.35b. A decrease in τ_i from QAD settings results in ringing (Figure 15.36c) and an increase results in a slow removal of offset (Figure

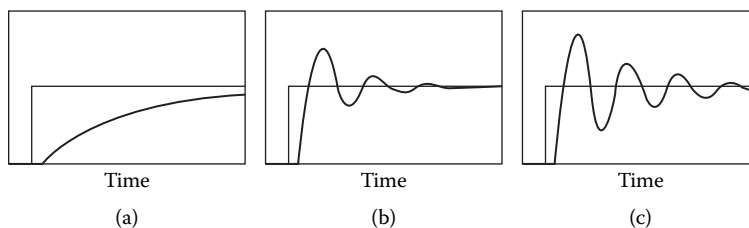


FIGURE 15.35 PI controller responses for a FOPDT process with varying amounts of proportional action. (a) K_c too low, (b) K_c tuned for QAD, (c) K_c too large.

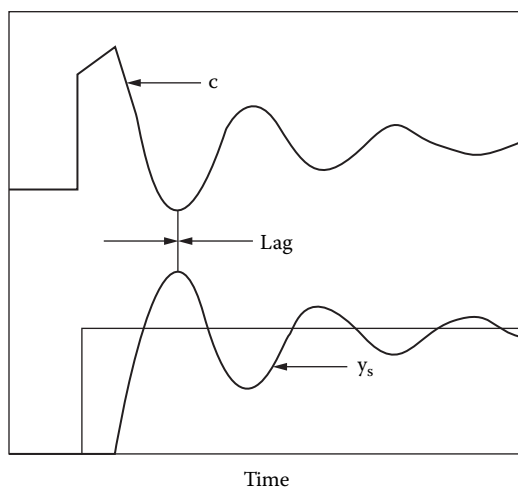


FIGURE 15.38 The lag between the controller output and controlled variables for a controller with too much proportional action.

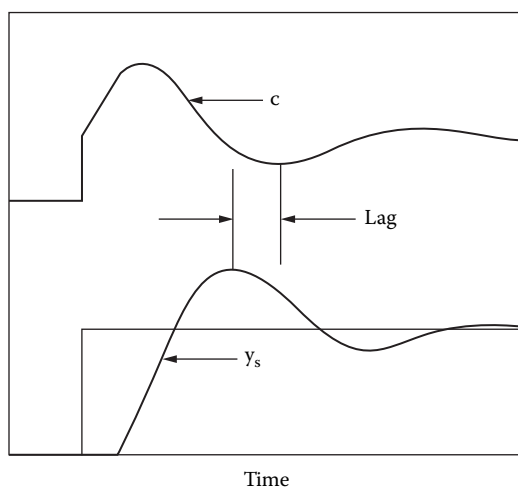


FIGURE 15.39 The lag between the controller output and controlled variable for a controller with too much integral action.

15.4.3.2 PID Control

The effect of proportional and integral action on the feedback behavior of a PID controller is similar to that observed for a PI controller. Figure 15.40a shows PID and PI control on a FOPDT process ($K_p = 1$, $\tau_p = 1$, $\theta_p = 0.1$). Figure 15.40b shows PID control and PI on another FOPDT process with more deadtime ($K_p = 1$, $\tau_p = 1$, $\theta_p = 2$). These results support the conclusion that derivative action is useful for processes that have a significant ratio of deadtime to time constant. Figure 15.41 shows a case that has too much derivative action in the PID controller. Note that the feedback response shows a “stairstep” behavior, which indicates that too much derivative action is being used. The stairstep behavior exists because, as the process moves toward the setpoint, excessive derivative action causes the process to stall or level out. When the process stalls, the proportional and integral actions act on the process to move the controlled variable toward the setpoint. When

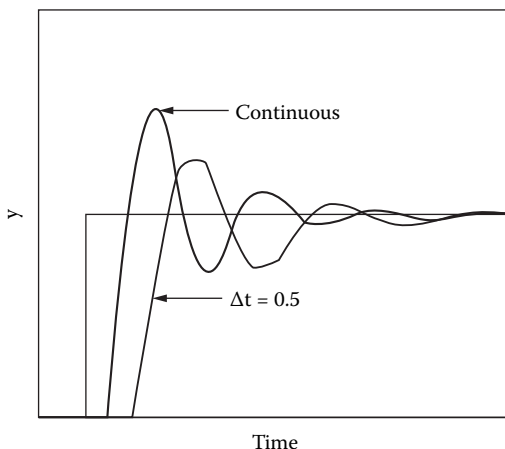


FIGURE 15.42 Comparison between a continuous PI controller and a PI controller applied each 0.5 time unit.

$$\Delta t \leq 0.05(\theta_p + \tau_p)$$

to obtain control performance approaching that of continuous control. For feedback control using an on-line GC, the control interval is set by the cycle time for the analyzer updates (typically 3 to 10 min). No advantage is gained by applying control action more frequently than the GC updates, since new information on the process response is available only when the GC updates. For sensors that provide continuous readings (e.g., temperature sensors), the maximum recommended control interval is typically equal to one sensor time constant. For level, pressure, and flow loops, sensor dynamics do not usually present a significant constraint for the choice of the control interval.

15.4.4 RECOMMENDED APPROACH TO CONTROLLER TUNING

The following procedure is recommended for tuning PID control loops:

1. Select the tuning criterion for the control loop. The tuning criterion depends on how the control loops affect the overall process objectives and can involve applying a compromise between performance and reliability.
2. Apply filtering to the sensor reading. Sensor filtering reduces the effect of sensor noise on the variability in the controlled variable but introduces lag to the feedback system, which is detrimental to control performance. Therefore, filtering should be applied carefully.
3. Determine if the control loop is a fast- or slow-responding control loop. The distinction between fast- and slow-responding control loops is concerned with the closed-loop response time of the system. If a set of controller settings can be tested using setpoint changes in a reasonable period of time (e.g., less than 10 min), the process is a fast-responding control loop. If not, it is a slow-responding control loop.
4. For fast-responding control loops, apply field tuning.
5. For slow-responding control loops, apply the ATV-based tuning procedure.

15.4.5 CONTROLLER RELIABILITY

Controller reliability has to do with whether a controller will stay in service during major upsets. Major upsets cause significant deviations from setpoint that result in variations in the process behavior for nonlinear processes, which can significantly affect the tuning performance. That is, when the inputs to a nonlinear process change, the effective gain, time constant, and deadtime can

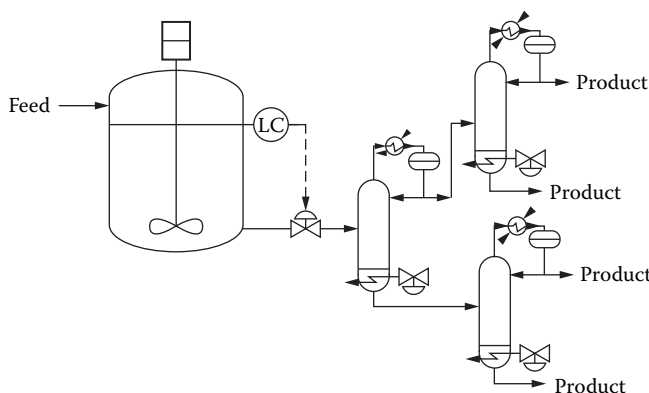


FIGURE 15.44 Schematic of a level controller that feeds a separation train.

leaving the CSTR represent major upsets for the composition controllers for the distillation columns in the separation train. Even though tight level control for the CSTR causes short-term variations in the feed to the first column, these upsets are much easier to handle than composition changes. Therefore, considering the overall process objectives, a tuning criterion corresponding to tight level control should be chosen for the level controller on the CSTR. These two examples indicate that it is important to consider how a control loop affects the overall process when selecting its tuning criterion.

If consideration of the overall process objectives does not place a limit on the aggressiveness of the tuning criterion, or if the overall process objectives dictate that minimum variability in the controlled variable of the loop in question is desirable, the selection of the tuning criterion should be based on a compromise between performance and reliability. The previous section indicates that process nonlinearity and disturbances determine the reliability of a controller. If a process is highly nonlinear and subject to large disturbances, controller reliability will likely be a problem, and a more conservative tuning criterion should be selected (e.g., a critically damped response). On the other hand, if the process is relatively linear and the disturbances are relatively mild, a more aggressive tuning criterion should be selected (e.g., a 1/6 decay ratio or 40% overshoot). Therefore, when control engineers choose a tuning criterion, they compromise between performance and reliability; they must use their knowledge of the process to evaluate the relative nonlinearity of the process and the relative degree of severity of the disturbances.

Even though QAD provides the best overall performance in terms of errors from setpoint, many companies are reluctant to have their control engineers tune even well-behaved control loops for QAD because of the 50% overshoot associated with QAD and because QAD is too close to the onset of instability. In addition, since QAD causes significant variation in the manipulated variable levels, QAD can result in unduly upsetting other parts of the process. For these reasons, it is probably better to tune well-behaved loops for decay ratios of 1/6 to 1/8. For a process that is more nonlinear with more severe disturbances, 1/10 amplitude damping or a critically damped response is more appropriate. In extreme cases, an overdamped tuning criterion may be the proper choice. No single tuning criterion works effectively for all control loops, because the process nonlinearity, disturbance type and magnitude, and operational objectives must all be considered when choosing the proper tuning criterion, and these factors change from control loop to control loop.

15.4.7 TUNING THE FILTER ON SENSOR READINGS

Sensor readings should usually be filtered to reduce the influence of sensor noise on feedback control performance. Filtering, however, adds lag to the closed-loop response. In certain cases, tuning a filter on a sensor can involve balancing the benefits of reducing the noise against the

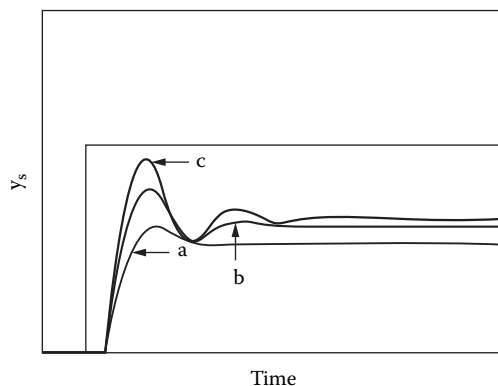


FIGURE 15.45 Selection of K_c during field tuning. (a) Results for initial value of K_c , (b) results for an increase in K_c , and (c) results for final value of K_c (1/6 decay ratio).

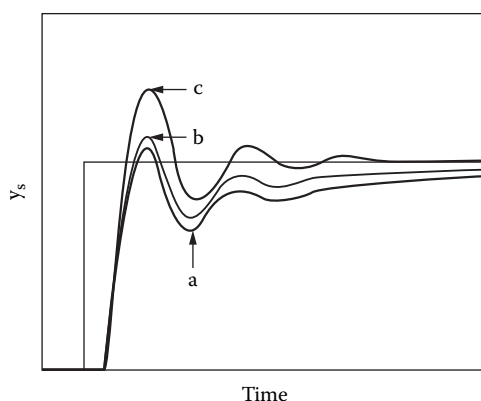


FIGURE 15.46 Selection of τ_i during field tuning. (a) Results for initial value of τ_i , (b) results for a decrease in τ_i , and (c) results for the final value of τ_i (1/6 decay ratio).

3. Using setpoint changes, increase K_c in small increments until the response meets the tuning criterion. (See Figure 15.45, which is based on a 1/6 decay ratio.) For tuning a P-only controller, the tuning procedure is completed.
4. Decrease K_c by 10%.
5. Use an initial value of τ_i , i.e., $\tau_i \cong 5\tau_p$. Estimate τ_p from process knowledge.
6. Decrease τ_i until offset is eliminated and the tuning criterion is met for setpoint changes. (See Figure 15.46, which is also based on a 1/6 decay ratio.)
7. Check to ensure that adequate levels of proportional and integral actions are being used.

15.4.9 SLOW-RESPONSE PROCESSES

For slow-response loops (e.g., certain temperature and composition control loops), field tuning can be a time-consuming procedure that leads to less than satisfactory results. Step test results can be used to generate FOPDT models, and tuning parameters can be calculated from a variety of techniques. This approach suffers from the fact that it takes approximately the open-loop response time of the process to implement a step test, and during that time, measured and unmeasured disturbances can affect the process, thus corrupting the results from the step test. In addition, it is unlikely that the selected tuning approach will result in the proper balance between reliability and

K_u and P_u can be used in one of several tuning schemes. One tuning approach is the Ziegler–Nichols (ZN) ultimate settings.³ Consider the ZN settings for a PI controller:

$$K_c^{ZN} = 0.45K_u$$

$$\tau_I^{ZN} = P_u / 1.2$$

ZN settings are fairly aggressive and can lead to ringing behavior for nonlinear processes due to the relatively small value of τ_I (i.e., large integral action).

Another tuning approach that was developed for processes that behave like an integrator plus deadtime system is the Tyreus and Luyben (TL) settings⁴:

$$K_c^{TL} = 0.31K_u$$

$$\tau_I^{TL} = P_u / 0.45$$

The TL settings are less aggressive, with considerably less integral action than the ZN settings. The TL settings are recommended for more sluggish processes that are well represented as integrator plus deadtime for a good portion of its step test (e.g., a sluggish distillation column). After the ZN or TL settings are calculated, they may require on-line tuning, particularly for the ZN settings, to meet the desired dynamic performance (e.g., 1/6 decay ratio or critically damped). For example, the ZN settings are tuned on-line as follows:

$$\begin{aligned} K_c &= K_u^{ZN} / F_T \\ \tau_I &= \tau_I^{ZN} \times F_T \end{aligned} \quad (15.13)$$

by adjusting F_T on line. Note that as F_T is increased, K_c decreases while τ_I increases by the same proportion (detuning). The tuning factor, F_T , can be adjusted to meet the performance requirements for each individual application. Therefore, on-line tuning has been reduced to a one-dimensional search for the proper level of controller aggressiveness for a PI controller. If the controller is too aggressive, F_T is increased. If the controller is too sluggish, decrease F_T .

Note that the procedure based on ATV identification with on-line tuning is applicable for tuning PI controllers. It should be pointed out that, for certain cases, after this procedure has been applied, it will be evident that the proper balance between proportional and integral action has not been used, e.g., if offset elimination is slow. In these cases, adjustments in the relative amount of proportional or integral action may be required. For example, if the TL settings were used and not enough integral action resulted, the 0.45 factor in the TL settings for integral action (i.e., $P_u/0.45$) could be increased to speed up offset elimination. Figures 15.35 and 15.36 can be helpful in determining if insufficient proportional or integral action is being used.

As an example of an ATV test, consider its application to a dynamic simulator of a C_3 (propylene/propane) splitter. Figure 15.48 shows an ATV test and an open-loop test on the same time scale for the bottom product composition control loop. Note that the four cycles of the ATV test required 6 to 8 hr, while the open-loop test required in excess of 60 hr. The ATV results were used with TL settings, and the results for three different tuning factors are shown in Figure 15.49.

Summarizing, identifying the ultimate gain and ultimate period of a slow-response loop using the ATV method is relatively fast, providing a “snapshot” of the process without unduly upsetting the system. In addition, the on-line tuning procedure provides a systematic method of selecting the proper degree of controller aggressiveness. Therefore, the ATV test with on-line tuning represents

of PI and P-only controls of level in a constant cross-section tank. He used these expressions to derive analytical expressions for the tuning parameters that result in a critically damped response for the closed-loop level control process:

$$K_c = \frac{-F'_{MAX}}{L'_{max}} \left\} P\text{-only control} \quad (15.14)$$

$$\left. \begin{aligned} K_c &= \frac{-0.736 F'_{MAX}}{L'_{max}} \\ \tau_I &= \frac{4A_c \rho}{-K_c} \end{aligned} \right\} PI \text{ control} \quad (15.15)$$

where A_c is the cross-sectional area of the tank, ρ is the density of the liquid, F'_{MAX} is the maximum expected step change in the feed rate to the tank, and L'_{MAX} is the desired level change that F'_{MAX} should cause under feedback conditions.

These tuning relations can be used for both tight level control and loose level control, depending on the selection of L'_{MAX} . If L'_{MAX} were selected to correspond to about a 2% level change, it would represent tight level control, and K_c would have a correspondingly high value. On the other hand, if L'_{MAX} were selected to correspond to a 40% level change, it would represent quite loose level control, and K_c would be correspondingly lower.

This analysis is based on an idealized model of the level of a tank and does not consider sensor or actuator dynamics and does not consider that horizontal tanks do not have a constant cross section. For these reasons, it is recommended that Equations (15.14) and (15.15) be used as initial estimates of the tuning parameters and that an on-line tuning factor, F_T , be used to tune for the desired level control performance:

$$K'_c = K_c / F_T$$

$$\tau'_I = \tau_I \times F_T$$

Example 15.2 Calculation of Initial Tuning Parameters for a Level Controller

Problem statement. Consider level control in a horizontal cylinder tank that is 6 ft in diameter and 20 ft long. Normally, the feed rate to the tank is 10,000 lb/hr of a dilute aqueous solution. Feed rate step changes are normally within the range of $\pm 10\%$ of the normal feed rate. The setpoint for the level is usually set at 20%. The pressure taps for the level indicator are located at the top and bottom of the tank. Determine the tuning parameters for a PI controller that will keep the level within $\pm 5\%$ of setpoint based on Equation (15.15) for $\pm 10\%$ feed rate changes.

Solution. By geometric analysis, the width of the liquid level in the tank at 20% full is 4.8 ft; therefore, the cross-sectional area is 96 ft². Using the density of pure water,

$$F'_{MAX} = (0.1)(10,000 \text{ lbs/h}) \left(\frac{\text{h}}{60 \text{ min}} \right) = 16.67 \text{ lbs/min}$$

$$K_c = \frac{-0.736(1000 \text{ lbs/h})}{5\%} = -147.4 \frac{\text{lbs/h}}{\%}$$

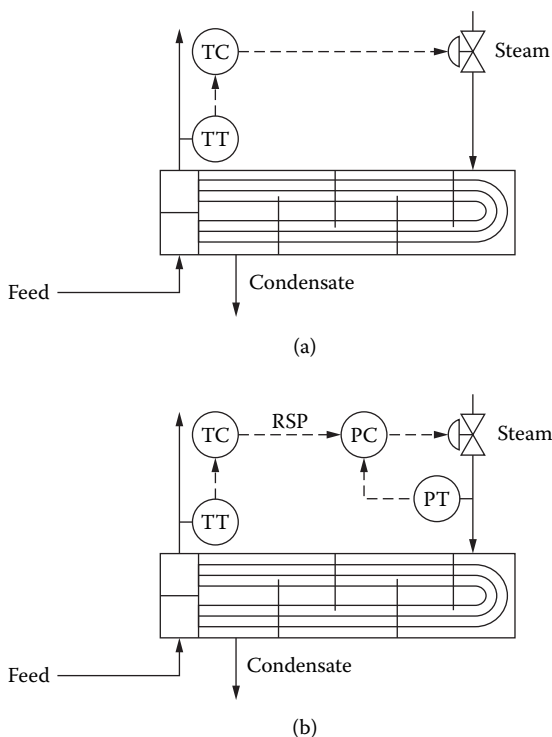


FIGURE 15.50 Schematic of a steam-heated heat exchanger with a temperature controller for controlling the temperature of the exiting process fluid. (a) Without cascade and (b) with cascade control.

feedback control using the GC can result in poor control performance, because the resulting deadtime to time constant ratio of the process is too large. For these cases, tray temperature control loops have a much smaller deadtime to time constant ratio because of the fast response of temperature sensors. Therefore, tray temperature control loops exhibit better control performance with shorter closed-loop response times than control directly off the GC. As the feed composition changes, the proper tray temperature setpoint changes. Therefore, adjustments to the setpoint for the tray temperature controllers are made by the composition control loop, which is the overall master loop for this cascade arrangement. This multiple-cascade arrangement works effectively, because the flow control loop is much faster than the temperature control loop, which is much faster than the composition control loop.

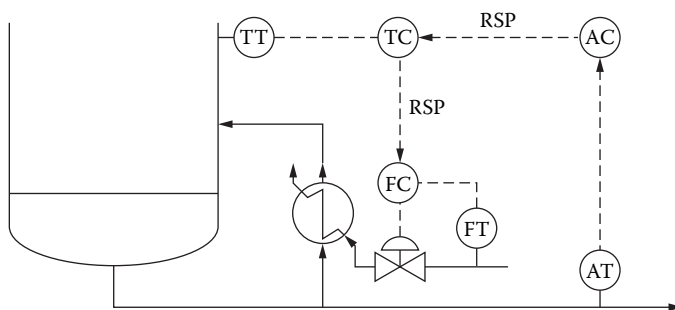


FIGURE 15.51 Schematic of a multiple-cascade configuration applied for bottoms composition control of a distillation column.

The dynamic element for this case can be simply a lag element, e.g., a digital filter described by Equation (15.10). The wastewater neutralization case (Figure 15.52) does not require dynamic compensation, since the process pH responses to feed rate changes and NaOH flow rate changes have similar dynamic behavior.

15.5.4 FEEDFORWARD CONTROL

Feedforward control can be applied to process control loops that are significantly affected by disturbances that are measurable (or estimated) on-line. A feedback controller reacts to deviations from setpoint caused by the disturbance until the process is returned to setpoint. As pointed out in Section 15.3.3, since the proportional and derivative terms are zero during steady-state operation at the setpoint, the integral term in the PID controller is responsible for long-term compensation for disturbances. A feedforward controller anticipates the effects of a measured change in a disturbance (i.e., a load change) and takes corrective action before the disturbance affects the process. In effect, the feedforward controller applies corrective manipulated variable changes corresponding to the integral action that a feedback controller would generate; therefore, when a feedback controller and feedforward controller are used together, the feedback controller has much less “work” to do to compensate for a measured disturbance.

Example 15.3 Feedforward Example

Figure 15.54a shows a feedback controller applied for the level control of a boiler drum. The feedback controller compares the measured value of the level with the setpoint for the level and adjusts the flow rate of the feedwater to the drum. Therefore, when changes in the demand for steam occur, changes in the drum level result. If large swings in steam demand occur, a large gain is required for the feedback controller to maintain the level near its setpoint. But for large controller gains, the process is more susceptible to oscillatory behavior in the level and feedwater flow rate to the drum. Also, high-gain controllers are sensitive to noisy measurements of the controlled variable, and, in this case, level indicators can have significant noise levels.

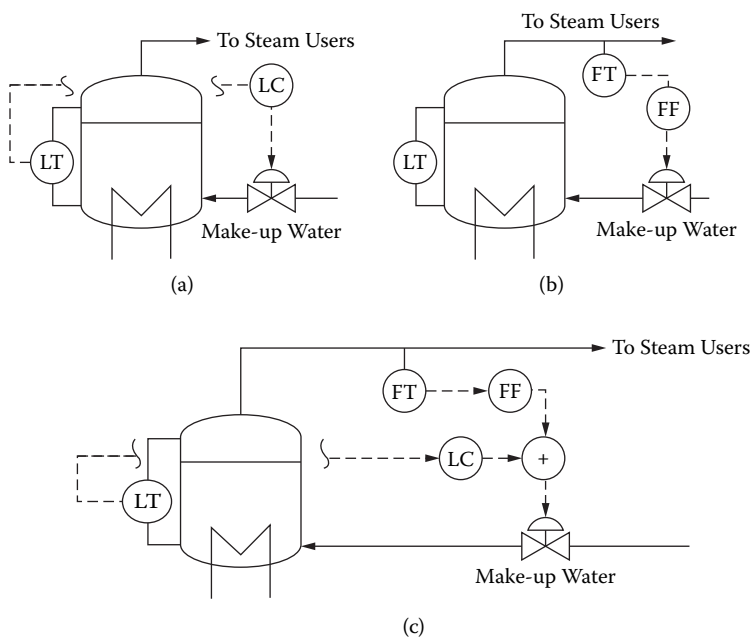


FIGURE 15.54 Boiler drum level control. (a) Feedback, (b) feedforward, and (c) feedback and feedforward combined.

the process to manipulated variable and disturbance changes) has a profound effect on the shape of the response.

15.5.4.2 Overview

Table 15.8 summarizes the advantages and disadvantages of feedforward and feedback control. Note that feedforward and feedback control are complementary, i.e., each can overcome the disadvantages of the other so that together they are superior to either method alone. Feedforward control does not offer a significant advantage for fast-responding processes, because a feedback-only controller can usually absorb disturbances efficiently for these cases. But for slow-responding processes or processes with significant deadtime, by the time a feedback-only controller starts to respond to the effects of a disturbance, the process can already be severely upset. For these cases, the disturbance can cause the controlled variable to change significantly from its setpoint, resulting in relatively large process parameter changes (K_p , τ_p , and θ_p). In some cases, this can lead to closed-loop instability. When feedforward is added to a slow process or a process with significant deadtime, the deviation of the controlled variable from setpoint can be significantly reduced, resulting in smaller process parameter changes. Therefore, feedforward can provide significantly more reliable feedback control performance when the feedforward control compensates for a major disturbance to the process. In general, feedforward is useful when (1) feedback control by itself is not satisfactory, i.e., for slow-responding processes or processes with significant deadtime, and (2) the major disturbance to a process is measured on-line.

Feedforward control provides a linear correction and therefore can provide only partial compensation to a nonlinear process. Nevertheless, feedforward control can be effective when properly implemented, since it can reduce the amount of feedback correction required. When tuning a feedforward controller for a nonlinear process, care should be taken to ensure that the feedforward controller is tuned with consideration to both increases and decreases in the disturbance level.

Figure 15.56 shows the effect of the ratio of τ_{ld}/τ_{lg} on the dynamic response of a lead/lag element. When τ_{ld}/τ_{lg} is greater than 1, overcompensation is used. That is, when the process responds faster to the disturbance than to the controller output, larger than steady-state changes in the controller output are required to compensate for dynamic mismatch. On the other hand, when τ_{ld}/τ_{lg}

TABLE 15.8
Comparison of Feedback and Feedforward Control

Advantages	Disadvantages
Feedback	
1. Does not require a measurement of the disturbance. 2. Can effectively reject disturbances for responding process. 3. Simple to implement.	1. Waits until the disturbance has affected the process before taking action. 2. Susceptible to disturbances when the process is slow or when significant deadtime is present. 3. Can lead to instability of the closed-loop system due to nonlinearity.
Feedforward	
1. Compensates for disturbances before they affect the process. 2. Can improve the reliability of the feedback controller by reducing the deviation from setpoint. 3. Offers noticeable advantages for slow processes or processes with significant deadtime.	1. Requires the measurement of the disturbance. 2. Does not compensate for unmeasured disturbances. 3. Since it is a linear-based correction, its performance deteriorates with nonlinearity.

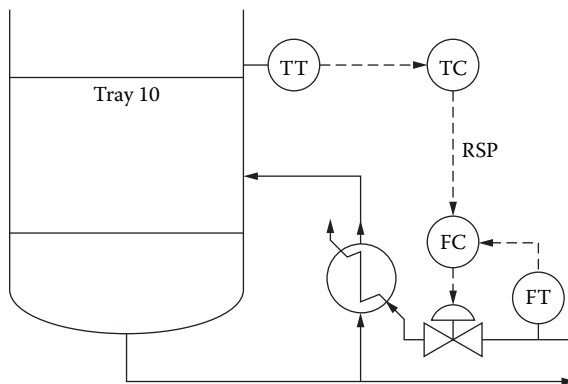


FIGURE 15.58 Schematic for inferential control of the bottoms product composition of a distillation column.

be used as the value of the controlled variable in a feedback control loop, greatly reducing the associated measurement delay.

There are three main reasons for using inferential measurement of a controlled variable: (1) Excessive analyzer deadtime undermines the performance of the feedback loop. (2) The total cost (i.e., the purchase price and maintenance cost) of an on-line analyzer can be excessive. Since inferential measurements are typically based on temperature, pressure, and flow measurements, they are much less expensive to install and maintain. (3) An on-line analyzer may not be available. In that case, an inferential measurement may be the only option for feedback control.

For an inferential control to be effective, the inferential measurement must correlate strongly with the controlled variable value, and this correlation should be relatively insensitive to unmeasured disturbances. The following are several examples that illustrate how inferential measurements can be effectively applied in the CPI.

15.5.5.1 Inferential Temperature Control for Distillation

Tray temperatures correlate very well with product compositions for many distillation columns; therefore, inferential control of distillation product composition is a widely used form of inferential control. Figure 15.58 shows the arrangement for inferential temperature control of the bottoms product composition for this column. Note that the tray temperature controller is cascaded to a flow controller.

15.5.5.2 Inferential Reaction Conversion Control

Consider an adiabatic fixed-bed reactor. For a single irreversible reaction, $A \rightarrow B$, the macroscopic energy balance assuming no phase change is given by

$$X_A C_{A_{in}} (-\Delta H_{rxn}) = \rho C_P (T_{out} - T_{in})$$

where X_A is the fractional conversion of reactant A, $C_{A_{in}}$ is the inlet concentration of A to the reactor, ΔH_{rxn} is the heat of reaction, ρ is the average density of the process stream, C_P is the average heat capacity of the process stream, T_{out} is the temperature of the outlet stream from the reactor, and T_{in} is the temperature of the inlet stream to the reactor. Rearranging the previous equation,

$$X_A = \frac{\rho C_P}{C_{A_{in}} (-\Delta H_{rxn})} (T_{out} - T_{in})$$

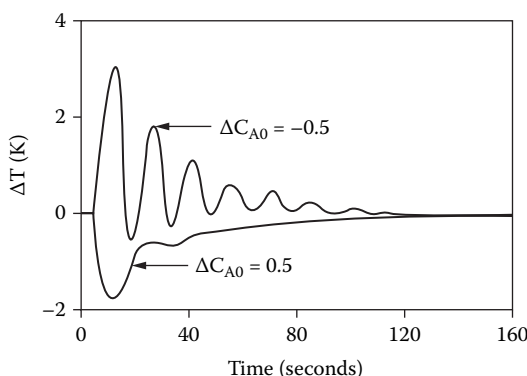


FIGURE 15.60 The effect of feed composition upsets on the PI feedback behavior for an endothermic CSTR.

Occasionally, the NO_x analyzers on a boiler fail. If the NO_x level is not measured, the power companies must pay a fine for emissions. Instead of installing additional on-line NO_x analyzers, which are quite expensive, some power companies have applied a type of inferential estimator to predict the NO_x level in their flue gas.

Instead of using one or two process measurements, all the measured process conditions (e.g., fuel feed rate, oxygen in the flue gas, heating value of the fuel, ambient air temperature, and so on) have been empirically correlated to predict the NO_x concentration in the flue gas. The empirical correlation is based on training an artificial neural network to predict the flue gas NO_x concentration from all the available data.

15.5.6 SCHEDULING CONTROLLER TUNING

In Section 15.4.5, it was demonstrated that nonlinear process behavior can result in a controller becoming unstable in certain situations; in others, it can become extremely sluggish (see Figure 15.60). Tuning PID controllers for the case with the largest process gain can eliminate unstable operation, but at the expense of largely sluggish performance. For some processes, certain measurements directly indicate whether the process parameters have increased or decreased and by how much; therefore, scheduling of the controller tuning based on process measurements can often compensate for process nonlinearity. The controlled variable and the feed rate are examples of such key process measurements that typically can be used to schedule the controller tuning.

Consider a heat exchanger used to heat a process stream with steam as the heating medium. As the feed to the heat exchanger flows through the tube bundle, it is heated by steam condensing on the shell side. As the feed rate changes, the residence time of the feed in the tubes exposed to the steam changes. Figure 15.61 shows the open-loop responses for three different feed rates for a step change in the setpoint of the steam pressure controller. The feed rate is represented by the average fluid velocity (v) in the tubes. Both the gain and the dynamic response change as the feed rate is changed. Table 15.9 lists the FOPDT parameters for each flow rate. Note that the gain and the deadtime each change by a factor of about 2.5. Using these FOPDT parameters, the controller settings for each flow rate are also listed in Table 15.9. Note that the controller gain changes by a factor of 5, but the reset time changes are more gradual. It is clear from these results that it is not reasonable to expect one set of PI controller settings to work effectively for significant changes in the feed rate to this heat exchanger. For example, if the temperature controller for the outlet of the heat exchanger were tuned for $v = 7$ ft/s, when the feed rate is reduced to $v = 4$ ft/s, the controller becomes unstable. Conversely, if the controller were tuned for the low flow rate condition, it would perform sluggishly for the high flow rate conditions. Figure 15.62 shows results with and without scheduling of the controller tuning based on feed rate for a step decrease in the feed rate corre-

examples of nonstationary behavior that results in much more gradual process gain changes. The following are several examples of such behavior in the CPI: (1) catalyst deactivation, (2) heat exchanger fouling, (3) fouling of trays in a distillation column, and (4) feed composition changes that affect the process parameters (K_p , τ_p , and θ_p).

These effects can be large enough that controller retuning is required. If an overall tuning factor, F_T , has been used, one can adjust F_T in a straightforward manner to compensate for the nonstationary behavior. Control methods that adjust controller tuning to adapt to nonstationary behavior are referred to as *adaptive control techniques*. Adaptive control techniques can be effectively applied for processes that vary slowly. A number of commercially available adaptive controllers are referred to as *self-tuning controllers* and can usually be installed on a DCS. While a range of approaches are used for self-tuning controllers, they are generally limited to processes that vary in a gradual, consistent manner.

15.5.7 OVERRIDE/SELECT CONTROL

Constraints are a natural part of industrial process control. As processes are pushed to produce as much product as possible, process limits are inevitably encountered. When an upper or lower limit on a manipulated variable is encountered, or when an upper or lower value of a controlled or output variable from the process is reached, it can become necessary to apply different control loops from those previously used. That is, effective industrial controller implementation requires that safeguards be installed to prevent the process from violating safety, environmental, or economic constraints. These constraints can be met using override/select controls.

Consider the furnace-fired heater shown in Figure 15.63. Under normal operating conditions, the fuel flow rate is adjusted to control the exit temperature of the process fluid. As the feed rate of the process fluid is increased, the furnace tube temperature increases. At some point, the upper limit on furnace tube temperature (an operational constraint) is encountered. The fuel flow rate to the furnace must be adjusted to keep the furnace tube temperature from exceeding its upper limit, at which point damage to the furnace tubes results. Figure 15.63 shows that the output of both control loops (the temperature controller on the process fluid and the temperature controller on the furnace tube temperature) are combined, and the lower fuel feed rate is actually applied. The “LS” symbol in Figure 15.63 is called a *low select* and indicates that the lower fuel feed rate is chosen. When the feed rate is sufficiently low that the temperature of the process fluid can be controlled

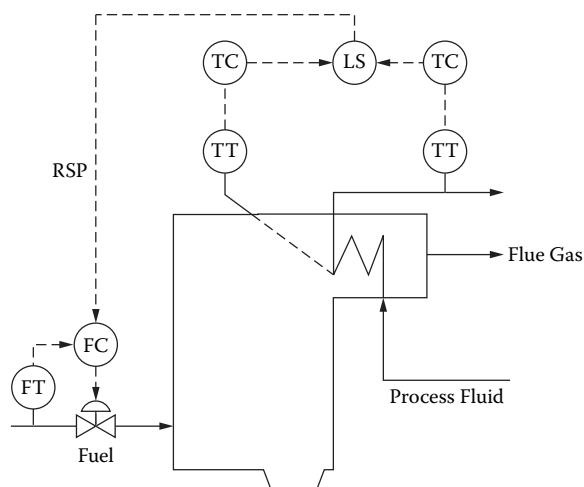


FIGURE 15.63 A schematic of a furnace-fired heater with low select firing controls.

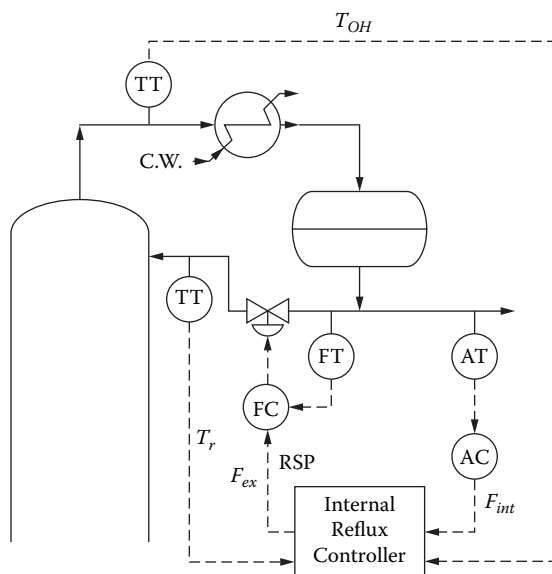


FIGURE 15.65 Schematic of an internal reflux controller applied for composition control of the overhead of a column.

This approach, called *internal reflux control*, is shown schematically in Figure 15.65. Note that the composition controller outputs the internal reflux flow rate, and the internal reflux controller calculates the external reflux flow rate, which is used as the setpoint for the flow controller on the reflux.

15.5.9 ANTIWINDUP STRATEGIES

Figure 5.17a shows the manipulated and controlled variables for a standard PI controller for which the manipulated variable reaches its upper limit, i.e., the control valve is fully open or fully closed, which is referred to as a *saturated control valve*. This can occur when a large disturbance enters the process. Since the manipulated variable cannot be increased further, the PI controller is unable to return the controlled variable to its setpoint. As long as there is an error between the controlled variable and its setpoint, the integral term in the PI controller [Equation (15.1)] continues to accumulate, which is referred to as *reset windup* or *integral windup*. After some time, the disturbance level returns to its original value. At this point, integral windup in the PI controller keeps the manipulated variable at its maximum level, even though the value of the controlled variable is now above its setpoint. In effect, before the process can return to steady state, an equal area above the setpoint must be generated to compensate for area “A” shown in Figure 5.66a.

This behavior occurs because the integral is allowed to continue accumulating after control of the process has been lost (i.e., the manipulated variable saturates). Figure 5.66b shows the same case as Figure 5.66a except that, when the manipulated variable saturates, the integral is not allowed to accumulate (windup). Note that when control returns to the process (i.e., when the manipulated variable is no longer saturated), the controlled variable moves directly back to its setpoint and does not exhibit prolonged deviations from setpoint as before. Because the integral action was turned off when the manipulated variable became saturated, the PI controller does not have to generate an area equivalent to area “A” above the setpoint.

Antireset windup can be implemented by simply not allowing the integral to accumulate when the manipulated variable is saturated. The manipulated variable is saturated when the control valve on the line supplying the manipulated variable is either closed or fully open. A saturated control valve can be identified when there is sustained offset between the manipulated variable level

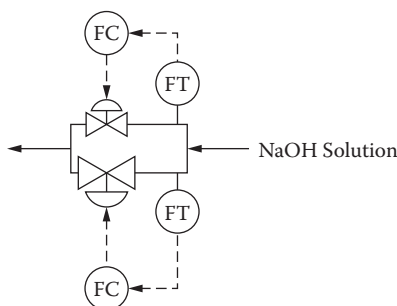


FIGURE 15.68 Schematic of a split-range flow controller.

is set equal to the current controlled variable value; therefore, there is no change in the manipulated variable level. After this, the internal setpoint is ramped toward the true setpoint, and the process gradually begins moving toward the true setpoint. After the internal setpoint reaches the true setpoint value, it remains constant. By selecting a proper setpoint ramping rate, smooth and consistent startups for control loops result.

15.5.11 SPLIT-RANGE FLOW CONTROL

Consider a wastewater neutralization process with a titration curve for the wastewater that exhibits a high gain at neutrality. To control the pH to ± 1.0 pH units at a setpoint of pH 7, the base flow rate must be metered accurately to within $\pm 0.5\%$. A single-flow control loop with a control valve with a positioner can meet this metering precision. But if the total flow rate of base were to range from 0.1 to 10 GPM, one flow control loop could not meter the base flow rate to within $\pm 0.5\%$ at both 0.1 and 10 GPM.

Two flow control loops that work together can meet this requirement, as shown in Figure 15.68. At low flow rates, the large control valve is closed, and the flow control loop with the smaller control valve can accurately meter the low-flow operation. As the total flow increases, the smaller control valve begins to approach saturation. Before this happens, the flow control loop with the larger control valve comes into service. At large flow rates (>1 GPM), the small control valve is completely open, and the flow control loop with the larger valve is accurately metering the base flow rate. This is an example of split-range flow control, which is used when accurate flow control is required over a wider operating range than one control valve can provide.

15.5.12 MIMO PROCESS CONTROL

A multiple-input/multiple-output (MIMO) process has two or more inputs and two or more outputs. A two-input/two-output system is shown schematically in Figure 15.69. Note that both c_1 and c_2 affect both y_1 and y_2 . When both inputs affect both outputs, the process is referred to as a *coupled process*. MIMO processes are frequently encountered in the chemical processing industries.

This section considers the application of PID controllers to coupled MIMO processes. A key issue when applying PID controllers to MIMO systems is deciding which manipulated variable should be used to control which controlled variable. This is referred to as choosing the manipulated/controlled variable pairings [(c , y) pairings] or the control configuration. The factors that affect the choice of (c , y) pairings are analyzed here.

15.5.12.1 SISO Controllers and (c , y) Pairings

Figure 15.70 shows two single-loop PID controllers applied to a two-input/two-output process (2×2 system). Applying single-loop PID controllers to a MIMO process is called *decentralized*

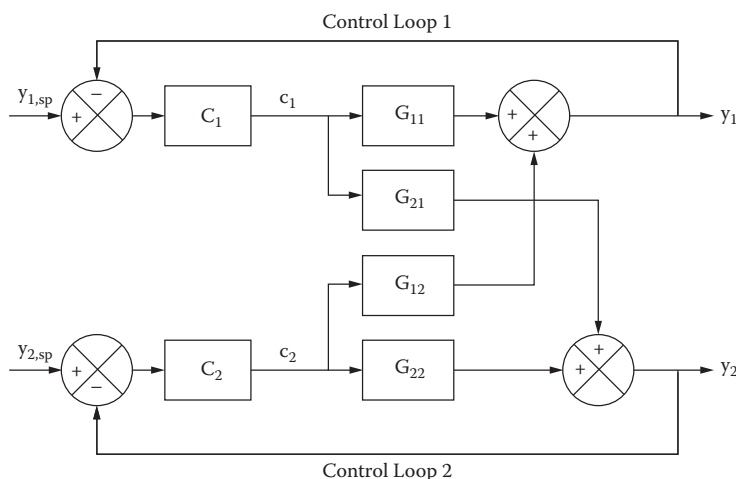


FIGURE 15.71 A block diagram of a 2×2 process with single-loop controllers showing the coupling effect of loop 2 on y_1 for changes in c_1 . Note that C represents a controller and P represents an input/output function.

Example 15.4 Configuration Selection for a C_3 Splitter

Problem statement. Evaluate the configuration selection problem for a C_3 splitter. A C_3 splitter separates a feed mixture primarily composed of propane and propylene into polymer-grade propylene ($<0.5\%$ propane) and a fuel-grade propane (approximately 2% propylene).

Solution. The nomenclature used here refers to a particular configuration as (c_1c_2) , where c_1 is assumed to be the controller output that is used to control the overhead composition, and c_2 is the controller output that is used to control the bottoms composition. If we limit ourselves to controlling the overhead composition with L , D , or L/D (the reflux ratio) and the bottoms composition with V , B , or V/B (the boilup ratio), there are a total of nine possible configurations. Here we limit the discussion to the following configurations: (L, B) , (L, V) , $(L/D, V/B)$, and (D, V) .

The steady-state RGAs for each of these configurations are listed below:

Configuration	RGA ¹ (λ_{11})
(L, B)	0.94
(L, V)	25.3
$(L/D, V/B)$	1.70
(D, V)	0.06

Based on these results, the (L, B) and $(L/D, V/B)$ configurations appear to be the most promising.

The dynamics of distillation columns can be understood by recognizing that product composition changes result from changes in the internal vapor/liquid traffic in the column. On the other hand, changes in B and D must depend on the level controllers to change the vapor/liquid traffic of the column; therefore, the dynamic response of the product compositions is significantly slower when B and D are changed, compared with changing L and V . The dynamic response to changes in L/D and V/B are intermediate between L and V on the fast side and B and D on the slow side. Based on this analysis, (L, B) is expected to perform better for the overhead composition control than for the bottoms, but there is no clear winner between the (L, B) and the $(L/D, V/B)$ configurations with regard to the overall dynamic response.

Table 15.10 shows the relative changes in each manipulated variable for a change in feed composition. This table is based on steady-state results in which the product compositions are maintained at a constant level. A lower relative change for a manipulated variable indicates a reduced sensitivity to feed composition changes for that manipulated variable. Note that L , L/D ,

a decentralized controller is to apply ATV tests for each manipulated variable/controlled variable pair. While an ATV test is applied to one loop, the other loops should be maintained in an open-loop condition.

Next, determine if any of the loops are significantly faster responding than the other loops. This can be done by comparing the values of the ultimate periods, P_u , obtained in the ATV tests. If the smallest value of P_u is at least five smaller than the next larger P_u , that loop alone should be implemented first, before tuning the other loops. It can be tuned as a single PID loop as discussed in Chapter 3. Next, ATV tests on the remaining loops should be rerun with the tuned fast loop in service (closed-loop operation). Then, the remaining control loops can be tuned using the following procedure.

Assume that it is required to tune PI controllers on a 2×2 MIMO process. The ATV results are used to select the controller gain and reset time based on, for example, Zeigler–Nichols tuning. Then, a single tuning factor, F_T , is applied to the tuning parameters for both control loops:

$$\left. \begin{aligned} K_c &= K_c^{ZN} / F_T \\ \tau_I &= \tau_I^{ZN} \times F_T \end{aligned} \right\} \text{First control loop}$$

$$\left. \begin{aligned} K_c &= K_c^{ZN} / F_T \\ \tau_I &= \tau_I^{ZN} \times F_T \end{aligned} \right\} \text{Second control loop}$$

F_T is adjusted until the proper dynamic response is obtained. While tuning, if the closed-loop response is sluggish, decrease the value of F_T . Likewise, if the controller exhibits periods of ringing, increase the value of F_T .

After F_T has been adjusted to tune the set of decentralized PI controllers, fine tuning of the controller settings should be used. For example, if one observes that one of the control loops is slow to settle at setpoint in a manner similar to Figure 15.3a, an increase in integral action for that loop should be tested. If one of the loops exhibits ringing, derivative action should be tested to determine if it improves the feedback control performance of that loop. In the latter case, derivative action should be tuned in the manner that was described in Section 15.3.

15.6 MODEL PREDICTIVE CONTROL

This section covers model predictive control (MPC). It describes what it is, how to design it, how to install it, and how to make it work. This work is both fun and useful, but there is one rule: *Understand the process*. This section contains tips and clues about how to analyze and learn process behavior.

15.6.1 WHAT IS MPC?

There are many ways to control plant operations. Among these are the following.

Batch control is used to produce batches of material to specification. For example, certain polymer reactors fall into this category.

Programmable logic controllers (PLCs) are typically used to control very high-frequency equipment such as steel mill rolls or compressors.

PID (the old standby of continuous control) is largely dedicated to controlling a single variable, such as flow in a pipe.

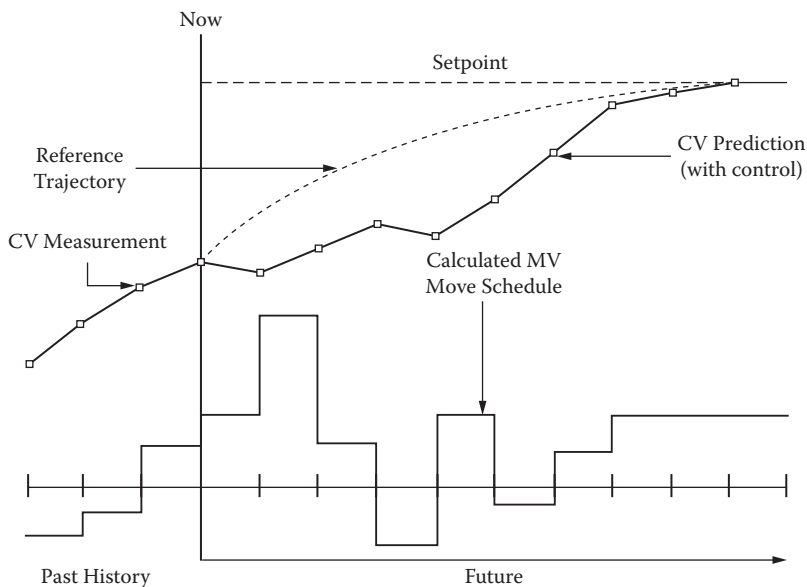


FIGURE 15.72 Representation of CV prediction and scheduled MV moves at each calculation step for MPC.

15.6.2 HISTORY OF MPC

Industrial model predictive control (MPC) is based on algorithms that were developed many years ago. They share several common traits:

- They are based on discrete linear dynamic models.

- The algorithm for identifying linear dynamic models is derived from plant data.

- The algorithm for calculating on-line control actions is based on plant models.

They have been refined and applied successfully over the past 40 years. Currently, DMC is the predominant industrial MPC.

15.6.3 WHEN SHOULD MPC BE USED?

Because MPC requires significant investments in software and time, it is best to observe certain considerations:

- There is significant economic payout. A typical MPC takes about a man-year to build.

- Software costs are typically about one third of the investment in engineering time.

- The process is interactive. This means that a single MV affects more than one CV.

- There are significant process constraints.

- The plant must have suitable infrastructure, particularly skilled engineers and operators, as well as modern and well-maintained instrumentation.

- All of the necessary final control elements must exist and be able to work properly.

One should not to use MPC if

- The problem is easily solved with one or two PID controllers or other standard control blocks. This happens when the process is naturally decoupled, i.e., either there are few

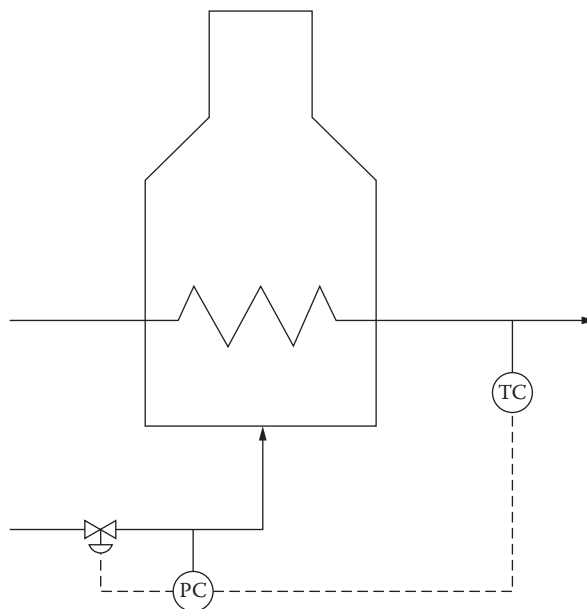


FIGURE 15.73 Fired heater outlet temperature control in the DCS.

15.6.4.1.2 Regulatory Control Strategy

Early in the project, learn which variables to keep in cascade, automatic, or manual modes. This is commonly referred to as the *state of the plant*. Normally, you want the PID loops to do as much work as possible, allowing the MPC to focus on higher-level functions.

The following are situations in which you probably want to leave the PID loops closed:

- Fired heater outlet temperature control
- Drum level control (see exceptions later)
- Controls on rotating equipment
- Properly functioning distillation tower temperature controls

The fired heater in Figure 15.73 shows the outlet temperature in the DCS. One reason for leaving this loop closed is that disturbances in these systems are usually very high in frequency and are rejected well by simple PID loops in the DCS.

Situations in which you may want to break the PID loops in the DCS, taking them out of cascade, or possibly putting them in manual, include the following:

- Distillation columns with temperature controllers on both overhead and bottom
- Process lines with two control valves in series (e.g., flow/level or flow/flow)
- Loops with very long dynamics (e.g., composition loop with an hour or more of deadtime)

Consider a distillation column that has a temperature controller on the overhead and one on the bottom as well. Usually, this configuration leads to instability, variable saturation, or both. The best solution is to break one of the temperature loops (put in manual) in the DCS before beginning the plant test. Leave the one closed at the end of the column, where composition matters the most.

In general, think very carefully about the state of the plant before doing plant tests. If you choose incorrectly, you can always repeat the tests, but this will cost you many weeks of engineering time and a loss of credibility with the plant operators.

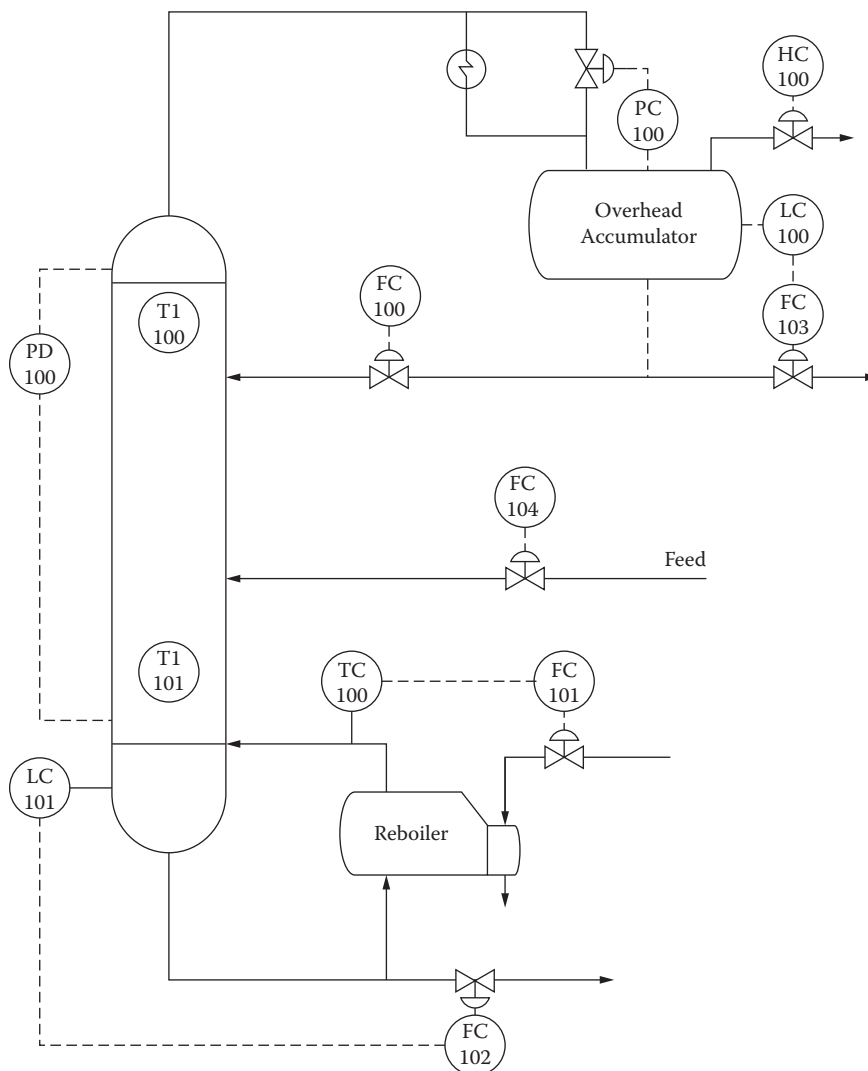


FIGURE 15.74 A distillation column with temperature control on the reboiler return.

as soon as a problem occurs in the plant, you will be blamed because you are doing something new. Be prepared, and don't let that happen.

For example, assume that you want to perform tests on the plant, represented by Figure 15.74. The plant is a simple distillation column with overhead accumulator pressure controlled by moving the hot vapor bypass, bottoms level maintained by bottoms product draw rate, and the overhead accumulator level controlled by adjusting the overhead product draw rate. Reflux is on flow control, and the reboiler is on temperature control. Typical move sizes for this plant are shown in Table 15.12.

15.6.4.2.1 Designing a Good Input Waveform

There are many ways to make moves to independent variables during a plant test. The most practical approach is as follows:

Use a series of step changes in a single variable.

Move only one independent variable at a time. If you move more, the resulting test data often become difficult to analyze visually.

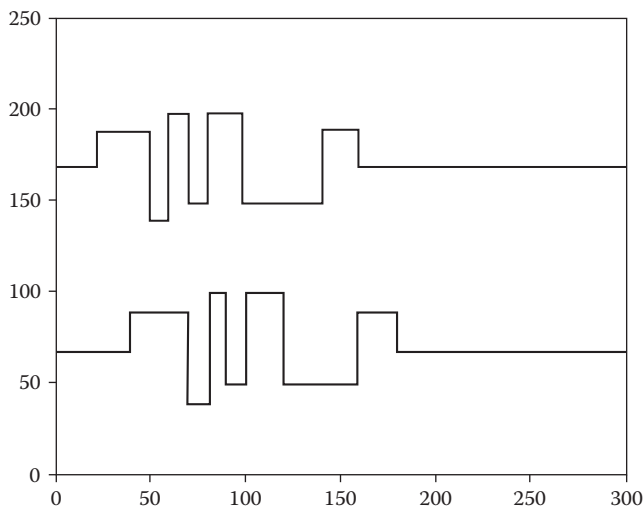


FIGURE 15.76 Plot of two correlated step tests (poor step test).

There are two theories of data collection:

1. Be cautious and collect everything. This minimizes the chance that you will forget something, but it maximizes the chance that you will acquire too much data to deal with later. This approach is a bit like packing five suitcases for an overnight trip.
2. Be practical and collect only what you need. If you carefully determine which data to collect, you minimize the data-processing problem but run the risk of missing useful data. This is like spending an hour to pack a small suitcase but forgetting your comb.

15.6.4.2.2.3 Laboratory Data

You need to identify which stream samples to collect during the plant test. Later, you will analyze the sample data to build inferred properties. Make sure you agree with the plant operations people about how much lab data you will need, for which streams, and how often it should be collected. Finally, remember that lab analyses are very expensive, so be careful to take just enough, but not too many, samples (30 to 60 samples per stream is about right). A good rule of thumb is to take at least ten data samples for each inferred properties coefficient being modeled. For a simple inferred property with 3 coefficients, at least 30 samples should be taken; e.g., $Y = a_1 x_1 + a_2 x_2 + a_3 x_3$, where a_i = the coefficients.

15.6.4.3 Conduct the Plant Test and Collect the Data

15.6.4.3.1 Preparation

The objective of doing a plant test is to get *good* data. The requirements of getting good data include

- The instrumentation must work properly.
- The PID controllers must be properly tuned.
- Control valves must be properly sized and functioning correctly.
- The process equipment must be in a normal state.

Before investing the time to conduct a plant test, you should spend a few days making sure that everything in the plant works properly. Move the setpoints to the main controllers to verify that the PID loops and final control elements work as they should. Look at the heat, mass, and

TABLE 15.13
Relative MPC Controller Sizes

	MVs	CVs	Comment
Very small controller	2–4	2–10	Will likely miss important constraints and interactions.
Reasonable controller size	5–40	10–40	About the right size.
Controller is too large	40+	40+	Human operators begin to have difficulty in understanding.

	AP100	PD100	PC100.VP	FC101.VP
FC100	–	+	+	+
TC100	+	+	–	+
HC100	0	0	+	0
PC100	–	–	+	–

FIGURE 15.78 Roughed-out gain matrix for the control design of the tower in Figure 15.73.

therefore benefits). Typically, a single controller spans a large part of a process unit. Table 15.13 illustrates the concept of proper controller size.

At this point in a control project, you should have a good idea of the controller structure—which variables are MVs, which are CVs, and which are DVs. Draw a matrix with the MV and DV tags as rows and the CV tags as columns (or vice versa). Using your newly gained knowledge of the process, write in a “+” or a “–” for each MV/CV pair (or DV/CV pair) where you expect to see a positive response and where you expect to see a negative response, respectively. Tape the matrix to your wall and look at it from time to time just to make sure you are on track as you proceed with more detailed analyses.

Be sure to look for patterns in your roughed-out matrix. For example, if two blocks have no common interactions, you may be able to divide it into two smaller controllers. Keep this in mind as you progress with the detailed analysis. See Figure 15.78 for an example.

15.6.4.4.2 Designing for Closed-Loop Optimization

Today's multivariable controllers are mainly linear algorithms. Depending on the process, there can be significant advantages to optimizing the process using a nonlinear model. Most nonlinear models today are steady-state, rigorous, heat and mass balance models and are built separate from the multivariable controller.

Even at this early stage in designing your controller, keep in mind that some of its targets may be set by a nonlinear optimizer. It is useful to decide which CVs or MVs will have their targets set by an optimizer. This becomes important later, particularly when tuning the controller.

15.6.4.4.3 Building the Power Model for the MPC Controller

Contemporary model building methodology is well established. Essentially, it is a matter of identifying which plant test data are usable; which variables should be CVs, MVs, or DVs; and what

TABLE 15.14
Economic Data for Distillation
Column in Figure 15.74

Tag	Description	Cost	Units
FC101	Steam flow	0.003	\$/lb
FC102	Bottoms product	12	\$/BBL
FC103	Overhead product	20	\$/BBL

TABLE 15.15
Process Gains for Distillation Column in Figure 15.73

	FC101 Steam (lb/hr)	FC102 Bottoms (BPD)	FC103 Overhead (BPD)
FC100 (reflux, BPD)	1090	0.2	-0.2
TCI 00 (reboiler, Dec F)	2800	-10	10

and the columns are the CVs. At the intersection of each row and column is a single model (blanks indicate that no relationship exists between a given MV/CV pair).

15.6.4.4.4 Plant Economics

Many multivariable control algorithms include a built-in optimizer that can be used to drive the plant in a better economic direction. To tune this part of the controller, reasonable economic data are required. These are often combined with process or simulation data to put them in a form that can be used by the controller.

The plant economics almost always end up as costs on controller CVs or MVs or both. They tell the controller which variables to minimize and which ones to maximize to achieve the proper objective (e.g., increased profit, reduced cost, reduced environmental cost, and so forth).

Let us use an example to illustrate. Imagine that you are designing a controller based on the distillation tower shown in Figure 15.74. The overhead product flow is measured by FC103, the bottoms product flow is measured by FC102, and the steam flow is measured by FC101. The controller manipulates reflux flow FC100, bottoms temperature TC100, fuel gas vent HC100, and tower pressure PC100. There are measured constraints, but for the time being we will generally ignore them and aim to maximize profits; we want plant conditions that maximize production of the more valuable product. To figure out how to make the controller push the plant in the correct direction (optimization), you will need the information in Table 15.14. Your job is to find a way to get this economic information into the controller so that it makes more overhead product, while attempting to save steam.

Since none of the economic variables in Table 15.14 appear in the controller, it is necessary to transform this information somehow to include it indirectly. To do this, you will need information on what effect the manipulated variables FC100 and TC100 have on plant economics. To do this, you will need more information. Fortunately, this is given in Table 15.15. These process gains were derived during plant tests. They represent the change in the economic variables that result from changes in the manipulated variables.

So, combining the information in Tables 15.14 and 15.15, we can compute the economic costs to be included in the controller as in Table 15.16. Note that one cost is positive and the other negative. The positive cost for reflux will cause the controller to reduce reflux flow. The negative cost for reboiler temperature will cause the controller to increase reboiler temperature. In practice,

15.6.4.5.3 Controller Tuning—Dynamics

All multivariable control algorithms include a way to tune how quickly they respond to setpoint changes or disturbances. Two general classes of tuning parameters affect the speed of response.

The first is often referred to as *reference trajectory* and can be thought of as a filter on setpoint changes. The filtered setpoint in essence becomes a trajectory—the controller attempts to move the MVs so that the CV follows their individual trajectories. Increased filtering produces slower controller action.

The second class of dynamic tuning focuses on how much the MVs move for a given disturbance (either setpoint change or unmeasured disturbance). This type of tuning parameter is commonly called *move suppression* and provides a mechanism to slow down some MVs relative to others. Move suppression is important when a given MV affects a critical piece of equipment, for example, a large compressor with many automatic overrides and shutdown interlocks.

The general procedure for tuning the dynamics of a new controller is to run the controller/simulation combination under many different combinations of setpoint changes and unmeasured disturbances. Typically, plant operators will provide valuable feedback for how much the MVs should move in different circumstances and how fast the CVs should get to setpoint and away from constraints.

15.6.4.5.4 Operator Training

In many states in the U.S.A., it is a legal requirement that all operator training take place before a multivariable closed-loop controller is activated in an operating plant for the first time. Even in places where this is not a legal requirement, common sense dictates that this step be carried out first.

Typically, the plant operators each receive an hour or two of training while working on their normal shift. In some exceptional cases, the operators receive formal classroom training. Better training leads to increased project success.

15.6.4.5.5 Watchdog Timer

A multivariable controller is expected to run continuously. Sometimes, however, the control software or control hardware fails. This situation should be detected quickly and the operator warned, normally by an alarm in the DCS.

The most common way of detecting and alarming this problem is to use a small program called a *watchdog timer* running in the DCS. The watchdog timer communicates frequently with the multivariable controller program. If the watchdog timer fails to get a response after a predetermined period of time, the watchdog forces each MV into its fallback (shed) position and writes an alarm to the operator.

15.6.4.6 Commission the Controller

After a controller has been designed, built, and tuned in an off-line environment, the next big step is to install it in the plant computing hardware and commission it. Since, at this stage, it becomes possible for the controller to directly modify how the plant is running, one must proceed methodically and with caution. Use checklists. Be observant and, at least initially, monitor all of the variables related to the controller frequently and thoroughly. Below is a good suggested procedure.

15.6.4.6.1 Use a Checklist

Installing a multivariable controller is not difficult, but, if done carelessly, it can lead to serious problems such as an off-specification product or equipment damage. To maximize the chances of a smooth installation, use a checklist. Here is a simple example.

1. Make sure that operators are trained on how the controller works. Do not proceed until they are.

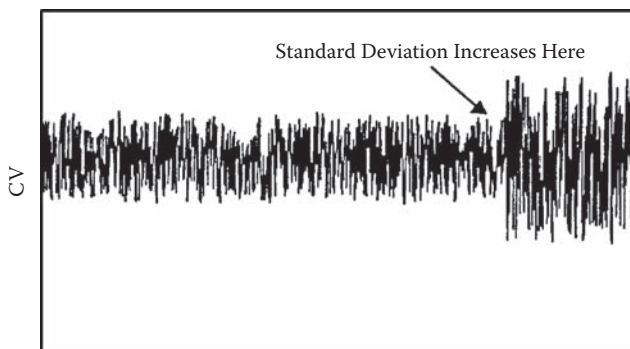


FIGURE 15.80 Standard deviation of a CV increases suddenly.

15.6.5.1 Commonsense Approach

Ninety percent of troubleshooting multivariable controllers is common sense. For example, below is a daily checklist that can be applied to diagnose the last 24 hr of operation for a MPC application.

15.6.5.1.1 Quick Screening

The first step in controller troubleshooting is to check overall controller behavior during the recent past. This quick screening is often a simple set of questions or a few simple reports. For example, here are some questions to ask each morning:

- What percent of time was the controller running?
- Which constraint set was most active?
- How many MVs are at bounds?
- How many CVs are at bounds?
- How many MVs are active (being manipulated by the controller)?
- What is the standard deviation of CVs that are at bounds?
- Is the controller pushing the plant in the right direction?
- How far apart are the MV bounds?

15.6.5.1.2 Deeper Analysis

If the quick screening turns up potential problems, deeper analysis can help narrow down the problem areas. One good way to do this is to examine time plots for all CVs and MVs for the last 24 hr. Abnormal behavior can be quickly traced to one or a few variables by this approach.

Figure 15.80 is an illustration of what happens when a multivariable controller develops a problem; in this case, a CV in the controller exhibits a sudden increase in standard deviation. Now, having narrowed the problem, an engineer can conduct even more detailed analyses.

15.6.5.2 Detailed Troubleshooting—Use a Checklist

Finally, once the problem behavior has been narrowed down, a good final step is to try to pinpoint the problem using a checklist. It is surprising how many problems can be found by running quickly through a checklist—for example,

- ☐ Controller is on, but MVs don't move
- ☐ Controller turned off by itself
- ☐ Operator turned controller off

15.6.5.3 Is the Controller Still Making Money?

In the final analysis, only one thing really matters—is the controller still making money? You should get in the habit of periodically evaluating the controller behavior; every few months is probably often enough. Check to see whether

The controller is pushing the plant in a direction that makes economic sense.

Controller economics match the current process economics.

Standard deviations of key variables are acceptable compared to a good base case.

CV and MV constraints still make economic sense and are safe.

The variable set is correct. (Should some be removed? Others added?)

The scope of the controller is still OK. (Should it be expanded? Made smaller?)

It is time to add a real-time nonlinear optimizer.

The operators are still adequately trained in the use of the controller.

REFERENCES, SECTION 15.2

1. Lucas, M. P., 1986. *Distributed Control Systems*. New York: Van Nostrand Reinhold, 4.
2. McMillan, G. K., G. E. Mertz, and V. L. Trevathan, 1998. Troublefree Instrumentation, *Chem. Eng., Nov.*: 80–88.
3. Liptak, B., 1995. *Instrument Engineers Handbook*. Philadelphia: Chilton.
4. McMillan, G. K., 1995. *Advanced Temperature Control*. Research Triangle Park, NC: Instrument Society of America, 133–155.

REFERENCES, SECTION 15.3

1. Riggs, James B., 1999. *Chemical Process Control*. Lubbock, TX: Ferret Publishing, 154–160.
2. Private communication, Jim Downs, Tennessee Eastman Company, Nov. 1998.

REFERENCES, SECTION 15.4

1. Marlin, T. E., 1995. *Process Control*. New York: McGraw-Hill, 393.
2. Astrom, K. J. and T. Hagglund, 1988. *Automatic Tuning of PID Controllers*. Research Triangle Park, NC: Instrument Society of America, 233.
3. Ziegler, J. G. and N. B. Nichols, 1942. Optimum Settings for Automatic Controllers, *Trans ASME* 64: 759.
4. Tyreus, B. D. and W. L. Luyben, 1992. Tuning PI Controllers for Integrator/Deadtime Processes. *Ind. Eng. Chem. Res.* 31: 2625.
5. Marlin, T. E., 1995. *Process Control*. New York: McGraw-Hill, 588–590.

REFERENCE, SECTION 15.5

1. Bristol, E. H., 1966. *IEEE Trans Auto. Con.*, AC-11: 133.

REFERENCES, SECTION 15.6

Cutler, C. R. Ramaker, B. L., 1979. Dynamic Matrix Control—A Computer Control Algorithm, AIChE National Meeting, Houston, TX.

16.4.2	Minimize Uncertainty in Input Data through Experimentation: Principles of Scale-Up	1313
	Additional Reading.....	1314
16.4.3	Units of Measurement and Communication	1314
16.4.4	Gather Input Data from Data Bases for Design and Process Improvement	1314
16.4.4.1	Checklist for Reactivity.....	1317
16.4.4.2	Checklist for Chemical Persistence	1317
	Additional Reading.....	1320
16.4.5	Gather Data for Troubleshooting	1321
	Additional Reading.....	1321
16.5	Sustainability from the Start	1322
16.5.1	Impact of Sustainability on Design.....	1323
16.5.2	Impact of Sustainability on Process Improvement	1323
	Additional Reading.....	1324
16.6	Operability and Control Considered Throughout	1324
16.6.1	Control and Design.....	1324
16.6.1.1	Design: Impact of Control on the Initial Design Statement	1324
16.6.1.2	Design: Impact of Control on the Evolving Flowsheet.....	1324
16.6.1.3	Design: Impact of Control on the Type of Equipment Selected.....	1325
16.6.1.4	Design: Impact of Control on the Sizing of Equipment	1325
16.6.1.5	Design: Impact of Control on Issues beyond Conceptual Design.....	1325
16.6.2	Control and Process Improvement	1326
16.6.3	Control and Troubleshooting.....	1326
	Additional Reading.....	1326
16.7	Consider Safety, Waste Minimization, and Environmental Sensitivity Throughout.....	1327
16.7.1	Step 1: Target Opportunities	1327
16.7.1.1	Know the Legal and Economic Context.....	1327
16.7.1.2	Identify the Opportunity.....	1327
16.7.2	Steps 2 through 5: Move from “Eliminate” to “Isolate” during the Design Process	1328
16.7.2.1	Step 2: Eliminate the Source	1328
16.7.2.2	Step 3: Minimize the Source	1330
16.7.2.3	Step 4: Minimize the Impact.....	1332
16.7.2.4	Step 5: Isolate the Source	1333
16.7.2.5	Step 6: Isolate the Impact	1333
16.7.3	For Process Improvement.....	1333
16.7.4	For Troubleshooting	1333
	Additional Reading.....	1333
16.8	Aids for Design, Process Improvement, and Troubleshooting.....	1333
16.8.1	Steady-State Flowsheeting.....	1336
16.8.2	Formulating a Well-Posed Problem	1336
16.8.3	Flowsheet Architectures.....	1338
16.8.3.1	Sequential Modular Architecture	1338
16.8.3.2	Equation-Based Architecture.....	1341
16.8.4	Importance of Thermodynamics Packages	1341
16.8.4.1	Vapor-Liquid Equilibrium	1342
16.8.4.2	At High Pressure or near the Critical Region	1342
16.8.4.3	Equation of State, EOS	1342

16.11.3.15 Thermal Energy: Solidify Liquids	1367
16.11.3.16 Thermal Energy: Heat Loss to the Atmosphere	1367
16.11.3.17 Thermal Energy: Refrigeration	1367
16.11.3.18 Thermal Energy: Steam Generation.....	1368
16.11.4 Homogeneous Separation.....	1368
Overall Guidelines	1368
16.11.4.1 Evaporation.....	1368
16.11.4.2 Distillation	1369
16.11.4.3 Freeze Concentration.....	1372
16.11.4.4 Melt Crystallization.....	1372
16.11.4.5 Zone Refining.....	1373
16.11.4.6 Solution Crystallization.....	1373
16.11.4.7 Precipitation.....	1374
16.11.4.8 Gas Absorption.....	1374
16.11.4.9 Gas Desorption/Stripping.....	1376
16.11.4.10 Solvent Extraction, SX.....	1376
16.11.4.11 Adsorption: Gas.....	1378
16.11.4.12 Adsorption: Liquid	1378
16.11.4.13 Ion Exchange.....	1379
16.11.4.14 Foam Fractionation.....	1380
16.11.4.15 Membranes: Gas.....	1381
16.11.4.16 Membranes: Dialysis.....	1381
16.11.4.17 Membranes: Electrodialysis	1382
16.11.4.18 Membrane Configurations.....	1382
16.11.4.19 Membranes: Pervaporation.....	1382
16.11.4.20 Membranes: Reverse Osmosis (RO).....	1384
16.11.4.21 Membranes: Nanofiltration.....	1385
16.11.4.22 Membranes: Ultrafiltration (UF).....	1385
16.11.4.23 Membranes: Microfiltration	1386
16.11.5 Heterogeneous Separations.....	1387
General Guidelines	1387
16.11.5.1 Gas-Liquid.....	1387
16.11.5.2 Gas-Solid	1388
16.11.5.3 Liquid-Liquid.....	1390
16.11.5.4 Liquid-Solid: General Selection.....	1391
16.11.5.5 Dryer.....	1392
16.11.5.6 Screens for "Dewatering".....	1396
16.11.5.7 Settlers	1396
16.11.5.8 Hydrocyclones	1397
16.11.5.9 Thickener.....	1397
16.11.5.10 CCD: Countercurrent Decantation.....	1397
16.11.5.11 Sedimentation Centrifuges	1398
16.11.5.12 Filtering Centrifuge	1399
16.11.5.13 Filter.....	1400
16.11.5.14 Leacher	1404
16.11.5.15 Liquid-Solid: Dissolved Air Flotation, DAF	1404
16.11.5.16 Liquid-Solid: Expeller and Hydraulic Press.....	1405
16.11.5.17 Solid-Solid: General Selection.....	1405
16.11.5.18 Froth Flotation.....	1405
16.11.5.19 Electrostatic	1406
16.11.5.20 Magnetic	1406

16.11.7.6	Dry Solids.....	1429
16.11.7.7	Pastes, Polymers, Foodstuffs, Clay, and Fertilizers.....	1429
16.11.8	Size Reduction.....	1429
16.11.8.1	Gas in Liquid (Bubbles in Liquid)	1429
16.11.8.2	Liquid in Gas (Sprays).....	1430
16.11.8.3	Liquid-Liquid.....	1430
16.11.8.4	Solids: Crushing and Grinding	1431
16.11.8.5	Solids: Modify Size and Shape: Extruders, Pug Mills, and Molding Machines.....	1432
16.11.8.6	Solids: Solidify Liquid to Solid: Flakers, Belts, and Prill Towers.....	1432
16.11.9	Size Enlargement.....	1432
16.11.9.1	Size Enlargement: Liquid-Gas: Demisters.....	1432
16.11.9.2	Size Enlargement: Liquid-Liquid: Coalescers	1433
16.11.9.3	Size Enlargement: Solid in Liquid: Coagulation/Flocculation.....	1433
16.11.9.4	Size Enlargement: Solids: Spray Drying	1433
16.11.9.5	Size Enlargement: Solids: Fluidization.....	1433
16.11.9.6	Size Enlargement: Solids: Spherical Agglomeration.....	1434
16.11.9.7	Size Enlargement: Solids: Disc Agglomeration	1434
16.11.9.8	Size Enlargement: Solids: Drum Granulator	1434
16.11.9.9	Size Enlargement: Solids: Briquetting.....	1434
16.11.9.10	Size Enlargement: Solids: Tableting.....	1434
16.11.9.11	Size Enlargement: Solids: Pelleting.....	1435
16.11.9.12	Size Enlargement: Solids: Sintering/Pelletizing	1435
16.11.9.13	Size Enlargement: Solids: Crystallization	1435
16.11.9.14	Solids: Modify Size and Shape: Extruders, Pug Mills, and Molding Machines.....	1435
16.11.9.15	Solids: Solidify Liquid to Solid: Flakers, Belts, and Prill Towers.....	1436
	Additional Reading	1436

Consult this chapter first if you need to accomplish any of the following:

- Design a piece of equipment
- Propose and design new equipment or a new process
- Evaluate a current piece of equipment or a process
- Suggest changes for equipment or a process
- Debottleneck by increasing the limiting capacity in a process
- Troubleshoot to correct faulty operation

We classify these problems as being design, process analysis and improvement, and troubleshooting.

Engineering is based on fundamentals and the dynamic balance among economic, operability, sustainability, safety, environmental, legal, ethical, and time constraints. It is *dynamic*, because the development of new technology, catalysts, and materials of construction, and the shifting economical, social, and political scenes, mean that the processes we develop, improve, and operate in the future will be dramatically different from past practice. We say it is based on fundamentals, because mass, energy, momentum, and charge will still be conserved.

The goal is a win-win balance (not a lose-lose compromise) among competing forces. Moderation and patient creative problem solving are the keys. Regrettably, plants have been built that have so many safety interlocks, so much heat integration, and such extremely minimized inventory that

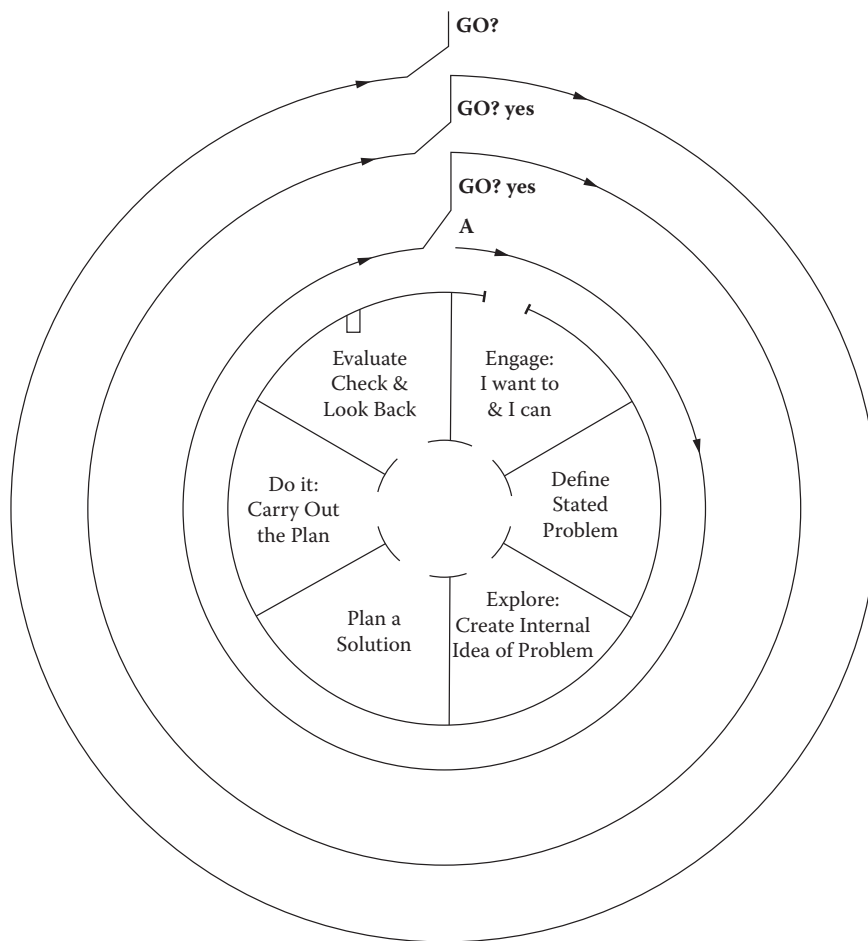


FIGURE 16.1 The problem solving strategy is applied many times in solving problems as illustrated for the first phases of the hierarchical conceptual design sequence.

suggesting the number of ideas or options considered at the different gates (Cooper, 1987). Listed in columns 5 and 6 are the different technical and economic dimensions of the overall task. Column 5 also shows when the three different types of problems (conceptual design, process improvement, and troubleshooting) are usually encountered. The “startup phase” includes conceptual design through construction.

2. The problem-solving process applies to design, process improvement, and troubleshooting. To manage the process, we usually consider the problem in a hierarchical series of cycles that reflect the systematic evolution of our ideas. For conceptual design, these stages in the cycle are listed across the top of Table 16.2 (based on Douglas, 1988). The constraints are usually (1) the production capacity, the purity of the products, and the anticipated disturbances; (2) economic (amount of capital available and the projected return); (3) time (when); (4) the budget, time, and resources for the design process; and (5) the potential for expansion.

For *process improvement*, the cyclical stages and criteria are as illustrated in Table 16.3. The constraints are usually (1) the existing plant, equipment, and layout, and (2) the existing feedstocks (although one might allow different trace contaminants) and economic constraints of budget and profitability. For process improvement and waste

TABLE 16.2
Full Problem-Solving Cycle Is Applied to Each of the Hierarchical Stages in Conceptual Design

Hierarchical Stages in Conceptual Design							
Criteria	II. Gather the Data for Inputs and Target Outputs; Set Goals		III. Preliminary Scouting of the Reactor	IV. Explore Mass Recycle	V. Explore Separations	VI. Explore Energy Integration	V. Polish
	I. Batch versus Continuous						
Technical feasibility	Use when difficult to scale up; identify as multiproduct, general multipurpose, or campaign operation of multipurpose.	Define product amount, purity, and range of production rates	Reaction conditions: Excess reagent? Heat removal method? Shift equilibrium? Add diluent? Combine reactor-separator?	Buildup of trace materials? Overall mass balance? Changes in corrosion?	Prefer not to add agents	Pinch technology	
Economic feasibility	< 2,500 Mg/a <0.1 kg/s	Use cost correlation to estimate investment; estimate product cost using %.			Use cost correlation based on flowrate		Minimum cost may not give minimum waste
Sustainability		Define risk and expected return; Define tax and insurance impacts TNS: renewable resources? Bioassimilation of feedstock, product, byproducts, intermediates, and wastes					

TABLE 16.3
Full Problem-Solving Cycle Is Applied to Each of the Hierarchical Stages for Process Improvement

Hierarchical Stages in Process Improvement								
Criteria	I. Better Inventory; Reduce Fugitives	II. Identify Realistic Needs for Process Units	III. Optimization of Reactor/ Separation	IV. Cycle Time Optimization; Improved Control	V. Process Modifications to Debottleneck: Simple Switch	VI. Process Modifications to Debottleneck; Redesign, Equipment Replacement	VII. Recycle Management; Heat and Mass Exchange Networks	VIII. Substitute Raw Materials, Reagents, Solvents, and Additives
Technical feasibility	Minimum risk with greatest economic potential	Realistic specifications for products, utilities;	Focus here because usually raw material cost predominates; consider issues from design		Relocate feed, replace internals, vertical condenser to horizontal condenser		Pinch technology	
	Incremental analysis		Purity of feedstocks; renewable? and bioassimilation?					
Control and operability	Minimum surge volume needed to damp out disturbances	Four levels	Better sensors, relocate sensors	Shift to statistical process control?	Impact on control	Impact on control, startup		
Hazard: safety, environmental, waste minimization	Main focus here!	Consider zero discharge; guidelines for acceptable risk	Minimize waste production		Minimize holdup	Increase in fouling? Increase in corrosion?		
Legal and ethical: social/political	Ethical concern for community; legal requirements							
People								

- (6) satisfaction of all legal and ethical concerns, and (7) providing the company with a good corporate image. More is given under "Qualitative Measures" in Section 16.3 and in Sections 16.5 through 16.7.
5. *The problem-solving process uses all available current computer assists such as flow-sheeting, the Web, data sourcing, and data-processing techniques.*
 6. The problem-solving process is usually a team effort, with many people contributing.

Additional Reading

- J. M. Douglas, *Conceptual Design of Chemical Processes*. New York: McGraw-Hill, 1988. This book and articles published by Douglas and his research group give more on the process of conceptual design.
- R. G. Cooper, *Winning at New Products*, 3rd ed. New York: Perseus Books Group, 2001. Gives more on the business aspects of the design process.
- D. J. Doyle, *Making Technology Happen*. Nepean, Ontario, Canada: Doyletech Corp., 1980. An excellent 120-page summary that integrates engineering, business, and entrepreneurship.

16.2 RULES OF THUMB FOR PROBLEM SOLVING*

Below are 18 rules of thumb about the process of problem solving.

1. Be aware. Be able to describe the thought processes being used and to identify where in the process you are.
2. Know the systematic stages for each cycle of the problem-solving process (as illustrated in Figure 16.1).
3. Focus on accuracy. Check and double check.
4. Actively write things down. Make charts and raw diagrams, write down goals, list measurable criteria, and record ideas in brainstorming.
5. Monitor and reflect. Mentally keep track of the problem-solving process and monitor about once per minute.
6. Be organized and systematic. Use an organized strategy such as those illustrated in Figure 16.1 and in Tables 16.2 to 16.4.
7. Define the "real" problem by creating a rich perspective of the problem. See it from many different points of view. Be willing to spend at least half the total available time defining the problem. Ask many "what-if" questions. Try to bound the problem space. "Swim with the data" to see how they respond. Identify the real problem by asking a series of "why" questions to generalize the situation. In Figure 16.1, this activity of identifying the real problem is called the *explore* stage and is the heart of the problem-solving process.
8. Be flexible.
9. Use your creativity effectively. Defer judgment; be succinct; list 50 ideas in 5 min; create a risk-free environment; encourage free and forced association of ideas; piggyback on previous ideas; use triggers, such as those listed in Table 16.5, to maintain the flow of ideas; don't be discouraged—in the last 2 min of a 5-min brainstorming session, over 85% of the ideas are impractical—but spend time to identify the treasures among the 15%. Use impractical and ridiculous ideas as steppingstones to innovative, practical options.
10. Critically assess the knowledge and data used. Too often, we hope that the data are applicable. A colleague, in designing a petrochemical plant, was unable to locate the physical properties of the organics. He decided to assume that they were the same as water and hoped that this would work out. Just a short time spent in critical assessment of this assumption would have saved six months of wasted work. Too often, we accept

* Reproduced with permission from Donald R. Woods, *Rules of Thumb in Engineering Practice*, pages 22 to 25, 2007 copyright Wiley-VCH Verlag GmbH & Co. KGaA, Weinheim, ISBN: 978-3-527-31220-7.

TABLE 16.5 (Continued)
Checklist of Triggers for Brainstorming

Name of Trigger to Change Point of View	Elaboration of How It Is to Be Used	Comments
Functional analogy	How else is the function achieved?	
Appearance analogy	How else might we get the appearance of this situation?	
Morphology	Break the problem situation into a series of parts. For each part list 10+ options. Then, systematically combine one option from each part and ask why not?	More mechanical; easy to computerize; most of the work is in setting up the parts and the options; fun and surprising to see some of the results.
Symbolic replacement	Replace the original problem by an interesting idea generated in the session; refocus.	Occurs naturally in many brainstorming sessions. Add this trigger explicitly if needed.
Juxtaposition	Bring in three completely random words and bridge to current situation. Example: "refrigerator, light switch, clock."	Very effective. Don't fake it by using words "you think will help." Use random words.
Personal analogy	Imagine yourself as part of the situation. Describe your feelings and what you are experiencing. Be imaginative.	Tricky. Works for some people; not for others. Effective with fluid dynamic problems.
Reversal	Do the reverse.	More challenging than one thinks. Focus systematically on the reverse of different elements of the situation at a time.
Book title	Create a title for a "best selling" novel. The title should sum up the current situation. "Will exchanging bring happiness to Mary Lou?"	Interesting. Worth a try for 1 min.
Letter, word, sentence	Focus on three different levels of detail corresponding to the big view (a sentence), an intermediate view (a word in the sentence), and a letter (in a word). In ion exchange this might be "the ions, the resin, the packed bed, the separation."	Very effective for most of our problems. Consider a 5-min brainstorm at each level.

data from the published literature, yet about 8% of published data are mistakes. "The temperature into the hydrodealkylation reactor is $>1150^{\circ}\text{C}$," states one reference. It should read $>1150^{\circ}\text{F}$. A major handbook published an incorrect value of the heat of vaporization through several editions. Check the data coming from computer programs and simulations. Check the physical property package estimates.

11. See challenges and failures as opportunities for new perspectives.
12. Spend time where it benefits you the most. Use Pareto's principle (80% of the results can be found from 20% of the effort). Find the key 20%.
13. Be an effective decision maker. Express the goal as results to be achieved rather than as actions to be taken. Make decisions based on some criteria that are explicit and measurable. Distinguish between *must* criteria (the process must have an internal rate of return of 35%) and *want* criteria (the process might have the potential to be licensed). Reject options that do not meet the must criteria. Use a rating system to score the want criteria.

16.3.1 ROLE OF ECONOMICS IN FINANCIAL REPORTING

Some basic knowledge of economics and financial reporting is essential for a professional engineer moving up the corporate ladder from a technical professional to a corporate manager. The engineer must recognize the importance of financial management and learn to speak and understand the language used by corporate management. The information in this section is beyond what one would encounter in college courses in business school economics or in engineering economics courses. A company financial report, sometimes called an annual report, contains much information. It is designed to tell the reader how well the company performed in the previous year and how this performance is measured against various standards. Two important documents in the annual report are the *balance sheet* and the *income statement*. Two ancillary documents often included are the *accumulated retained earnings* and the *changes in working capital*. As each of these documents is discussed, the reader should have Tables 16.6 and 16.7 available while reading the following sections. These are the financial documents for a fictitious chemical company, ALLCHEM, for the current year 20X6 with data for the previous year 20X5.

16.3.1.1 Balance Sheet (Anon., 1992; Couper et al., 2000)

The balance sheet is the financial status of the company on a given date. The choice of date is arbitrary and depends on the company's operations. A *consolidated* report means that all the financial data for the parent company as well as for the subsidiary companies are presented in one document. A balance sheet contains some real figures, e.g., cash and marketable securities; some estimated amounts or allowances, e.g., inventories and accounts receivable; as well as some fictitious figures, e.g., intangibles for which numbers are difficult to determine.

Two main parts of the balance sheet are the *assets*, which is what the company owns, and the *liabilities and stockholders' equity*, which is what the company owes. The total assets equal the total liabilities plus the stockholders' equity.

16.3.1.1.1 Assets

The assets of a company are divided into three categories: *current assets*, *fixed assets*, and *intangibles*.

Current assets are those that may be converted to cash within a year from the date of the balance sheet. The current assets include cash and money on deposit in a bank as well as *marketable securities* (e.g., commercial paper and/or government bonds) that can be easily converted to cash. *Accounts receivable* are goods sold to customers on a 30-, 60-, or 90-day basis for which full payment has not been received. An allowance is made for uncollected bills, because some customers were unable to pay. *Inventories* consist of raw materials on hand, goods in process, supplies, and finished goods ready for shipment. Raw materials are charged at cost, goods in process at raw material cost plus one half the conversion cost, and finished goods are valued at selling price. Frequently, inventory costs are carried at values slightly less than these figures to account for deterioration, decline in prices, and other factors. *Prepaid expenses* include prepaid insurance premiums as well as leases for equipment, computers, and office equipment. These expenses are listed under current assets because, although a company has paid for them, full benefit has not been received, but the company expects to do so within the year. The *total current assets* are the sum of cash and marketable securities, accounts receivable, and prepaid expenses.

Fixed assets include land, buildings, manufacturing equipment, office equipment, and so forth, that the company owns. These items are carried on the books at cost less the accumulated depreciation, except for land, which is generally entered at the same value year to year. The sum of these items is the *net fixed assets*.

Intangibles are assets that have substantial value to the company, such as patents, licenses, trademarks, goodwill, and so forth. There is no consistent way to evaluate these assets, so the company often balances both sides of the balance sheet by making this value "close" the sheet.

TABLE 16.7
Consolidated Income Statement for ALLCHEM, Inc.

CONSOLIDATED INCOME STATEMENT*		
	20X6	20X5
Net Sales (Revenue)	\$932,000	\$850,000
Cost of Sales and Operating Expenses		
Cost of Goods Sold	692,000	610,000
Depreciation and Amortization	40,000	36,000
Selling, General and Administrative Expenses	113,500	110,000
Operating Profit	\$86,500	\$94,000
Other Income (Expenses)		
Dividends and Interest Income	10,000	7,000
Interest Expense	(22,000)	(22,000)
Income Before Provision for Income Taxes	\$74,500	\$79,000
Provision for Federal Income Taxes	24,500	26,000
Net Profit for Year	\$ 50,000	\$ 53,000
ACCUMULATED RETAINED EARNINGS STATEMENT*		
Balance as of January 1	\$172,900	\$141,850
Net Profit for Year	50,000	53,000
Total for Year	\$222,900	\$194,850
Less Dividends Paid on		
Preferred Stock	700	700
Common Stock	14,600	21,250
Balance December 31	\$207,600	\$172,900

* All figures are in thousands of dollars.

Other assets, such as investments in affiliates or *deferred charges* for which full benefit has not been received, may be included before the total assets are summed.

Total assets are the sum of current assets, fixed assets, intangibles, and deferred charges.

16.3.1.1.2 Liabilities

The *total liabilities* are what a company owes and consist of the sum of *current* and *long-term liabilities*. *Current liabilities* are debts that must be paid within a year from the date of the balance sheet. The total current liabilities are the sum of the *accounts payable*, *notes payable*, *accrued expenses payable*, as well as *income taxes payable* from current assets. *Accounts payable* include such items as invoices for raw materials, supplies, and others, that a company has purchased from suppliers and for which payment is due on a 30-, 60-, or 90-day basis. *Notes payable* include monies owed to banks and other creditors as well as promissory notes. *Accrued expenses payable* include such entries as salaries, wages, interest on borrowed funds, insurance premiums, pensions, and so on. *Income taxes payable* are the debt owed to federal, state, and local governments. These taxes are usually paid on a quarterly basis and commonly isolated from other expenses.

Long-term liabilities are debts due after one year from the date of the financial report and include bonds, loans, and deferred income tax. *Bonds and loans* include *first mortgage bonds* (issued at a stated rate due in a stated year and backed by the company's property), *debenture bonds* (backed by the general credit of the company rather than by company property), and *long-term loans* from insurance companies and investment houses. *Deferred income taxes* are encouraged

each year as an operating expense. This *depreciation* is not a cash item. *Amortization* is the decline in useful value of a tangible asset, such as a patent. *Depletion* is the diminution of a natural resource, such as a coal mine. All of these paper allowances appear as one item in most income statements.

The *SARE expenses* are expenses associated with the maintenance of sales offices, paying corporate officers and their staffs, and research and engineering expenses not attributable to a specific project.

16.3.1.2.3 Operating Profit (Operating Income)

This entry is the difference between net sales or net revenue and all operating expenses.

Other income may be derived from dividends or interest received by the company from other investments, income from patents, licenses, and so forth. When other income is subtracted from the operating profit, the result is *income before provision for federal income taxes*.

Every company has a basic federal income tax rate that it must pay. However, the actual *federal income taxes* paid may be less than the basic rate, due to tax incentives, tax credits, depreciation write offs, capital gains, and so on.

16.3.1.2.4 Net Profit for the year after Income Taxes

This entry is obtained by subtracting the provision for federal income taxes from the income before provision for federal income taxes.

16.3.1.3 Accumulated Retained Earnings

Accumulated retained earnings is an important part of the financial report and is often found along with the income statement. It shows how much money the company has retained for growth and how much was paid out as dividends to stockholders. When the accumulated retained earnings increase, the company has more value. The balance of the accumulated retained earnings at the end of one year is the opening balance on January 1 of the next year. To that figure, the net profit after taxes for that year from the income statement is added, giving the total for the year. From the total for the year, the dividends paid to the preferred and common stockholders are subtracted, and the remainder is the balance of the accumulated retained earnings at the end of the year on December 31.

16.3.1.4 Changes in Financial Position

Scrutiny of the balance sheet and the income statement reveals how much money flowed through the company; how much profit was made; how the funds provided by the net profit, depreciation, sale of common stock, and other items were used; and how the cash generated affected the company operations. The changes in financial position show how the company managed its funds.

16.3.1.5 Other Financial Terms of Significance

Working capital, which allows a company to carry on day-to-day operations, is determined by subtracting current liabilities from current assets. (See also item 20 in Section 16.3.4.2.) *After-tax cash flow* is defined as the net profit after taxes plus depreciation. It is essential to have adequate cash flow to operate the company. *Earnings per share* interests common stockholders and stockbrokers. It is found by dividing the net profit after taxes by the number of shares of common stock.

Depreciation methods in use today are *straight-line* or *accelerated* depreciation. In the former method, the cost of the asset is divided by the asset's life. Accelerated methods were introduced in the 1950s to stimulate capital spending. In the intervening years, there have been many changes to the tax laws as well as how depreciation is handled. The net effect of accelerated depreciation was to provide a larger amount of depreciation in the early years of a venture, thereby increasing the cash flow when the plant is coming on stream and the market for a product is being established.

TABLE 16.8
Financial Ratios for ALLCHEM, Inc.

Liquidity

$$\text{Current Ratio} = \frac{\$391,200}{\$201,500} = 1.94$$

$$\text{Cash Ratio} = \frac{\$391,200 - 149,000}{\$201,500} = 1.20$$

Leverage

$$\text{Debt to Assets} = \frac{\$448,100 - 201,500}{\$705,700} \times 100 = 35\%$$

$$\text{Times Interest Earned} = \frac{\$74,500 - 22,000}{\$22,000} = 4.39$$

$$\text{Fixed Charge Coverage} = \frac{\$86,500}{\$22,000} = 3.93$$

Activity

$$\text{Inventory Turnover} = \frac{\$932,000}{\$149,000} = 6.25$$

$$\text{Average Collection Period} = \frac{\$135,000}{(\$932,000 / 365)} = 52.8 \text{ days}$$

$$\text{Fixed Assets Turnover} = \frac{\$932,000}{\$438,000} = 2.13$$

$$\text{Total Assets Turnover} = \frac{\$932,000}{\$705,700} = 1.32$$

Profitability

$$\text{Gross Profit Margin} = \frac{\$932,000 - 692,000}{\$932,000} \times 100 = 25.8\%$$

$$\text{Net Operating Margin} = \frac{\$74,500}{\$932,000} \times 100 = 7.99\%$$

$$\text{Profit Margin on Sales} = \frac{\$50,000}{\$932,000} \times 100 = 5.36\%$$

$$\text{Return on Net Worth} = \frac{\$50,000}{\$705,700 - 448,100} \times 100 = 19.4\%$$

(Return on Equity)

$$\text{Return on Total Assets} = \frac{\$50,000}{\$705,700} \times 100 = 7.09\%$$

The *fixed charge coverage* is obtained by dividing the income available for meeting fixed charges by the fixed charges. Some firms enter into long-term lease agreements, and these are a part of the fixed costs in doing business. The numerator of this ratio is the operating profit before deducting the interest expense, lease costs, and income taxes divided by lease costs and interest expenses.

16.3.1.8.3 Activity Ratios

Activity ratios measure how effectively a company manages its assets.

Additional Reading

Anon., *How to Read an Annual Report*. New York: Merrill Lynch, 1992.

J. R. Couper, *Process Engineering Economics*. New York: Marcel Dekker, 2003.

J. R. Couper, O. T. Beasley, and W. R. Penny, *The Chemical Process Industries Infrastructure*. New York: Marcel Dekker, 2000.

16.3.2 FINANCIAL ATTRACTIVENESS

In the free enterprise system, if profits are not maintained, the firm's growth might be stifled. The objective is to maximize profit on invested capital. The attractiveness of a venture is viewed by corporate officers and boards based on "quantitative" and "qualitative" measures of profitability. Although we use the term "profitability" loosely to measure a project's worthiness, it may not be a good measure. Drucker (1974) has said that "profitability is not a perfect measurement; no one has ever been able to define it, and yet it is a measurement despite all its imperfections."

16.3.2.1 Quantitative Measures

Although there are many quantitative measures of profitability, the four most commonly used are return on investment, payout period, net present value, and internal rate of return. The first two measures do not include the time value of money; however, the payout period can be modified to do so, as we shall see later.

The *return on investment* method is defined as the net profit after taxes divided by the total capital investment. Many variations on this measure have been used in the past. It does not include the time value of money but is simple enough that it can be used for simple screening purposes. The *payout period* is defined as the fixed capital investment divided by the after-tax cash flow. It indicates how long it will take to recover the fixed capital investment from the after-tax cash flow. Again, this is used for screening purposes. The payout period with interest takes into account the time value of money (Couper and Rader, 1986) but is a tedious calculation, and the results are not as informative as the net present value or the internal rate of return methods.

The *net present value* method is the most popular one in use today. An arbitrary time frame (i.e., time zero or the present time) is selected as the basis for the calculations. All investment expenditures made prior to time zero are compounded forward to time zero, and all income items are discounted back to time zero using an interest rate (or arbitrary "barrier return") set by management at a few percentage points above the *cost of capital*, depending on the project risk. The equation for determining the net present value is

$$\text{Net present value (NPV)} = \text{net present value of all cash flows derived from income minus net present value of all investment items}$$

If the NPV is positive, then the venture will earn more than the arbitrary barrier return. Conversely, if the NPV is negative, then the venture will earn less.

The *internal rate of return (IRR)* method is similar to the NPV method in principle. In the NPV method, the interest rate is stated, and the NPV is calculated. In the IRR method, an interest rate is sought by trial and error such that the NPVs sum to zero. That interest rate is the return that the venture will earn. There has been much discussion in the literature about which method is preferred (Couper et al., 2000).

16.3.2.2 Qualitative Measures

Before an investment decision is made, consideration must be given to certain qualitative factors and their impact on the decision-making process. In some cases, these may be the controlling factors. The qualitative measures or criteria are outlined in Tables 16.2 to 16.4.

TABLE 16.9
Cost of Capital

Balance Sheet 12/31/20X6	Millions (\$)	After-Tax Yield to Maturity (%)	After-Tax Weight Ave. Cost (%)
Long-Term Debt			
Revolving Account	5.0	4.5	0.02
4 3/8's debentures	12.0	4.0	0.05
6 1/2 DM	3.4	4.7	0.02
6 3/4 DM*	9.4	4.2	0.04
7 1/2 DM	74.5	4.2	0.30
9 3.8 DM	125.0	4.4	0.53
Other	23.2	4.4	0.10
	<hr/> 252.5		<hr/> 1.06
Deferred Taxes	67.7	0	0
Reserves	16.1	0	0
Preferred Stock	50.0	8.6	0.42
Shareholder's Equity	<hr/> 653.9	15.6	<hr/> 9.80
	1,040.2		11.28

* The after-tax weighted average cost of capital is 11.28%.

yield to obtain an after-tax weighted cost for each capital item. The after-tax weighted average costs are then summed to give the average weighted cost of capital. In the example, it is noted that the stockholders' equity is the predominate factor in the cost of capital calculation, while the bonds contribute about 10% to the cost of capital. Equity capital is an expensive way to obtain funds. The cost of capital should be reviewed periodically by the company's financial personnel because this figure is used as a basis for funding projects.

16.3.2.3.2 Minimum Acceptable Rate of Return

Every business enterprise has limitations on the amount of capital available for investment each year. A minimum rate of return or barrier rate is established by management for different projects, depending on the risk involved, the type of venture, the cost of capital, and the duration of the venture. Different styles of management often use different methods for establishing the minimum rate of return.

16.3.2.3.3 Risk

Companies release funds for capital expenditures on a quarterly, semiannual, or annual basis. Executive committees determine on a scheduled basis how the funds should be released, based on risk and measures of profitability. The riskier the project, the higher the barrier return. For the discussion here, let us assume a company has a venture classification system as follows: necessity projects, product improvement projects, process improvement projects, and new ventures.

Necessity projects are mandated by environmental, health, safety, legal, or image issues. The company must invest in these projects to stay in business and avoid fines and/or litigation. The calculation of an NPV is meaningless, as the company must comply. These projects have zero risk. *Product improvement projects* involve the addition of perhaps a processing step, requiring a low capital investment to improve quality so that more sales or increased sales price is possible. These projects are short term, and there is a low risk. The minimum rate of return for these projects is set at a few percentage points above the cost of capital.

11. *Other expenses.* Technical services for troubleshooting process problems may employ a young engineer at a salary of about \$50,000 to \$60,000 per year (2007). Expenses for environmental control often include the costs of incineration, chemical treatment of the waste, landfill, and perhaps notification, documentation, reporting, manifesting, and labeling under RCRA legislation. The most reliable source for these figures is the environmental engineering staff in the specific plant, with some elaboration as given in Section 16.7.
12. *Total direct conversion expense.* The sum of items 3 through 11 is the *total direct conversion expense*.
13. *Indirect conversion expenses* include (a) depreciation and (b) plant indirect expenses. (a) Depreciation is the major component of indirect expenses. For estimation purposes, the annual depreciation is assumed to be straight-line and is calculated by dividing the fixed capital investment by the number of years over which the investment is to be depreciated. (Accelerated depreciation is not normally entered into the manufacturing expense sheet but is used in cash flow analyses after backing out straight-line depreciation from the manufacturing expenses.) (b) Plant indirect expenses include many items such as *ad valorem* and real estate taxes, insurance, maintenance of yards, docks, and roads, cafeterias, fire protection, and security. Plant accounting departments often compile factors to be applied for each plant site. To estimate this expense, use 2 to 4% of the fixed capital investment per year.
14. *Total indirect conversion expense* is the sum of depreciation and plant indirect expenses.
15. *Total manufacturing expense* is the sum of the net raw material expense, the total direct conversion expense, and the total indirect conversion expense.
16. *Packaging, loading, and shipping expenses.* The packaging expense includes the container and the labor to package the product. The loading expense may entail moving the product from the manufacturing department to a centralized storage facility before shipping to a customer. Under the shipping expense may be labor charges for loading on trucks or rail cars and any materials, such as dunnage, required to protect the product containers. Transportation charges vary widely depending on whether the product is shipped by pipeline, barges or tankers, railroad cars, or tank trucks. Companies maintain good expense control records on this item. Depending on the manner in which a product is packaged and shipped, this expense could vary between \$0.013 and \$0.034 per kilogram of product (2000).
17. *Total product expense* is the sum of the total manufacturing expense and the packaging, loading, and shipping expenses.
18. *General overhead expenses* refers to the expense in maintaining sales offices throughout the country, staff engineering departments, research laboratories, and administrative offices. All products are expected to share in these burdens, so an appropriate charge is made for each product. Company accounting departments frequently develop formulas or factors based on sales. The charge is highly dependent on the amount of customer service provided. A factor between 6 to 15% of the annual sales revenue may be assessed. The former figure is for established commodity products, and the latter for new specialty or fine chemicals.
19. *Total operating expense* is the sum of the total product expense and the general overhead expense.

Example 16.2

The Acme Specialty Company is considering manufacturing Plasticizer M. The engineering department has estimated that a fixed capital investment of \$8 million will be required to produce 7.5 million kilograms of product per year. The product is expected to sell for \$1.24 per kilogram.

Indirect conversion expenses:

Depreciation: $\$8,000,000/7 \text{ yr} = \$1,143,000$

Plant indirect expenses: $\$0.03/\text{yr} \times \$8,000,000 = \$240,000$

Total indirect conversion expenses: $\$1,383,000$

Total manufacturing expenses: $\$6,299,000$ (answer a)

Packaging, loading, and shipping expense: $7,500,000 \text{ kg product} \times \$0.01/\text{kg} = \$75,000$

General overhead expenses: $\$9,300,000 \times 0.06 = \$10,000$

Total operating expenses: $\$6,984,000$ (answer b)

Actual operating expense reports, given in Table 16.10, form the basis for information needed for the income statement, Table 16.8, such as the cost of goods sold, depreciation, amortization and depletion, and general overhead expense. This information would be used in the quantitative measures of financial attractiveness.

Additional Reading

J. R. Couper, *Process Engineering Economics*. New York: Marcel Dekker, 2003.

J. R. Couper, O. T. Beasley, and W. R. Penny, *The Chemical Process Industries Infrastructure*. New York: Marcel Dekker, 2000.

J. R. Couper and W. H. Rader, *Applied Finance and Economic Analysis for Scientists and Engineers*. New York: Van Nostrand Reinhold, 1986.

P. Drucker, *Management: Tasks, Responsibilities and Practices*. New York: Harper & Row, 1974.

J. Hackney, *Control and Management of Capital Projects*. New York: McGraw Hill, 1992.

W. E. Wessel, 1952. *Chem. Eng.* 59 (7): 209–210.

16.3.4 ESTIMATION OF FIXED AND TOTAL CAPITAL INVESTMENTS

The fixed capital investment is the cost to build the manufacturing facility. Corresponding to the different levels in the gating process given in Table 16.1 are methods of cost estimation that have different levels of accuracy. Here we describe estimation methods for the conceptual design stages that use process cost correlations (which are usually accurate to ± 40 to 50%) and the “bare module” factor method ($\pm 30\%$). Some estimation methods provide improved accuracy but require vendor quotations; detailed estimates of material costs of piping, valves, and insulation; and estimates of installation labor hours and the mix of labor rates. Such methods are beyond the scope of this chapter.

The methods described here work well if clear definitions, unambiguous terminology, and correct methods to account for alloys, inflation, and location are used, and if care is taken to include all of the cost contributions.

16.3.4.1 Definitions and Terminology

Battery limits cost (BL). This includes the cost of the process itself and excludes the costs of utilities, storage, and services unless these are required only for this process.

BL cost estimation. The simplest and least accurate method uses a correlation of the cost with the capacity of final product. When more accuracy is needed, the process equipment is costed, and costs are attributed to all the components needed to convert the equipment items into a complete working BL process. Many different methods have been developed, depending on the accuracy needed.

Outside battery limits or offsite costs. Factory-site (as opposed to process-specific) facilities such as (a) access roads, rail spur lines, paving, unloading and loading facilities; (b) utilities facilities

different takeoffs are supports (0 to 25%), concrete (5 to 10%), electrical (3 to 5%, with 10 to 15% for fans and compressors and 30 to 75% for pumps), process and utility piping, vents, and sewers, including the "local" pipe rack within about 2 m of the equipment (15 to 60%), insulation (3 to 25%), and painting (1 to 3%). For carbon steel equipment, the material cost, m^* , is usually 60 to 70% of the FOB cost for process equipment handling fluids and 20 to 30% of the FOB cost for process equipment handling primarily solids. Instrumentation costs are handled separately in item 3. The other "material" cost within the module is the FOB cost, item 1.

The costs for the labor, L , include those to receive, uncrate, inspect, haul to the site, and install the equipment, and the labor to install all materials needed to provide the local environment to operate the equipment. If the unit is a skid-mounted package, then the labor cost is 20 to 45% of the FOB cost, which represents the minimum labor cost.

The sum of $L + m^*$ accounts for materials and labor within the BM but excludes the FOB cost (item 1) and excludes freight, tax and duties, instrumentation, buildings, land and site preparation, and long runs of piping needed to connect equipment modules separated by more than the usual distance because of safety. These latter costs are site specific and are added separately.

- (b) $L + M^*$. For ease in calculation, the FOB costs from item 1 are combined with $L + m^*$ costs and expressed as $L + M^* = L + m^* + FOB$. That is, $L + M^*$ cost = $FOB_{\text{carbon steel}} \times L + M^*$ factor. This approach would be used for the purposes of decisions made at Gate 3 in Table 16.1.

The $*$ indicates that the instrumentation costs have been excluded from the factor, and instrumentation is estimated in item 3. Typically, $L + M^*$ factors are in the range 1.2 to 3 times, depending on the type of equipment and the number of such pieces being installed. Table 16.11 gives example values of the factors. Care is needed, because published data report $L + M$ factors but use them as $L + M^*$; others confuse $L + m$ with $L + M$. All $L + M^*$ factors are based on FOB carbon steel equipment; the $L + M^*$ factor varies dramatically with material of construction. Section 16.3.4.5 gives the details.

The $L + M^*$ can be separated into a labor cost and total materials M^* cost if the L/M ratio is known. The L/M ratio ranges from 0.15 to 0.65, with 0.4 as the usual value. Figure 16.2 illustrates how the factors interact.

TABLE 16.11
Illustrative Breakdown of Material and Labor Components

	Centrifuge			Rotary Drum Filter			Crystallizer		
	Total	Labor, L	Material, M	Total	Labor, L	Material, M	Total	Labor, L	Material, M
FOB	1.00			1.00			1.00		
Setting		0.101		1.104	0.104			0.076	
Piping		0.109	0.25		0.07	0.59		0.17	0.41
Insulation		0.024	0.04		—	—		0.024	0.05
Paint		0.01	0.01			0.05		0.005	0.01
Elect		0.122	0.27		0.01	0.10		0.036	0.05
Concrete		0.038	0.09		0.01	0.13		0.048	0.06
Steel		0.049	0.10		0.01	0.15		0.048	0.07
$L+M^*$	2.21	0.453	0.76	2.224	0.204	1.02	2.06	0.407	0.65
L/M	0.26			0.10			0.24		

offsites. For grassroots plants, this is about 45 to 150% of the FOB cost, but the costs should be determined separately for each facility.

8. *Indirects*. Engineering home office expense includes the salaries paid to design engineers, computer time, administration of the contract, records, and drawings for this piece of equipment. This is usually about 10 to 20% of M or 9% of the $L + M$ cost, with larger values needed for small projects.
9. *Indirects*. Field expense includes the salaries for the onsite personnel during construction, security, and inspection during construction for this piece of equipment. This is usually about 20% of the $L + M$ module cost or 50 to 80% of L .
The total of the indirects, items 8 and 9, is 10 to 45% of the $L + M$ module cost, with small values for large projects.
10. *Total*. The sum of items 5, 6, 8, and 9 (with an allowance for modification of the offsites as needed, item 7) is referred to as the *direct* or *bare module costs (BM)*.
11. *Contractors' and subcontractors' fees*. This is usually 3 to 5% of the BM cost.
12. *Contingency* for strikes, tornados, floods, and unexpected delays in delivery. This is usually 10 to 15% of the BM cost and does not include engineering errors, engineering uncertainties in design, or uncertainties in quotations.
13. *Design contingency* for changes in the scope during construction. Allow 10 to 30% of the BM cost.
14. *Total*. The sum of items 10, 11, 12, and 13 is called the *total module cost (TM)* or the *fixed capital investment cost*.
15. *Royalties, licenses, know-how fees, and regulatory permits*.
16. *Land* and (a) the initial site preparation such as grading and drainage and (b) the special foundation costs such as pile driving and rock blasting. These costs are important for many wastewater treatment facilities, which are often located on low-grade land. This is often about 1 to 2% of the TM cost. Site development is sometimes expressed as 10 to 20% of the FOB cost.
17. *Spare parts* (these are especially important for remote factory sites). Use 4 to 8% of the FOB equipment cost for the MPI or 1 to 2% of the TM cost.
18. *Interest* during the construction period and/or the cost of borrowing capital and paying it back, as with a municipal bond. This can be estimated to be 6% of the TM cost.
19. *Legal fees*. An estimate might be 1% of the TM cost.
20. *Working capital*. This accounts for the initial charge of solvent, catalyst, heat transfer media, and initial inventory of raw materials and of product awaiting sale. For commodity and pseudocommodity products produced at a uniform rate, use 15 to 20% of the TM cost. For seasonal products such as herbicides and fertilizers, use 25 to 40% of the TM.
For specialty products like perfumes, cosmetics, and flavors with high raw material costs and relatively low TM costs, it may be preferred to express working capital as 15 to 40% of sales, with 30% being a reasonable value.
21. *Startup expenses*. These include a living allowance for the startup team, special tests and test equipment, and computer costs until the process is producing specification product. Estimate as 8 to 10% of the TM cost. Operator training is 0 to 4% of M . The total startup expense is 15 to 40% of M .

Although the 21 items usually represent the total capital investment, different items are excluded for different purposes. For example,

- Item 20. This cannot be included as the cost of fixed assets for government depreciation purposes.
- Item 18. For a municipal waste treatment facility, the project must be self-financed, because the municipality does not have a continual reserve. Hence, the cost of capital

TABLE 16.12
Inflation Indices

	CE Index (1957–59 = 100)	CE Instruments (1957–59 = 100)	MS; Process Industry (1926 = 100)	M&S Index: All Industry (1926 = 100)
1980	261.1	249.5	676	659.6
1981	297.0	287.9	744.9	721.3
1982	314.0	297.6	774.4	745.6
1983	316.9	308.4	786	760.7
1984	322.7	319.1	806.5	780.4
1985	325.3	322.8	813.4	789.6
1986	318.4	324.5	816.9	797.7
1987	323.8	330.0	830.4	813.6
1988	342.5	341.9	870.1	852.0
1989	355.4	352.1	914.2	895.1
1990	357.6	353.6	934.5	915.1
1991	361.3	353.8	951.8	930.6
1992	358.2	356.6	960.5	943.1
1993	359.2	358.4	975.3	964.2
1994	368.1	365.4	1000	993.4
1995	381.1	378.3	1037.3	1027.5
1996	381.7	372.2	1051.3	1039.2
1997	386.5	372.4	1068.3	1056.8
1998	389.5	365.5	1077	1061.9
1999	390.6	363.5	1083.1	1068.3
2000	394.1	368.5	1102.7	1089
2001	394.3	363.3	1109.0	1093.9
2002	395.6	363.5	1121.1	1104.2
2003	402.0	365.8	1143.5	1123.6
2004	444.2	374.3	1201.8	1178.5
2005	468.2	381.8	1295.1	1244.5
2006	499.6	420.1	1364.8	1302.3

16.3.4.3.2 Location

Construction costs differ depending on the location, since labor costs and productivity differ. The labor component for North America can be extracted from $L + M^*$ data through the L/M ratio data and adjusted to reflect location costs and productivity. Illustrative location indices, given in Table 16.13, compare construction costs for complete processes in U.S. dollars to the cost in U.S. dollars in a different country. Specialists in your company should be consulted to obtain pertinent data.

16.3.4.4 Estimating the $L + M$ Cost of Instrumentation

Three options to estimate the cost are to use an average cost per MPI, cost the control elements per MPI, and cost the instrumentation for different types of equipment.

Option 1: Main Plant Items and an Average Cost for Instrument

For typical process plants, use \$47,000 U.S. (CE instruments = 1000) per MPI; for highly automated batch processes, use \$69,000 to \$82,000 U.S. (CE instruments = 1000) per MPI. CE instruments is the *Chemical Engineering* inflation index for process instruments. Details are given in Section c and in Table 16.12. Scale the instrument cost to the correct time.

Option 2: Take-Offs for Different Types of Processes

Table 16.14, based on Navarrete (1995) and Page (1996), reports the number of different elements in the distributed control system (DCS) for the MPIs in different types of plants. The average number of field instruments decreases as the scope of the project increases.

TABLE 16.14
Number of Elements per MPI (Based on Page, 1996, and Navarrete, 1996)

Elements	Different Types of Plants			
	Usual Overall	Batch Process	Continuous Process	Storage Area
DCS Points	2	3.6	1.7	1.0
DCS wiring units	3	5.4	2.5	1.5
Field instruments	7.5–2.5	12	7	6.5
Air hookups	1	1.8	0.9	0.5

Total $L + M$ cost = DCS FOB cost + 2.1 (FOB cost for field instrumentation), where

DCS FOB, hardware including computer = \$5000 (CE = 1000)/point

FOB field instrumentation c/s equipment = \$1800 (CE = 1000)/balloon for carbon steel.

The alloy cost factors are low alloy $\times 1.33$, high alloy $\times 1.5$.

Option 3: Costs for Instrumentation of Particular Types of Equipment

Table 16.15 lists “typical” DCS (control loops, C; alarms, A; and transmitters, T) and the types of field instruments (indicators, I, and relief valves, R) for different types of equipment and their FOB cost. For this list, we give an estimate of the installed instrument cost in Table 16.15. These results are reasonably consistent with the previous two methods.

16.3.4.5 Accounting for Materials of Construction Other Than Carbon Steel

In Section 16.3.4.2, the $L + m^*$ costs were expressed as a fraction of the cited FOB cost (which is usually carbon steel fabrication). If the equipment is made of an alloy, the FOB cost of the equipment is larger, say \$70,000 instead of \$30,000. However, the $L + m$ costs of concrete, painting, insulation, and other components in the BM remain about the same as they were for the carbon steel equipment. To account for this, we need to multiply the FOB alloy cost by an $L + M^*$ factor that is smaller than the factor reported for carbon steel. This is counterintuitive, because we intuitively may think “alloys” = “more expense for everything.” The amount of reduction in the $L + M^*$ factor for carbon steel is determined from Figure 16.3.

Example 16.3

- The FOB cost of a carbon steel pressure tank is \$70,000, CE = 400. What is the $L + M$ cost if the $L + M^*$ factor is 2.5?
- The vessel needs to be 316 stainless steel. If the FOB alloy cost is 1.4 times the carbon steel cost, what is the $L + M$ cost?

Solution to Part a

The $L + M^*$ cost is $L + M^* \times \text{FOB} = 2.5 \times \$70,000 = \$175,000$.

Comment: In practice, a date or inflation index value and error range should be given with every cost estimate.

For preliminary estimates using FOB cost correlations and $L + M^*$ factors, the error is usually $\pm 30\%$.

In addition, we need to add the $L + M$ cost of instrumentation. For a pressure tank, from Table 16.15, the $L + M$ cost of instruments is \$8300 at CE = 1000. Therefore, the cost at

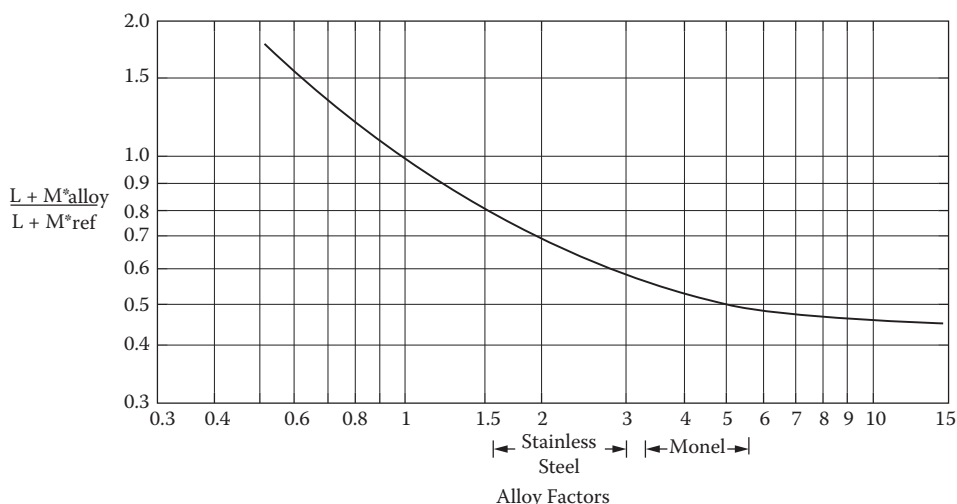


FIGURE 16.3 $L+M^*$ and alloys (reproduced with permission from Donald R. Woods, *Rules of Thumb in Engineering Practice*, page 377, 2007, copyright Wiley-VCH Verlag GmbH & Co. KGaA, Weinheim, ISBN: 978-3-527-31220-7).

CE = 400 would be found by the ratio of the indices = $\$8300 \times 400/1000 = \3320 . The $L + M$ cost at CE = 400 is $\$175,000 + 3,320 = \$178,320$ or $\$178,000 \pm 30\%$.

Solution to Part b

The FOB cost of the stainless steel vessel is $\$70,000 \times 1.4 = \$98,000$.

The $L + M^*$ ratio for an alloy of 1.4 is 0.82, from Figure 16.3. The $L + M^*$ factor for the alloy is therefore $L + M^*$ carbon steel \times correction factor = $2.5 \times 0.82 = 2.05$. Therefore, the $L + M^*$ cost is $\$98,000 \times 2.05 = \$196,000 \pm 30\%$ at CE = 400.

Comment: we need to add the cost of instruments = $\$3320$ from part a for an $L + M$ cost = $\$199,320$ or $199,000 \pm 30\%$ at CE = 400.

16.3.4.6 Different Methods for Different Levels of the Gating Process

For *preliminary evaluation* (Gate 1 in Table 16.1), correlations for complete processes scaled up for capacity and for time are commonly used. For a *conceptual design* (Gate 2), FOB equipment cost correlations based on flow rate are often used and scaled up to BM cost based on $L + M^*$ factors. For a *preliminary engineering design* (Gate 3), the equipment is sized more accurately; based on simple rules of thumb, the cost is estimated from FOB cost correlations related to equipment size and scaled up to BM cost based on $L + M^*$ factors. The process and FOB cost correlations are all of the form

$$\text{cost} = \text{cost}_{\text{reference}} \left(\frac{\text{size}}{\text{size}_{\text{reference}}} \right)^n$$

Tables of cost data are given for the reference cost corresponding to the reference size, for example, *flow rate*, *annual production*, *filter area*, the exponent n (e.g., usually $n = 0.6$ to 0.7), the range of the size variable over which the correlation is valid, and the error (e.g., $\pm 30\%$). Sometimes the costs for one piece of equipment will be correlated with a different exponent, n , for different size ranges. For example, for flow rates 10 to 100, $n = 0.4$. For flow rates 100 to 1,000, $n = 1.0$.

$$\begin{aligned}\text{FOB cost} &= \$900,000 \left(\frac{400}{1000} \right)^{0.56} \\ &= \$539,000\end{aligned}$$

$$\text{FOB cost at CE} = 400 = \$215,600$$

$$L + M^* \text{ cost} = \text{FOB} \times 2 = \$431,200$$

Accounting for instrumentation, from Table 16.15, estimate minimal controls needed as \$8,000 at CE = 1000 or $\$8,000 \times 400/1000 = \$3,200$. Hence, $L + M$ cost = $\$431,200 + 3,200 = \$435,000 \pm 35\%$ at CE = 400.

16.3.4.6.3 FOB Equipment Cost Correlations Based on Design Size and BM Module Factor Method

For this method, the size, materials of construction, and conditions of operation for the process equipment must be known. The calculation is the same as that used in Example 16.3. The difference is an increase in accuracy for the estimate of the FOB cost because the correlation requires an estimation of *size* of the unit instead of the *flow to the unit*. For example, for a bag filter, we could use a cost correlation based on feed gas flow rate to the filter or, for increased accuracy in engineering design, use a correlation based on the bag filtration area. Since the gas flow rate/unit filter area depends on the specific application, the cost correlation based on filtration area is site specific and therefore more accurate. Cost correlations based on flow rate are usually less accurate (± 25 to 40%) than those based on design size (± 15 to 30%). Rules of thumb, given in Section 16.11, can be used to obtain the size.

Additional Reading

- D. E. Garrett, *Chemical Engineering Economics*, New York: Van Nostrand Reinhold, 1989. Provides sound basic advice with data in appendices (general).
- The American Association of Cost Engineers is an excellent organization that publishes data and holds annual conferences. <http://www.aacei.org>.
- Richardson Engineering Services, *Process Plant Construction Estimating Standards*, vols. 1–4. Annual publications give FOB and take-off costs for equipment, piping, concrete, mechanical and electrical. <http://www.resi.net>.
- Woods, D. R. et al. have published a series of papers on estimating offsites:
- 1979. *Canadian Journal of Chemical Engineering* 57: 533–566 (utilities).
 - 1982. *Canadian Journal of Chemical Engineering*, 60: 173–201 (offsite industrial gases).
 - 1993, 1994. *Canadian Journal of Chemical Engineering*, 71: 575–590; 72: 342–351 (liquid disposal).
- Page, J. S. *Conceptual Cost Estimating Manual*, 2nd ed. Houston: Gulf Publishing, 1996. Gives FOB cost and erection man-hours for about 200 types of process equipment plus take-offs for site preparation, concrete, structural steel, buildings, piping, electrical, instrumentation, insulation, painting, paving, overheads, and indirects.
- Guthrie, K. M. *Process Estimating, Evaluation and Control*. Solana Beach, CA: Craftsman, 1974. The original classic that we still refer to often. A gold mine of data.
- J. Cran. 1981. *Improved Factor Method gives Better Preliminary Cost Estimates*. *Chemical Engineering*, April, 65–79.
- P. F. Navarrete. *Planning, Estimating and Control of Chemical Engineering Construction Projects*. New York: Marcel Dekker, 1995.

kinematic, and dynamic conditions. To achieve this, the dimensionless numbers are kept the same for small- and large-scale operations. *For example, a mix in the lab should not be done with a magnetic stirrer, because this does not match geometrically the large-scale operation from, say, a propeller agitator. For mechanical similarity, for some operations, operate at the same impeller Reynolds numbers for small- and large-scale equipment.*

For drops, bubbles, particles, or catalysts, we cannot scale down, because the area, volume, and surface/volume ratio change. For this situation, we often use the “element” strategy in which the small scale consists of a small slice of the real situation that contains the real size of the drops, bubbles, packing, or catalyst. Recurring sources of scale-up problems include (a) the inability to have similar equipment shape; (b) faulty accounting for the batch vs. continuous operation and the scale of operation; (c) changes in the surface/volume ratio that cannot be appropriately accounted for; (d) unexpected flow patterns; (e) flow instability and mixing characteristics, (f) wall, edge, and end effects; (g) materials of construction; (h) trace impurities; and (i) heat removal from gaseous, highly exothermic catalytic reactions.

Additional Reading

- A. Bisio and R. L. Kabel, *Scaleup of Chemical Processes*. New York: John Wiley & Sons, 1985. Chapters from 17 experts. Six of the 18 chapters are on reactors.
- H. F. Johnstone and M. Thring, *Pilot Plants, Models and Scale-Up Methods in Chemical Engineering*. New York: McGraw Hill, 1957. A classic on how and what to consider.
- S. J. Kline, *Similitude and Approximation Theory*. New York: McGraw Hill, 1960. A fundamental view of creating dimensionless groups.

16.4.3 UNITS OF MEASUREMENT AND COMMUNICATION

My calculations for the first plant I designed were 10% too small. That is because I was working in *short* tons (2000 lb), whereas my supervisor in this UK-based company assumed I was using *long* tons (2240 lb). The definitions of such terms as ton, yard, inch, gallon, and barrel vary around the world. Fortunately, the SI (Le Systeme International d'Unites) eliminates most ambiguity, and the use of the time unit of seconds and length unit of meters allows simple determination of force and energy without additional factors. However, care is still needed. Some engineers and texts use metric units instead of SI and assume they are using SI. Examples include the archaic use of mm mercury, bar, torr, and kg/cm² for pressure instead of Pa; the use of calorie instead of joule; and the use of minutes, hours, or days instead of the standard use of second.

Concerning powers, often the SI prefixes work well *provided* everyone knows the definitions. A common error is to use lowercase “m” or “MM” instead of capital “M” to represent 1000 kg. Care is needed to distinguish between gauge pressure and absolute pressure; it is recommended that all pressures (except for differences in pressure) be reported as kPa-g or kPa-a.

16.4.4 GATHER INPUT DATA FROM DATABASES FOR DESIGN AND PROCESS IMPROVEMENT

Data needed include expected variations in conditions; costs of materials, labor, equipment, and utilities; disposal limitations; sources; legal definitions and restrictions; environmental impact measures; and numerical values for the criteria. For all the species involved in the process, we need physical and thermodynamic data, and such reactivity and safety properties as flammability, corrosivity, abrasiveness, and propensity for dust explosions of solids, stability, environmental persistence and health indicators such as the LD₅₀, carcinogenicity, mutagenicity, and toxicity and those listed in Table 16.16.

TABLE 16.16 (Continued)
Definitions of Key Terms

LC ₅₀ lethal concentration	Administered via 4-hr inhalation will cause death 50% of the time within 14 days.
LEL	Lower explosive limit, the minimum concentration of combustible material that will support combustion.
Light liquid	One that contains a liquid compound to the extent >20% w/w that has a vapor pressure greater than 0.3 kPa at 20 °C.
Light liquid petroleum	One that has >10% evaporate at 150°C.
MAK	Maximale Arbeitsplatzkonzentration or maximum workplace concentration.
Mond rating	Ratings are based primarily on flammability.
Mutagenic	Risk of hereditary genetic defects.
NFPA	National Fire Protection Association. System gives a qualitative rating for health, flammability, and spontaneity. These values range from 0 to 4, with 4 being the most hazardous. These can be used for an initial screen to sensitize engineers to the potential hazard. Quantitative values are published elsewhere for each separate issue: health (TLV, STEL, IDLH); flammability explosivity (upper and lower explosive limits).
OSHA	Rating of employee exposure and working conditions.
Overpressure	Pressure exerted on an objective from an impacting shock wave.
PDEP corrosion index	Process Design and Engineering Practice qualitative rating on the corrosivity of pure components contacting carbon steel, copper, and 316 stainless steel. These can be used for an initial screen to sensitize engineers to the potential hazard (Woods, 1994).
PEL	Permissible exposure limits; typical worker can be exposed to this time-weighted average concentration of the substance for 8 hr per day, five days per week for a working lifetime, without ill effects.
RCRA	Resource Conservation and Recovery Act (U.S.). Legislation dealing with licenses, fees, and accountability for the processing of hazardous wastes.
STEL	Short-term exposure limit, a 15-min time-weighted average concentration. Example: TLV-STEL for monochloroethane is 1250 ppm or 3250 mg/m ³ .
Teratogenic	Risk of subsequent nonhereditary birth defects.
TWA	Time-weighted average.
TLV-STEL	Threshold limit values as measured by short-term exposure. A typical worker can be exposed to this time-weighted average concentration of the substance for 15 min without ill effects. (UK based on 10-min TWA), benzene, 50 ppm.
TLV-TWA	Threshold limit values as measured on a time-weighted average (sometimes referred to as the ACGIH permissible limit values). Typical worker can be exposed to this time-weighted average concentration of the substance for eight hours per day, five days per week for a working lifetime, without ill effects. Example: TLV-TWA for monochloroethane is 1000 ppm or 2600 mg/m ³ ; benzene, 10 ppm.
UFL UEL	Upper explosive limit; the maximum concentration of combustible material that will support combustion.
VCE	Vapor cloud explosion; occurs when a cloud of combustible material is within the flammable or explosive limits.
VOC	Volatile organic compound.

Data from each of the HON, OSHA, NFPA, Dow, and Mond hazard ratings should be gathered. Example 16.7 highlights the disadvantages of using only one type of hazard indicator and the importance of knowing the legal ratings.

Example 16.7

Acetophenone is on the HON and HON Section F list (defined in Table 13.16) as a hazardous chemical. Thus, legally we must monitor and minimize emissions from vents, storage vessels, and transfer racks, and discharges to wastewater, and minimize leaks from rotating shafts, sampling, and

TABLE 16.17
Bonds That Are Potentially Hazardous

Type		Examples	
Vinyl	$-\text{CH}=\text{CH}_2$	Styrene, vinyl chloride, ethyl acrylate	Exothermic polymerizations
	$>\text{C}=\text{CH}-\text{CC}-$	Vinyl acetylene	Contains peroxidisable hydrogen with potential for explosion
Congugated double bonds with carbon, nitrogen, and oxygen atoms	$-\text{CH}=\text{CH}-\text{CH}=\text{CH}-$	Butadiene, isoprene, chloroprene, cyclopentadiene	Exothermic polymerizations
	$-\text{CH}=\text{CH}-\text{CH}=\text{O}$	Acrolein, crotonaldehyde	Exothermic polymerizations
Adjacent double bonds	$-\text{CH}=\text{CH}-\text{C}=\text{N}$	Acrylonitrile	Exothermic polymerizations
	$-\text{CH}=\text{C}=\text{O}$	Ketene	Exothermic polymerizations
	$-\text{N}=\text{C}=\text{O}$	Methyl isocyanate, toluene diisocyanate	Exothermic polymerizations
Three-membered rings	$\begin{array}{c} \text{O} \\ \diagup \quad \diagdown \\ -\text{CH}-\text{CH}_2 \end{array}$	Ethylene and propylene oxide, epichlorhydrin	Exothermic polymerizations
	$\begin{array}{c} \text{NH} \\ \diagup \quad \diagdown \\ -\text{CH}-\text{CH}_2 \end{array}$	Ethylene imine	Exothermic polymerizations
Aldehydes	$-\text{CH}=\text{O}$	Acetaldehyde, buyraldehyde	Exothermic polymerizations: contains peroxidisable hydrogen with potential for explosion
	$>\text{CH}-\text{O}-$	Acetals, ethers, oxygen heterocycles	Contains peroxidisable hydrogen with potential for explosion
Isopropyl compounds	$-\text{CH}_2$	Isopropyl compounds, decahydronaphthalenes	Contains peroxidisable hydrogen with potential for explosion
	$>\text{CH}-$		
Allyl compounds	$-\text{CH}_2$	Allyl compounds	Contains peroxidisable hydrogen with potential for explosion
	$>\text{C}=\text{C}-\text{CH}_2-$		
Haloalkenes	$>\text{C}=\text{CH}-\text{X}$		Contains peroxidisable hydrogen with potential for explosion
Dienes	$>\text{C}=\text{CH}-\text{C}=\text{CH}<$		Contains peroxidisable hydrogen with potential for explosion

TABLE 16.20

Fate of Chemical Species: Distribution among Compartments and Degradation Rate within Each Compartment (Mackay and Paterson, 1991)

Synthetic Chemical Species	Illustrative Amount in the Compartment or Distribution among Compartments	Rate of Assimilation within a Compartment		Net Overall Rate of Assimilation in the Ecosphere
		Degradation Rate Constant, h ⁻¹	Comments	
Benzene	air [2500 ng/m ³]	8.6 × 10 ⁻⁴	partitions mainly to the air	about 50 to 200 h depending on the atmospheric temperature
	soil [0.01 µg/kg]	0		
	water [290 ng/L]	0.0048		
	biota [0.002 mg/kg]	0		
	suspended solids			
Benzopyrene	sediment [0.5 ng/g]	0		
	air [3.0 ng/m ³]	0		
	soil [0.04 mg/kg]	3.5 × 10 ⁻⁵		
	water [11 ng/L]	3.5 × 10 ⁻⁵		
	biota [0.26 mg/kg]	0		
Hexachlorobiphenol	suspended solids			
	sediment [190 ng/g]	0		
	air [1.4 ng/m ³]	0		> 8 years
	soil [0.04 mg/kg]	1.5 × 10 ⁻⁵		
	water [5 ng/L]	1.5 × 10 ⁻⁵		
Hexachlorobenzene	biota [0.2 mg/kg]	1.0 × 10 ⁻⁶		
	suspended solids			
	sediment [80 ng/g]	1.5 × 10 ⁻⁵		
	air [0.2 ng/m ³]	0.0144		> 10 years
	soil [0.0009 mg/kg]	1.9 × 10 ⁻⁵		
water [1.3 ng/L]	0			
	biota [0.01 mg/kg]	0	high bioconcentration potential	
	suspended solids			
	sediment [7 ng/g]	0		

Example 16.8

Mackay and Patterson (1981) estimated that 79% of DDT would end up in sediments, 98% of benzene in the air, and 61% of p-cresol in water. Hence, the biodegradation of most interest would be for DDT in sediments, for benzene in air, and for p-cresol in water.

Step 2. Estimate the bioassimilation of the species in the dominant compartment.

Additional Reading

- D. T. Allen and D. R. Shonnard, *Green Engineering: Environmentally Conscious Design of Chemical Processes*. Englewood Cliffs, NJ: Prentice Hall, 2002. <http://www.epa.gov/oppt/greenengineering>.
- D. R. Woods, *Data for Process Design and Engineering Practice*. Englewood Cliffs, NJ: Prentice Hall, 1994. Gives order of magnitude values of properties for more than 1200 compounds and a guide to sources for more accurate data. This includes the PDEP Corrosion Index referred to in Table 13.16.
- R. C. Reid, J. M. Prausnitz, and B. E. Poling, *The Properties of Gases and Liquids*, 4th ed. New York: McGraw Hill, 1987. Gives methods for estimating properties.
- R. King, *Safety in the Process Industries*. Oxford, UK: Butterworth-Heinemann, 1990.

TABLE 16.21
Non-Renewable Minerals (from Holmberg et al., undated)

Element	Amount in the Lithosphere, Eg	Rate of Global Mining/Rate of Global Weathering
Abundant		
Aluminum	1,200,000	0.02
Iron	720,000	1.4
Magnesium	15,000	< 0.01
Titanium	82,000	0.06
Scarce		
Cadmium	8.3	3.8
Chromium	1,200	16
Copper	760	24
Lead	200	12
Molybdenum	17	7.5
Mercury	1.2	3.8
Nickel	920	3.0
Zinc	1,200	8.1

A. S. Elstein et al., *Medical Problem Solving: An Analysis of Clinical Reasoning*. Cambridge, MA: Harvard University Press, 1978. Gives a superb description of how to troubleshoot when we must *hypothesize* about the cause. Written in a medical context, but most of the ideas apply directly.

16.5 SUSTAINABILITY FROM THE START

Robert's (1992) program, The Natural Step (TNS), is preferred to such options as life cycle, ecological footprinting, and green engineering. The four principles of TNS are as follows:

1. Substances extracted from the core, mantle, and crust of the Earth (such as oil and fossil fuels, metals, and other minerals) must not systematically accumulate in the ecosphere. The rate of mining from the Earth's crust must not be at a pace faster than the extracted species can be redeposited and reintegrated into the crust. The rate of extraction can be reduced by recycling or by substitution. Table 16.21 lists minerals and compounds present in the lithosphere that are deemed to be economically extractable based on today's best practice. Also shown is the ratio of annual rate of mining to the rate of natural weathering. All abundant minerals (except iron) have values < 1. However, all scarce metals have values > 1. For the sources of energy given in Table 16.22, shift toward renewable resources.
2. Substances produced by society must not systematically increase in the ecosphere. Yet some synthetic substances are produced at rates faster than they can be broken down and integrated into the cycles of nature.
3. The physical conditions for productivity and assimilation within the ecosphere cannot be systematically diminished. Forests, wetlands, prime agricultural land, and natural plants and animals cannot be systematically diminished. The assimilative capacity of the ecosystem must exceed any rates of pollution so that nature can regenerate itself. The rates of use of renewable resources do not exceed their rates of regeneration. Table 16.23 illustrates the net rate of natural regeneration.
4. Since we have limited resources and a human population with needs, the basic human needs must be met with the most resource-efficient methods possible. The satisfaction

Additional Reading

- K.-H. Robèrt, *The Necessary Step*. Stockholm: Ekerlids forlag. This is the original publication. However, sites on the Web provide more accessible data and examples. Search for "The Natural Step." Some example sites are <http://www.globalideasbank.org/BOV/BV-273.html>, <http://www.naturalstep.org>, and <http://iisd.iisd.ca/business/naturalorg.htm>.
- D. T. Allen and K. S. Rossetot, *Pollution Prevention for Chemical Processes*. New York: John Wiley & Sons, 1997. The authors do not use The Natural Step, but they provide excellent insight into sustainability.
- D. T. Allen and D. R. Shonnard, *Green Engineering: Environmentally-Conscious Design of Chemical Processes*. Englewood Cliffs, NJ: Prentice Hall, 2001.

16.6 OPERABILITY AND CONTROL CONSIDERED THROUGHOUT

Chemical processes must be controlled to make them operable, profitable, safe, and environmentally friendly. Issues of control affect process design, process improvement, and troubleshooting.

16.6.1 CONTROL AND DESIGN

Control is the heart of process design; how to control the plant effectively should be in the designer's mind right from the very beginning of the design process.

16.6.1.1 Design: Impact of Control on the Initial Design Statement

The initial design statement usually identifies the target product, amount, and purity. However, the initial design goal should also include the base case conditions, the expected setpoint changes, and the likely process disturbances.

16.6.1.1.1 Range of Setpoints

The range in production modes is determined by *setpoint*:

- Production rate (processes typically operate at 80% design capacity).
- Product specifications and the distribution among products on multiproduct processes.
- The range in product purity. The product purity has a major impact on both capital investment costs and operating costs. For example, for distillation, increasing the purity specifications by 1% may increase the energy requirement by about 10%. For sulfur removal from waste gases, for the same volume of gas treated, the fixed capital investment triples when the sulfur removal is changed from 90 to 99%.
- The different grades of a product customers want and may want in the future, for example, the grades of acid.

16.6.1.1.2 Range of Anticipated Process Disturbances

Anticipated disturbances include the range in feedstock composition, the range in expected utility properties (summer and winter temperatures of the cooling water and of the air), the slow drift in reaction kinetics, the gradual deactivation of the catalyst, and the gradual fouling of heat exchangers. Downs and Vogel (1993) provide a good example of a well-defined problem with the setpoint specifications in Table 7 and the disturbances in Table 8 in their paper.

16.6.1.2 Design: Impact of Control on the Evolving Flowsheet

Major issues include surge volume, recycle, and the control system:

Surge volume. As the flowsheet design progresses, sufficient (but not excessive) surge volume must be provided. The trade-off is between a steady-state and a safety viewpoint, in which the surge volumes are eliminated to minimize the capital cost and the volumes of hazardous

time constants, minimize sensor dynamics (especially sample systems for analyzers), and provide the required upstream and downstream lengths of straight pipe for flow meter and sensor reliability. Prevent maldistribution of flow in parallel systems. The selection and location of steam traps and air vents are important.

Consider using statistical process control, reexamine the types and locations of sensors, and use the four basic levels of control: (1) basic process control system, (2) alarm system, (3) safety interlock system, and (4) relief system. Consider active/passive controls. Active controls include sensors to detect hazardous or unsafe conditions; for example, a flame sensor that is used to shut down the fuel supply if no pilot flame is present and sensors for trace impurities that trigger deflagration. Passive controls (or self-regulating control systems) include fail-open and fail-shut valves, safety relief valves, and bursting disks to release pressure; large solvent or heat transfer fluid heat sinks to absorb heats of reaction should the cooling system fail; and the addition of a cold shot or reaction inhibitor. Prevent overheating by limiting the steam pressure; use tempered water instead of steam to ensure that the heating medium cannot overheat sensitive reactants. Include process conditions that have a negative temperature coefficient on reaction conditions. Self-limiting reactor configurations could be used. Marlin (2000) provides details.

16.6.2 CONTROL AND PROCESS IMPROVEMENT

To improve processes and remove bottlenecks, one of the first areas of focus is control. For batch processes, consider installing surge volumes to smooth out variations and make overall batch operations more efficient. Add the four levels of control.

The location and type of sensor can greatly affect controllability, safety, and on-time reliability. Controllability can also be improved when a different type of sensor is used. For example, a temperature sensor might be used to infer composition. Such a sensor is easy, robust, and accurate in measuring the temperature. However, the new specifications for the purity have shifted the composition to a range where temperature measurements are no longer sensitive to the composition. Refractive index measurements should be used.

Control can often be improved by using statistical process control. Montgomery and Runder (1994, Chapter 14) and Kourti and MacGregor (1996) describe this approach.

16.6.3 CONTROL AND TROUBLESHOOTING

When trouble occurs, one of the first steps is to put the system on manual control and see if the trouble disappears. Other suggestions are given in Section 16.11.1.1 on rules of thumb for process control.

Additional Reading

- T. Marlin, *Process Control*, 2nd ed, New York: McGraw Hill, 2000. <http://chemeng.mcmaster.ca>.
- J. J. Downs and E. F. Vogel, 1993. A Plant-Wide Industrial Process Control Problem. *Computer Chem. Eng.* 17, 3: 245–255.
- Luyben, M. L. et al., 1997. Plantwide Control Design Procedure. *AIChE Journal* 43, 3161–3174.
- Luyben, W. L., *Process Modeling, Simulation and Control for Chemical Engineers*. New York: McGraw Hill, 1989.
- Montgomery, D. C. and G. C. Runger, Statistical Process Control, chap. 14 in *Applied Statistics and Probability for Engineers*. New York: John Wiley & Sons, 1994.
- Kourti, T., and J. F. MacGregor, 1996. Multivariate Statistical Process Control methods for Monitoring, Diagnosing Process and Product Performance. *J. Qual. Tech.* 28: 409–428.

Use checklists, such as given in Table 16.24, to identify potential waste reduction and safety opportunities. Identify opportunities by challenging the nominal specifications.

16.7.2 STEPS 2 THROUGH 5: MOVE FROM “ELIMINATE” TO “ISOLATE” DURING THE DESIGN PROCESS

Guidelines for inherent safety, environmental protection, or waste minimization can be summarized in the following five steps that move from elimination to isolation.

16.7.2.1 Step 2: Eliminate the Source

Eliminate the source at the reactor and elsewhere in the process.

16.7.2.1.1 At the Reactor: Eliminate, Substitute, and Recycle

Eliminate

Eliminate reactants that pose problems with sustainability, the environment, and the hazard.

Substitute

Modify the reaction pathway, the operating conditions, the heat management system, and the reactor configuration.

Change the reaction pathway. Select reaction pathways between the raw material and the desired product to eliminate the use of hazardous intermediaries.

Change the operating conditions. Alter the reaction conditions to eliminate the hazards or production of toxic waste. Waste by-products from the reactor can be eliminated if the reaction to produce the by-products is reversible (as for biphenyl production in the hydrodealkylation process).

Change heat management systems. Substitute sources of thermal energy and provide active and passive control. For example, for the catalytic liquid-phase oxidation of a substituted acetophenone to produce carboxylic acid operating at 80°C, the reaction is very exothermic (–920 MJ/kmol acetophenone) and poses great potential for temperature runaway. Temperature runaway can be prevented by the use of a catalyst that deactivates at 100°C.

Change the reactor configuration to minimize hazard.

Recycle

Recycle by-products until the rate of production of the by-product equals its rate of consumption.

16.7.2.1.2 Elsewhere in the Process: Eliminate, Substitute, and Recycle.

Eliminate

Additives. Eliminate catalysts, solvents, and adsorbents. For example, use thermal hydrodealkylation instead of catalyzed hydrodealkylation.

Trace contamination. Eliminate by locating air and water intakes in pollution-free locations. For example, instrument air compressors for a plant site were incorrectly located beside ammonia refrigeration units. Throughout the plant, the ammonia reacted with the mercury to produce azides in the instruments.

VOCs. Eliminate by eliminating rotating shafts that must be sealed or by selecting a sealing mechanism that produces no emissions. Use welded pipe instead of flanges. Table 16.25 provides data for options.

The source of electrical hazards. Eliminate electric sparks and charge buildup; replace electrical with pneumatic instrumentation, replace electric-driven with steam-driven devices. Eliminate charge buildup by increasing conductance, e.g., increasing the conductivity of the atmosphere (via ionization) and increasing the conductivity of nonconductors (by humidification or additives).

TABLE 16.24 (Continued)
Potential Sources of Wastes and Safety Hazards

Waste from general operation and maintenance

Oils and lubricants
 Equipment cleaning
 Sampling and analytical losses
 Purges of internal environments at startup and shutdown

Safety hazards from general operation and maintenance

Poor housekeeping,
 Electrical lines and water
 Maintenance done on wrong equipment
 Inadequate isolation of equipment; venting of atmosphere;
 removal of toxics
 Insufficient room around equipment

Safety hazards from packaging and storage

Storage mass larger than safe maximum

Wastes from packaging and storage

Packing, use of non-reusable drums
 Failure to use disposable liners
 Damage during storage
 Storage vessel residue
 Fugitive via vents

Safety hazards because of fugitive emissions

Wastes from fugitive emissions

Seals around rotating shafts: valves, pumps, compressors,
 mixers
 Breathing from storage vessels

Safety hazard because of accidental spills

Wastes from accidents

Incidental spills

Wastes from metal sludges (approximately 0 to 150 kg/Mg product)

Wastes from slags and ashes (approximately 10 to 50 kg/Mg product)

Non-chemical industrial wastes (approximately 10 to 80 kg/Mg product)

Substitute

Mechanical gauges for mercury gauges. Nonhazardous additives: solvents, catalysts, filter aids, adsorbents, absorbents. Nonhazardous solvents can be identified by matching the Hildebrand hydrogen bond and polar solubilities parameters and the molar volumes. Example substitutions are water > nonpolar organic > aliphatics with flashpoint < 60°C > aliphatics with flashpoint > 60°C > aromatics > halohydrocarbons > polar organics > alcohols > organic acids > other oxygenates > nitrogen-bearing compounds > halogenated organics > chlorinated organics.

Recycle

Water. Caution: account for the buildup of trace amounts of other species; salts may precipitate if the concentration of salts becomes too high. Increased corrosion can occur because the recycle causes the buildup of unexpected species that enhance corrosion. Trace surfactants can build up and stabilize foams, causing foaming in distillation and stable emulsions in decanters. Although the buildup of trace species can be controlled by purging or by separation, the location of the purge stream can affect the overall performance. Purging minimizes but does not eliminate waste.

16.7.2.2 Step 3: Minimize the Source

If one cannot eliminate, one can at least minimize.

TABLE 16.26
Dust Emissions from Various Equipment Options

Source	Description of Equipment Option	Emission Rate, mg/s [King, 1990]
Vibratory screens	Open top	5.5 times top surface area in m ²
	Closed top with open port access: 15 cm diam. port	0.11
	20 cm diam. port	0.21
	30 cm diam. port	0.44
Bag dumping	Closed cover, no ports	Nil
	Manual slitting and dumping	3
	Fully automatic with negative pressure	Nil
Bagging machines	No ventilation	1.5
	Local ventilation	0.01
	Totally enclosed with negative pressure	Nil

Substitute

Employ less-hazardous species. *Use less-hazardous additives* (solvents, catalysts, filter aids, adsorbents, and absorbents) if nonhazardous ones are not available.

Attenuate or Minimize

Use equipment, seals, and valve stems that leak less. Tables 16.25 and 16.26 give estimates of VOC leak rates and dust generation from different types of equipment.

Minimize waste by changing the operating conditions: substitute continuous processing for batch processing to minimize cleanout cycles, and clean vessels with a dry ice spray instead of sandblasting. *Change the operating conditions.* Use hazardous materials under less hazardous conditions. Use hot water instead of steam and water instead of hot oil; use chemicals with higher flash temperatures. Use a vacuum to reduce the boiling temperature, reduce process temperatures and pressures, dissolve hazardous species in safe solvents, add diluents, and operate at conditions far from explosive limits and from reactor runaway conditions. Add inert gas (such as steam, nitrogen, or carbon dioxide) to combustible mixtures to reduce the concentration of oxygen to about 4% below the minimum. *Minimize the hazard from storage tanks* by providing double-walled tanks with water between the walls (provided that water does not react with the stored material). *Reduce the intensity of electric sparks;* ensure that the voltage used is so low that low-energy sparks do not ignite a flammable mixture. For mixtures of flammable vapors in air, these voltages are <0.01 to 1 mJ; for sensitive explosives, <0.001 mJ; for dust explosions, <0.1 mJ.

Recycle

Minimize the source through recycle.

16.7.2.3 Step 4. Minimize the Impact

If hazardous materials must be used and unsafe environments exist, *limit the potential for leakage;* use finned tube heat exchangers for vaporization on the shell side. *Develop special procedures during the startup phase,* when conditions go through the explosive limits. *Measure key variables to trigger safety measures;* for example, for reactors, include instrumentation to detect temperature runaways. For example, AIChE/CCPS (1995) recommends $d^2T/dt^2 > 0$ and $d(T_{\text{reactor}} - T_{\text{coolant}})/dt > 0$. Monitor the various streams for impurities. *Install explosion suppressors* in potentially explosive spaces for dusts, such as the exit ducts from grinders. *Dump cold liquid or inert solids* into systems on the verge of temperature runaway. *Add an inhibitor to neutralize* the catalyst for a potential temperature runaway (for example, add gaseous ammonia to neutralize the Lewis acid catalyst BF_3

TABLE 16.27
Software Aids

Vendor	Process Synthesis and Analysis	Physical Properties	Steady-State and Dynamic Simulation, Optimization	Equipment Sizing and Rating, Costing
Aspen Technology www.aspentech.com	Aspen Pinch TM ; minimize energy usage	Aspen Properties TM ; Databank, property and estimation methods	Aspen Plus TM ; steady-state simulation	Aspen AeroFtran TM Aspen
	Aspen Split TM ; conceptual design of azeotropic systems	Aspen OLI TM ; aqueous mixtures	Batchfrac TM ; batch distillation	Hetran TM Aspen Teams TM ; various heat exchanger design tools
	Aspen Water TM ; minimize water usage	DE'THERM TM ; compilation of pure physical properties	Ratefrac TM ; distillation and absorber column distillation	CFX ; computational fluid dynamics tool for unit design
	Aspen PEP Process Library TM ; comparison of processes		Aspen Plus Optimizer TM ; equation oriented optimization	FLARENET ; design, rating, and debottlenecking of flare systems
	development, route synthesis, and implementation		Aspen Custom Modeler TM ; new model builder	HTFS ; thermal design and simulation of heat exchangers
	DISTIL ; synthesis of column sequences for multicomponent azeotropic systems		Aspen OnLine TM ; online connection with knowledge capture	PIPESYS ; pipeline flow modeling
	HX-NET ; conceptual design tool for heat exchanger networks; uses pinch technology		Aspen ADSIM TM ; adsorption processes	STX/ACX ; rate and design shell-and-tube and air-cooled heat exchangers
	HYSYS, Concept-data regression and thermodynamic database access for conceptual design of separation systems		Aspen Chromatography TM ; chromatographic processes	
			Aspen FCC TM ; fluidized catalytic cracker simulation	
			Batch Plus TM ; batch process recipe oriented modeler	

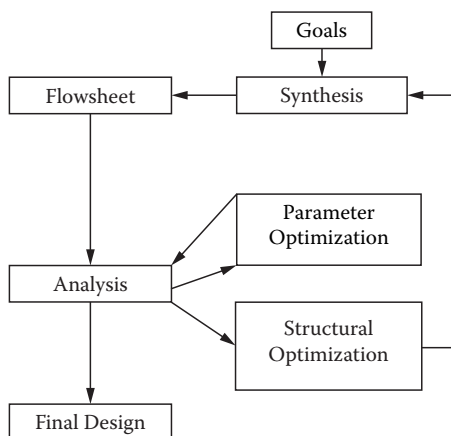


FIGURE 16.5 Synthesis, analysis, and optimization activities.

16.8.1 STEADY-STATE FLOWSHEETING

Software flowsheeting aids are usually used for the preliminary engineering design (step 3 in Table 16.1) or perhaps in the conceptual design (step 2). The flowsheeting activity is divided into three basic steps:

- Step 1. **Synthesis** or selecting the structure of the flowsheet: identification of the equipment, interconnecting and specifying the initial design values. In this step, a crude approximate flowsheet is created to consider recycles, purges, and possible separation schemes; make a simple, linear model to assess the effects of major parameters and structural variations; do necessary laboratory work; get more details for physical properties, thermodynamics, utilities, and process units; write unit models, if necessary; and fix the flowsheet layout.
- Step 2. **Analysis** or solving the heat and material balances; sizing and costing the equipment; evaluating the economic worth of the project; assessing the safety and environmental impact; and analyzing the operability.
- Step 3. **Optimization** of the structure and the parameters. For the structure, optimize the choice of equipment and the interconnection of units. For parameters, select values for the state variables (such as temperature, pressure, and level) within a given process configuration.

In an additional step 4, move from the steady-state condition to study the dynamics and controller effects and the operability.

The six key components in a process flowsheet simulator are the component database, the thermodynamic model solution package, the flowsheet graphic tool, the models of the unit operations, the data output generation, and the flowsheet solver strategy.

16.8.2 FORMULATING A WELL-POSED PROBLEM

To obtain a solution to a process model, first formulate a *well-posed problem* (Himmelblau, 1996). This requires that we (1) identify the stream variables entering and leaving a unit and the variables that describe the unit, (2) determine the number of independent equations for each unit, (3) calculate the degrees of freedom or number of decision variables for each unit, and (4) specify the values of variables equal to the number of degrees of freedom.

The *degrees of freedom* (DOFs) are the variables in a set of independent equations that must have their values assigned. $\text{DOF} = \text{no. of variables} - \text{no. of equations and constraints}$, or

Example 16.14

Determine the number of process variables, equations, and constraints and the overall DOF for a combination of a mixer and flash separator.

Mixer:

$$N_v: 3(N_{sp} + 2) + 1$$

$$N_c: N_{sp} + 1$$

$$N_d: 2N_{sp} + 6$$

Flash separator:

$$N_v: 3(N_{sp} + 2) + 1$$

$$N_c: 2N_{sp} + 5$$

$$N_d: N_{sp} + 2$$

Sum of DOF of individual units:

$$N_d = 3N_{sp} + 8$$

Less redundant variables and constraints:

$$\text{Stream 3} = \text{stream 4} \quad N_{sp} + 2$$

$$\text{Need one energy balance} \quad 1$$

$$\text{Total DOF} \quad N_d = \{3(N_{sp} + 8)\} - \{N_{sp} + 3\}$$

16.8.3 FLOWSHEET ARCHITECTURES

The two basic flowsheet software architectures are sequential modular and equation-based. In *sequential modular*, we write each unit model so that it calculates output(s), given feed(s), and unit parameters. This is the most commonly used flowsheeting architecture at present, and examples include Aspen+ plus Hysys (AspenTech), ChemCAD, and PROII (SimSci). In *equation-based* (or open-system) architectures, all equations are written describing material and energy balances as algebraic equations in the form $f(x) = 0$. This is the preferred architecture for new simulators and optimization, and examples include Speedup (AspenTech) and gPROMS (PSE plc). Each is discussed in turn.

16.8.3.1 Sequential Modular Architecture

Unit models are written to *calculate* output stream values, *given* input stream values and unit parameters. The recycle stream values are then calculated and checked against the estimated values for that iteration. If they agree within a tolerance, then the flowsheet has converged. This procedure is called *tearing* a recycle stream. The important questions for this approach are

1. How is a process flowsheet analyzed to determine whether there are recycles and which stream to tear (estimate)?
2. How do we handle many recycles, which may be nested?
3. How are calculated values for the recycle stream used for subsequent iterations?
4. What solution procedure should be used if not all the inputs to the process are known, but some outputs are specified?

16.8.3.1.1 Tearing

There are a number of approaches to develop better tearing strategies, but they require analysis of the number of components and number of recycles. Biegler et al. (1997) describe algorithms to minimize the number of tears and the number of recycle variables in the tears.

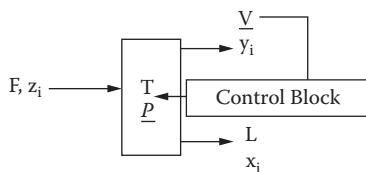


FIGURE 16.6 Symbols and configuration for the adiabatic flash in Example 16.15.

safety and operational constraints on the temperature and pressure in the vessel. A control block solves the equation:

$$Error = set\ point - value < tolerance$$

$$E = V_{sp} - V < error$$

The calculation procedure may proceed as follows:

For iteration k in the flash example,

1. If $k = 1, 2$, estimate P^k (make sure flash is in the two-phase region).
2. Calculate V^k .
3. Calculate $E^k = V_{sp} - V^k$.
4. If, $|E| < error$, exit

else, $|E| > error$, use secant method to calculate P^{k-1} :

$$P^{k+1} = P^k - \{(P^k - P^{k-1}) / (E^k - E^{k-1})\} E^k$$

In many problems, there are recycle loops and design specifications. Recycle loops require convergence blocks. *Explicit* iterations occur to satisfy material, temperature, and pressure agreement in a given recycle stream. Design specifications require control blocks. *Implicit* iterations occur to satisfy a specification by adjusting an input stream variable or equipment parameter.

For a design problem, converge the entire flowsheet (close all the recycles) for every intermediate value of the adjust variable. This is very expensive computationally and is a major drawback to the sequential modular approach. Alternative and sometimes faster approaches include

- Partially converge the flowsheet, a less stringent recycle tolerance, for the intermediate adjusted variable values.
- For each iteration of the control block, converge only the units between the specified and adjusted variables; solve the entire flowsheet after the adjust variable is converged.

These alternatives are not guaranteed to converge, and partially converged flowsheets may provide poor estimates for the monitoring of the specified variable.

16.8.3.1.5 Partitioning and Precedence Ordering

Partitioning locates groups of units that must be solved together. *Precedence ordering* solves these groups of units within a process in the proper computational order. A partition is unique, but the precedence ordering is not. Partitions may exist where the order of the solution may have groups of units calculated in serial or parallel order. An effective algorithm developed by Sargent and Westerberg is

TABLE 16.28
Select the Model for the System

System	Margules	VanLaar	Wilson	NRTL	UNIQUAC
Multi	?	?	OK	OK	OK
Azeotropic	OK	OK	OK	OK	OK
Liquid-liquid-vapor	OK	OK	NO	OK	OK
Self-associating	NO	NO	OK	OK	OK
Polymers	NO	NO	NO	NO	OK

16.8.4.1 Vapor-Liquid Equilibrium

Liquid activity models must be used in vapor-liquid equilibria calculations, with the appropriate model tested against available data. Models often used include Margules, Van Laar, Wilson, nonrandom two-liquid (NRTL), and universal quasi-chemical (UNIQUAC). For mixtures, mixing rules are used to combine pure component parameters. Table 16.28 suggests regions of applicability for different models.

16.8.4.2 At High Pressure or near the Critical Region

At high pressure or near the critical region, the thermodynamic functions for the liquid phase cannot be assumed to be independent of pressure. Simple equations of state are not adequate for vapor-phase predictions. Chao–Seader method includes the calculation of liquid-phase fugacity coefficient by Pitzer's correlation. Chao–Seader uses the Redlich–Kwong equation of state with a temperature range of -20 to 250°C and pressure $<10,000$ kPa. The Grayson–Streed extension of the model of Chao–Seader is used for systems rich in hydrogen and methane at a temperature range of -20 to 450°C and pressure $<20,000$ kPa. It is advisable to check the simulator manual.

16.8.4.3 Equation of State, EOS

Commonly used EOS models include the ideal, virial, PengRobinson, Soave–Redlich Kwong, and Lee–Kesler. The reduced form of the EOS is particularly significant. Substances with the same reduced properties are in *corresponding states*. Van der Waal's EOS is a poor predictor of state properties, but the experimental data do correlate well with reduced conditions. Many of the cubic EOS models are based on the van der Waal equation.

EOS models are used to determine liquid and vapor densities, vapor pressures, fugacities, thermal property deviations from ideal, and enthalpies. EOS parameters can be adjusted to fit some data listed above, but usually one EOS set of parameters cannot fit all of the pure component data well. Flowsheet simulators allow the user to mix EOSs to get the best match between EOS parameters and desired state variables. In general, EOSs are very good predictors of the vapor-phase properties and of the liquid-phase density and composition. Cubic EOSs are relatively simpler to use. The Lee–Kesler model (based on the theory of corresponding states, and using reduced temperature and pressures) can cover a wider range of pressures and temperatures. It is recommended practice not to extrapolate the EOS results outside of conditions for which the parameters were fitted. Check the simulator manual for temperature pressure and composition restrictions. Generally, the higher the pressure (>10 bar), the poorer the prediction. If polar molecules are present (alcohols, acids), then EOS should not be used. Use an activity model for the liquid phase or a specially fitted EOS for those systems.

16.8.5 TOOLS FOR FLOWSHEET DEVELOPMENT

Flowsheet development involves the selection of the equipment and the interconnects that integrate the equipment into a working system. Two approaches are used for the development of the flowsheet: mathematically based programming and the use of heuristics and evolutionary development.

- Himmelblau, D. M., *Basic Principles and Calculations in Chemical Engineering*, 6th ed. Englewood Cliffs, NJ: Prentice Hall, 1996.
- King, C. J., *Separation Processes*, 2nd ed. New York: McGraw-Hill, 1980.
- Seider, W. D., J. D. Seader, and D. R. Lewin, *Process Design Principles: Synthesis, Analysis and Evolution*. New York: John Wiley & Sons, 1999.
- Smith, R., *Chemical Process Design*. New York: McGraw-Hill, 1995.
- Turton, R., R. C. Bailie, W. B. Whiting, J. A. Shaeiwitz, *Analysis, Synthesis, and Design of Chemical Processes*. Englewood Cliffs, NJ: Prentice Hall, 1998.

16.9 PROCESS OPTIMIZATION

In Step 3, optimization of the structure and the parameters (Section 16.8.1), the two types of process optimizations are parameter and structural optimization. *Parameter optimization* is the process of determining the best value of a process unit parameter or stream quantity in terms of improving performance within a given set of constraints. Parameter optimization is usually a nonlinear continuous variable (over a range of variable values defined by upper and lower bounds). *Structural optimization* involves the determination of the best set of units and their interconnections such that the process configuration provides the best performance within a given set of constraints. Structural optimization requires discrete decisions. Pinch technology, described in Section 16.8.5, is a form of structural optimization.

16.9.1 DEFINE THE PROBLEM

The first key steps are to determine the *objective function*, the *decision variables* (or design variables or degrees of freedom), and the *constraints*. The *objective function* is the performance measure to be used to determine the degree of improvement in the process. Examples include maximizing profit, minimizing cost, maximizing production, and minimizing a waste stream. *Decision variables* are those variables that can be changed, within a given process design, to improve the objective function. Examples of continuous decision variables include the pressure or temperature of a stream, and the number of stages in an absorber column would be a discrete decision variable. *Constraints* are of three types: variable bounds, equality constraints, and inequality constraints. Variable bounds are the upper and lower limits on a variable due to operational, physical, or economic considerations. Equality constraints are functions of process variables that define a relationship that must be enforced in a feasible solution, e.g., material balance on a unit. Equality constraints reduce the dimensionality of a problem, since each equation reduces the number of independent decision variables. Inequality constraints are usually one-sided feasible regions (less-than or greater-than relationships) defined by a function of process variables; e.g., distillation columns must be operated within flooding constraints.

16.9.2 SELECT THE OPTIMIZATION SOLUTION SCHEME

Combinations of these objectives, variables, and constraints are so common that the optimization solution schemes are tailored for the function properties. A key step in solving an optimization problem is to match the appropriate solution algorithm with the problem type as outlined in Table 16.29.

Optimization algorithms all require the definitions of the objective function and decision variables, and constraints if applicable. In addition, most solution algorithms require a reasonable initial set of values for the decision variables, preferably a feasible starting point. Optimization algorithms generally follow a pattern:

1. Provide a starting set of decision variables.
2. Determine a *search direction* for the decision variable to improve the objective function.

16.9.2.2 Linear Programming

Linear programming is probably the most commonly used optimization method. Edgar et al. (2001) and Press et al. (1992) describe many available sophisticated algorithms.

16.9.2.3 Nonlinear Programming

Nonlinear programming problems are generally formulated as

$$\begin{array}{ll}\text{Min. or max.} & f(x) \\ \text{Subject to} & h(x) = 0 \\ & g(x) \leq 0 \\ & 1 \leq x \leq u\end{array}$$

where x is the set of decision variables bounded between 1 and u , $f(x)$ is the objective function, $h(x)$ is the set of equality constraints, and $g(x)$ is the set of inequality constraints. Nonderivative methods are generally slow and unreliable for problems with more than a few decision variables. Some variations on the simplex method have been made to incorporate constraints (Press et al., 1992). Most algorithms use derivative information, or approximations to the derivatives, for $f(x)$, $h(x)$, and $g(x)$. Example algorithms include successive linear programming, reduced gradient methods, and successive quadratic programming. Many programs are available to solve these classes of problems. Most optimization algorithms require continuity of the objectives and constraints within the exploratory region, which can be difficult for real process design problems. While some advances have been made in partitioning problems to seek the global optimum, this is still a relatively difficult area of optimization and not routinely used.

16.9.2.4 Discrete Decision Variables

Design problems in particular usually have discrete decisions. Few large-scale optimization algorithms are available that can handle nonlinear constraints with a mix of continuous and discrete variables.

16.9.3 LINKING OPTIMIZATION WITH THE FLOWSHEETING TOOL

The most important part of process optimization is linking the process flowsheeting tool to the optimization algorithm. With an *equation-based architecture*, the unit equations (material and energy balances, operating constraints, and specifications) are constraints in a general nonlinear programming formulation. The main problems are

- Problem size, as most process optimization problems have on the order of 10^4 to 10^6 constraints and at least 10 to 100 decision variables. Generally, this is done with sparse matrix algorithms or by partitioning the problem to take advantage of the equation structure due to the unit equations and recycles.
- Starting point for the decision variables, which generally requires a complete simulation of the process to be completed.
- Derivative information is required, which is especially problematic for thermodynamics packages and the avoidance of discontinuities in the search space.

With a *sequential modular architecture*, optimization is generally done on much smaller problems (usually less than 20 decision variables) using either of the following:

Key 3. Build trust. Trust glues relationships together. We build trust by *keeping* commitments to ourself and others; *clarifying* expectations that we have of ourself and of others; *showing* personal integrity, honesty, and loyalty to others, especially when they are not present; *apologizing* promptly and sincerely when we know we are wrong; *honoring* the fundamental *rights* listed above and avoiding the killers; *listening* and *understanding* another's perspective; *being truthful*; and *accepting others*, "warts and all." We destroy trust by the reverse of the builders of trust listed above and by selectively listening, reading, and using material out of context; not accepting experience of others as being valid; making changes that affect others without consultation; blind-siding by playing the broken record until we are eventually worn others out or subtly make changes in the context/issues/wording gradually so that they are unaware of what is happening until it is too late.

Key 4. The 12:1 rule applies to rebuild relationships. Twelve positive experiences are needed to overcome one negative experience.

Key 5. To improve and grow, we need feedback about performance. Give feedback to others to encourage and help them; it not for you to get your kicks by putting them down.

16.10.2 EFFECTIVE TEAMS

A team is not just a collection of individuals. In a collection of individuals, each has a personal goal, trusts only himself, and rarely reveals personal skills. Decisions are usually not made, and conflict is ignored. In a team, all unanimously accept common goals, each is clear about his role, trust and involvement levels are high, personal unique skills are used effectively, decisions are made by unanimity, and the team has methods for handling conflict. Our meetings and teamwork improve when we strive for the characteristics of teams. Some target behaviors of teams follow:

- Have a purpose for each team and each meeting. Set and follow agendas to get the task done.
- No agenda, no meeting! If a meeting must be held without a circulated agenda, then spent the first five minutes creating the agenda.
- The team must have the correct membership and resources to achieve the goal.
- The team should be empowered and accountable to achieve the goal.
- Both *task* (getting the job done) and *morale* (feeling good about the group work and about how you have interacted with the other group members) are important.
- Have a chairperson whose role is to facilitate the team process: this person thinks through the tasks to be done, decides on the need for a team meeting, identifies the time and place for the meeting, sets and circulates an agenda, facilitates the meeting, and starts and stops the meeting on time.
- Being the chairperson and being a leader are different; different people may become leaders at different times.
- Group evolution tends to follow a pattern described by such descriptors as "*forming, storming, norming, and performing*."
- Establish norms. Agree on terminology and procedures for problem solving, for brainstorming, for decision making. Agree on the role of the chair in decision making (e.g., *vote or no vote*); roles, minutes, and records of decisions (e.g., *format, details, who prepares them, whether they are circulated, their use for subsequent meetings*); how to handle conflict and the level of intervention; combating "groupthink"; how to handle emergencies and criteria; and procedures for asking a member of the group to resign.
- Each has a clear idea of roles and of group norms.
- When groups are functioning effectively, about 70% of the time is spent on the task, 15% on morale-building activities, and 15% on task process activities.
- The products from groups or teams are improved when members have different "styles," as outlined in Section 16.10.1.1.

TABLE 16.30
Rating Form for Teams

Assessment of your team & team meeting	Name: _____ Date: _____ unclear: <input type="checkbox"/> unclear: <input type="checkbox"/>
Purpose of team: _____	
Purpose of this meeting: _____	
Agenda for this meeting: detailed, clear, and circulated ahead of time <input type="checkbox"/> bare minimum circulated ahead of time <input type="checkbox"/> none <input type="checkbox"/>	

Three minute team task to seek consensus about the rating of the Task and Morale:

• **Teamwork: Task** all members clear about and committed to goals; all assume roles willingly; all influence the decisions; know when to disband for individual activity; all provide their unique skills; share information openly; the team is open in seeking input; frank; reflection and building on each other's information; team believes it can do the impossible; all are seen as pulling their fair share of the load.

The degree to which these descriptors describe your team's performance (as substantiated by evidence: meetings, engineering journal, interim report, presentations).

None of these behaviors	Few of these behaviors but major omissions	Most features demonstrated	All of these behaviors
<input type="checkbox"/> 1	<input type="checkbox"/> 2	<input type="checkbox"/> 3	<input type="checkbox"/> 4
<input type="checkbox"/> 5	<input type="checkbox"/> 6	<input type="checkbox"/> 7	<input type="checkbox"/> 8

• **Teamwork: Morale:** Trust high, written communication about any individual difficulties in meeting commitments; cohesive group; pride in membership; high *esprit de corps*; team welcomes conflict and uses methodology to resolve conflicts and disagreements; able to flexibly relieve tension; sense of pride; "we" attitude; mutual respect for the seven fundamental rights of all team members; absence of contempt, criticism, defensiveness, and withdrawal.

The degree to which these descriptors describe your team's performance (as substantiated by evidence: meetings, engineering journal, interim report, presentations).

None of these behaviors	Few of these behaviors but major omissions	Most features demonstrated	All of these behaviors
<input type="checkbox"/> 1	<input type="checkbox"/> 2	<input type="checkbox"/> 3	<input type="checkbox"/> 4
<input type="checkbox"/> 5	<input type="checkbox"/> 6	<input type="checkbox"/> 7	<input type="checkbox"/> 8

Each, in turn, gives a 30-second summary of his/her perception of his/her contribution. This is presented *without discussion*.

Individual, 30-second reporting of his/her contribution to this meeting:

Four-minute team task to reach consensus about the five strengths and the two areas for growth.

Strength of your team

Areas to work on for growth

D. R. Woods (2001)

This form should be completed after each meeting and copies used as evidence of growth.

has a causal effect on the controlled variable. The number of *final elements* is greater than or equal to the number of measured variables to be controlled, and we must provide an independent means for controlling every variable.

Final elements must provide the desired capacity with the required precision of flow throttling over the desired range, usually 10% to 95% of maximum flow. The valve characteristic should provide a linear closed-loop gain, *except* choose linear or quick-opening characteristics for valves that are normally closed but must open quickly. Select the valve failure position for safety. The valve body should satisfy such requirements as required flow at 0% stem position, plugging, pressure drop, or flashing. The nonideal final element behavior, such as friction and deadband, should be small, as required by each application. Control valves should have manual bypass and block valves to allow temporary valve maintenance when short process interruptions are not acceptable. However, the bypass should never compromise safety interlock systems.

Specifics

Include the same length of upstream straight-run piping before control valves as for orifices. This is particularly important for rotary valves.

Globe valves. Permissible stroke range: 10% to 90%; sliding stem gives the highest sensitivity, and the actuator stem feedback position more closely represents the final element position (but not for fouling or solids).

Rotary ball valves. Permissible stroke range: 20% to 80%. Δp across the valve is small, but accounts for the pipe reducers needed for installation. Be sensitive to the need for upstream straight pipes.

Rotary butterfly valves. Permissible stroke range: 25% to 65%.

Signal transmission. Use sensor-matched transmitters. All measurements used for control should be transmitted using high-level 4–20 mA transmission.

Feedback controller. Match the type to the process requirements as follows:

Manual. When close regulation of the variable near its desired value is not required, and when knowledge is required that is not available in the control computer.

On/off. When the system responded slowly to disturbances, and close regulation of the variable is not required.

Regulator. A self-contained P-only regulator offers low-cost and reliable control of noncritical variables that can be permitted to deviate from their setpoints for long periods.

PID. The proportional-integral-derivative algorithm is used for most single-loop applications.

PID control. Always determine the form of the PID algorithm being used. Select the PID modes: *P*, always; *I*, when the controlled variable should return to its set point; *D*, for processes that are undamped, unstable, or have a very large ratio of dead time/time constant.

Tuning. Typical values are $K_c = 0.8/K_p$, $T_I = 0.75 (\theta + \tau)$, and $T_d = 0.0$. The proportional band ($100/K_c$) and the reset time ($1/T_I$) can be calculated from these. When fine tuning, observe the behavior of both the controlled and manipulated variables. Always use an implementation that includes antireset windup protection for use when the manipulated variable encounters a constraint. Use an implementation that includes initialization that starts automatic control bumplessly from the last manual condition. The digital execution period should be fast with respect to the feedback dynamics, with $\Delta t \leq 0.05 (\theta + \tau)$ where possible.

Filtering. For control variables, when filtering is needed, use a first-order filter to reduce the effects of high-frequency noise. Do not excessively filter measurements unless absolutely necessary. The filter time constant, τ_f , should be much less than feedback dynamics.

For monitoring variables. Use filters to reduce the noise at frequencies higher than the effects being observed. Recall that “averaging” is a filter that is often performed by the DCS historian features.

Loop pairing. Where options exist, pair the most important variables with manipulated variables that have fast feedback dynamics and large capacity. Select pairings that give good integrity. For

Reciprocating piston compressors: 30 to 400,000 kPa; 5 to 10^4 dm³/s. Usually economical for >6 MPa and <150 dm³/s or any discharge pressure and flows <100 ad³/s.

Axial compressors: 20 to 2,000 kPa; 4×10^3 to 10^6 dm³/s.

Guidelines

Fans: Power: up to 7.5 kW/m³/s.

Blowers: Power: up to 125 kW/m³/s.

For compressors,

Adiabatic $pV^k = \text{constant}$

Isothermal $pV = \text{constant}$

Polytropic $pV^n = \text{constant}$: for uncooled internally, $n > k$; for internally cooled, $1 < n < k$, with $n \approx k$. $k = c_p/c_v = 1.04$, increases to 1.67 as the molar mass decreases with air = 1.4 and such gases as ethylene, carbon dioxide, steam, sulfur dioxide, methane, and ammonia = 1.2 to 1.3.

Temperature rise between feed 1 and exit 2:

$$T_2/T_1 = (p_2/p_1)^{[(n-1)/n]}$$

$$(n - 1)/n = (k - 1)\eta_p/k$$

$$\eta_p = \text{polytropic efficiency}$$

For each stage, keep the exit temperature $(T_2 - 298) < 120 - 150^\circ\text{C}$. For diatomic gases, $k = 1.4$, which limits the compression ratio (p_2/p_1) to 4; for triatomic gases, 6.

$\eta_p > \eta_{\text{adiabatic}}$. For uncooled compressors, polytropic, hydraulic, and temperature rise efficiencies are the same and range from 0.7 to 0.8 with the usual value of 0.72.

Rotary screw: Power: 100 to 750 kW/m³/s.

Centrifugal compressors: These deliver actual volumetric flows (cubic decimeters per second, and performance should not be expressed as mass, moles, or standard volumetric flow). Assume compression ratios to be equal in all stages. The maximum number of stages that can be on one shaft or fit in the "frame" = eight minus one stage for each side nozzle. The compression ratio is 2.5 to 4. The pressure coefficient = 0.5 to 0.65; assume 0.55. The pressure differential increases with increase in suction gas density (increased molar mass or suction pressure, or decrease inlet temperature, decrease in k). Power: Up to 7.5 kW/m³/s. Efficiency of large centrifugal compressors: 76 to 78%.

Centrifugal compressors operate between low volumetric flow rate "surge" conditions and high volumetric flow rate limited by the sonic velocity at the eye of the impeller. At "surge" conditions, the gas flow back through the compressor causes damage to the thrust bearings. The surge point is usually 0.33 to 0.5 of the normal operating capacity of the compressor. During startup, the machine goes through the surge region. The point of surge is a minimum for a single impeller. The range of stable operation decreases 5% with the addition of each impeller. High molar mass decreases the range of operation. Surge may be caused by a system disturbance (especially changes in the molar mass of the feed gas) and insufficient flow.

Surge is related to power used:

- When the molar mass of the inlet gas increases, the motor amps increase.
- If the molar mass increases by 20% and we control the suction drum pressure by recycling exit gas to the inlet (spill back control), the motor amps increase by 20%; if control is by throttle of the suction line, the motor amps increase by 10%. For every

Mechanical vacuum: 2 to 50 kW/m³/s air exhausted

Steam ejector:

1 stage: 0.002 to 10 kg steam/kg air exhausted/kPa abs

2 stage: 100 kg steam/kg air exhausted/kPa abs

3 stage: 1 Mg steam/kg air exhausted/kPa abs

4 stage: 2 Mg steam/kg air exhausted/kPa abs

5 stage: 40 Mg steam/kg air exhausted/kPa abs

Steam ejector, general:

down to 10 kPa abs., 1 to 200 kg/h air; 1.3 kg steam/kg air exhausted/kPa abs.

down to 30 kPa abs., 1 to 20 kg/h air exhausted; 0.1 kg steam/kg air exhausted

The compression ratio of the first-stage ejector is set primarily by the intercondenser cooling water temperature.

Assume discharge pressure to atmosphere after the last stage = average barometric pressure + 7 kPa.

Assume motive steam = minimum steam pressure in header less 5 to 10%. Pressure drop on shell side of surface condenser usually <5% of absolute design operating pressure.

A related topic is covered in Section 16.11.3.13 for interstage direct contact G-L condensers, although current practice is to use surface shell-and-tube condensers.

16.11.2.3 Liquid

Area of Application

Centrifugal pumps: head = fluid viscosity <300 mPa·s

end suction, single stage: head = 0.2 to 100 m; 0.05 to 4000 L/s; 0.05 to 0.7 kW/L/s; efficiency 40 to 60%

end suction, multistage: head = 50 to 800 m; 10 to 400 L/s; 0.2 to 10 kW/L/s; efficiency 40 to 60%

Peripheral: 10 to 300 m; 0.1 to 2 L/s; 4 kW/L/s

Centrifugal axial: fluid viscosity <300 mPa·s: 0.3 to 10 m; >150 L/s; 0.1 kW/L/s

Reciprocating pumps: fluid viscosity <5,000 mPa·s, diaphragm or piston: 1 to 1,000 m; <50 L/s; 0.1 to 3 kW/L/s

Rotary screw: fluid viscosity, usually above 10 Pa·s; 0.2 to 300 m; <120 L/s

Guidelines

Optimum exit pipe size selection:

pump liquids at >1.5 m/s

hydrocarbons with low conductivity <0.3 m/s

Suction pipe of larger diameter to prevent cavitation

NPSH requirement [m] = {rpm/(5400 volumetric flow rate [L/s])}^{1.33}

Centrifugal pumps operate on their operating head-capacity curve. Head-capacity curves are independent of the fluid, although the curve drops slightly at higher capacities for higher-viscosity fluids. For centrifugal pumps, the drive power required and pressure at the exit flange depend on the fluid density. Reciprocating pumps are constant-volume devices, producing essentially constant "pressure."

Pressure drop through pipes: 1 velocity head per 45 to 50 length/diameter; for water, 23 kPa/100 m pipe

Pressure allowance across a control valve for good operability: 20 to 50% of the dynamic head loss or 70 to 140 kPa

16.11.2.6 Solids

Choice depends on particle characteristics (size, flowability, corrosiveness, abrasiveness, handling characteristics, safety-hazard [static electrification, fumes, flammability]), and vertical versus horizontal distance. A related topic is covered in Section 16.11.2.5, and bins for storage (Section 16.11.6.35).

Area of Application

Belt conveyors: $<10^\circ$ incline; 10 to 100 m horizontal distance; capacity 3 to 270 kg/s. OK for most diameters of particles but not for particles that cake or are light and fluffy.

Bucket/belt elevators: usually for >25 m vertical; 15 to 150 Mg/h; usually not for particles $<150\text{ }\mu\text{m}$ dia. and not for particles that cake or are light and fluffy.

Screw conveyors: 2 to 75 m horizontal distance; 0.3 to 275 kg/s. Not for particles that cake or are light and fluffy. Can be used for inclines up to 20° .

Vibratory feeder: <20 m; 1 to 400 Mg/h; not for light and fluffy materials or particles $<150\text{ }\mu\text{m}$ dia.

Apron feeder: $<18^\circ$ incline; 2 to 12 m horizontal; 10 to 150 Mg/h; not for particles that cake or are light and fluffy or are fine with $<50\text{ }\mu\text{m}$ dia.

Pneumatic transportation: limited by solids loading that plugs pipe.

Dilute phase: pressure: continuous: particle dia. $60\text{ }\mu\text{m}$ to 0.3 cm; pressure drop <100 kPa. Distance <600 m. One-point collection and several-point delivery.

Dilute phase: vacuum: continuous: particle dia. $60\text{ }\mu\text{m}$ to 0.3 cm; Δp pressure drop <50 kPa. Distance <50 m. One-point delivery and several-point delivery.

Dense phase: pressure: batch: particle dia. $60\text{ }\mu\text{m}$ to 0.3 cm; pressure drop 550 to 700 kPa. High capacity (<10 kg/s) over long distances <2300 m. For materials that degrade easily or are highly abrasive.

Guidelines

Caution for all: dust explosions: dust explosion potential for particle dia. $<200\text{ }\mu\text{m}$. Minimum ignition temperature $>300^\circ\text{C}$; minimum ignition energy 10 to 30 mJ.

Belt conveyors: keep speeds <1 m/s for fines; otherwise speeds in the range 2.7 to 4 m/s; burden thickness (cm) = $0.17 (\text{volumetric capacity, dm}^3/\text{s}) / \{(\text{belt speed, m/s})(\text{belt width, m})\}$. Belt width 0.5 to 0.8 m.

Speed: 0.8 to 2 m/s.

Power: 0.02 to 0.4 kW/Mg/h per km horizontal distance.

Bucket conveyor: vertical: velocity <1.5 m/s; for material of density 0.4 Mg/m^3 capacity <16 kg/s; for 2 Mg/m^3 capacity <85 kg/s or $<40\text{ m}^3/\text{s}$. Power 0.15 to 0.35 kJ/kg or 0.013 to 0.023 kJ/kg/m of height.

Screw conveyors: 10 to 120 rpm and trough loading 15 to 95%, depending on the particle size, flowability, abrasiveness. Dia. 0.3 to 0.4 m. Power 10 to 20 kW/Mg/h per km horizontal distance.

Rotary, star valve feeder: used especially as solids feeders for dilute-phase pneumatic conveying to provide an air lock and to feed solids. Seal/wear depends on Δp and abrasiveness of powder. For pressure systems keep $\Delta p <80$ kPa; for vacuum systems $\Delta p <40$ kPa. Provide an air vent to take the air loss away from the gravity flow of the solids and to control the filling of the star.

Pneumatic conveying: dilute phase: pressure: continuous: nominal gas velocity 5 to 35 m/s with usual 11 to 25 m/s. Solids loading 3.5 to 15 kg solid/kg air with usual 6 to 15 kg solids/kg air or 1 to 7 m^3 solids/ m^3 air. Power 7 to 11 kJ/kg. Problems: about 30% air leakage out of the system. Rotary/star valve problem/bridging: overcome with bin

wheels are discussed in Section 16.11.3.14. Sections 16.11.3.15 through 16.11.18 discuss solidification of solids, heat loss to the atmosphere, refrigeration, and steam generation.

16.11.3.1 Drives

Area of Application

Gasoline/diesel engines: 200 to 800 rpm; >80 kW; efficiency: 28 to 38%.

Electric motors (synchronous): <500 rpm; 35 to 500 kW; use 480 V for motors up to 115 kW; 4160 V for >115 kW.

Electric motors (induction): >500 rpm; 10 to 15000 kW.

Steam turbine: single-stage, single-valve: 1000 rpm to 12,000 rpm; 50 to 1500 kW

Single-valve, multistage: 1500 to 2800 kW

Multivalve, multistage: 2800 to 30,000 kW

Gas combustion turbine: cogeneration

Guidelines

For less than 75 kW, select motor or turbine.

Gasoline-diesel engines usual application: 200 to 400 rpm; 500 to 1200 kW.

Electric motors: select synchronous for low speed; usual application for either synchronous or induction: 500 to 2100 rpm; 150 to 500 kW. Usually use total enclosed Fan cooled (TEFC) enclosure, efficiency: 84 to 95%.

Induction: available for large power requirements, relatively low efficiency, power factor is low if rpm <500 and at starting and fractional loads.

Synchronous: high efficiency at any speed, suitable for direct coupling for <1000 rpm. Power factor >1; constant speed without slip. Power consumption, kW = amps (0.001 volt \times PF \times 0.95 \times $\sqrt{3}$).

Power, kW	Volts, V
0.1 to 1	110
1 to 75	220 to 440 3 phase
50 to 200	440 to 2,300
175 to 2000	2,300 to 4,160
>2000	11,000 to 13,200

Steam turbines: competitive above 75 kW; condensing: 2 kg/h steam/kW with 1.8 m² condenser surface area per kg/h steam. Multivalve, multistage efficiency: 42 to 78%.

16.11.3.2 Thermal Energy: Furnaces

Multiuse including heating, boiling, reactions. Related topics are distillation (Section 16.11.4.2) and reactors (Section 16.11.6.4).

Area of Application

250 to 1300°C; <30 MPa; thermal efficiency: 70 to 75%.

Guidelines

Heat flux in radiant section: 10 to 60 kW/m² based on outside tube area with fluid velocity inside tubes 0.1 to 3 m/s. Use 1.5 m/s. In the convection section: 12 kW/m².

Equate heat duties in the radiant and convection sections; 80% efficiency based on net heating values.

Size radiant section to absorb 50% of the radiant energy with 1.22 m³ chamber per m² tube area.

175°C, consider Dowtherm J
 200 to 400°C, consider molten salt
 275°C, consider Dowtherm A
 310°C, consider Dowtherm G

Shell-and-tube:

Use shell-and-tube exchangers for gas-gas and for low-viscosity liquid-liquid systems (<200 mPa·s).

Use floating head if the temperature difference between shell-and-tube fluids exceeds 30°C (to minimize impact of thermal expansion).

Surface compactness: for ordinary tubes: 70 to 500 m²/m³; for finned tubes 65 to 3300 m²/m³.

Number of Shell Passes Affected by Temperature Ratio	No. of Shell Passes
$\frac{(t_{hot/in} - t_{hot/out}) + (t_{cold/out} - t_{cold/in})}{(t_{hot/in} - t_{cold/in})}$	
0–0.8	1
0.8–1.1	1 or 2
1.1–1.3	2
1.3–1.4	2 or 3
1.4–1.5	3

Tube velocity >1 m/s; for crude preheat exchangers, tube velocity is 1 to 2 m/s; for overhead water condensers, tube velocity is 1 to 3.5 m/s. To minimize fouling, keep tubeside velocities 3 to 4.5 m/s, reduce the wall temperature, and use single-flow channels.

Nozzle velocity <2 m/s and Δp , kPa = 0.75 to 0.9 (nozzle velocity, m/s)².

Baffle cut <30%; baffle pitch: minimum should be the maximum of 5 cm or 1/5 of ID shell diameter. The maximum should be the smaller of 0.75 m or shell ID diameter.

For shell-and-tube heat exchange: numerous related topics including evaporation (Section 16.11.4.1), distillation (Section 16.11.4.2), crystallization (Section 16.11.4.6), freeze concentration (Section 16.11.4.3), melt crystallization (Section 16.11.4.4), and PFTR reactors (Section 16.11.6.5 and .6). Approach temperature 5 to 8°C; use 0.4 THTU/pass; design so that the total pressure drop on the liquid side is about 70 kPa. Allow four velocity heads pressure drop for each pass in a multipass system. Put inside the tubes the more corrosive, higher-pressure, dirtier, hotter, and more viscous fluids. Recommended liquid velocities 1 to 1.5 m/s with maximum velocity increasing as more exotic alloys are used. Use triangular pitch for all fixed tube sheets and for steam condensing on the shell side. Try $U = 0.5 \text{ kW/m}^2\cdot^\circ\text{C}$ for water/liquid; $U = 0.3 \text{ kW/m}^2\cdot^\circ\text{C}$ for hydrocarbon/hydrocarbon; $U = 0.03 \text{ kW/m}^2\cdot^\circ\text{C}$ for gas/liquid, and $0.03 \text{ kW/m}^2\cdot^\circ\text{C}$ for gas/gas. Finned tubes: see air-cooled.

For shell-and-tube condensation: related topics include evaporation (Section 16.11.4.1) and distillation (Section 16.11.4.2). Prefer condensation outside horizontal tubes; use vertical tubes when condensing immiscible liquids to subcool the condensate. Assume pressure drop of 0.5 of the pressure drop calculated for the vapor at the inlet conditions. Baffle spacing is 0.2 to 1 times the shell diameter with the baffle window about 25%. Limit pressure drop for steam to 7 kPa on the shell side. $U = 0.5$ to $0.85 \text{ kW/m}^2\cdot^\circ\text{C}$.

For shell-and-tube boiling: approach temperature <25°C to ensure nucleate boiling. Related topics include evaporation (Section 16.11.4.1), distillation (Section 16.11.4.2), solution crystallization (Section 16.11.4.6), and reactors, PFTR nonadiabatic (Section 16.11.6.6).

Kettle: use for clean, relatively low-pressure, nucleate pool boiling; not for foams; 75 to 100% vaporized. $U = 1.1 \text{ kW/m}^2\cdot^\circ\text{C}$.

Area of Application

Use for highly exothermic reactions or for heating/cooling solids. Mixing provides uniform temperature in the bed and solids increase the heat transfer coefficients 5 to 25 times that of the gas alone.

Guidelines

Coils in fluidized bed: $U = 0.2$ to $0.4 \text{ kW/m}^2\cdot^\circ\text{C}$; bed to wall $U = 0.45$ to $1.1 \text{ kW/m}^2\cdot^\circ\text{C}$; solids to gas $U = 0.017$ to $0.055 \text{ kW/m}^2\cdot^\circ\text{C}$; gas-solid thermal conductivity 0.17 to $42.5 \text{ kW/m}\cdot\text{K}$.

16.11.3.5 Thermal Energy: Motionless Mixers

Related topics include reactors (Section 16.11.6.10), mixing (Section 16.11.7.3), size reduction, gas-liquid (Section 16.11.8.1), and liquid-liquid (Section 16.11.8.3).

Area of Application

Use for viscosity liquids $<50 \text{ mPa}\cdot\text{s}$ and liquid reactions (Section 16.11.6.9).

Guidelines

Cooling melts $U = 0.15$ to $0.25 \text{ kW/m}^2\cdot^\circ\text{C}$. Polymerization: $10 \text{ kW/m}^2\cdot^\circ\text{C}$. Internal heat transfer coefficient $h_{\text{inside}} = 3 \times$ value for fluid flowing in empty pipe of same diameter and length.

16.11.3.6 Thermal Energy: Direct Contact Liquid-Liquid Immiscible Liquids

A related topic is size reduction (Section 16.11.8.3).

Area of Application

Exchange heat across a liquid-liquid interface. Droplet diameter and area per unit volume estimated from size reduction (Section 16.11.8.3).

Guidelines

Tray, sieve: $U_v = 160 \text{ kW/m}^3 \cdot ^\circ\text{C}$

Wetted wall: $U_v = 20 \text{ kW/m}^3 \cdot ^\circ\text{C}$

Baffles: $U_v = 20 \text{ kW/m}^3 \cdot ^\circ\text{C}$;

Spray tower: $U_v = 2$ to $100 \text{ kW/m}^3 \cdot ^\circ\text{C}$

RTD: $U_v = 260 \text{ kW/m}^3 \cdot ^\circ\text{C}$

Pipeline: $U_v = 200$ to $1000 \text{ kW/m}^3 \cdot ^\circ\text{C}$

16.11.3.7 Thermal Energy: Direct Contact Gas-Solid Kilns

A related topic is reactors (Section 16.11.6.17).

Area of Application

Temperature 520 to 1700°C ; atmospheric pressure; particle diameter $7 \mu\text{m}$ to 20 mm ; solid residence time 2000 to $35,000 \text{ s}$.

Used for drying (Section 16.11.5.5), incineration, and gas-solid reactions (Sections 16.11.6.17 through 16.11.20).

Guidelines

Rotary cascading kiln dryer: heat transfer coefficient $U_m = 0.1 \text{ W/kg solids } ^\circ\text{C}$ for coarse materials and $0.4 \text{ W/kg } ^\circ\text{C}$ for fine materials.

Pneumatic or flash dryers: wall to gas/particle systems: $U = 0.1 \text{ kW/m}^2\cdot^\circ\text{C}$.

Spray dryer: volumetric heat transfer coefficients: $U_v = 0.13 \text{ to } 0.18 \text{ kW/m}^3\cdot^\circ\text{C}$.

Rotary steam tube dryer: heat transfer coefficient: $U = 0.03 \text{ to } 0.09 \text{ kW/m}^2\cdot^\circ\text{C}$.

Rotary cascading dryer: heat transfer coefficient: $U_m = 0.1 \text{ W/kg solids } ^\circ\text{C}$ for coarse materials and $0.4 \text{ W/kg}\cdot^\circ\text{C}$ for fine materials.

Continuous freeze dryer: overall heat transfer coefficient: $U = 0.001 \text{ to } 0.01 \text{ kW/m}^2\cdot^\circ\text{C}$, depending on the vacuum and residence time, with smaller values for lower total pressure and longer residence time.

16.11.3.11 Thermal Energy: Direct Contact Gas-Liquid Cooling Towers

Area of Application

Use of the latent heat of evaporation of 9% of hot water to cool the water by removing sensible heat from hot water; size range: 60 to 1500 L/s.

Guidelines

Volumetric heat transfer coefficients $U_v = 0.5 \text{ to } 15 \text{ kW/m}^3\cdot^\circ\text{C}$; gas superficial velocity 1 m/s; liquid loading $1 \text{ L/s}\cdot\text{m}^2$ cross-sectional area.

16.11.3.12 Thermal Energy: Direct Contact Gas-Liquid Quenchers

Area of Application

The quenching media can be any liquid. Gas flow rate 4 to 100 m^3/s .

Guidelines

Tray: heat transfer coefficient, $U = 7 \text{ to } 20 \text{ kW/m}^2\cdot^\circ\text{C}$. of tray area; volumetric heat transfer coefficient, $U_v = 3 \text{ kW/m}^3\cdot^\circ\text{C}$; superficial gas velocity = 1 to 1.6 m/s; mass loading liquid/gas = 10 to 20/1.

Packing: volumetric heat transfer coefficient, $U_v = 3 \text{ kW/m}^3\cdot^\circ\text{C}$; superficial gas velocity = 1 m/s; mass loading liquid/gas = 1.5 to 3/1.

Spray tower: volumetric heat transfer coefficient, $U_v = 1.8 \text{ to } 5 \text{ kW/m}^3\cdot^\circ\text{C}$; superficial gas velocity = 1 m/s; mass loading liquid to gas = 1 to 50/1.

Baffles: volumetric heat transfer coefficient, $U_v = 0.5 \text{ kW/m}^3\cdot^\circ\text{C}$; superficial gas velocity = 0.7 to 1 m/s; mass loading liquid to gas = 15 to 60/1.

16.11.3.13 Thermal Energy: Direct Contact Gas-Liquid Condensers

Area of Application

The condensing medium is water to condense steam or to cool gas. Use in steam ejector systems, although these are being replaced by indirect condensers. A related topic is vacuum service (Section 16.11.2.2). Body dia., 0.1 to 2.5 m; liquid flow rate, 3 to 700 L/s.

Guidelines

Liquid loading 43 to 85 $\text{L/s}\cdot\text{m}^2$ cross-sectional area. Height/diameter = 5/1. Keep temperature increase in the cooling water limited to 8.3°C for operating pressures $<6 \text{ kPa}$, limited to 17°C for operating pressures 6 to 25 kPa, limited to 25°C for operating pressures $>25 \text{ kPa}$; and keep overall temperature $<50^\circ\text{C}$ to minimize erosion and corrosion.

Gas cooling: $\Delta T = 16 \text{ to } 18^\circ\text{C}$.

Steam condensation: $\Delta T = 2.75^\circ\text{C}$; approach temperature at both ends of the condenser = 2.75°C .

16.11.3.18 Thermal Energy: Steam Generation

See thermal energy furnaces/boilers (Section 16.11.3.2). See Section 16.11.2.8 for steam distribution.

16.11.4 HOMOGENEOUS SEPARATION*

Overall Guidelines

1. Keep it simple.
2. Exploit differences in properties between the key target species.
3. Consider mixing/blending of streams before considering separation.
4. Remove lightest component, most abundant, least expensive first; or remove the most difficult last.
5. Leave high specific recoveries until last.
6. Try to avoid adding an agent to achieve the separation.
7. Try to avoid extremes in operating conditions.
8. Consider shifting from homogeneous phase separation to heterogeneous phase separation.
9. Consider reaction to shift the species to another form.

16.11.4.1 Evaporation

This is related to crystallization (Section 16.11.4.6).

Area of Application

$\alpha_{vp} = 20$ to 5000. Liquid feed concentration of target solute 2 to 50%; 1 to 40 kg/s feed rate. One product. Usually used when no solids, nonfoaming and doesn't thermally degrade, although special designs can accommodate these. Can be operated as multistage with up to 3 to 10 stages.

Guidelines

Dissolved solids elevate the boiling temperature between the solution and saturated vapor by 1.5 to 5.5°C.

Temperature-sensitive materials: use the Hickman decomposition hazard index, *HDHI*, which is expressed as the amount of time the material is kept under temperature (as measured by pressure, Pa) in units of Pa-s.

External short tube, vertical exchanger, natural circulation: OK for foaming but not for fouling, crystal formation, or suspended solids. Viscosities <20 mPa-s. Relative to agitated film retention time of 16:1 and volume 10:1. Overall heat transfer coefficient 1 to 1.5 kW/m²·°C. HDHI = 10⁸ to 10⁹ Pa-s. Area 3 to 1000 m².

External short tube, vertical exchanger, forced circulation: OK for foaming, fouling, crystal formation, and some suspended solids. Viscosities <150 mPa-s. Relative to agitated film retention time of 42:1 and volume 13:1. Overall heat transfer coefficient 0.75 to 3 kW/m²·°C, decreasing with increasing viscosity. Power 0.13 to 0.5 kW/m². HDHI = 10⁷ to 10⁸ Pa-s. Area 3 to 600 m².

External kettle reboiler, natural circulation: viscosities <200 mPa-s.

Internal calandria, vertical short tube: preferred for fouling and crystal forming systems. OK for foaming, fouling, crystal formation, and some suspended solids. Viscosities <1000 mPa-s. Relative to agitated film retention time of 168:1 and volume 3:1.

* Reproduced with permission from Donald R. Woods, *Rules of Thumb in Engineering Practice*, pages 87 to 135, 2007, copyright Wiley-VCH Verlag GmbH & Co. KGaA, Weinheim, ISBN: 978-3-527-31220-7. See this book for more details, especially about Good Practice, Trouble shooting and Capital Costs.

Prefer to remove the most valuable as distillate.

Prefer to remove components one by one as overhead.

Prefer separations that give equimolar splits.

Set the column pressure to try to use water as the coolant and steam as the energy source.

Overhead concentrations 95 to 99% mol.

Internals are trays, packing, or high-performance packing.

If trays are selected, then calculate the theoretical stages required.

Tray options: valve: usually cheaper than sieve, use for large-diameter columns at moderate to high pressures, moderate turndown ratio. Usually about 120 to 140 values per active m²; sieve: use for large-diameter columns at moderate to high pressures, moderate turndown ratio; bubble cap: use for columns with small liquid flow rate, high turndown ratio, heat transfer needed internally.

Typical $\Delta p/\text{HETS} = 0.4$ kPa.

Downcomer: unaerated liquid velocity 0.5 m/s; head loss via underflow clearance <0.3 kPa.

Allow 3 s liquid residence time and extend to 6 s for foaming systems. Weir overflow velocity = 5 to 20 L/s·m of outlet weir.

If packings are selected, then calculate the number of transfer units, NTU, required or number of theoretical stages (NTS).

Conventional random dumped packings: pall rings, Tellerettes, raschig rings, beryl or intalox saddles, lessing rings: use for columns <1 m dia., vacuum service, small pressure drop, high liquid flow rates, viscous liquids, minimum liquid holdup. Prefer Pall rings and Tellerettes; if ceramic, use saddles.

High-performance structured packing: Flexipac, gauze, Glitsch grid, Leva film: not for viscosities >2 mPa·s, pressures >200 kPa;

$\Delta p/\text{HETS}$ 0.001 to 0.5 kPa; very small superficial gas velocity.

To estimate the NTS,

1. Estimate minimum reflux ratio from the Underwood equation, or as an approximation if the distillate is almost pure:

$$R_{\min} = \frac{1}{(a-1)(X_{LK,Feed})}$$

Select operating reflux ratio that is 1.2 to 1.5 times minimum. For vacuum distillation, the reflux ratio usually is >10:1, especially for packed columns.

2. Estimate the minimum number of theoretical stages using the Fenske equation, or as approximations:

Douglas': T = absolute temperature for overhead distillate, D , and for the bottoms, W :

$$N_m = \frac{T_D + T_W}{3(T_W - T_D)}$$

Latour's: x = mol fraction:

$$N_m = 0.11 \frac{T_D + T_W}{(T_W - T_D)} \log_{10} \left[\frac{x_D}{x_W} \frac{(1-x_W)}{(1-x_D)} \right]$$

The number of theoretical trays = twice the minimum number, N_m .

If structured packing is selected: design for 70 to 80% of flooding; for foaming, use 40% of flooding. Usual liquid flow rate of 0.007 to 5 L/s·m². Usual gas density-weighted superficial velocity, F factor, of 0.5 to 2.5 m/s (kg/m³)^{0.5}. $\Delta p/\text{HETS} = 0.01$ to 0.05 kPa. If the $\Delta p > 1.2$ to 1.6 kPa/m, then the packing is flooded. HETS 0.12 to 0.45 m, with this increasing to 1.8 m for high liquid capacity Glitsch grid.

For *extractive distillation*, the solvent should have a boiling temperature 50 to 100°C higher than those of the products, with solubility parameters and molar volumes similar to those of one product but different from the other.

For molecular distillation, 0.2 to 0.5 g/s·m² with about 4.5 m²/unit; 80 to 90% efficient.

For *steam distillation*:

For direct heating, 25 to 120 kg/m³. For inert steam added, flow rate calculated.

For *HIGEE*:

Residence time 0.1 to 1 s; voidage 90 to 95%; 2 m dia. max., area per volume 2000 to 5000 m²/m³. 1000 rpm; film thickness 100 μm . Overall heat transfer coefficient $U = 10$ kW/m²·K. See also reactive distillation, Section 16.11.6.32.

For *batch distillation*: size based on cycle time: fill, distill, discharge bottoms, clean.

for $\alpha_{vp} = 2$, NTS = 10; reflux ratio 20:1

$\alpha_{vp} = 4$, NTS = 6; reflux ratio 12:1

$\alpha_{vp} = 10$, NTS = 3; reflux ratio 7.5:1

To convert TS to height of packing:

1 TS = 1 m of >5 cm dumped Pall rings or saddles

1 TS = 0.9 m of 4 cm dumped Pall rings or saddles

1 TS = 0.6 m of <2.5 cm dumped Pall rings or saddles

1 TS = 0.15 m of structured mesh packing in column of diameter <0.3 m

1 TS = 0.3 m of structured mesh packing in column of diameter >0.3 m

For *batch distillation*: As the more volatile species is removed, the separation becomes progressively more difficult. Too low a reflux gives an unattainable product, regardless of the number of trays. Gives high-purity recovery from a small concentration of a low-boiling species in a single operation. Keep the reflux holdup <10% to 15% of the initial batch charge.

16.11.4.3 Freeze Concentration

Area of Application

Liquid feed 1 to 30% w/w solute; operates below the freezing temperature of the *solvent*.

Guidelines

Don't exceed the K_{sp} of the solute. For juices, the solute concentration increases from about 10 to 50% when the freezing temperature is -10°C .

16.11.4.4 Melt Crystallization

Area of Application

Liquid concentration 60 to 90% w/w. Operates below the freezing temperature to solidify the target *solute*. Capacity usually <3 kg/s. Use for temperature-sensitive materials, when $\alpha_{vp} < 1.4$, when azeotropes form, or for solid product. A freeze test shows >50% reduction in impurities.

Guidelines

Design based on heat transfer. Limited by eutectic formation. Multistaging possible but usually <10 stages.

Suspension crystallization: crystals and melt same temperature; design on degree of supersaturation; separation of crystals from melt depends on density difference in countercurrent operation. Scraped wall crystallizer (Section 16.11.4.6).

If *fouling* is a problem, consider flash growth type Pachuca, draft tube MSMR units, or classified product removal CPR type: Oslo, krystall type.

May be operated batch or continuous.

Seed the process because the nucleation sets the crystal habit and influences crystal size distribution (CSD). Importance of "contact nucleation" where crystals strike pump and mixer impellers. Crystal growth kinetics increase with temperature increase. Crystal growth rate = 0.1 to 0.8 mm/h with growth approximately the same in all directions

Batch: size based on cycle time: fill, crystallize, dump, clean. Use for production capacity of <0.15 kg/s and where target is relatively uniform and narrow CSD; although reproducibility may be difficult between batches. Batch gives narrower CSD than continuous.

Continuous CPR with classified fines and classified product removal gives increased crystal size and narrow CSD. Multistaging in series gives larger crystals and narrow CSD.

16.11.4.7 Precipitation

Area of Application

Liquid feed; operates at temperatures above the freezing temperature of the solute, usually in the range 18 to 35°C. Solute formed by reaction is insoluble, key parameter is K_{sp} of product. Provides a sharp first cut removal of solute.

Guidelines

Design based on mass transfer. Reactions are usually very rapid and design is based on mixing to distribute the reactant. For most precipitation reagents, allow 5-min residence time. If secondary reagents are needed to change the oxidation state of the target species before precipitation, then example residence times are

Arsenic: 30 min

Hexavalent chromium or iron: 20 min

Either pre- or post-pH change, allow about 0.180 kg acid or base/m³ water.

16.11.4.8 Gas Absorption

See also heterogeneous gas-liquid separations, turbulent bed contactor (TCA, TVA) (Section 16.11.5.2), distillation (Section 16.11.4.2), reactors (Sections 16.11.6.11 through 16.11.6.17), and direct-contact heat exchange (Sections 16.11.3.11 through 16.11.13), with gas-liquid contacting characteristics described in Sections 16.11.8.1 and 16.11.8.2.

Area of Application

α = 2000 to 100,000, and gas feed concentration of target solute is 0.1 to 20%; 98% purity possible. Target species is soluble.

For high concentration and solubility plus particulates, use

Jets, venturis: very soluble gas only with target species Henry's law constant <10³ kPa/mol fraction; feed gas concentration >1 vol%. Efficiencies 50% to 85%.

Turbulent bed contactor: both gas absorption and removal of heavy, sticky particulates.

Related to Section 16.11.5.2.

For high concentration and solubility, use

Countercurrent packed column: Economic NTU usually <5 ; critical energy-consuming phase is the gas at about 3 kJ/m^3 with liquid-to-gas ratio about 0.7 to 1.5 L/m^3 . Liquid loading on usual packings 3 to $35 \text{ L/m}^2\cdot\text{s}$; (0.007 to 5 on structured packings) molar ratio liquid to gas 1.4 to 80; superficial gas velocity 1.4 to 2.2 m/s ; design on mass transfer in both gas and liquid. Power usage 0.15 to $0.6 \text{ kW}\cdot\text{s/m}^3$. $\Delta p_{\text{gas}} = 0.07$ to $0.4 \text{ kPa/theoretical stage}$; HETS = 0.5 to 1 m. For low liquid loadings and high gas flow rates, $HTU_G/HTU_L \approx 2$; for high liquid loading and low gas flow rates, 0.2.

Assume 99% absorption; set molar flow rates $F_L/F_G = 1.2$ to 2 times the minimum. Use the Kremser equation for the design of dilute units with molar absorption factor $F_L/F_G m = 1.2$ to 2; use 1.4. $\text{NTU}_{OG} = 20$ for 99% recovery.

Assume $\text{HTU}_{OG} = 0.6 \text{ m}$ with maximum packing height 12 m. Superficial gas velocity 1 m/s and/or superficial density-weighted velocity F -factor of 0.6 to $3.5 \text{ m/s (kg/m}^3)^{0.5}$. Use 2.5-mm Pall rings or Tellerettes of metal or plastic.

Countercurrent tray column: economic NTU usually <5 ; liquid-to-gas ratio 1.5 to 18 L/m^3 ; superficial gas velocity 1 to 1.6 m/s and/or superficial density-weighted velocity F -factor of 1.2 to $1.8 \text{ m/s (kg/m}^3)^{0.5}$. Power usage 0.5 to $2 \text{ kW}\cdot\text{s/m}^3$; $\Delta p_{\text{gas}} = 0.7$ to $1.5/\text{tray}$. HETS = 0.7 m. Tray efficiencies 10 to 20%.

Assume 99% absorption; use the Kremser equation for the design of dilute units with molar absorption factor for economic recovery of the solvent $F_L/F_G m = 1.4$ with general range 1.2 to 2. Tray spacing = 0.6 m with valve or sieve trays. See also Section 16.11.4.2 for such details as downcomer sizing.

For multitube cocurrent falling film: $U = 0.6 \text{ kW/m}^2\cdot\text{K}$.

16.11.4.9 Gas Desorption/Stripping

Area of Application

$\alpha = 2000$ to 100,000 and liquid feed concentration of target solute is 0.1 to 5%; 98% purity possible.

Guidelines

Because the target solute usually has low solubility in the liquid, usually the desorption is liquid-phase controlled.

For packings the goal is high liquid loadings, about $30 \text{ L/m}^2\cdot\text{s}$, and minimum gas flow rates. Superficial density-weighted velocity F -factor of $0.6 \text{ m/s (kg/m}^3)^{0.5}$.

Use Kremser equation for the design of dilute units with molar L /absorption factor for economic stripping of $F_G m/F_L = 1.2$ to 2 with starting value of 1.4; m = Henry's constant/total pressure. For packing, HETS = 1.83 m.

Edible oil deodorizing: high vacuum. For $<0.6 \text{ kg/s}$, irregular production, use batch. Requires processing time = 4 h/batch, low heat recovery. For $>0.6 \text{ kg/s}$, continuous with processing time = 1 h. Keep liquid films thin to promote mass transfer of volatiles and use astute distribution of sparge steam.

16.11.4.10 Solvent Extraction, SX

A related topic is size reduction (Section 16.11.8.3).

Area of Application

General: feed concentration 0.03 to 95% w/w; for minerals, typically 0.01 to 2% w/w; separation factor α = partition coefficient ratio with values 2 to 500 and should be >5 .

Lurgi contactor: HETS increases exponentially with diameter; 0.7 m at 1 m dia.; diameters <8 m; superficial velocity about 5.5 L/s-m².

Pulsed packed column: HETS increases exponentially with diameter; 0.7 m at 1 m dia.; max. diameter 2.5 m; superficial velocity about 5.5 L/s-m².

Pulsed sieve plate column: HETS increases exponentially with diameter; 0.4 m at 1 m dia.; max. diameter 3 m; superficial velocity about 5.5 L/s-m² sieve holes 3 to 8 mm; velocities through the holes <0.2 m/s to minimize the formation of small drops. Tray efficiencies about 20 to 30%.

Reciprocating plate: HETS increases exponentially with diameter; 0.35 m at 1 m dia.; max. diameter 1.5 m; superficial velocity about 11 L/s-m².

Rotating disk contactor, RDC, ARD contactor; Mixco, Scheibel, Treybal, Oldshue–Rushton, Kuehni: HETS is sensitive to rotor speed. HETS increases slightly with diameter; 0.5 m at 1 m dia.; superficial velocity about 5.5 L/s-m² with Kuehni 9.7 L/s-m². Mixco, Scheibel, Treybal, Oldshue–Rushton, diameter <2.5 m; RDC diameter <9 m.

Total flow through a column = 10 L/s-m² with a density difference of 0.2 Mg/m³.

Centrifugal: two to six units per machine, depending on the machine.

16.11.4.11 Adsorption: Gas

Area of Application

Use when feed concentration of the more volatile species is small, 0.15 to 10%, and when $\alpha_{ads} > 2$; when the target species is difficult to condense.

Guidelines

Select adsorbent based on pore size related to the target species.

Alumina: surface area: 210 to 350 m²/g; pore volume 0.21 cm³/g, temperature <320°C; superficial gas velocity 125 to 500 dm³/m²·s; usually adsorb 800 kg/m³ or 0.14 to 0.22 kg organics/kg dry solid; 0.15 kg water/kg dry solid. Lifetime: 150 cycles.

Silica: surface area: 750 to 830 m²/g; pore volume 0.4 to 0.45 cm³/g, temperature <230°C; superficial gas velocity 125 to 500 dm³/m²·s; usually adsorb 720 kg/m³; 0.3 to 0.6 kg organics/kg dry solid; 0.4 kg water/kg dry solid.

Four-Å molecular sieve: surface area: 640 to 80 m²/g; pore volume 0.27 cm³/g, temperature <300°C; superficial gas velocity 150 to 250 dm³/m²·s; usually adsorb 480 to 720 kg/m³; 0.05 kg nitrogen/kg dry solid; 0.22 to 0.36 kg water/kg dry solid. Lifetime: 400 cycles.

Activated carbon: surface area: 1000 to 1500 m²/g; pore volume 0.6 to 0.8 cm³/g, temperature <540°C; superficial gas velocity 100 to 600 dm³/m²·s; capacity depends on organic; range 0.06 to 0.2 kg organics/kg dry solid adsorbent.

For fixed bed: batch: size on cycle time: load, swing out of service, regenerate, swing back into service. Loading time: 100 to 3000 bed volumes (BV)/h with time based on the ratio of the adsorption isotherm to the feed concentration of the target species (usual range 50 to 300 corresponding to load times of 0.2 to 2 h). Regenerate with steam (at 3 to 5 kg steam per kg organic removed), solvent, reduced pressure, combustion, or via vacuum/pressure shift. Use superficial gas velocity of 60 to 600 dm³/dm²·s or recommended value for the adsorbent to determine *cross-sectional* area. Residence time 0.03 to 0.8 Bed volumes/second: (F/V) with depth >0.33 dia.

16.11.4.12 Adsorption: Liquid

A related topic is ion exchange (Section 16.11.4.13).

Area of Application

High-valence ionic species in liquid phase with $\alpha_{IX} = \Gamma^+(1 - c^+)/c^+(1 - \Gamma^+) = 1.01$ to 1.04 and feed concentration 0.02 to 2% w/w. Γ^+ = surface concentration of cations.

Guidelines

Select the ion exchange resin based on the pH of the environment and the valence of the target ion. For high efficiency, try to use weak electrolyte resin.

Weakly acidic cationic (WAC) exchange resin: carboxylic; pH >4; $T < 100^\circ\text{C}$; hydrogen or sodium form, depending on regeneration preference; loading 3.5 equivalent/L of resin; good selectivity; greatest affinity for alkaline earth metals in the presence of alkalinity.

Strongly acidic cationic (SAC) exchange resins: sulfonic; full range of pH, $T < 120^\circ\text{C}$; hydrogen or sodium forms; loading 1.9 equivalents/L resin; high capacity, high activity. Ionic sequence $\text{Ba} > \text{Pb} > \text{Sr} > \text{Ca} > \text{Ni} > \text{Mn} > \text{Be} > \text{Cd}^{2+} > \text{Cu} > \text{Co} > \text{Zn} > \text{Mg}$.

Weakly basic anionic (WBA) resin: aromatic polyamine; pH <7; temperature $< 50^\circ\text{C}$; chloride (more thermally robust) or OH form; loading 1.6 eq/L resin.

Strongly basic anionic (SBA) exchange resins: type I trimethyl amine; full range of pH; chloride (more thermally stable) or OH forms; loading 0.46 to 1 eq/L resin.

Ions being exchanged must have a higher valence than ions in bed from regeneration.

Batch:

Fixed bed: batch: size on cycle time: load, backwash/rinse, elute, standby. Try to match loading with off-line time. Load: loading feedrate 5 to 10 BV/h with loading time depends on the ratio of exchange capacity of the resin to the feed concentration of the target species. Usual ratio 10 to 100 corresponding with a loading time of 1.5 to 15 h. Backwash with a velocity to fluidize the bed for 1 to 10 BV (corresponding to about 1.5 h). Eluent feedrate 1 to 3 BV/h for typically 8 to 20 h. Standby is typically 20% of the backwash time. When the eluate is valuable, try to match the loading time with the backwash, eluate recovery, and standby.

Feed flow rate: superficial velocity 1 to 15 L/m²·s; use 5 L/m²·s. Superficial velocity <3 L/m²·s gives poor feed distribution; 5 to 10 bed volumes/hour; too deep a bed leads to excessive pressure drop; keep below 350 kPa. Add 2.5 m to height to allow for bed support and head room for backwashing. Typical bed depths 1 to 5 m; usual industrial bed cross section 5 m².

Use fixed bed if <20 L/s. Pressure, gravity, cocurrent, countercurrent, series, single bed, or mixed bed. Gravity is economical where the bed volume > 80 m³.

Loading times and elution-regeneration times should be approximately equal.

For WAC and WBA systems, the backwash, regeneration, and rinse cycles are 30 to 60 min.

Continuous:

Moving bed: use if >20 L/s.

Fluidized bed: use if slimes or fine particles in feed, elution time >> IX time, eluant is expensive. Use 16 to 20 mesh resin with superficial velocities of 40 L/m²·s. Try to operate at 50 to 200% bed expansion. Related topics include adsorption-liquid (Section 16.11.4.12).

16.11.4.14 Foam Fractionation

A related topic is size reduction, gas in liquid (Section 16.11.8.1).

Area of Application

Solute feed concentration usually 1 ppm to 0.1% with some applications up to 10% (10⁻³ to 10⁻⁹ mol).

Guidelines

Driving force for the rate of separation: concentration of target species.

Membrane: symmetric microporous with 0.1 to 10 mm pore diameter. Hydraulic permeability: 10^{-3} to 8 g/s·m²·MPa. Membrane-solute permeability 0.05 to 9 μm/s, depending on the solute and the membrane. Dialysis transfer coefficient: 1 to 10 μm/s.

16.11.4.17 Membranes: Electrodialysis

Area of Application

Diameter of the target species: 0.2 to 0.8 nm. Feed concentration <20% ionic. Feed range 0.005 to 5%.

Guidelines

Driving force for the rate of separation: electropotential

Membrane: ion exchange, homogeneous or microporous polymer with positively or negatively charged fixed ions

Hydraulic permeability: 10^{-3} to 8 g/s·m²·MPa

Pretreat feed until ferric < 0.3 mg/L

Mn < 0.1 mg/L

H₂S < 0.3 mg/L

Temperature: >10 and <43°C

Optimum feed concentration: 1000 to 5000 mg/L

Energy: about 5.5 to 9 MJ/m³ product

Pressure drop: horizontal stack 0.2 to 0.4 MPa; vertical stack 0.02 to 0.07 MPa

16.11.4.18 Membrane Configurations

Can be operated *dead-end* or *crossflow*: “batch” with 100% recycle of retentate; “continuous” with recycle ratios 15/1 to 30/1 and purge and “multistage,” where the purge from one stage becomes the feed of the next.

Batch process: stop feed because the membrane performance has deteriorated or because the target concentrations or volumes of permeate or retentate have been achieved. Deteriorated membrane performance can be (1) because of a buildup of particulates or biological deposits (this can be corrected by backflushing with permeate or cleaning with detergents, acids, or bases) or (2) because the membrane needs to be replaced (the life of a membrane is one or two to ten years, depending on the operating conditions and the type of membrane). See Table 16.32.

Membranes:

Hydrophilic: cellulosic (temperature <30°C), polyacrylic, nylon 66, ceramic. Life: polymers: 1 year; ceramic: <10 years.

Hydrophobic: polysulfones, polyolefins, carbon. Life: polymers: 1 to 2 years; fluoropolymers <4 years.

Neither hydrophilic nor phobic: sintered.

16.11.4.19 Membranes: Pervaporation

Area of Application

$\alpha = (c_{i3}/c_{j3})/(c_{i1}/c_{j1})$, where *i* is the target permeate species, *j* is the reject; 3 = permeate, and 1 = feed, separates dissolved organics = 1.3 to 41. Particle diameter, 0.2 nm. Target concentration 5 to 20% w/w, but 0.1 to 10% w/w for economical. Temperature <120°C.

Guidelines

Driving force for the rate of separation: concentration gradient in the vapor pressure.

Membrane: asymmetric: homogeneous, or microporous (cellulose acetate, polyamide, polysulfone, polyacrylonitrile); composite of a homogeneous polymer film on microporous substructure (cellulose acetate, polyamide, polysulfone, polyimide, polyvinyl alcohol).

Usual pore 0.1 to 0.2 μm .

0.1 μm PVA: water \gg methanol $>$ ethanol $>$ other organics.

Silicone rubber: methanol $>$ ethanol $>$ aldehydes $>$ ketones \gg water; paraffins $>$ olefins.

Cellulose esters: aromatics $>$ paraffins; olefins $>$ paraffins; dienes $>$ olefins; *n*-paraffins $>$ branch; low molar mass paraffins $>$ high molar mass paraffins.

Capacity/unit: feed < 1.5 kg/s.

Feed pressure: atmospheric.

Feed temperature: close to the normal boiling temperature; usually 50 to 100°C.

Permeate conditions: pressure 0.5 to 2 kPa absolute with condenser temperatures: -20 to $+30^\circ\text{C}$.

For dehydration, use a difference in partial vapor pressure at least one order of magnitude; the permeate flux doubles for an increase in temperature of 10°C .

Permeate flux: depends on membrane but in the range 0.008 to 5 $\text{g/s}\cdot\text{m}^2$.

Configuration: see Section 16.11.4.18.

Spiral wound, transverse hollow fiber.

Use *crossflow* with recycle ratio 15 to 30/1. Criterion: 10% of feed volume is permeate or purity of the permeate or retentate.

Membrane life: 2 to 4 years.

Cycle time: usually limited by life of membrane.

16.11.4.20 Membranes: Reverse Osmosis (RO)

Area of Application

$\alpha = 6$ to 25; feed concentration 0.05 to 20% w/w; with suggested economic feed concentration $< 0.5\%$; 99% purity possible. Diameter of the target species: 0.2 to 0.8 nm. Must have a difference in osmotic pressure. The osmotic pressure coefficient in mass ratio units for different solutes = 20 to 80 MPa $\cdot\text{kg/kg}$ at 25°C . The higher the valence, the better the rejection.

Guidelines

Driving force for the rate of separation: hydrostatic pressure.

Membrane: asymmetric: homogeneous or microporous; active dense 20- to 50- μm layer of cellulose acetate with total thickness 100 μm ; composite of a homogeneous polymer film on microporous substructure.

Pressure: 1.4 to 10 MPa (1.4 to 4.2 for brackish water; 5.6 to 10 for seawater). Inlet pressure $>$ twice the inlet osmotic pressure.

Temperature: $< 45^\circ\text{C}$.

Capacity/unit: < 7 L/s.

For cellulose acetate membranes: $1/\Theta^+ = A_p/B_p = 1$ to 500 with usual value 300 (dimensionless).

For aromatic polyamide membranes: $1/\Theta^+ = 0.7$ to 20.

A = permeate hydraulic permeability, $\text{g/s}\cdot\text{m}^2\cdot\text{MPa}$.

p = total operating pressure, MPa (1.4 to 10 MPa).

B = target solute transport coefficient, $\mu\text{m/s}$ (10^{-6} to 10 $\mu\text{m/s}$).

ρ = mass density of the feed stream.

Select diameter or channel spacing so that diameter of the target species is 0.1 of the diameter or channel spacing; except for spiral wound where, for 0.75-mm spacing, the particles must be <5 to $25\text{ }\mu\text{m}$; or 0.006 to 0.034 diameter of spacing; for 1-mm spacing, particles should be <25 to $50\text{ }\mu\text{m}$ or 0.025 to 0.05 of the diameter or channel spacing.

Permeate flux: depends on the membrane and configuration: hollow fibers/polysulfone: 0.005 to $0.016\text{ L/s}\cdot\text{m}^2$; spiral wound/polysulfone: 0.08 to $0.14\text{ L/s}\cdot\text{m}^2$; tubes/polysulfone: 0.06 to $0.2\text{ L/s}\cdot\text{m}^2$.

Liquid permeability increases 25% for every 10°C increase in temperature.

Power depends on target species and configuration: water treatment 1.8 kJ/L permeate; food application: 32 kJ/L permeate; electropaint: 60 kJ/L permeate. Configuration: hollow fiber 6 kJ/L ; plate and frame 9 kJ/L ; spiral 3 to 6 kJ/L ; tube 15 kJ/L ; or hollow fibers: 100 to 280 W/m^2 ; plate and frame: 180 to 280 W/m^2 ; spiral wound 25 to 120 W/m^2 .

Configuration: see Section 16.11.4.18.

Spiral wound, hollow fibers, plate and frame, and tubular (use for small flow, high value, and severe fouling applications).

For laminar flow operation of hollow fiber, plate and frame, and spiral wound, keep the operating pressure 0.1 to 0.2 MPa; for turbulent flow operation of plate and frame, spiral wound and tubes, operate at 0.5 to 0.7 MPa.

Use *dead-end* for low concentrations of particles $>0.1\text{ }\mu\text{m}$.

Use *crossflow* batch with 100% retentate recycle, continuous bleed with recycle ratio 15 to 30/1 and multistage: when a concentrated retentate is desired or when particle diameter $<0.1\text{ }\mu\text{m}$. Criterion to backwash/or clean: when 90% reduction in retentate volume is achieved; given quality or volume of permeate; the permeate flux $<15\%$ of initial flux; or when the viscosity of the retentate is 100 to $300\text{ mPa}\cdot\text{s}$. This corresponds to concentrations for pigments of 30 to 70%; for microorganisms of 1 to 10%.

Membrane life: 2 to 4 years.

Cycle time: clean by backwashing with permeate every 6, 24, 170, 360, 1000 h (depending on the criteria, the membrane, operating conditions, and the amount of pretreatment); example, 8 h on and 1 to 2 h off to clean; or short pulses every 150 to 300 s so that steady-state flux operation is never achieved.

Clean by steam, detergents, solvents, acids, or bases. Another option to lengthen cycle time is to add solids to the feed to mechanically wear away the gel layer. The choice affects membrane life. Steam cleaning gives 50 to 150 cycles before membrane replacement; nonsteam cleaning gives 200 to 500 cycles.

16.11.4.23 Membranes: Microfiltration

A related topic is filters (Section 16.11.5.13).

Area of Application

Particulate diameter 0.05 to $800\text{ }\mu\text{m}$; feed solids concentration $<75\%$ w/w; $<50\%$ v/v. Remove solid or gelatinous particulates by pore size in the membrane. Pore size: 0.2 to $1\text{ }\mu\text{m}$ with the membrane cutoff sizes in the range 0.05 to $10\text{ }\mu\text{m}$.

Guidelines

Driving force for the rate of separation: pressure.

Membrane: symmetric or asymmetric microporous. Ceramic, sintered metals, or polymers with pores 0.2 to $1\text{ }\mu\text{m}$. Symmetric polymers have a porosity of 60 to 85%; asymmetric ceramic membranes, porosity 30 to 40%, are used for high pressure and higher temperature $<200^\circ\text{C}$.

TABLE 16.33
Selection Guide within Section 16.11

		Major Feed Component		
		Solid	Immiscible Liquid	Gas/Vapor
Minor feed component	Solid	General 5.17	Settler 5.7	General 5.2
		Zone refine 4.5	Thickener 5.9	
		Screen 5.29	Screen, 5.6	
		Classifier 5.21–24	Hydrocyclone, 5.8	
		Separator 5.25–28	DAF 5.15	
		Flotation 5.18	Filter 5.13	
		Electrostatic 5.19	Centrifuges, 5.11, 5.12	
		Magnetic 5.20	Ultrafiltration, 4.22	
			Microfiltration, 4.23	
	Liquid	General options 5.4	General options 5.3	5.1 Knockout pots
		Dryer 5.5		Zigzag baffled chambers; wet
		Screen 5.6		cyclones; spray chambers, venturis,
		Leach 5.14		cross flow; wetted packing
		Expeller 5.16		
	Gas/vapor		Stripping 4.9	Homogeneous: membranes 4.15

$$v_{o\ max} = k((\rho_L - \rho_G/\rho_G))^{0.5}, \text{ where } k \text{ is usually } 0.13. \ k_{horiz} = 1.25 \ k_{vertical}$$

and use superficial design value of 0.5 to 0.85% of v_{max} . (This separation superficial gas velocity is used to design/size many types of equipment: distillation columns, demisters.)

Design liquid volume usually 80% with sufficient volume for 300 s residence time to satisfy process control requirements. Typical length-to-diameter ratio of 3:1 to 5:1.

Knockout pot (for low ratios of liquid/gas, as in demisters): use vertical cylinder. Size the same as horizontal with height of the vapor space 1.5 times dia. with 15 cm minimum above the top of the inlet nozzle and use lower value for k in the above equation. For the liquid phase: maximum liquid level at least 18 cm below bottom of inlet nozzle; liquid residence time about 300 to 600 s.

Steam traps: ball float, open bucket, inverted bucket, liquid expansion, and thermodynamic. Float: continuous discharge, operating principle of buoyancy, OK for low loads but not high pressure. Inverted bucket: intermittent discharge, operating principle = weight of the bucket, robust, okay for high pressure and corrosive condensate, use check valve before trap. Balanced pressure, thermostatic: operating principle = vapor pressure of fluid inside bellows. Thermodynamic/kinetic energy: intermittent, operating principle is Bernoulli's principle/impulse, poor air handling, larger sizes more susceptible to back pressure. Usually for steam pressure <1.2 MPa, affected by ambient temperature.

Select inverted bucket traps based on condensate flow rate, pressure differential, and "safety factor."

The other units are sized using approaches used for gas-solid separations (Section 16.11.5.2).

16.11.5.2 Gas-Solid

Area of Application

"Fumes" are particles <1 μm . In general: use cyclones and settling basins for solids loading >20 g/m³. Then, select bag filters unless fumes are also present, low temperatures (<100°C

shaking. Gas-to-cloth ratio of 25 to 150 $\text{dm}^3/\text{s}\cdot\text{m}^2$, but usually design on $<75 \text{ dm}^3/\text{s}\cdot\text{m}^2$. Usual range for woven fabric 7.5 to 50 $\text{dm}^3/\text{s}\cdot\text{m}^2$; for felted fabric, use 7.5 to 100 $\text{dm}^3/\text{s}\cdot\text{m}^2$; for microporous tubes, use 9 to 20 $\text{dm}^3/\text{s}\cdot\text{m}^2$. Gas loading depends on density of particles, size, inlet dust concentration, type of fabric. Batchwise loading with dust removal by reverse jet or blowring is about 0.04 kW/m^2 of bag area. Bag length: diameter $<33:1$.

Wet scrubbers: limited to lower temperatures $<100^\circ\text{C}$.

Wet cyclone: size on internal superficial gas velocity of 1 m/s; height to diameter of 3:1 and water usage of 0.4 L/m^3 ; water flow rate 1.3 to 2.5 $\text{L}/\text{m}^2\cdot\text{s}$.

Crossflow scrubber: $\Delta p = 0.3 \text{ kPa}/\text{m}$ of width; 1 to 1.5 m width usual; water flow rate 2.7 $\text{L}/\text{m}^2\cdot\text{s}$ of horizontal cross-sectional packing; size on actual inlet gas flow rate to the packing face of 1 $\text{m}^3/\text{m}^2\cdot\text{s}$.

Countercurrent wet packing: pressure drop 0.3 to 0.5 kPa/m of packing. Liquid loading about 0.4 L/m^3 gas or 0.6 to 1 $\text{L}/\text{s}\cdot\text{m}^2$; superficial gas velocity 0.5 to 1 m/s; mass loading liquid/gas = 0.7 to 1.5.

Turbulent bed contactor: Liquid loadings 20 $\text{L}/\text{m}^2\cdot\text{s}$; superficial gas velocity based on actual inlet gas flow rate 2 to 11 $\text{m}^3/\text{s}\cdot\text{m}^2$ horizontal cross section; mass loading liquid/gas = 4 to 8. Related topics include fluidized bed, drying (Section 16.11.5.5); heat transfer (Section 16.11.3.8); reactors (Section 16.11.6.27); mixing (Section 16.11.7.1), and size enlargement (Section 16.11.9.5).

Venturi scrubbers: size on throat velocity of 15 to 150 m/s selected based on particle size to be removed with 40 m/s (and 25 kPa pressure drop) for 1 μm and 120 m/s (and 25 kPa) for 0.1 μm . Water usage is in the range 0.5 to 5 L/m^3 gas, with pressure drop increasing as throat velocity increases; mass loading liquid/gas = 1.3 to 1.6.

Wet impingement baffle (Peabody) scrubbers: height/diameter 1.3:1 to 4.6:1; liquid loading 1 to 2 $\text{L}/\text{m}^2\cdot\text{s}$ of horizontal cross-sectional area; mass loading liquid/gas = 0.2 to 0.7.

Electrostatic precipitator: Batch process: load electrodes, then clean: via wet spray or mechanical rapping. For particle conductivity between 10^{-8} and 0.01 reciprocal ohm-m. Prefer negatively charged configuration. May need to adjust conditions to get particle conductivity into acceptable range. For particles $>10 \mu\text{m}$, use 38- m^2 plate area per m^3/s gas flow; 1 μm , use 100- m^2 plate area per m^3/s gas flow; 0.4 μm , use 120- m^2 plate area per m^3/s gas flow.

16.11.5.3 Liquid-Liquid

Usual drop size 200 μm ; interfacial tension 30 mN/m .

Area of Application

Decanter: drop diameter $>100 \mu\text{m}$; feed concentration $>2\%$ v/v.

Hydrocyclone: drop diameter $>20 \mu\text{m}$; feed concentration 6 to 60% v/v. Interfacial tension must be $>10 \text{ mN}/\text{m}$ to prevent drop breakup.

Sedimentation centrifuge: disc type: drop diameter >20 and $<200 \mu\text{m}$; feed concentration 6 to 60% v/v; suited for low surface tension, density differences $>0.02 \text{ Mg}/\text{m}^3$. Solids contamination $<0.1\%$ v/v. Use differential type for drop diameter $>200 \mu\text{m}$; feed concentration 6 to 60% v/v; suited for low surface tension, density differences $>0.05 \text{ Mg}/\text{m}^3$. Solids contamination $<0.1\%$ v/v.

Electrodecanter: drop diameter 9 to 500 μm ; feed concentration 0.8 to 8% v/v.

Fibrous bed coalescer: drop diameter 3 to 75 μm ; feed concentration $<3\%$ v/v. See size enlargement, Section 16.11.9.2.

API separator: drop diameter $>75 \mu\text{m}$; feed concentration 0.015 to 3% v/v.

Dissolved air flotation: drop diameter $>8 \mu\text{m}$ with feed concentration 0.005 to 0.015% v/v and drop diameter $<8 \mu\text{m}$; feed concentration 0.0075 to 0.1% v/v. See Section 16.11.5.15.

aid is 8- to 20- μm diameter to give a precoat bed of permeability 0.05 to 0.5 μm^2 ; a *medium* filter aid is 30- to 60- μm diameter to give a precoat bed of permeability 1 to 2 μm^2 ; a *coarse* filter aid is 70- to 100- μm dia. to give a precoat bed of permeability 4 to 5 μm^2 . For particle diameter less 1 μm , consider size increase via coagulation/flocculation, Section 16.11.9.3. An example coagulant is starch.

Effect of Recovery on the Choice

To recover liquid: in the order of preference of filters, Section 16.11.5.13, and filtering centrifuges, Section 16.11.5.12: deep bed, horizontal vacuum, pressure leaf, gravity flat table; cartridge, precoat drum, and plate and frame, or vertical basket filtering centrifuge. For high fluid viscosity, use plate and frame or horizontal filtering cone centrifuge.

To recover liquid: in order of preference of settlers, Section 16.11.5.7, thickeners, Section 16.11.5.9, and sedimentation centrifuges, Section 16.11.5.11: clarifier, settler, washing tray thickener, reactor-clarifier, hydrocyclone, batch tubular bowl centrifuge, batch automatic (horizontal or vertical bowl, disc with intermittent nozzle discharge); continuous disc bowl centrifuge with nozzle discharge.

To recover liquid and solids: in order of preference of filters: expellers and presses, Section 16.11.5.16.

To recover liquid and solids: in order of preference of settlers, Section 16.11.5.7, CCD, Section 16.11.5.10, and sedimentation centrifuges, Section 16.11.5.11: continuous countercurrent decanter circuit CCD, horizontal solid bowl centrifuge with scroll discharge.

To recover solids: in order of preference of filters: requiring good washing: pressure, vacuum, gravity table/pan, horizontal pressure or vacuum, horizontal belt, vacuum drum, cylindrical screen scroll discharge filtering centrifuge, and plate and frame. Requiring good washing and the crystals break easily: gravity, vacuum table/pan; vacuum, pressure, gravity drum, and plate and frame. If the cake is compressible, use low pressure, <200 kPa, or vacuum rotary drum. For dry solids: consider the following filtering centrifuges, Section 16.11.5.12: basket, basket automatic constant speed vertical, basket automatic variable speed horizontal; continuous conical with scroll conveyor, oscillating conical screen; cylindrical screen with pusher conveyor, or horizontal solid-screen scroll conveyor. To recover solids: in order of preference of thickeners, Section 16.11.5.9, and sedimentation centrifuges, Section 16.11.5.11: thickeners, deep thickener, rake thickener, and tray thickener or hydrocyclone, batch automatic solid bowl centrifuge, continuous conical bowl centrifuge, continuous contour bowl vertical or horizontal centrifuge.

16.11.5.5 Dryer

Use when the goal is solid recovery. Related topics are screens (Section 16.11.5.6), centrifugal filters (Section 16.11.5.12), and dewatering expellers (Section 16.11.5.16).

Area of Application

Particle diameter 20 μm to 1 cm; feed solid concentration >50% solids. Liquid contamination in exit solids 0 to 20% v/v liquid. Use batch for <40 g/s; use continuous for >280 g/s. Select initially on temperature sensitivity. Prefer "adiabatic" over conduction.

Indirect conduction options: (nonadiabatic) for temperature-sensitive solids ($T < 40^\circ\text{C}$).

Batch:

Pan/tray/shelf, jacketed, atmosphere, or vacuum (conduction): batch, feed: thin or thick liquids, soft or stiff pastes, moist crumb, grains (>150 μm) and grits (<150 μm). Product: solid cake. *Pan, agitated*, atmosphere or vacuum (conduction): batch, feed: thin or thick liquids, soft or stiff pastes, moist crumb, grains (>150 μm), and grits (<150 μm). Product:

Convection with hot gas through the bed: evaporative capacity 1.2 to 0.25 g water/s-m² as moisture goes from 0.9 to 0.025 kg/kg dry solids.

Convection plus radiation: evaporative capacity 0.8 to 0.15 g water/s-m² as moisture goes from 0.9 to 0.025 kg/kg dry solids.

Indirect conduction options:

Batch: size on cycle time: load, dry, discharge, clean.

Pan/tray/shelf, jacketed, batch (conduction): evaporative capacity 0.13 to 0.27 g water/s-m² tray area for crystals, 0.07 to 0.14 g water/s-m² tray area for finely divided solids; loading 10 to 35 kg wet paste/m² tray area; pressure 7 to 27 kPa. *Pan, agitated, batch, atmosphere* (conduction): area 1.5 to 15 m²; evaporative capacity 1 to 12 g water evaporated/s-m²; power 4 kW/m³. Heat transfer coefficient 10 to 50 W/m² °C; solids capacity 2.8 to 4.2 g dry solids/s-m³. *Pan, agitated, batch, vacuum* (conduction): evaporative capacity 1.35 to 6.8 g/s-m²; time 7.5 to 35 h. *Tray/pan/shelf* (conduction, vacuum): area 1 to 20 m²; evaporative capacity 0.27 to 7.7 g/s-m²; time 4 to 48 h. Heat transfer coefficient $U = 0.002$ to 0.5 kW/m²-K. *Rotary indirect, batch, vacuum* (conduction): area 2 to 35 m²; evaporative capacity 0.3 to 5 g water evaporated/s-m² with values increasing as initial feed moisture content increases; 0.7 to 5 g organic evaporated/s-m². Power 0.5 kW/m² area. *Cone/double cone, jacketed, batch, vacuum* (conduction): area 1 to 10 m²; evaporative capacity 2.7 to 5.4 g water evaporated/s-m² of actual surface area. Power 0.5 kW/m² area. Freeze, batch, vacuum (conduction) drying temperature serum, -9 to -12°C; plasma, -20 to -25°C; penicillin -28 to -32°C; size vacuum pump to remove the water vapor; avoid air leaks. Pressure 10 to 200 Pa or 1/4 to 1/2 the vapor pressure at the temperature; 7 to 8 h drying cycle.

Continuous:

Drum dryer, atmosphere (conduction): area 2 to 50 m²; evaporative capacity 7 to 11 g water/s-m²; residence time: 6 to 15 s; solids capacity 5 to 50 kg/m²; heat transfer coefficient 0.001 to 0.002 kW/m² °C; 1 to 10 rpm; 1 to 2.5 kW/m². 1 to 10 rpm; drive power 1 to 2.5 kW/m² drum surface area. Related topic is flakers, Section 16.11.9.15. *Fourdrinier machine* for paper: 37 cylinders, 1.5-m dia.; velocity of paper = 4 to 5 m/s; residence time 31 s; heat transfer coefficient $U = 0.34$ kW/m² °C. Water/solid = 0.4; 2.8 g water evaporated/s-m². *Screw, jacketed, atmosphere* (conduction): 2 to 30 rpm; area 4 to 60 m², volume 0.1 to 3 m³, 0.03 to 0.5 kg water evaporated/s. Heat transfer coefficient 4 to 60 W/m² °C with 4 to 10 for hollow screw and 5 to 35 for hollow paddles; power 140 MJ/Mg. *Continuous band, vacuum*; (conduction): 2.2 kg steam/kg water evaporated; solid capacity 2 to 5 g dry solids/s-m² belt area; belt size <8 m². *Continuous band, atmospheric* (conduction): evaporative capacity 0.8 g water/s-m²; dry solids output 2 g solid/s-m²; area 56 m². Freeze, continuous tray: 50-mm thick bed; vacuum 13 Pa absolute; heat transfer coefficient, $U = 0.01$ to 0.02 kW/m² °C; relatively independent of stirring speed but dependent on residence time. Residence time 10 to 200 s. *Dielectric*: 315°C.

Indirect convection options: for moderately temperature sensitive, sensitive, and very sensitive solids ($5 < T < 40^\circ\text{C}$).

Batch: size on cycle time: load, dry, discharge, clean.

Tray/shelf (indirect convection) crossflow: 0.05 to 0.2 g water evaporated/s-m² tray area; residence time 4 to 48 h; 1.5 to 5 m/s gas flow; steam 1.8 to 2 kg steam/kg water evaporated; power 8 to 15 kJ/kg; air temp. 50 to 110°C. solids capacity <6 g/s. *Open sand bed:* (natural convection) 1000 to 100,000 m² including piping, sand/gravel beds, and underground collection.

20°C higher than the exit solid temperature; heat transfer coefficient 0.1 W/kg solids °C for coarse materials and 0.4 W/kg °C for fine. $NTU = 0.5$ for vegetables. $NHTU$ (for air water) = 1.0 to $3.5 = \ln(T_{hot\ gas\ in} - T_{wet\ bulb}) / (T_{hot\ gas\ out} - T_{wet\ bulb})$. Drive power 0.075 to 0.16 kW/m² nominal circumferential area; area in the range 200 to 2500 m². Related topics are kilns (Section 16.11.3.7) and reactors (Section 16.11.6.20). *Open bed*: residence time: minutes; gas through bed 0.5 to 1 m/s.

16.11.5.6 Screens for "Dewatering"

See also Section 16.11.5.29, screens for solid-solid separation. Related topics are filters (Section 16.11.5.13), centrifugal filters (Section 16.11.5.12), and expellers (Section 16.11.5.16).

Area of Application

In general, particle diameter >1000 µm and solid concentration >3%. Special types include micro-screens for >20 µm.

Batch:

Deep bed or granular: batch, for 0.01 to 50 µm (see filter, Section 16.11.5.13). *Fixed bar screen*: batch, grizzly (the filter cloth is made of rods and bars) removal of very coarse material of diameter >2 to 5 cm; low concentration of solids <15 mg/L; bars at 30 to 60° to the horizontal that can be cleaned manually or automatically. *Microscreen* (rotary drum or disk). Batch, removal of particulates of diameter >20 µm; 20 mg/L solids feed concentration.

Continuous:

Fixed, inclined wedge wire screen (sieve bends, DSM): removal of particles >0.15 cm. Variable inclination from 65 to 45° to the horizontal; feed concentration 200 mg/L. For dewatering minerals, dewatering particles of diameter >40 µm. *Vibrating screens*: typical exit liquid concentration for <8-mm particle size, 20 to 45 vol% liquid; for >40-mm particle size, 2 to 10% v/v liquid. *Belt, gravity*: see Section 16.11.5.13.

Guidelines

Batch: consider cycle time: load, clean.

Bar screen: batch: fluid velocity through the screen 0.6 to 1.2 m/s; head loss 15 to max. 75 cm. Mechanical clean. *Rotating microscreen*: batch, fluid loading 3 to 6 L/s·m² of submerged area; usually 66% area submerged; solids loading 0.05 to 0.1 g/s·m²; head loss 7 to 14 cm to max. of 45 cm. Clean by backwash at 2 to 5% volumetric throughput capacity.

Continuous:

Fixed, inclined wedge wire screen, sieve bend: fluid loading 6.7 to 20 L/s·m²; or 10 to 40 L/s·m of width; solids loading 1.4 to 4.2 g/s·m²; exit solids concentration 12 to 15% w/w solids. For dewatering minerals, fluid capacity of 0.0015 to 0.03 L/s·m² with larger fluid capacity for larger size particles (1 to 2 mm) and smaller than the included angle of the bend. The bend in the screen is such that the oversized are continually sluiced off. *Vibrating screens*: see Section 16.11.5.29.

16.11.5.7 Settlers

Area of Application

Particle diameter <2 cm; solids concentration 0.2 to 50%.

Guidelines

Wash ratio 2 to 2.2 water to 1 solid. Wash ratio and the number of stages are selected for expected recovery.

16.11.5.11 Sedimentation Centrifuges

Primarily to recover liquid, although it can be used to recover solids. Incomplete separation.

Area of Application

Liquid contamination in the exit solids: 10 to 15% v/v liquid.

Batch:

Tubular bowl: batch, very fine particles with settling velocities 5×10^{-8} to 5×10^{-7} m/s; particle diameter 0.1 to 500 μm , feed concentrations 0.1 to 20% v/v; <5% w/w. Clarify low concentrations. *Vertical solid basket:* batch, particle diameter >30 μm ; feed solids concentration 3 to 5% w/w to prevent frequent cleaning. *Multichamber vertical solid basket, manual batch discharge:* particle settling velocity 2×10^{-6} to 7×10^{-5} m/s; particle diameter 1 to 50 μm ; feed solids concentration <4 to 5% v/v. Very dry product and higher capacity. *High-speed disc vertical solids retaining:* batch, particle settling velocity 8×10^{-8} to 2×10^{-7} m/s; particle diameter <1 μm ; feed concentration solids <1% w/w; <20% v/v.

Continuous:

High-speed disc, intermittent solids ejecting: particle diameter 1 to 500 μm ; feed concentration solids 2 to 6% v/v and <5% w/w. *High-speed disc, continuous nozzle discharge:* particle diameter 0.1 to 500 μm ; feed concentration solids 5 to 30% v/v; <10% w/w. Usually select when have a large amount of fines. *Horizontal scroll discharge:* (solid bowl decanter) 10^{-6} to 5×10^{-6} m/s; particle diameter 2 to 5,000 μm ; feed solids concentration 0.5 to 50% v/v. Usually >10% v/v. Only option when feed concentration >40% v/v solids.

Guidelines

Scaled up based on liquid handling capacity.

Batch: size on cycle time: separate, remove solids, clean.

Tubular bowl: batch, up to 50,000 rpm; 3×10^3 to 6×10^4 g; L/D 4 to 8; liquid flow rates 0.03 L/s at high rpm, 0.1 to 10 L/s at lower rpm. Clarify low concentrations. *Vertical solid basket:* batch, 450 to 3500 rpm, 900 to 1100 g; L/D = 0.8; 1.6 to 2.8 L/s; 70- to 120-cm diameter bowl; 200 to 500 g/s·m²; area 0.5 to 3 m²; 3 to 17 kW. *Multichamber vertical solid basket, batch discharge:* 4500 to 8500 rpm; 3×10^3 to 3×10^4 g; 0.7 to 2.8 L/s; 30- to 60-cm dia. bowl. *High-speed disc vertical solid basket:* <12,000 rpm; 3×10^3 to 3×10^4 g; L/D = 1; <28 L/s; 15- to 100-cm bowl diameter; cone 35 to 50°. Solids retaining: 5 to 20 L/s;

Σ , m ²	Bowl dia., cm
1000	10
10,000	20 to 30
100,000	60 to 90

Continuous:

Horizontal scroll discharge: 1600 to 6000 rpm; 1500 to 5000 g; L/D 1.5 to 3.5; 0.1 to 16 L/s;

discharge: particle diameter <6 mm; feed solids concentration 40 to 80% w/w. capacity 7 to 40 kg/s.

Guidelines

Batch: size on cycle times: accelerate to load speed, load and cake formation, accelerate to wash, wash, accelerate to full speed, spin dry, decelerate to unload speed, unload. Cake volume in the centrifuge is key. During load and cake formation, the particles migrate to the periphery to form a cake, the supernatant liquid moves through the bed to the cake surface, and then the liquid drains out of the interstices in the wet cake. The latter two times usually control. *Vertical basket*: batch with cycle: cake formation, wash, discharge, clean. Total cycle >10 min, e.g., 180 min. Cake buildup rate 200 to 1000 g/s·m²; area per unit: 2.8 m²; cake volume 0.009 to 0.5 m³; cake thickness 25 to 150 mm with smaller thickness in smaller diameter centrifuges. 600 to 2100 rpm; 300 to 800 G. Basket diameter 0.3 to 1.5 m; L/D = 0.5 to 0.6/1. Power 3 to 6 kW/m² filter area. Temperature <175°C. *Vertical basket, bottom discharge*: batch with cycles: accelerate to load speed, load and cake formation, accelerate to wash, wash, accelerate to full speed, spin dry, decelerate to unload speed, unload: 3 to 120 s. Cycle time for free draining 2 to 6 min; slower draining materials cycle time 20 to 30 min with some >60 min, area per unit 0.4 to 4.5 m²; cake volume 0.018 to 0.53 m³; about 67% of feed volume; cake thickness 50 to 150 mm with smaller thickness in smaller diameter centrifuges. 900 to 1800 rpm. Basket diameter 1 to 1.2 m; L/D = 0.5. *Horizontal basket, plough discharge*: batch with cycles: load 7 to 25 s; wash 5 to 25 s, spin dry 12 to 30s, unload cake 3 to 12 s; total cycle time 20 s to 15 min but usually <3 min. Cake buildup rate 500 to 3000 g/s·m²; area per unit 0.1 to 3.8 m²; cake volume 0.03 to 0.17 m³. Bowl dia. 0.3 to 1.2 m. 1000 to 2500 rpm; <1250 G. Power 25 to 40 kW/m² filter area.

Semibatch: particles move through the cycle continually. *Horizontal basket, pusher discharge*: 20 to 120 cycles/min: cake formation, wash, discharge. Cake buildup rate 1000 to 10,000 g/s·m²; area per unit: 1.4 m²; cake thickness <75 mm. Basket diameter 0.2 to 1.2 m; 300 to 600 G. Power 40 to 60 kW/m² filter area or 7 to 15 kJ/kg "salt" (about 3000 g/s·m²). Keep feed solids concentration >40% w/w for optimum. Example data: adipic acid, urea 1.4 kg/s·m²; crude sodium bicarbonate 1.45 kg/s·m²; phosphate rock 2.2 kg/s·m²; ammonium sulfate 2.36 kg/s·m²; and sodium chloride 3.1 kg/s·m²;

Continuous: *horizontal combo solid-screen, scroll discharge*: area per unit, 1.2 m²; power 12 to 15 kW/m² filter area. *Vertical or horizontal cone*: slip discharge: cake buildup rate 3000 to 20,000 g/s·m²; area per unit 4 m²; cone angle 20 to 35° and greater than angle of repose of the solids. 2500 G. rinsing efficiency: fair. *Vertical cone, scroll discharge*: diameter 0.5 to 1 m. 2500 to 3800 rpm; 1800 to 2500 G. Product solids 24%. *Horizontal cone oscillating/torsional vibration discharge*: cone angle 13 to 18°; cycles >20 cycles/min. 300 to 500 rpm; <500 G. Diameter 0.5 to 1 m; L/D = 0.5 to 1/1. Product 92% solids. Limited liquid handling capacity. Power 0.2 kW/Mg solids.

16.11.5.13 Filter

Table 16.35 relates filtration rate to process operation.

For *incompressible* cakes, the filtration rate is directly proportional to the specific cake resistance and the pressure/vacuum, and inversely proportional to the viscosity and cake thickness. The filtration rate is inversely proportional to the ratio of solids to filtrate, while the rate of cake formation is directly related to this ratio. For *compressible* cakes, the filtration rate is relatively independent of pressure. The more flocculated the solids, the more compressible will be the filter cake.

TABLE 16.36
Particle Diameter and Cake Permeability and Resistance

Particle Diameter, μm	Permeability $(\mu\text{m})^2$	Intrinsic Permeability, $\text{m}^4/\text{N}\cdot\text{s}$	Cake Resistance, m/kg
1	10^{-3} –0.1 depending on ϵ	10^{-13} – 10^{-10} depending on ϵ and liquid viscosity	10^{12}
10	0.1–10 depending on ϵ	10^{-12} – 10^{-8} depending on ϵ and liquid viscosity	10^{10}
100	10–1000 depending on ϵ	10^{-10} – 10^{-6} depending on ϵ and liquid viscosity	10^8
1 mm	1000– 10^5 depending on ϵ	2×10^{-8} – 10^{-4} depending on ϵ and liquid viscosity	10^6
10 mm	10^5 – 10^7 depending on ϵ		$<10^6$

Continuous: drum, gravity: particle diameter 40 to 5,000 μm ; feed solid concentration 0.08 to 0.8% w/w. Recover wet solid with good washing and fragile crystals (rank 2). *Drum, pressure:* particle diameter 5 to 200 μm ; feed solid concentration 0.75 to 5% w/w. Recover wet solid with good washing and fragile crystals (rank 2). *Drum, rotary vacuum:* particle diameter 1 to 700 μm ; feed solid concentration 5 to 60% w/w. Recover wet solid with good washing (rank 4). Recover wet solid with good washing and relatively compressible cake (rank 1). Recover wet solid with good washing and fragile crystals (rank 2). Dry solids capacity <50 kg/s. *Drum, precoat rotary vacuum:* particle diameter 0.5 to 80 μm ; feed solid concentration 0.02 to 0.1% w/w. Recover liquid (rank 4). *Disk, rotary vacuum:* particle diameter 15 to 500 μm ; feed fraction solids 0.02 to 0.70. Free flowing. *Table/pan gravity:* recover liquid (rank 1). Recover wet solid with good washing (rank 1). Recover wet solid with good washing and fragile crystals (rank 1). Particle diameter 40 to 50 μm ; feed fraction solids 0.02 to 0.20. Dry solids capacity 280 kg/s. *Table/pan vacuum:* particle diameter 40 to 50 μm ; feed fraction solids 0.02 to 0.20. dry solids capacity: 280 kg/s. *Belt, gravity:* recover wet solid with good washing (rank 3). Liquid contamination in exit solids 20 to 30% v/v liquid. *Belt, vacuum:* particle diameter 20 to 70 μm ; feed fraction solids 0.05 to 0.6. Dry solids capacity <30 kg/s. *Belt press:* dewater and handle flocculated solids. Rotary press: dewater and handle flocculated solids. Particle size 1 to 50 μm . Feed solids 0.1 to 25% w/w. Related to extruders, Section 16.11.7.7. *Ultrafiltration:* see Section 16.11.4.22. Particle diameter 0.4 to 200 nm; feed solids concentration <20% w/w. *Microfiltration:* see Section 16.11.4.23. Particle diameter 0.05 to 800 μm ; feed solids concentration <75% w/w. *Dissolved air flotation, DAF:* see Section 16.11.5.15. Particle diameter 0.1 to 50 μm with typical target diameter 2 μm ; feed solid concentration 0.002 to 0.08% w/w; >80% removal efficiency.

Guidelines

General porosity of cake over the usual range of pressure difference for filtration:

0.9: silica, polystyrene; 0.8 to 0.85: talc, zinc sulfide; 0.7: calcium carbonate; 0.6 titanium dioxide, ignition plug; 0.5 kaolin; 0.42 iron carbonyl.

Table 16.36 relates particle diameter to parameters important in filtration.

Batch:

Usually size unit on cycle and based on volume of cake removed. Select required cake volume in batch unit. Two thirds of the cake forms in 1/3 of filtration time: consolidation of the last 1/3 of the cake during the last 2/3 of the filtration time. Typically filtration cycle stops when the filtrate flux is <0.01 L/s·m². Cycle: filter, drain, 3 min, fill with wash, 2 min; wash to with volume = five times the cake void volume; air blow; unload, 6 min. *Leaf, pressure vertical:* cycle (for wet cake): filter 2 to 80 h; open, dump, close 0.4 to 4 h; cake volume/unit 0.1 to 2 m³ corresponding to 5 to 90 m² filter area; leaves on 75 mm spacing. Δp 250 to 400 kPa. Cake buildup flux: 0.001 kg/s·m².

speed 0.04 to 0.15 m/s. For feed concentrations $<5\%$, usually liquid dewatering controls: liquid load 2.5 to 3.5 L/s-m of belt width. For feed concentrations $>5\%$ solids throughput limiting: 0.15 to 0.275 kg/s-m of belt width. $\Delta p < 80$ kPa. *Rotary press*: <3 rpm; dewatering area: 1.25 to 5 m². Solids flux 0.003 to 0.127 kg/s-m², depending on the feed solids concentration in range 0.1 to 6% solids. Product 20 to 75% solids. See also Section 16.11.7.7. *Ultrafiltration*: see Section 16.11.4.22. *Microfiltration*: see Section 16.11.4. *Dissolved air flotation (DAF)*: see Section 16.11.5.15.

16.11.5.14 Leacher

Area of Application

Percolation leach: particle diameter >700 μm ; liquid concentration 0.8 to 20%; relatively fragile solid (e.g., seeds). *Immersion leach*: particle diameter <700 μm ; liquid concentration $<20\%$; relatively robust solids (e.g., minerals). *Combo leach*: high feed concentration of solute, relatively robust solid. *Supercritical solvent*: usually CO₂ for small capacity of high value products, especially for temperature sensitive foods, cosmetics, and pharmaceuticals.

Guidelines

Percolation leach: high solute leach rate; solvent percolation through the bed >3 mm/s; 3 to 10 L/s-m²; bed permeability >200 μm^2 ; low feed concentration of solute; 0.5 to 0.7 kg liquid solvent carryover from stage to stage/kg inert solid; solute diffusivities of essential oils 10^{-7} to 10^{-14} cm²/s; of sugar in sugar beets 10^{-5} cm²/s. Tend to use series of counter-current contactors with time for diffusion and separation in each stage. *Rotating cells/baskets*: capacity: 30 kg/s flaked soybeans in 10-m diameter unit; prepressed cottonseed $\times 0.66$; unpressed cottonseed $\times 0.33$; sugar cane $\times 0.33$; canola $\times 0.33$. *Buckets*: 10 kg/s flaked soybeans with 40 buckets. *Belt*: 10 kg/s flaked soybeans with belt 20 m long; 2 to 5 kg solvent makeup/Mg oil seed feed. *Drag chain*: 10 kg/s flaked soybeans with belt 20 m long.

Immersion leach: low solute leach rate. Product of residence time \times concentration of leachant for acid leach = constant for a given particles diameter. Tends to have a separate leacher followed by system to separate and wash solids. *Pachuca*: plus CCD, settler; particle diameter <70 μm ; solids 30 to 60% w/w; agitator 0.07 to 0.2 kW/m³; for CCD 1.5 to 2 kg liquid solvent carryover/kg inert solid. *Autoclaves*: plus CCD; particle diameter <70 μm ; solids 30 to 60% w/w; 0.7 to 1.3 kW/m³.

Combo leach: tend to use countercurrent contactors with time for diffusion and separation in each stage. *Sloped diffuser with rotating screw*: 10 kg/s sugar beets in 2 m diameter.

Tower with rotating screw: 10 kg/s sugar beets in 0.3-m diameter unit. *Trough-scroll*:

10 kg/s sugar beets in three troughs. *Rotary diffuser*: 10 kg/s sugar beets in 5-m dia. unit.

Supercritical solvents: batch process operating at $T > 31^\circ\text{C}$ and pressures >7.3 MPa. Solvency is intermediate between nonpolar and weakly polar solvents. Contact times $0.1 \times$ usual leach times.

16.11.5.15 Liquid-Solid: Dissolved Air Flotation, DAF

Area of Application

Particle diameter 0.1 to 50 μm with typical target diameter 2 μm ; feed solid concentration 0.002 to 0.08% w/w; $>80\%$ removal efficiency.

Guidelines

Bubble size 70 to 90 μm ; air: solids 0.005 to 0.1 kg/kg; liquid loading 0.5 to 2 L/s-m². Liquid residence time 20 to 200 min with a minimum depth of 1.8 m. If feed concentration is <400 mg/L, use about 50% recycle.

16.11.5.19 Electrostatic

Area of Application

For systems with dry particles, no slimes or organic coatings, a narrow range of both density differences and particle sizes, and a difference in conductivity. Particle diameter 40 to 3,000 μm ; usually 80 to 1000 μm ; feed concentration of target species 5 to 75%. Good conductors have relative permittivity >11 ; poor or nonconductors have relative permittivity <10 ; threshold voltage to make species conducting is 1 to 10 kV/cm.

Guidelines

Select voltage where one species conducts and the other does not. *Corona-active electrode rotary drum*: handles wide range of particle diameters from 75 to 1000 μm ; high capacity, <0.75 kg/s-m of drum width; high efficiency 95%; separates good from poor conductors. Zero to 40 kV DC, 0.5 to 1 mA/electrode; insensitive to humidity and temperature; often can recycle the middlings with recycling 10 to 30% OK. *Active electrode rotary drum*: trouble handling fines; capacity <0.5 kg/s-m of drum width, moderate efficiency; separates good from poor conductors or two semiconductors. Zero to 30 kV DC, 0.04 mA/electrode. The voltage gradient must be sufficient to charge target particles, operates best in a controlled environment.

For roughers and scavengers, set the active polarity so that the valuable minerals become conductors. For cleaners and recleaners, set the active polarity so that the gangue and middlings become the conductors. Collect middlings if the valuable target is trapped in the gangue; if the density of the nonconducting is heavier than the conducting and if the feed has a wide range of particle diameters.

16.11.5.20 Magnetic

Area of Application

For systems with a narrow range of both density differences and particle sizes; particle diameter >50 μm ; feed concentration of target species 0.4 to 40%. Magnetization = product of the mass magnetic susceptibility and the magnetic field, T m^3/kg . Ferromagnetic species: magnetization $>10^{-4}$ T m^3/kg . Paramagnetic species: magnetization $10^{-8} < \text{value} < 10^{-5}$ T m^3/kg .

Batch: cycle: load, clean. *Plate*: batch: magnetization $>10^{-4}$ T m^3/kg ; particle diameter >6 mm; feed concentration of magnetic $<0.01\%$ w/w. Primarily to remove tramp ferrous metal. *Grate*: batch: magnetization $>10^{-4}$ T m^3/kg ; particle diameter <1.8 mm; feed concentration of magnetic $<0.01\%$ w/w. Primarily to remove tramp ferrous metal. *WHGMS (wire, Kolm-Marston)*: batch: magnetization $>2 \times 10^{-9}$ T m^3/kg ; particle diameter 1 to 30 μm ; feed concentration of magnetic $<0.05\%$ w/w. Solids concentration in water 20%. *WHGMS (grooves, Jones)*: batch: magnetization $>2 \times 10^{-9}$ T m^3/kg ; particle diameter 200 to 1000 μm ; feed concentration of magnetic $<50\%$ w/w; solids concentration in water $<50\%$.

Continuous: pulley: magnetization $>10^{-4}$ T m^3/kg ; particle diameter >6 mm; feed concentration of magnetic $<0.01\%$ w/w. Primarily to remove tramp ferrous metal. *Belts/cross or inline*: magnetization $>10^{-4}$ T m^3/kg ; particle diameter >6 mm; feed concentration of magnetic 0.01 to 10% w/w. Primarily to remove tramp ferrous metal. *Belts/cross HGMS*: magnetization $>10^{-4}$ T m^3/kg ; particle diameter 150 to 1500 μm ; feed concentration of magnetic 0.5 to 2% w/w. Primarily to remove tramp ferrous metal. *Wet belt*: magnetization $>10^{-4}$ T m^3/kg ; particle diameter 100 to 2500 μm ; feed concentration of magnetic 0.3 to 2% w/w. *Dry drum/LGMS*: magnetization $>2 \times 10^{-5}$ T m^3/kg ; particle diameter 0.1 to 100 mm; feed concentration of magnetic 1.5 to 75% w/w. *Dry drum high-speed/MGMS*: magnetization $>2 \times 10^{-5}$ T m^3/kg ; particle diameter 100 μm to 30 mm; feed concentration of magnetic $<10\%$ w/w. *Dry rotor HGMS (induction)*: magnetization $>4 \times 10^{-8}$ T m^3/kg ; particle diameter 70 to 2000 μm ; feed concentration of magnetic <0.05 w/w. *Wet drum/LGMS*: magnetization $>10^{-4}$ T m^3/kg ; particle diameter 70 μm to 6 mm; feed concentration of magnetic

water. Particle cut diameter 30 to 1000 μm . Particle diameter $>1.5 \mu\text{m}$. Feed concentration of target solid 4 to 60% w/w.

Guidelines

Solids-to-gas ratio 2 to 8 w/w. Solids loading 2 to 4 $\text{kg/s}\cdot\text{m}^2$. *Zigzag*: cut diameter 100 to 10,000 μm ; capacity 0.01 to 0.08 kg/s . *Gas centrifugal separator*: cut diameter $>20 \mu\text{m}$; capacity $<15 \text{ kg/s}$. *Gas cyclone*: cut diameter 10 to 50 μm ; capacity $<15 \text{ kg/s}$. *Gas gravitational inertial classifier (GIC)*: cut diameter 50 to 200 μm ; capacity $<300 \text{ kg/s}$. *Gas Mikroplex spiral*: cut diameter 2 to 20 μm ; capacity 0.01 to 1 kg/s . *Gas Nauta-Kosakawa*: cut diameter 3 to 300 μm ; capacity 0.01 to 1 kg/s . *Gas classifiers for MSW*: cut diameter $>100 \mu\text{m}$ with capacities up to 20 kg/s .

16.11.5.23 Rake Classifiers

Superseded by hydrocyclones (Sections 16.11.5.21 and 16.11.5.8).

16.11.5.24 Spiral Classifiers

Area of Application

Bird number (mass of solids with a ± 0.1 density variation from the cut density) <15 ; particle cut diameter $>50 \mu\text{m}$ but usually 1000 to 20,000 μm .

Guidelines

Two types: cut diameter $>200 \mu\text{m}$, use *high weir configuration*; cut diameter $<200 \mu\text{m}$, use *submerged spiral*. Size based on the target exit overflow concentration and "limiting" particle diameter. Diameter of the limiting particle should have a settling velocity double that of the cut diameter (cut diameter is about 70% of the limiting diameter). Separation efficiency is 50%; that is, use double the cross-section area obtained from the settling velocity of the "limiting" particle diameter. Capacity 2 to 250 kg/s . Underflow solids capacity is a function of the spiral diameter and solids density; independent of the separation. Angle of inclination 16° .

High weir: 1 m^2 pool area produces about 5 kg/s dry solids in the overflow with 400 μm limiting diameter or about 280 μm cut diameter and 30% concentration. *Submerged weir*: 1 m^2 pool area produces about 0.5 kg/s dry solids in the overflow with 150 μm limiting diameter or about 100 μm cut diameter and 16% concentration. For both configurations, increase the area by a factor of 10, increase the amount of overflow solids by 10 with the same cut and limiting diameters and overflow concentrations. Rotational speed increases with the cut diameter.

16.11.5.25 Jig Concentrators

Area of Application

Bird no. (mass of solids with a ± 0.1 density variation from the cut density) <15 ; relative density ratio 2 to 2.5 and particle diameter 2 to 10 mm. Feed concentration 1.5 to 30% w/w.

Guidelines

Loading 1 to 8 $\text{kg/s}\cdot\text{m}^2$ with loading increasing with increase in particle diameter. Power 1 kW/m^2 and water usage 13 $\text{L/s}\cdot\text{m}^2$.

16.11.5.26 Table Concentrators

Area of Application

Bird number (mass of solids with a ± 0.1 density variation from the cut density) <15 ; relative density ratio >2 to 2.5; usual particle diameter 70 to 2000 μm ; only one valuable mineral. *Tilting frames*:

Guidelines

Screen: efficiency 85 to 95%; length/width of screen 2:1 to 1.5:1; rate of travel of solids along the screen face 0.3 to 0.5 m/s. The flux of solids passing through the screen is about: for coarse particle diameters, 2 to 5 kg/s·m²; for intermediate particle diameters, 0.4 to 4 kg/s·m²; for fine particle diameters, 0.08 to 0.4 kg/s·m², with fluxes decreasing as the density decreases.

Trommels: rotational speed should be slow enough that the particles free fall (about 45% of the transition rpm). L/D 2:1 to 5:1; residence time 30 to 60 s with flux rates of 0.03 to 0.1 kg/s·m².

16.11.6 REACTORS AND VESSELS*

Reactors are considered in Sections 16.11.6.1 through 16.11.6.33; vessels are discussed in Sections 16.11.6.34 and 16.11.6.35. For most process equipment, equipment is sized based on the optimization criterion of cost. For reactors, the optimization criterion may be selectivity, yield, flexibility, ability to control, or cost. Section 16.11.6.1 lists the general rules of thumb. Section 16.11.6.2 gives examples of the reactor type based on the type of reaction. Sections 16.11.6.3 onward give rules of thumb organized by reactor type.

Symbols: adiabatic factor = adiabatic temperature change accompanying complete consumption of the reactant without regard to equilibrium considerations; *Bd* = Bodenstein number; **D** = diffusivity; *D* = tube diameter; *D_p* = particle or catalyst diameter; *Eo* = Eotvos number; *GL* = gas-liquid; *GS* = gas-solid; *GLcS* = gas-liquid reaction with solid catalyst; *GrS* = gas reacting with a solid; *H* = height; *Ha* = Hatta number; heat generation potential = reaction activation energy/*RT_{inlet}*²; *L* = length of tubes; *Nu* = Nusselt number; OD = outside diameter; *Pe* = Peclet number; *R* = ideal gas law constant. *RTD* = residence time distribution; *Re* = Reynolds number; *T* = temperature; and β = volume of liquid in the reactor/volume of mass transfer liquid "film" in the reactor.

16.11.6.1 General Rules of Thumb

1. The rate of reaction doubles for a temperature increase of 10°C.
2. Prefer continuous to semicontinuous to batch.
3. Prefer PFTR to CSTR.
4. Prefer minimum inventory in reactor by providing better mixing, increased temperature or pressure, or changing the catalyst.
5. Prefer internally heated/cooled to externally heated/cooled.
6. Consider light and ultrasound as optional forms of energy.
7. For gas reactions, usually use plug flow tubular reactors (PFTRs), static mixers, or fluidized beds.
8. For gas fixed-bed catalytic reactions, use $L/D_p > 100$ and $D_p/D < 0.10$ to ensure good gas distribution and negligible back mixing.
9. For liquid reactions, usually use continuous stirred tank reactors (CSTRs) (unless the pressure is very high), static mixers.
10. Prefer operating temperatures below the boiling temperature or dilute the liquid with a safe solvent.
11. For gas-liquid reactions, usually use CSTR or bubble column.
12. For reactions using solid catalysts: although many of the reactors described below are classed as "continuous," whenever a solid catalyst is used, the performance of the catalyst decays over time. The catalyst needs to be regenerated or replaced periodically. Time

* Reproduced with permission from Donald R. Woods, *Rules of Thumb in Engineering Practice*, pages 196, 225 to 278, 2007, copyright Wiley-VCH Verlag GmbH & Co. KGaA, Weinheim, ISBN: 978-3-527-31220-7. See this book for more details, especially about Good Practice, Trouble shooting and Capital Costs.

Area of Application

Phases: gas, liquid, gas-liquid, liquid-liquid. Use if the order of the reaction is positive and >95% conversion is the target, and for consecutive reactions with an intermediate as the target product. *Gas* (or gas with homogeneous catalyst): residence time: 0.4 to 2000 s; heat of reaction: endothermic; reaction rate, fast; capacity: 0.001 to 200 L/s; good selectivity for: consecutive reactions and irreversible first order; volume of reactor 1 to 10,000 L; OK for high pressures. For temperatures <500°C. *Liquid* (or liquid with homogeneous catalyst): residence time: 0.4 to 2000 s; heat of reaction: endothermic; reaction rate, fast or slow; capacity: 0.001 to 200 L/s; good selectivity for consecutive reactions; volume of reactor 1 to 10,000 L; OK for high pressures. *Gas-liquid*: residence time: short; heat of reaction: primarily for endothermic reactions. Beware of highly exothermic reactions because of inability to control temperature; good selectivity for consecutive reactions in which the product formed can react further. See transfer line, Section 16.11.6.9, or bubble reactors, Section 16.11.6.11. *Liquid-liquid*: see transfer line, Section 16.11.6.9, or bubble reactors, Section 16.11.6.11.

Guidelines

Gas: residence time 0.5 to 1.3 s; gas velocity 3 to 10 m/s; $Re > 10^4$, $L/D > 100$. To eliminate backmixing, $Pe > 100$. *Liquid*: residence time 1 to 6 s; liquid velocity 1 to 2 m/s; $Re > 10^4$, $L/D > 100$. PFTR is smaller and less expensive than CSTR. PFTR is more efficient/volume than CSTR if the reaction order is positive with simple kinetics. For fast reactions, use small-diameter empty tube in turbulent flow. For slow reactions, use large-diameter empty tubes in laminar flow. If reaction is complex and a spread in RTD is harmful, consider adding motionless mixer (Section 16.11.6.10). *Examples*: hydrolysis of corn starch to dextrose; polymerization of styrene; hydrolysis of chlorobenzene to phenol; esterification of lactic acid. *Gas-liquid*: see transfer line, Section 16.11.6.9, or bubble reactors, Section 16.11.6.11. *Liquid-liquid*: see transfer line, Section 16.11.6.9, or bubble reactors, Section 16.11.6.11.

16.11.6.4 PFTR: Fire Tube

For temperatures >500°C, put tubes in furnace. Same area of application, guidelines, and good practice as empty tube, Section 16.11.6.3. Radiant heat flux in furnaces 30 to 80 kW/m². Reformers:

Gas oil: heat flux: 40 to 50 kW/m²; fluid velocity inside tubes 1.5 to 2.5 m/s
 Light oil: heat flux: 25 to 40 kW/m²; fluid velocity inside tubes 1.4 to 2.3 m/s
 Heavy oil: heat flux: 25 to 35 kW/m²; fluid velocity inside tubes 1.7 to 2.1 m/s

Cracking: ethylene as product from

Ethane: heat flux: 23 to 28 kW/m² at exit conditions with double values at inlet
 Propane: heat flux: 14 to 17 kW/m² at exit conditions with double values at inlet
 Butane or naphtha: heat flux: 11 to 15 kW/m² at exit conditions; at inlet the values are twice as large.

See thermal energy: furnaces, Section 16.11.3.2.

16.11.6.5 PFTR: Fixed-Bed Catalyst in Tube or Vessel: Adiabatic

Area of Application

Phases: gas, liquid, gas-liquid. Use if the order of the reaction is positive and >95% conversion is the target, and for consecutive reactions with an intermediate as the target product. *Gas or Liquid with fixed bed of solid catalyst*: residence time: 0.4 to 2000 s; heat of reaction: endothermic;

16.11.6.6 PFTR: Multitube Fixed-Bed Catalyst: Nonadiabatic*Area of Application*

Phase: gas, liquid. Use if the order of the reaction is positive and >95% conversion is the target, and for consecutive reactions with an intermediate as the target product. Exchange heat generated if the product of the adiabatic factor \times heat generation potential >10 .

Guidelines

Shell-and-tube exchanger with reactants and catalyst inside the tubes, 250 to 400 m²/m³. Tube diameter <50 mm. *Gas* with fixed bed of catalyst: use high mass gas velocity to improve heat transfer kg/s·m² > 1.35 . To ensure good gas distribution and negligible backmixing, $Pe > 2$; height/catalyst particle diameter $H/D_p > 100$ and $D_p/D < 0.10$. Gas velocity 3 to 10 m/s; residence time 0.6 to 2 s. Heat transfer coefficient $U = 0.05$ kW/m²·K. For fast reactions, catalyst pore diffusion mass transfer may control if catalyst diameter is >1.5 mm. *Liquids* with fixed bed of catalyst: to minimize backmixing, $Pe > 1$; use $L/D_p > 200$ and $D_p/D < 0.10$. Liquid velocity 1 to 2 m/s; residence time 2 to 6 s. Heat transfer coefficient $U = 0.5$ kW/m²·K.

16.11.6.7 PFTR: Multibed Adiabatic with Interbed Quench*Area of Application*

Phase: gas. For fast reactions that are strongly exothermic or endothermic. Use if the order of the reaction is positive and >95% conversion is the target, and for consecutive reactions with an intermediate as the target product.

Guidelines

Limit the height of the bed to keep temperature increase $<50^\circ\text{C}$ to minimize effects of radial temperature gradients. Bed can be shallow and wide. Quench can include injection of cold reactants, internal or external heat exchangers.

16.11.6.8 PFTR: Fixed Bed with Radial Flow

For fast reactions, strongly exothermic or endothermic reactions. Phases: gas with solid catalyst. Use to minimize pressure drop limitations.

16.11.6.9 PFTR: Transported or Slurry, Transfer Line

A related option is fluidized reactor (Section 16.11.6.27).

Area of Application

Phases: gas-solid, gas-solid reactant, gas-liquid, liquid-solid, gas-liquid-solid. *Gas plus catalytic solid*: gas residence time in milliseconds. Reaction rates very fast and very rapid deactivation of catalyst. Solid particle diameter 0.007 to 1.5 mm. *Gas plus solid reactant*: solid residence time, 0.8 to 300 s; gas residence time, <1 s; solid particle diameter 0.007 to 1.5 mm. *Gas-liquid*: see size reduction, Section 16.11.8.1. *Gas liquid plus solid catalyst*: for fast hydrogenation reactions. Compared with trickle bed, Section 16.11.6.15, or PFTR fixed bed with upflow, Section 16.11.6.5. (1) Catalyst particles are small, so less chance of diffusional resistance to mass transfer. (2) Better control of temperature (because of better heat transfer efficiency and high heat capacity of slurries), attractive for exothermic reactions. (3) No need to shut down for catalyst replacement or reactivation. (4) Partial wetting and need to maintain a coating film of liquid (as needed in the trickle bed) are not issues. (5) The space time yield is usually better in slurry reactors (under comparable conditions).

of liquid phase: 120 to 700 m²/m³ liquid phase. Volumetric ratio liquid to mass transfer liquid film, $\beta > 100$. Fast reaction systems, consider mass transfer: film diffusion. Power: cocurrent: 0.03 to 2 kW/m³; countercurrent: 0.04 to 1 kW/m³. See size reduction, Section 16.11.8.1. *Gas-liquid catalytic solid*: catalyst diameter, <0.1 mm. Operate semibatch. Holdup: volume fraction liquid 0.8 to 0.9; volume fraction catalyst 0.01; volume fraction gas 0.1 to 0.2. Gas holdup slightly less than for GL systems. Backmixing: solids backmixing $Pe = 2$ to 5 for superficial gas velocities of 2 to 7 cm/s; Liquid-phase backmixing about the same as gas-liquid systems; gas-phase backmixing, about the same as gas-liquid systems. Surface area: surface area solid 500 m²/m³; surface area gas-liquid 100 to 400 m²/m³; power 0.1 to 2 kW/m³ sufficient to keep catalyst in suspension. Heat transfer solid wall to mixture >1 kW/m²·K; presence of solids increases the heat transfer coefficient. Catalyst activity: variable but often able to avoid diffusion limitations because of small-diameter catalyst. Catalyst selectivity: OK. Catalyst stability: change catalyst between batches, heat exchange OK. Consider complications because of catalyst deposition and erosion. *Liquid-liquid*: superficial dispersed drop velocity 0.001 to 0.02 m/s with usual values 5.5 L/s·m². Smallest reactor volume. For example, for esterification: reactor volume divided by the daily production, m³·day/kg.

PFTR	0.7
3 CSTR in series	0.85
Batch STR	1.04
CSTR	1.22

RDC: sum of the superficial velocities for both phases is 1 to 2.5 cm/s; dia. <9 m for SX but usually <2.5 m for reactions. A related topic is SX (Section 16.11.4.10).

16.11.6.12 PFTR: Spray Reactor and Jet Nozzle Reactor

Area of Application

Phases: gas-liquid, liquid-liquid. *Gas-liquid*: residence time, very short. Reaction rates, very fast; need rapid absorption. Very high gas capacity. Used for neutralization reactions with one of the reactants in the gas phase. For surface area see size reduction, Section 16.11.8.2. *Gravity spray*: surface area 30 to 70 m²/m³; target species Henry's law constant 10³ to 10⁴ kPa/mol fraction; feed gas concentration 0.3 to 4 vol%. *Venturi jet nozzle*: surface area: 200 to 2500 m²/m³; very soluble gas only with target species Henry's law constant <10³ kPa/mol fraction; feed gas concentration >1 vol%. *Liquid-liquid*: surface area: 7 to 75 m²/m³. Related topics are solvent extraction (Section 16.11.4.10) and size reduction (Section 16.11.8.3).

Guidelines

Gravity spray towers: superficial velocity about 5.5 L/s·m²; mass transfer coefficients liquid phase: $1.5 \times 10^{-4} < k_L < 3 \times 10^{-4}$ m/s; for the gas phase $0.4 < k_G < 1$ mol/m²·atmos·s, or in other units, $0.01 < k_G RT < 0.25$ m/s; critical energy-consuming phase is the liquid; gas energy 8 kJ/m³; with liquid-to-gas ratio high; design on gas-phase controlling. Superficial gas velocity 1 m/s. Power usage 0.03 to 0.5 kW·s/m³. Δp gas = 0.6 to 1.2 kPa. Related topics are gas-solid separation (Section 16.11.5.2) and size reduction (Section 16.11.8.2). *Gas-liquid venturi*: Δp gas = 5 kPa, velocity in the throat 30 to 100 m/s and usually 100 m/s; mass transfer coefficient for liquid phase $k_L = 7 \times 10^{-4}$ m/s; for gas phase, $k_G = 10^{-2}$ to 3×10^{-2} m/s; gas-liquid surface area 150 to 300 m²/m³. For fluids with surface tension 40 to 70 mN/m and viscosity of liquid = 1 mPa·s; critical energy-consuming phase is the gas at about 20 kJ/m³ with liquid-to-gas ratio about 1.3 to 1.6 L/m³; design on gas-phase controlling. Power usage 0.04 to 8 kW·s/m³. Δp gas = 1.2 to 6 kPa. Related topics are gas-solid separation (Section 16.11.5.2) and size reduction (Section 16.11.8.2). *Liquid-liquid*: superficial velocity = 50% flooding.

because of flooding. Other recommended packings include Pall rings, mini-rings, Sulzer, Multinit, and tellerettes. *Liquid-liquid*: Superficial velocity of continuous phase = 30 to 50% of flooding. Backmixing less than in spray column or tray columns. The walls and packing must be preferentially wetted by the continuous phase. Packing size = 0.5 to 1 cm. Superficial velocities 0.001 to 0.02 m/s. Prefer diameter <0.6 m; superficial velocity about 5.5 L/s-m²; 2.5 cm Pall rings. Redistribute the dispersed phase every 1.5 to 2 m. *Gas-liquid bio solid*: gravity: trickling filter reactor: gas holdup 0.46 to 0.94; (carbon oxidation): *standard rate*: liquid superficial velocity 0.01 to 0.04 L/s-m², depth 1.8 to 3 m; recycle ratio 0; *high rate*: liquid superficial velocity 0.1 to 0.4 L/s-m², depth 0.9 to 2.4 m; recycle ratio 1/1 to 4/1; (carbon oxidation/nitrification combo): liquid superficial velocity = 0.095 to 0.18 L/s-m². Six-meter depth, recirculation ratio 1:1; (nitrification): liquid superficial velocity = 0.3 to 1.3 L/s-m². Biofilter reactor: media depth 1.5 to 6.5 m, usually 4 m; liquid recycle ratio 0.4; liquid loading: 2.3 L/s-m².

Rotating: RBC: (carbon oxidation) liquid residence time <1 h; 3 to 3.6 m dia.; 40% submerged; 1 to 2 rpm; bio layer 2 to 4 mm thick. Liquid loading 0.0005 to 0.004 L/s-m²; temperature >13°C; Module 10,000 m²; power = 3.5 kW; (nitrification): liquid loading 0.0004 to 0.0025 L/s-m². Temperature >13°C.

16.11.6.15 PFTR: Trickle Bed

Gas and liquid flow cocurrently down through a packed bed of catalyst. Porosity 0.38 to 0.42. (Contrast with packing described in Section 16.11.6.14.)

Area of Application

Phases: gas-liquid catalytic solid. Gas-liquid catalytic solid: use for very fast reactions; all reaction is in the liquid film and is mass transfer-controlled.

Guidelines

Gas-liquid with solid catalyst: catalyst particle diameter 1 to 5 mm. Operate close to the boundary between two-phase (trickle) and pulse flow. Superficial liquid velocity $0.005 < v_{Lo} < 9$ mm/s (although some operate in the range 0.8 to 25 L/s-m² or mm/s). The velocity should be reduced if liquid tends to foam. Superficial gas velocity is >0.010 m/s. Holdup volume fraction liquid 0.05 to 0.25. Static liquid holdup is constant for low Eotvos number, $Eo < 4$ (Eo = density liquid \times gravitational constant \times particle diameter squared/liquid-gas surface tension). Liquid holdup increases with Eo for $Eo > 4$. Dynamic liquid holdup increases with liquid flow rate but is independent of gas flow rate. The liquid axial backmixing is negligible if the height/particle diameter is >150. Holdup volume fraction catalyst 0.6 to 0.7. Holdup volume fraction gas 0.2 to 0.35. Surface area solid 1000 to 2000 m²/m³. Surface area gas-liquid 100 to 3500 m²/m³. Power input 1 to 100 kW/m³. Catalyst activity: variable but often reduced because of mass transfer limitation. Plug flow is favorable. Catalyst selectivity: often reduced because of mass transfer limitation; plug flow is favorable. Catalyst stability: should have stability because of difficulty in replacing. Heat exchange: challenging, so usually work adiabatically.

16.11.6.16 PFTR: Monolithic

Related topics are motionless mixer in tube (Section 16.11.6.10) and trickle bed (Section 16.11.6.15).

Area of Application

Phases: gas with solid catalyst; liquid with solid catalyst; gas-liquid with solid catalyst.

Guidelines

Prefer because of intensification with 1.4 to 4 times the surface/volume. Possible to install in pipelines. Use when mass transfer affects selectivity or reactivity. Perhaps not for highly exothermic

16.11.6.20 PFTR: Rotary Kiln

Phases: gas plus reactant solid. Related topics are incineration (Section 16.11.3.7) and drying (Section 16.11.5.5).

Area of Application

Solid residence time 2,500 to 20,000 s; gas residence time <1 s; solid particle diameter 7 μm to 20 mm. Sinter product: product diameter 80 to 150 mm; capacity 15 to 300 kg/s; product crush strength $>10^4$ kPa.

Guidelines

See heat transfer (Section 16.11.3.7) and related topic (drying, Section 16.11.5.5). Sintering: 0.012 kg/s·m³ volume. For fast reactions, bulk phase film diffusion may control, and pore diffusion may control if the solid diameter is >1.5 mm. Incineration: see heat transfer, Section 16.11.3.7.

16.11.6.21 PFTR: Shaft Furnace

Phases: Gas plus reacting solid.

Area of Application

Solid residence time 20,000 to 200,000 s; gas residence time <1 s; solid particle diameter 8 to 300 mm.

Guidelines

For fast reactions, bulk phase film diffusion may control, and pore diffusion may control if the solid diameter is >1.5 mm.

16.11.6.22 PFTR: Melting Cyclone Burner

Phases: Gas plus reacting solid.

Area of Application

Solid residence time 0.004 to 2 s; gas residence time <1 s; solid particle diameter, 0.002 to 0.4 mm.

Guidelines

For fast reactions, bulk phase film diffusion may control.

16.11.6.23 PFTR Via Multistage CSTR

$Bd = 2n$, where n = number of CSTRs in series. About 100 CSTR in series to provide negligible backmixing.

Area of Application

Phases: liquid, gas-liquid bio solids. *Liquid*: use for residence time >4 h; for systems where PFTR conditions are desired. Heat of reaction: highly exothermic reaction rate, slow. Capacity 0.2 to 100 kg/s. *Gas-liquid bio solids*: variety of reactor configurations to remove soluble BOD₅ from wastewater: aerated lagoon. *Pure-oxygen backmix-activated sludge*, CSTR in series: 85 to 95% removal, compact unit for use where space is limited.

Guidelines

Gas-liquid bio solids: aerated lagoon: three CSTRs in series: residence time: 1 day for each CSTR, removal 80 to 95%; GL bubble reactor: retention time less than a facultative lagoon, biomass suspended, plus subsequent settling = no recycle activated sludge reactor. Oxygen requirements control if residence time is <1 d; mixing controls if residence time is >1 d; length/width <1.5; depth 2.4 to 5.4 m; SS concentration = 1 to 5 g/L; power 0.011 to 0.023 kW/m³; 80 to 95% removal; food/microorganism ratio = 22 mg BOD₅/s·kg MLSS; depth 2.4 to 5.4 m; 0.01 to 0.25 kW/m³; SS

autoclaves <100 L. *Unique for CSTR*: phases: liquid, gas-liquid, liquid-liquid, liquid catalytic solid, gas-liquid catalytic solid, gas-liquid bio solid. Capacity 0.0001 to 100 L/s and usually >0.4 L/s; volumes 1 to 1,000,000 L. Autothermal reactions. Usually used if the concentration of reactants is low, and need low concentration of reactants for selectivity. CSTR is larger and more expensive than PFTR. For multiphase, STRs are characterized by high liquid holdups; holdup of the reactive phase is important if the reaction is slow, $Ha < 1$; phase ratio is easy to control. *Liquid*: <300,000 mPa·s; volume <75 m³. Use for kinetically controlled reactions that require long residence times. *Gas liquid*: surface area 60 to 500 m²/m³; surface area gas-liquid per volume of reactor: 200 to 2000 m²/m³ volume reactor; surface area gas-liquid per volume of liquid phase: 220 to 2500 m²/m³; liquid phase can handle viscous liquids and suspensions, only appropriate for smaller size reactors <10 to 20 m³. *Liquid-liquid*: surface area 400 to 3500 m²/m³ with area increasing with decreasing surface tension and increasing velocity. Drop diameter 4 to 5000 μm; for viscosities <10⁴ mPa·s. Phase ratio is easy to control. *Liquid with catalytic solid*: catalyst diameter <0.1 mm; surface area solid 500 m²/m³. *Gas-liquid with catalyst solid*: catalyst diameter <0.1 mm; surface area 50 to 1200 m²/m³; surface area solid 500 m²/m³; surface area gas-liquid 100 to 1500 m²/m³. *Gas-liquid bio solid*: aerobic sludge digesters: reduce the volume of and render biologically stable the sludge from a variety of sources: conventional activated sludge and primary clarifier.

Guidelines

Reactor size 8 to 32 m³, 1.5 MPa, with jacketed heat transfer surface 1.5 to 2.5 m²/m³ volume. Heat transfer coefficient $U = 0.06$ to 0.35 kW/m²·K for jacket to inside reactor contents; coil 0.7 to 0.8 kW/m²·K. Power = 0.2 to 2 kW/m³, see mixing, Section 16.11.7.3, and heat transfer, Section 16.11.3.3. *Liquid*: power input to promote heat and mass transfer: 1 to 6 kW/m³ reactor volume. *Gas-liquid*: holdup: liquid holdup >0.7, gas holdup <0.1; bubble diameter = 2.5 mm regardless of the agitation and has a mean upward velocity of about 0.27 m/s; superficial gas velocity, 0.05 to 1 m/s; backmix; complete; typical liquid mass transfer coefficient = $k_L a = 0.02$ to 0.2 1/s; volumetric ratio liquid to mass transfer liquid film, $\beta > 100$; power input 0.1 to 4 kW/m³. Height of liquid = tank diameter or use multiple impellers if height of liquid/tank diameter >2. Impeller diameter 0.3 to 0.5 of tank diameter. *Liquid-liquid*: holdup: volume fraction dispersed liquid 0.01 to 0.5 ; typical drop diameter is 150 μm; power input 0.2 to 3 kW/m³. A related topic is solvent extraction (Section 16.11.4.10). *Liquid with catalytic solid*: holdup: volume fraction catalyst 0.01 ; volume fraction liquid 0.99 ; power input to facilitate heat and mass transfer, suspend solids, and promote mass transfer: 1 to 4 kW/m³ reactor volume. *Gas-liquid with catalyst solid*: holdup: volume fraction catalyst 0.01 ; volume fraction liquid 0.8 to 0.9 ; volume fraction gas 0.1 to 0.2 . Power input 0.05 to 2 kW/m³. Catalyst activity: variable but often able to avoid diffusion limitations because of small-diameter catalyst. Catalyst selectivity: OK. Catalyst stability: change between batches. Heat exchange: OK. *Gas liquid bio solids*: aerobic sludge digesters: CSTR designed on the basis of VSS reduction. Mixing to keep the solids suspended plus oxygenation. Cell residence time for cells 12 to 22 days, depending on the source of the sludge. Typical organic load 4 to 26 μg VSS/s·m³; dissolved oxygen concentration 1 to 2 mg/L; air requirement for activated sludge = 0.25 to 0.33 dm³/s·m³; mixture of primary plus activated sludge = 0.4 to 0.5 dm³/s·m³; 1.42 kg O₂/kg biosolids digested. Oxygen usage 1.4 to 11 mg O₂/s·kg VSS, depending on the source of the sludge. For diffused air 0.33 to 1 dm³/s·m³, depending on the sludge; surface aeration = 0.025 to 0.033 kW/m³. Power = 0.015 to 0.02 kW/m³.

16.11.6.27 STR: Fluidized Bed (Backmix)

Related topics are heat transfer (Section 16.11.3.4 and Section 16.11.3.8), mixing (Section 16.11.7.1), dryers (Section 16.11.5.5), and size enlargement (Section 16.11.9.5).

Area of Application

Phases: gas-liquid bio solid; liquid plus bio solid. Liquid plus bio solid: anaerobic digesters: (conventional first stage): batch microbiological treatment of municipal sludge; no mixing: use for $<50 \text{ m}^3/\text{s}$. Other options include anaerobic ponds, facultative lagoons and ponds, and aerobic ponds.

Guidelines

Liquid plus bio solid: *anaerobic digesters*: (conventional first stage): Residence time 30 to 60 days (35°C); organic loading = 4 to 9 $\text{mg VS/s}\cdot\text{m}^3$; circular, diameter 6 to 35 m; depth = 6 to 14 m. *Anaerobic pond*: residence time: 5 days; surface loading 600 to 3500 $\mu\text{g BOD}_5/\text{s}\cdot\text{m}^2$ with 150 $\mu\text{g BOD}_5/\text{s}\cdot\text{m}^2$ for winter conditions; volumetric loading 3 to 100 $\text{kg BOD}_5/\text{s}\cdot\text{m}^3$. pH 6.7 to 7.1; depth 1 to 2.5 m. *Facultative lagoon*: residence time = 7 to 20 days, usually 4 to 8 days, longer in cold temperatures; loading 40 to 130 $\mu\text{g BOD}_5/\text{s}\cdot\text{m}^2$; depth 2.4 to 4.8 m; surface aeration power to oxygenate. *Facultative pond*: residence time: 7 to 50 days; surface loading 26 to 65 $\mu\text{g BOD}_5/\text{s}\cdot\text{m}^2$; depth 1 to 2.5 m; length/width = 3/1. No surface aeration; photosynthesis is source of oxygen; recycle ratio = 0.2 to 8, usually 4 to 8. *Aerobic pond*: residence time: 2 to 6 days; surface loading 130 to 260 $\mu\text{g BOD}_5/\text{s}\cdot\text{m}^2$; depth 0.15 to 0.45 m; recirculation ratio = 0.2 to 2. A related topic is aerobic lagoon (Section 16.11.6.23).

16.11.6.29 Mix of CSTR, PFTR with Recycle

Area of Application

Phases: gas-liquid and bio solid. Bio solid removes the soluble organics, COD or BOD_5 , from wastewater. Variety of reactor configurations. Related topics are trickling filter (Section 16.11.6.14), CSTR (Section 16.11.6.26), and CSTR in series (Section 16.11.6.23). *Conventional PFTR-activated sludge*: low-strength domestic wastewater, susceptible to shock loads; 85 to 95% removal. *Conventional backmix-activated sludge*: usual-strength domestic wastewater, resistant to shock loads, 85 to 95% removal. *Step aeration, modified aeration PFTR-activated sludge*: higher-strength domestic wastewater, 85 to 95% removal. *Contact stabilization*: PFTR: OK for domestic wastewater; unsuitable for most industrial wastewater, flexible, 80 to 90% removal. *Extended aeration backmix-activated sludge* (oxidation ditch): low organic loadings, small capacity: $<40 \text{ L/s}$; flexible, 75 to 95% removal. *High rate aeration backmix-activated sludge*: high-strength domestic wastewater, 75 to 90% removal.

Guidelines

Conventional PFTR-activated sludge: mean cell residence time = 5 to 15 days; food/microorganism ratio = 2.3 to 4.6 $\text{mg BOD}_5/\text{s}\cdot\text{kg MLVSS}$; volumetric loading = 0.3 to 0.6 $\text{kg BOD}_5/\text{m}^3$; MLSS = 1.5 to 3 g/L ; residence time = 4 to 8 h; recycle ratio = 0.25 to 0.5. Air requirements = 100 m^3/kg of input BOD_5 . Conventional backmix-activated sludge: mean cell residence time = 5 to 15 days; food/microorganism ratio = 2.3 to 7 $\text{mg BOD}_5/\text{s}\cdot\text{kg MLVSS}$; volumetric loading = 0.8 to 2 $\text{kg BOD}_5/\text{m}^3$; MLSS = 3 to 6 g/L ; residence time = 3 to 5 h; recycle ratio = 0.25 to 1. Air requirements = 100 m^3/kg of input BOD_5 . Step aeration, modified aeration PFTR-activated sludge: mean cell residence time = 5 to 15 days; food/microorganism ratio = 2.3 to 4.6 $\text{mg BOD}_5/\text{s}\cdot\text{kg MLVSS}$; volumetric loading = 0.6 to 1 $\text{kg BOD}_5/\text{m}^3$; MLSS = 2 to 3.5 g/L ; residence time = 3 to 5 h; recycle ratio = 0.25 to 0.75. Air requirements = 100 m^3/kg of input BOD_5 . Contact stabilization: PFTR with recycle: mean cell residence time = 5 to 15 days; food/microorganism ratio = 2.3 to 7 $\text{mg BOD}_5/\text{s}\cdot\text{kg MLVSS}$; volumetric loading = 1 to 1.2 $\text{kg BOD}_5/\text{m}^3$; MLSS = 4 to 10 g/L ; residence time = 3 to 6 h; recycle ratio = 0.25 to 1. Air requirements = 100 m^3/kg of input BOD_5 . Extended aeration-activated sludge backmix with recycle: mean cell residence time: = 20 to 30 days; food/microorganism ratio = 0.6 to 1.8 $\text{mg BOD}_5/\text{s}\cdot\text{kg MLVSS}$; volumetric loading = 0.16 to 0.4 $\text{kg BOD}_5/\text{m}^3$; MLSS = 3 to 6 g/L ; residence time = 18 to 36 h; recycle ratio = 0.75 to 1.5. Air requirements = 125 m^3/kg of input BOD_5 . High rate aeration-activated sludge, backmix with recycle:

16.11.6.34 Process Vessels

Area of Application

Used for a wide range of temperatures, pressures, and uses. Can be decanters, reflux drums, intermediate storage, towers, KO pots, reactors.

Guidelines

Operating pressure and temperature constrain practical size of vessel. Design codes for pressure vessels vary slightly with the country. In general, for operating pressures >10 MPa, vessel volume usually <1 m³. Pressure decreases as temperatures exceed 250°C. For temperatures above 350°C, consider carbon/molybdenum, and for temperatures $>500^\circ\text{C}$, consider austenitic steels. *Corrosion allowance* 1.5 mm for corrosion rates 0.08 mm/a; 3 mm for rates 0.09 to 0.3 mm/a; 4.5 mm for 0.31 to 0.4 mm/a; 6 mm for >0.4 mm/a. If pressure <400 kPa, use L/D of 2 to 3:1. For pressures >400 kPa, use L/D of 4 to 5:1. *For surge*, allow 2-min liquid residence time; for draw-off, use 15 min; for reflux, use 5 min, provided this allows sufficient time for controllers to function. Total volume = $1.3 \times$ holdup if the holdup volume is >3 m³.

16.11.6.35 Storage Vessels and Bins

Guidelines

For liquids, consider floating-head vertical cylinders for pressures <100 kPa; spheres, vertical cylinders with dome ends for pressures <250 kPa; small spheres and horizontal cylindrical tanks for pressures <800 kPa. For gases, consider pressure cylinders and small horizontal cylindrical tanks for pressures >800 kPa. For solids, bins, and hoppers: promote mass flow with cone angle to the vertical related to the wall friction angle of the solid.

Wall Friction Angle	Cone Angle with the Vertical	Wedge Angle with the Vertical
	$<$	$<$
30°	10°	20°
20°	25°	38°
10°	35°	48°
0°	45°	60°

Both bottom angle and surface smoothness are important. For a circular cone, the outlet should be at least six to eight times the diameter of the largest particle. For wedge hoppers, the discharge opening should be at least three to four times the diameter of the largest particle. The length of the slot opening should be at least three times the width. The desired mass flow requires the entire discharge opening to be active by the use of: tapered interface belt conveyor, a tapered shaft screw conveyor, a screw conveyor with an increasing pitch (providing the length:screw diameter is $<3:1$), or a combination of screw conveyor with a tapered shaft plus increased pitch, provided the length:screw diameter is $<6:1$.

16.11.7 MIXING*

The major situations are gas-solid, gas-liquid, liquid, and solids. Solids blending can include dry solids blenders; extruders for foodstuffs and polymers; and pug mills for clays, thick pastes, and fertilizers.

* Reproduced with permission from Donald R. Woods, *Rules of Thumb in Engineering Practice*, pages 282 to 291, 2007, copyright Wiley-VCH Verlag GmbH & Co. KGaA, Weinheim, ISBN: 978-3-527-31220-7. See this book for more details, especially about Good Practice, Trouble shooting and Capital Costs.

of linear distance along the basin. Diffusers 15 to 30 dm³ air/s·m² diffuser area. For 45-min detention time, 0.6 to 1 dm³/L. See related topics, flocculation (Section 16.11.9.3) and size reduction, gas in liquid (Section 16.11.8.1). *Anchor*: power = 4 to 9 kW/m³. *Gentle mechanical mixing, such as paddle reel or stator-rotor for flocculation* (see related topic, Section 16.11.9.3): 0.035 to 0.04 tapering to 0.001 to 0.009 kW/m³. *Motionless mixers*: for viscosity ratio <100:1 and Reynolds no., $Re > 10,000$, use turbulent vortex mixer; for viscosity ratio >100:1 and $Re < 10,000$, use helical element. For pipe diameter <0.3 m, element is $1.5 \times$ pipe diameter; for pipe diameter >0.3 m; element = pipe diameter. For $Re < 10$, use 18 elements with the number of elements reducing to 2 as Reynolds no. increases to >5000. *Annular sparger*: annular sparger blends liquids of equal viscosity and density in 50 pipe diameters; central injection blends liquids of equal viscosity and density in 80 pipe diameters; in mixing tee after 10 pipe diameters. For viscosity differences <10:1, inject the viscous liquid into the thin liquid. For *blending and heat transfer*, identify viscosity when turbulent mixing occurs. Usually, impeller Re of 200.

16.11.7.4 Liquid-Liquid

Related sections are solvent extraction (Section 16.11.4.10), size reduction (Section 16.11.8.3), and reactors (Sections 16.11.6.9 through 16.11.6.16, 16.11.6.23 through 16.11.25, and 16.11.6.30).

Area of Application

Fluid viscosity and volume to be mixed are the most significant factors. Propellers: viscosity <3000 mPa·s; volumes <750 m³. Turbines and paddles: viscosity <300,000 mPa·s; volumes <75 m³.

Guidelines

Propellers and turbines: power: 0.2 to 1.5 kW/m³ for mixing immiscible liquids, with values decreasing as the interfacial tension decreases, and for heat transfer. Power: 1 to 4 kW/m³ for emulsification and mass transfer.

16.11.7.5 Liquid-Solid

Area of Application

Stirred tank: crystallizers, see Section 16.11.4.6; and reactors, Sections 16.11.6.23 through 16.11.6.25. Liquid fluidized bed: reactors, Section 16.11.6.26; liquid adsorption, Section 16.11.4.12; ion exchange, Section 16.11.4.13; backwash fixed-bed operations such as deep-bed filters, Section 16.11.5.13; liquid adsorbers, Section 16.11.4.12; and ion exchangers, Section 16.11.4.13.

Guidelines

Stirred tank: paddles: power input: suspend solids, 0.2 to 1.6 kW/m³; $L/D = 0.7$ to $1.05/1$. Baffle, four @ 90°; baffle width = $0.08 \times$ tank diameter; off-the-wall distance = $0.015 \times$ tank diameter. Minimum level of liquid = $0.15 \times$ tank diameter for impeller:tank diameter 0.28:1 and minimum level = $0.25 \times$ tank diameter for impeller:tank diameter = 0.4:1. Use a foot bearing plus a single, main axial hydrofoil impeller diameter = $0.28 \times$ tank diameter located $0.2 \times$ tank diameter from the bottom plus a pitched blade impeller diameter = $0.19 \times$ tank diameter located $0.5 \times$ tank diameter from the bottom. *Liquid fluidized bed*: in general, particle diameter 0.5 to 5 mm with density and diameter of the particle dependent on the application. The superficial liquid velocity to fluidize the bed depends on both the diameter and the density difference between the liquid and the particle. Usually, the operation is particulate fluidization. Particle diameter 0.2 to 1 mm reactors; superficial liquid velocity 2 to 200 mm/s. *Fluidized adsorption*: bed expands 20 to 30%; superficial liquid velocity for usual carbon adsorbent = 8 to 14 mm/s. *Fluidized ion exchange*: bed expands 50 to 200%; superficial liquid velocity for usual ion exchange resin = 40 mm/s. *Backwash operations*: fixed-bed adsorption: superficial liquid velocity = 8 to 14 mm/s; fixed-bed ion exchange: superficial backwash velocity = 3 mm/s.

air sparged into the liquid. $k_L a = 0.0008$ 1/s. A related section is mixing (Section 16.11.7.3). *Bubble column*: superficial gas velocity, 0.03 to 0.04 m/s holdup <0.2 , $k_L a = 0.005$ to 0.01 1/s. $k_L a$ is independent of the diameter if column diameter >0.15 m; $k_L a$ is not affected by the type of gas sparger if the gas velocity exiting the orifice is >0.03 m/s. If <0.03 m/s, then use a sintered plate. Height: $3 < \text{height} < 12$ m; allow 0.75 of diameter or 1 m at the top for foam disengagement. Energy 0.01 to 1 kW/m³. *Spray column*: superficial gas velocity, 0.75 to 2 m/s; holdup <0.8 , energy: high for atomization; $k_L a = 0.0007$ to 0.015 1/s. *Packed column*: superficial gas velocity, 0.75 to 1.5 m/s for atmospheric pressure; 0.2 m/s for pressure operation and 2.5 m/s for high vacuum; holdup <0.95 ; energy 0.01 to 0.2 kW/m³; $k_L a = 0.005$ to 0.02 1/s; packing >6 mm; catalyst >3 mm. Column diameter/packing diameter >8 and prefer >30 to prevent liquid channeling. Redistributors every 3 to 4.5 m. Higher mass transfer coefficient, $k_L a = 0.15$ 1/s for cocurrent upflow in the bubble regime. *Tray column*: superficial gas velocity, 0.75 to 1.5 m/s for atmospheric pressure; 0.2 m/s for pressure operation and 2.5 m/s for high vacuum; holdup <0.8 ; energy 0.01 to 0.2 kW/m³; $k_L a = 0.01$ to 0.05 1/s. *Agitated tank*: superficial gas velocity, 0.05 to 1 m/s; holdup <0.1 , energy 0.1 to 4 kW/m³; $k_L a = 0.02$ to 0.2 1/s. Height of liquid = tank diameter or use multiple impellers if height of liquid/tank diameter is >2 . Impeller diameter 0.3 to 0.5 of tank diameter. *Motionless mixer*: superficial gas velocity, 1 to 2 m/s; holdup 0.5, energy 10 to 700 kW/m³; $k_L a = 0.1$ to 3 1/s. Volumetric flow rate of gas to liquid = 1 at the nozzle. *Pipe/tubes, transfer line*: superficial gas velocity, 0.01 to 0.4 m/s; holdup 0.05 to 0.95; energy 0.1 to 100 kW/m³. For <10 -cm dia. tubes, $k_L a = 0.01$ to 0.7 1/s.

16.11.8.2 Liquid in Gas (Sprays)

Area of Application

Pressure nozzle: spray diameter 70 to 10,00 μm ; capacity 0.03 to 0.3 L/s; low viscosity and clean fluids. *Spinning disc*: spray diameter 50 to 250 μm ; capacity 0.0015 to 0.4 L/s; for usual fluids and for viscous fluid or fluid containing solids. *Twin fluid*: spray diameter 2 to 80 μm ; capacity 0.03 L/s; increasing the ratio of atomizing fluid to liquid from 1 to 10, will decrease the spray diameter by a factor of 10. *Rayleigh breakup* to produce uniform drops of diameter $1.8 \times$ diameter of orifice. A related topic is prilling (Section 16.11.9.14). *Surface aerators*: for activated sludge oxidation (instead of diffused air aeration, Section 16.11.8.1). *Brush aerators*: for oxidation ditches. *Motionless mixers*: spray flow.

Guidelines

Pressure nozzle: pressure 0.45 to 14 MPa; increasing the pressure increases the capacity. *Spinning disc*: increasing the capacity increases the drop size. *Twin fluid*: high energy input. *Surface aeration*: 0.01 to 0.025 kW/m³ or 0.3 to 1.2 kg O₂/MJ. *Brush aeration*: 0.015 to 0.018 kW/m³ 0.6 to 0.8 kg O₂/MJ. *Motionless mixers*: spray flow: gas superficial velocity 3 to 25 m/s; liquid superficial velocity 0 to 0.6 m/s. Turbulent flow.

16.11.8.3 Liquid-Liquid

Liquid-liquid contacting for reactions, separations, mixing. See reactions, Section 16.11.6.26; separations, Section 16.11.4.10; and mixing, Section 16.11.7.4, for separate rules of thumb.

Area of Application

Mixer in tank: drop diameter 4 to 5000 μm ; capacity >0.05 L/s; for viscosities $<10^4$ mPa·s. *Colloid mill*: drop diameter 1 to 8 μm ; capacity 0.01 to 3 L/s; for viscosities $<10^4$ mPa·s but usually >1000 mPa·s. *Homogenizer*: drop diameter 0.1 to 2 μm ; capacity 0.03 to 30 L/s; for viscosities $<10^3$ mPa·s but usually <200 mPa·s; decrease the drop diameter by increasing the exit pressure. *High shear disperser*: for viscosities 10^3 to 5×10^6 mPa·s. *Roller mills*: for viscosities $>10^3$ mPa·s. *Motionless mixer*: drop diameter 100 to 1000 μm (about 0.15 times drop diameter for fluid velocity in a pipe

capacity occurs under choke feed; minimum of fines (breakup by compression). Product diameter determined by the adjustment clearance between compressing plates. *Gyratory crusher*: power 3 to 10 MJ/Mg; rpm 450 to 110; minimum of fines (breakup by compression), product diameter determined by the adjustment clearance between compressing plates. *Cone crusher*: selected as secondary and tertiary reducers; power 0.9 to 5 MJ/Mg; rpm 290 to 220; (breakup by compression) product diameter determined by the adjustment clearance between compressing plates. *Short head cone crusher*: power 3 to 12 MJ/Mg; (breakup by compression) product diameter determined by the adjustment clearance between compressing plates. Often, choke fed as tertiary crusher. *Roll crusher*: power 3 to 15 MJ/Mg; (breakup by compression) product diameter determined by the space between the rolls. Speed determines the capacity. *Roller mill*: 50 to 500 kPa, (breakup by compression) product diameter determined by the space between the rolls. Speed determines the capacity. *Shredders*: power 25 to 250 MJ/Mg. *Hammer mill*: power 2 to 80 MJ/Mg, (breakup by impact against a plate traveling at 20 to 60 m/s) product diameter determined by exit screen size. *Cage mill*: (breakup by impact against a plate traveling at 20 to 30 m/s) product diameter determined by exit screen size. Handles amorphous materials. *Pin-disc mill*: (breakup by impact against a plate traveling at 200 m/s) product diameter determined by feed flow rate and speed of the pins. Ideal for soft material. *Impact mill*: (breakup by impact against a plate traveling at 50 to 110 m/s) product diameter determined by exit screen size. *Autogenous mill*: length:diameter 0.2 to 0.5 with 0.33 usual (breakup by impact among particles). *Rod mill*: power 5 to 80 MJ/Mg; length:diameter 1.4:1 to 1.6:1 with length <6.8 m; 35 to 40% v/v rod charge to give total charge of 45% v/v. (Breakup by variety of mechanisms with revolving media.) *Ball mill*: power 30 to 10,000 MJ/Mg; length:diameter 1:1 to 2:1; 50% v/v charge of balls (breakup by variety of mechanisms with revolving media); large balls give coarse particles, small balls give fine particles. *Fluid energy mill*: about 6 to 9 kg air/kg of solid or 1 to 4 kg steam/kg solid; (breakup by impact with other particles traveling at 100 to 300 m/s) product size determined by the feedrate. Power 700 to 1000 MJ/Mg.

16.11.8.5 Solids: Modify Size and Shape: Extruders, Pug Mills, and Molding Machines

See size enlargement, Section 16.11.9.14.

16.11.8.6 Solids: Solidify Liquid to Solid: Flakers, Belts, and Prill Towers

See Section 16.11.9.15.

16.11.9 SIZE ENLARGEMENT*

16.11.9.1 Size Enlargement: Liquid-Gas: Demisters

Area of Application

In general, liquids should not bind to the inserts or walls; they should flow as rivulets or drops along the surface of the insert. *Vane separators*: droplet diameter >20 μm ; droplet concentration >0.1 mg/m^3 . *Mesh pads*: droplet diameter 3 to 20 μm ; droplet concentration 0.01 to 0.1 mg/m^3 . *Fiber beds designed for impaction* (usually cylindrical or “candles”): droplet diameter 0.2 to 3 μm ; droplet concentration 0.001 to 0.01 mg/m^3 . *Fiber beds designed for Brownian motion* (usually cylindrical or “candles”): <0.1 μm ; droplet concentration <10⁻³ mg/m^3 .

* Reproduced with permission from Donald R. Woods, *Rules of Thumb in Engineering Practice*, pages 298 to 309, 323 to 324, 2007, copyright Wiley-VCH Verlag GmbH & Co. KGaA, Weinheim, ISBN: 978-3-527-31220-7. See this book for more details, especially about Good Practice, Trouble shooting and Capital Costs.

Guidelines

Fluidized bed: 30 to 50 min for batch of 200 to 700 kg. Shallow bed, 0.3 to 0.6 m deep; gas velocity 0.1 to 2.5 m/s or 3 to 10 \times minimum fluidization velocity. Evaporation rates 0.005 to 1 kg/s·m² cross-sectional area.

16.11.9.6 Size Enlargement: Solids: Spherical Agglomeration*Area of Application*

Product diameter: 2 to 3 mm; batch; tensile strength of agglomerate: 10 to 100 kPa.

Guidelines

Power 10 to 40 kW/m³. Mixing time 30 to 300 s.

16.11.9.7 Size Enlargement: Solids: Disc Agglomeration*Area of Application*

Product diameter: 10 mm, fertilizer 1.5 to 3.5 mm; ore 10 to 25 mm. Capacity <25 kg/s. Tensile strength of agglomerate 10 to 200 kPa, depending on the binder. Produces more nearly uniform granules than drum (Section 16.11.9.8).

Guidelines

Rotational speed about 50% of critical speed or 30 rpm decreasing to 6 rpm as diameter increases. Disc area = 0.1 to 200 m². L:D = 0.1 to 0.22; angle of inclination with the horizontal 40 to 70°. Power = 7 to 9 kW·s/kg or MJ/Mg.

16.11.9.8 Size Enlargement: Solids: Drum Granulator*Area of Application*

Product diameter 2 to 5 mm; capacity 0.001 to 30 kg/s. Tensile strength of the agglomerate: 10 to 200 kPa, depending on the binder.

Guidelines

Drum volume: 5 to 100 m³. L:D = 2 to 4; angle of inclination with the horizontal, 10°. For fertilizer: 5 to 7 kW·s/kg or MJ/Mg. For iron ore: 2 kW·s/kg. 10 to 20 rpm. Product diameter controlled by speed, residence time, and binder.

16.11.9.9 Size Enlargement: Solids: Briquetting

Use of pressure to create agglomerate.

Area of Application

Product diameter 15 to 80 mm; capacity 1 to 30 kg/s. Crushing strength of agglomerate 1 to 10 MPa.

Guidelines

Constant product volume; operating pressure <50 MPa. Power 2 to 50 MJ/Mg.

16.11.9.10 Size Enlargement: Solids: Tableting

Use of pressure to create agglomerate.

Area of Application

Product diameter 15 to 100 mm; capacity 0.011 to 1.5 kg/s. Crushing strength of agglomerate 1.5 to 10 MPa.

velocity 0.35 m/s; draw ratio 4:1; extrude at 180°C; mass flow 0.2 g/s; thickness 34 μm . *Extruders for dewatering*: 1 to 4 kW·s/g or 1000 to 4000 kJ/kg. Related to rotary press (Section 16.11.5.13). *Extruders for foodstuffs*: rpm 30 to 40; shear 5 to 10 1/s; power 200 kJ/kg or 0.1 to 0.4 kW·s/g with values increasing with shear. *Extruders and cookers*: for foodstuffs: rpm 60 to 500; shear 20 to 180 1/s; power 75 to 500 kJ/kg. *Pug mills* for clays, thick pastes, and fertilizers: 0.004 kW·s/g or 3 to 12 kJ/kg.

16.11.9.15 Solids: Solidify Liquid to Solid: Flakers, Belts, and Prill Towers

Related topics are size decrease (Section 16.11.8.6) and dryers (Section 16.11.5.5), but use refrigeration (instead of steam) to solidify liquid.

Area of Application

Flaker: liquid feed: product: flakes about 1 cm \times 1 cm \times 1 mm thick; capacity <10 kg/s. *Chilled belt*: liquid feed: product: pastilles, flakes, pellets; capacity usually <10 kg/s per unit. *Prilling tower*: liquid feed, product diameter: spheres 1 to 3 mm. Capacity <5 kg/s per unit.

Guidelines

Flaker: 20 to 300 g/s·m². Heat transfer coefficient 350 W/m² C; power: 1 to 50 MJ/Mg, depending on the material; lower values for ammonium nitrate, benzoic acid, tetrachlorobenzene, sodium hydroxide; higher power usages for waxes and resins. *Chilled belt*: feeder: heated overflow weir, viscosities <1000 mPa·s, produces flakes 1 to 3 mm thick; overhead double roll, viscosities <10⁸ mPa·s, produces flakes; rotoformer to produce pastilles 1 to 10 mm diameter; heated strip former (for brittle products). Heat transfer coefficient 350 W/m² C; 20 to 300 g/s·m². Power 1 to 50 MJ/Mg, depending on the material. *Prilling tower*: gas velocities less than the terminal velocity of the prill, <1 to 2 m/s; gas-to-solids ratio 10 kg air/kg solids. Assume solid surface temperature = solidification temperature, volumetric heat transfer coefficient 5 W/m³ C. Height <60 m.

ADDITIONAL READING

For rules of thumb:

Woods, D. R. 2007. *Rules of Thumb in Engineering Practice*, Weinheim: Wiley-VCH.

For short cut methods:

Branan, C. R. 2005. *Rules of Thumb for Chemical Engineers*, 4th ed., Amsterdam: Elsevier.

Couper, J. R. et al. 2005. *Chemical Process Equipment*, 2nd ed., Amsterdam: Elsevier.

Coker, A. K. 2007. *Ludwig's Applied Process Design for Chemical and Petrochemical Plants*, 4th ed., Vol. 1, Amsterdam: Elsevier.

Ludwig, E. E. 1997. *Applied Process Design for Chemical and Petrochemical Plants*, 3rd ed., Vol. 2, Amsterdam: Elsevier.

Ludwig, E. E. 2001. *Applied Process Design for Chemical and Petrochemical Plants*, 3rd ed., Vol. 3, Amsterdam: Elsevier.

For trouble shooting:

Woods, D. R. 2007. *Successful Trouble Shooting*, Weinheim: Wiley-VCH.

17.4 Other Aspects of Process Safety Management	1467
Table of Symbols	1468
Conversion Factors	1469
Appendix A	1470
Appendix B	1478
Appendix C	1479
Appendix D	1481

17.1 INTRODUCTION

Chemical engineers are faced with a variety of safety concerns, from both federal and state authorities as well as management at the corporate and local levels. At the federal level, the “Process Safety Management” standard of the Occupational Safety and Health Administration (OSHA) [1] and the “Risk Management Program” rule of the U.S. Environmental Protection Agency (EPA) [2] present comprehensive requirements for the control of processes to prevent releases of hazardous materials. Similarly, several states (notably, New Jersey, Delaware, and California) require chemical plants and other facilities that handle chemicals to protect the public and employees. Further, many companies and insurers have even stricter requirements for process control and for preventing and reporting of process incidents, including those that do not cause injury or property loss.

This chapter presents methods for meeting the requirements of the federal regulations concerning public and employee safety. Additional information is provided for some aspects of process safety that are not included in this legislation but can affect the safety of operations in facilities handling hazardous materials. There are other resources for analysis and control of general industrial hazards [3, 4].

Calculation procedures presented here help to evaluate the consequences of leaks or spills of hazardous material. However, the methodology and equations can be used for other calculations that are frequently encountered in chemical engineering studies.

17.2 PROCESS SAFETY MANAGEMENT

Table 17.1 shows the aspects of process safety for which actions are required by OSHA in Title 29 of the Code of Federal Regulations, Part 1910, Section 119 (29 CFR 1910.119) [1] and by the EPA in Title 40 of the Code of Federal Regulations, Part 68 (40 CFR 68) [2]. This “Chemical Process Safety” section concentrates on the engineering aspects of “Process Safety Information”—on the “consequences of failure of engineering and administrative controls” and the “qualitative evaluation of a range of the possible safety and health effects of failure of controls” requirements of the OSHA and EPA “Process Hazards Analysis” and the “Off-Site Hazard Assessment.”

Appendices B and C of the OSHA Process Safety Management standard provide some guidance concerning the elements of the OSHA standard and, therefore, of similar elements of the EPA standard. To assist in compliance with the Offsite Consequence Analysis element of the EPA standard, dispersion-analysis Reference Tables 1 through 22 and calculation-methods Appendices A through E are provided in the accompanying rule [9].

The type and extent of the EPA requirements depend on the placement of a “stationary source” in Programs 1, 2, or 3. Program 1 eligibility is limited to sites having good histories and presenting no off-site hazards. Program 3 applies to sites subject to OSHA requirements and sites that are identified with the following North American Industrial Classification System [NAICS] codes: 32211, 32411, 32511, 325181, 325188, 325192, 325199, 325211, 325311, and 32532 [2]. Thus, program 3 applies to most large chemical-handling plants. Program 2 applies to other sources.

Additional guidance concerning management systems and calculation methods are provided in the following sections. Pertinent references are presented in Appendices C and D and are indicated by brackets [] in the text.

1. The owner or operator of a stationary source shall develop a management system to oversee the implementation of the risk management program elements.
2. The owner or operator shall assign a qualified person or position that has the overall responsibility for the development, implementation, and integration of the risk management program elements. When responsibilities for implementing individual requirements of this part are assigned to other persons, the names or positions of these people shall be documented, and the lines of authority shall be defined through an organization chart or similar document.

A PSM system has been defined as the “comprehensive sets of policies, procedures, and practices designed to ensure that barriers to episodic incidents are in place, in use, and effective” [6(G20)], and “the set of formal and informal procedures and activities used by a facility to control and direct process safety” [6(G20)].

The PSM system involves planning, organizing, implementing, and controlling activities at the corporate and site-management (“strategic”) levels, at the middle (“managerial”) level and at the employee (“task”) level [6(G8)]. It depends on the inherent and demonstrated hazards of the processes, their complexity, the numbers and potential exposures of employees, and many other factors, and guidance for PSM system design and implementation is available [6(G25); 6(G8); 6(G10)] (Table 17.2).

Each of the above aspects should normally be assigned to one or more persons in the organization, with periodic (e.g., monthly) reports concerning the success in implementation.

17.3.2 EPA OFF-SITE HAZARD ASSESSMENT

Important aspects of process safety are minimizing the frequency and size of releases of hazardous materials and minimizing the exposure of persons to the toxicity, fire, and explosion consequences of hazardous-materials releases. To evaluate the potential hazards of such releases, it is necessary to estimate the rates and durations (or quantities) of possible releases, and then evaluate the consequences of such releases. The following sections provide methods for estimating the rates of releases from process containers and piping.

The EPA standard requires that—for the “worst case” evaluations—the total quantity of toxic or flammable material is released from the vessel that contains the greatest amount, over a 10-min period, and a liquified gas is assumed to be released as a gas (that is, 100% “flashing” to gas or vapor). If the largest container contains liquid or a gas maintained as a liquid by refrigeration, it is assumed that a pool is formed instantaneously (1 cm deep), with evaporation of the hazardous

TABLE 17.2
Factors That Should Be Addressed in the PSM System

Elements of the PSM System	Some Components of the PSM System
New-project design review	Process design, siting, and hazards reviews
Legislation, standards/codes, and internal	Design, construction, operation, and maintenance guidance
Process knowledge	Process design, operating conditions, and protective systems
Training	Orientation, initial, and refresher
Human factors	Operator interactions with controls and equipment
Process and equipment integrity	Materials of construction, and maintenance procedures
Process risk management	Hazards identification and reduction of risk
Management of change	Procedures and authorizations
Incident investigation	Injury, loss, and near-miss, and communication
Audits and corrective actions	Self-examination and third-party studies of practices
Continuous improvement	Updating of control and safety system and practices
Accountability at all levels	Continuity of operations and protection against injury/loss

$$W_{lost} = [V_T M P_o 19.32 T_o] / [(14.7 / [Z_o P_o])] \text{ pounds for real gases} \quad (17.7)$$

$$t_c = (\ln [P_o t_c / 14.7]) / (0.035 D_H^2 [19.32 / V_T] [T_o / M]^{0.5}) \text{ seconds for ideal gases} \quad (17.8)$$

$$t_c = (\ln [P_o t_c / 14.7]) / (0.23 D_p^2 [19.32 / V_T] [T_o / M]^{0.5} [D_p / L]^{0.5}) \text{ for real gases} \quad (17.9)$$

The preceding equations assume that the temperature of the gas or vapor remains constant (isothermal conditions), and this would apply only if the initial temperature was near-ambient and the duration of leakage was very long.

The EPA standard states that the total quantity of gas or vapor is to be divided by 10 min, to obtain a rate of flow that could then serve as input to the dispersion tables.

17.3.2.2 Release Source Terms (Liquid Flow Rates)

The rate of liquid flow through a "hole" in process equipment is a function of (in descending order of importance) the diameter of the hole, the pressure within the equipment (including the "head" of liquid above the hole), the density of the liquid, and the viscosity of the liquid within the equipment.

17.3.2.2.1 Hole in Piping or Equipment

The following simplified equation can be used to estimate the rate of liquid flow through a hole [8, 10]:

$$w_{liquid} = 0.31 D_{hole}^2 [d P_g]^{0.5} \text{ pounds/second} \quad (17.10)$$

where P_g is the pressure upstream of the hole, and d is the density of the liquid (in psig and pounds/feet³, respectively).

17.3.2.2.2 Guillotine Failure of Piping

The following equation can be used to estimate the rate of liquid flow from the open end of a pipe:

$$w_{liquid} = 0.31 D_{hole}^2 [d P_g / (1 + [0.08 L / D])]^{0.5} \text{ pounds per second} \quad (17.11)$$

where L and D are the pipe length and diameter (in feet and inches, respectively).

17.3.2.2.3 Time to Empty a Container of Liquid

The time required to empty a tank of liquid is given by [10]

$$t_{empty} = 1.0 [D_{tank} / D_{hole}]^2 H_{liquid}^{0.5} \text{ minutes} \quad (17.12)$$

where D_{tank} and D_{hole} are the tank and hole diameters (in feet and inches, respectively), and H_{liquid} is the initial height of liquid above the hole. The above equation applies only if the pressure in the tank is atmospheric. If other conditions apply, a more complicated procedure should be used [11].

17.3.2.3 Release Source Terms (Two-Phase Flow)

A sudden release of pressure in a container of liquified gas or a liquid that is at a temperature above the atmospheric-pressure boiling point can result in a rapid conversion of some of the liquid to vapor, with a consequent swelling of the now two-phase fluid. Since this fluid is not totally gas or liquid, the equations that are used to calculate flow rates for these phases do not apply. Similarly, venting of a liquified gas or a liquid at a temperature above the atmospheric-pressure boiling point

17.3.2.5 Pool Formation from Liquid Spills

The hazards of a spill of a volatile toxic or flammable liquid are primarily dependent on the size of the spill, in terms of its diameter or area, since the rate of evaporation depends primarily on the surface area. If the spill is into a dike or curbed area, the area of the spill that is exposed to evaporation is the area of the confinement. If the spill is onto a surface without confinement, the spill area is related to the viscosity and is limited by the rate of evaporation at the outside edge of the spill.

The area of a confined pool would be governed by the dike area (or curbed area, if the spill can be contained by the curbing). The area of an unconfined spill on an essentially flat surface depends on the average depth of the pool. The following equation gives the approximate pool depth:

$$h_{pool} = 0.3W_{pool}^{0.5}/d_{liquid} = 0.1 G_{pool}^{0.5}/d_{liquid}^{0.5} \text{ inches} \quad (17.17)$$

where W_{pool} is the weight of liquid in the pool (in pounds), and G_{pool} is the volume of liquid in the pool (in gallons).

For the purposes of the EPA "worst case" evaluation, the pool is assumed to be 0.39 in. (1 cm) deep [2]. The above equation assumes that no vaporization occurs as the pool is developing.

17.3.2.6 Evaluation of Toxicity Hazards

17.3.2.6.1 Toxicity Hazards Analysis

Of the many routes of toxic-material entry into humans, inhalation is the most likely to occur and is the route specified in current legislation. Toxicity data have been developed for most of the important industrial chemicals [19] and form the basis for "threshold" or "allowable" concentrations to which persons can be exposed with no significant physiological effect. Evaluation of toxicity hazards is then based on the duration of exposures to concentrations above these "threshold" levels. The concentrations of toxic materials in air are primarily functions of vapor pressure and temperature (for toxic liquids); the rate of gas, vapor, mist, or dust release or generation; and distance from the source.

After the rate of toxic material entry into a cloud has been determined (using the equations in the preceding section), the effects of atmospheric conditions on the dispersion (dilution) of the material—particularly gas or vapor—can be evaluated.

Computer programs are available for calculating (1) gas and vapor concentrations; (2) concentration \times time products (doses); (3) cloud lengths, widths, and heights; and (4) travel times, as functions of (in decreasing order of importance) wind speed, atmospheric stability, surface roughness, and averaging time. Evaluation and listing of these programs are outside the scope of this publication, but resources are available [6(G40)].

The EPA has selected conservative models for (1) neutrally buoyant gases and vapors and (2) dense gases and vapors. For compliance with the EPA standard [2], the values of the variables that are shown in Table 17.3 were specified by the EPA and should be used [9].

For evaluation of flash-fire hazards involving dispersion of flammable gases and vapors, an averaging time of 0.1 min was used in the EPA tables. Only "passive" mitigation (such as a dike or a confining building) is to be considered for the "worst-case" evaluation, but "active" mitigation (such as valves, transfers, and operator responses) can be considered for the "alternative" evaluations.

Each of the EPA tables can be represented by one or two "exponential" equations, having the form

$$X = Kw_{vapor}^a/[MCv_{wind}]^b \text{ feet} \quad (17.18)$$

where w_{vapor} is the rate of vapor release to the atmosphere (in pounds per minute); M is the molecular weight of the vapor; C is the concentration of the vapor in air (in mg/L); v_{wind} is the wind speed

The equations in Table 17.4 thus can be used in “spreadsheet” calculations, with “logic” statements to determine which of the short-distance or long-distance equations applies, to interpolate between values in the EPA Reference Tables [9].

In the above equations, w_v is the rate of vapor release (as gas or vapor, or as vapor from the surface of a pool) in pounds per second, M is the molecular weight of the gas or vapor, C is the concentration of interest in parts per million by volume, and v_w is the wind speed in feet/second.

17.3.2.6.2 Consequence Analysis for Toxicity Hazards

The EPA standard requires that the consequences of a toxic-material release be described in terms of

1. The population within a circle with its center at the point of the release and a radius determined by the distance to the endpoint as determined from the dispersion analysis (release rate, gas or vapor properties, toxic endpoint, and atmospheric conditions). The population is to be estimated to two significant digits. U.S. Census data are available on CD-ROM disks individually, by section of the country, or as a set of 11 from the U.S. Bureau of the Census [301-457-4100].
2. The presence of institutions (such as hospitals, nursing homes, retirement centers, schools, day-care centers, and prisons); parks and recreational areas (such as stadiums and swimming pools); and major commercial, office, and industrial buildings (such as shopping malls and industrial parks) within the circle. Some schools and hospitals are shown on U.S. Geological Survey maps, and the locations of other concentrations of population generally may be found on local street maps. The EPA standard does not require a determination of the population at these locations.
3. The presence of environmental receptors (such as national or state parks, forests, or monuments, wildlife sanctuaries, preserves, refuges, or areas, and Federal wilderness areas) within the circle and as identified on U.S. Geological Survey maps.

The current EPA standard does not require an estimation of the number of persons that might be injured, the types or severity of injuries, the areas of environmental receptors that might be damaged, or the types or severity of damage that might result from a release of hazardous material.

17.3.2.6.3 Risk-Mitigation Methods for Toxic Materials

Mitigation efforts can take several forms [6(G4), 6(G24), 20]. However, the EPA standard allows consideration only of “passive” mitigation systems (that function without human, mechanical, or other energy input) when evaluating “worst case” scenarios. For “alternative” scenarios, the proper functioning of both “passive” and “active” mitigation devices or equipment can be assumed. Typical “post-release” mitigation methods for the protection of personal are as follows, in an approximate decreasing order of effectiveness in each category:

1. Lower “source strength” (reduction in toxic vapor/gas concentration)
 - a. “Passive” methods for liquids [2]
 - (1) Reducing both the evaporation rate and out-of-doors concentration (by design, so that a spill would be within a confining building)
 - (2) Minimizing the surface area of a spill pool (by confining the spill in a diked area)
 - b. “Passive” methods for gases or vapors
 - (1) Reducing the out-of-doors concentration (by design, so that a release would be within a confirming building)
 - c. “Active” methods for liquids [9]
 - (1) Dilution of spilled liquid, if miscible
 - (2) Neutralization/detoxification of spilled liquid
 - (3) Spill-area-limitation devices
 - d. “Active” methods for gases or vapors [9]

where e is the vapor cloud explosion efficiency (0.1, for 10%), $W_{\text{flammable}}$ is the weight of flammable vapor (in pounds) in the vapor/air cloud, and $H_{\text{combustion}}$ is the heat of combustion (in BTU/pound).

Heats of combustion for the materials that are listed in the EPA guidance are given in Appendix A. Also included in Appendix A are the heats of combustion for several of the materials that are listed in the OSHA standard.

For the “worst case” evaluation, the weight of flammable material in a vapor cloud is assumed to be the total quantity of the substance that could be released from a vessel or pipeline. For liquids, this assumption infers that the liquid is above its atmospheric-pressure boiling point and that 100% flashing to vapor occurs. Also, the entire quantity of vapor is assumed to have concentrations between the lower and upper flammability limits and that the entire quantity explodes, with an energy-conversion efficiency e of 0.10. For mixtures, the weight-average heat of combustion would be used in the above equation.

For “alternative” evaluations, the weight of flammable material in a vapor cloud can be calculated as the gas-release or vapor-release rate multiplied by the estimated time required to stop the release. For liquid releases, the vapor-release rate would be calculated from the liquid-release rate multiplied by twice the flashing fraction (to account for aerosol vaporization) or, for liquids released below the boiling point, as the rate of vaporization from a pool multiplied by the estimated time required to cover or dilute the pool. Also, a lower energy-conversion efficiency (such as 0.03) can be used in the calculation.

The EPA guideline for evaluation of the “far-field” (distant) explosion hazards is based on a “TNT” [TriNitro Toluene] model. Evaluation of the “near-field” (within the vapor cloud, or near the explosion center) requires departure from the blast-pressure and blast-impulse curves for TNT or modification of the distance/quantity relationship [22].

17.3.2.7.2 Consequence Analysis for Explosion Hazards

The EPA standard requires that the consequences of a flammable material release be described in terms similar to those listed for toxicity hazards in Section 17.3.2.6.2 above.

17.3.2.7.3 Risk-Mitigation Methods for Flammable and Explosive Materials

Mitigation of the effects of releases of flammable gases or vapors, or liquids above the boiling point, at high rates is very limited. Further, the EPA standard allows consideration only of “passive” mitigation systems (that function without human, mechanical, or other energy input) when evaluating “worst case” scenarios. For “alternative” scenarios, the proper functioning of both “passive” and “active” mitigation devices or equipment can be assumed.

Typical “post-release” mitigation methods are as follows, in an approximate decreasing order of effectiveness in each category:

1. Lower “source strength” (reduction in vapor concentration)
 - a. “Passive” methods
[None would apply to releases of flammable gases, vapors, or liquids]
 - b. “Active” methods [6(G4)]
 - (1) Dispersion with existing fans or air curtains, etc.
 - (2) Water or chemical sprays
2. Lower “source duration” (reduction in vapor-cloud size)
 - a. “Passive” methods
 - (1) Excess-flow valves, to limit the duration of a high-rate leak
 - (2) Check valves, for protection against back-flow toward a leak
 - b. “Active” methods
 - (1) Leak-sensor-actuated block or shutoff valves
 - (2) Leak-sensor-actuated de-inventory valves
 - (3) Operator-controlled remote-operated shutoff valves
 - (4) Operator-controlled de-inventory to a scrubber, absorber, adsorber, or condenser
 - (5) De-inventory to a stack, for high-elevation release

vapors that have a molecular weight >30 or where the product of vapor pressure and molecular weight >500 mm Hg.

17.3.2.8.2 Consequence Analysis for Flash-Fire Hazards

The EPA standard does not require an offsite consequence analysis for flash fires unless the flammability endpoint (LFL) is outside the property boundary, or unless there are locations within the property boundary to which the public has routine and unrestricted access during or outside business hours.

If either of these situations could exist, the EPA standard recommends that the consequences of a flash fire be evaluated as an "alternative" scenario for a flammable-liquid release and be described in terms similar to those listed under Toxicity Hazards.

17.3.2.8.3 Risk-Mitigation Methods for Flash Fires

Mitigation efforts can take several forms [6(G4), 6(G24), 20]. For "alternative" scenarios, the proper functioning of both "passive" and "active" mitigation devices or equipment can be assumed.

Typical "post-release" mitigation methods are as follows, in an approximate decreasing order of effectiveness in each category:

1. Lower "source strength" (reduction in concentration)
 - a. "Passive" methods for liquids [2]
 - (1) Minimizing the surface area of a spill pool (by confining the spill in a diked area)
 - (2) Designing so that spills would occur in a building, which would have "explosion-proof" electrical equipment and no other ignition sources
 - b. "Passive" methods for gases or vapors
[None would apply to releases of flammable gases or vapors]
 - c. "Active" methods for liquids [9]
 - (1) Dilution of spilled liquid, if miscible
 - (2) Spill-area-limitation devices
 - (3) Ventilating a building in which a spill had occurred [The concentration above a spill would decrease approximately as the 0.22 power ($v^{0.78}/v$) of the air velocity over the spill]
 - d. "Active" methods for gases or vapors
 - (1) Water or chemical sprays
 - (2) Dispersion with air curtains, fans, etc.
2. Lower "source duration" (reduction in duration of release)
 - a. "Passive" methods for gases, vapors, or liquids
 - (1) Excess-flow valves, to limit the duration of a high-rate leak
 - (2) Check valves, for protection against back-flow toward a leak
 - b. "Active" methods for gases, vapors, or liquids
 - (1) Leak-sensor-actuated block or shutoff valves
 - (2) Leak-sensor-actuated de-inventory valves
 - (3) Operator-controlled remote-operated shutoff valves
 - (4) Operator-controlled de-inventory to a scrubber, absorber, adsorber, or condenser
 - (5) Applying spill-covering materials to liquid spills: foam; sheeting; floating granular materials; water (if less dense); adsorbent or reactive
 - (6) De-inventory to a stack for elevation above ignition sources
 - (7) Leak-stopping: patching, plugging, freezing
3. Reduced off-site effects of a flammable-material release
 - a. "Passive" methods
[None would apply to releases of flammable gases, vapors, or liquids]
 - b. "Active" methods

1. Lower "source strength" (reduction in concentration)
 - a. "Passive" methods for liquids or liquified gases [2]
 - (1) Minimizing the surface area of a spill pool (by confining the spill in a diked area)
 - (2) Designing so that spills would occur in a building, which would have "explosion-proof electrical equipment and no other ignition sources
 - c. "Active" methods for liquids and liquified gases [9]
 - (1) Dilution of spilled liquid, if miscible
 - (2) Spill-area-limitation devices (personnel wearing flash suits over Level A protective clothing)
 - (3) Ventilating a building in which a spill had occurred [The concentration above a spill would decrease approximately as the 0.22 power ($v^{0.78}/v$) of the air velocity over the spill]
 - (4) Water or chemical sprays
 - (5) Dispersion with air curtains, fans, etc.
2. Lower "source duration" (reduction in duration of release)
 - a. "Passive" methods for liquids or liquified gases
 - (1) Excess-flow valves, to limit the duration of a high-rate leak
 - (2) Check valves, for protection against back-flow toward a leak
 - b. "Active" methods for liquids or liquified gases
 - (1) Leak-sensor-actuated block or shutoff valves
 - (2) Leak-sensor-actuated de-inventory valves
 - (3) Operator-controlled remote-operated shutoff valves
 - (4) Operator-controlled de-inventory to a scrubber, absorber, adsorber, or condenser
 - (5) Applying spill-covering materials to liquid spills: foam; sheeting; floating granular materials; water (if less dense); adsorbent or reactive
 - (6) De-inventory to a stack for elevation above ignition sources
 - (7) Leak-stopping: patching, plugging, freezing
3. Reduced off-site effects of a flammable-material release
 - a. "Passive" methods for pool fires involving flammable liquids or liquefied gases
[None would apply to releases of flammable liquids or liquified gases]
 - b. "Active" methods for pool fires involving flammable liquids or liquified gases
 - (1) Minimize the probability of ignition, by shutting off all ignition sources: welding; vehicles; sparking electrical tools and other "non-explosionproof" electrical equipment; flares; incinerators and boilers (unless protected with flame arresters in the air inlets), actuated by a site-wide alarm
 - (2) Off-site alarms (audible; radio; television; local authorities) to "shelter in place" by taking refuge in structures and avoiding exposure to the thermal radiation.

Pre-release methods for minimizing the size of a hazardous-material release (rate and duration, or quantity) and/or the frequency of any such release involve recognition of potential hazards early in the design of a facility and then incorporating appropriate mitigation features in the design [6(G4), 7, 20, 21].

17.3.2.10 Pressure-Vessel-Burst Hazards Evaluation

The explosive bursting of a pressure vessel is not at present identified by the EPA as a likely cause of off-site injury or property damage. However, if a pressure vessel is large and the pressure within the vessel is very high, explosive rupture of the vessel can create blast pressures and impulses at considerable distances from the vessel. The following evaluation is for pressure vessels that contain gas or vapor, or where most of the volume is occupied by gas or vapor; evaluation of the explosive-

TABLE 17.6
Probability Relationships for Hazard Distances

Type of Injury	Probability of Injury		
	1%	50%	99%
First-degree (sunburn)	[Not determined]	$X_{\text{fireball}} = 5.6W_f^{0.49}$	[Not determined]
Second-degree (blisters)	[Not determined]	$X_{\text{fireball}} = 5.3W_f^{0.48}$	[Not determined]
Third-degree (fatality)	$X_{\text{fireball}} = 5.0W_f^{0.46}$	$X_{\text{fireball}} = 3.6W_f^{0.46}$	$X_{\text{fireball}} = 2.5W_f^{0.46}$

17.3.2.10.1.2 Flammable Contents

If the gas or vapor that is confined in a pressure vessel is flammable, there may be a fireball hazard in addition to the explosion hazard, particularly if the cause of vessel rupture is fire exposure or impact.

The EPA equation for the second-degree burn hazard distance at which the combination of thermal-radiation intensity and duration of exposure would correspond to 5000 watts/m² and 40 seconds, respectively, is (approximately)

$$X_{\text{fireball}} = 0.10H_{\text{combustion}}^{0.5}W_{\text{flammable}}^{0.43} \text{ feet} \quad (17.27)$$

where $H_{\text{combustion}}$ and $W_{\text{flammable}}$ are the heat of combustion and weight of flammable material, respectively, in BTU per pound and pounds.

The preceding equation was developed for fireballs in which some of the flammable material was in the form of aerosol and in which the mixing of flammable material with air might be significantly slower (thus, “rich” conditions within the fireball) as compared with that of a flammable gas or vapor. The energy effects would be similar, although the cloud burning time might be shorter, and the maximum diameter of the cloud might occur at a lower elevation (as a result of faster mixing of the gas or vapor with air).

Relationships for hazard distances as a function of probability of injury are listed in Table 17.6 [26].

The equations in Table 17.6 were developed for propane (which has a heat of combustion near 12,000 calories/gram). For other materials, the weight of flammable material would be multiplied by the ratio of the heat of combustion (in calories/gram) to 12,000.

17.3.2.10.2 Consequence Analysis for Pressure-Vessel-Burst Hazards

The extent of injury and property damage from an explosion depends on both the blast overpressure and the blast impulse at the point of interest [30]. Table 17.7 presents examples of overpressure and impulse combinations as a function of distance for an explosion having an energy equivalent of 10,000 pounds of TNT, together with the approximate limits of various types of injury and property damage.

The EPA standard requires that the consequences of a flammable material release be described in terms similar to those listed under Toxicity Hazards.

17.3.2.10.3 Risk-Mitigation Methods for Pressure-Vessel-Burst Hazards

There are no “passive” or “active” methods for mitigating the blast or missile effects of an explosion after an explosion has taken place, other than the self-preservation actions of persons turning and running away if there is any visual (speed of light) warning. For this reason, all practical measures should be taken to prevent explosions in the design and operation of high-pressure and exothermic processes; thus, “pre-release” mitigation. This could include barricading, both to reduce the pressure effects outside the barricade and to limit the number, size, and range of missiles [6(G4), 7, 20, 21].

impact or a runaway reaction. Ignition simultaneous with release of flammable contents is less likely if the cause of container rupture is a liquid-full condition and solar or ambient heating.

The consequences of exposure to a fireball resulting from a BLEVE can be determined as described in the previous section.

17.3.2.11.2 Risk-Mitigation Methods for BLEVEs

There are no “passive” or “active” methods for mitigating the blast or missile effects of a BLEVE-type explosion after the BLEVE has taken place, other than the self-preservation actions of persons turning and running away if there is any visual (speed of light) warning. However, the primary cause of BLEVE is fire exposure, and several precautions can be taken during fire-fighting to minimize the risk of injury from BLEVE:

1. Provide water-spray cooling of fire-exposed containers either by remote-operated “monitors” or “water cannons” or by mobile “water cannons” placed near the fire-exposed containers “early” in the fire, with fire-lighters then retreating to a safe distance. The time available to set up and aim mobile “water cannons” would depend on the size of the container, its design pressure, the size of relieving devices, and the volatility of the contents.
2. Ensure that there are no fire-fighters or spectators in the “axial” directions for horizontal cylindrical containers, and evacuate buildings in the axial directions, since a BLEVE frequently projects parts to great distances (up to a quarter mile) in an axial direction.
3. Ensure that there are no fire-fighters or spectators within a radius of about 1000 feet (for a 55-ton tank car) to minimize exposure to a BLEVE fireball.

Because there are no reasonable methods for mitigating risk following the occurrence of a BLEVE, all practical measures should be taken to prevent the causes of a BLEVE. This could include fixed water-spray systems over process vessels containing flammable liquids or which could be exposed to flammable-liquid fire, ensuring that relief devices do not direct vented flammable vapors onto the container, systems for diverting spilled flammable liquid to locations that would not expose process vessels, and public-address systems to warn persons to evacuate locations where loss of process control could lead to a BLEVE [14].

17.3.2.12 Jet-Fire Hazards Evaluation

It is unlikely that a release of flammable fluid could result in a jet fire that would cause an off-site thermal-radiation hazard, and the EPA guidelines [9] do not provide guidance concerning jet-fire hazards assessment. However, the length of a jet flame can be calculated from [7]

$$L_{jet} = 0.37[W_{flammable}H_{combustion}]^{0.46} \text{ feet} \quad (17.29)$$

where $W_{flammable}$ is the rate of release of the flammable material (in pounds/second).

The hazard radius is usually assumed to be twice the jet-flame length [12].

There are no “passive” methods for mitigating the risk of exposure to a jet fire other than the self-preservation action of turning and running away from the fire or taking refuge in the “shadow” of intervening equipment or a structure. “Active” methods would include stopping the flow of flammable fluid to the leaking equipment and de-inventorying the equipment to another container or to a stack or flare.

17.3.2.13 “Condensed-Phase” Detonation Hazards Evaluation

Detonation of a self-reactive material or mixture of materials results in blast effects that can be related to an energy-equivalent weight of TNT, for which there are good blast-effects data. The

17.3.4 EMPLOYEE PARTICIPATION

The OSHA regulations require employee participation in several aspects of process safety [1(c)]:

1. Specifically, the conduct and development of Process Hazard Analyses
2. Generally, the development of the other elements of the Process Safety Management Standard, which would include
 - a. Compilation of Process Safety Information, particularly concerning the evaluation of the consequences of deviations from safe upper and lower limits of operating conditions
 - b. Development and review of Operating Procedures
 - c. Development of the Training program and, specifically, the frequency of refresher training
 - d. Development of the Contractor Safety program, particularly concerning the evaluation of the performance of contractors in training employees to safely perform their jobs, in following the safety rules of the facility, and unique hazards presented by contract employer's work
 - e. Participation in Pre-Startup Safety Reviews
 - f. Development of Mechanical Integrity (maintenance) procedures, including inspections and tests and the frequencies of such inspections and tests
 - g. Development of safe work practices, including lockout/tagout, confined space entry, opening process equipment, facility-entrance procedures, and hot-work procedures
 - h. Development of the Management of Change procedure
 - i. Participation in Incident Investigations
 - j. Development of Emergency Plans
 - k. Participation in Compliance Audits

A written plan of action concerning Employee Participation is required. Also, all of the information and the results of analyses, investigations, and audits are to be made available to employees and their representatives.

17.3.5 PROCESS SAFETY INFORMATION

The OSHA and EPA require a compilation of Process Safety Information concerning the regulated chemicals and the processes in which they are employed [1(d), 2(65)]. Although Material Safety Data Sheets (MSDS) may serve as resources for this information, it should be recognized that some of the quantitative data that may be important to hazards analysis are not at present required by the pertinent standard [40]. In particular, quantitative thermal-stability (self-reactivity), incompatibility, and corrosivity data are frequently not found in the MSDS publications shipped with chemicals; further, some materials that are considered to be "stable" by manufacturers and distributors are not stable (can decompose, polymerize, form peroxides, auto-oxidize, or auto-ignite) at the temperatures that are frequently employed or accidentally occur in chemical processes [33]. Under the "general duty" clause [41], the employer would be responsible for determining the degree of stability or regions of instability of chemicals used in processes.

17.3.6 PROCESS HAZARDS ANALYSIS

A Process Hazards Analysis (PHA) is described as [1(C)]:

1. "An organized and systematic effort to identify and analyze the significance of potential hazards associated with the processing or handling of highly hazardous chemicals."

The employer is obliged to determine a priority order for the analysis of processes involving regulated materials and to use an appropriate method [1(e), 2(67)]. The prioritizing should consider (1) the potential severity of an incident, (2) the number of potentially affected employees, (3) the operating history of the process (such as the frequency of incidents), and (4) the age of the process. The method selection should consider (1) the amount of existing knowledge about the process, (2) type of operation (batch, semi-batch, or continuous), (3) size and complexity of the process, and (4) previous operating experience with the process (length of time, and frequency of hazardous or "near-miss" incidents).

In addition to the Process Hazards Analysis, the following are to be addressed in the PHA report:

1. Previous incidents with potential for catastrophic consequences.
2. Applicable engineering and administrative controls.
3. Setting of the facility.
4. Human factors.
5. A qualitative evaluation of safety and health effects of failure of controls.

Updating and revalidation of Process Hazards Analyses is required at least every 5 years after May 26, 1997, for OSHA and after June 21, 1999, for the EPA.

17.3.7 OPERATING PROCEDURES

The OSHA and EPA require that written operating procedures be developed and implemented for processes in which regulated chemicals are used. These procedures are to provide guidance for operators for each step of operation, including [1(f), 2(69)]:

1. Initial startup of a process, following construction.
2. Startup following a normal shutdown, a shutdown for maintenance, or an emergency shutdown.
3. Normal operations.
4. Temporary operations, with modified materials, equipment, or conditions.
5. Emergency operations, to regain control of a process.
6. Emergency shutdown, if control of a process is not recoverable.
7. Normal shutdown.

These procedures are to describe the steps to be performed, how the steps are to be performed, the desired values of the operating variables at each step, the limits for process variables, the reasons why the limits are not to be exceeded, steps to be taken to correct deviations from the desired operating conditions, the data to be recorded, the samples to be collected, and the safety and health precautions to be taken. Of particular importance are the conditions under which emergency shutdown is required, and the assignment of shutdown responsibility to qualified operators to ensure that emergency shutdown is executed in a safe and timely manner.

The operating procedures also should include precautions to ensure quality control and inventory control, and descriptions of safety systems and their functions. The operating procedures should be reviewed and corrected to reflect current operating practices or validated at least annually.

17.3.8 TRAINING

Initial and periodic refresher re-training (at least every 3 years) are required by the OSHA and EPA standards. This training is to ensure that each employee involved in operating a process (1) understands and adheres to the current operating procedures of the process (including emergency shutdown); (2) understands the specific safety and health hazards; (3) can perform the safe work

TABLE 17.9
"Non-Routine" Work Regulations

Nonroutine Work	References	Examples
Hot work (welding, etc.)	[25] 29 CFR 1910.252	Lees [7], p. 21/28
Lockout/tagout	[25] 29 CFR 1910.147	"Hazards in the Workplace" [41], p. 39
Confined-space entry	[25] 29 CFR 1910.146	"Hazards in the Workplace" [41], p. 17
Hot work (electrical)	[25] 29CFR 1910.269(j; 1); 333(a)(2); (c)(ii); 335	"Hazards in the Workplace" [41], p. 97
Personal protective equipment	[25] 29 CFR 1910.132; 120	"Personal Protective Equipment" [41], p. 5

17.3.12.2 Opening Process Equipment or Piping

It is often necessary to open process equipment or piping for cleaning, maintenance, or modification. The "work-permit" procedure should address the following:

1. Establishing the levels and areas of authorizations (operations, maintenance; landlord, supervisor, site manager) required for the work to proceed.
2. Evaluating the hazards of the material(s) that might be in the equipment or piping.
3. Positively identifying the equipment or piping to be opened.
4. Determining whether the equipment or piping (a) can be and has been drained and depressurized, or (b) cannot be or has not been drained or depressurized, including a study of piping to identify undrained low points, unvented high points, and potential syphons.
5. Determining whether the equipment or piping has been flushed, purged, or evacuated.
6. Locking shut and tagging valves, using blind-flanges, or disconnecting sources of hazardous material associated with the equipment or piping to be opened, locking open vent valves, and locking off energy sources such as pumps, compressors, and electrical tracing.
7. Safeguarding against external hazards, such as ignition sources if the piping or equipment could contain flammable material, and sealing off drains or other possible sources of noxious liquids, vapors, or gases.
8. Preparing a safe working position, through proper use of platforms, scaffolds, ladders, safety harness, ventilation, etc.
9. Isolating the area, by barricades or shields, to exclude inadequately protected persons, particularly at lower elevations.
10. Preparing or maintaining exits from the work area, in event of a release of hazardous material.
11. Preparing for accidental releases or spills from the equipment or piping to be opened, by establishing spill control, having fire extinguishers ready, etc. ("contingency planning").
12. Ensuring the presence and testing of safety showers, eyewash fountains, or other washing or flushing facilities.
13. Establishing the types and degree of protection that should be worn for "drained" and "undrained" equipment or piping, considering the flammability, corrosivity, toxicity, thermal, and pressure hazards and quantity of material that might remain in the equipment or piping.
14. Providing for one or more standby "buddy" persons, who is equally protected, at a safe distance from the work area but maintaining visual contact with the worker.
15. Developing and implementing the procedure for gradually loosening bolts or connections, with periodic tests for "residual" pressure, to avoid exposure from unexpected sprays, pressure impacts, or other discharges.

1. Sign-in and sign-out of visitors, with dates, times, printed name, and signature.
2. A warning statement concerning the hazardous materials that are used in the area to be visited.
3. Protective-equipment requirements (such as eye and head protection).
4. The layout of the area (using, for example, a map of the area).
5. Whether or not an authorized employee is required to escort the visitor at all times in the area.
6. An alarm provided to initiate evacuation, and the desired response to such an alarm.

17.3.12.5 Hot-Tapping

Hot-tapping is the drilling of a hole into, and fitting a branch on, a pipe while it is still on line, by welding or “strapping” a sleeve on the pipe. The “work-permit” procedure for hot-tapping should address the following [7, 44]:

1. Establishing the levels and areas of authorizations (operations, maintenance; landlord, supervisor, site manager) required for the work to proceed.
2. Establishing the pipeline fluid conditions: liquid at temperatures below the atmospheric-pressure boiling point; liquified gas at temperatures above the atmospheric-pressure boiling point; or gas, temperature, and pressure.
3. Establishing the pipe material, the wall thickness, and the condition of the pipe (particularly internal or external corrosion); and the effect of welding on the pressure-resistance strength of the pipe, if welding is to be performed.
4. Establishing the type of fitting to be placed on the piping and the attaching method(s), and whether or not reinforcing pads are required.
5. Positively identifying the piping to be hot-tapped.
6. Preparing a safe working position, through proper use of platforms, scaffolds, ladders, safety harness, ventilation, etc.
7. Isolating the area, by barricades or shields, to exclude inadequately protected persons.
8. Eliminating external hazards, such as ignition sources if the piping contains flammable material, and sealing off drains or other possible sources of noxious liquids, vapors, or gases.
9. Preparing and maintaining access to and exits from the work area, in the event of a release of hazardous material.
10. Preparing for accidental releases or spills from the piping to be hot-tapped, by establishing spill control, having fire extinguishers ready, etc. (“contingency planning”).
11. Ensuring the presence of, and testing of, safety showers, eyewash fountains, or other washing or flushing facilities.
12. Establishing the types and degree of protection (eye, face, head, hands, feet, and body) that should be worn for the work, considering for flammability, corrosivity, toxicity, thermal, and pressure hazards.
13. Providing for one or more standby “buddy” persons, who is equally protected, at a safe distance from the work area but maintaining visual contact with the worker.

17.3.13 MANAGEMENT OF CHANGE

The development and implementation of a procedure for the control of changes in process chemicals, technology, equipment, and procedures are required by OSHA and EPA [1(1), 2(75)]. Replacement of a defective component “in kind” (same manufacturer, model, and size, and other characteristics) would not require following the procedure. Replacement of a defective, obsolete, or obsolescent device with a “similar” device would require a “minimal” procedure, with limited authorizations.

TABLE 17.10
OSHA and EPA Emergency Requirements

Requirement	OSHA Standard	EPA Standard
Procedures and measures for emergency response	Emergency escape procedures (types of evacuation) and routes	Provide to the local emergency planning committee
Procedures for employees who remain to operate critical operation before they evacuate	Required	Not required
Procedures to account for all employees after emergency evacuation	Required	Not required
Rescue and medical duties for those employees who are to perform them	Required	Not required
First-aid and emergency medical treatment of persons exposed to regulated substances	Required [29 CFR 1910.119(f)(1)(iii)(C)]	Documentation required (for off-site treatment)
Preferred means of reporting fires and other emergencies	Required (to other employees)	Required (to public and local emergency response agencies)
Names or titles of persons who can be contacted for further details	Required	Required [40 CFR 68.15(b)]
Establish an alarm system, with distinctive signals for brigade members and other purposes	Required [29 CFR 1910.165]	Not required
Training for evacuation aides	Those employees who are to assist in safe and orderly emergency evacuation	Not required
Training for all employees	Initially and following any changes	Required
Procedures for handling small releases	Required	Not required
Hazardous waste operations and on-site emergency response requirements	Required unless releases are "incidental" and can be absorbed, neutralized, or otherwise controlled at the time of release by employees, and where there is no "reasonable possibility" for employee exposure to safety or health hazards.	Not required
Emergency response equipment	Required: Annual testing of alarm (or every two months if not a "supervised" system)	Required: Inspection, testing, and maintenance of emergency response equipment
Procedures to review and update the emergency response plan	Not specifically required	Required
Ensure that employees are informed of changes to the plan	Required	Required

The EPA requires, in addition, periodic audits by the implementing agency, such as the state or local air permitting agency. The frequency of such audits would be based on (1) accident history, (2) quantities of regulated substances, (3) proximity to public receptors, and (4) hazards identified in the Risk Management Program [2(220)].

17.3.17 TRADE SECRETS

The OSHA standard requires that all pertinent information be provided to employees involved in (1) compiling Process Safety Information, (2) performing Process Hazards Analysis, (3) developing

TABLE OF SYMBOLS

English units, with °K.

A_p	Area of the pool (the area of a dike, or $[\pi/4] D_p^2$ for an unconfined pool, in feet ²).
C	Concentration of interest, in parts/million, by volume.
$[C]$	Number of carbon atoms in the molecule.
C_d	Coefficient of discharge, which is a function of Reynold's number (~ 0.62); dimensionless.
C_L	Heat capacity of the liquid or liquified gas or vapor, in BTU/pound/°F.
C_p	Specific heat of a fluid at constant pressure, in BTU/pound/°F.
D_h	Diameter of the hole, in inches.
D_p	Diameter of the pool, in feet.
D_p	Inside diameter of the pipe, in inches.
D_T	Diameter of the vertical cylindrical tank, in feet.
f	Fanning friction factor; dimensionless.
g_c	Conversion constant (32.2 ft/lb _m /lb _f /sec ²).
G_p	Volume of the liquid in the pool, in gallons.
$[H]$	Number of hydrogen atoms in the molecule.
H_c	Heat of combustion of the flammable material, in BTU/pound.
$H_{L,Pb}$	Enthalpy of the liquid at the container-burst pressure, in BTU/pound.
$H_{L,14.7}$	Enthalpy of the liquid at atmospheric pressure, in BTU/pound.
$H_{V,14.7}$	Enthalpy of the vapor at atmospheric pressure, in BTU/pound.
H_v	Latent heat of vaporization, in BTU/pound.
K	Slope of a line on probability graph paper.
k	Specific-heat ratio; dimensionless.
L	Length of the pipe from the source container to the open end, in feet.
LFL	Lower flammable limit, in volume-percentage.
M	Molecular weight of the gas or vapor.
N_M	Mach number for gas or vapor flow; dimensionless.
N_{Re}	Reynold's number; dimensionless.
$[O]$	Number of oxygen atoms in the molecule.
OB	Negative or positive oxygen balance.
P_a	Pressure outside the equipment (usually 14.7 psia).
P_b	Bursting pressure of the container, in psia.
P_f	Final pressure (usually 14.7 psia).
P_g	Gauge pressure in the vapor space above the liquid, in psig.
P_o	Initial absolute pressure within the equipment, in psia.
P_o	"Virtual" absolute pressure, for subsonic flow, in psia.
P_s	Saturation vapor pressure of the flashing liquified gas at the temperature of interest, in psia.
q	Thermal-radiation intensity, in BTU/second/feet ² .
R	"Ideal gas law" constant, which is equal to 19.32 psia/feet ³ /lb-mole/°K.
r_c	Critical pressure ratio, given by $(2/[k + 1])^{(k/(k-1))}$.
RH	Relative humidity, in %.
S	Entropy value (similar to values of enthalpy H), in BTU/lb/°F.
$[S]$	Number of sulfur atoms per molecule.
$[Si]$	Number of silicon atoms per molecule.
t	Time required to empty a container of fluid, in seconds.
T_a	Ambient temperature, in °K (typically about 298°K [25°C/77°F]).
T_b	Atmospheric-pressure boiling point, in °K.
T_c	Critical temperature, in °K.
T_f	Final temperature, in °K.
T_p	Temperature of the liquid in the pool, in °K.
T_o	Initial temperature, in °K.
v	Velocity of liquid or gas through a pipe, in feet/second.
vp	Vapor pressure, in mm Hg.

APPENDIX A

OSHA AND EPA LISTED CHEMICALS

The EPA and OSHA regulations [A-1, A-2, and A-3] apply to facilities from which a release of hazardous material could occur, at or above the quantities specified, as shown in **bold** in Table 17.A.1. Also shown are the Immediately Dangerous to Life and Health [IDLH] concentrations (for 30-minute exposure) [A-4]; the Lower Flammable Limits and Heats of Combustion for combustible materials; and the EPA toxic, thermal-radiation, and overpressure “endpoints” for public-exposure evaluations. “N/L” indicates that the chemical is not listed in the pertinent document. Estimated values are shown with a superscript (°). Where no inhalation-toxicity data were available, the oral dose that caused 50% fatalities is shown only to indicate qualitatively the systemic toxicity (for example, an oral LD50 of 1000 mg/kg would be considered relatively nontoxic). The data are for pure chemicals, except where otherwise indicated, that is, without added diluents. Additional hazardous-properties information can be obtained via the “Sax No.” [A-6].

REFERENCES

- A-1. U.S. Department of Labor, Occupational Safety and Health Administration. “Process Safety Management of Highly Hazardous Chemicals.” Title 29, Subtitle B, Chapter XVII, Part 1910, Subpart H, Paragraph 119, Code of Federal Regulations [29 CFR 1910.119], vol. 57, no. 36, p. 6403; Federal Register, February 24, 1992.
- A-2. U.S. Environmental Protection Agency. “Risk Management Program Rule,” Title 40, Part 68, Subpart F, Code of Federal Regulations [40 CFR 68], vol. 61, p. 31717; Federal Register, June 20, 1996.
- A-3. U.S. Environmental Protection Agency. “List of Regulated Substances and Threshold Quantities for Accidental Release Prevention.” Title 40, Part 68, Subpart C, Paragraph 130, Tables 1–4, Code of Federal Regulations [40 CFR 68], vol. 59, no. 20, p. 4495; Federal Register, January 31, 1994; rev. October 1997.
- A-4. U.S. Department of Health and Human Services, National Institute for Occupational Safety and Health. “Pocket Guide to Chemical Hazards,” June 1994.
- A-5. American Conference of Governmental Industrial Hygienists. “Threshold Limit Values for Chemical Substances,” 1995.
- A-6. Lewis, R.J. *Sax's Dangerous Properties of Industrial Materials*. 9th ed., New York: Van Nostrand Reinhold, 1996.
- A-7. U.S. Department of Labor, Occupational Safety and Health Administration. “Hazard Communication.” Title 29, Subtitle B, Chapter XVII, Part 1910, Subpart Z, Paragraph 1200(c), Code of Federal Regulations [29 CFR 1910.1200]; Federal Register, July 1, 1995.
- A-8. National Fire Protection Association. *Fire Protection Guide to Hazardous Materials*. 11th ed. Quincy, MA: NFPA, 1994.
- A-9. U.S. Environmental Protection Agency. “Technical Guidance for Hazards Analysis – Emergency Planning for Extremely Hazardous Substances”, December 1987: 2–13, Appendix C, .
- A-10. American Industrial Hygiene Association. *Emergency Response Planning Guidelines*. Fairfax, VA: AIHA, 1995.

TABLE 17.A.1 (Continued)
OSHA and USEPA Listed Chemicals

OSHA Highly Hazardous Chemical or EPA Regulated Substance	"Sax" No.	Mole Wgt.	OSHA Threshold Quantity (pounds)	IDLH Conc. (ppm)	EPA Threshold Quantity (pounds)	Toxic Endpoint		Lower ^c Flammable Limit (v%)	Heat of Comb. (cal/g)
						(mg/l)	(ppm)		
Carbonyl fluoride	CCA500	66.0	2500	N/L	N/L	0.0054	2 ^j		
Cellulose nitrate >12.6% n	CCU250	504.3	2500	N/L	N/L	Oral: 5000 mg/kg		Solid	
Chlorine	CDV750	70.9	1500	10	2500	0.0087	3	Not combust.; oxidizer	
Chlorine dioxide	CDW450	67.5	1000	5	1000	0.0028	1	10	
Chlorine monoxide	N/L	86.9	10,000 ^a	23,500 ^d	10,000 (Flamm.)	8.4	2350 ^h	23.5	240
Chlorine pentafluoride	CDX250	130.4	1000	N/L	N/L	0.3	57 ⁱ	Not combust.; oxidizer	
Chlorine trifluoride	CDX750	92.4	1000	20	N/L	0.0038	1 ^g	Not combust.; oxidizer	
Chloro diethylaluminum	DHI885	110.6	5000	N/L	N/L	0.11	24 ^j	Pyro.	
Chloro dinitrobenzene	CGM000	202.6	5000	N/L	N/L	Oral: 780 mg/kg		2.0	750
Chloroform	CHI500	119.4	N/L	500 Ca	20,000	0.49	100	Not combust.	
Bischloro methyl ether	BIK000	115.0	100	Ca	1000	0.00025	0.05	5.7 ^e	
Chloromethyl methylether	CIO250	80.5	500	Ca	5000	0.0018	0.5	4.6 ^e	
Chloropicrin	CKN500	164.4	500	2	N/L	0.0013	0.2 ^g	Not combustible	
Chloropicrin/methyl bromide	N/L	Mix	1500	N/L	N/L	Vendor's MSDS		Not combustible	
Chloropicrin/methyl chloride	N/L	Mix	1500	N/L	N/L	Vendor's MSDS			
2-chloro,1-propylene	CKS000	76.5	10,000 ^a	4500 ^d	10,000 (Flamm.)	1.4	450 ^h	4.5	5520
1-chloro,1-propylene	PMR750	76.5	10,000 ^a	4500 ^d	10,000 (Flamm.)	1.4	450 ^h	4.5	5520
Crotonaldehyde	COB250	70.1	10,000 ^b	50	20,000	0.029	10	2.1	7730
Cumene hydroperoxide	IOB000	152.2	5000	N/L	N/L	0.012	2 ⁱ	1.0 ^e ; expl.	
Cyanogen	COO000	52.0	2500	N/L	10,000 (Flamm.)	0.021	10 ⁱ	6.0	5055
Cyanogen chloride	COO750	61.5	500	N/L	10,000	0.03	12	Not combustible	
Cyanuric fluoride	TKK000	135.1	100	N/L	N/L	0.0002	0.03 ⁱ	5.1 ^e	
Cyclohexylamine	CPF500	99.2	10,000 ^b	N/L	15,000	0.16	40	1.5	
Cyclopropane	CQD750	42.1	10,000 ^a	2400 ^d	10,000 (Flamm.)	0.41	240 ^h	2.4	11,175
Diacetyl peroxide >70%	ACV500	118.0	5000	N/L	N/L	Oral: 283 mg/kg		Oxid.; expl.	
Diazomethane	DCP800	42.1	500	2	N/L	0.00034	0.2 ^h	6.7 ^e	
Dibenzoyl peroxide	BDS000	242.2	7500	N/L	N/L	Oral: 5700 mg/kg		Oxid.; expl.	
Diborane	DDI450	27.7	100	15	2500	0.0011	1	0.8	
Teritributyl peroxide	BSC750	146.3	5000	N/L	N/L	Oral: 10,200 mg/kg		1.0 ^e ; oxid.	

TABLE 17.A.1 (Continued)
OSHA and USEPA Listed Chemicals

OSHA Highly Hazardous Chemical or EPA Regulated Substance	"Sax" No.	Mole Wgt.	OSHA Threshold Quantity (pounds)	IDLH Conc. (ppm)	EPA Threshold Quantity (pounds)	Toxic Endpoint		Lower ^c Flammable Limit (v%)	Heat of Comb. (cal/g)
						(mg/l)	(ppm)		
Hydrogen bromide	HHJ000	80.9	5000	30	N/L	0.0099	3 ^h	Not combustible	
Hydrogen chloride	HHX000	36.5	5000	50	5000	0.030	20	Not combustible	
Hydrogen cyanide	HHH000	27.0	1000	50	2500	0.011	10	5.6	5970
Hydrogen fluoride	HHU500	20.0	1000	30	N/L	0.016	20	Not combustible	
Hydrogen peroxide >52 wt%	HIB000	34.0	7500	75	N/L	0.010	7.5 ^h	Not combust.; oxidizer	
Hydrogen selenide	HIC000	81.0	150	1	500	0.00066	0.2	6.7 ^e	
Hydrogen sulfide	HIC500	34.1	1500	100	10,000	0.042	30	4.0	
Hydroxylamine	HLM500	33.0	2500	N/L	N/L	Oral: 29 mg/kg		Solid: expl.	
Iron pentacarbonyl	IHG500	195.9	250	N/L	2500	0.00044	0.05	Not combustible	10,940
Isobutane	MOR750	58.1	10,000 ^a	1800 ^d	10,000 (Flamm.)	0.43	180 ^h	1.8	
Isobutyronitrile	IIX000	69.1	<10,000 ^b	N/L	20,000	0.14	50	1.9 ^e	
Isopentane	EIK000	72.2	10,000 ^a	1400 ^d	10,000 (Flamm.)	0.41	140 ^h	1.4	10,780
Isoprene	IMS000	68.1	10,000 ^a	1500 ^d	10,000 (Flamm.)	0.42	150 ^h	1.5	10,510
Isopropylamine	INK000	59.1	5,000	750	10,000 (Flamm.)	0.18	75 ^h	2.0	8760
Isopropyl chloride	CKQ000	78.5	10,000 ^a	2800 ^d	10,000 (Flamm.)	0.90	280 ^h	2.8	5690
Isopropyl chloroformate	IOL000	122.6	<10,000 ^b	N/L	15,000	0.1	20	2.7 ^e	
Ketene	KEU000	42.0	100	5	N/L	0.00086	0.5 ^h	5.2 ^e	5860
Methacrylaldehyde	MGA250	70.1	1000	N/L	N/L	0.036	12.5 ⁱ	2.2 ^e	
Methacryloyl chloride	MDN899	104.5	150	N/L	N/L	0.0006	0.14 ⁱ	2.7 ^e	
Methacryloyl oxyethyl isocyanate	IKG700	155.2	100	N/L	N/L	0.00025	0.04 ⁱ	1.5 ^e	
Methane	MDQ750	16.0	10,000 ^a	5000 ^d	10,000 (Flamm.)	0.33	500 ^h	5.0	12,010
Methyl acrylonitrile	MGA750	67.1	250	N/L	10,000	0.0027	1	2.1 ^e	
Methylamine, anhydrous	MGC250	31.1	1000	100	10,000 (Flamm.)	0.13	100 ^h	4.9	7540
Methyl bromide	MHR200	95.0	2500	250 Ca	N/L	0.78 ^f	200	Not combustible	
Methyl butene	MHT000	70.1	10,000 ^a	1500 ^d	10,000 (Flamm.)	0.43	150 ^h	1.5	10,680
Methyl chloride	MIF765	50.5	15000	2000 Ca	10,000	0.82	400	8.1	3250
Methyl chloroformate	MIG000	94.5	500	N/L	5000	0.0019	0.5	7.4 ^e	
Methyl ether	MIW500	46.1	10,000 ^a	3400 ^d	10,000 (Flamm.)	0.64	340 ^h	3.3	6920
Methyl fluoroacetate	MKDOO0	92.1	100	N/L	N/L	0.00025	0.07 ⁱ	3.9 ^e	
Methyl fluoro-sulfate	MKG250	114.1	100	N/L	N/L	0.00023	0.05 ⁱ	8.6 ^e	

TABLE 17.A.1 (Continued)
OSHA and USEPA Listed Chemicals

OSHA Highly Hazardous Chemical or EPA Regulated Substance	"Sax" No.	Mole Wgt.	OSHA Threshold Quantity (pounds)	IDLH Conc. (ppm)	EPA Threshold Quantity (pounds)	Toxic Endpoint		Lower ^c Flammable Limit (v%)	Heat of Comb. (cal/g)
						(mg/l)	(ppm)		
Propane	PMJ750	44.1	10,000 ^a	2100 ^d	10,000 (Flamm.)	0.38	210 ^h	2.0	11,120
Propargyl bromide	PMN500	119.0	100	N/L	N/L	0.0000 ^f	0.01	3.4 ^e ; Expl.	
Propionitrile	PMV750	55.1	<10,000 ^b	N/L	10,000	0.0037	1.5	2.6 ^e	
Propyl chloroformate	PNH000	122.6	<10,000 ^b	N/L	15,000	0.010	2	2.7 ^e	
Propylene	PMO500	42.1	10,000 ^a	2000 ^d	10,000 (Flamm.)	0.34	200 ^h	2.0	10,980
Propyleneimine	PNL400	57.1	<10,000 ^b	100 Ca	10,000	0.12	50	2.3 ^e	
Propylene oxide [epoxypropane]	PNL600	58.1	<10,000 ^b	400 Ca	10,000	0.59	250	2.3	
Propyl nitrate	PNQ500	105.1	2500	500	N/L	0.21	50 ^h	2.0; Expl.	
Propyne [methyl acetylene]	MPX590	40.1	10,000 ^a	1700 ^d	10,000 (Flamm.)	0.28	170 ^h	1.7	11,080
Sarin ["gb" nerve gas]	IPX000	140.1	100	N/L	N/L	0.0001 ^f	0.01	1.9 ^e	
Selenium hexafluoride	SBS000	193.0	1000	2	N/L	0.0016	0.2 ^h	Not combustible	
Silane	SDH575	32.1	10,000 ^a	1400 ^d	10,000 (Flamm.)	0.18	140 ^h	Pyro.	10,630
Stibine [antimony hydride]	SLQ000	124.8	500	5	N/L	0.0026	0.5 ^h	6.8 ^e	
Sulfur dioxide, liquid	SOH500	64.1	1000	100	5,000	0.0078	3	Not combustible	
Sulfur pentafluoride	SOQ450	254.1	250	1	N/L	0.0010	0.1 ^h	Not combustible	
Sulfur tetrafluoride	SOR000	108.1	250	N/L	2500	0.0092	2	Not combustible	
Sulfur trioxide [as sulfuric acid]	SORS00	80.1	1000	0.3	10,000	0.010	3	Not combustible	
Tellurium hexafluoride	TAK250	241.6	250	1	N/L	0.001	0.1	Not combustible	
Tetrafluoroethylene	TCH500	100.0	5000	10,000 ^d	10,000 (Flamm.)	4.1	1000 ^h	11.0	310
Tetrafluorohydrazine	TCI000	104.0	5000	N/L	N/L	0.002	0.5 ⁱ	Explosive	
Tetramethyl lead	TDR500	267.3	1000	4.7	10,000	0.0040	0.4	1.4 ^e	
Tetramethyl silane	TDV500	88.2	10,000 ^a	1300 ^{d,e}	10,000 (Flamm.)	0.047	130 ^h	1.3 ^e	10,010
Tetra nitromethane	TDY250	196.0	<10,000 ^b	4	10,000	0.0040	0.5	Oxid.; Expl.	
Thionyl chloride	TFL000	119.0	250	N/L	N/L	0.024	5 ⁱ	Not Combust.; Oxidizer	
Titanium tetrachloride	TGH350	189.7	N/L	N/L	2500	0.020	2.5	Not Combustible	
Toluene diisocyanate	TGM740	174.2	<10,000 ^b	2.5 Ca	10,000	0.0070	1	0.9	
Trichloro chloromethyl silane	CIY325	183.9	100	N/L	N/L	0.0003 ^f	0.04	8.8 ^e	
Trichloro dichlorophenyl silane	DGF200	280.4	2500	N/L	N/L	0.008	0.7	2.2 ^e	
Trichloro silane	TID500	135.5	5000	7000 ^d	10,000 (Flamm.)	3.9	700 ^h	7.0	900
Trifluoro chloroethylene	CLQ750	116.5	10,000	8400 ^d	10,000 (Flamm.)	4.0	840 ^h	8.4	440

APPENDIX B

FIRE-HAZARD PROPERTIES OF OSHA AND EPA LISTED HAZARDOUS MATERIALS

Flammable Liquid	Liquid Density (g/ml)	Boiling Point (°C)	Heat of Combust. (cal/g)	Heat of Vapor (cal/g)	Specific Heat (cal/g/°C)	$H_v/H_v+C_L(T_b-T_a)$ for $T_a=25^\circ\text{C}$ (dimensionless)	Burning Rate (kg/sec-m ²)	Rate/Ratio (kg/sec-m ²)
Ammonia	0.82	33.3	5400	328	1.10	16.5	Not Determined	—
Butane	0.57	0.5	10,970	92	0.55	119	0.078	0.00065
Carbon Disulfide	1.26	46	3240	85	0.24	36	Not Determined	—
Cyclohexane	0.78	80.7	11,160	86	0.55	89	0.090	0.00101
DiMethyl Amine	0.68	6.8	8595	140	0.73	61	Not Determined	—
Ethane	0.54	88.6	11,400	117	0.57	97	0.122	0.00125
Ethyl Chloride	0.89	12.3	4780	92	0.37	52	Not Determined	—
Ethylene Oxide	0.88	10.6	6850	139	0.48	49	Not Determined	—
Ethyl Ether	0.71	34.5	8110	90	0.52	90	0.085	0.00094
Hydrogen	0.07	252.9	28,790	107	2.32	269	0.017	0.00006
Hydrogen Cyanide	0.69	26	5970	272	0.62	22	Not Determined	—
Methane	0.42	161.5	12,010	122	0.83	98	0.078	0.00079
Pentane	0.63	36	10,730	92	0.53	116	0.076	0.00065
Propane	0.49	42.1	11,120	102	0.58	109	0.099	0.00091
TetraFluoro-Ethylene	1.52	75.9	310	40	0.28	7.8	Not Determined	—
Vinyl Chloride	0.91	13.3	2480	100	0.30	25	Not Determined	—

References: SFPE "Handbook" [25], 2–50; NFPA *Handbook* [26], 21–37.

24. U.S. Department of Labor, Occupational Safety and Health Administration. "Occupational Safety and Health Standards." Title 29, Subtitle B, Chapter XVII, Part 1910, Subpart I, of the Code of Federal Regulations, 29 CFR 1910.38(a) and 29 CFR 1910.132; July 1995.
25. Prugh, R. W. "Quantitative Evaluation of Fireball Hazards", *Process Safety Progress* 13(2) (April 1994): Table II.
26. Society of Fire Protection Engineers. *Handbook of Fire Protection Engineering*. Bethesda, MD: SFPE, 1988: 2–54, 2–61, 2–63, 2–83.
27. National Fire Protection Association. *Fire Protection Handbook*. 16th ed. Quincy, MA: NFPA, 1986: 21–37.
28. U.S. Army. "Structures to Resist the Effects of Accidental Explosions." Technical Manual TM 5–1300. Hyattsville, MD: USACE, 1990: 2–11, 2–13; Figures 2-7, 2-15; Table 2-1.
29. Prugh, R.W. "The Effects of Explosive Blast on Structures and Personnel" (paper 4c). In the *Proceedings of the 32nd Loss Prevention Symposium*, March 10, 1998.
30. Prugh, R. W. "Evaluation of Unconfined Vapor Cloud Explosion Hazards." In *International Conference on Vapor Cloud Modeling*, November 4, 1987: 720.
31. U.S. Army. *Engineering Design Handbook – Explosives Series – Properties of Explosives of Military Interest*. AMCP 706-177 (AD-764-340). Hyattsville, MD: USACE, 1971: 4; and individual compounds.
32. Meyer, R. *Explosives*. 3rd ed. Berlin: Wiley-VCH, 1987: 255; and individual compounds.
33. Urben, P.G. *Bretherick's Handbook of Reactive Chemical Hazards*. 5th ed., vols. 1, 2. New York: Butterworth-Heinemann, 1995: 74.
34. American Society of Testing and Materials. *Chemical Thermodynamic and Energy Release Evaluation [CHETAH]*. Version 7.0. West Conshohocken, PA: ASTM, 1994.
35. U.S. Army. *Engineering Design Handbook – Principles of Explosive Behavior*. AMCP 706-180. Hyattsville, MD: USACE, 1972: 3–2.
36. U.S. Department of Transportation. "Hazardous Materials Regulations." Title 49, Subtitle B, Chapter 1, Subchapter C, Code of Federal Regulations, 49 CFR 172.101, 49 CFR 173.50, and 49 CFR 173.21(j); October 1995.
37. Manufacturing Chemists Association (now Chemical Manufacturers Association). *Case Histories of Accidents in the Chemical Industry*. Vols. 1–4. Washington, DC: MCA, 1962, 1966, 1969, 1975.
38. Marsh & McLennan Protection Consultants. *Large Property Damage Losses in the Hydrocarbon – Chemical Industries* [published annually].
39. Lenoir, E.M., and J.A. Davenport. "A Survey of Vapor Cloud Explosions – Second Update", *Process Safety Progress* 12(1) (January 1993): 12.
40. U.S. Department of Labor, Occupational Safety and Health Administration. "Hazard Communication", Title 29, Subtitle B, Chapter XVII, Part 1910, Subpart Z, Paragraph 1200, Code of Federal Regulations [29 CFR 1910.1200(g)]; July 1995.
41. J. J. Keller & Associates. "OSHA Compliance Manual – 29 CFR 1910 Plant Safety." April 1997: OSHA-19.
42. Thompson Publishing Group. *Risk Management Program Handbook*. Paragraphs 414, 418, 420, 424, 434, 458, 460, 710 (updated monthly).
43. U.S. Department of Labor, Occupational Safety and Health Administration. "Occupational Safety and Health Standards", Title 29, Subtitle B, Chapter XVII, Part 1926, Subpart P, Paragraph 650, Code of Federal Regulations [29 CFR 1926.650]; July 1989.
44. American Institute of Chemical Engineers. *Loss Prevention*. Vol. 9. New York: AIChE, 1975: several pertinent articles on "hot-tapping".
45. Kletz, T.A. *Plant Design for Safety*. Newport, Australia: Hemisphere Publishing, 1991: 11, 132, 134.
46. Crowl, D.A., ed. *Inherently Safer Chemical Processes*. Center for Chemical Process Safety. New York: AIChE, 1996.
47. Furr, A.K. *CRC Handbook of Laboratory Safety*. 4th ed. Boca Raton, FL: CRC Press, 1995.
48. Kletz, T.A. *Learning from Accidents in Industry*. New York: Butterworth-Heinemann, 1988: 149.
49. Kletz, T.A. *What Went Wrong?* Houston, TX: Gulf Publishing, 1985: 73, 143.
50. Kletz, T.A. *Computer Control and Human Error*. Houston, TX: Gulf Publishing, 1995.
51. Kletz, T.A. *Lessons from Disaster – How Organizations Have No Memory and Accidents Recur*. Rugby, UK: Institution of Chemical Engineers, 1993.
52. American Petroleum Institute. "Management of Hazards Associated with Location of Process Plant Buildings." API Recommended Practice 752. Washington, DC: API, 1995.
53. Mecklenburgh, J.C. *Process Plant Layout*. New York: Halsted Press, 1985.
54. Wells, G.L. *Safety in Process Plant Design*. London: George Godwin Ltd., 1980: 145, 255.

46. "Chemical Process Safety: Case Histories," G-46, 1993.
47. [Title Not Yet Assigned], G-47 (not issued).
48. [Title Not Yet Assigned], G-48 (not issued).
49. [Title Not Yet Assigned], G-49 (not issued).
50. "RELEASE: A Model with Data to Predict Aerosol Rainout in Accidental Releases," G-50, 1998.
51. "Evaluating Process Safety in the Chemical Industry: A User's Guide to Quantitative Risk Analysis," G-51, 2000.
52. [Title Not Yet Assigned], G-52 (not issued).
53. "Practical Compliance with the EPA Risk Management Program," G-53, 1999.
54. "Local Emergency Planning Committee Guidebook: Understanding the EPA Risk Management Program Rules," G-54, 1999.
55. [Title Not Yet Assigned], G-55 (not issued).
56. "Guidelines for Improving Plant Reliability," G-56, 1998.
57. [Title Not Yet Assigned], G-57 (not issued).
58. "Electrostatic Ignitions of Fires and Explosions," G-58, 1997.
59. [Title Not Yet Assigned], G-59 (not issued).
60. "Estimating the Flammable Mass of a Vapor Cloud," G-60, 1999.
61. "Understanding Explosions," G-61, 2003.
62. "Guidelines for Process Safety in Batch Reaction Systems," G-62, 1999.
63. "Guidelines for Consequence Analysis of Chemical Releases," G-63, 1999.
64. "Deflagration and Detonation Flame Arrestors," G-64, 2002.
65. [Title Not Yet Assigned], G-65 (not issued).
66. "Layers of Protection Analysis," G-66, 2001.
67. "Avoiding Static Ignition Hazards in Chemical Operations," G-67, 1999.
68. "Guidelines for Process Safety in Outsourced Manufacturing Operations," G-68 2000.
69. [Title Not Yet Assigned], G-69 (not issued).
70. [Title Not Yet Assigned], G-70 (not issued).
71. "Revalidating Process Hazards Analyses," G-71, 2000.
72. [Title Not Yet Assigned], G-72 (not issued).
73. [Title Not Yet Assigned], G-73 (not issued).
74. [Title Not Yet Assigned], G-74 (not issued).
75. "Wind Flow and Vapor Cloud Dispersion at Industrial and Urban Sites and Surface Roughness," G-75, 2002.
76. "The Design and Evaluation of Physical Protection Systems," G-76, 2002.
77. [Title Not Yet Assigned], G-77 (not issued).
78. [Title Not Yet Assigned], G-78 (not issued).
79. "Guidelines for Analyzing the Security Vulnerabilities of Fixed Chemical Sites," G-79, 2002.
80. [Title Not Yet Assigned], G-80 (not issued).
81. "Essential Practices of Managing Chemical Reactivity Hazards," G-81, 2003.
82. "Guidelines for Investigating Chemical Process Incidents," 2nd ed., G-82, 2003.
83. "Guidelines for Fire Protection in Chemical, Petrochemical, and Hydrocarbon Processing Facilities," G-83, 2003.
84. "Guidelines for Facility Siting and Layout," G-84, 2003.
85. "Guidelines for Safe Handling of Powders and Bulk Solids," G-85, 2005.
86. [Title Not Yet Assigned], G-86 (not issued).
87. [Title Not Yet Assigned], G-87 (not issued).
88. [Title Not Yet Assigned], G-88 (not issued).
89. [Title Not Yet Assigned], G-89 (not issued).
90. [Title Not Yet Assigned], G-90 (not issued).
91. [Title Not Yet Assigned], G-91 (not issued).
92. [Title Not Yet Assigned], G-92 (not issued).
93. "Dust Explosions", 3rd Ed., G-93 (2003).
94. [Title Not Yet Assigned], G-94 (not issued).
95. "Guidelines for Safe Handling of Powders and Bulk Solids," G-95, 2004.
96. "Guidelines for Mechanical Integrity Systems," G-96, 2006.

18.4.2	Lessons Learned: 3-Mile Island and Chernobyl.....	1496
18.4.3	Next Generation Designs: VHTR Reactors	1497
18.5	OSHA	1497
18.6	The "Superfund" Law	1498
18.6.1	Amendment to the Superfund Law: SARA	1498
18.7	EPCRA (Emergency Planning and Community Right to Know Act)	1498
18.8	Toxic Substances Control Act (TSCA).....	1498
18.8.1	TSCA General Sections References	1499
18.9	Resource Conservation and Recovery Act (RCRA).....	1499
18.10	Spill Prevention Control and Countermeasures (SPCC) Act	1499
18.11	Greenhouse Gases and (Global Warming) Climactic Change	1499
18.11	Summary	1500
	Acknowledgments	1500

18.1 BACKGROUND

Increased attention to both local and global environmental issues over the past few decades has resulted in heightened focus on these issues. This new attention has increased the workload, knowledge base, and responsibilities of environmental professionals. Issues ranging from the impact of pollution on human health, global climactic change, national security risks, and nuclear fuel processing pose serious concerns.

As with any issue within our society, consideration to health and environment is made with attention to economics and commerce. Known cases exist where deleterious financial impact resulted from negative consumer perceptions of a corporation's environmental or human health-related policies. "Green marketing" wears a friendly neighbor label and instills a barrier-to-entry against competitive products.

The costs associated with environmental and personal safety policies (the "compliance burden") pose real challenges to corporations. However, these costs serve as prudently invested dollars when weighed against the ramifications of environmental policy inaction, whether as regulatory fines or market share loss. Adherence to the various Code of Federal Regulations (CFR) that apply to a large number of U.S. industries can prevent public embarrassment and help maintain customer loyalty.

This chapter will focus on statutes and mandates of the U.S. Environmental Protection Agency (EPA) enforceable by various federal regulations, as well as discuss the state of engineering and management tools available for managing corporate compliance, and provide numerous online resources suitable for in-depth investigation of each topic.

As a quick reference, government agencies that have important bearing on the environment can be contacted via the following sites:

- | | |
|--|--|
| • The U.S. Environmental Protection Agency (EPA) | www.EPA.gov |
| • The U.S. Nuclear Regulatory Commission (NRC) | www.nrc.gov |
| • The U.S. Department of Energy (DOE) | www.doe.gov |
| • Occupational Safety & Health Administration (OSHA) | www.osha.gov |
| • U.S. Department of Health and Human Services (HHS) | www.hhs.gov |

18.2 THE CLEAN AIR ACT (<http://epa.gov/air/caa/>)

18.2.1 BACKGROUND AND POLLUTANT TYPES

The Clean Air Act (CAA) establishes monitoring and reporting mechanisms, air pollution inventories and reporting thresholds, and economic incentives for controlling and/or reducing pollutant

to assist in determining a chemical's standing relative to its level of hazard within several categories. When available, even more detailed information is preferred.

18.2.1.4 Maximum Achievable Control Technology Standards

To limit the risk of hazardous air pollutant exposure over time, the EPA mandates that all major sources of HAP emissions operate under Maximum Achievable Control Technology (MACT) standards. The EPA intends to augment and add to the current list of MACT standards; additionally, there are "catch-all" regulations for all major sources of HAPs. One such example is the "MACT Hammer," which allows states to implement MACT standards for industries not currently addressed by EPA definitions. A list of such MACT standards, including the Miscellaneous Organic NESHAP (MON), can be referenced at http://www.dep.state.pa.us/dep/deputate/airwaste/aq/permits/neshaps/hammer_table.pdf.

18.2.2 COMPLIANCE REQUIREMENTS

To implement the CAA, the EPA administers regulations via six discrete "Titles." These titles are defined as follows (courtesy of the EPA):

Title I – Air Pollution Prevention and Control (<http://epa.gov/air/caa/title1.html>)

- Part A – Air Quality and Emission Limitations
- Part B – Ozone Protection (replaced by Title VI)
- Part C – Prevention of Significant Deterioration of Air Quality
- Part D – Plan Requirements for Nonattainment Areas

Title II – Emission Standards for Moving Sources (<http://epa.gov/air/caa/title2.html>)

- Part A – Motor Vehicle Emission and Fuel Standards
- Part B – Aircraft Emission Standards
- Part C – Clean Fuel Vehicles

Title III – General (<http://epa.gov/air/caa/title3.html>)

Title IV – Acid Deposition Control (<http://epa.gov/air/caa/title4.html>)

Title V – Permits (<http://epa.gov/air/caa/title5.html>)

Title VI – Stratospheric Ozone Protection (<http://epa.gov/air/caa/title6.html>)

Requirements associated with Title V are of vital importance to industry, state, and local agencies. A facility's air permit defines the air pollutant threshold limits available to it. The permit declares essential operational parameters of the holder's facility with regard to product and raw material throughputs, and establishes the basic relationships between those throughputs and regulated pollutant emissions amounts.

18.2.3 SOURCE DELINEATIONS UNDER TITLE V

The EPA applies NESHAP, as well as other classifications, in defining an emitter's standing under the Title V program. Where new sources of emissions are created, or where existing sources are modified, other regulations (including both new source review (NSR) and new source performance standards [NSPS]) must be considered.

Agencies grant permits to manufacturers or distributors generally based on one of three regulated emitter definitions, as follows:

mode of operation (NSPS). All new and modified major sources of HAPs must comply with MACT standards.

These modifications may be positive or negative with regard to Title V permitted emission levels, but such a change requires an update to the air pollutant inventory under SIP rules. In many cases, a net zero change in emissions will be sought by combining parallel activities—one positively divergent, one negatively divergent. Substituting non-HAP for a HAP classified solvent in cleaning operations is a simple example whereby reduction of use in one area may allow for increased use, or possibly retooling, in another.

18.2.6 NEW REGULATIONS

The Miscellaneous Organic NESHAP (MON) is structured to reduce the floor levels of major sources and to reassess the definitions of and methods by which MACT standards and levels are achieved (<http://www.epa.gov/ttn/atw/mon/monpg.html>)

Certain sites currently classified as minor emissions sources will find themselves classified as major sources under MON, and adherence to the requirements of the MACT guidelines posed by the major source classification will likely be costly. It is recommended that manufacturers of VOC-related products acquaint themselves with the MON and make necessary preparations. Costs associated with major source classification within MON often range upwards of \$5–10 million per facility.

18.2.7 TITLE IV (ACID RAIN) AND TITLE VI (STRATOSPHERIC OZONE) CONSIDERATIONS

18.2.7.1 The Title IV (Acid Rain) Permit (<http://epa.gov/air/caa/title4.html>)

The environmental, health, and cultural impacts of acid rain were well documented in the late 20th century. Acid rain results from combustion of the sulfur and nitrogen contents of fossil fuels. Sulfur and nitrogen oxides combine with atmospheric water to form acids. The prevalence of mobile (e.g., automotive and aircraft) sources globally hints at the requirement for control of Title IV compounds and precursors.

Automotive catalytic converters (<http://www.all-catalytic-converters.com/techtip1.html>) alleviate this issue (as well as those associated with smog formation) within the mobile source category; however, they are not the perfect solution to emissions problems.

Within the stationary source category, acid rain forming compounds primarily result from combustion-based power plant facilities.

18.2.7.2 Permitting Requirements

Title IV addresses “affected sources,” which comprise “affected units.” These affected units are subject to emissions reductions or limitations under Title IV, and are granted allowances per annum, with each allowance equal to 1 ton of SO₂ per year.

Under Title IV, facilities must document and report annually regarding the aggregate amount of acid-rain precursors in the form of SO₂ and NO_x. Determination of these amounts are traditionally handled by stack testing, with the emissions factor subsequently calculated in units of pound of species emissions per pound of fuel combusted, per hour of operation, or other. Title IV thresholds are subject to penalty when exceeded. Additionally, in the case of violation, the EPA can enforce a mandatory emissions reduction in the subsequent year to offset the excess emission value.

Power generation facilities are evaluated within the Title IV requirements versus baselines established within the National Acid Precipitation Assessment Program (NAPAP) Emissions Inventory. Descriptions of source and unit types applicable under Title IV can be found at <http://epa.gov/air/caa/caa402.txt>.

Available sorbent surface area, vapor-liquid stream mixing, and reactivity will dictate the effectiveness of such "dry sorbent injector" scrubbers.

5. Biofilters. Although relatively new, biofiltration has been used in some instances for reduction of emissions and odors. Biofilters consist of microbes grown on porous media, and in small-scale implementations, they provide >90% reduction in emissions levels.
6. Cogeneration. Several new technologies combine destructive oxidation technologies with cogenerative site-based power facilities. The energy utilized in emissions oxidation can sometimes be reclaimed to yield economic benefits.

18.2.10 CONSULTATION

In general, numerous professional consulting service providers can help prepare Title V permits, annual emissions inventory reports, and other state-specific documents. An Internet search can identify potential regional candidates.

The EPA expects that EMIS systems be implemented at all major categorization facilities, and site implementation of such systems typically constitutes the first requirement of an EPA corrective action plan. As stated above, more accurate systems of emissions estimation can lead to reduced compliance burden and potentially eliminate the need for source classification adjustment.

In all cases, adherence to the full range of Federally Applicable Requirements, the crux of which are provided above, combined with the goal of maintaining operational flexibility, should be the objective of any permit-focused environmental engineer.

18.3 THE CLEAN WATER ACT

(<http://www.epa.gov/r5water/cwa.htm>)

The Clean Water Act (CWA) provides water quality standards (WQS) for surface waters in the United States. The CWA gives the EPA the authority to implement pollution control and regulatory strategies.

Water quality criteria (WQC) provide chemical-specific numerical values of amount (magnitude), interval of test, and frequency of occurrence that must be met in tandem to meet the requirements of the WQS. For chemicals with WQC documented at EPA, states and Indian tribes must also assign WQC (not necessarily of identical values per the EPA metrics).

The EPA typically allows exemptions from the WQS for locations downstream of point source discharges ("stream mixing") as well as for relatively rare conditions where a significant increase in flow diminishes water quality (for example, storm sewer flooding). Waivers based on mixing are regulated and require that mixing zones do not extend throughout a body of water or from bank to bank of a river or stream. Additionally, waivers will not allow deleterious impact to designated use (DU) zones. A contiguous region meeting WQS must be maintained.

18.3.1 EXISTING USE

Designated use nomenclatures indicate the level of quality to which a community aspires; the "existing use" establishes a benchmark. The intent of the existing use delineation assures that no commercial, public, or private activity reduces water quality to subexisting use levels, and regulating bodies will not authorize subexisting use conditions ("Tier I rule").

The EPA protects zones that significantly exceed current WQS from negative impacts, thus making it difficult to impact a water body while ensuring the quality remains above its minimum. Prior to initiation of such an adverse activity, several criteria must be met as defined under the "Tier II rule."

Certain waterways are designated as outstanding national resource waters, and no significant degradation in water quality is permitted for any significant period of time ("Tier III rule"). These

TABLE 18.1
General Publicly Owned Treatment Works Water Allowance Limits

Pollutant	Effluent Limit/7-Day Average	Effluent Limit/30-Day Average
5-day BOD	45 mg/L	30 mg/L
TSS	45 mg/L	30 mg/L
pH	N/A	6–9
Removal specification	N/A	85% of BOD 5 and TSS

BOD, biochemical oxygen demand; TSS, total suspended solids.

5bmou.doc. This example provides an historical review of the environmental performance of the waterway in question, with focus on mercury contamination. Additional information on waste quality is available at http://en.wikipedia.org/wiki/water_quality.

Often, NPDES permits are either granted as individual or general permits, and contain specific mass amounts of defined pollutants eligible for discharge (effluent limits at pipe end) from the permitted operation. To ensure compliance, internal auditing plans and quality control policies are defined. Further requirements for using best management practices, monitoring, and reporting are included.

Detailed information on NPDES permits is available at <http://www.epa.gov/watertrain/cwa/cwa40.htm>.

As with the CAA, the CWA establishes performance standards (the maximum effluent concentrations allowable) and control technology guidelines applicable to various industries and sectors. These guidelines reflect data compiled from numerous industry sources, and define expected discharge levels as a function of best available technology economically achievable (BAT or BATEA). More information on effluent streams is at <http://www.epa.gov/waterscience/guide/>.

For cases where application of BAT to effluent stream discharges will not meet the requirements of a water source's DU, and for which TMDL limits are not established, the permitting agency will apply water quality–based effluent limits (WQBEL). WQBEL includes an analysis of the level of effluent stream dilution required to retain DU levels. Where WQBEL is employed, a high risk has been assigned to the water source, and economics will often be secondary to technology.

18.3.4 PUBLICLY OWNED TREATMENT WORKS

Both primary and secondary levels of sequential treatment specifications exist for POTW plants. The former involves the settling and filtering of solids (activated sludge). Table 18.1 provides typical limits imposed on secondary treatment criteria.

The EPA offers supplemental information regarding activated sludges involving biosolids, including rules and standards (see <http://www.epa.gov/watertrain/cwa/cwa42.htm>).

18.3.5 “WET WEATHER FLOW” CONDITIONS

Due to heavy rainfall, wastewater overflows from sewers or industrial facilities may result in underperformance versus WQS. Nevertheless, affected sewer systems, typically combined sewer overflow (CSO) or municipal separate storm sewer systems (MS4), remain subject to NPDES regulations. CSO systems, found in older residential or municipal areas, allow transportation of both rainwater and raw sewage within a common stream; MS4 systems separate the two flows.

Attention to the public health challenges posed by CSO sewers focus on control of pathogen dispersion. From NPDES perspectives, CSO systems are restricted from discharging untreated sewage during periods of dry weather.

The hydropower dam presents an interesting case study, as dams by definition cause great variance between existing and DU classifications and the final state of the dammed water.

18.4 NUCLEAR POWER GENERATION

Currently, nuclear energy serves as the second largest source (behind coal) of electrical power in the United States. Nuclear sources are inherently clean, but significant risks and therefore governmental regulations apply to the waste disposal methods.

The Nuclear Regulatory Commission (<http://www.nrc.gov/>) oversees all permitting, guidelines, and definition of operational requirements via the Office of Nuclear Reactor Regulation.

18.4.1 HAZARDOUS WASTE DISPOSAL

Nuclear reactor facilities undergo hazardous waste management procedures every 12 to 24 months. Older fuel rods are removed, generating approximately 2000 metric tons of used radioactive material annually (the National Energy Institute presents the analogy of one football field covered to the depth of 5 yards during the past 40 years).

Based on laws against the proliferation of nuclear weapons, nuclear waste cannot be recycled, and is assigned a once-through single use designation. Department of Energy policies as administered by the U.S. Department of Energy Office of Health, Safety, and Security can be consulted at <http://www.hss.energy.gov/NuclearSafety/techstds/standard/standard.html>.

The Office of Environmental Management maintains the DOE's waste management policies. Two discrete levels of nuclear wastes are considered:

1. Low-Level Waste
 - a. Radioactive by-products of NRC-licensed or DOE-permitted activities that are not high-level waste.
 - b. Radioactivity, containing mostly beta and gamma emissions, persists for 5 to 50 years; contains elements with atomic numbers less than that of uranium (92), and is eligible for disposal via authorized independent or government-approved facilities, as determined by the Low-Level Waste Disposal Facility Federal Review Group (LFRG).
2. High-Level Waste
 - a. Irradiated nuclear fuel ("spent fuel"), plus both liquid products of reprocessing and the solids into which such liquids have been incorporated.
 - b. Contains numerous radioactive materials of high levels of radiation and with long half-lives. Such materials are generated either through nuclear power generation or Department of Defense activities. In general they are assigned for disposal at the U.S. Government Yucca Mountain National Depository.

For the centralized disposal of high-level nuclear wastes, Yucca Mountain, Nevada, was selected in large part because of national security concerns.

18.4.2 LESSONS LEARNED: 3-MILE ISLAND AND CHERNOBYL

The incident at Unit 2 of the 3-Mile Island (Pennsylvania) reactor during March 28 to April 1, 1979, led to the formation of the Institute of Nuclear Power Operations (INPO). The INPO sets objectives, guidelines, and criteria for all U.S.-based nuclear power generating facilities. In 1985, this group established the National Academy for Nuclear Training, which accredits all plant operators and supervisors.

In April 1986, fundamental flaws in Soviet reactor designs, combined with procedural human error, resulted in a steam explosion and the expulsion of 5% of the Chernobyl-4 (Ukraine, USSR)

Variances are not retroactive. During the period of operation prior to receipt of a variance, if issued, OSHA may provide an interim order, allowing continued activity based on current methods. Details of such an interim order are subject to site publication and employee-employer review.

18.6 THE “SUPERFUND” LAW

The “Superfund” law derives from citizen concerns over the health impacts of decades of accumulated hazardous wastes within or near communities. More accurately labeled the Comprehensive Environmental Response, Compensation, and Liability Act (CERCLA), the Superfund governs the removal and destruction of toxics and also establishes disposal procedures through the Office of Superfund Remediation Technology Innovation (OSRTI). Prioritization activities are within the jurisdiction of the OSTRI.

18.6.1 AMENDMENT TO THE SUPERFUND LAW: SARA

The Superfund Amendments and Reauthorization Act (SARA) provides guidelines to improve Superfund enforcement methods and criteria. SARA also refines the Hazardous Rankings System, and by OSTRI prioritizes remediation activities. Rules and regulations under the Superfund and its SARA amendment are accessible at <http://www.epa.gov/superfund/action/index.htm>.

18.7 EPCRA (EMERGENCY PLANNING AND COMMUNITY RIGHT TO KNOW ACT)

EPCRA, also known as “Title III of SARA,” protects local communities from the hazards of toxic pollutant discharge (<http://www.epa.gov/region5/defs/html/epcra.htm>). EPCRA mandates regulations surrounding the maintenance and site availability of such forms as MSDS, toxic chemical release forms, and emergency and hazardous chemical inventory forms (see http://www4.law.cornell.edu/uscode/html/uscode42/usc_sup_01_42_10_116_20_II.html

Under EPCRA, state emergency planning commissions and local emergency planning councils must be formed. EPCRA ensures the documentation of quantity and location of hazardous materials present in excess of Toxic Substance Controls Act (TSCA) thresholds. SARA Title III information must be submitted to state and local (including fire) agencies under SARA Sections 312 and 313.

EPCRA, in combination with the Pollution Prevention Act (PPA), administers the toxic release inventories (TRI) program. Industry and federal facilities emitting toxic materials must report on annually released quantities under SARA Section 313 (Form R). Although the EPA does not host a site containing all TRI materials, versions of this document can be obtained via the Government Printing Office (<http://www.access.gpo.gov/>). An executive summary, including requirements for submittal to the TRI via Form R submittals, is available at <http://www.epa.gov/tri/tri-data/tri01/press/executivesummarystandalone.pdf>.

18.8 TOXIC SUBSTANCES CONTROL ACT (TSCA)

More than 75,000 chemicals enter, are manufactured within, and/or are consumed within the United States each year. The TSCA (<http://www.epa.gov/region5/defs/html/tsc.htm>) provides methods for categorizing newly created and existing chemicals, and supplements the Clean Air Act and the Toxic Release Inventory portion of EPCRA. The TSCA assists in quantifying types and amounts of chemicals both produced and released to the environment annually.

Commercial activities that result in the creation of new chemicals must receive authorization from the EPA prior to production or distribution. To receive such authorization, a pre-manufacture notice (PMN) must be filed with the EPA's Office of Pollution Prevention and Toxic Substances.

Although few dispute that current industrial processes, automobiles, power production, etc., impact GHG levels, there is still much debate regarding human-induced and naturally occurring variations. Recently excavated ice core samples indicate that CO₂ levels are rising at a much faster rate than at any time in the past 400,000 years. Such cores show current atmospheric CO₂ levels of 380 ppmv, exceeding previous cyclical highs by roughly 18%. The following links to graphical data can assist in drawing conclusions:

- <http://www.grida.no/climate/vital/02.htm> (400,000-year CO₂ atmospheric measurements, Vostok ice sheet, Antarctica)
- <http://www.grida.no/climate/vital/06.htm> (recent data from Mauna Loa test site, altitude 4000 meters)
- <http://www.grida.no/climate/vital/07.htm> (CO₂ levels, 1870 to 2000)

Although the scientific community generally believes that decreasing polar ice cap size and commensurate rising ocean levels correlate with increased GHG levels and global warming, the full ramifications of the evidence remain contested.

18.11 SUMMARY

The daily tasks of compliance management in the face of potentially changing government regulations are facilitated by a strong industry complement of consulting expertise. Additionally, software packages of varied types are available to assist in automating difficult compliance tasks.

Environmental engineering issues span a wide gamut of technologies and requirements both mundane and essential. Ensuring compliance with government regulations, though never a glorified chore, nonetheless provides a necessary function that ensures the protection of interests ranging from the economic to the vital.

The roles of environmental engineers in ensuring and monitoring the healthy progress of developing nations, assisting in defining the directions of new and necessary technologies, and in protecting our children and ecosystems cannot be underestimated.

The economic impact of a dearth of environmental stewardship is too great to gamble.

ACKNOWLEDGMENTS

The authors thank the EPA (<http://www.epa.gov/>) for providing many of the links cited above for public use. "Exit links" provided by the EPA have been referenced in many instances. The EPA or the authors do not verify the accuracy and content of these links.

Additionally, the authors wish to thank their colleagues at Greenfield Environmental, Inc., for their general assistance and numerous contributions.

19.5.3 Correlation for $k_L a$	1528
19.5.3.1 Bubble Column	1528
19.5.3.2 Mechanically Agitated Vessel	1528
19.5.4 Power Consumption	1528
19.5.5 Scale-Up	1529
References	1529

19.1 INTRODUCTION

Biochemical engineering involves the scale-up of biological processes. One of the earliest examples of the successful scale-up of a biological process was the production of penicillin during World War II. Industrial microbiologists used stirred-tank fermenters to culture molds on a large scale. During the 1960s and 1970s, biochemical engineering grew rapidly with the increased needs for the development of biological processes in the food, beverage, and pharmaceutical industries. The activities in bioprocessing grew even further as Arab oil embargos prompted the use of renewable energy sources, such as biomass. For example, cellulose, a major component of wood, can be broken down enzymatically to glucose, hence producing ethanol via yeast fermentation.

The research for the utilization of renewable resources dwindled in the early 1980s because of the reduction in energy prices. However, the area found another opportunity to grow as biologists discovered a way to manipulate genes of living organisms. The manipulation of genes is known as genetic engineering or biotechnology.

19.1.1 BIOTECHNOLOGY

Biotechnology is broadly defined as “commercial techniques that use living organisms, or substances from those organisms, to make or modify a product, including techniques used for the improvement of the characteristics of economically important plants and animals and for the development of microorganisms to act on the environment” [1]. This very broad definition includes not only the newly developed recombinant DNA technology, but also the traditional areas involving agriculture, animals, human health, and industrial microbiology. Since ancient days, people utilized microorganisms to produce fermented beverages (alcohol, sweet refreshments) and food (cheese, soy sauce, fermented vegetables, sweets, and bread), though they did not understand those biological changes. People crossbred plants and animals for better yields.

However, in recent years, the term biotechnology is being used to refer to novel techniques such as recombinant DNA. This technique is also known as genetic engineering, a misleading description of scientific endeavors. The applications are numerous, as listed in Table 19.1. Previously expensive and rare pharmaceuticals (such as insulin for diabetics, a human growth hormone to treat children with dwarfism, interferon to fight infection, vaccines to prevent diseases, and monoclonal antibody for diagnostics) are now produced from genetically modified microbial cells or hybridoma cells inexpensively and in large quantities. Disease-free seed stocks and healthier, higher-yielding food animals have been developed. Important crop species can be modified to have traits that resist stress, herbicides, and pests. Furthermore, recombinant DNA technology can be applied to develop genetically modified microorganisms so that they will produce various chemical compounds with higher yields than available from unmodified microorganisms.

19.1.2 BIOCHEMICAL ENGINEERING

In order to cultivate genetically modified cells in large quantities, we need to develop a large-scale process that is technologically efficient and economically viable. A typical biological process (bioprocess) involving microbial cells can be illustrated as in Figure 19.1. Raw materials are treated and mixed with other ingredients that are required for cells to grow well. The liquid medium,

TABLE 19.2
Characteristics of Bioprocessing

Advantages	Disadvantages
The reaction conditions are mild: typically atmospheric conditions.	Complex product mixture and low productivity make the product separation expensive.
Enzyme catalysts are highly specific. A great variety of enzymes exist that can catalyze a very wide range of reactions.	Cells tend to lose desirable characteristics. Enzymes are sensitive and unstable in harsh conditions.
The major raw material for bioprocesses is biomass, which is renewable.	Fermenter and medium have to be sterilized and kept in sterile conditions.

enzymes involved on the process such amylase and glucose isomerase) and laundry additives (protease enzyme).

Lastly, the word *fermentation* needs to be discussed due to the confusion caused by different definitions of the word. Traditionally, fermentation was defined as the process for the production of alcohol or lactic acid from glucose. A broader definition of fermentation, which has been adopted in this handbook, is an enzymatically controlled transformation of an organic compound.

19.2 CELLS AND ENZYMES

19.2.1 MICROBIAL CELLS

The three major categories of life are the animal kingdom, the plant kingdom, and the protists (Table 19.3). Protists have a relatively simple biological organization and do not differentiate into separate cell types. The microorganisms classified as the protists are further divided into two categories: eukaryotes and prokaryotes. Prokaryotes are small and simple. It is the unit of structure of bacteria and blue-green algae. The more complex eukaryotic cell has internal unit membrane systems that segregate many of the functional components of the cell. Since eukaryotic cells are also the unit of structure of animals and plants, in modern biology, life is broadly classified into two categories: eukaryotes and prokaryotes (Table 19.3). Among the protists, bacteria and fungi are two most important microorganisms for industrial applications. Table 19.4 gives several examples of microorganisms used industrially.

TABLE 19.3
Major Categories of Life

Type	Haeckel	Modern
Multicellular	Animals Plants	Eukaryotes
Unicellular	Protists Algae Protozoa Fungi Molds Yeasts Bacteria Blue-green algae	
		Prokaryotes

TABLE 19.5
Typical Growth Medium for Yeasts

Glucose	100 g
Yeast extract	8.5 g
NH ₄ Cl	1.32 g
MgSO ₄	0.11 g
CaCl ₂	0.06 g
Anti-foam	0.2 mL
Water to make	1 L

The most common growth pattern for yeasts is budding, which is an asexual process. A small bud (or daughter cell) is formed on the surface of a mature cell.

Molds are filamentous fungi. A single reproductive cell or spore is germinated to form a long thread, or hyphae, which branches repeatedly as it elongates to form a vegetative structure called a mycelium. The most important classes of molds industrially are *Aspergillus* and *Penicillium*. Molds can produce antibiotics, industrial chemicals, enzymes, and food additives. The production of penicillin was scaled up between 1941 and 1945 from virtually nothing to more than 650 billion units per month; meanwhile, its cost dropped from \$20 to 60¢ per 100,000 units [2]. The dramatic development was due to the improvements in composition of the medium, the development of the submerged culture technique, the production of mutant strains of *Penicillium chrysognum*, and the refinements of downstream separation techniques [3].

19.2.1.4 Culture Media

There are two main types of culture media: natural and synthetic. They vary widely in form and composition, depending on the species of organism to be cultivated and the purpose of the cultivation.

Natural media (or complex media) usually contain peptones, beef extract, or yeast extract. When a solid medium is desired, a solidifying agent such as gelatin or agar may be incorporated into the medium.

Synthetic media (or chemically defined media) consist of dilute solutions of chemically pure compounds. They may be simple such as inorganic ammonium salt plus minerals and a sugar, or complex such as purified casein with added vitamins, minerals, and a sugar. They can be produced with constant compositions year after year. Table 19.5 shows a typical growth medium for the cultivation of yeasts.

The medium must be sterilized to eliminate any living organisms in the vessel, often by moist heat (steam under pressure) in an autoclave. Generally, the autoclave is operated at approximately 15 psig at 121°C. The time of sterilization depends on the nature of the material, the type of container, and the volume; test tubes of liquid media can be sterilized in 15 to 20 minutes at 121°C.

Inoculation is the seeding of a culture vessel with the microbial material (inoculum). The inoculum is introduced with a metal wire or loop that is rapidly sterilized just before its use by heating it in a flame. Transfers of liquid culture are often made by using a sterilized pipette.

19.2.2 ANIMAL CELLS

Animal cells are classified as eukaryotic cells, and they can be cultivated in nutritional medium outside the donor's body. Such cultured cells grow in number and size. Tissue culture methodologies are employed to study cancer cells and malignant tumors, to determine tissue compatibility in transplantation, and to study specific cells and their interactions.

value-added, low market-volume products are economically feasible to be produced from plant cell culture techniques. Potential products are

1. Food products: color, flavors, oils, sweeteners, and spices
2. Pharmaceuticals: alkaloids, steroids, shikonin, rosmarinic acid
3. Agricultural chemicals

Plant tissue cultures can be divided into two major types: unorganized growth cultures and organized growth cultures.

Unorganized growth cultures lack any recognizable structure of the original plant. Callus cultures are amorphous cell aggregates arising from the unorganized growth of explants on an aseptic solid nutrient medium. *Suspension (or cell) cultures* consist of cells and cell aggregates, growing dispersed in liquid medium. They are usually initiated by placing pieces of a friable callus culture in moving liquid medium. Suspension culture is generally preferred for mass propagation of plant cells because it can be maintained and manipulated similar to submerged microbial fermentation.

Organized growth cultures maintain their original organ structure such as root cultures and embryo cultures. *Root cultures* can be established from root tips taken from many plants. The “hairy root” clones that are produced can be cultivated to produce metabolites. *Embryo cultures* may be established from embryos removed from sterilized seeds, ovules, or fruits. Embryo cultures can be employed for the rapid production of seedlings from seeds that have a protracted dormancy period.

19.2.4 CELL GROWTH MEASUREMENT

Microscopic counts: The number of cells in a culture can be counted under a microscope using a hemocytometer, which has counting chambers etched on the surface of a glass slide. A sample of cell suspension is allowed to flow under the cover slip and to fill the counting chambers. Dense suspensions need to be diluted.

Viable plate count: An aliquot of cell suspension is spread over the agar surface. The plate is then incubated until colonies appear, and the number of colonies is counted. To obtain the appropriate number of cells per unit volume, the sample has to be diluted. For the larger dilution, it is common to use the serial dilution technique. For example, to make $1/10^6$ dilution, three successive $1/100$ dilutions or six successive $1/10$ dilutions can be made.

Cell dry weight: An aliquot of cell suspension is centrifuged to discard the supernatant. The cells are thoroughly washed with distilled water and recentrifuged to eliminate all soluble matter. The washed cells are dried in an oven and weighed. This is the most direct and probably the most reliable method. However, such determinations are time consuming and relatively insensitive to small changes of cell mass.

Turbidity: The cell mass can be estimated optically by determining the amount of light scattered by suspended cells. A calibration curve is obtained by measuring the absorbency of a sample with a known cell concentration. The measurements are usually made at a wavelength between 600 and 700 nm.

19.2.5 ENZYMES

Enzymes are biological catalysts and proteins, which are produced by living organisms. Almost every reaction in a cell requires the presence of a specific enzyme. Their major function is to catalyze the making and breaking of chemical bonds. Therefore, like any other catalysts, they increase the rate of reaction without themselves undergoing permanent chemical changes. An enzyme is highly specific and catalyzes only one or a small number of chemical reactions. The rate of an enzyme-catalyzed reaction is usually much faster than that of the same reaction when

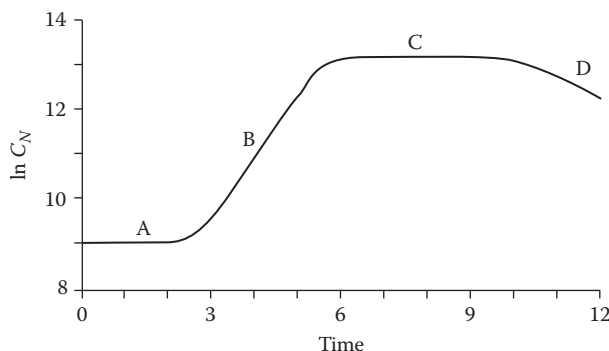


FIGURE 19.2 Typical growth curve of unicellular organisms: (A) lag phase; (B) exponential growth phase; (C) stationary phase; (D) death phase.

The lag phase is the initial period when the change of cell number is negligible; the cells may grow in size, but not in number. The length of the lag period depends on the type and age of the microorganisms, the size of the inoculum, and other culture conditions. The lag usually occurs as the cells adjust to the new medium before growth begins, and as the cells produce the enzymes necessary for the metabolization of the available nutrients.

At the end of the lag phase, growth begins and cell concentration increases exponentially. As the available nutrients are exhausted in the medium, the rate of growth declines and growth eventually stops. The stationary phase is usually followed by a death phase, in which the organisms in the population die due to the depletion of the cellular reserves of energy or due to the accumulation of toxic products.

19.3.1.2 Unstructured Cell Kinetic Models

Cell growth involves numerous complicated networks of biochemical and chemical reactions. A simple unstructured kinetic model was formulated based on the assumptions that

- Cells can be represented by a single component, such as cell mass or cell number.
- The cell suspension can be regarded as a homogeneous solution.

The rate of the cell growth r_X is proportional to cell concentration C_X as

$$r_X = \frac{dC_X}{dt} = \mu C_X \quad (19.1)$$

where μ is the specific growth rate [hr^{-1}]. Equation (19.1) can be integrated from time t_0 to t to give

$$C_X = C_{X_0} \exp[\mu(t - t_0)] \quad (19.2)$$

where C_{X_0} is the cell concentration at t_0 when the exponential growth starts. Equation (19.2) shows the increase of cells exponentially with respect to time. The cell concentration C_X can be replaced by cell number density C_N .

Actually, M does not remain constant during the exponential period, because it will be affected by the culture condition, such as substrate and production concentrations, which are constantly

$$\mu = \mu_{\max} \left(\frac{C_S}{K_S + C_S} \right) \left(1 - \frac{C_P}{C_{Pm}} \right)^n \quad (19.5)$$

19.3.1.3 Structured Models

Unstructured distributed models such as Monod's equation satisfactorily predict the growth behavior in many situations. However, they cannot account for lag phases, sequential uptake of substrates, or changes in mean cell size during the growth cycle of a batch culture. Structured models recognize the multiplicity of cell components and their interactions. Many different models have been proposed based on the assumptions made for cell components and their interactions.

A general structured model equation can be derived by the following assumptions:

1. The system is defined as multiple cells that do not contain any abiotic phase of culture. The mass of the system is m on a dry basis and the specific volume is \hat{v} .
2. There are c components in the cell and the mass of the j th component per unit volume of the system is \hat{C}_{X_j} .
3. There exist kinetic rate expressions for p reactions occurring in the system and the rate of the j th component formed from the i th reaction per unit volume of the system is $\hat{r}_{X_{i,j}}$.

Then, during batch cultivation, the change of the j th component in the system with respect to time can be expressed as [6]

$$\frac{d(m\hat{v}\hat{C}_{X_j})}{dt} = m\hat{v} \sum_{i=1}^p \hat{r}_{X_{i,j}} \quad (19.6)$$

If the specific volume \hat{v} is assumed constant with time, the above equation can be rearranged to

$$\frac{d\hat{C}_{X_j}}{dt} = \sum_{i=1}^p \hat{r}_{X_{i,j}} - \frac{\hat{C}_{X_j}}{m} \frac{dm}{dt} \quad (19.7)$$

where the last term represents the dilution of intracellular components by the growth of biomaterial. All variables denoted by circumflexes in the preceding equations are intracellular properties. Since the structural models recognize the multiplicity of cell components and their interactions in the cell, it makes more sense to express the model with intrinsic variables.

The concentration terms in the preceding equations can be expressed as mass per unit culture volume V instead of that per biotic system volume $m\hat{v}$. The two different definitions of concentration are related as

$$\hat{C}_{X_j} = \frac{V}{m\hat{v}} C_{X_j} \quad (19.8)$$

Substituting the above equation into Equation (19.7) and simplifying for the constant V yields

$$\frac{dC_{X_j}}{dt} = \frac{m\hat{v}}{V} \sum_{i=1}^p \hat{r}_{X_{i,j}} \quad (19.9)$$

$$k_1 C_S C_E = k_2 C_{ES} \quad (19.14)$$

Since we assume that the total enzyme contents are conserved, the free-enzyme concentration C_E can be related to the initial enzyme concentration C_{E_0} :

$$C_{E_0} = C_E + C_{ES} \quad (19.15)$$

From the previous three equations, C_E and C_{ES} can be eliminated by substituting Equation (19.14) into Equation (19.15) for C_E and rearranging for C_{ES} as

$$C_{ES} = \frac{C_{E_0} C_S}{\frac{k_2}{k_1} + C_S} \quad (19.16)$$

Substitution of Equation (19.16) into Equation (19.13) results in the Michaelis-Menten equation.

$$r = \frac{dC_P}{dt} = -\frac{dC_S}{dt} = \frac{k_3 C_{E_0} C_S}{\frac{k_2}{k_1} + C_S} = \frac{r_{\max} C_S}{K_M + C_S} \quad (19.17)$$

The Michaelis constant K_M is equal to the dissociation constant K_1 or the reciprocal of equilibrium constant K_{eq} as

$$K_M = \frac{k_2}{k_1} = K_1 = \frac{C_S C_E}{C_{ES}} = \frac{1}{K_{eq}} \quad (19.18)$$

When K_M equals C_S , r is equal to one-half of r_{\max} , according to Equation (19.17). The value of K_M equals the substrate concentration when the reaction rate is half of the maximum rate r_{\max} , as shown in Figure 19.3. K_M is of importance since it characterizes the interaction of an enzyme with a given substrate.

Another kinetic parameter in Equation (19.17) is the maximum reaction rate r_{\max} , which is proportional to the initial enzyme concentration. To express the enzyme concentration in molar units, one needs to know the molecular weight of the enzyme and the exact amount of pure enzyme added.

Enzyme concentration may be expressed in mass units instead of molar units. However, the amount of enzyme is not well quantified in mass units because the actual contents of an enzyme can differ widely depending on its purity. Therefore, enzyme concentration is expressed as an arbitrarily defined unit based on its catalytic ability. For example, one unit of an enzyme, cellobiase, is defined as the amount of enzyme required to hydrolyze cellobiose to produce 1 μmol of glucose per minute. Whatever unit is adopted for C_{E_0} , the unit for $k_3 C_{E_0}$ should be the same as that of r , $\text{kmole/m}^3/\text{s}$. Care should be taken for the consistency of units when enzyme concentration is not expressed in molar units.

19.3.2.2 Briggs-Haldane Approach

In this approach, the change of the intermediate concentration is assumed to be negligible. From the mechanism described by Equations (19.11) and (19.12), the rates of product formation and of substrate consumption are

This solution procedure requires the knowledge of elementary rate constants, k_1 , k_2 , and k_3 . The elementary rate constants can be measured by experimental techniques, such as pre-steady-state kinetics and relaxation methods [12], which are more complicated compared to the methods to determine K_M and r_{\max} . A numerical solution with the elementary rate constants often provides a more precise picture of what is occurring during the enzyme reactions.

19.3.2.4 Evaluation of Michaelis-Menten Parameters

The kinetic parameters can be estimated by making a series of batch runs with different levels of substrate concentration. Then the initial reaction rate is calculated as a function of initial substrate concentration. The results can be plotted graphically so that the validity of the kinetic model can be tested and the values of the kinetic parameters estimated. The most straightforward way is to plot r against C_S as shown in Figure 19.3. The asymptote for r will be r_{\max} and K_M is equal to C_S when $r = 0.5 r_{\max}$. However, this is an unsatisfactory plot in estimating r_{\max} and K_M because it is difficult to estimate asymptotes accurately and also to test the validity of the kinetic model.

Therefore, the Michaelis–Menten equation (Equation (19.17)) is usually rearranged so that the results can be plotted as a straight line. Some of the better known methods are

Langmuir plot [13]:
$$\frac{C_S}{r} = \frac{K_M}{r_{\max}} + \frac{C_S}{r_{\max}} \quad (19.26)$$

Lineweaver-Burk plot [14]:
$$\frac{1}{r} = \frac{1}{r_{\max}} + \frac{K_M}{r_{\max}} \frac{1}{C_S} \quad (19.27)$$

Eadie-Hofstee plot [15,16]:
$$r = r_{\max} - K_M \frac{r}{C_S} \quad (19.28)$$

If the Michaelis–Menten equation is applicable, the Langmuir plot of C_S/r versus C_S will result in a straight line with slope $1/r_{\max}$ and intercept K_M/r_{\max} . Similarly, the Lineweaver-Burk plot of $1/r$ versus $1/C_S$ results in a straight line with slope K_M/r_{\max} and intercept $1/r_{\max}$. The Eadie-Hofstee plot of r versus r/C_S results in a straight line with slope $-K_M$ and intercept r_{\max} .

The Lineweaver-Burk plot is the most popular among the three because it shows the relationship between the independent variable C_S and the dependent variable r . However, $1/r$ approaches infinity as C_S decreases, which gives undue weight to inaccurate measurements made at low substrate concentrations. On the other hand, the Eadie-Hofstee plot gives slightly better weighting of the data than the Lineweaver-Burk plot. A disadvantage of this plot is that the rate of reaction r appears in both coordinates while it is usually regarded as a dependent variable. Therefore, the Langmuir plot (C_S/r versus C_S) is the most satisfactory of the three, since the points are equally spaced.

19.3.2.5 Inhibition of Enzyme Reactions

An inhibition (I) decreases enzymes activity, causing the rate of reaction to decrease competitively or noncompetitively (I). A competitive inhibitor has a strong structural resemblance to the substrate. Therefore, both the inhibitor and substrate compete for the active site of an enzyme as

$$K_M = \frac{k_2}{k_1} = \frac{k_6}{k_5}$$
$$r_{i,\max} = \frac{r_{\max}}{1 + \frac{C_1}{K_1}} \quad (19.34)$$
$$K_1 = \frac{k_4}{k_3} = \frac{k_8}{k_7}$$

Therefore, the maximum reaction rate will be decreased by the presence of a noncompetitive inhibitor, while the Michaelis constant K_S will not be affected by the inhibitor.

19.4 BIOREACTOR DESIGN

A bioreactor is a reactor in which enzymes or living cells catalyze the biochemical transformations. It is frequently called a fermenter whether the transformation is carried out by living cells or in vivo cellular components (enzymes). Fermentation originally referred to the metabolism of an organic compound under anaerobic conditions. However, modern industrial fermentation includes both aerobic and anaerobic cultures of organisms. Currently, bioreactor and fermenter can be regarded as synonyms.

19.4.1 BIOREACTORS

19.4.1.1 Stirred-Tank Bioreactor (or Fermenter)

In laboratories, cells are usually cultivated in Erlenmeyer flasks on a shaker. The gentle shaking effectively suspends the cells, enhances the oxygenation through the liquid surface, and aids the transfer of nutrients without damaging the structure of the cells.

For a large-scale operation, the stirred-tank fermenters (STF) are widely used (Figure 19.4). They are employed for both aerobic and anaerobic fermentation of a wide range of cells including microbial, animal, and plant cells. The mixing intensity can be varied widely by choosing suitable impellers and by varying agitating speeds. The mechanical agitation and aeration are effective for the suspension of cells, oxygenation, mixing of the medium, and heat transfer. The STF was one of the first large-scale fermenters developed in the pharmaceutical industries for the production of

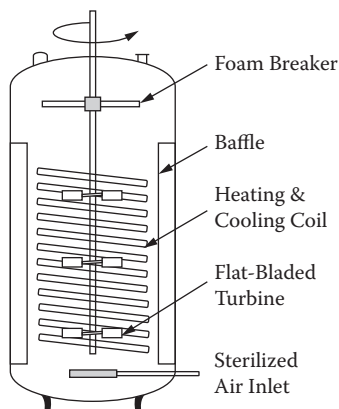


FIGURE 19.4 Schematic diagram of a stirred-tank fermenter.

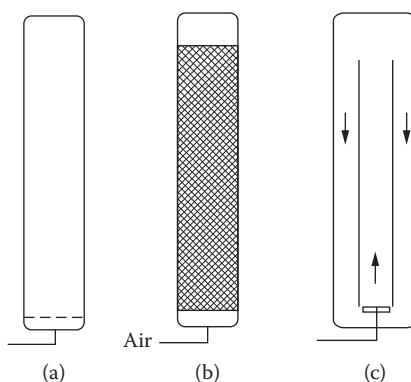


FIGURE 19.5 Alternative fermenters: (a) bubble column; (b) packed column; (c) air lift.

of the cells. Since the fermenter does not have any moving parts, a bubble-column fermenter is energy efficient with respect to the amount of oxygen transfer per unit energy input. As the cells settle, high cell concentrations occur in the lower portion of the column without any separation device. However, bubble-column fermenters are limited to aerobic fermentation. Furthermore, the rising bubbles may not provide adequate mixing for optimal growth. As the cell concentration increases in a fermenter, high airflow rates are required to maintain the cell suspension and mixing. The increased airflow rate can cause excessive foaming and high retention of air bubbles, which decreases the productivity of the fermenter. As bubbles rise in the column, they often coalesce rapidly, leading to a decrease in the oxygen-transfer rate. Therefore, column fermenters tend to be inflexible and limited to a relatively narrow range of operating conditions.

To overcome the weaknesses of the column fermenter, alternatives have been proposed. A tapered column fermenter can maintain a high airflow rate at the lower section of the fermenter where the cell concentration is high. Several sieve plates can be installed in the column for the effective gas-liquid contact and the breakup of the coalesced bubbles. The cylindrical column can be divided into multiple stages with stirrers. This configuration is analogous to stirred-tank fermenters connected in series. To enhance the mixing, the fermentation broth can be recirculated by using a pump.

A loop fermenter is a tank or column fermenter with a liquid circulation loop. Depending on how the liquid circulation is induced, it is often classified into three types: air-lift, stirred loop, and jet loop. The liquid circulation of the air-lift fermenter, Figure 19.5c, is induced by sparged air, which creates a density difference between the bubble-rich liquid in the riser (inner column) and the bubble-depleted liquid in the downcomer (space between the inner and the outer tubes). The liquid circulation and mixing are enhanced by installing a propeller or by circulating liquid externally using a pump. However, the addition of a propeller or pump diminishes the advantages of an air-lift fermenter as being simple and energy efficient.

19.4.2 MODE OF BIOREACTOR OPERATIONS

19.4.2.1 Batch or Plug-Flow Bioreactors

An ideal stirred bioreactor is assumed to be well mixed so that the contents are uniform in composition at all times. The plug-flow bioreactor (PFB) is an ideal tubular-flow bioreactor without radial concentration variations. The nutrient concentration of an ideal batch bioreactor after time t will be the same as that of a steady-state PFB at the longitudinal location of the residence time. Therefore, the following analysis applies for both the ideal batch bioreactor and the steady-state PFB.

The growth yield ($Y_{X/S}$) is defined as the amount of cell produced per substrate consumed as

$$Y_{X/S} = \frac{\Delta C_X}{-\Delta C_S} = \frac{C_X - C_{X_0}}{-(C_S - C_{S_0})} \quad (19.39)$$

Substitution of Equation (19.39) into Equation (19.38) and integration of the resultant equation gives a relationship that shows how the cell concentration changes with respect to time:

$$(t - t_0)\mu_{\max} = \left(\frac{K_S Y_{X/S}}{C_{X_0} + C_{S_0} Y_{X/S}} + 1 \right) \ln \frac{C_X}{C_{X_0}} + \frac{K_S Y_{X/S}}{C_{X_0} + C_{S_0} Y_{X/S}} \ln \frac{C_{S_0}}{C_S} \quad (19.40)$$

19.4.2.1.2 Enzyme Reactions

Assume that an enzyme reaction is initiated at $t = 0$ by adding enzyme and the reaction mechanism can be represented by the Michaelis-Menten equation

$$-\frac{dC_S}{dt} = \frac{r_{\max} C_S}{K_M + C_S} \quad (19.41)$$

Equation (19.41) is similar in form to the Monod equation, but is quite different when you compare it with Equation (19.37), which has an extra term, C_X .

An equation expressing the change of the substrate concentration C_S with respect to time can be obtained by integrating Equation (19.41), as follows:

$$\int_{C_{S_0}}^{C_S} - \left(\frac{K_M + C_S}{C_S} \right) dC_S = \int_0^t r_{\max} dt \quad (19.42)$$

and

$$K_M \ln \frac{C_{S_0}}{C_S} + (C_{S_0} + C_S) = r_{\max} t \quad (19.43)$$

With known values of r_{\max} and K_M , the change of C_S with time in a batch reactor can be predicted from this equation.

19.4.2.2 Continuous Stirred-Tank Bioreactor

For an ideal continuous stirred-tank bioreactor (CSTB), the concentrations of the various components of the outlet stream are assumed to be the same as the concentrations in the bioreactor. Continuous operation of a bioreactor can increase the productivity of the reactor significantly by eliminating the downtime and the ease of automation.

19.4.2.2.1 Cell Cultivation

Microbial populations can be maintained in a state of exponential growth for extended time by using a system of continuous culture, operated either as chemostat or as a turbidostat. In a chemostat, the flow rate is set at a particular value and the rate of growth of the culture adjusts to this flow rate. In a turbidostat, the turbidity is set at a constant level by adjusting the flow rate. It is easier to operate a chemostat than a turbidostat, because the former is at a constant flow rate, whereas

rate. Hence, the specific growth rate of a microorganism is controlled by changing the medium flow rate. If the growth rate is expressed by the Monod equation, then

$$D = \mu = \frac{1}{\tau_m} = \frac{\mu_{\max} C_S C_X}{K_S + C_S} \quad (19.47)$$

The equality of the specific growth rate and the dilution rate of the steady-state CSTB is helpful in studying the effects of various components of the medium on the specific growth rate. By measuring the steady-state substrate concentration at various flow rates, kinetic models can be tested and the value of the kinetic parameters can be estimated. By rearranging Equation (19.47), a linear relationship can be obtained as follows:

$$\frac{C_S}{\mu} = \frac{K_S}{\mu_{\max}} + \frac{C_S}{\mu_{\max}} \quad (19.48)$$

$$\frac{1}{\mu} = \frac{K_S}{\mu_{\max}} \frac{1}{C_S} + \frac{1}{\mu_{\max}} \quad (19.49)$$

$$\mu = \mu_{\max} - K_S \frac{\mu}{C_S} \quad (19.50)$$

These are similar to the equations for the Langmuir, the Lineweaver-Burks, and the Eadie-Hofstee plots that were discussed earlier with the Michaelis-Menten kinetics.

From Equation (19.47), C_S can be calculated with a known residence time and the Monod kinetic parameters as

$$C_S = \frac{K_S}{\tau_m \mu_{\max} - 1} \quad (19.51)$$

However, the preceding expression is only valid when $\tau_m \mu_{\max} > 1$. If $\tau_m \mu_{\max} < 1$, the growth rate of the cells is less than the rate of cells leaving with the outlet stream. Consequently, all of the cells in the fermenter will be washed out.

If the growth yield ($Y_{X/S}$) is constant, then

$$C_X = Y_{X/S}(C_{S_i} - C_S) \quad (19.52)$$

Substituting Equation (19.51) into Equation (19.52) yields the correlation for C_X as

$$C_X = Y_{X/S} \left(C_{S_i} - \frac{K_S}{\tau_m \mu_{\max} - 1} \right) \quad (19.53)$$

Similarly, one can derive a relationship for the product concentration C_P as

$$C_P = C_{P_i} + Y_{P/S} \left(C_{S_i} - \frac{K_S}{\tau_m \mu_{\max} - 1} \right) \quad (19.54)$$

TABLE 19.9
Solubility of Oxygen in Water at 1 atm^a

Temperature (°C)	Solubility	
	mmol O ₂ /L	mg O ₂ /L
0	2.18	69.8
10	1.70	54.5
15	1.54	49.3
20	1.38	44.2
25	1.26	40.3
30	1.16	37.1
35	1.09	34.9
40	1.03	33.0

^a Data from *International Critical Tables*. 1928. Vol. III, 271. New York: McGraw-Hill Book Co.

19.5.2 DETERMINATION OF OXYGEN-ABSORPTION RATE

The oxygen absorption rate per unit volume q_a/v can be estimated by

$$\frac{q_a}{v} = K_L a (C_L^* - C_L) = k_L a (C_L^* - C_L) \quad (19.58)$$

where a is the interfacial area per unit volume and C_L^* is the liquid-side oxygen concentration in equilibrium with the gas-phase oxygen. Because the oxygen is a sparingly soluble gas, the overall mass-transfer coefficient K_L is approximately equal to the individual mass-transfer coefficient k_L . An objective in fermenter design is to minimize power consumption and airflow rate. To increase the oxygen absorption rate, larger k_L , a , and, $C_L^* - C_L$ are needed. Since the concentration difference is limited because the value of C_L^* is low, the main parameters of interest are the mass-transfer coefficient and the interfacial area.

19.5.2.1 Estimation of Equilibrium Oxygen Concentration C_L^*

Table 19.9 lists the dissolved concentration of oxygen in water that is in equilibrium with pure oxygen at atmosphere pressure at various temperatures. Since air supplies the oxygen to a bioreactor, the maximum concentration of oxygen is about one-fifth of the solubility listed, according to Henry's law:

$$C_L^* = \frac{P_{O_2}}{H_{O_2}(T)} \quad (19.59)$$

where P_{O_2} is the partial pressure of oxygen and $H_{O_2}(T)$ is Henry's law constant of oxygen at a temperature, T . The value of Henry's law constant can be obtained from the solubility listed in Table 19.9.

19.5.2.2 Sodium Sulfit Oxidation Method

One of the simplest techniques to determine $k_L a$ is the sodium sulfite oxidation method [19], which is based on the oxidation of sodium sulfite to sodium sulfate in the presence of a catalyst (Cu^{++} or Co^{++}) as

19.5.3 CORRELATION FOR $k_L a$

19.5.3.1 Bubble Column

Akita and Yoshida [21] correlated the volumetric mass-transfer coefficient $k_L a$ [s^{-1}] for the absorption of oxygen in various aqueous solutions in bubble columns, as follows:

$$k_L a = 0.6 D_{AB}^{0.5} \nu_c^{-0.12} \left(\frac{\sigma}{\rho_c} \right)^{-0.62} D_T^{0.17} g^{0.93} H^{1.1} \quad (19.64)$$

where

D_{AB} = diffusivity of A through B [m^2/s]

ν_c = kinematic viscosity [m^2/s]

σ = interfacial tension [kg/s^2]

ρ_c = the density of liquid [kg/m^3]

D_T = tank diameter [m]

g = gravity constant [m/s^2]

H = the height of the liquid level in a tank [m]

19.5.3.2 Mechanically Agitated Vessel

For aerated mixing vessels in an aqueous solution, the mass-transfer coefficient is proportional to the power consumption. Van't Riet [22] correlated the data of several investigators as follows:

1. For "coalescing" air-water dispersion,

$$k_L a = 0.026 \left(\frac{P}{v} \right)^{0.4} V_S^{0.5} \quad (19.65)$$

2. For "noncoalescing" air-electrolyte solution dispersions,

$$k_L a = 0.002 \left(\frac{P}{v} \right)^{0.7} V_S^{0.2} \quad (19.66)$$

where

P = power dissipated by impeller during agitation [W]

v = volume of the liquid [m^3]

V_S = superficial gas velocity [m/s]

These correlations are applicable for volumes up to about 2.6 m^3 .

19.5.4 POWER CONSUMPTION

Power consumption by agitation is a function of physical properties, operating conditions, and vessel and impeller geometry. For fully baffled agitated vessels,

9. A.J. Brown. 1902. *Journal of the Chemical Society* 81: 373–388.
10. L. Michaelis, M.L. Menten. 1913. *Bio-chem Zeitschr* 49: 333–369.
11. G.E. Briggs, J.B.S. Haldane. 1925. *Biochemical Journal* 19: 338–339.
12. J.E. Bailey, D.F. Ollis. 1986. *Biochemical Engineering Fundamentals*, 111–113. New York: McGraw-Hill.
13. J.J. Carberry. 1976. *Chemical and Catalytic Reaction Engineering*, 364–366. New York: McGraw-Hill.
14. H. Lineweaver, D. Burk. 1934. *Journal of the American Chemical Society* 56: 658–666.
15. G.S. Eadie. 1942. *Journal of Biological Chemistry* 146: 85–93.
16. B.H.J. Hofstee. 1952. *Journal of Biological Chemistry* 199: 357–364.
17. K. Schüugerl. 1982. *International Chemical Engineering* 22: 591–610.
18. J. Monod. 1949. *Annual Review of Microbiology* 3: 371–394.
19. C.M. Cooper, G.A. Fernstrom, S.A. Miller. 1944. *Industrial & Engineering Chemistry* 36: 504–509.
20. H. Taguchi, A.E. Humphrey. 1966. *Journal of Fermentation Technology Japan* 44: 881–889.
21. K. Akita, R. Yoshida. 1973. *Industrial & Engineering Chemistry Process Design and Development* 12: 76–80.
22. K. Van't Riet. 1979. *Industrial & Engineering Chemistry Process Design and Development* 18: 357–364.
23. J.Y. Oldshue. 1985. In *Mixing of Liquids by Mechanical Agitation*, ed. J.J. Ulbrecht, G.K. Patterson, 309–342. New York: Gordon and Breach Science Publishers.

and boiling points, respectively, of water at 0°C and 100°C (depending on barometric pressure). The current discussion will be limited to the most popular thermometers. More advice and information on various sensors relative to their installation and operation are in the literature.

20.2.1 THERMOCOUPLES

Two dissimilar wires are connected in two places to form a loop. The first connection is positioned where the temperature is to be measured; the second connection is positioned where the temperature is known. This temperature difference causes a potential (or voltage) difference in the wires. Tables are available for predicting the temperature changes of several combinations of two dissimilar wires [3]. Temperature ranges for common thermocouples are as follows:

Chromel/alumel	−180°C to 1370°C
Iron/constantan	−180°C to 760°C
Copper/constantan	−180°C to 400°C
Platinum 10% rhodium/platinum	0°C to 1760°C
Tungsten/tungsten 26% rhenium	0°C to 2850°C
Tungsten 5% rhenium/tungsten 26% rhenium	0°C to 2850°C

Thermocouples unfortunately develop only relatively small voltage (electromotive force, or emf) changes for a temperature difference of 1°C. Hence errors of predicted temperatures are often relatively large. The first three thermocouples often have errors of 2°C to 3°C or 0.5% to 0.75%. The latter three (and more expensive) thermocouples typically have smaller errors. With specially constructed thermocouples having purer metals, better connections, etc., errors are reduced by perhaps 50% as compared with the values reported above.

Thermocouples tend to be relatively inexpensive, but the instruments to measure voltages and to record the temperatures are generally more expensive. To obtain reliable temperature measurements, the following factors are important relative to the installation of the thermocouple plus other types of thermometers:

1. The tip of the thermocouple (or other thermometer) often cannot be inserted directly in the liquid, gas, slurry, etc., due to chemical attack or erosion of the thermocouple. Obtaining a leak-proof system is frequently a problem.
2. A thermowell is often employed for the temperature probe in order to protect it against direct contact with the material being investigated. A gas such as air is often in the thermowell in direct contact with the thermocouple. As a result, the thermocouple may become oxidized or corroded, causing the calibration to change. Thermocouples for ethylene furnaces operated at about 800°C to 1000°C often need to be replaced after several months of operation.
3. Sometimes appreciable heat transfer may occur in both the thermocouple and the thermowell, e.g., in ethylene furnaces. In these furnaces, there are large temperature gradients along the length of the thermocouple.
4. Frequently, thermocouples are provided with protective sheaths, and their purchasing price is considerably higher.

A well-designed system, including thermocouple, thermowell, and often protective sheath, generally provides more reliable measurements.

20.2.2 RESISTANCE THERMOMETERS AND THERMISTORS

For these thermometers, the electrical resistance of a metal or metal oxide changes with temperature. This resistance change can be measured by three-wire or four-wire null bridges (or Wheatstone

4. Gas or suspended solids or liquids in the space between the material being measured and the radiation detector measuring the radiation.
5. Wavelengths of the radiation being recorded by the measuring device. Wavelengths being emitted from the object being investigated vary significantly with its temperature often in range of 0.3 to 100 microns. At ambient temperatures, wavelengths in the visible range predominate, but at about 1000°C, infrared wavelengths of about 2 to 20 microns predominate. At still higher temperatures, even shorter wavelengths result, i.e., near infrared, ultraviolet, etc. Modern pyrometers often record the emissions of two or more wavelengths.
6. Most desired instrument for recording the radiation of the object being investigated.
7. Method of collecting radiation from the object being investigated. The size of the aperture or opening to view the object plus area being sighted is important.

Several temperature readings sometimes need to be recorded. In an ethylene furnace, for example, a hydrocarbon feedstock is pyrolyzed to produce an ethylene-rich stream. At the inlet to the coil reactor, much lower temperatures occur as compared with the outlet. In addition, the ceramic wall of the furnace is often relatively close to that of the hot combustion gases. These gas temperatures are much higher than those of the metal walls. Normally, the measuring detector collects information at different locations inside the furnace through a small aperture on the wall of the furnace. De Witt and Albright [4] report the results of a test of a furnace for distilling crude oil in a refinery about 20 years ago. In this test, flat targets were employed in which calibrated thermocouples were embedded. One target was essentially at the temperature of the combustion gas (and hence was considerably hotter) while another target was cooled to a much lower temperature. The pyrometers of those tests resulted in temperature measurements that were too low for the low-temperature target. Newer instruments and improved methods of predicting the temperatures have since significantly improved the accuracy of measurements.

Emissivities of different metals vary greatly. Liptak et al. [1] report values for common metals including 0.03 for gold and 0.94 for dull oxidized wrought iron. Calibrations based on emissivities correct to a high degree predicted values. Part of the radiant energy is adsorbed by intervening smoke, carbon dioxide, etc. Narrow-band pyrometers use only a narrow band of the spectrum, often in the red zone. By proper selecting of the band, the desired temperature of the solid, gas, or glass can be predicted. They recommended the wavelength in microns for vacuum depositions (0.2 to 0.3); furnaces, refractory metals, etc. (0.653); metal processing (0.6 to 1.0); textiles, plastics, food products (2.0 to 2.6); thin film polymers (3.43 ± 0.14); and carbon dioxide gas (4.8 to 5.6).

20.2.4 FILLED-BULB AND GLASS-STEM THERMOMETERS

These thermometers contain either mercury, alcohol, etc., as liquids. The thermal expansion of these liquids is greater than the glass, so the height of liquid in the glass capillary rises as the temperature increases. A major problem is that the glass can be easily broken. Furthermore, mercury causes toxicity problems if the thermometer breaks. Visual observations are usually required to read the thermometers. Often these instruments are restricted to temperatures from about -40°C to 400°C. Their advantages are low costs, long life if properly protected, and reasonable accuracy. They still are widely used in experimental setups and for various home uses.

Some filled-bulb thermometers take account of the pressure increase in the capillary stream. This increase is due to the vapor-pressure rise of the liquid phase plus the rise due to the compression of the gas. A relatively high pressure may hence occur. Bending the capillary tube is sometimes used, and the tube straightens to a degree as the pressure rises. The amount of straightening can be calibrated with a pointer on a dial to measure the temperature.

momentum is imparted to flowing fluid by providing harmonic vibrations. Sometimes a U-bend is provided, and in other designs, two tubes are operated in parallel. Costs of these units tend to be high, but the electromagnetic detectors often provide highly reliable flowrate predictions. Reigner [6], however, indicates they are not reliable for two-phase flows such as aerated liquids. Omega Engineering [7] also provides important recommendations.

3. Displacement flowmeters for both liquids and gases. In some cases, positive displacement pumps are employed for liquids.
4. Rotameters can often be used for liquids and gases, but safety issues such as loss of toxic materials if the tube breaks are concerns.
5. Weirs and flumes are sometimes employed.
6. Flowmeters are available for granular solids.

20.4 PRESSURE MEASUREMENTS

Measuring pressure is obviously of great importance in chemical processes, and numerous instruments and techniques are available. Key considerations in selecting the best instrument for a specific application include the following:

1. Range of pressures to be measured may vary from high vacuums to several thousand atmospheres.
2. Short-time pulsations of pressure. For example, some pumps cause rapid pulsations.
3. Desired accuracy and precision of pressure reading.
4. Temperature range of materials being measured.
5. Character or nature of materials including corrosiveness, freezing point, viscosity, etc. Sometimes special precautions are needed in transferring pressure from process stream to pressure measuring device. For common Bourdon tubes, fluids such as silicone oils, light hydrocarbon oils, glycerine, etc., are employed for such transfers.
6. The required or preferred method of reading or recording the pressure. Pressures, for example, can be read usually from a gauge or a recorder.

Methods and instruments for measuring pressure are available for \$100 or less up to several thousand dollars. It should be emphasized that many pressure devices read pressure differences between the process stream and atmospheric pressure.

1. Pressure gauges containing Bourdon tubes are widely used for either pressures from atmospheric to high pressures, such as over 700 bars, or from atmospheric to high vacuums. With pressure changes, the tube changes shape causing a needle to change direction so the pressure can be read. Gauges calibrated by the manufacturer often have inaccuracies up to $\pm 2.0\%$ over at least a portion of their range. Better accuracy can be obtained with more carefully manufactured and hence more expensive gauges.
2. Pressure gauges involving spring and bellows, bell-cased mounting, diaphragms, and other devices have also been developed.
3. Strain-gauge transducers are also employed for pressure measurements; mechanical strain caused by pressure changes causes the electrical resistance of the transducer to change. Semiconductors such as germanium or silicon are often employed. Thermal errors are minor at near-ambient temperatures. A wide range of prices occurs for such transducers.
4. Manometers are employed for relatively small pressure changes. Often costs are low.
5. Dead-weight piston gauges are employed to calibrate pressures up to large pressures. Well-designed gauges of this type are relatively expensive.

21.3.4	Microbiologically Influenced Corrosion (MIC).....	1566
21.3.4.1	Effect on Materials of Construction	1567
21.3.4.2	Mitigation Methods	1567
21.4	Failure Modes	1567
21.4.1	Embrittlement Phenomena	1567
21.4.2	Carbon and Low-Alloy Steel	1569
21.4.2.1	Stainless Steel.....	1571
21.4.3	High Alloys.....	1572
21.4.4	Hydriding	1572
21.4.5	High-Temperature Effects	1572
21.4.5.1	Mechanical Effects	1572
21.4.5.2	Metallurgical Effects	1573
21.4.6	Low-Carbon Stainless Steel	1574
21.4.6.1	Chemically Stabilized Stainless Steel.....	1574
21.4.7	Hydrogen Gas.....	1577
21.4.8	Nitriding.....	1578
21.4.9	Oxidation	1579
21.4.10	Sulfidation and Sulfidic Corrosion.....	1579
21.5	The Process of Materials Selection.....	1581
21.5.1	Designing a Template.....	1581
21.5.2	Materials Selection Criteria.....	1588
21.5.2.1	Product Contamination.....	1588
21.5.2.2	Reliability	1588
21.5.3	Organizing the Materials Selection Procedure	1589
21.5.4	Materials Selection Procedure: Exceptions.....	1589
21.5.4.1	Piping.....	1589
21.5.4.2	Pumps	1589
21.5.4.3	Fabricated Equipment	1589
21.5.5	Grouping Process Regions	1590
21.5.6	Materials Selection Procedure.....	1590
21.5.6.1	Low Temperature	1590
21.5.6.2	High Temperature.....	1590
21.5.6.3	Corrosion	1591
21.5.6.4	Upset Conditions: Review.....	1592
21.5.7	Materials Selection Diagram.....	1593
21.6	Conclusions.....	1594
	References	1595

21.1 AN OVERVIEW OF THE MATERIALS SELECTION PROCESS

In selecting metals and alloys as materials of construction, one must have knowledge of how materials fail, for example is, how they corrode, become brittle with low-temperature operation, or degrade as a result of operating at high temperatures. Corrosion, embrittlement, and other degradation mechanisms such as creep will be described in terms of their threshold values. Transient or upset operating conditions are common causes of failure. Examples include start-ups and shut-downs, loss of coolant, the formation of dew point water, and hot spots due to the formation of scale deposits on heat transfer surfaces. Identification and documentation of all anticipated upset and transient conditions are required.

Corrosion debris is a related problem. In some applications, materials with nominally low corrosion rates produce considerable corrosion debris. Such problems are always associated with units that contain large surface areas exposed to the corroding fluid. Examples include heat

Operating Temperature (Minimum/Maximum): _____		
Operating Pressure (Minimum/Maximum): _____		
Commodity: _____	Phases: _____	Liquid Water (Y/N): _____
Corrodents: _____		
Crack-Inducing Agents: _____		
Metallurgy: _____		
PWHT (Y/N): _____	Valve Trim *: _____	Corrosion Allowance: _____
Notes: _____		
<p>* For most services, valve trim will be 13Cr stainless steel. Use full hard facing for temperatures >600°F (315°C).</p>		

FIGURE 21.1 A simplified materials selection template. (Copyright Marcel Dekker, Inc.; reprinted with permission [5].)

21.1.4 SPECIAL REQUIREMENTS

The required design life will generally affect materials selection and/or the determination of the recommended corrosion allowance. Normally, the user or process licensor will define design life requirements. It is helpful to define the design life requirements in the “Notes” addendum of the template.

Materials selection for some projects is affected by special objectives such as minimal capital cost, minimal maintenance, short project schedule, extended design life, concerns about product purity, or the consequences of a leak or rupture. If such objectives are governing, they should be included in the materials selection design basis in the “Notes” addendum of the template. Occasionally, objectives may be in conflict, such as minimal capital cost vs. short schedule. When this occurs, compromises are made. Or a superior material may not be selected if its delivery would delay start-up. Safety and environmental concerns must always be considered.

21.1.5 MATERIALS SELECTION TEMPLATE

A materials selection template, containing critical design and operating conditions for each piece of equipment and piping run, is used as part of a structured method to select suitable materials of construction. It is usually prepared by a plant or project process engineer, and is customized for the plant or project (see Figure 21.1 for an example of a simple template).

The template serves two major purposes: (1) it organizes all the technical information needed for materials selection; and (2) on a large job or project, the template is a convenient means to transmit process and materials selection information to design engineers.

21.2 BASIC METALLURGY

Metallurgical descriptions often contain jargon and arcane words, as explained below.

21.2.1 HEAT TREATMENTS

21.2.1.1 Annealing

For carbon and low-alloy steels, full annealing requires heating to a temperature of 1350°F to 1750°F (730°C to 955°C). The steel is held at this temperature long enough to ensure through-

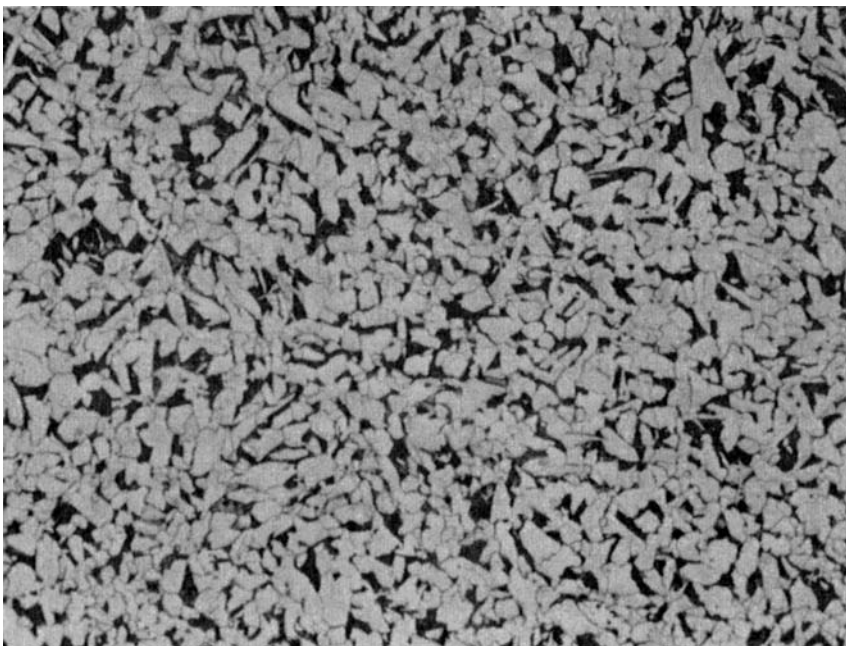


FIGURE 21.3 Carbon steel that has been normalized. © Copyright by Marcel Dekker, Inc.; reprinted with permission [5].

21.2.1.4 Stress Relief/Postweld Heat Treatment

Residual stresses can be introduced into a metal by fabrication processes such as forging or rolling, by uneven heating or cooling, or by welding. The magnitude of such stresses is usually on the order of the yield strength, but sometimes approaches the tensile strength.

To stress relieve or postweld heat treat carbon and low-alloy steels, they are typically heated to 1100°F to 1350°F (595°C to 730°C) for extended time, followed by air cooling. The minimum time is specified by the relevant engineering code, and the temperature must be less than the lower transformation temperature of the steel, which is the lowest temperature at which austenite starts to form, for example, 1333°F (720°C) for plain carbon steels. In order to avoid degrading the required mechanical properties of a heat treated alloy, subsequent fabrication heat treatment temperatures, such as those for stress relief and PWHT, must not exceed the tempering temperature (discussed in the next section).

The yield strengths of metals and alloys decrease with increasing operating temperature. Residual stresses in excess of the reduced yield strength are eliminated via plastic deformation. Upon cooling, the maximum residual stress possible is the yield strength at the holding temperature. For carbon steels, heat treatment will reduce residual stress by about two-thirds. When done for the purpose of removing residual stresses caused by cold work, the process is termed stress relief.

As the liquid metal in a weld solidifies, it becomes at least partially constrained by the surrounding parent metal. When the weld metal cools to ambient temperature, the resulting residual stress in the weld is approximately equal to the ambient temperature yield strength of the parent metal. Stress relief heat treatment for welds is called postweld heat treatment. An additional benefit of such treatment is a reduction of the hardnesses of the weld metal and heat-affected zone (HAZ), thus reducing the risk of stress corrosion cracking.

Stress corrosion cracking in heat treated weldments indicates that postweld heat treatments are sometimes ineffective. Sometimes this result can be attributed to microalloying. (Microalloying is discussed later.) In some cases, subsequent stress corrosion cracking can be traced to an improperly

generate the cooling rates necessary to develop martensite. Hence, tempering is primarily for stress relief rather than for softening martensite. Many codes, such as the ASME Boiler & Pressure Vessel Code, Section VIII [1] and materials specifications such as ASTM A516, permit such thick sections, properly quenched and tempered, to be equivalent to normalized material. Tempering is also sometimes done in conjunction with other heat treatments such as normalizing in order to soften and/or toughen the steel. In some cases, stress relief may be a secondary or even a primary objective.

Fabricators occasionally propose multiple heat treatments or heat treatments having unusually long holding times or unusually high holding temperatures. The user should be wary of such proposals. Some multiple heat treatments may cause degradation of carbon and low-alloy steels with loss of strength and/or loss of toughness. The fabricator should be required to demonstrate, by testing, that the proposed procedure will not result in material degradation.

21.2.2 MICROSTRUCTURAL TERMS

21.2.2.1 Austenite

Austenite is a high-temperature form of carbon steel, having a face-centered cubic crystal structure. The lowest temperature at which ordinary carbon steel can be fully austenitic is 1333°F (720°C). During normalizing heat treatments, the holding temperature and time are specified so that the alloy becomes fully austenitic. For the common carbon steels, the austenitizing temperature is typically specified as 1650°F (900°C).

Austenite has a much higher solubility for carbon than other forms of steel. Heating the steel to an austenitizing temperature causes any carbides present to dissolve. Alloys capable of forming austenite at high temperatures, but that transform to other crystal structures at lower temperatures, are said to be hardenable by heat treatment. Martensitic steels are an example. Most carbon and low-alloy steels are hardenable by heat treatment.

When alloying elements such as nickel or manganese are added to carbon steel, the austenitic microstructure becomes stable at low temperatures. For example, most austenitic stainless steel and high-nickel alloys exhibit stable austenitic microstructures at temperatures approaching absolute zero. These alloys have excellent low-temperature fracture toughness and are resistant to hydrogen embrittlement from causes other than cathodic charging. Most austenitic alloys are not hardenable by heat treatment, the major exception being a few precipitation hardenable types.

21.2.2.2 Ferrite

Ferrite is essentially pure iron with a body-centered cubic crystal structure. Ferrite forms from austenite at about 1675°F (915°C), as the austenite cools from a normalizing heat treatment. Because ferrite does not contain enough carbon to permit the formation of martensite, it is not hardenable by heat treatment. The most common truly ferritic steel is Type 405 SS, a ferritic stainless steel. The generic term "ferritic steel" often refers to carbon or low-alloy steels that contain other phases in addition to ferrite. Such steels are usually hardenable by heat treatment. Ferritic steels become brittle at low temperatures. This phenomenon is reversible, that is, the steels regain their former toughness after being warmed up. Ferritic steels are also susceptible to hydrogen embrittlement.

21.2.2.3 Martensite

Martensite is formed from high-temperature austenite, in heat-treatable alloys, by cooling the austenite fast enough to prevent the formation of ferrite. For some heat-treatable alloys, quenching in water or some other liquid such as oil or a molten salt is often required. Some steels have sufficient alloying additions that quenching is not necessary. Air cooling produces the martensitic microstructure in Type 410 SS and other martensitic stainless steels. Since martensite is usually brittle, it is normally subsequently tempered. The tempering temperature is less than the austenite

TABLE 21.1
Typical Carbon Equivalent (CE) Limits for Carbon Steels

Wall Thickness	1/2"	5/8"	3/4"	7/8"	1.0"
	(12.7 mm)	(15.9 mm)	(19 mm)	(22 mm)	(35.4 mm)
Max. CE Value	0.4	0.39	0.37	0.35	0.34

deformation disappears with the removal of the stress. Plastic deformation (sometimes called permanent strain) is permanent, i.e., plastic deformation remains after removal of the stress that caused it.

Galling is related to adhesive wear. When two metals of similar chemistry and hardness are in moving contact and under pressure, in the absence of lubrication, surface asperities (high points) tend to momentarily weld together. Continued movement ruptures these very local welds, resulting in metallic particles being torn from one or both surfaces. These particles result in rapidly increasing friction. Galling is an extreme form of adhesive wear, causing gross surface damage. Austenitic stainless steels are the most common susceptible materials. Examples include threaded fasteners (galling occurs in the threaded region) and valve closures.

Hardenable describes alloys that can be hardened and strengthened by cold working, for example, strain-hardened bolting. Hardenability describes the ability of an alloy to be hardened and strengthened, usually by heat treatments such as quenching and tempering.

Heat-affected zone (HAZ) is the volume of parent metal in which the mechanical properties and/or the microstructure have been changed by the heat of welding or thermal cutting. For most welds in carbon and low-alloy steels, the HAZ is a band, usually about 1/8 in. (3 mm) wide, adjacent to the fusion line of the weld. In austenitic stainless steels, a narrow, secondary HAZ may be generated some distance from the fusion line as illustrated in Figure 21.4.

Hot working causes plastic deformation to occur at a temperature high enough to prevent the material from becoming strain hardened. Instead, it spontaneously “recovers” plastic deformation. Hot-worked materials therefore do not have the internal energy characteristic of cold-worked materials. In practice, hot-work threshold temperatures are dictated by factors such as tool life. These temperatures range from as low as 350°F (175°C) for aluminum alloys to as high as 2300°F (1260°C) for steels and nickel alloys.

Oxide stabilized refers to materials, such as aluminum and the stainless steels, whose corrosion resistance depends on the formation and stability of a very thin surface oxide layer that is inert, easily “healed” if damaged, and tenacious. When the oxide layer has been disrupted and not healed, the material usually has little corrosion resistance. Both active and passive states sometimes exist adjacent to each other on the surface, resulting in rapid local corrosion. Crevice corrosion in stainless

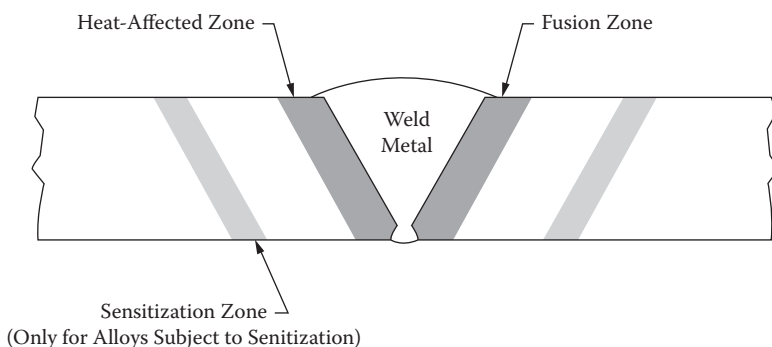


FIGURE 21.4 The typical features of a weld. © Copyright by Marcel Dekker, Inc.; reprinted with permission [5].

castings. Wrought products tend to have a uniform, fine, partially isotropic grain structure. However, they are normally more expensive, reflecting the fabrication costs of hot working, machining, welding, etc.

Castings typically have lower strength, lower toughness, higher defect concentrations, and coarse anisotropic grain structures. Depending on the casting process, the surface may be less corrosion resistant than the bulk material. Because of this, corrosion tests should represent the expected surface condition of the casting. The advantages of castings include relatively low cost, ease of obtaining complex shapes, and minimal machining. In some alloys, the silicon addition and/or cast grain structure produces exceptional corrosion resistance. For example, austenitic stainless steel castings are more resistant to chloride stress corrosion cracking than are their wrought equivalents. In addition, castings are often less weldable, usually because of their greater silicon and/or carbon contents. Thus, repairability may be an issue and may be enhanced by specifying tighter compositions. A common example is the use of Grade CA-6NM (12Cr-4Ni-Mo) (UNS J91540) instead of Grade CA-15 (13Cr) (UNS J91150) for 12Cr castings. (The CA-6NM alloy has a much lower carbon allowable than the CA-15 alloy.) When choosing between wrought and cast components, the lower flaw density and/or better repairability of the wrought product or the lower cost or a unique property of the cast product should be considered.

Welding results in a metallurgical discontinuity* with different microstructures than the parent metal. Mechanical properties of the weld metal usually differ. Even with PWHT, weldments retain a residual stress field. Heat affected zones often contain a coarsened grain structure and/or "hard spots." Corrosion testing of the welds may be a critical part of the testing program.

As discussed earlier, cold work can change the mechanical properties of a material, including adversely affecting the fracture toughness. For applications such as bolting that will not be exposed to crack-inducing agents, cold working is deliberately used to increase yield strengths. However, cold-worked areas are typical sites for the development of strain aging (see Section 21.4). In addition, cold-worked areas can be susceptible to corrosion pitting, stress corrosion cracking, hydrogen embrittlement, and other damaging phenomena. For applications in which excessive cold working may be harmful, it is normal practice to stress relieve materials that have received more than 5% permanent outer fiber strain.

21.2.6 METALS AND ALLOYS

21.2.6.1 Cast Iron

Cast irons typically contain at least 2 wt% carbon; the cast carbon steels used for plant construction rarely contain more than 0.35%. The high carbon content of cast iron makes it difficult to weld. Two types of cast iron are commonly used:

1. *Gray cast iron* such as ASTM A48 material is plain cast iron, composed of ferrite containing graphite stringers. Figure 21.5 shows the microstructure. It is relatively brittle and is used for applications in which toughness is not a concern, including utility services, as pump cases, and valve bodies.
2. *Ductile cast iron* (also known as *nodular* or *spheroidal iron*) contains a small amount of magnesium, which greatly improves ductility and toughness; an example is ASTM A536. Figure 21.6 shows the microstructure. Nodular cast iron is occasionally used in valve bodies, in pumps in various utility services, and in large reciprocating compressors. Malleable cast iron such as ASTM A47 material is a related alloy that is relatively expensive. Mildly acidic water can graphitize both gray and ductile cast iron as the iron

* A metallurgical discontinuity is an interruption in the normal physical structure of a metal. Examples include welds, cracks, laps, seams, bolted closures, inclusions, and porosity. A metallurgical discontinuity may or may not be a defect, that is, a discontinuity that is regarded as harmful.

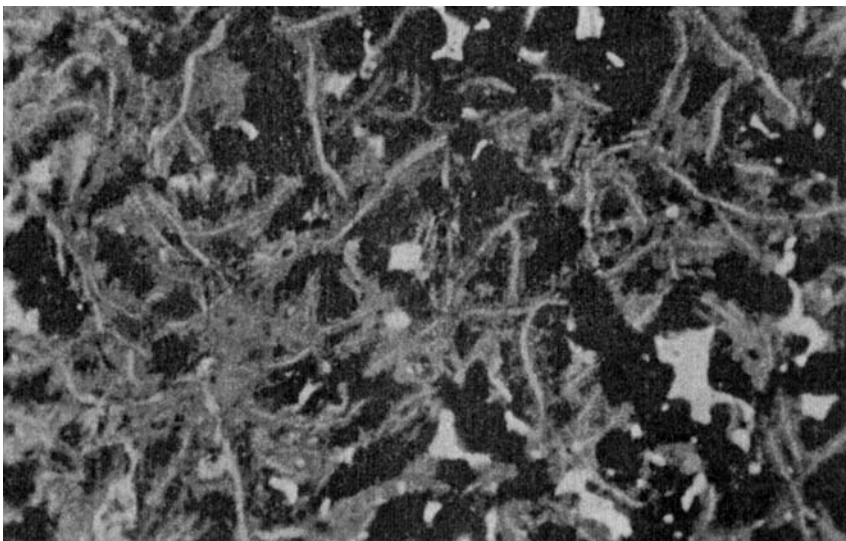


FIGURE 21.7 “Graphitization” of a gray cast iron pipe, caused by long-term service in slightly acidic water. © Copyright by Marcel Dekker, Inc.; reprinted with permission [5].

is slowly leached from the casting forming a network of graphite (Figure 21.7), resulting in low mechanical strength.

Three specialty cast irons are occasionally employed. Corrosion and erosion resistant *silicon cast irons* such as those of ASTM A518 find use in acid and abrasive services. They are relatively brittle and difficult to machine, limiting their usefulness. *White cast irons* such as ASTM A532, containing up to 25% chromium, are used in highly abrasive services such as pumping abrasive slurries; they are also relatively brittle. Nickel-rich cast irons, known as *Ni-resist cast irons* (such as those of ASTM A436), find use in both low- and high-temperature applications that require resistance to wear, and as seawater alloys. Because of its brittleness, cast iron is normally not permitted for hydrocarbon streams.

21.2.6.2 Carbon Steel

Carbon steels are the most widely used materials of construction. Unalloyed carbon steels typically contain nominal amounts of manganese, silicon, phosphorus, and sulfur. They are normally supplied with a pearlitic-ferritic microstructure (see Figure 21.3) produced by air cooling a hot-formed product (e.g., hot-rolled plate) or by a normalizing heat treatment. They are available as either killed carbon steel or plain carbon steel.

21.2.6.2.1 Killed Carbon Steel

Raw liquid steel is saturated with gaseous oxygen. By adding an oxygen scavenger such as silicon to the liquid steel before it is poured, the oxygen is removed as slag. The resulting “killed” steels are cleaner and contain fewer defects than “unkilled” (sometimes called “wild” steels) or partially deoxidized steels. ASTM A106 pipe, A105 forgings, and A516 plate are examples. Cast carbon steel products are also killed, even though typical ASTM specifications do not mention this requirement. Vacuum degassing is less commonly used to remove nitrogen, oxygen, hydrogen, and carbon dioxide.

Steels killed with silicon, such as ASTM A515 plates, tend to have a coarse grain structure usually with a silicon content of 0.15 to 0.30 wt%. They characteristically have relatively high brittle-ductile transition temperatures, making them unsuitable for applications requiring low-

The mechanical properties of several Cr-Mo low-alloy steels are improved by adding vanadium. Examples include vanadium-enhanced 1Cr-1Mo for turbine rotors and vanadium-enhanced 1Cr-1/2Mo bolts, widely used for temperatures up to 1100°F (595°C). Vanadium-enhanced versions of the 2-1/4Cr-1Mo and 3Cr-1Mo plate and forging alloys are employed in heavy-wall vessel construction. These alloys can permit substantially reduced wall thicknesses. Alloys such as AISI 4140 steel (1Cr-0.2Mo, with carbon between 0.37 and 0.49%) (UNS G41400) are used as rotating equipment shafts, bolts, high-strength forgings, etc.

Ni-Mn (with either 3-1/2 or 9Ni) alloys are used for moderately low-temperature services, in the range of -50°F to -320°F (-46°C to -195°C). They are commonly used in liquified petroleum gas and liquified natural gas plants. (See ASTM A203, A333, A334, A350, A352, and A420 for various product forms of these materials.) Type 304L SS, while more costly, may result in a lower fabricated cost by avoiding welding problems.

Various enhanced strength plate steels are used in pressure vessels for high-pressure applications. Conventional carbon steels would require excessive wall thickness. Most enhanced steels also have increased low-temperature toughness. Postweld heat treatment is usually mandatory for these materials. Plate materials of this class include A302 (Mn-Mo and Mn-Mo-Ni steels), A517 (high-strength, low-alloy steels, quenched and tempered), A537 (Mn-Si steels; depending on section thickness, some grades can be qualified by impact testing at temperatures of -90°F (-68°C) or colder), A542 (micro-alloyed Cr-Mo steels, quenched and tempered), and A543 (Cr-Ni-Mo steels, quenched and tempered).

Alloying steels for improved corrosion resistance in chemical and hydrocarbon plants is based on chromium and molybdenum additions. The lowest of these alloys, 1Cr-1/2Mo and 1-1/4Cr-1/2Mo, are often used above 800°F (425°C). Low-alloy Cr-Mo steels (with 5% or greater Cr) are resistant to high-temperature sulfidic corrosion. However, the Cr-Mo alloys find their most critical use in high-temperature, high-pressure hydrogen service. The most commonly used alloys are the 1-1/4Cr-1/2Mo, 2-1/4Cr-1Mo, and 3Cr-1Mo steels. 9Cr-1Mo is available as piping, but is not commonly used in pressure vessel construction. A vanadium-enhanced version of 9Cr-1Mo is used in heavy wall vessels intended for high-pressure, high-temperature hydrogen service. All Cr-Mo alloys are air-hardenable and usually require PWHT. (See ASTM A182, A199, A217, A335, A336, A387, A541, and A739).

Weathering steels, many often classified as HSLA steels, are a common class of low-alloy steels employed for corrosion resistance. They commonly have small chromium and copper additions to form a stable patina-type rust in mildly corrosive atmospheres. These steels are used primarily in structural applications. (See ASTM A242, A588, and A618 for various product forms.)

21.2.6.4 Stainless Steel

21.2.6.4.1 Straight Chromium Stainless Steels

The 12Cr stainless steels are the least expensive and most commonly used alloys in this class. They are available in both ferritic and martensitic microstructures. Type 405 SS and Type 410S (ferritic) and Type 410 SS (martensitic) are corrosion resistance, particularly in wet CO₂ and in hot (T > 500°F [260°C]) services containing organic sulfur compounds or hydrogen sulfide. Type 410 SS, because it is martensitic, is used only when welding is not required. For welding, either Type 405 SS or Type 410S SS is specified. All 400-series stainless steels often grain coarsen in welds, causing relatively high brittle-ductile transition temperatures. Martensitic grades, being air-hardenable, often produce very brittle HAZs. Consequently, straight chromium stainless steels are usually not recommended for pressure containment utilizing welded construction. Their major use is in heat exchanger tubing, valve and pump internals, vessel internals, and as clad or weld overlaid linings in pressure vessels and heat exchangers.

Four hundred-series alloys are resistant to chloride stress corrosion cracking, but not chloride pitting. Accordingly, they are rarely used in aqueous chloride services. However, "superferritic"

The austenitic stainless steels do not require PWHT as a hardness control measure. They are sometimes stress relieved or postweld heat treated to reduce residual stresses, thereby improving their resistance to stress corrosion cracking. The austenitic stainless steels are sometimes chosen in preference to the Cr-Mo low-alloy steels because PWHT can be avoided (the fusion zones of welds of the Cr-Mo low-alloy steels may be air hardenable).

The workhorse alloy of the 300-series is Type 304 SS, while the workhorse casting alloy is CF-8M. The low-carbon grades (Type 304L for the wrought alloy, CF-3M for the cast alloy) are preferred for welded construction. The low-carbon grades (as well as the stabilized grades such as Types 321 SS and 347 SS) are also preferred if sensitization is a problem. Type 316 SS (its small molybdenum addition differentiates it from Type 304 SS) is specified when chloride pitting or crevice corrosion is a problem. Type 316 SS also has a higher maximum allowable stress. The high-carbon H grades such as Type 304H SS are specified for high-temperature use ($T > 1000^{\circ}\text{F}$ [540°C]), since they have an allowable stress advantage over the conventional grades. The H grades should be used with caution if service-induced carburization may be a problem.

Higher chromium-nickel austenitic alloys are used extensively in high-temperature applications such as heaters, in both cast and wrought form. Examples include Type 310 stainless steel (25Cr-20Ni), a cast analogue called HK-40 (25Cr-20Ni) (UNS J94204), the Alloy 800-series (20Cr-32Ni, with Ti and Al) (UNS N08800, N08810, and N08811), and proprietary alloys such as the "HP-Mod" materials. These alloys can have problems such as weldment cracking, embrittlement, carburization, nitriding, oxidation, and metal dusting. (These phenomena are discussed in Section 21.4.) Industry experience or consultation with alloy specialists is recommended before material selection.

Galling is sometimes a problem with austenitic stainless steels; lubricants such as molybdenum bisulfide and graphite, and coatings are sometimes employed. The problem is also avoided by using two mating surfaces with a hardness difference of at least 50 BHN. With components such as valve closures, the hardness differential is usually obtained by using a hard face weld overlay or electroless nickel plating on one of the two components. In threaded connectors, the differential is usually obtained from cold working one of the components. Sometimes the hardness differential is obtained by specifying two materials having appropriately different hardnesses. Some users have employed electroplated or vapor-diffused aluminum on fasteners (preferably on the male component). Galling may also be mitigated by specifying one component to be a free machining grade such as Type 303 SS. Free machining materials are, however, sensitive to stress cracking problems. For example, NACE MR0175 [2] does not allow free machining grades in wet sour service.

Wrought austenitic stainless steels are more susceptible to chloride stress corrosion cracking than are the cast austenitic alloys. Accordingly, cast austenitic stainless steel valve bodies and pump casings are often useful in services in which higher alloys are necessary for the wrought components (pipe, tubing, fittings, plate, etc.). Ferritic stainless steels such as Type 410 SS are also subject to chloride pitting. Superferritic grades are an alternative to the plain ferritic grades if the component can be fabricated in thin sections, such as for heat exchanger tubing; for neutral or near-neutral pH applications, high-nickel stainless steels such as Alloy 20 Cb-3 (20Cr-35Ni-2.5Mo-Cb) (UNS N08020) have elevated chloride stress corrosion cracking threshold temperatures.

Alloys resistant to chloride stress corrosion cracking include: (1) "superaustenitic" alloys with high chromium and nickel content, as well as 2% to 6% molybdenum; Alloy AL-6XN (21Cr-25Ni-6.5Mo-N) (UNS N08367) is an example of a superaustenitic stainless steel; (2) nickel-chromium alloys such as Alloy 825 (22Cr-42Ni-3Mo, Ti stabilized) (UNS N08825), with nickel contents of approximately 40% or more; (3) duplex austenitic-ferritic alloys such as Alloy 2205 (22Cr-5Ni-3Mo-N) (UNS S31803); and (4) Ni-Cu alloys such as Alloy 400 (67Ni-30Cu) (UNS N04400).

Unless heavily cold worked, the austenitic stainless steels are resistant to hydrogen stress cracking such as that caused by hydrogen sulfide. They are also resistant to hydrogen embrittlement caused by phenomena other than cathodic charging. If sensitized, austenitic stainless steels can also be susceptible to intergranular corrosion.

and other applications where both high strength and superior corrosion resistance are desirable. Their corrosion resistance is superior to the 12Cr stainless steels but is somewhat inferior to Type 304 SS. They can be susceptible to both chloride stress corrosion cracking and hydrogen stress cracking.

Further information on stainless steels is available from the trade organization:

Specialty Steel Industry of North America
3050 K. Street, N.W.
Washington, DC 20007
Tel. (202) 342-8630
www.ssina.com

21.2.6.5 Common Alloys and Metals

21.2.6.5.1 Nickel Alloys

Nickel alloys plus nickel are widely used for services, including acids, caustics, corrosive waters, and for numerous corrosive process applications and low- and high-temperature applications. For further information contact:

Nickel Institute
55 University Ave., Suite 1801
Toronto, Ontario, Canada M5J 2H7
Tel. (416) 591-7999
www.nickelinstitute.org

21.2.6.5.2 Copper Alloys

Copper alloys, including brasses and bronzes, find extensive use in heat transfer systems exposed to corrosive waters (primarily brackish or saline waters). Naval brasses such as UNS C46400, usually as a cladding on carbon steel, are used for tubesheets and plate components. Inhibited admiralty alloys such as UNS C44300 and the 70/30 (UNS C71500) and 90/10 (UNS C70600) Cu/Ni alloys are often used for piping and heat exchanger tubes. The Cu/Ni alloys are usually preferred, as they have better impingement resistance and can tolerate higher velocities. Aluminum bronzes such as UNS C60800 are relatively high-strength alloys used for pump and valve components. The upper temperature permitted by most engineering codes for copper alloys 400°F (205°C). A few alloys with higher allowable temperatures include aluminum bronzes and Cu/Ni alloys.

Most copper alloys are unsuitable with ammonia, sometimes in even trace amounts and for wet sour services. Most are corroded by caustics. Some brass alloys contain zinc in excess of 15%. Unless properly “inhibited” by arsenic, antimony, or phosphorus, such alloys can “dezincify” in brackish or saline waters. To evaluate copper alloys, contact an alloy specialist or the copper alloy trade organization:

Copper Development Association
260 Madison Ave., 16th Floor
New York, NY 10016
Tel. (212) 251-7200
www.copper.org

21.2.6.5.3 Cobalt Alloys

Cobalt alloys are used for hardfacing to improve the resistance to abrasion, galling, and/or impact; Stellite 6* (60Co-29Cr-5W) (UNS R30006) is an example. Most alloys are in closure

* Registered trademark of Deloro Stellite Group, Goshen, Indiana.

The Aluminum Association, Inc.
1525 Wilson Boulevard, Suite 600
Arlington, VA 22209
Tel. (703) 358-2961
www.aluminum.org

21.2.6.5.6 Chromium

Chromium is a refractory metal having a melting point of 3375°F (1857°C). Neither chromium metal nor chromium-based alloys are widely in the hydrocarbon or chemical industries. Chromium plating is useful for aesthetic purposes, and “hard” chromium plating finds some use in hardface applications. It is extensively used as an alloy addition to low-alloy steels (usually for the purpose of stabilizing carbides) and in cast irons (to produce wear-resistant products) and nickel alloys (for increased corrosion resistance). Chromium is the main alloying addition in the 400-series stainless steels and is used extensively in the 200- and 300-series stainless steels.

21.2.6.5.7 Titanium

Titanium is a reactive refractory metal with a melting point of 3034°F (1668°C). It and its alloys find heat transfer applications in hydrocarbon and chemical process industries. It is resistant to both organic and inorganic corrodents; it is employed in heat exchanger tubing for corrosive processes on one side and corrosive cooling water such as seawater on the other side; it finds use for wet chlorine and for concentrated hot caustic solutions. It can be useful in mildly reducing applications, such as wet alkaline sour overhead condensing systems. However, titanium (and the other reactive and refractory metals) are generally unstable in strongly reducing environments. It can also become unstable in the presence of powerful oxidizers including dry chlorine, red fuming nitric acid, and liquid oxygen. Titanium is embrittled by the formation of hydrides.

Only three titanium alloys are commonly used in the chemical industries, grades 2, 7, and 12. Grade 2 is pure titanium, while grade 7 has a small Pd (palladium) addition. Grade 12 has small molybdenum and nickel additions and has a corrosion resistance between that of grades 2 and 7. Grade 7 alloy is intended for most severe services, and is especially useful in hot, low pH, chlorine-saturated brines. Grade 12 is useful to about 500°F (260°C) for pH <4, and grade 7 is resistant to such corrosion at temperatures of at least 500°F (260°C). Titanium alloys lose strength rapidly with increasing temperature. The upper temperature limit permitted by the common engineering codes 600°F (315°C). Titanium alloys are available in most, if not all, product forms.

21.2.6.5.8 Zirconium

Zirconium, having a melting point of 3365°F (1852°C), is a reactive refractory metal, but it and its alloys are relatively difficult to fabricate. Welded construction should be heat treated at 1425°F (775°C) and cooled rapidly to achieve the best corrosion resistance. These materials, although expensive, can be very useful in severe applications, such as hot concentrated alkalis and inorganic acids. They are favored in high-temperature processes for the production of urea, hydrogen peroxide, many organic acids, including formic and acetic acids, etc., and for high-temperature organic processes utilizing hydrogen chloride. It is one of the better metals for hydrochloric acid and sulfuric acid, being resistant up to 70% at the boiling point and up to 75% at 265°F (130°C). Stress corrosion cracking sometimes occurs in 64% to 69% sulfuric acid at elevated temperatures. An advantage of zirconium over nickel alloys is that it can handle these acids when oxygen or other oxidants are present. It is not suitable, however, for hydrofluoric acid. Corrosion of zirconium sometimes produces compounds that are pyrophoric; the corrosive products can ignite when equipment is taken out of service. Zirconium is resistant to oxidizing acids such as nitric acid. Its corrosion rate is less than 5 mpy* (0.1 mm/yr) in zero to 70% acid at temperatures up to 500°F (260°C). However, it is susceptible to stress corrosion cracking in concentrations exceeding 70%.

* mpy = mils per year, where a mil is 0.001.

Thermodynamically, an anode has a higher Gibbs free energy. For example, both cold work and residual tensile stresses increase the local free energy in metals and alloys. For two dissimilar metals, the different inherent corrosion resistances of the two metals translate into one having a greater Gibbs free energy. Because of the induced current and in accordance with Ohm's law,* corrosion rates become a function of current flow and electrical resistance.

21.3.1.1 Cathodes

In hot-formed carbon steel, the cathode is often the area covered by mill scale (Fe_3O_4), while the anode sites are cracks in the mill scale.

The cathode area is sometimes the noncold-worked area in a component that has been partially cold worked, for example, the straight-run tubing in a U-bend heat exchanger bundle.

In heat exchangers, pumps, and vessels, the internals are often the more corrosion-resistant alloys as compared with the material of the pressure retaining component. Thus, the internals are cathodic with respect to the pressure retaining component and the pressure retaining component is in effect a galvanic anode.

21.3.1.2 Anodes

The anode area may be the metal under a deposit on an otherwise clean surface.

For crevices such as in those in socket welds, the metal in the crevice is likely to be anodic. Crevice corrosion and under-deposit corrosion can be serious problems in oxide-stabilized materials such as aluminum and the stainless steels. Crevices and deposits can also accelerate corrosion in metals (such as carbon steel) that do not exhibit both active and passive states. However, the rate of corrosion is much slower in such materials because they lack the galvanic driving force of the active-passive states characteristic of the oxide-stabilized metals and alloys. The anode areas in crevices and under deposits are typically smaller than the cathode areas. This difference accelerates the corrosion rate.

The welding-induced sensitized area in a stainless steel is usually anodic.

21.3.2 CORROSION CONTROL

The rate of corrosion at the anode is directly proportional to the anode current density (expressed as amps per unit area). This knowledge aids in developing methods to control or eliminate corrosion.

21.3.2.1 Barrier Coatings

Barrier coatings prevent or reduce current flow between the corrodent and the metal surface.

21.3.2.1.1 Inhibitors

Inhibitors act to control corrosion, particularly in piping systems. They form a very thin (perhaps monomolecular) adsorbed layer that acts as a barrier. Film-forming amines are a common example. Because inhibitors may locally de-adsorb, they are usually continuously injected. For large-diameter pipelines, batch inhibition may be necessary. Inhibition is usually not permitted in processes for high-purity products.

Chemical inhibition is usually not effective in applications involving turbulent flow (such as pumps and control valves) or in systems having deposits that prevent the inhibitor from contacting the metal surface to be protected. In most pipeline systems using inhibitors, regular cleaning by "pigging" is used. It is performed using pipeline pressure to push a mechanical cleaning device through the pipeline.

* $V = IR$, where V is the electrical potential (in volts), I is the current (in amperes), and R is the resistance (in ohms).

impressed current electrode, and a potentiostat provide a potential that keeps the material in the passive state. The most common application is for stainless steel tanks in strong mineral acids and for coolers in sulfuric acid plants. The technique should only be used with expert advice. A similar application, without an impressed current system, involves spreading the cathode current over a large anode area. This minimizes the cathode area and thus minimizes the total cathode current available for corrosion on a carbon steel tank. It has been shown that turning the entire tank bottom (uncoated) into an anode, by abrasive blasting, reduces local pitting rates.

21.3.2.1.5 Passivation

Passivation consists of exposing a clean metal surface to an oxidizing environment to form an oxide film. This surface is much more corrosion resistant than it would be in an unpassivated state. In materials such as carbon steel, which form weak oxides, passivation can be destroyed rather easily. In oxide-stabilized alloys such as the stainless steels, this corrosion resistance is not easily destroyed.

Passivation is usually part of a chemical cleaning process using a sodium nitrite solution. (Chromates, once used extensively, are now considered to be too toxic.) Austenitic stainless steels are usually passivated in air after pickling and neutralization. *Pickling* is a chemical process to descale or clean new stainless steel. (See ASTM A380 for recommended procedures.) For heavily oxidized materials, the pickling process removes the chromium-depleted surface beneath the layer of scale. The acid solutions used contain sufficient nitric acid (a good oxidizer) so that a subsequent passivation step is unnecessary.

21.3.2.1.6 Polarization

Polarization occurs because of ion concentration buildup near the anode and/or cathode. Once the ion concentration reaches saturation, corrosion essentially stops. Polarization can occur when: (1) Hydrogen ions concentrate at an active cathode in the absence of a cathodic depolarizer. Dissolved oxygen acts as a cathodic depolarizer. (2) Metal ions saturate the electrolyte around an anode. (Soluble Fe^{++} may saturate the anode, perhaps as the result of the precipitation of an insoluble iron salt, inhibiting the diffusion of Fe^{++} . For example, insoluble surface compounds such as carbonate scales in a fresh water often occur on carbon steel.)

Examples of polarization are: (1) In deaerated, but otherwise corrosive, water, hydrogen polarization all but shuts down the corrosion mechanism. For example, seawater deaerated to less than about 10 ppbw is noncorrosive to carbon steel. (2) Many waters form insoluble dense scales on the corroded surface. The scale acts as a barrier to the diffusion of new corrodent and dissolved oxygen to the substrate surface. Scaling tendencies and corrosivities of waters can be estimated by analysis [12]. Polarization is prevented by: (1) Ions such as sulfides and cyanides that are "cathode poisons." Instead of the hydrogen ions forming hydrogen gas, which acts to polarize the cathode, cathode/poisons promote the formation of nascent hydrogen atoms. This hydrogen then diffuses into the substrate material. In ferritic steels, the following may result: hydrogen embrittlement, hydrogen stress cracking, and various forms of hydrogen induced cracking, including blistering. (2) By fluid flow phenomena such as turbulent flow or particulate erosion. (3) Cathodic depolarizers; the most common is dissolved oxygen.

The selection of materials must also consider oxidation/reduction processes that occur in the absence of an aqueous electrolyte. Examples include sulfidation, destructive oxidation of alloys in air or steam at high temperatures, carburization, nitriding, fuel ash corrosion, and high-temperature hydrogen attack.

21.3.3 STRESS CORROSION CRACKING

Failures due to stress corrosion cracking, while not common, may occur without warning, with catastrophic consequences. This cracking occurs only if both of the following conditions occur simultaneously: (1) a susceptible material and (2) an appropriate combination of stress (*tensile stress is required*), temperature, crack-inducing agent, pH, aeration, etc. For example, chloride

substance. (3) For thin-ligament pressure-containing components where leaks could develop quickly and would require unscheduled maintenance (e.g., tube-to-tubesheet welds). (4) In new equipment or piping where subsequent inspection and/or repairs after long-term service would be excessively expensive. For example, sites where congestion may make it difficult to mobilize the necessary repair equipment (e.g., cranes).

Shot peening, in which hard shot is impinged on a surface, produces surfaces that are in residual compression, thus making them resistant to stress corrosion cracking.

Cladding or *overlays* are sometimes applied to carbon and low-alloy steel to avoid stress corrosion cracking problems. For example, carbon steel clad with Type 304L SS is often used in severe amine services.

Paint coatings are occasionally used to minimize stress corrosion cracking. They are often provided for external stainless steel surfaces exposed to wet chlorides, marine atmospheres, or in services under wet insulation. For under-insulation surfaces, some users coat only the welded areas where chloride stress corrosion cracking usually occurs. Paint coatings are also sometimes used to minimize stress corrosion cracking in old equipment that may be exposed to a crack-inducing agent. Internal coatings in vessels and tanks are occasionally employed.

Crack-inducing agents generally require the presence of an electrolyte in order to be active. For example, H_2S cracks carbon steel only in the presence of water or other electrolytes. The most common electrolytic crack-inducing agents for carbon and low-alloy steels are aqueous solutions of amines, caustics such as caustic soda (NaOH), hydrogen sulfide, dilute sulfuric acid, hydrofluoric acid, and mixtures of carbon monoxide and carbon dioxide. The austenitic stainless steels are sensitive to chloride stress corrosion cracking, caustic stress corrosion cracking, and, at high temperatures, to intergranular stress cracking by liquid zinc. When sensitized, these materials often experience intergranular stress corrosion cracking by weak oxidizing acids such as polythionic acid. High-strength aluminum alloys can be susceptible to chloride stress corrosion cracking. Most copper alloys are rapidly cracked by liquid mercury.

A few crack-inducing agents do not require an electrolyte, e.g., the attack of copper alloys by ammonia. Accordingly, the template should include the information necessary to determine if a crack-inducing agent is either active or can become active.

21.3.4 MICROBIOLOGICALLY INFLUENCED CORROSION (MIC)

This corrosion is defined as the corrosion of materials caused by microorganisms. The combination of unexpected attack and rapid failure is sometimes a concern. Generally it occurs in stagnant water systems or the water legs of mixed-phase, quiescent process streams at ambient temperatures (but may occur at temperatures up to 200°F [93°C]). Most materials of construction are susceptible. A typical MIC problem is the pitting corrosion in the bottom of a pipeline, before commissioning, due to microbial activity in residual hydrotest water. Systems subject to stagnant operation, shut-downs, or velocities less than 2 ft/sec (0.6 m/sec) are at risk. In some media, such as seawater, colonization by microorganisms may occur at velocities up to about 5 ft/sec (1.5 m/sec). For stagnant water or quiescent water-wet systems, exposures exceeding 30 days often lead to severe MIC.

The microorganisms responsible for MIC are primarily bacteria and fungi. They may be anaerobes (which do not function in the presence of oxygen), or aerobes (which require oxygen), or a mixture of several microorganisms living in colonies. While strictly anaerobic environments are not common in nature, anaerobes can develop in even highly aerated systems. For example, anaerobic conditions can be established under the slime film formed by some aerobic microbes. Common organisms include sulfate-reducing bacteria, sulfur/sulfide-oxidizing bacteria, iron/manganese-oxidizing bacteria, aerobic slime formers, methane producers, and acid-producing bacteria and fungi. They usually form discrete biodeposits, either nodules or flat shiny deposits. An exception is when they exist in high concentrations in anaerobic soil environments, where they do not need to form either a film or a deposit to become active. Under such conditions, these organisms often cause corrosion.

embrittlement. In practice, most fractures involve ductile crack propagation due to plastic instability occurring in pressure-containing components that have been thinned by corrosion or erosion.

Risk of fracture differs from brittleness. A brittle material will not fracture as long as the applied stress is below the crack propagation threshold. In practice, brittle materials such as gray cast iron and glass can be used safely if the applied stresses are kept small so that inherent flaws in the material do not propagate into unstable cracks (i.e., brittle fracture). In ductile materials, the risk of fracture usually depends on the thickness in a locally thinned area. Evaluating the risk of fracture involves employing *fitness-for-service* or *remaining life assessment* techniques. In some localities, such analysis is a regulatory requirement. A conservative rule-of-thumb is to require further evaluation only if the corrosion allowance has been consumed. A less conservative criterion is to evaluate if the remaining minimum thickness is insufficient to limit the pressure hoop stress* to the specified minimum yield strength of the pressure-containing material. For simple cylindrical geometries such as vessel shells and piping, the pressure hoop stress can be adequately estimated by the “Barlow formula”:

$$\text{Stress } (\sigma) = \frac{(P)(r)}{t} \quad (21.2.)$$

where P is pressure, r is the internal radius, and t is the remaining thickness.

Fracture-safe design is when there is little likelihood of a serious accident even if a through-thickness crack occurs. For each metal and alloy, there is a combination of critical crack size, stress intensity, and thickness above which cracks will no longer propagate in a ductile manner. Brittle fractures of this type are rarely encountered in low- to medium-strength carbon and low-alloy steels; they typically have tensile strengths of 70 ksi (480 MPa). As a result, fracture mechanics is not commonly used in most plant designs, except in the chemical and hydrocarbon industries for high-pressure processes in which relatively high-strength materials of construction are employed. The ASME Boiler and Pressure Vessel Code, Section VIII, Div. 3 [1], is used in such cases.

Leak-before-break is a common application of fracture-safe design, used to ensure that a pressure-retaining system will leak before breaking. This design procedure utilizes fracture mechanics to ensure that the applied stress is insufficient to cause a through-thickness crack to propagate in a brittle manner. Propagation of a through-thickness crack will be ductile. The crack will start leaking before there is a break. The 10% rule is one application of leak-before-break; it involves piping and equipment in relatively low-pressure services. For carbon and low- to medium-strength low-alloy steels, brittle fracture will not occur if the combined stress in tension is less than about 10% of the material's tensile strength. (This will hereafter be referred to as the “10% rule”). For carbon and low-alloy steel equipment, in compliance with the 10% rule, leak-before-break will prevail. This principle has been incorporated into many engineering codes. While low-stress conditions do not permit brittle fracture, stable crack propagation by other mechanisms such as stress corrosion cracking can still be active.

Embrittlement refers to a loss of ductility and fracture toughness. Embrittlement causes crack growth to change from ductile to brittle. In most cases, brittle or embrittled materials have a threshold temperature range above which they respond to crack propagation stresses in a ductile manner. Cracking below the threshold temperature is at least partially brittle. Such cracking is often catastrophic. Cracking above the threshold temperature is by a ductile mechanism. Embrittlement examples include: (1) The term “embrittlement” is applied to the ambient temperature brittleness of an alloy that has become embrittled by high-temperature service. (2) Process fluids can embrittle an otherwise ductile material. Hydrogen embrittlement is an example of this effect. (3) In carbon

* Pressure hoop stress is the circumferential tangential (tensile) stress on a cylinder as a result of internal pressure.

0 to 100°F (−18°C to 38°C). The risk rapidly diminishes >175°F (80°C). Hence, low-alloy steels such as the Cr-Mo steels are usually not pressurized, if in gaseous hydrogen service, until the operating temperature is brought up to 250°F (120°C). Ordinary low- to medium-strength steels (with tensile strengths of up to 70 ksi [480 MPa]) are moderately susceptible to this embrittlement. Between 70 and 90 ksi (480 and 620 MPa) tensile strength, steels are susceptible to it. Higher-strength steels (with tensile strengths in excess of about 90 ksi [620 MPa]) can be severely embrittled. Bolting is the most common product form in which hydrogen embrittlement is observed in plants, since they are often electroplated without a subsequent hydrogen bakeout (the electroplated material does not allow trapped dissolved hydrogen to escape by diffusing to a free surface).

For carbon and low-alloy steels, the relationship between susceptibility to hydrogen embrittlement and strength is very similar to that between susceptibility to hydrogen stress cracking and strength. This embrittlement often occurs in carbon steels, low-alloy steels, and ferritic or martensitic stainless steels subject to hydrogen stress cracking environments. The measures to minimize embrittlement are essentially the same as those to minimize the risk of stress corrosion cracking (hardness controls, control of microalloying additions, PWHT, etc.)

Hydrogen embrittlement is normally not a problem in most chemical plants, because the material strengths are too low to propagate cracks. Four situations should, however, be given special attention: (1) The rate and extent of hydrogen embrittlement are affected by the amount of residual cold work; hence, stress relieve components that have been cold worked. Five percent cold work is often used as the threshold. Designs should avoid sharp notches, as these can subsequently become cold worked. (2) Metals for high-temperature, high-pressure hydrogen service are often at risk, especially upon cooldown. Such components (usually Cr-Mo low-alloy steels) may be subject to brittle fracture if exposed to tensile or bending stresses during maintenance, revamp fabrication, etc. (3) Hard HAZs may be susceptible to both hydrogen embrittlement and hydrogen stress cracking. Welding and joint configurations are generally not susceptible to these phenomena. However, if a carbon steel parent metal has excessive microalloying, or if the weld cools too rapidly, excessive HAZ hardness can be created when a thin section is welded to a thick section, as in tube-to-tubesheet welds. Heat-affected zone hardnesses of 200 BHN or less are not likely to be affected by dissolved hydrogen. Similarly, hard spots susceptible to cracking can form at the fusion zone in dissimilar metal welds involving relatively high-carbon plain or low-alloy steels to stainless steels or Cr-Ni alloys. (4) *Delayed hydrogen cracking* (also called *underbead cracking* or *cold cracking*) is sometimes associated with hydrogen embrittlement; it is a form of hydrogen stress cracking. The problem occurs in freshly made welds, usually because of hydrogen generated during welding if a moist welding flux is used. However, such cracking can occur in repair welds because of hydrogen dissolved in the steel while in service. Cracking in repair welds is prevented by a bakeout. The delayed hydrogen cracking mechanism requires an incubation period before cracking occurs. Such cracking may not be visible if the weld is inspected immediately after it is completed. Inspection should be delayed 2 or 3 days after welding. The primary mitigation measures are (a) bakeout, if necessary; (b) preheat; and (c) control of welding flux to avoid moisture absorption.

Caustic embrittlement is a misnomer. The loss of ductility causes a reduction in load-carrying capability because of the formation of cracks due to caustic stress corrosion cracking.

Low-temperature embrittlement occurs in carbon and low-alloy steels at temperatures below their brittle-ductile transition temperature range. The effect is reversible: when the alloy is heated above the transition range, ductility is restored. This embrittlement is avoided by following the Charpy impact test requirements of the relevant engineering codes. The need to test depends primarily on the material, its thickness and the minimum design temperature.

Aluminum, copper, and other face-centered cubic metals and alloys (such as the austenitic stainless steels and nickel-base alloys) do not become brittle at low temperatures, except if heavily cold worked. Most such alloys are exempt from impact testing for design temperatures down to −320°F (−195°C). Some types, such as Type 304, are exempt down to −425°F (−255°C). The exemption temperatures for weld metals and HAZs are usually higher than those for the parent metal.

Duplex stainless steels are susceptible to 885°F (475°C) embrittlement and to sigma-phase formation, and they are usually not selected for temperatures above 650°F (345°C). Because of their ferrite content, they are susceptible to low-temperature embrittlement. However, the duplex stainless steels tend to have relatively low brittle-ductile transition temperatures. The engineering codes typically require the duplex stainless steels to be qualified for low-temperature service by impact testing. They can be susceptible to hydrogen embrittlement, but are less susceptible than are the ferritic and martensitic stainless steels.

21.4.3 HIGH ALLOYS

High alloys with little exception suffer some embrittlement if exposed to sustained high-temperature service due to the formation of intermetallic compounds. Conditions and rates of embrittlement vary with the alloy. Check with alloy manufacturers for specific information. High alloys containing enough nickel to ensure an austenitic microstructure are, like austenitic stainless steels, unaffected by low-temperature embrittlement.

21.4.4 HYDRIDING

Hydriding is a common problem for all refractory metals, including titanium, zirconium, columbium, and tantalum. Galvanic cells that promote hydriding can be particularly damaging. Instances of iron sacrificial anodes causing hydriding in titanium heat exchanger components have been reported. Hydriding is related to hydrogen embrittlement. Hydrides are brittle, thermodynamically stable compounds. Re-refining the metal is required to destroy the hydrides.

Titanium is the most common material of construction that can be hydrided; it has a threshold temperature of ~175°F (80°C). Hydriding can be caused by: (1) Titanium can absorb hydrogen directly from anhydrous process streams containing hydrogen gas. Because only a small amount of moisture is necessary to inhibit such embrittlement, it is relatively uncommon. (2) Nascent hydrogen generated by a corrosion reaction involving cathodic poisons (such as sulfides, cyanides, and arsenic or antimony compounds) diffuses into titanium to form hydrides. (3) Cathodic protection of titanium charges the metal with hydrogen (most often the cathodic protection is inadvertent, being caused by a materials mismatch, such as titanium tubes rolled into a nontitanium tubesheet).

21.4.5 HIGH-TEMPERATURE EFFECTS

21.4.5.1 Mechanical Effects

More expensive materials of construction are often needed at high temperatures. Whenever possible, determine if the maximum design temperature can be reduced.

Creep frequently occurs. Most metals and alloys exhibit a temperature above which the grain boundaries become weaker than the grains themselves. Fabricated equipment such as furnaces, heaters, and combustion gas turbines often experience creep. Creep begins for carbon steel at ~750°F (400°C), for Cr-Mo steels at ~900°F (480°C) and higher, and for conventional austenitic stainless steels at 1050°F to 1100°F (565°C to 595°C). A safe estimate for the creep threshold temperature of a material is the upper temperature limit permitted by ASME Section VIII, Div. 2 [1]. Engineering codes such as ASME B31.3 [4] for piping and ASME Section VIII, Div. 1 [1] for vessels contain provisions for creep design. If creep is a concern, coarse grained materials are favored. Carbon steels killed with silicon are usually recommended when creep is a concern, e.g., ASTM A106 for pipe and ASTM A515 for plate.

Stress rupture can occur as a result of sustained operation in the creep range. Stress rupture design keeps allowable stresses much lower than for noncreep designs. The stress rupture design life is the expected period of *secondary* creep, during which cracking damage slowly accumulates, often over several years. During this period, component dimensions such as heater tube diameter

outside. (2) *Prevent the formation or ingress of water.* Purge with a dry inert gas such as nitrogen and then maintain a slightly positive pressure. (3) *Use a neutralizing wash.* Both ammonia and soda ash solutions are used to maintain a basic pH. Refer to NACE RP0170: "Protection of Austenitic Stainless Steel from Polythionic Acid Stress Corrosion Cracking During Shutdown of Refinery Equipment" [14] for recommended practices.

External polythionic acid attack may occur in plants having atmospheric sulfide pollution including gas applications with water condensation. However, the problem does not usually occur on external surfaces in fired equipment because excess air causes sulfates to form, instead of sulfides. Wet sour systems containing carbon steel heat transfer surfaces may generate substantial iron sulfide. Such systems should not be flushed or drained into stainless steel piping or equipment prior to a shut-down unless appropriate precautions are taken. Several metallurgical methods address intergranular corrosion caused by sensitization.

21.4.6 LOW-CARBON STAINLESS STEEL

The "L" grades such as Type 304L SS with a low carbon content, limit the level of sensitization. However, they have lower allowable stresses than either the conventional grades or the stabilized grades. The low-carbon grades are typically chosen for services in which welded fabrication is required but the operating temperatures will be less than the sensitization threshold, about 800°F (425°C). With a low-carbon content, the rate of sensitization is low, and the postweld cooling rate in the HAZ is fast enough to avoid significant sensitization. 29Cr-4Mo (UNS S44700) is an example of a low-carbon ferritic stainless steel.

21.4.6.1 Chemically Stabilized Stainless Steel

Types 321, 347, and 348 SS and their H grades, and Types 316Ti and 316Cb SS are resistant to sensitization. They contain carbon scavengers (titanium in Type 321 and Type 316Ti and niobium in Type 347, Type 348, and Type 316Cb) that inhibit chromium depletion. These materials are referred to as *stabilized alloys*.

ASTM specifications for austenitic stainless steels, including the stabilized grades, are usually provided in the solution annealed condition, in which these alloys are not resistant to sensitization caused by long-term, high-temperature service. ASTM specifications warn the user that solution annealing the stabilized grades may result in inferior resistance to intergranular corrosion. With these specifications, the mill solution annealing heat treatment should be followed by a *stabilization anneal*. A widely used practice is to hold the alloy at about 1650°F (900°C) for 2 to 4 hours followed by air cooling to promote stable carbides, formed from either titanium for Types 321 and 316Ti SS or from niobium for Types 347, 348 SS, and 316Cb, without chromium depletion. The purchaser should specify stabilization annealing.

Special alloy composition requirements may be necessary to assure proper stabilization annealing [15]. These requirements limit the ratios of Ti/C in Type 321 stainless steel and of Cb/C in Type 347. The protection provided by a stabilization anneal can be partially destroyed by welding, since some chromium carbides may form. For full protection, welds made after the stabilization anneal should be restabilized. Type 321 SS is more susceptible to this welding effect than is Type 347.

Several stabilized nickel-based high alloys (such as Alloy 825 (22Cr-42Ni-3Mo, Ti stabilized) (UNS N08825) are resistant to sensitization. They are usually furnished in the stabilization annealed condition but may be made susceptible to sensitization by subsequent PWHTs. The alloy manufacturer should be consulted before undertaking stress relief or PWHTs.

Hot bending may cause cracking in stabilized stainless steel pipe, and should be avoided. Virtually all nonstabilized Cr-Ni and nickel-based high alloys are susceptible to sensitization and intergranular corrosion. If fabrication involves aggressive pickling, or if the alloy is to be exposed to polythionic acid or other oxidizing acids, sensitization and resistance to intergranular corrosion should be considered. Check the technical literature or consult with the alloy manufacturer.

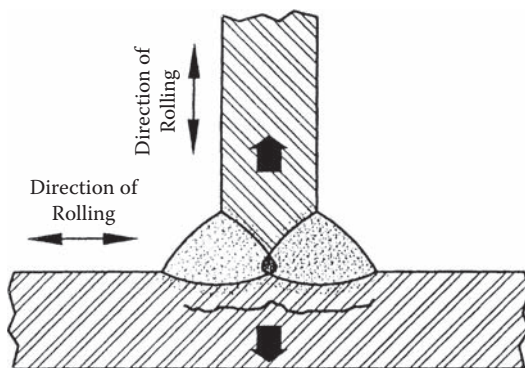


FIGURE 21.11 Lamellar tearing in a T-joint. © Copyright by Marcel Dekker, Inc.; reprinted with permission [5].

Welds of dissimilar metals result in: (1) *Warping, buckling, and/or excessive residual stresses* caused by different thermal expansion coefficients. (2) “*Hard spots*” in *heat-affected zones and fusion zones* are caused by formation of hard intermetallic compounds such as carbides. The heating/cooling cycle can harden HAZs and can cause a sensitized HAZ in nonstabilized alloys. (3) *Galvanic effects* between a sensitized HAZ and its adjacent parent metal can also occur.

Lamellar tearing is an unusual type of failure in plate and plate products, as the weldment cools (Figure 21.11); restraint causes the region just below the weld to be in tension and tearing can occur. (Poor through-thickness toughness is usually caused by the presence of a relatively high density of nonmetallic inclusions, that is, a “dirty” steel.) Lamellar tearing is normally not a problem in plate <1 in. (25 mm) thick.

Methods to avoid lamellar tearing include (1) *Materials control* utilizes plate with a low concentration of nonmetallic inclusions, using purchasing specifications developed for plate resistant to hydrogen-induced cracking (HIC). ASTM A770, “Standard Specification for Through-Thickness Tension Testing of Steel Plates for Special Applications,” can be used to ensure plate with proven through-thickness toughness. ASTM A435, “Standard Specification for Straight-Beam Ultrasonic Examination of Steel Plates,” ensures that the plate manufacturer or vendor has inspected the plate for injurious nonmetallic inclusions. (2) A *welding technique* option is to use a “butter” layer of low-strength weld metal on the surface of the plate for which lamellar tearing is to be avoided. This technique may require adjusting the weld joint efficiency if the minimum specified tensile strength of the filler metal is less than that of the base metal. Another option is to modify the joint or weld to minimize restraint. Using fillet welds rather than full penetration welds is sometimes useful.

Postweld inspection for lamellar tears is difficult unless the tears penetrate to the surface (usually at the toe of the weld). Dye penetrant inspections are reliable for tears that penetrate the surface. For embedded tears, ultrasonic inspection is sometimes used, but tears are difficult to differentiate from noninjurious inclusions.

Carburization is the development of a carbide-rich layer at high temperatures on a metallic surface exposed to a reducing hydrocarbon environment. Mild carburization of ordinary 300-series austenitic stainless steels is sometimes observed, e.g., in the plenum of a fluid catalytic cracking unit. Special alloys, such as the Alloy 800 series (20Cr-32Ni with Ti and Al) (UNS N08800/8810/8811) or HP-Mod, are generally used in the cracking tubes of ethylene furnaces. Carburization can cause premature failures such as cracking, due to the large difference in the coefficients of thermal expansion between the parent alloy and the carburized layer. Thermal cycling is the normal cause of such failures. Metal loss can also occur by the mechanism known as *metal dusting*. It is observed in the “syngas” process to convert natural gas to hydrogen. This very limited mechanism usually involving reducing hydrocarbon process streams is worst for Fe-Cr or Fe-Cr-Ni alloys having chromium contents of 25% [16] and is very sensitive to temperature. The proba-

As a result, most users employ a *positive materials identification* program, which includes welds as well as parent metals. Positive materials identification testing should be done on installed materials. When this is not practicable, alternatives such as testing immediately before installation are permitted.

Hydrogen attack is accelerated by inclusions and slag-type defects. Therefore, killed steels and inclusion-free welds are often specified. To further protect materials exposed to hydrogen, PWHT is recommended for all Cr-Mo alloy steels. Components cold worked more than 5%, such as cold-formed heads, should be stress relieved. Pockets, such as those created by strip linings, should be avoided. When the metal is exposed to infrequent and short-term transient combinations of high temperature and moderate hydrogen partial pressure, a significant incubation time often occurs before the effects of such attack become detectable. Investigation of incubation times can often justify the choice of a lower cost material of construction. API Publication No. 941 [3] provides details on incubation times. Such analyses are particularly valuable in applications such as bypass loops in which gaseous hydrogen may be blocked in or is stagnant and subsequently heated during start-ups or shut-downs.

To summarize, when selecting materials for gaseous hydrogen service

1. The Nelson curves, utilizing the maximum operating temperature plus 25°F (14°C), should be used.
2. Carbon steels should be killed or otherwise fully deoxidized.
3. Low-alloy steels such as the Cr-Mo steels should be postweld heat treated.
4. Cold-worked materials should be stress relieved.
5. Seamless tubing and pipe are preferred, as they avoid potential problems associated with longitudinal welds.

Hardness controls should be specified as follows:

1. NACE RP0472 [13]. The maximum weld metal hardness permitted for carbon steel is 200 BHN. Weld procedure qualification testing should be done to ensure that HAZ hardnesses do not exceed 248 BHN.
2. NACE MR0175 [2]. This practice, which limits the hardnesses of parent metals and HAZs, should be required. Recommended hardness limits for the weld metal of Cr-Mo low-alloy steels is 225 BHN for $\text{Cr} < 3$ and 241 BHN for $3 < \text{Cr} < 9$.

Designs for gaseous hydrogen service should include the following features: (1) Plate materials, including clad plate, should be ultrasonically examined for laminations (see ASTM A578). Weld repair of laminations should not be permitted. (2) Pressure-containing and internal attachment welds should be full penetration. (3) Pocketed weldments such as reinforcement pads should be vented. Internal attachment welds that cannot be full penetration, such as tray support welds, should also be vented.

Since hot high-pressure H_2 can crack the Cr-Mo steels favored for this service, the following should be kept in mind: (1) Hydrogen embrittlement can occur at operating temperatures at about <250°F (120°C). This concern is usually addressed by not pressurizing at operating temperatures <250°F (120°C). (2) Delayed hydrogen cracking that can occur in weld repairs subsequent to service. This concern is addressed by an appropriate bakeout prior to repair welding.

21.4.8 NITRIDING

Stainless steels and many higher alloys such as Alloy 800 slowly develop a brittle nitride layer if exposed to a nitriding atmosphere at temperatures exceeding about 750°F (400°C). By far the most common nitriding atmosphere is ammonia or a mixture rich in ammonia. Nitriding of stainless

600°F (315°C). The term *sulfidic corrosion* refers to corrosion of carbon and low-alloy steels by sulfur compounds while the term *sulfidation* is normally used for higher alloys. Sulfidic corrosion is usually associated with sulfur in crude oil (as organic sulfides and/or as H₂S). Severe pitting and general wastage can occur in carbon and alloy steels above 500°F (260°C). Corrosion rates are estimated using the McConomy and Couper-Gorman curves.

The original McConomy curves [17] have been found by experience to usually be conservative [18]. They are used for services containing no hydrogen gas. The total sulfur content (in wt%) is not a precise indicator of the corrosivity of a crude oil since not all organic sulfur compounds are corrosive to carbon and alloy steels, even at elevated temperatures. The curves apply to sour crude oils and sour crude fractions, operating at temperatures of >500°F (260°C). They are used for processes containing gases having hydrogen partial pressures no greater than 50 psia (0.34 MPa). They provide *average* corrosion rates and are used to predict the time-to-first leak or to estimate corrosion allowances. (For low-pressure applications, some users utilize the entire wall thickness for making time-to-first leak estimates.) Because of uncertainties, McConomy curve estimates often do not agree with previous plant experience. In such cases, one obviously relies on plant experience with similar operating conditions.

The Couper-Gorman curves [19] are used for sour services with hydrogen gas having a partial pressure of at least 50 psia (345 kPa). Materials selected in compliance with the Couper-Gorman curves must also satisfy the restrictions involving gaseous hydrogen service. When the McConomy or Couper-Gorman curves indicate that carbon steel is appropriate, silicon-killed steels are generally preferred, as they are more resistant to sulfidic corrosion than are aluminum-killed steels. However, coarse-grained silicon-killed steels may be precluded by a requirement for the low-temperature toughness provided by the fine grain practice steels killed with aluminum. When these two curves indicate that the corrosion rates of both carbon or low-alloy steels are sufficiently low, consider the effect of corrosion on downstream equipment. For some processes, equipment such as reactors contain catalyst beds that may be plugged by sulfides. Hence corrosion-resistant steels are needed.

For temperatures at which sulfidic corrosion rates are excessive, two alternatives may be needed: (1) Refractory linings in both vessels and piping. A low iron-containing refractory is required, because spalling of the refractory has been associated with iron oxide contaminants in the refractory. (2) Aluminum diffusion coatings on steel. These coatings are applied by proprietary processes for vapor-diffusing aluminum on and into the steel. For heater tubing, the useful temperatures are extended to 800°F (425°C). Such coatings on low-alloy steels protect heater tubes from external sulfidic corrosion, corrosion-resistant alloys used for close-tolerance components such as internal bolting, and very thin components such as screens and catalyst baskets. Imperfections of the coatings can lead to early failure.

For applications requiring corrosion-resistant alloys, either low-carbon or stabilized stainless steels such as Type 321 SS are normally selected. Sensitization-induced polythionic acid corrosion is a concern in such applications. High-nickel alloys and copper-based alloys often corrode rapidly in the presence of high-temperature sulfur compounds.

Pure liquid sulfur is stored in pits made of Type V concrete. Carbon steel piping is usually specified for the liquid. Nitrogen blanketing or alloys such as Alloy 20 Cb-3 or Type 310 SS are employed since liquid sulfur and air are highly corrosive to carbon steel.

Sulfur and sulfur compounds may cause *sulfidation* of nickel-based alloys >600°F (315°C). The threshold temperature depends on both the process chemistry and the alloy composition. At least one user regards the threshold to be as low as 300°F (150°C) for Alloy 400 (67Ni-30Cu) (UNS N04400) in the presence of hydrogen sulfide. Copper-based alloys corrode quickly and should generally be avoided. Sulfidation can cause pitting, intergranular attack, or fluxing of molten sulfides. Ordinary austenitic stainless steels are subject to fluxing by molten Fe-Ni sulfides. Alloy manufacturer literature and assistance should be sought for differentiating among alloys.

Example 21.2. General Template for a Refinery**STREAM OR EQUIPMENT NUMBER:** _____**Design Temperature** (Minimum/Maximum): _____**Design Pressure** (Minimum/Maximum): _____**Commodity:** _____ **Phases:** _____ **Liquid Water** (Y/N): _____**Corrodents** (1): _____**Crack-Inducing Agents** (2): _____**Upset Conditions:** _____

Liquid Water (Y/N): _____

Corrodents (1): _____

Crack-Inducing Agents (2): _____

Autorefrigeration (Y/N): _____

If Yes, indicate minimum temperature: _____

Other: _____

Wet Sour Service (Y/N): _____

If Yes, indicate severity: _____

Metallurgy: _____**PWHT** (Y/N): _____ **Valve Trim:** _____ **Corrosion Allowance:** _____**Notes:** _____

The template should (1) Accommodate all of the processes and services to be analyzed plus process chemistries. (2) Contain all design information such as temperatures and pressures. Any anticipated operating conditions that affect mechanical design should be indicated. Examples include pressure and/or thermal cycling. This information will be used to prepare the piping and equipment data sheets and to alert designers to special conditions such as cyclic operation. (3) Contain the maximum operating temperatures and pressures. For most mature plant technologies, materials selection is based on operating conditions rather than design conditions. The major exception is for the minimum temperature, for which engineering codes require materials resistant to brittle fracture. (4) Define any upset (nonstandard) and transient design conditions. (5) Contain "Notes" to indicate supplementary materials selection information such as referring to NACE or API documents. The "Notes" section helps describe upset conditions, or a materials testing requirement such as positive materials identification. (6) Include, as an attachment, an addendum (referred to as the "Notes" addendum). It defines temperature, pressure, and concentration threshold values for applicable corrosion and other materials degradation phenomena, as obtained from data supplied by process licensors, or from testing in plants, pilot plants, laboratories, or the open literature. Addendum information helps evaluate risks of early failure. Examples include: (a) a widely used threshold definition for "sour" water is a dissolved H_2S concentration of at least 50 ppmw; (b) austenitic stainless steels are generally resistant to chloride stress corrosion cracking in neutral saline water at less than 140°F (60°C); (c) sensitization-induced intergranular corrosion of low-carbon austenitic stainless steel welded construction is normally not a problem at less than 800°F (425°C).

Example 21.3. General Template for a Refinery

Stream Description	Units	References	Stream No.		
			1	2	Etc.
Commodity					
Phase (Liq/Vap/Solids)	L/V/S				
Design Temperature: Min/Max	°F				
Design Pressure: Min/Max	psig				
Operating Temperature: Normal/Min/Max	°F				
Operating Pressure: Normal/Min/Max	psig				
Fluid Velocity	ft/sec				
Free Water	Yes/No	Note 5			
Crack-Inducing Agents		Note 4			
Chloride	ppmw	Note 4			
Cyanide	ppmw	Note 4			
Hydrogen (partial pressure)	psia	Note 4			
Hydrogen sulfide	Note 4	Note 4			
Amine	wt%	Note 4			
NaOH or other caustics	wt%	Note 4			
Other		Note 4			
Corrodents		Note 3			
Sulfur	Notes 1&2	Notes 1&2			
Acids	wt%				
Acid gases	mole%				
Acid salts	wt%				
pH					
Other		Note 3			
Upset Conditions		Note 6			
Wet Sour Service	yes/no				
If yes, simple or severe					
Metallurgy		Note 7			
Corrosion Allowance	inch				
Valve Trim					
Notes					

Example 21.4. Ammonia Plant Template**STREAM OR EQUIPMENT NUMBER:** _____**Design Temperature** (Minimum/Maximum): _____**Design Pressure** (Minimum/Maximum): _____**Commodity:** _____ **Phases:** _____ **Liquid Water (Y/N):** _____**Corrodents (1):** _____**Crack-Inducing Agents (2):** _____**Upset Conditions:** _____

Liquid Water (Y/N): _____

Corrodents (1): _____

Crack-Inducing Agents (2): _____

Autorefrigeration (Y/N): _____

If Yes, indicate minimum temperature: _____

Other: _____

Metallurgy: _____**PWHT (Y/N):** _____ **Valve Trim:** _____ **Corrosion Allowance:** _____**Notes:** _____**Notes for Example 21.4.**

- (1) Corrodents (only if liquid water or other electrolyte is present).
 - (a) Indicate wt% for any acids.
 - (b) Indicate partial pressure for wet CO₂.
 - (c) Be alert to the danger of metal dusting in hot, high-alloy streams with CO/CO₂ ratios >0.5.
- (2) Crack-inducing agents (list only if liquid water, or other electrolyte, is present [except for NH₃ and H₂]; indicate concentration of the following agents, if present above their threshold concentrations):
 - (a) Anhydrous ammonia: water content in wt%. 0.1 wt% water is required to inhibit stress corrosion cracking in carbon steel. Note that inhibition will be ineffective in vapor spaces.
 - (b) Hydrogen, if the partial pressure is 100 psia.
 - (c) In lines and equipment in the CO₂ recovery unit (in wt% caustic or wt% amines).
 - (d) Chlorides, any concentration (in ppmw).

21.5.2 MATERIALS SELECTION CRITERIA

While the normal criteria for materials selection address design life, sometimes other criteria govern. Examples include using design conditions rather than operating conditions as the basis for materials selection, requirements for unusual reliability or unusually long life, and corrosion debris or product contamination concerns. Such information is sometimes referred to as the *materials selection design basis*. It is helpful to indicate this information in the “Notes” addendum of the template.

21.5.2.1 Product Contamination

Food, drug, polymer, and fine chemical processes are generally sensitive to contamination, including flaking of scales. While carbon steels may have acceptably low corrosion rates, they often result in iron contamination. Damage by *corrosion debris* is a closely related consideration. Examples include processes in which downstream catalysts are damaged by corrosion debris or where debris can affect flow or heat transfer efficiencies or may cause mechanical problems. The amount of corrosion debris depends primarily on the amount of exposed surface area. Packed beds and heat transfer surfaces of heat exchangers are usually the primary sources of corrosion products. Even though the corrosion rate of the exposed material may be acceptable from the design life, the relatively large exposed surface area may contaminate the product.

21.5.2.2 Reliability

Some systems demand operating reliability. For example, fire water systems must have fast response and operation under severe conditions, including hydraulic surges and fire exposure. The latter is often cited as the reason for not using plastic or fiberglass piping in corrosive fire water systems. In other cases, reliability may not be very important, permitting the choice of less expensive materials of construction, for example, drain valves in low-pressure benign services. Some users have design standards and materials selection limitations that override materials selected. Galvanized steel is sometimes prohibited where a plant fire could cause liquid zinc to drip onto austenitic stainless steel piping, vessels, or equipment. Process licensors sometimes override selections made in accordance with a template. Normally, such recommendations are more conservative than those of the template. Nevertheless, process licensor recommendations are always subject to review.

In selecting a material, always remember the “common sense” of materials selection: (1) Ease of maintenance, replacement, and/or reparability of the component being evaluated. For example, for a design that calls for 100% spares (e.g., one pump running, one on standby), ease of maintenance or replacement may permit selection of less expensive, or even nonrepairable, materials such as cast iron pump internals. In some cases, reparability may influence selection, such as using cast steel, which is repairable by welding, instead of cast iron. (2) Plant experience is particularly useful for processes having a broad base of experience and for selecting materials for water services. In some cases, plant experience may indicate that a lower grade of material is adequate even if the available nomographs and corrosion charts indicate otherwise, for example, some high-temperature sulfur services in chemical and hydrocarbon plants. (3) Once the design, operating and upset conditions have been defined for a piping run or equipment item, it is normal to assume that all components are subject to the same exposure factors. Some components may, however, be exposed to less than the full set of template conditions. Blinds in a piping run are a good example. Such blinds are usually used only to isolate the piping run from equipment or other runs, for the purpose of hydrostatic testing or as part of a maintenance procedure. Most blinds will never experience normal operating or upset conditions. In applications in which the piping run requires special materials, the blinds often can be made of carbon steel. Care taken to differentiate among such service-related applications is often rewarded with significant cost savings.

usually supplied with off-the-shelf materials of construction. Most often, any deviations in materials proposed by the fabricator or supplier will exceed the minimum material of construction selected in accordance with the template. However, the proposed materials should be reviewed for compliance with template requirements, including any special fabrication specifications such as PWHT for process reasons, NACE MR0175 [2], and safety and design life requirements.

Equipment to be subjected to two or more sets of process conditions may require two or more templates. Examples include: (1) For shell and tube heat exchangers, use one template for the shellside and another for the tubeside. (2) For separators and distillation towers, use one template for the overhead section and another for the bottoms section. Towers with multiple feeds and/or draws usually require multiple templates.

21.5.5 GROUPING PROCESS REGIONS

When different sections of the process are exposed to essentially the same environment, they can be grouped together for materials selection. The following example is for a refinery; only four types of commodities are needed. (1) *Hydrogen and hydrogen mixtures*. Either pure hydrogen gas or commodities that are mixtures of hydrogen gas with other components, such as hydrocarbons. (2) *Hydrocarbons*. Commodities that are hydrocarbons or mixtures of hydrocarbons with other materials such as water, hydrogen, steam, etc. (3) *Noncorrosive gases*. Commodities such as nitrogen and dry plant air at ambient temperature. (4) *Other services*. Commodities such as amines, cooling water, fire water, and chemicals such as sulfur, caustics, acids, oxidants, etc.

21.5.6 MATERIALS SELECTION PROCEDURE

The first step is to consider the effect of the design temperatures.

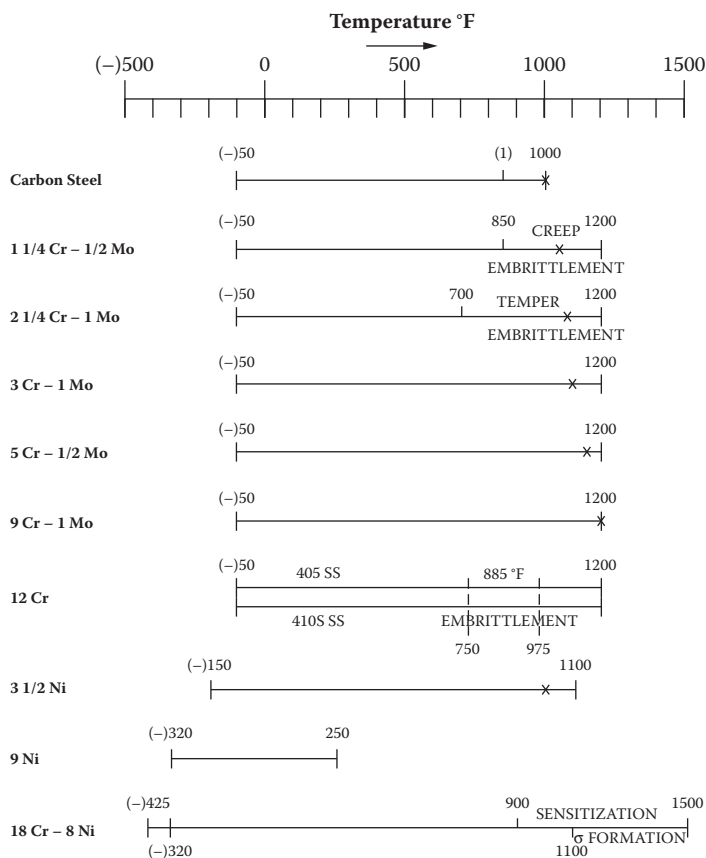
21.5.6.1 Low Temperature

Ensure that the upset conditions listed in the template have been considered in establishing the minimum design temperature. A candidate material of construction must comply with minimum code requirements for low-temperature toughness. As the template information is subsequently reviewed for the effects of corrosion, crack-inducing agents, embrittlement, etc., make sure that the low-temperature toughness requirements are retained after making any changes in materials.

21.5.6.2 High Temperature

The preliminary material of construction should be checked for the risk of thermally induced degradation at the maximum design temperature: (1) Is it susceptible to thermally induced embrittlement or thermal degradation that could cause failure during high-temperature service? For example, creep embrittlement and spheroidization or graphitization. (2) Will sustained operation at the maximum design temperature cause the material to be brittle at lower operating temperatures? Sigma-phase embrittlement of stainless steels is an example. (3) Will sustained operation at the maximum design temperature cause the material to be susceptible to corrosion at lower temperatures? Polythionic acid attack of stainless steels is an example.

The material is upgraded as necessary, always ensuring that it has adequate toughness at the minimum design temperature. The suitability of the upgraded material for the anticipated corrosion/degradation environment will be evaluated later. If sustained operation at the maximum design will cause the material to be brittle at lower operating temperatures, the design engineer should prepare appropriate operating instructions. Next, the candidate material is evaluated for the anticipated external environment, e.g., external chloride stress corrosion cracking, induced by a marine atmosphere. Next, the following considerations of corrosion, upset and transient conditions, and final review are organized to use the grouped process regions mentioned above.



X Forms excessive scale above this temperature if exposed to air or steam.

(1) Weakens by graphitization of carbides at prolonged temperature above 850 °F.

FIGURE 21.12 Materials selection as a function of temperature. (The upper value of the temperature range represents the limit for which code-allowable stresses are available.) © Copyright by Marcel Dekker, Inc.; reprinted with permission [5].

21.5.6.4 Upset Conditions: Review

Several items on the template should be reviewed, as follows:

1. All material selections for conditions above 1000°F (540°C), to avoid oxidation, scaling, or spalling problems. Figure 21.12 is useful for evaluating such problems, including thermally induced embrittlement >700°F (370°C).
2. For carbon steel in hydrogen stress cracking services, determine if heavy section/sharp thickness gradients such as thick nozzles will be required. Such gradients may indicate a need for HIC-resistant plate and PWHT to prevent stress-oriented hydrogen-induced cracking. Determine where HIC-resistant plate is to be used for vessels, heat exchangers, and/or piping. Determine if normalizing and PWHT should be specified.
3. Review all carbon steel templates for which PWHT is indicated. Consider the maximum operating pressure. If it is <65 psia (0.45 MPa) or if the combined stress in tension is less than the 10% rule, PWHT may be unnecessary.
4. Corrosion allowance is probably unnecessary for pressures <65 psia (0.45 MPa), particularly for piping.

numbers and equipment designations utilized on the respective templates. This PFD should show design temperatures and pressures for all piping and equipment. There should be sufficient room to create a "Notes" section, which includes any special materials selection requirements such as concerns about product contamination or operating reliability. Templates should be included as attachments.

The preliminary material selections are entered on the simplified PFD, along with corrosion allowances and any special features such as hardness controls or PWHT. Use arrows with legends, color codes, dotted or dashed lines, or some other method to identify the material/corrosion allowance/fabrication requirements for each pipe run and piece of equipment. In most cases, the "Notes" section simplifies the identification process, since many of the process services will refer to common notes. Examples include NACE hardness controls, PWHT, requirements for internal and/or external paint coatings, anodic or cathodic protection, and design-related measures such as a requirement for self-draining. This generates the materials selection diagram. The MSD is useful for several activities:

1. Compare the metallurgies, corrosion allowances, and fabrication requirements of the incoming and outgoing lines for each piece of equipment versus those of the equipment. This is a consistency check. Highlight any inconsistencies for later resolution.
2. If materials selection depends on corrosion control by process-related measures (such as chemical treatment), these should be indicated on the MSD. Indicate the intended injection points and the type of chemical to be injected. Examples include corrosion inhibitors, scale inhibitors, biocides, pH control chemicals, wash water, etc. Also indicate the location of proposed corrosion monitoring and sampling sites. If anodic or cathodic protection is to be part of the corrosion control design, the MSD or its "Notes" section should indicate the piping and/or equipment to be protected.
3. If degradation processes such as high-temperature embrittlement or autorefrigeration will affect operating procedures such as pressurization during start-up, indicate such limitations as general notes to the MSD.
4. Check for large pressure drops such as those that can occur at control valves. Determine if pressure drops will induce corrosive flashing. Flash spools or splash plates may be required downstream of the affected control valve.
5. Check for potential "mixing point" corrosion problems. A typical example of this type of problem occurs where a nominally noncorrosive electrolyte such as water is mixed with a dry acid gas or acid salt. The turbulence associated with mixing usually requires a "mixing" spool of corrosion-resistant material for at least 10 pipe diameters downstream of the mixing point. Neutralization may also be required.
6. Indicate convenient specification breaks. Specification breaks are points where the materials of construction change from one type to another.
7. Indicate the need for check valves, to protect upstream piping and equipment from damage by corrosive reverse flows. In most cases, an upgrade of the upstream piping is less expensive and more reliable than a corrosion-resistant alloy check valve.

If review of the MSD causes any changes in the templates, make sure that the changes are documented.

21.6 CONCLUSIONS

The procedure we have discussed is not a "cook book" process. Prior plant experience should always be an important part of the materials selection process. Common sense plays a key role in evaluating candidate materials. Time should be taken to determine the leeway provided by ease of maintenance, repairability, and sparing. In some cases, these considerations require upgrading of the materials or fabrication procedures (e.g., PWHT). In other cases, it may make sense to recom-

18. Gutzeit, J. 1986. In *High Temperature Sulfidic Corrosion of Steels, Process Industries Corrosion-Theory and Practice*, eds. B. J. Moniz and W. I. Pollock, 367–372. Houston, TX: NACE International.
19. Couper, A.S., and J.W. Gorman. “Computer Correlations to Estimate High Temperature H₂S Corrosion in Refinery Streams.” *Materials Protection and Performance* 10(1) (1971): 31–37.
20. American Petroleum Institute. Current edition. *Centrifugal Pumps for General Refinery Service*. API Standard 610. Washington, DC: API.
21. American Society of Mechanical Engineers. Current edition. *Specification for Horizontal End Suction Centrifugal Pumps for Chemical Processes*. ASME B73.1M. New York: ASME.
22. American Society of Mechanical Engineers. Current edition. *Specification for Vertical In-Line Centrifugal Pumps for Chemical Processes*. ASME B73.2M. New York: ASME.
23. American Petroleum Institute. Current edition. *Recommended Practice for Calculation of Heater Tube Thickness in Petroleum Refineries*. API Recommended Practice 530. Washington, DC: API.

22.4.7	Strange Behavior of Super-Compactible Materials	1627
22.4.8	Critical Pressure Drop	1628
22.5	Solid/Liquid Separation Equipment and Operation	1629
22.5.1	Batch Pressure Filters	1630
22.5.1.1	Pressure Nutsches	1630
22.5.1.2	Leaf Filter	1631
22.5.1.3	Candle Filter	1632
22.5.1.4	Bag Filters	1633
22.5.1.5	Cartridge Filters	1634
22.5.1.6	Filter Presses	1634
22.5.2	Continuous Filters	1636
22.5.2.1	Rotary Drum and Disc Filters	1636
22.5.2.2	Horizontal Belt Filter	1639
22.5.2.3	Indexing Belt Filter	1639
22.5.3	Deep-Bed Filter	1640
22.5.4	Cross-Flow Filters	1641
22.5.5	Membrane Filters	1641
22.5.6	Thickening and Clarification	1643
22.5.7	Centrifugation	1645
22.5.8	Hydrocyclone	1646
22.5.9	Expression Equipment	1647
22.6	Cake Washing	1648
22.6.1	Displaced Washing and Repulping	1648
22.6.2	Terms and Definitions for Displacement Washing	1648
22.6.3	Washing Curves	1649
22.7	Laboratory SLS Test	1650
22.7.1	Laboratory SLS Test	1650
22.7.2	Problems in Laboratory Tests	1653
22.7.2.1	Samples	1653
22.7.2.2	Adverse Effect of Sedimentation on Filtration Experiments	1653
22.7.2.3	Wall Friction in C-P Cell and Small-Scale Cells	1653
22.7.2.4	Test Numbers	1653
22.8	SLS System Design	1654
22.8.1	Selection of SLS Equipment	1654
22.8.1.1	Specifications of a SLS System	1654
22.8.1.2	Selection of Equipment and Process	1654
22.8.1.3	Comparison of SLS Equipment	1656
22.8.2	Decision Network for Design for Cake Filtration Systems	1656
22.8.3	Selection of Filter Media	1658
22.8.3.1	Introduction	1658
22.8.3.2	Woven Filter Media	1659
22.8.3.3	Selection of Filter Media	1659
22.8.4	Selection of Pumps in Filtration Operation	1660
22.8.5	Cycle Analysis in Selection of Filter Aids	1661
22.8.6	Scale Up	1663
	Table/Figure Source Lines	1664
	References	1665

TABLE 22.1
Terminology in Relation to Size Range

Size (μm)	Terminology	Examples	Solid/Liquid Separation Method
0–0.001	Ionic	Aqueous salts	Nanofiltration, reverse osmosis, chromatography
0.001–0.1	Macro-molecular	Virus, colloids	Ultrafiltration
0.1–10	Fine particle	Pigments, clay, bacteria	Microfiltration, cake filtration, deep-bed filtration, centrifugation
10–100	Medium size	Bacteria, yeast, fibers, fine sand	Cake filtration, gravity sedimentation, floatation, cycloning
100–1000	Large	Coarse sand	Screens, shakers

22.1.4.2 Straining

Screens with openings smaller than the particles are used to remove the particles (Figure 22.1a). Screens, strainers, and bag filters belong to this category. Bar screens and trash rakes are employed for removal of large debris. Traveling, passive, vibrating, and rotating screens are employed. Sieves have openings ranging from 25 μm (400 mesh) to 8 mm (2 1/2 mesh). Larger sizes are specified by the actual size of the aperture. Shale shakers are screens used for separating cuttings from drilling fluids in the production of petroleum. Bag filters represent the simplest and most commonly used type.

22.1.4.3 Cake Filtration

In cake filtration (Figure 22.1b), solids and liquid are separated by filter medium, which retains the solids as a cake and permits the liquid to pass through under pressure, vacuum, or centrifugal forces. At the start of filtration, some particles may pass through the medium, and the filtrate may be turbid. Once the cake is formed, it becomes the primary filter medium and particles finer than the openings of the medium can be separated.

22.1.4.4 Cross-Flow Filtration

Cross-flow filtration (Figure 22.1c) is principally used on difficult to filter materials. When a cake of low permeability forms, filtration rates can drop to unacceptable values. The cake thickness can be reduced by introducing shear forces at the cake surface. Low-shear cross-flow operation is accomplished by pumping slurries through channels with porous walls or through porous tubes. Rotating turbines or mixers are used in high-shear devices. Cross-flow filtration is essentially a filter-thickening operation in which the suspension thickens as it flows through the unit. Ultimately, the concentration reaches a point where pumping or mixing is no longer feasible. Due to the fine

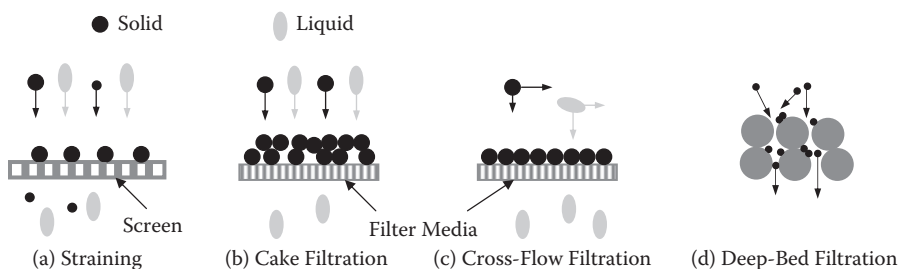


FIGURE 22.1 Schematic mechanisms of three types of filtration.

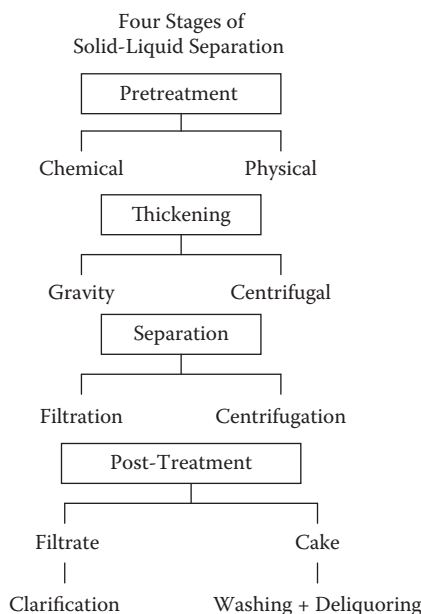


FIGURE 22.2 Stages of solid/liquid separation.

render it hydrophobic. Frothers are added to the vigorously agitated mixture. Air bubbles attach to the collector-mineral particles, which then rise and are removed along with the froth or foam.

22.1.5 STAGES OF SOLID/LIQUID SEPARATION

Separation of solids from liquids usually consists of four stages including pretreatment, thickening, separation, and post-treatment, as shown in Figure 22.2.

An overall perspective is essential to solution of SLS problems which are basically complex. Engineers must consider the four steps and their interrelationships in approaching system design or improving existing operations.

Frequently, slurries settle slowly, and are difficult to filter or centrifuge. Pretreatment techniques such as coagulation and flocculation or filter aid addition can be employed to improve separation characteristics. When a suspension consists of fine particles that are difficult to separate, increasing the effective size through aggregation or flocculation leads to improved separability. Aggregated particles are called flocs. A floc is illustrated in Figure 22.3. Degradation of flocs by shear forces is a problem in coagulation and flocculation. It is necessary to study the effects of pumping and

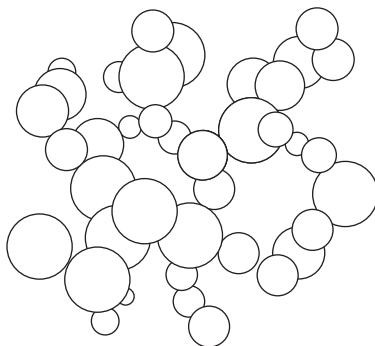


FIGURE 22.3 Arrangement of flocculated particles.

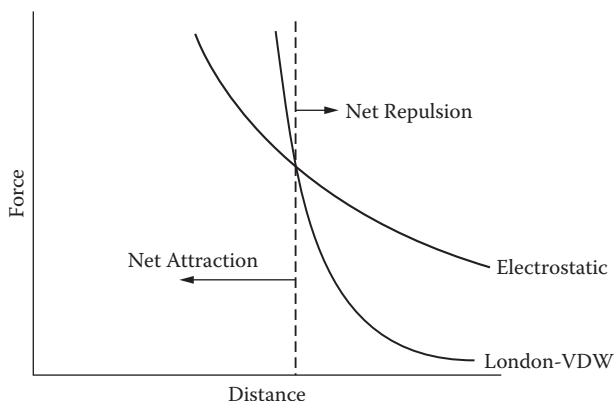


FIGURE 22.4 Interparticle forces.

electrostatic charges. Pretreatment operations aim at neutralization of the repulsive force and stimulation of particle aggregation.

22.2.1 INTERPARTICLE FORCES AND ZETA POTENTIAL

Most particles suspended in water and wastewater, e.g., clays, silica, hydrated metal oxides, paper fibers, biological cells, etc., possess negative surface charges in the neutral pH range. The repulsive electrostatic forces due to the electrostatic surface charge and the attractive London–van der Waals (LVDW) force represent the two principal forces among particles. In Figure 22.4, the electrostatic and LVDW forces are shown as a function of the distance r between particles. Repulsive electrostatic forces vary with the inverse square (r^{-2}) of the distance between particles. Attractive LVDW forces vary inversely with the sixth power (r^{-6}) of the distance. In order for particles to be coagulated, the LVDW forces must be greater than the electrostatic forces. In Figure 22.4, as the distance r decreases, the LVDW force increases very rapidly; and at the point, where the two forces intersect, the net force is zero. At a shorter distance, the net force is attractive; and the particles form aggregates that increase the ease of separation. The magnitude of electrostatic force of colloidal particles is evaluated by the term “zeta potential” explained as follows:

A particle in a suspension with negative electrostatic surface charge is shown in Figure 22.5. Positive ions in the solution are attracted to the negatively charged surface where they may be strongly adsorbed. The adsorbed layer remains rigidly attached and forms what is known as the Stern layer with a thickness equal to δ . Outside the Stern layer is a diffuse layer in which negative ions outnumber positive ions and balance the excess in the Stern layer. The electrostatic potential at the particle surface A decreases through the Stern layer along AB and along BC in the diffuse layer and reaches zero at point C , where the bulk of the solution is encountered. The Stern layer and diffuse layer are called double layers. They are important in determining forces between colloidal particles. Zeta potential BC is the difference between the charge at the edge of the Stern layer and the bulk of the suspending liquid, as shown in Figure 22.5a,b. High zeta potential leads to stability of colloidal systems. The relationship of colloid stability to values of zeta potential is shown in Table 22.2.

Zeta potential can be measured by tracking the rate of a negatively or positively charged particle moving across an electric field. The most common commercial instrument is the zeta meter. It can be expensive and requires some operational experiences to get reliable testing results.

22.2.2 COAGULATION AND FLOCCULATION

Coagulation generally refers to aggregation by charge neutralization with inorganic salts, and flocculation is brought about by large molecular weight polyelectrolytes. Coagulation and floccu-

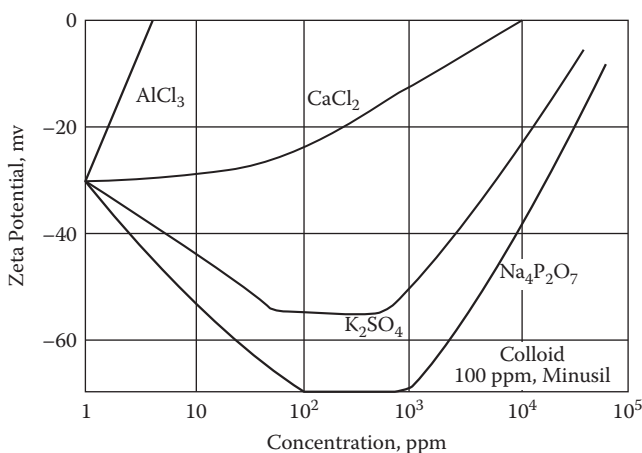


FIGURE 22.6 An example of the impact of type and dosage of electrolyte on zeta potential.

TABLE 22.3
Inorganic Coagulants

Chemical Name	Common Name	Formula
Acids		
Hydrochloric acid		HCl
Sulfuric acid		H ₂ SO ₄
Bases		
Calcium hydroxide	Slaked lime	Ca(OH) ₂
Sodium hydroxide		NaOH
Salts		
Aluminum chloride		AlCl ₃
Aluminum chlorohydrate		Al(OH) ₂ Cl
Aluminum sulfate		Al ₂ (SO ₄) ₃
Calcium chloride		CaCl ₂
Calcium oxide	Quick lime	CaO
Ferrous chloride		FeCl ₂
Ferric chloride		FeCl ₃
Ferrous sulfate	Copperas	FeSO ₄
Ferric sulfate		Fe ₂ (SO ₄) ₃
Sodium aluminate	Soda alum	NaAlO ₂

power of the valence. Although not precisely correct, the rule correctly predicts that the quantity of AlCl₃ to achieve zero potential is much less than that of CaCl₂. In general, Al⁺³ and Fe⁺³ have proven to be more effective in the coagulation of negatively charged particles. On the other hand, the pyrophosphate ion P₂O₇⁻⁴ is highly effective in increasing the negative nature of the particles and leads to a highly stable colloidal suspension. This property makes phosphate ions useful components of detergents.

In addition to coagulation with electrolytes or polyelectrolyte by controlling the zeta potential, agglomeration is usually accomplished by employing a long-chain polymer to provide mechanical bridging, which is called flocculation. Coagulation and flocculation can occur simultaneously or with some degree of overlapping.

1. Settling velocity, supernatant turbidity, and volume fraction of solids of the sediment (average solidosity)
2. Filtration rate, specific cake resistance, CST (capillary suction time; slurry is poured into a small cylinder placed on a filter paper [see Figure 22.62a]. A cake is formed and filtrate is sucked out radially. The time required to pass between two fixed radii is termed CST), filtrate turbidity, and cake solidosity
3. Determining the time from coagulant addition to the first appearance of a visible floc
4. Visually recording and comparing flocs as they are formed
5. Floc density measurements
6. Zeta potential

Criteria (1) can be evaluated by sedimentation experiments and (2) can be tested by vacuum, pressure filtration, or CST experiments. Filtration and CST experiments will be discussed in Section 22.7.

A jar test procedure based on the bench stirrer method is basically as follows:

1. Choose the desired coagulant and/or flocculant and the desired dosage.
2. Prepare the coagulant and flocculant samples according to the guidelines in the previous section.
3. Measure and pour slurry samples into each beaker (Figure 22.7).
4. Mix the coagulant or flocculant at a chosen dosage with slurry: place the beakers with slurry under the bench stirrer with paddles centered in the beakers, approximately 1 in. from the surface of the sludge sample. Use graduated syringes or graduated cylinders to add various dosages of chemicals to each of the beakers. Mix the chemicals and slurry for 30 to 60 sec, with a paddle speed of 200 rpm for thorough chemical/particles mixing. Then reduce the speed to 30 rpm for sufficient time (1 to 15 min) to allow the flocs to grow.
5. Results evaluation based on specific criteria.

A jar test evaluation based on sedimentation rate as a function of coagulant or flocculant concentration is shown in Figure 22.8. Intervening time between coagulant and flocculant additions is a third variable. Results of CST (Dentel 1993) as a function of polymer dosage from CST test are shown in Figure 22.9. Minimum dosage of coagulants or flocculants can be determined from the two plots.

In wastewater and sludge treatment plants, the lab-scale jar test is used to predict full-scale performance of additives. Testing in the full-scale plant under controlled conditions is ideal but is seldom done. Tiller undertook full-scale tests in urban wastewater treatment plants using belt presses or centrifuges (Tiller and Li 2001b, 2002). Normally, the optimization of polymer usage is determined by the dryness of the dewatered sludge and overall economics are often neglected. In Tiller's test, an economic analysis based on the cost of the polymer and the cost of gas to dry solids is shown in Figure 22.10. Although increased polymer dosage led to increased cake solids as shown in Figure 22.11, the cost of additional polymer exceeded the cost of drying the sludge. Therefore, the total cost increases as more polymer is used.

22.3 PRETREATMENT—FILTER AIDS

"Filter aids" are inert materials that can be used in filtration pretreatment. The principle characteristics of filter aids are (1) increasing cake permeability, (2) increasing cake porosity, and (3) increasing cake rigidity (decreasing cake compactibility).

There are two objectives related to the addition of filter aids. One is to form a layer of second medium that protects the basic medium (filter cloth) of the system. This is commonly referred to

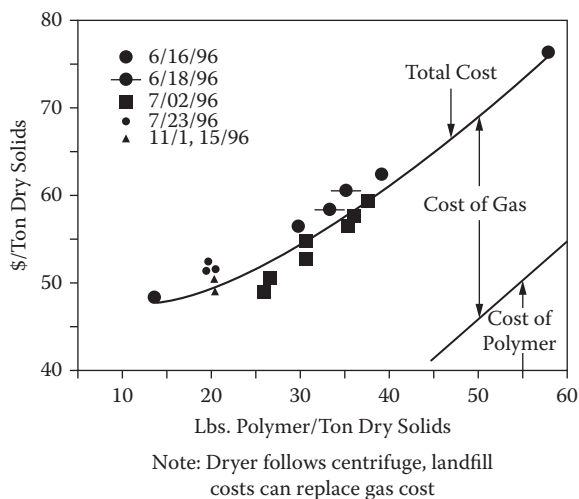


FIGURE 22.10 Tiller's full-scale test results, 1 lbm = 0.4535 kg.

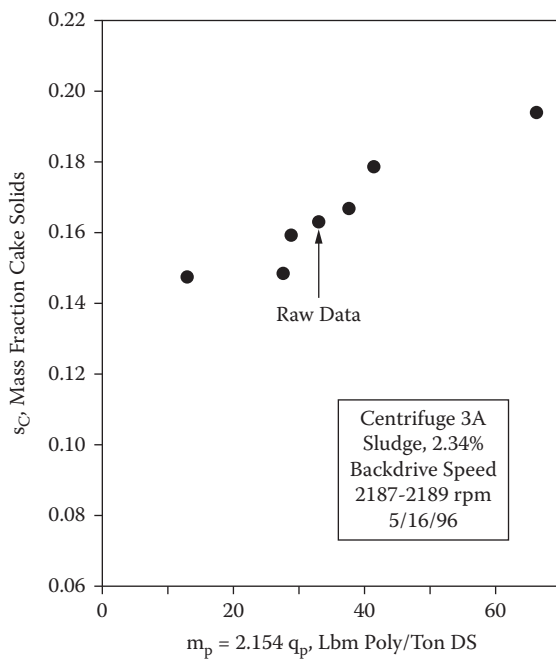


FIGURE 22.11 Cake water content against polymer dosages in Tiller's full-scale test, 1 lbm = 0.4535 kg.

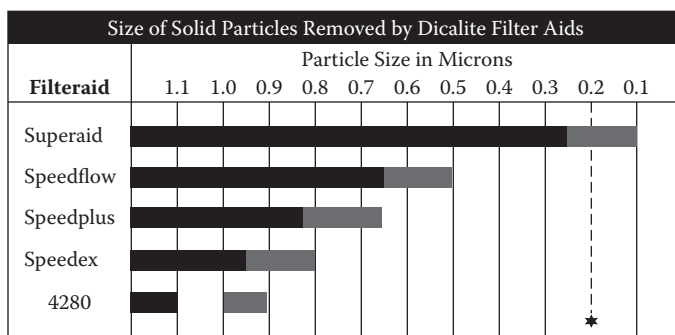


FIGURE 22.14 Chart showing the sizes of particles removed by five grades of Dicalite DE filter aids.

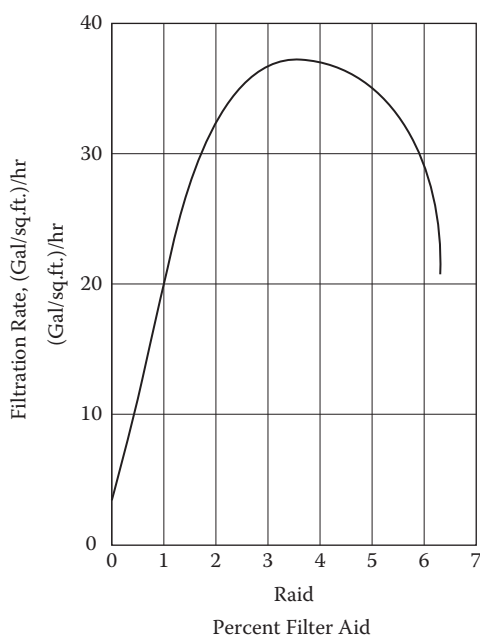


FIGURE 22.15 Optimum amount of filter aids for maximum flow.

Usually, as a filter aid is added to a system, the average flow rate is increased. However, the added solids not only decrease the percentage of product solids in the cake, but also fill the cake space sooner in batch pressure filters. Therefore, cycle analysis must be applied for determination of the optimum amount of filter aid addition. Discussion and calculation of cycle rates are presented in Section 22.8.5.

22.3.2 PERLITE

Perlite is another important silica based mineral filter aid. It is a particular variety of naturally occurring glassy volcanic rock, characterized by onionlike, splintery breakage planes (Figure 22.13b). After crushing, this rock will expand with heat to about 10 times its original volume.

There are differences between DE and perlite. First, the bulk density of perlite is less than that of DE. The density difference affects dosage and percentage of product solids in a cake. Second, a packed bed of perlite will not produce the same degree of clarity as diatomite. However, due to the potential industrial hygiene issues by inhalation, perlite has replaced DE in some applications.

$$q = \frac{dv}{dt} = \frac{p}{\mu(\alpha_{av}\omega_c + R_m)} \quad (22.2)$$

Although the usual definition encountered in the literature employs w_c , mass of solids/unit area, there are distinct advantages accruing to the use of volumetric units in simplicity of formulas, correlations, and predictive power. The dimensions of α depend on whether ω_c (m^3/m^2) or w_c (kgm/m^2) is used. The two quantities are related by $w_c = \rho_s \omega_c$, where ρ_s is density of solids. Resistance takes the form of $R = p/\mu q$ with dimensions $1/L$. Cake resistance is given by

$$R_c = \alpha_{av}\omega_c = \alpha_{av}^* w_c \quad (22.3)$$

where the superscript is used to differentiate the two types of specific resistance. The units of α_{av} and α_{av}^* are, respectively, $1/L^2$ and L/M . A closely packed bed of $10\text{ }\mu\text{m}$ spheres would be expected to have a specific resistance α of about $3.0\text{E}(12)\text{m}^{-2}$. The resistance of the bed to flow would depend entirely on the size and shape of the pores and would be independent of the mass inside the particles. Using α^* requires that $3.0\text{E}(12)\text{m}^{-2}$ be divided by the particle density, thereby leading to different values for every material for geometrically identical beds. Correct comparison of the resistances of different materials can only be made with the specific resistance as used in Equation (22.2) with dimensions of L^{-2} .

Integration of Equation (22.2) to obtain filtrate volume as a function of time t requires:

1. Specification of pump characteristics, that is, p as a function of q with constant pressure and constant rate being important special cases.
2. Relation between v and ω_c or w_c as obtained from a volumetric or mass balance over slurry, cake, and filtrate.
3. Equations relating the average values of the specific resistance α_{av} , permeability K_{av} , and volume fraction of solids in the cake ϵ_{sav} to the pressure drop Δp_c across the cake.

Before using Darcy's law to theoretically develop Equation (22.2), simplified procedures used by many authors (Rushton et al. 1996; Svarovsky 1990) will be employed to derive volume vs. time equations. Although widely used and valuable in interpreting data, highly significant information important to full-scale operation is missed when Equations (22.1) and (22.2) are the sole basis for developing the theory of cake filtration.

Although Equation (22.2) is often considered to be a "fundamental" formula governing filtration, it must be used with caution. It is very useful in analysis when viewed as an empirical approximation. It provides an instantaneous picture of the relationship among the variables, which include the instantaneous flow rate q , applied pump pressure p , and volume ω_c or mass w_c of solids/unit area.

22.4.2 MATERIAL BALANCE

Volumetric and mass balances are necessary in developing filtrate volume/unit area v as a function of t . A schematic diagram in Figure 22.16 shows how the slurry relates to the cake and filtrate. Quantities necessary for balances include:

	Total Solids	Concentration of Solids	
		Slurry	Cake
Volume basis	ω_c , vol./unit area	ϕ_s , vol. fraction	ϵ_{sav} , av. vol. fraction
Mass basis	w_c , mass/unit area	s , mass fraction	s_c , av. mass fraction

$$v = \left(\frac{1}{s} - \frac{1}{s_c} \right) w_c = \left(\frac{s_c}{s} - 1 \right) \frac{L}{s_c / \rho_s + (1 - s_c) / \rho_L} \quad (22.10)$$

It is clear that the volumetric balance leads to easier to handle expressions.

22.4.3 VOLUME VS. TIME

Solving for ω_c in Equation (22.5) yields

$$\omega_c = \frac{\phi_s}{1 - \phi_s / \epsilon_{sav}} v = cv \quad (22.11)$$

Substituting for ω_c in Equation (22.2) and rearranging the terms leads to

$$\frac{p}{\mu} dt = (\alpha_{sv} cv + R_m) dv \quad (22.12)$$

Historically, this equation has been integrated assuming α_{av} , ϵ_{sav} , and c to be constant even though they vary. When the variation is not large, integration from $t = 0$, $v = 0$ to (t, v) yields a parabolic relation in the form

$$\frac{pt}{\mu} = \alpha_{av} c \frac{v^2}{2} + R_m v \quad (22.13)$$

This is the well-known parabola that has been used extensively to calculate α_{av} and R_m based on v vs. t data for constant pressure filtrations performed in the laboratory. It must be used with caution.

22.4.4 DATA ANALYSIS

A simplified but useful approach to analysis of constant pressure data can be developed with the use of Equations (22.12) and (22.13) placed in resistance form. Dividing Equation (22.12) by dv and Equation (22.13) by v produces

$$\frac{p}{\mu} \frac{dt}{dv} = \frac{p}{\mu q} = \alpha_{av} cv + R_m \quad (22.14)$$

$$\frac{p}{\mu} \frac{t}{v} = \frac{p}{\mu q_{av}} = \frac{1}{2} \alpha_{av} cv + R_m \quad (22.15)$$

where $q_{av} = v/t$ is the average rate and $q = dv/dt$ is the instantaneous rate. Substituting R_c for $\alpha_{av} cv$ leads to

$$R = p / \mu q = R_c + R_m \quad (22.16)$$

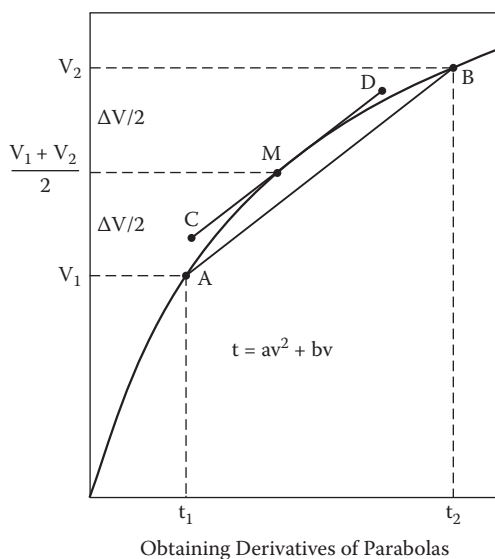


FIGURE 22.19 Tangent representing dt/dv as parallel to arc.

Example 22.1

An aqueous suspension of calcium silicate ($\rho_s = 1950 \text{ kg/m}^3$) at 20°C was filtered at a constant pressure of 68.9 kPa in a small press with an area of 428.7 cm^2 . The slurry concentration was 0.495% by weight and the average moisture content of the cake was 70.63% by weight. Calculate the specific and medium resistances on the basis of the following data (Hosseini 1977):

Time, sec.	70	93	120	152	187	227	270
Vol. of filtrate, liters	5	6	7	8	9	10	11

It is necessary to calculate the volumetric slurry concentration ϕ_s and the average cake porosity ϵ_{sav} . Using Equation (22.8) with ϕ_s and s replacing ϵ_{sav} and s_c leads to

$$\phi_s = \frac{0.00495 / 1950}{0.00495 / 1950 + (1 - 0.00495) / 1000} = 0.002545 \quad (22.18)$$

where the density of water at 20°C is 1000 kg/m^3 . The suspension is very dilute. Calculating ϵ_{sav} based on $s_c = 1.0$ $0.7063 = 0.2937$,

$$\epsilon_{sav} = \frac{0.2937 / 1950}{0.2937 / 1950 + 0.7063 / 1000} = 0.1758 \quad (22.19)$$

The volume/unit area ω_c of inert solids is related to the filtrate volume/unit area by

$$\omega_c = v / \left(\frac{1}{0.002545} - \frac{1}{0.1758} \right) = v / (393 - 5.7) = 0.00258v \quad (22.20)$$

The ratio $p/\mu = 68,900/0.001 = 6.89\text{E}(7)$ is required for calculating the resistance terms

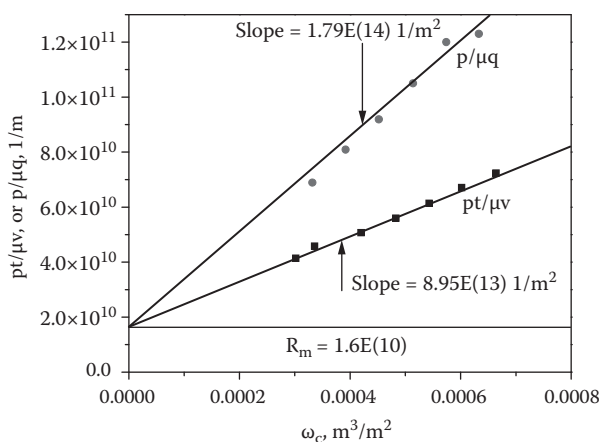


FIGURE 22.20 Resistance plot used to obtain medium and specific resistances.

The lines shown in Figure 22.20 yield $R_m = 1.6E(10)$ 1/m, and $\alpha = 1.69(14)$ 1/m². The specific resistance on a mass basis can be obtained from Equation (22.3) as

$$\alpha_{av}^* = \alpha_{av} / \rho_s = 1.69E(14) / 1950 = 8.67E(10) \text{ m / kg} \quad (22.27)$$

The use of units m/kgm predominates in the literature. If regression techniques had been employed with the points in Figure 22.20, two lines with different intercepts and slopes not in the ratio of 2/1 would have resulted. The construction and methodology illustrated in example 22.1 represent a compromise, and there is generally no precise answer.

22.4.5 DEVIATIONS FROM PARABOLIC THEORY

The equations employed in Example 22.1 require that the t versus v relation be a perfect parabola in constant pressure filtration. Errors are both theoretical and experimental. Introducing a suspension into a filter and suddenly increasing the pressure to the operating value results in a transient state in which a finite time is required to reach equilibrium conditions. If high pressures are involved, it is undesirable to raise the pressure too suddenly. Most slurries undergo some sort of pretreatment and mixing to improve filtration characteristics. If insufficient time is allowed for equilibrium to be reached, the cake permeability and porosity of successive layers will change continuously. Aging is an almost universal problem making it unwise to use other than fresh slurries. Biological solids are particularly susceptible to change.

Sedimentation in the filter vessel is a difficult problem that is frequently neglected. If vertical surfaces are involved, the cake will be thicker at the bottom compared with the top. In filters with horizontal surfaces, dense particles settle and increase the slurry concentration at the cake surface. Destruction of aggregates may occur during pumping, pouring, and mixing. Tiller, Hsyung, and Cong (1995) analyzed the sedimentation problem and developed approximate techniques to obtain the average specific resistance.

Slurries frequently involve a wide range of particle sizes that include submicron particles in the Brownian diffusional region. When cakes are deposited, the finest particles may diffuse into the filtrate and continuously clog the supporting medium, leading to increasing values of R_m . Tiller and Leu (1984) showed that clogging was a major problem in the removal of ash and asphaltenes from liquefied coal.

Processing of liquefied coal in a pilot plant at Wilsonville, Alabama, provides a good example of filtration operations that deviate from the simple constant pressure equations. After liquefying

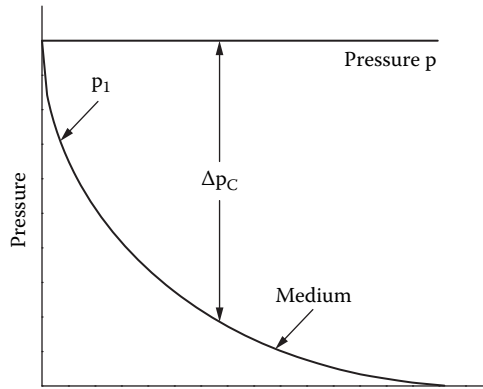


FIGURE 22.22 Variation of Δp_c .

$$p_1 = \mu q R_m \quad (22.28)$$

The time required for p_1 to drop to a negligible value may vary from seconds to a relatively lengthy period. Nevertheless, it is apparent that as long as $R_m > 0$, there cannot be a filtration with constant Δp_c , and the simplified analysis shown in Figures 22.18 and 22.20 must be used with caution.

In Figure 22.23, a plot of $p/\mu q$ vs. ω_c is illustrated for a constant pressure filtration in which R_m is not negligible. As Δp_c increases with time, the slope of the curve and α_{av} also increase. The total resistance is given by the curve ABD , and the cake resistance R_c is represented by BC . In accord with Equation (22.3), α_{av} is obtained by dividing R_c by $\omega_c(AC)$. As point moves up the curve, the angle of the triangle ABC increases and ultimately approaches the slope given by BD . The pressure drop across the cake can be calculated from

$$\Delta p_c = \left(\frac{R_c}{R_c + R_m} \right) p \quad (22.29)$$

Equation (22.29) can be used when pressure is constant or a function of time.

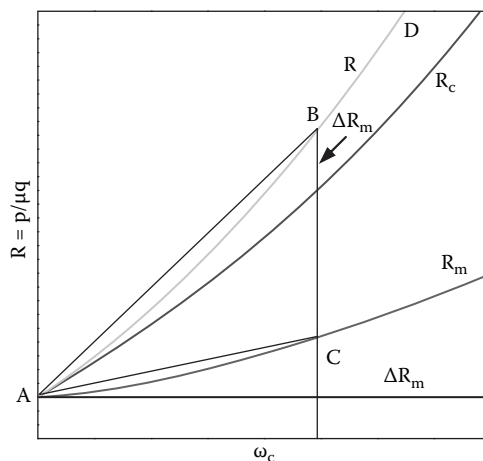


FIGURE 22.23 Medium and cake clogging.

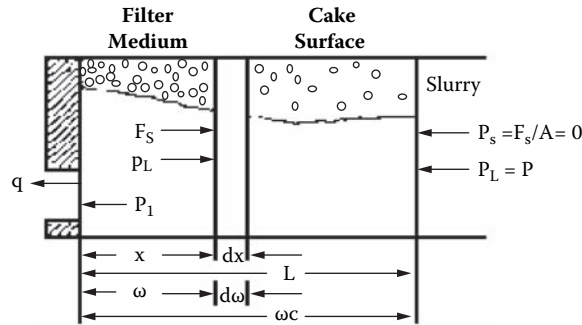


FIGURE 22.25 Diagram of a filter cake with spatial x and the material coordinate.

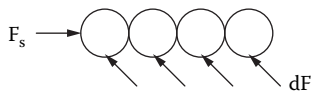


FIGURE 22.26 Fractional drag in a particulate bed.

area A must be balanced by an equal force at position x . Assuming that there is point contact among particles and that the local liquid pressure p_L is effective over the entire cross-sectional area leads to

$$Ap_L + F_s = Ap \quad (22.30)$$

Dividing Equation (22.30) by A and then defining the compressive drag or effective pressure by $p_s = F_s/A$, we have

$$p_L + p_s = p \quad (22.31)$$

The drag on the particle is an accumulation of form drag force resulting from friction along the surface of the particles and is transmitted through the point contacts over which the stress acts. The term p_s is a fictitious pressure used for convenience. It is called “effective pressure” in soil mechanics. In actual cakes, of course, there is a small area of contact, and the pressure at the contact points is much larger than the average given by p_s .

In thickening and centrifugation when gravitational and centrifugal stresses are involved, Equation (22.31) is replaced by more complex expressions Tiller and Hsyung (1993).

The quantities p_L and p_s vary with position and time and are functions of (x, t) . The applied pressure is either constant or a function of time alone. If we take differentials with respect to x in the interior of the cake at constant t , we have

$$dp_s + dp_L = 0 \quad (22.32)$$

The effective pressure increases and hydraulic pressure decreases as the liquid flows from the upstream face of the cake toward the filter medium.

Variations of the hydraulic and solid or effective pressures in a typical filter cake are illustrated in Figure 22.27. The liquid pressure drops from the pump pressure at the cake surface to a value p_1 at the medium. At the surface of the cake where $p_L = p$, the effective pressure is zero as no drag on the particles has developed. Consequently, the surface layer of the cake is unstressed, and the solidosity has its minimum value at that point. The solidosity reaches a maximum at the medium

$$K\alpha\varepsilon_s = 1 \quad (22.37)$$

As K , α , and ε_s are functions of frictional effective pressure p_s rather than hydraulic liquid pressure p_L , it is necessary to replace dp_L by $-dp_s$ in Equation (22.34). Making this substitution yields

$$q = -\frac{K}{\mu} \frac{dp_s}{dx} = -\frac{1}{\mu\alpha} \frac{dp_s}{d\omega} \quad (22.38)$$

To integrate the particulate Equation (22.38), K and α must be provided as functions of p_s .

22.4.6.3 Empirical Constitutive Equations

Empirical models of local solidosity, permeability, and specific resistance as functions of p_s can be in many forms. Tiller and Leu (1980) presented the following equations:

$$\left(\frac{\varepsilon_s}{\varepsilon_{so}}\right)^{1/\beta} = \left(\frac{K}{K_o}\right)^{-1/\delta} = \left(\frac{\alpha}{\alpha_o}\right)^{1/n} = 1 + \frac{p_s}{p_a} \quad (22.39)$$

in which p_a is an empirical parameter; and β , δ , n are cake compactibility coefficients. They provide a measure of the rate of change of ε_s , α , K with p_s . As a rough approximation, the exponents can be related by

$$\delta / 5 = n / 4 = \beta \quad (22.40)$$

22.4.6.4 Integration of the Darcy Equation

Combining the boundary conditions at the cake surface ($x = L$ or $\omega = \omega_c$, $p_s = 0$) and at the medium ($x = 0$ or $\omega = 0$, $p_s = \Delta p_c = p - p_1$) with the empirical constitutive equations ([Equation (22.39)]; assuming q is independent of x and is only a function of t , the particulate structure Equations (22.38) can be integrated to yield

$$\int_0^L \mu q dx = \mu q L = K_{av} \Delta p_c = \int_0^{\Delta p_c} K_o \left(1 + p_s / p_a\right)^{-\delta} dp_s = \frac{K_o P_a}{1 - \delta} \left[\left(1 + \frac{\Delta p_c}{p_a}\right)^{1-\delta} - 1 \right] \quad (22.41)$$

and

$$\int_0^{\omega_c} \mu q d\omega = \mu q \omega_c = \Delta p_c / \alpha_{av} = \int_0^{\Delta p_c} \frac{dp_s}{\alpha_o \left(1 + p_s / p_a\right)^n} = \frac{p_a}{\alpha_o (1 - n)} \left[\left(1 + \frac{\Delta p_c}{p_a}\right)^{1-n} - 1 \right] \quad (22.42)$$

These two equations give an instantaneous view of the cake and provide relationships among q , ω_c , L , K_{av} , α_{av} , and p_c . Equations (22.41) and (22.42) can be easily solved for q as a function of L or ω_c and Δp_c . Dividing Equation (22.42) by (22.41) leads to

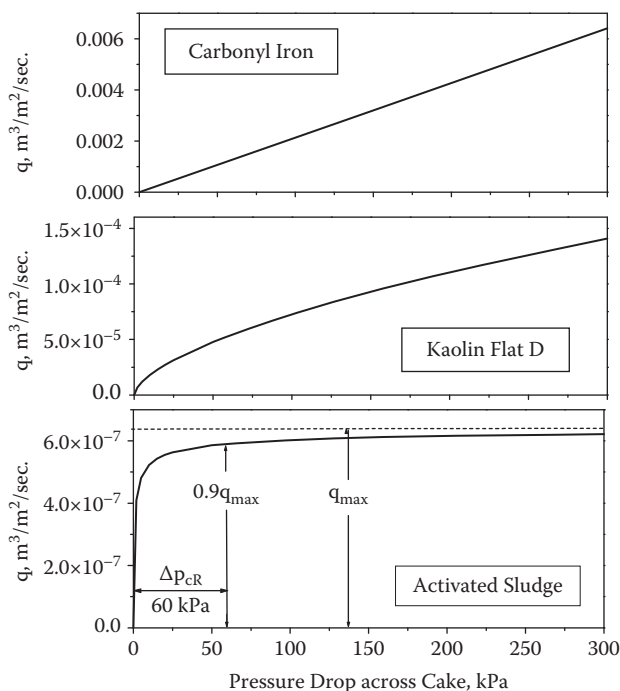


FIGURE 22.28 Variation of q against Δp_c .

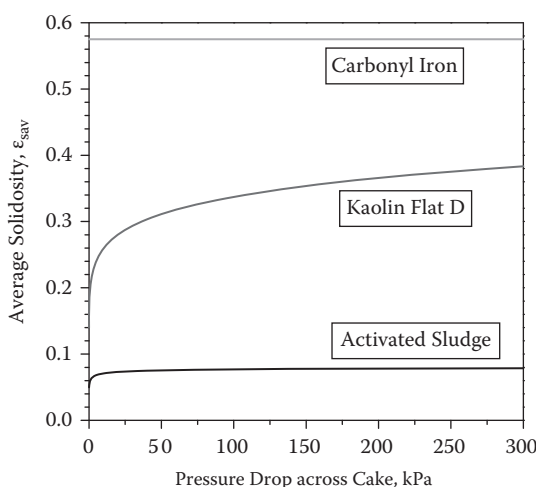


FIGURE 22.29 Variation of ϵ_{sav} against Δp_c .

incompressible materials like carbonyl iron, it increases with a power of Δp_c , which is less than unity for compactible materials like kaolin. Unfortunately, for super-compactible materials with $n > 1$ and $\delta > 1$, increasing the pressure drop beyond some low value has negligible effect on the flow rate and average solidosity, and both q and ϵ_{sav} approach maximum values.

22.4.8 CRITICAL PRESSURE DROP

As Δp_c approaches infinity, the limiting values of the flow rate and average solidosity become

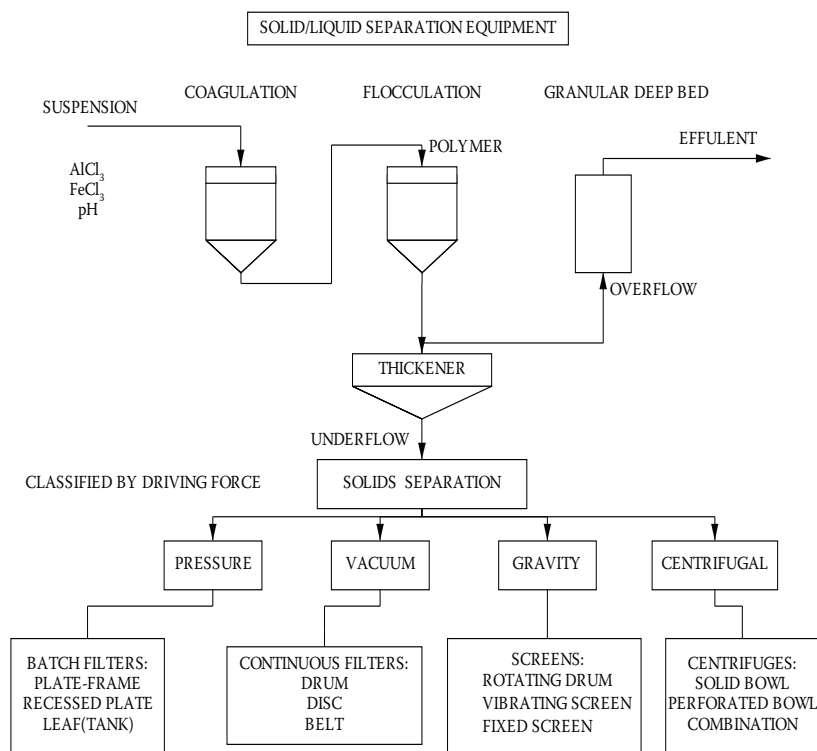


FIGURE 22.30 Equipment used for the four stages of solid/liquid separation.

and small screens have openings of less than 0.5 in. Slot openings in rotary screens run from 0.01 to 0.1 in. (254–2540 μm). Micro-screens frequently fall in the 15 to 60 micron range.

In vacuum filtration, the driving force (~ 20 in Hg = 10 psi, 1 psi = 4895 Pa) is slightly higher than the gravity. The vacuum operation frequently is tied in with continuous equipment such as drum, disc, or belt filters, in which cake is removed continuously. As the permeability of cakes diminishes, pressure becomes an important element in producing a satisfactory flow rate. Pressure filters are operated in the range of 30 to 60 psi and sometimes up to 100 psi. In contrast to vacuum filters, pressure filters normally operate in batch mode. In addition to vacuum and pressure, centrifugal forces are also used to increase the driving force in separation of particles from liquids.

Solid/liquid separation equipment can be also classified according to the principle of each unit operation, which is presented in Section 22.1.4. A list of equipment based on operating principle is given in the next section.

22.5.1 BATCH PRESSURE FILTERS

Pressure filters are usually operated batch-wise. The batch pressure filters can be classified as tank (pressure vessel) filters or presses. Tank filters have filter elements of different types mounted in pressure vessels. Tank filters are divided into pressure nutsches, leaf filters, candle or tubular filters, bag filters, and cartridge filters. Presses (see Figure 22.38) consist of a series of filter surfaces (plates). The elements are mounted on a frame and are pressed together mechanically.

22.5.1.1 Pressure Nutsches

Nutsche filters contain a single horizontal filtering surface in a pressure vessel. Gas is used to provide pressure for filtration and avoid the use of a high-pressure pump. Due to the limited filtration

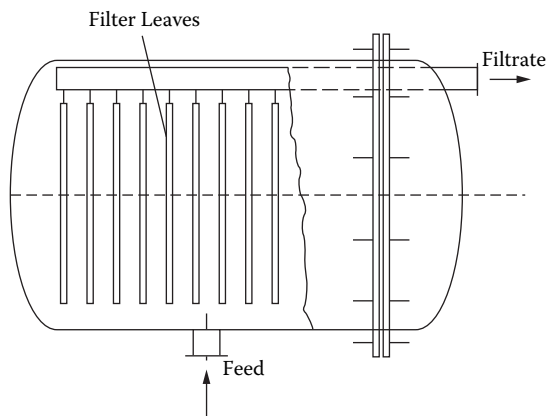


FIGURE 22.33 Horizontal-vessel, vertical-leaf filter.

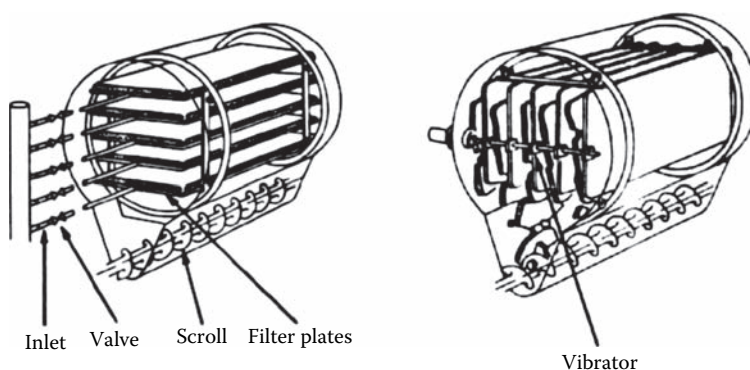


FIGURE 22.34 A Sparkler leaf filter with leaves in horizontal position during precoat, filtration, washing, and drying and vertical position during the cleaning cycle.

cm. A space of ~ 2.0 cm must be maintained between the cakes to prevent arching and facilitate discharge. Cake discharge from the vertical leaves can be accomplished by manual means, vibration, rotation at a slow speed against blades, blow back of gas, or by flushing with liquid. Horizontal leaves assure uniform deposition and washing. However, cakes are not easy to remove from the horizontal leaves. Centrifugal action provided by rotating of leaf bundles is used for cake discharging in some designs of horizontal leaf vertical tank filters. In general, cake can be discharged more easily from vertical leaf-type filters. A kind of leaf filter from Sparkler Filter, Inc. uses leaves in horizontal position during precoat, filtration, washing, and drying, but in vertical position during discharging and cleaning as shown in Figure 22.34. The design combines advantages of horizontal leaf and vertical leaf, and can provide completely automatic operation.

Pressure vessel filters are useful where noxious vapors are involved, and a completely closed system is desirable.

22.5.1.3 Candle Filter

Tubular filter elements contained in a matching vessel are known as candle filters. A typical candle filter (Purchas 1981) is shown in Figure 22.35. The filter vessel may contain one or more filter candles. The advantage of candle filters is the capability of back pulsing (with dry gas) or back-washing (with liquid) to automatically discharge the cake as shown in Figure 22.36. Some designs

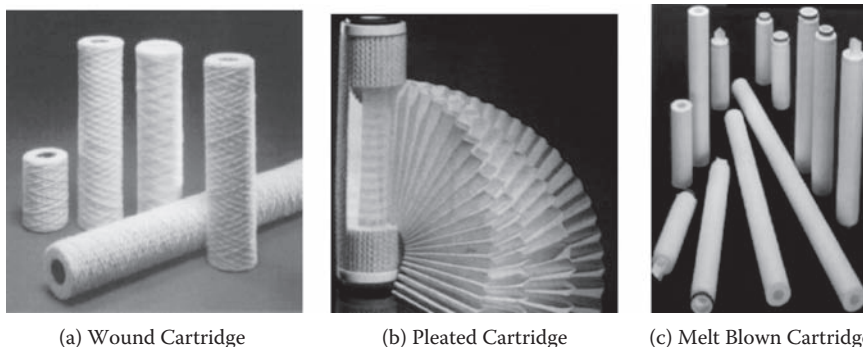


FIGURE 22.37 a–c: Cartridge filters.

completely plugged. Otherwise, a liquid full bag needs to be removed, resulting in product loss and industrial hygiene concerns for the operators.

22.5.1.5 Cartridge Filters

Cartridge filters are very commonly used. In industrial processes, usage of bag filters or cartridge filters is greater than other SLS equipment combined. Three types of cartridge filters are shown in Figure 22.37.

In string wound cartridge, fiber yarn is wound around a mandrel to form a depth medium. Filtration is primarily done by deep-bed filtration and the separation efficiency is poorer than the pleated type. Because string wound cartridges are less expensive, they are commonly used as the prefilter in front of the more expensive pleated cartridges. Pleated cartridges are fabricated by pleating fabric sheet to provide additional surface area and strength. The filtration mechanism is surface straining so the filtration efficiency curve is steeper. They are used when high collection efficiencies for specific particles are required. The mechanisms of melt blown or resin bonded cartridges are deep-bed filtration, that will be discussed later.

A term called the β ratio is commonly used to describe the filtration efficiency of cartridge filters. The β ratio is calculated by

$$\beta \text{ ratio} = C_{\text{feed}} / C_{\text{filtrate}} \quad (22.52)$$

where C_{feed} and C_{filtrate} represent the particle count per unit volume in the feed and filtrate.

22.5.1.6 Filter Presses

Filter presses play an important role in SLS since the nineteenth century. They are used when enclosed operation is not required. An excellent treatment of practical problems encountered with presses was provided by Alliot (1920). There are basically three types of filter presses: plate and frame, recessed, and membrane (diaphragm).

A plate and frame filter press is illustrated in Figure 22.38. A filter medium (usually cloth or paper) placed over a grooved plate serves as the support for the cake, which is deposited in an adjoining frame. Plates and frames are alternated as shown in Figure 22.38. The media serves as the gasket when mechanical closure is effected. Where washing is desired, every other plate is constructed so that liquid can be passed from one plate through the cake to the opposite plate. Thus the wash liquid passes through two cakes. Feed to a plate and frame press is generally through openings at the bottom corner. Large, dense particles tend to settle out, producing a nonuniform

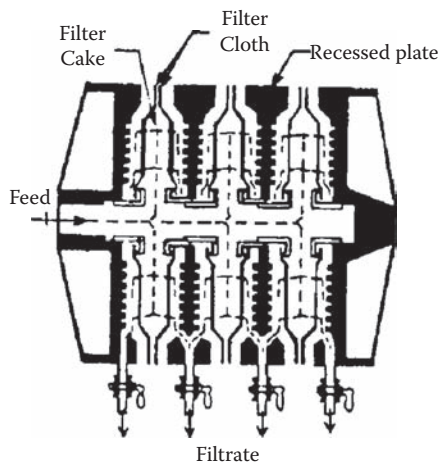


FIGURE 22.40 The recessed plate provides space for cakes and eliminates the need for frames.

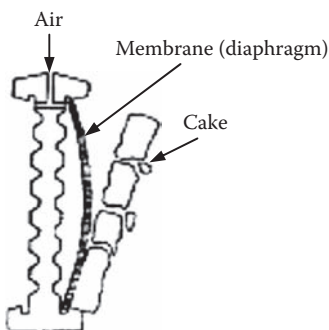


FIGURE 22.41 The membrane filter press.

A membrane filter press is shown in Figure 22.41. The impermeable flexible membranes, or diaphragms, are attached on the recessed plates. At the end of cake formation, the membranes can be inflated by air or pressured water to squeeze the cake for further cake deliquoring. This type of filter provides drier cakes compared with traditional plate and frame of recessed plate filter presses.

22.5.2 CONTINUOUS FILTERS

Continuous filters can be classified into rotary drum (Figure 22.42), disc (Figures 22.42, 22.43, 22.44), horizontal belt (Figure 22.45), table, and tilting pan. Drum filters are further divided according to the method used for cake removal. Most continuous filters use vacuum, and are best suited for materials that permit a reasonably fast rate of cake buildup. Continuous filters work best on medium-sized particles in the range of 5 to 50 μm . Larger particles generally exert minor capillary forces; therefore, cake drying or “drainage” can be accomplished by sucking air through the cakes under vacuum.

22.5.2.1 Rotary Drum and Disc Filters

The salient features of rotary drum and disc filters are illustrated in Figure 22.42. The rotary drum consists of a cylindrical drum having a permeable surface revolving partially submerged in a slurry. Disc filters consist of a series of thin discs revolving on a common shaft and partially submerged in a slurry, which is also shown in Figure 22.43. Continuous filters are normally used for materials

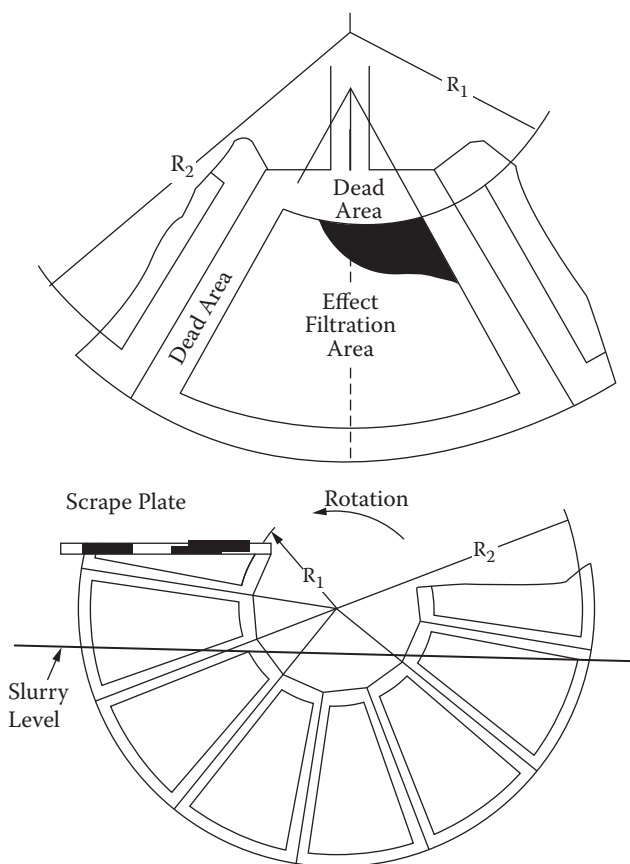


FIGURE 22.44 Horizontal filter illustrating filtration, washing, and drainage stages.

2. Cake formation period.
3. Emergence from slurry with suction causing some drainage to occur.
4. Application of a spray for displacement washing.
5. Drainage period that is frequently called *drying*, although no evaporation takes place. Steam heating reduces viscosity and surface tension and permits improved drainage. Displacement by influx of air may occur.
6. Cake discharge.

Although processes requiring the three steps of cake formation, washing, and drainage (drying) can be more easily done on a drum or horizontal belt filter, drainage can also be accomplished with discs. As illustrated in Figure 22.43, the filter consists of a series of discs *A* that rotate on a common axis in a slurry. The cake is scraped off at *C* and dropped into discharge chutes *D*. Each chute receives solids from facing sides of adjacent discs. The discs are divided into sections that have individual connections to the vacuum and air for the filtering, drainage, and blow zones. Piping is enclosed in the central revolving barrel connected to a wear plate that contacts a control block. Filtration takes place on both sides of the disc. Vacuum is applied inside, and the filter cake is deposited on the disc surface as it rotates through the slurry with only a part of the disc being submerged. At the end of the cycle, the vacuum is broken and the cake discharged. Cake removal from a rotary drum filter is carried out by a number of methods that are related to the properties of the cake and how it sticks to the medium. In Table 22.7, the minimum cake thickness for discharge is shown for different types of drums.

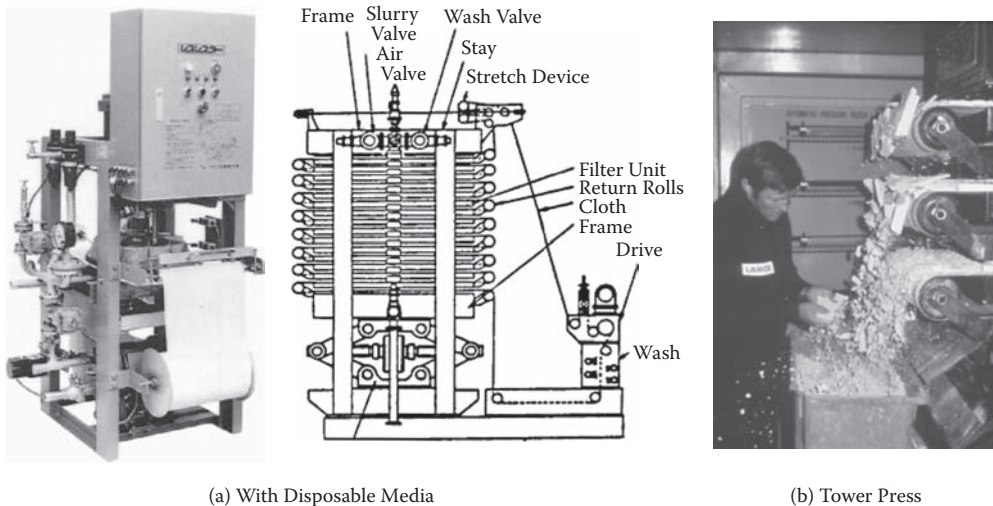


FIGURE 22.46 Indexing belt figures.

able media are employed when solids tend to stick to or blind the media (Figure 22.46a). They are especially useful for small waste stream clarifications. A few of these filters can be stacked to increase the filtration area and are called tower presses (Figure 22.46b). In tower presses, only permanent belts are used.

22.5.3 DEEP-BED FILTER

Deep-bed filters are employed for slurries with very dilute concentration ($<100 \text{ ppm} = \text{mg/L}$). The deep beds are in the form of granular media (sand, crushed anthracite coal, garnet) or cartridges (Figure 22.37), which are cylinders containing a variety of materials for trapping the particles. An example of the widely application of cartridge filters is removing particles from lubricating oils in automobiles and trucks.

A typical depth-type cartridge is shown in Figure 22.47. They are disposable. The illustration shows an outer region with large pores and high permeability and an inner region with smaller pores. This gradient design provides filtration efficiency without sacrificing on-line life.

Sand and anthracite are the two most commonly used media in granular bed filters. Single, dual, or multiple media can be used. Finer granular provides higher filtration efficiency but has a

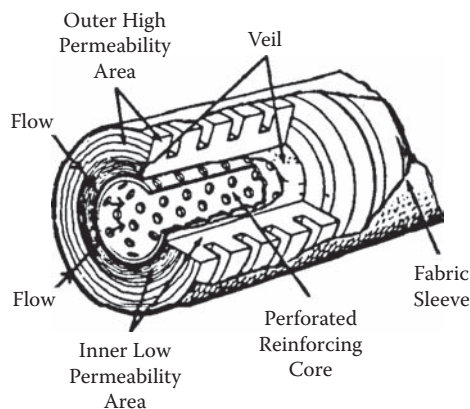


FIGURE 22.47 Johns-Manville cartridge.

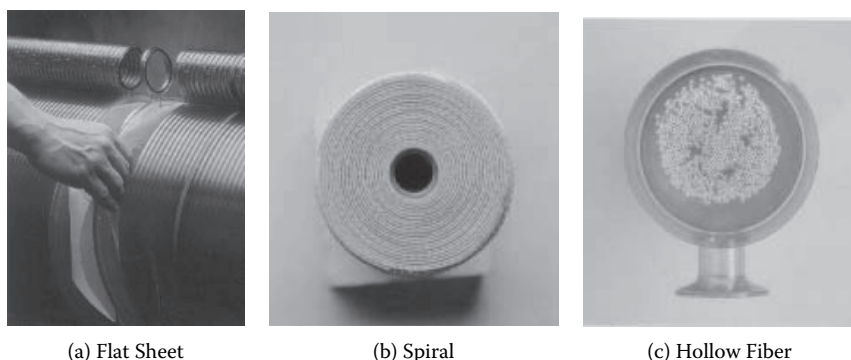


FIGURE 22.49 Typical continuous thickener.

UF and NF, a term called molecular weight cut off (MWCO) is used. MWCO means molecules with molecular weight greater than the MWCO will be rejected by this membrane.

Membrane filters come in three configurations: flat sheet, spiral, and hollow fiber (Figure 22.49). Flat sheet membranes can be attached to the plates and by stacking many plates to achieve a large filtration area. The suspension flows across the membrane surface while the permeate flow through the membrane to the collection channels at the edge of the plates. This configuration is most suitable when concentrated suspension is encountered (a few wt%). The manufacturers tend to make special cassettes or plates that are not interchangeable with other suppliers' products.

Spiral elements are the most popular form of membrane filter today due to their relatively low cost. The membrane in a spiral element is wrapped with spacer sheets into a cylinder (Figure 22.49b). The suspension is flowing in parallel to the axis of the cylinder and the permeate flows spirally into the center collecting chamber. Although the design favors low solid concentrations, it is possible to run suspensions with high solid concentrations in a spiral membrane filter.

In hollow fiber systems (Figure 22.49c), a bundle of hollow fibers are contained within a shell and the suspension flows inside the hollow fiber and the permeate is collected in the shell side. Hollow fibers are best suitable for applications without solid particles. In addition to the above three types, there are also rotating discs, annual gap, and vibrating disc systems for membrane cross-flow filtration.

There are two modes that can be used to operate a membrane filter, concentration or diafiltration. In concentration operations, the permeate passes through the membrane and is collected as a filtrate while the retentate (the unfiltered part) is recycled back to the feed vessel. As more and more permeate is removed, the solid concentration in the retentate increases until the desired concentration is reached or the cross flow becomes inefficient due to the high viscosity. The retentate concentration can be calculate as (Cheryan 1998)

$$C_{retentate} = C_{initial} \left(\frac{V_{initial}}{V} \right)^R \quad (22.53)$$

where $C_{retentate}$ and $C_{initial}$ are the solid concentration in the retentate and the initial suspension, and $V_{initial}$ and V are the initial volume and current volume of the retentate in the feed tank. R is the rejection ratio of the species of interest. $R = 1 - C_{permeate}/C_{retentate}$.

In the diafiltration mode, fresh liquid is added to the retentate to maintain a constant retentate volume. This method is useful if some dissolved material in the retentate needs to be extracted to the permeated side. The concentration of retentate can be calculated as (Cheryan 1998)

where A is the area of the clarifier and Q_o is the overflow rate. The particle settling rate can be estimated with the Stokes' settling equation

$$u_{S,Stoke} = \frac{(\rho_s - \rho_L)gd_p^2}{18\mu} \quad (22.56)$$

where ρ_s and ρ_L are densities of particle and liquid, respectively, g is the gravity acceleration, d_p is the particle diameter, and μ is the liquid viscosity. In a real suspension with a large range of particle size distribution, a cut particle size would be used for Equation 22.56. With known settling velocity u_s , Equation (22.55) can be used to design a clarifier to retain certain sized particles.

Stokes' equation is derived based on a spherical particle settling in an infinite liquid without the interference of other particles. Equation (22.56) becomes less accurate when the solid concentration increases. For suspensions with higher solid concentrations (approximately >1 wt%), the solid particles tend to settle together due to particle–particle interactions. It is called zone settling. For this type of settling, Stokes' law no longer applies and the settling rates are no longer dependent on the particle size but more dependent on the solid concentrations. Although there are correlations to calculate the zone settling velocity, it is better to run a settling test to obtain the settling velocity.

Almost all the design methods for continuous gravity thickener in the zone settling region are based on the following equation (Coe and Clevenger 1916):

$$G_T = \frac{u_s}{\frac{1}{C} - \frac{1}{C_u}} \quad (22.57)$$

where G_T is the total solid flux in the thickener, C and C_u are the solid concentration in the thickener and in the underflow, and u_s is the zone settling velocity corresponding to C that can be obtained by a batch settling test as shown in Figure 22.51. With known $u_s \sim C$ values, solid flux G_T as a function of C at a desired C_u can be calculated based on Equation (22.57), and is shown in Figure 22.52. The smallest G_T at point A represents the bottleneck for solid flux in the thickener. The area (A) of the thickener is designed based on this limiting flux ($G_{T,min}$):

$$A = \frac{Q_{feed} \cdot C_{feed}}{G_{T,min}} \quad (22.58)$$

For even higher solid concentrations where the particles are in contact with each other, “free settling” phenomena is replaced by “compression” or “consolidation.” The Coe and Clevenger–type design methods are not sufficient. Sediment height and consolidation effect need to be included in the thickener design (Tiller and Tarnig 1995).

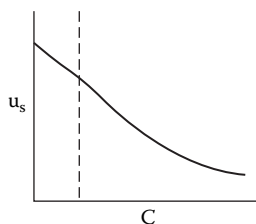


FIGURE 22.51 Settling test for thickener.

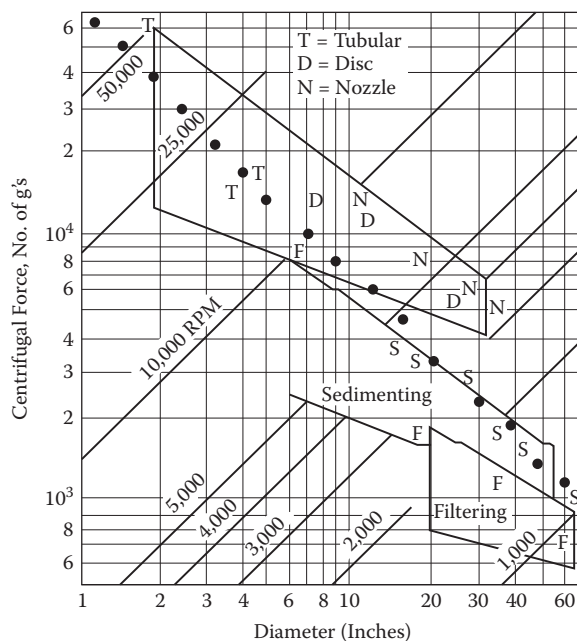


FIGURE 22.54 Classification of centrifuges.

In general, sedimenting centrifuges have smaller diameters and operate at higher speeds in comparison with filtering centrifuges. As a rough guide, centrifuges are designed to operate below the heavy dotted lines in Figure 22.54. The precise location of the dotted line depends up the elasticity and strength of the materials of construction.

In Figure 22.54, centrifuges are classified according to bowl diameter and the number of g -forces, which is defined by $r_b \Omega^2 / g$, where r_b is the bowl radius. For a dilute suspension with particles in the free-settling region, the higher acceleration for small diameter units leads to improved rates of sedimentation. Tubular and disc types are used primarily for clarification where the throughput rate of solids is small. Solid bowl decanters can be used for processing large solid flow rates.

Compaction forces developed in filtering centrifuges differ markedly from those encountered in sedimenting centrifuges. In sedimenting centrifuges, the solids flow radially toward the bowl and displace liquid, which must then flow radially inward and resulting drag on the particle delays sedimentation and compaction. In a filtering centrifuge, liquid and solids flow in the same direction. Frictional drag due to the liquid flow through the cake adds to the centrifugal body force. The relative magnitudes of the centrifugal and drag induced stresses are important to understanding operating conditions necessary to produce the desired compaction (Tiller and Hsyung 1993).

22.5.8 HYDROCYCLONE

The hydrocyclone also utilizes the centrifugal forces to separate solid particles. With centrifuges, the equipment is rotating, but hydrocyclones are stationary and the centrifugal force is generated by the rotating of the liquid. A hydrocyclone is normally composed of a cylindrical and a conical part (Figure 22.55). The feed slurry is tangentially fed into the cylindrical section, the clear liquid (overflow) comes out of the top of the cylindrical section (called the vortex finder), and the stream with more solids is discharged from the conical end (underflow).

The construction of hydrocyclones is very simple and therefore very economical compared to all the other solid/liquid separation equipment. However, low efficiencies in separation is the major disadvantage.

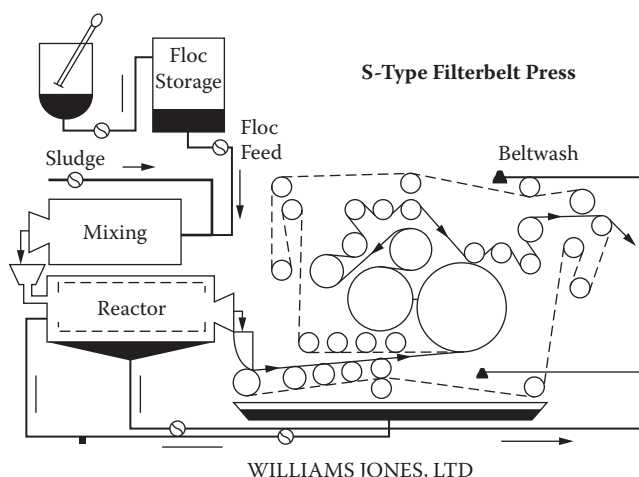


FIGURE 22.56 Deliquoring of flocculated, fragile cakes.

moving belts. A belt filter press is a common type of equipment used for deliquoring activated sludge at many wastewater treatment plants.

A laboratory instrument called a crown press is the best bench device to simulate belt filter press performance.

There are also compression filters which are operated at high pressures. These units are operated in batch mode. The filter press discussed earlier can be equipped with a diaphragm to squeeze the cake after filtration. They are commonly called membrane presses although they have nothing to do with the microfiltration membranes. One variation of the membrane press is the horizontal diaphragm press which also has a diaphragm to compress the cake, but the filter surface is horizontal instead of vertical as in membrane presses. For very high pressure expression, tubular presses can provide squeezing pressures as high as 2000 psi.

22.6 CAKE WASHING

22.6.1 DISPLACED WASHING AND REPULPING

Cake washing can be classified by (1) displacement washing: using clear liquid to displace mother liquor in the cake; and (2) repulping: diluting with liquid, and filtering again. Initial liquid leaving the cake in displacement washing as shown in Figure 22.57 has a concentration equal to that of the mother liquor. When approximately half (a large variation in this value can be encountered with non-Newtonian liquids, nonuniform cakes, or where there is cake cracking) of the original liquid has been displaced, fresh wash breaks through, and the exit concentration begins to drop rapidly. Displacement becomes inefficient, and solute removal is controlled by diffusion from relatively stagnant areas. Where high degrees of solute removal are essential, it may be useful to follow displacement washing by reslurrying and replacing the displacement process. Only displaced washing will be discussed in this section.

22.6.2 TERMS AND DEFINITIONS FOR DISPLACEMENT WASHING

Wash ratio j : a ratio equaling the total volume of wash liquid exiting a cake to the volume of void of the cake.

Mother liquid concentration, C_o : concentration of liquid remaining in the cake before washing.

in the cake, and it diffuses in accord with concentration gradients established in the interstices of the particulate bed. The average value of all of the accumulated wash C_{wav} divided by C_o lies above the instantaneous curve. The average value of solute in the liquid in the cake C_{av} is also shown in Figure 22.58.

The washing curves can be obtained by experimental data of C_w as the function of time, and instantaneous volume of washing liquid with time. Interpretation of experimental data must be approached with caution. At the beginning of the washing cycle, the conduits leading from the filter unit will be full of filtrate. Any curves that are drawn to show the percentage of solute remaining in the cake must take into account the solute in the body of the filter as well as solute in the cake.

22.7 LABORATORY SLS TEST

22.7.1 LABORATORY SLS TEST

Separations can be classified as dealing with homogeneous or heterogeneous systems, e.g., fluid/particle systems. Homogeneous separations such as distillation, absorption, and extraction represent mature technologies where the fundamentals have been translated into well-developed design procedures with competing software programs being widely available. On the other hand, heterogeneous separations or fluid/particle separations involve more complex, less-well-understood phenomena. Parameters such as settling velocity in sedimentation and porosity and permeability of filter beds in filtration are very much depended on experimental results. Laboratory testing necessarily plays an important role in control and design of fluid/particle separation systems.

Objectives of laboratory SLS tests include

- Cake filtration characteristics such as porosity, permeability, specific resistance, and cake compactibility parameters n , β , δ , $\alpha_o \epsilon_{so}$, or p_a in Equation (22.29)
- Selection of filter media
- Selection of filter aids
- Selection of coagulations and flocculants
- Cake washing efficiency
- Settling velocity for thickener design and scale-up

Parameters involved in SLS tests fall into the following criteria:

- Particle characteristics: Particle size distribution, mean particle size, particle shape, density, chemical content, etc.
- Slurry characteristics: Concentration, pH, conductivity, zeta potential, particle settling velocity, rheology characteristics, etc.
- Sedimentation characteristics: Variation of interface of slurry and clear liquid against time, zone-settling region and compaction region, settling velocity
- Filtration characteristics: Volume of filtrate versus time, filtrate rate, volume of filter cake, cake porosity, clarity of filtrate, clogging of filter media, effect of slurry concentration on filtrate rate and filtrate clarity, effect of slurry viscosity on filtrate rate and media clogging, etc.

Major methods for obtaining test data in SLS can be classified as follows:

1. Flow under gravitational head
 - a. Filtration with falling head
 - b. Filtration with constant head

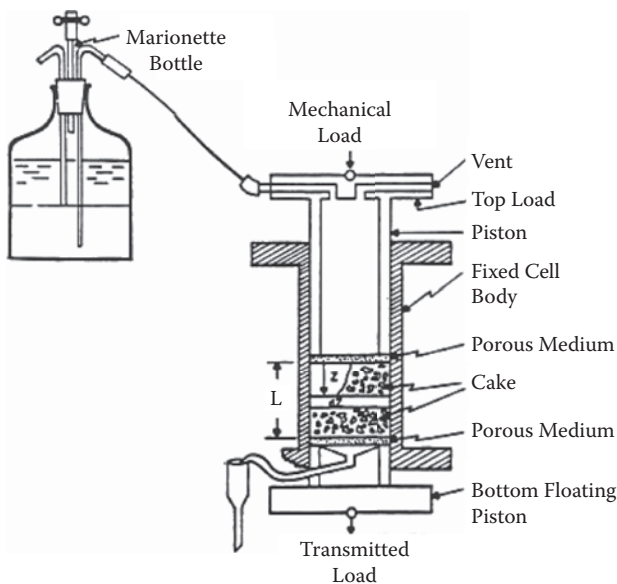
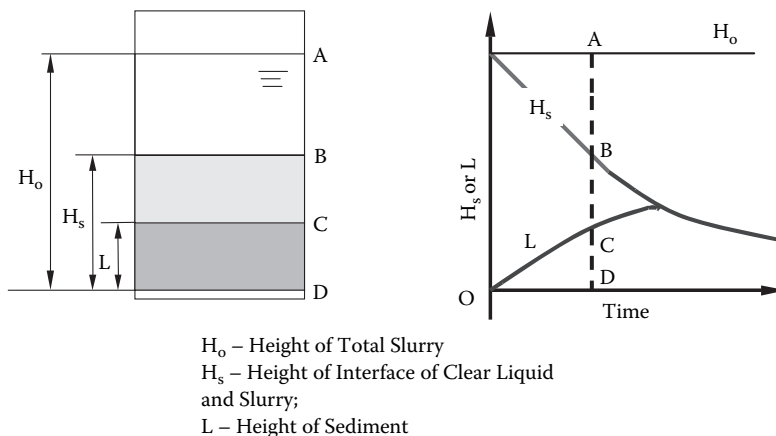


FIGURE 22.61 Compression permeability cell.

3. Constant rate filtration
4. Variable pressure and variable rate filtration
5. Compression-permeability cell (Figure 22.61)
6. Capillary suction time apparatus (Figure 22.62)
7. Batch sedimentation test
8. Flocculation and coagulation jar test (Figure 22.7)
9. Lab scale belt press (crown press)
10. Lab scale filtering or sedimenting centrifuges.

Constant pressure filtration under vacuum or in a small bomb powered by gas pressure has been the favorite method for obtaining filtration data. Constant rate filtration offers the advantage of providing data for different pressures in one run. It simulates the industrial filter operation where



(a) Batch Sedimentation Cylinders

(b) Batch Sedimentation Results

FIGURE 22.62 Capillary suction time apparatus.

pressures be utilized. Ideally, a very low pressure in the neighborhood of 300 mm of water (0.5 psi) should be used. Capillary suction apparatus employing Whatman #17 has a suction pressure of approximately 14.85 kPa (2.15 psi). Determination of compactibility necessitates the use of gravity, vacuum, or pressure. Due to the limited data obtained, errors from wall friction, or sedimentation during tests, most compressibility coefficients reported in the literature are of questionable quality.

22.8 SLS SYSTEM DESIGN

For a particulate application involving SLS, how to choose the best equipment, to use batch or continuous operation, which filter medium to select, and what is the optimum operating conditions are concerns of engineers. Although theories are available for some SLS operations, solutions for equipment selection, process design, and optimization are still very much dependent on test and experience, and are frequently qualitative or semi-qualitative. In this section, strategy and decision networks for selection of SLS equipment, introduction of filter media, centrifugal pumps for filtration operation, and selection of filter aids by cycle analysis will be discussed.

22.8.1 SELECTION OF SLS EQUIPMENT

22.8.1.1 Specifications of a SLS System

In approaching the initial selection of equipment, questions include what are the product (liquid or solid), the feed and production rates of the system, the required filtrate clarity, and the liquid and solute contents in the cake. The product may be solids, liquid, or both. For example, in the liquefied coal manufacturing process, the dissolved carbon in the liquid represents the main product. At the same time, minerals in the original coal end up as cake along with unconverted carbon, which is also a valuable component and can be used for the production of hydrogen. As far as the SLS operation is concerned, both cake solids and filtrate are of value in liquefied coal processes.

Purchas (1977) provided a conceptual model for initial specifications of a SLS system as illustrated in Figure 22.63.

22.8.1.2 Selection of Equipment and Process

The selection depends to a great extent on the rate of growth of the cake. This rate has a major effect on the following choices: batch versus continuous process; pressure or vacuum; gravity filters; and separation technique (filters, centrifuges, etc.). Table 22.8 (features of slurry), Table 22.9 (selection of filters), and Table 22.10 (comparison of separation processes) aid in this effort.

The basic strategy for equipment selection relating to cake buildup rate in Table 22.8 can be summarized as follows:

1. Continuous filtration is suitable for material of rapid cake buildup.
2. Medium-speed filtering materials are suited to vacuum equipment and filtering centrifuges like peeler or vertical basket centrifuges.
3. Slow filtering materials require pressure equipment or sedimenting centrifuges.
4. Dilute materials that result in high-resistance cakes are generally best handled in batch pressure filters and filter aids can be considered. If the solid concentration is less than 100 ppm, deep-bed filters become options.
5. Rapid settling slurries lend themselves to gravity separation or filtering centrifuges with wedge wire screen (like pusher or screen bowl centrifuges).

Flood, Porter, and Rennie (1977) developed Table 22.9 as an expanded version 5 to Table 22.8.

TABLE 22.10
Comparison of SLS Equipment Performance

	Solid Dryness	Liquid Clarity	Thickening	Washing	Classification	Particle Breakage
Strainers						
Screen strainers		G			G	G
Bag filters	F		—		—	G
Cartridge filters	F		—		—	G
Screens	F	F-P	G	G		G
Membrane filters					—	G
Deep-Bed Filters						
Granular (batch)			F	—	—	—
Granular (continuous)			F			—
Cake Filters						
Gravity filters	F	G		G	—	
Batch, semi-batch vacuum filters	G	G			—	
Continuous vacuum filters	G	G		F	—	
Batch, semi-batch pressure filters					—	G
Continuous pressure filters				F	—	G
Compression filters		F	—	F	—	
Filtering centrifuges	G				—	F-P
Precoat filters	—		—	—	—	—
Settlers						
Gravity, clarifier			G	—	—	
Gravity, thickener		G			—	
Tubular centrifuge			—	—	—	F
Disc centrifuge, solid bowl			—	—	—	G
Disc centrifuge, desludger					—	F
Disc centrifuge, nozzle		G	G	F		F
Solid bowl centrifuge	F-G	E-G				
Hydrocyclones			G	F		

Note: E, excellent; G, good; F, fair; P, poor; —, should not be considered.

Source: From Chen (2002).

22.8.1.3 Comparison of SLS Equipment

Fitch (1974) discussed the general problem of matching process specifications to SLS equipment and the necessity of considering trade-offs involving such items as filtrate clarity, cake dryness, reliability, maintenance, versatility, and cost. In Table 22.10, a comparative profile of all major types of SLS equipment is given. It should be emphasized that a wide range of performance occurs because of the endless variation in slurries, and the descriptive terms would undoubtedly vary some if another author were to prepare the same table.

22.8.2 DECISION NETWORK FOR DESIGN FOR CAKE FILTRATION SYSTEMS

A series of decisions must be made concerning the following factors in designing new or improving existing cake filtration systems:

TABLE 22.11
Classification of Filter Media

Type	Construction	Example
Flexible media	Woven fabric or woven wire	Including the wide variety of metallic, natural, and synthetic fabrics
	Nonwoven preformed	Including felt, melt blown, and similar materials
	Nonwoven, non-preformed	Cellulose pulp, asbestos
	Membranes	Organic or inorganic
Rigid media	Fixed	Including sintered metal, porous carbon, porous ceramic, formed plastics
	Loose	In packed beds of sand, carbon, and other loose materials

ical and hydraulic compression. A highly compactible material has very little reduction in porosity except in a layer close to the medium. There is little frictional drag in the first part of the cake, which results in a lack of consolidation except in the skin close to the medium. Comparatively, mechanical pressure directly applied on the cake can be quite effective. However, as the porosity decreases, cake permeability also decreases; and the rate of expression may drop substantially.

22.8.3 SELECTION OF FILTER MEDIA

22.8.3.1 Introduction

The filter medium is the part of a filter that retains the solids while allowing passage of the fluid through its pore structure. It is one of the essential components of the filtration process, and is sometimes called "heart of filter." In practical operations, the suspension is normally composed of particles with a wide range of particle sizes and shapes, therefore, there are several mechanisms for particle capture.

Appropriate selection of filter media is one of the most important factors to ensure efficient performance of filtration equipment. The filtration performance requirements are application specific and may include (Cheremisinoff et al. 1983):

- Retention of particles
- Sufficient flow rate
- Easy cake release
- Gasket action
- Chemical and biological stability
- Abrasion resistance
- Dimensional stability with respect to stretching and shrinking
- Strength
- Fray or unraveling stability
- Washability for reuse or low price for disposability

According to materials and construction, filter media can be grouped as flexible and rigid media. The flexible media include woven (fabric or wire), nonwoven preformed, and nonwoven nonpreformed filter media. The rigid media can be classified as fixed or loose media as shown in Table 22.11. Among the various types of filter media, the woven flexible media is most commonly used for cake filters.

TABLE 22.13
Performance of Woven Fabrics by Different Weave Patterns in Descending Order

Maximum Filtrate Clarity	Minimum Resistance to Flow	Minimum Moisture in Cake	Easier Cake Discharge	Maximum Cloth Life	Least Tendency to Blind
Satin	Plain	Plain	Satin	Satin	Plain
Twill	PRD	PRD	Twill	Twill	PRD
PRD	Twill	Twill	Plain	PRD	Twill
Plain	Satin	Satin	PRD	Plain	Satin

Note: PRD, plain reverse Dutch weave.

Source: From Purchas (1967).

TABLE 22.14
Desired Physical and Filtration Performance of Filter Media for Different Filters

Filters	Requirements						
	Strength	Abrasion Resistance	Tensile Strength	Gasket Action	Stability to Stretching and Shrinking	Easy Cake Release	Washability
Plate and frame	✓	✓		✓		✓	✓
Rotary drum	✓	✓				✓	✓
Leaf filter					✓		✓
Disc	✓	✓			✓	✓	
Filtering centrifuges	✓	✓		✓			✓
Belt filters	✓		✓		✓	✓	✓
Belt press	✓		✓		✓	✓	✓

ments on physical and filtration performance of filter media for different filters are summarized in Table 22.14.

22.8.4 SELECTION OF PUMPS IN FILTRATION OPERATION

Pumps employed for slurries can be classified as (1) centrifugal, (2) progressive cavity or screw, (3) diaphragm, (4) piston pump, and (5) compressed gas either alone or combined with a pump. Pressure versus flow rate for various types of pumping mechanisms is illustrated in Figure 22.67. Arrows point in the direction of increasing time. Although constant pressure operation has dominated the literature and laboratory practice, generally diaphragm and single-screw rotary pumps are the best choices. Centrifugal pumps are widely employed in filtration in spite of their tendency to degrade aggregates because of large shear forces resulting from high-velocity impellers. Progressive cavity or screw pumps are capable of pumping high viscosity and high solid content slurries without particle breakup. The cost is high and maintenance may be a problem if the stator wears or seals leak. Piston pumps operate at constant rates that can be easily adjusted. There is a minimum breakup of particles. Abrasion can cause wear if particles invade the clearance between piston and cylinder. Severe pulsation is possible unless adequate damping devices are incorporated in the piping. Diaphragm pumps have some of the characteristics of piston pumps. However, with air driven pumps, the rate drops as pressure builds up. Progressive cavity, piston, and diaphragm pumps are also called positive displacement pumps. Gas driven filtration is only applicable in a

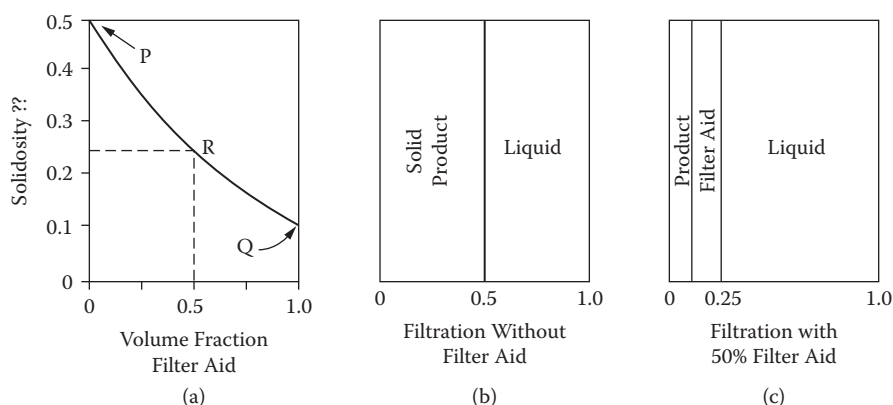


FIGURE 22.68

product solids corresponding with point *R* in Figure 22.68a. With the increase of the filter aid, the cake has 75% liquid, 25% solids, and the amount of product is reduced to one fourth of the quantity present in Figure 22.68b. As the active solid component in the filter has been reduced to 25% of the original amount in Figure 22.68b, four cycles will be necessary to yield the same quantity of active solids. It can easily be shown that after the addition of filter aids, overall cycle rates will be reduced and more cycles are required to produce the same amount of solids.

An example involving the addition of a perlite filter aid to a clay suspension with a volumetric concentration of $\phi_s = 0.058$ will be discussed. Constant rate filtration (Camacho 1975) with different fractions of perlite was used to obtain cake resistance α_{av} and cake solidosity ϵ_{sav} as functions of Δp_c . The specific problem to be analyzed is a constant pressure filtration at 200 kPa (29 psi) of this clay suspension. For constant pressure and constant rate filtration with minimal medium resistance, maximum cycle flux is reached when the filtration time equals the time required to dump the cake, clean the filter, and start the next cycle (Rushton et al. 1996). In this example, it is assumed that the dead time between cycles is 15 minutes. With t (filtration) = 15 minutes, a cake thickness of $L = 0.014$ m results when the cycle rate is maximized for this highly resistant, moderately compactible clay.

Calculations involved in the analysis include (1) concentration of slurry after addition of perlite ϕ_{sF} ; (2) time required to produce a cake of 0.014 m t ; (3) number of cycles with filter aid addition f (volume fraction of filter aids in the total cake solids) to get the same amount of product solids without filter aid addition when $f = 0$; (4) volume/unit area of filtrate produced in 15 min; (5) the cycle rate based on liquid; and (6) cycle rate based on product clay solids. The calculated results are shown in Table 22.15.

TABLE 22.15
Cycle Rate Calculation Involving Filter Aids

1	2	3	4	5	6	7	8	9
f	$\alpha_{av}(\text{m}^{-2})$	ϵ_{sav}	ϕ_{sF}	t , sec for $L = 0.014$ m	v , m^3/m^2 $t = 15$ min	Number of Cycles	Cycle Rates ($\text{m}^3\text{m}^2/\text{hr}$) Liquid	Solid
0	2.21E(15)	0.47	0.058	3615	0.0496	1	0.0496	0.00328
0.1	2.22E(15)	0.45	0.064	2951	0.0466	1.04	0.0464	0.00312
0.2	7.27E(13)	0.33	0.071	43	0.233	1.42	0.0501	0.00365
0.333	4.09E(13)	0.26	0.085	11	0.265	1.81	0.029	0.00242
0.667	2.32E(13)	0.18	0.156	0.314	0.115	2.61	0.0021	0.00084

can be found in the treatment of separation operations by these authors. An excellent discussion of equipment is provided by Purchas (1981).

TABLE/FIGURE SOURCE LINES

FIGURE 22.5(A) Thomas Riddick, Control of Colloid Stability through Zeta Potential, Zeta Meter Inc, 1968.

FIGURE 22.6 Thomas Riddick, Control of Colloid Stability through Zeta Potential, Zeta Meter Inc, 1968.

TABLE 22.3 Thomas Riddick, Control of Colloid Stability through Zeta Potential, Zeta Meter Inc, 1968.

FIGURE 22.9 Frank M. Tiller et al., "Minimizing Total Cost Involving Use of Polyelectrolytes with Wastewater Centrifugation," *Advances in Filtration and Separation Technology*, vol. 16, American Filtration & Separations Society, 2002.

FIGURE 22.10 Frank M. Tiller et al., "Minimizing Total Cost Involving Use of Polyelectrolytes with Wastewater Centrifugation," *Advances in Filtration and Separation Technology*, vol. 16, American Filtration & Separations Society, 2002.

FIGURE 22.11 Frank M. Tiller et al., "Minimizing Total Cost Involving Use of Polyelectrolytes with Wastewater Centrifugation," *Advances in Filtration and Separation Technology*, vol. 16, American Filtration & Separations Society, 2002.

FIGURE 22.19 Frank M. Tiller, "Tutorial: Interpretation of Filtration Data, I," *Fluid/Particle Separation Journal*, vol. 3, no. 2, American Filtration & Separations Society, p. 91, 1990.

FIGURE 22.21 Frank M. Tiller, et al., "Filtering Coal Liquids: Clogging Phenomena in the Filtration of Liquefied Coal," *Chemical Engineering Progress*, December 1981, *AIChE*, p. 65, Figure 10, 1981.

FIGURE 22.24 Frank M. Tiller, "Filtering Coal Liquids: Clogging Phenomena in the Filtration of Liquefied Coal", *Chemical Engineering Progress*, December 1981, *AIChE*, Page 66, Figure 12, 1981

FIGURE 22.25 Frank M. Tiller, et al. Role of Porosity in Filtration: XIII. Behavior of Highly Compactible Cakes," *AIChE Journal*, vol. 44, *AIChE*, p. 2159, vol. 44, 1999.

FIGURE 22.26 Frank M. Tiller, et al. Role of Porosity in Filtration: XIII. Behavior of Highly Compactible Cakes", *AIChE Journal*, vol. 44, *AIChE*, p. 2159, vol. 44, 1999.

FIGURE 22.27 Frank M. Tiller, et al. Role of Porosity in Filtration: XIII. Behavior of Highly Compactible Cakes," *AIChE Journal*, vVol.44, *AIChE*, p. 2159, vol. 44, 1999.

TABLE 22.5 Source: Frank M. Tiller, et al, "Explaining Strange Behavior of Highly Compactible Materials," *Chemical Processing*, Sep. 2000, *AIChE*, September, 2000.

TABLE 22.6 Frank M. Tiller, Wenping Li, "Determination of the Critical Pressure Drop for Filtration of Super-Compactible Cakes," *Water Science and Technology*, Vol. 44, No. 10, 2001, IWA, Table 3, Figure 3, Figure 4, no. 10, 2001.

FIGURE 22.28 Frank M. Tiller, Wenping Li, "Determination of the Critical Pressure Drop for Filtration of Super-Compactible Cakes," *Water Science and Technology*, vol. 44, No. 10, 2001, IWA, Table 3, Figure 3, Figure 4, No. 10, 2001.

FIGURE 22.29 Frank M. Tiller, Wenping Li, "Determination of the Critical Pressure Drop for Filtration of Super-Compactible Cakes", *Water Science and Technology*, vol. 44, no. 10, 2001, IWA, Table 3, Figure 3, Figure 4, no. 10, 2001.

FIGURE 22.35 Frank M. Tiller, et al., "The Role of Porosity in Filtration Part X: Deposition of Compressible Cakes on External Radial Surfaces," *AIChE Journal*, vol. 31, no. 8, *AIChE*, p. 1242, Figure 1, August 1985.

FIGURE 22.38 Frank M. Tiller, et al., "Hydraulic Deliquoring of Compressible Filter Cakes, Part I: Reverse Flow in Filter Presses," *AIChE Journal*, vol. 29, no. 2, *AIChE*, p. 298 Figure 1, Figure 2; p. 299, Figure 3, March 1983.

FIGURE 22.39 Frank M. Tiller, et al., "Hydraulic Deliquoring of Compressible Filter Cakes, Part I: Reverse Flow in Filter Presses," *AIChE Journal*, vol. 29, no. 2, *AIChE*, p. 298 Figure 1, Figure 2; p. 299, Figure 3, March 1983.

FIGURE 22.40 Frank M. Tiller, et al., "Hydraulic Deliquoring of Compressible Filter Cakes, Part I: Reverse Flow in Filter Presses," *AIChE Journal*, vol. 29, no. 2, *AIChE*, p. 298 Figure 1, Figure 2; p. 299, Figure 3, March 1983.

FIGURE 22.41 Frank M. Tiller, et al., "Hydraulic Deliquoring of Compressible Filter Cakes, Part I: Reverse Flow in Filter Presses," *AIChE Journal*, vol. 29, no. 2, *AIChE*, p. 298 Figure 1, Figure 2; p. 299, Figure 3, March 1983.

- Purchas, D.B. 1967. *Industrial filtration of liquids*. Cleveland, OH: CRC Press.
- Purchas, D.B. 1977. *Solid/liquid separation equipment scale-up*. Croydon, UK: Uplands Press Ltd.
- Purchas, D.B. 1981. *Solid/liquid separation technology*. Croydon, UK: Uplands Press Ltd.
- Riddick, Thomas M. 1968. *Control of colloid stability through zeta potential*. New York: Zeta Meter Inc.
- Risbud, ... 1974. Mechanical expression, stresses at cake boundaries and new compression-permeability cell. PhD diss., University of Houston, Texas.
- Rushton, A., A.S. Ward, and R.G. Holditch. 1996. *Solid-liquid filtration and separation technology*. New York: VCH Publishers, 411.
- Svarovsky, Ladislav. 1990. *Solid-liquid separation*. 3rd ed. London, Boston: Butterworth & Co., 29–30.
- Tiller, F.M. 1978. Characteristics of staged, delayed-cake filters. *Filtration and Separation* May/June: XXX.
- Tiller, F.M. 1974. Continuous processes for cake filtration. *Chemical Engineering* April: 29.
- Tiller, F.M., and T.M. Garrett. 1997. Developing methodology for improving dewatering characteristics of wastewater sludge with emphasis on optimal use of polyelectrolytes to minimize costs. Report to Greater Houston Wastewater Program, University of Houston, Texas.
- Tiller, F.M., S. Haynes, and W.M. Lu. 1972. The role of porosity in filtration vii: effect of side-wall friction in compression-permeability cells. *AIChE Journal* 18: 13–19.
- Tiller, F.M., and L.L. Horng. 1983. Hydraulic deliquoring of compressible filter cakes, part I: reverse flow in filter presses. *AIChE Journal* 29: 297–305.
- Tiller, F.M., and N.B. Hsyung. 1993. Unifying the theory of thickening, filtration, and centrifugation. *Water Science Technology* 28: 1.
- Tiller, F.M., N.B. Hsyung, and D.Z. Cong. 1995. Role of porosity in filtration: II. Filtration with sedimentation. *AIChE Journal* 41: 1153.
- Tiller, F.M., and J.H. Kwon. 1999. Role of porosity in filtration: XIII. Behavior of highly compactible cakes. *AIChE Journal* 44: 2159.
- Tiller, F.M., and W.F. Leu. 1980. Basic data fitting in filtration. *Journal of the Chinese Institute of Chemical Engineers*. 11: 61.
- Tiller, F.M., and W. Leu. 1984. Solid-liquid separation for liquefied coal industries. Final Report for Project 1411–1, July.
- Tiller, F.M., and P.J. Lloyd. 1978. *Theory and practice of solid/liquid separation*. Houston, TX: University of Houston.
- Tiller, F.M., and D. Tarng. 1995. Try deep thickeners and clarifiers *Chemical Engineering Progress* March: 75–80.
- Tiller, F.M., and Wenping Li. 1999. Comparing % cake solids in filtration, thickening, sedimenting centrifugation and expression. *Fluid/Particle Separation Journal* 12: 173.
- Tiller, F.M., and Wenping Li. 2000. Explaining strange behavior of highly compactible materials. *Chemical Processing* September.
- Tiller, F.M., and Wenping Li. 2001. Optimizing candle filters for super-compactible materials. *Advances in Filtration and Separation Technology* 15.
- Tiller, F.M., and Wenping Li. 2001. Cost minimization study of a full scale urban wastewater treatment plant. Proceedings of the 6th European Biosolids and Organic Residuals Conference; West Yorkshire, UK; November, 11–14.
- Tiller, F.M., and Wenping Li. 2002. Minimizing total cost involving use of polyelectrolytes with wastewater centrifugation. *Advances in Filtration and Separation Technology* 16.
- Tiller, F.M., and Wenping Li. 2003. Dangers of lab-plant scaleup for solid/liquid separation systems. *Chemical Engineering Communications*.

23.1 INTRODUCTION

The solid/liquid separation operation of drying converts a solid, semi-solid, or liquid feedstock into a solid product by evaporation of the liquid via application of heat. In the special case of freeze drying, which takes place below the triple point of the liquid being removed, drying occurs by sublimation of the solid phase directly into the vapor phase. This definition thus excludes conversion of a liquid phase into a concentrated liquid phase (evaporation); mechanical dewatering operations such as filtration, centrifugation, sedimentation, etc.; supercritical extraction of water from gels to produce extremely high porosity aerogels (extraction); or so-called drying of liquids and gases by use of molecular sieves (adsorption), etc. Phase change and production of a solid phase as an end product are essential features of the drying process. Drying is an essential operation in the chemical, agricultural, biotechnology, food, polymer, ceramics, pharmaceutical, pulp and paper, mineral processing, and wood processing industries.

Drying is perhaps the oldest, most common, and most diverse of chemical engineering unit operations. Over 500 types of dryers have been reported in the literature, while over 100 distinct types are commonly available. It competes with distillation as the most energy-intensive unit operation due to the high latent heat of vaporization and the inherent inefficiency of using hot air as the (most common) drying medium. Various studies report national energy consumption for industrial thermal drying operations ranging from 10% to 15% for the United States, Canada, France, the U.K., etc., to 20% to 25% for Denmark and Germany. The latter figures have been obtained recently based on mandatory energy audit data supplied by industry and hence are more reliable.

Energy consumption in drying ranges from a low value of under 5% for the chemical manufacturing industries to 35% for papermaking operations. Capital expenditures for dryers are estimated to be in the order of only \$800 million per annum for the United States. Thus, the major costs for dryers are in their operation rather than in their initial investment costs.

Drying of various feedstocks is needed for one or several of the following reasons: need for easy-to-handle free-flowing solids, preservation and storage, reduction in cost of transportation, achieving desired quality of product, etc. In many processes, improper drying may lead to irreversible damage to product quality and hence a nonsalable product.

Unique features of drying make it fascinating and challenging:

- Product size may range from microns to tens of centimeters (in thickness or depth)
- Product porosity may range from zero to 99.9%
- Drying times range from 0.25 sec (drying of tissue paper) to 5 months (for certain hardwood species)
- Production capacities may range from 0.10 kg/hr to 100 t/hr
- Product speeds range from zero (stationary) to 2000 m/sec (tissue paper)
- Drying temperatures range from below the triple point to above the critical point of the liquid
- Operating pressure may range from a fraction of a millibar to 25 atmospheres
- Heat may be transferred continuously or intermittently by convection, conduction, radiation, or electromagnetic fields

Clearly, no single design procedure applies to all or even several of the dryer variants. It is therefore essential to revert to the fundamentals of heat, mass, and momentum transfer coupled with knowledge of the material properties (quality) when attempting a design of a dryer or analysis of an existing dryer. Mathematically speaking, all processes involved, even in the simplest dryer, are highly nonlinear and hence scale-up of dryers is generally very difficult. Experimentation at laboratory and pilot scales coupled with field experience and know-how is essential to the development of a new dryer application. Dryer vendors are necessarily specialized and normally offer only a narrow range of drying equipment. The buyer must therefore be reasonably conversant with

TABLE 23.1
Thermodynamic and Transport Properties of Air-Water System

Property	Expression
P_v	$P_v = 100 \exp[27.0214 - (6887/T_{abs}) - 5.32 \ln(T_{abs}/273.16)]$
Y	$Y = 0.622RHP_v/(RHP_v)$
c_{pg}	$c_{pg} = 100926 \times 10^3 - 4.0403 \times 10^{-2} + 6.1759 \times 10^{-4}T^2 - 4.097 \times 10^{-7}T^3$
k_g	$k_g = 2.425 \times 10^{-2} - 7.889 \times 10^{-5}T - 1.790 \times 10^{-8}T^2 - 8.570 \times 10^{-12}T^3$
ρ_g	$\rho_g = PM_g/(RT_{abs})$
μ_g	$\mu_g = 1.691 \times 10^{-5} + 4.984 \times 10^{-8}T - 3.187 \times 10^{-11}T^2 + 1.319 \times 10^{-14}T^3$
c_{pv}	$c_{pv} = 1.883 - 1.6737 \times 10^{-4}T + 8.4386 \times 10^{-7}T^2 - 2.6966 \times 10^{-10}T^3$
c_{pw}	$c_{pw} = 2.8223 + 1.1828 \times 10^{-2}T - 3.5043 \times 10^{-5}T^2 + 30601 \times 10^{-8}T^3$

Source: Mujumdar (1995b) and Pakowski et al. (1991).

properties of humid air. Table 23.1 summarizes the essential thermodynamic and transport properties of the air-water system. In Table 23.2, a listing of brief definitions of various terms encountered in drying and psychrometry is given. It also includes several terms not explicitly discussed in the text.

Figure 23.1 is a psychrometric chart for the air-water system. It shows the relationship between the temperature (abscissa) and absolute humidity (ordinate, in g water per kg dry air) of humid air from 0°C to 130°C at one atmosphere absolute pressure. Lines representing percent humidity and adiabatic saturation are drawn according to the thermodynamic definitions of these terms. Equations for the adiabatic saturation and wet-bulb temperature lines on the chart are as follows (Geankoplis 1983):

$$\frac{Y - Y_{as}}{T - T_{as}} = -\frac{c_s}{\lambda_{as}} = -\frac{1.005 + 1.88Y}{\lambda_{as}} \quad (23.1)$$

and

$$\frac{Y - Y_{wb}}{T - T_{wb}} = -\frac{h / M_{air} k_y}{\lambda_{wb}} \quad (23.2)$$

The ratio $(h/M_{air}k_y)$, termed the psychrometric ratio, lies between 0.96 and 1.005 for air-water vapor mixtures; thus it is nearly equal to the value of humid heat c_s . If the effect of humidity is neglected, the adiabatic saturation and wet-bulb temperatures (T_{as} and T_{wb} , respectively) are almost equal for the air-water system. Note, however, that T_{as} and T_w are conceptually quite different. The adiabatic saturation temperature is a gas temperature and a thermodynamic entity while the wet-bulb temperature is a heat and mass transfer rate-based entity and refers to the temperature of the liquid phase. Under constant drying conditions, the surface of the drying material attains the wet-bulb temperature if the heat transfer is by pure convection. The wet-bulb temperature is independent of surface geometry as a result of the analogy between heat and mass transfer.

Most handbooks of engineering provide more detailed psychrometric charts including additional information and extended temperature ranges. Mujumdar (1995aORb) includes numerous psychrometric charts for several gas-organic vapor systems as well.

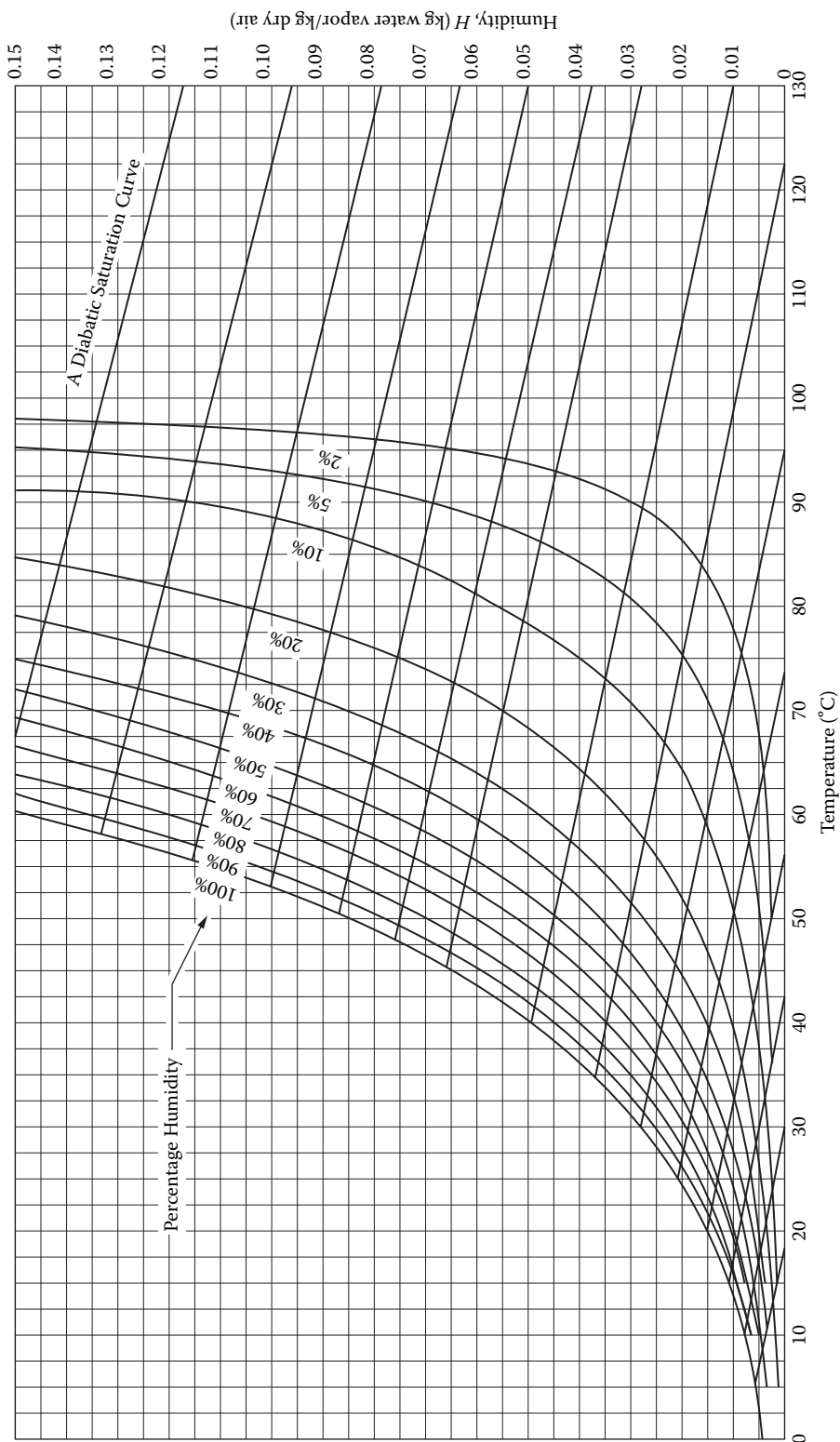


FIGURE 23.1 Humidity chart for mixtures of air and water (pressure of 101.325 kPa).

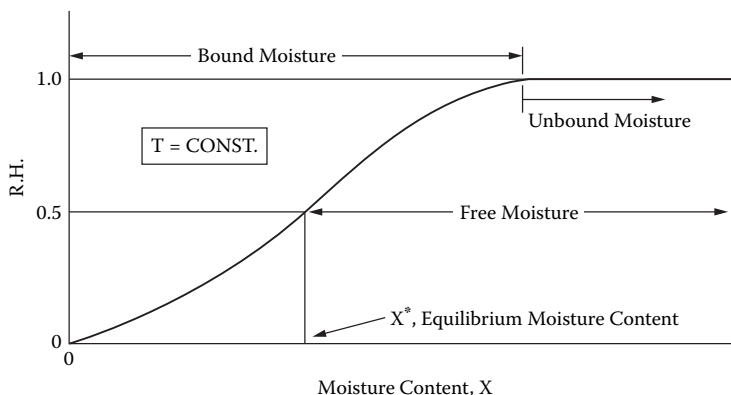


FIGURE 23.4 Various types of moisture.

For hygroscopic solids, the enthalpy of the attached moisture is less than that of pure liquid by an amount equal to this binding energy, which is also termed the enthalpy of wetting, ΔH_w (Keey 1978). It includes the heat of sorption, hydration, and solution and may be estimated from the following equation:

$$\left. \frac{d(\ln \psi)}{d(1/T)} \right|_{X=\text{constant}} = -\frac{\Delta H_w}{R_g T} \quad (23.4)$$

A plot of $\ln(\Psi)$ against $1/T$ is linear with a slope of $\Delta H_w/R_g$, where R_g is the universal gas constant ($R_g = 8.314 \times 10^3 \text{ kg kgmol}^{-1} \text{ K}^{-1}$). Note that the total heat required to evaporate bound water is the sum of the latent heat of vaporization and the heat of wetting; the latter is a function of the moisture content X . The heat of wetting is zero for unbound water and increases with decreasing X . Since ΔH_w is responsible for lowering the vapor pressure of bound water, at the same relative humidity, ΔH_w is almost the same for all materials (Keey 1978). For most materials, the moisture binding energy is positive; generally it is a monotonically decreasing function of the moisture content, with a value of zero for unbound moisture.

In general, water sorption data must be determined experimentally. Some 80 correlations, ranging from those based on theory to those that are purely empirical, have appeared in the literature. Two of the most extensive compilations are due to Wolf et al. (1985) and Iglesias and Chirife (1982). Aside from temperature, water sorption is also affected by the physical structure as well as the composition of the material. The pore structure and size, as well as the physical and/or chemical transformations during processing can cause significant variations in the moisture binding ability of the solid.

23.2.1.3 Water Activity

In drying of some materials, which requires careful hygienic attention, e.g., food, availability of water for growth of microorganisms, germination of spores, and participation in several types of chemical reactions becomes an important issue. This availability, which depends on relative pressure or water activity a_w , is defined as the ratio of the partial pressure p of water over the wet solid system to the equilibrium vapor pressure p_w of water at the same temperature. Thus, a_w , which is also equal to the relative humidity of the surrounding humid air, is defined as

$$a_w = \frac{p}{p_w} \quad (23.5)$$

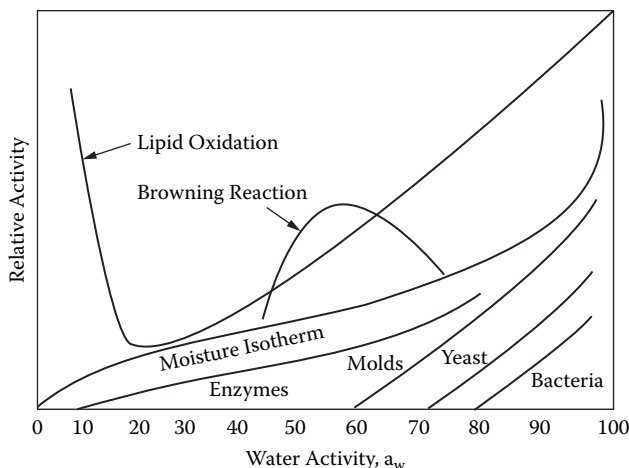


FIGURE 23.6 Deterioration rates as a function of water activity for food systems.

Figure 23.6 shows the general nature of the deterioration reaction rates as a function of a_w for food systems. Aside from microbial damage, which typically occurs for $a_w > 0.70$, oxidation, nonenzymatic browning (Maillard reactions), and enzymatic reactions can occur even at very low a_w levels during drying. Laboratory or pilot testing is essential to ascertain that no damage occurs in the selected drying process since this cannot in general be predicted.

23.2.2 DRYING KINETICS

Consider the drying of a wet solid under fixed drying conditions. In the most general cases, after an initial period of adjustment, the dry-basis moisture content X decreases linearly with time t following the start of the evaporation. This is followed by a nonlinear decrease in X with t until, after a very long time, the solid reaches its equilibrium moisture content X^* and drying stops. In terms of free moisture content, defined as

$$X_f = (X - X^*) \quad (23.6)$$

the drying rate drops to zero at $X_f = 0$.

By convention, the drying rate N is defined as

$$N = -\frac{M_s}{A} \frac{dX}{dt} \text{ or } -\frac{M_s}{A} \frac{dX_f}{dt} \quad (23.7)$$

under constant drying conditions. Here ($\text{kg m}^{-2} \text{ h}^{-1}$) is the rate of water evaporation, A is the evaporation area (may be different from heat transfer area), and M_s is the mass of bone dry solid. If A is not known, then the drying rate may be expressed in kg water evaporated per hour.

A plot of N versus X (or X_f) is the so-called drying rate curve. This curve must always be obtained under constant drying conditions. Note that, in actual dryers, the drying material is generally exposed to varying drying conditions (e.g., different relative gas-solid velocities, different gas temperatures and humidities, different flow orientations). Thus, it is necessary to develop a methodology in order to interpolate or extrapolate limited drying rate data over a range of operating conditions.

Figure 23.7 shows a typical “textbook” drying rate curve displaying an initial constant rate period, where $N = N_c = \text{constant}$. The constant rate period is governed fully by the rates of external

It is easy to see that N_c can be calculated quite easily using empirical or analytical techniques to estimate the external heat/mass transfer rates (Keey 1978; Geankoplis 1993). Thus,

$$N_c = \frac{\sum q}{\lambda_s} \quad (23.8)$$

where $\sum q$ represents the sum of heat fluxes due to convection, conduction, and/or radiation, and λ_s is the latent heat of vaporization at the solid temperature. In the case of purely convective drying, the drying surface is always saturated with water in the constant rate period and thus the liquid film attains the wet-bulb temperature. The wet-bulb temperature is independent of the geometry of the drying object due to the analogy between heat and mass transfer.

The drying rate in the falling rate period(s) is a function of X (or X_p) and must be determined experimentally for a given material being dried in a given type of dryer.

If the drying rate curve (N versus X) is known, the total drying time required to reduce the solid moisture content from X_1 to X_2 can be simply calculated by

$$t_d = - \int_{X_1}^{X_2} \frac{M_s}{A} \frac{dX}{N} \quad (23.9)$$

Table 23.5 lists expressions for the drying times for constant rate, linear falling rates, and a falling rate controlled by liquid diffusion of water in a thin slab. The subscripts c and f refer to the constant and falling rate periods, respectively. The total drying time is, of course, a sum of drying times in two succeeding periods. Different analytical expressions are obtained for the drying times t_p depending on the functional form of N or the model used to describe the falling rate, e.g., liquid diffusion, capillarity, evaporation-condensation. For some solids, a receding front model (wherein the evaporating surface recedes into the drying solid) yields a good agreement with experimental observations. The principal goal of all falling rate drying models is to allow reliable extrapolation of drying kinetic data over various operating conditions and product geometries.

The expression for t_f in Table 23.5 using the liquid diffusion model (Fick's second law of diffusion form applied to diffusion in solids with no real fundamental basis) is obtained by solving analytically the following partial differential equation:

$$\frac{\partial X_f}{\partial t} = D_L \frac{\partial^2 X_f}{\partial x^2} \quad (23.10)$$

subject to the following initial and boundary conditions:

$$X_f = X_i \text{ everywhere in the slab at } t = 0$$

$$X_f = 0, \text{ at } x = a \text{ (top, evaporating surface), and} \quad (23.11)$$

$$\frac{\partial X_f}{\partial x} = 0 \text{ at } x = 0 \text{ (bottom, non-evaporating surface)}$$

The model assumes one-dimensional liquid diffusion with constant effective diffusivity D_L , and no heat effects. X_2 is the average free moisture content at $t = t_f$ obtained by integrating the analytical

TABLE 23.6
Approximate Ranges of Effective Moisture Diffusivity in
Some Materials

Material	Moisture Content (kg/kg, DB)	Temperature (°C)	Diffusivity (m ² /sec)
Alfalfa stems	3.70	26	2.6×10^{-10} – 2.6×10^{-9}
Animal feed	0.01–0.15	25	1.8×10^{-11} – 2.8×10^{-9}
Apple	0.10–1.50	30–70	1.0×10^{-11} – 3.3×10^{-9}
Asbestos cement	0.10–0.60	20	2.0×10^{-9} – 5.0×10^{-9}
Banana	0.01–3.50	20–40	3.0×10^{-13} – 2.1×10^{-10}
Biscuit	0.10–0.60	20–100	8.6×10^{-10} – 9.4×10^{-8}
Carrot	0.01–5.00	30–70	1.2×10^{-9} – 5.9×10^{-9}
Clay brick	0.20	25	1.3×10^{-8} – 1.4×10^{-8}
Egg liquid	—	85–105	1.0×10^{-11} – 1.5×10^{-11}
Fish muscles	0.05–0.30	30	8.1×10^{-11} – 3.4×10^{-10}
Glass wool	0.10–1.80	20	2.0×10^{-9} – 1.5×10^{-8}
Glucose	0.08–1.50	30–70	4.5×10^{-12} – 6.5×10^{-10}
Kaolin clay	<0.50	45	1.5×10^{-8} – 1.5×10^{-7}
Muffin	0.10–0.95	20–100	8.5×10^{-10} – 1.6×10^{-7}
Paper, thickness direction	~0.50	20	5×10^{-11}
Paper, in-plane direction	~0.50	20	1×10^{-6}
Pepperoni	0.16	12	4.7×10^{-11} – 5.7×10^{-11}
Raisins	0.15–2.40	60	5.0×10^{-11} – 2.5×10^{-11}
Rice	0.10–0.25	30–50	3.8×10^{-8} – 2.5×10^{-6}
Sea sand	0.07–0.13	60	2.5×10^{-8} – 2.5×10^{-6}
Soybeans	0.07	30	7.5×10^{-13} – 5.4×10^{-12}
Silica gel	—	25	3.0×10^{-6} – 5.6×10^{-6}
Starch gel	0.20–3.00	30–50	1.0×10^{-10} – 1.2×10^{-9}
Tobacco leaf	—	30–50	3.2×10^{-11} – 8.1×10^{-11}
Wheat	0.12–0.30	21–80	6.9×10^{-12} – 2.8×10^{-10}
Wood, soft	—	40–90	5.0×10^{-10} – 2.5×10^{-9}
Wood, yellow poplar	1.00	100–150	1.0×10^{-8} – 2.5×10^{-8}

Source: Zogzas et al. (1996), Marinos-Kouris and Marouris (1995), and other sources.

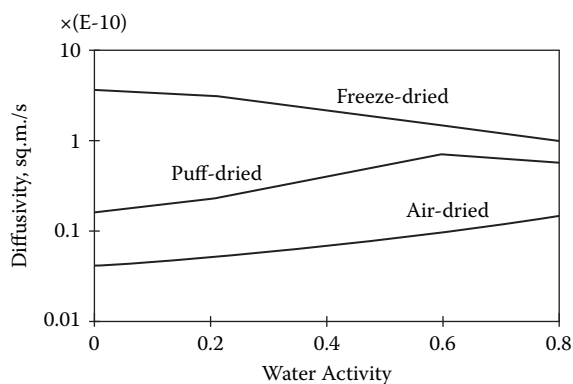


FIGURE 23.8 Moisture diffusivity in dehydrated potatoes.

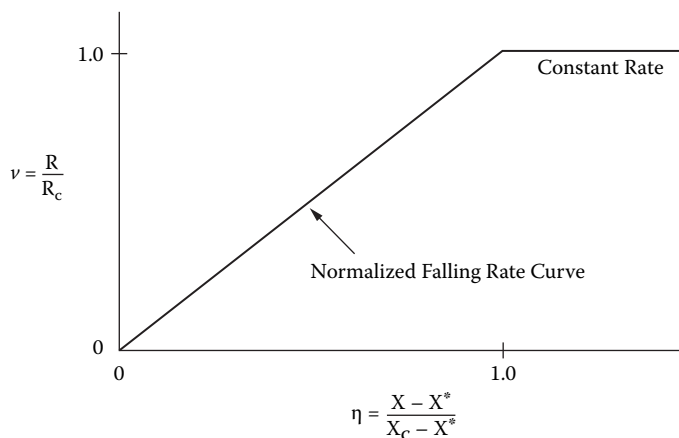


FIGURE 23.9 Characteristic drying rate curve.

drying processes for the purposes of engineering design, analysis, and optimization. A mathematical description of the process is based on the physical mechanisms of internal heat and mass transfer that control the process resistances, as well as the structural and thermodynamic assumptions made to formulate the model. In the constant rate period, the overall drying rate is determined solely by the heat and mass transfer conditions external to the material being dried, such as the temperature, gas velocity, total pressure, and partial pressure of the vapor. In the falling rate period, the rates of internal heat and mass transfer determine the drying rate. Modeling of drying is complicated by the fact that more than one mechanism may contribute to the total mass transfer rate and the contributions from different mechanisms may change during the drying process.

Diffusional mass transfer in the liquid phase, as discussed earlier, is the most commonly assumed mechanism of moisture transfer used in modeling drying that takes place at temperatures below the boiling point of the liquid under locally applied pressure. At higher temperatures, the pore pressure may rise substantially and cause a hydrodynamically driven flow of vapor, which, in turn, may cause a pressure driven flow of liquid in the porous material.

For solids with continuous pores, a surface tension driven flow (capillary flow) may occur as a result of capillary forces caused by the interfacial tension between the water and the solid particles. In the simplest model, a modified form of the Poiseuille flow can be used in conjunction with the capillary forces equation to estimate the rate of drying. Geankoplis (1993) has shown that such a model predicts the drying rate in the falling rate period to be proportional to the free moisture content in the solid. At low solid moisture contents, however, the diffusion model may be more appropriate.

The moisture flux due to capillarity can be expressed in terms of the product of a liquid conductivity parameter and moisture gradient. In this case, the governing equation has, in fact, the same form as the diffusion equation.

For certain materials and under conditions such as those encountered in freeze drying, a “receding-front” model involving a moving boundary between “dry” and “wet” zones often describes the mechanism of drying much more realistically than does the simple liquid diffusion or capillarity model. Examination of the freeze drying of a thin slab of frozen material indicates that the rate of drying is dependent on the rate of heat transfer to the “dry-wet” interface, and the mass transfer resistance offered by the porous dry layer to permeation of the vapor that sublimates from the interface. Because of the low pressures encountered in freeze drying, Knudsen diffusion effects may be significant. Liapis and Marchello (1984) have discussed models of freeze drying involving both unbound and bound moisture.

TABLE 23.8
Classification of Dryers

Criterion	Types
Mode of operation	Batch Continuous*
Heat input-type	Convection,* conduction, radiation, electromagnetic fields, combination of heat transfer modes Intermittent or continuous*
State of material in dryer	Adiabatic or nonadiabatic Stationary, moving, agitated, dispersed, etc.
Operating pressure	Vacuum* Atmospheric
Drying medium (convection)	Air* Superheated steam Flue gases
Drying temperature	Below boiling temperature* Above boiling temperature Below freezing point
Relative motion between drying medium and drying solids	Concurrent Countercurrent Mixed flow
Number of stages	Single* Multi-stage
Residence time	Short (<1 min) Medium (1–60 min) Long (>60 min)

* Most common dryer type in industry.

23.3.1.1 Batch Dryers: Classification (Baker 1997)

Particulate Solids: Major Classes—Layer (Packed Bed); Dispersion Type

1. Layer type
 - a. Contact (conduction or indirect type), e.g., vacuum tray, agitated bed, rotary batch
 - b. Convection (atmospheric tray)
 - c. Special types (e.g., microwave, freeze, solar)
2. Dispersion type
 - a. Fluidized bed/spouted bed
 - b. Vibrated bed dryer

23.3.1.2 Continuous Dryers: Classification

Major Classes—Layer; Dispersion Type

1. Layer type
 - a. Contact (conduction or indirect type), e.g. drum, plate, vacuum based, agitated bed; indirect rotary, etc.
 - b. Convection, e.g., tunnel, spin-flush, throughflow, conveyor, etc.
 - c. Special, e.g., microwave, radio frequency, freeze, solar, etc.

Microwave dryers are expensive in terms of both the capital and operating (energy) costs. They have found limited applications to date. However, they do have special advantages in terms of product quality when handling heat-sensitive materials. They are worth considering as devices to speed up drying in the tail end of the falling rate period. Similarly, RF dryers have limited industrial applicability. They have found some niche markets, e.g., drying of thick lumber and coated papers. Both microwave and RF dryers must be used in conjunction with convection or under vacuum to remove the evaporated moisture. Standalone dielectric dryers are unlikely to be cost-effective except for high-value products. See Schiffmann (1995) for a detailed discussion of dielectric dryers.

It is possible, indeed desirable in some cases, to use combined heat transfer modes, e.g., convection and conduction, convection and radiation, convection and dielectric fields, etc., to reduce the need for increased gas flow that results in lower thermal efficiencies. Use of such combinations increases the capital costs, but these may be offset by reduced energy costs and enhanced product quality. No generalization can be made a priori without tests and economic evaluation. Finally, the heat input may be steady (continuous) or time-varying; also, different heat transfer modes may be deployed simultaneously or consecutively depending on the individual application. In view of the significant increase in the number of design and operational parameters resulting from such complex operations, it is desirable to select the optimal conditions via a mathematical model.

23.3.2 SELECTION OF DRYERS

In view of the enormous choices of dryer types one could possibly deploy for most products, selection of the best type is a challenging task that should not be taken lightly, nor should it be left entirely to dryer vendors who typically specialize in only a few types. The user must take a proactive role and employ vendors' experiences and bench-scale or pilot-scale facilities to obtain data that can be assessed for a comparative evaluation of several options. A wrong dryer for a given application is still a poor dryer, regardless of how well it is designed. Note that minor changes in composition or physical properties of a given product can influence its drying characteristics, handling properties, etc., leading to a different dried product and, in some cases, severe blockages in the dryer itself. Thus, tests should be carried out with the "real" feed material and not a "simulated" one when feasible.

Although here we will focus only on the selection of the dryer alone, it is very important to note that in practice one must select and specify a drying system that includes pre-drying stages (e.g., mechanical dewatering, evaporation, pre-conditioning of feed by solids backmixing, dilution, or pelletization and feeding) as well as the post-drying stages of exhaust gas cleaning, product collection, partial recirculation of exhaust gas, cooling of product, coating of product, agglomeration, etc. The optimal cost-effective choice of a dryer will depend, in some cases, significantly on these stages. For example, a hard pasty feedstock can be diluted to a pumpable slurry, atomized, and dried in a spray dryer to produce a powder, or it may be pelletized and dried in a fluid bed or in a through circulation dryer, or dried as is in a rotary or fluid bed unit. Also, in some cases, it may be necessary to examine the entire flowsheet to see if the drying problem can be simplified or even eliminated. Typically, nonthermal dewatering is an order-of-magnitude less expensive than evaporation, which, in turn, is many-fold more energy efficient than thermal drying. Demands on product quality may not always permit one to select the least expensive option based solely on heat and mass transfer considerations. Often, product quality requirements have overriding influence on the selection process.

As a minimum, the following quantitative information is necessary to arrive at a suitable dryer:

- Dryer throughput; mode of feedstock production (batch/continuous)
- Physical and chemical properties of the wet feed as well as the product desired (specifications); expected variability in feed characteristics
- Upstream and downstream processing operations

TABLE 23.9
Typical Checklist for Selection of Industrial Dryers

Physical form of feed	Granular/particulate/sludge/crystalline/ liquid/pasty/suspension/solution/ continuous sheets, planks, odd-shapes (small large)
Average throughput	Sticky, lumpy, other kg/hr (dry/wet); continuous kg per batch (dry/wet)
Expected variation in throughput (turndown ratio)	
Fuel choice	Oil Gas Electricity
Pre- and post-drying operations (if any)	
For paniculate feed products	Mean particle size Size distribution Particle density Bulk density Rehydration properties
Inlet/outlet moisture content	Dry basis Wet basis
Chemical/biochemical/microbiological activity	
Heat sensitivity	Melting point Glass transition temperature
Sorption isotherms (equilibrium moisture content)	
Drying time	Drying curves Effect of process variables
Special requirements	Material of construction Corrosion Toxicity Nonaqueous solvents Flammability limits Fire hazard Color/texture/aroma requirements (if any)

is fragile and toxic at the same time. If it were not toxic, a through circulated rotating shelf dryer (e.g., Turbo dryer) may be more economic.

In Table 23.10, Kemp (1998) gives results that were obtained from the proprietary dryer selection algorithm developed by Separation Processes Service (SPS) of AEA Technology, Harwell, United Kingdom. Although only one choice is reported here, it should be noted that, in most cases, alternate dryers can also be recommended with nearly equal performance. If local cost of equipment and energy are factored in along with the value of the dried product itself, the results may be different as well.

A further caution to be exercised when selecting dryers is not to be biased by the way the product is made in the laboratory. Drying as well as filtration, at extremely small scales, are very different from that at a scale that is several orders-of-magnitude larger. Some materials may start to form hard lumps under their own weight—this may not show in pilot tests if the product depth is under the critical depth needed to produce lumps. A double-cone vacuum dryer, for example, has a tendency to form snowballs on full-scale but not necessarily on pilot-scale equipment (Kemp 1998).

Table 23.11 lists some key recommendations on dryer selection based on specific properties of the material. It is not all-inclusive, nor does it cover all special physical and/or chemical

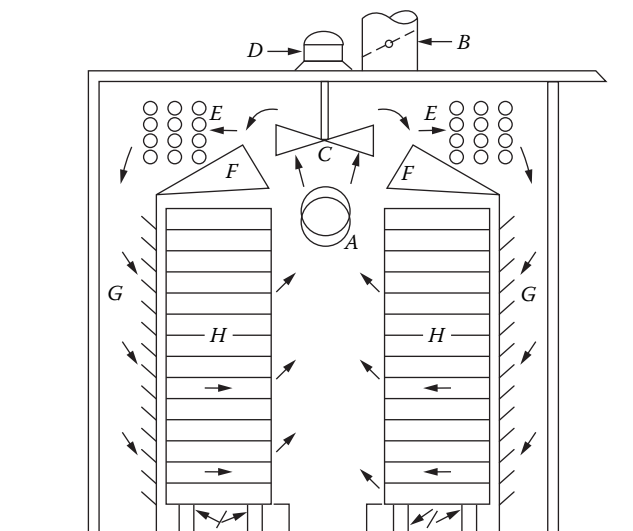


FIGURE 23.10 Schematic of a batch tray dryer.

23.4 DRYING EQUIPMENT

In this section, a number of dryer types commonly used in practice will be discussed based on their different capabilities of handling different types of feedstock, e.g., particulate/granular solids and slurries and suspensions. Some other selected dryers (e.g., infrared, microwave, radio-frequency dryers) will also be mentioned.

23.4.1 DRYERS FOR PARTICULATES AND GRANULAR SOLIDS

23.4.1.1 Tray Dryers

By far the most common dryer for small tonnage products, a batch tray dryer (Figure 23.10) consists of a stack of trays or several stacks of trays placed in a large insulated chamber in which hot air is circulated with appropriately designed fans and guide vanes. Often, a part of the exhausted air is recirculated with a fan located within or outside the drying chamber. These dryers require a large amount of labor to load and unload the product. Typically, the drying times are long (10 to 60 hours). The key to successful operation is the uniform air flow distribution over the trays as the slowest drying tray decides the residence time required and hence dryer capacity. Warp of trays can also cause poor distribution of drying air and hence poor dryer performance.

The batch tray dryer can often be converted into a continuous unit. Figure 23.11 shows the so-called Turbo dryer, which consists of a stack of coaxial circular trays mounted on a single vertical shaft. The product layer fed into the first shelf is leveled by a set of stationary blades that scratch a series of grooves into the surface layer of the solid particles. The blades are staggered to ensure mixing of the material. After one rotation, the material is wiped off the shelf by the last blade and falls onto the next lower shelf. Up to 30 trays or more can be accommodated.

Hot air is supplied to the drying chamber by turbine fans. In the design shown, the air is heated by internal heaters. The wet granular material is fed at the top and it falls under gravity to the next tray through radial slots in each circular shelf. A rotating rake mixes the solids and thus improves the drying performance. Such dryers can be operated under vacuum for heat-sensitive materials or when solvents must be recovered from the vapor. In a modified design, it is possible to heat the trays by conduction and apply vacuum to remove the moisture evaporated.

In this type of dryer, a wide assortment of granular products of diverse shapes, sizes, and size distributions can be processed by proper design of the internal flights and lifters. Special internals are needed for materials that tend to form large lumps, which must be broken to avoid major problems in the later stages of drying. The lifters lift the material to the top of the drum where it showers down in the form of cascades. Major heat and mass transfer steps occur during the flight of the particles from the top to the bottom of the drum by gravity. The drying medium is in cross-flow with respect to the cascading particles. Clearly, particles with terminal velocities below the cross-flow gas velocity will be entrained and collected in the gas cleaning equipment. The cascading action often causes severe attrition of fragile materials, especially when the drum diameter is large.

Although numerous attempts have been reported that permit calculation of the average particle residence times in rotary dryers, the design of commercial units is still based on pilot tests. Empirical rules (often proprietary) are generally based on prior experience with similar material and similar designs of rotary dryer hardware. The drying process is essentially intermittent. It is intense during the cascading motion under gravity when the particles contact the cross-flowing hot gas stream. When the particles settle on the drum wall as a bed carried upward by the revolving shell, there is a "soaking" or "tempering" period when the temperature and moisture content fields in the particles tend to equalize before the particles are exposed to the convective drying condition again.

Rotary dryers can be designed for drying times from 10 to 60 minutes. If a large retention time is needed for removing the internal moisture in the falling rate period, it is possible to use a smaller shell diameter at the wet end for surface moisture removal with low holdup of material in the drum and then increase the shell diameter at the dry end to allow a longer retention time with a larger holdup. In some designs, it is possible to use a pneumatic conveyor to carry the product out of the dryer.

Thermal efficiencies of rotary dryers vary widely in the range of 30% to 60%. For good efficiency, the product holdup (typically 10% to 15% of volume) should be such as to cover the flights or lifters fully. The lifters should be carefully designed to ensure good cascading action, avoiding large clusters of material falling from the flights. Length-to-diameter ratios of 4 to 10 are common in industrial practice.

Rotary dryers can be operated at very high temperatures to accomplish various reactions in addition to or instead of simple drying; these units are referred to as kilns. It is necessary to line the shell of rotary kilns with suitable refractory materials.

In order to enhance the drying rates in the rotary dryer without raising the gas temperature or gas flowrate excessively, it is possible to introduce steam heated tubes or coils within the shell. Aside from providing additional energy for drying, such internals can also help with redistribution or delumping of the material. Of course, it is possible to use internal heaters only if the material does not stick to the walls of the internals.

A new variant of the classical rotary dryer uses a central axial header for drying gas that is injected at discreet intervals along the length of the rotating shell directly into the "kilning" bed of particles. This type of flow distribution is more effective for heat and mass transfer and results in volumetric heat and mass transfer coefficients up to two times larger than those in the cascading dryer. However, this design is not suited for all types of materials.

Rotary dryers are very flexible, very versatile, and are especially suited for high production rate demands. On the negative side, they are typically less efficient, demand high capital costs, and significant maintenance costs, depending on the material being dried. They are not recommended for fragile materials and for low production rates.

Finally, it is useful to note that while most of the continuous rotary dryers are operated under near atmospheric pressure, the term vacuum-rotary dryer refers to an entirely different class of dryers. It is, in fact, an indirect-type batch dryer because of the difficulty of maintaining vacuum under continuous feeding and discharge conditions. Here, the horizontal cylindrical shell is stationary while a set of variously designed agitator blades revolves on a central shaft to agitate the material contained in the dryer shell. Heat is supplied by heating the shell jacket using condensing steam or a thermal fluid. In larger units, the central agitator shaft and the blades may also be heated.

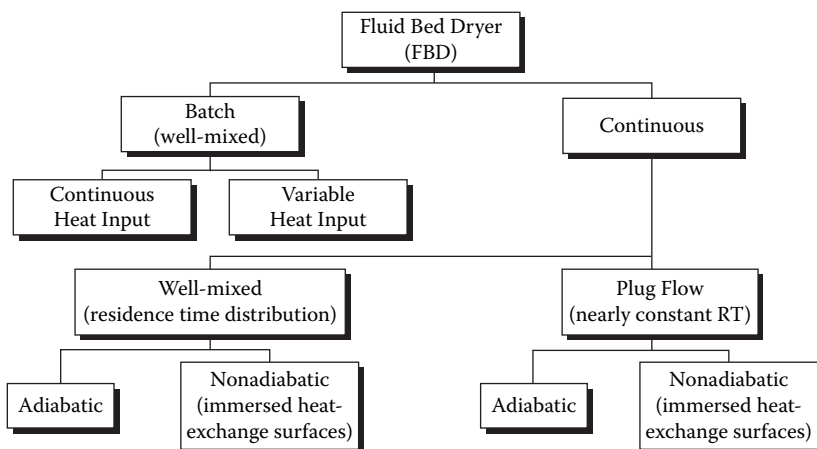


FIGURE 23.14 Coarse classification scheme for fluidized bed dryer.

Also, when handling fairly wet feedstocks, such as filter cakes, mixing of the wet feed into a highly agitated bed of drier particles allows smoother fluidization.

Plug-flow fluidized bed dryers are recommended when it is very important to ensure an almost uniform particles residence time in the dryer. Such dryers may be rectangular geometry trough with large aspect ratios. If floor space is a problem, the trough can be made into a spiral channel. In the straight trough configuration, it is possible to have gas temperature distribution along the length of the dryer. The inlet region can use higher air temperature to enhance the drying rate while toward the end, when the product has lower moisture content, the air temperature can be lowered; in many cases, ambient air is used to cool the product prior to storage or packaging.

When drying large particles, which are difficult to fluidize, a spouted bed or one of its many variants may be used instead of the conventional fluidized bed in which the air is distributed uniformly through a low open area—supporting grid. In a spouted bed, the air enters as a jet and causes a regular recirculatory motion of the particles within the vessel. Due to several limitations, the conventional spouted bed has not found significant commercial application as a dryer, however.

When handling difficult-to-fluidize granular products (because of large size, wide size distribution, or surface stickiness), mechanical assist may be needed to cause the particle bed to be dispersed. Mechanical agitation of the bed or application of vertical vibration at frequencies in the range of 5 to 20 Hz at half-amplitudes of 3 to 5 mm eases separation of the particles. In fact, very low velocities of the drying air are needed to cause pseudo-fluidization by vibration; the resulting drying rates are comparable to those obtained at higher velocities (and hence higher power consumption and particle attrition) in a conventional fluidized bed. The power required for vibration is rather small compared to that used for air handling in a fluidized bed. For fragile solids, e.g., crystals, weak agglomerates, tea leaves, etc., a vibrated fluidized bed may be preferable to conventional fluidized beds. It is used also for large, complex-shaped particles, e.g., chopped or cut fruits and vegetables.

23.4.1.4 Freeze Dryers

Highly heat-sensitive solids, such as some certain biotechnological materials, pharmaceuticals, foods with high flavor content, etc., may be freeze dried at a cost that is at least one order-of-magnitude higher than that of spray drying—itself not an inexpensive drying operation. Here, drying occurs well below the triple point of the liquid (often at temperatures in the vicinity of -40°C) by sublimation of the frozen moisture into vapor, which is then removed from the drying chamber by mechanical vacuum pumps or steam jet ejectors. Generally, freeze drying yields the highest quality

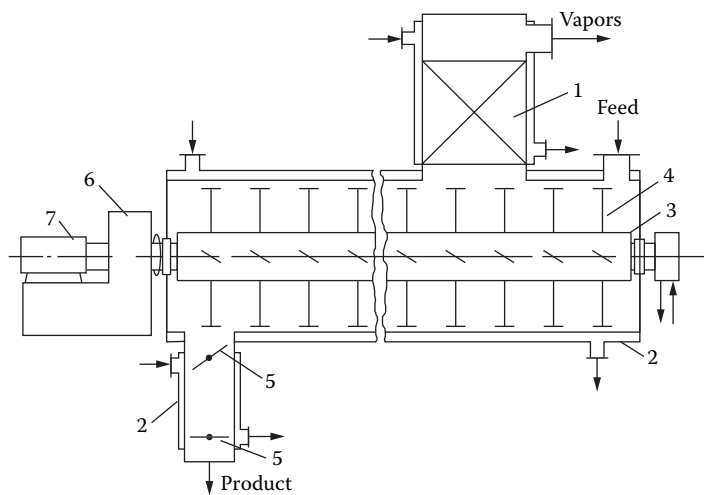


FIGURE 23.16 Continuous vacuum paddle dryer: (1) vapor filter; (2) steam jacket; (3) shaft with paddles; (4) paddles; (5) valves; (6) shaft drive; (7) shaft oscillator.

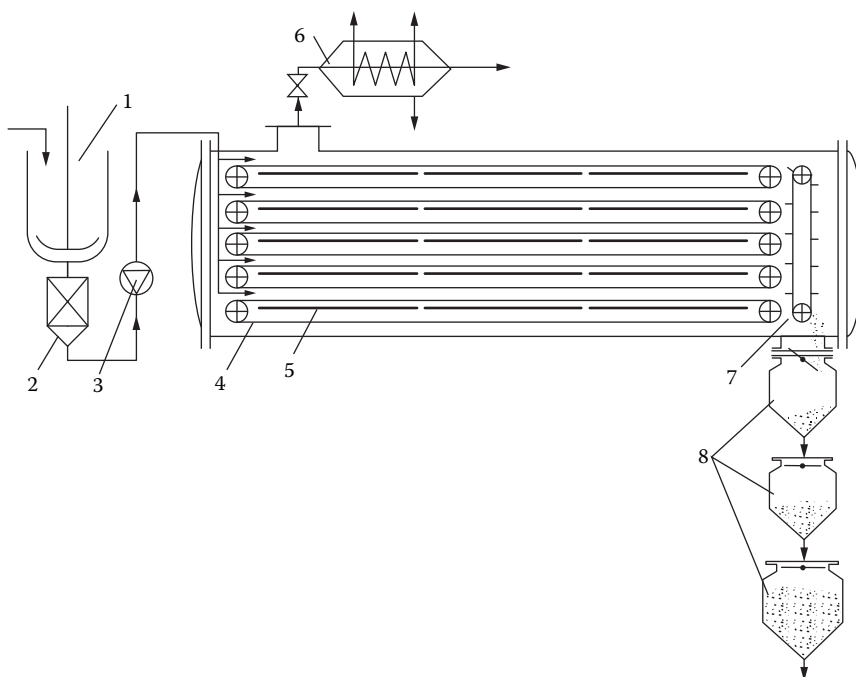


FIGURE 23.17 Band vacuum dryer installation: (1) feed mixer; (2) filter; (3) feed pump; (4) band; (5) heating panels; (6) vapor condenser; (7) scraper; (8) product collector system.

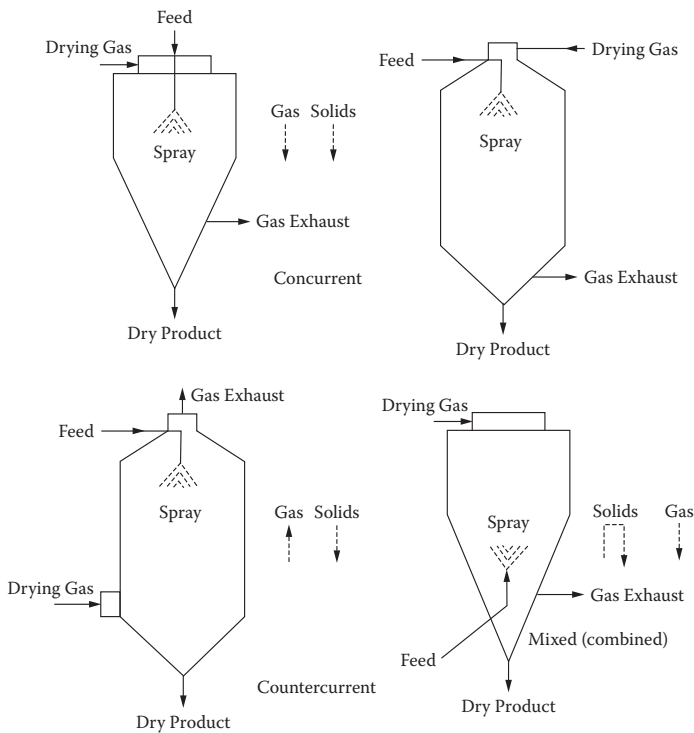
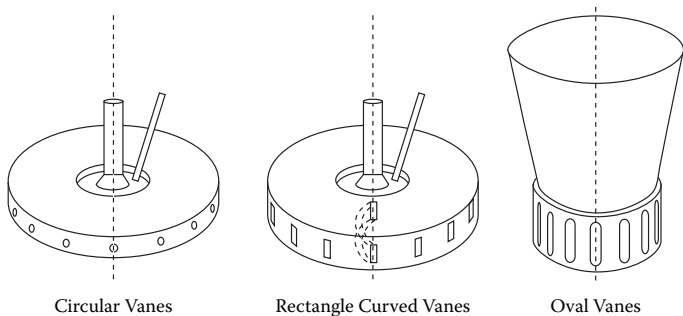
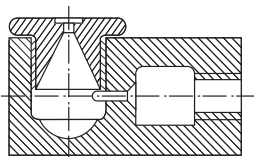


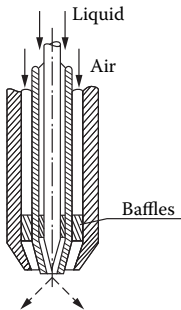
FIGURE 23.19 Schematic diagrams of co-current, countercurrent, and missed flow spray dryer configurations.



(a) Various Designs of Wheel Atomizers



(a) Pressure Nozzle



(a) Pneumatic Nozzle with External Mixing

FIGURE 23.20 Atomizers.

TABLE 23.15
Spray Dryer System Layout

System Layout	Characteristics
Open cycle	General; all aqueous feeds
Closed cycle	Recovery of solvents; prevention of vapor emissions; elimination of explosion or fire hazards
Semi-closed	Prevent powder explosion (keep O ₂ content low), yet use higher inlet temperature
Self-inertizing	

TABLE 23.16
Selection of Dry Powder Collection System

Requirement	Recommended System
Low cost, efficient, easy to clean	Cyclones
Medium cost, very efficient, high running cost	Bag filter
Large air volumes	Electro-static precipitator
Product recovery; fines	Cyclone + wet scrubber

Collection of the dried powder from the spray dryer is also an important issue. Table 23.16 lists general recommendations for the selection of the dry powder collection system.

Since the choice of the atomizer is very crucial, it is important to note the key advantages and limitations of the wheel and pressure nozzles most common in practice. Although both types may be used for same feedstocks, the product properties (bulk density, porosity, size, etc.) will be different.

Rotary wheel (or disk) atomizers

Advantages

- Handle large feed rates with a single wheel
- Suited for abrasive feeds with proper design
- Negligible clogging tendency
- Change of rpm controls particle size
- More flexible capacity

Limitations

- Higher energy consumption compared to pressure nozzles
- More expensive
- Broad radial spray requires large drying chamber (cylindrical-conical type)

Pressure nozzles

Advantages

- Simple, compact, cheap
- No moving parts
- Low-energy consumption

Limitations

- Low capacity (flow rates)
- High tendency to clog
- Erosion can change spray characteristics

Figure 23.21 shows schematics of two spray dryers, one fitted with a wheel atomizer (cylindrical-conical) and the other with a nozzle atomizer (single or two-fluid), which is a cylindrical vessel.

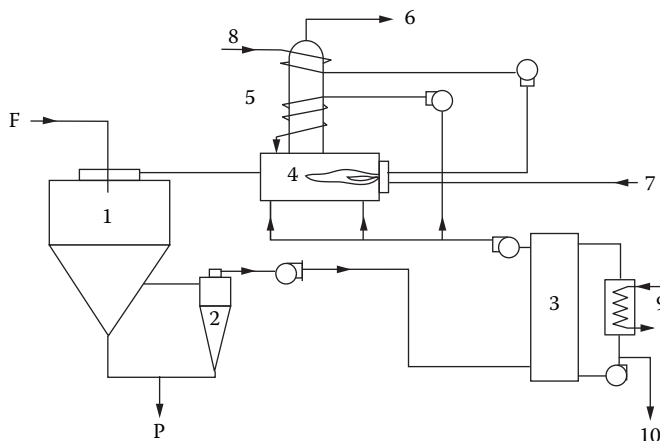


FIGURE 23.22 Self-inertizing spray drying system: (1) drying chamber with rotary atomizer; (2) cyclone; (3) scrubber condenser; (4) direct-fired heater; (5) heat exchanger for waste-heat recovery; (6) exhaust to atmosphere; (7) fuel; (8) combustion air; (9) cooler; (10) condensate; F, feed; P, product.

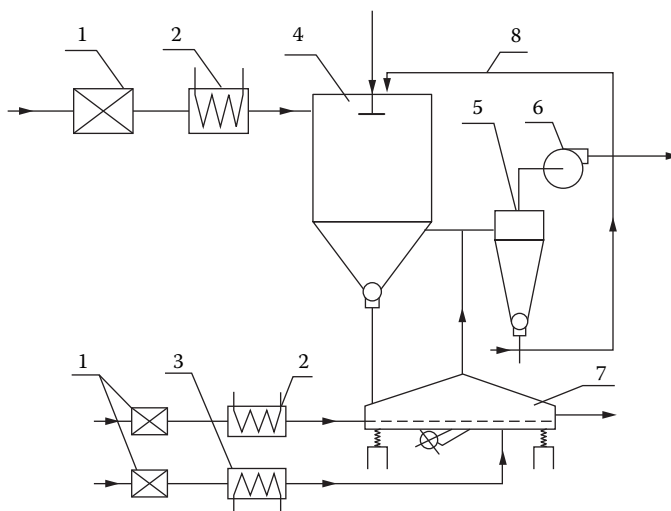


FIGURE 23.23 A two-stage spray drying process for milk: (1) air filter; (2) heater; (3) cooler; (4) spray dryer; (5) cyclone; (6) exhaust fan; (7) fluidized bed dryer; (8) return line of fine powder.

the surface moisture from droplets is removed fully, along with some internal moisture. The final moisture content is achieved in a fluidized bed located at the bottom of the spray chamber as an integral part of it. This two-stage drying process is very efficient and economic. The fluidized bed drying unit can be replaced with a through circulation band dryer at the bottom of the chamber; this concept is the basis of the so-called filtermat dryer used for sticky and sugar-rich materials, which are hard to dry. The bottom section of the spray chamber in this case is much wider, unlike the spray-fluidizer.

23.4.2.2 Drum Dryers

In drum dryers, slurries or pasty feedstocks are dried on the surface of a slowly rotating steam-heated drum. A thin film of the paste is applied on the surface in various ways. The dried film is removed (doctored off) once it is dry and is collected as flakes (rather than powder). Figure 23.24

listed here: two-stage dryers, flash or pneumatic dryers, spin-flash dryers, Roto-Louvre dryer, tunnel dryers, band dryers, infrared, microwave, and radio frequency dryers.

Flash and spin-flash dryers can be used for the removal of surface moisture from a variety of feeds ranging from particulates to pastes in medium to high tonnages. The residence time in these dryers is very short (10 to 30 seconds), although, in some cases, it is enhanced by automatic aerodynamic recirculation of the heavier (larger or wetter) particles through the dryer tube. Band dryers are used for relatively free-flowing particulate materials for medium tonnages, and, in some cases, very large circulation conveyor dryers are used to replace rotary dryers. Most of the dryers mentioned here have several variants that make them more efficient or desirable for a given application; here we will cover only the most basic dryer concepts.

23.4.3.1 Two-Stage Dryers

When both surface and internal moistures must be removed from large quantities of feedstock, it is desirable to consider two-stage operation, where the two stages may be the same dryer type (e.g., fluidized bed) or may be different. The fundamental advantage of such a system is that one can then remove the surface moisture rapidly using dryers or conditions suitable for its rapid removal (e.g., using higher gas temperatures or velocities), and using a dryer allowing longer residence time or gentler drying conditions as the second stage. A plug-flow continuous fluidized bed dryer can be zoned along its length by lowering the gas temperature from inlet to outlet, for example.

Figure 23.25 shows a two-stage arrangement, where the top first stage is a well-mixed fluidized bed dryer for a filter cake, which is difficult to fluidize unless it is mixed with a fluidized bed of lower moisture content. In this figure, the first stage also uses internal heating panels to increase the drying rate since this stage receives drying air, which is the exit air from the lower second stage. The lower stage, which receives the output of the first stage by gravity through a centrally located discharge tube, is a spiral plug-flow fluidized bed dryer, which controls the particle residence time to yield a uniform product.

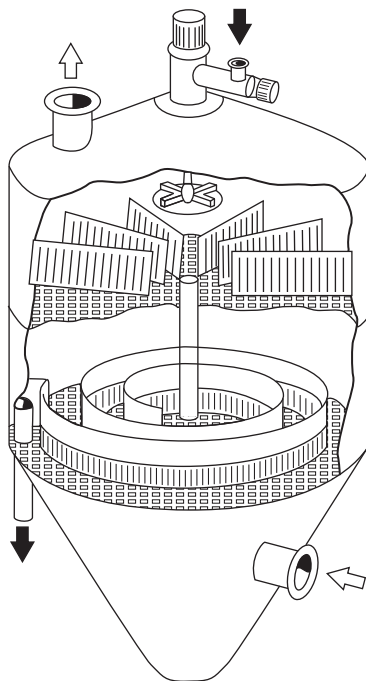


FIGURE 23.25 Schematic of a two-stage fluid bed.

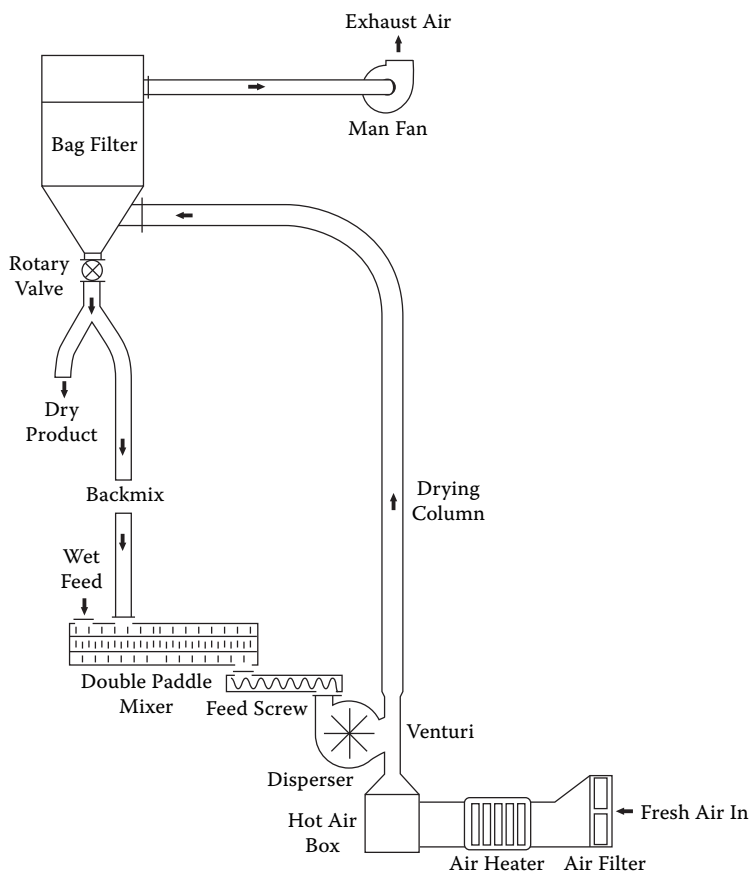


FIGURE 23.27 Flash dryer fitted with back mixer and bag filter.

Flash dryers may be used to dry heat-sensitive solids in view of the short exposure time to the drying medium. They have low capital cost, although, in some cases, the ancillary equipment (disperser, blender [if solids backmixing is needed prior to dispersion], heat exchangers, product collection devices, etc.) may cost much more than the basic flash dryer tube itself. Because of the risk of fire and explosion, care must be taken to avoid flammability limits in the dryer. The dryer must be designed with suitable rupture disks to minimize damage in the event of an explosion. The dryer has small "foot print" (e.g., small floor area) since the flash tube generally rises vertically so the flow of particulates against gravity increases the residence time in the tube of a given length. When it is feasible, a flash dryer should be considered. It does cause attrition, however. It can be used as the first stage of a two-stage dryer system to remove only the surface moisture rapidly and cheaply while a higher residence time dryer (e.g., fluidized bed) may be deployed as the second stage. Removal of the surface moisture also helps fluidize the material well, aside from reducing the size of the fluidized bed unit.

Design of the feed system is crucial for a flash dryer. For free-flowing powdery solids, a screw feeder or a rotary valve is effective. Pasty or sticky materials need to be pre-conditioned by blending them with dried product using a single- or twin-shaft paddle blender and then dispersing them mechanically using a kicker mill or one of several other designs of rotating disperser. The product may be collected in cyclones or baghouses and the very fine material removed prior to exhaust in wet scrubbers.

Flash dryers utilizing superheated steam as the drying medium often have unique quality and energy advantages over air drying systems. More recently, flash dryers consisting of inert media

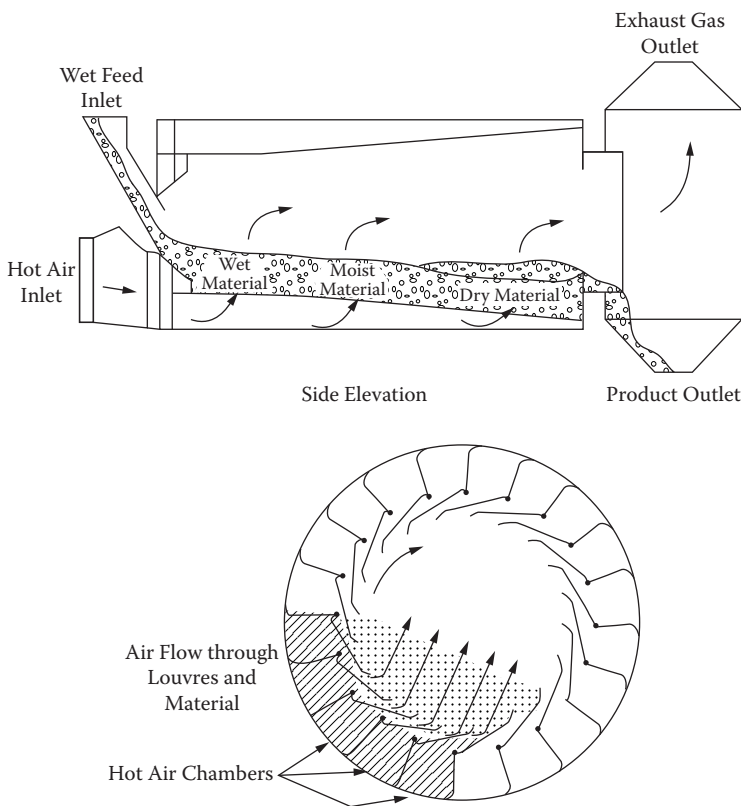


FIGURE 23.29 Roto-louvre dryer.

rotary dryer. Hence, the size of the dryer may be reduced by up to 50%. However, the additional complexity of the equipment increases the initial cost. Product handling is gentler and results in less attrition.

23.4.3.5 Tunnel Dryers

In this simple dryer concept, cabinets, trucks, or trolleys containing the material to be dried are transported at an appropriate velocity through a long insulated chamber (or tunnel). The hot drying gas flows in concurrent, countercurrent, cross-flow, or mixed-flow fashion (Figure 23.30). In the concurrent mode, the hottest and driest air meets the wetted product and hence results in high initial drying rates but with relatively low product temperature (wet-bulb temperature of surface moisture is present). Higher gas temperatures can be used in concurrent arrangements while in countercurrent dryers, the inlet drying gas must be at a lower temperature if the product is heat sensitive. If the material to be dried is not heat sensitive and low residual moisture content is a requirement, then one may employ higher gas temperatures in the countercurrent arrangement as well. Combination flow or cross-flow arrangements are used less commonly. The latter offer high drying rates, but the tunnels must be designed to fit the trolleys snugly so the drying gas flows through the material much like a through-circulation packed bed dryer. Total drying times often range from 30 minutes to 6 hours.

23.4.3.6 Band Dryers

For relatively free-flowing granules and extrudates, which may undergo mechanical damage if they are dispersed, band dryers (Figure 23.30) are a good option. It is essentially a conveyor dryer in which a perforated band supports the bed of drying solids. Drying air at rather low velocities flows

TABLE 23.17
Basic Characteristics of Microwave and Radio Frequency Techniques

Characteristics	Microwave	Radio Frequency
Frequency/wavelength (free space)	896 MHz/30.0 cm	13.56 MHz/22.2 m
	915 MHz/32.8 cm	27.12 MHz/11.1 m
	2450 MHz/12.2 cm	40.68 MHz/7.4 m
Power source	Magnetron (klystron)	Class C triode
Typical efficiency	~50%	~60%
Maximum power of a single unit	60 kW at 915 MHz	600 kW
	6 kW at 2450 MHz	
Principal mechanism of heat generation	Dipole oscillation	Ionic conduction
Loss factor	May be low	Must be relatively high
Penetration depth	Medium or low	High
Product shape	Any	More or less regular
Product size	Small and medium	May be large
Generator service life	2000–5000 hr	5000–10,000 hr
Generator-to-applicator capital cost ratio	0.5	2.3

into the interior, as limited by Fourier's law of heat conduction. This type of heating provides the following advantages:

- Enhanced diffusion of heat and mass
- Development of internal pressure gradients that enhance drying rates
- Increased drying rates without increasing surface temperatures
- Better product quality

When an alternating electromagnetic field is applied to a "lossy" dielectric material, heat is generated due to friction of the excited molecules with asymmetric charges, e.g., water. This is a result of ionic conduction or dipole oscillations (Kudra and Strumillo 1998). The radio frequency range extends from 1 to 300 MHz while the microwave range is from 300 to 3000 MHz. However, only specific frequency ranges are permitted for industrial heating applications, i.e., in RF, ranges 13.56, 27.12, and 40 MHz and for MW, 915 (896 in Europe) and 2450 MHz. Bound and free water have different loss factors. Because loss factors increase with temperature, there is a danger of runaway, i.e., an accelerated heating rate causing a thermal damage to the material.

Table 23.17 summarizes the basic characteristics of MW and RF techniques. The main limitation of MW and RF drying is that the technique is highly capital intensive. It also consumes high-grade energy, i.e., electricity, and the conversion efficiency to the dielectric field is only in the order of 50%. Thus, these techniques are suited only for special applications involving very high-value products, extremely long drying time to remove traces of moisture, or to obtain products of special characteristics not obtained otherwise. It is therefore not surprising that MW/RF drying is used only in special niche applications. Further, these techniques are used mainly to boost drying capacity (to remove free water rapidly without generation of large thermal gradients in the material) or to remove the last few percent of water that comes out very slowly. Generally, dielectric heating is combined with convection or vacuum to reduce the energy consumption. Microwave vacuum drying and microwave freeze drying have found to date only limited commercial applications. Microwave freeze drying is typically carried out at well below the triple point of water. Typical conditions are pressure in the range of 500 Pa and temperature of -40°C . Use of excessive power as well as maldistribution of power due to nonhomogeneities in the frozen

ized, bed superheated steam dryer is marketed commercially for drying of beat pulp. It yields a higher quality fiber that can be used for human consumption while the same product dried in hot air gives a lower quality fiber that is used for animal feedstocks. Higher pressures are typically not cost-effective, although the specific volume of superheated steam is reduced and its enthalpy per unit volume increased at higher pressures.

In general, superheated steam drying should be considered if one or more of the following conditions apply:

1. Energy cost is very high; product value is low or negligible (e.g., commodities like coal, peat, newsprint, tissue paper, and waste sludges that must be dried to meet regulatory requirements).
2. Product quality is much superior (e.g., newsprint, which yields superior strength properties in steam and permits use of lower chemical pulp content to attain same strength and runnability).
3. Risk of fire, explosion, or other oxidative damage is very high (e.g., coal, peat, pulps, etc.). Lower insurance premiums may partially offset added investment cost of a steam dryer.
4. Quantity of water to be removed as well as production capacity required are high. This affords economy of scale.

Such dryers are superior only for continuous operation because of the inherent problems associated with start-up and shut-down when water condensation on the product as well as presence of noncondensables (air) cause problems. See Mujumdar (1995a) for detailed information on superheated steam drying.

23.4.3.10 Drying of Boards and Sheets

Drying of sheet-form materials or materials in the form of large and small pieces often occurs for paper, textile, coated or impregnated fabrics, wood processing, food processing, polymer and photographic film production as well as in the graphic arts industries. Figure 23.32 outlines several possible dryers when the feedstock is other than particulate or liquid-like. The main dryer types suited for such materials will now be reviewed very briefly.

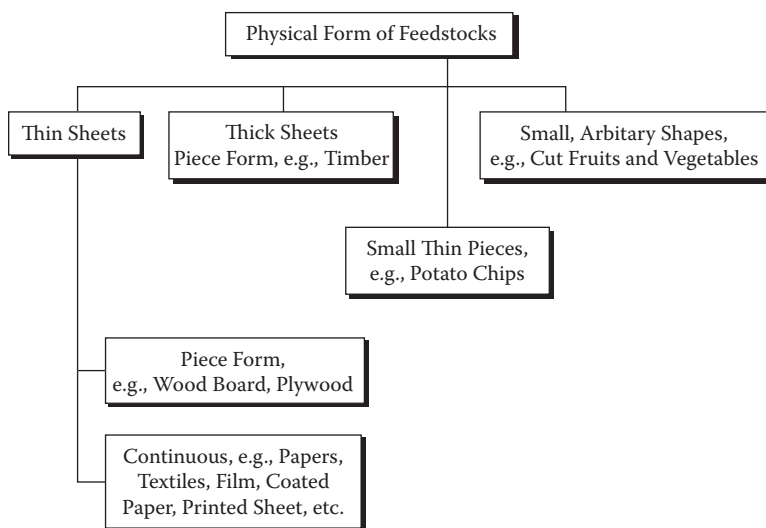


FIGURE 23.32 Classification of feedstock by physical form.

NOMENCLATURE

A	Evaporation area, m^2
a_w	Water activity
c_p	Specific heat, $\text{J kg}^{-1} \text{K}^{-1}$
c_s	Humid heat, $\text{J kg}^{-1} \text{K}^{-1}$
D_L	Effective diffusivity, $\text{m}^2 \text{s}^{-1}$
D_{Lo}	Effective diffusivity at reference temperature, $\text{m}^2 \text{s}^{-1}$
E_a	Activation energy, J
ΔH_w	Enthalpy of wetting, J kg^{-1}
h	Convective heat transfer coefficient, $\text{W m}^{-2} \text{K}^{-1}$
k_g	Thermal conductivity, $\text{W m}^{-1} \text{K}^{-1}$
k_y	Convective mass transfer coefficient, $\text{kgmol s}^{-1} \text{m}^{-2} \text{mol frac}^{-1}$
M_{air}	Molar mass of air, kgmol^{-1}
M_s	Mass of bone dry solid, kg
N	Drying rate, $\text{kg m}^{-2} \text{h}^{-1}$
P_v	Vapor pressure of pure water, Pa
p	Partial pressure, Pa
p_w	Equilibrium vapor pressure of water, Pa
R_g	Universal gas constant, $8.314 \text{ J mol}^{-1} \text{K}^{-1}$
	Temperature, $^{\circ}\text{C}$
T_{abs}	Absolute temperature, K
T_{wb}	Wet-bulb temperature, $^{\circ}\text{C}$
t	Time, sec (or hr)
X	Total moisture content, $\text{kg water/kg dry solid}$
X_c	Critical moisture content, $\text{kg water/kg dry solid}$
X_f	Free moisture content, $\text{kg water/kg dry solid}$
X^*	Equilibrium moisture content, $\text{kg water/kg dry solid}$
Y	Absolute air humidity, $\text{kg water vapor/kg dry air}$

GREEK LETTERS

η	Normalized moisture content
λ	Latent heat of vaporization, J kg^{-1}
μ_g	Dynamic viscosity, $\text{kg m}^{-1} \text{s}^{-1}$
v	Normalized drying rate
ρ_g	Density, kg m^{-3}
Ψ	Relative humidity of air

SUBSCRIPTS

a^s	Adiabatic saturation
c	Constant rate period
f	Falling rate period
g	Gas
s	Solid
v	Vapor
w	Water
w^b	Wet-bulb

- Turner, I., and Mujumdar, A.S., eds. 1997. *Mathematical modeling and numerical techniques in drying technology*. New York: Marcel Dekker.
- van Meel, D.A. 1958. Adiabatic convection batch drying with recirculation of air. *Chemical Engineering Science* 9: 36–44.
- van't Land, C.M. 1991. *Industrial drying equipment: selection and application*. New York: Marcel Dekker.
- Waananen, K.M., Litchfield, J.B., and Okos, M.R. 1993. Classification of drying models for porous solids. *Drying Technology—An International Journal* 11: 1–40.
- Wolf, W., Spiess, W.E.L., and Jung, G. 1985. *Sorption isotherms and water activity of food materials*. Amsterdam: Elsevier.
- Zogzas, N.P., Maroulis, Z.B., and Marinos-Kouris, D. 1996. Moisture diffusivity data compilation in foodstuffs. *Drying Technology—An International Journal* 14: 2225–2253.

TABLE 24.1
Common Screening Applications

Material	Scalping	Fines Removal	Grading
Carbon black, activated carbon	X		X
Ceramics, refractories	X		X
Detergents	X	X	
Electrolytics			X
Explosives, propellants	X		X
Fertilizers	X	X	X
Food additives	X	X	X
Herbicides, pesticides			X
Inorganics	X	X	X
Metal powders	X	X	X
Petroleum coke			X
Pharmaceuticals	X		
Pigments, toners	X		
Plastic beads			X
Plastic pellets	X	X	
Plastic resins	X		
Salts	X	X	X
Sugar, starch	X	X	X

sentative sample and determining the weight of particles within size ranges. This is most commonly accomplished by sieve analysis. In this technique, standardized test sieves with precise apertures defined by standards organizations such as ASTM, ISO, TYLER, DIN, and others, are used (Table 24.2). Sieves used in North America are defined by the ASTM E11 specification.

These test sieves are arranged in a stack from coarsest to finest with a collection pan below the finest sieve. The sample of material to be analyzed is introduced to the top sieve, and the stack is exposed to a combination of motions that cause the material to stratify through the sieves. After a set period of time, the stack is disassembled, and the weight of material retained on each sieve is measured and recorded as a percent of the total sample (Table 24.3).

While mechanical sieve analysis is the most common method for characterizing particle size distribution, other measurement techniques such as laser diffraction and video imaging are often utilized. Laser diffraction has the advantage of being able to measure small particles that cannot be effectively measured by sieves. It is particularly useful for fine powders. Video imaging systems have the advantage of being able to characterize not only particle size, but also particle shape. While their use may expand in the future, to date, neither laser diffraction nor video analysis has been embraced by many processors of granular materials, who continue to rely on mechanical sieve analysis techniques. Regardless of the measurement technique used, particle size distribution generally resembles a bell-shaped curve (Figure 24.1). Figure 24.1 also indicates the portion of the solids that might be separated in fines removal or scalping.

Performance, specifically screening machine capacity, is greatly influenced by the location, the desired separation point on the distribution curve. A typical capacity curve is shown in Figure 24.1. For scalping operations at the coarse end of the particle distribution (right side of curve), very high screening capacities are achievable. This is because most of the particles are much smaller than the screen opening and pass through quite easily, with multiple particles passing simultaneously. The capacities are also quite high for fines removal (left side of curve) because, again, the fine particles that should pass through the screen are much smaller than the screen opening. The capacities, in this case, are not quite as high as with scalping because the fine particles must first work their way through the bed of material that is traveling across the screen surface.

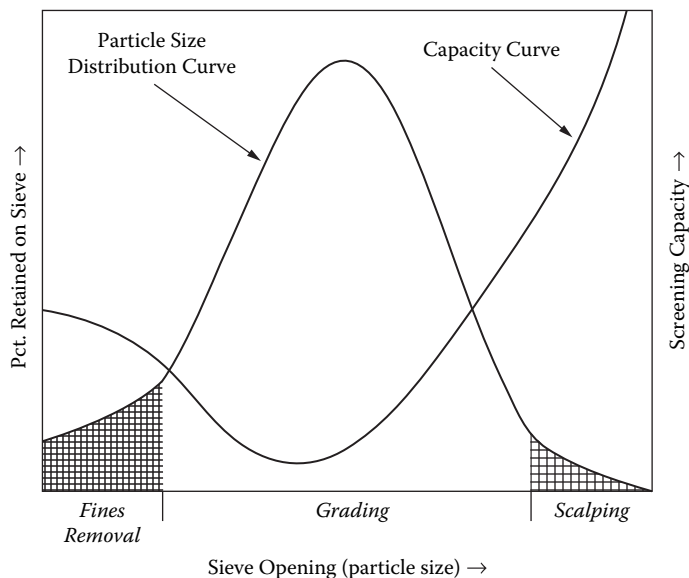


FIGURE 24.1 Particle size distribution curve.

Capacities are lowest when grading. This is because the required separations use screen openings that are near the peak of the particle size distribution curve, where there are numerous particles approximately the same size as the screen opening. These near-size particles that are smaller than the screen opening and should pass through the screen often require multiple exposures to the opening to pass through. In addition, the near-sizes that are slightly larger than the screen opening temporarily block openings, thus limiting the number of screen openings available for the smaller particles. Accurate gradations require relatively low feed rates and highly effective screening motions.

Particle shape affects screening performance. Particles can be various shapes: granular, spherical, cylindrical, etc. Regular shapes such as spherical often allow for relatively sharp separations. Screening of irregular shapes (e.g., elongated, sliver-like, plate-like) generally produce inaccurate separations since the particles enter the screen openings at many different angles. Particle shape can also cause screen blinding, in which particles slightly larger than the screen openings plug the openings. Crystalline particles and spherical particles are particularly prone to blinding.

Another material characteristic that affects screening performance is bulk density. In general, the higher the bulk density, the higher the screen capacity. There are two reasons for this. One is that the force that causes a particle to pass through an opening is proportional to the particle's mass. Consequently, heavy materials like metal powder screen quite readily. However, lightweight materials like sawdust are generally screened at very low-mass flow rates. The second reason is that screening is essentially a volumetric process, as volume defines the depth of material on the screen surface. So, for a given volumetric flow through a screener, the material with the higher bulk density will result in the higher screening rate for a given bed depth, i.e., mass flow.

Flowability of a material, indicated by its angle of repose, affects screening performance since materials that do not flow well do not spread out on the screen surface and properly present themselves to the screen openings. Materials with poor flow characteristics do not convey well along the screen surface. This leads to deeper bed depths and lower screening efficiency. While a material's angle of repose gives some indication of flowability, it is best to evaluate flowability by measuring the material's conveying rate under actual screening conditions.

Surface moisture generally has a significant negative impact on screening performance. Moisture level is measured directly using specialized laboratory equipment in which the solid granular sample is weighed before and after drying. Moisture can cause particles to agglomerate, thus

TABLE 24.4
Comparison of "10 Mesh" Screens

Mesh	Wire Diameter		Opening		% Open Area
10	0.020 in.	0.51 mm	0.080 in.	2.03 mm	64.0%
10	0.025 in.	0.64 mm	0.075 in.	1.91 mm	56.3%
10	0.028 in.	0.71 mm	0.072 in.	1.83 mm	51.8%
10	0.032 in.	0.81 mm	0.068 in.	1.73 mm	46.2%
10	0.035 in.	0.89 mm	0.065 in.	1.65 mm	42.3%

U.S. No. 10 Test Sieve: 2.00 mm (0.078 in.) opening.

Tyler No. 10 Test Sieve: 1.70 mm (0.065 in.) opening.

length separations. Screen clothing for chemical applications is commonly constructed of Type 304 stainless steel.

Screens can be woven of synthetic material such as nylon and polyester. These alternatives offer performance advantages in certain screening applications. Another alternative is perforated steel plate. Weld profile and finish should also be consistent with the materials being screened. These plates are also effective and are quite durable. However, they have a low percentage of open area and therefore have lower capacity for a given screen area.

24.3 SCREEN MOTION AND CONFIGURATION

Screening machines are available in various shapes, sizes, and types of motion (Figure 24.3).

The two most common screen motions used in screening machines are vibratory and gyratory. Vibratory is characterized by a short stroke, high-frequency motion commonly used for coarse separations and for screening applications where a high degree of separation accuracy is not required. For finer separations, or when separation accuracy is a priority, gyratory motion is preferred due to its longer stroke and lower speed. Other types of screen motion such as drum screens or centrifugal screens are used for specialized applications.

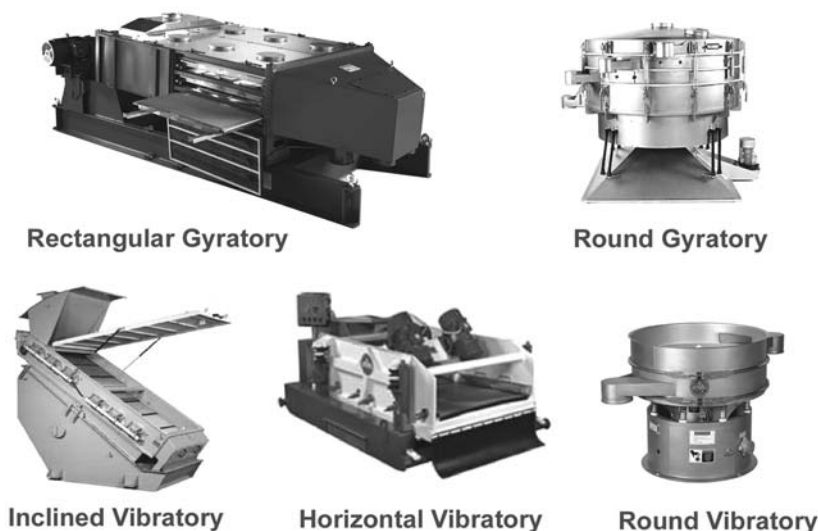


FIGURE 24.3 Screener types.

24.4 SPECIFYING SCREENER PERFORMANCE

Screening machines are evaluated on their ability to maximize both product quality and screening efficiency. One or more of the fractions, or flows, produced is considered to be “product.” This product has imposed on it a quality specification defining the acceptable particle size distribution. Often, this specification consists simply of particle size limits. For example, in a scalping application, the product quality specification may be stated as “0% + 10 U.S. allowable,” i.e., a sample of material that passes through the screen should contain no material coarser than a No. 10 U.S. test sieve. Similar specifications can also be applied to define acceptable results of a fines removal operation. For example, a fines specification of 3% maximum allowable –60 U.S. means that the analysis of a sample taken from the material that passed over the screen would contain no more than 3% by weight passing the No. 60 U.S. test sieve.

Limits and tolerances can also be applied to define product quality in grading applications. Certain industries have arrived at other particle size quality measurements to be applied to their products. The fertilizer industry commonly uses SGN (size guide number) to define the desired mean particle size and UI (uniformity index) to define the allowable variation from that mean particle size. Industrial sands are characterized by the GFN (grain fineness number) that approximates the theoretical sieve opening that would equate to the mean grain size. Abrasives, such as shot and grit, have exacting specifications that set limits and tolerances on the product. Filter media, such as activated carbon, are specified in terms of ES (effective size) and UC (uniformity coefficient), which are analogous to the SGN and UI used in the fertilizer industry. Regardless of the product specification, the key factor affecting product quality is the screen opening selected. So, if a screener is not producing adequate product quality, typically a screen with a different opening must be used.

Although product quality is important, it is not the sole criteria for evaluating screening performance. The other key measure of screening performance is screening efficiency. Screening efficiency is generally measured in one of two ways. The most common of these is referred to as “yield.” Yield is the amount of material separated as product as a percentage of that product fraction which is available in the feed. Thus yield measures the efficiency by which the screener produces the desired, on-specification product.

A more exacting measure of screening efficiency is referred to as product recovery efficiency. It is expressed as a percentage based on the amount of on-size product in the product fraction separated by the screener, divided by the amount of on-size material available in the feed to the screener. Product recovery is calculated as follows:

$$\text{Efficiency (Product Recovery)} = \frac{\text{percent on-spec material in product} \times \text{percent product production rate}}{\text{percent on-size material available in feed}}$$

The product production rate is defined as the percent of material separated by the screener as product times the feed rate to the screener. Production rates are meaningful only if the quality of the product meets the product specifications.

The example shown in Figure 24.4 is a typical screening application in which a screener is used to extract on-size product from a process flow. The example illustrates the relationship between product quality, product yield, and product recovery efficiency.

Product quality is always a factor in system design, but it is screening efficiency that determines production rates and overall system efficiencies. For systems that include recycle loops, screening efficiency can have a compound effect on overall system performance. Clearly, the more efficiently a screener extracts on-size product, the higher the production rate. Often, the reject streams from the screener are recycled and reintroduced to the screener. In such cases, on-size material that was mistakenly rejected by the screener will be needlessly reprocessed, resulting in higher energy costs

and all fractions. As this is often impractical in a production unit, it is preferable to record and analyze these data in a pilot production or laboratory setting. Because of the wide variety of applications and types of screening equipment, no reliable formulas are available to predict performance based solely on process conditions. For this reason, most manufacturers of screening equipment have test laboratories where empirical methods are used to predict screener performance. These tests are used to formulate reliable estimates of product quality, product yield, screening efficiency, and screener capacity. A screener's capacity should always be specified by the feed rate to the machine rather than the product rate produced from the machine.

Sometimes, a manufacturer will define a screening machine's capacity in terms of a screen loading per screen area, for example, 5000 kg/hr/m². This loading is specific for a granular solid mixture and for specific equipment. Loadings vary considerably with application requirements, and even when handling the same application, screeners of different types can have very different loading capacities. Continuing the example, a screener with a screen area of 10 m² would have a capacity of about 50,000 kg/hr (5000 × 10). Or, for a feed rate of 30,000 kg/hr, a screen area of about 6 m² (30,000 ÷ 5000) is needed.

If the required feed rate for a system is relatively high, two possible alternatives occur: one large screener or multiple smaller screeners. While the latter approach typically involves higher installed cost, it offers several advantages. First, smaller screeners tend to be easier to operate because the components to be serviced are more manageable. Second, a dual-machine system allows the entire flow to be diverted to one machine while the other is being serviced. Of course, operating in such condition will necessitate a reduction in overall system processing rate or compromised screening performance.

Beyond screening performance, an evaluation of screening equipment should include various features affecting performance, durability, and maintainability. For example, the method of screen attachment must be appropriate for the application. Specifically, screen clothing must be tensioned at the proper force level to ensure the screen deck remains taut under the material load. While coarse screens (>10 mm) can be tensioned by hand and fixed with mechanical fasteners, finer screen clothing should be tensioned by spring loaded devices or factory set pre-tensioning and attachment. If several screen decks are required to make the necessary separations, it is often desirable to use a single-screening machine with multiple decks installed. This is typically the most cost-effective approach if the amount of screen area required on each deck is approximately the same. If the number of decks required exceed three, it is often more cost-effective to use two separate screening machines arranged in series. This eliminates the complexity involved with a four- or five-deck screener and also allows for tailoring the screener sizes to the amount of screen area required for each separation.

A key element of any screening machine is the drive system. Two types of drive systems are generally used. Drives used on screeners (typically of the vibrating type) in which the screen box are mounted on springs or cables allow the box to move freely in a cyclical motion. The drive consists of a rotating eccentric weight and is attached to the screen box. This intentionally out-of-balance system produces a motion in the screen box that is synchronous with the drive speed and proportional to the ratio of the drive weight to the sprung weight of the screen box. Screen box stroke can therefore be increased or decreased by adjusting the drive weight. One drawback is that screener motion is dampened when a large amount of material is introduced to the screen box, resulting in a significant loss of screening performance.

The other type of screening machine drive system is the positive displacement or crank drive. In this system (typically used for gyratory screen motion), an eccentric crank produces the motion. The advantage is that screen motion is fixed at the designed stroke regardless of material load. The positive displacement drives must employ rotating weights, for counterbalancing the moving assembly. Gyratory screeners are more expensive than vibratory screeners.

When installing a screening machine, the surrounding structure should be properly designed to withstand the forces generated by the screening equipment. In addition to the static load of the

results can identify various problems that may have developed since the last sampling. For example, if an analysis of material passing through a screen reveals the presence of particles larger than the installed screen opening, then one can infer that the screen has a tear in it or one of the seals in the machine has failed. Conversely, if an analysis of material passing over a screen reveals an unusually high percentage of fine material, then one can infer that the screen is blinded or the machine is overloaded, either of which would lead to poor fines removal performance.

Screener maintenance involves both preventive and corrective maintenance. Preventive maintenance includes lubrication, cleaning, and routine inspection of all critical components per the manufacturer's instructions. Corrective maintenance most commonly involves repair or replacement of the screen media. Screen media life is a function of many process variables. Some factors that lead to short screen media life are operating with high screen loadings, using very fine screen wire, and screening of abrasive materials. For example, a relatively coarse 5 mm opening screen with a large diameter wire might last several years, while a fine screen with a 100 micron opening might last only a few days or weeks. When designing processes that are expected to have low screen media life, consideration must be given to frequent servicing of the screen media. If the effects of a torn screen are intolerable, it may be necessary to establish a mean time to failure value for the screen media and make preemptive replacements before failures are expected.

Because most screening machines have relatively massive moving or rotating components, it is imperative that appropriate safety precautions be taken when working on or around the equipment. The manufacturers' manuals and labeling detail the safety considerations. Extra precaution must be taken when processing materials that present explosion hazards. Manufacturers of screening machines will often include special provisions for grounding the various subassemblies and components of the machine to ensure that an electrostatic charge differential does not develop between such components and result in a spark that could trigger an explosion. Machine maintenance can necessitate the removal of these grounding provisions, and care must be taken that they be properly replaced and secured before the machine is returned to operation.

Most screening machines are designed and fabricated such that their useful service lives are measured in decades rather than years in most applications. However, some applications can dramatically shorten service life. Abrasive materials can cause premature wear, particularly when process rates are high. Some materials attack the screener's metal components. Salts, such as sodium chloride, calcium chloride, and ammonium sulfate, are particularly aggressive. In such cases, selection of the materials of construction is critical to maximizing screener service life. In this matter, it is best to work closely with the manufacturer, sharing all pertinent process parameters so recommendations can be made based on their experience with similar systems.

upsets. Changes in moisture, particle size and size distribution, particle attrition, and even changes in raw material supplier, for example, affect the performance of mechanical and pneumatic conveyors. Actual operation must be considered before making a final choice of a conveyor. Often, material samples are tested or are sent to conveyor manufacturers for tests. Testing "similar" materials often helps.

Flow theories plus laboratory tests often permit the design of storage silos and hoppers. The following can be determined: power consumption for withdrawing solids and granules from hoppers and bins, prediction of frictional wear of conveyor and silo surfaces during handling of bulk materials, and attrition of particles during storage and handling. The American Society for Testing Materials (ASTM), Subcommittee D18.24, is currently developing improved Standard Testing Methods for Bulk Solids.

25.3 BELT CONVEYORS

A belt conveyor is made up of an endless belt that traverses between two or more pulleys and is supported at intermediate points by idler rolls. These conveyors can handle a wide range of materials, from fine powders to large lumpy stone or coal, at rates varying from several tons per hour to over 5000 ton/hr. Belt speeds vary from 35 to 300 m/min with belts extending over considerable distances. Such belts are widely used. Figure 25.1 shows a typical belt. It can be arranged horizontally and with inclined or declined sections combined with convex and concave curves in the belt. The desired path of travel is limited only by the strength of the belt and the permissible angle of incline or decline for the particular situation.

Bulk materials are sometimes conveyed on flat belts supported on horizontal idlers on the carrying and return runs. However, in most industrial systems, in order to increase the handling capacity, the belt is formed into a trough shape after it has been loaded with material and it is supported along the carrying run by troughing idlers. The most common troughing idler consists of three rolls. The belt is realigned to a flat position over the head pulley to discharge the material and returns supported on horizontal rolls. The viscoelastic properties of the conveyor belt and the distribution of stresses during start-up and shut-down must be considered when designing long conveyor belts and belts with horizontal curves.

Solids being transferred vary in size of particles; dusty material sometimes results in dust explosions. The materials can also vary in abrasiveness, be free-flowing, or cohesive, or friable. Wet or sticky materials, however, are often a problem if they are not continuously cleaned from the belt surface.

Material characteristics are typically used to determine the required belt width, the carrying capacity of a particular belt, and the maximum inclination at which the belt can be operated.

The angle of repose and angle of surcharge: The angle of repose is the angle a freely formed heap of bulk material makes with the horizontal. The measured value of this angle, when taken together with observations of particle shape and size, moisture, and flowability, determines the angle of surcharge. This is defined as the angle (to the horizontal) that a material assumes while the material is on a moving conveyor belt. For most materials, the angle of surcharge is 5° to 15° less than the angle of repose, but with some very free flowing materials it may be 20° less to avoid spillage from the edge of the belt. Because the cross-section area of the heap is defined by the belt trough geometry and the angle of surcharge, the belt speed required for a desired transport rate of a material with a known density can be easily determined.

The size and proportion of lumps: The larger the lump, and the greater the number, the wider the belt must be to prevent lumps from spilling from a horizontal conveyor; they are more likely to fall off of inclined conveyors.

Fluidizing or air retention properties: Materials that are easily aerated and have long air retention time limit belt inclination and speed.

25.3.1 CARRYING IDLERS

The most commonly used troughed carrying idler consist of three rolls with two outer rolls inclined at 20°, 35°, or 45° from the horizontal. Carrying capacity increases with the troughing angle. In the past, the multi-ply belts in use were stiffer and did not conform well to idlers having troughing angles over 20°. The newer belts, having carcasses of synthetic fiber blends, are more flexible and can be designed for higher angles. Idlers of 35° to 45° are gaining in popularity. It is important that the belt is centered on the idlers.

The mechanical design of the idler rolls is a function of the particular service under which the conveyor operates. Minimum industrial standards for roll dimensions, bearings, and application criteria for different service conditions have often been established. Idler life is determined by a combination of factors such as bearings, seals, shell thickness, load density, and operating environment.

Bearing rating and life are the only variables for which laboratory tests can provide standard values. CEMA therefore uses bearings as a guide for establishing idler ratings. In rating the idler bearing life, CEMA uses the term "useful life" (BU) representing the statistical point in hours where a minimum of 90% of the bearings will still be functional with no increase in torque or noise. The minimum required load ratings for equal-length roll idlers for service conditions ranging from light duty to heavy duty based on 90,000 hours minimum bearing life at 500 rpm have been determined for belt widths ranging from 18 to 96 inches, for 20°, 35°, and 45° troughing angles and for flat return idlers. These ratings form the basis for the minimum design requirements for CEMA-rated idlers. Actual figures for idlers are obtained from the idler manufacturer. Whereas bearing life is useful as an indicator of idler life, other factors such as bearing seal effectiveness may be more important in determining idler life.

Specialized idlers are available for certain applications. Examples are plastic disc catenary idlers for wet corrosive materials; two-roll idlers, where the rolls are oriented in a "V" for a lighter duty conveying system; and suspended idler supports for severe service.

25.3.2 BELTS

Conveyor belts are manufactured in widths up to 2500 mm. Belts are susceptible to damage and are often the most expensive portion of the total system. The belt consists of two principal elements: the covers (top and bottom) and the carcass. The covers protect the carcass against environmental effects, wear, and cutting. Covers are generally natural or synthetic rubber, thermosetting elastomers, and thermoplastic materials. The carcass provides the tensile strength required to start and move the loaded belt, the traverse flexibility and longitudinal flexibility to allow the belt to both support the load and conform to the shape of the idlers when running empty and to properly wrap around pulleys, and the strength to absorb the impact forces at the loading point. Carcasses have one or more plies of a woven fabric bonded together with an elastomeric compound. Woven materials include cotton, rayon, nylon, polyester, polyamides (nylon), and glass, in the pure form or in blends. The fabrics are constructed with warp yarns that run lengthwise along the belt and filling (weft) yarns that run crosswise. There are a variety of weaves available for specific applications. New high-tenacity synthetic fibers and improvements in belt construction have led to belts with load capacities equal to or exceeding those of the previous belts with fewer plies. A more recent development in belt technology has been the solid-woven carcass belts impregnated and covered with poly-vinyl-chloride (PVC) or urethane plastisol. Steel cable belts made with a single layer of parallel steel cables completely imbedded in rubber and enclosed between one or more fabric plies are available for even higher tensile loadings. A more recent development in high-tensile strength belts has been the use of Kevlar (DuPont) high-strength (aromatic polyamides) fibers in woven, cord, solid woven, and cable construction. Careful cost analyses are needed in selecting the type of belt to be used.

25.5 BUCKET ELEVATORS

A series of metal or plastic buckets are used to lift solid particles. These buckets are attached to an endless belt or chain. The buckets are first filled with the solid particles, and the buckets are unloaded after the moving belt has lifted the buckets. Continuous elevators can handle a wide range of materials, from light to heavy, free-flowing granular and pulverized materials with lumps up to 100 mm. This elevator handles material rather gently. Bucket speeds range from 30 to 46 m/min. The lower speeds are used in order to properly fill the buckets when fluffy, low-density materials are handled. Capacities range up to 75 m³/hr on standard elevators.

Super-capacity elevators are continuous-type elevators in which buckets are mounted between two strands of chains. This arrangement makes it possible to handle a larger volume because the bucket can be extended in back of the chain. Elevators of this type are capable of handling up to 375 m³/hr.

25.6 VIBRATING CONVEYORS

A vibrating conveyor consists of a trough supported by tuned springs and/or hinged links, having a drive system. The drive system is arranged to oscillate the trough, causing solid particles to be moved along the trough. Such conveyors are sometimes called oscillating conveyors. There are two types: reciprocating and vibrating.

On a reciprocating conveyor, material is carried forward in a horizontal direction by frictional contact with the trough. Inertia causes the material to be left in that position as the trough is quickly returned to its initial position. These conveyors are useful for granular free-flowing materials with a minimum of attrition. They provide gentle handling of food products, such as friable flakes and pellets, pharmaceuticals, powdered and granular chemicals, and minerals. Vibrating conveyors are uniquely suited for handling metal parts, abrasive, hot, and dusty materials, and can be designed to withstand heavy impact loads from materials such as rocks, iron and steel casting, and metal and wood scrap.

Tubular troughs are useful where dust-tight operation is required. Inclined flat bottom troughs with a sawtooth-shaped carrying surface can be used for conveying granular materials up to 10° to 20° slopes. Troughs can be provided with multiple discharge openings and can be designed to handle materials at temperatures up to 900°C (1652°F). Tubular or rectangular troughs wound in a vertical spiral can be used for vertical conveying of granular materials. This type of conveyor also operates at sub-resonance and is shop or field fine-tuned by weight adjustment on the trough before being put in service. This design requires fewer moving parts than the direct drive machine, but requires more attention to design and tuning. The exciters usually operate at frequencies of 15 to 20 Hz.

Excitation can also be supplied by an electromagnetic exciter that uses a rectified, pulsed AC power supply, or AC supply to an apposed electromagnet/permanent magnet drive. These units operate at very short strokes and frequencies of 50 to 60 Hz.

Compressed air or hydraulically driven reciprocating piston or rotary exciters are sometimes used in short conveyors. They are particularly useful where explosion hazards limit the use of electrical drives.

25.7 EN-MASSÉ CONVEYORS

An en-masse conveyor consists of an endless chain or cable pulling a series of spaced skeleton or solid plug flights through an enclosed casing or housing. Material is introduced through an opening in the casing, where it is captured by the flights and drawn through the casing until it reaches an opening in the housing where it discharges by gravity.

En-masse conveyors are compact and totally enclose the bulk material; they handle many materials with little particle attrition; they can have a L-shaped or a Z-shaped path, therefore

transported, distances and heights of transport, etc. Manufacturers of conveyors can generally aid in the selection of a preferred conveyor. Both operating and capital costs need be considered in selecting the preferred conveyor.

26.7	Corrosion Processes.....	1805
26.7.1	Thermodynamics of Corrosion Processes.....	1806
26.7.2	Kinetic Aspects of Corrosion Reactions.....	1808
26.7.3	Mass Transfer Effects.....	1810
26.7.4	Metal Passivation.....	1811
26.7.5	Types of Corrosion and Methods of Corrosion Prevention.....	1812
26.7.5.1	Uniform Attack.....	1812
26.7.5.2	Galvanic Corrosion.....	1812
26.7.5.3	Crevice Corrosion.....	1813
26.7.5.4	Pitting.....	1814
26.7.5.5	Stress Corrosion Cracking.....	1815
26.7.5.6	Hydrogen Embrittlement.....	1815
26.8	Batteries and Fuel Cells.....	1816
26.8.1	Batteries.....	1816
26.8.1.1	Battery Performance Characteristics.....	1816
26.8.2	Fuel Cells.....	1821
26.8.2.1	Fuel Cell Types.....	1822
	Nomenclature.....	1824
	References.....	1826

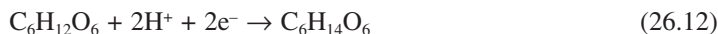
26.1 INTRODUCTION

Electrochemical methods of producing energy (primary and secondary batteries and fuel cells), fabricating materials (e.g., electroplating, electrowinning, and electromachining operations), purifying chemical compounds (electrodialysis membrane separations), and synthesizing chemicals (e.g., the industrial electrosynthesis of chlorine, caustic soda, and organic chemicals) are attractive due to their inherent energy efficiency, the moderate temperature of operation, and the ease of measuring and controlling current and voltage. Electrochemical routes are often less polluting than chemical schemes because electrons perform the oxidation and reduction reactions rather than chemical reagents. The application of electrochemistry to real-world systems requires the same understanding of chemical engineering fundamentals (thermodynamics, reaction kinetics, and mass transport) as needed for traditional chemical or petrochemical processes, with two exceptions. There is the need to consider the ionic species in an electrolyte that may react heterogeneously at an electrode surface and to include electrical potential effects, which drive both electrochemical reactions and the mass transfer of ionic species in solution.

The merging of electrochemistry and chemical engineering into electrochemical engineering formally began in the 1950s. Since its inception, this subfield of chemical engineering has grown considerably. This chapter provides an overview of electrochemical principles and applications. First, thermodynamics, kinetics, and mass transfer, as applied to electrochemical systems, are reviewed. Next, specific examples of electrochemical processes/applications are presented, including electroplating and etching, environmental clean-up technologies, corrosion of metals, electrochemical reactor design, organic and inorganic electrochemical syntheses, and batteries and fuel cells.

26.2 FUNDAMENTALS

All electrochemical cells consist of at least two electrodes, an anode where oxidation reactions occur and a cathode for reduction reactions, with a conductive electrolytic solution between the anode and cathode. To maintain an overall charge balance, the electrons produced at the anode are consumed at the cathode; an external wire connecting the electrodes provides the pathway for electron flow. The electrical circuit is completed by current flow through the electrolyte solution,

Anode Oxidation Reactions*Cathode Reduction Reactions*

Examples of half-cell and overall reactions for industrially important electrochemical processes and commercial electrochemical devices are listed in Table 26.1.

Knowing that a given combination of anode and cathode half-cell reactions will proceed spontaneously does not ensure that the electrode reaction rates will be sufficiently high for practical applications. Reaction kinetics at the anode and cathode and mass transfer of reactants/products to/from the electrodes may play important roles in an electrochemical cell and may influence the choice of cell design and operating conditions. These important points will be addressed later in this chapter.

Since electrode reactions involve electron transfers, the measurement of current with units of amperes (where 1 ampere = 1 coulomb/sec) quantifies the rate of an oxidation or reduction reaction at an electrode. For the following generalized electrode reaction



we see that χ/n moles of oxidized species (denoted as *Ox*) or ε/n moles of reduced species (abbreviated *Red*) react for each mole of electrons that is transferred into or out of the electrode.

Since the charge of an electron is 1.6×10^{-19} coulombs, one mole of electrons contains a total charge of 96,487 coulombs. This quantity, known as Faraday's constant, relates the current to the molar rate of product formation or reactant consumption in an electrochemical reaction. Molar rate expressions for the forward and backward reactions of Equation (26.13) are integrated to give Faraday's Law:

$$M_{\text{oxid}} = \frac{\int_0^{t^*} I(t) dt}{\left[\frac{n}{\chi} \right] F} \quad \text{and} \quad M_{\text{red}} = \frac{\int_0^{t^*} I(t) dt}{\left[\frac{n}{\varepsilon} \right] F} \quad (26.14)$$

In the next three sections of this chapter, fundamental theories and principles of thermodynamics, reaction kinetics, and mass transfer processes, as applied to electrochemical systems, are reviewed.

26.2.1 THERMODYNAMICS

Thermodynamics is used in the analysis of electrochemical cells: (1) to predict which electrode reactions occur spontaneously in the anodic and cathodic directions if the two electrodes are in equilibrium with their respective adjacent solutions and are connected to one another via an external wire, and (2) to quantify chemical potentials and activity coefficients in nonideal electrolytic solutions.

26.2.1.1 Thermodynamics of Electrochemical Cells

In chemical systems, the state variable used to determine the spontaneity of a given reaction in the forward or reverse direction is the Gibbs free energy. For the electrochemical cell shown in Figure 26.1, we stipulate that the two electrodes are connected through a high-resistance voltmeter to essentially stop any current flow, in which case the overall cell reaction [given by Equation (26.3)] is at thermodynamic equilibrium. The Gibbs energy for this or any overall cell reaction at standard state conditions (where the temperature is 25°C, the pressure is one atmosphere, and the activities of reactants and products are unity) is given by

$$\Delta G^\circ = \sum \Delta G^\circ_{\text{products}} - \sum \Delta G^\circ_{\text{reactants}} \quad (26.17)$$

where ΔG° denotes the standard state Gibbs energy. When the cell is not at standard state conditions, we can further write

$$\Delta G = \Delta G^\circ + RT \ln K = \Delta G^\circ + RT \ln \frac{\prod_i (a_{i,P})^{x_{i,P}}}{\prod_i (a_{i,R})^{y_{i,R}}} \quad (26.18)$$

where K is the equilibrium constant of the reaction, R and T are the gas constant and absolute temperature, the $a_{i,P}$ and $a_{i,R}$ terms are the activities of the product and reactant species, respectively, $x_{i,P}$ and $y_{i,R}$ are the stoichiometric coefficients of the products and reactants in the reaction (e.g., ϵ and χ in Equation 26.13), and Π denotes the arithmetic product. When ΔG° or ΔG is < 0 , the forward reaction as written is spontaneous, whereas the reverse reaction is spontaneous when the Gibbs energy change is > 0 . Electrochemists use the electric potential (E) rather than the Gibbs energy to assess the spontaneity of a given set of anode/cathode reactions. At constant temperature and pressure, the Gibbs energy and emf (electric potential) are related by

$$\Delta G^\circ = -nFE^\circ \quad \text{and} \quad \Delta G = -nFE \quad (26.19)$$

where n is the number of electrons participating in the anode or cathode reactions ($n = 2$ for the Zn/Cu example above). Since the overall reaction in an electrochemical cell is given by the combination of anode and cathode “half-cell” reactions, the cell emf can also be decomposed into two individual electric potentials. An abbreviated listing of such standard half-cell reactions and their associate reduction potentials is in Table 26.2. Extensive listings of potentials are in electrochemical texts and chemical handbooks [see, for example, references (1–4)].

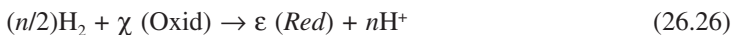
$$\begin{aligned}
 \Delta G^o &= \Sigma \Delta G^o(\text{products}) - \Sigma \Delta G^o(\text{reactants}) \\
 &= [\Delta G^o(\text{CH}_3\text{OH}) + \Delta G^o(\text{H}_2\text{O})] - [\Delta G^o(\text{HCOOH}) + 2\Delta G^o(\text{H}_2)] \\
 &= [-39.9\text{kcal/mol} - 56.7\text{kcal/mol}] - [86.4\text{ kcal/mol} + 0] \\
 \Delta G^o &= -10.2\text{ kcal/mol} = -42.6\text{ kJ/mol}
 \end{aligned}
 \tag{26.24}$$

From Equation (26.19) (with $n = 2$), E^o is computed from this value of ΔG^o

$$E^o = \frac{-\Delta G^o}{nF} = \frac{42.6 \times 10^3}{2F} = +0.22\text{ V vs. SHE} \tag{26.25}$$

Once the two half-cell reactions in an electrochemical cell have been assigned/identified and the standard half-cell potentials have been either ascertained from standard reduction potential tables or computed using Gibbs energy data, one can determine which reaction proceeds spontaneously in the anodic and cathodic directions. Using Equation (26.19) and our definition of zero potential, the half-cell reaction with the more negative standard reduction potential is the anode in an electrochemical cell and the reaction with the more positive half-cell potential proceeds in the cathodic direction. For the Cu/Zn cell given by Equation (26.3), we see from Table 26.2 that $(E^o)_{\text{Cu/Cu}^{2+}} = +0.337\text{ V vs. SHE}$ (an abbreviation for the standard hydrogen electrode) and $(E^o)_{\text{Zn/Zn}^{2+}} = -0.763\text{ V vs. SHE}$, hence Zn will spontaneously oxidize and cupric ions will be reduced in the cell shown in Figure [26.1]). The standard reduction potentials in Table 26.2 are invariant in sign and independent of the position of the half-cell electrode reactions in an electrochemical cell. The cell potential (as defined by Equation 26.21), on the other hand, depends on the relative positions of the two electrodes (i.e., which electrode is on the left). For example, if the Zn electrode is the left-hand electrode in the cell, E_{cell} will be $0.34\text{ V} - (-0.76\text{ V}) = +1.1\text{ V}$, whereas the cell potential will be $-0.76\text{ V} - (0.34\text{ V}) = -1.1\text{ V}$ if the copper electrode were positioned on the left.

To determine the potential of a half-cell reaction when the reactants and products are not at unit activity, the Nernst equation is used. Consider again the general half-cell reaction given by Equation (26.13). When this reaction is combined with the standard hydrogen electrode reaction (Equation (26.20)), the overall cell reaction is



Combining Equations (26.18) and (26.19) for this reaction results in the following formula:

$$E^e = E^o + \frac{RT}{nF} \ln \frac{(a_{\text{Red}})^\varepsilon (a_{\text{H}^+})^n}{(a_{\text{Oxid}})^\chi (a_{\text{H}_2})^{n/2}} \tag{26.27}$$

where E^e is defined as the equilibrium half-cell potential with respect to the standard hydrogen electrode. For simplicity, the activities in Equation (26.27) are replaced with concentrations. Also, by definition of the standard hydrogen electrode, $a_{\text{H}^+} = a_{\text{H}_2} = 1$, in which case we arrive at the Nernst equation:

$$E^e = E^o + \frac{RT}{nF} \ln \frac{(C_{\text{Red}})^\varepsilon}{(C_{\text{Oxid}})^\chi} \tag{26.28}$$

solution containing only anions or cations (i.e., only neutral salt molecules, containing both cations and anions, can be dissolved in a solvent during an activity measurement experiment). To circumvent this problem, electrochemists have defined the electrochemical potential of neutral salt molecules in terms of mean activities and mean activity coefficients. For a salt $M_{\nu+}X_{\nu-}$ that dissociates completely into one type of cation species and one anion species when dissolved in a solvent, one can write the following equation:



Relationships for the electrochemical potential of a neutral salt electrolyte ($\bar{\mu}_e$) are written as,

$$\begin{aligned} \bar{\mu}_e &= (\bar{\mu}_e)^o + \nu RT \ln a_{\pm} \\ &= (\bar{\mu}_e)^o + \nu RT \ln (\gamma_{\pm} m_e) \\ &= (\bar{\mu}_e)^o + \nu RT \ln (f_{\pm} C_e) \end{aligned} \quad (26.34)$$

where m_e and C_e are the molal and molar concentrations of the salt, respectively, a_{\pm} is the mean activity of the salt, $\nu = (\nu+) + (\nu-)$, $\bar{\mu}_e = (\nu+)\bar{\mu}_{+} + (\nu-)\bar{\mu}_{-}$, and γ_{\pm} and f_{\pm} are the mean molal and mean molar activity coefficients, which are defined in terms of the individual ion activity coefficients

$$(a_{\pm})^{\nu} = (a_{+})^{\nu+} (a_{-})^{\nu-} \quad (26.35)$$

$$(\gamma_{\pm})^{\nu} = (\gamma_{+})^{\nu+} (\gamma_{-})^{\nu-} ; (f_{\pm})^{\nu} = (f_{+})^{\nu+} (f_{-})^{\nu-} \quad (26.36)$$

In Equation (26.34), $\bar{\mu}_e$ is dependent on the electrical state of the system through the mean activity coefficient terms, which in turn are related to the individual ion activities.

Values of electrolyte activities, as measured by osmotic pressures, freezing point depression, and other experimental methods are in the literature (References 5 and 6, for example) or one can calculate activity coefficients based on models of molecular-level interactions between ions in electrolyte solutions. For illustrative purposes, mean molal activity coefficients for various salts at different aqueous molal (m_e) concentrations at 25°C are listed in Table 26.3 [7].

Numerous models predict the activity coefficient of individual ions in solution. The one by Debye and Hückel [8] considers only electrostatic (columbic) interactions between cations and anions in a dilute solution of a single, completely dissociated salt. It is assumed that ion-ion interactions (as opposed to other phenomena such as ion-solvent interactions, ion solvation effects, and variations in the solvent dielectric constant with salt concentration) cause the ion activity coefficients to deviate from 1.0. From a practical point, only the Debye-Hückel activity coefficient relationship is needed, along with some knowledge of the theory's shortcomings, which restrict its application. For a dilute electrolytic solution containing a binary salt (i.e., a salt with one type each of cation and anion species), the ion activity coefficient from Debye-Hückel theory is given by

$$\ln \gamma_i = \ln f_i = \frac{z_i^2 A \sqrt{I_s}}{1 + B \alpha \sqrt{I_s}} \quad (26.37)$$

where α is the mean diameter of the ion (nm) and

TABLE 26.4
Debye-Hückel Activity Coefficient Parameters
for Aqueous Solutions of Any Binary Salt

Temperature (°C)	0	25	50	75
A (kg/mol) ^{1/2}	1.1324	1.1762	1.2300	1.2949
B (kg/mol) ^{1/2} /nm	3.248	3.287	3.326	3.368

Data from [4].

$$\ln \gamma_i = -z_i^2 A \sqrt{I_s} \quad (26.42)$$

Equation (26.41) predicts to within approximately 10% mean molal activity coefficients for salt concentrations up to 0.1 molal. The more accurate form of the activity coefficient equation [Equation (26.40)] allows the model to be extended to salt concentrations up to 0.5 molal. To expand the applicability of the Debye-Hückel theory to higher concentrations, additional terms are added to Equation (26.40), such as [4]

$$\ln \gamma_{\pm} = \frac{z_+ z_- A \sqrt{I_s}}{1 + B \alpha \sqrt{I_s}} + \frac{4 (v_+) (v_-) \Theta}{(v_+) + (v_-)} m \quad (26.43)$$

where values of the parameter Θ for various aqueous electrolytes at 25°C [9] are listed in Table 26.5. For additional activity correlations and for a review of activity coefficients in multicomponent solutions, the reader is directed to [10, 11].

TABLE 26.5
 Θ Parameter for Activity Coefficients in
Aqueous Electrolytes at 25°C

HCl	0.27
HClO ₄	0.30
LiCl	0.22
NaOH	0.06
NaCl	0.15
NaNO ₃	0.04
NaF	0.07
KOH	0.13
KCl	0.10
KBr	0.11
KClO ₃	-0.04
AgNO ₃	-0.14
RbCl	0.06
RbNO ₃	-0.14
CsOH	0.35
CsCl	0.00
CsI	-0.01
CsNO ₃	-0.15

Data from [9].

potential) produces a large current density. Electrode reactions with a low-exchange current density, on the other hand, are slow and are often referred to as irreversible because large overpotentials are required for appreciable current densities. Mathematically we can write an equation for i_o in terms of the chemical kinetic rate constants for the reaction in the anodic and cathodic directions (k_a and k_c , respectively) and the concentrations of the reduced and oxidized species at the electrode surface (C_{Red} and C_{Ox} , respectively) [4, 12]:

$$i_o = n F k_c^{(1-\beta)} k_a^\beta C_{Ox}^{(1-\beta)} C_{Red}^\beta \quad (26.46)$$

Figures 26.2 and 26.3 show typical current density-overpotential plots where i varies exponentially with η_s , in accordance with the Butler-Volmer equation. In Figure 26.2, the effect of varying β on i - η_s curves is shown (as β decreases, i increases at a given value of η_s). The increase in current density at a given η_s for increasing values of i_o is shown in Figure 26.3. From these two figures it can be concluded that electrochemical reactions that follow Butler-Volmer kinetics will be facile when the kinetic parameter β is small and the value of i_o is large.

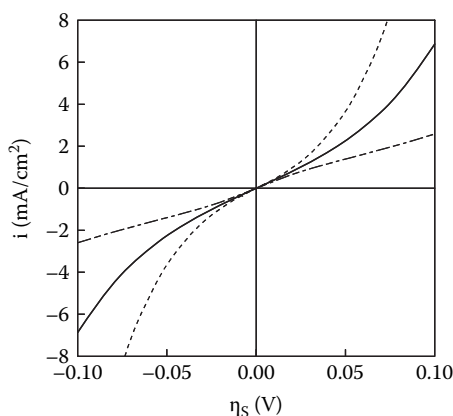


FIGURE 26.2 Current density-surface overpotential plots showing the effect of the transfer coefficient for a redox reaction [Equation (26.45)] with $n = 1$, $T = 298\text{K}$, and $i_o = 1.0 \text{ mA/cm}^2$. - - - $\beta = 0.74$; — $\beta = 0.5$; — · — $\beta = 0.25$.

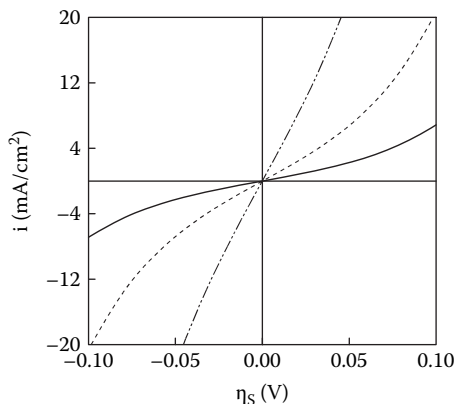


FIGURE 26.3 Current density-surface overpotential plots showing the effect of the exchange current density for a redox reaction [Equation (26.45)] with $n = 1$, $T = 298\text{K}$, and $\beta = 0.5$. — $i_o = 1.0 \text{ mA/cm}^2$; - - - $i_o = 3.0 \text{ mA/cm}^2$; — · — $i_o = 5.0 \text{ mA/cm}^2$.

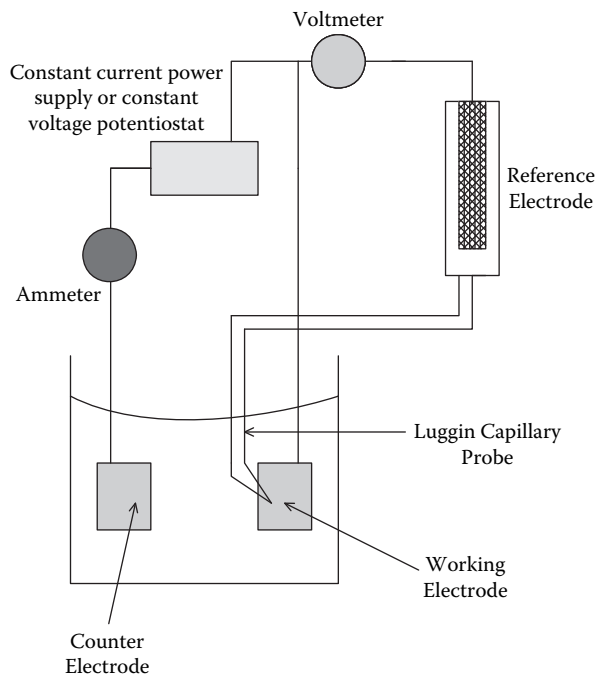


FIGURE 26.4 Three-electrode electrochemical cell for the collection of current-voltage data at the working electrode.

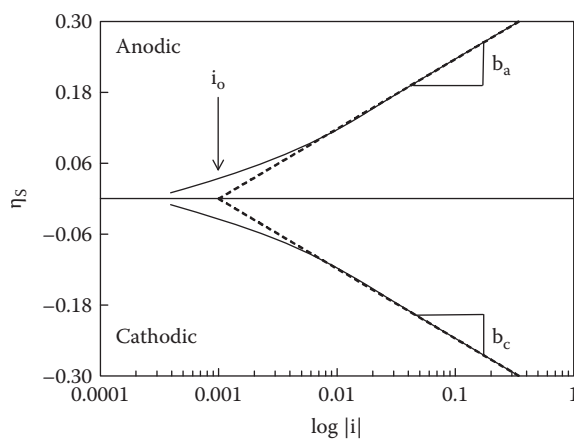


FIGURE 26.5 Surface overpotential vs. current density plots for a kinetically controlled redox reaction. Overpotentials less than zero refer to the reaction proceeding in the cathodic direction. The anodic and cathodic Tafel lines are drawn for high overpotentials.

is governed by the usual processes of diffusion (where concentration or activity gradients are the driving force for transport) and convection, which is dependent on bulk fluid motion. Because of the electric field between the anode and cathode, there is an additional mode of transport for charged species in solution, called migration, where the driving force is the gradient in the electric potential.

26.2.3.1 Transport Equations

The analysis of mass transfer in electrochemical cells requires the use of equations that describe the condition of electroneutrality (which applies for the entire electrolyte outside the double layer at an electrode), species fluxes, mass conservation, current density, and fluid hydrodynamics. Often, mass transport events are rate limiting, as compared to kinetics processes at the electrode surface, in which case the overall electrode reaction rate is solely dependent on species mass transfer (e.g., during high-rate electroplating of some metals and for those electrochemical reactions where the concentration of reactant in solution is low).

Isothermal mass transport in electrochemical systems is described by the following relationships [4], which are strictly applicable for infinitely dilute electrolyte solutions:

1. The equation for electroneutrality in the bulk electrolytic solution,

$$\sum_i z_i C_i = 0 \quad (26.53)$$

where z_i is the charge number of species i ($z < 0$ for anions and $z > 0$ for cations) and C is concentration with units of mol/cm³.

2. The molar flux (N_i) equation for charged ions in solution, with diffusion, migration, and convection terms,

$$N_i = -D_i \nabla C_i - z_i u_i F C_i \nabla \Phi + C_i v \quad (26.54)$$

where D_i is the diffusivity, u_i is the electric mobility of ion species i in solution and v is the fluid velocity.

3. A material balance equation for species i in the bulk electrolyte,

$$\frac{\partial C_i}{\partial t} = -\nabla \cdot N_i + R_i \quad (26.55)$$

where R_i represents the rate of homogeneous chemical reaction in solution that produces or consumes species i .

4. The current density equation,

$$i = F \sum_i z_i N_i \quad (26.56)$$

To apply the above equations to electrochemical mass transfer, the solution velocity [v in Equation (26.54)] must be known, which requires the solution of a separate set of fluid mechanics equations. Also, the transport parameters, D_i and u_i , must be specified, as will be discussed in some detail below.

Manipulation of Equations (26.53)–(26.56) leads to a number of important mass transfer relationships. When the molar flux, current density, and electroneutrality equations are combined

$$D = \frac{z_+ u_+ D_+ + z_- u_- D_-}{z_+ u_+ + z_- u_-} \quad (26.65)$$

The convective diffusion equation for a binary electrolyte dissolved in an incompressible fluid is derived by combining the anion and cation flux relationships (using Equation [26.54]) with the corresponding material balance equations [Equation (26.55)], with $R_i = 0$ and $\nabla \cdot \mathbf{v} = 0$) to give

$$\frac{\partial C}{\partial t} + \mathbf{v} \cdot \nabla C = D \nabla^2 C \quad (26.66)$$

where D is the average ion diffusivity, as defined by Equation (26.65). Curiously, this equation for the movement of charged species in solution has no term explicit in the electric potential, although there is an electric potential gradient driving force acting on the ionic species when current is flowing between the anode and cathode. Thus, for the binary electrolyte case, one does not need a full description of the electric potential distribution between the anode and cathode to determine the concentration distribution of ion species in solution. This result greatly simplifies the mathematical analysis of transport in electrochemical systems. Also, the absence of an electric potential term in Equation (26.66) means that the convective transport equation for a binary electrolyte is of a similar form as that used in heat transfer and nonelectrolytic mass transfer systems. Consequently, many solutions to nonelectrochemical convective transport problems in the literature can be utilized by electrochemical engineers, as shown below.

To increase the electrolyte conductivity, an additional ionic component that does not participate in the electrochemical reactions is often added to a solution. This nonreactive component is called a supporting electrolyte or indifferent electrolyte. In the presence of a supporting electrolyte, there is a lowering of the electric field in solution, due to the electrolyte's high conductivity. Transport of the minor ionic species in solution is due primarily to diffusion and convection, in accordance with Equation (26.54) with $\nabla \Phi = 0$. Also, in the presence of a supporting electrolyte, the convective diffusion equation for a minor component in solution is written as

$$\frac{\partial C_i}{\partial t} + \mathbf{v} \cdot \nabla C_i = D_i \nabla^2 C_i \quad (26.67)$$

This equation is similar in form to that obtained for the case of no supporting electrolyte (Equation (26.66)) except for the use of an individual ion concentration and diffusion coefficient.

To illustrate the use of the transport equations, the following problem is posed. An electrochemical cell containing vertical flat sheets of copper as the anode and cathode is operated with an aqueous CuSO_4 electrolyte. The copper plates are connected to a DC power supply so that oxidation and reduction reactions proceed at the anode and cathode ($\text{Cu}^{2+} + 2\text{e}^- \rightarrow \text{Cu}$ at the cathode; $\text{Cu} \rightarrow \text{Cu}^{2+} + 2\text{e}^-$ at the anode). For the case when there is no forced or natural convection during current flow, we derive a simple expression between the constant applied current density and the steady-state cupric ion concentration profile. The cation flux and current density equations for the flat plate electrode/no convection cell are

$$N_+ = -v_+ D \frac{dC}{dy} + \frac{t_+ i}{z_+ F} \quad (26.68a)$$

$$i = z_+ F N_+ \quad (26.68b)$$

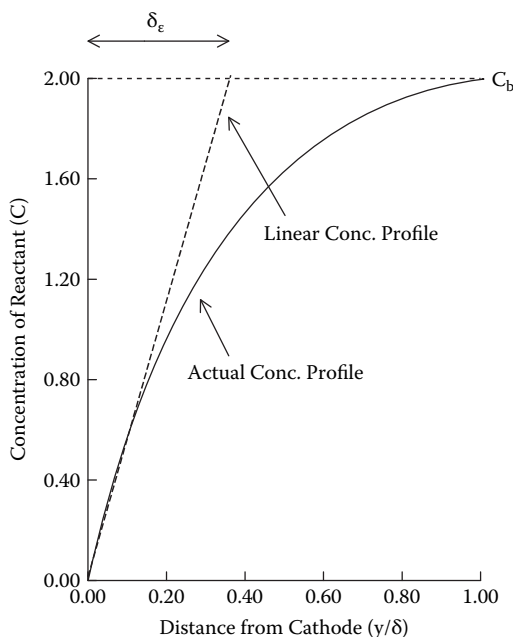


FIGURE 26.6 Concentration profile of reacting species near an electrode surface under mass transfer controlled conditions.

electrochemical systems. One assumes that there is a small region very close to the electrode surface where all fluid velocities are zero and transport to and from the electrode surface occurs by diffusion (and migration) only, hence the terminology stagnant diffusion layer. Within this motionless fluid, the concentration profiles of the electro-active species are linear, as was the case in the example given above. The actual concentration profile in the mass transfer boundary layer is nonlinear, due to the presence of finite fluid velocities near the electrode (the velocity is only zero at the electrode surface). A typical nonlinear concentration profile and the region over which the concentration differs from that in the bulk fluid, which defines the actual mass transfer boundary-layer thickness (denoted as δ), are shown in Figure 26.6. The effective mass transfer boundary layer is also shown in this figure, where the linear concentration profile is tangent to the actual concentration variation at the electrode surface.

Equation (26.69) (or Equation (26.70) for the case of a supporting electrolyte) was originally derived under the assumption of no convective velocities. These same relationships can be utilized within the effective mass transfer boundary layer when fluid stirring exists. A current density/concentration equation with fluid stirring can now be generated starting with Equation (26.69) or Equation (26.70). The dC/dy term in Equation (26.69) is replaced by $\Delta C/\delta_e$ (where δ_e is the effective mass transfer boundary-layer thickness):

$$i = \frac{-z_+ v_+ DF \left. \frac{dC}{dy} \right|_{y=0}}{(1-t_+)} = \frac{-z_+ v_+ DF \left(\frac{C_\infty - C_o}{\delta_e} \right)}{(1-t_+)} \quad (26.73)$$

where $y = 0$ is the location of the electrode surface, and C_∞ and C_o are the concentrations of the reacting species in the bulk and at the electrode surface, respectively. Similar arguments can be used to generate a linear concentration profile current density equation when an excess supporting electrolyte is present (starting with Equation (26.70)).

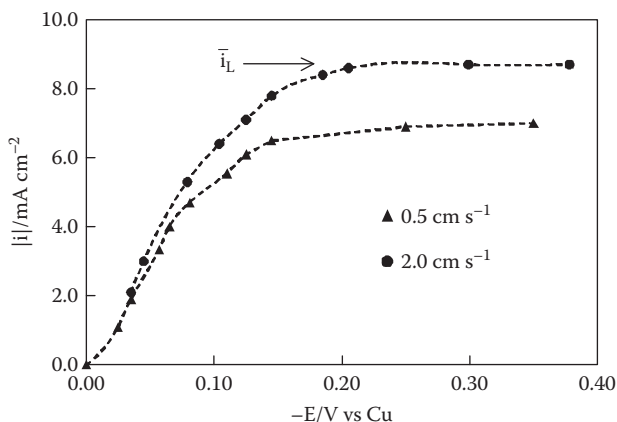


FIGURE 26.7 Current density (i) – voltage (E) plots showing the limiting current density during copper plating at a vertical flat plate cathode with assisting (upward) natural and force convection stirring (the forced convection fluid velocity is either 0.5 or 2.0 cm/sec). Data from [15]. Copyright Elsevier (1993).

+ $2e^- \rightarrow H_2$). As one would expect, the data in Figure 26.7 show that i_L increases (δ_e decreases) as the forced convection velocity is increased from 0.5 to 2.0 cm/sec.

There may be situations where there is a significant amount of hydrogen gas evolution during metal deposition. In this case, i_L may not be easily observed in a current density-voltage plot, as is the case in Figure 26.8 [16] for copper deposition at a rotating disk electrode from a $CuSO_4$ solution containing H_2SO_4 as the supporting electrolyte and Gleam-PC, a polyethylene glycol-based copper plating additive manufactured by LeaRonald, Inc. In order to determine the limiting current density, separate current density-voltage measurements must be made in the absence of $CuSO_4$. Such data gives the hydrogen evolution rate on the cathode as a function of cathode potential. Subtraction of the hydrogen current densities for the i - V curve representing hydrogen evolution and copper reduction then gives the copper deposition limiting current density, as shown in Figure 26.8.

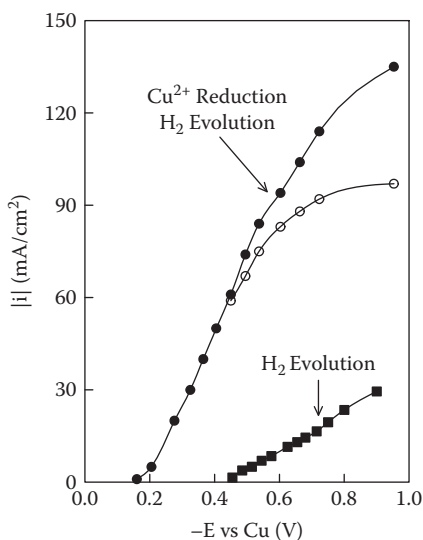


FIGURE 26.8 Current density (i) – voltage (E) plots for simultaneous cupric ion reduction + hydrogen gas generation and only hydrogen gas generation. The open circle curve (obtained by subtracting the two solid line curves) shows the Cu^{2+} limiting current. Data from [16]. Reproduced by permission of ECS—The Electrochemical Society.

or

$$Sh = 0.62 \left[\frac{r^2 \omega}{\nu} \right]^{1/2} \left[\frac{\nu}{D} \right]^{1/2} \quad (26.81)$$

where ω is the disk rotation speed (with units of s^{-1}), r is the disk radius, ν is the kinematic viscosity ($\nu = \mu/\rho$), and the characteristic length for the Sh number is the disk radius (r). For this system, the fluid velocity can be varied by changing the disk rotation speed. The above correlation has been generated theoretically by Levich and verified in numerous experimental studies [17–19]. The corresponding limiting current correlation is

$$|i_L| = 0.62 z_+ F C_\infty D^{2/3} \nu^{-1/6} \omega^{1/2} \quad (26.82)$$

2. Laminar flow parallel to a flat plate [20]:

$$Sh = 0.677(Re)^{1/2}(Sc)^{1/3} \quad (26.83)$$

where both Sh and Re are defined in terms of the flat plate length, measured in the direction of fluid flow, hence the value of k_d in this correlation represents an average mass transfer coefficient over the entire plate length.

3. Laminar flow in a tube [21]:

$$Sh = 1.07(Re)^{1/3}(Sc)^{1/3} \left(\frac{d}{L} \right)^{1/3} \quad (26.84)$$

In the above equation, L is the tube length, the characteristic length in Sh is the tube diameter d , and Re is defined in terms of the tube diameter and the average velocity in the tube. Equation 26.84 does not take into account possible disruptions in the laminar flow condition at the entrance of the tube, nor can it be used at distances far down the tube (it has been shown that the correlation is accurate for $L < 5000d$) [4].

4. Natural convection at a vertical flat plate [22, 23]:

$$Sh = 0.66(ScGr)^{1/4} \quad (26.85)$$

where Gr and Sh are defined in terms of the plate length in the direction of the natural convection fluid flow.

5. Combined forced and free convection at a vertical flat plate, where the forced convection velocity is in the same direction as the natural convection flow (the so-called assisting mixed convection case). Here, researchers have combined Sherwood numbers for the pure forced and natural convection cases in the following way [15, 24–26]:

$$Sh_{mixed}^{3.2} = Sh_N^3 + Sh_F^3 \quad (26.86)$$

where Sh_N for natural convection is given by Equation (26.85) and Sh_F (forced convection) is defined by Equation (26.83). Additional limiting current correlations can be found in [27].

TABLE 26.7
Equivalent Conductances of Cations and Anions in 25°C
Water at Infinite Dilution

Ion	z_i	λ_i (S-cm ²)/equiv	Ion	z_i	λ_i (S-cm ²)/equiv
H ⁺	+1	349.8	OH ⁻	-1	197.6
Li ⁺	+1	38.69	Cl ⁻	-1	76.34
Na ⁺	+1	50.11	Br ⁻	-1	78.3
K ⁺	+1	73.52	I ⁻	-1	76.8
NH ₄ ⁺	+1	73.4	NO ₃ ⁻	-1	71.44
Ag ⁺	+1	61.92	HCO ₂ ⁻	-1	54.6
Mg ²⁺	+2	53.06	SO ₄ ⁻	-1	80
Ca ²⁺	+2	59.50	IO ₄ ⁻	-1	54.38
Sr ²⁺	+2	59.46	ClO ₄ ⁻	-1	67.32
Cu ²⁺	+2	54	BrO ₃ ⁻	-1	55.78
Zn ²⁺	+2	53	HSO ₄ ⁻	-1	50
La ³⁺	+3	69.5	CH ₃ COO ⁻	-1	40.9

Data from [4].

driven cell. One can reverse the direction of spontaneous anode and cathode reactions in an electrochemical cell by introducing a power supply in the external circuit between the electrodes. In such a driven cell, the negative terminal of the power supply is connected to the cathode and the positive lead is connected to the anode.

We have already discussed equilibrium electrode potentials and how they can be used to determine the tendencies for anodic de-electronation and cathodic electronation reactions at the electrode–solution interfaces in an electrochemical cell. For a self-driven cell, the current density will set up a number of current-produced potentials, known as overpotentials, that decrease the overall cell potential from its equilibrium value. In the development of energy-producing devices such as batteries and fuel cells, the variation of the cell potential with current is often more important than its open circuit, equilibrium potential. By proper engineering designs, one seeks to lower these overpotentials in order to obtain as much energy as possible from the cell. Similarly, in a driven cell, the open circuit, equilibrium potential represents the minimum thermodynamic potential driving force needed to carry out the anodic and cathodic reactions. Once these reactions begin and current flows, overpotentials are generated that increase the cell potential above that at open circuit. These overpotentials need to be minimized to ensure operation of the cell with the lowest possible energy input.

The overpotentials (denoted as η) that must be taken into account when designing and operating both driven and self-driven electrochemical cells describe energy consuming processes that occur during current passage. Due to the electrical conductivity of the electrolyte that separates the anode and cathode, the IR drop (sometimes called the resistance or ohmic overpotential η_{ohm}) depends on the magnitude of the current density, the distance between the anode and cathode, and the conductivity of the electrolyte solution. Normally, the concentration of ionic species in the bulk electrolyte is constant during current flow and variations in concentration are relegated to Nernst diffusion layers adjacent to the electrode surfaces, as described above. For this situation, the composition and conductivity of the bulk electrolyte are constant and one can write for η_{ohm}

$$|\eta_{ohm}| = \frac{|i|}{\kappa} \Delta y \quad (26.93)$$

$$i = i_o [e^{(1-\beta)nF\eta_s/RT} - e^{-\beta nF\eta_s/RT}] \quad (26.97)$$

where i_o is a function of the electrode surface concentrations of reactants and products. By definition, $\eta_s < 0$ favors reduction reactions, whereas $\eta_s > 0$ favors anodic reactions.

We now estimate the anode/cathode potential difference during current flow for driven and self-driven cells. First, we define the cell potential (V) as the difference in the anode and cathode potentials. For a self-driven cell, the cell voltage at a given current density will be less than the difference in equilibrium electrode potentials (ΔE_e) due to the presence of various overpotentials,

$$V = \Delta E_e - |\eta_s(\text{anode})| - |\eta_c(\text{anode})| - |\eta_s(\text{cathode})| - |\eta_c(\text{cathode})| - |\eta_{ohm}| \quad (26.98)$$

where $\Delta E_e = E_e(\text{cathode}) - E_e(\text{anode})$. Since the thermodynamic quantity ΔE_e is always greater than zero for a self-driven system, the overpotentials in Equation (26.98) decrease the magnitude of the available anode/cathode electric potential difference. For a driven electrochemical cell, Equation (26.98) also holds, but $E_e(\text{cathode}) - E_e(\text{anode}) < 0$ and the various overpotentials add to ΔE_e . Thus, the anode/cathode voltage drop will be greater than that predicted from thermodynamic arguments alone.

In the remaining sections of this chapter, overviews of various electrochemical processes/systems are presented. Where appropriate, these overviews refer back to the fundamental principles and theories presented above.

26.3 ELECTROCHEMICAL REACTORS AND REACTOR DESIGN

An important task of electrochemical engineers is to design and operate electrochemical reactors (cells) for the manufacture of chemical products, including inorganic compounds (e.g., Cl_2 and concentrated NaOH), organic chemicals (e.g., adiponitrile), and purified metals (e.g., aluminum electrorefining). This aspect of electrochemical engineering deals with fundamental electrochemistry, heat and mass transfer, fluid flow, reactor configuration, scale-up, ancillary equipment for product purification, capital and operating costs analyses, and process optimization.

The configuration of an electrochemical reactor in an industrial process is geared to certain performance criteria. For example, in an organic electrochemical synthesis, reactors are designed to maximize product yield and current efficiency. A number of practical and general rules should be considered when deciding upon the design of an electrochemical reactor. The most general rules include (1) *simplicity of cell design and operation*, to lower capital and operating costs, minimize reactor down-time, and facilitate plant expansion; (2) *operational stability and reliability*, to ensure product purity and to enable automated operation; (3) *low cell cost and long lifetime*, to improve process economics; and (4) *safety of operation*, to minimize the dangers associated with electrical sparking and the possible production of explosive side-products during reactor operation.

26.3.1 CHARACTERIZING THE PERFORMANCE OF AN ELECTROCHEMICAL REACTOR

There are numerous ways of quantifying the energy efficiency and product selectivity of an electrochemical reactor, for both scale-up calculations and capital/operating cost analyses. Although products are formed at both the anode and cathode in such reactors, the cell performance is normally characterized in terms of the electrode where the desired product is generated.

1. Current efficiency: The current efficiency (CE) of an electrochemical reaction is defined as the ratio of the electric charge used in forming the product of interest to the total

26.3.1.1 Initial Design Experiments

The first step in designing an electrochemical reactor is to identify the electrode and electrolyte components and to determine baseline operating conditions. Data are collected using bench-scale batch or semicontinuous reactor experiments, with a single anode and cathode, to determine (1) the choice of electrode materials, (2) the nominal operating current density and voltage of the reactor, (3) the cell temperature and pressure, (4) the proper reactant concentration, (5) the type of solvent and the type and concentration of supporting electrolyte, and (6) the method and extent of electrolyte agitation. The following general rules assist in designing an electrochemical reactor.

Choice of Electrode Materials

The anode and cathode should be stable in the electrolysis medium, allow the desired oxidation/reduction reactions at the highest possible rates with minimal by-product formation, and be of reasonable cost. In actuality, the electrodes may corrode or undergo physical wear during reactor operation, which may limit their lifetime. Often, if an expensive electrode material is needed for a given reaction, it can be plated or physically coated on a less costly, inert, and electronically conducting substrate. Common anode and cathode materials are listed in Table 26.8.

The form and shape of the electrodes are tailored for the specific reactor configuration. Typical shapes include flat metal sheets, perforated or expanded metal grids, metal foams and meshes, and three-dimensional packed bed electrodes formed by stacking metal meshes, pressing catalyst powders, or by use of microporous carbon felts and cloths (three-dimensional electrodes are particularly attractive for low-current density reactions because the electrode surface per unit reactor volume can be made very large) [28].

Electrolysis Medium

The reaction medium normally consists of a solvent into which the electroactive species is dissolved. Often, a supporting electrolyte salt is added to increase the conductivity of the solution. The concentration of electroactive species should be made as high as possible in order to pass the maximum feasible current through the reactor. When choosing a solvent, one must consider such factors as proton activity (the required pH for the electrode reactions), dielectric constant (which affects ion conductivity), solubility of electrolyte salts and other inorganic/organic substrates, accessible temperature range, vapor pressure, viscosity, toxicity, and price. Water is the solvent of choice, based on its low cost, high-salt solubility, and lack of toxicity. The solubility of organic compounds in an aqueous electrolytic solution, however, may be limited, necessitating the use of other protic solvents (e.g., methanol or acetic acid). In some cases an aprotic solvent such as

TABLE 26.8
Common Electrode Materials

Cathodes	Anodes
High hydrogen overpotential metals such as Hg, Pb, Sn, Zn, and metal amalgams (Zn-Hg)	Precious metals on an inert substrate (e.g., Ti) including Pt, Ir, and Pt-Ir
Graphite and other forms of carbon (including porous carbon and carbon powders bound in an inert polymer matrix)	Graphite or other forms of carbon
Steels and stainless steels	PbO ₂ on Ti, Nb, or carbon
Coatings of low hydrogen overpotential metals (e.g., Ni, Ni/Zn, Ni/Al) on steel	Ni (for alkaline media)
Low hydrogen overpotential Raney metal powders pressed into a bed or bound in a polymer matrix	Dimensionally stable anodes such as mixed Ru-Ti oxide or Ti for Cl ₂ production or IrO ₂ on Ti for O ₂ generation
Precious metal powders (Pt, Pd, and Pt on carbon)	Magnetite (Fe _{3-x} O ₄)
Hastelloys (such as Bi-Mo-Fe and Ni-Mo-Cr alloys)	Conducting ceramics, such as Ti ₄ O ₇
TiO _x	

TABLE 26.10
Factors to Consider during Preliminary Reactor Design

Batch vs. continuous reactor operation
Single vs. multiple anodes and cathodes
Two-dimensional vs. three-dimensional electrode geometry
Monopolar vs. bipolar electrical connections
Divided vs. undivided
Open vs. closed cells
Static vs. moving electrodes
Finite interelectrode gap vs. zero gap or capillary cells

are to remain unmixed (to prevent unwanted side reactions at the electrodes, to isolate electrode products, and/or to prevent the formation of explosive or toxic mixtures), an ion-exchange membrane or some other kind of ionically conducting separator is placed between the anode and cathode chambers (the divided cell configuration). For simplicity of design and operation, most electrochemical reactors utilize flat plate electrodes.

Electrochemical reactors operate on DC current and, thus, high-voltage alternating current must be rectified and transformed before being sent to the cells. When the reactor contains multiple electrodes, electrical connections can be made using either a monopolar or bipolar design (see Figure 26.9). In a monopolar reactor, there are alternating anodes and cathodes, and both sides of each flat sheet electrode have the same polarity. External electrical contact is made to each electrode and the cell voltage is applied between each anode and cathode. In a bipolar design, electrical connections are made only to the two end electrodes, and the opposite faces of each electrode will have opposite polarities. Monopolar reactors require a low-voltage, high-current power supply, whereas the current is low and voltage high for a similar reactor geometry with bipolar connections. Although the electrical connection scheme is much simpler in a bipolar reactor, there may be leakage currents between cells (also known as bypass or shunt currents).

To minimize the cell voltage in an electrochemical reactor, the anode and cathode electrodes are placed as close as possible to minimize the resistance (IR) overpotential. Such voltage minimization is achieved in zero-gap and capillary cells [31, 32], by placing the electrodes directly adjacent to the membrane/diaphragm that separates the anode and cathode compartments. Figure 26.10 shows a bipolar capillary gap cell that was used in electro-organic processing [29], where

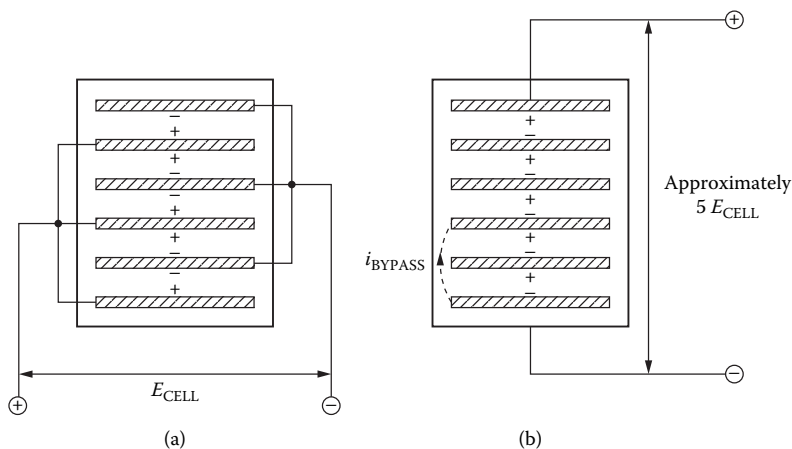


FIGURE 26.9 Electrical connections in multi-electrode cells. (a) Monopolar connection, (b) Bipolar connection (showing bypass current). From [30] (with kind permission from Springer Science and Business Media).

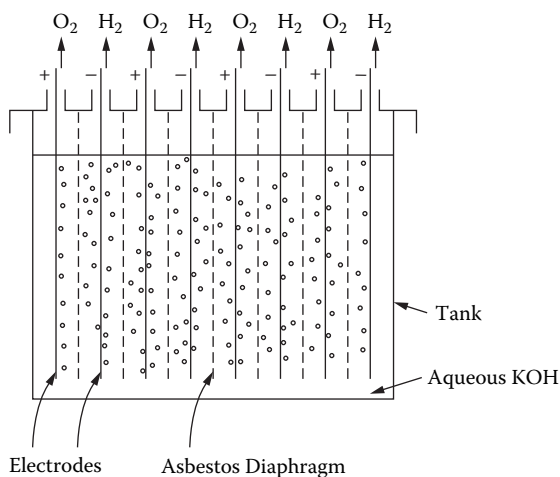


FIGURE 26.11 Tank cell with flat sheet electrodes for the electrolysis of water [30] (with kind permission from Springer Science and Business Media).

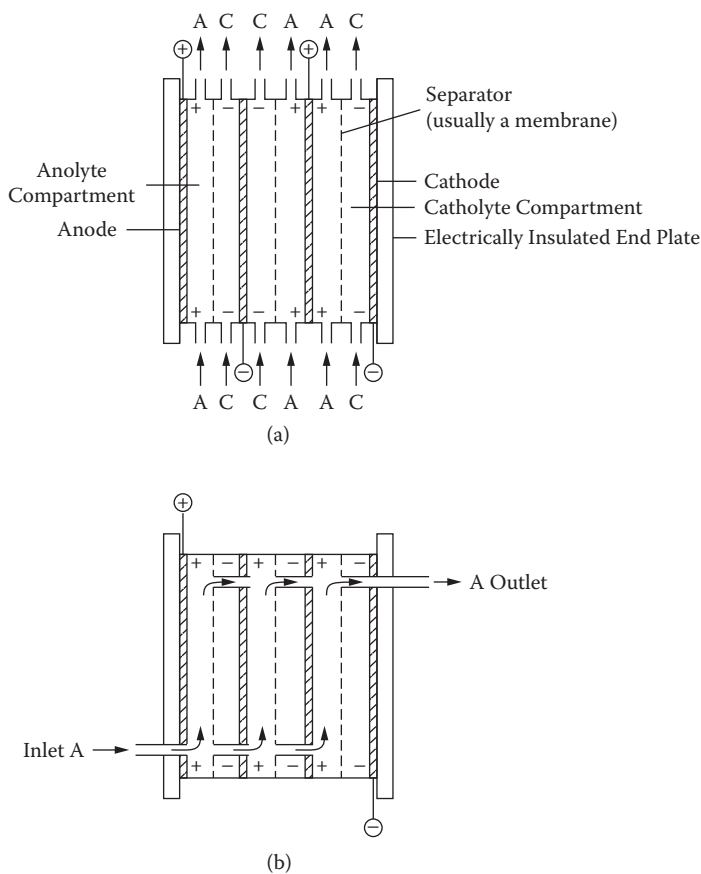


FIGURE 26.12 Plate and frame (filter-press) electrochemical flow cells. (a) Monopolar connection with external fluid flow manifolding. (b) Bipolar connections with internal manifolding [30] (with kind permission from Springer Science and Business Media).

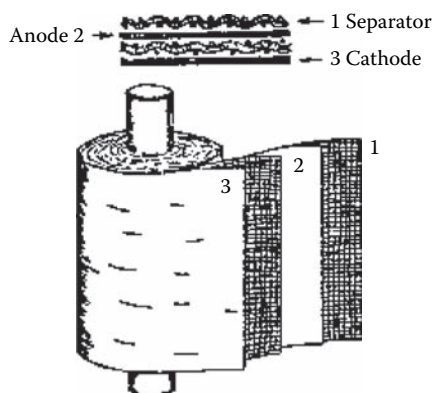


FIGURE 26.14 The Swiss-roll cell [30] (with kind permission from Springer Science and Business Media).

c to give a 5- to 6-mm thick sandwich that is rolled around an anode rod and inserted into a cylindrical container. Electrolyte flow is usually in the axial direction, through the mesh electrodes. Electrical connection to the rolled anode is provided by the anode rod, whereas a bolt through the side of the container makes electrical contact with the cathode. The close inter-electrode spacing (as small as 0.2 mm) minimizes the electrolyte IR drop and provides a high space-time-yield (a high electrode area per unit reactor volume), while the mesh spacers and electrodes promote turbulence and enhance mass transfer.

26.4 INORGANIC AND ORGANIC ELECTROCHEMICAL SYNTHESIS

26.4.1 INORGANIC PROCESSES

26.4.1.1 Aluminum Electrorefining

In our natural environment, metals are most stable in an oxidized state, e.g., Fe_2O_3 or Al_2O_3 . As a consequence, one step of metal ore refining is the reduction of the metal oxide to its zero oxidation state. An electrochemical reduction process, where the electrolysis medium is a molten salt, is preferred for very electropositive metals (e.g., aluminum, sodium, lithium, and magnesium) and for metal refining where the chemical route suffers from environmental problems.

The electrolytic production of aluminum is carried out in Hall-Heroult cells that have changed little in nearly 100 years [39]. The Hall-Heroult process operates at a high temperature (about 1250 K) and utilizes a molten salt electrolyte of alumina (Al_2O_3) and cryolite (Na_3AlO_2), with additives such as calcium fluoride and aluminum trifluoride. The cathode reaction is the reduction of Al^{3+} , with a consumable carbon anode. The overall reaction in the Hall-Heroult cell (shown schematically in Figure 26.15) is



The cells are strong steel boxes, lined with alumina (to act as a refractory), a thermal insulator, and carbon. The cathode is a liquid pool of aluminum that lies at the base of the cell, above a current collector consisting of a number of carbon blocks inlaid with steel bars. A frozen crust of electrolyte protects the cell housing from erosion. The cell has ports for the periodic addition of alumina through the crust, for the removal of Al metal, and an extractor to vent anode gases (mainly CO_2). As the carbon anode is consumed, it is lowered to maintain a constant anode/cathode gap (about 5 cm). In a typical plant for the production of 70,000 tons of Al per year, 200 Hall-Heroult cells, each 3 m \times 8 m in size with 15 m² of anode area, are arranged in series. The operating current density is

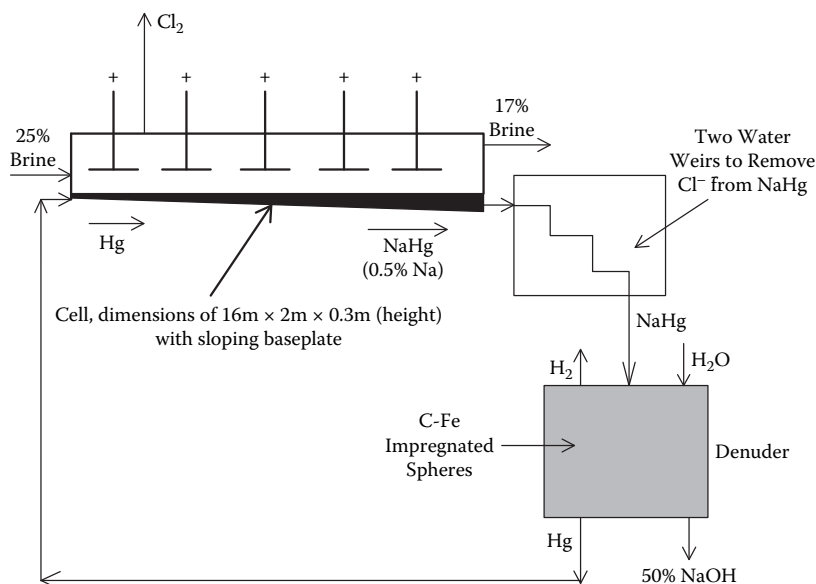


FIGURE 26.16 A schematic diagram of a mercury cell and the coupled Hg denuder [30] (with kind permission from Springer Science and Business Media).

A schematic diagram of a mercury cell is shown in Figure 26.16. The cell consists of a large shallow trough with a sloping base. Mercury flows along the bottom of the cell and acts as the cathode, while graphite or RuO_2 -coated titanium (dimensionally stable anode) is used as the anode, with an anode/cathode gap of about 1 cm. Brine at an NaCl concentration of about 25% and a temperature of 60°C enters the cell and is electrolyzed, exiting at a concentration of about 17%. Cl_2 exits the top of the cell and the sodium amalgam leaves the base, where it is first washed with water to remove NaCl and then enters a denuder where a concentrated (50%) NaOH solution is generated from the amalgam and the proper amount of water. Hydrogen gas is vented from the top of the denuder and the Hg is recycled to the cells. Mercury cells typically operate at a current density of 1.0 A/cm^2 , at an anode/cathode cell voltage of -4.4 V . Energy consumption is approximately 3150 kWh per ton of NaOH. Due to environmental concerns over the use of Hg, this cell design is being phased out in the U.S. and Japan and replaced by diaphragm and membrane cells.

In a diaphragm cell (shown schematically in Figure 26.17), an asbestos separator is deposited directly onto a steel cathode (or a cathode composed of steel with a nickel coating to lower the overpotential for hydrogen evolution) to physically inhibit mixing of the NaOH cathode product and brine feed (typically about 30%). The anode (graphite or dimensionally stable anode) is placed close to the cathode. A small fraction of the brine feed is allowed to diffuse through the asbestos diaphragm and H_2 and NaOH are formed on the opposite (cathode) side of the separator. The concentration of NaOH at the cathode is restricted to below 12%, otherwise OH ions will diffuse across the diaphragm and react with Cl_2 to form hypochlorite. A high pH brine also increases the rate of oxygen evolution (from water) at the anode, which lowers the current efficiency of the process and contaminates the Cl_2 gas. Also, the NaOH solution leaving the cathode contains some NaCl impurity. To synthesize a higher quality/higher concentration caustic product, water can be evaporated from the catholyte to give a 50% caustic solution. Removal of water also results in the crystallization of NaCl, but it is difficult to lower the salt concentration to $<1\%$. Of course this added purification step is energy intensive and adds to the overall cost of the process. Diaphragm cells operate at an elevated temperature of 60°C to 80°C , a current density of about 0.2 A/cm^2 , and a cell voltage of -3.45 V . When the water evaporation step to produce 50% caustic is added to the electrical energy for the electrolysis, a total of 3260 kWh is required per ton of NaOH.

energy-intensive (expensive) than traditional reformer processes (e.g., natural gas reforming), but the electrochemical route may be cost-effective for small-scale hydrogen production plants and/or where low-cost hydroelectric power is available. With the above two electrode reactions, the thermodynamic cell voltage is -1.23 V and independent of solution pH. Industrial water electrolyzers are designed to minimize the cell voltage. Typical cell configurations include tank cells, filterpress cells, and zero-gap cells utilizing a solid polymer electrolyte [28].

26.4.2 ORGANIC ELECTROCHEMICAL SYNTHESSES

In an organic electrochemical process, heterogeneous electron transfer reactions at the anode and cathode replace chemical oxidizing or reducing agents in solution. Electrons may be added or removed directly from an organic species at the electrode surface or the electron transfer reactions can generate anion or cation radicals, which initiate radical, electron-transfer, nucleophilic/electrophilic and acid/base reactions. The electrode potential influences the nature of the organic product or the electro-generated intermediate and its production rates. The field of organic electrochemical synthesis encompasses not only the oxidation or reduction of suitable functional groups, but also more intricate reactions, such as anodic or cathodic substitution, addition, coupling, cleavage of bonds, and polymerization [29, 41–44]. Thousands of organic compounds have been synthesized in the laboratory by means of electrochemical methods. In over 100 cases, the electrochemical process was sufficiently promising to build either pilot- or commercial-scale plants (see for example, Table 6.2 in [30] and Chapter 30, Table 2, in [29]). Several types of chemical transformations that can be performed electrochemically are presented in Table 26.11.

Electrochemical methods for the production of organic compounds are attractive for a number of reasons:

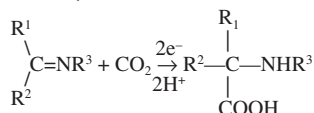
1. High yields and high selectivity are attained under appropriate electrolysis conditions; the desired compounds may be produced at a lower cost, as compared with traditional methods.
2. Electrical energy is used instead of chemical reagents (e.g., LiAlH_4 for organic reductions); accordingly, electrochemical processes may be less expensive with less pollution. Also, it may be possible to regenerate electrochemically spent redox agents in situ, so that large quantities of product can be produced from a small inventory of reagents.
3. Reactions occur at moderate temperature and pressure.
4. Oxidation and reduction reaction rates can be controlled by the current or electric potential.

Possible complications of an electrochemical route are listed below.

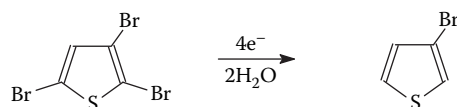
1. The rate of electron transfer at the anode or cathode may be slow for a complex reorganization of the substrate. This problem may be circumvented by: (a) three-dimensional packed, stacked, or fluidized bed electrodes with a high ratio of surface area to volume; (b) mediated reactions (a fast redox reaction at the electrode followed by a bulk solution homogeneous reaction with the organic substrate which consumes the electro-generated reagent); and (c) phase-transfer catalysts, where the active species is electro-generated, usually in an aqueous phase and then transferred by the catalyst into a nonaqueous phase where it reacts with a water-insoluble organic.
2. The high charge requirement of 96,487 coulombs (1 Faraday) per mole of electrons is a detriment for multiple electron transfer steps. Consequently, ideal candidates are (a) the synthesis of high value-added products, (b) compounds that cannot be made by traditional catalytic methods, and (c) organic compounds with a high molecular weight

TABLE 26.11 (Continued)
Examples of Organic Electrochemical Reactions

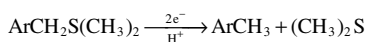
Carboxylation



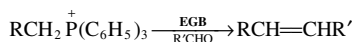
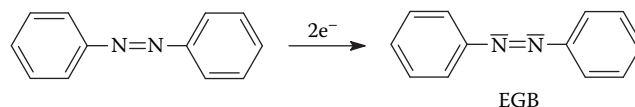
Selective Dehalogenation



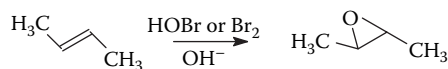
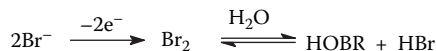
Desulfurization



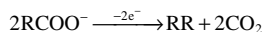
In Situ Electro-Generated Base (EGB)



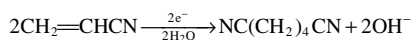
In Situ Electrogeneration of Oxidant and Base



Oxidative Coupling by Decarboxylation (Kolbe Reaction)



Electrohydrodimerization (Reductive Coupling)



(where the number of Faradays per unit mass of product is low even though the required number of Faraday's per mole is large).

- Solubilizing an inorganic supporting electrolyte salt in the organic starting material or dissolving the organic substrate in an aqueous electrolyte solution is often a problem. To address this problem, the following have been used: (a) nonreactive aprotic solvents; (b) a single or mixed polar organic solvent (such as an alcohol or alcohol/water mixture, which can solubilize the organic reactant); (c) special supporting electrolyte salts, such

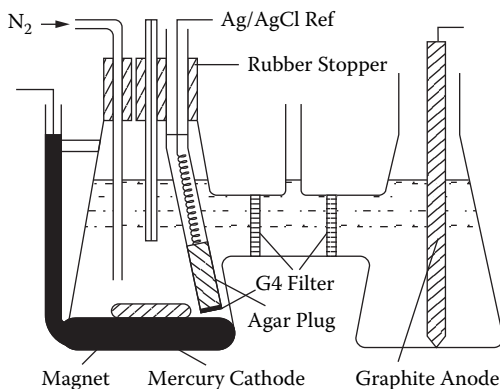


FIGURE 26.18 H-cell for semi-macroscopic electro-organic syntheses [48]. (Used with permission from the *Journal of Chemical Education*, Vol. 48, No. 2, 1971, 136–137; © 1971, Division of Chemical Education, Inc.)

26.4.2.1.2 Separator Materials

The separator for a divided electrochemical reactor should ideally be chemically inert and an electric insulator, with a porosity that allows for the facile movement of supporting electrolyte cations and/or anions but prevents the passage and intermixing of organic compounds. Inert porous materials, such as sintered glass, ceramic refractories, filter paper, nylon cloth, and porous plastic provide a barrier for inter-diffusion. Ion-exchange membrane separators (such as DuPont's Nafion[®] perfluorosulfonic acid cation-exchange membranes) generally provide effective barriers (see Section 26.6.3 and Table 26.15 for more information regarding ion-exchange membranes).

26.4.2.1.3 Electrode Materials

The proper choice of electrode materials is important when designing a cell [57]. A general discussion of electrode materials was presented in Section 26.3.1.1. Factors that must be considered include: the catalytic properties of the electrode material, substrate absorption, the presence of solution-phase impurities (often due to electrode corrosion/degradation when using water as the electrolyte solvent), the physical state of the electrode, and the electrode history [58]. Popular cathode materials for organic electrochemical reactions include:

Mercury—The very high hydrogen overvoltage of Hg is useful for organic reduction reactions in protic solvents, where competing H₂ gas electrogeneration must be suppressed. The liquid state of mercury places certain restrictions on the design of such electrochemical cells (see Figure 26.18). Environmental concerns over the toxicity of mercury also limit its use.

Lead and Cadmium—The hydrogen overvoltage on Pb and Cd is high, and they are easy to work mechanically. For many reactions, a lead or cadmium cathode yields the same chemical products as mercury.

Tin—Electrodes composed of Sn are used mostly for the reduction of nitro compounds.

Nickel and Platinum—These two metals (in the form of Raney nickel and Pt-black) are used for electrocatalytic organic hydrogenation reactions (i.e., the electrochemical generation of hydrogen on the catalytically active, high surface area cathode followed by the chemical reaction of adsorbed hydrogen with the organic substrate).

Aluminum and Iron (Steel)—These metals are widely used in large-scale electro-organic processes, due primarily to their low cost.

The choice of anode material for electro-organic reactions is limited, due to anodic dissolution of most metals. The most common materials are

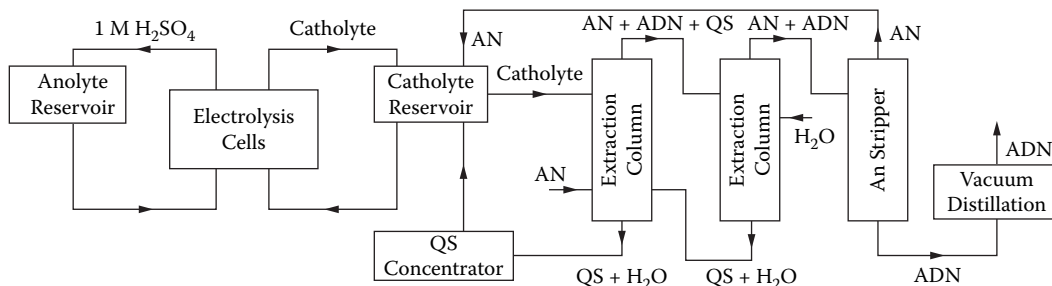


FIGURE 26.19 Schematic diagram of the adiponitrile process flowsheet. AN = acrylonitrile, ADN = adiponitrile, QS = quaternary ammonium salt [30] (with kind permission from Springer Science and Business Media).

26.4.3 MONSANTO'S ELECTROHYDRODIMERIZATION PROCESS

In 1965, the Monsanto Company started production of adiponitrile from acrylonitrile via an electrochemical route [Equation (26.113)]. Adiponitrile was then converted to either adipic acid or hexamethylenediamine by chemical means; these two compounds are reactants in the production of nylon 66.



The key to this process [63, 64] was the addition of a quaternary ammonium salt (tetraethylammonium p-toluenesulfonate or tetraethylammonium ethylsulphate) to the reaction medium, which increased the solubility of acrylonitrile in the aqueous electrolyte and generated an aprotic organic layer on the cathode surface that inhibited the synthesis of propionitrile by-products (formed by the simple reduction of acrylonitrile).

Initially, divided electrochemical cells were employed (24 cells, each with 16 anode/cathode pairs in a bipolar filterpress design), with a lead cathode, a lead-silver anode, and a cation-exchange membrane separator. Due to the low conversion rate per pass, the cells were operated in a batch recycle mode with an external catholyte reservoir. A fraction of the reservoir was bled continuously into an extraction plant and fresh acrylonitrile was added to the reservoir. In the downstream extraction plant, quaternary ammonium salt supporting electrolyte and unreacted acrylonitrile were recovered and recycled, and adiponitrile was isolated and purified. Adiponitrile and acrylonitrile were extracted from the aqueous electrolyte in a sieve tray column by addition of acrylonitrile starting material. The organic phase from this unit was washed with water to remove the last traces of supporting electrolyte salt, and the adiponitrile and acrylonitrile were then separated by distillation. The final stage of the process was a vacuum distillation purification of adiponitrile. A schematic flowsheet is shown in Figure 26.19 [30].

During the 1970s, both a larger plant and a second plant were built. These expansions employed a second-generation, undivided cell design, with an emulsified reaction medium composed of 7% acrylonitrile in an aqueous solution of 15% disodium hydrogen phosphate with a low concentration (0.4%) of a quaternary ammonium salt. More information on the Monsanto adiponitrile process are found in [28–30, 42 (Part III), 65, 66].

26.4.4 ELECTROCATALYTIC REDUCTION (HYDROGENATION) REACTIONS IN A SOLID POLYMER ELECTROLYTE (PROTON EXCHANGE MEMBRANE) REACTOR

Many electro-organic reduction reactions are performed using an aqueous reaction medium (the H atoms in water supply the necessary hydrogen for the reaction) and a high hydrogen overpotential cathode such as lead or cadmium to minimize unwanted H_2 gas evolution (from the electro-reduction

cathode chamber and flows past the backside of the cathode. Ion (proton) conductivity between the anode and cathode occurs through the wetted cation-exchange membrane, so that pure organic and distilled water (or H_2 gas) can be circulated in the cathode and anode chambers, respectively. In this regard, the SPE reactor represents a significant advancement in electrochemical reactor design since inorganic supporting electrolyte salts are not needed (such salts would have to be removed from the reaction medium downstream from the reactor, often with considerable difficulty). The close proximity of the anode and cathode on an MEA (the electrodes are separated by the ion-exchange membrane, which is at most 200 μm thick) and the high ion-exchange capacity of the cation-exchange membrane ensures facile H^+ transport between the anode and cathode.

Solid polymer electrolyte reactors have been examined previously for oxidation and organic electrochemical reduction of organic compounds [56, 72–78]. Ogumi and co-workers studied the electrochemical hydrogenation of nitrobenzene to aniline using a Cu-Pt cathode/Nafion membrane/Pt anode MEA [76] and the reduction of cyclo-octene, diethyl maleate, ethyl crotonate, and n-butyl methacrylate (dissolved in either ethanol, diethyl ether, or n-hexane) with MEAs composed of Pt, Au, or Au-Pt cathode layers deposited onto the surface of a Nafion membrane [72]. In addition, electrochemical reduction of edible oils (such as soybean or cottonseed) results in a quite different product [79].

The high temperature of a chemical catalytic hydrogenation process promotes the undesirable *cis*-to-*trans* isomerization of fatty acid double bonds; recent studies have shown that the injection of *trans* fatty acids in edible oils increases cholesterol blood levels and contributes to coronary heart disease. The low-temperature electrochemical hydrogenation scheme reduces such isomerization.

A schematic diagram of the SPE oil hydrogenation reactor and the principle reactions associated with electrochemical H_2 generation and oil hydrogenation are shown in Figure 26.20. The key component of the reactor is an MEA, composed of either RuO_2 or Pt/C powder (for the anode) and either Pt-black or Pd-black powder (for the cathode) that are hot-pressed as thin films onto the opposing surfaces of a cation-exchange membrane. During reactor operation at a constant applied current, water or H_2 gas is back-fed to the RuO_2 anode, where it is oxidized electrochemically to produce H^+ . Protons migrate through the membrane under the influence of the applied electric field and contact the Pt or Pd cathode where they are reduced to atomic and molecular hydrogen. Oil is circulated past the backside of the cathode and unsaturated triglycerides react with the electro-generated hydrogen species. The SPE reactor was operated successfully with a low anode/cathode voltage drop for a variety of oil feeds at a constant temperature between 50°C and 80°C and an applied current density between 0.10 and 0.490 A/cm^2 . Partially hydrogenated oil products had a lower percentage of total *trans* isomers (6% to 10%) and a somewhat high saturated fat (stearic acid) content, as compared to the products from a traditional chemical catalytic reaction scheme [80].

Various factors that might affect the oil hydrogenation current efficiency were investigated [81, 82], including the type of cathode catalyst, catalyst loading, the cathode catalyst binder loading, current density, and reactant flow rate. The current efficiency ordering of different cathode catalyst powders was found to be $\text{Pd} > \text{Pt} > \text{Rh} > \text{Ru} > \text{Ir}$ (this is the same order as for chemical reactions). Oil hydrogenation current efficiencies with a Pd-black cathode decreased with increasing current density and ranged from about 70% at 0.050 A/cm^2 to 25% at 0.490 A/cm^2 (current efficiencies less than 100% were attributed solely to H_2 gas evolution at the catalytic cathode). The optimum cathode catalyst loading for both Pd and Pt was 2.0 mg/cm^2 . When the oil feed flow rate was increased from 80 to 300 mL/min , the oil hydrogenation current efficiency at 0.10 A/cm^2 increased from 60% to 70%. A high (70%) current efficiency was achieved at 80 mL/min by inserting a nickel screen turbulence promoter into the oil stream. The concentration of *trans* isomers ranged from about 2% (with a Pt cathode) to about 9% with Pd-black. When a second metal (Ni, Cd, Zn, Pb, Cr, Fe, Ag, Cu, or Co) was electrodeposited onto a Pd-black powder cathode, substantial increases in the fatty acid selectivities were observed (due presumably to changes in oil adsorption/desorption on the catalyst surface) [82].

TABLE 26.12
Components and Operating Conditions of Various Plating Baths

Metal	Plating Bath Composition	Operating Conditions (temp., curr. density, curr. plating efficiency)	Additives	Anode
Cu	CuSO ₄ (200–500 g/L) H ₂ SO ₄ (25–50 g/L)	20°C –40°C 20–50 mA/cm ² 95%–99% current efficiency	Dextrin, gelatin, S-containing brighteners, sulphonic acids	P-containing rolled Cu
Ni	NiSO ₄ (250 g/L) NiCl ₂ (45 g/L) H ₃ BO ₃ (30 g/L)	40°C –70°C 20–50 mA/cm ² pH 4–5 95% current efficiency	Coumarin, saccharin, benzenesulphonamide, acetylene derivatives	Ni
Ag	KAg(CN) ₂ (40–60 g/L) KCN (80–100 g/L) K ₂ CO ₃ (10 g/L)	20°C –30°C 3–10 mA/cm ² 99% current efficiency	S-containing brighteners	Ag
Sn	SnSO ₄ (40–60 g/L) H ₂ SO ₄ (100–200 g/L)	20°C –30°C 10–30 mA/cm ² 90%–95% current efficiency	Phenol, cresol	Sn
Zn	NH ₄ ZnCl ₃ (200–300 g/L) NH ₄ Cl (60–120 g/L)	25°C 10–40 mA/cm ² pH 5 98% current efficiency	Dextrin, organic additives	Zn
Cr	CrO ₃ (450 g/L) H ₂ SO ₄ (4 g/L)	45°C –60°C 100–200 mA/cm ² 8%–12% current efficiency	Complex fluorides to increase current efficiency	Pb-Sb or Pb-Sn coated with PbO ₂

electric conductivity of the plating solution; (3) complexing agents (such as cyanide, hydroxide, and sulphamate ions) to suppress unwanted reactions at the plating surface; and (4) a variety of organic additives, including brighteners (e.g., aromatic sulphones or sulphonates, thiourea, and coumarin for nickel plating), levelers, structure modifiers, and wetting agents that improve the morphology and uniformity of the electroplate thickness, as well as the physical appearance, and physical properties of the deposit.

Most electroplating processes use a DC power supply and cells of simple geometry. Where possible, the anode in an electroplating cell is made from the same metal as that being plated at the cathode so that the concentration of the metal ion in solution remains nearly constant during the plating processes (so long as the anode and cathode current efficiencies are matched). Electrolyte stirring is accomplished by either moving the cathode through the plating bath or by pumping the electrolyte over the cathode surface. Representative examples of plating conditions are listed in Table 26.12 [30].

Electroplating is rarely used for coatings of thickness >75 μm . The upper limit on deposit thickness is governed by cost and time factors, the generation of unacceptably high internal stresses in the deposit, and/or irregular deposit growth. Most plating processes operate at a current density between 10 and 70 mA/cm² and are completed in a few seconds to several hours.

The key factors that control the rate of electrodeposition and the structure, physical properties, uniformity, and composition of electrodeposited metals and alloys are (1) thermodynamics (where the electric potential is based on the standard electromotive series); (2) electrode kinetics (which may vary with the structure of the electrodeposit); and (3) mass transport (which is important at high current densities, where the delivery of reactant to the cathode surface affects the local deposition rate and the structure of the deposit).

The normal goal in plating is to achieve a uniform distribution of the metal or alloy deposit, regardless of the geometry of the system. For the deposition of a single metal, the thickness of

2. *Secondary current distribution* [85, 86]. Here, mass transfer effects are not controlling, but reaction kinetics are considered because of a non-negligible electrode polarization (i.e., electrode reactions that require an appreciable surface overpotential to sustain a high reaction rate). Once again, Laplace's Equation (Equation [26.120]) is solved for the potential distribution, but the boundary condition for Φ on the electrode surface ($y = 0$) is given by

$$-\kappa \nabla \Phi = f(\eta_s) \text{ at } y = 0 \quad (26.122)$$

where $f(\eta_s)$ denotes a current density/voltage electrode kinetic expression (such as the Butler-Volmer electrochemical rate equation given by Equation (26.45) in Section 26.2.2 or simplified versions thereof) and η_s (the surface overpotential) is defined as $V - \Phi$ (where V is the imposed potential of the electrode and Φ is the electric potential in solution adjacent to the electrode). For example, when the surface overpotential is sufficiently small, the Butler-Volmer kinetic equation reduces to a linear form and Equation (26.122) is written

$$-\kappa \frac{\partial \Phi}{\partial y} = (\alpha_c + \alpha_a) \frac{i_o F}{RT} \eta_s \text{ at } y = 0 \quad (26.123)$$

where α_a and α_c are the anodic and cathodic transfer coefficients, with $\alpha_a = (1 - \beta)n$ and $\alpha_c = \beta n$. A boundary condition expression also can be generated using the linear Tafel equation to relate i and η_s (when η_s is large). The secondary current distribution depends on the same electrode geometry conditions as the primary current distribution, but it also depends on electrode kinetic parameters (such as the transfer coefficient, α , and the exchange current density i_o in Equation (26.123)). The secondary current distribution on an electrode is finite at the electrode edges and is more uniform than the primary current distribution, as can be seen in Figure 26.21 for a rotating disk.

The uniformity of the secondary current distribution has been related to the value of the Wagner (Wa) number [87], which expresses the ratio of the polarization resistance at the electrode-electrolyte interface to the ohmic resistance of the electrolyte:

$$Wa = \frac{\kappa \left(\frac{\partial \eta_s}{\partial i} \right)_{i_{av}}}{L} \quad (26.124)$$

where $d\eta_s/di$ is the slope of the electric potential/current density curve at the average current density on the electrode (e.g., for Tafel kinetics, $\partial \eta_s / \partial i$ is given by the cathodic Tafel slope) and L is a characteristic electrode length. When Wa becomes large, i.e., when the kinetic polarization resistance dominates, the current distribution on the electrode becomes perfectly uniform and independent of geometry. An example of the secondary current distribution near the leading edge of a planar electrode in a parallel plate flow channel and the effect of Wa on the ratio $(i - i_\infty)/i_\infty$ (where i_∞ is the current density far from the electrode's leading edge) is shown in Figure 26.22 [33].

3. *Tertiary current distribution*. This method of analysis applies to those systems where there is significant mass transport and electrode polarization effects. Electrode kinetics is considered, with electrode surface concentrations of reactant and/or products that are no longer equal to those in the bulk electrolyte due to finite mass transfer resistance. The analysis of tertiary current distributions is complex, involving the solution of coupled

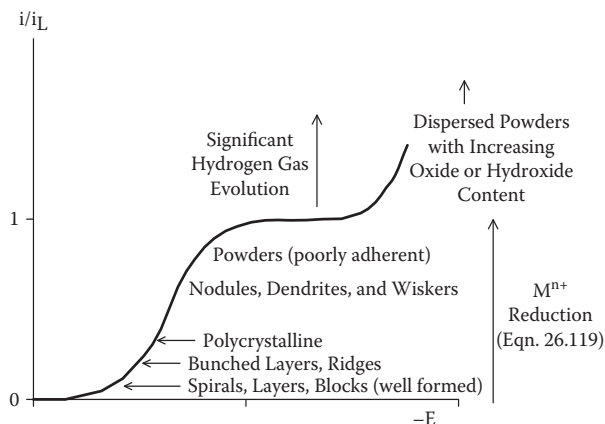


FIGURE 26.23 Variation in metal electrodeposit structure as a function of the applied current density and limiting current density. Figure from [92] (copyright Elsevier 1994).

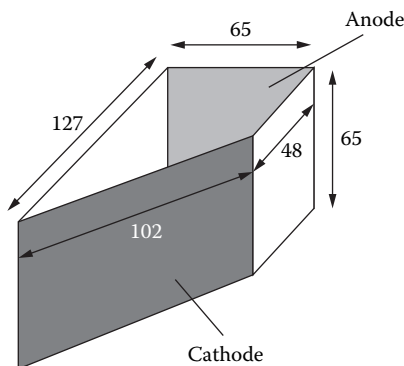


FIGURE 26.24 The classical Hull cell for electroplating. All dimensions are in mm. Figure from [94] (copyright Elsevier 1994).

current distribution in an impinging jet cell [97] and the effects of current density, electrolyte composition, electrolyte velocity, and nozzle height on the metal-thickness distribution [98].

The plating rate and the quality of the electrodeposit can also be increased by using a laser beam during the plating process. Such a technique has enhanced plating rates by factors of 1000 for nickel, copper, and gold [99, 100]. The elevated rates have been attributed to localized heating of the substrate by the laser beam [101]; higher temperatures increase the electrodeposition reaction rates when mass transfer is not controlling. Figure 26.23 shows that better quality electrodeposits are formed at current densities well below the mass transfer limiting current density. With a laser-enhanced electroplating technique, finely detailed electrodeposits can be created, with plated spots as small as 4 μm in diameter [102] (such plating precision is important when fabricating micro-circuitry and electronic devices). More recently, laser-enhanced plating, combined with an impinging jet has achieved localized high-speed plating of metal spots and fine lines of high quality [103]. In addition to increasing convective mass transport, the electrolyte jet limits the region of plating and also acts as a light pipe for the laser beam.

26.5.3 ELECTROLESS PLATING

During a normal electrolytic metal deposition process, the electrons required for the reduction of the metal ions are supplied by an external current source. In an electroless deposition process, the

TABLE 26.13
Compositions and Operating
Conditions of Electroless Plating Baths

Plating Bath	Bath Composition
Acid nickel	Nickel chloride: 20 g/dm ³ Sodium hypophosphite: 20 g/dm ³ Sodium acetate: 10 g/dm ³ Sodium succinate: 15 g/dm ³ pH: 4.5 Temperature: 93°C
Alkaline nickel	Nickel chloride: 30 g/dm ³ Sodium hypophosphite: 10 g/dm ³ Ammonium citrate: 65 g/dm ³ Ammonium chloride: 50 g/dm ³ pH: 8–10 Temperature: 90°C
Copper	Copper sulphate: 12 g/dm ³ Formaldehyde: 8 g/dm ³ Sodium hydroxide: 15 g/dm ³ Rochelle salt: 14 g/dm ³ EDTA: 20 g/dm ³ pH: 11 Temperature: 25°C

26.5.4 ALLOY PLATING

During alloy plating, more than one metal is deposited on the electrode. The relative importance of current distribution and mass transfer may differ for different metals and current densities; a non-uniform current density may lead to an electrodeposit of varying thickness during metal deposition and nonuniform partial currents lead to variations in alloy composition [94,105]. Thus, electroplating of specialty alloys requires tight control of the plating operating conditions, including the electrolyte bath composition (the ratio of metal ion concentrations in solution), the plating temperature, the current density, and the electrolyte flow conditions. For example, when nickel and iron are simultaneously plated onto a rotating disk cathode from a $\text{NiCl}_2/\text{FeCl}_2/\text{H}_3\text{BO}_3/\text{NaCl}$ bath at pH 3 and 25°C, the alloy composition and current efficiency for electrodeposition are dependent on the plating current density i_p and the electrolyte agitation rate, as shown in Figures 26.25 and 26.26 [106]. In this system, iron deposition is mass transfer controlled and Ni^{2+} reduction is kinetically controlled. The loss in current efficiency (<100%) is due to H_2 evolution, which is mass transfer controlled and independent of the electrode potential in the voltage regime where Ni and Fe co-deposit.

Some examples of alloy plating baths and plating conditions are listed in Table 26.14 [30]. For additional information on alloy as well as pure metal electrodeposition, see [92, 94, 105, 107–112].

26.5.5 ELECTROCHEMICAL METAL REMOVAL PROCESSES

Electrochemical metal removal processes have been developed and utilized by industry for a variety of different applications. Electropolishing as an industrial finishing operation was first demonstrated by Jaquet in 1930 [113]. Metals such as aluminum, steel, brass, copper, and silver/nickel alloys are anodized to produce a highly reflective mirror finish. The surface to be polished is the anode with a current density in the range of 0.100 to 0.800 A/cm². The electrolyte is typically phosphoric

TABLE 26.14
Alloy Plating Bath Compositions and Operating Conditions

Alloy	Plating Bath Composition	Operating Conditions (temp., curr. density, metal plating current efficiency)	Anode
70% Cu—30% Zn (brass)	$K_2Cu(CN)_3$ (45 g/L)	40°C–50°C	Brass
	$K_2Zn(CN)_4$ (50 g/L)	5–10 mA/cm ²	
	KCN (12 g/L)	60–80% current efficiency	
	sodium tartrate (60 g/L)		
40% Sn—60% Cu (bronze)	$K_2Cu(CN)_3$ (40 g/L)	60°C–70°C	Bronze or mixture of Sn and Cu
	Na_2SnO_3 (45 g/L)	20–50 mA/cm ²	
	NaOH (12 g/L)	70–90% current efficiency	
	KCN (14 g/L)		
65% Sn—35% Ni	$NiCl_2$ (250 g/L)	60°C–70°C	Separate Ni and Sn plates
	$SnCl_2$ (50 g/L)	10–30 mA/cm ²	
	$NH_4F \cdot HF$ (40 g/L)	97% current efficiency	
	NH_4OH (30 g/L)		
80% Ni—20% Fe	$NiSO_4$ (300 g/L)	50°C–70°C	Ni + Fe
	$FeSO_4$ (100–200 g/L)	20–50 mA/cm ²	
	H_3BO_3 (45 g/L)	90% current efficiency	
	NaCl (30 g/L)		
	$NiCl_2$ (0.2 M)	25°C	
	$FeCl_2$ (0.005 M)	5–30 mA/cm ²	
	H_3BO_3 (0.4 M)	pH 3	
	NaCl (0.5 M)	70–97% current efficiency	

Large volumes of electrolyte are circulated past the metal anode surface at very high velocities (typically 9 to 60 m/sec) in order to remove quickly dissolving metal ion product (so there is no precipitation of metal hydroxide salts on the anode) and heat generated during the machining process. Normally a highly conductive electrolyte with an inexpensive salt (e.g., NaCl or $NaNO_3$) is employed with small interelectrode spacing (0.10 to 1.5 mm). Complex features and shapes, including fine holes, angled holes, engine casting, and turbine components, can be produced with great precision and reproducibility. In contrast to conventional mechanical metalworking techniques, electromachining leaves the metal without scratches, unwanted sharp edges, and burrs. In addition, the machined surface is almost free of all induced stresses. More recently, electromachining has been used in the electronics industry to drill fine holes (0.25 to 0.4 mm in diameter) in tough cast alloys and to fabricate groove patterns and holes in thin metal foils. A review of such micromachining operations in the electronic industry has been compiled by Datta and Romankiw [116].

26.6 ENVIRONMENTAL CLEAN-UP PROCESSES

Effluent and waste water treatments are of growing importance due to legislation that limits toxic discharge, plus the need to recycle and reuse raw materials. Electrochemical processes are inherently less polluting because oxidation and reduction reactions at the electrodes involve “clean” electrons, as opposed to chemical oxidizing and reducing agents where the spent reagents themselves may be toxic. Several useful electrochemical methodologies have been developed to treat streams containing dissolved metal ions and/or organics, including the removal and recovery of trace metal ions in solution, the destruction of organics via electrochemically generated oxidants, and water purification by electrodialysis membrane processes.

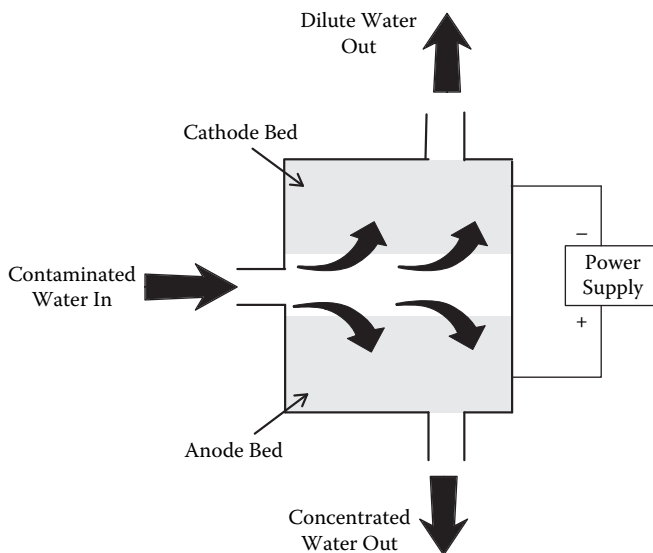


FIGURE 26.27 Schematic diagram of a flow-through packed bed reactor for the removal of dissolved metal ions.

flow-through particle bed electrode reactors have been mathematically modeled in order to better understand and improve the metal ion removal rate (see 4, Chapter 22). A schematic diagram of a flow-through particle bed electrode reactor is shown in Figure 26.27.

In this reactor, the feed solution enters via a central channel between the anode and cathode beds and then flows in the upward and downward vertical directions (where the majority of the solution passes through the porous cathode). When the cathode bed is filled to capacity with deposited metal, the polarity of the electrode beds is reversed and the metal is electrochemically etched into a small liquid volume to create a concentrated solution. The longer the contact time of the metal-laden solution in the porous cathode, the greater the extent of metal removal (where the contact time is inversely proportional to the catholyte flow rate and directly proportional to the cathode bed thickness). To maximize the energy efficiency for metal removal, the entire bed should operate at or near the metal reduction limiting current density, but this is difficult to achieve because of unwanted hydrogen gas evolution. The relevant differential equations are solved to obtain the metal ion concentration, electric potential, and current density distributions in the cathode bed are [125]

1. A material-balance relationship:

$$\frac{dC}{dy} = -\frac{ak_d C}{v} \quad (26.131)$$

2. A charge-balance equation:

$$\frac{di}{dy} = -nFak_d C = nvF \frac{dC}{dy} \quad (26.132)$$

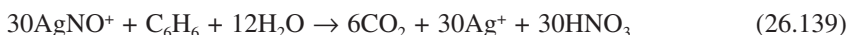
3. Ohm's law in solution:

rate divided by the cross-sectional bed area available for flow (width \times length \times porosity) must be equal to the superficial fluid velocity.

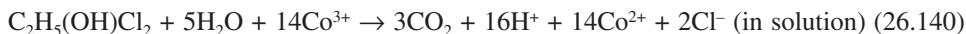
26.6.2 ELECTROCHEMICAL DESTRUCTION OF ORGANICS

Anodic oxidation processes can effectively destroy toxic organic compounds in aqueous waste streams. The oxidation reaction may occur directly at the anode or indirectly in solution via an oxidizing agent that is electrochemically generated, reacts homogeneously in the bulk solution with the organic, and then is regenerated at the anode [124]. For many organic-laden waste streams, the electrolyte conductivity is low and a supporting electrolyte salt must be added (this salt may have to be removed eventually from the waste stream). It may also be necessary to add a solvent (e.g., water or alcohol) to the stream to increase the solubility of the electrolyte salt.

The electro-oxidation of various organic compounds directly at an anode (e.g., the oxidation of phenol to CO_2 in water) has employed either a Pt or SnO_2 anode [126–128]. SnO_2 is often preferred to minimize organic intermediates and to reduce the total organic carbon content in the water solution. Farmer and co-workers [129], studied the indirect oxidation of organic compounds using Ag^{2+} or Co^{3+} as the oxidizing agent. With HNO_3 , the electrochemical oxidation of Ag^+ to Ag^{2+} forms an AgNO_3^+ complex. This complex then reacts with an organic pollutant (such as ethylene glycol, benzene, or a chlorinated hydrocarbon) to produce CO_2 . For benzene destruction with AgNO_3^+ , the following oxidation reaction occurred:



By re-oxidizing spent Ag^+ at the anode, the organic oxidizing agent is regenerated continuously in the electrochemical reactor, thus minimizing the amount of Ag^{2+} required to destroy the organic compound. Unfortunately, for most organic electrochemical degradation reactions (including Equation (26.139)), the total charge required to oxidize the pollutant to CO_2 is very large (30 Faraday's per mole of benzene for the above reaction, where one Faraday is the charge equivalent of one mole of electrons). Thus, a reactor for organic destruction to a low-molecular-weight innocuous compound such as to CO_2 must operate at a very high current density (which may generate secondary reactions at the anode and lower the current efficiency for organic oxidation) and the electrical cost per pound of degraded organic contaminant is usually high. Whereas Ag^{2+} cannot be used to degrade chlorinated hydrocarbons (due to the formation of insoluble AgCl), Co^{3+} is an effective oxidizing agent for many chlorinated hydrocarbons such as 1,2-dichloro-2-propanol [130]. The relevant homogeneous oxidation and heterogeneous electrochemical reactions for this organic pollutant are



Kaba et al. [131] employed a $\text{Ce}^{3+}/\text{Ce}^{4+}$ redox couple and ultrasonic solution agitation to degrade human biomass waste using either a Pt or PbO_2 anode and a 12M H_2SO_4 electrolyte. The total organic carbon content of the electrolyte decreased by a factor of about 3 and the total nitrogen dropped by a factor of 2 after a 70-hour electrolysis.

Since electrochemical oxidation of organics does not yield a useful product, this technology has been driven more by governmental regulation rather than a favorable return on investment. Hence, the development of electrochemical processes for organics destruction has not progressed beyond laboratory-size or pilot-plant reactors.

TABLE 26.15
Commercially Available Cation-Exchange and Anion-Exchange Membranes

Membrane Manufacturer	Chemical Composition	Ion-Exchange Capacity (mmol/g)
Cation-exchange membranes	Sulfonated polystyrene	2.4
CMV (Asahi Glass Co. Ltd.)	Carboxylated perfluorinated polymer	0.9
Flemion (Asahi Glas Co. Ltd.)	Sulfonated styrene/cross-linked with	1.4
K101 (Asahi Chemical Industry Co., Ltd.)	divinyl benzene	1.5
R-5010-L (Pall RAI, Inc.)	Sulfonated low density polyethylene	0.91
Nafion (DuPont de Nemours and Co., Inc.)	Perfluorosulfonic acid	2.0
CL-25T (Tokuyama Soda Co. Ltd)		
Anion-Exchange Membranes		
A 111 (Asahi Chemical Industry, Co. Ltd)	Styrene/divinylbenzene butadiene	1.2
AMV (Asahi Glass Co., Ltd)		1.9
103QZL386 (Ionics Inc.)		2.1
ACM (Tokuyama Soda Co. Ltd)		1.5

Clearly, the most important components of an electrodialysis process are the anion- and cation-exchange membranes. Ion-exchange membranes should possess (1) high permselectivity, where the membrane is highly permeable to counterions and impermeable to co-ions; (2) low electrical resistance, so that the transmembrane flux of ions will be high for a given electric potential driving force; (3) good mechanical strength and dimensional stability (i.e., low swelling/shrinkage); and (4) high chemical stability (since the membranes are routinely exposed to acid and alkali solutions as well as various oxidizing agents).

For cation-exchange membranes, one of the following charged moieties is normally attached to the polymer: $-\text{SO}_3^-$, $-\text{COO}^-$, $-\text{HPO}_2^-$, $-\text{AsO}_3^{2-}$, or $-\text{SeO}_3^-$, whereas an anion-exchange membrane will contain one of the following: $-\text{NH}_3^+$, $-\text{RNH}_2^+$, $-\text{R}_3\text{N}^+$, $=\text{R}_2\text{N}^+$, $-\text{R}_3\text{P}^+$, or $-\text{R}_2\text{S}^+$. These ionic groups have significant effects on the selectivity and ionic conductivity of the ion-exchange membranes. For example, sulfonic acid groups (SO_3^-) are completely dissociated over the entire pH range, but carboxylic acid groups (COO^-) are undissociated in acid solutions (at a pH <3). Similarly, quaternary ammonium groups ($-\text{R}_3\text{N}^+$) in anion-exchange membranes are completely dissociated over the entire pH range, whereas primary ammonium moieties ($-\text{NH}_3^+$) are only weakly dissociated. Table 26.15 lists some commercially available cation- and anion-exchange membranes and their associated ion-exchange capacities (with units of mmol per gram of dry membrane).

The permselectivity of an ion-exchange membrane is governed by the solubility of counterions and coions at the membrane-solution interfaces and by transport processes in the membrane. One approach to describe mathematically counterion and co-ion solubility in an ion-exchange membrane is Donnan equilibrium theory [138]. For a cation-exchange membrane (with negatively charged fixed ions of concentration X) immersed in a single 1:1 salt solution (at a concentration C^b), the counterion concentration inside the membrane (C_+) is given by

$$C_+ = \frac{X}{2} + \left[\left(\frac{X}{2} \right)^2 + \left(\frac{f_+^b}{f_+^m} C^b \right)^2 \right]^{1/2} \quad (26.142)$$

where f_{\pm}^b is the mean molar activity coefficient of the salt in the external bulk solution and f_{\pm}^m is the activity of salt inside the membrane. A similar relationship can be derived for the concentration of anions in an anion-exchange membrane. Once the counterion concentration in the membrane is known, the coion concentration is computed from the macroscopic electroneu-

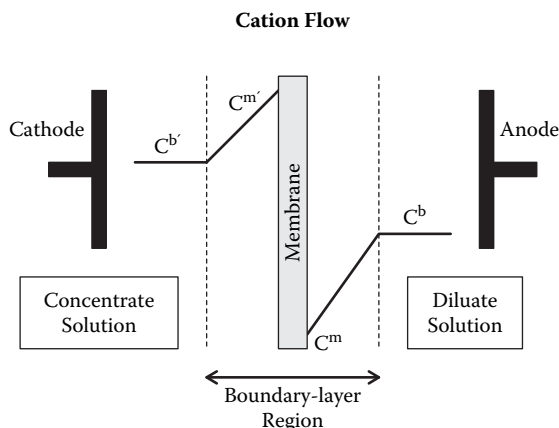


FIGURE 26.29 Schematic diagram of cation concentration profiles on the diluate and concentrate sides of a cation-exchange membrane during current flow.

Another structure/function transport model, often referred to as the “capillary” or “electrokinetic” model, predefines the microlevel structure of an ion-exchange membrane as an array of pores of known dimensions with a specified distribution of ion-exchange sites on the pore walls. Equations describing solute and solvent transport and theories for molecular-level ion/solvent and ion–membrane interactions are then generated, based on this pore structure [151]. The fundamental transport equation for the molar flux of ionic species is the Nernst-Planck equation

$$N_i = -\frac{z_i F D_i C_i}{RT} \nabla \Phi - D_i \nabla C_i + v C_i \quad (26.144)$$

When the radius of the membrane pores is of the same order of magnitude as the Debye screening length, electroneutrality within the pores is no longer valid. A non-zero space charge produces coupling between electrical forces, mass transfer, and fluid flow within the pore. This coupling manifests itself in two ways: (1) the interaction of fluid flow and the electric field generates a body force term in the momentum balance equation, and (2) the electrostatic potential in the space charge region of the pore causes counterion enrichment and coion exclusion. Also, the interaction between the space-charge region and the driving forces for transport directed parallel to the pore wall results in such electrokinetic phenomena as streaming potentials and electroosmosis [152]. For examples of electrokinetic transport models as applied to ion-exchange membranes, see [151, 153, 154].

Two important design parameters for an electrodialysis stack are the limiting current density and current utilization. The transport of charged species to the anode or cathode through a set of ion-exchange membranes leads to a concentration decrease of counterions in the boundary layer at the membrane surface that faces the dilute compartment and an increase at the surface facing the concentrated solution (Figure 26.29). The decrease in salt concentration at the membrane surface of the diluate limits the ion flux (or current density) through the membrane. At the absolute limiting current density, the ion concentration at the surface of the cation- and/or anion-exchange membrane drops to zero. The limiting current density (i_L) in this situation is given by [132, 155]

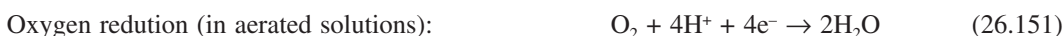
$$i_L = \frac{C^b z_+ F k_d}{t_+ - t_+^*} \quad (26.146)$$

basically rooted in electrochemistry. The corrosion cell may be viewed as a short-circuited electrochemical cell, where a voltage difference between the anode and cathode provides the driving force for spontaneous oxidation and reduction reactions. The anode and cathode may be physically separated from one another or, more commonly, may occur on a single heterogeneous metal surface, where discrete microcells arise due to differences in metal composition and/or spatial variations in the composition of the solution in contact with the metal surface.

The primary oxidation reaction involves the anodic electrochemical dissolution of metal species M, according to the following reaction:



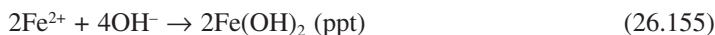
This reaction is driven to the right and controlled by one or more reduction reactions, typically,



The overall reaction in a corrosion cell is the sum of an anodic and cathodic reaction. For the case of metal dissolution and O_2 reduction, the overall reaction is



Dissolved metal ions can either pass into the bulk solution or react immediately with OH^- to form insoluble metal oxides/hydroxides that coat the metal surface. For iron corrosion, iron hydroxide species react further with water and oxygen to form rust ($Fe(OH)_3$) according to the following reaction sequence:



The rate of a corrosion reaction is affected by pH (via H^+ reduction and hydroxide formation), the partial pressure of O_2 (the solubility/concentration of oxygen in solution), fluid agitation, and electrolyte conductivity. Corrosion processes are analyzed using the thermodynamics of electrode reactions, mass transfer of the cathode reactants O_2 and/or H^+ , and the kinetics of metal dissolution reactions [157, 158].

26.7.1 THERMODYNAMICS OF CORROSION PROCESSES

We have seen in Section 26.2.1 that thermodynamics (i.e., equilibrium half-cell potentials) can be used to determine which of two half-cell reactions proceeds spontaneously in the anodic or cathodic direction when the two reactions occur on the same piece of metal or on two metal samples that are in electrical contact with one another. The half-cell reaction with the higher equilibrium potential will always be at the cathode. Thus, under standard conditions any metal dissolution (corrosion) reaction with an E° less than 0.0 V vs. SHE will be driven by proton reduction while metal dissolution reactions with an E° less than +1.23 V vs. SHE will be driven by dissolved

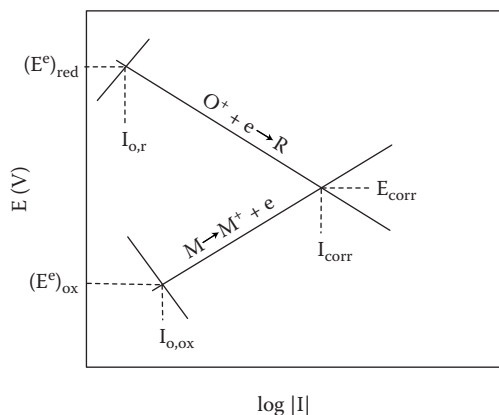


FIGURE 26.31 Current-voltage plots for metal corrosion, showing Tafel lines for metal (M) oxidation and oxidant (O) reduction. The intersection of the Tafel lines gives the corrosion potential and corrosion current.

26.7.2 KINETIC ASPECTS OF CORROSION REACTIONS

Almost all metals corrode, but many metals corrode very slowly under normal environmental conditions, due in part to kinetic limitations of the metal dissolution reaction. Thus, the rate of metal corrosion can be anticipated and controlled by developing kinetic rate expressions for metal oxidation reactions. There is a major difference, however, between “classical” electrochemical metal dissolution kinetics and metal dissolution in a corrosion system, that difference being the occurrence of one or more oxidation and reduction reactions on the same metal.

As stated above, wet-metal corrosion involves a metal dissolution (oxidation) reaction coupled to a reduction reaction. Electrons produced at anodic sites pass through the metal, and are consumed by reduction reactions so that there is no net charge build-up in the metal. For this situation, “mixed potential theory” is applicable. The basic premises of this theory are (1) any electrochemical reaction can be divided into two or more partial oxidation and reduction reactions, and (2) the sum of the rates (as quantified by the current densities) of all anodic reactions must be equal to the current densities for all cathodic reduction reactions on an isolated corroding metal sample because there is no net accumulation of charge. During metal corrosion, the open circuit (zero net current) electrode potential of the corroding metal, also known as the corrosion potential (E_{corr}), lies between the potentials of the relevant anodic and cathodic half-cell reactions. The partial anodic or cathodic current that flows at E_{corr} is called the corrosion current (I_{corr}) and is directly related to the rate of metal corrosion (g/sec) through Equation (26.14) in Section 26.2.2. The corrosion rate in mils of metal lost per year (abbreviated mpy, where 1 mil = 10^{-3} inches) is related to the current density at the corrosion potential (designated as i_{corr} with units of A/cm²) by the following equation:

$$mpy = 394 \times \frac{i_{corr}}{nF} \times \frac{M}{\rho} \quad (26.157)$$

where M is the molecular weight of the corroding metal (g/mole) and ρ is the metal density (g/cm³).

Tafel plots of E vs. $\log I$, such as those shown in Figure 26.31, are often used to determine the rate of a corrosion process. For a corroding metal (anode) that is driven by a single kinetically controlled reduction reaction (such as hydrogen evolution from an acid-containing solution), one can write the following Tafel equations for cathodic proton reduction and anodic metal dissolution:

$$E - E_{H_2}^e = -\beta_{H_2} (\log I - \log I_{o,H_2}) \quad (26.158)$$

Combining the anodic and cathodic Tafel equations results in the following modified Butler-Volmer rate expression:

$$I = I_{corr} \left(\exp \left[\frac{2.3(E - E_{corr})}{b_a} \right] - \exp \left[\frac{2.3(E_{corr} - E)}{|b_c|} \right] \right) \quad (26.162)$$

Using the above equation, the deviation in the corroding metal potential away from its open circuit potential (E_{corr}) generates a net anodic or cathodic current (in the same way that a deviation of the electrode potential away from E^e for a single electrode reaction produces an oxidation or reduction current). The magnitude of the current, as given by Equation (26.162), depends on the level of electrode polarization ($E - E_{corr}$), the cathode and anodic Tafel slopes (b_c and b_a , respectively), and I_{corr} (which is analogous to the exchange current in the Butler-Volmer equation).

For a small electrode polarization (denoted as ΔE , which can be no more than ± 20 mV) that produces a current of I , the exponential terms in Equation (26.162) can be linearized, resulting in the following current-voltage expression:

$$I = 2.3 \cdot I_{corr} \left[\frac{\Delta E}{b_a} + \frac{\Delta E}{|b_c|} \right] \quad (26.163)$$

When a metal corrodes, there is no external flow of current (electrons) to indicate the metal dissolution rate. One can, however, place the corroding metal in a three-electrode electrochemical cell (working electrode, counter electrode, and reference electrode, as shown in Figure 26.4), polarize the working electrode metal either anodically or cathodically away from its open circuit (corrosion) potential by no more than ± 20 mV (this potential difference is measured between the working and reference electrodes), and then measure the resulting current. For this case, Equation (26.163) can be rearranged to give the following equation for the corrosion current

$$I_{corr} = \frac{b_a \cdot |b_c|}{2.3(b_a + |b_c|)} \cdot R_p \quad (26.164)$$

where R_p is known as the polarization resistance and is given by $\Delta I/\Delta E$ (i.e., the slope of the linear portion of an experimental I vs. E plot, for small polarizations of the working electrode). Once I_{corr} is known for a metal specimen of area A , then i_{corr} can be determined and the metal corrosion rate in mpy can be calculated using Equation (26.157).

The use of Tafel plots for the analysis of metal corrosion systems indicates how dissolved O_2 in solution and the subsequent O_2 reduction (which is under kinetic control) accelerates metal corrosion. Due to the high value of E^e for O_2 reduction (+1.23 V vs. SHE), the intersection of the oxygen reduction and metal dissolution Tafel lines occurs at high values of E_{corr} and I_{corr} . When the reduction of both H^+ and O_2 drives metal corrosion (with the reduction reactions under kinetic control), one simply adds together the current-voltage Tafel lines for the two reduction reactions. A new line is then drawn for the sum of the cathodic currents on the corroding metal. The intersection of this new line with the metal oxidation Tafel line gives E_{corr} and I_{corr} .

26.7.3 MASS TRANSFER EFFECTS

In some situations, the oxygen or proton reduction reaction during metal corrosion will be mass transfer (diffusion) controlled, due to poor fluid agitation and/or a low concentration of H^+ or dissolved oxygen in solution (this is especially true for O_2 , which has a low solubility in water at

initially displays dissolution behavior similar to nonpassivating metals (i.e., there is an increase in the anodic dissolution current with increasing electrode potential). As the potential increases, the dissolution rate is so high that the concentration of dissolved metal ions adjacent to the anode surface exceeds its solubility limit and a salt film precipitates on the metal. The maximum current achievable before salt film formation is called the critical current (I_c in Figure 26.34). At a designated potential known as the passivation potential (E_{pp} in Figure 26.34), there is a sharp decrease in the metal dissolution current (often by several orders of magnitude) to a value defined as the passive current I_p . The drop in metal dissolution rate at E_{pp} is due to a drastic change in the composition and properties of the precipitated salt film on the metal surface, with a reduction in film porosity and the conversion of the film from an ionic conductor to an electronic conductor. For an appreciable electrode potential range above E_{pp} , the current remains low (at I_{pass}) and independent of potential. This regime is termed the passive region. Finally, at a very high anodic potential, metal dissolution commences again, as the protective passive film breaks down. In this transpassive region, the dissolution current once again increases with increasing electrode potential. As will be discussed below, the presence of a passive film on certain metals has been exploited as a convenient way of protecting the underlying metal from further corrosion.

26.7.5 TYPES OF CORROSION AND METHODS OF CORROSION PREVENTION

26.7.5.1 Uniform Attack

Uniform attack or general overall corrosion is the most common form of corrosion, causing most metal destruction on an overall tonnage basis. During this form of corrosion, the metal becomes thinner and eventually fails. Although widespread, the form of corrosion is not of too great a concern because the corrosion rate can be accurately predicted using simple tests (immersing the metal specimen in the liquid of interest for an extended period of time and measuring the weight loss or performing electrochemical polarization experiments to determine the corrosion current) so that the metal lifetime can be estimated. As an example, this type of corrosion would occur when a steel or zinc plate is immersed in a dilute sulfuric acid solution, with rusting (corrosion) over the entire metal surface.

Prevention—Uniform corrosion can be prevented or reduced by (1) the proper choice of metal for a given environment; (2) the use of metal coatings, such as a paint coating or nonoxidizing organic inhibitors (e.g., benzotriazole or organic amines [160]) in solution that adsorb onto and protect the metal surface; or (3) cathodic protection (discussed below).

26.7.5.2 Galvanic Corrosion

A potential difference exists between any two dissimilar metals that are exposed to a corrosive or electrically conductive solution. When the two metals are in contact, the potential difference causes electrons to flow between the two metals. To a first approximation, the determination of the equilibrium potential of the two reactions on the metals (see Section 26.2.1.1) can be used to predict which metal will corrode (that metal with the lower equilibrium electrode potential will become the anode and will corrode). The greater the difference of the potentials of the two metals, the greater the driving force for corrosion and the greater the metal dissolution rate. Examples of galvanic corrosion are: (1) corrosion of aluminum tubing that is connected to brass (Cu-Zn alloy) fittings, (2) corrosion of a steel hot water tank where copper tubing is connected to the tank, and (3) corrosion of steel pump shafts and valve stems because of contact with graphite packing. Galvanic corrosion is usually greatest near the junction of the two metals. Anode/cathode area effects also play an important role during galvanic corrosion. A large cathode and small anode is unfavorable because the anode current density will be greater than that at the cathode even though both the anodic and cathode currents are equal.

to a corrosive environment [157, 162]. Such corrosion is associated with a small volume of stagnant solution in holes, under gasket surfaces, beneath surface deposits, and under bolts and rivet heads. When two overlapping metal parts, for example, are exposed to aerated seawater, there is initially uniform corrosion over the entire metal surface, where metal dissolution is driven by oxygen reduction (low concentrations of dissolved oxygen being present in the seawater). After a short time, oxygen within the crevice is depleted due to poor fluid mixing and oxygen reduction ceases. Dissolution of metal in the crevice, however, continues (driven by O_2 reduction outside the crevice) and the metal cation concentration in the crevice increases. To maintain charge neutrality, Cl^- ions migrate into the crevice solution and the resulting metal chloride salt hydrolyzes into H^+ , Cl^- , and an insoluble metal hydroxide precipitate. The production of protons and chloride anions accelerates metal dissolution in the crevice. The increase in metal dissolution increases Cl^- migration, which in turn further heightens the rate of metal corrosion in the crevice. The corrosion process within the crevice drive oxygen reduction on the adjacent metal surface outside the crevice (this metal surface is actually cathodically protected by metal corrosion in the crevice). Thus, during crevice corrosion, metal attack is localized within shielded areas while the remaining metal surface suffers little or no damage. The unfavorable cathode/anode area ratio means very rapid disintegration of metal within the crevice. There is usually a long incubation period associated with crevice corrosion (when dissolved O_2 within the crevice is depleted). Once crevice corrosion starts, it often proceeds at an accelerating rate. Metals or alloys that depend on oxide films or passive layers for corrosion resistance are particularly susceptible to crevice corrosion (the films are destroyed by H^+ and/or Cl^-).

Prevention—Crevice corrosion is prevented or minimized by: (1) closing crevices and overlapping metal parts by continuous welding, caulking, or soldering; (2) removing solid deposits from metal surfaces; and (3) increasing fluid stirring to minimize the difference in dissolved O_2 concentration within and outside of a crevice [163].

26.7.5.4 Pitting

Pitting is a destructive and insidious form of corrosion, where localized dissolution occurs in small holes or pits on the metal surface [157, 161]. Although metal weight loss is small, equipment failure occurs due to perforation of the metal. Pitting occurs in passivating metals, where certain aggressive species in solution, e.g., chlorides, bromides, and hypochlorites, break down the passive oxide film. An autocatalytic and accelerating metal dissolution process then begins at film rupture. As is the case for crevice corrosion, rapid metal dissolution creates an excess of metal cations within the pit and the electromigration of Cl^- ions into the pit to maintain electroneutrality. The subsequent hydrolysis of metal chloride species produces H^+ and metal hydroxides (which precipitates at the pit entrance). The solubility of oxygen drops to virtually zero as the solution in the pit acidifies. Cathodic reduction of oxygen on the large metal surfaces adjacent to the pit drives the dissolution reactions, in a manner similar to crevice corrosion.

Prevention—The methods outlined above to combat crevice corrosion also apply to pitting. Metals that are resistant to pitting should be used as alloying agents; their passive films are more protective and more stable to halogen attack. For example, the addition of 2% molybdenum to 18-8 (type 304) stainless steel to produce 316 stainless steel significantly increases pitting resistance.

Anodic Protection—Anodic protection procedures make use of a passive film on a metal surface to minimize corrosion. Normally, the application of an anodic current to a metal structure would increase its electrochemical dissolution rate. With metals that exhibit active-passive behavior (e.g., Ti, Ni, Fe, Cr, and their alloys), application of an anodic current or an anodic potential results in passive film formation and a dramatic reduction in the metal corrosion rate. There are essentially two methods of anodically protecting a metal: (1) the imposition of an anodic potential greater than the passivating potential (E_{pp} in Figure 26.34) or (2) the use of oxidizing inhibitors (e.g., NO_3^- , CrO_4^{2-} , SO_4^{2-} , CH_3COO^- , or OH^-) [164] at a sufficiently high concentration so that the mixed

almost reversible process, especially in steels, thus heating the metal to 200°F to 300°F liberates trapped hydrogen), which often restores the mechanical properties of the metal; and/or (3) using alloying agents (e.g., nickel and molybdenum) that are not susceptible to hydrogen embrittlement.

26.8 BATTERIES AND FUEL CELLS

26.8.1 BATTERIES

Batteries are electrochemical reactors that convert chemical energy into electrical energy. The thermodynamic relationship for this conversion is given by Equation (26.19):

$$E = -\frac{\Delta G}{nF}$$

where E is the electromotive force (voltage) of the battery system, ΔG is the free energy change for the overall battery reaction (the sum of the primary anode and cathode reactions), and n is the number of electrons involved in the battery reactions. The available thermodynamic voltage depends on the chemical reactants. In a battery, reactants for the oxidation and reduction reactions do not meet directly, but are consumed at different sites, the anode and cathode, which causes electrons to flow through an external circuit between the battery terminals. The energy transfer is manifested as a voltage (a measure of the energy difference of electrons at the anode and cathode) and current (the flow of electrons through the external circuit connecting the anode and cathode). All batteries have four common features: (1) the anode and cathode electrodes must be electronically conducting; (2) the electrolyte between the anode and cathode must be ionically conducting; (3) there must be physical separation of the electrodes and the fuel and oxidant reactants; and (4) the available fuel and oxidant materials for the electrode reactions must be contained within the battery itself. Primary batteries [166–170] are designed only for a single discharge, while a secondary battery is expected to be capable of repetitive charge/discharge cycles. The original chemistry of a primary battery cannot be restored by electrical means internal to a cell due to (1) irreversibility in phase changes and chemical interconversion of the electrode active material; (2) isolation, electrically or electronically, of active material; and/or (3) local poor conductivity of electrode materials in the discharged state [169]. In contrast to primary batteries, secondary batteries [168, 171, 172] can be recharged electrically to their original condition many times by passing current through them in the opposite direction to that of the discharge current. Thus, the anode and cathode battery reactions in a secondary battery must be reversible.

26.8.1.1 Battery Performance Characteristics

Battery performance is related to the available voltage and current while the battery is discharging. The terminal voltage of a battery depends on the thermodynamic free-energy change of the anode and cathode reactions, according to Equation (26.19) and by the various activation (kinetic), concentration, and resistance overpotentials that lower the battery's voltage (as discussed in Section 26.3.4):

$$E_{cell} \equiv E^C - E^A = (E^e)^C - (E^e)^A - |\Sigma \eta^A| - |\Sigma \eta^C| - |\eta_{ohm}| \quad (26.165)$$

where the superscripts A and C refer to the anode and cathode, respectively. According to the above equation, one should choose the anode and cathode reactions with a large $(E_e^C - E_e^A)$. At the same time, the various overpotentials (primarily the kinetic and resistance overpotentials) must be minimized, by ensuring fast electrode reactions and by designing the battery with a low electrical resistance (e.g., a high-conductivity electrolyte, a small interelectrode gap, and a low-resistance

TABLE 26.16
Commercial Primary Battery Systems

Common Name	Overall Cell Reaction	Nominal Voltage	Approximate Power Density (Wh/cm ³)	Comments
Leclanche	$\text{Zn} + 2\text{MnO}_2 + 2\text{NH}_4\text{Cl} = \text{Zn}(\text{NH}_3)_2\text{Cl}_2 + \text{H}_2\text{O} + \text{Mn}_2\text{O}_3$	1.5	0.20	Low cost; general purpose; wide range of sizes
Zinc chloride	$4\text{Zn} + 8\text{MnO}_2 + \text{ZnCl}_2 + 9\text{H}_2\text{O} = 8\text{MnOOH} + \text{ZnCl}_2 \cdot 4\text{ZnO} \cdot 5\text{H}_2\text{O}$	1.5	0.20	Intermediate cost and performance
Alkaline	$2\text{Zn} + 3\text{MnO}_2 = 2\text{ZnO} + \text{Mn}_3\text{O}_4$	1.5	0.25	Sets standard for cylindrical cells
Silver	$\text{Zn} + \text{Ag}_2\text{O} = 2\text{Ag} + \text{ZnO}$	1.6	0.50	Good pulse power, higher voltage than Zn/HgO or Zn/Air
Mercury	$\text{Zn} + \text{HgO} = \text{Hg} + \text{ZnO}$	1.35	0.50	Sets the standard for button-size cells
Zinc-air	$2\text{Zn} + \text{O}_2 (\text{air}) = 2\text{ZnO}$	1.4	1.0	Twice the capacity of a mercury battery
Li/CuO	$2\text{Li} + \text{CuO} = \text{Li}_2\text{O} + \text{Cu}$	1.5	0.60	Potential replacement for leclanche and zinc chloride batteries
Li/FeS	$2\text{Li} + \text{FeS} = \text{Li}_2\text{S} + \text{Fe}$	1.6	0.40	Replacement for Zn/HgO and Zn/Ag ₂ O
Li/SO ₂	$2\text{Li} + 2\text{SO}_2 = \text{Li}_2\text{S}_2\text{O}_4$	2.8	0.4	Military battery; low temperature; excellent storage
Li/SOCl ₂	$\text{Li} + \text{SOCl}_2 = \text{LiCl} + \text{SO}_2$	3.6	1.0	High voltage; high-energy density
Li/CF _x	$x\text{Li} + \text{CF}_x = x\text{LiF} + \text{C}$	2.7	0.50	High voltage; long shelf-life; wide operating temperature
Li/MnO ₂	$\text{Li} + \text{MnO}_2 = \text{LiMnO}_2$	2.8	0.50	High voltage; long shelf-life; wide operating temperature
Li/I ₂	$2\text{Li} + \text{I}_2 = 2\text{LiI}$	2.8	0.60	Battery for heart pacemaker

Data from [167–170].

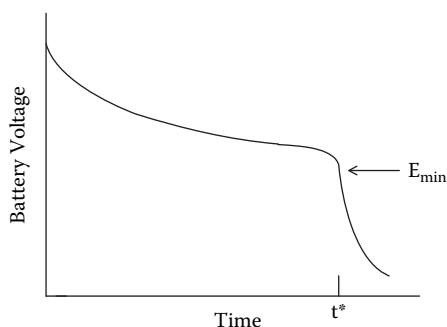


FIGURE 26.38 Voltage vs. time curve during battery discharge at a constant current.

In the lead-acid battery, the actual capacity is well below its theoretical value due to the formation during discharge of poorly conducting PbSO_4 , which forms a barrier between the electroactive PbO_2 and the current collector. Examples of various primary and secondary batteries are listed in Tables 26.16, 26.17, and 26.18.

TABLE 26.17
Commercial Secondary (Rechargeable) Battery Systems

Common Name	Overall Cell Reaction	Nominal Voltage	Approximate Power Density		Comments
			Wh/l	Wh/kg	
Lead-Acid	$\text{Pb} + \text{PbO}_2 + 2\text{H}_2\text{SO}_4 = 2\text{PbSO}_4$	2.10	80	35	Lowest cost; largest sales
Nickel-Cadmium	$\text{Cd} + \text{NiOOH} + 2\text{H}_2\text{O} = \text{Cd}(\text{OH})_2$	1.30	80	38	High rate; available sealed
Nickel-Iron	$\text{Fe} + 2\text{NiOOH} + 2\text{H}_2\text{O} = \text{Fe}(\text{OH})_2 + 2\text{Ni}(\text{OH})_2$	1.37	90	30	Very long cycle life; almost indestructible; old technology
Nickel-Hydrogen	$\text{H}_2 + 2\text{NiOOH} = 2\text{Ni}(\text{OH})_2$	1.35	90	45	Special space battery; very long cycle life; high self-discharge
Silver-Zinc	$\text{Zn} + \text{AgO} + \text{H}_2\text{O} = \text{Zn}(\text{OH})_2$	1.86	200	100	Two-step discharge; limited cycle life; high-energy density
	$+ \text{Ag}_2\text{OZn} + \text{Ag}_2\text{O} + \text{H}_2\text{O} = \text{Zn}(\text{OH})_2 + \text{Ag}$	1.60			
Lithium-MoS ₂	$\text{Li} + \text{MoS}_2 = \text{LiMoS}_2$	2.3	150	80	Small sealed cell

Data from [168, 169, 171, 172].

TABLE 26.18
Battery Systems Formerly/Currently in Various Stages of Development

Common Name	Overall Cell Reaction	Nominal Voltage	Approximate Power Density		Comments
			Wh/l	Wh/kg	
Nickel-Zinc	$\text{Zn} + 2\text{NiOOH} + \text{H}_2\text{O} = \text{Zn}(\text{OH})_2 + \text{Ni}(\text{OH})_2$	1.65	95	60	Limited cycle life; high rate capability
Zinc-Bromine	$\text{Zn} + \text{Br}_2 = \text{ZnBr}_2$	1.85	75	65	Bromine complexed by quaternary ammonium salt; circulating electrolyte
Lithium-FeS	$\text{Li} + \text{FeS} = \text{LiFeS}$	1.33	90	95	Low cost; high temperature fused salt
Sodium-Sulfur	$2\text{Na} + 3\text{S} = \text{Na}_2\text{S}_3$	2.1	120	160	Solid $-\text{Al}_2\text{O}_3$ separator; high temperature operation
Aluminum-Air	$4\text{Al} + 3\text{O}_2 + 2\text{H}_2\text{O} = 2\text{Al}_2\text{O}_3 \cdot \text{H}_2\text{O}$	1.6		300	Circulating electrolyte; low cost; low-energy efficiency
Lithium-TiS ₂	$\text{Li} + \text{TiS}_2 = \text{LiTiS}_2$ (intercalate)	2.1		150	Room temperature; organic electrolyte
Solid-State Lithium	$\text{C}_6 + \text{LiMO}_2 = \text{Li}_x\text{C}_6 + \text{Li}_{1-x}\text{MO}_2$	3.4–3.7		90–120	

Data from [169, 173–176].

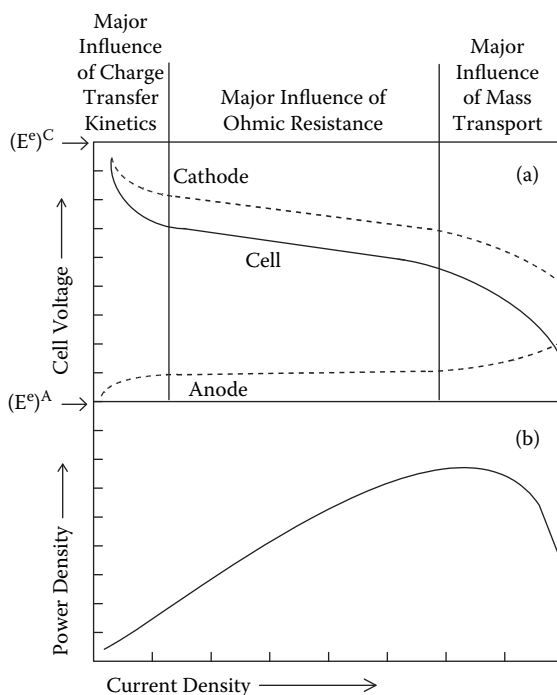


FIGURE 26.40 Typical current density/voltage (a) and current density/power density (b) plots for a fuel cell.

theoretical anode/cathode cell potential, which is about 90% to 95% that of ΔH_o at moderate temperatures. Consequently, the intrinsic maximum energy conversion efficiency of a fuel cell is much greater than that of a heat engine (typically 30% to 40%, as determined by the Carnot efficiency) [177–179]. The actual operational efficiency of a fuel cell is in the range of 30% to 60% due to activation (kinetic), concentration (mass transfer), and resistance overpotentials, which lower the cell voltage, according to Equation (26.166). The current density regimes where these overpotentials dominate in a typical fuel cell are shown in Figure 26.40a, and the resulting power density vs. current density curve is shown in Figure 26.40b.

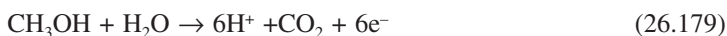
26.8.2.1 Fuel Cell Types

A summary of the electrolyte, anode, and cathode gases, operating temperature, and efficiency of different fuel cells is presented in Table 26.19.

Considerable research is currently in progress to find applications for fuel cells. Fuel cells may be useful for large-scale power generation during intermittent peak electricity demand and for load leveling (where electricity is stored in a fuel cell during off-peak hours) [179, 192, 193]. Automobiles equipped with fuel cells are being tested [194–196], but the cost of an automotive fuel cell power plant is too high. Military and space applications of fuel cells are also being explored [177, 179, 192] and portable power applications (replacement for lithium batteries) look promising. Research is in progress to develop cheaper sources of hydrogen gas (the fuel used in most fuel cells) and to find improved methods to store and transport hydrogen.

Molten Carbonate Fuel Cells—The anode fuel is hydrogen, with the following oxidation reaction:





and the cell operates normally at a temperature of about 80°C. High-temperature operation (120°C to 140°C) with vaporized methanol has also been studied, to improve the oxidation kinetics and minimize anode catalyst poisoning by CO (a by-product of the methanol oxidation reaction). The problem of methanol crossover (leakage) through the solid polymer electrolyte cation-exchange membrane is yet to be solved completely. An alternative approach is to reform methanol and then pump the resulting H₂ gas product to a PEM H₂/O₂ fuel cell.

Alkaline Fuel Cells

This low-temperature fuel cell uses H₂ and O₂ reactants and a highly alkaline aqueous KOH electrolyte. The advantages of this fuel cell are the faster oxygen reduction reaction in the alkaline electrolyte and the possibility of using low-cost, nonprecious metal electrode catalysts, such as Ag-loaded carbon powder. The greatest problem with alkaline fuel cells is that the electrolyte reacts with traces of CO₂ to produce insoluble carbonates.

Solid Oxide Fuel Cells

Such fuel cells operate at high temperatures (~1000°C) and utilize a ceramic oxide material to separate the anode and cathode. At elevated temperatures, the ceramic electrolyte becomes conductive to oxide anions. In these fuel cells, either hydrogen or hydrogen/carbon monoxide mixtures (produced by reforming natural gas) are consumed at the anode and air or oxygen is fed to the cathode. This is a promising fuel cell for large, high-power applications, including industrial and large-scale central electricity generating stations.

NOMENCLATURE

a_i	Activity of species i
a	Electrode area per unit volume (cm ⁻¹)
A	Area (cm ²)
b_a, b_c	Anodic and cathodic Tafel slopes (V/decade)
C	Concentration (mol/cm ³)
C_∞, c^b	Bulk solution concentration (mol/cm ³)
CE	Current efficiency of an electrode reaction (%)
d	Tube diameter in Equation (26.80) (cm)
D	Diffusion coefficient of the electrolyte (cm ² /sec)
D_i	Diffusion coefficient of species i (cm ² /sec)
e	Charge of an electron (1.6021×10^{-19} C)
E	Electromotive force (EMF) (V)
E^e	Equilibrium reduction potential (V)
E°	Standard reduction potential (V)
f_i	molar activity coefficient of species i
f_\pm	Mean molar activity coefficient
F	Faradays constant (96487 C/equiv.)
g	Acceleration of gravity (cm/s ²)
G	Gibbs energy (J)
Gr	Grashof number (defined by Equation [26.79d])
H	Enthalpy (J)
i	Current density (A/cm ²)
i_L	Mass-transfer limited current density (A/cm ²)
i_o	Exchange current density in the Butler-Volmer equation (A/cm ²)
I	Current (amps)

ρ	Density (g/cm ³)
Φ	Electric potential (V)
ω	Rotation speed of disk (compare Equation (261.81)) (rad/sec)

REFERENCES

1. Johnthan Dean, ed. *Handbook of Lange's Chemistry*. 13th ed. New York: McGraw-Hill, 1985: 2-6, 6-19.
2. A.J. Bard and L.R. Faulkner. *Electrochemical Methods: Fundamentals and Applications*. New York: John Wiley & Sons, 1980.
3. J.O'M Bockris and A.K.N. Reddy. *Modern Electrochemistry*. New York: Plenum Press, 1973.
4. J.S. Newman. *Electrochemical Systems*. 2nd ed. Englewood Cliffs, NJ: Prentice-Hall, 1991.
5. E.A. Guggenheim. *Thermodynamics*. Amsterdam: North-Holland Publishing, 1959.
6. G.N. Lewis and M. Randall. *Thermodynamics* 2nd ed. New York: McGraw-Hill, 1961.
7. R.A. Robinson and R.H. Stokes. *Electrolyte Solutions*. New York: Academic Press, 1959.
8. P. Debye and E. Hückel. *Physik Zeit* 24 (1923): 185.
9. E.A. Guggenheim and J.C. Turgeon. *Transactions of the Faraday Society* 51 (1955): 747.
10. G. Prentice. *Electrochemical Engineering Principles*. Englewood Cliffs, NJ: Prentice-Hall, 1991.
11. H.S. Harned and R.A. Robinson. *Multicomponent Electrolyte Solutions*. Oxford, UK: Pergamon Press Ltd., 1968.
12. Klaus J. Vetter. *Electrochemical Kinetics*. New York: Academic Press, 1967.
13. Paul Delahay. *Double Layer and Electrode Kinetics*. New York: Interscience Publishers, 1965.
14. N. Tanaka and R. Tamamushi. *Electrochimica Acta* 9 (1964): 963.
15. S. Roy and P.N. Pintauro. *Electrochimica Acta* 38 (1993): 1461.
16. S. Roy and P.N. Pintauro. *Journal of the Electrochemical Society* 140 (1993): 3167.
17. B. Levich. *Acta Physicochimica URSS* 17 (1947): 837.
18. V.G. Levich. *Physicochemical Hydrodynamics*. Englewood Cliffs, NJ: Prentice-Hall, 1962.
19. A.C. Riddiford. "The Rotating Disk System." *Advances in Electrochemistry and Electrochemical Engineering* 4 (1966): 47.
20. C.W. Tobias and R.G. Hickman. *Zeit Physik Chemie* (1965) 229: 145.
21. T.K. Ross and A.A. Wragg. *Electrochimica Acta* (1965)10:1093.
22. N. Ibl and U. Braun. *Chimia* 21 (1967): 395.
23. C.R. Wilke, M. Eisenberg, and C. W. Tobias. *Chemical Engineering Progress* 49 (1953): 674.
24. A.A. Wragg and T.K. Ross. *Electrochimica Acta* 12 (1967): 1421.
25. E. Ruckenstein. *Advances in Chemical Engineering*. Vol. 13. New York: Academic Press, 1987: 11.
26. J. Jorne and T. Cheng. *Chemical Engineering Science* 42 (1987): 1635.
27. J.R. Selman and C.W. Tobias. In *Advances in Chemical Engineering*. Vol 10. T. Drew, ed. New York: Academic Press, 1978: 211.
28. H. Wendt and G. Kreysa. *Electrochemical Engineering: Science and Technology in Chemical and Other Industries*. Berlin: Springer, 1999.
29. M.M. Baizer and H. Lund, eds. *Organic Electrochemistry*. 2nd ed. New York: Marcel Dekker, 1983.
30. D. Pletcher and F.C. Walsh. *Industrial Electrochemistry*. London: Chapman and Hall, 1993.
31. F. Beck and H. Guthke. *Chem Ing Tech* 41 (1969): 943.
32. L. Ebersson, K. Nyberg, and H. Sternerup. *Chemica Scripta* 3 (1973):12.
33. F. Goodridge and K. Scott. *Electrochemical Process Engineering: a Guide to the Design of Electrolytic Plant*. New York: Plenum Press, 1995.
34. D. Degner. "Scale-Up of Electroorganic Processes: Some Examples for a Comparison of Electrochemical Syntheses with Conventional Syntheses." In *Techniques of Electroorganic Synthesis, III*. N.L. Weinberg and B.V. Tilak, eds. New York: John Wiley & Sons, 1982.
35. J.R. Backhurst, J.M. Coleman, F. Goodridge, R.E. Plimley, and M. Fleischmann, *Journal of the Electrochemical Society* 116 (1969): 1600.
36. F. Goodridge and A.R. Wright. "Porous Flow-Through and Fluidised Bed Electrodes." In *Comprehensive Treatises of Electrochemistry*. Vol. 6. E. Yeager, J. O'M. Bockris, and S. Sarangapany, eds. New York: Plenum Press, 1983.

80. W. An, J.K. Hong, P.N. Pintauro, K. Warner, and W. Neff. *Journal of the American Oil Chemists' Society* 75 (1998): 917.
81. P.N. Pintauro, M.P. Gil, K. Warner, G. List, and W. Neff, *Industrial & Engineering Chemistry Research* 44 (2005): 6188.
82. W. An, J.K. Hong, P.N. Pintauro, K. Warner, and W. Neff. *Journal of the American Oil Chemists' Society* 76 (1999): 215.
83. J.W. Dini. *Electrodeposition: The Materials Science of Coatings and Substrates*. Park Ridge, NJ: Noyes Publications, 1993.
84. J. Newman. *Journal of the Electrochemical Society* 113 (1966): 501.
85. J. Newman. *Journal of the Electrochemical Society* 113 (1966): 1235.
86. W.R. Parrish and J. Newman. *Journal of the Electrochemical Society* 116 (1969): 169.
87. C. Wagner. *Journal of the Electrochemical Society* 98 (1951): 116.
88. N. Ibl. *Comprehensive Treatise of Electrochemistry*. Vol. 6. E. Yeager, ed. New York: Plenum Press, 1983: 239.
89. W.R. Parrish and J. Newman. *Journal of the Electrochemical Society* 117 (1970): 43.
90. K. Viswanathan and D.-T. Chin. *Journal of the Electrochemical Society* 124 (1977): 709.
91. J. Newman. *Advances in Electrochemistry and Electrochemical Engineering*. C.W. Tobias, ed. 5 (1967): 87.
92. R. Winand. *Electrochimica Acta* 39 (1994): 1091.
93. M. Matlosz, C. Creton, C. Clerc, and D. Landolt *Journal of the Electrochemical Society* 134 (1987): 3015.
94. D. Landolt. *Electrochimica Acta* 39 (1994): 1075.
95. D.-T. Chin and K. L. Hsueh. *Electrochimica Acta* 31 (1986): 561.
96. A. Bensmaili and F. Coeuret, *Journal of the Electrochemical Society* 137 (1990): 3086.
97. R. C.alkire and J.B. Lu, *J. Electrochem. Soc.*, 134 (1987): 294.
98. C. Karakusand C.-R. Chin. *Journal of the Electrochemical Society* 141 (1994): 691.
99. R. J. von Gutfeld and J. Cl. Puippe. *Oberfläche-Surface* 11 (1981): 294.
100. L. Kulynych, L. Romankiw, and R. J. von Gutfeld. *IBM Technical Disclosure Bulletin* 23 (1980): 1262.
101. J.Cl. Puippe, R.E. Acosta, and R.J. von Gutfeld. *Journal of the Electrochemical Society* 128 (1981): 2539.
102. R.J. von Gutfeld, E.E. Tynan, R.L. Melcher, and S.E. Blum. *Applied Physics Letters* 35 (1979): 651.
103. M.H. Gelchinski, L.T. Romankiw, D.R. Vigliotti, and R.J. von Gutfeld. *Journal of the Electrochemical Society* 132 (1985): 2575.
104. P. Bindra and J. Roldan. *Journal of the Electrochemical Society* 132 (1985): 2581.
105. A. Brenner. *Electrodeposition of Alloys: Principles and Practice*. Vols. 1, 2. New York: Academic Press, 1963.
106. P. C. Andricacos, C. Arana, J. Tabib, J. Dukovic, and L.T. Romankiw. *Journal of the Electrochemical Society* 136 (1989): 1336.
107. A. T. Kuhn, ed. *Techniques in Electrochemistry, Corrosion, and Metal Finishing – a Handbook*. London: Chichester, 1987.
108. J. Edwards. *Electroplating: a Guide for Designers and Engineers*. Middlesex, UK: Finishing Publications, 1983.
109. F.A. Lowenheim, ed. *Modern Electroplating*. 3rd ed. New York: Wiley, 1974.
110. W. Canning and Co., Ltd. *The Canning Hanbook: Surface Finishing Technology*. 23rd ed. Birmingham, UK: W. Canning in association with Spon, 1982.
111. J.W. Dini. *Electrodeposition: the Materials Science of Coatings and Substrates*, Park Ridge, NJ: Noyes Publications, 1993.
112. C.W. Ammen. *The Electroplater's Handbook*. Blue Ridge Summit, PA: Tab Books, 1986.
113. P.A. Jaquet. *Nature* 135 (1935): 1076.
114. J.F. Wilson. *Practice and Theory of Electrochemical Machining*. New York: Wiley Interscience, 1971.
115. J.A. McGeough. *Principles of Electrochemical Machining*. London: Chapman and Hall, 1974.
116. M. Datta and L.T. Romankiw. *Journal of the Electrochemical Society* 136 (1989): 185C.
117. W.N. Brooks. *AIChE Symposium Series* 98 (1986): 1.
118. L. Carlsson, B. Sandegren, D. Simonsson, and M. Rihovsky. *Journal of the Electrochemical Society* 130 (1982): 342.

162. H.H. Ulig. *Corrosion and Corrosion Control: an Introduction to Corrosion Science and Engineering*. New York: Wiley, 1971.
163. L.L. Shreir. *Corrosion and Corrosion Control*. 2nd ed. Vols. 1, 2. London: Butterworth, 1976.
164. H. Bohni and H. Uhlig. *Journal of the Electrochemical Society* 116 (1969): 906.
165. J.C. Scully. *The Fundamentals of Corrosion*. 2nd ed. Oxford, UK: Pergamon Press, 1975.
166. G.W. Heise and N.C. Cahoon, eds. *The Primary Battery*. Vols. I, II. New York: Wiley, 1971, 1976.
167. P. Bro. *Interface* 4 (1995): 42.
168. D. Linden, ed. *Handbook of Batteries*. 2nd ed. New York: McGraw-Hill, 1995.
169. A.J. Salkind and R. J. Brodd. *Electrochemical Society Proceedings* 87-3 (1987): 127-145.
170. P. Bro and S.C. Levy. *Quality and Reliability Methods of Primary Batteries*. New York: Wiley, 1990.
171. *Rechargeable Batteries Application Handbook*. London: Butterworth-Heinemann, 1992.
172. P.D. Bennet, K.R. Bullock, and M.E. Fiorino. *Interface* 4 (1995): 26.
173. R. Ishikawa, T. Hazama, M. Miyabashi, and H. Andoh. In *Proceedings of the International Workshop on Advanced Batteries*. Osaka, Japan; February 22-24, 1995.
174. S. Megahed and B. Scrosati. *Interface* 4 (1995): 34.
175. G. Pistoia. *Lithium Batteries*. New York: Elsevier, 1994.
176. D.S. Clive Tuck. *Modern Battery Technology*. Chichester, UK: Ellis Horwood, Ltd., 1991.
177. J.H. Hirschenhofer, ed. *Fuel Cell Handbook*. 4th ed. Orinda, CA: Business/Technology Books, 2000.
178. S.A. Angrist, ed. *Direct Energy Conversion*. 3rd ed. Boston: Allyn and Bacon, 1976.
179. K. Kordesh and G. Simader. *Fuel Cells and Their applications*. New York: VCH Publishers, 1996.
180. W. Vielstich, A. Lamm, and H.A. Gasteiger, eds. *Handbook of Fuel Cells: Fundamentals, Technology, and Applications*. New York: Wiley, 2003.
181. T. Fuller. *Interface* 3 (1997): 26.
182. W. Vielstich, A. Lamm, and H.A. Gasteiger. *Handbook of Fuel Cells: Fundamentals Technology and Applications. vol. 4, Fuel Cell Technology and Applications. Pt. 2*. Chichester, England: Wiley, 2003.
183. C. Zawodzinski, M.S., Wilson, and S. Gottesfeld. In *Proton Conducting Membrane Fuel Cells I*. Electrochemical Society Symposium Series 65-23. Pennington, NJ: The Electrochemical Society, Inc., 1995: 57.
184. R. Lemons. *Journal of Power Sources* 29 (1990): 251.
185. M. Wakizoe, O.A. Velev, and S. Srinivasan. *Electrochimica Acta* 40 (1995): 335.
186. G. Hoogers, ed. *Fuel Cell Technology Handbook*. Boca Raton, FL: CRC Press, 2003.
187. T.A. Zawodzinski, J. Davey, J. Valerio, and S. Gottesfeld. *Electrochimica Acta* 40 (1995): 297.
188. S.T. Narayanan, A. Kindler, B. Jeffries-Nakamura, et al. In *Proton Conducting Membrane Fuel Cells I*. Electrochemical Society Symposium Series 65-23. Pennington, NJ: The Electrochemical Society, Inc., 1995: 261.
189. S. Surampudi, S.R. Narayanan, E. Vamos, H. Frank, and G. Halpert. *Journal of Power Sources* 47 (1994): 377.
190. J.S. Wainright, J-T. Wang, D. Weng, R.F. Savinell, and M. Litt. *Journal of the Electrochemical Society* 142 (1995): L121.
191. S.C. Singhal and K. Kendall, eds. *High Temperature Solid Oxide Fuel Cells: Fundamentals, Design, and Applications*. Amsterdam: Elsevier, 2003.
192. J. Larminie and A. Dicks. *Fuel Cell Systems Explained*. New York: Wiley, 2000.
193. E.A. Gillis. *Chemical Engineering Progress* October (1980): 88.
194. M.S. Vreeke, D.T. Mah, and C.M. Doyle. *Journal of the Electrochemical Society* 145 (1998): 3668.
195. F. Barbir, ed., *PEM Fuel Cells: Theory and Practice*. New York: Elsevier Academic Press, 2005.
196. J. Motavalli. *Forward Drive: The Race to Build "Clean" Cars for the Future*. San Francisco: Sierra Club Books, 2001.

27.2 UNITED STATES PATENTS AND RELATED RIGHTS AND DOCUMENTS

27.2.1 UTILITY PATENT

The most common and well-known type of patent is the "utility patent." Utility patents cover functional features of an invention with utility as a key requirement. Inventions that qualify for utility patents include articles of manufacture, compounds or compositions of matter, manufacturing processes, and methods of using articles, compounds, or compositions.

The term of enforceability of a utility patent extends from its issue date to its expiration date. This is in contrast to certain other countries, where a patent once issued may qualify for enforcement retroactively to a publication date that precedes the issuance of the patent. When originally created by federal law, U.S. patents expired 17 years from the issue date. This was changed in 1995 by federal legislation implementing the GATT (General Agreement on Tariffs and Trade) Treaty for international harmonization of patent laws. Under the 1995 legislation, a utility patent applied for after June 8, 1995, will expire 20 years from the filing date of the earliest United States application that the patent derives benefit from. Thus, a utility patent issuing on an original application filed in the United States Patent and Trademark Office (USPTO) after June 8, 1995, expires 20 years from the filing date of the application; and a utility patent issuing on an application filed either before or after June 8, 1995, as a continuation, continuation-in-part, or division of an application filed before June 8, 1995, expires 20 years from the filing date of the previously filed application regardless of the status of that application. A patent that was either (a) issued prior to June 8, 1995, and had not yet expired by that date, or (b) issued after June 8, 1995, on an application filed before that date expires either 17 years from the issue date or 20 years from the filing date, whichever results in a longer period of time between issuance and expiration. The term of a patent is generally not extendable beyond these expiration dates, except for those patents that were issued as the result of an appeal before the USPTO Board of Patent Appeals and Interferences, and for patents on inventions requiring federal regulatory approval prior to commercialization.

A utility patent bestows on its owner the right to exclude others from making, using, offering to sell, or selling the invention as defined by the scope of the patent claims, within the geographical boundaries of the United States and its territories and possessions. Thus, patents to articles of manufacture, compounds, or compositions of matter are infringed by the unauthorized manufacture, use, offer of sale, or sale of the article, compound, or composition within these boundaries. Patents to methods of use are infringed by the unauthorized practice of the patented method within these boundaries. Patents to manufacturing processes are likewise infringed by the unauthorized practice of the patented process within these boundaries, but are also infringed by the importation into the United States of a product that was produced outside the United States by the patented process, or by the offer of sale, the sale, or the use of such a product in the United States. No patent insulates its owner from potential liability as an infringer of another patent.

27.2.2 DESIGN PATENT

Design patents are issued only for articles and cover only the ornamental features of the article rather than functional features. The term of enforceability of a design patent extends from its issue date to an expiration date 14 years from the issue date, and remains unaffected by GATT implementation legislation. Like a utility patent, a design patent bestows on its owner the right to exclude others from making, using, or selling a product that embodies the patented design, within the geographical boundaries of the United States and its territories and possessions.

27.2.3 PROVISIONAL PATENT APPLICATION

A provisional patent application is a document filed in the USPTO as a preliminary step toward applying for a utility patent. The primary advantage of a provisional patent application is the official

publication or 100 years from the year of creation, whichever expires first. Copyrights for works created before January 1, 1978, and still in force on that date have a duration of 28 years from the securing of the copyright, subject to renewal for an additional 47 years.

Copyrights need not be federally registered to be effective, but federal registration is required before suing an infringer, and early registration offers advantages to the copyright owner when enforcing the copyright, particularly in terms of the monetary damages and costs that the successful owner can collect. Copyrights are registered with the United States Copyright Office.

27.3 PATENTS OUTSIDE THE UNITED STATES

As in the United States, patents in countries throughout the world are generally enforceable only in the countries where the patents are issued. There is no global patent; patents must be applied for in each country where patent rights are desired.

Patent treaties between certain groups of countries serve to simplify the process of applying for patents in multiple countries within the groups and to promote consistency in standards for patentability. Included among the multi-country patent treaties are the European Patent Convention (31 countries), the Eurasian Patent Convention (9 countries), the African Regional Industrial Property Organization (ARIPO) (16 countries in western Africa), the African Intellectual Property Organization (OAPI) (16 countries in eastern Africa), the Gulf Cooperation Council (6 countries in the Persian Gulf), and the Patent Cooperation Treaty (PCT) (encompassing the latter 4 conventions plus approximately 60 additional countries including the United States). Each of these treaties offers the establishment of a filing date for a patent application in each of its member countries by filing the application at a single location. In addition, the European Patent Convention, the ARIPO, the OAPI, and the Gulf Cooperation Council each provide a single examination applicable to all of their own member countries.

The oldest and most widely used treaty is the Paris Convention, which permits an application initially filed in a single country to be subsequently filed in other countries with recognition of its original filing date, provided that the subsequent filings are made within a year of the original filing. The Paris Convention has approximately 170 signatory countries worldwide (including the United States). The Paris Convention can be used for foreign filings through any of the other treaties listed above.

The purpose of a patent in any country is to confer a state-recognized property right to an invention. The laws of individual countries differ in such matters as the types of inventions that can be patented, the degree to which an invention must advance the state of the art, the types of prior documents and activities that will defeat patentability, and whether or not the patentee can be required to issue licenses to others and under what conditions, and what constitutes infringement. U.S. patent law, for example, is notable for its difference from the patent laws of certain other countries in the patentability of pharmaceutical compositions and medical procedures (both patentable in the United States), and in cases where competing inventors apply for conflicting patents on the same invention (the United States awards the patent to the first to invent, while most other countries award the patent to the first to file, although, as of the date of publication of this chapter, legislation is pending in the United States to change the standard to first-to-file).

27.4 REQUIREMENTS FOR PATENTABILITY

To qualify for a patent in the United States, an invention must meet the fundamental requirements of novelty, utility, and nonobviousness.

27.4.1 NOVELTY

Novelty is met by the presence of any element or feature of the invention distinguishing it from the "prior art," the legal term used to designate certain categories of information that are considered

that is available to those in the technical field of the invention, or any commercial activity in the United States. The type of search and the manner in which it is conducted will determine what type of prior art is found.

27.5.3 PATENTS AS PRIOR ART

A form of prior art commonly encountered is previously issued patents. The discovery of a relevant patent cannot only affect the patentability of a subsequent invention, but can also raise the possibility of infringement of the patent by the subsequent inventor. These considerations are often independent and must be addressed separately. The freedom to *patent* a new invention over a prior patent requires scrutiny of everything disclosed in the prior patent. The most relevant portion of the prior patent for this purpose is its specification (the text preceding the patent claims), since the specification often contains description or disclosure that does not appear or is not reflected in the claims, or is peripheral to the invention appearing in the claims. The freedom to *practice* a new invention requires scrutiny of the claims of the prior patent, and is achieved when the new invention avoids fully meeting the recitations in each of the claims.

Free to patent but not to practice. An invention of this type is one that falls within the scope of one of the claims of a prior patent that is still in force, while still offering a patentable distinction over what is disclosed in the patent. This includes such inventions as those representing an improvement in a process or product whose initial discovery is the subject of the prior patent that claims the process or product in a generic manner, and inventions whose use requires the concurrent use of the invention claimed in a prior patent. An example is an invention residing in a new reaction to achieve a particular product, followed by an invention residing in a new catalyst or new reaction conditions to enhance the rate, product yield, or selectivity of the reaction without departing from the reaction itself. For inventions in this category, anyone seeking to practice the second invention will require permission from the owners of both patents. The owner of any one of the two patents will likewise require a license from the owner of the other patent to practice the second invention.

Free to practice but not to patent. This describes an invention that is fully disclosed in a prior patent (that is still in force), although outside the scope of the claims of that patent. This category also includes an invention that is fully disclosed (and possibly claimed) in a prior patent that is either expired, dedicated to the public, or declared invalid.

Free to neither patent nor practice. Inventions of this type are those that are fully disclosed in the specification of a prior patent and fall within the scope of the claims of that patent. The discovery of two patents, two patent applications, or a patent and an application claiming the same invention can lead to an "interference," a procedure that determines which of the two competing parties has priority over the other, usually in terms of the date of invention, and awards the patent to the prevailing party.

Free to patent and to practice. Inventions of this type are those that are distinct from anything disclosed in the prior patent and fall outside the scope of the patent claims.

27.5.4 RECORD KEEPING

The date of conception of an invention can often be used to remove a prior patent or publication from consideration as prior art. Laboratory notebooks or other written records are particularly useful for this purpose, provided they bear a fully contained description of the idea conceived or the work performed, and each page is signed and dated by the inventor. The value of the record as evidence is strengthened when the inventor's signature is supplemented by the signature and date of a witness, and further strengthened when the signatures are notarized.

patent application can have trade secret status until the application becomes a patent or is published prior to issuance, as often occurs in countries outside the United States. One can thus apply for a patent with the option of maintaining the invention as a trade secret if a patent is not granted.

Unlike patents, there is no limitation on the duration of a trade secret that is not otherwise extinguished by non-secret disclosure.

27.7 INTELLECTUAL PROPERTY BETWEEN THE EMPLOYER AND EMPLOYEE

The obligations of an inventor to the inventor's employer extend to both patents and trade secrets, and to both present and past employers. Issues regarding these obligations often arise when the inventor changes jobs.

27.7.1 PATENTS—OWNERSHIP AND OTHER RIGHTS AND OBLIGATIONS

While patents are by law issued in the name of the inventor, the patent of an employed inventor is most often owned by the employer, the transfer having been made through an assignment executed by the inventor as a requirement of employment. When no assignment has been executed, the employer may still claim ownership through a contract obligating the employee to assign. The contract is often an express contract included in a more general employment contract. If no employment contract has been signed, the contract to assign patent rights can be inferred from statements of policy in such documents as employee handbooks or company memoranda issued by the employer. Whether express or implied, the employer's claim to ownership of patent rights can be challenged on such grounds as a failure of the employer to clearly explain the obligation, an open disagreement and lack of acquiescence by the employee in the obligation, or the claim that an invention did not involve any materials, facilities, or trade secret information of the employer and bore no connection to work performed for the employer. The latter is often supported by state law.

When neither a patent assignment clause in an employment contract or in a policy statement in an internal company document exists, employer ownership of patent rights can be implied for employees who are hired to invent, i.e., those hired either for a specific project or problem or for their expertise in a specific area. If the inventor is an officer or director of a corporation or other business entity, a special obligation to assign may exist as part of the officer's or director's fiduciary duty toward the entity.

When an inventor refuses to sign the documents required to apply for a patent, a present or former employer claiming ownership of the invention can apply for a patent in the inventor's name, provided that an appropriate showing of the respective rights and obligations can be made. The inventor will be informed by the USPTO of the existence of the application, and the USPTO will independently invite the inventor to participate in the application process.

Employers that do not claim ownership in patented inventions may claim a "shop right," which is a nonexclusive, royalty-free (although nontransferable) right to use the invention. Shop rights arise when an inventor has used the employer's resources to conceive the invention, reduce it to practice, perform scale-up, or develop the invention for commercial use. Shop rights can be voided by actions of either the inventor or the employer that are inconsistent with a shop right, or by express agreement or the payment of compensation by the employer to the inventor, the compensation voiding the royalty-free aspect of the shop right.

27.7.2 TRADE SECRETS—OBLIGATIONS TO PRESENT AND PAST EMPLOYERS

Trade secrets are some of the most valuable assets of employers. Present employees are obligated to respect the trade secrets of their employers by maintaining confidentiality of the secrets. Former employees have a greater obligation because they are prohibited from using or disclosing the trade

28.1 INTRODUCTION

At some point in your work—after you have used all the resources at your disposal, such as this handbook—you will have to write up your results and share them with the world, possibly giving a verbal presentation as well. This moment of communication is the point at which you begin to exist as an engineer or scientist. It is these nontechnical skills, the so-called “soft skills,” that set you apart from others in your field. If readers or listeners of your work are constantly distracted or, worse, amused, by how you present yourself in writing or speaking, they may begin to question what you are trying to say. As Professor Lanham notes, these errors reveal you—and in a way that you don't want to be revealed.

Effective writing and editing involves many considerations, and a brief checklist shows how detailed the process can become. In no particular order, each exercise at writing involves the following:

- Coherence and unity
- Transitions
- Subject-verb agreement
- Clarity and logic
- Pacing
- Conciseness
- Sentence patterns
- Sentence variety
- Awkwardness
- Pronoun reference
- Correct modification
- Word choice

Anyone using this guidebook will likely have already been exposed to a large body of written material and probably be an experienced writer. Many of these steps will be handled in the course of writing, and rarely does one person at this level have trouble with all of the above. What's more likely is that he or she may have a blind spot, say, dangling modifiers and conciseness. For that person, it becomes a matter of identifying the problems and working on them. This is where paying attention becomes important.

Tip: Keep a record of the comments made on your writing and look for patterns.

Welcome the information, for it will help you improve. Technical writing is a skill like any other: the more you practice, the better you get. But remember: it is also possible to practice bad habits. Anyone who has ever played golf will know the truth of this. Practice doesn't make perfect—it ingrains. Perfect practice makes perfect.

A complete writing/speaking treatise is beyond the scope of this chapter, but there are some basic areas and problems that, once corrected, can lead to rapid improvement. Certain errors tend to occur often in technical writing and speaking, and these are dealt with first. Some suggestions follow on refinements of style, along with examples.

28.1.1 SOME PRELIMINARIES

Audience Analysis. This staple of all communication goes beyond merely thinking about the occupations or titles of your readers/listeners. At some point, the following considerations will come into play as you plan your communication. The more of these you can match, the likelier your message will be received successfully. Clearly, it is unrealistic to expect to match more than, say, the cognitive needs and style, but be aware that your readers will likely be reading you through a lens colored by these variables.

Variables affecting a receiver's (reader/listener) behavior:

important aspect of style—the use of sentence combining—and concludes with some thoughts about the prevailing practice of avoiding the use of the first person.

28.2.1 PARAMEDIC METHOD

Although there are five steps to the method, they are not sequential. For example, number 4 may be considered a first step; numbers 1 to 3 can be done at the same time; and number 5 acts as a final check. According to this method,

1. Circle the prepositions.
2. Circle the “is” forms (be, am, is, are, was, were).
3. Put the action where it belongs—in a simple active verb.
4. Start fast—no mindless “zero-content” openings.
5. Read your draft aloud and listen for sound patterns.

Circle the Prepositions. Prepositional phrases act as adjectives or adverbs, adding qualifying detail. Used properly, they do their little jobs quite effectively, but in technical writing they often march along in a parade of details—an ineffective catalog because all details are treated the same way without regard to levels of importance. Consider the following example (from T.P. Johnson. *Effective Communication for Engineers*, 6), which contains eight prepositional phrases.

Before

The unlikelyhood **of** meeting orders **from** the majority **of** its new customers is **of** concern **to** the company, due **to** tardiness **in** the installation **of** its new manufacturing line.

Written in this way, all the details are equally weighted—nothing is more important than anything else. Read aloud, the sentence also lacks any life. The two- or three-word phrases all tramp along in the same rhythm. This is a poetic device (of two unstressed syllables and a stressed) that poets use to slow down the movement of the verse. Rarely is that a goal of technical writing. After a few such sentences, it is not surprising that readers find themselves nodding off.

The sentence gains new energy with the use of dependent clauses that subordinate details with respect to their importance.

After

The company does not know whether it can meet most new-customer orders, because its new manufacturing line is not yet installed.

This revision has zero prepositional phrases and two dependent clauses. It also exemplifies steps 2 and 3 in the paramedic method. See Section 28.2.2 for more about dependent clauses. Prepositional phrases are, of course, an integral part of writing and are not to be avoided. It is only their excessive use and without thought to what is being said that creates problems. The lack of such phrases in this sentence is only coincidental.

Circle the “Is” Forms (be, am, is, are, was, were). The “to be” verbs are important, but by their nature they make existence statements rather than action statements. When overworked, they rob a sentence of energy. For example,

Before

The calibration of the thermocouple **was** accomplished by the technician.

Sentence Combining. Look for short sentences, especially if related by information, and combine them. Common sense has to prevail here. The goal is not just to write long sentences. Balance is important, but usually a series of short statements indicates undeveloped ideas or ideas lacking proper emphasis. The use of dependent clauses is at the heart of improving style by sentence combining. The following sentences illustrate what is involved.

Before

Before starting experiments each day, the spectrophotometer was calibrated. This was accomplished by determining the absorbance of a standard solution of dye.

After

We first calibrated the spectrophotometer by determining the absorbance of a standard solution of dye.

Before (The following example contains undifferentiated statements.)

The temperature difference is the driving force in a heat exchanger. The temperature difference can be the difference between the temperatures of the steam and the water.

After

The temperature difference, which is the driving force in a heat exchanger, is the difference, for example, between the temperatures of the steam and the water.

or, depending on the emphasis

The temperature difference, which is the difference between the temperatures of the steam and the water, is the driving force in a heat exchanger.

Before (This example contains an awkward shift from active to passive.)

To begin the experiment, we adjusted the water flow rate to the desired value. The exit stream valve was then opened and the other steam exit valves were closed.

After

To begin the experiment, we adjusted the water flow rate to the desired value, opened the exit stream valve, and closed the other steam exit valves.

28.2.3 AVOIDANCE OF FIRST PERSON?

One of the ironies of writing in the engineering profession is the disappearance of the author. At every stage of the work, the engineer is the chief actor in the drama. From the birth of the idea to the presentation of the results to the world, he or she is the central figure. Yet, when it comes time to tell the world, the writer has to disappear. By being forced to drop the use of the word "I," the writer adopts the third person, which leads to more pronouns and passive verbs, and this in turn leads to all the problems with dangling and misplaced modifiers.

A workable compromise might be the use of the first person in moderation. For example, in certain sections of a report it makes sense to let the author's voice come through. A description of apparatus, for example, rightly focuses on the devices themselves, unless the writer wants to

28.3 GRAMMATICAL PROBLEMS COMMON TO ENGINEERING WRITING

Handbooks, textbooks, usage manuals, and any number of general works are filled with the problems common to technical writing. Improvement in these typical areas will immediately improve your writing overall.

28.3.1 AGREEMENT

Problems in subject-verb and noun-pronoun agreement in technical writing often arise because the verb is separated from the subject by one or more clauses that often contain a plural element. In the following examples, the writers allowed themselves to be misled by the plurals in the intervening words:

The **kerosene hold-up** in the column at agitator speeds of 200, 250, and 300 rpm **are** shown in Figure 5.

Interstage eddy flow at the two agitator speeds also **confirm** the above prediction.

28.3.2 AGREEMENT AND AMBIGUITY

The following sentence illustrates a number of problems:

The exit temperature of the water and the water flow rate was observed to give an approximation of how the constants functioned.

In this example, the writer creates several problems. First, it appears that the water flow rate also has a temperature! The order of the first two statements implies that the preposition “of” applies to both items. Writing “water flow rate” first would remove that problem and make it clear that the verb should be “were.” Were observed to give what? That is, a dangling modifier (infinitive, see below) is next. Here’s what must have been the original meaning:

To give an approximation of how the constants functioned, we observed the water flow rate and the exit temperature of the water.

28.3.3 CONCISENESS—OR, WORDINESS FROM INSECURITY

First, conciseness is not the same as brevity. Clarity is the goal. Sometimes, a sentence with 40 words may be more concise than one with half that many. Wordiness is almost always the sign of an early draft. In an early draft, one’s main concern is to get the ideas down; revision is for later.

An effective way of achieving conciseness is through subordination of sentences (see also Section 28.2.2). Another step is to write confidently. The following are examples of degrees of authorial insecurity: “I feel that,” “It should be noted,” and “The reason is that.” If something should be noted, then do so. The note itself is sufficient. To preface it by saying “It should be noted that” or “It is worthy to note that” is to show your insecurity in your own words.

I feel that the approach will not work under these conditions.

If you trust yourself and your work, be bold:

The approach will not work under these conditions.

It should be noted that the average value does fall within the range of literature values for a fouled system.

The error and the humor can be seen by considering the following sentences:

The rabbits were seen using binoculars.

The skeleton was discovered while digging for gold.

Just as the rabbits are holding binoculars and Mr. Bones is digging here, in the previous sentences the permeability is using pressure, models are using linear regression, and runs are using flow patterns! Sometimes the absurdity is immediately evident:

After drying in the sun for a few days, the workers finished the roadway.

And if attention is not paid, a dangling modifier can strain common sense:

After exiting the first exchanger, the water temperature was measured again by another thermocouple.

The inoculum was prepared a period of time before arriving in the laboratory.

28.3.5 SMOTHERED VERB

A smothered verb is also referred to as nominalization. A sure-fire way to make writing sound impressive, or so think ineffective writers, is to convert a verb into a noun and then add another weak verb to the sentence. This is guaranteed to add more words to your text. Consider the following sentence:

The experimental engineer calibrated the thermocouple.

Simple and straightforward but not very “impressive.” What you will often find in student writing is the following version:

The calibration of the thermocouple was accomplished by the technician.

The main action of the sentence is contained in the act of calibrating. The verb has been *nominalized*—turned into a noun; two prepositional phrases have been added (“of the thermocouple” and “by the experimental engineer”); and another verb created (“was accomplished”).

Another example:

We compared the permeabilities during co- and countercurrent flow by graphing the permeability versus run number.

With the onus on the use of first person, this sentence quite easily becomes

The comparison of the permeabilities during co- and countercurrent flow was done by graphing the permeability versus run number.

But it could just as easily have been written

The permeabilities during co- and countercurrent flow were compared by graphing the permeability versus run number.

With no gain in clarity or meaning, the writers of these sentences have taken a perfectly good concise sentence and larded it with fat! Whenever possible, keep the main action of the sentence in the main verb.

about the work. An *informative* abstract, however, contains information from the report, including the facts on which the conclusions are based, the conclusions themselves, and any recommendations made. Basically, it is a miniature report or distillation of an entire report.

Table of Contents. Keep the reader in mind and include everything that will make the work accessible to the reader. Remember to include figures and tables in a separate listing.

Introduction. The importance and relevance of the project and the objectives of the work are presented here. The level of detail depends on the type of report or the intended audience. A proposal or memorandum will require a different opening than a formal report, laboratory report, or technical manual. In any case, you should state your subject and purpose for writing and include some idea of the scope of the work. Again, the level of detail and size of the report/project will determine how much detail is needed in the introduction. For a technical manual, most of the detail should be left to the body of the report, with the introduction doing just that: introducing.

Method/Theoretical Information. Ideas, principles, theories, and techniques as well as relevant equations that apply to the project are included here. Derivations, calibrations, and other ancillary material are usually put in an appendix. Be careful not to turn this section into a list of equations. Provide enough information, both as introductory material and as transitions, to demystify the equations. In short, keep readers' needs in mind as you write.

Apparatus and Procedure. Describe the main features of the apparatus including schematics as well as major pieces of equipment. Use the past tense if reporting on work already completed. Use present tense when describing an apparatus or procedure in general.

Results and Discussion. In general, use plots (figures) rather than tables to discuss your results. Describe what is shown in the figures and tables and tell what it means. Do not make the reader figure it out. For tables and figures in the main body, describe each in a caption and refer to each in the text. Do not put all your figures and tables in the Results and Discussion section; show examples of some plots and discuss the general results. Present results of your statistical work, including regression, propagation of error, and analysis of variance. It is acceptable to refer to the appendix for some details.

Conclusions and Recommendations. Results and Discussion have led to concrete conclusions. Discuss those here as short sentences in a numbered list that must be supported by the data and the theory. Relate your conclusions to the objectives presented in the introduction and add the recommendations supported by the results of your project.

Notation. List symbols used in alphabetical order, English first and Greek in a second list. (Be sure to also introduce them in the report the first time they are used, in an indented table.)

References. List books and articles referred to in the report (see Section 28.4.5).

Appendices. Appendices contain details needed to support your results and to be used by people who may continue your work. Make it easy for them by organizing the material under subtitles or sub-appendices listed in the table of contents. Use enough words in appendices to define units and manipulations, but do not worry about smooth text with introductions and transitions. Include data sheets, sample calculations including error propagation, tables of intermediate variables in the calculations, working plots, calibration curves, and all the figures and tables that you did not include in the main body.

28.4.1 RELATED FORMAT MATTERS: EQUATIONS, TABLES, FIGURES, REFERENCES

Equations. State the nature or origin of each equation that you use (definition, balance, kinetic expression, or empirical correlation) to take the mystery out of your development. For example,

The rate of heat transfer in a heat exchanger is frequently reported as follows:

These results agree with those in Jones and McLaughlin (4, 77).

The derivation below follows that in Bird, Stewart, and Lightfoot (2, 255).

Hardcastle et al. (6, 215) showed that this method is incorrect.

The style of reference lists varies widely from one discipline to another, from one journal to another, and from one corporation to another. Professional societies often have a style that is used in all their journals. See Section 28.6 for lists of professional and general style guides.

Several types of references are needed. The following examples cover general usage:

Authored Text

Bird, R.B., W.E. Stewart, and E.N. Lightfoot, *Transport Phenomena*, New York: Wiley, 1960, chapter 12.

Greenkorn, R., and D. Kessler, *Transfer Operations*, New York: McGraw-Hill, 1972, 78–82.

Edited Text

CRC Handbook of Chemistry and Physics, 87th ed., R.C. Weast, ed., Cleveland, OH: CRC Press Inc., 2006.

Journal Article

Kramers, H., and P.J. Kreyger, *Chem. Eng. Sci.*, 6 (42) (1956).

Online Sources. In addition to the information provided in the previous examples (author, title, publication source, page numbers), these citations require the medium (online), the computer network (e.g., Internet), date, and electronic address (the URL).

28.5 BASIC PRINCIPLES OF ORAL REPORTING IN THE WORKPLACE

An oral report is simply a conversation—with attention to some constraints imposed by the situation. If, as you are walking down the hall, the boss asks, “How’s the project coming?”, your response is basically an oral report. Rather than have, say, a dozen such strolls—to talk with everyone who might have an interest or a stake in your work, it is more practical to talk to all of them at once. So why is this situation so much more fraught with terror than the former? It need not be. What is different about it? For one, with more people in the room you have to make eye contact with more than one person. Because they are further away from you, you have to speak louder. And since sound waves dampen rather quickly, you need to enunciate clearly so that even the last row will understand you. You also may not know the expectations or biases of all of your listeners, so it is best to err on the side of caution and to dress formally and maybe speak a little more formally than in everyday conversation. And the same holds true for the level of formality and quality of visuals or other materials. But these are all practical accommodations dictated by the situation.

For some reason we develop this fear of “The Formal Presentation.” Not confident in ourselves or our speaking style, we adopt a “false formal” style that quickly sounds like the worst nineteenth-century legalese. See Section 28.5.2 for some tips on dealing with anxiety.

Oral presentations come in all types and lengths—from the stroll down the hall to a professional conference or major policy address. Though dramatically different, they all share some common features.

Target the audience: What is obvious to you may not be so to them. Consider their:

information (which will be easy if you have practiced the talk). Also, practice “dropping” the eyes instead of bending down to look at notes. This motion is not as large as a movement of the head and is not as noticeable. Look back at the screen only for as long as it takes you to orient yourself.

Voice. Why should the audience show any enthusiasm if you do not? Enunciate clearly—sloppiness here may signal a lack of preparation. Worse yet, the audience may see it as a sign of disrespect, which is a sure way to lose their sympathy. You will also have to speak up if the room is fairly large. Have a friend signal to you if you are not making yourself heard. If talking too fast is your habit, focus on enunciating clearly. Consonants take time to form and doing so will give you the slowdown you need. There's no excuse, in a formal presentation, for “wanna,” “gonna,” and so on. Mispronouncing technical terms is especially bad practice. Like a performer in a one-person show on Broadway, you are in control of your material.

Tip: Always give yourself positive cues. A basketball player who thinks, “Don't miss this freethrow!” is in trouble already. He or she has given the muscles no positive action to perform. Focusing on what is in one's control is important. That player should be focusing on technique, not outcome. In the same way, focusing on enunciating clearly will accomplish more than telling yourself, “Don't talk too fast” or “Slow down”—both of which detract from your concentration.

Accent. Don't worry about any accent you may have or think you have. Accents vary in all countries from region to region, but there's no excuse for sloppy pronunciation. Look up the pronunciation of words that give you trouble.

Movement. Don't be afraid to gesture when speaking, if it is natural for you to do so. Purposeful movement (gestures also) can help in several ways:

- Uses nervous energy and puts it to work
- Attracts attention; emphasizes points
- Adds confidence; keeps speaker and audience awake
- Refreshes the visual scene for the audience

Speakers on the radio gesture emphatically even though they are out of sight of the audience. Use normal descriptive gestures that everyone uses in conversation to indicate length, height, speed, roundness, and so forth.

Notes. They should be unobtrusive. Avoid holding an 8.5 x 11 sheet of paper. Make notes very brief, using key words or phrases.

Timing. Clearly, the most important element for your professional audience will be your explanation of your results. In planning your talk, do this part first; then, with the time available, fill in the other sections.

Visuals. Time limitations and volume of material to cover make it necessary that you use an overhead projector, slide projector, or some computer-aided variation. Quality is very important here. If your lettering is too small or sloppy, your audience will not only have trouble reading what you have written but will likely form a negative opinion about the quality of your work or effort. In general:

- Print, using large lettering
- Use brief action statements, not complete sentences
- Put only one equation on a slide (unless they are very brief)
- Draw a neat schematic of the apparatus, highlighting the main features
- Label axes of graphs; include data points and confidence intervals

American Institute of Chemical Engineers. (See the journals for general format requirements.)

American Institute of Physics. *AIP Style Manual*. 4th ed. Woodbury, NY: American Institute of Physics, 1990.

28.6.3 USAGE GUIDES

The American Heritage Guide to Contemporary Usage and Style. New York: Houghton Mifflin, 1996.

Fowler's Modern English Usage. 3rd rev. ed. R. W. Burchfield, ed. New York: Oxford University Press, 2004.

28.6.4 MANUALS AND GUIDES

Alred, G.T., C.T. Brusaw, and W.E. Oliu. *Handbook of Technical Writing*. 8th. rev. ed., New York: St. Martin's Press, 2006.

The Chicago Manual of Style. 15th ed. Chicago: University of Chicago Press, 2003.

National Information Standards Organization. *Scientific and Technical Reports—Preparation, Presentation and Preservation*. ANSI/NISO Z39.18 – 2005. Baltimore, MD: NISO, 2005.

Turabian, K.L., et al. *A Manual for Writers of Term Papers, Theses, and Dissertations*. 7th ed. Chicago: University of Chicago Press, 2007.

Strunk, W., and E.B. White. *The Elements of Style*. 4th ed. New York: Allyn & Bacon, 1999. *Principles of English Usage in the Digital Age*. San Francisco: Hardwired, 1996.

28.6.5 GRAPHICS

Tufte, E.R. *The Visual Display of Quantitative Information*. 2nd ed. Cheshire, CT: Graphics Press, 2001.

28.6.6 ORAL PRESENTATIONS

Dayne, M.B. *The Performers Voice*, New York: Norton, 2005.

Hoff, R. *I Can See You Naked*. Kansas City, MO: Andrews and McMeel, 1992. Out of print but if found, a delightful and perceptive account for giving all kinds of professional presentations.

1. Confidential information: What is confidential information? Incidences have occurred in which an employer claims that specific information is confidential. Yet the company has permitted the information to be published in the open technical literature. Often the engineer is not certain just what is and what is not confidential.
2. What information can an employee take from one company to a second? Often details on the manufacture of a new catalyst are considered proprietary; yet if the employee developed a new method of designing a heat exchanger, the information might not be considered proprietary. An engineer supposedly improves and becomes more of an expert while he is with the first employer.
3. Assuming an engineer becomes convinced that a process or certain equipment has serious safety problems, but the employer insists that the current set-up is safe. What course of action should the engineer follow? With current laws, an engineer can be held liable for suppressing information on potential hazards. At the very least, it is recommended that the engineer address written correspondence on this matter to the top management of his company.
4. Stolen information: Situations have occurred in which an individual leaving one company fills his briefcase with confidential reports. When an employee at either the first or second company learns of this, what action should he take?
5. Technical reports have been published in which incorrect or misleading information has been published on a competitor's process.

Many industries and individuals find that they need to consult to an increased extent with attorneys in planning their actions and programs.

29.2 CASE STUDIES

The following case examples have been used by the author in numerous talks to engineers, students, and others throughout the United States. Several examples were published in the magazine *Chemical Engineering* (September 2, 1963, 87–90; December 9, 1963, 177–184; September 22, 1980, 177–184; September 2, 1987, 40–43; and September 28, 1987, 108–120). The author has, on occasion, modified the original. In some cases, he has used personal experiences. The questions raised in these talks are first reported. The answers received during these presentations are summarized.

29.2.1 CASE OF THE EAGER APPLICANT

Mr. A of ABC Chemical Co. interviews engineer X of XYZ Chemical Co. for an opening in ABC. ABC and XYZ are competitors. As engineer X explains his capabilities, he discloses confidential information about XYZ. Such information is of value to ABC.

Engineer X is obviously a top-notch engineer and he would be able to do the required engineering for ABC.

Questions

- (a) Is it ethical for Mr. A to pass on the confidential information to the engineers of ABC? The information was volunteered freely by engineer X.
- (b) If the information was passed on, is it ethical for engineers in ABC to use the information if they recognize how it was obtained?
- (c) Should ABC hire engineer X?
- (d) Should ABC inform XYZ that engineer X talks too much?

Comments

Most engineers consider this as a grey area. I agree. Is this new heat exchanger truly proprietary? Ken has had courses on heat exchangers in college. Is this new exchanger based on a truly new and unexpected concept?

Ken needs to report to Yum Yum that an improved exchange is possible but also to report possible legal problems. If Ken believes that the new exchanger is really his idea and that it is a logical extension of his scientific growth, then he should receive a favorable legal report first. If there is any question on the ethics, Yum Yum should inform Superbouncy, who would likely license at a rather low cost.

29.2.4 SPY IN SKY

Engineer Z of Super Plastics, Inc. is to estimate production costs of a new type of polyethylene produced by a competitor. She reviews the literature and her analysis indicates that the design and size of reactor are of key importance. She needs more information on the size of the reactor. Driving by the plant gives her a good idea on auxiliary equipment but not of the reactor. She is convinced that aerial photography would provide important information.

Questions

- (a) Are photos taken from the road ethical?
- (b) Are photos taken from an airplane ethical?
- (c) Are photos taken from a helicopter ethical?

Comments

Most engineers and students agree by a large majority to a yes answer for question (a). Less than 50% vote affirmatively to question (b) and almost none to question (c). Yet, if the competitor really has information that should be hid, that company could either hide it by placing siding around the reactor or by building dummy reactors.

Engineers do not like the idea of snooping on a competitor by aerial photography. Yet a U.S. government agency is known to have used it on at least one occasion. In another case, I have been told that one company aurally spied on another.

29.2.5 CASE OF REACTOR THAT MAY RUN AWAY

Engineer L works for KO Acid Co. and has just been assigned a new supervisor (engineer M). Engineer L is asked to make laboratory batch runs of a process described in a memo from Alpine Chemical Co. Rumor is that this memo arrived with the new supervisor, who had a job with Alpine Chemical 30 days ago. If batch laboratory runs are satisfactory, plant runs will be started shortly with engineer L in charge. Batch runs are conducted. Three runs result in major boilover of strong acid, including two on the day before the first plant run is to be made.

Questions

- (a) Should engineer L ask about the ethics of the situation from the new supervisor, who seems unfriendly?
- (b) Should engineer L perform the batch runs as requested if circumstantial evidence indicates that the memo was taken without permission from Alpine?
- (c) Should engineer L perform the plant runs as requested? Take any action relative to ethics before making the plant runs?
- (d) If engineer L resigns from KO Acid, does he have any responsibilities to other employees who may be endangered if there is a "runaway"?

used by company B; company B reported no specific experimental evidence on the dangers of the other catalyst. *They merely postulated on the dangers.* Many people did not agree that this other catalyst was that dangerous.

- (c) As a result of the report distributed by company B, several companies felt obligated to test the hypothesis publicized by company B. These other companies asked company B to be a participant and pay their share of the costs of the testing. Company B declined.
- (d) Tests indicated that company B's postulate was incorrect.

Comments

If you were an engineer of either company A or company B, what action if any should you take when you learned of your company's actions?

1. If the digits to be discarded begin with a digit less than 5, the digit preceding the first discarded digit is not changed.

Example: 6.974 951 5 rounded to 3 digits is 6.97

2. If the digits to be discarded begin with a digit greater than 5, the digit preceding the first discarded digit is increased by one.

Example: 6.974 951 5 rounded to 4 digits is 6.975

3. If the digits to be discarded begin with a 5 and at least one of the following digits is greater than 0, the digit preceding the 5 is increased by 1.

Example: 6.974 851 rounded to 5 digits is 6.974 9

4. If the digits to be discarded begin with a 5 and all of the following digits are 0, the digit preceding the 5 is unchanged if it is even and increased by one if it is odd. (Note that this means that the final digit is always even.)

Examples:

6.974 951 5 rounded to 7 digits is 6.974 952

6.974 950 5 rounded to 7 digits is 6.974 950

REFERENCE

Taylor, B. N., *Guide for the Use of the International System of Units (SI)*, NIST Special Publication 811, 1995 Edition, Superintendent of Documents, U.S. Government Printing Office, Washington, DC 20402, 1995.

Factors in **boldface** are exact

To convert from	to	Multiply by	
abampere	ampere (A)	1.0	E+01
abcoulomb	coulomb (C)	1.0	E+01
abfarad	farad (F)	1.0	E+09
abhenry	henry (H)	1.0	E-09
abmho	siemens (S)	1.0	E+09
abohm	ohm (Ω)	1.0	E-09
abvolt	volt (V)	1.0	E-08
acceleration of free fall, standard (g_n)	meter per second squared (m/s^2)	9.806 65	E+00
acre (based on U.S. survey foot) ⁹	square meter (m^2)	4.046 873	E+03
acre foot (based on U.S. survey foot) ⁹	cubic meter (m^3)	1.233 489	E+03
ampere hour (A · h)	coulomb (C)	3.6	E+03
ångström (Å)	meter (m)	1.0	E-10
ångström (Å)	nanometer (nm)	1.0	E-01
apostilb (asb)	candela per meter squared (cd/m^2)	3.183 098	E-01
are (a)	square meter (m^2)	1.0	E+02

To convert from	to	Multiply by	
British thermal unit _{IT} per hour (Btu _{IT} /h)	watt (W)	2.930 711	E-01
British thermal unit _{th} per hour (Btu _{th} /h)	watt (W)	2.928 751	E-01
British thermal unit _{IT} per hour square foot degree Fahrenheit [Btu _{IT} /(h · ft ² · °F)]	watt per square meter kelvin [W/(m ² · K)]	5.678 263	E+00
British thermal unit _{th} per hour square foot degree Fahrenheit [Btu _{th} /(h · ft ² · °F)]	watt per square meter kelvin [W/(m ² · K)]	5.674 466	E+00
British thermal unit _{th} per minute (Btu _{th} /min)	watt (W)	1.757 250	E+01
British thermal unit _{IT} per pound (Btu _{IT} /lb)	joule per kilogram (J/kg)	2.326	E+03
British thermal unit _{th} per pound (Btu _{th} /lb)	joule per kilogram (J/kg)	2.324 444	E+03
British thermal unit _{IT} per pound degree Fahrenheit [Btu _{IT} /(lb · °F)]	joule per kilogram kelvin [J/(kg · K)]	4.1868	E+03
British thermal unit _{th} per pound degree Fahrenheit [Btu _{th} /(lb · °F)]	joule per kilogram kelvin [J/(kg · K)]	4.184	E+03
British thermal unit _{IT} per pound degree Rankine [Btu _{IT} /(lb · °R)]	joule per kilogram kelvin [J/(kg · K)]	4.1868	E+03
British thermal unit _{th} per pound degree Rankine [Btu _{th} /(lb · °R)]	joule per kilogram kelvin [J/(kg · K)]	4.184	E+03
British thermal unit _{IT} per second (Btu _{IT} /s)	watt (W)	1.055 056	E+03
British thermal unit _{th} per second (Btu _{th} /s)	watt (W)	1.054 350	E+03
British thermal unit _{IT} per second square foot degree Fahrenheit [Btu _{IT} /(s · ft ² · °F)]	watt per square meter kelvin [W/(m ² · K)]	2.044 175	E+04
British thermal unit _{th} per second square foot degree Fahrenheit [Btu _{th} /(s · ft ² · °F)]	watt per square meter kelvin [W/(m ² · K)]	2.042 808	E+04
British thermal unit _{IT} per square foot (Btu _{IT} /ft ²)	joule per square meter (J/m ²)	1.135 653	E+04
British thermal unit _{th} per square foot (Btu _{th} /ft ²)	joule per square meter (J/m ²)	1.134 893	E+04
British thermal unit _{IT} per square foot hour [(Btu _{IT})/(ft ² · h)]	watt per square meter (W/m ²)	3.154 591	E+00
British thermal unit _{th} per square foot hour [Btu _{th} /(ft ² · h)]	watt per square meter (W/m ²)	3.152 481	E+00
British thermal unit _{th} per square foot minute [Btu _{th} /(ft ² · min)]	watt per square meter (W/m ²)	1.891 489	E+02
British thermal unit _{IT} per square foot second [(Btu _{IT})/(ft ² · s)]	watt per square meter (W/m ²)	1.135 653	E+04
British thermal unit _{th} per square foot second [Btu _{th} /(ft ² · s)]	watt per square meter (W/m ²)	1.134 893	E+04
British thermal unit _{th} per square inch second [Btu _{th} /(in ² · s)]	watt per square meter (W/m ²)	1.634 246	E+06
bushel (U.S.) (bu)	cubic meter (m ³)	3.523 907	E-02
bushel (U.S.) (bu)	liter (L)	3.523 907	E+01
calorie _{IT} (cal _{IT}) ¹¹	joule (J)	4.1868	E+00
calorie _{th} (cal _{th}) ¹¹	joule (J)	4.184	E+00
calorie (cal) (mean)	joule (J)	4.190 02	E+00
calorie (15 °C) (cal ₁₅)	joule (J)	4.185 80	E+00

To convert from	to	Multiply by	
cubic inch (in ³) ¹⁴	cubic meter (m ³)	1.638 706	E-05
cubic inch per minute (in ³ /min)	cubic meter per second (m ³ /s)	2.731 177	E-07
cubic mile (mi ³)	cubic meter (m ³)	4.168 182	E+09
cubic yard (yd ³)	cubic meter (m ³)	7.645 549	E-01
cubic yard per minute (yd ³ /min)	cubic meter per second (m ³ /s)	1.274 258	E-02
cup (U.S.)	cubic meter (m ³)	2.365 882	E-04
cup (U.S.)	liter (L)	2.365 882	E-01
cup (U.S.)	milliliter (mL)	2.365 882	E+02
curie (Ci)	becquerel (Bq)	3.7	E+10
darcy ¹⁵	meter squared (m ²)	9.869 233	E-13
day (d)	second (s)	8.64	E+04
day (sidereal)	second (s)	8.616 409	E+04
debye (D)	coulomb meter (C · m)	3.335 641	E-30
degree (angle) (°)	radian (rad)	1.745 329	E-02
degree Celsius (temperature) (°C)	kelvin (K)	$T/K = t/^{\circ}\text{C} + 273.15$	
degree Celsius (temperature interval) (°C)	kelvin (K)	1.0	E+00
degree centigrade (temperature) ¹⁶	degree Celsius (°C)	$t/^{\circ}\text{C} \approx t/\text{deg.cent.}$	
degree centigrade (temperature interval) ¹⁶	degree Celsius (°C)	1.0	E+00
degree Fahrenheit (temperature) (°F)	degree Celsius (°C)	$t/^{\circ}\text{C} = (t/^{\circ}\text{F} - 32)/1.8$	
degree Fahrenheit (temperature) (°F)	kelvin (K)	$T/K = (t/^{\circ}\text{F} + 459.67)/1.8$	
degree Fahrenheit (temperature interval)(°F)	degree Celsius (°C)	5.555 556	E-01
degree Fahrenheit (temperature interval) (°F)	kelvin (K)	5.555 556	E-01
degree Fahrenheit hour per British thermal unit _{IT} (°F · h/Btu _{IT})	kelvin per watt (K/W)	1.895 634	E+00
degree Fahrenheit hour per British thermal unit _{th} (°F · h/Btu _{th})	kelvin per watt (K/W)	1.896 903	E+00
degree Fahrenheit hour square foot per British thermal unit _{IT} (°F · h · ft ² /Btu _{IT})	square meter kelvin per watt (m ² · K/W)	1.761 102	E-01
degree Fahrenheit hour square foot per British thermal unit _{th} (°F · h · ft ² /Btu _{th})	square meter kelvin per watt (m ² · K/W)	1.762 280	E-01
degree Fahrenheit hour square foot per British thermal unit _{IT} inch [°F · h · ft ² /(Btu _{IT} · in)]	meter kelvin per watt (m · K/W)	6.933 472	E+00
degree Fahrenheit hour square foot per British thermal unit _{th} inch [°F · h · ft ² /(Btu _{th} · in)]	meter kelvin per watt (m · K/W)	6.938 112	E+00
degree Fahrenheit second per British thermal unit _{IT} (°F · s/Btu _{IT})	kelvin per watt (K/W)	5.265 651	E-04
degree Fahrenheit second per British thermal unit _{th} (°F · s/Btu _{th})	kelvin per watt (K/W)	5.269 175	E-04
degree Rankine (°R)	kelvin (K)	$T/K = (T/^{\circ}\text{R})/1.8$	
degree Rankine (temperature interval) (°R)	kelvin (K)	5.555 556	E-01
denier	kilogram per meter (kg/m)	1.111 111	E-07
denier	gram per meter (g/m)	1.111 111	E-04

To convert from	to	Multiply by	
foot pound-force per second (ft · lbf/s)	watt (W)	1.355 818	E+00
foot to the fourth power (ft ⁴) ¹⁷	meter to the fourth power (m ⁴)	8.630 975	E-03
franklin (Fr)	coulomb (C)	3.335 641	E-10
gal (Gal)	meter per second squared (m/s ²)	1.0	E-02
gallon [Canadian and U.K. (Imperial)] (gal)	cubic meter (m ³)	4.546 09	E-03
gallon [Canadian and U.K. (Imperial)] (gal)	liter (L)	4.546 09	E+00
gallon (U.S.) (gal)	cubic meter (m ³)	3.785 412	E-03
gallon (U.S.) (gal)	liter (L)	3.785 412	E+00
gallon (U.S.) per day (gal/d)	cubic meter per second (m ³ /s)	4.381 264	E-08
gallon (U.S.) per day (gal/d)	liter per second (L/s)	4.381 264	E-05
gallon (U.S.) per horsepower hour [gal/(hp · h)]	cubic meter per joule (m ³ /J)	1.410 089	E-09
gallon (U.S.) per horsepower hour [gal/(hp · h)]	liter per joule (L/J)	1.410 089	E-06
gallon (U.S.) per minute (gpm)(gal/min)	cubic meter per second (m ³ /s)	6.309 020	E-05
gallon (U.S.) per minute (gpm)(gal/min)	liter per second (L/s)	6.309 020	E-02
gamma (γ)	tesla (T)	1.0	E-09
gauss (Gs, G)	tesla (T)	1.0	E-04
gilbert (Gi)	ampere (A)	7.957 747	E-01
gill [Canadian and U.K. (Imperial)] (gi)	cubic meter (m ³)	1.420 653	E-04
gill [Canadian and U.K. (Imperial)] (gi)	liter (L)	1.420 653	E-01
gill (U.S.) (gi)	cubic meter (m ³)	1.182 941	E-04
gill (U.S.) (gi)	liter (L)	1.182 941	E-01
gon (also called grade) (gon)	radian (rad)	1.570 796	E-02
gon (also called grade) (gon)	degree (angle) (°)	9.0	E-01
grain (gr)	kilogram (kg)	6.479 891	E-05
grain (gr)	milligram (mg)	6.479 891	E+01
grain per gallon (U.S.) (gr/gal)	kilogram per cubic meter (kg/m ³)	1.711 806	E-02
grain per gallon (U.S.) (gr/gal)	milligram per liter (mg/L)	1.711 806	E+01
gram-force per square centimeter (gf/cm ²)	pascal (Pa)	9.806 65	E+01
gram per cubic centimeter (g/cm ³)	kilogram per cubic meter (kg/m ³)	1.0	E+03
hectare (ha)	square meter (m ²)	1.0	E+04
horsepower (550 ft · lbf/s) (hp)	watt (W)	7.456 999	E+02
horsepower (boiler)	watt (W)	9.809 50	E+03
horsepower (electric)	watt (W)	7.46	E+02
horsepower (metric)	watt (W)	7.354 988	E+02
horsepower (U.K.)	watt (W)	7.4570	E+02
horsepower (water)	watt (W)	7.460 43	E+02
hour (h)	second (s)	3.6	E+03
hour (sidereal)	second (s)	3.590 170	E+03
hundredweight (long, 112 lb)	kilogram (kg)	5.080 235	E+01
hundredweight (short, 100 lb)	kilogram (kg)	4.535 924	E+01
inch (in)	meter (m)	2.54	E-02

To convert from	to	Multiply by	
lambert ¹⁸	candela per square meter (cd/m ²)	3.183 099	E+03
langley (cal _m /cm ²)	joule per square meter (J/m ²)	4.184	E+04
light year (l.y.) ¹⁹	meter (m)	9.460 73	E+15
liter (L) ²⁰	cubic meter (m ³)	1.0	E-03
lumen per square foot (lm/ft ²)	lux (lx)	1.076 391	E+01
maxwell (Mx)	weber (Wb)	1.0	E-08
mho	siemens (S)	1.0	E+00
microinch	meter (m)	2.54	E-08
microinch	micrometer (μm)	2.54	E-02
micron (μ)	meter (m)	1.0	E-06
micron (μ)	micrometer (μm)	1.0	E+00
mil (0.001 in)	meter (m)	2.54	E-05
mil (0.001 in)	millimeter (mm)	2.54	E-02
mil (angle)	radian (rad)	9.817 477	E-04
mil (angle)	degree (°)	5.625	E-02
mile (mi)	meter (m)	1.609 344	E+03
mile (mi)	kilometer (km)	1.609 344	E+00
mile (based on U.S. survey foot) (mi) ⁹	meter (m)	1.609 347	E+03
mile (based on U.S. survey foot) (mi) ⁹	kilometer (km)	1.609 347	E+00
<i>mile, nautical</i> ²¹	meter (m)	1.852	E+03
mile per gallon (U.S.) (mpg) (mi/gal)	meter per cubic meter (m/m ³)	4.251 437	E+05
mile per gallon (U.S.) (mpg) (mi/gal)	kilometer per liter (km/L)	4.251 437	E-01
mile per gallon (U.S.) (mpg) (mi/gal) ²²	liter per 100 kilometer (L/100 km)	divide 235.215 by number of miles per gallon	
mile per hour (mi/h)	meter per second (m/s)	4.4704	E-01
mile per hour (mi/h)	kilometer per hour (km/h)	1.609 344	E+00
mile per minute (mi/min)	meter per second (m/s)	2.682 24	E+01
mile per second (mi/s)	meter per second (m/s)	1.609 344	E+03
millibar (mbar)	pascal (Pa)	1.0	E+02
millibar (mbar)	kilopascal (kPa)	1.0	E-01
millimeter of mercury, conventional (mmHg) ¹³	pascal (Pa)	.1.333 224	E+02
millimeter of water, conventional (mmH ₂ O) ¹³	pascal (Pa)	9.806 65	E+00
<i>minute</i> (angle) (')	radian (rad)	.2.908 882	E-04
<i>minute</i> (min)	second (s)	.6.0	E+01
minute (sidereal)	second (s)	.5.983 617	E+01
nit	candela per meter squared (cd/m ²)	1.0	E+00
nox	lux (lx)	1.0	E-03
oersted (Oe)	ampere per meter (A/m)	.7.957 747	E+01
<i>ohm centimeter</i> (Ω · cm)	ohm meter (Ω · m)	1.0	E-02
ohm circular-mil per foot	ohm meter (Ω · m)	.1.662 426	E-09

To convert from	to	Multiply by	
pica (printer's)	millimeter (mm)	4.217 518	E+00
pint (U.S. dry) (dry pt)	cubic meter (m ³)	5.506 105	E-04
pint (U.S. dry) (dry pt)	liter (L)	5.506 105	E-01
pint (U.S. liquid) (liq pt)	cubic meter (m ³)	4.731 765	E-04
pint (U.S. liquid) (liq pt)	liter (L)	4.731 765	E-01
point (computer) (1/72 in)	meter (m)	3.527 778	E-04
point (computer) (1/72 in)	millimeter (mm)	3.527 778	E-01
point (printer's)	meter (m)	3.514 598	E-04
point (printer's)	millimeter (mm)	3.514 598	E-01
poise (P)	pascal second (Pa · s)	1.0	E-01
pound (avoirdupois) (lb) ²³	kilogram (kg)	4.535 924	E-01
pound (troy or apothecary) (lb)	kilogram (kg)	3.732 417	E-01
poundal	newton (N)	1.382 550	E-01
poundal per square foot	pascal (Pa)	1.488 164	E+00
poundal second per square foot	pascal second (Pa · s)	1.488 164	E+00
pound foot squared (lb · ft ²)	kilogram meter squared (kg · m ²)	4.214 011	E-02
pound-force (lbf) ²⁴	newton (N)	4.448 222	E+00
pound-force foot (lbf · ft)	newton meter (N · m)	1.355 818	E+00
pound-force foot per inch (lbf · ft/in)	newton meter per meter (N · m/m)	5.337 866	E+01
pound-force inch (lbf · in)	newton meter (N · m)	1.129 848	E-01
pound-force inch per inch (lbf · in/in)	newton meter per meter (N · m/m)	4.448 222	E+00
pound-force per foot (lbf/ft)	newton per meter (N/m)	1.459 390	E+01
pound-force per inch (lbf/in)	newton per meter (N/m)	1.751 268	E+02
pound-force per pound (lbf/lb) (thrust to mass ratio)	newton per kilogram (N/kg)	9.806 65	E+00
pound-force per square foot (lbf/ft ²)	pascal (Pa)	4.788 026	E+01
pound-force per square inch (psi) (lbf/in ²)	pascal (Pa)	6.894 757	E+03
pound-force per square inch (psi) (lbf/in ²)	kilopascal (kPa)	6.894 757	E+00
pound-force second per square foot (lbf · s/ft ²)	pascal second (Pa · s)	4.788 026	E+01
pound-force second per square inch (lbf · s/in ²)	pascal second (Pa · s)	6.894 757	E+03
pound inch squared (lb · in ²)	kilogram meter squared (kg · m ²)	2.926 397	E-04
pound per cubic foot (lb/ft ³)	kilogram per cubic meter (kg/m ³)	1.601 846	E+01
pound per cubic inch (lb/in ³)	kilogram per cubic meter (kg/m ³)	2.767 990	E+04
pound per cubic yard (lb/yd ³)	kilogram per cubic meter (kg/m ³)	5.932 764	E-01
pound per foot (lb/ft)	kilogram per meter (kg/m)	1.488 164	E+00
pound per foot hour [lb/(ft · h)]	pascal second (Pa · s)	4.133 789	E-04
pound per foot second [lb/(ft · s)]	pascal second (Pa · s)	1.488 164	E+00
pound per gallon [Canadian and U.K. (Imperial)] (lb/gal)	kilogram per cubic meter (kg/m ³)	9.977 637	E+01
pound per gallon [Canadian and U.K. (Imperial)] (lb/gal)	kilogram per liter (kg/L)	9.977 637	E-02

To convert from	to	Multiply by	
square mile (based on U.S. survey foot) (mi ²) ⁹	square meter (m ²)	2.589 998	E+06
square mile (based on U.S. survey foot) (mi ²) ⁹	square kilometer (km ²)	2.589 998	E+00
square yard (yd ²)	square meter (m ²)	8.361 274	E-01
statampere	ampere (A)	3.335 641	E-10
statcoulomb	coulomb (C)	3.335 641	E-10
statfarad	farad (F)	1.112 650	E-12
stathenry	henry (H)	8.987 552	E+11
statmho	siemens (S)	1.112 650	E-12
statohm	ohm (Ω)	8.987 552	E+11
statvolt	volt (V)	2.997 925	E+02
stere (st)	cubic meter (m ³)	1.0	E+00
stilb (sb)	candela per square meter (cd/m ²)	1.0	E+04
stokes (St)	meter squared per second (m ² /s)	1.0	E-04
tablespoon	cubic meter (m ³)	1.478 676	E-05
tablespoon	milliliter (mL)	1.478 676	E+01
teaspoon	cubic meter (m ³)	4.928 922	E-06
teaspoon	milliliter (mL)	4.928 922	E+00
tex	kilogram per meter (kg/m)	1.0	E-06
therm (EC) ²⁵	joule (J)	1.055 06	E+08
therm (U.S.) ²⁵	joule (J)	1.054 804	E+08
ton, assay (AT)	kilogram (kg)	2.916 667	E-02
ton, assay (AT)	gram (g)	2.916 667	E+01
ton-force (2000 lbf)	newton (N)	8.896 443	E+03
ton-force (2000 lbf)	kilonewton (kN)	8.896 443	E+00
ton, long (2240 lb)	kilogram (kg)	1.016 047	E+03
ton, long, per cubic yard	kilogram per cubic meter (kg/m ³)	1.328 939	E+03
<i>ton, metric</i> (t)	kilogram (kg)	1.0	E+03
tonne (called "metric ton" in U.S.) (t)	kilogram (kg)	1.0	E+03
ton of refrigeration (12 000 Btu _{IT} /h)	watt (W)	3.516 853	E+03
ton of TNT (energy equivalent) ²⁶	joule (J)	4.184	E+09
ton, register	cubic meter (m ³)	2.831 685	E+00
ton, short (2000 lb)	kilogram (kg)	9.071 847	E+02
ton, short, per cubic yard	kilogram per cubic meter (kg/m ³)	1.186 553	E+03
ton, short, per hour	kilogram per second (kg/s)	2.519 958	E-01
torr (Torr)	pascal (Pa)	1.333 224	E+02
unit pole	weber (Wb)	1.256 637	E-07
<i>watt hour</i> (W · h)	joule (J)	3.6	E+03
<i>watt per square centimeter</i> (W/cm ²)	watt per square meter (W/m ²)	1.0	E+04
watt per square inch (W/in ²)	watt per square meter (W/m ²)	1.550 003	E+03

- local equilibrium model, 1145–1146
 - mass conservation and transport, 1141–1144
 - mass transfer resistances, 1146–1148
 - modified Wheeler and Robell method, 1146, 1155
 - pressure drop, 1149–1150
 - rate phenomena, 1140–1141
 - thermodynamics, 1132–1140
 - adsorption equilibrium and heats of adsorption, 1133–1134
 - isotherm equations, 1135–1139
 - mixture equilibria, 1139–1140
 - sources of equilibrium data, 1134–1135
 - A-FBR, *see* Adiabatic fixed-bed reactor
 - AIChE, *see* American Institute of Chemical Engineers
 - AIChE efficiency model, 1050
 - Air-lift reactors, 808, 811
 - Algebraic equations, 40, 81–92
 - nonlinear equations, 85–92
 - system of linear equations, 81–85
 - Aluminas, 1130
 - American Institute of Chemical Engineers (AIChE), 28
 - Analysis of variance (ANOVA), 243
 - Analytical solution of groups (ASOG) method, 345
 - Aniline
 - comparison of fluid-bed models for catalytic reduction (by hydrogen) of nitrobenzene to, 883–893
 - reduction of nitrobenzene to, 878–883
 - ANOVA, *see* Analysis of variance
 - Applied reaction kinetics, 739
 - Argument principle, 151
 - Arrhenius equations, chemical reaction engineering, 743
 - ASOG method, *see* Analytical solution of groups method
 - Austenite, 1546
 - Average absolute deviation (AAD), 365, 366
 - Azeotrope(s)
 - composition, 292
 - distillation, 993–1000
 - embedded, 997
 - prediction of, 999
- B**
- BACL eos, *see* Boublik–Alder–Chen–Kreglewski eos
 - Batch distillation, 1002–1005
 - Batteries, 1816–1820
 - BC, *see* Bubble column
 - Bernoulli equation, 103, 419
 - Berty reactor, 770
 - Bidirectional reflectance distribution function (BRDF), 574
 - Bingham plastic, 399, 426, 639
 - Bingham plastic fluids, 426–428
 - all flow regimes, 428
 - laminar flow, 427–428
 - Biochemical engineering, 1501–1530
 - agitation and aeration, 1525–1529
 - correlation for $k_L a$, 1528
 - oxygen-absorption rate, 1526–1527
 - power consumption, 1528–1529
 - scale-up, 1529
 - biochemical engineering, 1502–1504
 - bioreactor design, 1518–1525
 - alternative fermenters, 1519–1520
 - batch or plug-flow bioreactors, 1520–1522
 - continuous stirred-tank bioreactor, 1522–1525
 - stirred-tank bioreactor (or fermenter), 1518–1519
 - biotechnology, 1502
 - cells and enzymes, 1504–1509
 - animal cells, 1506–1507
 - cell growth measurement, 1508
 - enzymes, 1508–1509
 - microbial cells, 1504–1506
 - plant cells, 1507–1508
 - kinetics, 1509–1518
 - cell kinetics, 1509–1513
 - enzyme kinetics, 1513–1518
 - Biomass, 1133
 - Bioreactor design, 1518–1525
 - alternative fermenters, 1519–1520
 - bioreactor operations, 1520–1525
 - batch or plug-flow bioreactors, 1520–1522
 - continuous stirred-tank bioreactor, 1522–1525
 - stirred-tank bioreactor (or fermenter), 1518–1519
 - Boiling heat-transfer correlations, 532–535
 - critical heat flux in pool boiling, 533
 - natural and forced convection vaporization, 533–535
 - nucleate boiling, 532–533
 - Bolles–Fair correlation, 1057
 - Bolles–Fair model, 1056
 - Bonded fixed capital cost, 1305
 - Boublik–Alder–Chen–Kreglewski (BACK) eos, 301
 - Box–Hill criterion, 876, 877
 - Boyko–Kruzhilin equation, 527
 - Brainstorming, triggers for, 1281–1282
 - BRDF, *see* Bidirectional reflectance distribution function
 - Bubble column (BC), 902
 - Bubbling-bed reactor, 826
 - Buckingham's theorem, 78, 80
 - Buckingham–Reiner equation, 427, 428
 - Bulk solids, conveying of, 1729–1736
 - air-activated gravity conveyor, 1735
 - belt conveyors, 1730–1733
 - belts, 1732–1733
 - carrying idlers, 1732
 - bucket elevators, 1734
 - en-masse conveyors, 1734–1735
 - materials characterization, 1729–1730
 - pneumatic conveyors, 1735
 - screw conveyors, 1733
 - vibrating conveyors, 1734
- C**
- Calorimetry, 22
 - Capital investment (conceptual process design), estimation
 - of fixed and total, 1300–1312
 - accounting for materials of construction other than carbon steel, 1308–1310
 - accounting for time and location, 1305–1306
 - cost contributions for one type of MPI, 1301–1305
 - definitions and terminology, 1300–1301

- classification of reactors and their description, 799–849
 - comparison of gas-liquid reactors, 849
 - kinetic energy (stirred tank reactors), 839–848
 - potential energy (film contactors), 849
 - pressure energy, 800–839
- column-type equipment, 799
- complete dispersion, 842
- computational fluid dynamics, 740
- contact mass, 944
- core-in-shell pellet, 900
- critical impeller speed, 842, 843
- Davidson model, 885, 888
- dead-end reactor, 840
- Denbigh reaction, 749
- design of continuous reactor, 949
- disguises, 764
- effectiveness factor, 759, 760
- ejector, 848
- Eley–Rideal models, 758
- emulsion phase, 823
- film contactors, 800
- flooding, 841
- fluidized catalytic cracking units, 827
- fractional gas holdup, 940
- Fryer–Potter model, 891
- gas dispersion, 841
- gas-foil impellers, 842
- gas-solid reactions, 764
- Geldart's classification, 823
- gradientless reactors, 739
- gulf streaming, 834
- heat transfer coefficient, 857, 862
- helical coil reactor, 859
- heterogeneous fluidization, 821
- heterogeneous reactions, 753
- homogeneous model, 776
- homogenization number, 841
- ideal reactors, 741
- internal diffusional effect, 768
- isothermal effectiveness factor, 759
- isotherms, 756
- Jayaraman–Kulkarni–Doraiswamy model, 891
- jet-loop reactors, 847
- Kunii–Levenspiel model, 887
- Langmuir–Hinshelwood–Hougen–Watson model, 758
- LHHW kinetics, 763
- liquid-phase axial mixing, 849
- liquid-solid reactions, 764
- Lockhart–Martinelli correlation, 913
- macroscopic models, 773
- methylchlorosilanes, 944
- microenvironmental aspects of solid catalysts, 756
- minimum fluidization velocity, 812
- mixed-flow model, 885
- mixing time, 841
- Miyauchi model, 889, 890
- multiphase reactors, 741
- multiple reaction, 742
- NINA reactor, 879
- nomenclature, 741, 956–961
- nonisothermal effectiveness factors, 762
- nonisothermicity, 782
- operating at the edge, 763
- overlapping regimes, 790
- oxydesulfurization of coal, 919
- particulate fluidization, 821
- pellet regeneration, 894
- plate efficiency, 807
- point of incipient fluidization, 812
- pseudo-steady-state assumption, 774
- radial-flow reactors, 819
- random pore models, 773, 783
- rate constant, 742
- reaction analysis, 739
- reaction-controlled regime, 817
- reaction coordinates, 749
- reaction order, 742
- reaction rate, 743
- reaction rate definitions, 745
- reaction and reactor fundamentals, 741–753
 - complex (multiple and multistep) reactions, 742
 - extension to complex (multiple) reactions, 745–750
 - ideal reactors, 750–753
 - reaction rates, 743–745
 - scope, 741
 - simple reactions, 741–742
 - stoichiometry, 742–743
- reactions with interface, 753–799
 - fluid-fluid reactions, 785–797
 - gas-liquid-solid reactions, 797
 - gas-solid catalytic reactions, 753–770
 - gas-solid noncatalytic reactions, 770–785
 - solid-liquid reactions, 797
- reaction space, 743
- reactor analysis, 739
- regimes of operation, 841
- residence time, 743
- rotating biological contactors, 848
- Runge–Kutta fourth-order method for different tube diameters, 882
- secondary bubble size, 802
- segregated flow, 753
- sequential discrimination algorithm, 876
- shape factor, 760
- shape selectivity, 754
- sharp interface model, 770
- Sherwood number, 764
- shrinking core model, 770, 774
- simulated moving-bed reactors, 740
- single-pellet reactor, 770
- sintering, 784
- slugging, 833
- solid catalysts in organic synthesis, 755
- solid-liquid mass transfer coefficient, 930
- sparger region, 802
- stages reactors, 828
- standleg moving granular bed filter, 897
- stirred cell, 789, 791, 796
- stoichiometric reactions, 742
- supported aqueous phase catalyst, 754
- supported organic phase catalyst, 756
- surface aeration, 847

- brainstorming, triggers for, 1281–1282
- building of reliable database, 1313–1321
 - gathering of data for troubleshooting, 1321
 - gathering of input data from databases for design and process improvement, 1314–1320
 - input data from scientists, 1313
 - minimizing uncertainty in input data through experimentation, 1313–1314
 - units of measurement and communication, 1314
- business cycle, 1275
- capital cost indices, 1305
- capital stock, 1287
- common stock, 1287
- company good citizenship, 1293
- cost of capital, 1293, 1294
- debt-to-assets ratio, 1289
- deflagration, 1315
- depreciation, 1288
- detonation, 1315
- dust emissions from various equipment options, 1332
- earnings statement, 1287
- employee morale, 1293
- energy exchange (rules of thumb), 1359–1368
 - direct contact gas-liquid condensers, 1366–1367
 - direct contact gas-liquid cooling towers, 1366
 - direct contact gas-liquid quenchers, 1366
 - direct contact gas-solid fluidized beds, 1365
 - direct contact gas-solid kilns, 1364–1365
 - direct contact gas-solid multiple hearth furnaces, 1365
 - direct contact liquid-liquid immiscible liquids, 1364
 - drives, 1360
 - fluid heat exchangers, condensers, and boilers, 1361–1363
 - fluidized bed (coils in bed), 1363–1364
 - furnaces, 1360–1361
 - gas-gas thermal wheels, pebble regenerators, and regenerators, 1367
 - gas-solid drying of solids, 1365–1366
 - heat loss to atmosphere, 1367
 - motionless mixers, 1364
 - refrigeration, 1367
 - solidify liquids, 1367
 - steam generation, 1368
- energy sources, 1323
- engineering economics, 1283–1312
 - estimation of fixed and total capital investment, 1300–1312
 - financial attractiveness, 1292–1295
 - operating expense estimation, 1295–1300
 - role of economics in financial reporting, 1284–1292
- explore stage of problem solving, 1280
- financial ratios, 1289, 1290
- flowsheeting, 1333, 1336
- gating process, 1273, 1275, 1310
- HAZOP studies, 1327
- heats of reaction, 1319
- heterogeneous separations (rules of thumb), 1387–1410
 - air classifiers, 1407–1408
 - countercurrent decantation, 1397–1398
 - dense media concentrators, 1409
 - dryer, 1392–1396
 - electrostatic, 1406
 - filter, 1400–1404
 - filtering centrifuge, 1399–1400
 - froth flotation, 1405
 - gas-liquid, 1387–1388
 - gas-solid, 1388–1390
 - general guidelines, 1387
 - hydrocyclones, 1397, 1407
 - jig concentrators, 1408
 - leacher, 1404
 - liquid-liquid, 1390–1391
 - liquid-solid (dissolved air flotation), 1404
 - liquid-solid (expeller and hydraulic press), 1405
 - liquid solid (general selection), 1391–1392
 - magnetic, 1406–1407
 - rake classifiers, 1408
 - screens, 1409–1410
 - screens for “dewatering,” 1396
 - sedimentation centrifuges, 1398–1399
 - settlers, 1396–1397
 - sluice concentrators, 1409
 - solid-solid (general selection), 1405
 - spiral classifiers, 1408
 - table concentrators, 1408–1409
 - thickener, 1397
- Holmes–Rahe scale, 1283
- homogeneous separation (rules of thumb), 1368–1387
 - adsorption, gas, 1378
 - adsorption, liquid, 1378–1379
 - distillation, 1369–1372
 - evaporation, 1368–1369
 - foam fractionation, 1380–1381
 - freeze concentration, 1372
 - gas absorption, 1374–1376
 - gas desorption/stripping, 1376
 - ion exchange, 1379–1380
 - melt crystallization, 1372–1373
 - overall guidelines, 1368
 - precipitation, 1374
 - solution crystallization, 1373–1374
 - solvent extraction, 1376–1378
 - zone refining, 1373
- income statement, 1284, 1286, 1287
- interpersonal skills and teamwork, 1347–1349
 - effective teams, 1348–1349
 - interpersonal skills, 1347–1348
 - key principles, 1347–1348
 - self-awareness, 1347
- inventory-sales ratio, 1291
- inventory-turnover ratios, 1291
- Lee–Kesler model, 1342
- liabilities, 1286
- marketing activities, 1275
- materials reacting aggressively with water, 1319
- membranes
 - configurations, 1382
 - dialysis, 1381–1382
 - electrodialysis, 1382
 - gas, 1381
 - microfiltration, 1386–1387

solidify liquid to solid, 1436
 spherical agglomeration, 1434
 spray drying, 1433
 tableting, 1434–1435
 size reduction (rules of thumb), 1429–1432
 gas in liquid (bubbles in liquid), 1429–1430
 liquid in gas (sprays), 1430
 liquid-liquid, 1430–1431
 solids, crushing and grinding, 1431–1432
 solids, modify size and shape, 1432
 solids, solidify liquid to solid, 1432
 stockholders' equity, 1287
 structural optimization, 1344
 sustainability from the start, 1322–1324
 impact of sustainability on design, 1323
 impact of sustainability on process improvement, 1323–1324
 The Natural Step, 1322, 1323
 total module cost, 1304
 transportation (rules of thumb), 1353–1359
 ducts and pipes, 1359
 gas-liquid (two-phase flow), 1357
 gas moving (pressure service), 1353–1355
 gas moving (vacuum service), 1355–1356
 liquid, 1356–1357
 pumping slurries (liquid-solid systems), 1357
 solids, 1358–1359
 steam, 1359
 VOC release from various equipment options, 1311
 Wegstein acceleration, 1339
 wiredrawing, 1359
 Condensation, special cases in, 530–531
 condensation of multicomponent vapor, 530
 condensation in presence of noncondensable gas, 530
 condensation of superheated vapor, 530–531
 enhanced surfaces, 530
 Cone and fillet tank (CFT), 843
 Construction materials, *see* Materials of construction (steels and other metals), selection of
 Continuous stirred tank reactor (CSTR), 751
 endothermic, 1175, 1176
 mathematics, 41
 nonlinear equations, 45
 ordinary differential equations, 47
 singularity theory, 177
 steady-state multiplicity, 173
 Controlled variable (CV), 1247
 Core-in-shell (CIS) sorbent, 893
 COR equation, *see* Chain-of-rotators equation
 Corporate image, 1293
 Corrosion
 current, 1808
 potential, 1808
 processes, 1805–1816
 crevice corrosion, 1813–1814
 galvanic corrosion, 1812–1813
 hydrogen embrittlement, 1815–1816
 kinetic aspects, 1808–1810
 mass transfer effects, 1810–1811
 metal passivation, 1811–1812
 pitting, 1814–1815

 stress corrosion cracking, 1815
 thermodynamics, 1806–1807
 uniform attack, 1812
 COSMO, 12
 CPI, *see* Chemical process industries
 CRE, *see* Chemical reaction engineering
 Critical impeller speed, 842
 CS equation of state, *see* Carnahan-Starling equation of state
 CSTR, *see* Continuous stirred tank reactor
 CV, *see* Controlled variable

D

DAF, *see* Dissolved air flotation
 Darcy equation, 1626–1627
 Database, building of reliable, 1313–1321
 gathering of data for troubleshooting, 1321
 gathering of input data from databases for design and process improvement, 1314–1320
 input data from scientists, 1313
 key terms, 1315–1316
 minimizing uncertainty in input data through experimentation, 1313–1314
 units of measurement and communication, 1314
 Davidson model, 885, 888
 DCS, *see* Distributed control system
 DDB, *see* Dortmund Data Bank
 Deactivating catalyst, modeling of complex reaction on, 870–878
 Dead-end reactor, 840
 Debt-to-assets ratio, 1289
 Debye-Hückel theory, 18
 Degrees of freedom (DOFs), 1336
 Denbigh reaction, 749
 Design Institute for Physical Properties (DIPPR), 28
 Dew point, 984
 Difference equations, processes governed by, 42–44
 scalar difference equations, 42–43
 vector difference equations, 43–44
 Differential Chapman-Kolmogorov equation, 167
 Differential ebulliometry, 24
 Differential pressure (DP) cell 1193
 Differential scanning calorimetry (DSC), 23
 Differential thermal analysis (DTA), 23
 Dimensionless numbers, 504–507
 Colburn *j*-factor, 506
 Graetz number, 506
 Grashof number, 507
 Nusselt number, 505
 Peclet number, 506–507
 Prandtl number, 506
 Reynolds number, 504–505
 Sieder-tate term, 507
 Stanton number, 506
 DIPPR, *see* Design Institute for Physical Properties
 Dirac delta function, 184
 Dirichlet problem, 118
 Dissolved air flotation (DAF), 1402, 1404
 Distillation, 969–1072
 AIChE efficiency model, 1050

estimation and measurement of activity coefficients, 980–981
 summary, 981–983
 V-grid, 1021
 VLE relationships, 981
 window area, 1024
 Distributed control system (DCS), 1184–1187
 approach, 1185–1186
 background, 1184
 fieldbus technology, 1186–1187
 programmable logic controllers, 1186
 structure, 1184–1185
 Disturbance variable (DV), 1247
 DOFs, *see* Degrees of freedom
 Dortmund Data Bank (DDB), 14
 Downcomers, 1016, 1026
 DP cell, *see* Differential pressure cell
 Drying, principles and practice, 1667–1716
 basic principles and terminology, 1669–1682
 drying kinetics, 1676–1682
 equilibrium moisture content, 1671–1674
 psychrometry, 1669–1670
 thermodynamic properties of air-water mixtures and moist solids, 1669–1676
 water activity, 1674–1676
 classification and selection of dryers, 1683–1689
 batch dryers, 1684
 classification of dryers, 168
 continuous dryers, 1684–1685
 direct dryers, 1685
 indirect dryers, 1685–1686
 selection of dryers, 1686–1689
 drying equipment, 1690–1713
 band dryers, 1708–1709
 drum dryers, 1702–1703
 dryers for particulates and granular solids, 1690–1697
 dryers for slurries and suspensions, 1697–1703
 drying of boards and sheets, 1712–1713
 flash dryers, 1705–1707
 fluidized bed dryers, 1693–1694
 freeze dryers, 1694–1695
 infrared dryers, 1709
 microwave and radio frequency drying, 1709–1711
 rotary dryers, 1691–1693
 roto-louvre dryer, 1707–1708
 selected dryers and drying systems, 1703–1713
 spin-flash dryers, 1707
 spray dryers, 1697–1702
 superheated steam drying, 1711–1712
 tray dryers, 1690
 tunnel dryers, 1708
 two-stage dryers, 1704–1705
 vacuum dryers, 1695–1697
 nomenclature, 1714
 DSC, *see* Differential scanning calorimetry
 DTA, *see* Differential thermal analysis
 Dualflow trays, 1022
 Duhamel's principle, 120, 121
 DV, *see* Disturbance variable

E

Earnings before interest and taxes (EBIT), 1291
 EBIT, *see* Earnings before interest and taxes
 Ebulliometry, 23
 Economics, *see* Engineering economics
 EDD model, *see* Engulfment, deformation, and diffusion model
 EL-ALR, *see* External-loop air-lift reactor
 Electrochemical engineering, principles and applications, 1737–1830
 activation overpotential, 1765
 anodic metal dissolution reaction, 1795
 aqueous electrolytes, activity coefficients in, 1748
 assisting mixed convection case, 1762
 batteries and fuel cells, 1816–1824
 batteries, 1816–1820
 fuel cells, 1821–1824
 Butler-Volmer rate expression, 1751
 capillary model, 1804
 cathodic protection, 1813
 concentration overpotentials, 1765
 corrosion current, 1808
 corrosion potential, 1808
 corrosion processes, 1805–1816
 crevice corrosion, 1813–1814
 galvanic corrosion, 1812–1813
 hydrogen embrittlement, 1815–1816
 kinetic aspects, 1808–1810
 mass transfer effects, 1810–1811
 metal passivation, 1811–1812
 pitting, 1814–1815
 stress corrosion cracking, 1815
 thermodynamics, 1806–1807
 uniform attack, 1812
 critical current, 1812
 electrocatalytic reduction (hydrogenation) reactions in solid polymer electrolyte (proton exchange membrane) reactor, 1784–1786
 electrochemical reactors and reactor design, 1766–1774
 characterizing of electrochemical reactor performance, 1766–1769
 choosing of electrochemical reactor, 1769–1774
 electroplating and electroetching, 1787–1796
 alloy plating, 1794
 basic principles, 1787–1791
 electrochemical metal removal processes, 1794–1796
 electroless plating, 1792–1794
 high-speed and laser-assisted plating, 1791–1792
 environmental clean-up processes, 1796–1805
 electrochemical destruction of organics, 1800
 electrodialysis, 1801–1805
 metal ion removal, 1797–1800
 Faraday's constant, 1740
 Faraday's Law, 1740
 fundamentals, 1738–1766
 driven vs. self-driven cells and concept of overpotential, 1763–1766
 kinetics of electrode reactions, 1749–1753

- new source reviews and modifications, 1489–1490
- source delineations under Title V, 1488–1489
- Title IV (acid rain) and Title VI (stratospheric ozone) considerations, 1490–1491
- Title VI (stratospheric ozone) permit, 1491
- Clean Water Act, 1492–1496
 - existing use, 1492–1493
 - National Permit Discharge Elimination System, 1493–1494
 - publicly owned treatment works, 1494
 - Section 319 (nonpoint source pollution), 1495
 - Section 404 (wetland protection), 1495
 - Sections 303, 305, and Section 401 certification, 1495–1496
 - total daily maximum load levels, 1493
 - “wet weather flow” conditions, 1494–1495
- Emergency Planning and Community Right to Know Act, 1498
- greenhouse gases and (global warming) climactic change, 1499–1500
- nuclear power generation, 1496–1497
 - Chernobyl, 1496–1497
 - hazardous waste disposal, 1496
 - Three-Mile Island, 1496–1497
 - VHTR reactors, 1497
- OSHA, 1497–1498
- Resource Conservation and Recovery Act, 1499
- SARA, 1498
- Spill Prevention Control and Countermeasures Act, 1499
- “Superfund” law, 1498
- Toxic Substances Control Act, 1498–1499
- Enzyme(s), 1508–1509
 - commercial applications, 1509
 - kinetics, 1513–1518
 - Briggs–Haldane approach, 1514–1515
 - evaluation of Michaelis–Menten parameters, 1516
 - inhibition of enzyme reactions, 1516–1518
 - Michaelis–Menten approach, 1513–1514
 - numerical solution, 1515–1516
 - nomenclature, 1509
- EPA listed chemicals, 1470, 1471–1477
- EPA listed hazardous materials, fire-hazard properties of, 1478
- EPA off-site hazard assessment, 1440–1457
 - BLEVE hazards evaluation, 1455–1456
 - “condensed-phase” detonation hazards evaluation, 1456–1457
 - evaluation of toxicity hazards, 1444–1447
 - explosion-hazards evaluation, 1447–1449
 - flash-fire hazards evaluation, 1449–1451
 - jet-fire hazards evaluation, 1456
 - pool-fire hazards evaluation, 1451–1452
 - pool formation from liquid spills, 1444
 - pressure-vessel-burst hazards evaluation, 1452–1454
 - release source terms (gas or vapor flow rates), 1441–1442
 - release source terms (liquid flow rates), 1442
 - release source terms (two-phase flow), 1442–1443
 - vapor formation as result of adiabatic flashing, 1443
- EPCRA, *see* Emergency Planning and Community Right to Know Act
- Equation(s)
 - Arrhenius, 743
 - Bernoulli, 103, 419
 - Boyko-Kruzhilin, 527
 - Buckingham-Reiner, 427, 428
 - chain-of-rotators, 302
 - Chapman-Kolmogorov, 167
 - Clapeyron, 352
 - Colebrook, 437
 - complete local-composition, 341
 - Darcy, 1626–1627
 - elliptic, 118
 - Euler-Lagrange, 163, 164
 - filmwise condensation, 524–530
 - Flory-Huggins, 334–336
 - fluid statics, 408–410
 - Fokker-Planck, 167, 168
 - Fredholm, 42, 136, 140
 - Galerkin finite element, 114
 - Gibbs-Duhem, 281, 283
 - Hagen-Poiseuille, 419, 420, 435
 - ideal-gas, 258
 - integral, 42, 50
 - integrodifferential, 42
 - Îto stochastic, 53
 - Kremser, 725–726
 - Lagrange, 102
 - Laplace, 128
 - Maxwell–Stefan diffusional, 1054
 - multicomponent isotherm, 1140
 - Navier-Stokes, 618, 848
 - nonlinear, 45
 - nonrandom two-liquids equation, 338
 - ordinary differential, 47
 - parabolic, 119
 - partial differential, 48
 - Peng–Robinson, 11, 299
 - perturbation, 299
 - Poisson, 128, 130
 - polymer chain-of-rotator, 306
 - population balance, 52
 - pure component isotherm, 1138
 - radiative transfer, 583–585
 - Redlich–Kister, 330
 - Redlich–Kwong, 298, 1342
 - Ricatti, 105
 - Soave–Redlich–Kwong, 11
 - stochastic differential, 166
 - Tafel, 1751
 - UNIQUAC, 343, 369
 - van der Waals, 295, 330
 - van Laar, 330–332
 - vector difference, 43
 - Vogel–Tammann–Fulcher, 15
 - Volterra, 42, 132, 136
 - Wagner, 6
 - Weymouth, 440
 - Wheeler–Robell, 1146
 - Wilson's local-composition, 336–338

- moving systems, 410–411
- static forces on solid boundaries, 411–418
- Hagen-Poiseuille equation, 419, 420, 435
- hydraulic diameter, 435
- inviscid fluid, 396
- minimum required NPSH, 447
- Newtonian fluid, 399
- obstruction meters, 454
- pipe flow, 419–443
 - analysis, 431–433
 - Bingham plastic fluids, 426–428
 - compressible flows, 438–443
 - economical diameter, 433–435
 - fitting losses, 428–431
 - flow regimes, 419
 - Newtonian fluids, 419–422
 - noncircular conduits, 435–437
 - power law fluids, 422–426
 - pressure-flow relations, 419
 - turbulent drag reduction, 437–438
- Poiseuille flow, 398
- power law model, 400, 402, 422
- properties of gases, 440
- pumps and compressors, 443–453
 - centrifugal pump characteristics, 444–449
 - compressors, 449–453
 - pump types, 443–444
- rheological properties, 395
- shear limiting viscosity, 401
- shear rate, 396
- shear thinning, 400
- Sisko model, 401
- structural viscosity, 401
- vapor lock, 447
- Weymouth equation, 440
- Fluid-fluid reactions, 785–797
 - laboratory reactors for, 788–797
 - theory of mass transfer accompanied by irreversible chemical reaction, 786–788
- Fluidized catalytic cracking (FCC) units, 827
- Foaming systems, capacity discount factors for, 1018
- Fokker-Planck equation, 167, 168
- FOPDT model, *see* First-order plus deadtime model
- Forced convection, correlations for common geometries in, 507–520
 - flow across circular cylinder, 512–513
 - flow across tube banks, 513–519
 - heat transfer in packed and fluidized beds, 519–520
 - inside annular channels, 510–511
 - inside round tubes, 507–510
 - internally enhanced tubes, 510
- Fourier transform, 122, 157–160
 - application, 158–160
 - application of Fourier cosine transform, 160
 - application of Fourier sine transform, 159–160
 - application of Fourier transform, 158
 - convolution property, 157
- Fractionation Research, Inc. (FRI), 1065
- Fredholm equations, 42, 140
- Fredholm equations, methods of solution for, 136–142
 - degenerate kernels, 136–137

- method of Fredholm resolvent kernels, 137–138
- method of iterated kernels, 138–139
- method of regularization, 142
- numerical solution of nonhomogeneous Fredholm equation of second kind, 139–140
- solution of ill-posed Fredholm equations of first kind, 140–142
- symmetric kernels, 139
- Fredholm integral equations, 136
- Fredholm resolvent kernels, 137
- FRI, *see* Fractionation Research, Inc.
- Froth regime, 1043
- Fryer-Potter model, 891
- Fuel cells, 1816–1824
- Fugacity, definition of, 321

G

- Galerkin finite element equation, 114
- Garcia-Fair model, 1053
- Gas(es)
 - foil impellers, 842
 - holdup expression, 667
 - inducing impellers, 846
 - properties of, 440
 - superficial velocities of, 1357
- Gas chromatograph (GC), 1193
- Gas-liquid critical state, 285
- Gas-liquid mass transfer, interfacial area for, 929
- Gas-liquid mixing, 660–671
 - equipment and its function, 662–63
 - gas residence time, 668–669
 - impeller characteristics, 663–665
 - mass transfer, 661–662
 - mass transfer and gas holdup, 666–668
 - scale-up, 669–671
 - scope, 660–661
- Gas-liquid reaction(s)
 - absorption of NO_x gases for manufacture of nitric acid (system with multiple complexities), 917–918
 - effect of various parameters, 917–918
 - lesson, 918
 - nomenclature, 917
 - optimum design, 918
 - problem, 917
- air oxidation of sodium sulfide (simple reaction with typical problems of gas-liquid reactions), 900–916
- bubble column, 902
- external-loop air-lift reactor, 907–908
- horizontal sparged contactor, 908–909
- lesson, 916
- nomenclature, 900–901
- packed column, 913–916
- pipeline contactor, 910–913
- problem, 901–902
- sectionalized bubble column, 905–906
- solution, 902

industrially important, 786

- boiling heat-transfer correlations, 532–535
- design equations for filmwise condensation, 524–530
- mechanisms of condensation, 523–524
- mechanisms of vaporization, 531–532
- special cases in condensation, 530–531
- special cases in vaporization, 535–536
- conduction heat transfer, 481–503
 - extended surfaces, 487–493
 - mechanisms of conduction and basic equation, 481–482
 - numerical methods, 503
 - one-dimensional steady-state conduction, 482–486
 - thermal contact resistance, 486–487
 - transient conduction in simple solids, 497–503
 - two- and three-dimensional steady-state conduction, 493–496
- friction factor, 519
- Graetz-Nusselt problem, 508
- heat exchangers, 536–563
 - design principles, 550–560
 - fouling, 562–563
 - logic of design process, 560–562
 - types and selection, 537–550
- single-phase convection heat transfer, 503–523
 - correlations for common geometries in forced convection, 507–520
 - dimensionless numbers, 504–507
 - film coefficient of heat transfer, 504
 - mechanisms of convection, 503–504
 - single-phase heat transfer in natural convection, 520–523
- Stanton number, 506
- TEMA standards, 544
- transition boiling regime, 532
- Helgeson–Kirkham–Flowers (HKF) correlation, 19
- Helical coil reactor, 859
- Helmholtz energy, 12, 273, 317
- Higbie model, 602
- HKF correlation, *see* Helgeson–Kirkham–Flowers correlation
- Homogeneous gas-phase complex reaction, 869–870
- Homogeneous liquid phase simple reaction, 852–869
 - cost evaluation, 865–867
 - nomenclature, 852–854
 - problem, 854
 - reactant on shell side, 867–869
 - shell-side calculations, 862–865
 - solution, 854–860
 - tube-side calculations, 860–862
- Horizontal sparged contactor (HSC), 908
- HSC, *see* Horizontal sparged contactor
- Hydrogen embrittlement, 1815
- IAPWS, *see* International Association for the Properties of Water and Steam
- Ideal Adsorbed Solution theory, 1141
- Ideal gas
 - definition, 313
 - equation, 258
 - Gibbs energy, 316
 - Helmholtz energy, 316
 - law, fluid flow and, 409
 - properties, 8
- Ideal reactors, 741, 750–753
 - batch reactor, 750
 - continuous flow reactors, 751–752
- Ideal-solution law, 325
- IEM model, *see* Interaction by exchange with the mean model
- Immiscible liquid-liquid mixing, 671–682
 - characterization, 671–672
 - coalescence of suspended drops, 677–678
 - creation of dispersion (maintaining drop suspension), 678–679
 - dispersion of drops, laminar flow, and low viscosity, 673–674
 - dispersion of higher-viscosity drops turbulent flow, 676–677
 - dispersion of low-viscosity drops turbulent flow, 674–676
 - drop sizes, 672–673
 - equipment used for liquid-liquid mixing, 681
 - population-balance methods, 678
 - processes, 681–682
 - simultaneous suspension, dispersion, and coalescence, 680
- Industrial mixing technology, 615–707
 - Bingham plastic, 639
 - blending, 630–639
 - flow patterns, 633
 - mixing time (laminar flow), 639
 - mixing time (turbulent and transitional flows), 635–638
 - nature of turbulent flow, 632–633
 - scope, 630
 - shear rates, 633–635
 - turbulent, transitional, and laminar flow blending, 630–632
 - Dämköhler number, 646
 - degree of mixing, 630
 - dimpled jacket, 701
 - engulfment, deformation, and diffusion model, 647
 - equilibrium, 675
 - gas holdup expression, 667
 - gas-liquid mixing, 660–671
 - equipment and its function, 662–63
 - gas residence time, 668–669
 - impeller characteristics, 663–665
 - mass transfer, 661–662
 - mass transfer and gas holdup, 666–668
 - scale-up, 669–671
 - scope, 660–661
 - half-pipe jacket, 700
 - heat transfer in mixing equipment, 697–705
 - external auxiliary devices, 701–702
 - heat transfer in agitated vessels, 699
 - heat-transfer surfaces and effective area, 700

- processes governed by, 50–52
 - boundary-value problems with mixed derivative boundary condition, 51–52
 - determination of pore size distribution in porous media, 50–51
 - particle size distribution in continuous comminution process, 50
- Volterra integral equations, 131–132
- Integral transforms, 155–163
 - Fourier transform, 157–160, 186–187, 188, 189
 - application of Fourier cosine transform, 160
 - application of Fourier sine transform, 159–160
 - application of Fourier transform, 158
 - convolution property, 157
 - Hankel transform, 162–163, 190
 - application, 162–163
 - property, 162
 - Laplace transform, 156–157, 185–186
 - application, 156–157
 - convolution property, 156
 - Mellin transform, 160–161, 190
 - application, 161
 - convolution property, 160
 - tables of, 185–191
 - Fourier cosine transforms, 189
 - Fourier sine transforms, 188
 - Fourier transforms, 186–187
 - Hankel transforms, 191
 - Laplace transforms, 185–186
 - Mellin transforms, 190
- Integrodifferential equations, processes governed by, 52
- Intellectual property, *see* Patents and intellectual property
- Interaction by exchange with the mean (IEM) model, 647
- Internal rate of return (IRR), 1292
- International Association for the Properties of Water and Steam (IAPWS), 3
- International Solvent Extraction Conferences (ISECs), 712
- International Union of Pure and Applied Chemistry (IUPAC), 21
- Inventory-sales ratio, 1291
- IRR, *see* Internal rate of return
- ISA, *see* Instrument Society of America
- ISECs, *see* International Solvent Extraction Conferences
- Isochores, 286
- Isothermal flash, 985
- Îto stochastic equation, 53
- Îto stochastic integral, 168–170
 - application, 169–170
 - one-dimensional Îto formula, 169
- IUPAC, *see* International Union of Pure and Applied Chemistry

J

- Jayaraman–Kulkarni–Doraiswamy model, 891
- Jet-loop reactors, 847
- Jet mixing, 694–697
 - correlations, 695–697
 - equipment, 694–695
 - principles, 694

K

- Kirchhoff's laws, 575
- K–L model, *see* Kunii–Levenspiel model
- Kremser–Brown relationship, 1088
- Kremser equation, 725–726
- Kronecker delta, 120, 395
- Kunii–Levenspiel (K–L) model, 887

L

- Lagrange equation, 102
- Langmuir–Hinshelwood–Hougen–Watson (LHHW) model, 758
- Langmuir isotherm, 756
- Laplace equation, 128
- Laplace transform, 156–157
 - application, 156–157
 - convolution property, 156
- Laurent series, 149
- LCUs, *see* Local control units
- Least squares regression, 233–245
 - analysis of variance, 243–245
 - generalized multiple linear regression, 239–243
 - basic algorithm, 240–241
 - estimation of uncertainty, 241–243
 - nonlinear regression, 245
 - simple linear least squares regression, 234–239
 - basic algorithm, 234–237
 - estimation of uncertainty, 237–239
- Lewis fugacity rule, 355
- LHHW kinetics, 763
- LHHW model, *see* Langmuir–Hinshelwood–Hougen–Watson model
- Lignin extraction, 714
- Lime, carbonation of, 925–934
- Linear equations, processes governed by, 44–45
 - steady-state continuous countercurrent staged extraction, 44–45
 - steady-state first-order reactions in stirred tank reactor, 45
- Linear partial differential equation, 115
- Linear program (LP), 1247
- Linear stability analysis, 179
- Liquid-liquid equilibrium, 11
- Liquid-liquid extraction (LLE), 709–735
 - design of extraction systems, 720–726
 - countercurrent extractors, 723–725
 - Kremser equation, 725–726
 - phase diagrams, 721–723
 - dispersion, mass transfer, and coalescence, 712–713
 - distribution coefficients, 716–720
 - empirical distribution models, 720
 - nonreactive systems, 716–717
 - reactive systems, 718–720
 - thermodynamic models, 716
 - economic analysis for vertical contactors, 729–732
 - entrainer, 712
 - industrial extraction equipment, 726–728
 - mixer settlers, 726

- normalizing, 1543
- pearlite, 1547
- preheat, 1543
- quench and temper, 1545–1546
- stainless steel, 1554–1558
- stress relief/postweld heat treatment, 1544–1545
- Mathematics in chemical engineering, 35–197
 - activities related to mathematics, 41
 - Adams-Bashforth methods, 99
 - Adams-Moulton rule, 100
 - algebraic equations, 40, 81–92
 - nonlinear equations, 85–92
 - system of linear equations, 81–85
 - arithmetic-geometric means inequality, 59
 - asymptotic approximations and expansions, 170–173
 - boundary-value problem, 41, 108, 113, 152, 154
 - branch cut, 147
 - breakage kernel, 50
 - Buckingham's π -theorem, 78
 - Budan's rule of signs, 86
 - calculus of variations, 163–166
 - application, 165
 - Euler-Lagrange differential equation, 163–164
 - Euler-Lagrange equations for functional involving n -order derivative, 165
 - Euler-Lagrange equations for functional of n -dependent variables, 164–165
 - Euler-Lagrange equations for functional of two independent variables, 165
 - Cardano's formula, 87
 - Cauchy integral formula, 148
 - Cauchy-Riemann equations, 136
 - Cauchy-Schwartz inequality, 58
 - chaotic problems, 40
 - Chebyshev's inequality, 59
 - complex variables, 143–155
 - analytic functions, 144–149
 - argument principle and Rouché theorem, 151–152
 - conformal mapping, 152–155
 - properties of complex numbers, 143–144
 - residue theorem, 149–151
 - computational fluid dynamics, 131
 - Cramer's rule, 84
 - d'Alembert's solution, 124
 - degenerate kernels, 136
 - Descartes's rule of signs, 86
 - diagonal matrix, 82
 - difference equations, 92–100
 - method of solution for homogeneous equations, 92
 - method of solution for inhomogeneous equations, 92–94
 - numerical solutions to ordinary differential equations, 94–100
 - difference kernel, 133
 - differential and integral calculus, 60–66
 - derivative, 61–62
 - functions, limits, and continuity, 60
 - implicit function theorem, 64
 - integrals, 64–66
 - L'Hôpital's rule, 63–64
 - mean value theorem, 62–63
 - dimensional analysis, 78–81
 - applications, 79–81
 - theory, 78
 - dimensional matrix, 78
 - dimensions of commonly used physical quantities, 79
 - Dirac delta function, 184
 - Dirichlet problem, 118
 - drag coefficient, 80
 - Duhamel's principle, 120, 121
 - elliptic equations, 118
 - empiricism, 39
 - entire function, 146
 - equations, 40–53
 - difference equations, 42–44
 - integral equations, 50–52
 - integrodifferential equations, 52
 - linear equations, 44–45
 - nonlinear equations, 45–47
 - ordinary differential equations, 47–48
 - partial differential equations, 48–50
 - stochastic differential equations, 52–53
 - Euler-Lagrange equation, 163, 164
 - evolution equations, 118
 - Fokker-Planck equation, 167, 168
 - Fourier transforms, 122
 - Fredholm equations, 42
 - Fredholm integral equations, 136
 - Fredholm resolvent kernels, 137
 - Galerkin finite element equation, 114
 - gauge functions, 171
 - Green's function, 108, 110, 130, 136
 - harmonic function, 146
 - Hölder inequality, 59
 - identity matrix, 82
 - imaginary number, 143
 - inflection point, 61
 - initial-value problems, 41
 - integral equations, 42, 131–143
 - Fredholm integral equations, 136
 - methods of solution for Fredholm equations, 136–142
 - methods of solution for Volterra equations, 132–136
 - Volterra integral equations, 131–132
 - integral transforms, 155–163
 - Fourier transform, 157–160
 - Hankel transform, 162–163
 - Laplace transform, 156–157
 - Mellin transform, 160–161
 - integrodifferential equations, 42
 - iterated kernels, 138
 - Îto stochastic equation, 53
 - Jacobian matrix, 90
 - kernels for different transforms and integration limits, 155
 - Kronecker delta, 120
 - Laplace equation, 128
 - Laurent series, 149
 - linear partial differential equation, 115
 - linear stability analysis, 179
 - Lyapunov's function, 179, 180, 181
 - Markov process, 167

MIMO process, *see* Multiple-input/multiple-output process
 MIMO process control, 1242–1246
 SISO controllers and (c, y) pairings, 1242–1245
 tuning decentralized controllers, 1245–1246
 Minimum approach temperature (MAT), 1343
 Mixed-flow model, 885
 Mixed-flow reactor (MFR), 751
 Mixer settlers, 726
 Mix point, 722
 Mixtures, phase behavior of, 291–294
 gas-gas equilibrium, 294
 gas-liquid equilibrium, 291–293
 liquid-liquid equilibrium, 293–294
 Miyauchi model, 889, 890
 Model(s)
 activity-coefficient, 329–343
 complete local-composition equation, 339–341
 Flory-Huggins equation, 334–336
 nonrandom two-liquids equation, 338–339
 Redlich-Kister equation, 330
 regular solutions, 332–334
 UNIQUAC equation, 341–343
 van Laar equation, 330–332
 Wilson's local-composition equation, 336–338
 AIChE efficiency, 1050
 Bingham plastic, 426
 Bolles-Fair, 1056
 capillary, 1804
 Carreau-Yashuda, 402
 cell, 815
 chain-of-spheres, 302
 Davidson, 885, 888
 distillation, 972–975
 contacting stage, 973–975
 multiple stages, 975
 phase equilibrium, 972–973
 dumbbell rotator, 302
 electrolyte-NRTL, 18
 Eley-Rideal, 758
 Ellis, 401
 engulfment, deformation, and diffusion, 647
 EOS, 8
 FOPDT, 1181
 Fryer-Potter, 891
 Garcia-Fair, 1053
 gas-solid equilibrium, 372–374
 Gibbs energy models of liquid solutions, 347–350
 Hang-Chao-Hilson complete local-composition, 371
 Higbie, 602
 interaction by exchange with the mean, 647
 Jayaraman-Kulkarni-Doraiswamy, 891
 Kunii-Levenspiel, 887
 Langmuir-Hinshelwood-Hougen-Watson, 758
 Lee-Kesler, 1342
 liquid-liquid equilibrium, 367
 mixed-flow, 885
 Miyauchi, 889, 890
 noncompetitive adsorption, 759
 predictive control (MPC), 1246, 1247
 random pore, 773, 783
 SAFT, 11

Separations Research Program, 1061
 sharp interface model, 770
 shrinking core, 774
 Sisko, 401
 SUPERTRAPP, 17
 TBP reaction, 714
 thermodynamic, LLE and, 716
 Thiele-Geddes, 993
 two-zone, 778
 UNIFAC, 717, 981–983
 UNIQUAC, 1342
 Vacancy Solution, 1141
 volume reaction, 776
 Modified Accelerated Cost Recovery System (MACRS), 1289
 Monochromatic radiation, 568
 Moving-bed reactors, 837
 MPC, *see* Model predictive control
 MPI, *see* Major plant items
 M&S index, *see* Marshall & Swift index
 Multicomponent vapor, condensation of, 530
 Multiphase reactors, 741
 Multiple-input/multiple-output (MIMO) process, 1242
 Multitubular reactor, 860
 Multivariable control (MVC), 1247
 Multivariable controller
 general method for designing, 1249–1261
 commissioning of controller, 1260–1261
 conducting of plant test and collection of data, 1254–1255
 design of plant test, 1251–1254
 post audit, 1261
 structuring of controller and analysis of data, 1255–1259
 tuning of controller, 1259–1260
 understanding of process, 1249–1251
 troubleshooting, 1261–1263
 checklist, 1262–1265
 commonsense approach, 1262
 controller still making money, 1264
 Murphree point efficiency, 975
 MV, *see* Manipulated variable
 MVC, *see* Multivariable control

N

National Chemical Laboratory (NCL), 945
 National Institute of Standards and Technology (NIST), 28
 Natural convection, single-phase heat transfer in, 520–523
 horizontal cylinder, 523
 horizontal plates, 522–523
 other geometries, 523
 two horizontal parallel plates, 523
 vertical plane surface, 521–522
 Navier-Stokes equations, 618, 848
 NCL, *see* National Chemical Laboratory
 Nernst's law, 717, 725
 Net positive suction head (NPSH), 1325
 Newtonian fluids, 419–422
 all flow regimes, 420–422

P

Partial differential equations, 115–131
 classification of second-order equations, 118–119
 computational fluid mechanics, 131
 elliptic equations, 128–131
 Green's function, 130–131
 Poisson integral formula, 129–130
 first-order partial differential equations, 115–118
 hyperbolic equations, 124–128
 d'Alembert's solution, 124–126
 separation of variables, 126–128
 parabolic equations, 119–124
 inhomogeneous boundary conditions, 122
 inhomogeneous equation, Duhamel's principle, 120–121
 inhomogeneous equation in infinite domain, 123–124
 separation of variables, 119–120
 similarity solutions, 122–123
 processes governed by, 48–50
 dynamics of chromatography, 49–50
 dynamics of tubular reactor, 48–49
 Patents and intellectual property, 1831–1839
 intellectual property between employer and employee, 1838–1839
 patents, 1838
 rights and obligations created or eliminated by
 express agreement, 1839
 trade secrets, 1838–1839
 patents outside United States, 1834
 preliminary steps for inventor, 1835–1837
 minimizing chances for invalidation, 1837
 patents as prior art, 1836
 prior art searching, 1835–1836
 record keeping, 1836
 representation before USPTO, 1835
 requirements for patentability, 1834–1835
 nonobviousness, 1835
 novelty, 1834–1835
 utility, 1835
 trade secrets, 1837–1838
 United States patents and related rights and documents, 1832–1834
 copyrights, 1833–1834
 design patent, 1832
 provisional patent application, 1832–1833
 trademarks, 1833
 utility patent, 1832
 PBT, *see* Profiled bottom tank
 PC, *see* Pipeline contactor
 PCOR equation, *see* Polymer chain-of-rotator equation
 PCS, *see* Principle of corresponding states
 Pearlite, 1547
 Peclet number, 506–507, 855
 Peng–Robinson (PR) equation, 11, 299
 Peng–Robinson–Stryjek–Vera (PRSV) eos, 349
 Perturbed hard-chain theory (PHCT), 301
 PFDs, *see* Process flow drawings
 PFR, *see* Plug-flow reactor
 PFTR, *see* Plug flow tubular reactor

PHCT, *see* Perturbed hard-chain theory
 Physical and chemical properties, 1–34
 apparatus calibration, 21
 aqueous electrolyte solutions, 17–20
 density and enthalpy, 18–19
 transport properties, 19–20
 vapor-liquid equilibria and activity coefficients, 17–18
 binary interaction parameter, 11
 Burnett method, 22
 calorimetry, 22
 combining rule, 11
 corresponding-states methods, 7
 COSMO, 12
 differential ebulliometry, 24
 ebulliometry, 23
 electrolyte-NRTL model, 18
 equation of state, 11
 experience, 21
 flow calorimetry, 23
 fugacity coefficient, 12
 gas saturation method, 24
 Gibbs energy, 12
 group-contribution methods, 7, 20
 Hagen-Poiseuille relationship, 25
 Helgeson–Kirkham–Flowers correlation, 19
 Helmholtz energy, 12
 Henry's law, 13
 ideal-gas law, 9
 ideal mixture volume, 9
 ionic strength, 19
 isochors, 22
 Knudsen method, 24
 liquid-liquid equilibrium, 19
 major data sources, 27–30
 Beilstein, 29–30
 DDB, 29
 DECHEMA, 29
 DIPPR, 28
 Gmelin, 30
 Landolt-Börnstein, 29
 NEL, 29
 NIST, 28
 process simulation software, 30
 measurement of fluid thermophysical properties, 20–27
 density, 22
 electrolyte solutions, 27
 general considerations, 21–22
 heat capacity and caloric properties, 22–23
 liquid-liquid equilibria, 25
 mixture vapor-liquid equilibria, 24–25
 pure-component vapor pressure, 23–24
 thermal conductivity, 26–27
 viscosity, 25–26
 when experiments are necessary, 20–21
 model-substance approach, 18
 oscillating-cup method, 26
 Peng–Robinson equation, 11
 phase equilibria for mixtures, 10–14
 activity-coefficient methods, 12–13
 equation-of-state methods, 11–12

- monolithic, 1418–1418
- motionless mixer in tube, 1415
- multibed adiabatic with interbed quench, 1414
- multiple hearth, 1419
- multitube fixed bed catalyst, 1414
- packing, 1417–1418
- rotary kiln, 1420
- shaft furnace, 1420
- spray reactor and jet nozzle reactor, 1416
- thin film, 1419
- transported or slurry, transfer line, 1414–1415
- traveling grate, 1419
- trays, 1417
- trickle bed, 1418
- via multistage CSTR, 1420–1421
- Poisson equation, 128, 130
- Polymer chain-of-rotator (PCOR) equation, 306
- Polymers, 1132
- Polynomial equations, 85–88
 - bounds on real roots, 86
 - Budan's rule of signs, 86
 - Cardano's formula, 87
 - Descartes's rule of signs, 86
 - quadratic formula, 86
 - quartic formula, 88
 - Routh-Hurwitz criterion, 85
- Population balance equations, 52
- Potentiometry, 27
- Pourbaix diagrams, 1807
- Powder materials, *see* Granular and powder materials, dry screening of
- Power law fluids, 422–426
 - all flow regimes, 426
 - laminar flow, 422
- Poynting factor, 12, 325
- Prandtl number, 506
- PR equation, *see* Peng–Robinson equation
- Pressure swing adsorption (PSA), 1122
- Prigogine–Flory–Patterson theory of polymer liquids, 302
- Principle of corresponding states (PCS), 287
- Probability distributions, 201–202, 203–212
 - binomial distribution (discrete variable), 204
 - characteristic parameters of, 202–203
 - chi-square distribution for sample variance (continuous variable), 210–211
 - continuous probability density distributions, 201–202
 - discrete probability distributions, 201
 - F* distribution for ratio of sample variances (continuous variable), 211
 - geometric distribution (discrete variable), 205
 - normal or Gaussian distribution (continuous variable), 206–207
 - Poisson distribution (discrete variable), 205–206
 - t* distribution of sample means (continuous variable), 207–210
- Process control, 1173–1265
 - adaptive control techniques, 1238
 - adjustable-speed pumps, 1191
 - advanced PID control, 1227–1246
 - antiwindup strategies, 1240–1241
 - bumpless transfer, 1241–1242
 - cascade control, 1227–1228
 - computed manipulated variable control, 1239–1240
 - feedforward control, 1230–1233
 - inferential control, 1233–1236
 - MIMO process control, 1242–1246
 - override/select control, 1238–1239
 - ratio control, 1229–1230
 - scheduling controller tuning, 1236–1238
 - split-range flow control, 1242
 - ATV tests, 1223, 1246
 - boiler drum level control, 1230
 - booster relays, 1191
 - cavitation, 1190
 - closed-loop dynamic behavior, 1181–1182
 - comparison of feedback and feedforward control, 1232
 - controller cycle time, 1186
 - controller/DCS system problems, 1199
 - control loop hardware and troubleshooting, 1182–1200
 - actuator systems (final control elements), 1187–1191
 - distributed control system, 1184–1187
 - sensor systems, 1191–1194
 - troubleshooting control loops, 1194–1200
 - coupled process, 1242
 - decentralized control, 1242–1243
 - definition of symbols for control diagrams, 1176
 - derivative kick, 1202
 - direct-acting controller, 1201
 - direct-acting final control element, 1190
 - distillation column, bottoms composition control of, 1228
 - error from setpoint, 1177
 - finite control element, common problems with, 1196
 - first-order plus deadtime model, 1179–1181
 - FOPDT model, 1181
 - general dynamic behavior, 1177–1179
 - generalized feedback system, 1177
 - integral windup, 1240
 - interactive PID controller, 1205
 - internal reflux control, 1240
 - model predictive control, 1246–1264
 - description, 1246–1247
 - general method for designing multivariable controller, 1249–1261
 - history, 1248
 - multivariable controller troubleshooting, 1261–1264
 - when to use, 1248–1249
 - move suppression, 1260
 - multiple-input/multiple-output process, 1242
 - nonstationary process, 1237
 - PID algorithm, 1205
 - PID controllers, 1201–1213
 - algorithms, 1201–1206
 - analysis of P, I, and D action, 1206–1207
 - analysis of typical control loops, 1209–1213
 - controller design issues, 1208–1209
 - PID tuning, 1213–1227
 - controller reliability, 1218–1219
 - effect of tuning parameters on dynamic behavior, 1214–1218

jet-loop, 847

kinetic energy (stirred tank reactors), 839–848

- blending, 841, 845
- blending in gas-liquid systems, 844–845
- dead end systems, 846–848
- gas dispersion, 841–843
- heat transfer, 844
- heat transfer in gas-liquid systems, 846
- solid suspension, 843–844
- suspension in gas-liquid-solid systems, 845–846

mixed-flow, 751

moving-bed, 837

multiphase, 741

multitubular, 860

NINA, 879

nonisothermal nonadiabatic fixed-bed reactor, 813

pressure energy, 800–839

- gas-liquid reactors, 800–812
- gas-solid catalytic fixed-bed reactors, 813
- gas-solid catalytic fluidized-bed reactors, 821–835
- gas-solid noncatalytic reactors, 835–839
- liquid-liquid reactors, 812
- solid-liquid reactors, 812–813, 821

radial-flow, 819

radial flow fixed-bed reactor, 813

simulated moving-bed, 740

single-pellet, 770

SPE oil hydrogenation, 1786, 1787

staged, 828

steady-state adiabatic, 386

stirred-tank, 45

three-phase catalytic reactor, 936

three-phase sparged, 921

tubular

- dynamics of, 48
- steady-state multiplicity, 174

turbulent-bed reactor, 826

Real number system, 53–54

- logarithm, 54
- powers and roots, 53–54

Redlich–Kister equation, 330

Redlich and Kwong (RK) equation, 298, 1342

Regularization, method of, 142

Relay feedback experiment, 1223

Resistance temperature detectors (RTD), 1192, 1351

Resource Conservation and Recovery Act (RCRA), 1327, 1499

Retreat-curve impellers (RCI), 623

Retrograde condensation, 292

Reynolds number, 80, 504–505, 518, 689, 764, 864, 912

RF-FBR, *see* Radial flow fixed-bed reactor

RFT, *see* Radial-flow turbines

Ricatti equations, 105

RIM, *see* Reaction injection-molding systems

RK equation, *see* Redlich and Kwong equation

Robin boundary condition, 129

Robin problem, 118

Rotating biological contactors (RBC), 848

Rouché theorem, 151–152

RTD, *see* Resistance temperature detectors

RTE, *see* Radiative transfer equation

S

Safety, *see* Chemical process safety

Safety interlock system (SIS), 1351

SAFT, *see* Statistical associating fluid theory

Sales, administration, research, and engineering (SARE)

- expenses, 1287

SAP catalyst, *see* Supported aqueous phase catalyst

SARE expenses, *see* Sales, administration, research, and engineering expenses

SBC, *see* Sectionalized bubble column

Scalar difference equations, 42

Schmidt number, 1761

SCM, *see* Shrinking core model

Sectionalized bubble column (SBC), 905

Sensor systems, 1191–1194

- chemical composition analyzers, 1193
- flow measurements, 1193
- level measurements, 1193
- pressure measurements, 1193
- repeatability, accuracy, and dynamic response, 1192
- sampling system, 1193
- temperature measurements, 1192
- thermowells, 1192
- transmitters, 1194

Separations Research Program (SRP) model, 1061

Sharp interface model (SIM), 770

Sherwood number, chemical reaction engineering, 764

Shock wave velocity, 1146

Shrinking core model (SCM), 770, 774

Sieder-tate term, 507

Silicas, 1130–1131

SIM, *see* Sharp interface model

Simulated moving-bed reactors, 740

Simulated moving-bed systems, 1122

Single-pellet reactor, 770

SIS, *see* Safety interlock system

Sisko model, 401

SLE, *see* Solid-liquid extraction

SLS, *see* Solid/liquid separation

Slugging, 833

Slurry reactor, oxydesulfurization of coal in, 919–925

Soave–Redlich–Kwong (SRK) equation, 11

Software

- CFD, 618, 632
- design, process improvement, and troubleshooting, 1334–1335
- mathematical, 182–183
- MPC modeling software, 1257
- security, process safety management, 1467
- solvent extraction, 729

Solid(s)

- bulk, conveying of, 1729–1736
 - air-activated gravity conveyor, 1735
 - belt conveyors, 1730–1733
 - bucket elevators, 1734
 - en-masse conveyors, 1734–1735
 - materials characterization, 1729–1730
 - pneumatic conveyors, 1735
 - screw conveyors, 1733
 - vibrating conveyors, 1734

Stochastic differential equations, 42, 166–170
 connection between Fokker-Planck equation and, 167–168
 differential Chapman-Kolmogorov equation, 167
 Itô stochastic integral, 168–170
 application, 169–170
 one-dimensional Itô formula, 169
 processes governed by, 52–53
 Stochastic processes, 166
 Stokes's law, 654
 Stripping operating line, 986
 Sublimation pressure, 284, 372
 Sublimation pressure curve, 296
 SUPCRT92, 19
 Super-compactible materials, filtration of, 1623–1629
 Darcy's law, 1625–1626
 effective pressure, 1623–1625
 empirical constitutive equations, 1626
 integration of Darcy equation, 1626–1627
 Superheated vapor, condensation of, 530–531
 SUPERTRAPP model, 17
 Supported aqueous phase (SAP) catalyst, 754
 Supported organic phase (SOP) catalyst, 756

T

Tafel equation, 1751
 TBP, *see* Tri-*n*-butyl phosphate
 TCs, *see* Thermocouples
 Temperature-measuring devices, 1531–1535
 bi-metallic thermometers, 1535
 filled-bulb and glass-stem thermometers, 1534
 pyrometric cones, 1535
 radiation and infrared pyrometers, 1533–1534
 resistance thermometers and thermistors, 1532–1533
 thermocouples, 1532
 Temperature swing adsorption (TSA), 1122, 1162–1163
 Tetrachloroethane chlorinates, 871
 The Natural Step (TNS), 1322
 Thermal energy
 direct contact gas-liquid condensers, 1366
 direct contact gas-liquid cooling towers, 1366
 direct contact gas-liquid quenchers, 1366
 direct contact gas-solid fluidized beds, 1365
 direct contact gas-solid kilns, 1363
 direct contact gas-solid multiple-hearth furnaces, 1365
 direct contact liquid-liquid immiscible liquids, 1364
 fluid heat exchangers, 1361
 fluidized bed, 1363
 furnaces, 1360
 gas-gas thermal wheels, 1367
 gas-solid drying of solids, 1365
 heat loss to atmosphere, 1367
 motionless mixers, 1364
 refrigeration, 1367
 solidify liquids, 1367
 steam generation, 1368
 Thermocouples (TCs), 1192
 Thermodynamics, fluid phase and chemical equilibria, 255–392
 absolute temperature, 267

acentric factor, 288
 adiabatic system, 257
 analytical solution of groups method, 345
 athermal solutions, 334
 azeotrope, 292
 Boublik–Alder–Chen–Kreglewski eos, 301
 bubble-point curve, 291
 Carnot cycle, 265
 chain-of-rotators equation, 302
 chemical reaction equilibria, 375–391
 chemical reaction equilibrium, 375–376
 equilibrium constants, 376–384
 open systems with reaction, 385–388
 phase rule for chemically reacting species, 384–385
 stoichiometric formulation, 388–391
 Clapeyron equation, 352
 compressed liquid states, 355
 degree of freedom, 290
 dew-point curve, 291
 dimer theory, 306
 energy functions, 276
 enthalpy balance, 261
 entropy, 264
 equilibrium ratio, 355
 extensive property of system, 257
 first law of open systems, 261
 fluid-phase equilibria, 351–375
 gas-solid equilibrium models, 372–374
 liquid-liquid equilibrium models, 367–372
 vapor-liquid equilibrium of ideal mixtures, 355–358
 vapor-liquid equilibrium by ϕ - ϕ models, 364–367
 vapor-liquid equilibrium by ϕ - ϕ models, 358–364
 vapor-liquid equilibrium in single-component fluid, 351–355
 free-energy-matching mixing rules, 349
 free volume, 296
 fugacity, 279
 fugacity coefficient, 322
 function of temperature, 377
 gas-liquid critical state, 285
 Gauss-Jordan elimination, 390
 Gibbs-Duhem equation, 281, 283
 Gibbs phase rule, 385
 Hang–Chao–Hilson complete local-composition model, 371
 heat exchangers, 262
 Helmholtz free energy, 273
 ideal gas definition, 313
 ideal-gas equation, 258
 ideal-solution law, 325
 intensive property of system, 257
 isobaric process, 257
 isochores, 286
 Lewis fugacity rule, 355
 light component, 355
 liquid solutions, 325–351
 activity coefficient, 363
 activity-coefficient models, 329–343
 Gibbs energy models of liquid solutions, 347–350
 group contribution methods, 343–346
 ideal and excess solution properties, 328–329

Volterra integral equations, 131–132
Volume reaction model, 776
VTPR, 12

W

Weber number, 674, 689
Wegstein acceleration, 1339
Wet corrosion, 1805
Weymouth equation, 440

Wheeler–Robell equation, 1146
White noise, 53
Wien's displacement law, 570
Wilson's local-composition equation, 336–338

Z

Zeigler–Nichols tuning, 1246
Zeolites, 1131

